NOAA TECHNICAL MEMORANDUM NWS CR-112

POSTPRINT
Fourth NWS Winter Weather Workshop
September 19-22, 1995

National Weather Service
Central Region Headquarters
Scientific Services Division
Kansas City, Missouri

July 1996

U.S DEPARTMENT OF Commerce / National Oceanic and Atmospheric Administration / National Weather Service

NOAA TECHNICAL MEMORANDA
National Weather Service, Central Region Subseries

The National Weather Service Central Region (CR) subseries provides an informal medium for the documentation and quick dissemination of results not appropriate, or not yet ready, for formal publication. The series is used to report on work in progress, to describe technical procedures and practices, or to relate progress to a limited audience. These Technical Memoranda report on investigations devoted primarily to regional and local problems of interest mainly to regional personnel, and hence will not be widely distributed.

Papers 1 through 15 are in the former series, ESSA Technical Memoranda, Central Region Technical Memoranda (CRTM); Papers 16 through 36 are in the former series, ESSA Technical Memoranda, Weather Bureau Technical Memoranda (WBTM). Beginning with Paper 37, the papers are part of the series, NOAA Technical Memoranda NWS.

Papers that have a PB or COM number are available from the National Technical Information Service, U. S. Department of Commerce, 5285 Port Royal Road, Springfield, VA 22151. Order by accession number shown in parenthesis at the end of each entry. Prices vary for all paper copies. Microfiche are $4.50. All other papers are available from the National Weather Service Central Region, Scientific Services, Room 1836, 601 East 12th Street, Kansas City, MO 64106.

ESSA Technical Memoranda

CRTM 1 Precipitation Probability Forecast Verification Summary Nov. 1965 - Mar. 1966, SSD Staff, WBCRH, May 1966.
CRTM 2 A Study of Summer Showers Over the Colorado Mountains. William G. Sullivan, Jr., and James O. Severson, June 1966.
CRTM 3 Areal Shower Distribution - Mountain Versus Valley Coverage. William G. Sullivan, Jr., and James O. Severson, June 1966.
CRTM 4 Heavy Rains in Colorado June 16 and 17, 1965. SSD Staff, WBCRH, July 1966.
CRTM 5 The Plum Fire. William G. Sullivan, Jr., August 1966.
CRTM 6 Precipitation Probability Forecast Verification Summary Nov. 1965 - July 1966. SSD Staff, WBCRH, September 1966.
CRTM 7 Effect of Diurnal Weather Variations on Soybean Harvest Efficiency. Leonard F. Hand, October 1966.
CRTM 8 Climatic Frequency of Precipitation at Central Region Stations. SSD Staff, WBCRH, November 1966.
CRTM 9 Heavy Snow or Glazing. Harry W. Waldheuser, December 1966.
CRTM 10 Detection of a Weak Front by WSR-57 Radar. G. W. Polensky, December 1966.
CRTM 11 Public Probability Forecasts. SSD Staff, WBCRH, January 1967.
CRTM 12 Heavy Snow Forecasting in the Central United States (an Interim Report). SSD Staff, January 1967.
CRTM 13 Diurnal Surface Geostrophic Wind Variations Over the Great Plains. Wayne E. Sangster, March 1967.
CRTM 14 Forecasting Probability of Summertime Precipitation at Denver. Wm. G. Sullivan, Jr., and James O. Severson, March 1967.
CRTM 15 Improving Precipitation Probability Forecasts Using the Central Region Verification Printout. Lawrence A. Hughes, May 1967.
WBTM CR 16 Small-Scale Circulations Associated with Radiational Cooling. Jack R. Cooley, June 1967.
WBTM CR 17 Probability Verification Results (6-month and 18-month). Lawrence A. Hughes, June 1967.
WBTM CR 18 On the Use and Misuse of the Brier Verification Score. Lawrence A. Hughes, August 1967 (PB 175 771).
WBTM CR 19 Probability Verification Results (24 months). Lawrence A. Hughes, February 1968.
WBTM CR 20 Radar Prediction of the Topeka Tornado. Norman E. Prosser, April 1968.
WBTM CR 21 Wind Waves on the Great Lakes. Lawrence A. Hughes, May 1968.
WBTM CR 22 Seasonal Aspects of Probability Forecasts: 1. Summer. Lawrence A. Hughes, June 1968 (PB 185 733).
WBTM CR 23 Seasonal Aspects of Probability Forecasts: 2. Fall. Lawrence A. Hughes, September 1968 (PB 185 734).
WBTM CR 24 The Importance of Areal Coverage in Precipitation Probability Forecasting. John T. Curran and Lawrence A. Hughes, September 1968.
WBTM CR 25 Meteorological Conditions as Related to Air Pollution, Chicago, Illinois, April 12-13, 1963. Charles H. Swan, October 1968.
WBTM CR 26 Seasonal Aspects of Probability Forecasts: 3. Winter. Lawrence A. Hughes, December 1968 (PB 185 735).
WBTM CR 27 Seasonal Aspects of Probability Forecasts: 4. Spring. Lawrence A. Hughes, February 1969 (PB 185 736).
WBTM CR 28 Minimum Temperature Forecasting During Possible Frost Periods at Agricultural Weather Stations in Western Michigan. Marshall E. Soderberg, March 1969.
WBTM CR 29 An Aid for Tornado Warnings. Harry W. Waldheuser and Lawrence A. Hughes, April 1969.
WBTM CR 30 An Aid in Forecasting Significant Lake Snows. H. J. Rothrock, November 1969.
WBTM CR 31 A Forecast Aid for Boulder Winds. Wayne E. Sangster, February 1970.
WBTM CR 32 An Objective Method for Estimating the Probability of Severe Thunderstorms. Clarence L. David, February 1970.
WBTM CR 33 Kentucky Air-Soil Temperature Climatology. Clyde B. Lee, February 1970.
WBTM CR 34 Effective Use of Non-Structural Methods in Water Management. Verne Alexander, March 1970.
WBTM CR 35 A Note on the Categorical Verification of Probability Forecasts. Lawrence A. Hughes and Wayne E. Sangster, August 1970.
WBTM CR 36 A Comparison of Observed and Calculated Urban Mixing Depths. Donald E. Wuerch, August 1970.

NOAA Technical Memoranda NWS

NWS CR 37 Forecasting Maximum and Minimum Surface Temperatures at Topeka, Kansas, Using Guidance from the PE Numerical Prediction Model (FOUS). Morris S. Webb, Jr., November 1970 (COM 71 00118).
NWS CR 38 Snow Forecasting for Southeastern Wisconsin. Rheinhart W. Harms, November 1970 (COM 71-00019).
NWS CR 39 A Synoptic Climatology of Blizzards on the North-Central Plains of the United States. Robert E. Black, February 1971 (COM 71-00369).
NWS CR 40 Forecasting the Spring 1969 Midwest Snowmelt Floods. Herman F. Mondschein, February 1971 (COM 71-00489).
NWS CR 41 The Temperature Cycle of Lake Michigan 1. (Spring and Summer). Lawrence A. Hughes, April 1971 (COM 71-00545).
NWS CR 42 Dust Devil Meteorology. Jack R. Cooley, May 1971 (COM 71-00628).
NWS CR 43 Summer Shower Probability in Colorado as Related to Altitude. Alois G. Topil, May 1971 (COM 71-00712).
NWS CR 44 An Investigation of the Resultant Transport Wind Within the Urban Complex. Donald E. Wuerch, June 1971 (COM 71- 00766).
NWS CR 45 The Relationship of Some Cirrus Formations to Severe Local Storms. William E. Williams, July 1971 (COM 71- 00844).
NWS CR 46 The Temperature Cycle of Lake Michigan 2. (Fall and Winter). Lawrence A. Hughes, September 1971 (COM 71-01039).

(Continued on Back Cover)

NOAA TECHNICAL MEMORANDUM NWS CR-112

POSTPRINT
Fourth NWS Winter Weather Workshop
September 19-22, 1995

National Weather Service
Central Region Headquarters
Scientific Services Division
Kansas City, Missouri

July 1996

UNITED STATES DEPARTMENT OF COMMERCE
Michael Kantor
Secretary

National Oceanic and Atmospheric Administration
D. James Baker
Under Secretary

National Weather Service
Elbert W. Friday, Jr.
Assistant Administrator

PREFACE

The Fourth National Weather Service Winter Weather Workshop was held September 19-22, 1995 in Kansas City, Missouri. The National Weather Service Central Region Headquarters hosted this workshop. Support was provided by the National Weather Service Headquarters, Office of Meteorology. The American Meteorological Society was a collaborating organization.

This volume contains unrefereed articles by participants who provided written versions of their presentations. Copies of visual aids used during laboratory sessions are also included. A complete listing of abstracts is contained in the workshop manual.

Program/Arrangements Committee

- Dr. Preston Leftwich, Workshop Chairperson, NWS Central Region Headquarters, Scientific Services Division, Kansas City, Missouri.
- Dr. Richard Livingston, Chief, Scientific Services Division, NWS Central Region Headquarters, Kansas City, Missouri.
- Dr. Douglas Wesley, NWS Forecast Office, Cheyenne, Wyoming (Current affiliation NWS Forecast Office, Denver, Colorado.).
- Peter Browning, NWS Office, Pleasant Hill, Missouri.
- Samuel Beckman, NWS Training Center, Kansas City, Missouri.
- Kathy Hoxsie, NWS Central Region Headquarters, Kansas City, Missouri (Current affiliation NWS Office, Gaylord, Michigan.).
- Deborah White, NWS Central Region Headquarters, Scientific Services Division, Kansas City, Missouri
- Paula Guarino, Meteorological Services Division, NWS Central Region Headquarters, Kansas City, Missouri.

Efforts of the presenters, laboratory leaders, session chairpersons and numerous assistants led to a successful workshop. Special thanks go to Deborah White for her excellent work in the production of both the workshop manual and this volume.

For further information, please contact:

National Weather Service
Central Region Headquarters
Scientific Services Division - W/CR3
Federal Building, Room 1836
601 East 12th Street
Kansas City, Missouri 64106

FOURTH NWS WINTER WEATHER WORKSHOP
SEPTEMBER 19-22, 1995

Adams Mark
I-70 at Truman Sports Complex
Kansas City, Missouri

Session 1 - Program Overviews

1. THE COOPERATIVE PROGRAM FOR OPERATIONAL METEOROLOGY, EDUCATION, AND TRAINING (COMET®): WINTER WEATHER TRAINING PROGRAMS
   Roger V. Pierce - NWS Office of Hydrology; Gregory P. Byrd and Ron L. Alberty - COMET/UCAR; Julie A. Hall - NWS Office of Meteorology, Boulder, CO

Session 2 - Operational Forecast Models

2. A COMPARISON BETWEEN THE 40KM MESO-ETA AND 80 KM NGM DURING A HYBRID SYNOPTIC-LAKE EFFECT SNOW STORM OVER THE EASTERN GREAT LAKES
   Michael T. Eckert - Weather Forecast Branch, HPC, NCEP, Camp Springs, MD

3. THE PREDICTION OF RAPIDLY DEEPENING CYCLONES BY NCEP'S NESTED GRID MODEL (NGM) & GLOBAL SPECTRAL MODEL (AVN) WINTER 1989/90 - AUTUMN 1991 & WINTERS 1993/94 & 1994/95
   Robert J. Oravec - Weather Forecast Branch, HPC, NCEP, Camp Springs, MD; Richard H. Grumm - NWS Forecast Office, State College, PA

4. COMMON COLD SEASON BIASES IN NCEP'S MEDIUM RANGE FORECAST MODEL (MRF)
   Robert T. Oravec - Weather Forecast Branch, HPC, NCEP, Camp Springs, MD

Session 3 - Applications of Technology I

5. THE USE OF GOES-8 MULTISPECTRAL IMAGERY FOR THE DETECTION OF AIRCRAFT ICING REGIONS
   Gary P. Ellrod - NOAA/NESDIS Office of Research and Applications, Washington, DC

6. FORECASTING PRECIPITATION ON THE EAST SLOPES OF THE ROCKY MOUNTAINS: NEW OBSERVING SYSTEMS DURING THE 1994-95 WINTER
   Douglas A. Wesley and Jim L. Hatten - NWS Forecast Office, Cheyenne, WY; Julie A. Hall - NWS Office of Meteorology, Boulder, CO

7. CONTRIBUTIONS OF NWS MODERNIZED TECHNOLOGIES FOR THE HEAVY LAKE SNOW EVENT OVER NORTHEAST OHIO AND NORTHWEST PENNSYLVANIA ON 4 JANUARY 1995
   Louis A. Giordano, Richard R. Redmond and Paul A. Jendrowski - NWS Forecast Office, Moon Township, PA

Session 4 - Applications of Technology II

Session 5 - Poster Previews

Session 6 - Heavy Snow Case Studies

SESSION 1
PROGRAM OVERVIEWS

1. The Cooperative Program for Operational Meteorology, Education, and Training (COMET®): Winter Weather Training Programs

The Cooperative Program for Operational Meteorology, Education and Training (COMET®): Winter Weather Training Programs

Roger V. Pierce,[1] Gregory P. Byrd[2], Julie A. Hall[3], and Ron L. Alberty[4]

1. INTRODUCTION

New technologies such as the Weather Surveillance Radar 1988 Doppler (WSR-88D), Automatic Surface Observing System (ASOS), and Geostationary Operational Environmental Satellite (GOES) 8 and 9 are quickly becoming available for field personnel utilization. In order for data provided by these different sources to be fully utilized by forecasters throughout the nation, additional training and deployment of new software packages will be needed. A suite of software packages is available in the Pre-Advanced Weather Interactive Processing System (Pre-AWIPS) era (Pierce 1995). The use of these new data sources for application to winter weather forecasting is applied to most courses taught by the COMET Residence Program. These applications to winter weather are the focus of this paper.

2. COMET COURSE DESIGNS AND TARGET PERSONNEL

COMET Residence Courses are influenced primarily by the COMET Residence Program Advisory Committee (RPAC) chaired by Dr. Ron L. Alberty, COMET Deputy Director and Residence Program Manager. Members of the RPAC include National Weather Service (NWS) operational employees, COMET representatives, NWS regional office representatives, and university faculty. This group will ensure that COMET teaching philosophies meet the needs of NWS training initiatives.

COMET teaching methods use visiting university and operational scientists to convey recent research results to field operations personnel. A case study approach is used to teach advanced level scientific concepts, but job specific topics are not emphasized (Spangler et al., 1994).

The COMET teaching philosophy, as described by Spangler et al. (1994), is as follows:

1. Instruction will be by university and operational scientists.
2. Recent research results will be transferred to operations.
3. A case study approach will be taken.
4. Although training and education toward a particular profession is provided by the Residence Program, specific job training will generally not be provided.
5. Courses will be taught at an advanced level.

Goals for each COMET course are based on the needs each course is designed to fulfill. These goals are defined and agreed upon by the RPAC.

1. Corresponding author address: Roger V. Pierce, NWS, Office of Hydrology, UCAR/COMET, P.O. Box 3000, Boulder, Colorado 80307.
2. Dr. Gregory Byrd, Senior Meteorologist, UCAR/COMET, P.O. Box 3000, Boulder, Colorado 80307.
3. Julie Hall, NWS, Office of Meteorology, UCAR/COMET, P.O. Box 3000, Boulder, Colorado 80307.
4. Dr. Ron Alberty, COMET Deputy Director and Residence Program Manager, UCAR/COMET, P.O. Box 3000, Boulder, Colorado 80307.

Personnel attending Residence Program courses are selected from the NWS, Air Weather Service, Naval Meteorology and Oceanography Command, and organizations representing the national and international meteorology community.

3. RESIDENCE PROGRAM COURSES

Eight courses are being planned for calendar year 1996, some of which will be offered up to four times (Alberty, 1995). The signature course of the program is the Mesoscale Analysis and Prediction (COMAP) course designed for NWS Science and Operations Officers (SOO). This eight-week course is broken into two four-week segments and is taught at the graduate level. The first section covers synoptic and mesoscale cool season events. The second four weeks are devoted to mesoscale convection, related warm season meteorology, and selected hydrology topics.

To emphasize the importance of understanding hydrology in meteorology, the Residence Program offers a three-week course titled Hydromet. The Hydrologic Training Council of the NWS has oversight of this course along with the RPAC. Primary course attendees are members of NWS River Forecast Centers (RFC) and service hydrologists. Operational meteorology and hydrology are presented in this course with a focus on quantitative precipitation forecasting (QPF) and the use of new technologies such as the WSR-88D precipitation estimations (Pierce, 1995).

For management personnel of operational organizations, the COMET Residence Program offers a Managers Course—a science-based, short course that enables managers to become more familiar with new technologies and the advances in science and data sources now available to field personnel.

To assist in keeping senior operational scientists current in science and technological advances, the Residence Program is planning several one-week intensive training sessions. These symposiums will be topic specific and will enable forecasters to take information back to the home office for use in local training programs. QPF is an area of expanding significance in NWS operations and will be one of the first topics covered. Satellite meteorology is a topic that will also be offered in 1996.

With its title as the focus, Mesoscale Meteorology is designed as a three-week course for operational forecasters to enhance skills in new technologies and science.

Other COMET courses are presented in conjunction with various universities and international organizations such as the World Meteorological Organization (WMO). These courses are also topic specific and concentrate on education and significant advances in science for the instructor.

4. WINTER WEATHER INSTRUCTION

Each COMET course has segments devoted to synoptic scale and mesoscale meteorological events occurring in the cool season. Precipitation patterns on different scales are addressed, and techniques for analysis and forecasting such events are evaluated. In addition, students study temperature forecasting of the three-dimensional atmosphere. The processes are not just limited to the use of diagnostic charts, but extend to greater complexity to quantitatively analyze the physical conditions being generated in the atmosphere.

Courses are taught differently depending on the attendees and the course goals. A combination of lecture and Displaced Real-Time (DRT) workstation exercises are used to convey to students new techniques or understanding of the science of hydrometeorology. Because the courses focus on laboratory exercises using case studies, lecture sessions are kept to 40 to 60 percent of the classroom time. In fact, the concept of the "lecturette"—short 10- to 15-minute lectures on given topics related

to and presented prior to the exercise material—is an extremely effective venue for learning. Students are able to work at their own pace and instructors have the opportunity to move about the classroom giving individual instruction to students as needed.

Certain theoretical topics are best presented in lectures with varying presentation media. The Residence Program employs a large projection screen viewing system, videos, slides and overheads, and excerpts from the COMET Distance Learning Program modules to enhance the lecture format.

Once into the cool season exercise, students work in pairs at workstations, at their own pace, with supervision. Interaction between exercise leaders—experts on individual topics—and students is encouraged. A beneficial teaching concept includes prompts and directed questions to individual students by exercise leaders. Lecturettes or short discussions are frequently used in this period of learning. COMET instructors have found that a short break is necessary for periods greater than 1 hour; this time allows instructors to ensure that all students are following the material and understanding the concepts.

At the end of the DRT exercise, a final discussion of the exercise is conducted. Leaders of the exercise point out individual characteristics of the event and verification data. The data are collected from many different sources depending on the type of case being presented. This final wrap up of the case study gives participants the opportunity to discuss things missed in the analysis and forecast process and ways to better evaluate the situation to avoid such errors in the future.

An objective in all courses is to evaluate traditional ways of viewing data. Many of these analysis techniques can be modified to make the best use of new technologies. The profiler data network is an example of this new technology. Other tools, such as numerical meteorological forecast model output, make better use of more familiar data but make the display process user specific. A good example of this is the General Meteorological Package (GEMPAK), which makes use of the gridded data from National Meteorological Center (NMC) model guidance but displays the data in user defined formats.

In addition to numerical guidance, new satellite data and display systems are available in the COMET classroom. National Centers Satellite (NSAT) display system, part of the National Centers AWIPS (N-AWIPS), has the capability of displaying the advanced GOES 8 and 9 satellite data as well as WSR-88D images. Alphanumeric products are becoming available through National Centers Weather (NWX) and are also part of N-AWIPS. The NWS Techniques Development Laboratory (TDL) Forecast Systems Laboratory (FSL) and the AWIPS Program Office are collaborating with COMET software engineers on new developments and advances in display software capabilities.

Interaction between all these different software applications is very important to the DRT exercise process. The use of DRTs as a major part of teaching is paramount to COMET courses (Pierce, 1995; Spangler, 1994). Teaching with a case study approach using the tools of the future operational forecast setting is beneficial in that case studies are used to analyze forecast settings similar to the way they would be approached in a forecast facility using the latest techniques and equipment. Students are given the opportunity to assess familiar meteorological forecast problems with the added practice of analysis in a modern setting.

5. CLASSROOM DESIGN

Designed by COMET computer staff, the classroom setting is a network of ten Hewlett Packard 755 workstations on the COMET local area network. The design of this network allows access to these workstations through file transfer protocol (FTP) by instructors from the data source locations.

In this way, local staff and visiting instructors may compile exercise materials well in advance of courses. Data may then be transferred to each workstation for students to work with, as if in an individual forecast operational area. Students can then fully exercise the software using the data, skills, and techniques described in prior lecture material. Through the use of projection screen technology, individual data sets can be displayed for comparison and immediate feedback of results (Pierce, 1995).

6. CASE STUDY DEVELOPMENT

Winter weather phenomena are characterized by both synoptic and mesoscale events. Case studies are collected individually to fit specific needs as defined by COMET lead instructors, course coordinators, and requests from users. The RPAC also has an input as to the type of events needed to enhance instruction materials related to specific hydrometeorological problems. Once the need is defined, COMET case study meteorologist, Ms. Julie Hall, an NWS Office of Meteorology employee stationed in Boulder, begins watching for a storm system that appears to meet the requirements of the individual request. In addition, COMET staff and others assist the case study meteorologist in identifying potential case study events.

Once the case study meteorologist is alerted to the upcoming event, a number of data gathering computer software systems are put into operation. In the spring of 1995, the Residence Program established a new process whereby data may be collected in real- or near real-time. This process makes use of live data feeds used in weather briefings and daily weather analysis. As the event unfolds and meteorologists observe the event, a near real-time analysis can take place before a final archive of the data occurs. Collecting and analyzing the data is a continuously evolving process.

Currently, COMET data collection capabilities rely on data feeds from several sources. Satellite data makes use of internet and the Regional and Mesoscale Meteorology Advanced Meteorological Satellite Demonstration and Interpretation System (RAMSDIS) as a source of data for ingest into the COMET file server. All gridded numerical model data comes from an NMC data feed through FSL. The WSR-88D data comes via internet and an agreement between Unidata—a University Corporation for Atmospheric Research (UCAR) program—and the WSI Corporation—an NWS Next Generation Weather Radar (NEXRAD) Information Dissemination Service (NIDS) vendor. Profiler data and other data such as upper air, surface data, and alphanumeric products are provided through a data feed from FSL. The FSL data connections are dependent on an NWS Automation of Field Operations and Services (AFOS) data connection to the NWS Denver Forecast Office.

It is critical that the case study meteorologist be aware of the type of event and location so that the appropriate site-specific data collection occurs. For instance, to collect radar data, NIDS products for up to 25 WSR-88D sites can be ingested on a routine basis. These 25 sites, where data are collected, must cover the geographic area where the case study is to be developed. The RAMSDIS high resolution satellite products are also site specific; therefore, the location of the event needs to be specified to effectively activate the appropriate radars and RAMSDIS location for data collections.

It is not an easy task to ensure that all these different computer systems are connected and the data ingest process continues. During times of peak weather activity, and especially when courses are in session, COMET computer staff assume a "data watch" posture, intensifying data monitoring activities both at the office and at home. Not only is this data available to anyone on the COMET network in a real- and near real-time basis, but it is also held in storage on a product dependent basis for up to three days.

Sometimes, as in the forecasting process, an event may not unfold as expected. If the data has been collected on such an event, it may not be saved to tape for long-term archive. In the case of surprise events, the WSR-88D data, satellite data, and other related information could have been ingested for daily routine use and could be saved before being overwritten by later data. This process lends some flexibility to case study development, minimizing the amount of needed personnel.

In the event that data is inadvertently missing, it can be collected from other sources. As in past case study development, NMC, National Climatic Data Center (NCDC), and FSL archives can be used to recreate events. This process, however, requires sifting through the many volumes of data to choose those things which best highlight the event. If the data can be observed by staff, and collected in near real-time, the number of personnel hours to complete a case can be reduced.

7. WINTER SEASON CASE STUDIES

Winter (cool season) case studies used in COMET classes attempt to incorporate different meteorological events including snowstorms, heavy rainfall events, ice storms, and cold outbreaks using synoptic and mesoscale analysis. Case studies developed include a lake effect snow case from January of 1995 (Byrd et al., 1995). The highlights of this case include the synoptic scale evolution of the lake effect event, lake effect dynamics, and mesoscale modeling of the event. Other winter season events are collected to demonstrate the use of satellite imagery, and the WSR-88D is used to diagnose the meteorological events. Related topics such as Q-vector computations, thickness advection, conveyor belt, positive isothermal vorticity advection (PIVA), ageostrophic circulations and thermal wind balance, and mesoscale features, such as the evolution of a front range snowstorm, are captured within the case studies.

COMET staff has collected East Coast "Nor'easter-type" case studies. The February 3-5, 1995, event is being consolidated and evaluated for further refinement into a case study. COMET staff is developing West Coast cases based on the January and March 1995 precipitation events in California. These cases are of particular importance to the COMET hydrologic program. An attempt is being made to collect cases highlighting different hydrometeorologic events and geographic locations. However, as the analysis of these events continues, the findings indicate that many synoptic scale features are plainly evident, regardless of the geographic location. Nevertheless, interaction between the synoptic features and local mesoscale phenomena, such as terrain, are some of the factors that can create the greatest forecast challenge.

At this time, all case studies are for classroom use only although staff members are performing additional work to make these cases available to the wider university and forecast communities. The medium in which the cases are made available is a logistical issue. In addition to logistics, case study support for operational questions and expert analysis will require considerable COMET staff time. These and other issues are being resolved as quickly as possible. The COMET program intends on making the first case available in the fall of 1995.

The first case that will be available, the March 11-14, 1993, "Storm of the Century," has received wide publicity and has been studied at length. Prior research will provide COMET staff with an immediate source of expert analysis. COMET staff will aim to provide all possible data sources in a user-friendly format. This case has been used in many courses; however, only a limited number of individuals have been exposed to its finer details, so there is still demand for its use in a wider domain.

In addition to the standard case study computer base format, Dr. James T. Moore of St. Louis University and Mr. Matt Kelsch of FSL have developed a teaching document for this case involving

introductory synoptic and mesoscale lecture and workshop material for Hydromet (Moore, Kelsch, and Crawford, 1995, 1994, 1993). Key features highlighted in this case are the rapid cyclogenesis in the Gulf of Mexico with eventual severe convective event and storm surge in Florida. The rare snowstorm in the southeastern United States, northeast into New England, is also highlighted. It makes use of isentropic analysis and has highly defined jet structures which lead to enhanced snowfalls. This case has WSR-88D data available for some locations along the storm track. This is one of the first cases used in the Residence Program with the WSR-88D data. All cases currently being prepared include a suite of basic products available from the WSR-88D.

8. SUMMARY

COMET staff continues to produce successful, advanced studies training courses for operational forecasters and meteorologists. Using a case study approach, the COMET program includes data from the latest sources through the use of the most advanced display systems. To increase the advantages for the student in using these data, the instructors are chosen from a group of experts in the university and operational communities. The setting for the courses includes a modern classroom equipped with the most advanced multimedia communications systems. A committee of operational and university personnel guide the program in its endeavors to meet the needs of forecasters and meteorologists. Through the continued use of these advisors, and the intent to keep the main goals of facilitating the flow of knowledge from the university to the operational community at hand, the program will continue to enjoy success well into the future.

9. ACKNOWLEDGMENTS

The authors would like to thank the following for their review of this manuscript: Dr. Timothy C. Spangler, COMET Director; Dr. Charles N. Hoffeditz, NWS OH/Hydrologic Services; Dr. Danny L. Fread, Director, NWS OH; Dr. Lee Larson, Chief, NWS OH/HRL; Ms. Hanne Mauriello, COMET Administrator; Ms. Kay Miloshevich, COMET Administrative Assistant; and Ms. Elaine Hauschildt, Editorial Assistant, NWS OH/HRL.

This paper is funded by a cooperative agreement #NA37WD0018-01 from the National Oceanic and Atmospheric Administration (NOAA). Views expressed herein are those of the authors and do not necessarily reflect the views of NOAA or any of its subagencies.

10. REFERENCES

Alberty, R.L., 1995: Minutes of the Residence Program Advisory Committee, Boulder, Colorado, June 1-2, 1995. UCAR/COMET Memoranda, July 1995.

Byrd, G.P., R.J. Ballentine, J. Case, J.L. Hall, D. Rock-Kiessling, and R.S. Weinbeck, 1995: Mesoscale Model Simulation of the 4-5 January 1995 Lake-effect Snowstorm. 4th United States and Canada Workshop on Great Lakes Operational Meteorology, September 13-15, Syracuse, New York.

Moore, J.T., M. Kelsch, and K.C. Crawford, Contributing Authors: COMET Hydrometeorology Course, *Forecasting Heavy Precipitation From Meso- and Synoptic Scale Systems*, Boulder, Colorado, January 1993, June 1994, and June 1995.

Pierce, R.V., 1995: *Post Print, 27th Conference on Radar Meteorology*, Vail, Colorado, October 9-13, 1995, AMS Post print, paper 4.4, October 1995 (to be presented October 9, 1995).

Spangler, T.C., V.C. Johnson, R.L. Alberty, B.E. Heckman, L. Spayd, and E. Jacks, 1994: COMET: An Education and Training Program in Mesoscale Meteorology, *BAMS*, **75**, pp. 1249-1259.

Stewart, N.O., K.C. Crawford, and T.C. Spangler, 1993: NWS, NOAA Tech. Memo NWS ER-87, April 1993. *Post Print Volume, Third National Heavy Precipitation Workshop,* Pittsburgh, Pennsylvania, November 16-26, 1992.

SESSION 2
OPERATIONAL FORECAST MODELS

2. A Comparison Between the 40km Meso-ETA and 80 km NGM During a Hybrid Synoptic-Lake Effect Snow Storm over the Eastern Great Lakes

3. The Prediction of Rapidly Deepening Cyclones by NCEP's Nested Grid Model (NGM) & Global Spectral Model (AVN) Winter 1989/90 - Autumn 1991 & Winters 1993/94 & 1994/95

4. Common Cold Season Biases in NCEP's Medium Range Forecast Model (MRF)

A Comparison Between the 40km Meso-ETA and 80km NGM During a Hybrid Synoptic-Lake Effect Snow Storm over the Eastern Great Lakes

Michael T. Eckert[1]

1. INTRODUCTION

Snowstorms over the Great Lakes are normally of the synoptic or lake effect type. A third type is the hybrid synoptic-lake effect snow, which takes on characteristics of both synoptic and lake effect snows. This is due to the presence of a synoptic scale convergence zone moving across the Great Lakes, while cold air is in place. Quantitative Precipitation Forecasting (QPF) for this type of system is very difficult due to the multiple characteristics. The NGM model (Hoke, et al.) was the main forecast tool until the ETA was released in 1993 (Black, et al., 1993). In mid-1994, the Meso-ETA began running with a horizontal resolution of 40km and 50 layers (presently 29km and 50 layers).

The Fall of 1994 was very unusual over the Great Lakes and Northeastern U.S. in that many major cities recorded their latest ever occurrence of measurable snow due to a mild period. In late November, the development of an upper trough over the northeastern U.S. led to the first intrusion of Arctic air into the Northeastern U.S. (Figure 1).

On November 21-22, 1994, a Pacific origin cold front moved through the eastern U.S. Following this front, an Arctic surge of very cold air pushed across the Great Lakes region November 22-23, 1994. Brief periods of heavy snow accompanied the Arctic front. Snow amounts were generally one-to-two inches. Liquid equivalents were from one-to-two tenths of an inch. East of Lakes Superior, Ontario, and Georgian Bay, where enhancement of snowfall rates occurred, snows of 5-10 inches and liquid equivalents of two-to-five tenths of an inch occurred (Figure 2).

2. MODEL ANALYSIS (11/22/94 1200 UTC)

The NGM and Meso-ETA initial analysis from the surface to 500mb were very similar. The one difference noticed in all the analysis and forecasts was more detail in the Meso-ETA. This is attributable to the higher resolution of this model. (Only the Meso-ETA is shown when the analysis or forecasts are similar). Several mid-level shortwaves moved from Canada into the Northeastern U.S. and contributed to the deepening upper trough. Deep layered cold advection was increasing across the region as seen by the intense 1000-500mb thickness packing (Figure 3).

3. MODEL COMPARISON (11/23/94, 0000 UTC)

Twelve-hour 500mb forecasts from the NGM and Meso-ETA showed one shortwave moving into New England. A stronger shortwave was between James Bay and Lake Superior. Both models showed 700 mb cold advection over the Great Lakes with a thermal ridge forming from Lake Huron northward in response to the approaching shortwave. The surface pressure forecasts also showed cold advection with a weak thermal ridge building across Michigan. The first significant difference between the models began at this time as the Meso-ETA developed an elongated area of 700mb

1. Corresponding author address: Michael T. Eckert, National Centers for Environmental Prediction, Hydro-Meteorological Prediction Center, Forecast Operations Branch, 5200 Auth Road, Ste. 410, Camp Springs, MD 20746.

divergence from Lake Superior to Lake Ontario (Figure 4). The NGM showed an area of 700mb divergence over Lake Erie (Figure 5).

The 1000mb divergence forecasts, from the NGM and Meso-ETA, were quite similar. The models both showed a band of convergence from Lake Superior to Lake Ontario. This field is a good predictor of Lake Effect Snows (Burrows 1991) (Figures 6 & 7). Overlaying the Meso-ETA 700mb and 1000mb divergence fields reveals a strong low level convergence/middle level divergence couplet developing.

4. MODEL COMPARISON (11/23/94, 1200 UTC)

The 24-hour forecast from the models showed the strong 500mb shortwave elongated from Northern New England across the Upper Great Lakes. A cold front was positioned along the axis of Lakes Ontario, Huron/Georgian Bay and Superior (Figure 8). Cold advection was present from the surface through 700mb. Similar to the 12-hour forecasts, the Meso-ETA showed a strong low level convergence/middle level divergence couplet over Lakes Ontario, Huron, Superior and Georgian Bay (Figures 9 & 10). The NGM showed some 700-mb divergence over the east end of Lake Ontario and a broad area of 1000mb convergence over the Great Lakes (Figures 11 & 12).

5. QUANTITATIVE PRECIPITATION FORECASTS (11/22/94 1200 UTC TO 11/23/94 1200 UTC)

Precipitation forecasts, from the NGM and Meso-ETA, were very different for this 24-hour period. The NGM forecasted less than one-tenth of an inch of liquid precipitation from eastern Lake Superior to western Lake Ontario (Figure 13). The Meso-ETA indicated a band of one-tenth to five-tenths liquid precipitation from eastern Lake Superior to east of Lake Ontario. Of special note are the maximum amounts on the lee end of the lakes (Figure 14).

6. CONCLUSIONS

Comparisons of QPFs between the coarser resolution NGM and finer resolution Meso-ETA during a Hybrid Synoptic-Lake Effect Snow Event clearly show the Meso-ETA's superiority in QPF. The Meso-ETA can likely better model the interactions between fronts and the great lakes since the resolution is finer. For this event, synoptic scale forcing from the strong shortwave moving through the region supported the development of a surface front. Low level convergence along the front was enhanced as it moved into the seasonally normal mid-lake convergent zone. This low level convergence zone played a significant role in the snow production to the lee of the lakes, but the mid-level shortwave, 700mb divergence and possibly upslope flow also played an important role. Of high interest is the 1000mb convergent/700mb divergent couplet over the great lakes (Figure 15). As with all types of weather when a strong gradient (couplet), vertical or horizontal exists, the magnitude of the event is usually increased.

7. REFERENCES

Black, T.L., 1994: The New NMC Mesoscale Eta Model: Description and Forecast Examples. *Wea. Forecasting*, 9, 265-278.

Burrows, W.R., 1991: Objective Guidance for 0-24 Hour and 24-48 Hour Mesoscale Forecasts of Lake-Effect Snow Using CART. *Wea. Forecasting*, 6, 357-378.

Niziol, T.A., 1987: Operational forecasting of lake effect snowfall in western and central New York. *Wea. Forecasting*, 1, 311-321.

_____, 1993-1995: Personal Conversations.

Petersen, R.A., PCGRIDDS.

Reinking, R.F., R. Caiazza, F.A. Kropfli, B.W. Orr, B.E. Martner, T.A. Niziol, G.P. Byrd, R.S. Penc, R.J. Zamora, J.B. Snider, R.J. Ballentine, A.J. Stamm, C.D. Bedford, P. Joe, A.J. Koscielny, 1993: The Lake Ontario Winter Storms (LOWS) Project. *Bull.* AMS, 74, 1828-1849.

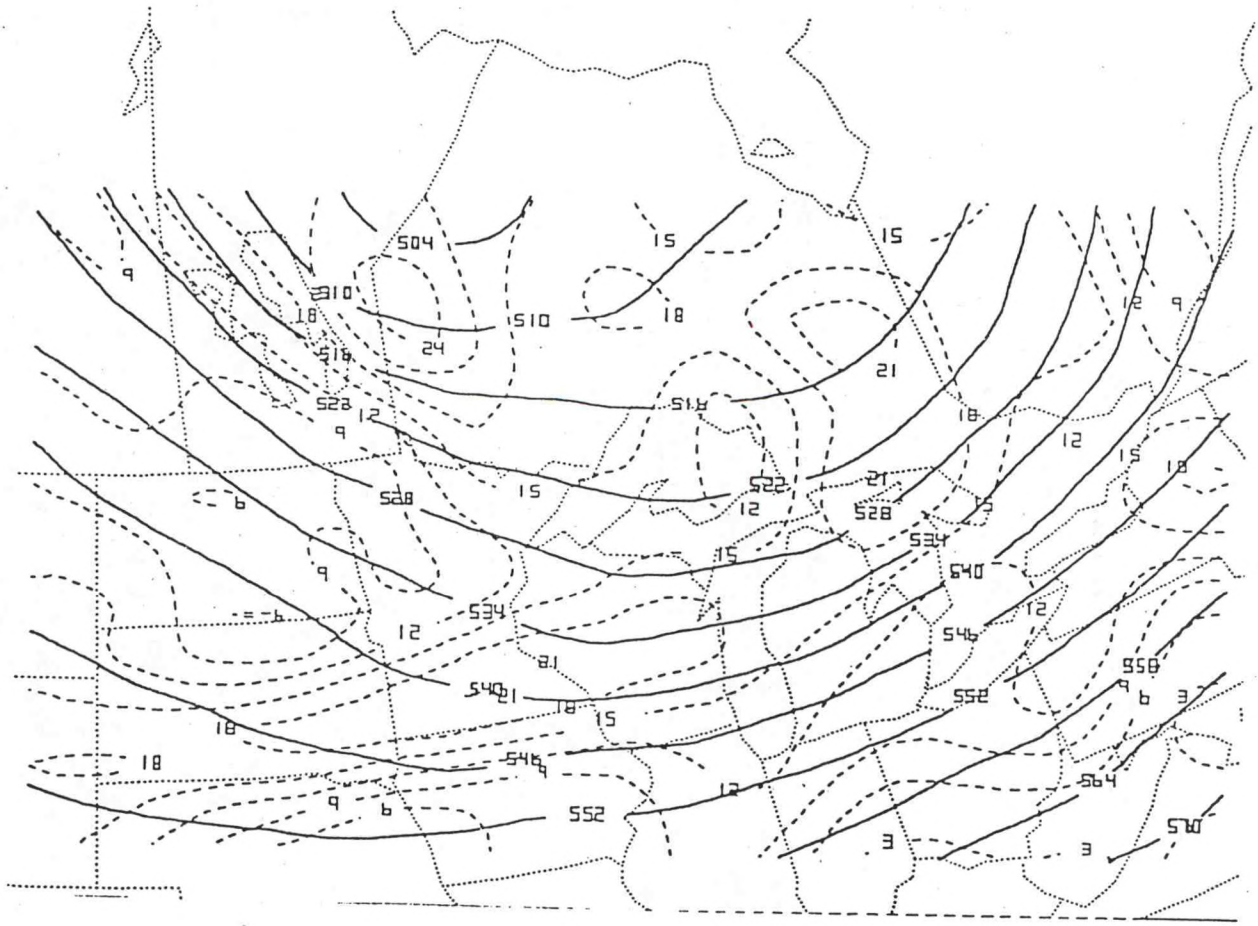

Figure 1. Meso-ETA 500mb heights/vorticity, 11/22/94 1200 UTC.

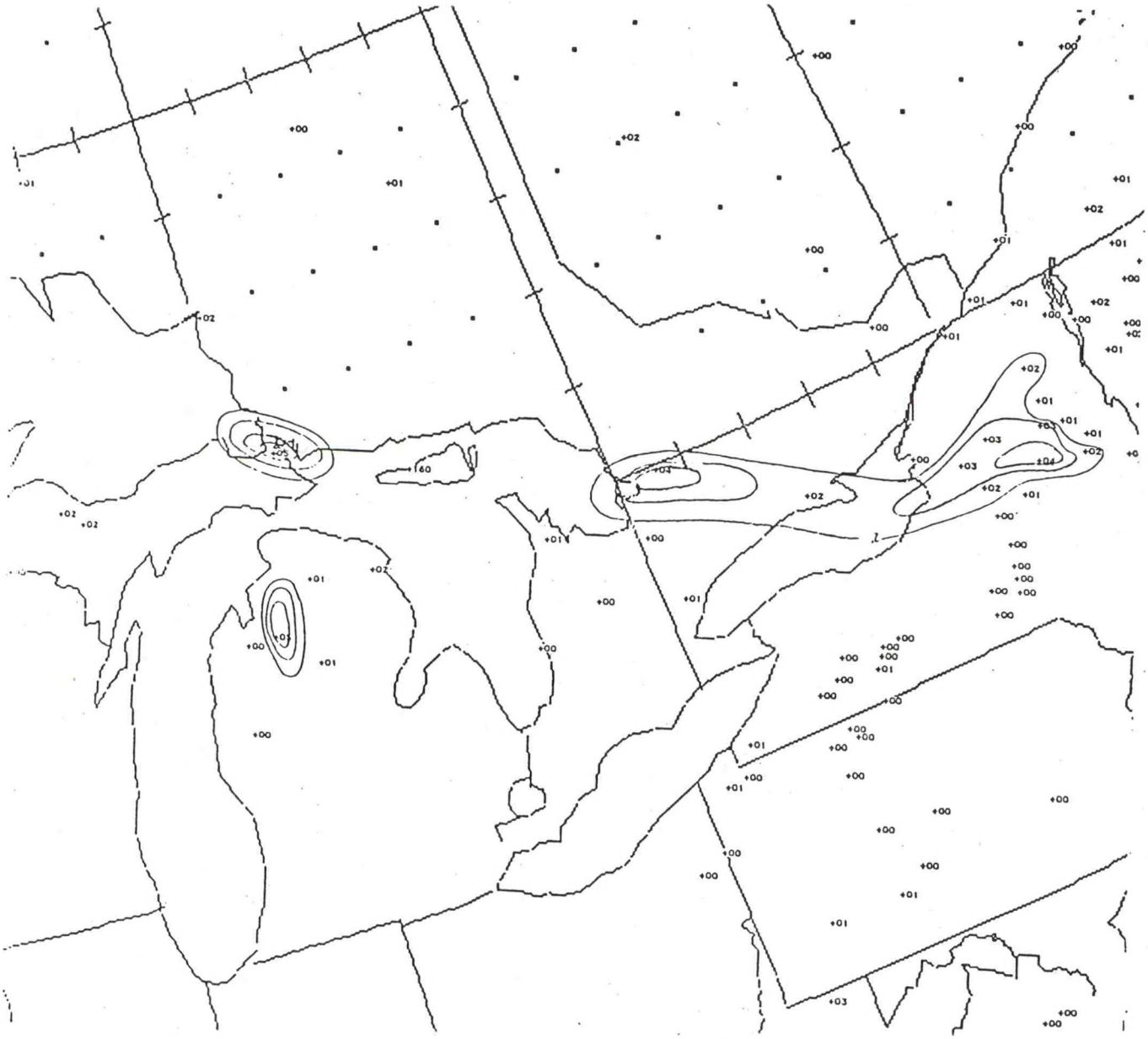

Figure 2. Actual QPF (tenths-of-inches), 11/22-23/94 1200 UTC to 1200 UTC.

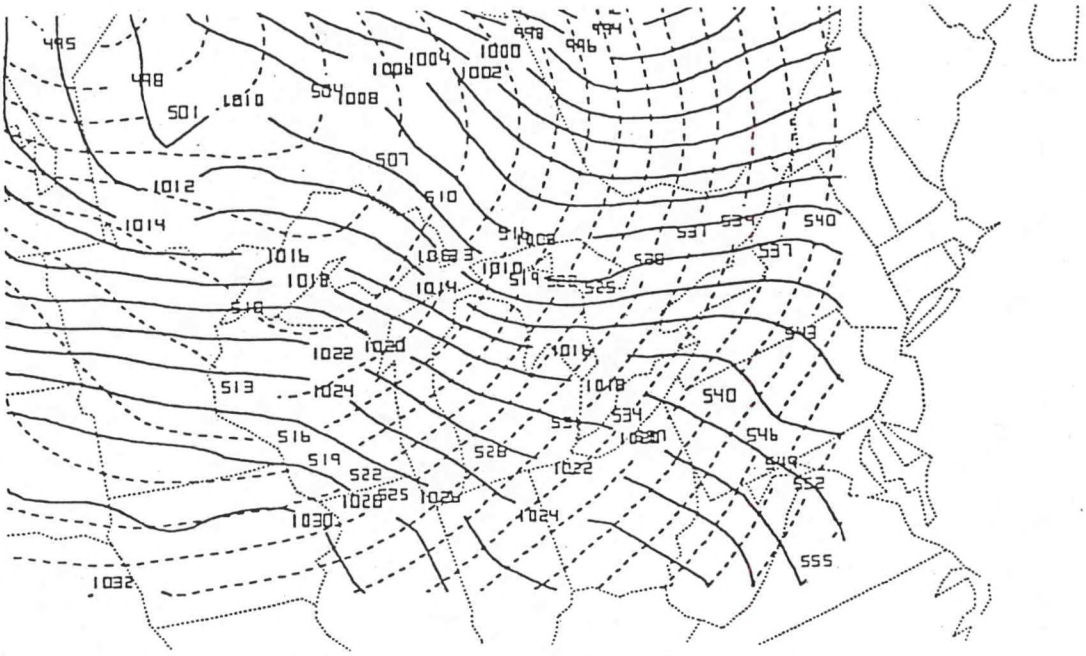

Figure 3. Meso-ETA MSL pressure & 1000-500mb thickness, 11/22/94 1200 UTC.

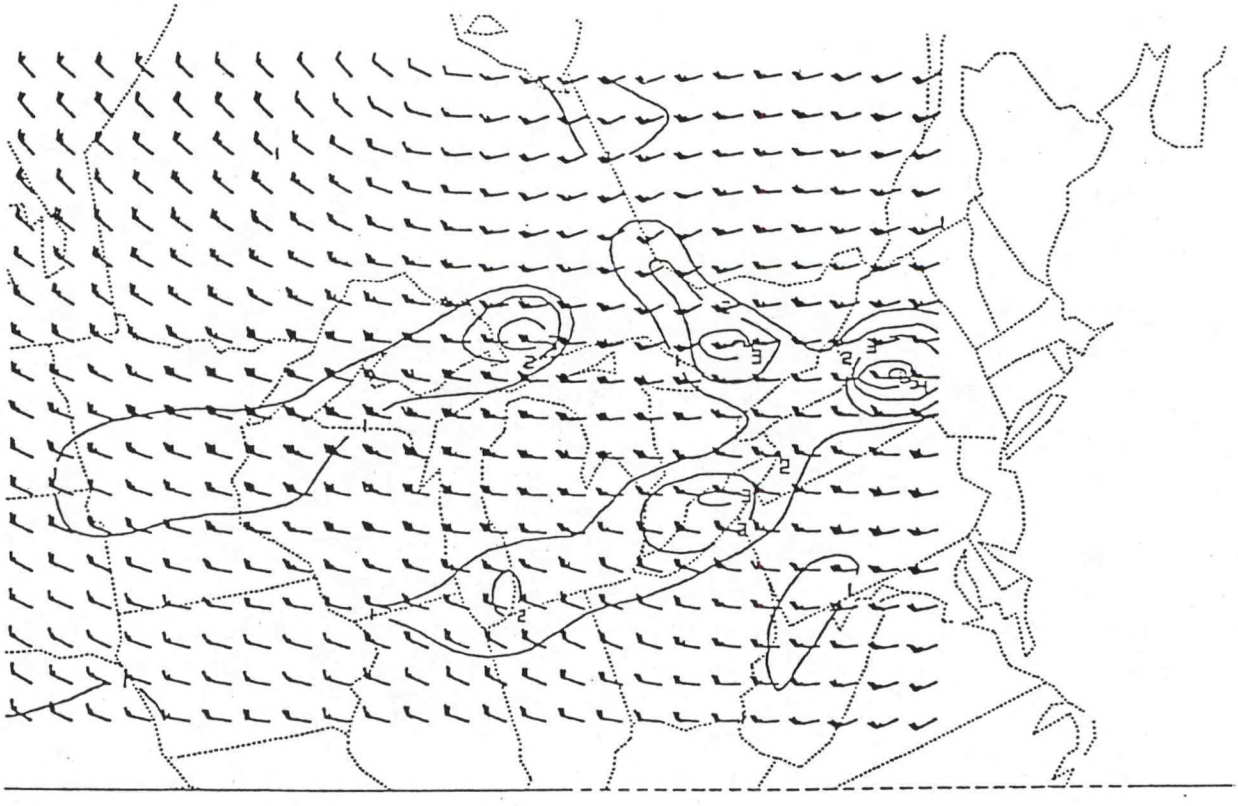

Figure 4. Meso-ETA 700mb winds (ms^{-1}) & divergence (s^{-1}) 11/23/94 0000 UTC.

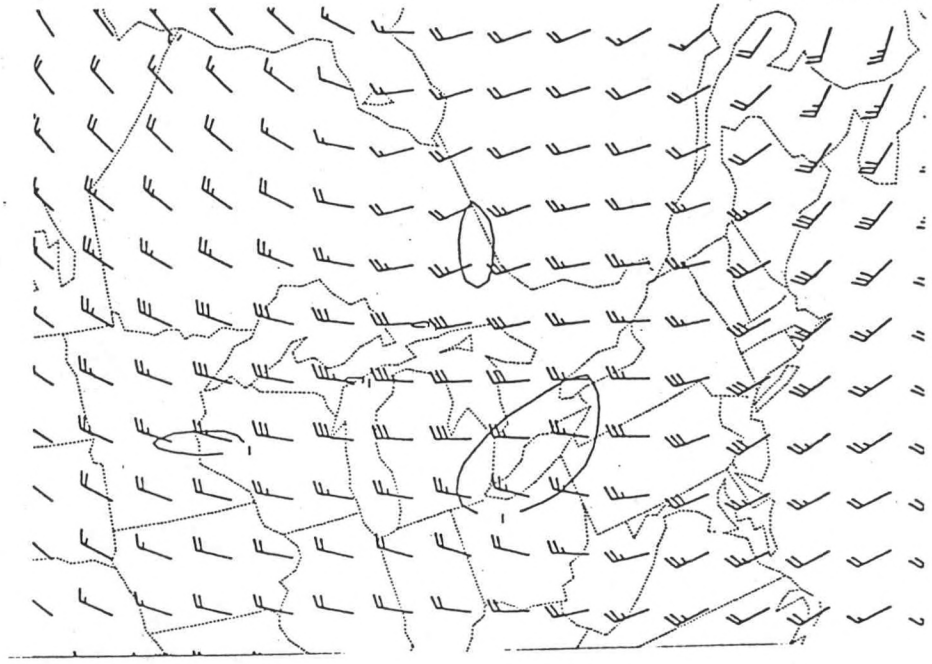

Figure 5. NGM 700mb winds (ms^{-1}) & Divergence (s^{-1}) 11/23/94 0000 UTC.

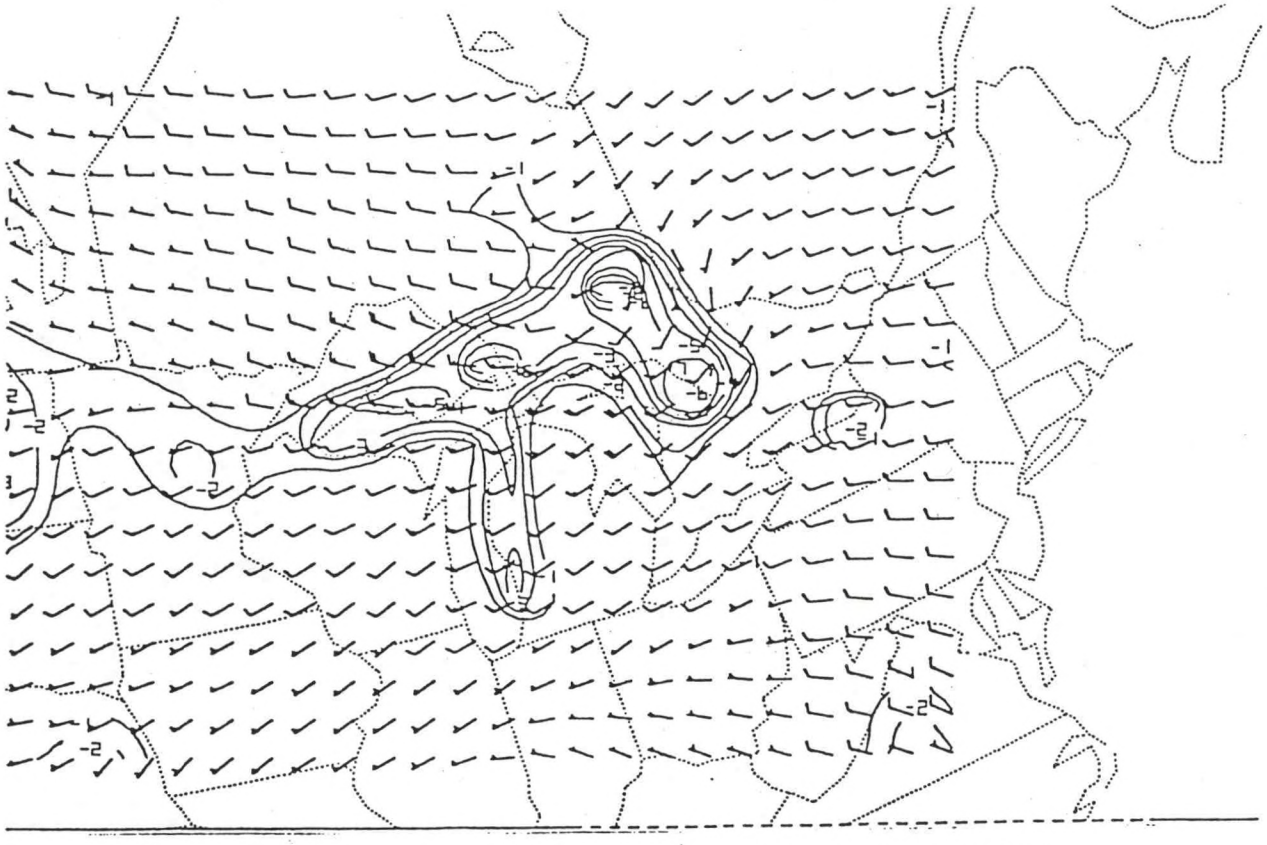

Figure 6. Meso-ETA 1000mb winds (ms^{-1}) & divergence (s^{-1}) 11/23/94 0000 UTC.

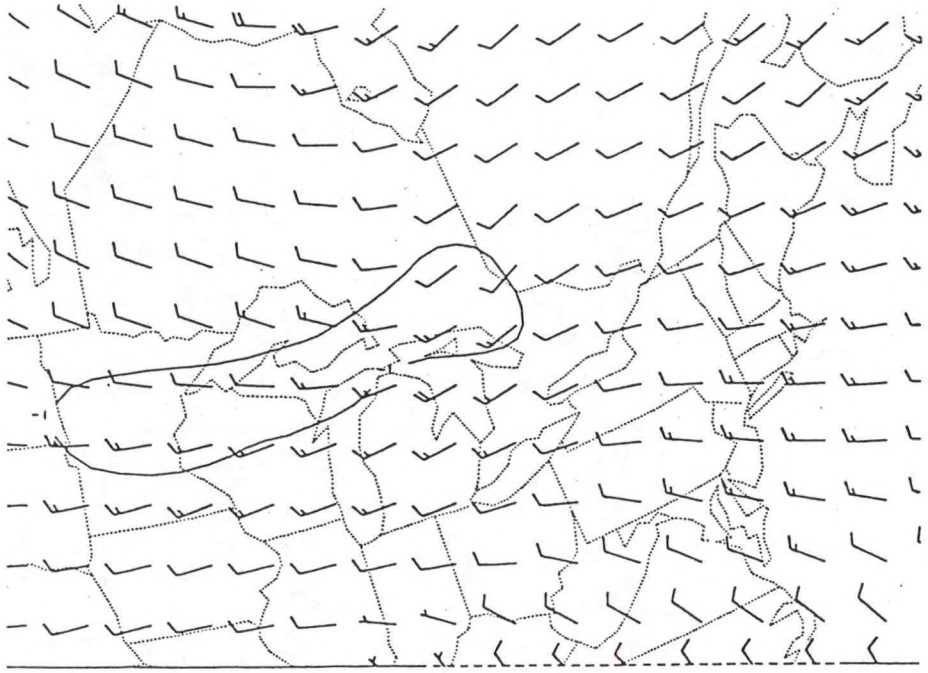

Figure 7. NGM 1000mb winds (ms^{-1}) & divergence (s^{-1}) 11/23/94 0000 UTC.

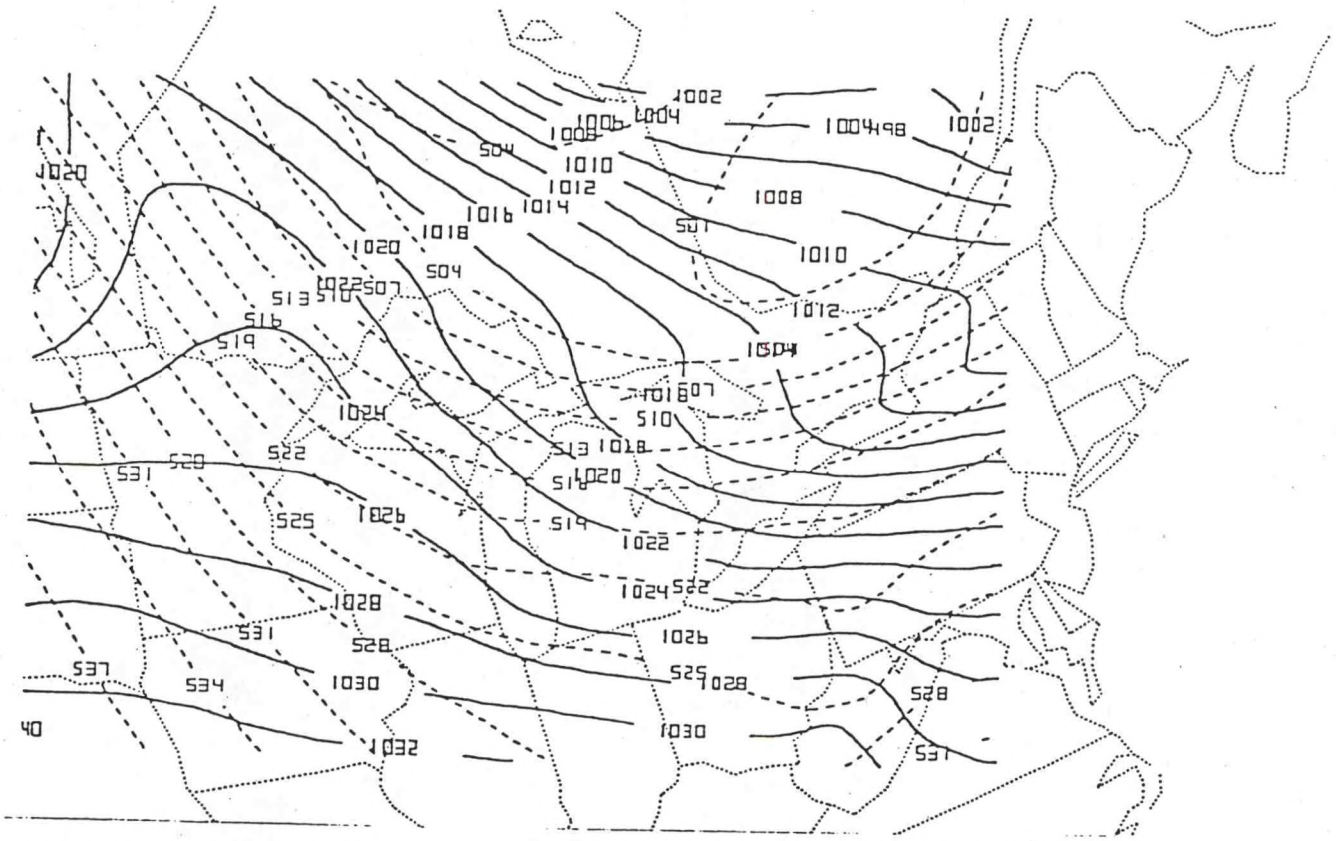

Figure 8. Meso-ETA MSL pressure and 1000-500mb thickness, 11/23/94 1200 UTC.

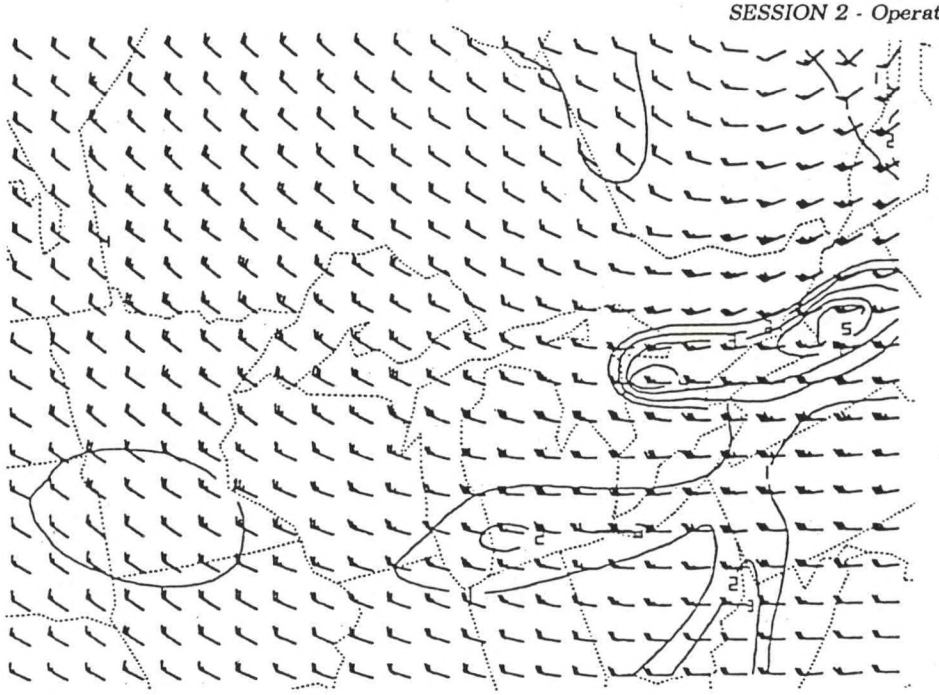

Figure 9. Meso-ETA 700mb winds (ms^{-1}) & divergence (s^{-1}) 11/23/94 1200 UTC.

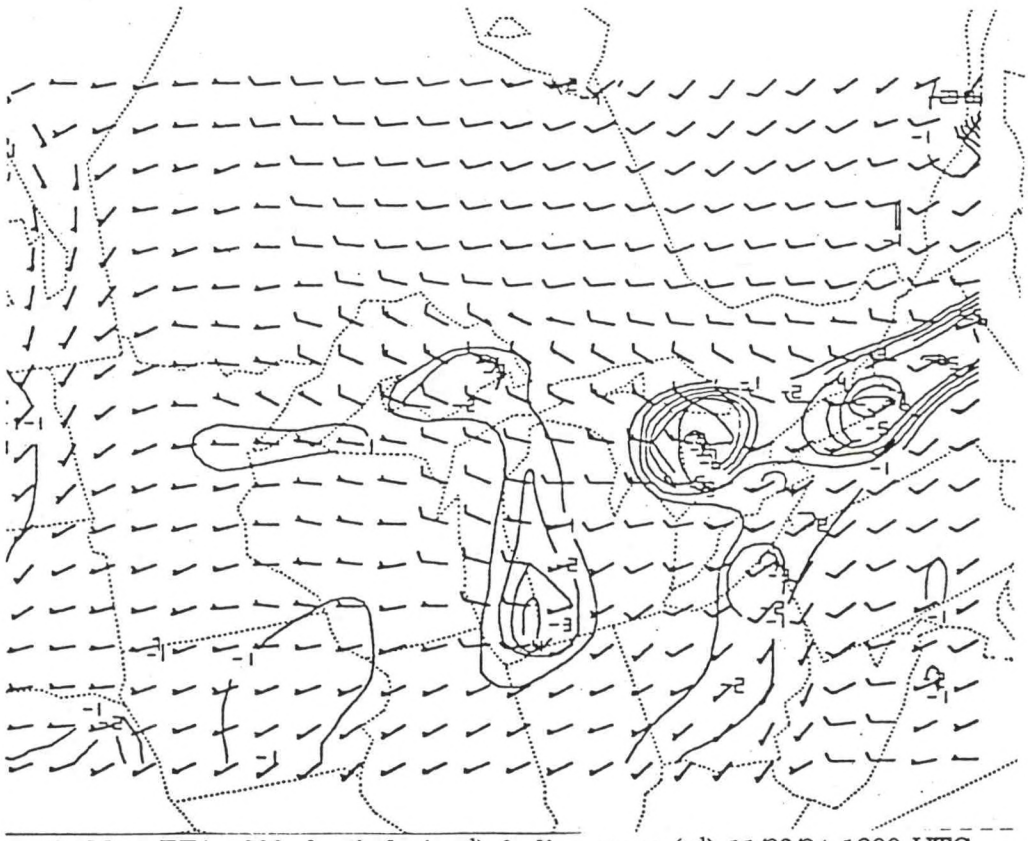

Figure 10. Meso-ETA 1000mb winds (ms^{-1}) & divergence (s^{-1}) 11/23/94 1200 UTC.

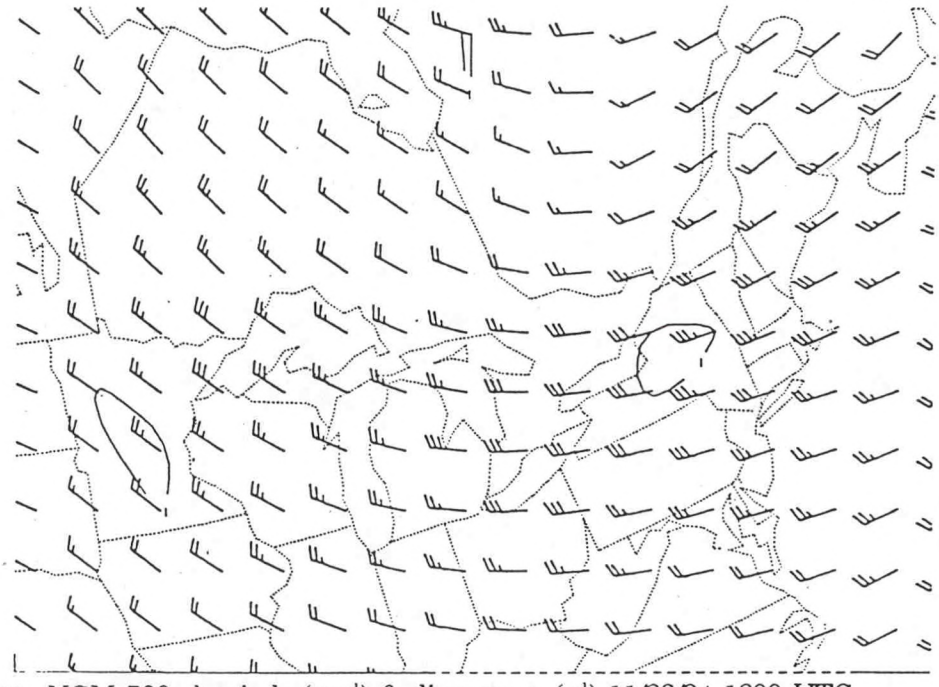

Figure 11. NGM 700mb winds (ms^{-1}) & divergence (s^{-1}) 11/23/94 1200 UTC.

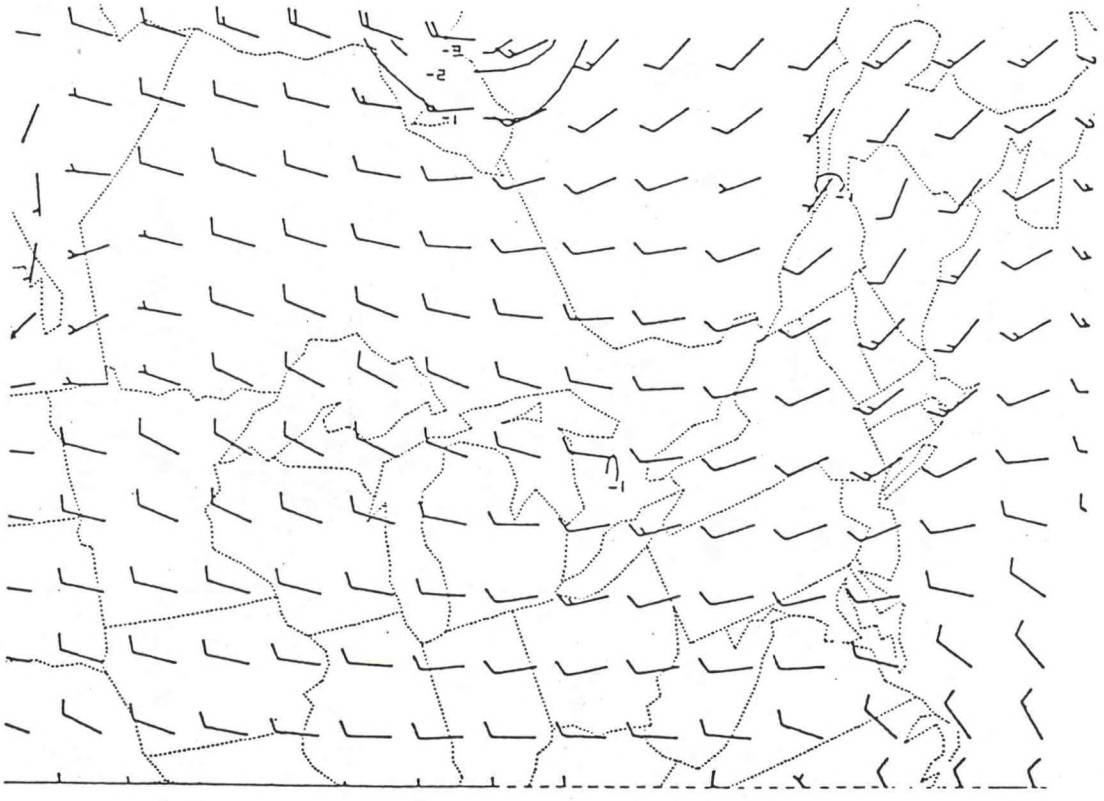

Figure 12. NGM 1000mb winds (ms^{-1}) & divergence (s^{-1}) 11/23/94 1200 UTC.

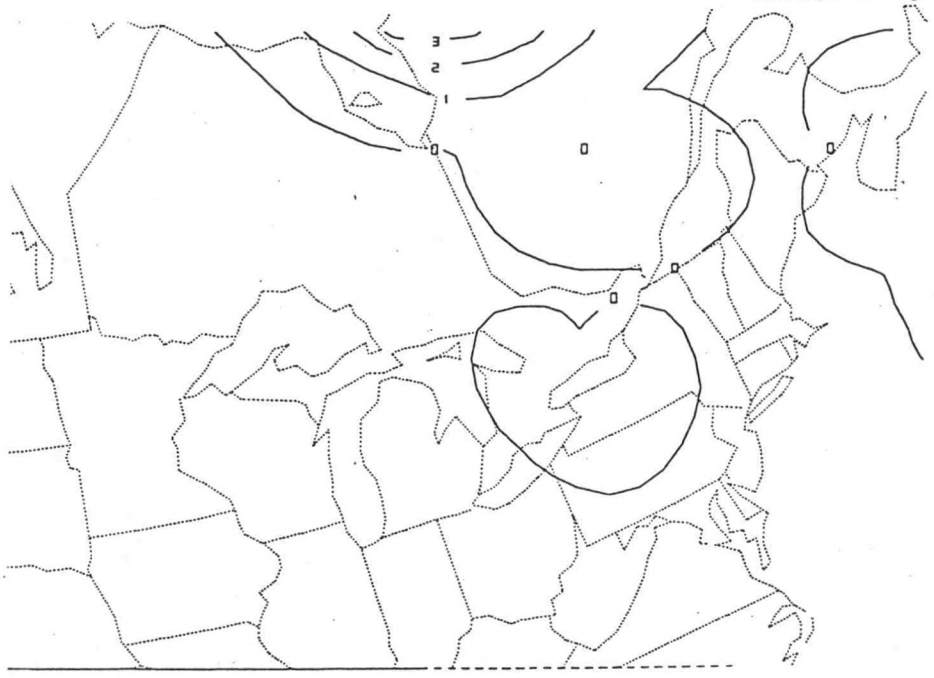

Figure 13. NGM 24-hour QPF (tenths-of-inches) 11/22-23/94 1200 UTC to 1200 UTC.

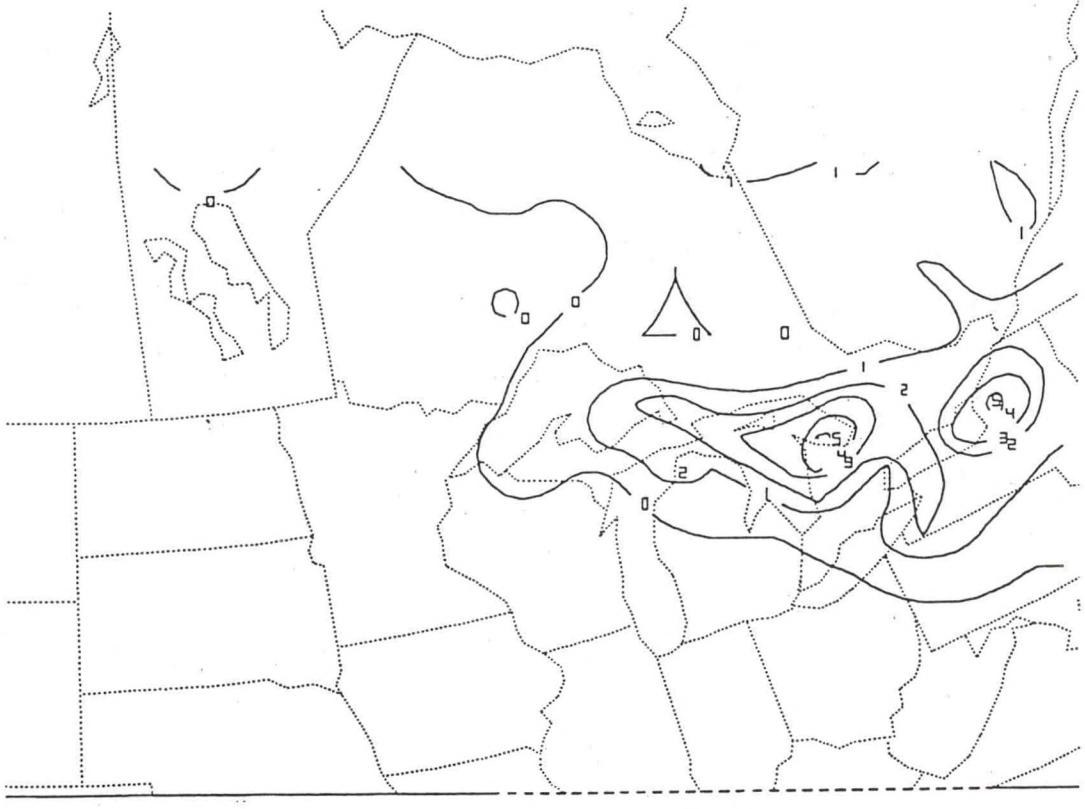

Figure 14. Meso-ETA 24-hour QPF (tenths-of-inches) 11/22-23/94 1200 UTC to 1200 UTC.

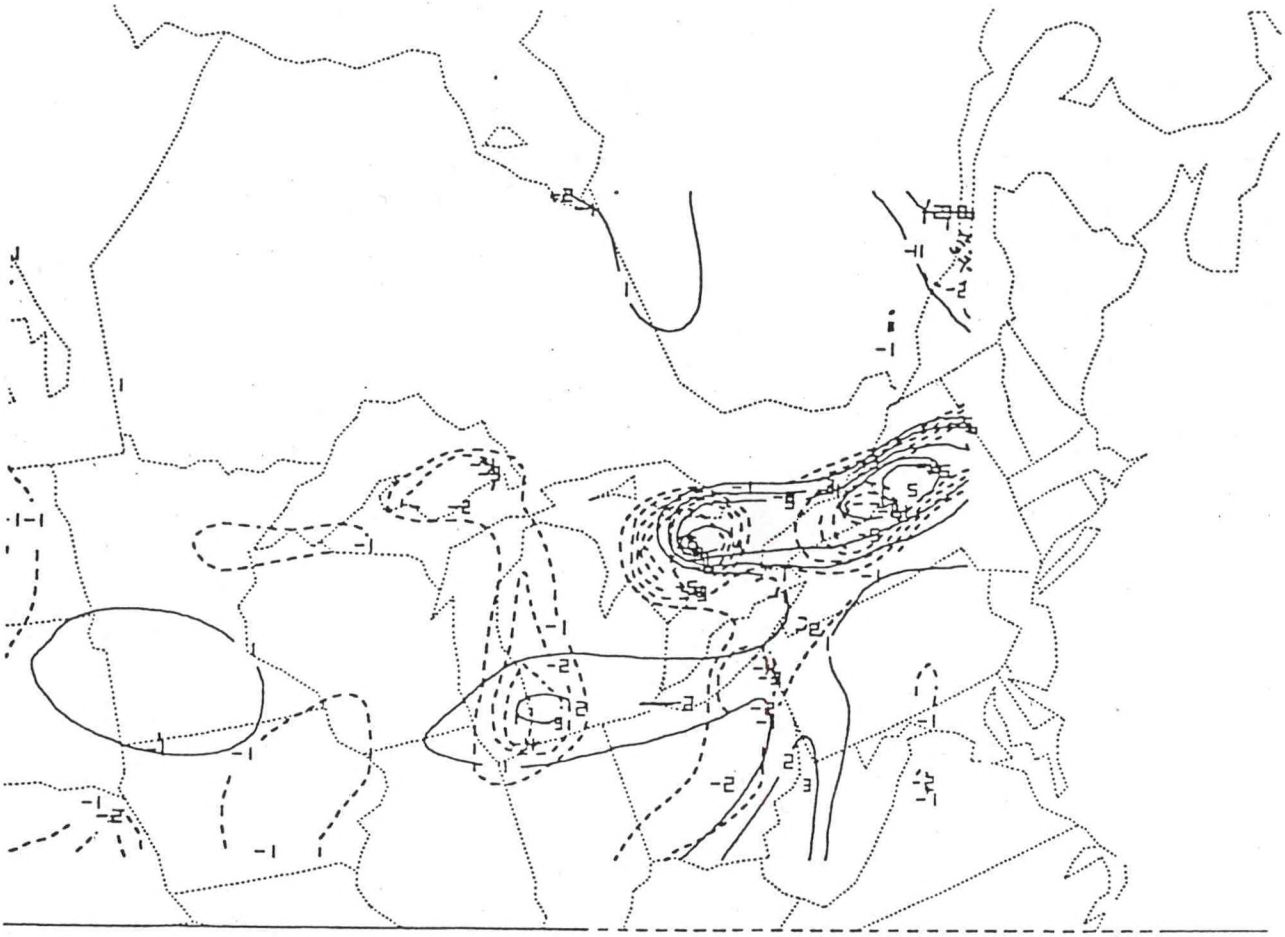

Figure 15. Meso-ETA 1000mb (dashed) & 700mb (solid) divergence (s^{-1}), 11/23/94 1200 UTC.

The Prediction of Rapidly Deepening Cyclones by NCEP's Nested Grid Model (NGM) & Global Spectral Model (AVN) Winter 1989/90 - Autumn 1991 & Winters 1993/94 & 1994/95

Robert J. Oravec[1], and Richard H. Grumm[2]

1. INTRODUCTION AND METHODOLOGY

A study of Rapidly Deepening Cyclones (RDC) forecast by The National Centers for Environmental Prediction's (NCEP) Nested Grid Model (NGM) and Global Spectral Model (AVN) was conducted for the two and one-half year period from the Winter of 1989/90 through the Autumn of 1991 and from the Winter 1993/94 through the Winter of 1994/95. In this study, the Winter season was defined from December through February and the Autumn season from September through November. The Winter seasons in this study included the Winters of 1988/89, 1989/90, 1990/91, 1993/94 and 1994/95 (hereafter WI89, WI90, WI91, WI94, and WI95); and three Autumn seasons 1989, 1990, and 1991 (hereafter AU89, AU90, and AU91). In these studies, a RDC is defined as a cyclonic circulation with a 12-h pressure fall of 12 mb or greater. Data for this study were produced during the model tracking and verification study conducted over the past five and one-half years at the Hydrometeorological Prediction Center (HPC) of NCEP (formerly the Meteorological Operations Division of NMC). In the model tracking and verification study, model forecast cyclone and anticyclone centers were tracked at 12-hour intervals for all available model runs in the NGM and AVN. The initialized analyses (00-h forecasts) from each of the models was used to represent the verifying atmosphere for the periods of this study. The model tracking was done using the VAS Data Utilization Center (VDUC), a Man Computer Interactive Data Access System (McIDAS).

Numerous studies have been done on the skill of NCEP (NMC) numerical models with respect to their skill in predicting cyclone central pressure since the early 1970's. Initial studies of the six-layer primitive equation model (PE) by Leary (1971) and subsequent studies of the LFM-II by Silverberg and Bosart (1982) and the NGM by Grumm and Siebers (1989), Mullen and Smith (1990) and Grumm et al. (1992) all found a bias in the operational models of forecasting the central pressure of cyclones too high. The results from these studies revealed, however, a trend of improving model forecast skill with each subsequent implementation of a higher resolution model at NCEP.

Specialized studies of model skill in predicting RDCs have been conducted by Sanders and Gyakum (1980) using the six and seven layer PE model, Sanders (1986b) using the LFM, Sanders (1987), Sanders and Auciello (1989), and Oravec and Grumm (1993) using the NGM. Similar to the other studies of model cyclone pressure errors, the model skill in forecasting RDC also has shown improvement with improved model physics in subsequent NCEP models.

2. SEASONAL DISTRIBUTIONS

The distribution of RDCs in each 5 by 5 latitude/longitude grid from the NGM for WI89-WI91, WI94-WI95, from the AVN for WI94-WI95, and from the NGM for AU89-AU91 are shown in Figure 1. Figure 1 reveals that the RDCs occurred primarily over the ocean regions. The axis of RDCs in the Atlantic from both the NGM and AVN stretched from off the mid-Atlantic coast northeastward

1. Corresponding author address: Robert J. Oravec, National Centers for Environmental Prediction, Hydrometeorological Prediction Center, Forecast Operations Branch, Camp Springs, Maryland.
2. Richard H. Grumm, National Weather Service Forecast Office, State College, Pennsylvania.

through the Maritimes of Canada to a position to the south of Greenland. Figure 1 shows a southwestward displacement in the axis of RDCs from the autumn to the winter seasons in the Atlantic. In the northeastern Pacific, there was a much smaller distribution of RDCs than in the Atlantic in both winter study periods in the NGM and in the AVN. However, this region of the Pacific was found to have a much larger RDC distribution during the autumn season. Examination of Figure 1 reveals a westward shift in the axis of the RDCs across northeastern North America from WI89-WI91 and WI94-WI95 in the NGM. This westward shift is likely due to a westward shift in the mean 500 mb trough position between these two periods.

3. POSITION AND PRESSURE ERRORS

Position errors for RDCs and all cyclones from WI94 and WI95 in both the NGM and AVN are shown in Figure 2a. Examination of Figure 2a reveals a nearly linear increase in the position errors with time for both RDC and all cyclones in both the NGM and AVN. However, the positions errors for the RDCs are substantially less than the position errors for all cyclones during the study period. In addition Figure 2a reveals that the position errors for the AVN's RDCs and for all AVN lows were less than their NGM counterparts at all time periods. The smaller position errors for RDCs compared to all cyclones in both the NGM and AVN is likely due to better initialization of these RDCs. The superior performance of the AVN compared to the NGM is consistent with results found in Grumm and Siebers (1990). Comparison of the position errors for RDCs in the NGM between the WI89-91 and WI94-95 in Figure 2b reveals improved skill between the earlier and later time periods. This improvement in skill can not be attributed to improved physics in the NGM as it has not undergone any changes between the aforementioned time periods. This decrease in position error for the RDCs in the NGM is likely due to a farther westward positioning of the mean 500 mb trough over eastern sections of North America which allowed for more data near the center of these RDCs for the numerical models. This farther westward positioning of the mean 500 mb trough for the WI94-95 time period is also seen in the westward shift of the NGM RDC distribution in Figure 1.

Mean pressure errors for RDCs and all cyclones from WI94 and WI95 in both the NGM and AVN are shown in Figure 3a. Except for the 12- to 24-hour period for RDCs in the AVN, there is an increase in the mean pressure errors with time for both RDCs and all cyclones. Figure 3a, however, reveals a significant difference between the pressure error characteristic between RDCs and all cyclones in both the AVN and NGM. In this study, RDCs from both the NGM and AVN were found to have a positive pressure error (models forecast central pressure to be too high), which is opposite to the negative pressure error (model forecast central pressure to be too low) that is exhibited by all cyclones in both the NGM and AVN. The results of Figure 3a for the NGM RDCs confirms results from Grumm et al. (1992) that the NGM is often too slow to deepen deepening lows. Similar to the position errors of Figure 2a, the AVN showed superior skill compared to the NGM with both RDCs and all cyclones, with the exception of the 12-hour period for RDCs where the NGM had a lower error. Figures 2a and 3a both reveal that the position and pressure errors for RDCs in the AVN at the 60- and 72-hour forecast periods are superior to the 48-hour forecast of the NGM. Similar to the results for the position errors, Figure 3b reveals an increase in the model skill with respect to pressure errors for RDCs in the NGM between the WI89-91 and WI94-95 time periods.

4. NGM PRESSURE CHANGE CHARACTERISTICS FOR RDCS

Figure 4 illustrates the NGM's ability to forecast the character of the pressure change over the RDCs. In this figure, three categories are used : 1) cyclones that are forecast to deepen and actually deepen (DD); 2) cyclones that are forecast to deepen and actually fill (DF); 3) cyclones that are forecast to fill and actually deepen (FD). Figure 4 includes only cyclones that either had a forecast or observed pressure fall of 12 mb in a 12-hour period. Figure 4 reveals that the NGM does an

excellent job in determining the pressure change characteristic of RDCs. In this study period, the NGM never forecast a cyclone to become a RDC which verified as a filling cyclone, and only once did it forecast a cyclone to fill and it became a RDC. Nearly all of the RDCs in the study from the NGM were forecast to be deepening cyclones. Figure 4 also illustrates the results seen in Figure 3a with the NGM generally too slow to deepen deepening lows, and with respect to RDCs having an overall positive mean pressure error.

5. SUMMARY AND CONCLUSIONS

A study of NGM model skill in forecasting RDCs was conducted over two separate periods, from the WI90 through the AU91, and from the WI94-WI95, and in the AVN from the WI94-WI95. Seasonal distributions revealed a majority of the RDCs occurred over oceanic regions in both winter and autumn in both the NGM and AVN. There was an observed southwestward shift in the axis of RDCs between the Fall and Winter seasons, and a westward shift in the axis of the RDCs between the WI90-WI91 and WI94-WI95 periods in the NGM. A much smaller distribution of RDCs was observed over the northeastern Pacific in both models at both time periods during the winter months. However, this region of the northeastern Pacific was found to be have a much higher distribution during the Autumn season. Position and mean pressure errors revealed superior skill (smaller errors) for the RDCs in both the NGM and AVN when compared to all cyclones for the respective time periods. The AVN, however, revealed superior skill compared to the NGM in both position and mean pressure errors for the RDCs during the WI94-WI95 period. Comparisons between the WI90-WI91 and WI94-WI95 periods for RDCs in the NGM revealed increased skill for the latter period. This was likely due to a more favorable mean 500 mb trough position which was over a more data rich land region of northeastern North America than the former period when the axis of the RDCs were over data poor oceanic regions. This study also revealed excellent NGM skill in forecasting the sign of the pressure change for RDCs.

6. REFERENCES

Grumm, R.H., and A.L. Siebers, 1990: Systematic Model Forecast Errors of Surface Cyclones in the NGM and AVN, January, 1990. *Wea. and Forecasting*, **5**, 672-682.

_____, and _____, 1989: Systematic Surface Cyclone Errors in NMC's Nested Grid Model November 1988 - January 1989. *Wea. and Forecasting*, 4, 246-252.

_____, R.J. Oravec, and A.L. Siebers, 1992: Systematic Model Forecast Errors of Surface Cyclones in NMC'S Nested Grid Model, December, 1988 through November, 1990. *Wea. and Forecasting.*, 7, 65-87.

Gyakum, J.R., 1983: On the Evolution of the QEII Storm. I: Synoptic Aspects. *Mon. Wea. Rev.*, 111, 1137-1155.

_____, J.R. Anderson, R.H. Grumm, and E.L. Gruner, 1989: North Pacific Cold Season Surface Cyclone Activity: 1975-1983. *Mon. Wea. Rev.*, **117**, 1141-1155.

Leary, C., 1971: Systematic errors in operational National Meteorological Center primitive-equation surface prognoses. *Mon. Wea. Rev.*, **99**, 409-413.

Mullen, S.L., and B.B. Smith, 1990: An Analysis of Sea-Level Cyclone Errors in NMC's Nested Grid Model (NGM) During the 1987-88 Winter Season. *Wea. and Forecasting*, **5**, 433-447.

Sanders, F., and J.R. Gyakum, 1980: Synoptic-Dynamic climatology of the "bomb". *Mon. Wea Rev.*, **108**,1590-1606.

_____, 1986: Explosive Cyclogenesis over the West-Central North Atlantic Ocean, 1981-84. Part II: Evaluation of the LFM Model Performance. *Mon. Wea Rev.* ,**114**,2207-2218.

_____, 1987: Skill of NMC Operational Dynamical Models in Prediction of Explosive Cyclogenesis. *Wea. and Forecasting*, **2** , 322-336.

_____, and E. Auciello, 1989: Skill in Prediction of Explosive Cyclogenesis over the Western North Atlantic Ocean, 1987-1988: A Forecast Checklist and NMC Dynamical Models. *Wea. and Forecasting.*, **4**, 322-336.

Silberberg, S.R., and L.F. Bosart, 1982: An analysis of systematic cyclone errors in the NMC LFM-II model during the 1978-79 cold season. *Mon. Wea. Review.*, **109**, 784-811.

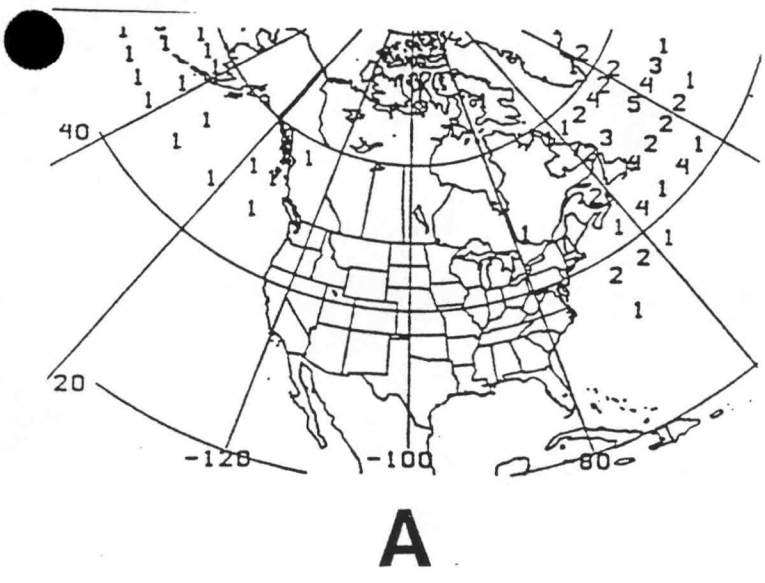

A

B

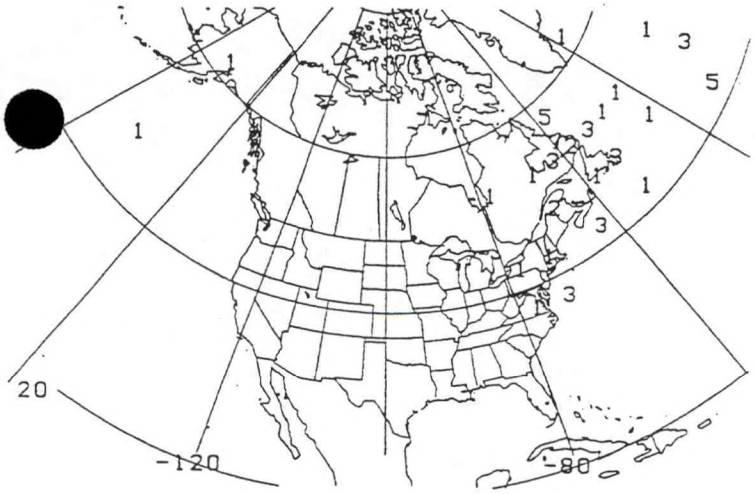

C

D

Figure 1. The distribution of rapidly deepening cyclones (a) NGM WI89-WI91, (b) NGM WI94-WI95, (c) AVN WI94-WI95, and (d) NGM AU90-AU91.

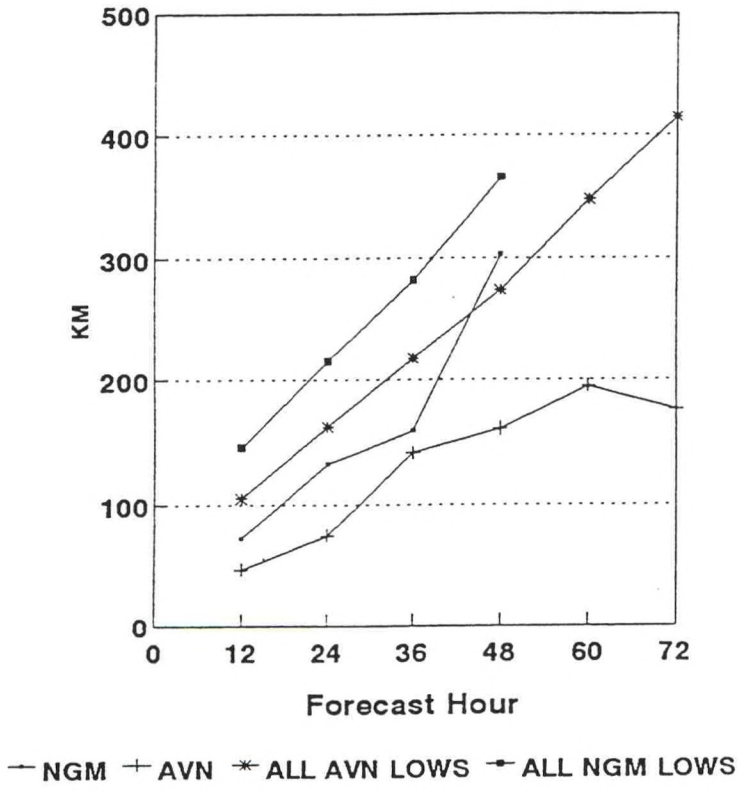

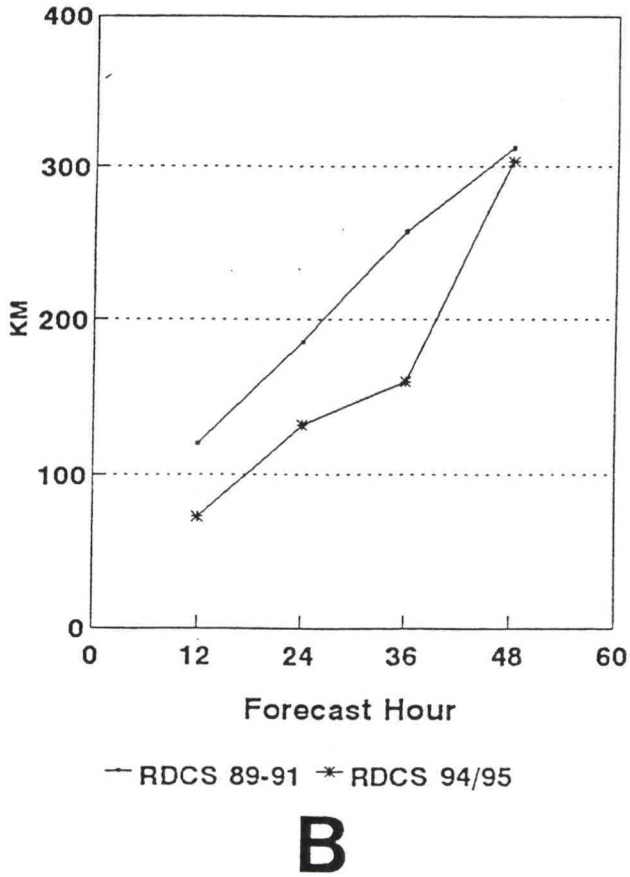

Figure 2. The position errors for (a) RDCs in the NGM, AVN and all lows in the NGM and AVN WI94-WI95, and (b) RDCs in NGM during WI89-WI91 and WI94-WI95.

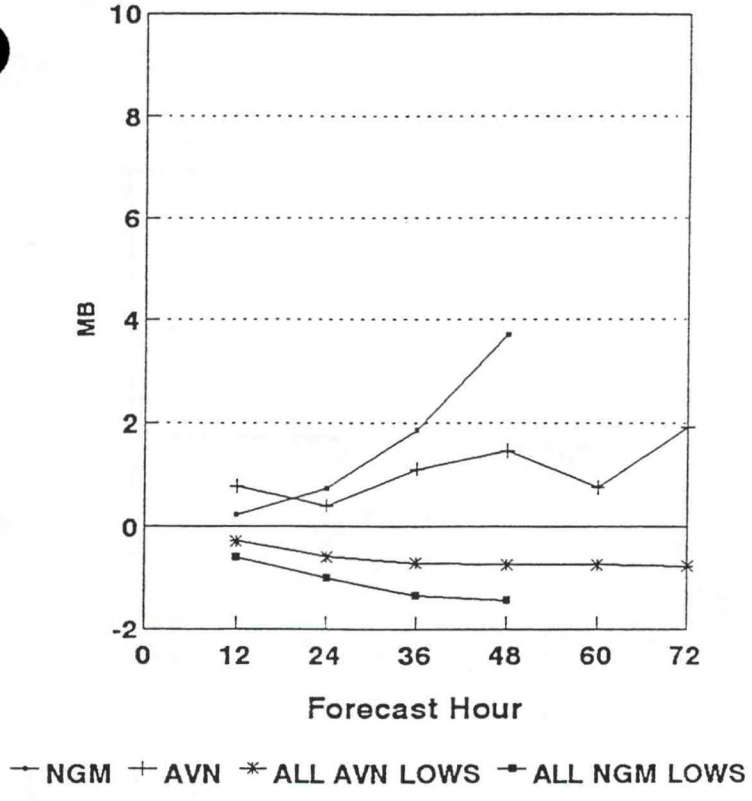

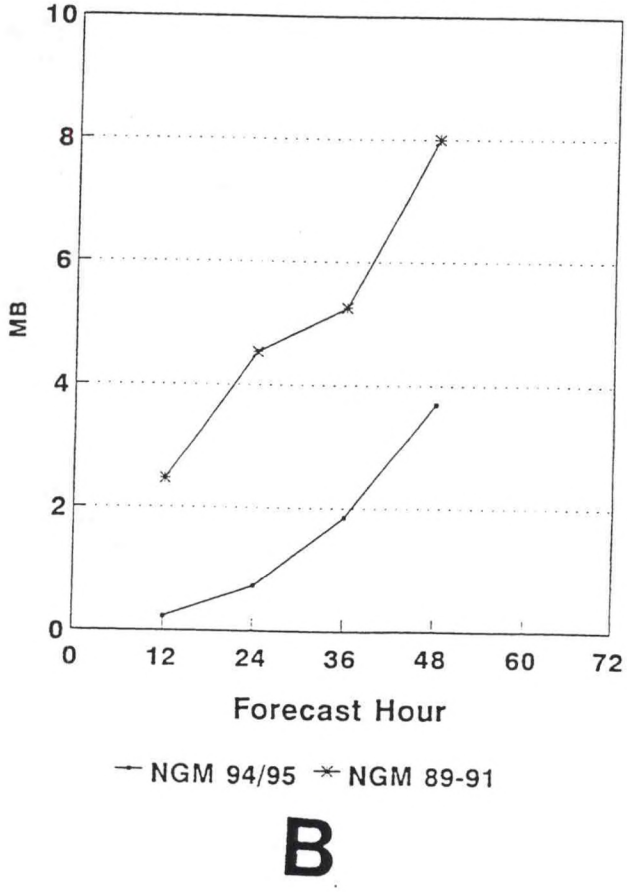

Figure 3. The pressure errors for (a) RDCs in NGM, AVN, and all lows in the NGM and AVN WI94-WI95, and (b) RDCs in NGM during WI89-WI91 and WI94-WI95.

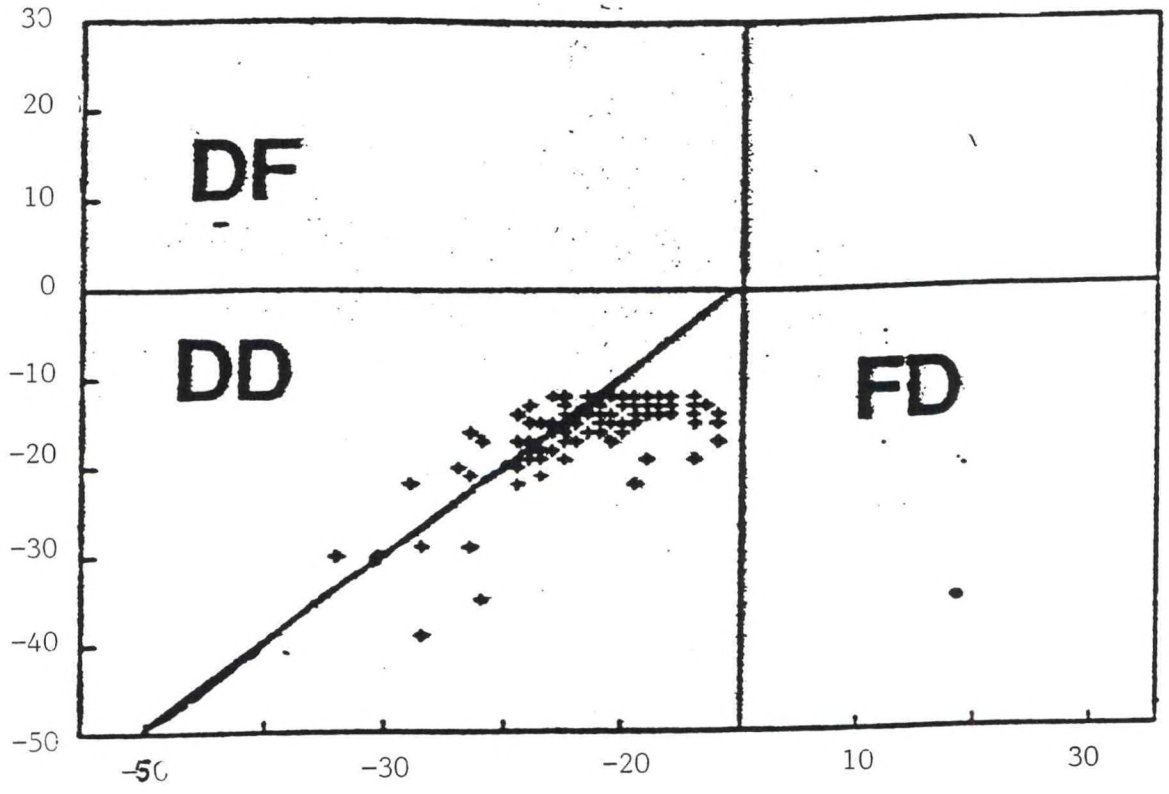

Figure 4. A scatter diagram of the 12-h forecast of the 12-h cyclone pressure change forecast for RDCs in the NGM. The three categories are listed in the text. The line bisecting the diagram represents a perfect forecast by the NGM.

Common Cold Season Biases in NCEP's Medium Range Forecast Model (MRF)

Robert J. Oravec[1]

1. INTRODUCTION

This paper will discuss some of the common cold season forecast problems that are encountered by the NCEP's HPC medium range forecasters. These problems often occur in conjunction with significant disagreements among the operational medium range forecast models (MRF, ECMWF and the UKMET). Examples of some of the more common forecast problems and biases will be given along with the rational used by NCEP's HPC medium range forecasters to produce the days 3 through 5 forecasts.

The cases that will be discussed will be:

- Model biases with the southward surge of cold air in the lee of the Rockies and the relationship between this southward surge and the problems the numerical models often have resolving the amount of upstream 500 mb troughing that is occurring over the Pacific Northwest, downstream of a highly amplified upper ridge over the Gulf of Alaska.

- The difficulties experienced during the winter of 1994-95 handling the split flow pattern that was present for a good portion of the winter. Specifically, a case examining the biases the MRF has in moving closed 500 mb lows in the southern stream component of this split flow.

- A case illustrating problems with phasing between northern and southern streams during split flow patterns.

2. EXAMPLES

One of the most common problems during the cold season across the middle section of the nation is the speed at which low level Arctic air moves southward. Often all numerical models, especially those in the medium range, are too slow with this southward surge. However, the forecasters can not always just speed up the low level cold surge to compensate for the model bias as the southward surge is often related to the direction of the 500 mb flow aloft. Generally, the more northerly the 500 mb flow is over the mid section of the nation the faster the southward surge of Arctic air will be. Unfortunately, it is also often difficult to gage the direction of the 500 mb flow for the days 3 through 5 period since the medium range numerical models will often show significant differences upstream over the pacific northwest. This often occurs downstream of a highly amplified upper ridge over the northeastern Pacific/Gulf of Alaska region, with the medium range models often forecasting different degrees of 500 mb trough development downstream of this upper ridge over the Pacific Northwest and subsequently differing directions of the 500 mb flow downstream over the mid section of the nation.

1. Corresponding author address: Robert J. Oravec, National Centers for Environmental Prediction, Hydrometeorological Prediction Center, Forecast Operations Branch, Camp Springs, Maryland.

The MSLP and 500 mb analysis valid at 1200 UTC 1 March 1995 is shown in Figure 1b. At this time a large Arctic anticyclone had surged southward through the middle section of the nation with the associated frontal boundary stretching from off the Pacific Northwest coast eastward through the southern Rockies and then southward in the lee of the Rockies and into eastern Mexico. At 500 mb a closed high was present over the Gulf of Alaska with broad cyclonic flow downstream of it across the United States. Note the strength of the 500 mb trough over the Pacific Northwest at this time and the direction of the flow downstream of it over the mid section of the nation.

The day 3, 4, and 5 MSLP and 500 mb from the MRF and ECMWF valid on 1200 UTC 1 March 1995 are shown in Figure 2. Comparison of Figure 2 and Figure 1b reveals the MRF bias of being much too slow with the southward surge of the low level Arctic air across the mid-section of the U.S. This is most evident on the day 5 forecast where the MRF's forecast frontal boundary is over southern South Dakota, southern Montana and it verified over eastern Mexico. Meanwhile, the ECMWF was much farther to the south with the forecast Arctic frontal boundary and was very consistent over the three model cycles which produced these forecasts and had much superior forecasts. The superior ECMWF forecast is likely due to superior modeling of the upstream trough over the Pacific Northwest. Examination of Figure 2 reveals that the MRF forecast the 500 mb trough over the Pacific Northwest to be too strong, especially with the day 4 and 5 forecasts. This subsequently allowed the downstream flow to be too west southwesterly across the mid section of the nation. The ECMWF, however, forecasted a much weaker 500 mb trough over the Pacific Northwest and subsequently allowed the 500 mb flow to have a more northerly component across the mid section of the nation which allowed for the low level Arctic air to move faster to the south. The stronger MRF 500 mb trough over the Pacific Northwest on day 5 also did not allow the Arctic air to move westward into pacific northwest. The HPC medium range forecasters correctly identified the biases exhibited by the MRF and were much more progressive to the south than the MRF across the mid section of the nation and farther to the west over the Pacific Northwest with the low level Arctic air (Figure 1a).

The second example will illustrate MRF biases with respect to the movement of closed lows in the southern stream component of split flow across North America. During the winter of 1994/95 an active split flow regime persisted across North America with several well defined closed lows moving in the southern stream. This forecast problem often begins over the southwestern U.S. and translates downstream across the remainder of the nation as closed lows in this southern stream flow begin to move east northeastward. The typical bias of the MRF is to move these closed lows too quickly to the northeast. In addition to problems with timing, the medium range models, especially the MRF, will often have problems forecasting the interactions between the southern stream closed low and the northern stream flow. This will often lead to phasing or partial phasing of the closed low with northern stream shortwaves which can cause the forecast position of the closed low to be significantly too far to the north and/or too progressive. The example given here occurred from the January 15-17, 1995, with this example illustrating the forecast difficulties experienced by the MRF as this southern stream closed moved into the southeastern U.S. on January 16.

Figure 3b shows the 1200 UTC MSLP and 500 mb analysis across the U.S. At 500 mb the split flow pattern is clearly seen with a well defined southern stream closed low just to the east of the South Carolina coast, and a weaker northern stream 500 mb trough moving through the eastern Great Lakes. At the surface these two streams are well represented by respective surface lows and frontal boundaries. This example will concentrate on the forecast that verified at 1200 UTC January 16 and will illustrate some of the above mentioned biases of the MRF with closed lows, while also showing the excellent forecast by the ECMWF and the NCEP medium range forecasters.

The days 3, 4, and 5 MSLP and 500 mb forecasts from the MRF and ECMWF verifying at 1200 UTC January 16 are shown in Figure 4. Comparison of Figure 4a with Figure 3b reveals two of the above mentioned biases. The bias of the MRF to be too progressive with southern stream closed lows is evident in the day 3 forecast with the MRF forecasting the closed low to be over northwestern Virginia when it verified off the South Carolina coast. The day 4 forecast illustrates the problem the MRF often has in phasing the northern and southern streams. These streams often remain distinctly separate as is evident in the 1200 UTC January 16 analysis.

Comparison of Figure 4a with Figure 3b shows the significant differences that can occur at the surface due to the timing and phasing problems in the split flow. The most dramatic example is on the day 4 MRF forecast which exhibited the phasing problem with the northern stream. The MRF day 4 forecast showed strong cold advection along and off the east coast with a 986 mb low near James Bay. Due to the aforementioned timing and phasing problems, broad warm advection verified along the eastern seaboard with a pressure error of approximately 38 mb in the vicinity of James Bay.

During periods of a well defined split 500 mb flow where the southern stream component has embedded closed lows, HPC medium range forecasters are often suspicious of any model forecast where these closed low are very progressive. Often during these situations other medium range guidance, ECMWF, UKMET, or MRF ensemble forecasts, will forecast a much slower eastward progression. In these situations the slower model forecast is often followed.

This was the situation during the January 15-17, 1995 forecast. During this time period, the ECMWF model provided superior guidance with the eastward movement of the southern stream closed low. Unlike the MRF, the ECMWF was very consistent with its forecast over the three day period. At all of these days the ECMWF was much slower to move the closed low eastward and did not phase the northern and southern streams, but kept them distinctly separate (Figure 4b). This ability of the ECMWF to keep the northern and southern streams separate appears to be one of the biggest strengths of this model during split flow regimes. While the ECMWF has been observed to have a bias of over-deepening shortwaves into closed lows, when there is a high degree of likelihood that one will exist, as was the case during the winter of 1994-95, it often is the superior model with the subsequent movement. Subsequently, the ECMWF's MSLP forecasts (Figure 4b) were far superior to the MRF's and very consistent over the three day period. Comparison of Figure 4b with Figure 4a reveals the very large differences between the MRF and ECMWF.

The manual HPC medium range forecasts for the above mentioned three day period are shown in Figure 3a. Over three separate forecast runs of the medium range models the HPC medium range forecasters correctly recognized the biases of MRF in the split flow regime. Subsequently, the HPC medium range forecasters trended toward the ECMWF forecasters. While the HPC forecasters followed the ECMWF significantly that day, they still made improvements to the ECMWF as they repositioned the forecast surface low slightly from inland positions across the southeastern U.S. to a position off the South Carolina coast where it verified.

The final example illustrates the phasing problem the MRF has between southern and northern streams during period of split flow. The bias of the MRF is to forecast too much interaction between the northern and southern streams, which often lead to phasing between these two streams and over-amplification of the downstream 500 mb trough over eastern North America.

This was the case during with the December 8, 1994 forecast by the MRF. Figure 5 shows the day 3, 4 and 5 forecast of the MRF from the 0000 UTC 8 December 1994 model run, along with the corresponding 500 mb analysis verifying at 1200 UTC on December 11, 12 and 13, 1994. The analyses

in Figure 5 clearly show the two streams remaining distinctly separate over the three day period. However, the MRF forecast for this period reveals the forecast phasing between the northern and southern streams, which produced a much stronger 500 mb trough over eastern North America than was observed. The position of the 540 DM height contour is highlighted in both the analysis and MRF forecast to illustrate this above mentioned bias.

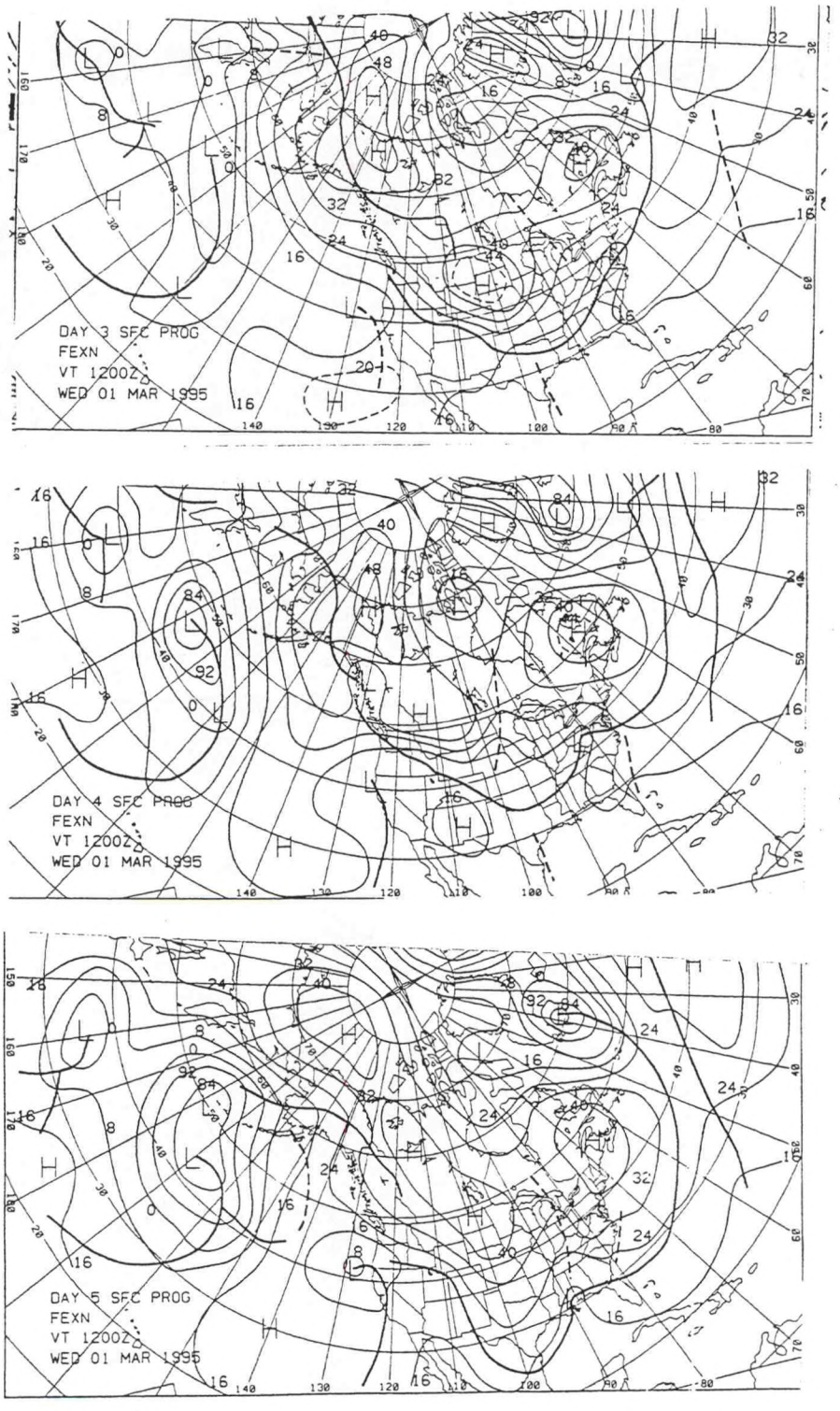

Figure 1a. The days 3,4, and 5 HPC medium range forecasts valid 1200 UTC 1 March, 1995.

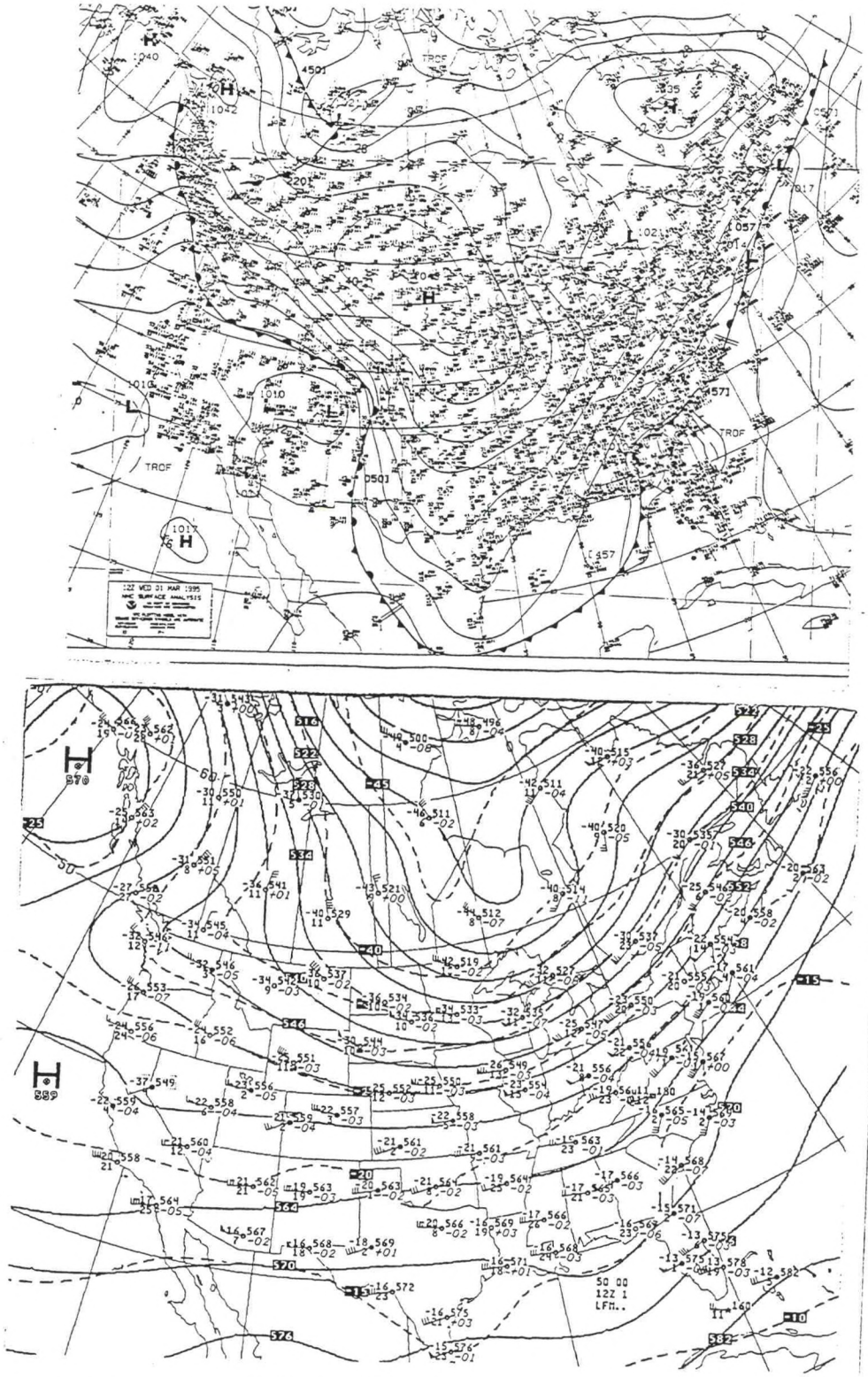

Figure 1b. The 1200 UTC 1 March 1995 MSLP and 500 mb analyses.

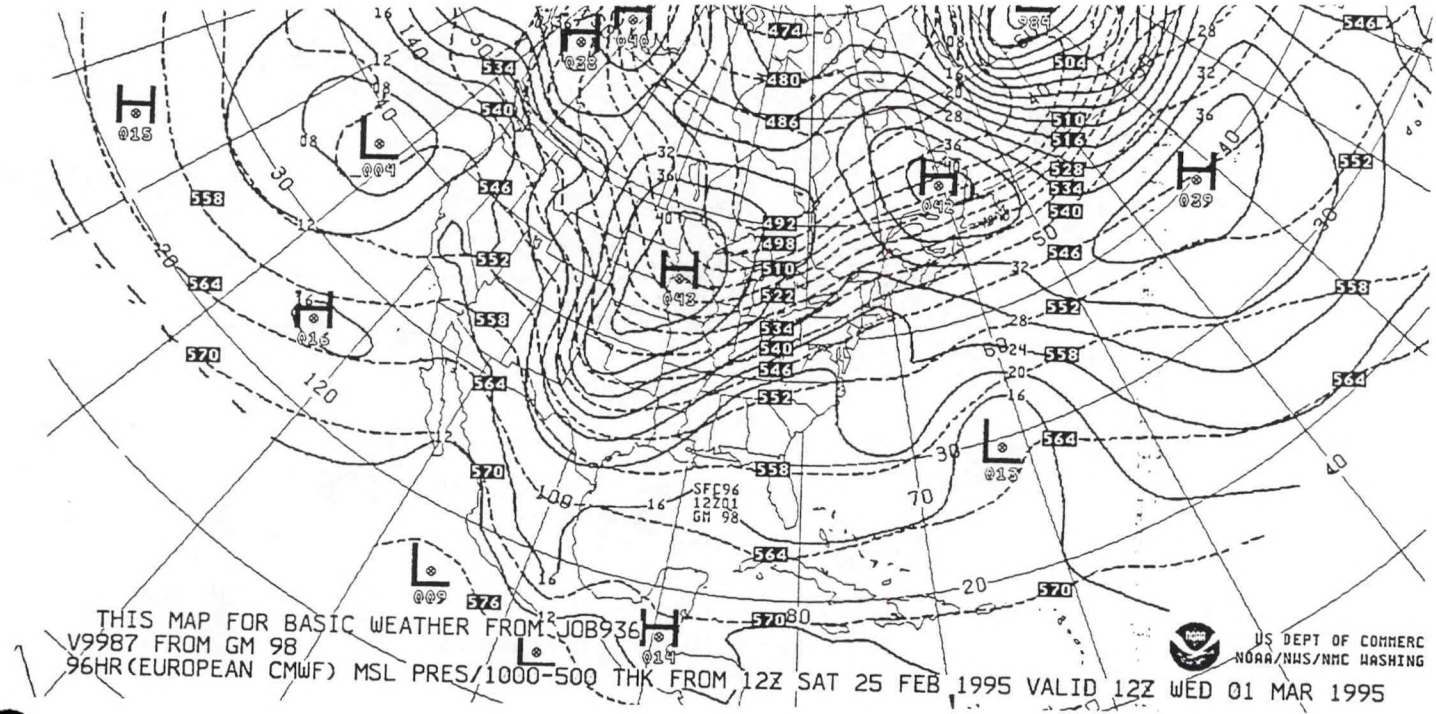

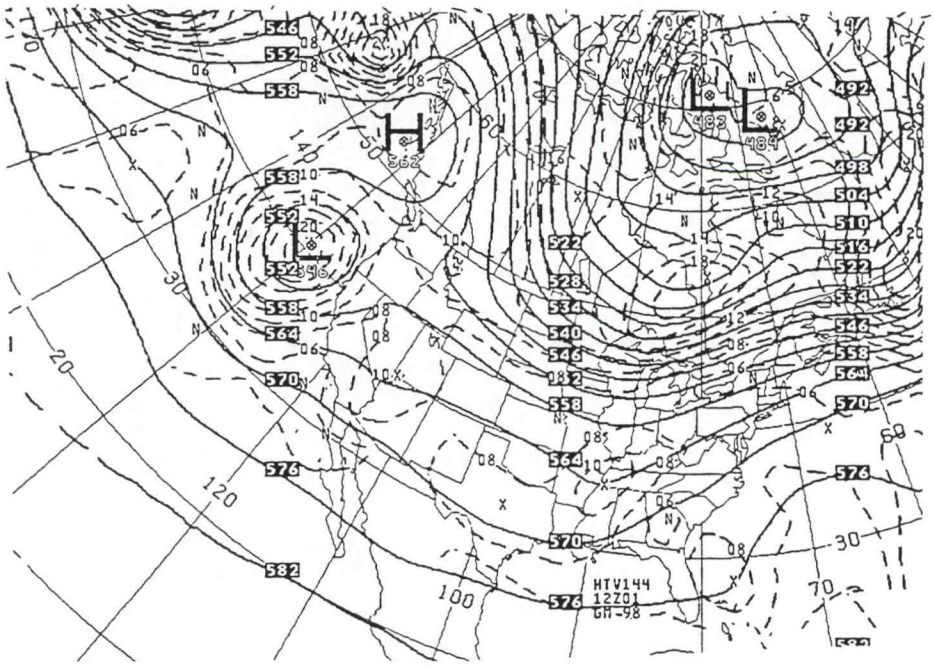

Figure 2a. The day 3 MSLP and 500 mb forecasts valid 1200 UTC 1 March 1995 from the ECMWF.

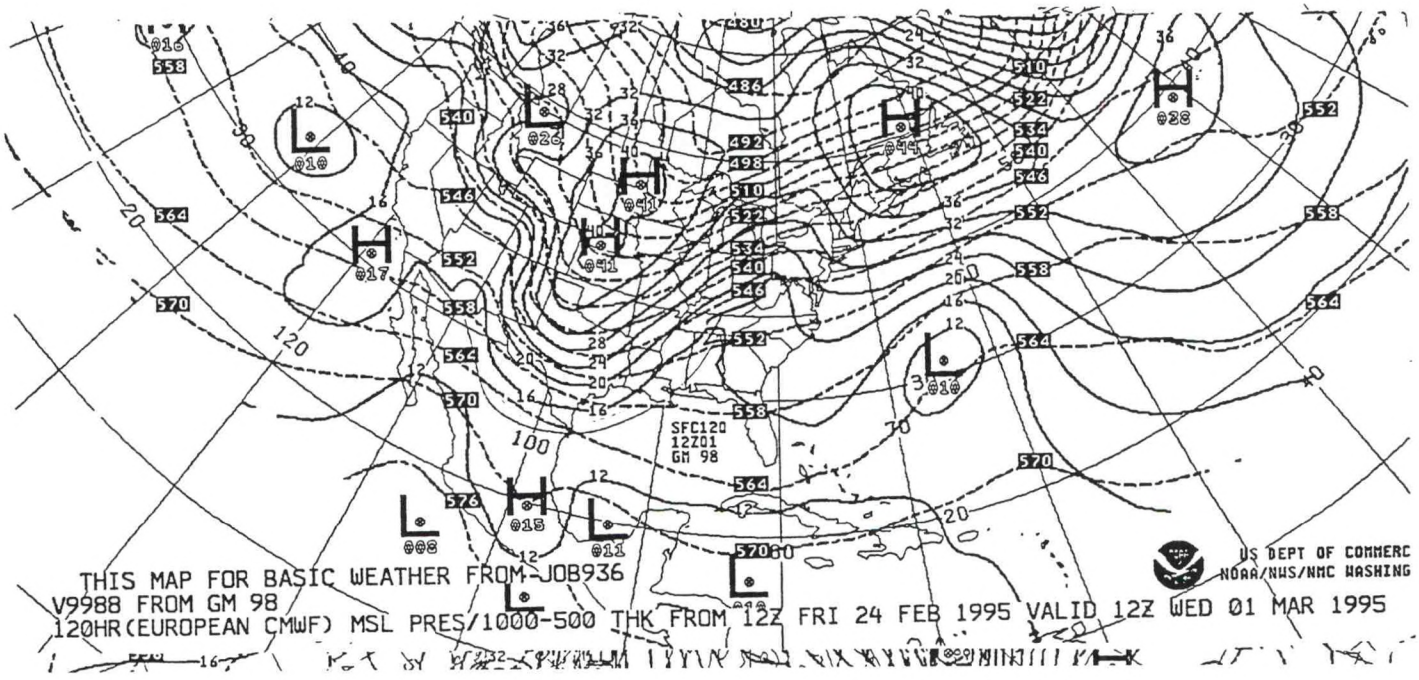

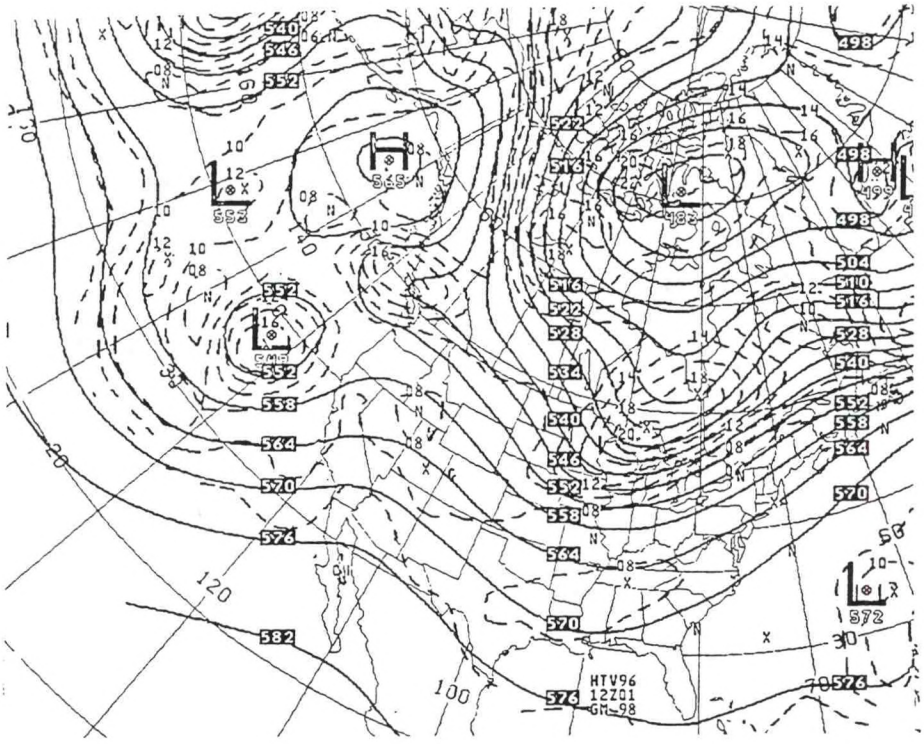

Figure 2a. The day 4 MSLP and 500 mb forecasts valid 1200 UTC 1 March 1995 fromthe ECMWF.

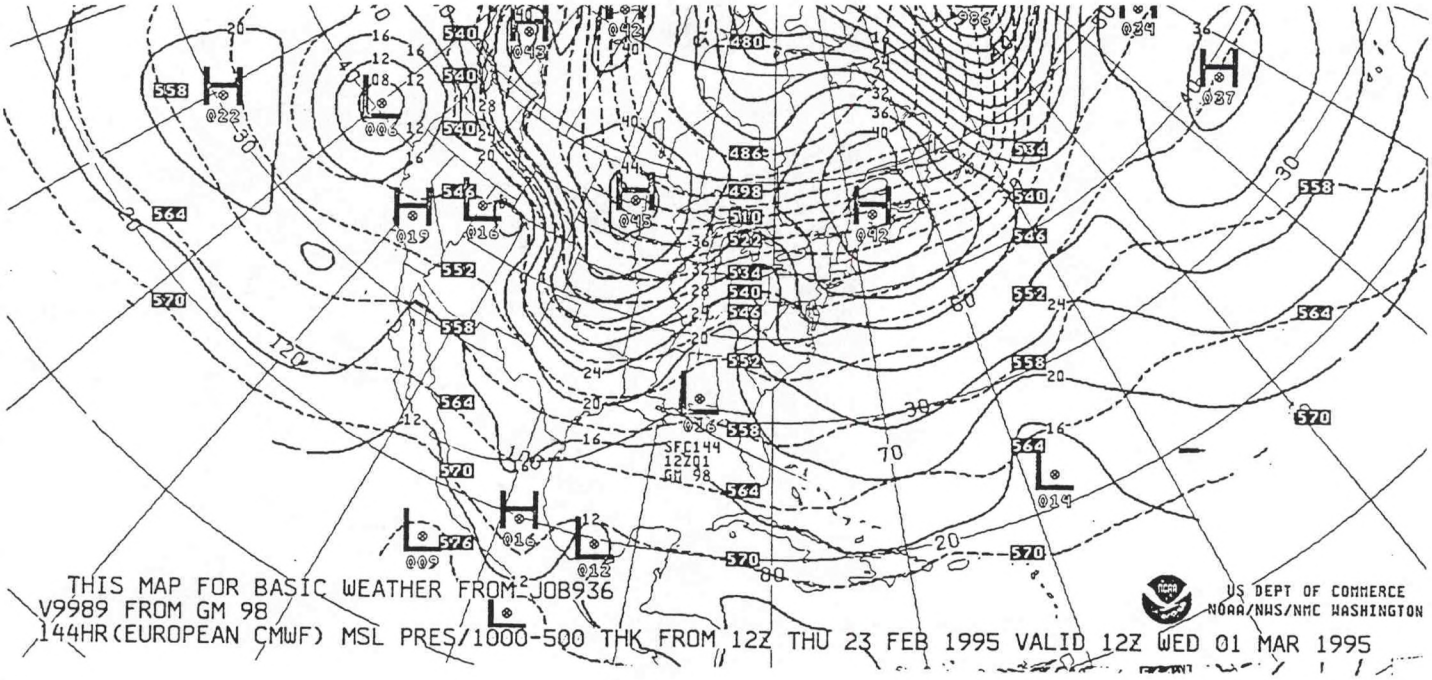

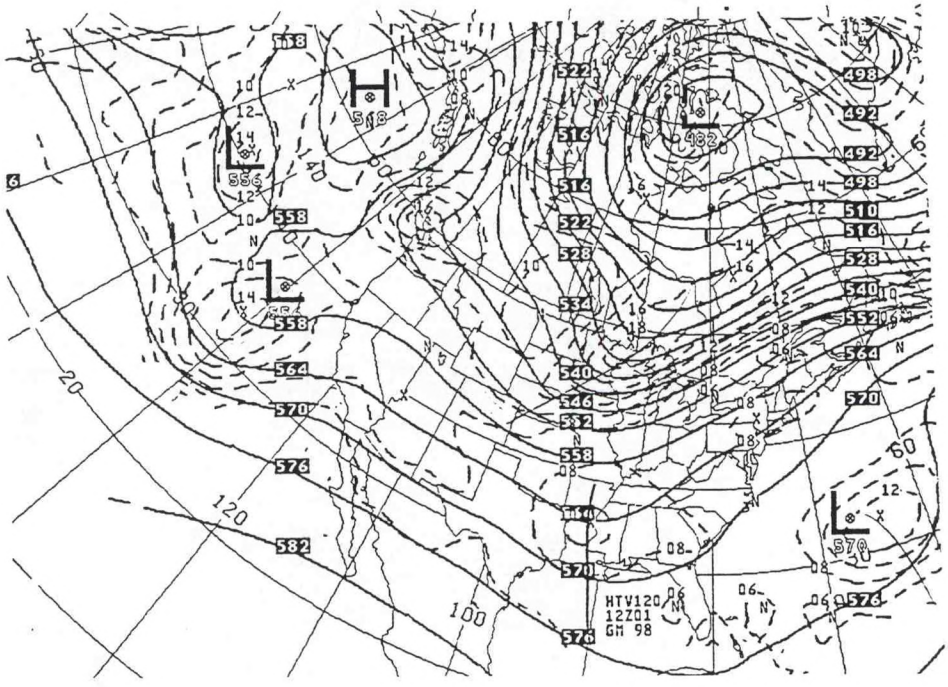

Figure 2a. The day 5 MSLP and 500 mb forecasts valid 1200 UTC 1 March 1995 from the ECMWF.

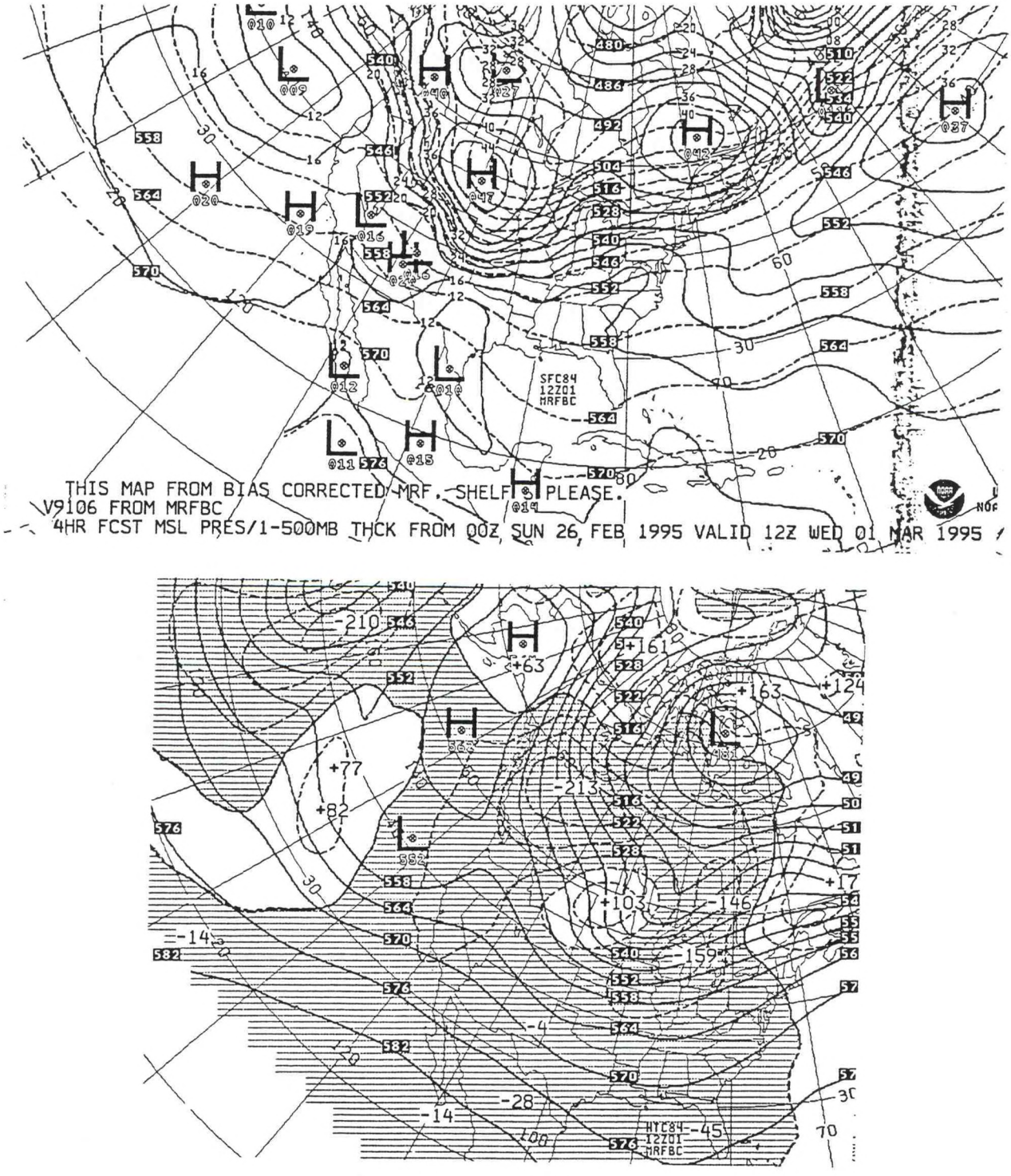

Figure 2b. The day 3 MSLP and 500 mb forecasts valid 1200 UTC 1 March 1995 from the MRF.

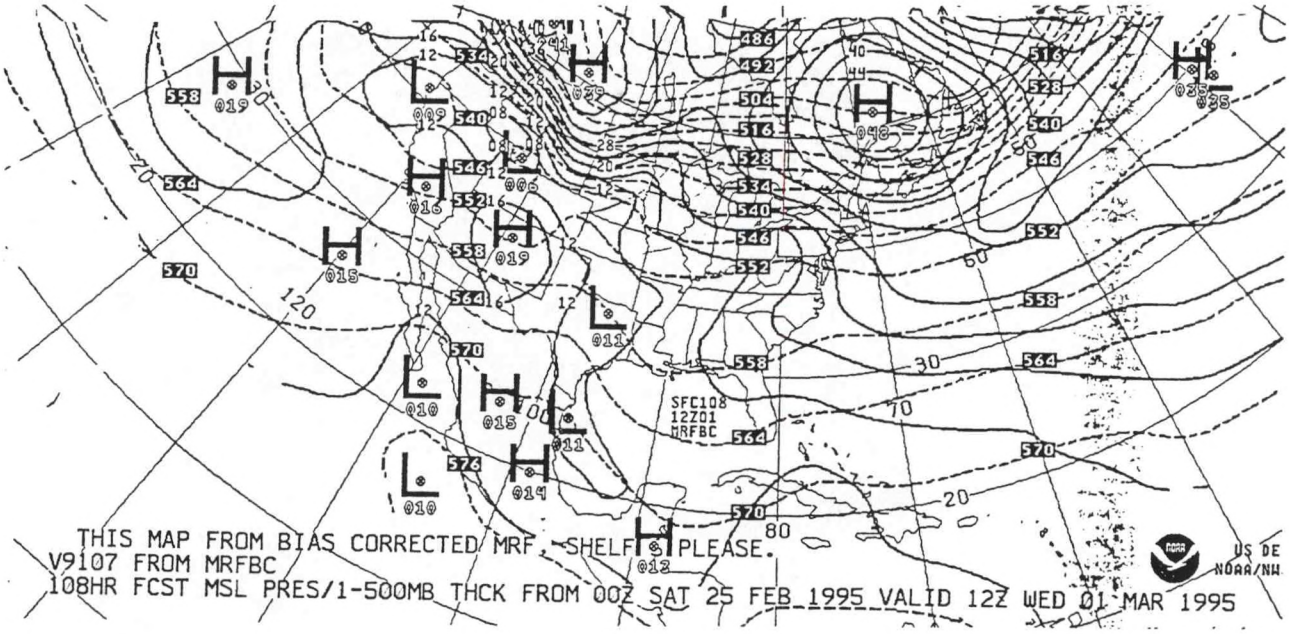

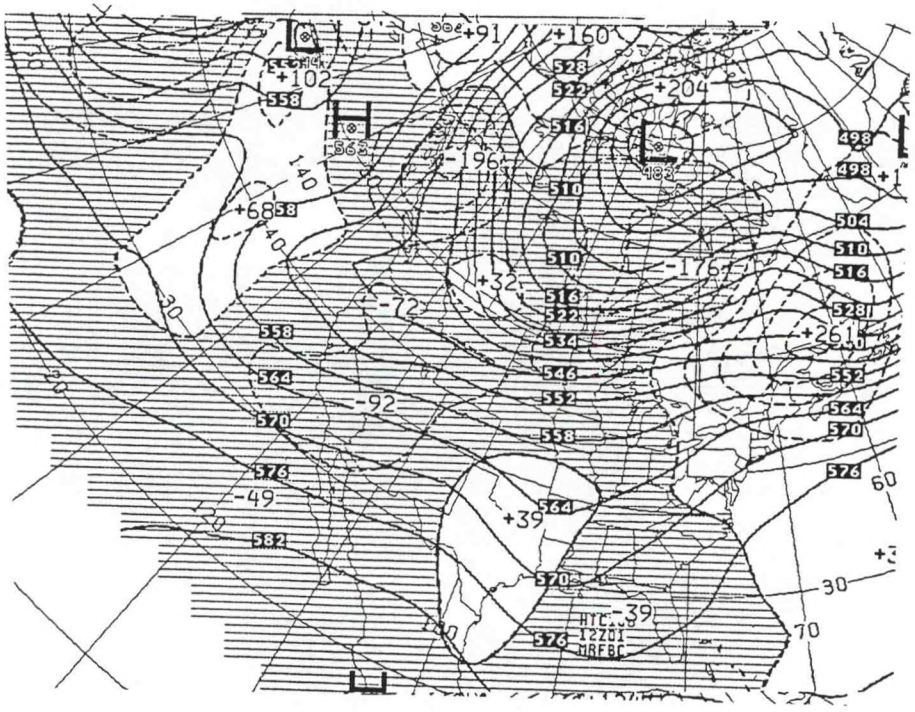

Figure 2b. The day 4 MSLP and 500 mb forecasts valid 1200 UTC 1 March 1995 from the MRF.

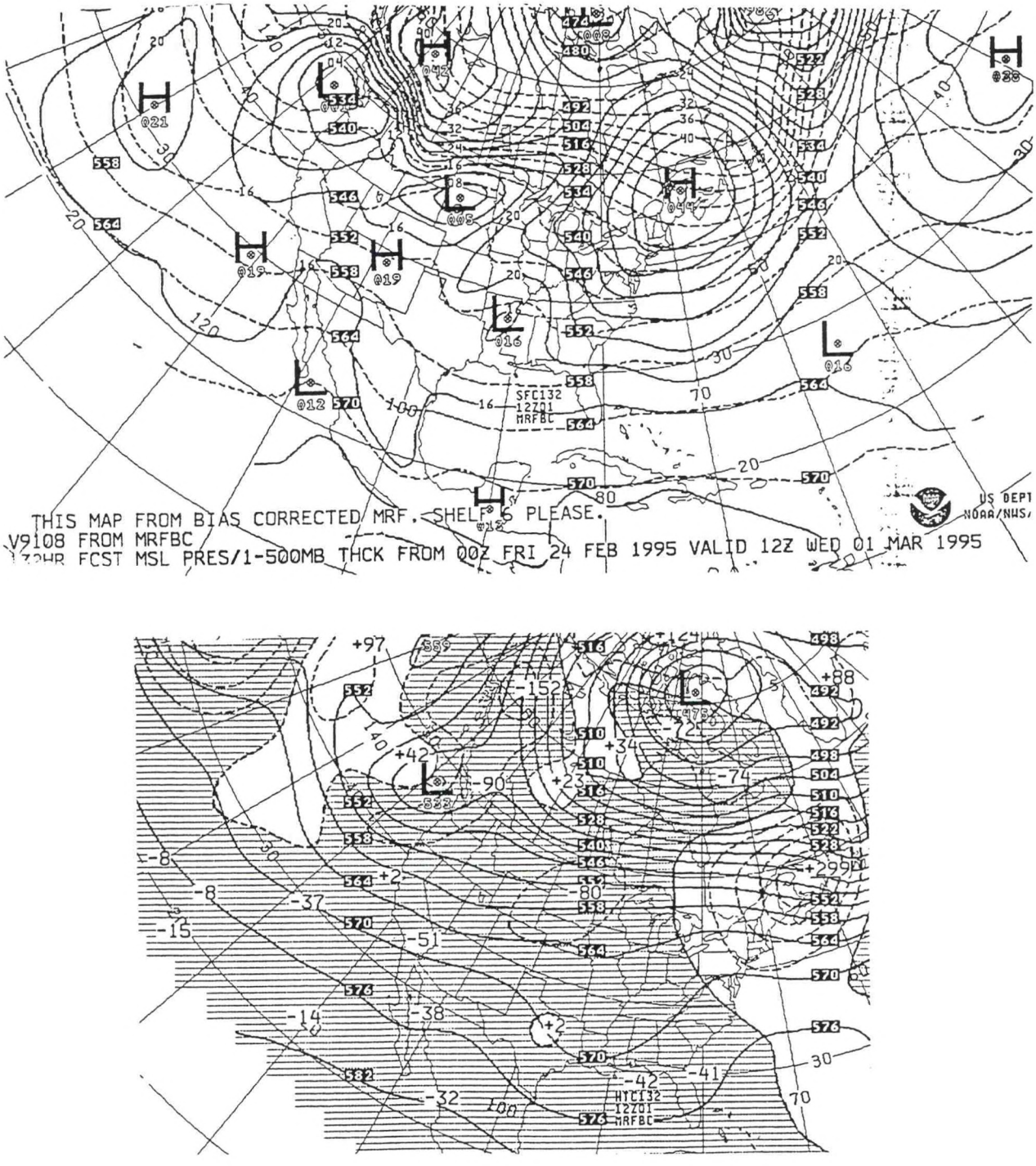

Figure 2b. The day 5 MSLP and 500 mb forecasts valid 1200 UTC 1 March 1995 from the MRF.

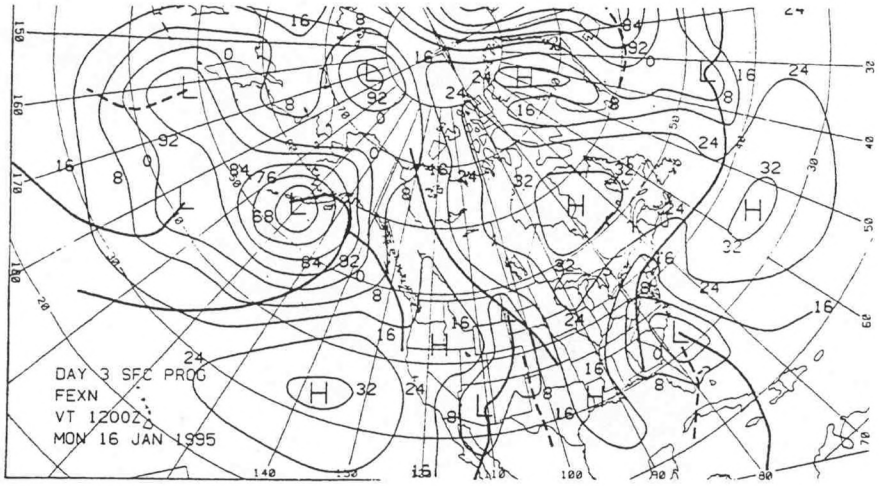

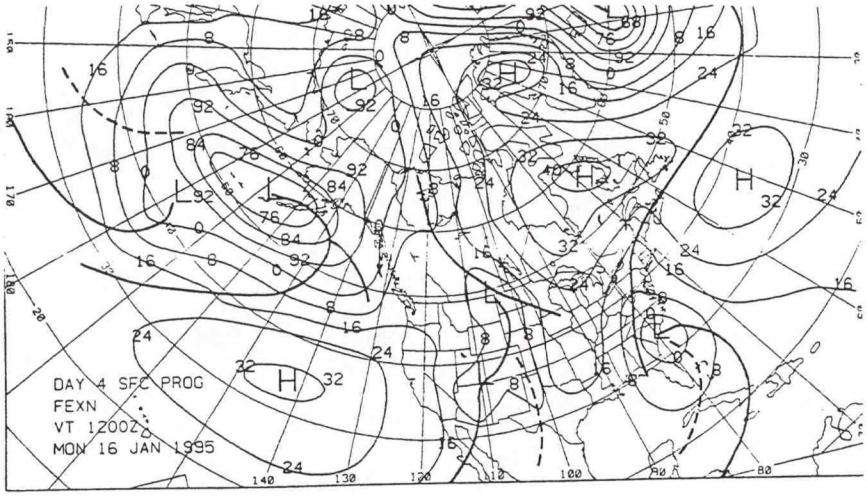

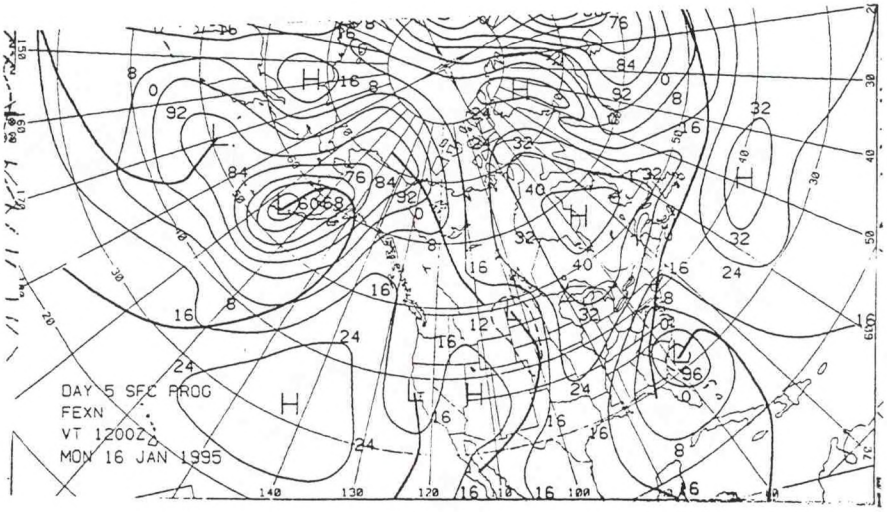

Figure 3a. The days 3, 4, and 5 HPC medium range forecasts valid 1200 UTC 16 January 1995.

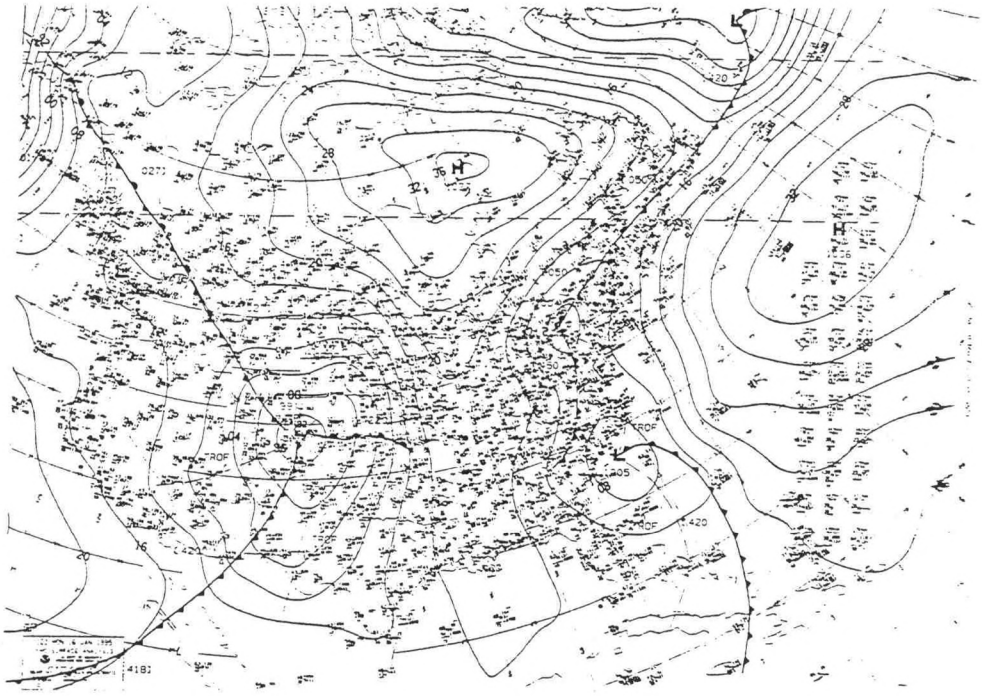

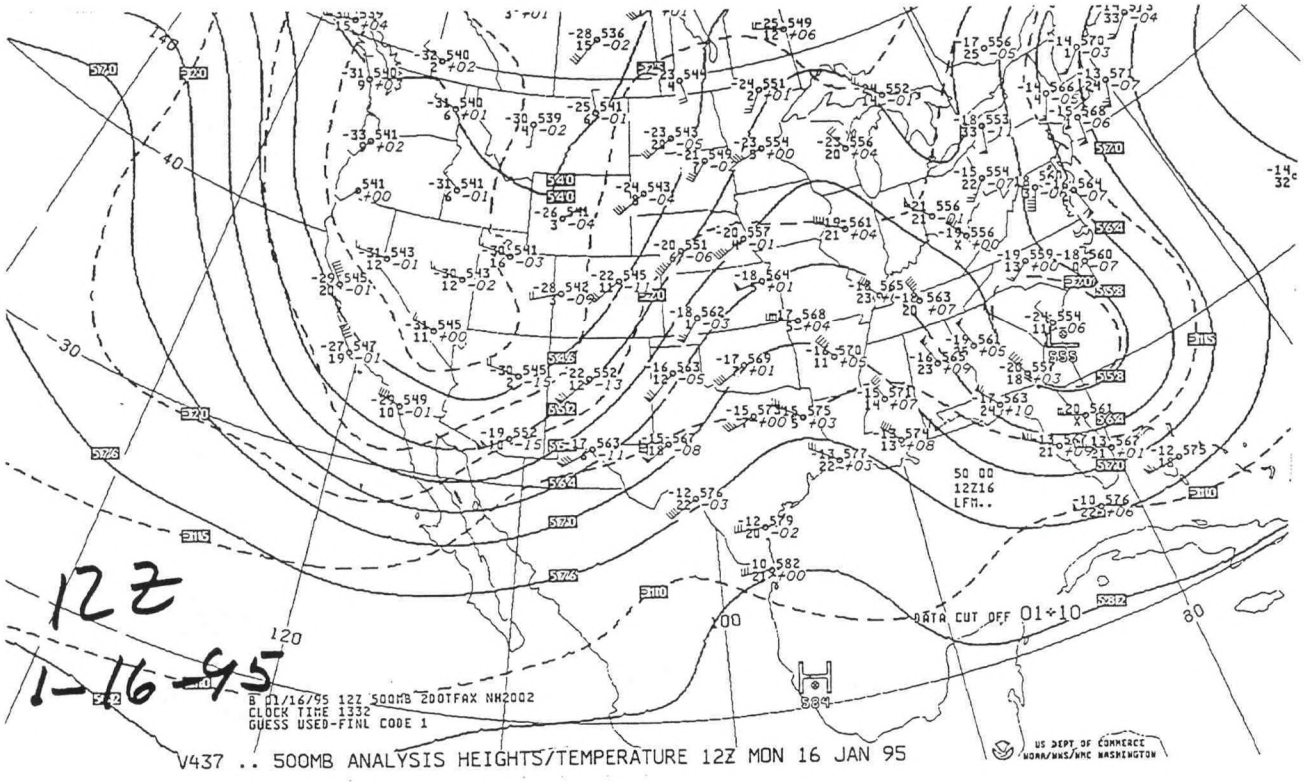

Figure 3b. The 1200 UTC 16 January 1995 MSLP and 500 mb analyses.

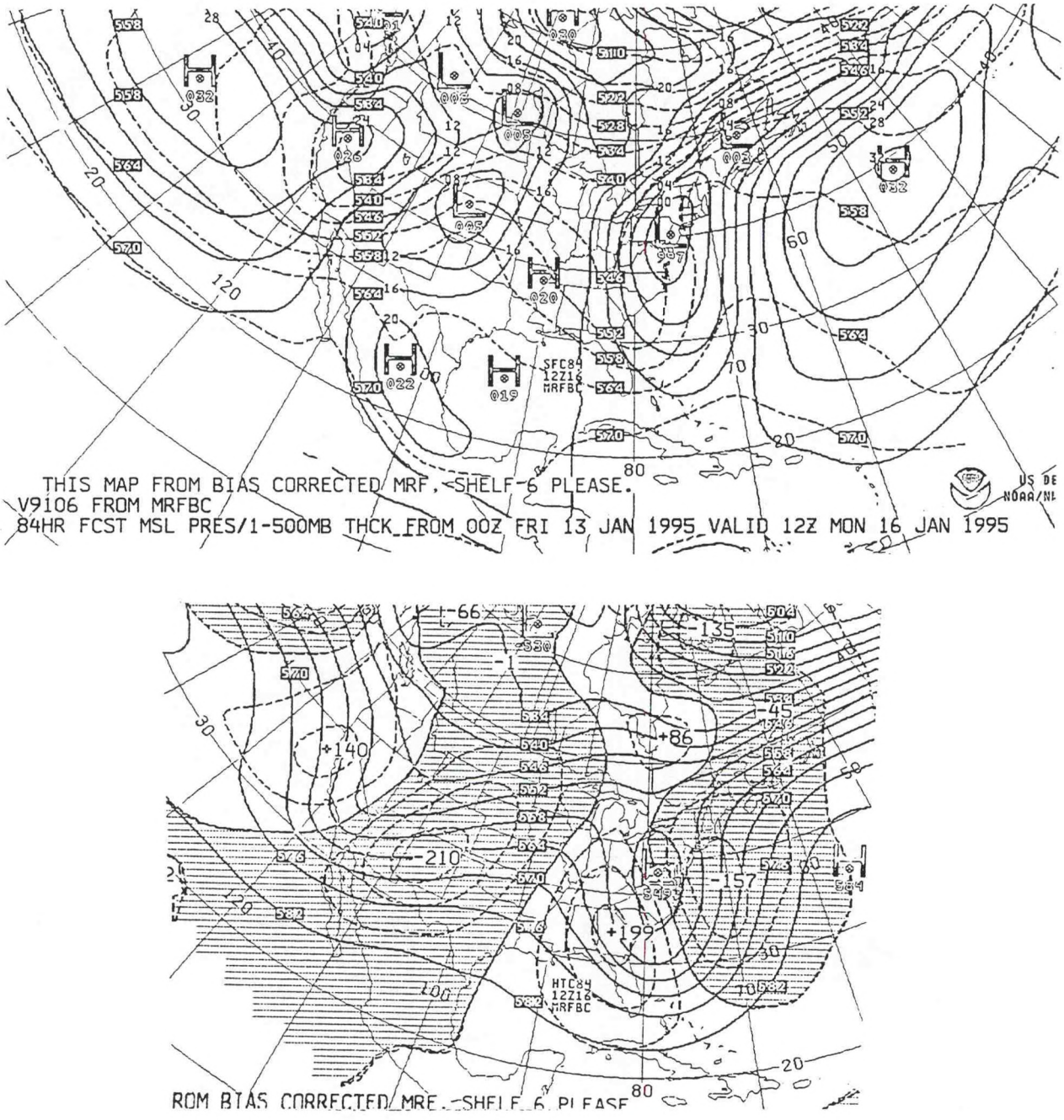

Figure 4a. The day 3 MSLP and 500 mb forecasts valid 1200 UTC 16 January 1995 from the MRF.

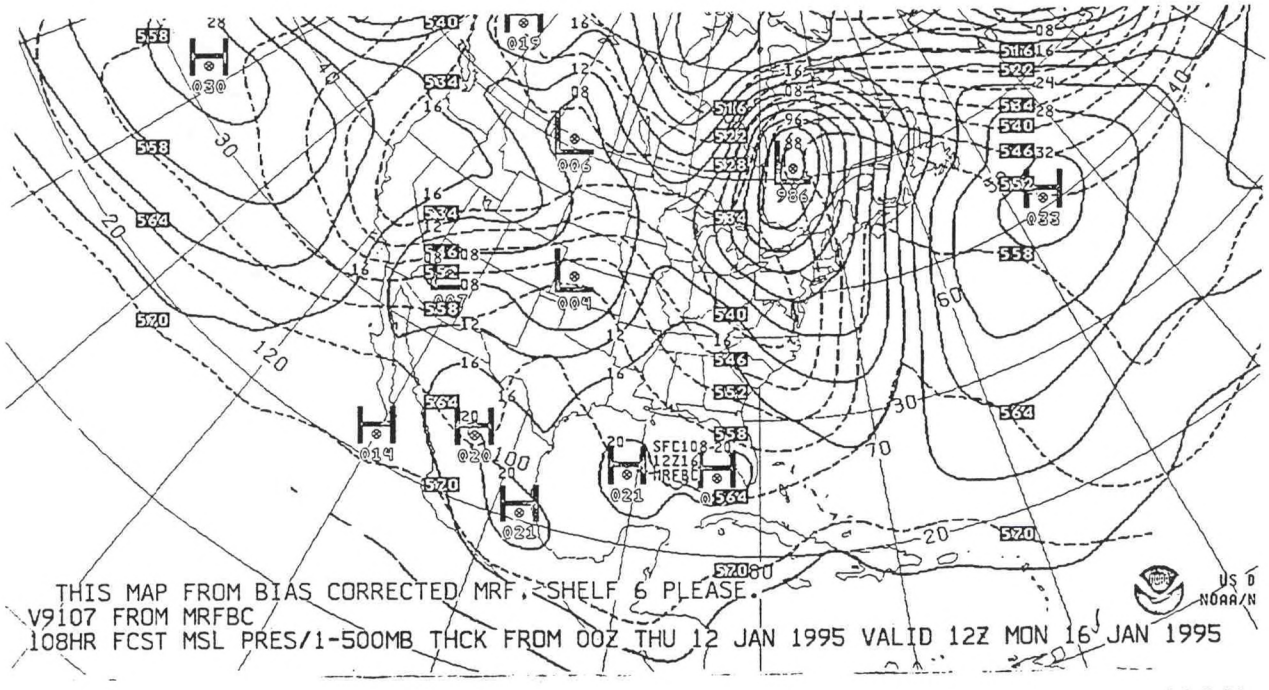

Figure 4a. The day 4 MSLP and 500 mb forecasts valid 1200 UTC 16 January 1995 from the MRF.

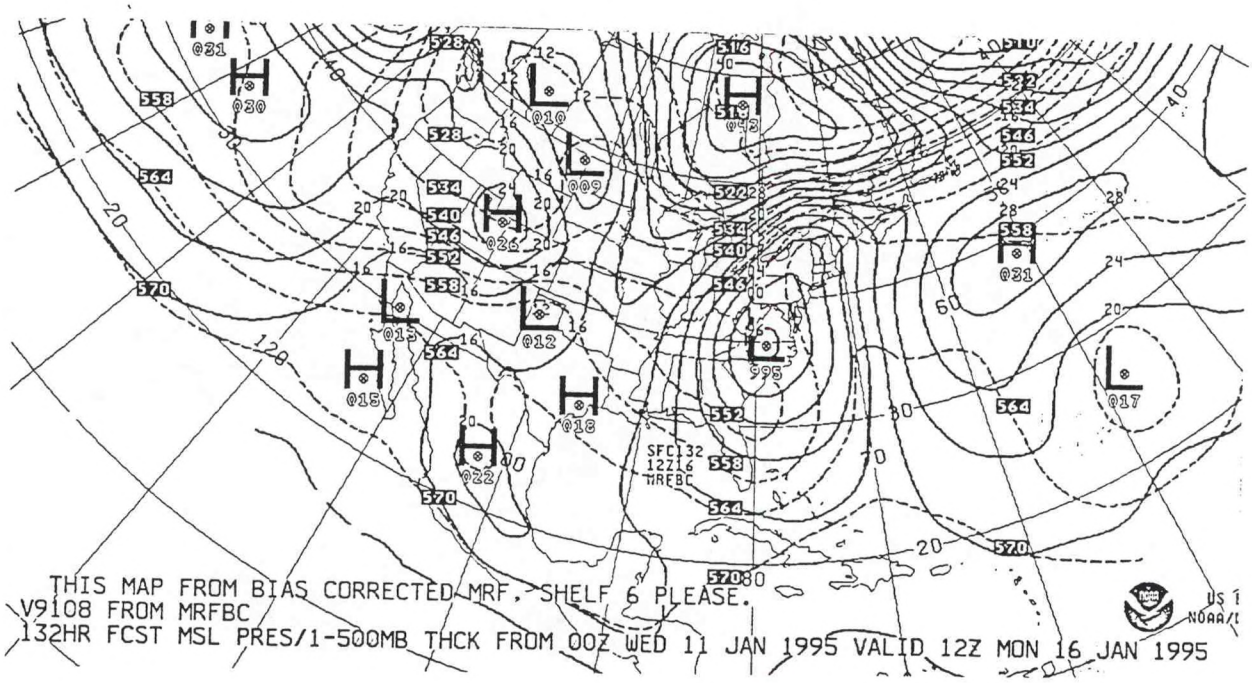

Figure 4a. The day 5 MSLP and 500 mb forecasts valid 1200 UTC 16 January 1995 from the MRF.

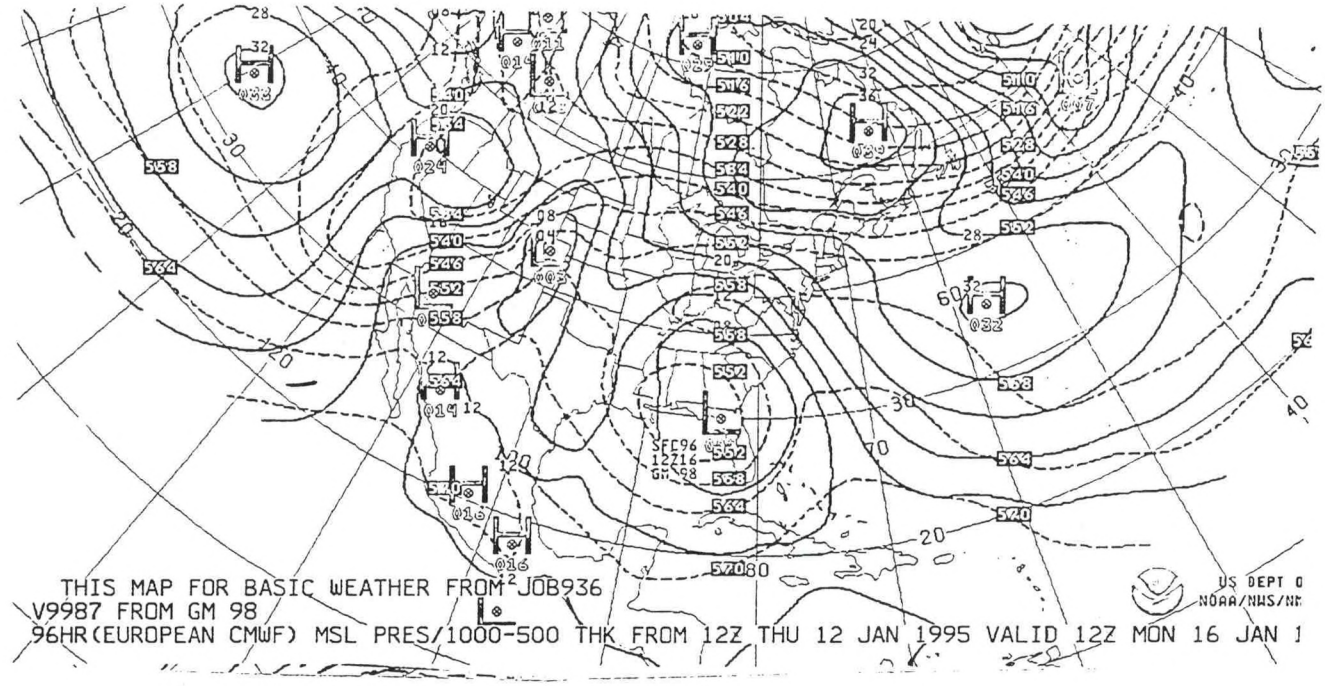

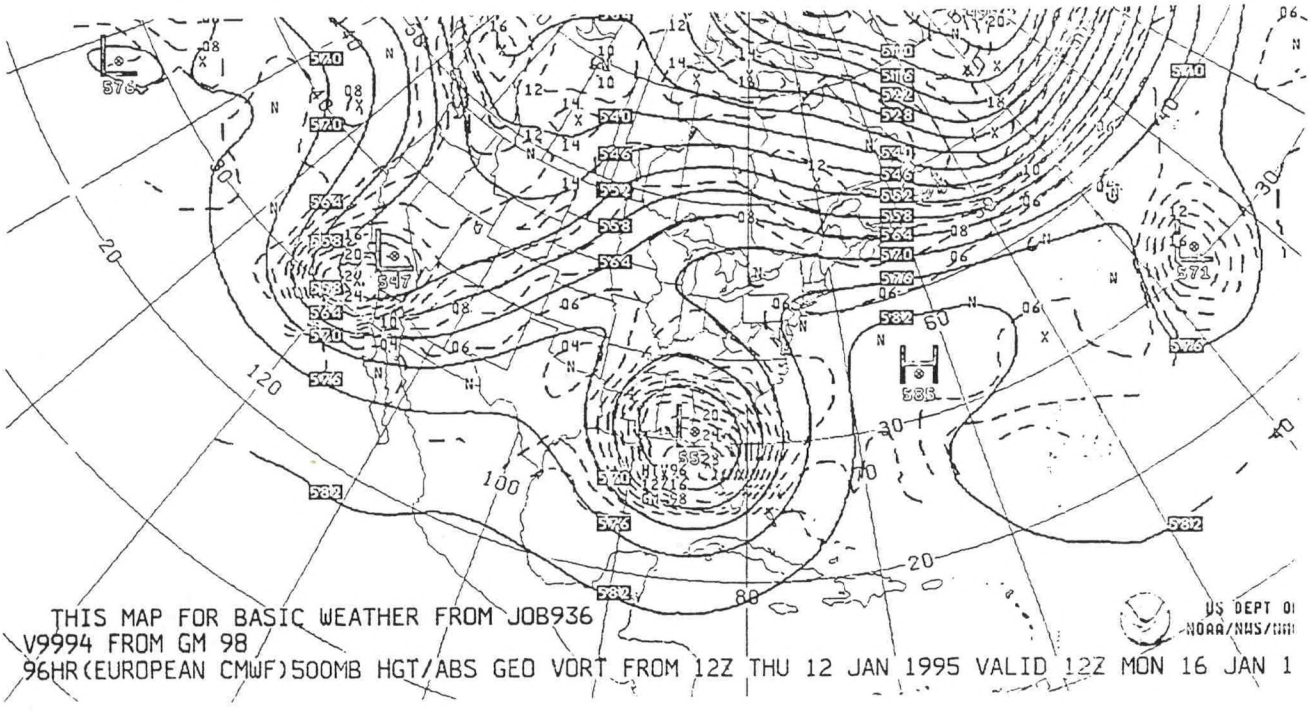

Figure 4b. The day 3 MSLP and 500 mb forecasts valid 1200 UTC 16 January 1995 from the ECMWF.

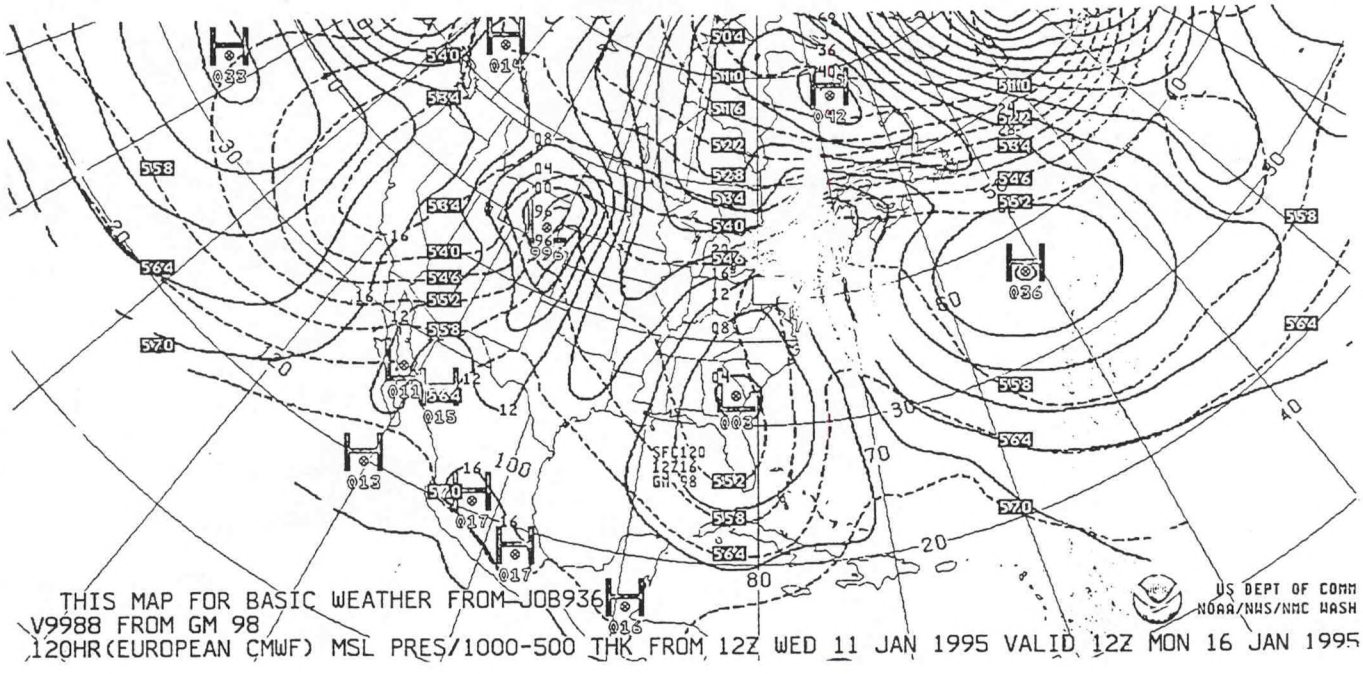

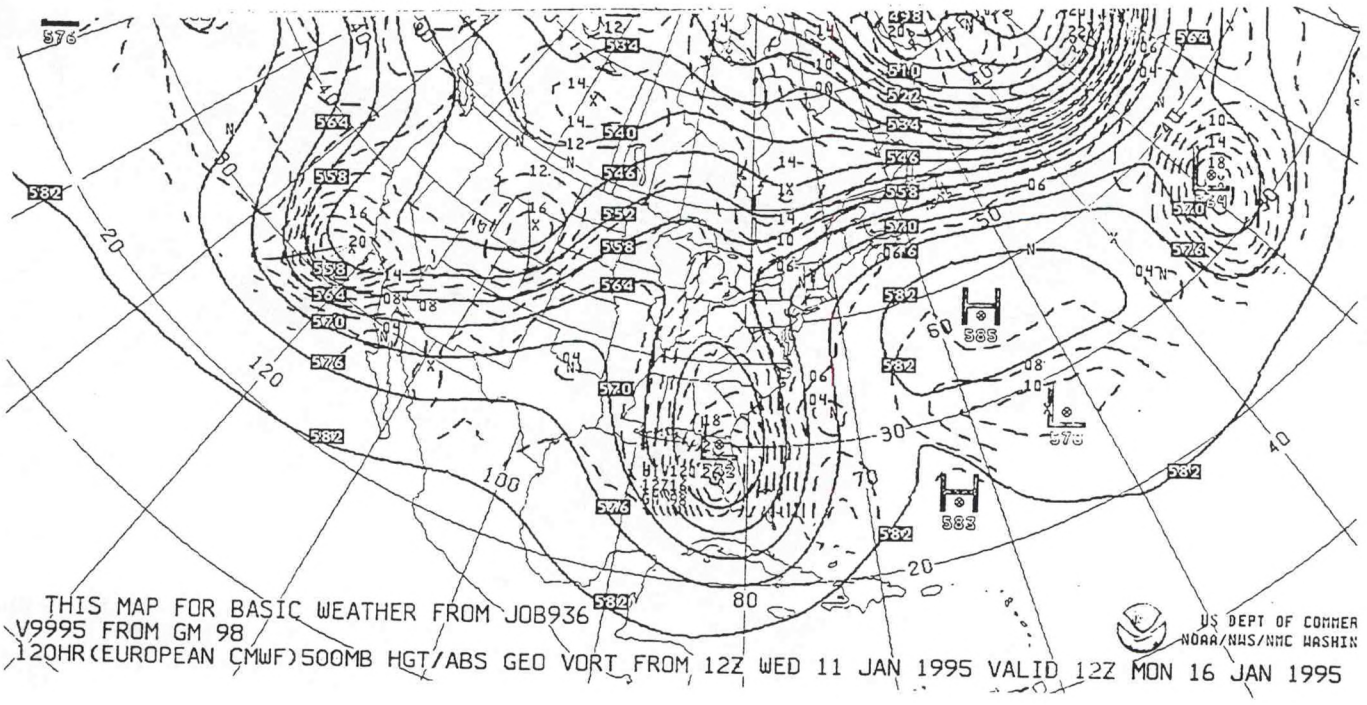

Figure 4b. The day 4 MSLP and 500 mb forecasts valid 1200 UTC 16 January 1995 from the ECMWF.

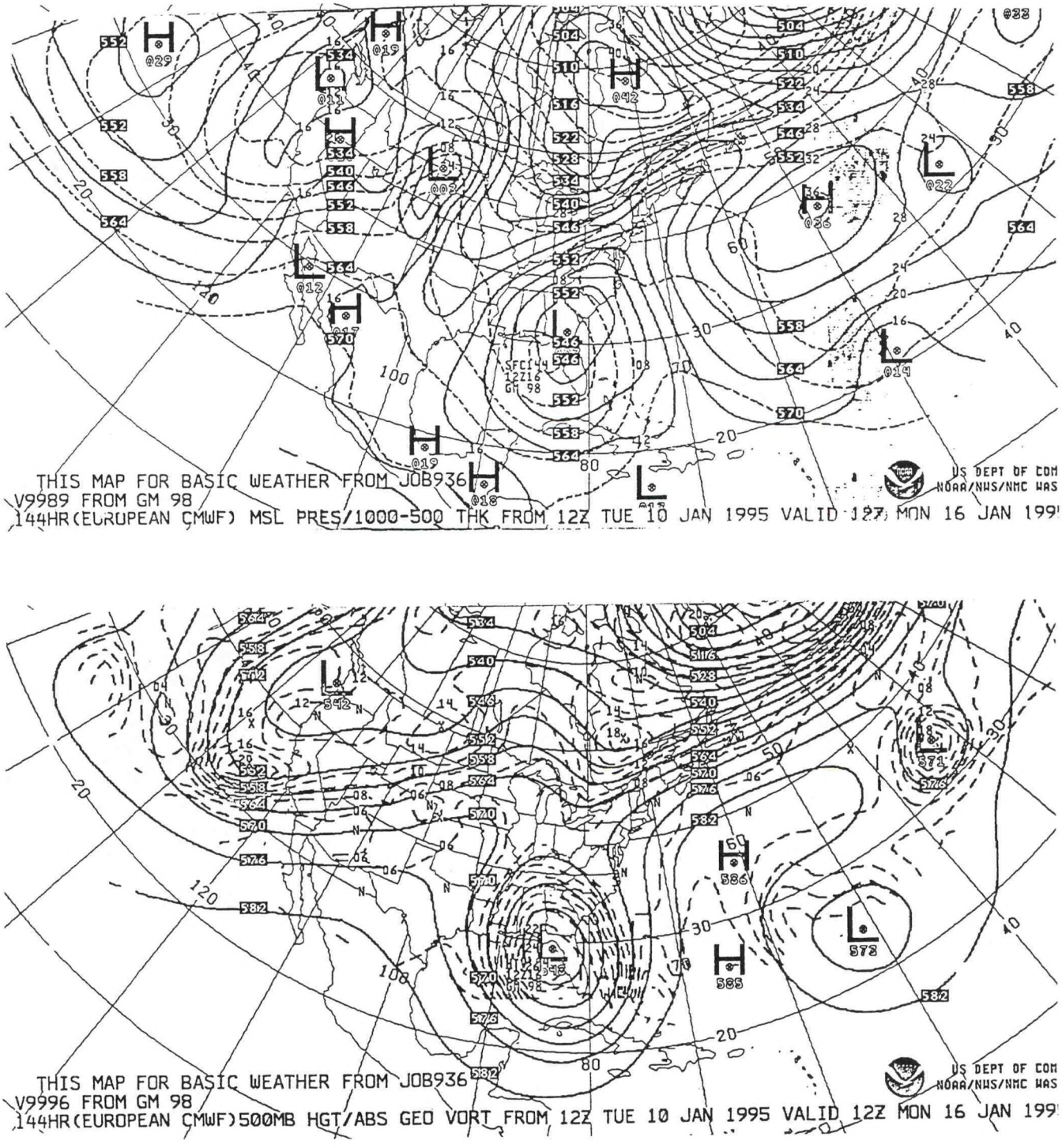

Figure 4b. The day 5 MSLP and 500 mb forecasts valid 1200 UTC 16 January 1995 from the ECMWF.

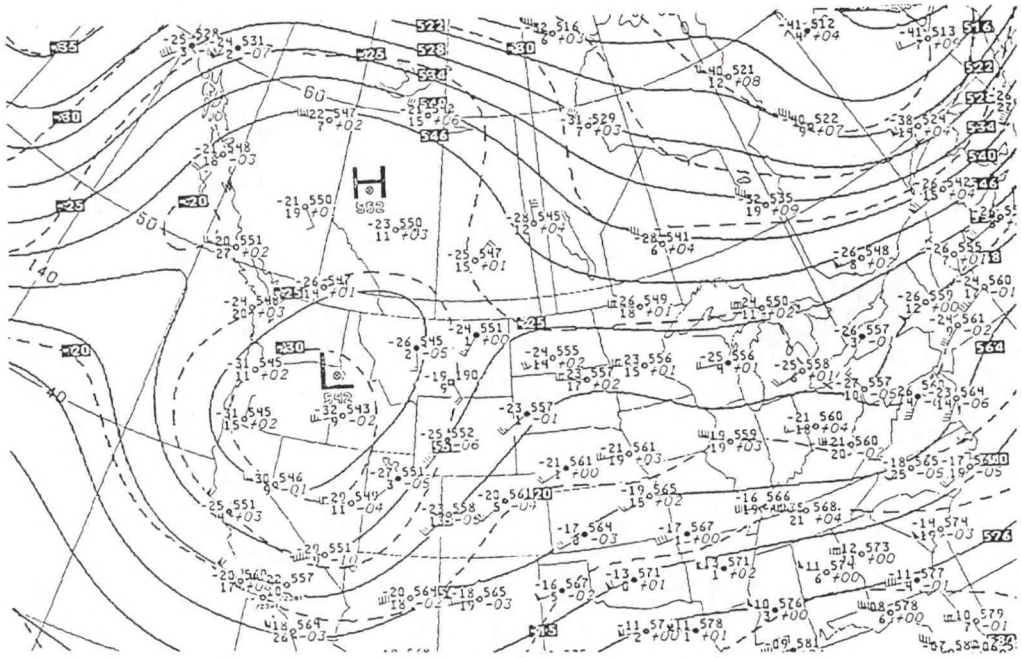

Figure 5a. The 500 mb analyses for 1200 UTC December 11, 1994.

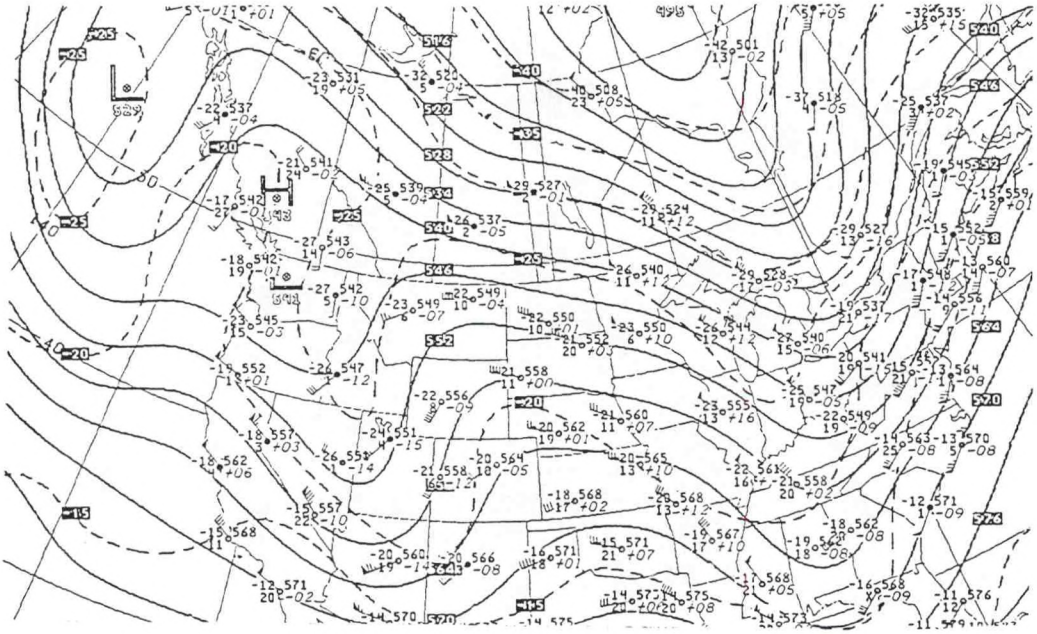

Figure 5a. The 500 mb analyses for 1200 UTC December 12, 1994.

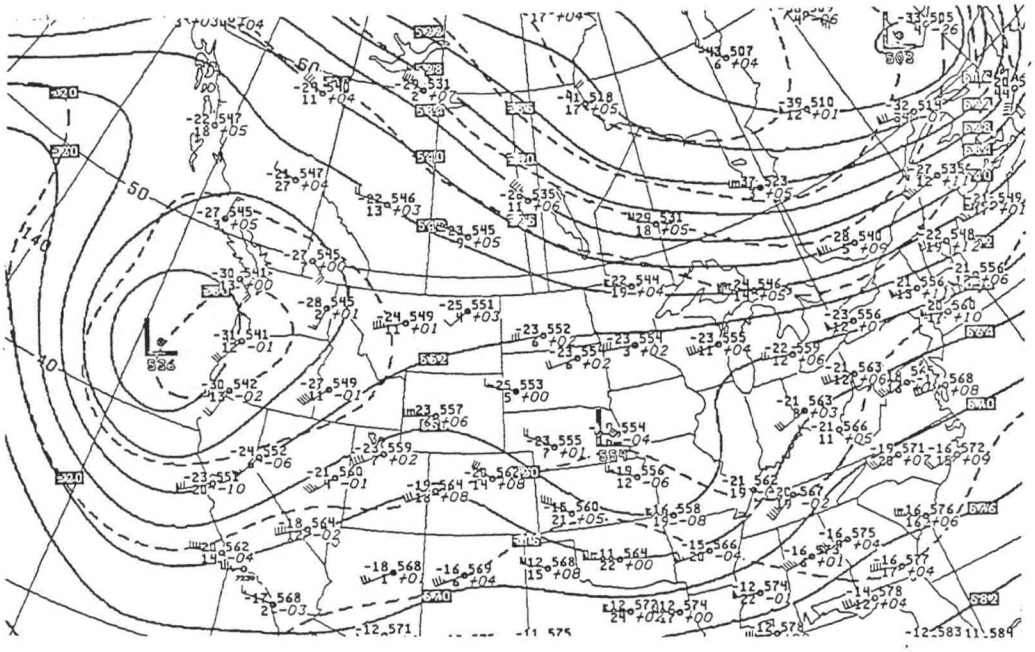

Figure 5a. The 500 mb analyses for 1200 UTC December 13, 1994.

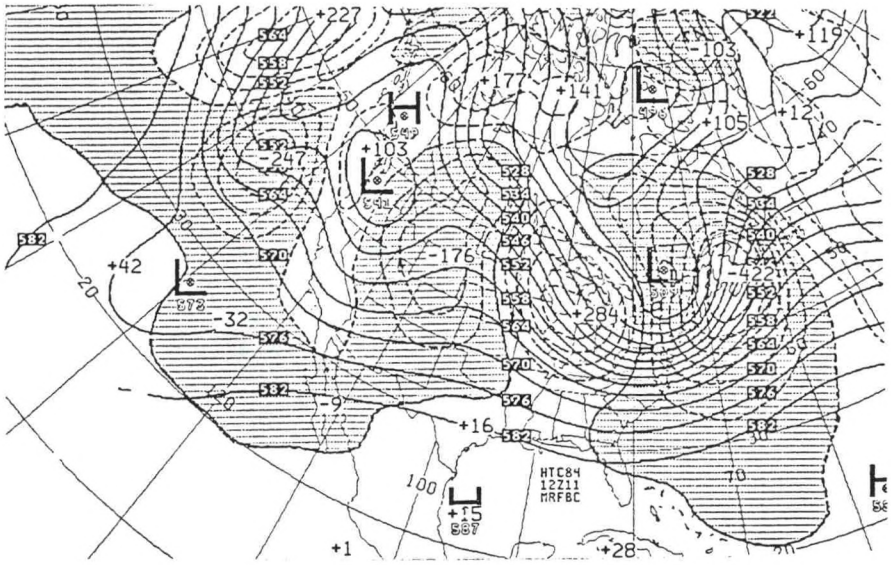

Figure 5b. The MRF day 3, 4, and 5 forecasts valid December 11, 1994.

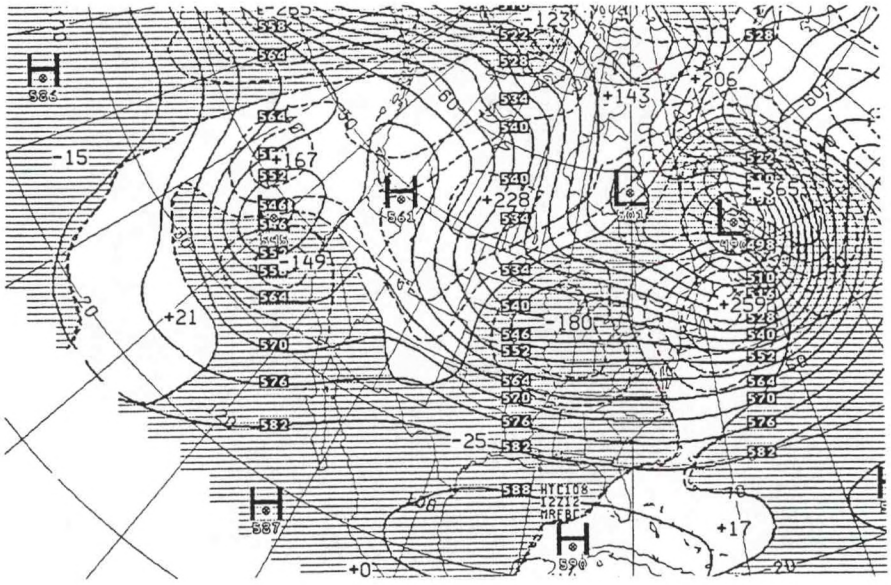

Figure 5b. The MRF day 3, 4, and 5 forecasts valid December 12, 1994.

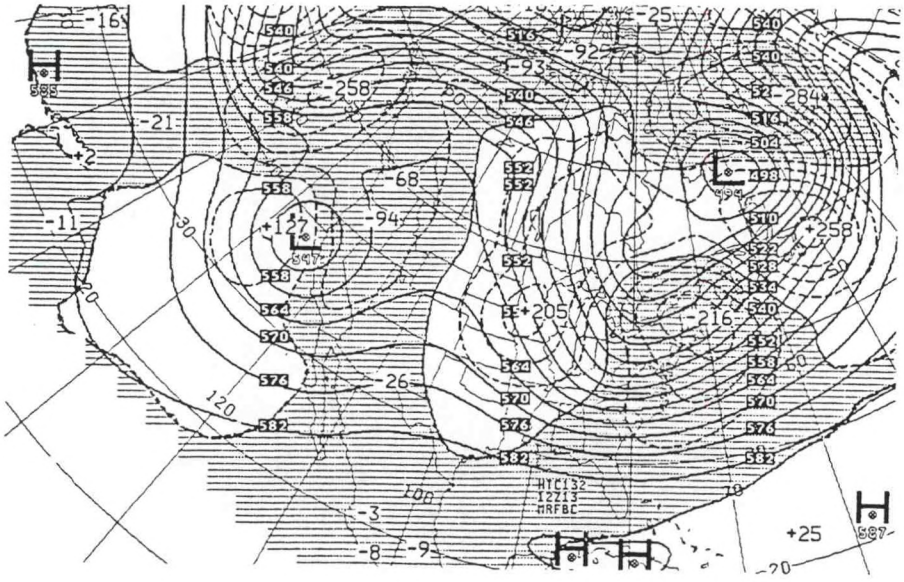

Figure 5b. The MRF day 3, 4, and 5 forecasts valid December 13, 1994.

SESSION 3
APPLICATIONS OF TECHNOLOGY I

5. The Use of GOES-8 Multispectral Imagery for the Detection of Aircraft Icing Regions

6. Forecasting Precipitation on the East Slopes of the Rocky Mountains: New Observing Systems During the 1994-95 Winter

7. Contributions of NWS Modernized Technologies for the Heavy Lake Snow Event over Northeast Ohio and Northwest Pennsylvania on 4 January 1995

The Use of GOES-8 Multispectral Imagery for the Detection of Aircraft Icing Regions

Gary P. Ellrod[1]

1. INTRODUCTION

Aircraft icing is a serious hazard for many types of aircraft, especially light, fixed wing or rotary aircraft due to their relatively slow cruising speeds and limited altitude range. The crash of an ATR-72 commuter plane, due to severe icing on October 31, 1994, brought this hazard to the forefront again. Meteorological conditions related to aircraft icing in clouds have been summarized in the literature (e.g., Schultz and Politovich 1992, Hansman 1989, WMO 1954). Among the conditions identified as important are: (1) liquid phase clouds, (2) temperatures in the 0° to -20°C range, (3) large liquid water content, (4) large droplet diameters (>50μm), (5) weak upward vertical velocity (UVV) to replenish the available supercooled water, and (6) large depth and horizontal extent of the cloud layer(s) for longer duration of flight under icing conditions. In addition, the presence of conditionally unstable lapse rates, resulting in embedded convection, increases the threat of significant icing, even in stratiform cloud systems (Forbes et al., 1993). Icing type is largely a function of temperature and cloud droplet size. Clear icing, the most dangerous type because of its tenacity, occurs at relatively warm temperatures (0° to -8°C) with larger drop diameters and liquid water content.

The availability of geostationary satellite imagery from the advanced GOES I-M series can be used to infer the presence and spatial extent of some of the above factors. There are five spectral channels on the GOES I-M imagers, three of which should be helpful in diagnosing potential aircraft icing zones. This paper will describe techniques that can be used to apply satellite imagery from GOES-8/9 to the analysis and short range forecasting of icing conditions.

2. GOES IMAGER APPLICATIONS

Visible imagery (CH1, 1 km resolution), can show the horizontal extent of clouds and a relative measure of cloud thickness and water content via the observed brightness of the cloud layers. Visible data can also assist in the identification of cloud phase and embedded convection using pattern recognition techniques (textural changes, shadows). Cloud top temperatures are obtainable from the 10.7μm infrared (IR) window channel (CH4, 4 km). From IR imagery, an estimate of cloud top height and cloud thickness can be made when combined with cloud base height information from surface observations or pilot reports. If the cloud top temperature is in the favorable range (0° to -20°C), icing may be present, if other cloud parameters are also conducive to icing. Since UVV tends to decrease near the cloud tops, accumulation of large droplets needed for heavy icing often occurs there.

Another IR channel (CH2, 4km), centered at 3.9 μm, has properties that can also be useful in icing analysis. This shortwave IR window channel senses both a thermal and reflected solar contribution during daylight hours (Scorer 1986). The reflected component is useful because it provides information on both the phase and microphysical properties of the cloud layers. Solar reflectance in this channel is much greater with liquid phase clouds than with ice phase clouds. The reflectance at 3.9 μm is also strongly dependent on cloud droplet size (Kleespies 1995). This

1. Corresponding author address: Gary Ellrod, Office of Research and Applications (NOAA/NESDIS), Washington, DC.

relationship as seen in California coastal stratus clouds is shown in Figure 1. Note that for droplet sizes larger than 6 μm, optical depth is not a significant factor. Reflected light in this channel has the effect of increasing the radiance sensed by the satellite, resulting in higher brightness temperatures than would occur with only emitted radiation. If the image is displayed as temperature with the normal convention (cold shown as white), the warming would result in a darker gray appearance of the clouds. The warming effect for larger droplets conducive to heavier rime or mixed icing would be significant, but much less than the warming due to small droplets.

3. ICING DATA (WINTER '94-95)

Digital IR brightness temperatures and visible brightness count values were collected for 49 reports of aircraft icing during the winter of 1994-95. The icing data was obtained on 13 days between December 16, 1994 and April 13, 1995 in stratiform cloud systems over the northeastern United States. Icing intensity ranged from light to severe, although a majority of the reports were of moderate or greater intensity. There was no adjustment of icing intensity for aircraft type. Imagery in each channel was also studied for any qualitative information that would help to locate regions of heavier icing.

As expected, temperatures in CH4 IR for the icing events ranged between 0°C and -25°C. There was no observed correlation between IR temperature and icing intensity. In most cases, CH2 IR was warmer than CH4 by a significant amount, depending on the time of day and observed CH1 brightness. As seen in Figure 2, the bispectral temperature difference (dT) was as much as 30° - 35°K for sunlit conditions where CH1 brightness values were high. For the icing data collected, dT values were greater than a line defined by the equation:

$$dT = 0.23B - 14.7 \qquad (1)$$

where B is CH1 brightness counts. In little or no sunlight, dT became negative, since the emissivity of CH2 is, in general, less than CH4 (Hunt 1973). For cold ground scenes observed during daytime, dT values will usually be much smaller than those observed for icing cases.

Thin cirrus can produce a false icing signature, since its dT value will sometimes be above the line in Figure 2. Because of this, the use of an additional IR window channel on GOES, centered at 12.0μm, may be required to eliminate thin cirrus signatures. This problem does not occur at night, because cirrus appears much warmer in CH2 than in CH4, while the opposite is true for liquid phase clouds. There is little difference in temperatures in CH2 and CH4 at night for cloud-free regions. It may be possible to combine this information to generate a single satellite product from GOES to display areas of maximum icing risk. A preliminary decision tree (that does not include CH5 techniques) is shown in Figure 3. This approach could be effective in the absence of obscuring cirrus cloud layers.

4. EXAMPLE: APRIL 13, 1995

On April 13, 1995, there were numerous reports of aircraft icing from the Ohio Valley to the Middle Atlantic states. A cold front was crossing Ohio, preceded by a large area of warm advection and associated stratiform cloudiness. Moderate icing was reported between 3,000 and 7,000 ft above Mean Sea Level (MSL) in the Ohio Valley, and as high as 10-12,000 ft MSL in Pennsylvania and New Jersey. Severe icing was reported in northern New Jersey by a commercial airliner. Figure 4 is a GOES-8 CH1 visible image at 1315 UTC showing some of the icing reports. Stratus coverage is extensive over the region, with no evidence of embedded convection.

The CH4 IR image (Figure 5) at the same time shows that cloud top temperatures ranged from -2° to around -15°C and were thus in the ideal range for icing conditions. Temperatures decreased toward the northeast and east, probably due to the presence of one or more higher layers. In contrast to CH4, CH2 IR data showed considerably more horizontal variation in cloud top temperature (Figure 6). The stratus clouds are warmer in CH2 than CH4, as shown by the averaged temperatures plotted in Figure 6, ranging from +5 to +15°C. The warmest temperatures in CH2 tended to occur near the edges of the cloud layers, such as in western Kentucky, or southeast New York. The region of severe icing in northern New Jersey was characterized by cooler CH2 temperatures, shown as lighter gray shades. This suggests the presence of larger cloud droplets. It should be noted that some thin cirrus was also present, that perhaps contributed to the cooler cloud top temperatures in that area.

5. SUMMARY AND CONCLUSIONS

GOES-8 image data in three spectral channels (Visible, 11 μm IR, 3.9 μm IR) has been analyzed for 49 reports of aircraft icing on 13 days during the winter of 1994-95. Preliminary results suggest that it may be possible to assess the potential for aircraft icing in situations of stratiform clouds by combining data from all three channels. The use of an additional IR channel (12 μm) may be required to screen false alarms caused by thin cirrus.

Although there is normally little skill in predicting icing intensity from any data source, CH2 IR imagery may show regions where heavier icing is possible, by observing spatial variations in cloud top temperatures. Cooler temperatures within supercooled cloud layers may show areas of larger droplets that are less reflective in daytime.

Satellite imagery seems to be a relatively under-utilized source of data in icing analysis and forecasting. Some work has been done using microwave imagery over the oceans from polar-orbiting satellites (Curry and Liu 1992) and over land and water using NOAA Advanced Very High Resolution Radiometer (AVHRR) IR and numerical model data (Lee and Clark 1995). Multispectral imagery available at more frequent intervals (15-30 min vs 6-12 hr) from the GOES-8/9 satellites show potential to improve the assessment of icing risk over continental as well as oceanic regions.

6. REFERENCES

Curry, J. and G. Liu, 1992: Assessment of aircraft icing potential using satellite data. *J. Appl. Meteor.*, **31**, 605-621.

Forbes, G.S., Y. Hu, B. Brown, B. Bernstein, M. Politovich, 1993: Examination of conditions in the proximity of pilot reports of aircraft icing during project Storm-Fest. *Preprint Volume, 5th Intl. Conf. on the Aviation Weather System*, Vienna, Virginia, AMS (Boston) 282-286.

Hansman, R.J., 1989: The influence of ice accretion physics on the forecasting of aircraft icing conditions. *Preprint Volume, 3rd Intl. Conf. on the Aviation Weather System*, Anaheim, California, 154-158.

Hunt, G.E., 1973: Radiative properties of terrestrial clouds at visible and infrared thermal window wavelengths. *Quart. J. Roy. Meteor. Soc.*, **99**, 346-369.

Kleespies, T., 1995: The retrieval of marine stratiform cloud properties from multiple observations of varying solar illumination. *J. Appl. Meteor.*, **34**, 1512-1524.

Lee, T.F., and J.R. Clark, 1995: Aircraft Icing Products from Satellite Infrared Data and Model Output. *Preprint Volume, Sixth Conf. on Aviation Weather Systems*, Dallas, Texas, 234-236.

Schultz, P. and M. Politovich, 1992: Toward the improvement of aircraft-icing forecasts for the continental United States. *Wea. and Forecasting*, 7, 491-500.

Scorer, R., 1986: *Cloud Investigation by Satellite*. J. Wiley & Sons.

WMO, 1954: Meteorological aspects of aircraft icing. WMO Tech. Note No. 3, WMO - No. 30. TP9, World Meteorological Organization, Geneva, 18pp.

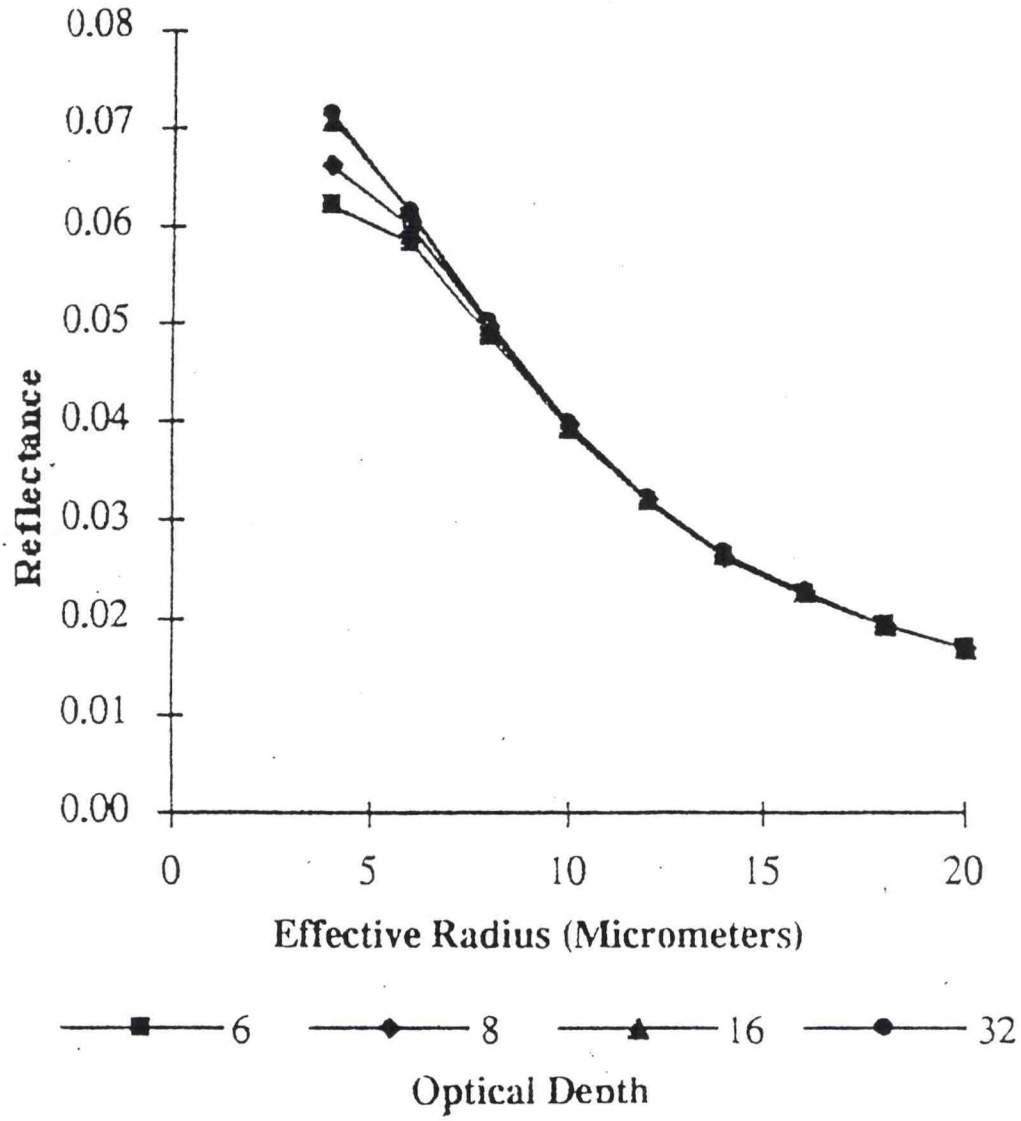

Figure 1. Cloud reflectance at 3.9 μm versus effective radius for various optical depths in California stratus clouds. Satellite zenith angle and solar zenith angle are 45°. (From Kleespies, 1995.)

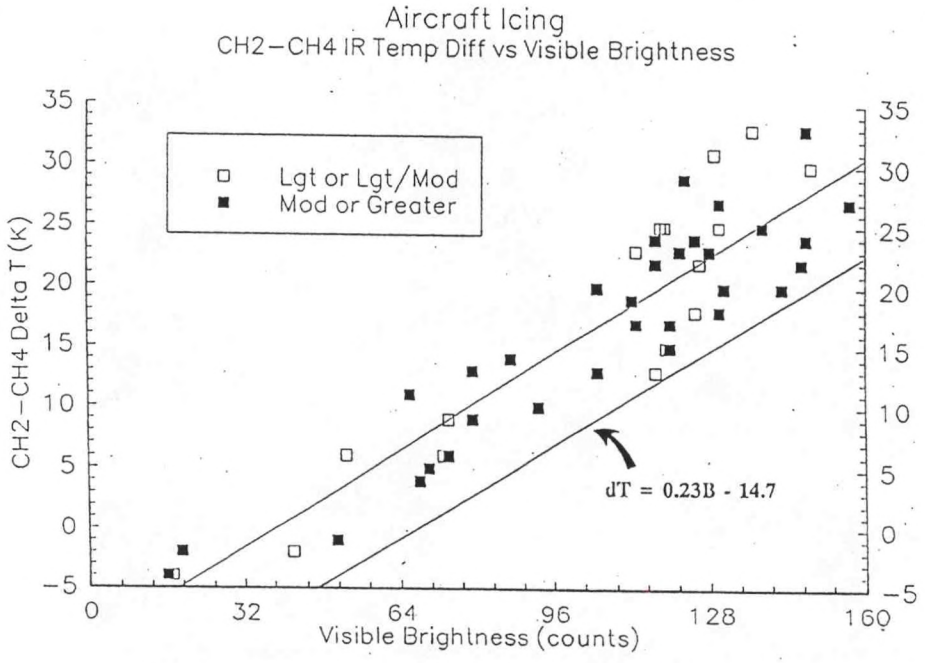

Figure 2. Temperature difference between GOES-8 CH2 and CH4 IR versus CH1 (visible channel) brightness count value observed for 52 icing reports of the indicated intensities.

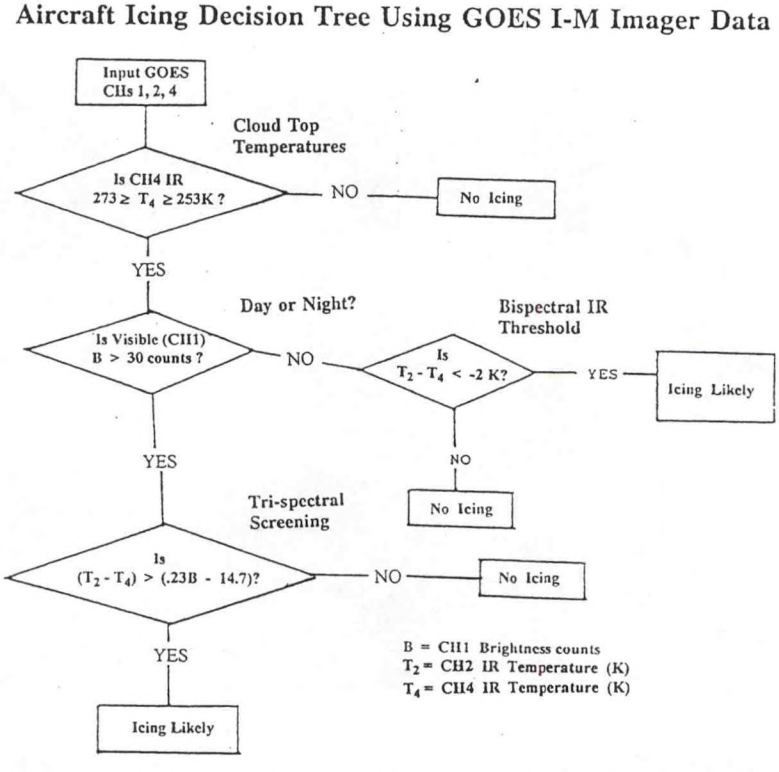

Figure 3. Decision tree for the identification of icing potential using three GOES imager channels.

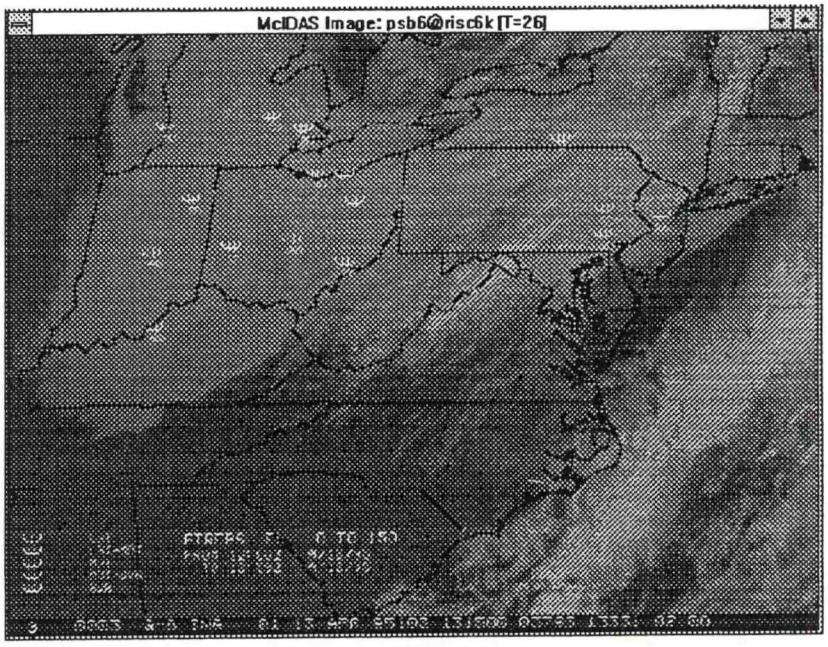

Figure 4. GOES-8 CH1 visible image at 1315 UTC 13 April 1995. Aircraft reports of icing and altitude (100's of ft) between 1200 and 1400 UTC are plotted on the image.

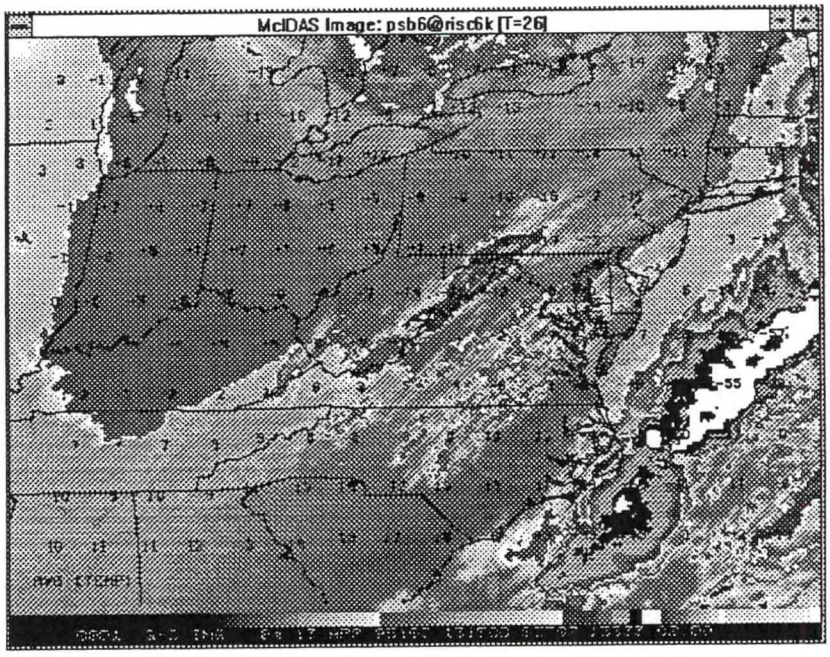

Figure 5. GOES-8 CH4 IR image at 1315 UTC 13 April, 1995. Mean temperatures (°C) are plotted on the image.

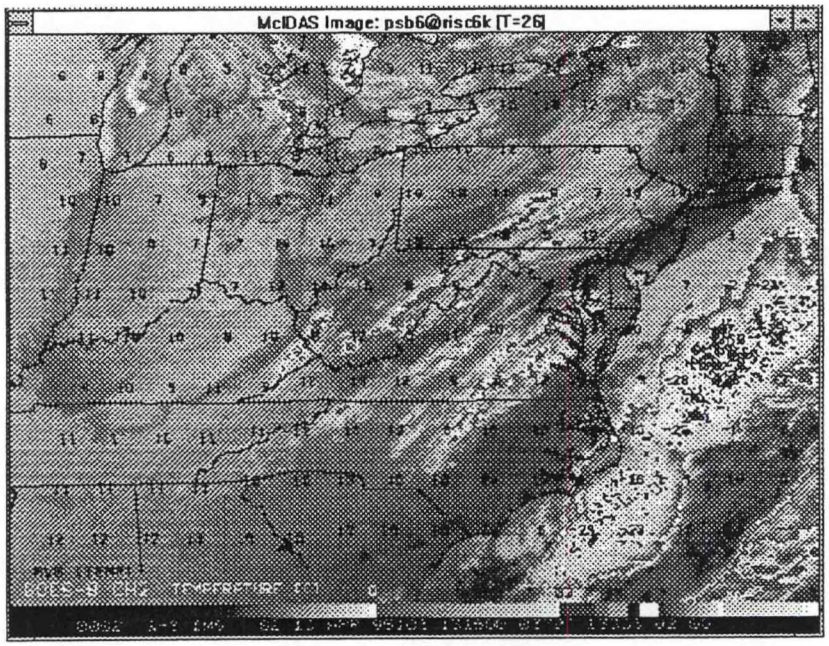

Figure 6. Same as Figure 5, except for GOES-8 CH2 IR.

Forecasting Precipitation on the East Slopes of the Rocky Mountains: New Observing Systems During the 1994-95 Winter

Douglas A. Wesley[1], James L. Hatten[2], and Julie Hall[3]

1. INTRODUCTION

The WSR-88D Doppler radar and RAMSDIS (RAMM Advanced Meteorological Demonstration and Interpretation System) satellite display systems were operational during the 1994-95 winter at NWS Forecast Office (WSFO) Cheyenne (CYS), Wyoming, representing major advances in observational data sets available to operational forecasters. During many snow and freezing drizzle events these systems were used extensively for both prognostic and diagnostic purposes. Forecasters and researchers at this office documented the detailed structure and evolution of snow bands for the first time in this portion of the High Plains. Implementation of these systems has resulted in marked improvement in both the resolution and accuracy of short-term snowfall forecasts in this region due to both the improved radar and satellite sensitivity and the availability of wind profiles in real-time. The vastly improved resolution of the new satellite and radar data has also enabled the initiation of a significant enhancement of the quality and usefulness of many other forecast products.

This paper will summarize applications of the 88D and RAMSDIS systems toward improving snowfall and freezing precipitation forecasts during a significant snowstorm. Some resulting advances in understanding the physical mechanisms of formation and movement of snow bands will be described. Of the 10 cases of significant winter precipitation at Cheyenne during the 1994-5 winter, one event will be investigated in detail: the February 9-11 snowfall. Up to 30 cm of snow fell in extreme southeast Wyoming during the deepening phase of an arctic air mass invasion. Organized narrow bands of enhanced reflectivity oriented west-northwest to east-southeast (parallel to the upper level winds) formed behind the leading edge of the cold air mass. These bands moved slowly southward and contained reflectivity maxima of 35-40 dBZ. Efficient microphysical and thermodynamical conditions led to snowfall rates of up to 5 cm/hr. Preliminary analyses indicated that a combination of frontal forcing, conditional symmetric instability and upslope flow was responsible for multiple band formation. Details of the evolution of this storm will be presented in the following section.

2. CASE STUDY: FEBRUARY 9-11, 1995

Strong northwesterly flow aloft characterized this event over southeast Wyoming (Figure 1 shows the 500 mb analyses at 1200 GMT 10 February). An upper level jet maximum was present over northwest Montana and the Idaho panhandle; this feature did not affect dynamics during significant snowfall over southeastern Wyoming. Note that southeastern Wyoming was located on the anticyclonic side of the core of the jet stream. Close examination of meteorological fields at lower levels in the atmosphere (Figure 2 shows the 850 mb analyses at the same time) revealed significant information about the characteristics of northerly flow at Cheyenne. Canadian frontal passage occurred at approximately 02 GMT 10 February, signaled by the onset of strong northerly winds. Note the strong convergence at 850 mb associated with this front over southeastern Wyoming and northeastern Colorado at 1200 GMT.

1. Corresponding authors address: Douglas A. Wesley, NWS Forecast Office, Cheyenne, Wyoming (Current affiliation, NWSFO Denver, Colorado.).
2. Jim L. Hatten, NWS Forecast Office, Cheyenne, Wyoming.
3. Julie A. Hall, NWS, Office of Meteorology, UCAR/COMET, P.O. Box 3000, Boulder, Colorado 80307.

Light snow began falling at 0245 GMT, but the snowfall rate was insignificant until about 0425 GMT when visibility decreased to 1½ mi.. The 88D reflectivity scan at 0.5 degrees for 0543 GMT showed that an intense band of snow had developed (Figure 3) just behind the front, apparently due to uplift along the cold frontal surface, which was located about 2000 feet above the ground. The band had moved past CYS with maximum reflectivity exceeding 30 dBZ. Additional evidence for frontal forcing of this initial period of snowfall was found in the 88D velocity-azimuth display (VAD) profile (Figure 4). Note the deepening and strengthening of low-level northerly flow during this 97-minute period, which corresponded to a period of significant snow accumulation at CYS. When this tendency ceased, snowfall correspondingly decreased rapidly. The bowed shape of the band to the south and west of CYS appeared to be the result of a local acceleration of northerly winds due to the elevated terrain in this region (Wesley et al. 1995 and Marwitz and Toth, 1993).

After a temporary letup in snowfall from about 07 GMT to 15 GMT, a 6-hour period of mostly moderate to heavy snowfall occurred with multiple banding. Generally, snow bands were stationary, narrow (5 to 15 km in width) and oriented west-northwest to east-southeast (Figure 5). At any given time, 2 to 4 distinct bands were evident on the 88D reflectivity scans, and propagation of the pattern was southward as northern bands dissipated and new southern bands formed. Several clues for the forcing mechanism of these bands pointed toward conditional symmetric instability (CSI):

1. Near-saturated conditions through a deep layer,
2 Large vertical speed shear,
3. Large-scale pattern of forced weak upward motion,
4. Bands parallel to the mid-level thermal wind.

A thermodynamic cross-section of gridded data at 1200 GMT (Figure 6) extending from just west of Bismarck North Dakota to near Durango, Colorado was examined. Over the CYS vicinity contours of θ_E were sloped steeper than those of constant momentum, indicating the potential of banded upward motion forced by CSI. Convective instability was also present in a small region over CYS, as well as in a shallow ground-based region to the north. Radar signatures of precipitation in the CYS region were dominated by the CSI bands as opposed to upright convection. To the north, shallow upright convection was capped by a strong stable layer.

Thus, in and near CYS, CSI appeared to be forcing upward motion in a favorable thermodynamic environment as temperatures in the 700 to 600 mb layer (-12°C to -16°C) favored rapid dendritic crystal growth (Auer et al., 1982); snow crystal types observed at CYS during heavy snow were large aggregates of rimed dendrites. On the RAMSDIS system pronounced bands of enhanced cold tops on the 10.7 μm imagery, oriented along the mid-level thermal wind vector, were present during this time (Figure 7). These bands were about 50 km in width, which corresponds closely to more traditional scales of CSI forcing. Note that the horizontal resolution of the IR satellite data prevented individual snow band signatures.

During actual forecast operations in this storm, assessment of the potential or presence of CSI banding did not occur until the bands were in the formative phase. However, during subsequent preparation of nowcasts, highlights and statements, the detailed 88D data was utilized extensively to delineate locations and trends of snow bands.

During the weakening period of the storm, after about 2200 GMT 10 February, the VAD wind profile (Figure 8) indicated a speed reduction and decreasing depth of low-level northerly winds. Snowfall intensity decreased rapidly during this phase, and intense snow bands were located in northern Colorado.

3. CONCLUSION

Integration of sensitive Doppler radar and advanced satellite data into operations at CYS has made a significant impact on documenting and forecasting winter storms. The data makes meso-γ analyses of snow band evolution possible, and this information has improved forecast products. Vertical wind profiles yield valuable information about storm dynamics that had not been available before the 1994-95 winter. The February 9-11 storm is an excellent example of the advantages of the availability of these types of data in operations. In this case, distinct snow bands forced primarily by CSI produced heavy snowfall over southeastern Wyoming. Utilizing 88D velocity and reflectivity, as well as detailed infrared satellite imagery, both the prognostic (real-time) and diagnostic assessments of the evolution of the snow bands were enhanced significantly. These applications will continue to expand during the 1995-96 winter at CYS.

4. REFERENCES

Auer, A.H., Jr,. and J.M. White, 1982: The Combined Role of Kinematics, Thermodynamics and Cloud Physics Associated with Heavy Snowfall Episodes. *J. Meteor. Soc. Japan,* **60**, 500-507.

Marwitz, J., and J. Toth, 1993: The Front Range Blizzard of 1990: Part I: Synoptic and Mesoscale Structure. *Mon. Wea. Rev.,* **121,** 402-415.

Snook, J.S., 1992: Current Techniques for Real-Time Evaluation of Conditional Symmetric Instability. *Wea. & Forecasting,* 7, 432-439.

Wesley, D.A., B.C. Bernstein and R.M. Rasmussen, 1995: Snowfall Associated with a Terrain-Generated Convergence Zone During the Winter Icing and Storms Project. *Mon. Wea. Rev.,* **123**, 2957-2977.

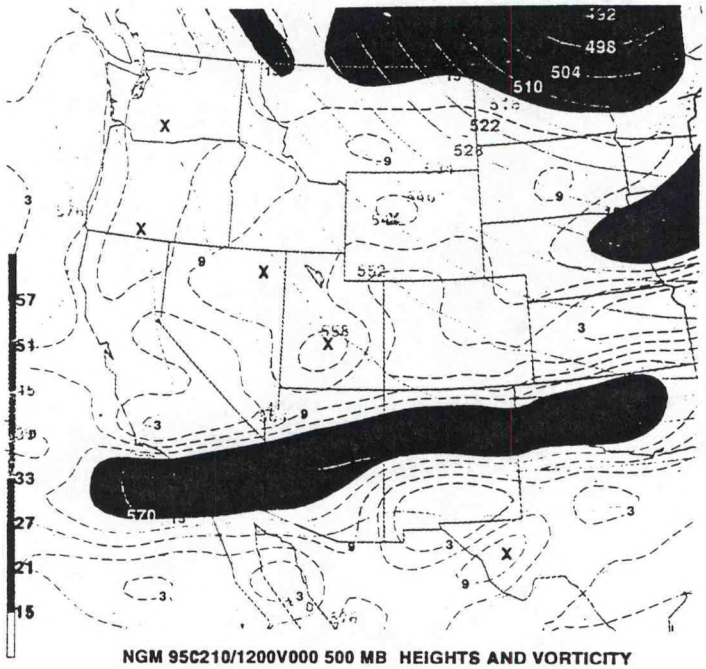

Figure 1. 500 mb analyses for 1200 GMT 10 February 1995. Heights are in dm (solid), vorticity in 10^{-5}/s (dashed). Vorticity values above 1.5 x 10^{-4}/s are shaded.

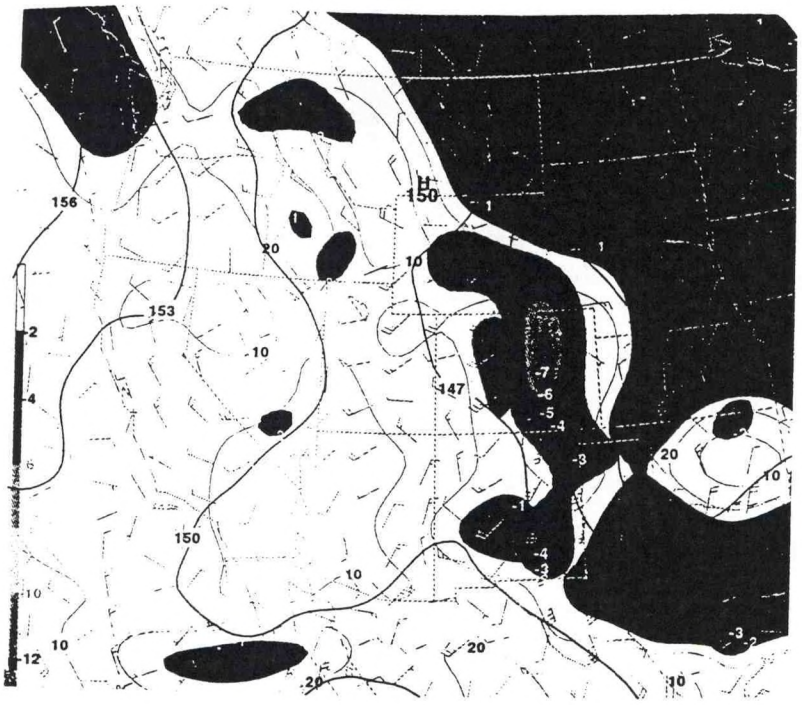

Figure 2. 850 mb analyses for 1200 GMT 10 February 1995. Heights are in dm (solid bold), divergence in 10^{-4}/s (solid). Divergence values below -2 x 10^{-4}/s are shaded.

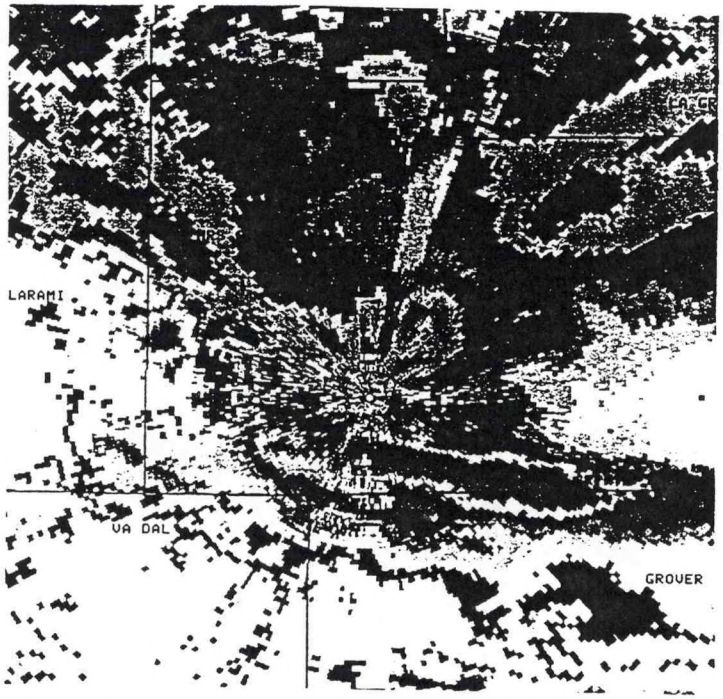

Figure 3. CYS 88D reflectivity scan at 0.5° for 0543 GMT 10 February. Intense east-west snow band has just passed CYS (radar is co-located at the forecast office in the center of the scan) and is moving southward. Maximum reflectivity within this band is above 28 dBZ.

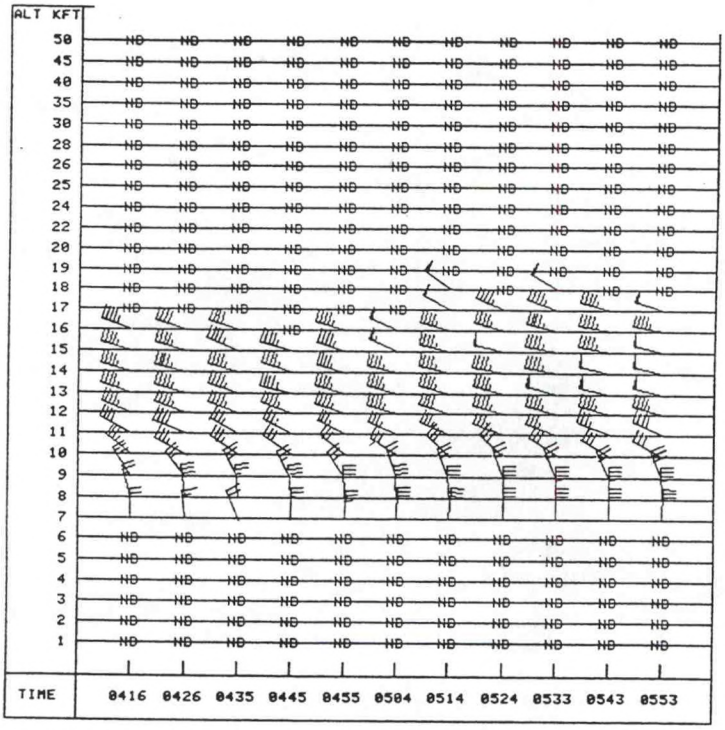

Figure 4. CYS 88D VAD wind profile for a period after surface frontal passage at CYS.

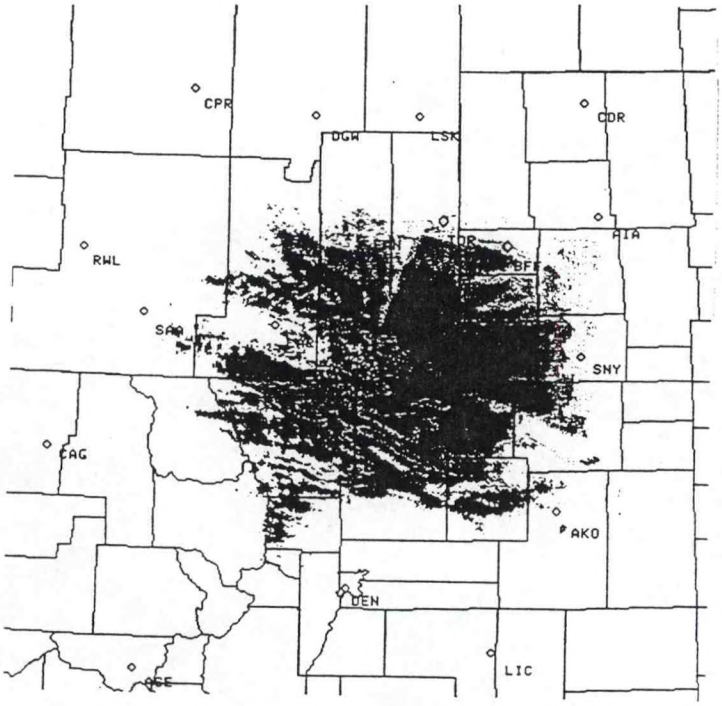

Figure 5. As in Figure 3, for 1644 GMT. CSI bands (see text) are oriented WNW-ESE and are imbedded in a general area of weak reflectivity (5-15 dBZ). Reflectivity maxima within bands are above 28 dBZ.

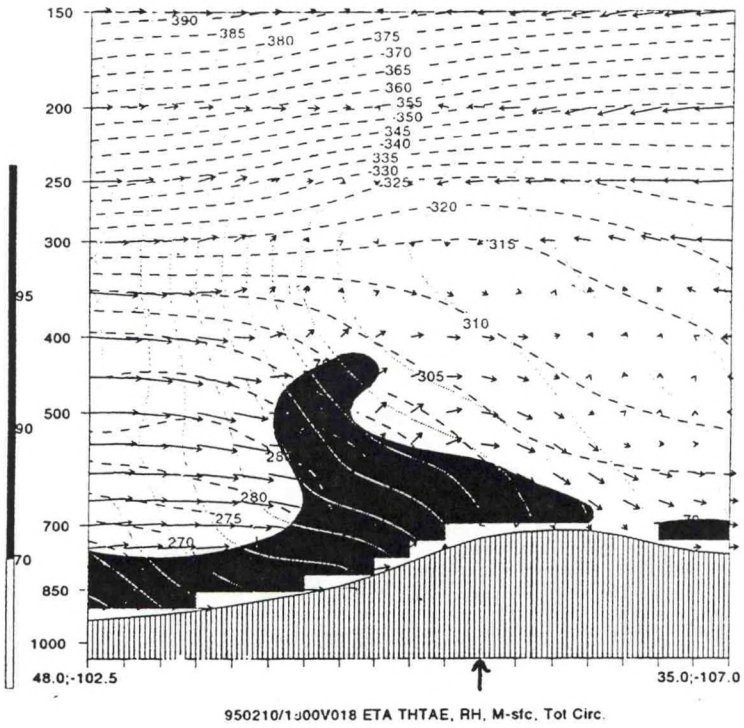

Figure 6. Vertical cross section from near Bismarck ND to near Durango CO, contouring values of θ_E (dashed), constant momentum (dotted), relative humidity and total circulation. RH values above 75% are shaded.

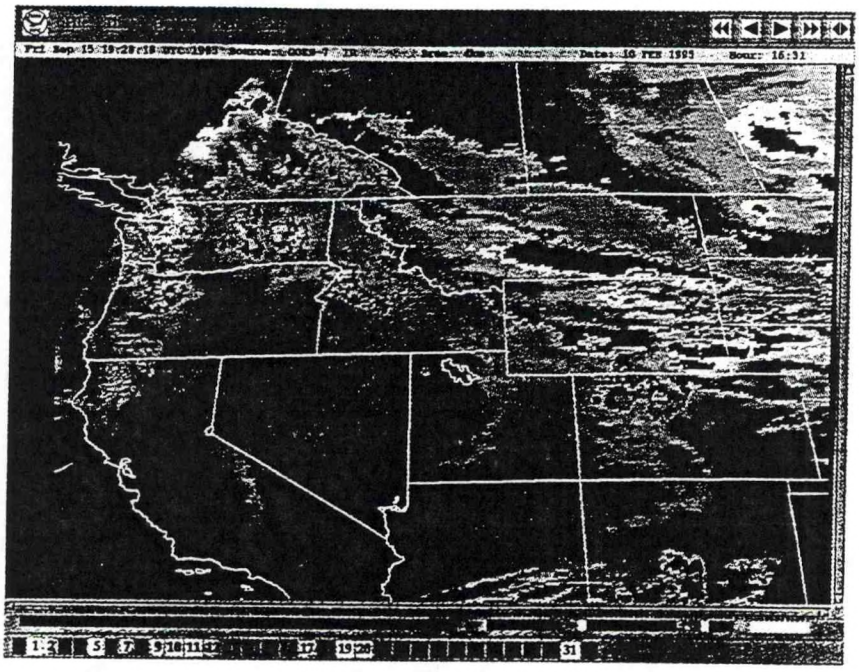

Figure 7. RAMSDIS infrared (10.7 μm) image at 1631 GMT 10 February. Darkest regions imbedded within white regions are coldest tops, which exhibit temperatures below -45°C.

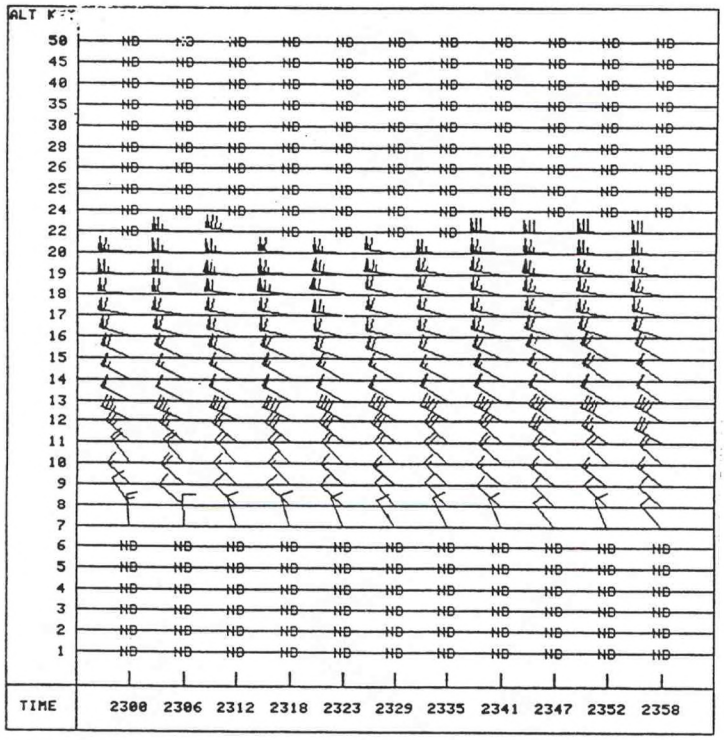

Figure 8. As in Figure 4 during the dissipating stage of storm.

Contributions of NWS Modernized Technologies for the Heavy Lake Snow Event over Northeast Ohio and Northwest Pennsylvania on 4 January 1995

Louis A. Giordano[1], Richard R. Redmond[2], and Paul A. Jendrowski[3]

1. INTRODUCTION

On January 4, 1995, heavy lake-effect snow bands brought more than 15 cm (6 inches) of snow to six counties in the Lake Erie shoreline area between Cleveland (CLE), Ohio and Erie (ERI), Pennsylvania. The highest snow amounts (Figure 1) were 30 cm (12 inches) in west central Erie County, Pennsylvania and 25 cm (10 inches) in western Lake County and northern Geauga County, Ohio. The first reports of heavy snow were from Erie County, Pennsylvania during the morning of January 4 and the last reports were from the Cleveland, Ohio area late that evening. The lake shore corridor from Cleveland to Erie experiences lake-effect snow events like this one a couple times in a typical winter.

Synoptic meteorological analyses (Figure 2) indicated this heavy snow event was associated with Type I snow bands as classified by Niziol et al. (1995). Such bands develop when the prevailing direction of the low-level arctic winds are nearly parallel to the long axis of Lake Erie, that is, from 250 to 280 degrees. The strong mesoscale convergence pattern that develops within the cold unstable flow of air over the warm lake results in several narrow and elongated bands of heavy snow with the elongated axis parallel to the prevailing wind direction. The bands are typically 20-50 km in width and 50-200 km in length and have life spans of several hours. They tend to become topographically anchored along the south shoreline due to frictional convergence effects. Consequently, some locations within 50 km of the lake shore can experience prolonged periods of heavy snow and deep accumulations while nearby areas further inland remain free of snow.

As part of the National Weather Service (NWS) Lake Effect Snow (LES) Project, a study was made of the various hydrometeorological data sets that were available during this heavy snow event for predicting and observing this meso-beta scale phenomena. Particular attention was given to data sets from recently deployed forecast tools and observational systems such as high resolution gridded fields from numerical weather prediction models and observed clouds/precipitation and velocity fields from WSR-88D radar, digital satellite data, and a mesonet of surface observations including ASOS.

These forecast procedures and remote sensor technologies, both individually and collectively, can contribute to more precise forecasts of the timing and location of such heavy lake-effect snow bands. Section 2 shows examples of the gridded forecasts fields. Section 3 points out the value of hourly sounding forecasts. Section 3 also examines how observed clouds, precipitation, and velocity fields from WSR-88D radar, digital satellite images, and a mesonet of surface observations can more precisely detect various characteristics of the snow bands. Such detections can lead to improved short-term forecasting.

1. Corresponding authors address: Louis A. Giordano, NWSFO Pittsburgh Pennsylvania.
2. Richard R. Redmond[1], NWSFO Pittsburgh Pennsylvania.
3. Paul A. Jendrowski, NWSFO Honolulu, Hawaii.

2. PC-GRIDDS

Model depictions generated from high resolution gridded fields, for example PC-GRIDDS (Zubrick and Thaler 1993), enable forecasters to more completely analyze numerical model output than what was possible in the past. PC-GRIDDS provides the following improvements: a greater variety of output fields, more diverse combinations of fields, more numerous levels, more frequent time intervals (6 h), and more flexible isopleths. The ensuing discussion focuses on the 1200 UTC 3 January 1995 NGM (Hoke et al. 1989), which was available in both AFOS and PC-GRIDDS versions. ETA and AVN runs were also available but will not be discussed since their solutions were similar to the NGM.

On January 4, the low-level flow (Figure 2) across Lake Erie was cold enough to generate lake-effect snow per Dockus's (1985) criteria. This criteria was the 850 mb temperature be -10°C, or colder, and at least 13°C colder than the lake water temperature, which on 4 January was 6°C. The 850 mb temperature below -10°C provides ample instability for convection to develop and ample coldness for the convective precipitation to reach the surface as snow. However, for snow showers to become heavy, three additional criteria need to be met. Cloud tops must exceed 2 km AGL (Byrd et al. 1991) to ensure a sufficient convective depth. Low-level winds have to be from 250-290 degrees to ensure sufficient lake fetch and moisture availability. In-cloud wind profiles must have directional changes less than 30 degrees (Niziol and McLaughlin 1992) to ensure minimal disruption of the growing convective towers.

The cloud top criteria for lake-effect heavy snow stems from Byrd et al. (1991) who found 2.3 to 3.1 km AGL to be the typical boundary layer top for intense Type I snow bands off Lake Ontario. Irregardless of the boundary layer instability, snow showers can be inhibited from reaching such heights if there is subsidence and consequently warmer and drier air to act as a cap immediately above the 850 mb level (about 1.5 km AGL).

For January 4, the NGM vertical velocity fields for 700 mb (about 3 km AGL) distributed via AFOS showed downward motion throughout the event. Furthermore, information about subsidence and the capping inversion near 850 mb was not available in the AFOS products. In contrast, PC-GRIDDS provided NGM vertical velocity fields for several levels. These fields could be examined as single plane-views of individual levels, superimposed plane-views of several levels, or as time versus height cross-sections. The cross-section for a point over Lake Erie about 75 km northeast of CLE (Figure 3) showed low-level upward motion would exist in the surface layer and at 850 mb throughout January 4, while the downward motion was restricted to 700 mb and higher levels. This PC-GRIDDS depiction provided an indication that the lake-effect convective instability could grow beyond 850 mb and so reach sufficient height for heavy snow shower development.

PC-GRIDDS (Figure 3) also provided wind profiles in the cross-section format, which permitted overlays onto such other fields as temperature, moisture, and vertical velocity. The wind profile showed little directional shear throughout January 4 with the overall low-level wind direction turning gradually from southwest into west. Such a wind profile met the final two criteria for Type I snow band development. Low-level winds from the southwest indicated New York and Pennsylvania shoreline counties would be downwind of the initial snow bands. Later winds from the west indicated the Ohio shoreline and Pennsylvania interior counties would eventually be downwind. In conclusion, the NGM forecast fields shown in Figures 2 and 3 clearly exhibited for this lake-effect situation how software like PC-GRIDDS can help operational forecasters quickly access information that they previously had to infer from AFOS products.

3. SHARP-ANALYZED MODIFIED NGM HOURLY SOUNDINGS

With the PC-GRIDDS indicating the potential for heavy snow shower development, SHARP (Hart and Korotky 1991) analyses of modified NGM soundings were next explored to see how they could help with forecasting hour-by-hour developments. NGM soundings can furnish detailed hourly visualizations of the atmosphere's thermodynamic and kinematic structure for specific points. There have been some recent successes in using NGM 16-level hourly soundings to forecast lake-effect snow (Niziol and McLaughlin 1992), and in using SHARP-analyzed NGM soundings to forecast both shallow cold-season and deeper warm-season convective events (Nierow and Kane 1993).

NGM hourly soundings (Hoke et al. 1989) for a point near CLE were inserted into SHARP (Hart and Korotky 1991) via software developed by Nierow and Kane (1993). This software also accommodated the manual input of surface data, which was employed to better simulate the warmer and moister conditions that existed over the lake.

A. Objective Surface-Layer Modification

One obstacle to using SHARP with NGM soundings was determining realistic lake surface air temperature and dew point values for input. Despite NGM improvements in parameterizing heat transfer and evaporation processes over water surfaces, NGM low-level temperatures and dew points in vicinity of the Great Lakes usually underestimate the actual warming and moistening and, therefore, degree of instability (Niziol et al. 1995). Prior studies of NGM hourly soundings overcame this inadequacy by comparing the 850 mb temperature with the observed lake water temperature to get a simple index of instability (Niziol and McLaughlin 1992). However, since SHARP can be used to analyze the thermodynamic structure of the entire sounding and compute such instability parameters as CAPE (B+), more realistic values of lake surface air temperature and dew point were needed for input.

The approach was to use Equations 1-4 after Phillips (1972) to objectively transform upwind land surface air temperatures (T_U) and dew points (D_U) into warmer and moister lake surface air temperatures (T_L) and dew points (D_L). The lake water temperature (T_W) and residence time (R) of the air over the lake were the main factors used in the transformation. Per the observations of Phillips, T_L was constrained from exceeding 40% of the initial difference between T_U and T_W. This likewise constrained D_L. Temperature units were Celsius. Time units were minutes.

$$\text{For } (T_U - T_W) \leq -10.5°C$$

$$T_L = -0.63 + 0.75\ T_U + 1.55\ (\log R) + 0.11\ T_W \qquad (1)$$

$$T_L \leq T_U + 0.4\ (T_W - T_U) \qquad (2)$$

$$D_L = -3.86 + 0.64\ D_U + 2.25\ (\log R) + 0.24\ T_W \qquad (3)$$

$$D_L \leq T_L \qquad (4)$$

For the January 4 event, the average residence time of boundary layer air over Lake Erie was about 6 h (360 min) as low-level winds were from the west at 7 to 10 m s^{-1} (25 to 35 km h^{-1}) and the fetch across Lake Erie from the west end near Toledo (TOL), Ohio and Detroit (DTW), Michigan to the CLE-ERI corridor ranged from 130 to 260 km. For input into SHARP, values of T_L and D_L for a particular hour, HH, were determined by using Equations. 1-4 with T_U and D_U values taken from averages of NGM MOS temperatures and dew points for TOL and DTW 6 hours earlier (HH-6). Surface wind direction and speed for hour HH were determined by using arithmetic averages of NGM MOS for CLE and ERI from hour HH. Observed values were substituted for any MOS values unavailable during the first 12 hours.

SHARP offered a choice of parcels to lift for the instability analysis. Considering winds were 7-10 m s^{-1}, there was ample mechanical turbulence to have a well-mixed boundary layer. So the parcel chosen to be lifted was one representative of the mean thermal and moisture properties of the lowest 100 mb.

B. Verification of Results

Table 1 is a summary of the resulting SHARP analyses of the modified NGM hourly soundings. Figures 4 and 5 are the forecast sounding and hodograph valid for 0000 UTC 5 January, during the time of peak instability near CLE. Although SHARP may have depicted the surface-based superadiabatic lapse rate to extend through too deep a layer, the overall size and vertical extent of the lifted parcel's buoyant energy appeared to be realistic.

The modified NGM soundings (Table 1) had 2.6°C as the maximum value for the lifted index at 850 mb (LI_8) computed by subtracting the sounding's 850 mb temperature from that of the lifted parcel. The 850 mb level was chosen as it is near the midpoint of the snow shower's convective layer. This maximum LI_8 agreed with Byrd et al. (1991) who had measured sounding temperatures within intense Type I snow showers as much as 2.5°C warmer than their environment.

NGM soundings forecasted convective layers with maximum parcel levels (MPL) up to 2.5 km (8.3 kft) AGL. This was in the 2.3 to 3.1 km range observed by Byrd et al. (1991) which is also the range frequently noted by forecasters for maximum radar precipitation echo tops. Indeed, the Cleveland WSR-88D echo top (ET) observations from 2333 UTC 4 January through 0216 UTC 5 January showed maximum precipitation tops in an intense Type I band near CLE to be frequently 2.4 km (8 kft) AGL with the tops of the vertical wind profile (VWP) observations (Figure 6) likewise extending to that level. (Note WSR-88D ET and VWP products have *kft MSL* for height units and CLE's elevation is 233 m or 764 ft.) The VWP tops help corroborate the ET values near CLE by inferring a lack of scatterers, in this case snow and ice crystals, in the "no data" region above 2.4 km AGL.

NGM sounding MPL temperatures were as cold as -27°C at 0000 UTC 5 January, which was in the range of -25°C to -30°C observed for cloud top temperatures by GOES 8 satellite infrared sensors (LaDue and Weaver 1995). LaDue and Weaver (1995) also noted that GOES 8 visible sensors observed glaciated tops further substantiating cloud top temperatures colder than -20°C. Such cold cloud top temperatures with the corresponding preponderance of ice crystals have favorable microphysical implications for heavy snow development (Rogers 1979).

C. Forecast Implications

Considering the apparent accuracy of these modified NGM hourly soundings in simulating the over-lake boundary layer near CLE, the next step was to investigate which sounding parameters could be most useful for forecasting when and where the intense snow bands would occur. The idea

was to examine the highly unstable albeit shallow Type I snow band environment in the same way one would examine a deep, unstable summertime thunderstorm environment.

A chronological analysis of radar and surface data showed the lake snow event began around 0000 UTC 4 January when surface observations, including ASOS, first showed snow showers with visibilities less than 4.8 km (3 mi). Around 0800 UTC, the Cleveland WSR-88D reflectivity data (Figure 7a) first showed intense Type I snow bands forming in the middle of Lake Erie north of Erie, Pennsylvania. Two distinct Type I bands slowly propagated south at 5.5 km h^{-1} over the next 12 hours. They brought heavy snow first to Erie (ERI), Pennsylvania, 1100-1500 UTC (Figure 7b), then to Ashtabula, Ohio (labeled A in Figure 1) 1200-1600 UTC and to Perry, Ohio (P) in Lake County 1200-1700 UTC (Figures. 7b and 7c), and lastly to the northeast sections of Cleveland, Ohio and Cuyahoga County (B and C) 1300-1900 UTC (Figure 7c). During this period, the two strong bands merged as the band orientation rotated slowly clockwise from west southwest-east northeast to west-east. During 2000-0000 UTC 5 January, this single strong band weakened and several other bands appeared. During 0100-0600 UTC, a new heavy snow band redeveloped over Cleveland and northern Cuyahoga County penetrating inland into northern Geauga County (Figure 7d). The orientation of this band was west northwest-east southeast. Shortly after 0600 UTC, this snow band diminished to flurries.

The strong surface convergence pattern typically associated with these intense snow bands (Byrd et al. 1991) was frequently detected by the mesonet of surface observations from such varied sources as SAO, SAWRS, marine coastal, nuclear power plant tower, and ASOS test sites (Figures 7c and 7d). Observations south of the band tended to have southwest winds, while sites north of the band had northwest winds.

Forecasting this event, the onset and sustenance of lake-effect snow showers, 2300 UTC 3 January through 0700 UTC 5 January, corresponded to modified NGM soundings (Table 1) with CAPE values greater than 20 J kg^{-1} (or LI_8 values -1°C or less) with MPL values higher than 1.5 km (5 kft) AGL. The changing orientation of the snow bands corresponded to the changing in-cloud (1 km AGL) wind direction, which varied from about 260 deg at onset to nearly 300 deg at demise.

The snow showers were heaviest near CLE (Figure 7d) when CAPE values exceeded 50 J kg^{-1} (or LI_8 values -2° or less), MPL values exceeded 2.1 km (7 kft) AGL with MPL temperatures -23°C or less, and the absolute value of in-cloud (1-3 km AGL) wind directional shear was less than 2 x $10^{-3}s^{-1}$ (Figures 8a and 8b). The corresponding in-cloud wind direction change was less than 10 deg (Table 1).

The 1 km wind direction was very effective in determining both the band orientation and areal extent of the heavy snow. The 1 km wind direction from 280-290 deg at 0000 UTC 5 January (Figure 5) coincided with the orientation of the intense snow bands that developed near Cleveland at that time (Figure 7d). The most frequent 1 km wind direction during the entire heavy snow event was also from 280–290 deg. The areal extent of the heavy snow observed with this event (Figure 1) closely corresponded to that projected by NWSFO Cleveland locator charts using these winds (Figure 9).

Table 1

SHARP analyses of modified 0-48 h NGM soundings for CLE vicinity valid from 1200 UTC 3 January 1995 to 1200 UTC 5 January 1995. All heights are AGL.

Hour	850 mb Temp.	850 mb LI	CAPE	EL	MPL	MPL Temp.	0-3km Mean Wind	1 km Wind	1-3 km (L3-L6) Dir Chg.	Dir. Shear	Spd. Shear
UTC	*°C*	*°C*	*J kg^{-1}*	*kft*	*kft*	*°C*	*deg kt*	*deg kt*	*deg*	*$10^{-3}s^{-1}$*	*$10^{-3}s^{-1}$*
Jan 3											
12	-10.5	+3.0	0	2.1	----	----	260 30	258 29	+11	+2.7	+5.2
13	-10.5	+3.2	0	2.1	----	----	254 31	250 31	+13	+3.3	+5.3
14	-10.5	+3.2	0	2.1	----	----	253 30	250 30	+13	+3.3	+5.8
15	-10.5	+3.1	0	2.1	----	----	252 29	249 28	+13	+3.3	+6.1
16	-10.7	+2.8	0	2.1	----	----	253 31	252 30	+ 7	+1.9	+5.8
17	-10.9	+2.4	0	2.2	----	----	254 32	257 30	+ 1	+0.3	+6.4
18	-11.3	+1.9	1	2.6	----	----	254 32	259 28	- 2	-0.6	+7.5
19	-11.7	+1.3	2	2.8	3.3	-11	255 32	258 26	- 2	-0.6	+8.4
20	-12.3	+0.6	3	3.1	4.0	-12	255 33	257 26	- 1	-0.3	+9.0
21	-13.1	-0.2	7	3.9	4.6	-13	258 32	258 25	- 1	-0.3	+9.3
22	-13.7	-0.6	10	4.2	4.9	-14	260 32	261 25	- 3	-0.9	+8.9
23	-14.5	-1.2	25	4.5	5.7	-16	263 32	264 26	- 5	-1.4	+8.3
Jan 4											
00	-15.1	-1.4	31	4.6	5.8	-16	265 30	272 26	-12	-3.2	+7.7
01	-15.9	-1.7	41	4.7	6.2	-17	268 29	279 25	-18	-4.5	+7.2
02	-16.7	-1.8	44	4.7	6.1	-18	269 27	280 24	-19	-4.5	+6.9
03	-17.1	-1.8	45	4.6	6.1	-18	268 26	278 22	-17	-3.9	+6.8
04	-17.7	-1.9	45	4.6	5.9	-18	268 27	276 23	-14	-3.2	+6.6
05	-17.9	-1.8	38	4.6	5.8	-18	268 27	275 24	-13	-3.0	+6.4
06	-18.3	-1.7	33	4.5	5.7	-19	268 29	276 25	-15	-3.6	+6.5
07	-18.7	-1.7	33	4.6	5.8	-19	269 29	277 25	-16	-3.9	+6.8
08	-19.1	-1.6	32	4.6	5.8	-20	270 29	278 25	-16	-4.0	+7.1
09	-19.3	-1.5	30	4.6	5.8	-21	272 30	278 26	-15	-3.8	+7.3
10	-19.5	-1.4	24	4.4	5.5	-21	272 31	277 26	-13	-3.4	+7.3
11	-19.5	-1.0	17	4.3	5.2	-21	272 31	280 27	-13	-3.5	+7.3
12	-19.9	-1.1	21	4.3	5.3	-21	275 32	282 28	-13	-3.5	+7.1
13	-20.3	-1.2	27	4.4	5.5	-21	276 33	285 29	-13	-3.5	+6.8
14	-20.7	-1.3	30	4.4	5.5	-22	280 32	288 29	-13	-3.4	+6.5
15	-21.3	-1.7	35	4.5	5.7	-22	282 31	290 28	-13	-3.3	+6.3
16	-21.7	-1.7	39	4.5	5.9	-22	283 29	290 26	-11	-2.7	+6.1
17	-21.7	-1.8	41	4.6	6.1	-23	282 27	288 24	- 8	-1.9	+5.9
18	-21.7	-1.8	43	4.7	6.2	-24	281 26	285 23	- 4	-0.9	+5.6
19	-21.5	-1.8	43	4.7	6.3	-24	280 26	282 23	0	0.0	+5.2
20	-21.3	-1.9	49	5.1	6.7	-25	280 26	280 24	+ 3	+0.6	+4.7
21	-21.1	-2.0	60	5.4	7.4	-25	281 26	280 25	+ 4	+0.8	+3.9
22	-21.1	-2.0	70	5.6	7.8	-26	283 27	282 27	+ 4	+0.8	+3.0
23	-21.3	-2.5	94	5.9	8.3	-27	285 27	283 28	+ 5	+1.0	+2.5
Jan 5											
00	-21.3	-2.4	95	5.9	8.2	-27	286 27	285 28	+ 4	+0.8	+1.9
01	-21.5	-2.5	96	5.8	8.1	-26	290 27	290 29	+ 3	+0.6	+1.4
02	-21.7	-2.5	82	5.5	7.5	-25	294 27	294 29	+ 3	+0.6	+1.4
03	-21.9	-2.6	75	5.2	7.0	-24	296 26	295 27	+ 5	+0.9	+1.8
04	-21.9	-2.5	65	5.0	6.6	-23	297 25	295 26	+ 7	+1.2	+2.1
05	-21.9	-2.3	55	4.7	6.1	-22	297 24	294 25	+10	+1.8	+2.6
06	-21.7	-2.0	48	4.5	5.8	-21	299 24	294 25	+15	+2.7	+3.5
07	-20.9	-1.3	32	4.2	5.2	-20	300 23	292 24	+22	+4.0	+4.6
08	-19.9	-0.2	15	3.9	4.6	-20	300 23	289 23	+27	+4.9	+5.4
09	-18.5	+1.0	6	3.2	3.9	-19	298 22	287 22	+29	+5.1	+5.6
10	-17.1	+2.1	0	2.9	----	----	293 21	283 21	+29	+5.0	+5.4
11	-15.7	+3.5	0	2.8	----	----	287 21	277 21	+28	+4.9	+5.4
12	-14.5	+4.6	0	2.6	----	----	280 22	270 23	+29	+5.4	+5.8

4. SUMMARY AND RECOMMENDATIONS

Topographically-induced mesobeta phenomena, such as heavy lake-effect snow, can be more precisely forecasted in space and time by using high-resolution gridded forecast fields like PC-GRIDDS and hourly model soundings. Also the application of more fundamental meteorological analyses to these data sets can lead to improved understanding and forecasting. For example, this study has demonstrated how the usage of SHARP to assess model-forecasted CAPE, MPL, in-cloud directional windshear, and in-cloud mean wind direction can lead to a precise 6-48 h forecast of where and when the snow showers will be heavy.

This study has also shown how WSR-88D radar and GOES-8 satellite data sets can help detect not only the precise locations of the heavy snow bands, but also other important meteorological characteristics. These include precipitation-top height, cloud-top temperature, and wind field environment. In the present study, these were used to verify model forecasts, but in future operational settings they could also be used for short-term forecasting. In addition, work is being conducted (LaDue and Weaver 1995) to use these data sets to make short-term forecasts of snow amounts for specific locations.

Mesonets of hourly surface data can also augment the detection and short-term forecasting of heavy lake snow. In this particular event, wind direction and visibility changes helped determine the local passage of the intense Type I snow bands.

One recommendation for improving the 6-48 h forecast of heavy lake-effect snow for specific locations (for example, one county-zones) along the south shore of Lake Erie is to use a network of SHARP-analyzed modified meso-ETA soundings along the entire south shore of Lake Erie from Toledo, Ohio to Buffalo, New York. To make best use by operational forecasters, the resulting huge amount of data needs to be presented in some condensed form such as Figures 8a and 8b or as an interactive computer software display such as BUFKITe (Mahoney and Niziol 1995).

Another recommendation for improving short-term (0-6 h) forecasts is to allow operational forecasters quick access to GOES-8, WSR-88D, and ASOS observations, as each of these data sets is now updated every few minutes. The ability to overlay and composite these various observational and forecast data sets onto a common grid would also be most helpful.

5. ACKNOWLEDGMENTS

The authors wish to thank the following: Gary Carter, NWS Eastern Region Headquarters, Jim Weyman and Bob Higgins, WSFO Pittsburgh (PBZ), for their helpful review comments, Joe Palko, WSFO PBZ, for helping to draft Figure 8, Tom Niziol, WSFO Buffalo, for sharing his expertise and references on lake-effect boundary layer modification, and Louise Barton, Cleveland Electric Illuminating Company, for providing wind data for the Perry OH Nuclear Power Plant.

6. REFERENCES

Dockus, D., 1985: Lake-Effect Snow Forecasting in the Computer Age. *Nat. Wea. Digest,* **10,** 5-19.

Hart, J.A., and J. Korotky, 1991: The Sharp Workstation V1.50 User's Manual. DOC, NOAA, NMC, NWS, NSSFC, Kansas City, 30 pp.

Hoke, J.E., N.A. Phillips, G.J Dimego, J.J. Tuccillo, and J.G. Sela, 1989: The Regional Analysis and Forecast System of the National Meteorological Center. *Wea. Forecasting,* **4,** 323-334.

LaDue, J.G., and J. Weaver, 1995: Multisensor Applications to Lake Effect Nowcasting. NOAA Technical Memorandum NWS CR-112, Kansas City, Missouri.. Postprint, Fourth Nat. Winter Weather Workshop, Kansas City, NWS. (In press.)

Mahoney, E., and T.A. Niziol, 1995: BUFKITe - An ETA Profile Toolkit for the Buffalo WSFO (v95b). DOC, NOAA, NWS. [Available from WSFO Buffalo NY.]

Nierow, A., and R. Kane, 1993: An Evaluation of NGM Forecast Soundings in Predicting Potential for Significant Weather Situations. *Preprints 13th Conf. on Weather Analysis and Forecasting,* Vienna, AMS (Boston), 143-149.

Niziol, T.A. and S. McLaughlin, 1992: The Use of High Resolution Data from the NGM for Prediction of Lake-Effect Snows. Postprint Third NWS Winter Weather Workshop, Portland, NOAA/NWS, 179-192.

Niziol, T.A., W.R. Snyder, and J.S. Waldstreicher, 1995: Winter Weather Forecasting Throughout the Eastern United States. Part IV: Lake Effect Snow. *Wea. Forecasting, 10,* 61-77.

Phillips, D.W., 1972: Modification of Surface Air over Lake Ontario in Winter. *Mon. Wea Rev., 100,* 662-670.

Rogers, R.R., 1979: *A Short Course in Cloud Physics.* Pergamon, 235 pp.

Zubrick, S.M. and E. Thaler, 1993: Enhancements to the Operational Forecast Process Using Gridded Model Data. *Preprints 13th Conf. on Weather Analysis and Forecasting,* Vienna, AMS, 5-9.

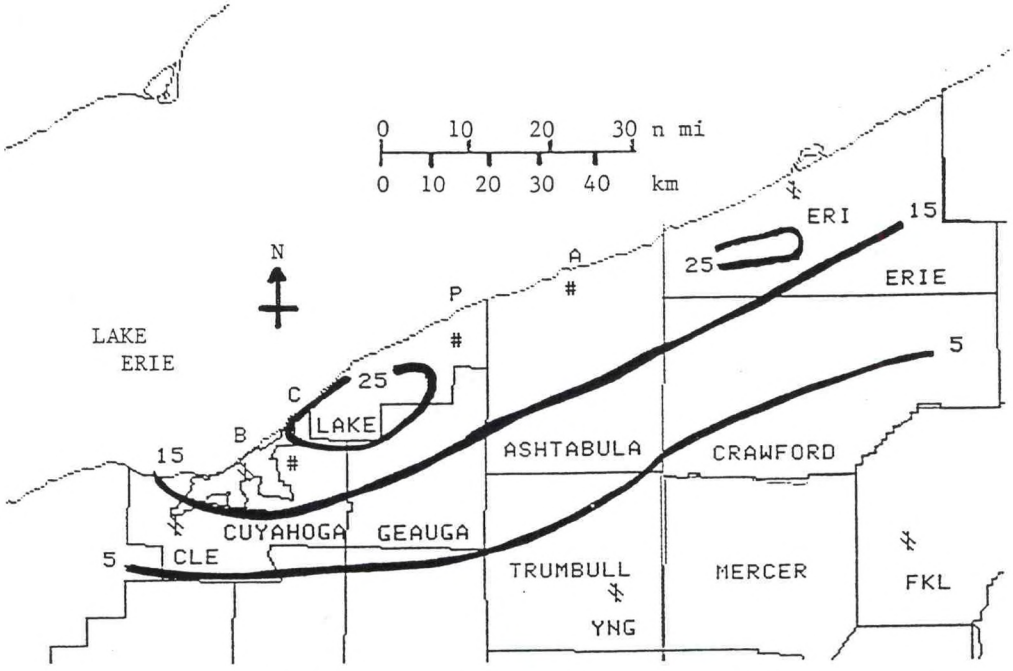

Figure 1. Observed 24-h snowfall (cm) ending 0600 UTC 5 January 1995. (Surface observation sites are denoted as follows: Ashtabula OH Lighthouse [A], Perry OH Nuclear Power Plant [P], Cuyahoga County Airport [C], and Burke Lake front Airport [B].)

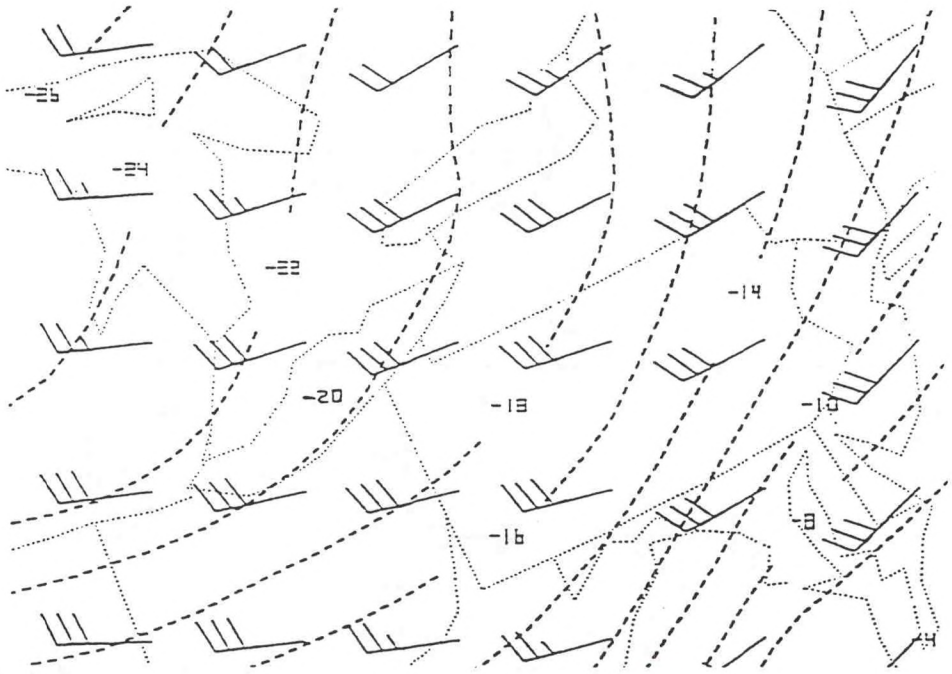

Figure 2. NGM PC-GRIDDS 24-h 850 mb temperature and wind forecast valid at 1200 UTC 4 January 1995.

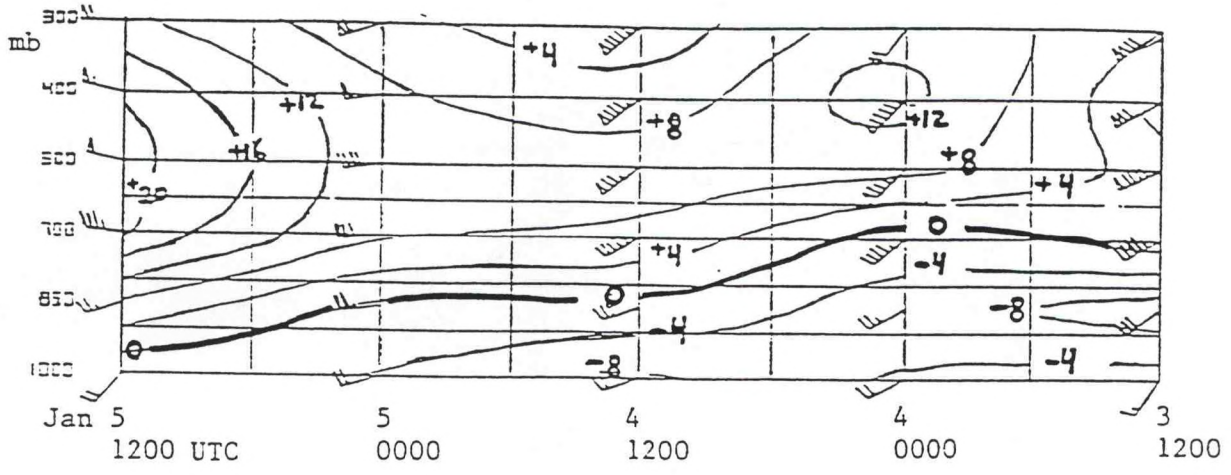

Figure 3. NGM PC-GRIDDS time vs height cross-section for location 42EN 81EW (75 km northeast of CLE) showing vertical velocity (10^{-6} bar s^{-1}) and horizontal winds (kts, barbs) 0-48 h forecasts valid from 1200 UTC 3 January 1995 to 1200 UTC 5 January 1995.

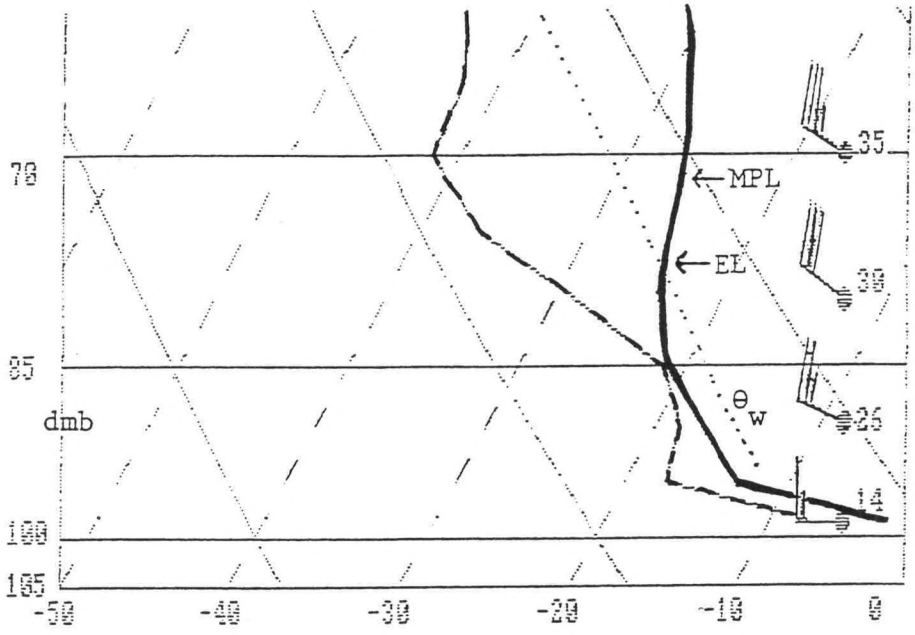

Figure 4. SHARP-analyzed modified 36-h NGM sounding for CLE vicinity valid at 0000 UTC 5 January 1995.

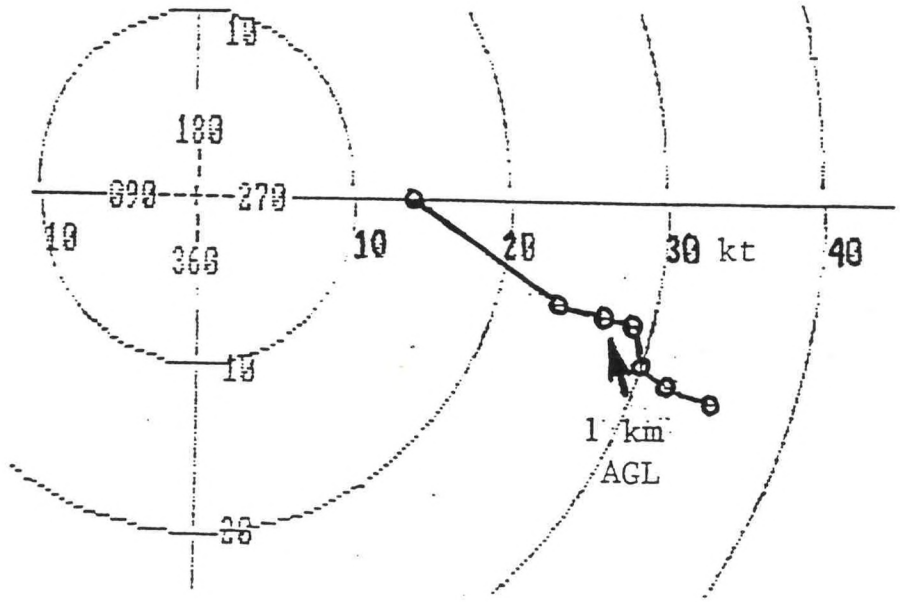

Figure 5. SHARP-analyzed modified 36-h NGM hodograph for CLE vicinity valid at 0000 UTC 5 January 1995.

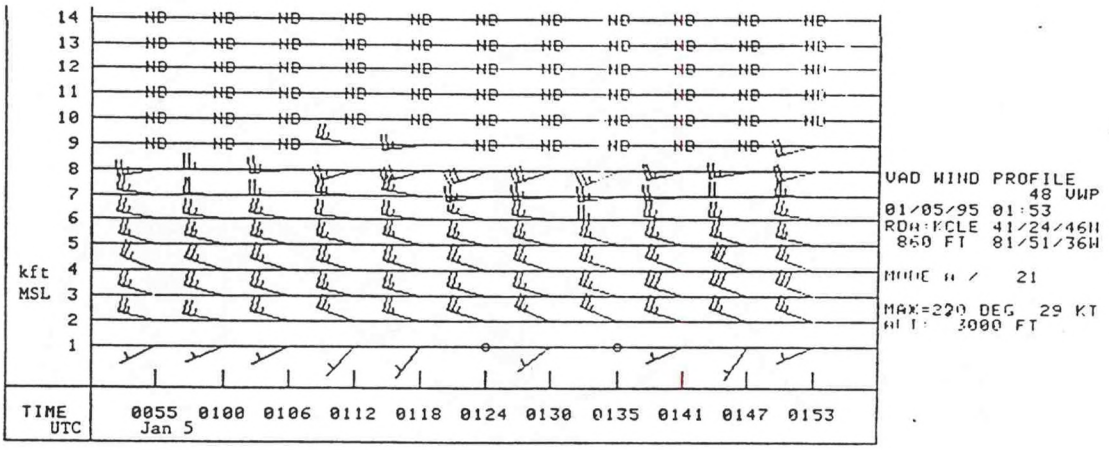

Figure 6. KLE WSR-88D Vertical Wind Profile (VWP) valid at 0153 UTC 5 January 1995. Wind barbs in kts.

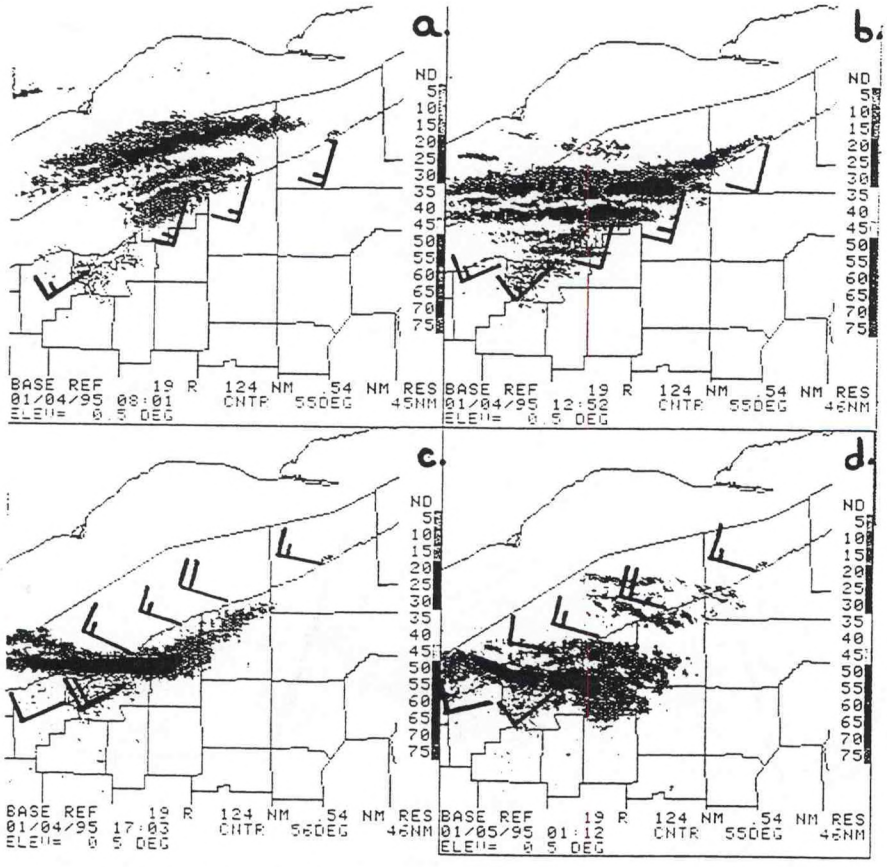

Figure 7. KCLE WSR-88D base reflectivity (elevation 0.5 deg, resolution 0.54 n mi) at 0801 UTC 4 January 1995 (a), 1252 UTC 4 January 1995 (b), 1703 UTC 4 January 1995 (c), and 0112 UTC 5 January 1995 (d). Intensities greater than 19 dBZ shaded black. Surface mesonet wind observations denoted by wind barbs in kts.

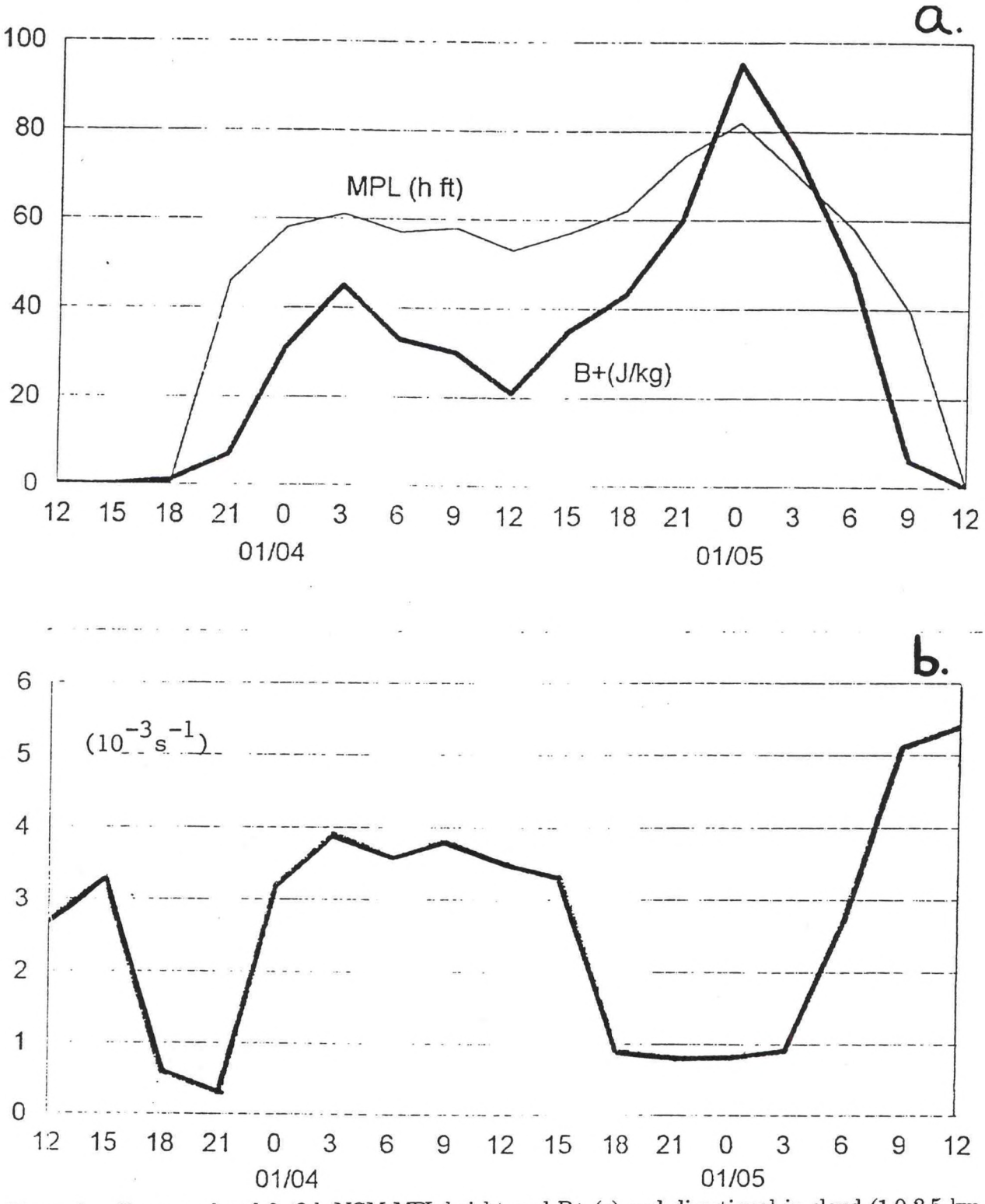

Figure 8. Sharp-analyzed 0-48 h NGM MPL height and B+ (a) and directional in-cloud (1.0-2.5 km AGL) wind shear (b) valid from 1200 UTC 3 January 1995 to 1200 UTC 5 January 1995.

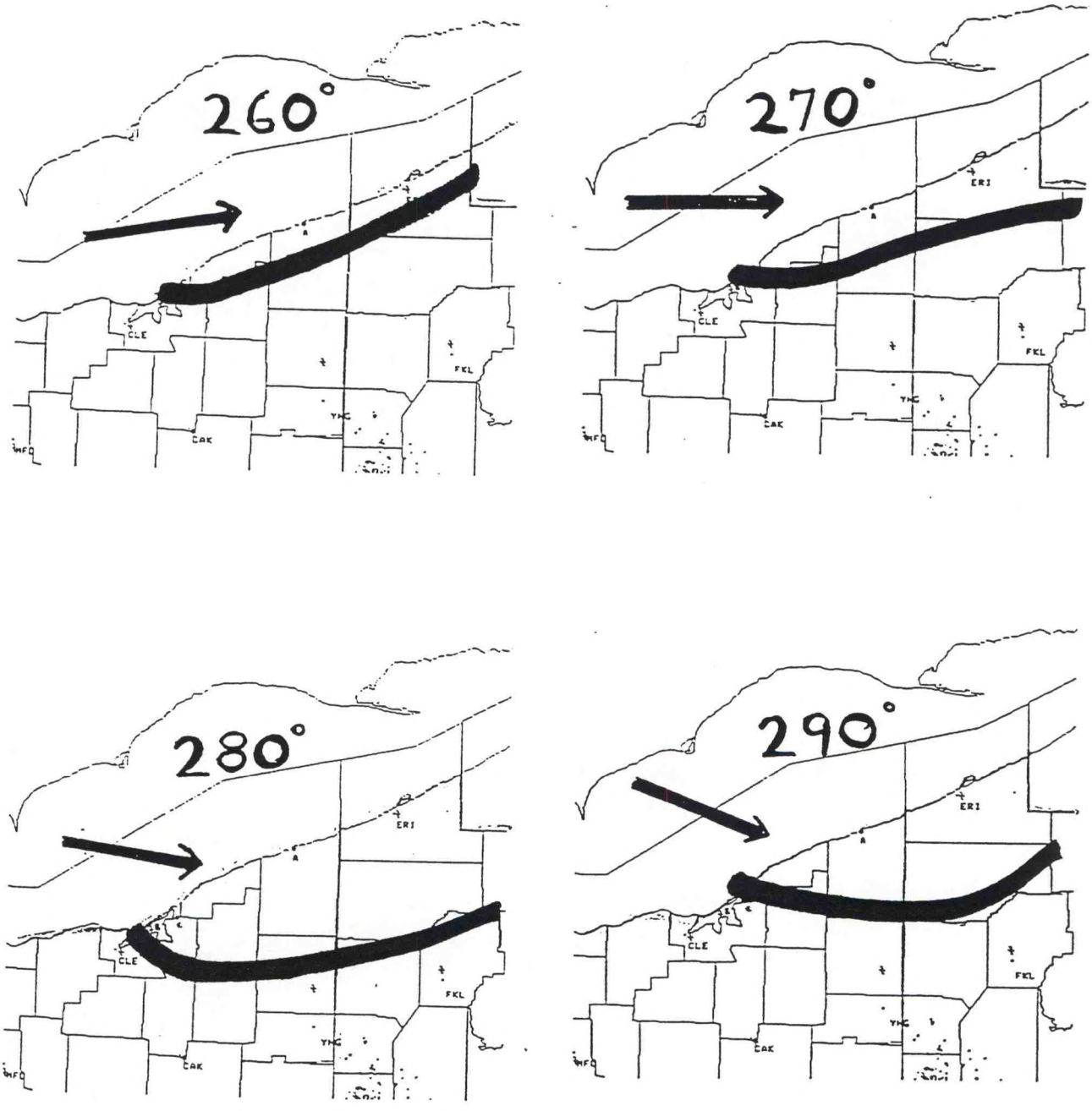

Figure 9. Lake Erie lake-effect snow locator charts developed by NWSFO Cleveland. The chart indicates to forecasters where the heaviest snow will occur based on the boundary layer wind direction.

SESSION 4
APPLICATIONS OF TECHNOLOGY II

8. Numerical Model Prediction and WSR-88D Depiction of Conditional Symmetric Instability for the 18 January 1995 Heavy Snowfall Event Across Northeastern Oklahoma and Northwestern Arkansas

9. A Wind Profiler and PCGRIDDS Analysis of a Tropopause Fold and Associated Cyclogenesis

10. Short and Medium Term Road Ice Predictions for Winter Road Maintenance

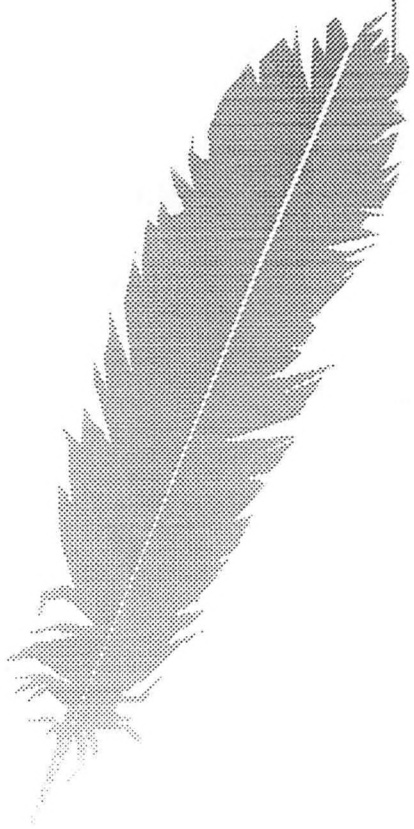

Numerical Model Prediction and WSR-88D Depiction of Conditional Symmetric Instability for the 18 January 1995 Heavy Snowfall Event Across Northeastern Oklahoma and Northwestern Arkansas

Peter L. Wolf[1]

1. INTRODUCTION

During the late afternoon and evening of January 18, 1995, heavy snow fell across portions of northeastern Oklahoma and northwestern Arkansas, with some locations receiving 10 inches or more in less than 12 hours (Figure 1). Strong moisture inflow and vertical motion led to widespread snowfall. Mesoscale bands of heavy snow that appeared convective in nature, in an air mass that was stable to vertical and horizontal motions, indicated the presence of conditional symmetric instability (CSI). The usefulness of model gridded data for predicting mesoscale snow bands due to CSI or the co-existence of CSI and dynamic forcing, and the depiction of the bands on WSR-88D radar imagery will be presented.

2. THE FORECAST

Gridded data from the numerical models indicated the potential for heavy precipitation on January 18 across eastern Oklahoma and western Arkansas from a developing winter storm. The models showed this potential up to 48 hours in advance of the event. However, low-level temperature forecasts for the event generated prior to 0000 UTC 18 January were too high to support snowfall. The 0000 UTC 18 January model forecasts showed low-level temperatures more conducive to snowfall. This along with anticipated cooling due to lift, evaporation and melting led forecasters to expect snow to become the primary precipitation type during this event.

A strong shortwave trough was forecast to intensify over the southern Plains on January 18. The models indicated a coupled upper jet configuration, as shown on Figure 2, with an anticyclonic jet over the Midwest and a cyclonic jet over southern Texas. The location and curvature of the jets resulted in strong upper-level divergence across Missouri, Arkansas and eastern Oklahoma. This, plus low-level moisture flux convergence and strong frontogenetical forcing ahead of the intensifying cyclone, led to forecasts of strong vertical motion over the area. These features indicated the potential for a significant and widespread precipitation event.

The models also predicted an important air mass characteristic, CSI, which played a role in the development of mesoscale bands of very heavy precipitation. (Only introductory information about CSI, relevant to operational forecasting, is provided here. Refer to Bennetts and Hoskins 1979, Emanuel 1983, Moore and Blakley 1988, Sanders and Bosart 1985, or Snook 1992, from which this material originates, for detailed information about CSI and predicting it with theta-e and angular momentum surfaces). CSI is a form of instability that exists in the presence of horizontal and vertical stability. In a saturated air mass which is stable to vertical or horizontal displacements, but exhibits CSI, air parcels displaced along slantwise theta-e surfaces become unstable and accelerate in the direction of displacement. This mesoscale acceleration can lead to "slantwise" convection.

1. Corresponding author address: Peter L. Wolf, NWS Office, Tulsa, Oklahoma.

Several important conditions must be met for CSI to exist. The air mass must be nearly saturated. The air mass must have low static stability, but should not be convectively unstable. Convective instability leads to upright convection rather than "slantwise" convection. A third condition is for either strong vertical or horizontal (anticyclonic) speed shear, or both, to exist such that air parcels traveling along a theta-e surface encounter increasing momentum with height. Another condition is for air parcels to be displaced along theta-e surfaces (isentropic lift), since CSI alone will not cause stationary parcels to move.

A favored area for low-level CSI to exist in strong extra-tropical cyclones is within the "cold conveyor belt", a low-to-mid level feature where saturated air, vertical shear, and low static stability all may exist (Carlson 1980 for a description of the cold conveyor belt). Frontogenetical forcing and other forcing mechanisms are also present within or in the vicinity of the cold conveyor belt. Precipitation on radar imagery and cloudiness on satellite imagery often take on a convective appearance within the cold conveyor belt.

Cross-sections of theta-e and angular momentum surfaces from model gridded data files, taken normal to the thermal wind, can be used to predict CSI. A saturated air mass exhibits CSI where the slope of the theta-e surface is greater (more vertical) than the slope of the angular momentum surface. If a saturated air parcel moving up a "slantwise" theta-e surface encounters increasing environmental momentum, CSI is released and the parcel accelerates. Another way to view this (as described in Bluestein 1986) is to assume air parcels move along angular momentum surfaces (conserve momentum). CSI exists where theta-e values decrease with height along an angular momentum surface. Decreasing theta-e with height is a more conventional sign of instability in a saturated air mass. The amount of instability increases as the angle between the theta-e and angular momentum surfaces seen on a cross-section increases.

The cross-section shown on Figure 3 is a 24-hour forecast from the 0000 UTC 18 January 1995 NGM, and is taken from northwest to southeast across northeastern Oklahoma and northwestern Arkansas, normal to the thermal wind. The cross-section is also normal to the cold conveyor belt located over the area between the 850 mb and 700 mb levels. CSI was forecast to exist below 500 mb, and be greatest below 800 mb, over extreme northeastern Oklahoma and northwestern Arkansas. To the west over north central Oklahoma, CSI was not indicated, while to the east over central and eastern Arkansas, convective instability was indicated. The large angle between the theta-e and angular momentum surfaces below 800 mb on the cross-section indicated substantial low-level instability along a slantwise plane. The Eta model also showed CSI, but not as dramatically as the NGM. Model forecasts produced 36 and 48 hours prior to the event also hinted at CSI.

During the pre-dawn hours of January 18, forecasters determined from the latest data that sufficient cooling due to evaporation, lift and melting would lead to a rain-to-snow changeover. From all indications (CSI, dynamic forcing, etc), the heaviest snow would fall across extreme northeastern Oklahoma. A winter storm warning was issued for that area (Figure 1) for 4 to 8 inches of accumulation, and a winter weather advisory was issued elsewhere across northeastern and east-central Oklahoma for lower accumulations. No advisory was issued initially for southeastern Oklahoma due to little or no expected accumulation, but was issued later when light accumulations became more likely.

3. THE STORM

During the morning of January 18, a cold rain spread across eastern Oklahoma and western Arkansas. Low-level cooling led to a mixture of rain, sleet and wet snow by midday across

northeastern Oklahoma. By late afternoon, wet snow was observed across much of northeastern Oklahoma and northwestern Arkansas.

Toward evening, locally heavy snow developed across northeastern Oklahoma and northwestern Arkansas, while rain changed to wet snow across east-central Oklahoma. The Inola, Oklahoma WSR-88D radar showed the formation of mesoscale bands of heavy snow (Figures 4 and 5). The superior quality of the WSR-88D imagery led to the design of useful and accurate short-term forecasts which described where the heaviest snow would fall.

Figure 4 shows a nearly stationary band of heavy snow over far northeastern Oklahoma, with reflectivity values of 35 to 40 dBZ, producing snowfall at rates greater than an inch per hour. The orientation of this band became more south to north during the evening as the thermal wind field became oriented more south to north. Figure 5 shows several south-to-north oriented snow bands over eastern Oklahoma. Other bands likely developed over extreme eastern Oklahoma and northwest Arkansas, but were low-topped and too far from the Inola WSR-88D radar to be detected and displayed.

Snowfall totals for the storm are shown on Figure 1. A maximum of 14 inches, most of which fell in 6 hours, was reported at Blue-jacket in Craig County, Oklahoma. This location was beneath the snow band shown on Figure 4 for several hours. Heavy snowfall was observed across northwestern Arkansas and southwestern Missouri as well.

Figure 1 also shows the areas covered by the initial warning and advisory products issued 12 hours before the snowfall began. The products accurately indicated which counties would get 1 to 3 inches and 4 to 8 inches of snow, respectively. Craig County, which received the heaviest snowfall in Oklahoma, was not in the initial winter storm warning. However, the remarkable display of the snow bands by the WSR-88D radar (Figure 4) led forecasters to include this county in the warning as the heavy snow began.

4. DISCUSSION

Prior to and during the event, the latest technology was used to design and issue accurate, timely and useful meteorological products. Model gridded data helped forecasters determine the potential for heavy snow, and led to the correct issuance of a winter storm warning only for extreme northeastern Oklahoma rather than for all of eastern Oklahoma. The gridded data accurately indicated the potential for mesoscale bands of heavy snow across northeastern Oklahoma. Timely short-term forecasts, which pin- pointed where the heaviest snow would fall, were produced as a result of the superior WSR-88D detection and display of the snow.

Low-level CSI, released by isentropic lift (Moore and Kaster 1993), provided the mesoscale "slantwise" acceleration to produce bands of heavy snow across northeastern Oklahoma. CSI may not have been the only cause. Frontogenetical forcing between 850 mb and 700 mb, and dynamic support for vertical motion due to a favorable upper-level jet stream configuration, may also have contributed to snow band development. Dynamic forcing modified the environment (leading to cold conveyor belt development) such that CSI, or even elevated convective instability in similar situations, could exist. The co-existence of dynamic forcing and the mesoscale acceleration due to CSI led to the formation of well-defined snow bands.

For the January 18 event, the models accurately predicted the co-existence of strong dynamic forcing and CSI over northeastern Oklahoma and northwestern Arkansas, indicating that mesoscale snow band development was a likely scenario. As illustrated in this case, snowfall amounts can vary

greatly across a forecast area when mesoscale snow bands develop. The phrase "locally heavier amounts" may be a necessity in the public forecast when predicting accumulations in environments that favor mesoscale snow band development.

5. CSI COMMAND FILE

A PCGRIDDS command file can be produced to display the data fields needed to diagnose a CSI environment. The following commands (separated by commas), are run successively to display angular momentum, theta-e, and relative humidity contours for a chosen cross-sectional area: LOOP, SSUM NORM GEOS SMLT FFFF DIST, THTE CIN3 DASH &, RELH CI10 GT70 DOTS &, ENDL.

6. ACKNOWLEDGMENT

The author would like to thank Steve Amburn, SOO, and Steve Piltz, WCM, for their reviews of this paper, and comments which improved the text.

7. REFERENCES

Bennetts, D.A., and B.J. Hoskins, 1979: Conditional symmetric instability - A possible explanation for frontal rainbands. *Quart. J. Roy. Meteor. Soc.,* **105**, 945-962.

Bluestein, H.B. 1993: *Synoptic-Dynamic Meteorology in Midlatitudes Vol. 2: Observations and Theory of Weather Systems.* Oxford University Press, New York, 545-561.

Browning, W.D. and M.P. Foster, 1995: Forecast and detection of conditional symmetric instability: a case study. *Preprints, 14th Conf. on Weather Analysis and Forecasting,* Dallas, TX, AMS (Boston), 199-203.

Carlson, T.N., 1980: Airflow through mid-latitude cyclones and the comma cloud pattern. *Mon. Wea. Rev.,* **108**, 1498-1509.

Emanuel, K.A., 1983: The Lagrangian parcel dynamics of moist symmetric instability. *J. Atmos. Sci.,* 40, 2368-2376.

Funk, T.W., C.W. Hayes, M.B. Sholz, and K.A. Kostura, 1995: Vertical motion forcing mechanisms responsible for the production of a mesoscale very heavy snow band. *Preprints, 14th Conference on Weather Analysis and Forecasting,* Dallas, TX, AMS (Boston), 176-181.

Moore, J.T., and P.D. Blakley, 1988: The role of frontogenetic forcing and conditional symmetric instability in the Midwest snowstorm of 30-31 Jan. 1982. *Mon. Wea. Rev.,* **116**, 2155-2171.

Moore, J.T., and M.A. Kaster, 1993: Physical processes organizing wintertime frozen precipitation events in the Midwest. *Preprints, 13th Conference on Weather Analysis and Forecasting,* Vienna, VA, AMS (Boston), 512-515.

Sanders, F., and L.F. Bosart, 1985: Mesoscale structure in the megalopolitan snowstorm of 11-12 February 1983. Part I: Frontogenetical forcing and conditional symmetric instability. *J. Atmos. Sci.,* 42, 1050-1061.

Snook, J.S., 1992: Current techniques for real-time evaluation of conditional symmetric instability. *Wea. Forecasting,* 7, 430-439.

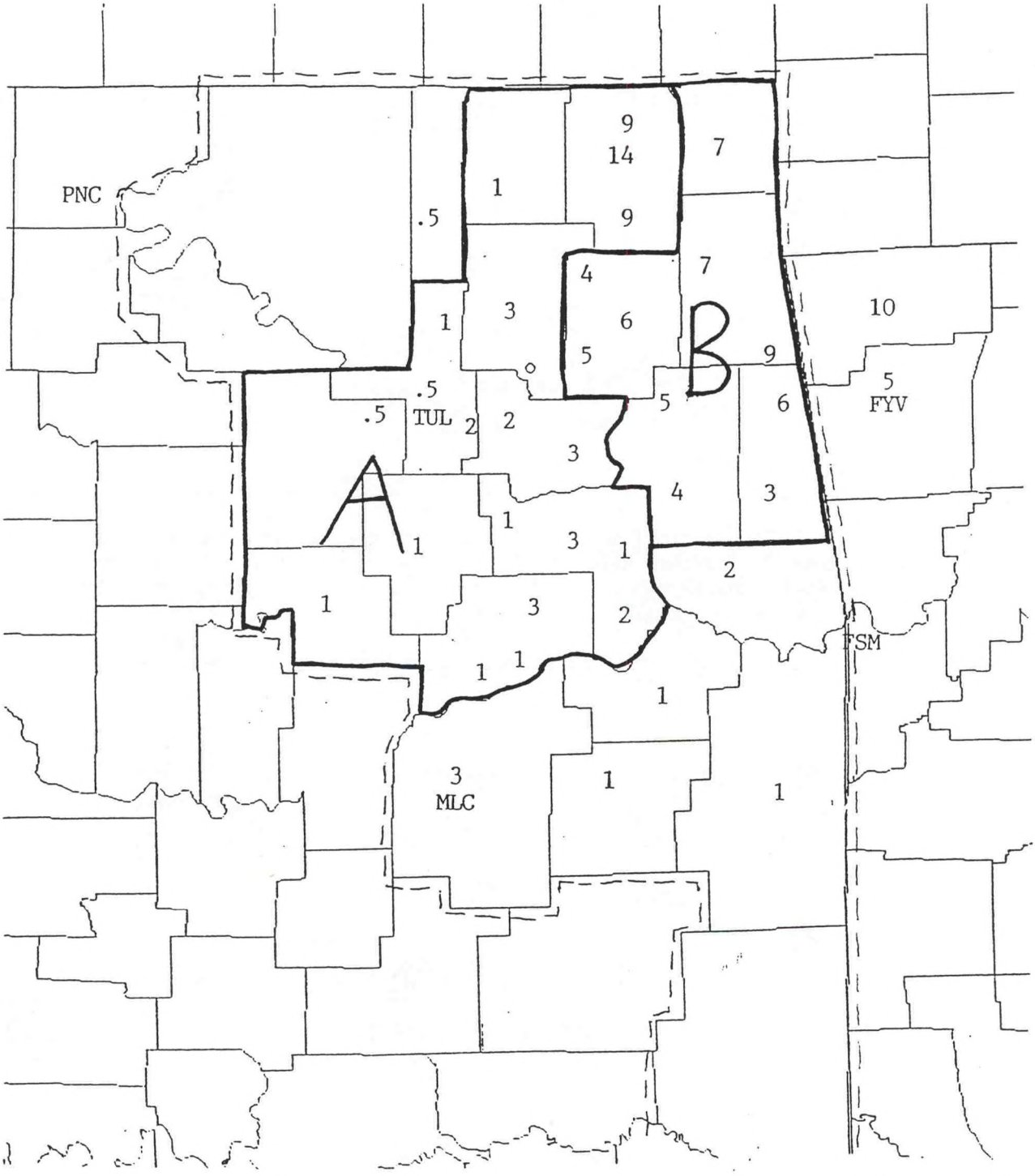

Figure 1. Snowfall totals, in inches, for the January 18, 1995 storm. Areas A and B represent the counties covered by the Winter Weather Advisory and the Winter Storm Warning, respectively, issued about 12 hours before the snowfall began. The dashed line outlines the eastern Oklahoma forecast area of WFO Tulsa, Oklahoma.

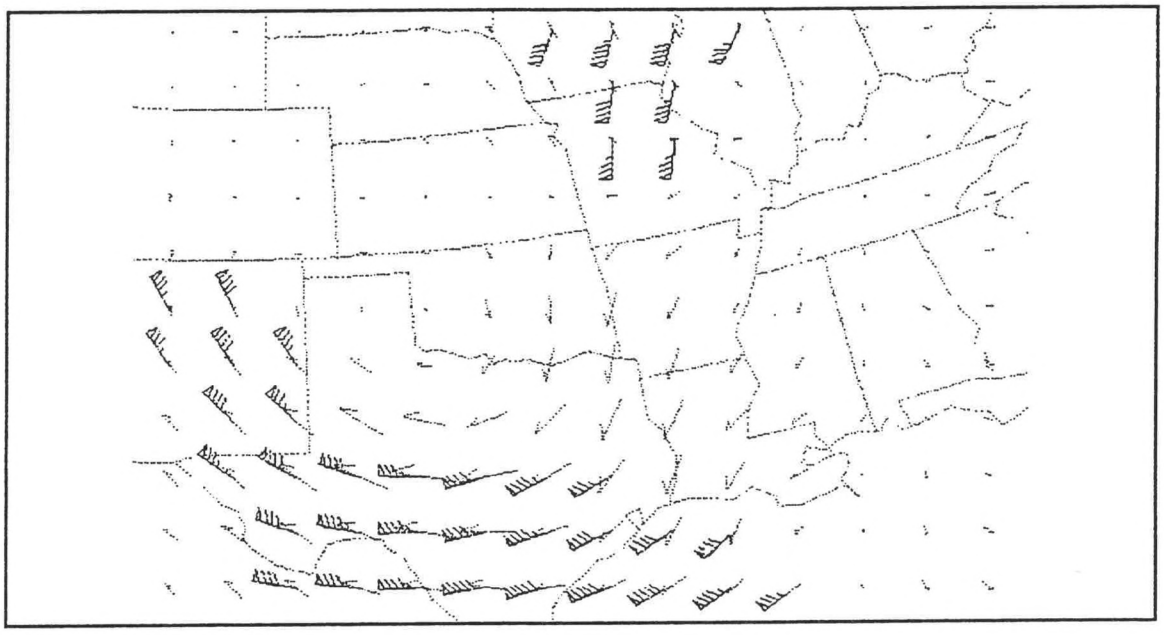

Figure 2. 24-hour NGM forecast of 300mb winds in excess of 75 knots (wind barbs) and 300 mb ageostrophic wind vectors (arrows), valid at 0000 UTC 19 January 1995. The coupled upper jet configuration resulted in strong upper level divergence over Arkansas and eastern Oklahoma, as indicated by the diverging ageostrophic wind vectors.

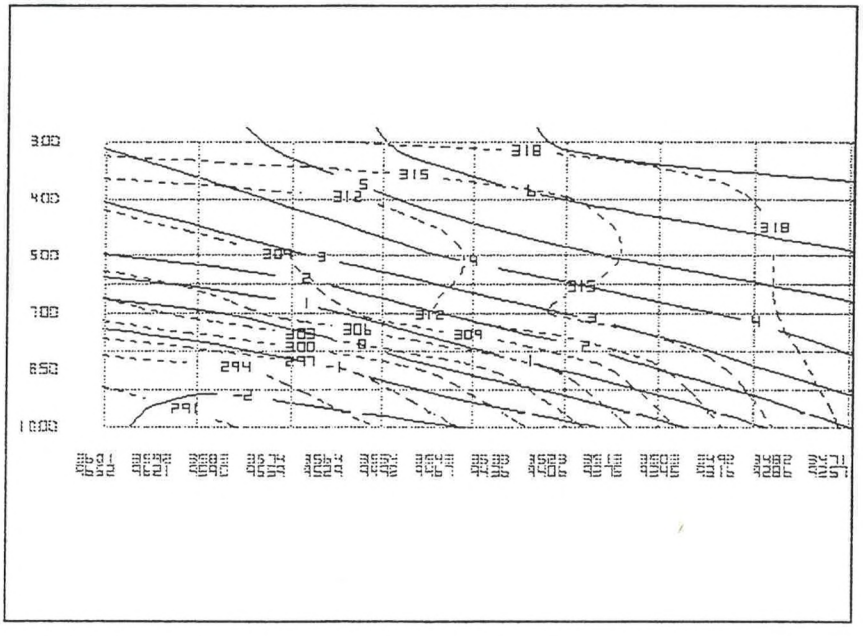

Figure 3. A 24-hour forecast cross-sectional plot of angular momentum (solid) an theta-e (dash) surfaces across northeastern Oklahoma (left half of the illustration) and northwestern Arkansas (right half), valid at 0000 UTC 19 January 1995. Relative humidities (not shown) were forecast to be 90 percent or greater below the 600 mb level.

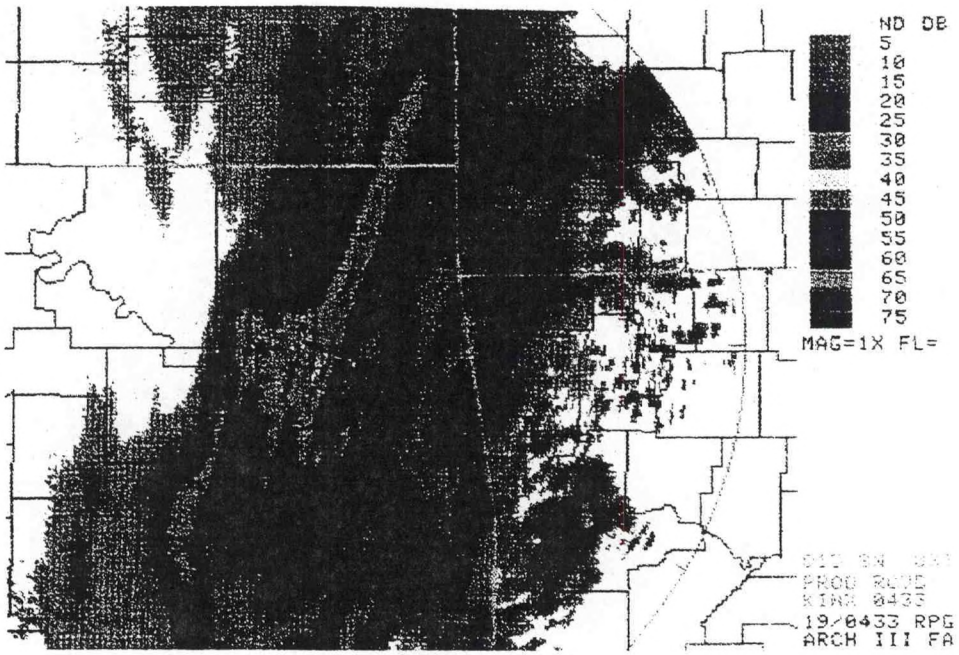

Figure 4. WSR-88D 0.5 degree base reflectivity image at 0039 UTC 19 January 1995. A well-defined mesoscale snow band is shown over northeastern Oklahoma.

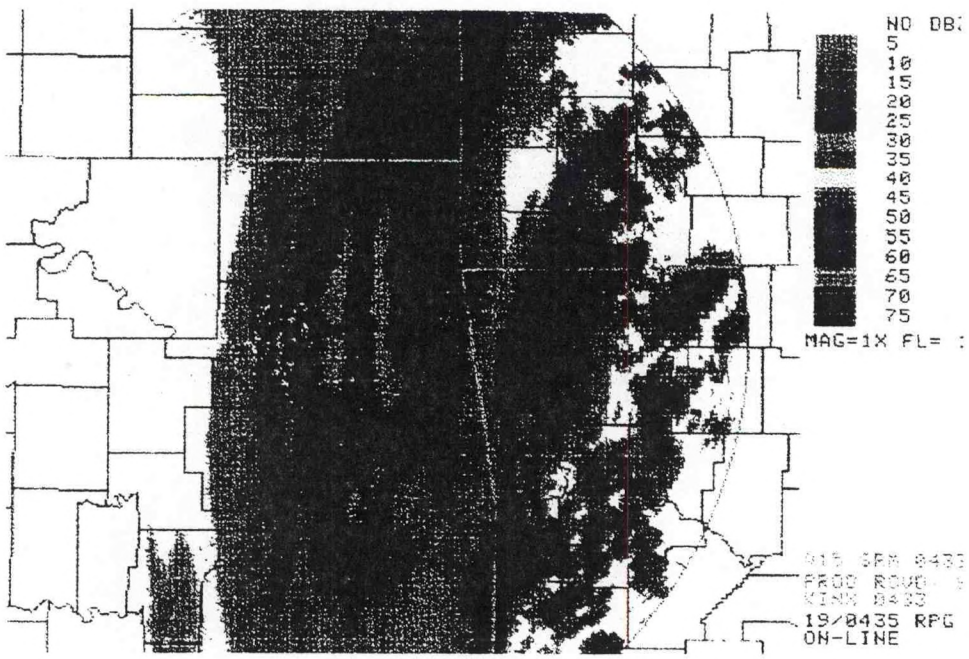

Figure 5. WSR-88D 0.5 degree base reflectivity image at 0324 UTC 19 January 1995. Several snow bands are shown over northeastern Oklahoma.

A Wind Profiler and PCGRIDDS Analysis of a Tropopause Fold and Associated Cyclogenesis

Mark Mitchell[1], Kyle Carstens[2], R.W. Arritt[3], and T.D. Rink[4]

1. INTRODUCTION

Intrusions of stratospheric air into the upper-troposphere can and often do intensify developing low pressure systems (Reed 1955; Reed and Danielson 1959). This stratospheric air can be identified by its relative warmth when compared to the surrounding upper-tropospheric air. Temperature variations in the upper-troposphere and lower stratosphere can be strong indications that cyclone development in the lower troposphere is occurring (Hirschberg and Fritsch 1991). These areas can often be identified by areas of warm advection downstream of the stratospheric air. However, warm advection may not always be a sure sign that a stratospheric intrusion is occurring. The warm, stable conditions that exist in the stratosphere represent sources of high potential vorticity. This potential vorticity can be used as a "tracer" of stratospheric air, and is coincident with warming of the upper troposphere as a stratospheric intrusion is occurring (Hirschberg and Fritsch 1991).

In the following paper we will show how a stratospheric intrusion with its accompanying potential vorticity can interact with a mid-latitude cyclone to enhance cyclogenesis. Then we will examine a cyclone that did undergo rapid cyclogenesis as it moved through the wind profiler network. Derivative products from clear-air Doppler radars, such as wind profilers, have the potential to provide valuable information regarding the height of the tropopause and the occasional intrusions of stratospheric air (Nastrom et al., 1989). We will use model gridded forecasts as well as wind profiler data to show how a stratospheric intrusion may have been responsible for cyclogenesis in this case.

2. POTENTIAL VORTICITY

Potential vorticity (P) can be defined as,

$$P = -(\zeta_\theta + f)\,\partial\theta/\partial p \tag{1}$$

where $(\zeta_\theta + f)$ is the absolute vorticity measured on an isentropic surface, and $\partial\theta/\partial p$ is the static stability. Potential vorticity is conserved on an isentropic surface and can be used to follow a parcel of stratospheric air as it intrudes into the troposphere.

The typical parcel of stratospheric air is warmer and drier than the levels below it in the troposphere. As a result, higher static stability values exist in the stratosphere than in the troposphere. So, when a tropopause fold occurs, allowing warm, dry stratospheric air to move down adiabatically, the static stability of the air decreases, and there is a corresponding increase in the absolute vorticity to keep P conserved. Adding positive amounts of absolute vorticity to the middle and upper levels of the troposphere increases synoptic scale rising motion.

1. Corresponding authors address: Mark Mitchell, NWS Forecast Office, Minneapolis, MN.
2. Kyle Carstens, NWS Forecast Office, Minneapolis, MN.
3. R.W. Arritt, Iowa State University.
4. T.D. Rink, Iowa State University.

In his study of the Presidents' Day Cyclone of February 18-19, 1979, Uccellini et al. (1985), found that a stratospheric intrusion can reach as low as 700 to 850 mb into the troposphere. In addition, as it reaches the lower to middle troposphere it does not only increases the absolute vorticity in this region, but it also increases the mass convergence, which leads to further deepening of the surface low. Uccellini et al. (1985) also found that the tropopause folds were closely integrated with sinking motion related to the deformation pattern created by an upper tropospheric jet streak.

The edge of stratospheric air in the troposphere can generally be marked by potential vorticity values greater than 10 x 10^{-6} K mb^{-1} s^{-1} (Reed and Danielson 1959; Shapiro 1976). This unit is defined as a potential vorticity unit (PVU). As Uccellini et al. (1985) pointed out, when these values reach down into the lower to middle troposphere (i.e., 850-700 mb) significant cyclogenesis are likely to occur.

3. CASE STUDY - NOVEMBER 19-21, 1994

A. Synoptic Overview

During the third weekend in November 1994 a developing mid-latitude cyclone made its way across the Rockies and into the Central Plains. Upon reaching the Central Plains the cyclone deepened rapidly. Flooding rains occurred from southern Kansas northward to southern Minnesota.

Early in the day on November 20, 1994 a surface low over the Oklahoma/Texas Panhandle deepened rapidly due to significant upper level dynamics, specifically a stratospheric intrusion extending well into the troposphere. Between 1200 UTC and 1500 UTC the most rapid intensification occurred when the central surface pressure dropped 3 to 4 millibars in three hours.

At 1200 UTC, the surface low was located in extreme southwest Kansas, while the associated 500 mb low was positioned over northwest New Mexico. Development of this storm system was being fueled by a stratospheric intrusion that ETA model gridded data, at 1200 UTC 20 November, initialized over northeast New Mexico. Figures 1 and 2 portray the forecasted potential vorticity at 300 mb from the ETA model run at 1200 UTC 20 November for the 00 hour (initial) and 12 hour forecast respectively. A plot of tropopause pressure and temperature from the upper air run at 1200 UTC 20 November verifies the position of the potential vorticity maximum showing a region of low tropopause heights and relatively warm temperatures centered over central New Mexico (Figure 3). In addition to the stratospheric intrusion, a coupled jet streak feature was also enhancing development of the system. The ETA 00 hour forecast at 300 mb from the model gridded forecast for 1200 UTC 20 November showed the left front quadrant of a jet streak over southwest Texas and the right rear quadrant of a weaker jet streak over the western Great Lakes were aligned over the panhandles of Texas and Oklahoma.

B. Profiler and PCGRIDDS Analysis

One of the many products that can be derived from the wind profiler network is the thermal wind. Assuming the thermal wind approximation is valid for a given situation, the type of advection can be inferred from a wind profile. As was discussed earlier in Section 2, warm advection downstream of a tropopause fold is one of the ways that an intrusion of stratospheric air can be detected. Figures 5 and 6 show the temperature advection at 300 mb along with the thermal wind from 250 mb to 400 mb from the ETA model gridded data from 1200 UTC for the 00 hour forecast (valid at 1200 UTC 20 November) and the 12 hour forecast (valid at 0000 UTC 21 November) respectively. These ETA model representations also show that the cyclone had completed its most intense period of cyclogenesis between 1200 UTC and 1800 UTC.

A cross-section of potential vorticity and normalized wind roughly from Rapid City, SD southward into Central Mexico using the ETA initial grid at 1200 UTC 20 November showed a potential vorticity maximum reaching downward just below 700 mb (Figure 4). An intrusion of stratospheric air this deep into the troposphere will usually lead to significant cyclogenesis (Uccellini et al. 1985).

The surface low deepened as it moved northeast into northeast Kansas and southeast Nebraska by 0000 UTC 21 November. The central surface pressure changed little and even began to increase after 1800 UTC. The 12 hour forecast from the ETA model gridded data from 1200 UTC 20 November showed the potential vorticity maximum at 300 mb weakening and moving to northeast Oklahoma and southeast Kansas (Figure 2).

Data from the wind profiler network was used to verify the positioning of the stratospheric intrusion as it moved through the Central Plains. Figures 5 and 6, which are representations of the model forecast thermal wind at 300 mb indicate a thermal ridge (i.e., backing of the thermal wind with time) in the same general vicinity as the potential vorticity maximum. Thermal wind displays from the wind profilers are also able to show the backing pattern with time in the upper gates. Figure 7 is a thermal wind profile from Western Oklahoma. It shows this backing pattern quite nicely between 1300 UTC and 2100 UTC 20 November from 9 to 11 km AGL. A strong area of warm advection precedes the thermal ridge around 1600 UTC roughly between 9.5 to 11 km AGL. Model gridded data showed the thermal ridge, as indicated by the thermal wind, and the potential vorticity maximum moving across western Oklahoma right around 1800 UTC. This is roughly the time that the profiler data shows a change over from warm to cold advection and thermal ridge passage. Figure 8 is a thermal wind profile from Southeastern Kansas. This profile also shows the beginnings of the backing of the thermal wind with time indicating thermal ridge passage. The initial stages of the thermal ridge can be seen between and 8 and 11 km AGL from 1900 UTC to 2300 UTC 20 November. Again a strong area of warm advection in advance of the thermal ridge is shown by 2100 UTC between 9.5 and 11 km AGL. Model gridded data forecast the intrusion of stratospheric air to pass over this region around 0000 UTC 21 November (Figure 2 and Figure 5). The profiler appears to be indicating the passage of the warm stratospheric air at about the time it was forecast.

4. CONCLUSIONS

Potential vorticity can be used as a tracer on stratospheric air as it descends into the troposphere. This type of analysis is useful, because it allows the forecaster to track areas of warm stratospheric air that have the potential to enhance the development of mid-latitude cyclones.

PCGRIDDS and profiler data were used to examine a specific case of a rapidly deepening low pressure area over the central United States. Profiler and conventional upper air data proved useful in verifying model predictions of stratospheric air intrusions, both in intensity and location. Model forecasts of potential vorticity and stratospheric intrusions can be very important in the determination of cyclogenesis. If the model misplaces a potential vorticity maximum and in turn the intensity and location of cyclogenesis, errors can occur in forecasts of significant weather events (Barnes and Colman 1994). Verification of atmospheric model output with "real-time" data can provide the forecaster with added confidence regarding the model solution.

5. ACKNOWLEDGMENTS

A publication [or report] pursuant to University Corporation for Atmospheric Research (UCAR) Subaward No. S94-42212 pursuant to National Oceanic and Atmospheric Administration Award No. NA37WD0018-01.

Additional thanks to Rich Naistat (SOO), WSFO Chanhassen, MN for his critique and valuable insights toward development of the manuscript.

6. REFERENCES

Barnes, S.L. and B.R. Colman, 1994: Diagnosing and operational numerical model using Q-vector and potential vorticity concepts. *Wea. and Forecasting,* **9,** 85-102.

Hirschberg, P.A. and J.M. Fritsch, 1991: Tropopause undulations and the development of extratropical cyclones. Part 1: Overview and observations from a cyclone event. *Mon. Wea. Rev.,* **119,** 496-517.

Nastrom, G.D., J.L Green, M.R. Peterson, and K.S. Gage, 1989: Tropopause folding and the variability of the tropopause height as seen by the Flatland VHF radar. *J. Appl. Meteor.,* **28,** 1271-1154.

Reed, R.J, 1955: A study of a characteristic type of upper-level frontogenesis. *J. Meteor.,* **12,** 226-237.

_____, and E.F. Danielson, 1959: Fronts in the vicinity of the tropopause. *Arch. Meteor. Geophys.* Bioklim., **A11,** 1-17.

Shapiro, M.A., 1976: The role of turbulent heat flux in the generation of potential vorticity in the vicinity of upper-level jet stream systems. *Mon. Wea. Rev.,* **104,** 892-906.

Uccellini, L.W., D. Keyser, K.F. Brill and C.H. Wash, 1985: The President's Day cyclone of 18-19 February 1979: Influence of upstream trough amplification and associated tropopause folding on rapid cyclogenesis. *Mon. Wea. Rev.,* **113,** 941-961.

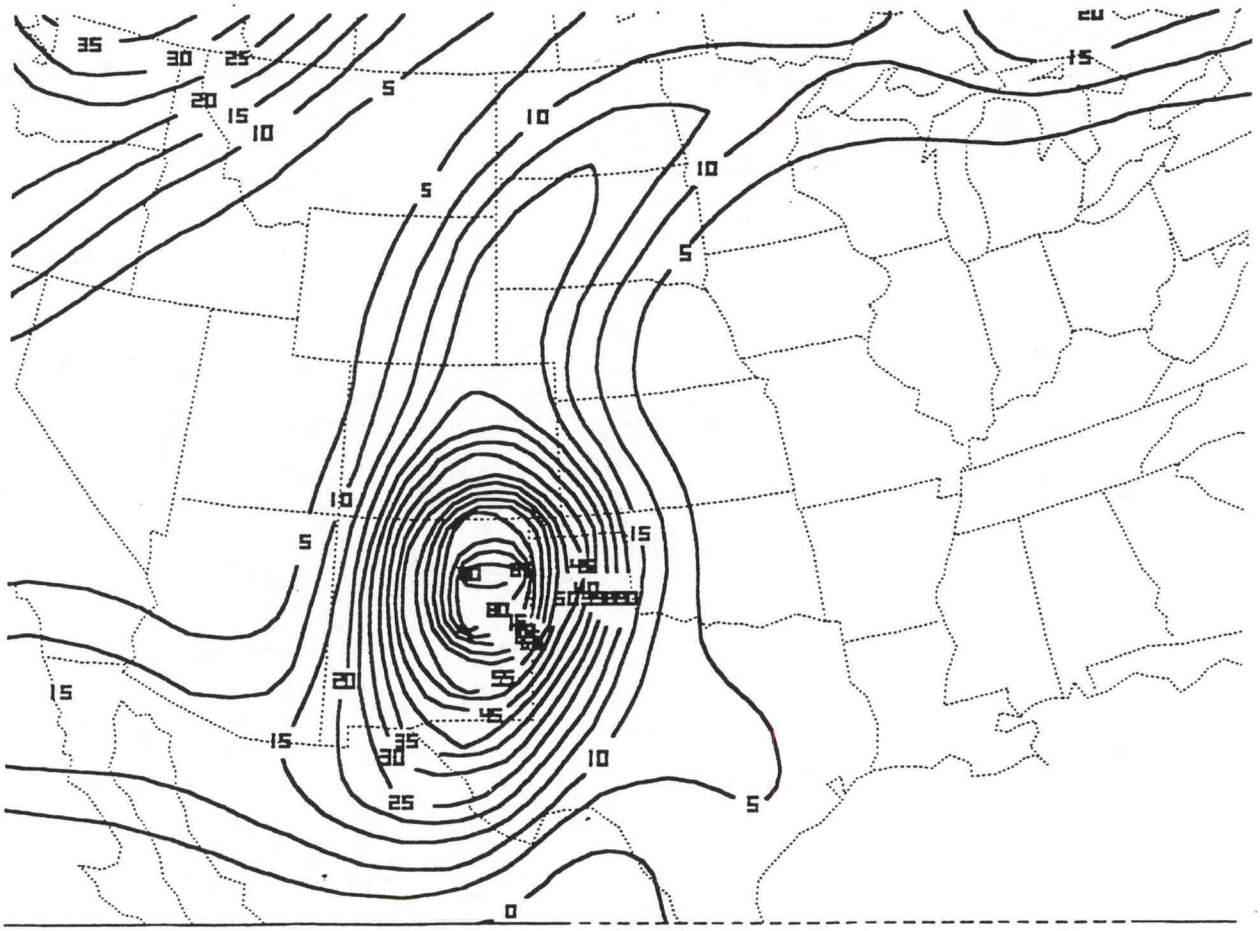

Figure 1. Potential vorticity (10^{-6}Kmb^{-1}s^{-1}) at 300 mb. ETA 00 hour (initial forecast) valid 1200 UTC 20 November 1994.

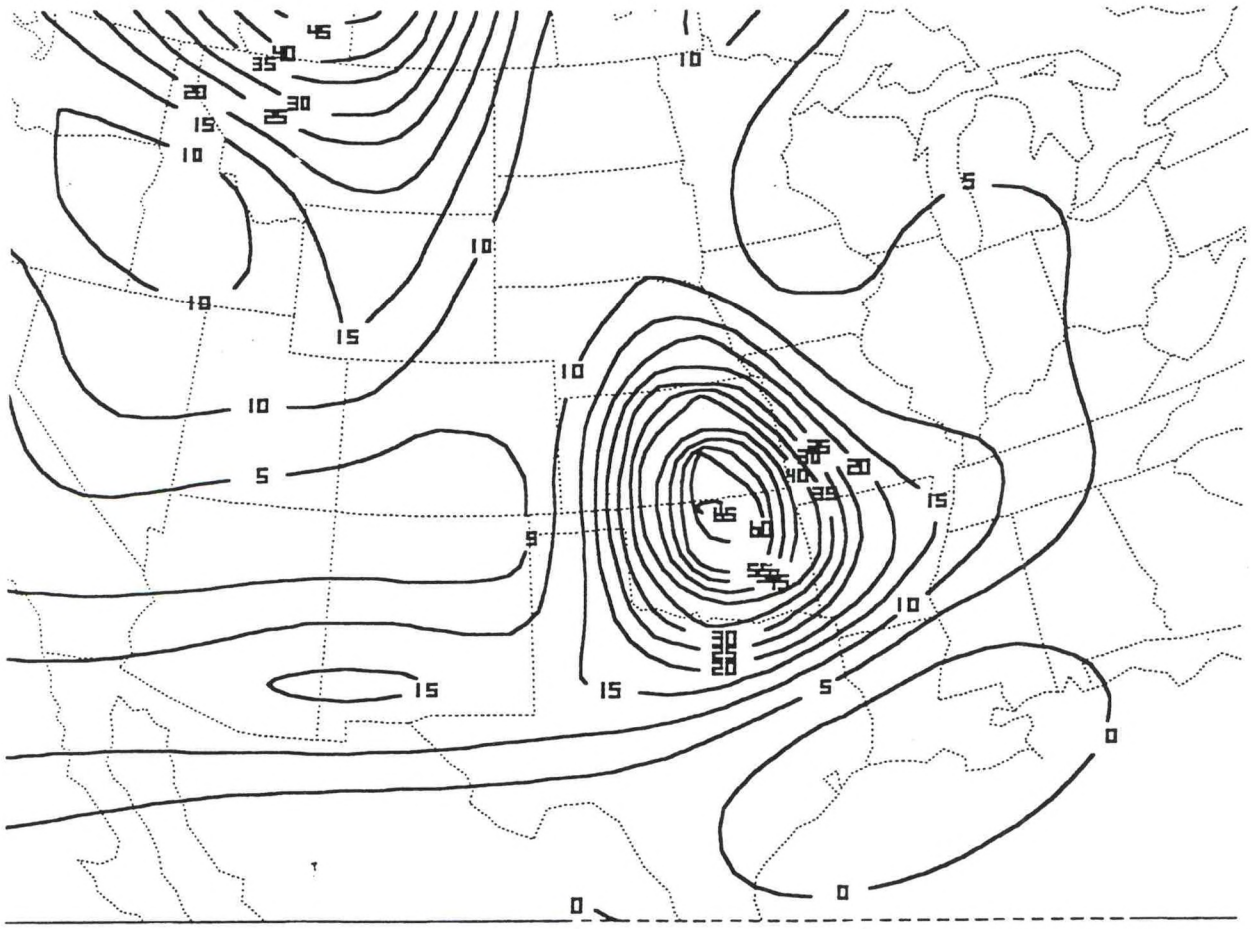

Figure 2. Same as Figure 1 except, ETA 12 hour forecast valid 0000 UTC 21 November 1994.

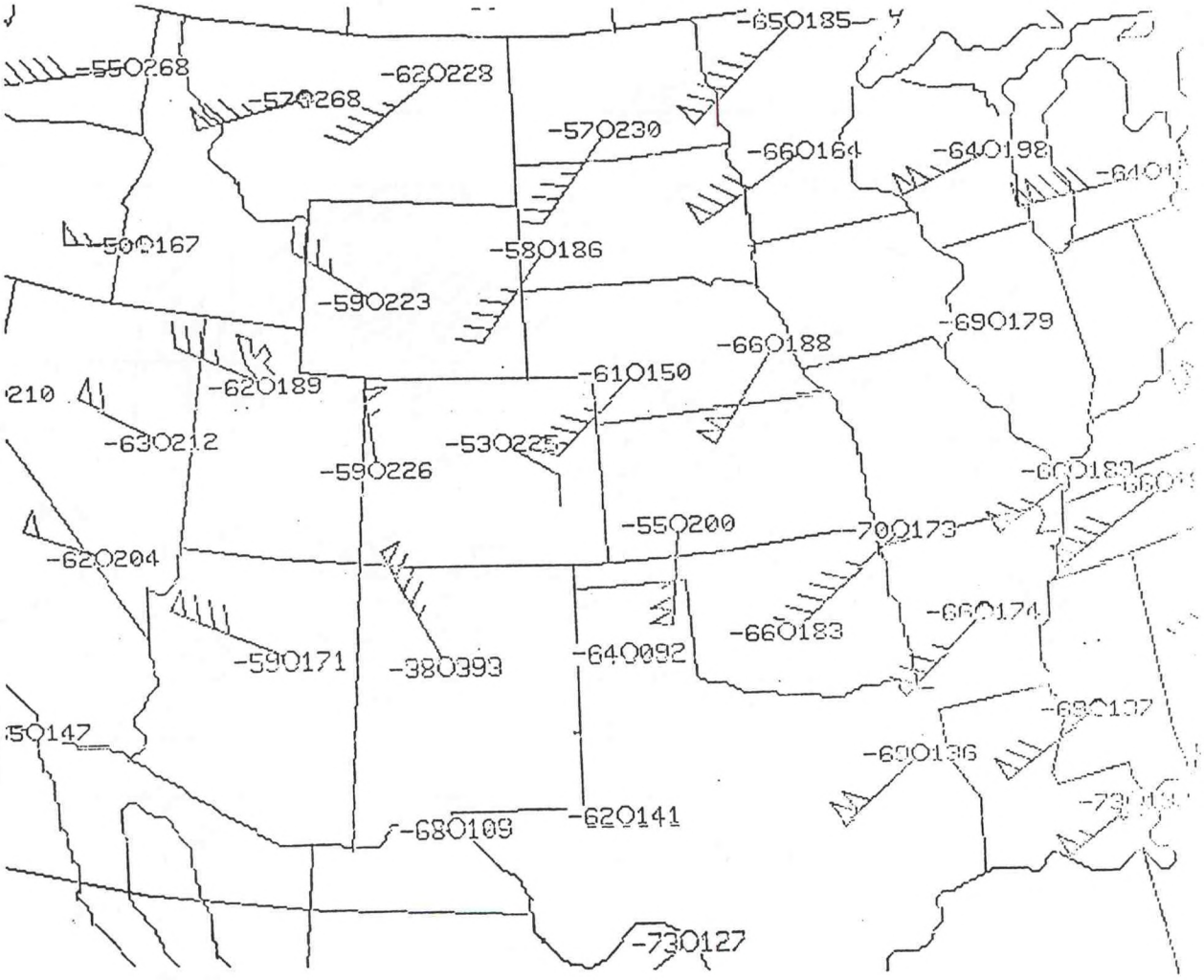

Figure 3. Plot of tropopause height pressure and temperature for 1200 UTC 20 November 1994.

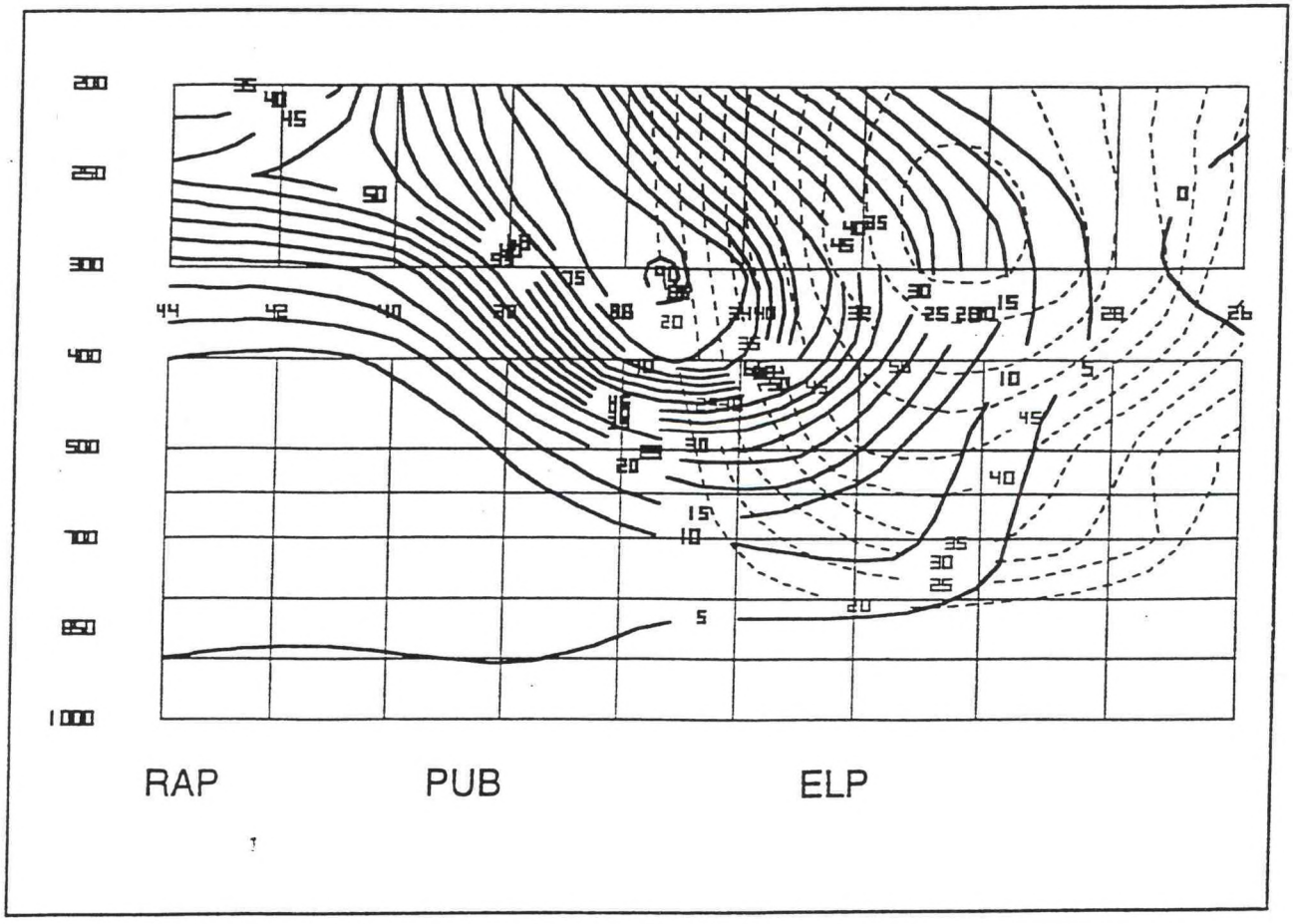

Figure 4. Cross-section of potential vorticity (x 10^{-6}Kmb^{-1}s^{-1}) and normalized wind (m/s). ETA 00 hour forecast valid 1200 UTC 20 November 1994. Normalized wind is dashed, potential vorticity is solid.

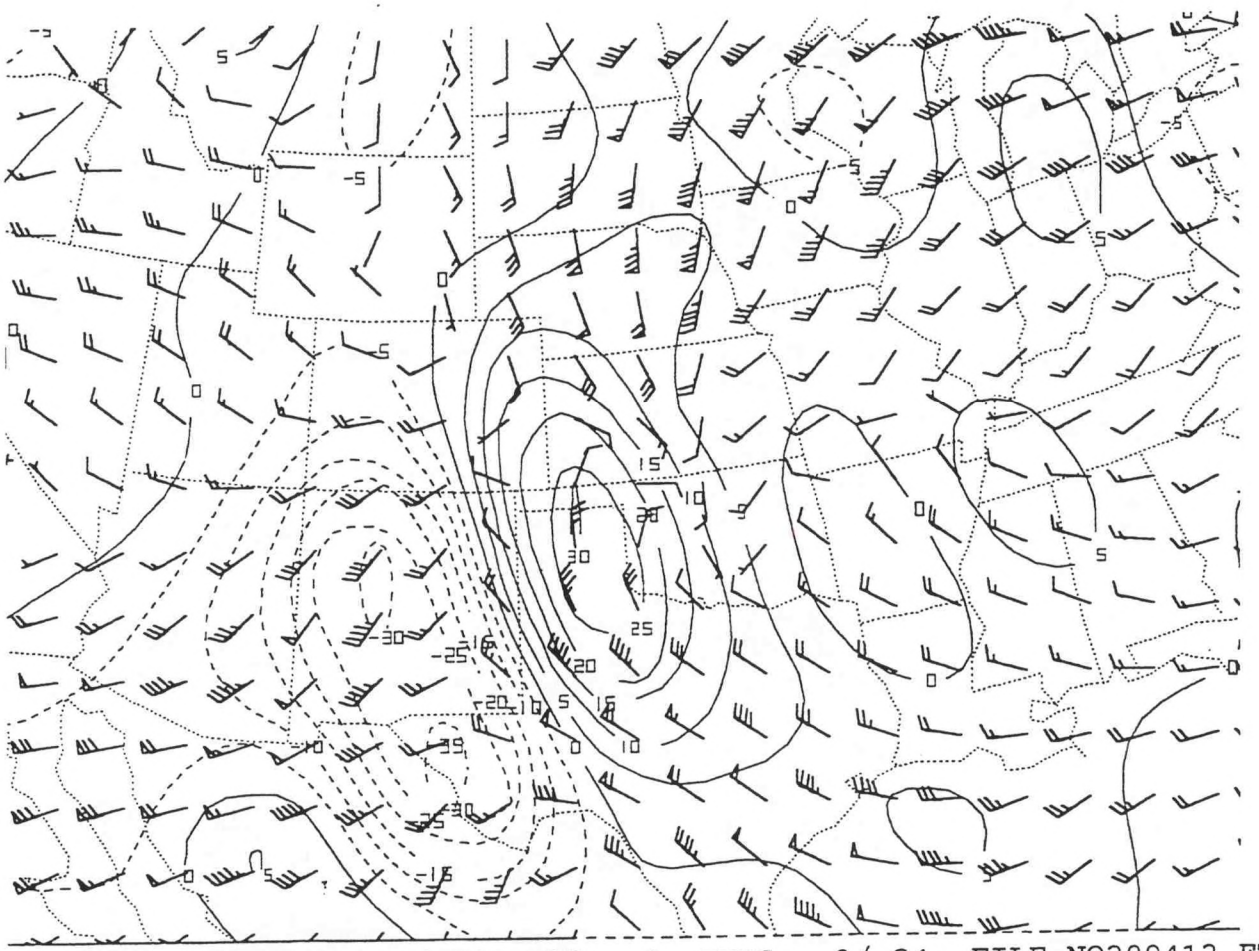

ETAX:LVL= 300:LYR=1000/ 500:FHR= 0 :FHRS= 0/ 24::FILE=NO209412.ETC
94/11/20/12--VDIF BKNT 250 BKNT 400&HRLY ADVT TEMP WIND CI.5 DNEG 300

ETAX:LVL= 250:LYR=1000/ 500:FHR= 0 :FHRS= 0/ 24::FILE=NO209412.ETC
94/11/20/12--VDIF BKNT 250 BKNT 400&HRLY ADVT TEMP WIND CI.5 DNEG 300

Figure 5. Temperature advection ($^{\circ}C/hr \times 10^{-1}$) at 300 mb and Thermal Wind for the layer 400 mb-250 mb. ETA 00 hour forecast valid 1200 UTC 20 November 1994.

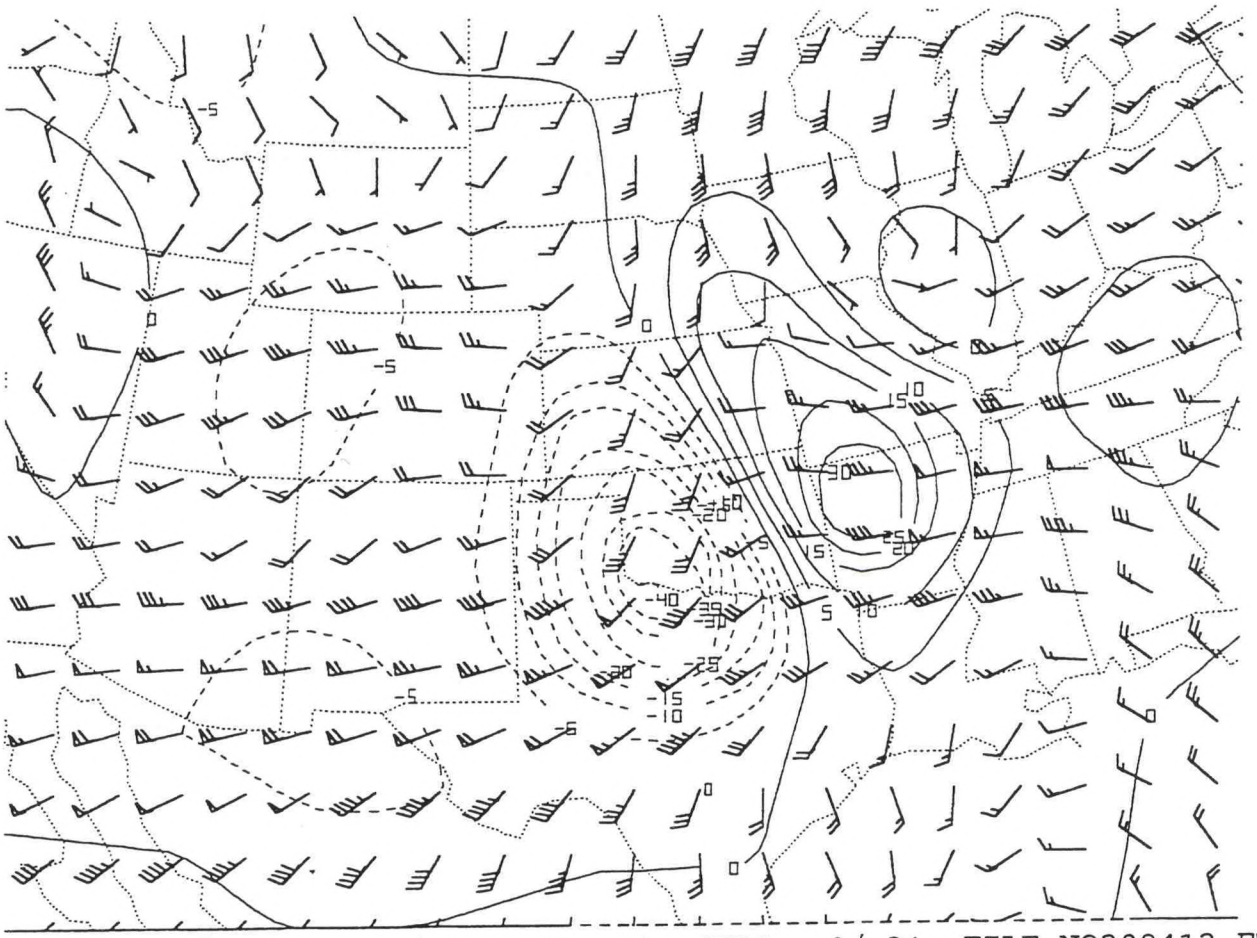

ETAX:LVL= 300:LYR=1000/ 500:FHR= 12 :FHRS= 0/ 24::FILE=NO209412.ETC
94/11/20/12--VDIF BKNT 250 BKNT 400&HRLY ADVT TEMP WIND CI.5 DNEG 300 F12

ETAX:LVL= 250:LYR=1000/ 500:FHR= 12 :FHRS= 0/ 24::FILE=NO209412.ETC
94/11/20/12--VDIF BKNT 250 BKNT 400&HRLY ADVT TEMP WIND CI.5 DNEG 300 F12

Figure 6. Same as Figure 5 except for ETA 12 hour forecast valid 0000 UTC 21 November 1994.

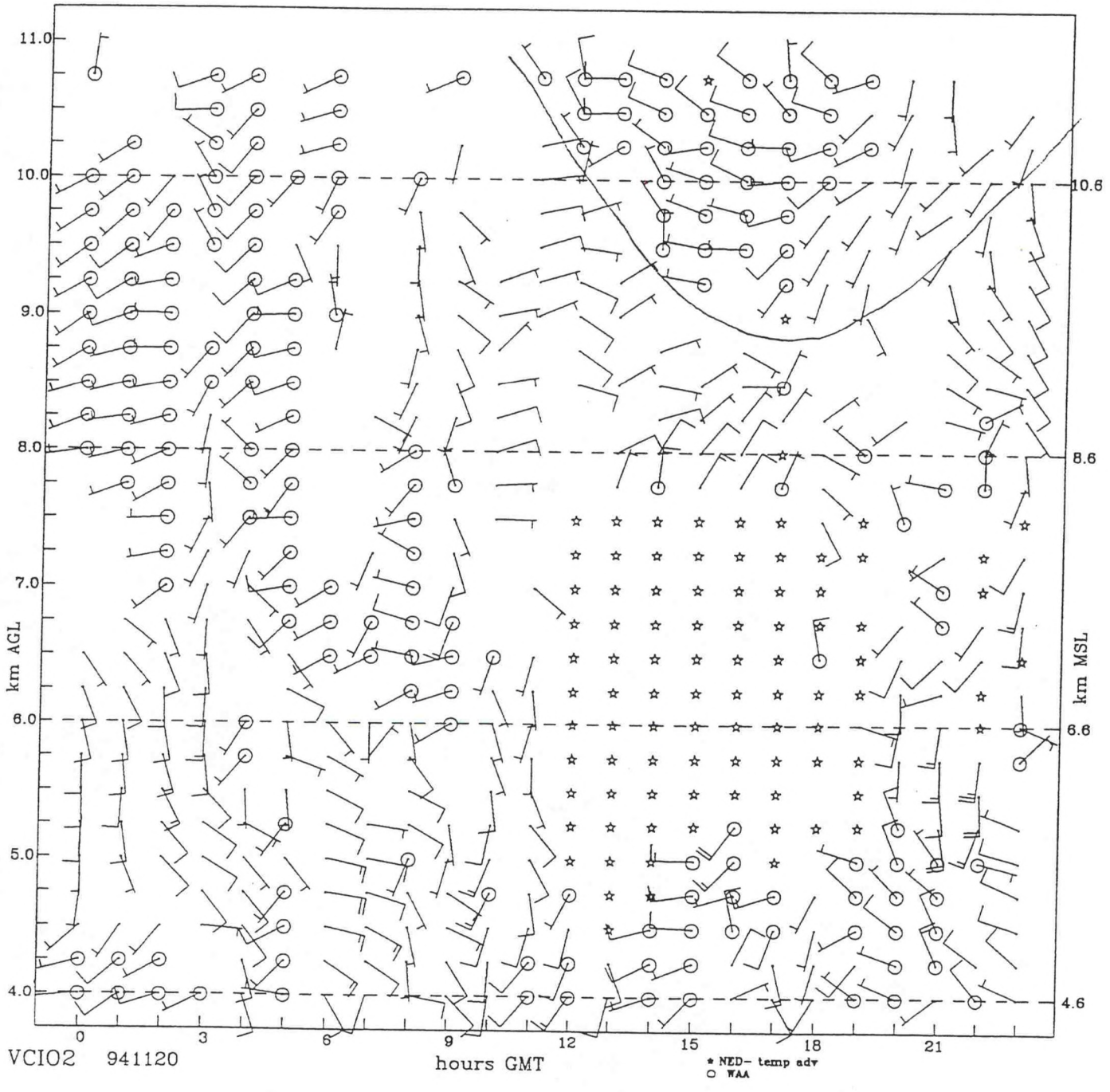

Figure 7. Thermal winds plot from Vici, Oklahoma (Western Oklahoma). November 20, 1994, barbs are in m/s, 1000 meter intervals, and circles indicated warm advection, no circles indicate cold advection.

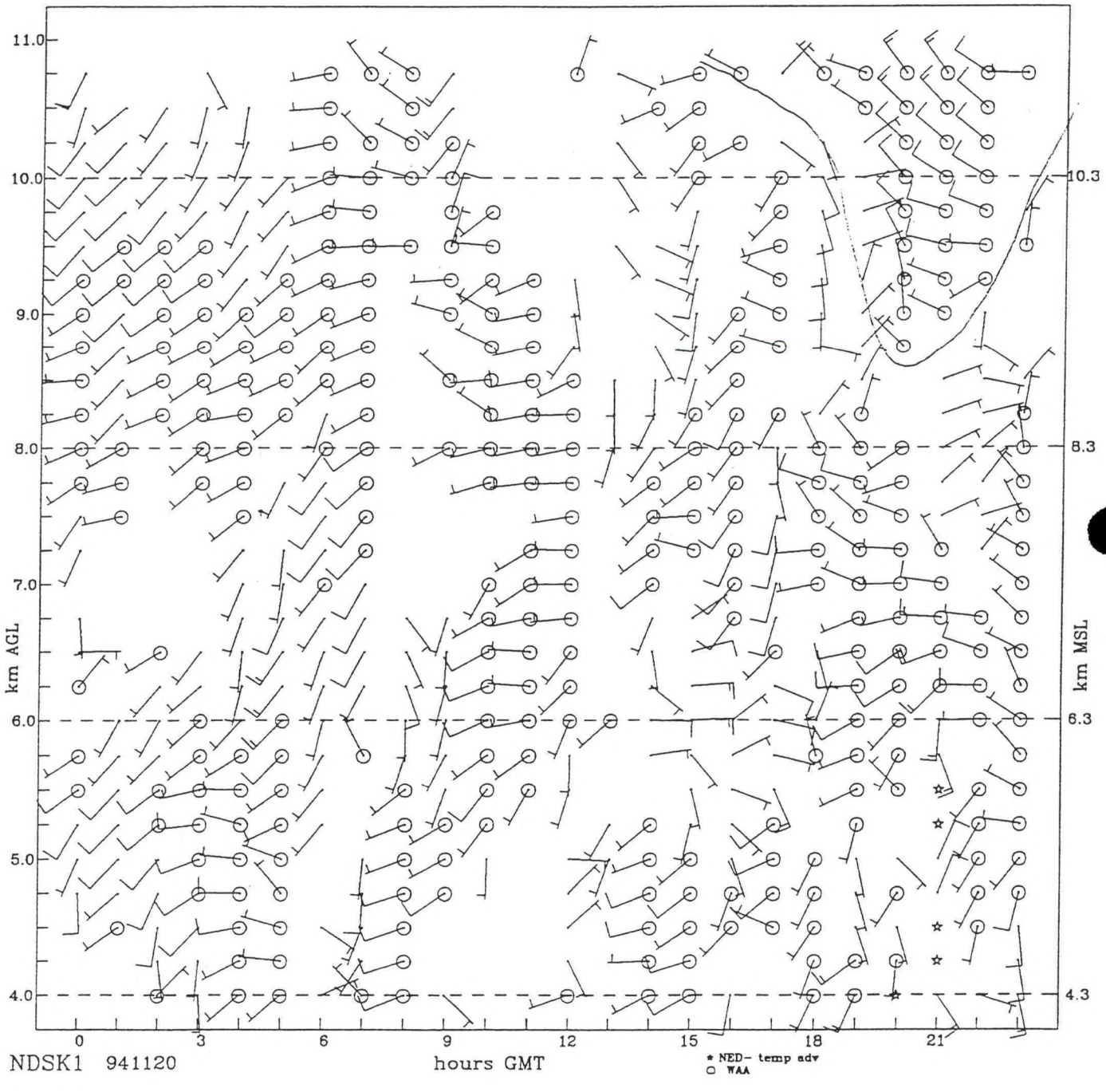

Figure 8. Same as Figure 7 except for location is Neodesha, Kansas (Southeast Kansas).

Short and Medium Term Road Ice Predictions for Winter Road Maintenance

J. Shao[1] and P. J. Lister[2]

1. INTRODUCTION

A numerical road surface temperature and surface state prediction model (called Icebreak model) is described and validated for its 24 hour forecast and 1 to 3 hour automated nowcasts. The comparison between model predictions and sensor measurements show that its 24 and 1 to 3 hour forecasts of minimum, maximum and overall (every hour in all days) temperatures are little biased. The root-mean-square (RMS) error of minimum temperature forecasts is about O.8°C for 24 hour forecast, and less than 0.5°C, 0.7°C and 0.9°C for 1, 2 and 3 hour nowcasts, In average, its accuracy of predicting frost and no frost nights is over 97 percent for both 24 hour forecast and 1 to 3 hour nowcasts. More than 75 percent of dry, wet and ice surface states are accurately predicted in 24 hour period, and the accuracy is over 80 percent for dry and ice states in nowcasting. More than 75 percent wet state nowcasting is correct in most countries.

The weather conditions in winter in North America, Western and North Europe and some other countries (e.g., Japan) are so serious that snow, ice and frost frequently occur on road surface, giving slippery and dangerous driving conditions. In Sweden alone, the number of road accidents due to snow or ice on road surface is about 2,000 every year (Wendt 1993). With the rapid upsurge in motor vehicle numbers and the more crucial role of road transport for economic development in future, winter road maintenance to produce safer and more efficient road transport is becoming a major concern of road authorities and highway engineers. The direct protection of roads from snow and ice may take a variety of forms, but the most common way of preventing an icy road is to spread a de-icing chemical such as salt. However, an excess of salt usage costs both extra labor and extra money. More importantly, it has been found that frequent use of salt leads to attendant problems of vehicle and bridge corrosion, water and soil pollution, delay in growth of trees and shrubs, and death of some buds and young shoots (OECD 1989; Keyser 1981; Highway Research Board 1967). In Britain, the cost of corrosion of motor vehicles in the early 1970's was estimated about £50-60 million per year (Bishop 1969). In order to provide a safe driving condition and minimize the damage to the vehicles and environment, the practice of salting (and gritting) should be taken only when necessary. This requires information about when and where ice or frost is to occur, well in advance of the occurrence of ice or frost. A recent survey commissioned by the UK Met. Office shows that about £170 million ($272 million) and 25 to 50 lives have been saved each year with road ice prediction system in the UK (Thomes 1994). In Wisconsin, USA, the use of winter weather system which includes a numerical road ice prediction model and remote automatic roadside weather stations can save $75,500 and reduce salt usage by 2,500 tons during a single winter storm (Stephenson 1988).

To provide such information, several numerical models (Shao & Lister 1995 a & b; Shao et al., 1994; Shao 1990; Kempe 1990; Rayer 1987; Thornes 1984; Nysten 1980) have been developed in the last decade. Of these models, one is called Icebreak (Shao 1990) and aims to provide forecasts of road surface temperature and surface state from 1 hour to 72 hours ahead. This paper presents the results of worldwide validation of the model for its 24 hour forecast and nowcasting (1 to 3 hours) at different sites (such as bridge, open or porous asphalt/concrete, dense or conventional asphalt/concrete).

1. Corresponding author address: J. Shao, Vaisala TMI Ltd., Vaisala House, 349 Bristol Road, Birmingham, B5 7SQ UK.
2. P. J. Lister, Vaisala TMI Ltd., Vaisala House, 349 Bristol Road, Birmingham, B5 7SQ, UK.

2. DESCRIPTION OF THE MODEL

The model is based on an unsteady one-dimensional heat conduction equation, i.e.:

$$C_m \frac{\partial T}{\partial t} = \frac{\partial}{\partial z} (\kappa \frac{\partial T}{\partial z}) \quad (1)$$

where C_m is the heat capacity, κ is the conductivity, T(z, t) is the temperature at time t and depth z. It is assumed that the road surface and underlying sub-layers are horizontally homogeneous so that heat transfer in a lateral direction can be neglected. The model considers a vertical pillar with unit cross-section area, extending to a depth (usually one meter but variable, depending on local climatic conditions) deep enough to eliminate the diurnal oscillation of temperature. Its lower boundary condition is straightforward and treated as a constant of local climatic soil temperature at the depth. The upper boundary condition is complicated and is expressed by an energy balance equation which contains both surface temperature and time. The energy balance equation is expressed as:

$$(1-\alpha_s)S + L^1(T_s) + H(T_s) + LE(T_s) + G(T_s) = 0 \quad (2)$$

where S is the solar irradiance, α_s is the surface albedo, L^1 is the net longwave irradiance, H and LE are the sensible and latent heat flux densities, G is the ground conductive heat flux density, and T_s is the road surface temperature.

By discriterizing the heat conduction equation and paramiterizing the energy balance equation, road surface temperature is generated forward. To off-set the influence of topographical shading effect on energy balance, the model introduces in a separate algorithm to simulate the shading effect and adjust the energy budget at the road surface. The prediction of road surface state, such as dry, wet, frost or icy, is carried out by considering surface temperature, past and current precipitation status and the exchange of moisture between the road surface and the overlying atmosphere.

It needs to be mentioned that in the model, it assumes that ice or frost will occur when surface temperature drops down to and below 0°C and road surface has been or is to be moist or wet. This assumption is not always true, especially when road is salted when freezing point can be actually well below 0°C. Therefore, it can be expected that the model will under-predict wet state or over-predict ice state. At the current stage, information about the amount of residual salt and freezing point has not yet become available to the model. The lack of such information will unavoidably have a negative influence on the accuracy of state prediction by the model.

In a medium term (namely 24 hour ahead) forecast, meteorological parameters (such as air temperature, dew point, wind speed, cloud cover and precipitation) are input from meteorologist's forecasts. Such external input is in a 3-hourly interval and usually updated daily. For the short term forecast (i.e., 1 to 3 hour ahead, called nowcasting), it is unreasonable to require the input to be updated every hour or so, especially if the model is not being run within a meteorological institute with easy access to meso-scale model output. Therefore, a fully automatic and intelligent prediction model, requiring no external resources, is desired. For this purpose, statistic and logical-reasoning methods are employed in the Icebreak model to project required meteorological parameters, based on sensor measurements of air temperature, dew point, wind speed, precipitation, road surface

temperature and state at the site in previous 24 hours. The generated inputs are then fed into the model to produce nowcasts of surface temperature and surface state. More details about the model can be found in the papers by Shao & Lister (1995 a & b) and Shao et al. (1994).

3. TESTING SITES

In meteorological modeling, it is quite often the case that a model performs well in one region or country but fails in another due to variety and complexity of weather or atmospheric conditions, and local topographical environment. For this reason, the validation of the Icebreak model is carried out at different sites (conventional asphalt/concrete, porous asphalt/concrete, bridge, open or shaded topography) in different countries.

To provide an objective measure of accuracy and reliability of medium term forecast of the model, a retrospective analysis using measured input is carried out. Seven sites in four countries, where actual cloud observation data is provided, are chosen for the validation. In such a retrospective validation, air temperature, dew point, wind speed and precipitation are sensor measurements at each test site. Total cloud amount (in octas) and single dominant cloud type (O for no cloud, 1, 2 and 3 for low, medium and high cloud) are observations by professional meteorologists near the site. The input is in a 3-hourly interval, starting at noon and lasting for the next 24 hours. For the validation of nowcasting, it can be carried out at more sites, since nowcasting only requires sensor measurements, not human observations at all. The total number of sites for nowcasting reaches 17 in 7 countries.

At these test sites, some are of 2 to 4 surface sensors buried in different lanes or sections of the road near the forecast site. The total number of sensors for the validation of 24 hour forecast is 13. For nowcasting, it is 41. Table 1 gives brief information on these test sites.

4. VALIDATION OF 24 HOUR FORECAST

The validation of the model is twofold: temperature and state. The validation in temperature is carried out by comparing model forecasts with measurements (forecast minus actual) in terms of bias and root-mean-square (RMS) error. Therefore, a negative bias in the comparison means that the model forecast is colder (or earlier in comparing time of frost) than actual. The comparison of overall temperature is based on every hourly predictions and measurements for all days, while the comparison of maximum and minimum is on daily basis. The prediction of surface state is categorized into dry, wet (including moist) and ice (including frost). It is compared to actual state on an hourly basis.

The results of 24 hour comparison is shown in Table 2. It is seen from the table that all temperature predictions at these sites are almost unbiased. Their RMS errors are less than 1.4°C for overall temperature, less than 2.5°C for maximum and less than 1°C for minimum. The accuracy in predicting frost (surface temperature <=0°C) and no frost (surface temperature >0°C) is generally higher than 92 percent. The error of predicting the time when frost first occurs varies from 1 hour earlier to 66 minutes later.

TABLE 1
Description of test sites for model validation

Country	Site Code	Sensor	No. of Days	Open Asphalt	Bridge	24 hr fcst.	1-3 hr ncst.
Finland	UT001	1	65	No	No	Yes	No
Italy	CP001	1	27	No	No	Yes	No
	CP002	1	27	No	Yes	Yes	No
	SM001	1	53	No	No	Yes	Yes
UK	ST009	1	10	No	No	Yes	Yes
		2	10	Yes	No	Yes	Yes
	LEEM1	1	169	Yes	No	Yes	Yes
		2 & 3	169	No	No	Yes	Yes
Austria	TR001	1, 2 & 3	9	No	Yes	No	Yes
	TR002	1	6	Yes	No	No	Yes
		2 & 3	6	Yes	Yes	No	Yes
	TR003	1 & 2	6	No	Yes	No	Yes
	TR004	1	6	Yes	Yes	No	Yes
		2	6	No	No	No	Yes
		3	6	Yes	No	No	Yes
		4	6	No	Yes	No	Yes
	TR001	1	6	Yes	No	No	Yes
		2	6	Yes	Yes	No	Yes
		3	6	No	No	No	Yes
		4	6	No	Yes	No	Yes
Switzerland	WD001	1 & 2	33	No	Yes	No	Yes
Holland	GM004	1	18	No	No	Yes	Yes
		2	18	No	No	No	Yes
	GN001	1, 2 & 3	19	No	No	Yes	Yes
	NM002	1, 2 & 3	9	No	No	No	Yes
Norway	RL002	1 & 2	32	No	No	No	Yes
	RL004	1 & 2	36	No	No	No	Yes
	RL005	1 & 2	31	No	No	No	Yes
	RL006	1 & 2	40	No	No	No	Yes
Japan	CA001	1	53	No	No	No	Yes

TABLE 2
Comparison of 24 hour temperature forecast, accuracy (%) of frost/no frost prediction and time error (minutes) in predicting frost

Site	Sensor	Overall Bias	Overall RMS	Maximum Bias	Maximum RMS	Minimum Bias	Minimum RMS	Accuracy (%)	Time error
UT001	1	-0.17	1.40	0.19	1.63	-0.04	0.7	96.9	9
CP001	1	0.19	1.24	0.23	1.87	-0.14	0.65	100.0	-
CP002	1	0.21	1.24	-0.23	1.64	-0.24	0.68	100.0	-
SM001	1	0.01	1.36	0.07	2.45	-0.06	0.77	94.3	-2
ST009	1	-0.08	1.04	-0.30	1.62	0.14	0.95	100.0	30
	2	-0.07	1.08	-0.02	1.69	0.08	0.95	100.0	-60
LEEM1	1	-0.02	1.39	0.03	2.21	-0.07	0.81	93.5	66
	2	-0.04	1.21	0.29	1.82	-0.18	0.77	94.1	25
	3	-0.13	1.36	-0.40	2.26	-0.12	0.85	92.3	60
GM004	1	-0.26	0.95	-0.27	1.83	-0.04	0.72	94.4	-45
GN001	1	-0.08	1.21	-0.32	1.54	0.13	0.7	100.0	-15
	2	-0.07	1.20	-0.26	1.45	0.07	0.73	100.0	-23
	3	-0.04	1.19	-0.22	1.33	0.01	0.67	100.0	-8
Mean	-	-0.04	1.22	-0.09	1.80	-0.04	0.77	97.3	3

To gain visual judgement on model performance, Figure 1 displays the averaged hourly error of 24 forecast at a convectional asphalt site in Italy. It shows that the forecasts well fitted sensor measurements, especially at night. Figure 2 exhibits hourly bias and standard deviation (SD) of 24 hour temperature predictions at the bridge site of Ponte Po (CP002) in Italy. It is seen from the figure that the model prediction at the site has a colder bias near dawn and a warmer basin the morning. A significant diurnal variation of SD can also be seen in the figure, with a much smaller SD at night (<=0.9°C) and a much lager SD near noon (2.6°C). This reflects the fact that solar radiation which plays an important role in road surface energy balance at daytime is difficult to be calculated due to any possible change or uncertainty of cloud amount and cloud type during the 3 hour interval of input. The prediction of daily minimum at Leeming site (sensor 1, open asphalt) is plotted against actual in Figure 3. It is clear that all predictions are well in accordance with the actual.

The sensor measurements of road surface state are only available at some of the test sites. The results of comparison of predictions to measurements at these sites are displayed in Table 3. Generally, the model prediction coincides with the actual states. Its accuracy for each state is at or over 75 percent.

5. VALIDATION OF NOWCAST

Unlike a 24 hour forecast, a nowcast does not necessarily need forecast input from a meteorologist, as inputs required by the model are projected by the model itself This leads to more sites coming into this validation test. The results of temperature comparison between nowcasts and actual are given in Tables 4 (a-c). The results show that:

A. The model has a near-zero bias for all temperature forecasts and the smallest RMS error in minimum temperature and the largest RMS error in maximum temperature.

B. While its bias remains near zero, the averaged RMS error of the model increases as nowcasting period increases from 1 to 3 hour (especially for maximum temperature).

C. The averaged RMS error of minimum temperature forecasts is less than 0.5°C, 0.7°C and 0.9°C respectively for 1, 2 and 3 hour forecasts.

D. The accuracy of frost and no frost predictions varies from 81. percent to 100 percent and its average is over 97 percent for 1 to 3 hour forecasts.

E. The mean error in predicting the time when temperature falls at or below 0°C is only 4 minutes earlier, 9 and 22 minutes later than actual for 1, 2 and 3 hour predictions.

TABLE 3

Hourly comparison of 24 hour surface state predictions to measurements (San Pietro, Italy, 19/01/1994-20/02/1994)

Actual State	Dry			Wet			Ice		
UT001:									
No. of observations		867			171			457	
Forecast state	Dry	Wet	Ice	Dry	Wet	Ice	Dry	Wet	Ice
No. of forecasts	644	47	176	25	118	28	75	39	343
Percetage (%)	74.3	5.4	20.3	14.6	69.0	16.4	16.4	8.5	75.1
CP001:									
No. of observations		495			126			0	
Forecast state	Dry	Wet	Ice	Dry	Wet	Ice	Dry	Wet	Ice
No. of forecasts	420	75	0	6	120	0	-	-	-
Percetage (%)	84.8	15.2	0.0	4.8	95.2	0.0	-	-	-
CP002:									
No. of observations		401			220			0	
Forecast state	Dry	Wet	Ice	Dry	Wet	Ice	Dry	Wet	Ice
No. of forecasts	320	81	0	31	189	0	-	-	-
Percetage (%)	79.8	20.2	0.0	14.1	79.8	0.0	-	-	-
SM001:									
No. of observations		748			344			127	
Forecast state	Dry	Wet	Ice	Dry	Wet	Ice	Dry	Wet	Ice
No. of forecasts	557	167	24	53	272	19	21	10	96
Percetage (%)	74.5	22.3	3.2	15.4	79.1	5.5	16.5	7.9	75.6
Average (%)	78.4	15.8	5.9	12.2	80.8	5.5	16.5	8.2	75.4

TABLE 4a

Results of comparison of 1 hour predictions of overall, maximum and minimum temperatures; accuracy of frost/no frost predictions and time error (min) in predicting frost

Site	Sensor	Overall		Maximum		Minimum		Accuracy	Time
		Bias	RMS	Bias	RMS	Bias	RMS	(%)	error
SM001	1	0.0	0.59	0.01	1.43	0.02	0.21	98.1	13
ST009	1	-0.06	0.78	-0.62	1.25	-0.02	0.47	100.0	0
	2	-0.08	0.84	-0.53	1.31	-0.54	0.55	100.0	0
LEEM1	1	0.04	0.75	-0.03	1.23	0.03	0.45	96.2	13
	2	0.03	0.63	0.0	0.98	0.07	0.44	95.6	10
	3	0.0	0.79	-0.09	1.30	0.03	0.51	95.6	21
TR001	1	0.14	0.40	-0.07	0.31	0.28	0.39	100.0	7
	2	0.07	0.39	-0.13	0.66	0.11	0.20	100.0	13
	3	-0.01	0.45	-0.44	0.94	0.07	0.13	100.0	13
TR002	1	-0.07	0.36	0.25	0.39	-0.12	0.29	100.0	10
	2	-0.09	0.27	0.08	0.20	-0.13	0.22	100.0	20
	3	0.03	0.28	0.27	0.42	0.05	0.20	100.0	0
TR003	1	-0.06	0.31	-0.22	0.70	0.03	0.15	100.0	-20
	2	0.0	0.30	0.12	0.55	0.18	0.35	100.0	-10
TR004	1	0.01	0.40	0.58	0.74	-0.05	0.34	100.0	-10
	2	-0.20	0.36	-0.13	0.25	-0.25	0.34	100.0	-80
	3	-0.02	0.38	0.47	0.61	0.07	0.24	100.0	0
	4	0.0	0.36	0.18	0.20	0.07	0.32	100.0	0
TR005	1	-0.20	0.45	0.22	0.42	-0.13	0.27	100.0	-10
	2	-0.17	0.45	0.23	0.49	0.0	0.34	100.0	-10
	3	-0.07	0.34	-0.18	0.44	-0.03	0.13	100.0	-20
	4	-0.08	0.47	0.0	0.44	0.07	0.25	100.0	-20
WD001	1	0.05	0.53	0.06	0.60	0.20	.05	87.9	0
	2	0.01	0.54	0.02	0.56	0.07	0.57	93.9	8
GM004	1	-0.14	0.86	0.36	1.25	-0.14	0.60	100.0	0
	2	0.23	1.05	0.81	1.71	0.14	0.83	100.0	0
Figure	1	-0.35	1.54	-0.72	1.76	0.03	0.46	100.0	-68
	2	-0.33	1.53	-0.62	1.67	0.02	0.48	100.0	-68
	3	-0.32	1.49	-0.65	1.54	0.03	0.48	100.0	-68
NM002	1	0.02	0.90	0.11	0.69	-0.16	0.74	100.0	0
	2	-0.01	0.82	0.10	0.61	-0.09	0.63	100.0	0
	3	0.11	0.89	0.11	0.61	-0.01	0.71	100.0	0
RL002	1	0.09	1.23	-0.50	1.69	0.22	0.82	93.8	32
	2	0.13	1.19	-0.18	1.51	0.20	0.81	93.8	32
RL004	1	0.13	1.07	0.0	1.46	-0.03	0.64	97.2	-3
	2	0.07	1.01	-0.09	1.31	-0.01	0.59	91.7	-6
RL005	1	0.02	0.94	0.44	1.55	0.0	0.57	93.5	7
	2	-0.09	0.97	0.20	1.65	-0.10	0.55	96.8	-11
RL006	1	0.11	0.97	0.06	1.53	0.09	0.31	100.0	40
	2	0.04	1.32	-0.41	1.26	0.05	0.32	100.0	23
CA001	1	-0.02	0.91	-0.27	1.03	0.24	0.95	100.0	0
Mean	-	-0.03	0.73	-0.03	0.96	0.02	0.45	98.4	-4

TABLE 4b

Results of comparison of 2 hour predictions of overall, maximum and minimum temperatures; accuracy of frost/no frost predictions and time error (min) in predicting frost.

Site	Sensor	Overall		Maximum		Minimum		Accuracy	Time
SM001	1	0.04	1.15	0.68	2.5	-0.1	0.53	98.1	-8
ST009	1	-0.01	0.96	0.07	1	-0.1	0.47	100.0	0
	2	-0.06	1.01	0.39	1.06	-0.1	0.52	100.0	0
LEEM1	1	0.02	1.36	-0.2	1.86	-0.1	0.77	96.2	47
	2	0.01	1.184	-0.06	1.44	-0.15	0.76	95.0	38
	3	-0.01	1.63	0.18	2.24	-0.14	0.87	95.0	34
TR001	1	0.09	0.63	-0.1	0.37	0.12	0.51	100.0	7
	2	0.04	0.64	-0.02	0.65	-0.02	0.33	100.0	13
	3	-0.04	0.73	-0.49	0.95	-0.06	0.28	100.0	20
TR002	1	-0.04	0.63	0.4	0.69	-0.3	0.58	100.0	40
	2	-0.08	0.40	0.43	0.72	-0.23	0.45	100.0	20
	3	0.06	0.60	0.73	0.85	-0.08	0.41	100.0	30
TR003	1	-0.04	0.64	0.25	0.98	-0.1	0.22	100.0	10
	2	0.02	0.6	0.3	0.72	-0	0.31	100.0	10
TR004	1	0	0.6	0.68	0.76	-0.1	0.41	100.0	20
	2	-0.19	0.48	0.1	0.42	-0.4	0.47	100.0	-70
	3	0.05	0.64	0.78	0.93	0	0.28	100.0	10
	4	0.09	0.7	0.73	0.86	0.12	0.32	100.0	10
TR005	1	-0.24	0.66	0.33	0.5	-0.2	0.43	100.0	0
	2	-0.19	0.73	0.5	0.66	-0	0.39	100.0	10
	3	-0.05	0.42	0.15	0.76	-0.1	0.19	100.0	-20
	4	-0.02	0.67	0.23	0.6	0.08	0.25	100.0	10
WD001	1	0.05	1.01	0.33	1.12	-0	0.8	87.9	11
	2	-0.01	1.01	0.18	0.93	-0.2	0.86	93.9	38
GM004	1	-0.17	1.04	-0.1	0.81	-0.2	0.75	100.0	0
	2	0.06	1.19	0.25	1.31	-0.1	0.88	100.0	0
GN001	1	-0.41	1.61	-0.4	2.05	-0.9	0.68	100.0	-86
	2	-0.38	1.61	0.3	2.03	-0.1	0.68	100.0	-86
	3	-0.34	1.6	-0.2	1.87	-0.1	0.66	100.0	-52
NM002	1	0.12	1.22	0.06	0.83	-0.1	1.12	100.0	30
	2	0.07	1.15	0.01	0.75	-14	0.94	100.0	0
	3	0.2	1.21	0.09	0.77	-0.1	0.97	100.0	30
RL002	1	0.09	1.63	-0.2	1.85	-0	1.06	90.6	39
	2	0.13	1.58	0.15	1.79	-0	1.05	90.6	49
RL004	1	0.2	1.51	0.01	1.6	-0.3	1.07	95.2	28
	2	0.12	1.46	-0.2	1.59	-0.4	1.07	95.2	5
RL005	1	0.11	1.2	0.72	2.48	-0.1	0.73	85.7	8
	2	-0.02	1.27	0.52	2.59	-0.2	0.72	96.4	9
RL006	1	0.06	1.4	0.17	1.84	-0.1	0.6	100.0	90
	2	0.03	1.96	-0.5	1.58	-0.1	0.64	100.0	30
CA001	1	0.03	1.52	-0.1	1.72	-0.1	1.43	98	11
Mean	-	-0.02	1.06	0.16	1.24	-0.1	0.65	98	9

TABLE 4c

Results of comparison of 3 hour predictions of overall, maximum and minimum temperatures; accuracy of frost/no frost predictions and time error (min) in predicting frost

Site	Sensor	Overall		Maximum		Minimum		Accuracy	Time
		Bias	RMS	Bias	RMS	Bias	RMS	(%)	error
SM001	1	-0.04	1.47	0.49	3.18	-0.10	0.78	92.5	-4
ST009	1	0.06	1.17	1.09	2.90	0.21	0.51	100.0	0
	2	0.09	1.34	1.40	3.23	0.23	0.54	100.0	0
LEEM1	1	0.07	1.65	-0.17	1.88	-0.13	1.01	94.4	79
	2	0.04	1.47	-0.03	1.56	-0.18	1.00	93.2	37
	3	0.02	1.95	0.06	2.18	-0.15	1.13	95.1	61
TR001	1	0.10	0.61	-0.23	0.42	0.14	0.53	100.0	17
	2	0.05	0.82	-0.73	1.19	-0.01	0.26	100.0	17
	3	-0.03	0.74	-0.97	1.25	-0.03	0.23	100.0	34
TR002	1	-0.04	0.63	0.04	0.69	-0.32	0.58	100.0	40
	2	-0.02	0.56	0.83	1.23	-0.12	0.66	100.0	50
	3	0.14	0.71	1.35	1.62	0.0	0.63	100.0	0
TR003	1	-0.01	0.79	1.15	1.68	0.05	0.52	100.0	10
	2	0.03	0.86	1.43	1.98	0.07	0.52	100.0	20
TR004	1	0.05	0.86	2.02	2.39	-0.12	0.50	100.0	30
	2	-0.19	0.57	0.53	1.18	-0.40	0.52	100.0	-60
	3	0.11	0.89	1.85	2.25	-0.03	0.38	100.0	40
	4	0.13	0.94	1.55	2.08	0.05	0.35	100.0	50
TR005	1	-0.24	0.80	1.15	2.06	-0.13	0.54	100.0	10
	2	-0.12	0.84	1.68	2.33	0.07	0.62	100.0	-10
	3	0.02	0.60	0.98	1.56	-0.05	0.35	100.0	10
	4	0.01	0.85	1.40	2.25	0.12	0.47	100.0	10
WD001	1	0.01	1.32	0.29	1.38	-0.22	1.01	81.8	11
	2	-0.07	1.29	0.26	1.39	-0.31	1.05	87.9	71
GM004	1	-0.25	1.40	0.08	1.38	-0.47	0.94	100.0	0
	2	-0.19	1.37	0.66	1.75	-0.35	0.93	100.0	0
GN001	1	-0.43	1.66	-0.32	1.83	-0.13	0.93	100.0	-52
	2	-0.40	1.66	-0.19	1.81	-0.15	0.92	100.0	-43
	3	-0.37	1.67	-0.20	1.62	-0.19	0.88	100.0	-60
NM002	1	0.16	1.43	0.06	0.87	-0.30	1.44	100.0	60
	2	0.10	1.39	0.03	0.85	-0.38	1.39	100.0	30
	3	0.25	1.43	0.07	0.88	-0.31	1.35	100.0	60
RL002	1	0.23	1.84	-0.26	2.05	-0.14	1.15	90.6	49
	2	0.28	1.78	0.09	1.87	-0.14	1.31	90.6	32
RL004	1	0.16	1.93	-0.31	1.75	-0.90	2.05	93.8	32
	2	0.07	1.85	-0.66	1.77	-0.93	2.06	93.8	14
RL005	1	0.26	1.34	0.72	2.01	-0.21	0.63	85.0	15
	2	0.10	1.36	0.48	1.93	-0.32	0.72	85.0	0
RL006	1	0.21	1.58	-0.12	2.13	-0.09	0.70	100.0	146
	2	0.01	1.53	-0.57	1.66	-0.12	0.75	100.0	60
CA001	1	0.06	2.03	0.30	2.31	-0.27	1.96	100.0	19
Mean	-	0.01	1.24	0.43	1.76	-0.16	0.85	97.2	22

The averaged frequency of temperature nowcasts falling into certain error bands is displayed in Figures 4 and 5. The figures show that both temperature predictions fall into a narrow (-1 to +1°C) band. For minimum, its 95 percent, 87 percent and 83 percent of 1, 2 and 3 hour predictions are within this error band. For overall temperature, the figures are 82 percent, 72 percent and 65 percent respectively.

The results of comparison in surface state (Table 5) demonstrate that over 80 percent of dry and ice state predictions were correct for up to 3 hours. The accuracy of wet state prediction is relatively low, especially in Austria. However, if Austrian sites where heavy salting was possible are excluded, the accuracy reaches 75 percent.

Table 5
Accuracy (%) of hourly surface state nowcasts compared to sensor measurements
(Note: "-" means that no such state occurs during the test period.)

Site	Sensor	1 hour			2 hour			3 hour		
		Dry	Wet	Ice	Dry	Wet	Ice	Dry	Wet	Ice
SM001	1	80.7	95.5	96.9	76.3	91.9	91.6	73.0	88.3	90.1
TR001	1	98.8	26.9	100.0	96.3	15.4	88.9	89.1	33.3	88.9
	2	96.6	21.9	96.6	95.2	18.8	89.7	90.0	15.6	89.7
	3	98.2	0.0	97.6	97.0	0.0	90.2	94.9	0.0	90.2
TR002	1	87.5	16.7	-	86.5	21.4	-	86.5	21.4	-
	2	92.8	-	-	91.3	-	-	88.4	-	-
	3	97.1	6.3	100.0	97.1	9.4	100.0	92.6	7.8	66.7
TR003	1	89.1	32.6	100.0	85.9	25.6	66.7	82.6	16.3	100.
	2	87.5	20.6	-	85.6	17.6	-	79.8	23.5	-
TR004	1	86.4	16.7	-	86.4	16.7	-	85.6	16.7	-
	2	98.0	31.8	-	96.0	34.1	-	90.0	30.7	-
	3	88.1	16.7	-	86.5	25.0	-	84.1	25.0	-
	4	89.5	43.8	-	85.1	31.3	-	83.3	25.0	-
TR005	1	87.8	26.1	-	87.0	17.4	-	83.5	21.7	-
	2	87.1	18.2	-	86.2	18.2	-	82.8	18.2	-
	3	90.0	62.5	-	88.5	50.0	-	86.9	62.5	-
	4	89.6	46.2	-	88.0	46.2	-	84.0	23.1	-
WD001	1	85.6	81.6	96.2	82.8	75.8	91.7	74.4	73.1	85.7
	2	83.6	87.7	97.7	79.0	84.7	90.6	75.1	82.5	84.4
RL002	1	89.3	89.8	79.2	88.0	83.8	75.0	88.0	81.7	75.0
	2	87.3	87.5	78.3	86.0	80.2	78.3	86.8	79.7	69.6
RL004	1	93.7	77.3	75.0	91.6	62.8	78.6	87.9	46.7	71.4
	2	95.0	78.6	81.3	92.4	63.2	85.7	88.8	48.5	85.7
RL005	1	95.7	89.5	93.2	95.4	81.4	79.4	89.9	81.9	82.1
	2	96.9	84.1	95.8	96.6	90.1	78.6	84.1	80.1	62.5
RL006	1	95.7	80.5	87.9	93.4	85.2	92.9	91.9	78.8	78.6
	2	95.0	79.6	100.0	93.3	86.2	100.0	89.5	78.9	76.9
CA001	1	92.7	97.2	100.0	87.3	90.0	95.4	85.2	83.2	85.0
Mean	-	91.3	52.4	89.6	89.3	48.6	84.9	86.0	46.1	80.6

6. CONCLUSIONS

The validation of the Icebreak model carried out in this test for 24 hour forecast and 1 to 3 hour nowcasts shows that:

A. Both 24 hour forecasts and 1 to 3 hour nowcasts show a near-zero bias in predicting minimum, maximum and overall road surface temperatures.

B. In 24 hour forecast, its mean RMS error is about 0.8°C, 1.2°C and 1.8°C for minimum, overall and maximum temperatures. The mean accuracy of frost and no frost prediction is about 97 percent. In average, it is about 3 minutes later to predict the first hour when frost occurs. In average, over 75 percent of surface states (dry, wet and ice) are correctly predicted.

C. In nowcasts, its averaged RMS error is within a range of 0.5~0.9°C, 0.7~1.2°C and 1.0~1.8°C for minimum, overall and maximum temperature forecasts for 1~3 hours ahead. Over 95 percent of minimum temperature forecasts are within an absolute 2°C error band for up to 3 hours ahead. Its average accuracy of frost and no frost prediction is over 97 percent for up to 3 hours, and its frost time prediction is 4 minutes earlier, 9 and 22 minutes later for 1, 2 and 3 hour nowcasts. Over 80 percent dry and ice state predictions are correct for up to 3 hours. The accuracy is over 75 percent for wet state if Austrian site are excluded.

7. ACKNOWLEDGMENTS

The authors wish to thank many anonymous meteorologists, highway engineers and staff members of Vaisala in Austria, Holland, Italy, Japan, Norway, Switzerland and the UK for their generosity of collecting and providing data for the tests in this paper.

8. REFERENCES

Bishop, R.R., 1969: Corrosion of motor vehicles by de-icing salt. RRL Report No 232. Road Research Laboratory, Ministry of Transport, Crowthorne.

Department of Transport, 1987: Winter maintenance of motorways and other trunk roads -Statement of service and code practice.

Highway Research Board, 1967: Environmental considerations in use of deicing chemicals. Highway Research Record No. 193. Highway Research Board, National Research Council, Washington, D.C.

Kempe, C., 1990: An estimation of the value of special weather forecasts in a pilot project for road authorities in Sweden. Proceedings of the Technical Conference on Economic and Social Benefits of Meteorological and Hydrological Services, Geneva, WMO.

Keyser, J.H., 1981: Chemical and abrasives for snow and ice control. Handbook of Snow, ed, by D.M. Gray & D.H. Male. Pergamon Press, Toronto. 580-612.

Nysten, E., 1980: Determination and forecasting of road surface temperature in the cost 30 automatic road station (CARS). Tech. Report No. 23. Finnish Met. Institute, Helsinki, 32 pp.

OECD, 1989: Road Transport Research Program - Curtailing usage of de-icing agents in winter maintenance. Organization for Economic Co-operation and Development, Paris, 125 pp.

Ponting, M., 1989: Flighway weather forecasting during winter - A cost-benefit study of the need for improved forecasting and communications for effective highway maintenance. MSC thesis, University of Birmingham, UK.

Rayer, P.J., 1989: The Meteorological Office forecast road surface temperature model. Meteorol.. Mag., 116: 180-191.

Shao, J. , and P.J. Lister, 1995a: An automated nowcasting model of road surface temperature and state for winter road maintenance. Submitted to *J. Appl. Meteor.*

_____, and _____, 1995b: The prediction of road surface state and simulation of the shading effect. *Boundary-Layer Meteor.*, 73, 411-419.

_____, _____, and A. McDonald, 1994: A surface temperature prediction model for porous asphalt pavement and its validation. *Meteorol.. Appl.*, 1: 129-134.

_____, 1990: A winter road surface temperature prediction model with comparison to others. Ph.D. thesis, University of Birmingham, UK, 245 pp.

Stephenson, T.E., 1988: Wisconsin's winter weather system. Proceedings of the 4th International Conference on Weather and Road Safety, Florence, Italy,. Academia Dei Georgofili, 61-101.

Thornes, J.E., 1984: The prediction of ice formation on motorways. Ph.D. thesis, University College, London.

_____, 1994: Salt of the Earth. Surveyor.

Wendt, K., 1993: Benefits of nowcasting to road maintenance in wintertime in Sweden. Proceedings of the 1st European Conference on Applications of Meteorology, Oxford, UK. 27.

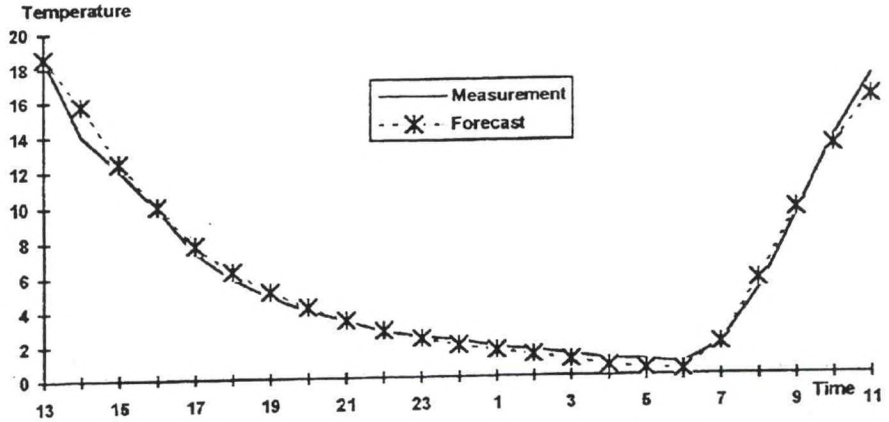

Figure 1. Comparison of averaged hourly predictions with sensor measurements (24 hour forecast, San Pietro, Italy, January 19 - March 15, 1994.

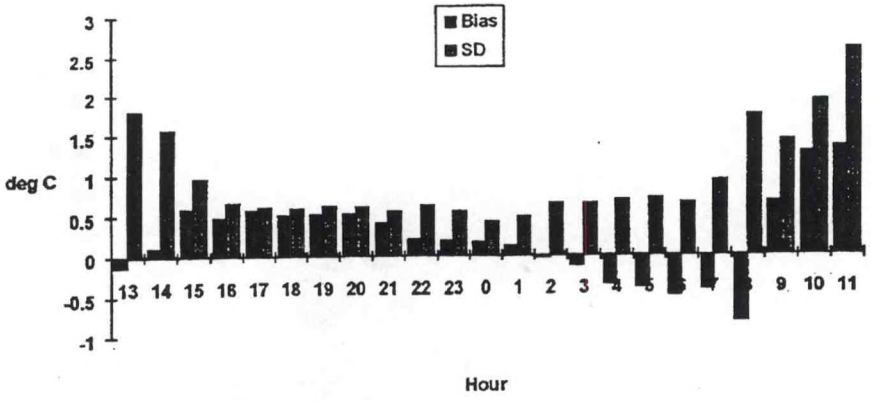

Figure 2. Hourly bias and standard deviation of temperature forecasts (CP002, Italy, October 1- 30, 1994).

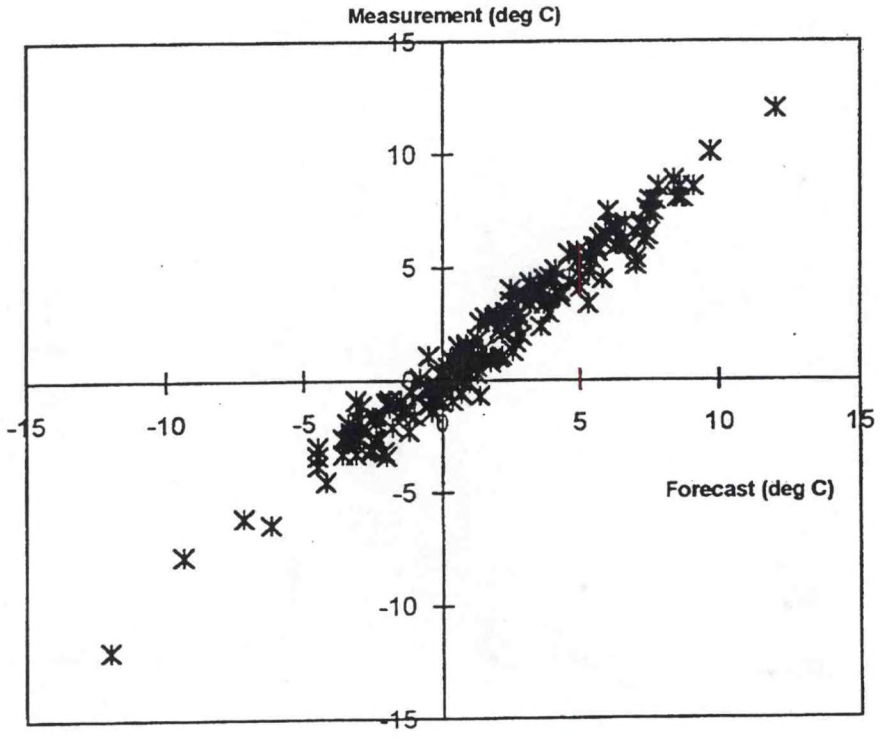

Figure 3. 24-hour minimum temperature forecasts against sensor measurements (Leeming, November 1, 1992 - April 29, 1993).

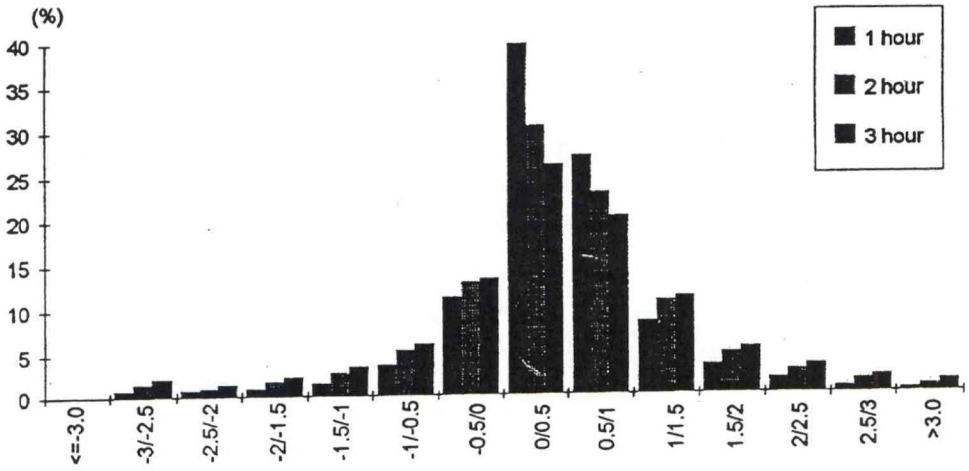

Figure 4. Distribution of mean difference of overall temperature nowcast minus actual in 0.5°C error bands.

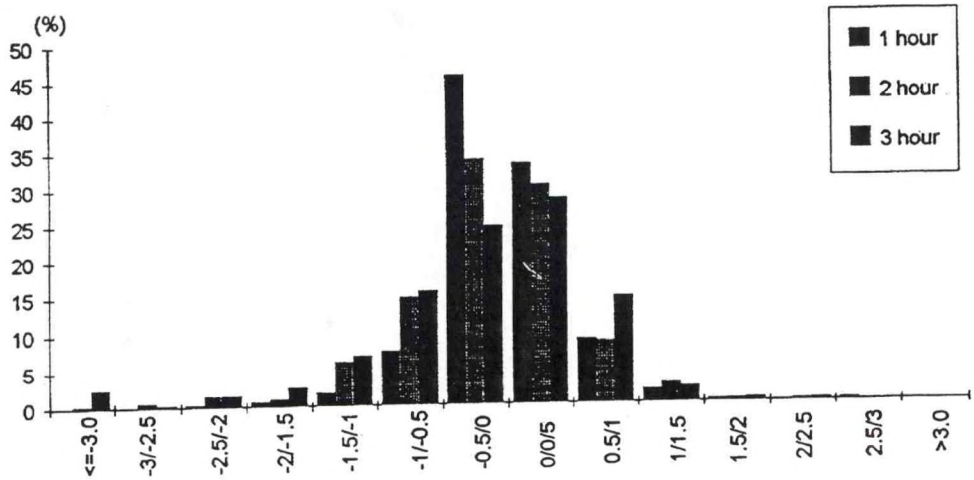

Figure 5. Distribution of mean difference of minimum temperature nowcast minus actual in 0.5°D error bands.

SESSION 5
POSTER PREVIEW

11. A Case Study of Heavy Snow Resulting from Dissipating Thunder-Storms in the Lower Ohio Valley

12. Heavy Snowfall Tracks for Des Moines, Iowa

13. A Study of the Thanksgiving 1993 Snowstorm - Enhancement of Heavy Snow over Northeast South Dakota in Response to Tropopause Undulation

14. Combining Satellite, Radar and Ground Truth Data in Nowcasting Lake Effect Snow Intensity

15. National Severe Storms Laboratory and Storm Prediction Center Freezing Precipitation Forecast Experiment for Winter of 1993-1994

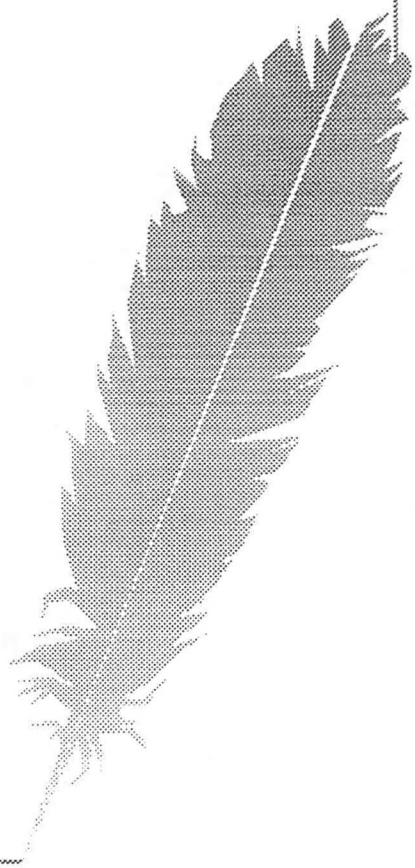

A Case Study of Heavy Snow Resulting from Dissipating Thunderstorms in the Lower Ohio Valley

Tim Troutman[1]

1. INTRODUCTION

The March 8-9, 1994 heavy snow event in the Lower Ohio Valley was an unusal late winter storm that resulted in snow amounts over a foot in southeast Missouri. Five-to-eight inch snowfall amounts were also common in southern Illinois, southwestern Indiana and western Kentucky. The purpose of this study is to demonstrate the use of wind profiler and satellite data were important tools to help predict this significant snow event.

2. SYNOPTIC SETTING

The synoptic weather pattern that prevailed across the U.S., which would lead to cyclogenesis, was characterized by a "split" 500-mb flow pattern, with the westerlies along the Northern plains and Canadian border and the southern jet stream extending northeastward from southern California into the southeast part of the U.S. A southern stream closed low was forecast to move from southeast Arizona on 0000 UTC 8 March, and merge with a weaker short-wave trough moving toward the southeast, embedded in a weak northwest flow, by 0000 UTC 10 March. The merging resulted in the associated surface low (as inferred from the mean sea-level pressure field) taking a more westerly track than expected, from central Louisiana on 1200 UTC 9 March to eastern Kentucky by 0000 UTC 10 March. The ETA, NGM and AVN National Meteorological Center (NMC) forecast models all predicted the surface low track well, which took the forecast position of the low west of the Appalachian mountains by 0000 UTC 10 March (Figure 1).

By 0000 UTC 9 March, all three models showed an area of developing precipitation ahead of (or downstream) of the developing surface cyclone in eastern Texas. That prediction seemed reasonable since already at 1800 UTC 8 March, the precipitation area had expanded rapidly to the northeast. Precipitation was believed to be in an area of warm advection, isentropic lift, and abundant moisture that had been transported northward toward the lower Ohio Valley from the Gulf of Mexico.

Initially, forecasters thought that an area of moderate to heavy snowfall would occur on the northwest fringe of the precipitation shield associated with the surface low, tracking from northern Oklahoma into central Illinois. Due to the NMC Heavy Snow forecast and the quantitative precipitation forecast across the lower Ohio Valley for one half to one inch of water equivalent, forecasters in Illinois and Kentucky issued Winter Storm watches early in the afternoon on March 8 for potential snowfall amounts of up to eight inches.

The NGM predicted 700-mb vertical velocity valid at 1200 UTC 9 March, displayed values as high as 9 microbars per second over the lower Ohio Valley. This would suggest significant warm air advection and isentropic lifting downstream from the developing cyclone, allowing heavy snow to occur. Strong warm advection was also noted from wind profiler data from 850 to 300-mb to the northwest of the surface low in Texas. These factors led the National Severe Storms Forecast Center to put Oklahoma and Arkansas in the slight risk category for severe thunderstorms from the period of 1900 UTC 8 March to 1200 UTC 9 March.

1. Corresponding author address: Tim Troutman, NWS Office, Old Hickroy (Nashville), Tennessee.

The models further indicated the possibility of strong isentropic lift over Oklahoma and Arkansas from 1800 UTC 8 March to 0000 UTC 9 March. "Upper air" analyses of the Paducah, Kentucky and Nashville, Tennessee, soundings were used in this case study due to the proximity of the reporting stations. Soundings implied that warm advection and isentropic lift were occurring across the lower Ohio Valley due to veering winds with height. Paducah, Kentucky's 0000 UTC 9 March sounding showed low level cold advection from 1000 to 850-mb due to backing winds with height. But from 850 to 810-mb, a small layer of warm advection had occurred during the previous 12 hours, with temperatures having warmed from -3° C to 0° C (Figure 2).

The Nashville, Tennessee, 0000 UTC 9 March sounding (Figure 3) showed much more pronounced warm advection in the 840 to 790-mb layer, with temperatures having warmed to +3° C around 800-mb. A mid-level southwest 50 knot jet was evident just above 700-mb, which further suggested warmer air was advecting northeastward ahead of the surface system. At 1200 UTC 9 March, warm advection continued over the area, as both the Paducah, Kentucky and Nashville, Tennessee, soundings had winds veering with height (not shown). The temperature at Paducah, Kentucky, warmed to 0° C at 850-mb.

3. USING WIND PROFILER DATA TO EVALUATE THE POTENTIAL FOR HEAVY SNOW DEVELOPMENT

Wind Profiler data across the Midwest was very important in the prediction of heavy snow in the lower Ohio Valley. At 2100 UTC 8 March, the 850-mb plan view plot (8ma) depicted an 850-mb trough in the wind field extending into southeast Oklahoma (Figure 4). This feature aided the development of strong to severe thunderstorms in south central Oklahoma to the north of the MSLP cyclone track. The organized area of thunderstorms progressed northeast into northern Arkansas by 0100 UTC 9 March, producing thundersnow and thundersleet throughout much of Arkansas.

The 850-mb profiler data also showed that the trough slowly extended northeast into central Arkansas by 0600 UTC 9 March (not shown) with winds converging across Arkansas ahead of the low. TheWinnfield, Louisiana profiler showed winds had increased from 30 knots at 2300 UTC 8 March to 40 knots by 0700 UTC 9 March. The Okalona profiler showed winds increasing from 30 knots at 0200 UTC to 50 knots by 1000 UTC. The 850-mb trough continued to move northeast from northern Arkansas at 1300 UTC 9 March, to central Tennessee by 1500 UTC.

AT 0000 UTC 9 March, the 700-mb plan view plot (7ma) indicated both speed and directional convergence occurring over part of Arkansas (not shown). The DeQueen profiler, in southwest Arkansas, showed a 55-knot southwest jet, while the site in Bloomfield, Missouri, depicted a 40-knot southwest wind and the Conway profiler showed northerly winds of only 10 knots. This implied speed convergence across north Arkansas and directional wind convergence as well. The speed and directional wind convergence, in addition to veering winds in the lower and mid levels, helped to provide an air mass capable of producing thunderstorms and continued thunderstorm development for several hours. Other factors that led to the development of thunderstorms in Oklahoma and Arkansas were the isentropic lifting that was occurring and the availability of deep moisture. The progression of the low pressure system to the northeast and its continued strengthening also contributed to further thunderstorm development.

4. USING INFRARED SATELLITE IMAGERY TO EVALUATE STORM SNOW TOTALS

Three "bands" of thunderstorms developed in southern Oklahoma and Arkansas and were easily defined by Infrared (IR) satellite enhancements from 2000 UTC 8 March to 0600 UTC 9 March. The 2000 UTC 8 March IR and visible satellite imagery indicated a developing thunderstorm area in

Oklahoma, with the coldest storm tops in southeast Oklahoma (not shown). The IR imagery indicated that the thunderstorm area continued to move northeast along the 700-mb steering level, with the convective area extending south from near Monett, Missouri, to near Fort Smith, Arkansas, by 2200 UTC 8 March.

Movement of the convective area continued parallel to the alignment of the 700-mb height contours, with the IR imagery at 2300 UTC 8 March indicating cold cloud tops continuing across south central Missouri (not shown). A 700-mb trough at 2300 UTC 8 March extended southwest from the Conway, Missouri, profiler site to near the Purcell, Oklahoma, profiler. The same thunderstorm area then moved into southern Illinois and western Kentucky by 0000 UTC 9 March and into southwestern Indiana by 0200 UTC. A second area of colder cloud tops developed over northwest Arkansas by 0100 UTC 9 March and moved northeast over the same area in south central Missouri by 0200 UTC 9 March (Figure 5). Heavy snowfall in excess of an inch an hour was reported from 0100-0400 UTC 9 March at Cape Girardeau, Missouri. Three inches of snow fell at CGI between 0500 to 0700 UTC 9 March.

This same dissipating thunderstorm area also produced three periods of heavy snow in the Evansville, Indiana area. The IR imagery from 0200 UTC 9 March (Figure 5) indicated that the first band of cold cloud tops was moving northeast into the immediate Evansville area. By 0300 UTC, a second area of colder cloud tops was advancing northeast out of southeast Missouri and then moved into the Evansville areas by 0400 UTC (not shown), with an inch of new snow reported at Evansville by 0600 UTC. The third and last significant period of heavy snow occurred in southeast Missouri at 0600 UTC, as colder cloud tops moved across this region (Figure 6). This snow area progressed into the Evansville area by 0700 UTC, with two more inches of snow reported between 0800-1000 UTC.

5. CONCLUSION

This type of snow event generally occurs across the lower Ohio Valley at least once a year with the snow amounts usually under-predicted. The availability of profiler, satellite data and improved forecasting techniques should continue to allow for improved snow event forecasting in the future.

6. ACKNOWLEDGEMENTS

Special thanks goes to Henry Steigerwaldt, SOO at NWSO Nashville, Tennessee for his review and suggestions regarding this paper.

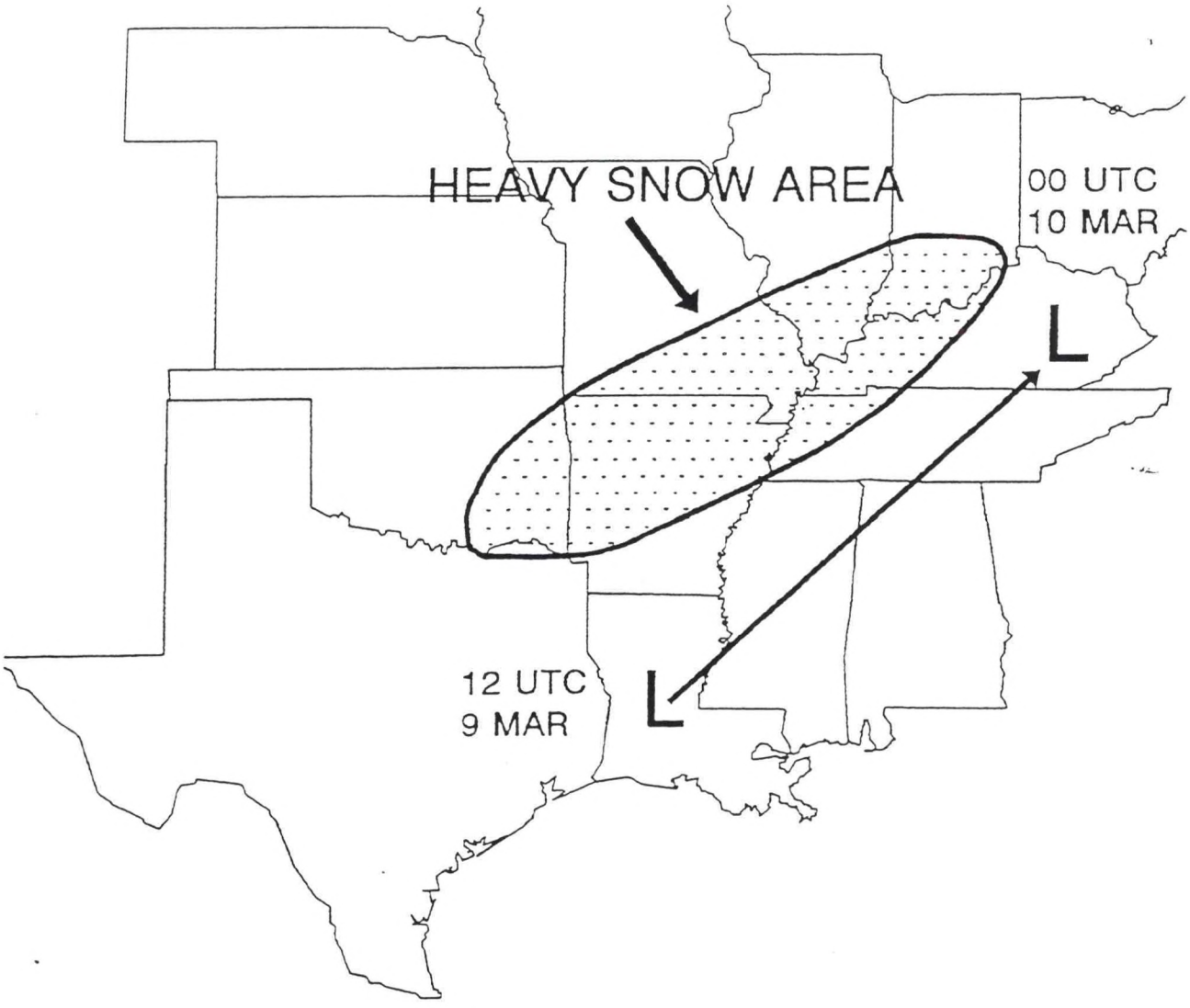

Figure 1. Forecast track of surface low and resultant heavy snow area.

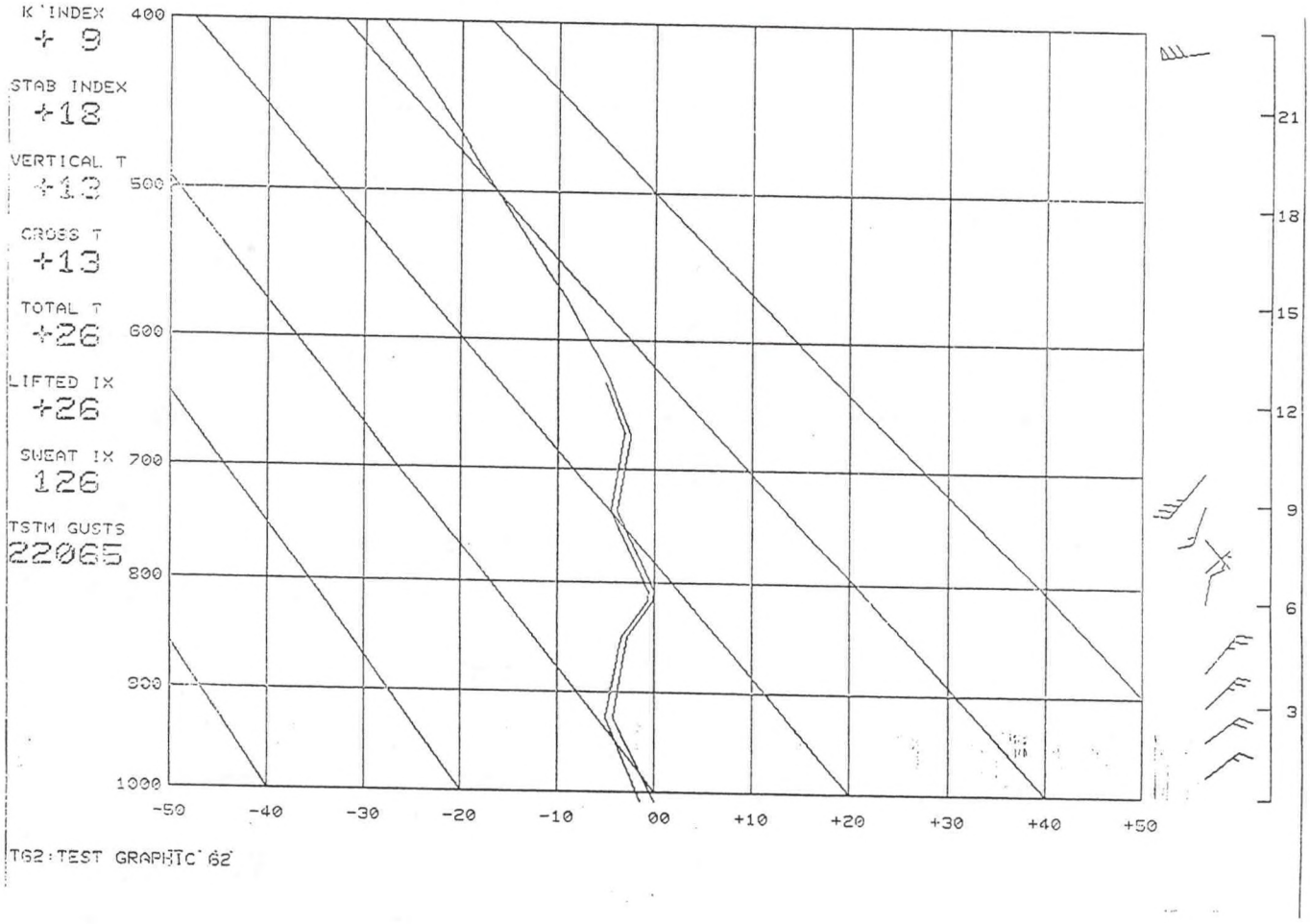

Figure 2. Paducah, Kentucky 0000 UTC 09 March 1994 upper air sounding.

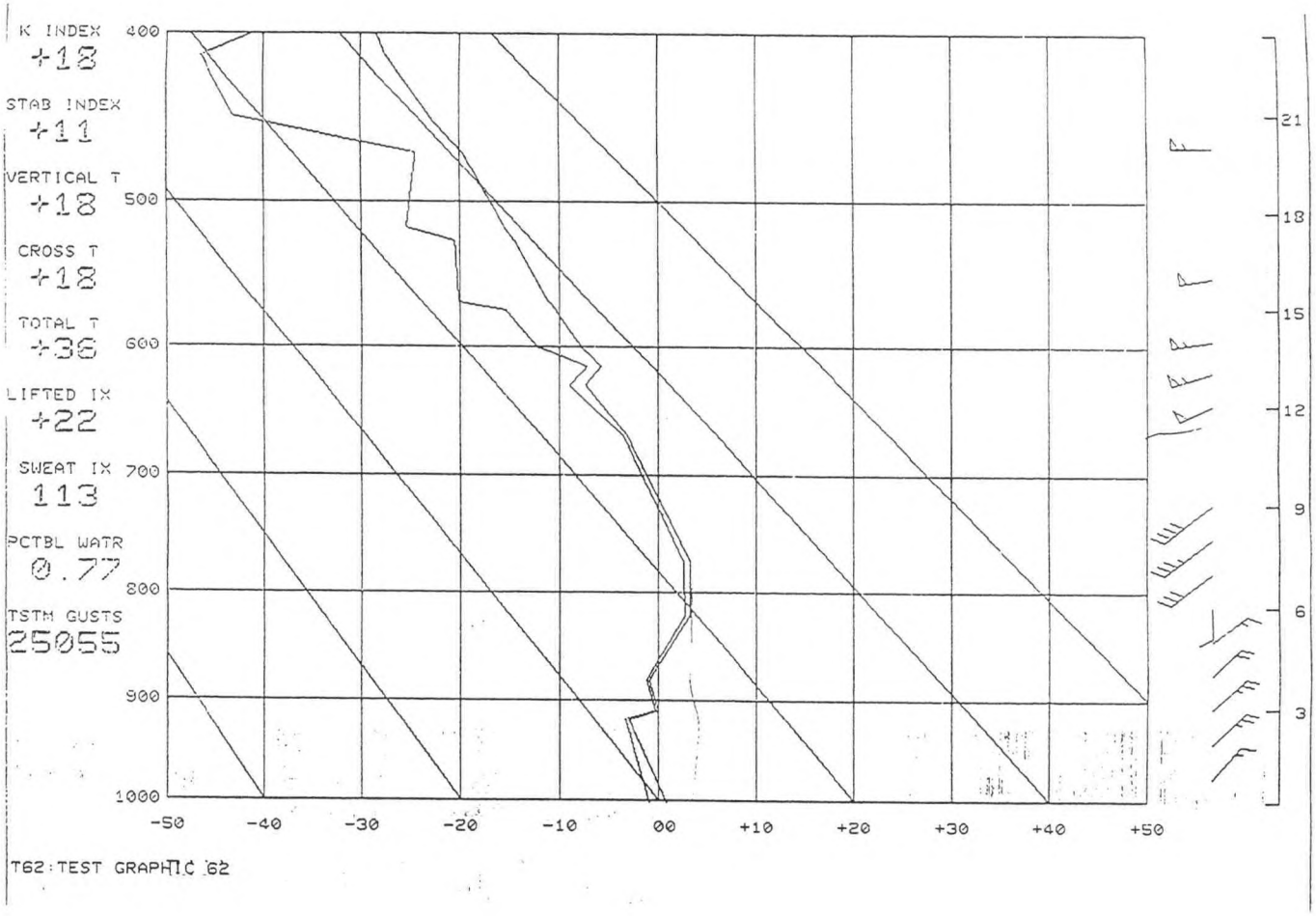

Figure 3. Nashville, Tennessee 0000 UTC 09 March 1994 upper air sounding.

Transmission of material in this release is embargoed until after 8:30 A.M. (EDT) Tuesday, August 13, 1996

CONSUMER PRICES IN NEW YORK-NORTHEASTERN NEW JERSEY INCH UP 0.1% IN JULY; 2.7% INCREASE OVER YEAR

The Consumer Price Index for the New York-Northeastern New Jersey area inched up 0.1 percent in July, John L. Wieting, Regional Commissioner for the U.S. Department of Labor's Bureau of Labor Statistics, reported today. The July index largely reflected a rise in the shelter sector and higher prices for dairy products, fruits and vegetables, cereals and bakery products and medical care. These increases were about offset by declines in apparel, typical for July, gasoline, fuel oil and meats, poultry and fish. For the year ended July 1996, consumer prices increased 2.7 percent.

With the New York-Northeastern New Jersey Consumer Price Index for All Urban Consumers at 166.7 in July (1982-84=100), $16.67 was required to purchase what $10 could in the 1982-84 base period. The purchasing power of the dollar was 60.0 cents in 1982-84 dollars and 20.8 cents in 1967 dollars.

The Consumer Price Index for Urban Wage Earners and Clerical Workers (CPI-W) held unchanged in July. The CPI-W rose 2.8 percent over the year.

Data in this report are not seasonally adjusted. Accordingly, month-to-month changes may reflect the impact of seasonal influences. The New York-Northeastern New Jersey area comprises the five boroughs of New York City, Nassau, Suffolk, Westchester, Rockland, Putnam, and Orange Counties in New York State; Bergen, Essex, Hudson, Hunterdon, Middlesex, Monmouth, Morris, Ocean, Passaic, Somerset, Sussex, and Union Counties in New Jersey; and Fairfield County and parts of Litchfield and New Haven Counties in Connecticut.

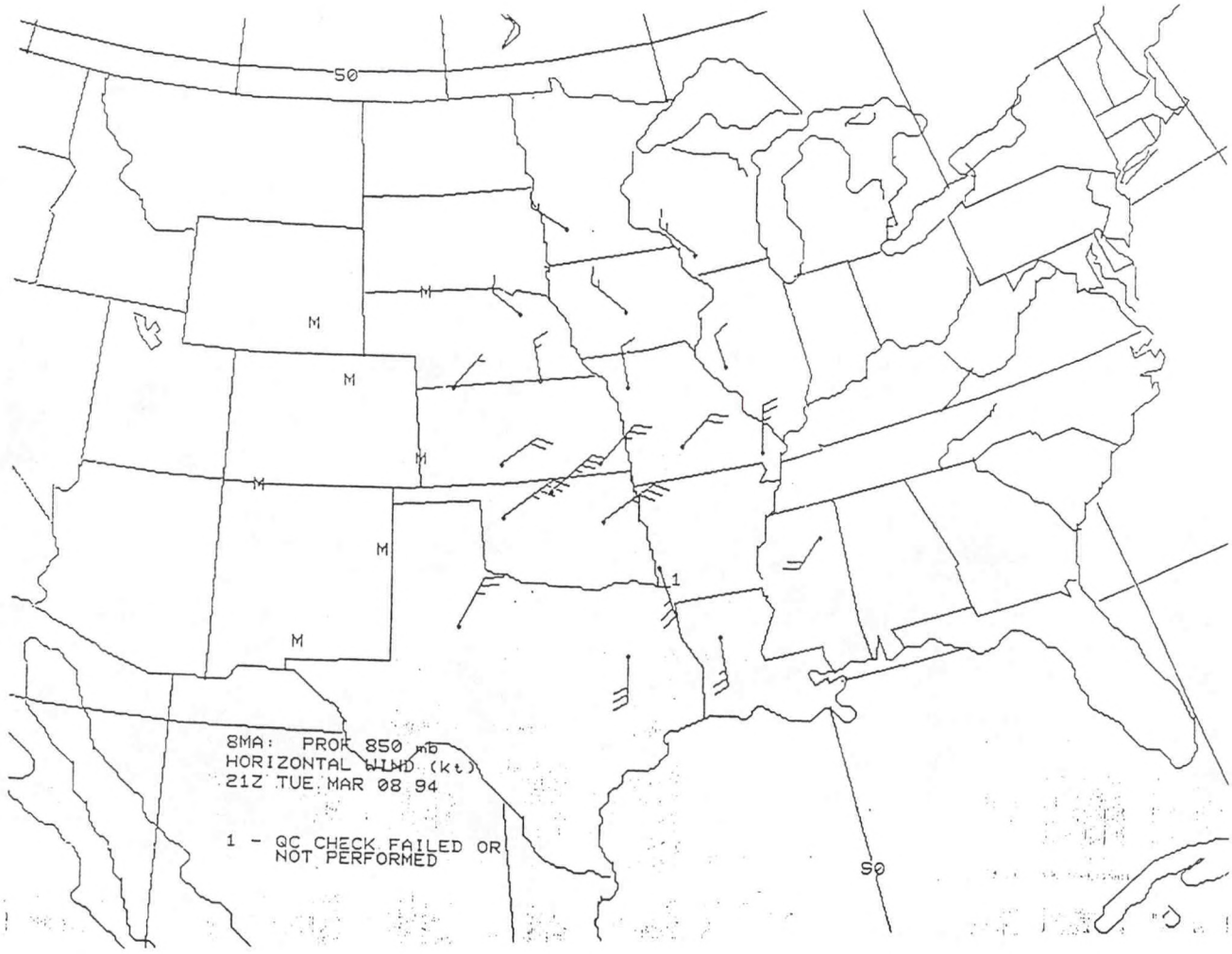

Figure 4. 2100 UTC 08 March 1994 850 mb wind profiler plan view plot.

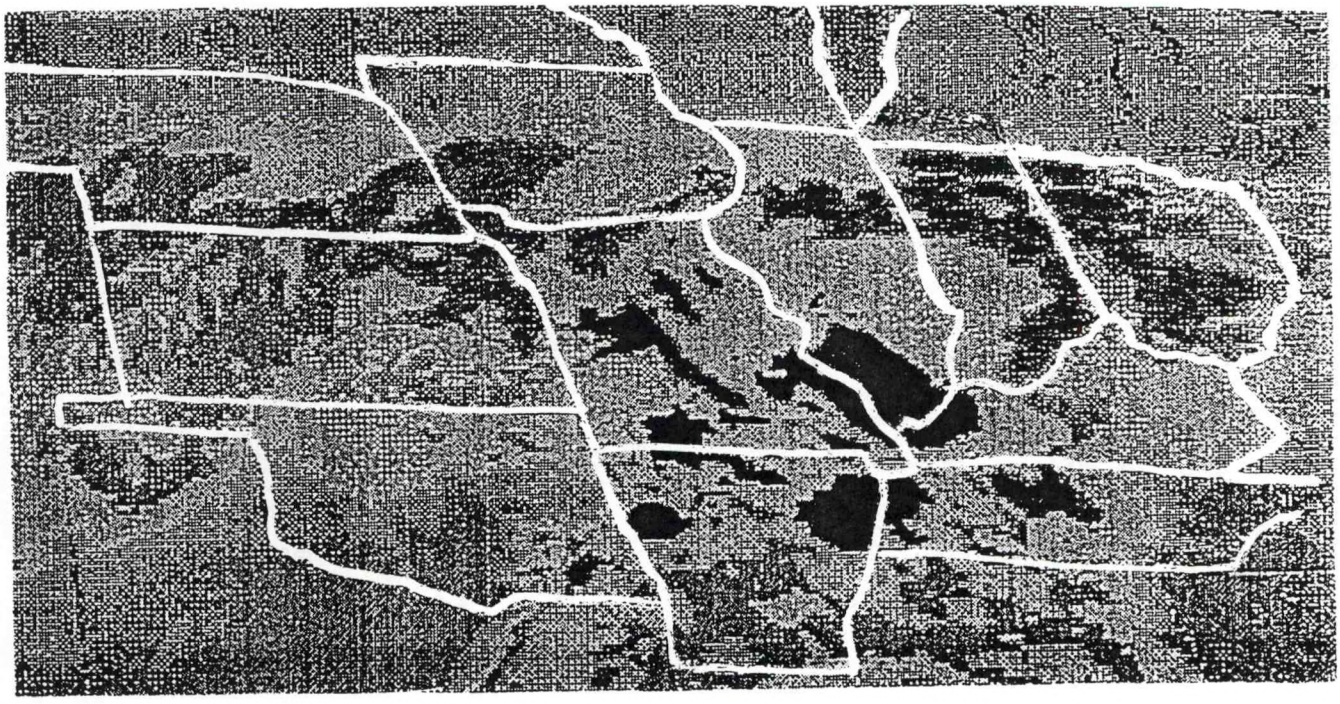

Figure 5. 0100 UTC 09 March 1994 infrared satellite imagery.

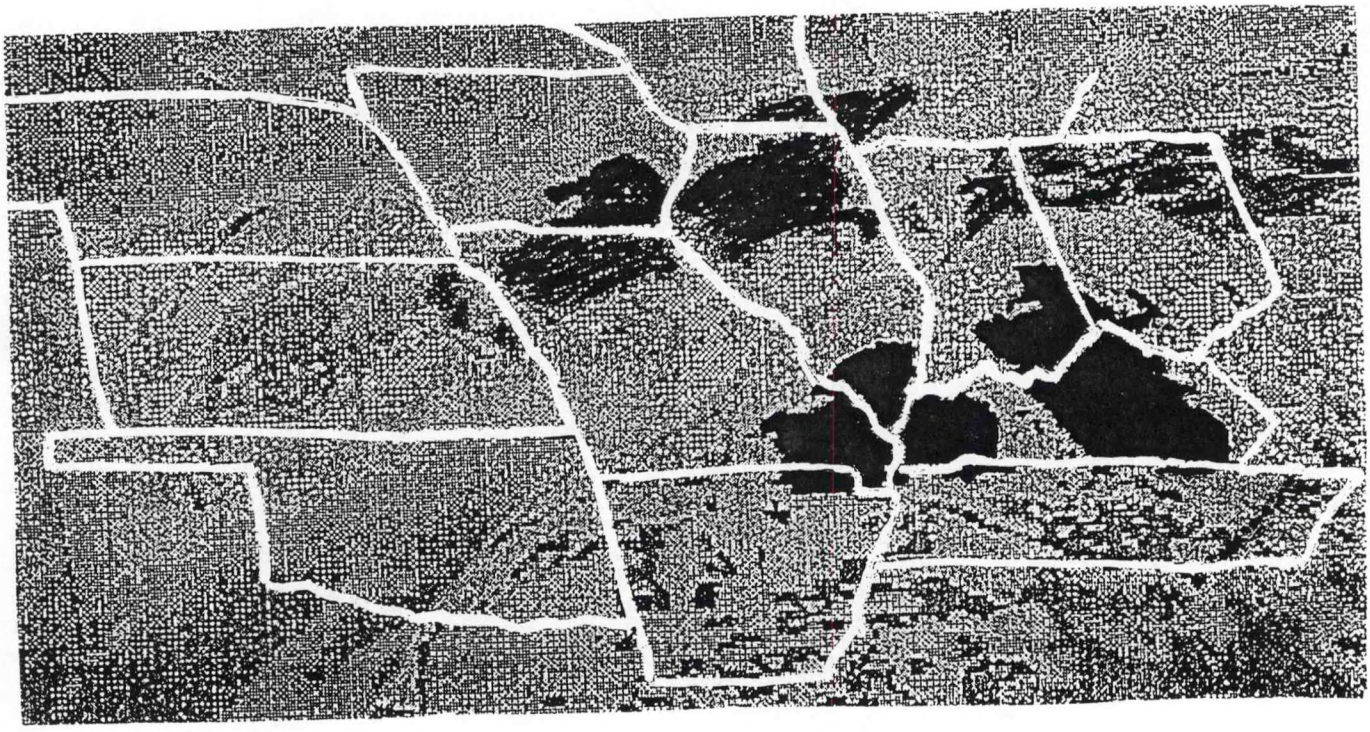

Figure 6. 0600 UTC 09 March 1994 infrared satellite imagery.

Heavy Snowfall Tracks for Des Moines, Iowa

Kimberly A. Schafer[1]

1. INTRODUCTION

In 1994, a study was completed at NWSFO Des Moines, Iowa, that compiled information on the frequency of snowfall amounts in the Des Moines area. Petersen (1994) showed that snowfalls of greater than 5 inches are infrequent to the area. The focus of this study was an attempt to define the weather patterns that produced heavy snowfall in Des Moines. For the purpose of this study, heavy snowfall events have been defined as those which had storm totals of 6 inches or more of snow.

2. DATA

Petersen's study compiled snowfall amounts from 1885 to 1993. A total of 1255 snowfall events were recorded. Two hundred and eleven events had storm total snowfall of 5 inches or more. Due to the lack of information prior to the year 1968 and the large amount of data to analyze, only snowfalls of 6 inches or more since 1968 were included in this study. Two additional heavy snowfall events have occurred since 1993; they have been included in the study providing a total of 38 events to review.

The original data provided the storm total, the month, and the year of each event. In order to review the weather patterns of the 38 events, the exact date of the snowfall was needed. Once the dates were obtained, surface and 500 mb maps were located for the days surrounding each storm.

Tables 1 and 2 (below) show the breakdown of the storms included in the study. Table 1 shows the breakdown of the heavy snowfall events by the total snowfall amounts. Table 2 shows the breakdown of the heavy snowfall events by their storm track.

TABLE 1
STORM TOTALS

Snow Amount	No	Percentage
6 inches	12	31.5
7-8 inches	12	31.5
9-12 inches	10	26.0
more than 12 inches	4	11.0

TABLE 2
STORM TRACK CATEGORIES

Storm Track	No	Percentage
Track One - passing through Iowa (Figure 1)	13	34
Track Two - passing across Southern Missouri (Figure 2)	6	16
Track Three - passing through Southeast Missouri (Figure 3)	7	18
Late Developing Storms	3	8
Undefined	4	11

1. Corresponding author address: Kimberly A. Schafer, NWS Forecast Office Des Moines, IA.

3. RESULTS

The surface weather patterns which produced the heavy snowfall events were broken down into six categories. The six categories consist of: three defined storm tracks, late developing systems, inverted troughs, and storms with no defined track.

The majority of the weather patterns were defined by three distinct storm tracks. Each storm track is 200 miles wide, allowing for a 100 mile variance on either side of the average track. The first track, which is most often associated with heavy snowfall events in Central Iowa, indicates a low pressure system developing over the Oklahoma Panhandle. It then passes through Missouri and Southeast Iowa before ending up in Lower Michigan (Figure 1).

The second and third tracks, developing over the Oklahoma Panhandle and North Central Texas respectively, both pass through Southeast Missouri and are often thought to be too far south for heavy snowfall to occur in Iowa (Figures 2 & 3). Tracks two and three, although not moving through Iowa, produced 13 of the 38 heavy snowfall events studied. This is the same number of storms produced by storms following track one. To account for the heavy snowfall provided by tracks two and three, compare Figures 2 and 3 with the 500 mb height falls track. The 500 mb height falls track corresponds closely to the 500 mb low track shown in Figure 4. Each of the surface low tracks are to the right of the 500 mb track. A study completed by Weber (1979) found that when this occurs, the heavy snow band will fall parallel to and left of the 500 mb height falls center track, therefore Central Iowa would receive heavy snowfall. Physically, regions of geopotential height falls are often similar to those with quasi-geostrophic forcing for upward vertical motion.

The three remaining categories include weather patterns that are more troublesome to forecasters. Three of the cases represent late developing systems (two produced snowfall amounts in the highest categories listed in Table 1). Late developing storms refer to those storms in which the surface low developed farther east than the classical High Plains or panhandle region. In each of the cases, high pressure was present north of the Dakotas and extended as far south as the Minnesota/Iowa border. Within the next 24 hours low pressure developed in southern Missouri and progressed northeast through central Illinois and lower Michigan. The 500 mb maps corresponding to the late developing storms were relatively zonal, with a short wave intensifying over the Rockies and moving east over Iowa during the storm. The resulting low pressure systems deepened as they moved east, depositing heavy snowfall across the Great Lakes Region.

The fourth category, inverted troughs, can be divided into two sub-categories by evaluating the 500 mb pattern. Three of the storms had 500 mb patterns in which a trough was located over the southwest portion of the United States, with split flow over the Midwest. As a shortwave moved east over Iowa, the northern part of the state was under westerly flow while southwesterly flow dominated south of the Iowa/Missouri border. The northern stream provided the cold air which was overrun by the moist southern stream. The 500 mb patterns of the remaining two storms revealed low pressure systems in Canada just north of Washington state. A trough extended southeast across the United States to the Gulf of Mexico, deepening as it moved east over the Midwest.

To further evaluate the inverted trough storms, 700 mb height and temperature maps were investigated. The results were similar in all of the cases. Each map revealed southerly flow bringing warm, moist gulf air into central Iowa. At the surface, high pressure dominated the Midwest 24 hours before heavy snow began. An inverted trough developed and progressed east across the Midwest. The band of heavy snow fell behind the wind shift line associated with the inverted

trough. It is recommended that when encountering this situation, forecasters look for areas of pressure rises and falls east of the Rocky Mountains along with areas of precipitation which, when combined with the Gulf flow, might be capable of producing heavy snowfall (Weber 1979, Steigerwaldt 1991).

The remain four storms do not fit into any of the above categories. They will be discussed individually. Two of the storms are closely related to those represented by Track one, with the exception that the surface low is too far north to fit the defined track. The 500 mb maps associated with the two storms revealed a weak low passed over Iowa from Nebraska. This track is also farther north than those associated with Track one. The surface lows in both cases were well defined, strong, closed lows which provided strong low level forcing for heavy snowfalls despite a weak upper air flow.

Another of the remaining storms was closely related to Track three, but it passed through central Iowa, placing it too far north to fit the defined storm track. The 500 mb maps associated with this storm followed the same pattern as those in Figure 4. Like the two previous cases, this storm was also a well defined closed low pressure system from the surface to 700 mb. Upper air analysis indicates strong moisture inflow and concentrated warm air advection induced upward vertical motion and heavy snowfall across central Iowa.

The final storm was not related to any of the others, making it potentially troublesome to forecasters. At the surface, the storm developed along the southeast border of Texas in the Gulf of Mexico. It then moved north through Louisiana, Tennessee, Illinois, eastern Iowa, and Wisconsin. Cold air was present at 850 mb along with an amplified low pressure pattern at 500 mb. Low pressure centers at each level tracked south and east of Iowa, keeping the state in sufficiently cold air for 6 inches of snow in Des Moines.

After examining the surface maps, the 500 mb maps were compared, and an attempt was made to relate the surface storm tracks to the 500 mb patterns. A majority (76%) of the 500 mb maps fell into a single pattern and were represented in each of the surface storm track categories. A 500 mb low developed at the base of a trough over Northern Arizona and New Mexico, and then progressed east to the Oklahoma Panhandle. From the Panhandle region it moved northeast through northern Missouri, eastern Iowa, and southern Wisconsin. From Wisconsin the low continued northeast across the Great Lakes Region (Figure 4). The low and the associated shortwave trough both deepened as they moved toward Iowa. However, they usually weakened east of the Mississippi River. These results agree with Weber's (1979) study of Midwestern storms.

The nine remaining 500 mb storm patterns fit into a second grouping. Despite the small number, they occurred in four of the six surface weather pattern categories. The path of the 500 mb low center was generally zonal, passing across the continental United States just south of the Canadian border (Figure 5). The southward extending shortwave troughs associated with these storms tended to be weaker than those described above. However, the shortwave deepened over the Midwest, providing the source of lift needed to initiate snowfall over central Iowa.

4. CONCLUSION

This study found that approximately two-thirds of heavy snowfall producing storms in central Iowa can be defined by three surface storm tracks and a single 500 mb track. Forecasters should be aware of these storm tracks when evaluating weather situations which include heavy snow.

The remaining storms, which do not have an organized surface low to the west, will be the most troublesome to forecasters. Forecasters should look at the 500 mb level for trough development over and just east of the Rocky Mountains, the 700 mb level for warm air advection, and for Gulf moisture moving north toward Iowa.

5. ACKNOWLEDGEMENTS

Thank you to Karl Jungbluth for his input and help in editing.

6. REFERENCES

Miller, C.J., and J.K. Last, 1990: An analysis of the southeast Iowa-west central Illinois snow event of 10 December, 1989. Central Region Technical Attachment 90-34. DOC, NOAA, NWS, Central Region, Scientific Services Division, Kansas City, MO.

_____. _____, _____: Forecasting Techniques Handbook, National Weather Service Forecast Office-Des Moines, Iowa. Heavy snow forecasting techniques (excerpts from Hanks, et. al., Snow forecasting procedures for the Central U.S.).

NOAA, DOC, NWS, NMC: Daily Weather Maps. Meteorological Operations Division and Climate Analysis Center, Washington , D.C.

Petersen, E.T., 1994: Storm total and 24-hour snowfall frequencies for Des Moines. *Iowa Technical Journal*, **2-2**, 4-5.

Steigerwaldt, H., 1991: Heavy snow events without the aid of sea level low and little or no positive vorticity advection at the 500 mb level. Central Region Technical Attachment 91-25. DOC, NOAA, NWS, Central Region, Scientific Services Division, Kansas City, MO.

Weber, E.M., 1979: Major mid-west snowstorms. Air Weather Service Technical Note 79-2, Third Weather Wing, Offutt AFB, NE.

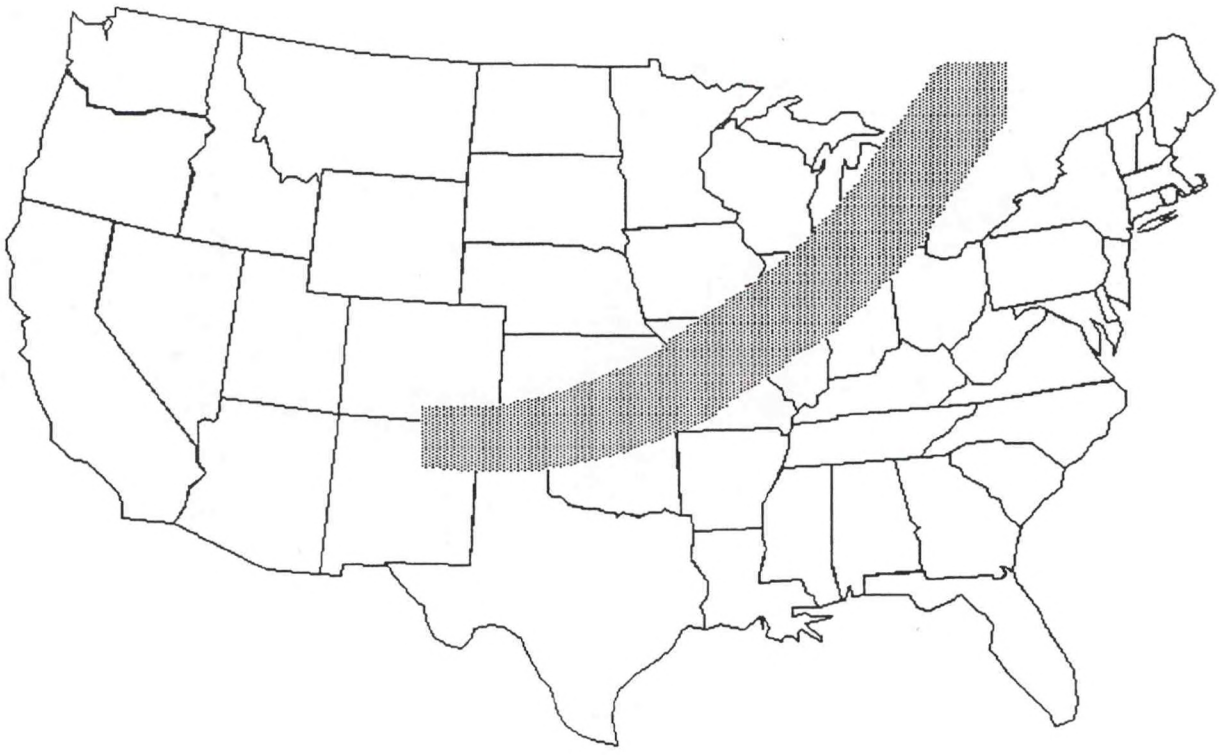

Figure 1. Surface low Track 1.

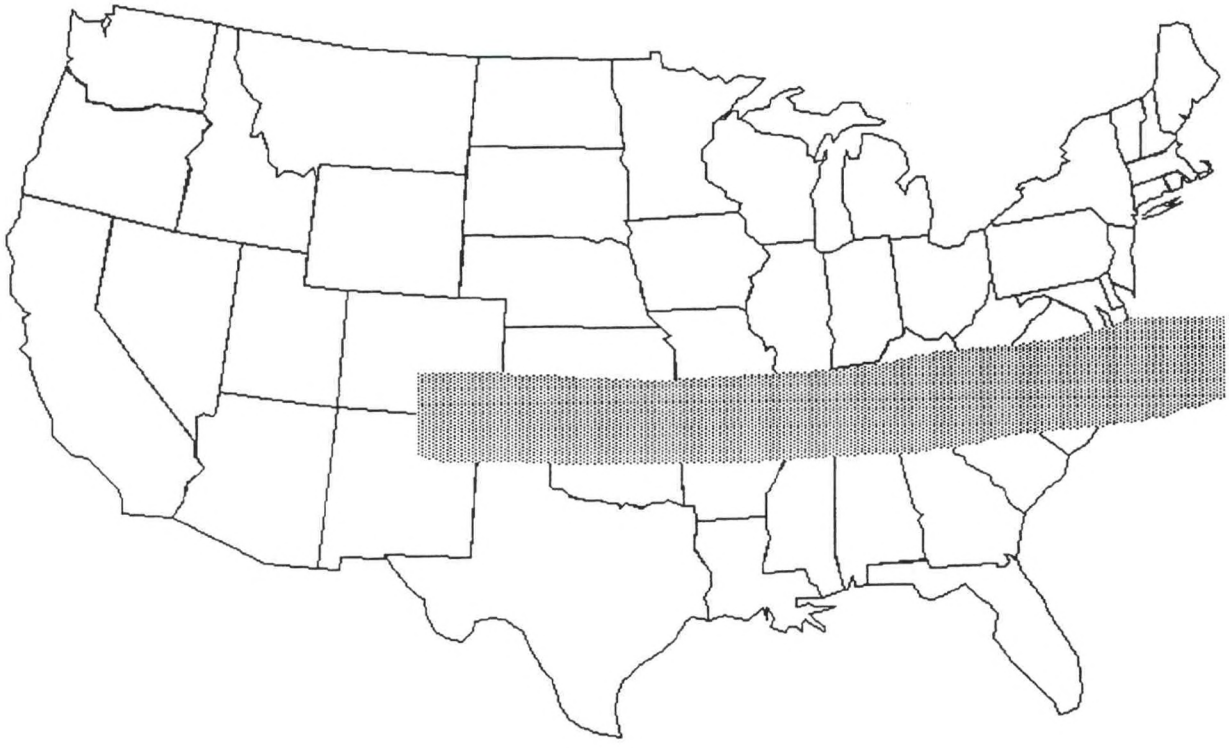

Figure 2. Surface low Track 2.

Figure 3. Surface low Track 3.

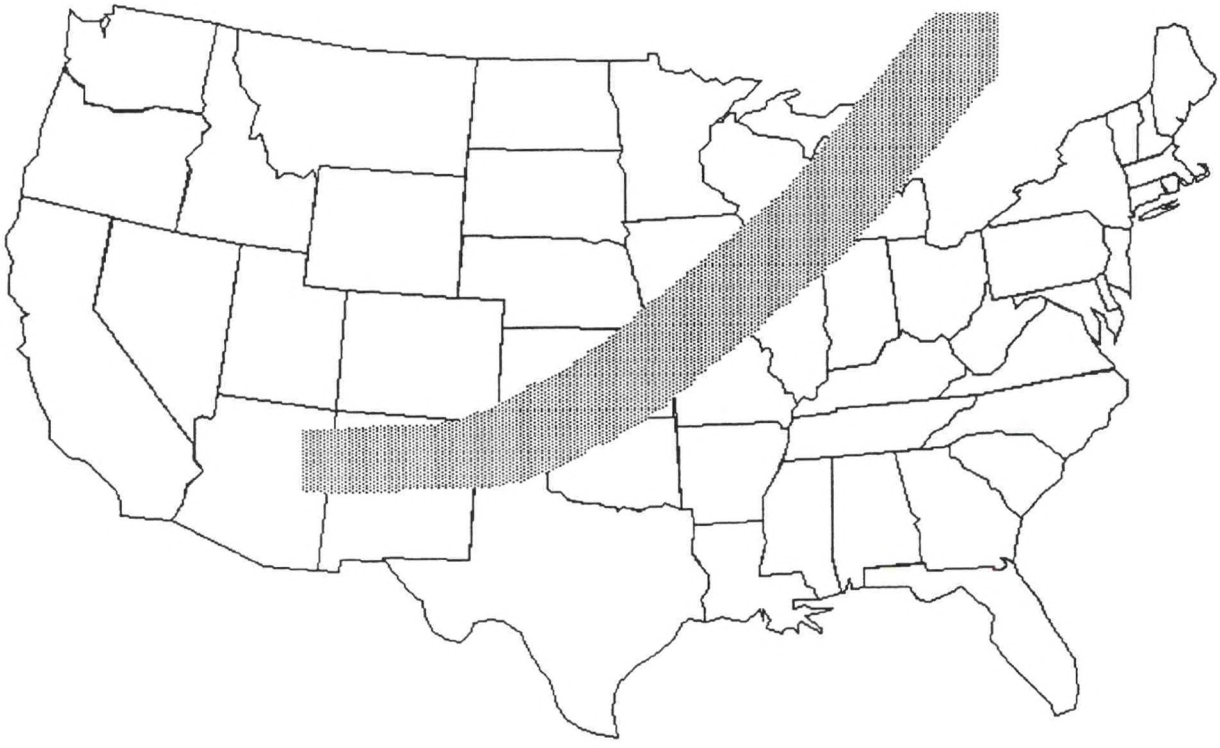

Figure 4. The main 500 mb low center track.

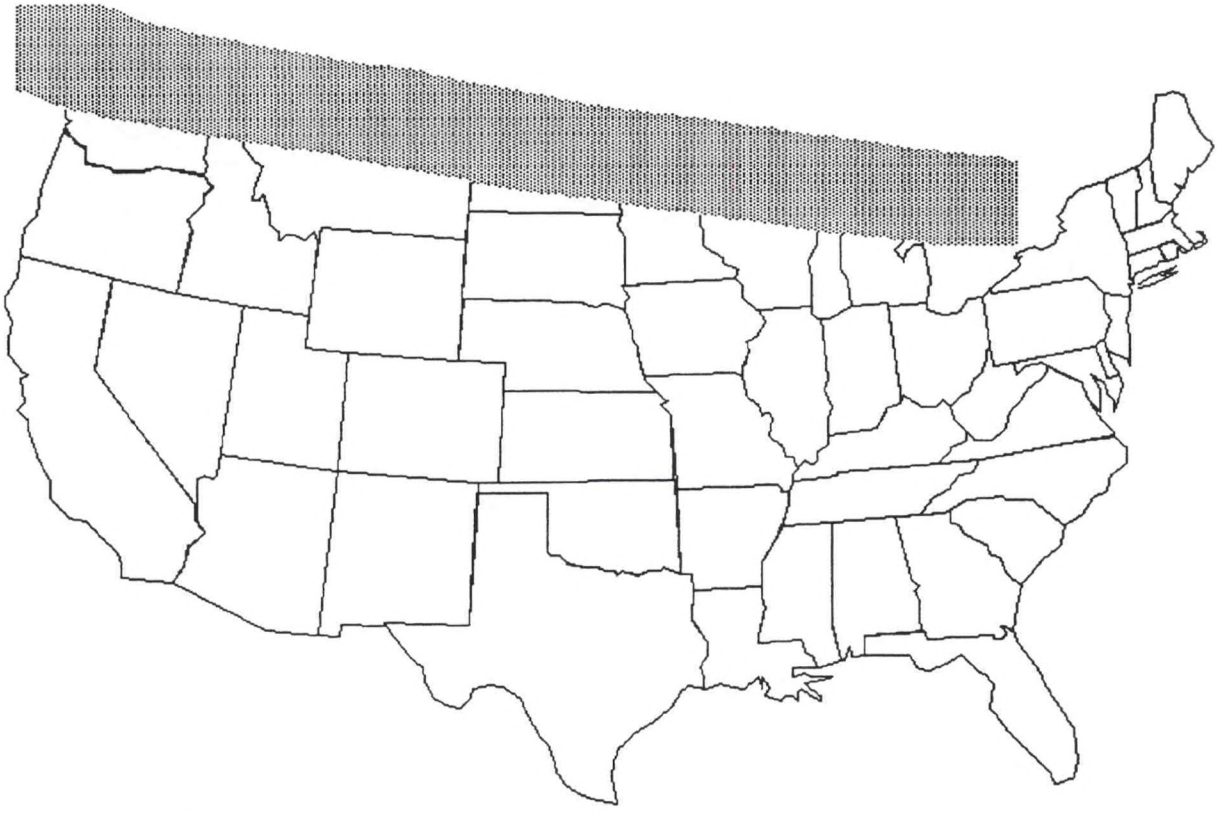

Figure 5. The secondary 500 mb low center track.

A Study of the Thanksgiving 1993 Snowstorm-Enhancement of Heavy Snow over Northeast South Dakota in Response to Tropopause Undulation

Dennis J. Blondin[1] and Debra D. (Murtha) Blondin[2]

1. INTRODUCTION

Heavy snowfall occurred in the northeast portion of South Dakota between November 21-28, 1993. A large area surrounding Aberdeen, South Dakota received snowfall amounts more than 24 inches (Figure 1). Snowfall occurred over much of the Northern Plains during this time, but the snowfall over northeastern South Dakota far exceeded amounts found throughout the rest of the region. The one exception was the orographically induced heavy snowfall in the Black Hills.

This study will investigate the presence of dynamic lift through a look at quasi-geostrophic diagnostics and jet streak circulations. The purpose of this study is to examine the relationship between the location of a stratospheric intrusion of warm air and potential vorticity into the upper troposphere to the unusually heavy snowfall that occurred over northeast South Dakota. This relationship will be shown through the use of gridded data sets from the Nested Grid Model (NGM) which were run on macros commonly found in PCGRIDDS. The greatest snowfall occurred between 0600 UTC 24 November and 0600 UTC 25 November with 12 inches recorded at Aberdeen. Therefore, this study will focus primarily on the 24-hour period.

2. SYNOPTIC OVERVIEW AND JET STREAK INFLUENCES

On November 23, 1993, a strong stationary front extended across the Northern Plains from southern Wisconsin to southwestern Kansas. An arctic high pressure system was centered over southern Saskatchewan that created a broad area of east to northeast winds from the Great Lakes to the Western Plains. South of the front, an expansive area of southerly winds was directed toward the stationary front from Kansas to Ohio. This front had remained stationary for nearly 36 hours prior to the development of a surface low along the front over western Iowa between 0000 UTC and 1200 UTC 23 November.

During this period, the northern and southern branches of the jet stream were aligned parallel to the surface front. By 1200 UTC 23 November, the entrance region of a jet streak in the northern branch was located over northern Minnesota while the exit region of a jet streak in the southern branch was pushing eastward through Nebraska into Iowa (Figure 2). Looking downstream, the cross-section in Figure 3 shows the thermally direct circulation in the entrance region of the northern jet streak depicted by the counterclockwise pattern of ageostrophic motion. Upward vertical motion was found south of the jet streak and subsidence north of the jet. The thermally indirect circulation in the exit region of the southern jet streak is evident in the clockwise pattern of ageostrophic motion. The upward vertical motion was located north of this jet streak while subsidence was found to the south. The coupling of the thermally direct and indirect circulations focused upward vertical motions over the Northern Plains causing low pressure to develop along the stationary front between 0000 UTC and 1200 UTC 23 November over western Iowa (Hakim and Uccellini, 1992).

1. Corresponding author address: Dennis J. Blondin, Nexrad Weather Service Office, Pocatello, Idaho.
2. Debra D. (Murtha) Blondin, Nexrad Weather Service Office, Pocatello, Idaho.

By 0000 UTC 25 November, the northern jet had moved east while the southern jet streak moved around the upper level low pressure over the northern Rocky Mountains (Figure 4). The left exit region of the southern jet pushed into southeastern South Dakota that continued to enhance the upward vertical motion over the eastern Dakotas. This, in turn, created a large area of upper level divergence over North Dakota and northern South Dakota that is evident in the 300 mb ageostrophic winds (Figure 5).

The contribution to upward vertical motion caused by the jet streaks was shown previously. Now we show how the omega equation can be used to show upward vertical motion. The two terms of the omega equation include differential vorticity advection and a thermal forcing term. Positive differential vorticity advection occurred in the layer between 500 mb and 300 mb with the maximum located over northeast South Dakota and western Minnesota (Figure 6). Positive values imply vorticity increasing with height over this area. The Laplacian of temperature advection was used to represent the thermal forcing term. Negative values of the Laplacian of temperature advection at 700 mb were found over much of North Dakota, eastern South Dakota and western Minnesota (Figure 7). Negative values indicate low level warm advection that contributes to upward vertical motion.

Another way to look at the omega equation is through the examination of Q-vectors. Q-vector divergence (convergence) corresponds to downward (upward) vertical motion (Hoskins et al., 1978). A large area of Q-vector convergence at 300 mb is shown over the eastern Dakotas and central Nebraska in Figure 8 and lends further support to the existence of upward vertical motion. The examples have shown that according to quasi-geostrophic theory upward vertical motion would exist over the eastern Dakotas. This was true with upward vertical motion greater than 3 mb per second between 700 mb and 300 mb across much of the eastern Dakotas and eastern Nebraska (Figure 9).

Abundant moisture was available over the area with 1000 to 500 mb average relative humidity exceeding 70 percent over much of the Dakotas and central Nebraska (not shown). Layer moisture advection from 1000 to 500 mb was also evident over the Northern Plains at 0000 UTC 25 November 1993 (not shown). In addition, there was significant isentropic lift as supported by positive values of pressure advection over the eastern Dakotas (not shown). This isentropic up glide motion continued to enhance the lift and saturate the atmosphere over the eastern Dakotas.

All parameters point to the possibility of heavy snowfall over the Northern Plains and the eastern Dakotas in particular. A combination of many factors show there was significant moisture and lift over northeastern South Dakota. Enhanced lift over the eastern Dakotas was caused by the coupling of the jet streaks, upper level divergence, Q-vectors and isentropic up glide. Another source of possible lift over northeastern South Dakota may have been caused by a tropopause undulation near the upper level low pressure system over the Rocky Mountains.

3. TROPOPAUSE UNDULATION

Earlier, we discussed the direct and indirect thermal ageostrophic circulations associated with jet streaks. By 0000 UTC 25 November, the entrance region of the southern jet streak was over southern Idaho and had a direct thermal ageostrophic circulation associated with it. This circulation caused convergence and subsidence in the left entrance region of the jet streak over Idaho and Montana. This subsidence and warming of the lower stratospheric air acted to lower the tropopause and cause a tropopause undulation.

A warm pool indicative of a tropopause undulation was found over western Montana and Wyoming while a cold pool was located over the Ohio Valley by 0000 UTC 24 November 1993

(Figure 10). Figure 11 shows how the warm pool intensified and moved slowly southeast into Wyoming by 0000 UTC 25 November. The upper level low, apparent from the wind circulation, also moved slowly southeast into the warm pool of air. A cold pool of air formed over Wisconsin by 0000 UTC 25 November as the tropopause undulation strengthened. This created a strong temperature gradient ahead of the undulation across the Dakotas and central Nebraska that is a common characteristic associated with a typical tropopause undulation (Hirschberg and Fritsch, Part I, 1991). The warm temperature advection at upper levels over eastern South Dakota and Nebraska intensified as southwesterly flow continued across the strengthening temperature gradient (Figure 12). It was shown in Hirshberg and Fritsch that the upper level warm advection greatly affects the low level pressure changes than equal temperature changes at low levels. Therefore, the strong warm advection at upper levels acted to significantly decrease the surface pressure. This, in turn, intensified the low level convergence and enhanced the vertical velocities over northeastern South Dakota.

The subsidence in the left entrance region of the jet streak allowed a downward extrusion of high potential vorticity from the stratosphere (Hirschberg and Fritsch, Part 11, 1991). This is evident in Figure 13 where the isentropic potential vorticity maxima at 1200 UTC 24 November and 0000 UTC 25 November were found in the warm pool over Montana and Wyoming.

Figure 14 shows a cross-section taken from central Idaho to near Green Bay, Wisconsin, of potential vorticity units (PVU) and vertical velocities (Gibson, 1995). The location of the cross-section is displayed in Figures 11 and 12. The tropopause is typically found between 1 and 1.5 PVU's- Note how the range of 1 to 1.5 PVU's descends to 500 mb or lower, most likely over the state of Wyoming. The high values of potential vorticity that descended into the troposphere represent the warm temperatures associated with the sinking stratospheric air and the resultant upper level warm advection ahead of the undulation that enhanced the upward vertical motion over northeast South Dakota.

Figure 15 shows the ageostrophic circulation in the plane of the cross-section along with the vertical velocities from central Idaho to near Green Bay, Wisconsin from 1200 UTC 24 November to 0000 UTC 25 November 1993. The area of greatest upward vertical motion occurred over northeast South Dakota and corresponded to the layer of lower stability (where the potential temperature surfaces were farther apart; not shown) between 500 mb and 250 mb. The vertical velocities were maximized here due to the decreased stability and the upper level warm advection. Note how as the undulation shifted slightly cast the vertical velocity maxima moved east over northeast South Dakota.

4. CONCLUSION

A coupled jet structure over the Northern Plains on November 23, 1993 enhanced upward vertical motion over northeastern South Dakota through the direct and indirect thermal ageostrophic circulations. The increased vertical velocities provided enough lift to saturate the atmosphere to cause an initial period of significant snowfall.

Subsidence and warming associated with convergence in the left entrance region of a jet streak over western Montana on November 24, created a tropopause undulation. High potential vorticity from the stratosphere was extruded downward with this subsidence. As this air warmed, a strong upper level temperature gradient formed over the Dakotas. The strong upper level warm advection over eastern South Dakota acted to lower the surface pressure and enhance the upward vertical velocities. As the strong upward vertical velocities moved over northeastern South Dakota, a second period of significant snow fell. The two events together helped snowfall totals exceed two feet over the northeastern portion of South Dakota.

Through the use of gridded data, meteorologists can readily analyze the presence of tropopause undulations in strong low pressure systems. Some common characteristics of tropopause undulations include a warm temperature pool in the upper troposphere, potential vorticity maxima in or near the warm pool, and strong upper level warm temperature advections downstream of an undulation. Recognizing these phenomena can aid forecasters in determining areas of enhanced upward vertical motion and heavy precipitation potential.

5. ACKNOWLEDGEMENTS

I would like to thank Ron Holmes and the NWS Central Region SSD for reviewing this paper. Thanks also to Chris Gibson for the potential vorticity macros.

6. REFERENCES

Bell, G.D., and L.F. Bosart, 1993: A Case Study Diagnosis of the Formation of an Upper Level Cutoff Cyclonic Circulation over the Eastern United States. *Mon. Wea. Rev.*, **121**, 1635-1655.

Gibson, C., 1995: Operational Use of Potential Vorticity to Identify the Location, Strength and Movement of Upper-Level Fronts. WR Technical Attachment 95-15. DOC, NOAA, NWS Western Region, Scientific Services Division, Salt Lake City, UT, 5pp.

Hakim, G.J., and L.W. Uccellini, 1992: Diagnosing Coupled jet-Streak Circulations for a Northern Plains Snow Band from the Operational Nested-Grid Model. *Wea. Forecasting*, **7**, 26-48.

Hirschberg, P.A., and J.M. Fritsch, 1991: Tropopause Undulations and the Development of Extratropical. Cyclones. Part 1: Overview and Observations from a Cyclone Event. *Mon. Wea. Rev.*, **119**, 496-517.

_____, and _____, 1991: Tropopause Undulations and the Development of Extratropical Cyclones. Part 11: Diagnostic Analysis and Conceptual Model. *Mon. Wea. Rev.*, **119**, 518-550.

Hoskins, B.J., I. Draghici, and H.C. Davies, 1978: A New Look at the Omega-Equation. *Quart. J. Roy. Meteor. Soc.*, **104**, 31-38.

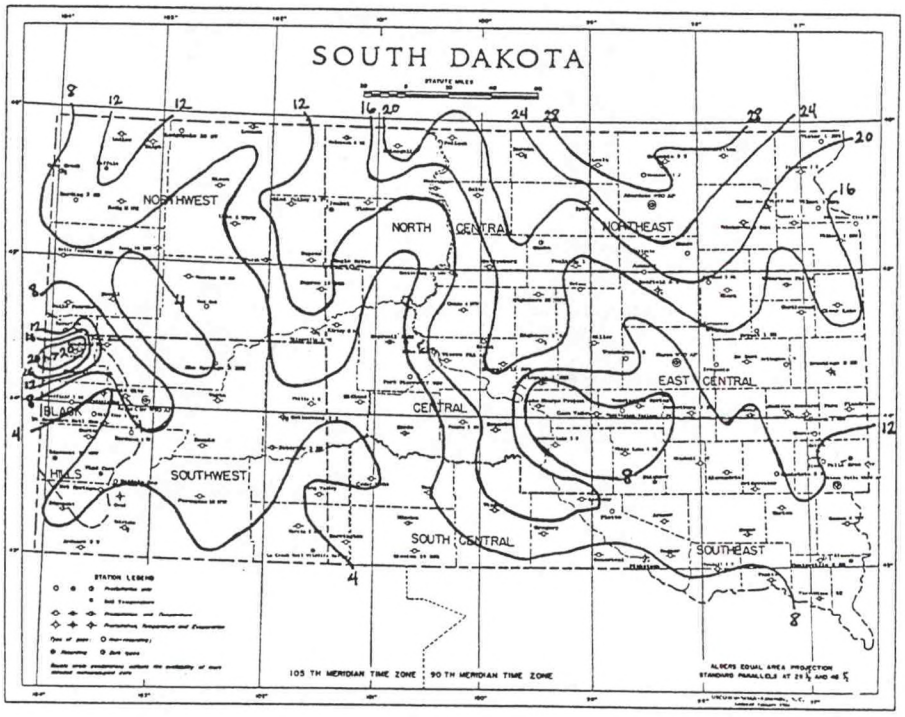

Figure 1. Total snowfall (inches) over South Dakota between November 21 and 28, 1993.

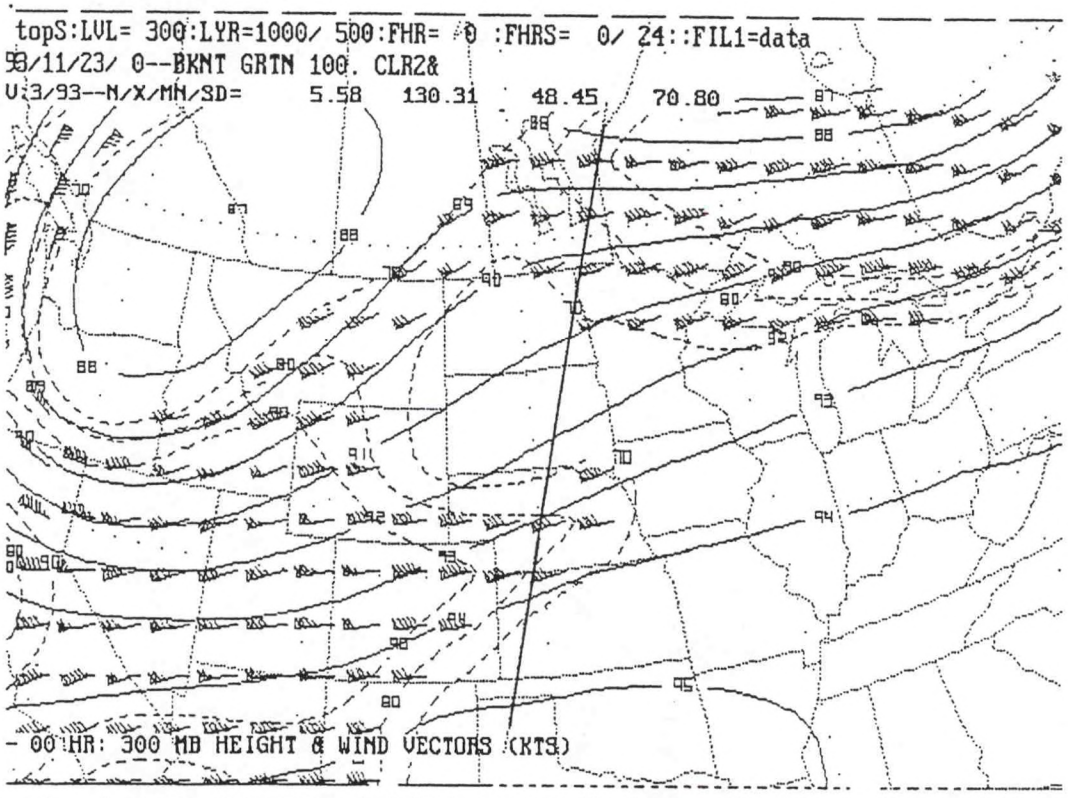

Figure 2. Analysis of 300 mb wind (kts), isotachs (dashed), and height (x 10 dm solid) for 0000 UTC 23 November 1993. Thick solid line A-B shows cross-section taken through jet streaks.

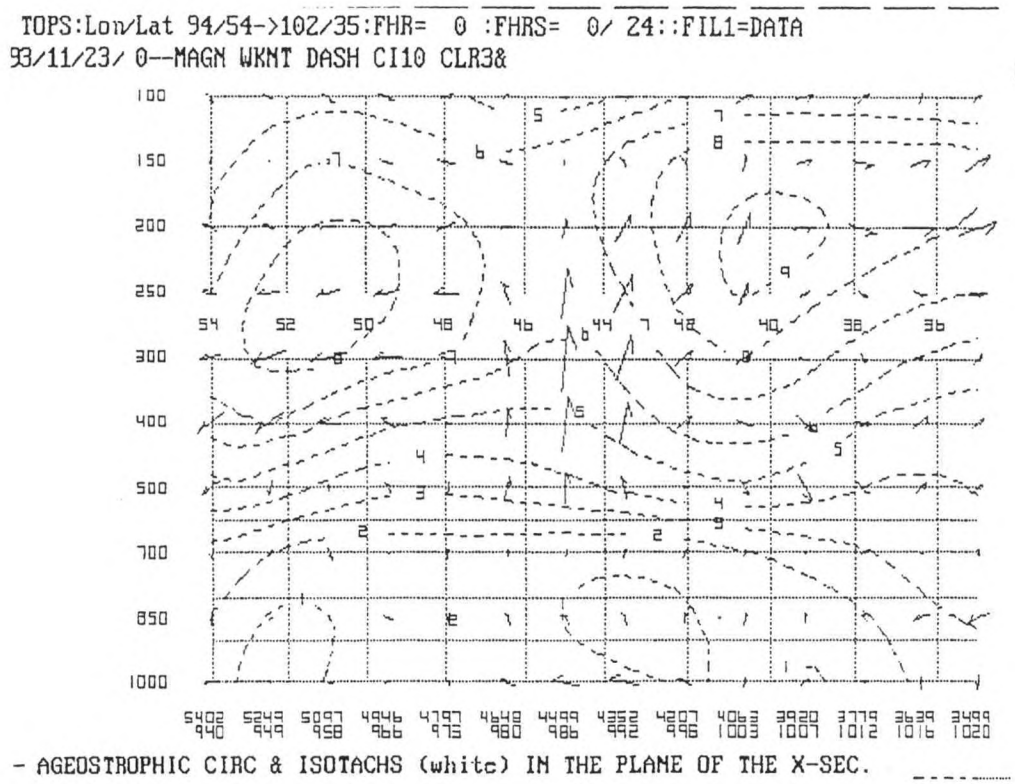

Figure 3. Cross-sectional analysis of ageostrophic circulation (arrows) and isotachs (kts) for 0000 UTC 23 November 1993. Isotachs are for winds normal to the plane of the cross-section.

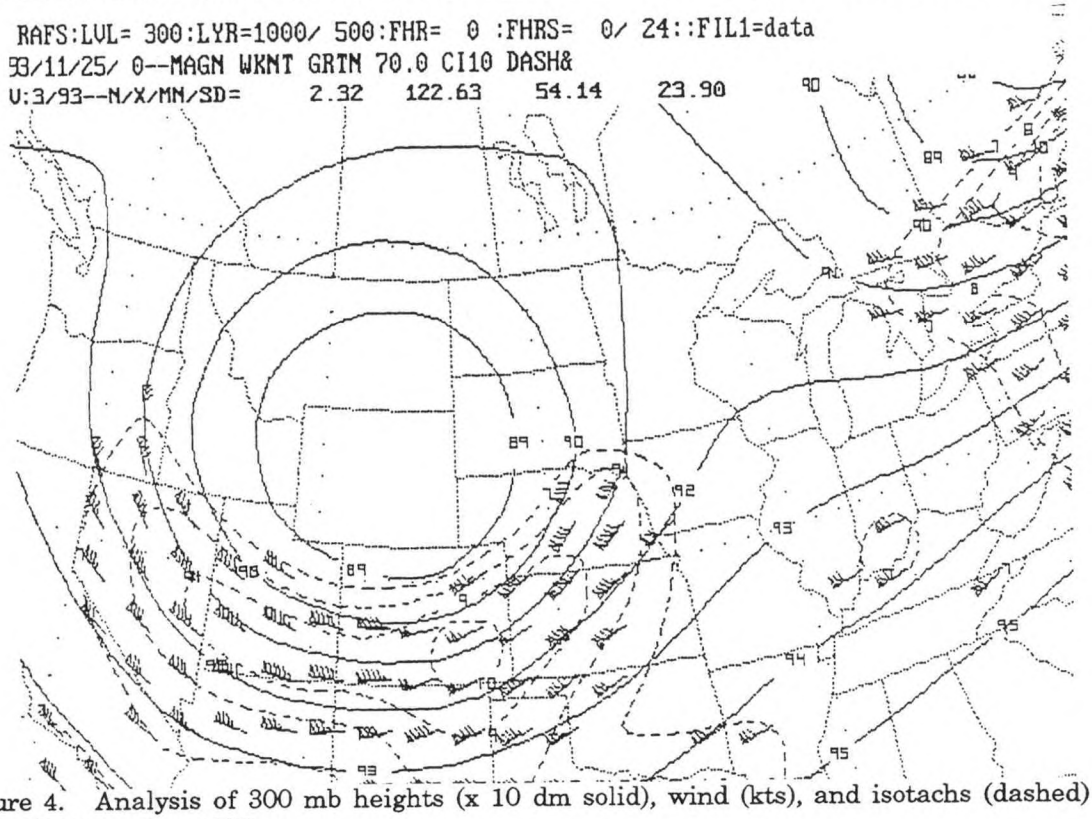

Figure 4. Analysis of 300 mb heights (x 10 dm solid), wind (kts), and isotachs (dashed) for 0000 UTC 25 November 1993.

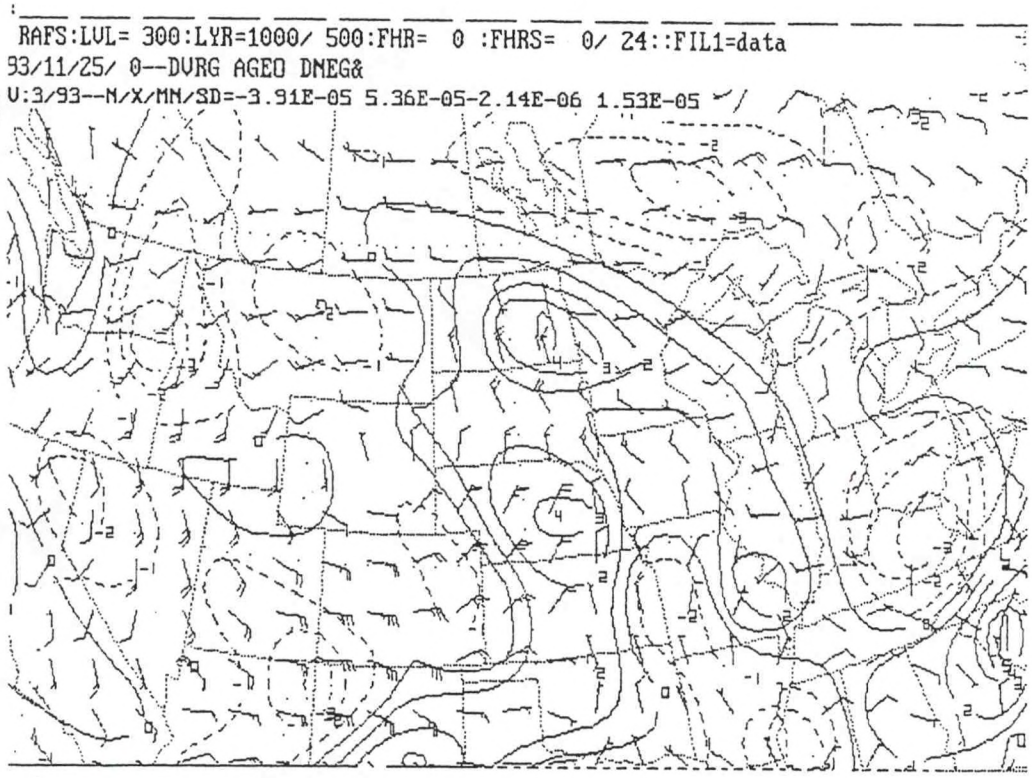

Figure 5. Analysis of 300 mb ageostrophic wind (m s^{-1}) for 0000 UTC 25 November 1993. Solid contours outline areas of ageostrophic wind divergence. Dashed contours outline areas of ageostrophic wind convergence.

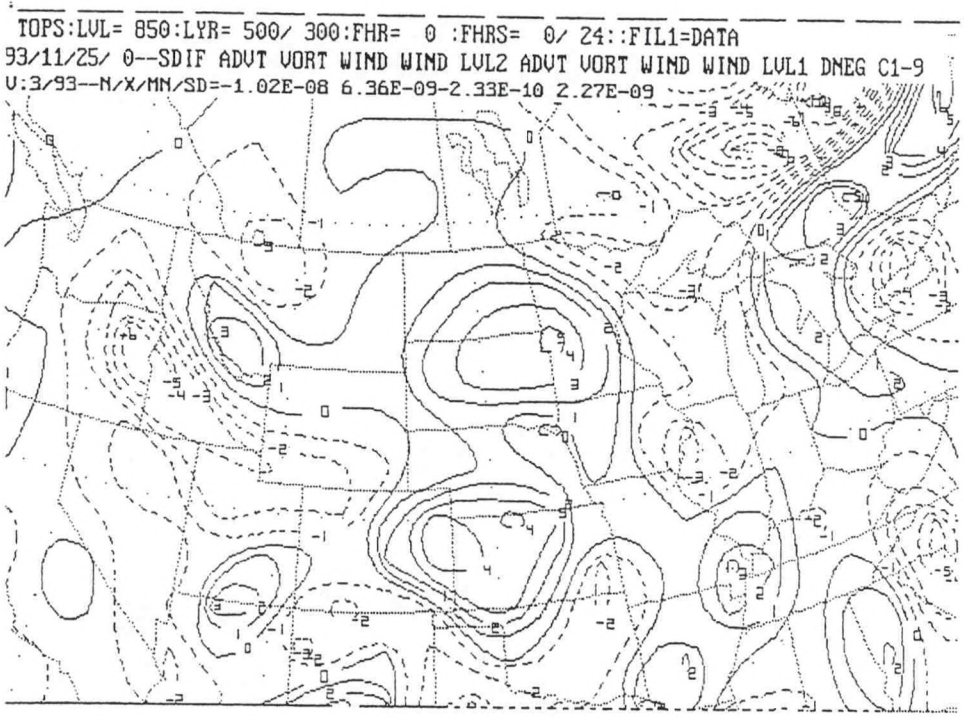

Figure 6. 500-300 mb layer difference of vorticity advection (x 10^{-9} s^{-2}) for 0000 UTC 25 November 1993. Positive values show a positive contribution to the vorticity advection term of the omega equation.

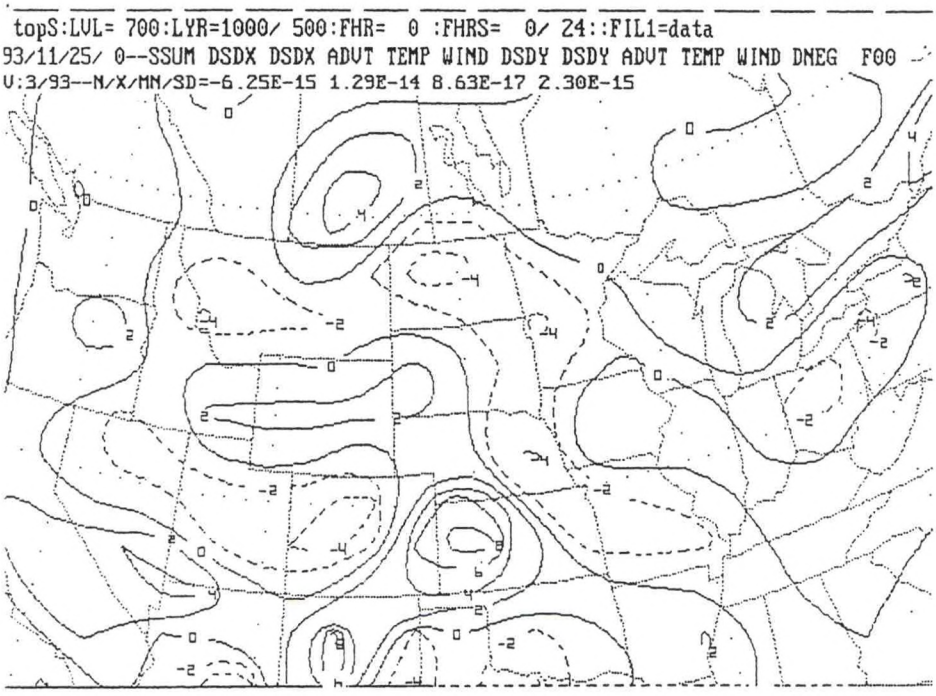

Figure 7. 700 mb analyses of Laplacian of temperature advection (x 10^{-15} m kg^{-1} s^{-1}) for 0000 UTC 25 November 1993. Negative values show a positive contribution to the temperature advection term of the omega equation.

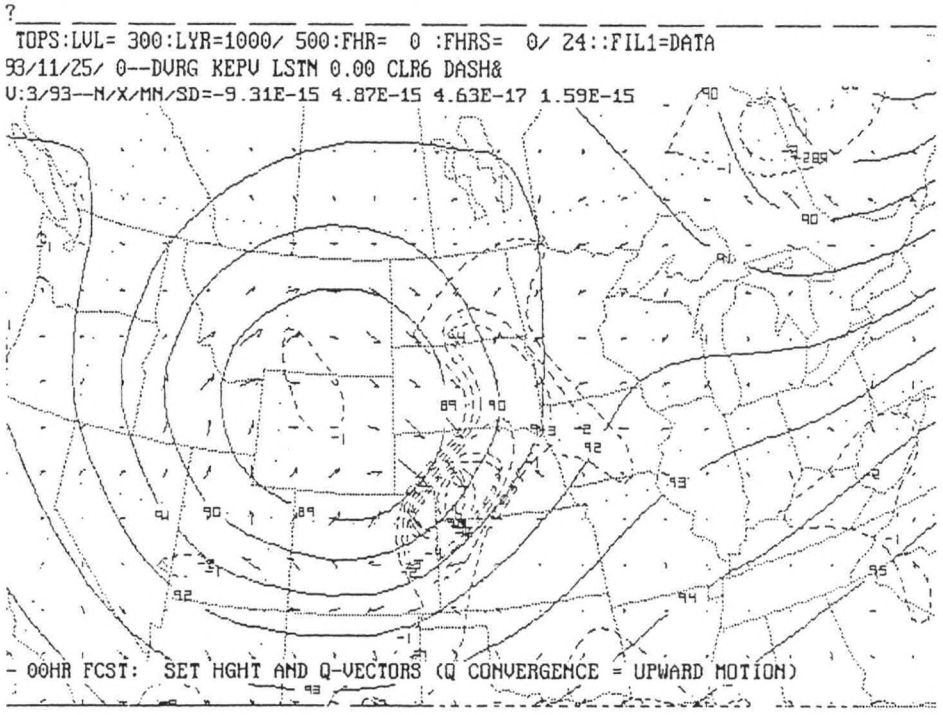

Figure 8. Analysis of 300 mb height (x 10 dm solid), Q-vectors (arrows), and convergence of Q-vectors (x 10^{-15} m kg^{-1} s^{-1}) for 0000 UTC 25 November 1993. Dashed lines show Q-vector convergence.

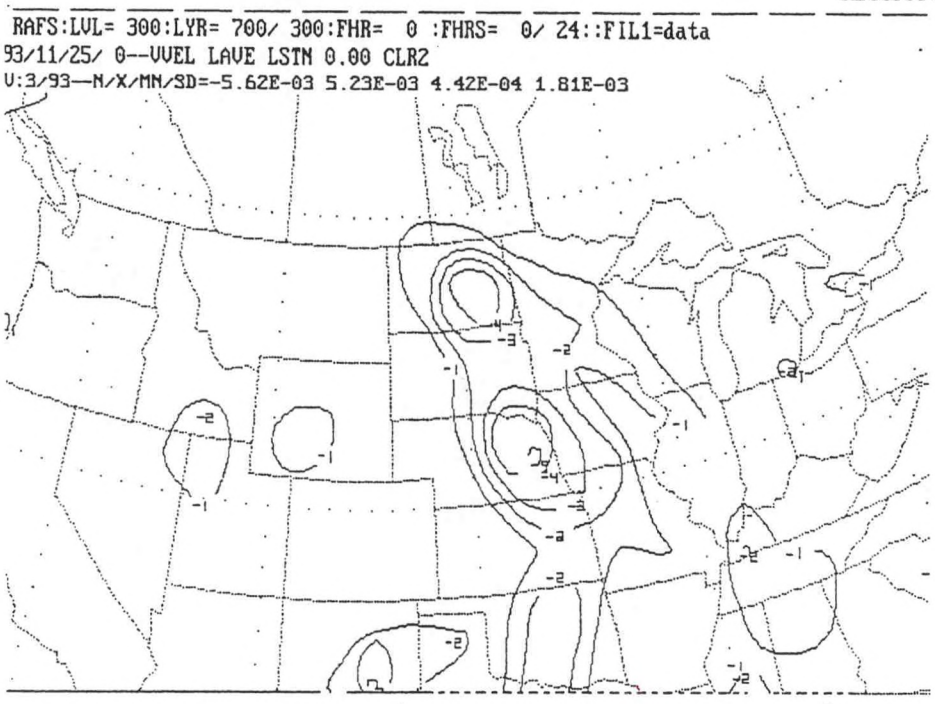

Figure 9. Analysis of 700 mb to 300 mb average upward vertical velocities (microbars per second) for 0000 UTC 25 November 1993.

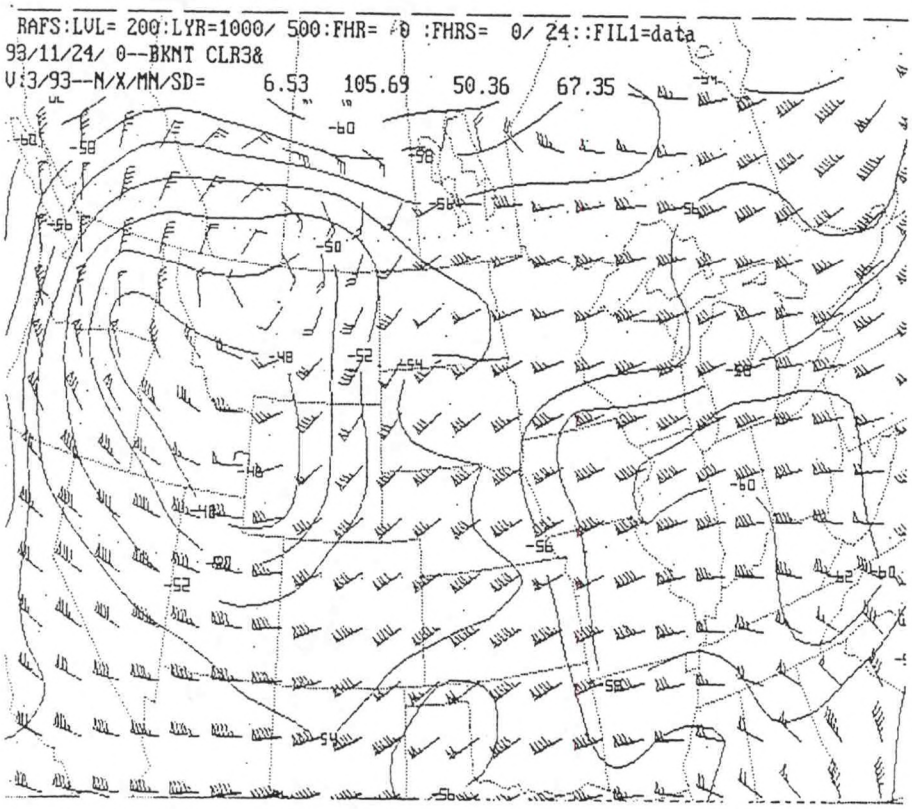

Figure 10. Analysis of 200 mb temperatures (°C) and winds (kts) for 0000 UTC 24 November 1993.

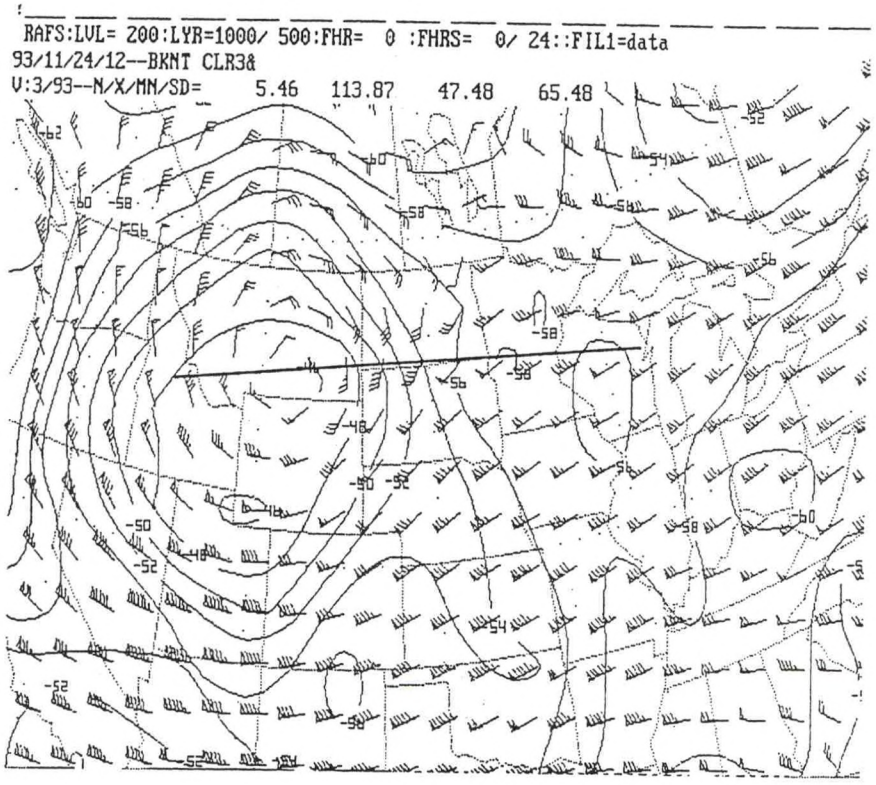

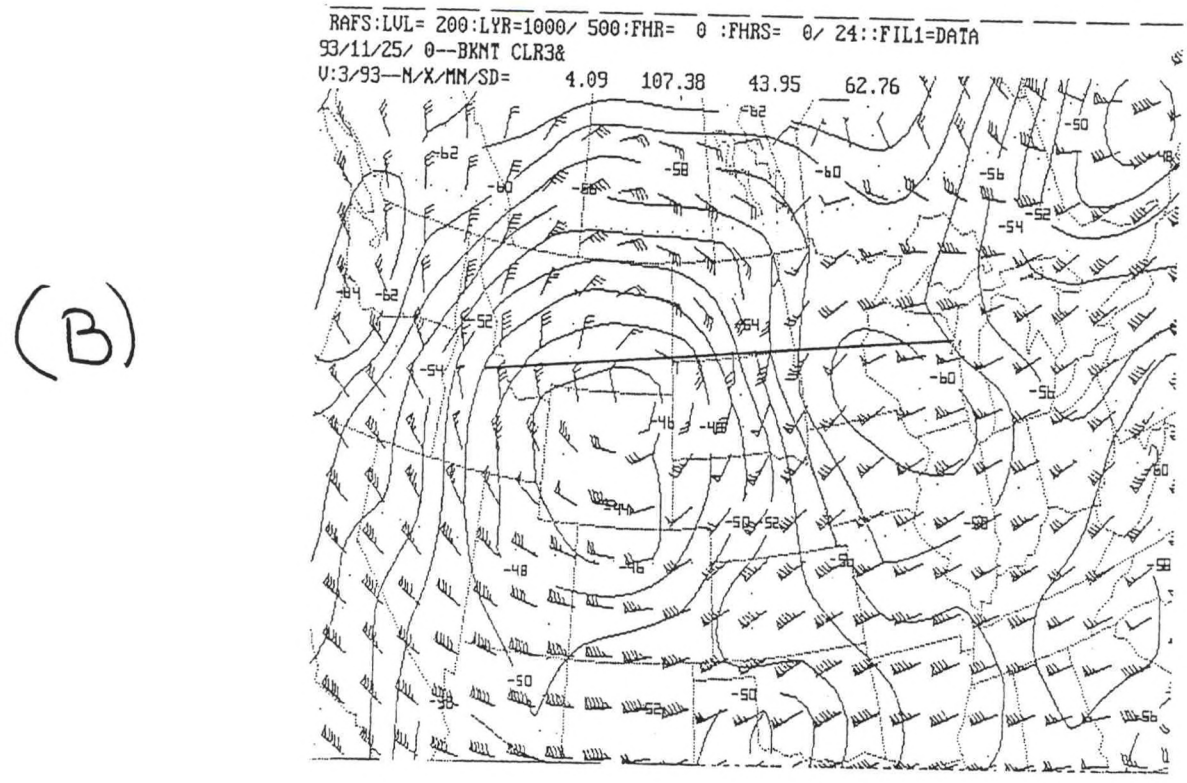

Figure 11. Analysis of 200 mb temperatures (°C) and winds (kts): (a) 1200 UTC 24 November; (b) 0000 UTC 25 November 1993. Heavy solid line represents cross-section.

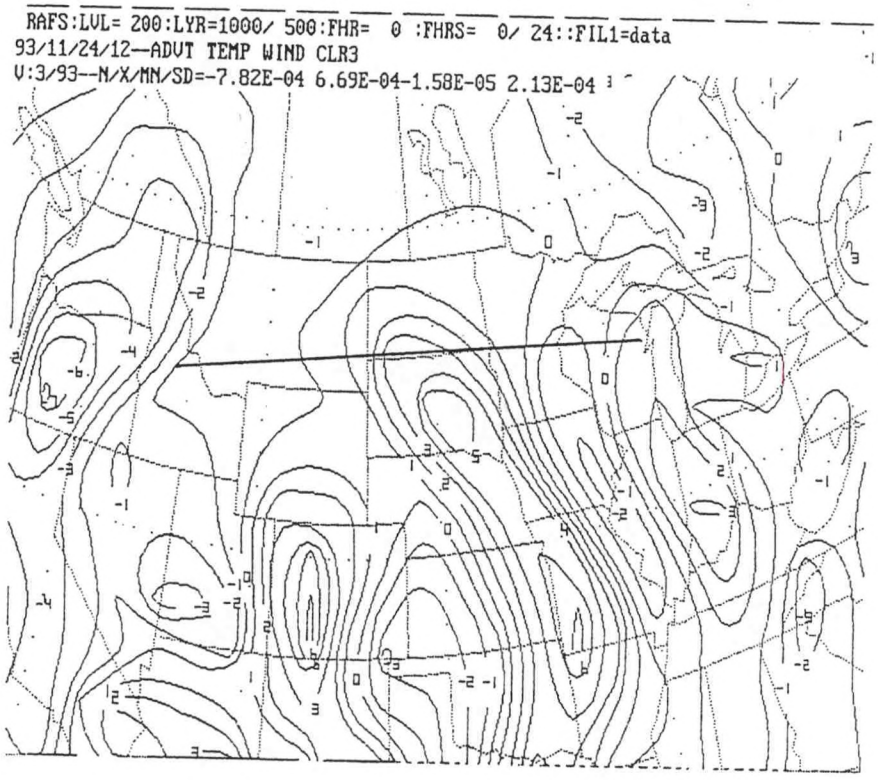

(A)

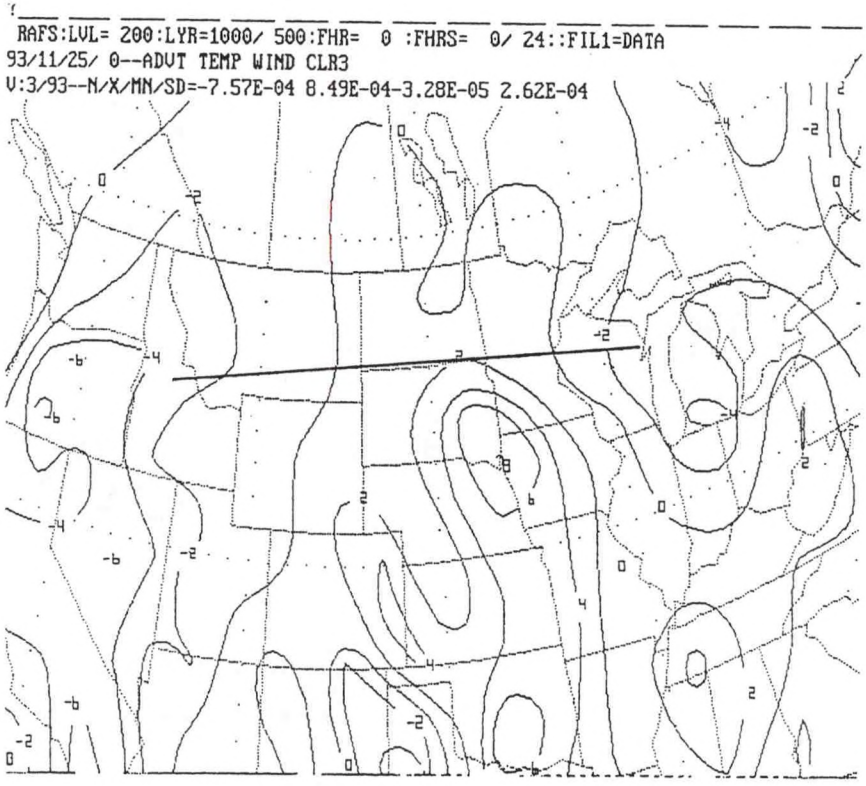

(B)

Figure 12. Analysis of 200 mb temperature advection (x 10^{-4}K s^{-1}): (a) 1200 UTC 24 November; (b) 0000 UTC 25 November 1993. Positive values indicate warm temperature advection. Heavy solid line represents cross-section.

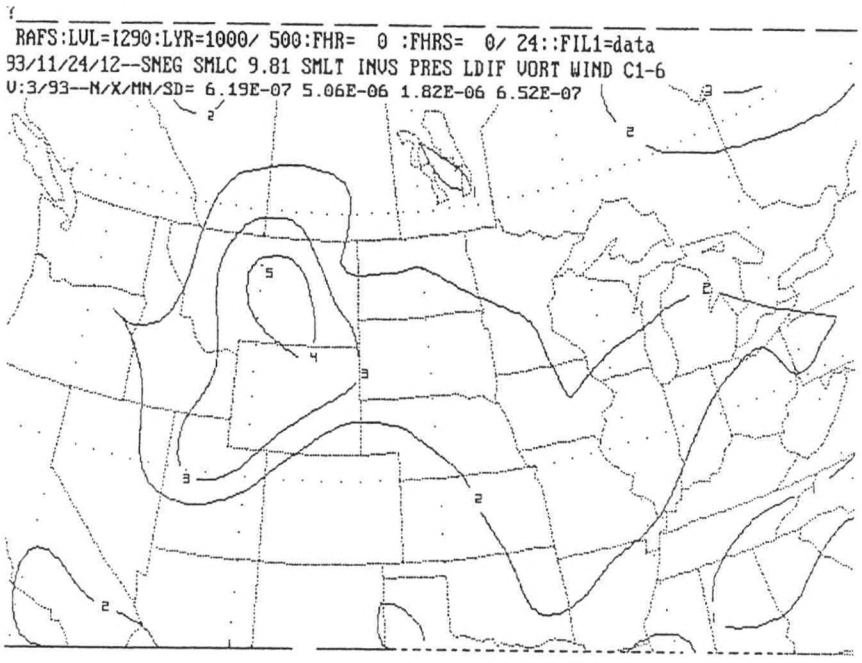

(A)

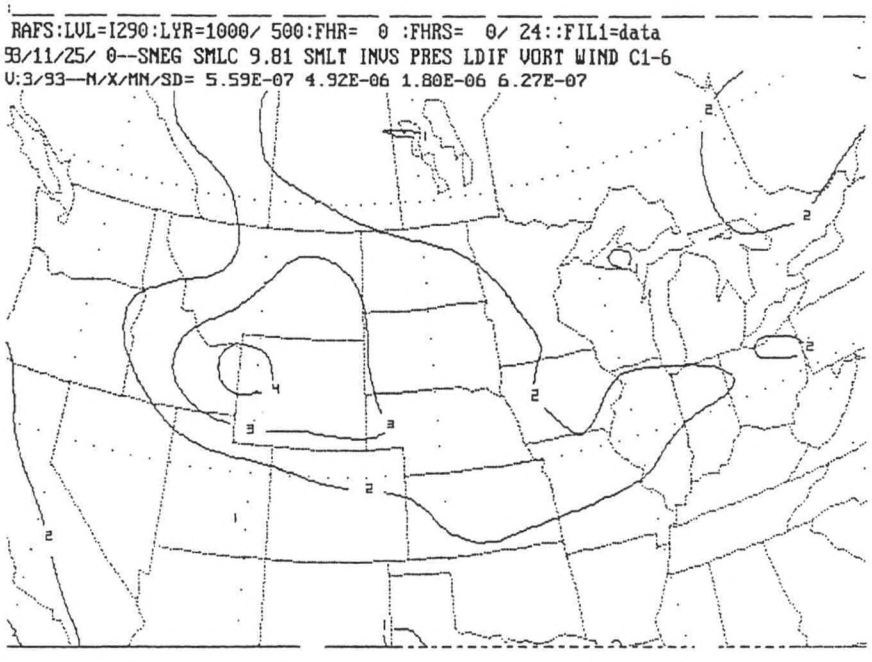

(B)

Figure 13. Analysis of isentropic potential vorticity (10^{-6}m2K kg^{-1}s^{-1}) on 290 K surface: (a) 1200 UTC 24 November; (b) 0000 UTC 25 November 1993.

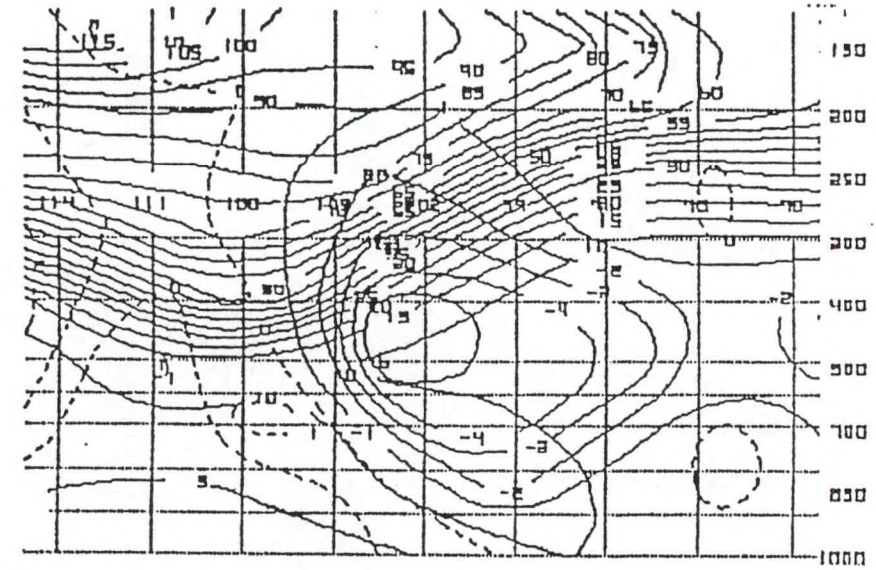

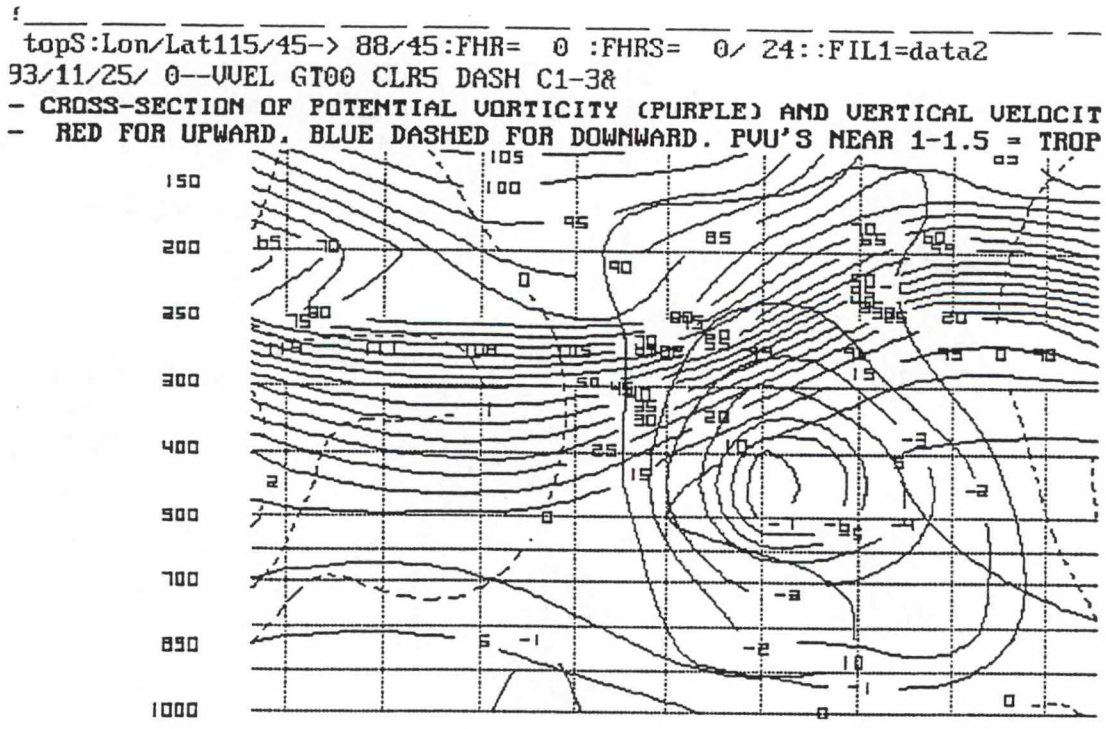

Figure 14. Cross-sectional analysis of potential vorticity units (1 PVU = 10-6m2Ks^{-1}kg^{-1}) and vertical velocities (microbars per second) from central Idaho to near Green Bay, Wisconsin (GRB): (a) 1200 UTC 24 November; (b) 0000 UTC 25 November 1993. Thick solid lines are potential vorticity. Thin solid and dashed lines are vertical velocities. Aberdeen, South Dakota, is represented by ABR.

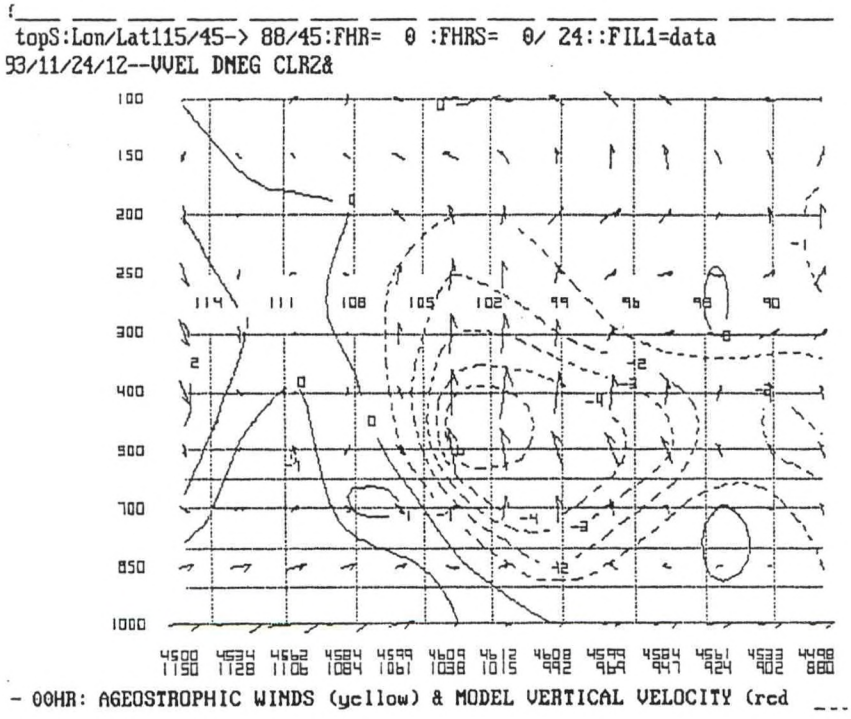

(A)

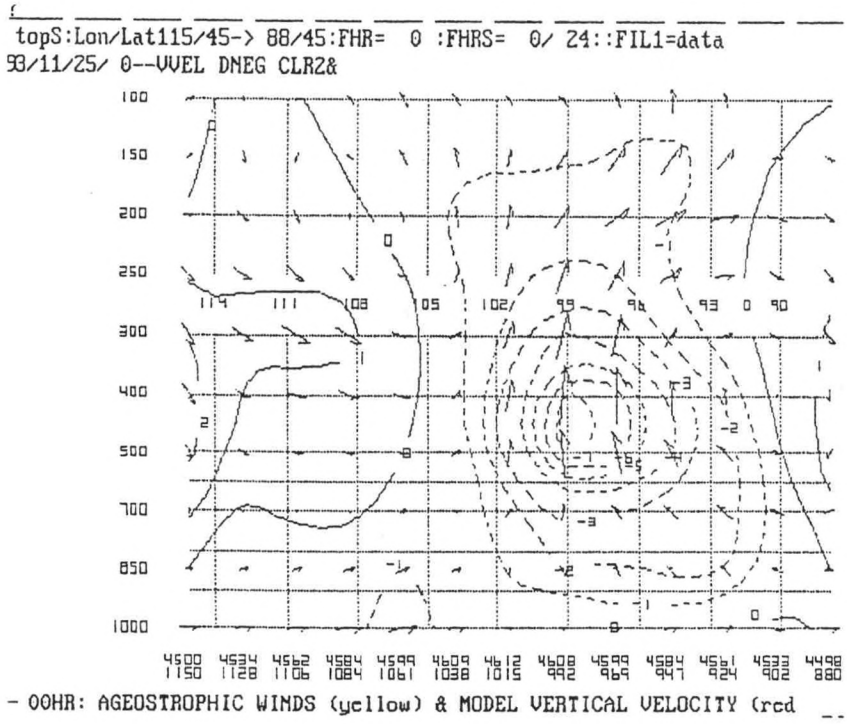

(B)

Figure 15. Cross-sectional analysis of ageostrophic circulation (arrows) and vertical velocities (microbars per second): (a) 1200 UTC 24 November; (b) 0000 UTC 25 November 1993. Dashed contours represent upward vertical velocities. Aberdeen, South Dakota, is represented by ABR.

Combining Satellite, Radar and Ground Truth Data in Nowcasting Lake Effect Snow Intensity

James G. LaDue[1]

1. INTRODUCTION

In the winter of 1994 to 1995, the National Weather Service (NWS) instituted Lake Effect Snow (LES) study as a result of concerns about whether the operational deployment of the WSR-88D radar network would be able to monitor lake effect events. The WSR-88D radar network has been unable to provide complete coverage of lake effect events because of their shallow nature. However, other data sources have become available to be utilized by the LES study. Two new Geostationary Operational Environmental Satellites (GOES-8 and 9) have been set into orbit with the ability to do multi-spectral scanning over the entire Great Lake basin in 15 minute intervals or less (Menzel and Purdom 1994). At the ground level, local NWS field offices have been implementing local, high density snow spotter networks. Other data sources including aircraft data, and Standard Airways Observations (SAO) continue to be available.

This study is an attempt to integrate the operational radar, satellite and surface ground truth data in order to provide a more accurate nowcast of lake effect snow intensity and location. An analysis of a case study lake effect event will be presented.

2. METHODOLOGY

Radar, satellite and ground truth data were analyzed for a lake effect event that occurred on January 4, 1995 over Lake Erie and Ontario. The following datasets were used for the study:

A. WSR-88D 0.5° reflectivity from Cleveland (CLE), Ohio and Binghamton (BGM), New York.

B. GOES-8 10.7 μm infrared imagery.

C. Contoured snow spotter data provided by NWS Buffalo, New York.

The first part of this study, GOES-8 10.7 μm and the BM WSR-88D radar data was averaged over 6-hour periods from 0000 UTC 4 January to 0000 UTC 5 January and compared to a contoured analysis of snow spotter reports east of Lake Ontario. These analyses were completed using operational software in the RAMM Advanced Meteorological Satellite Demonstration and Interpretation System (RAMSDIS) (Schrab et. al. 1994). The purpose of this study was to spatially compare the trends of cloud top temperature, reflectivity and observed snow accumulation.

The second part of this study involved point to point comparisons of SAO visibility, WSR-88D CLE base reflectivity (dBZ), 10.7 μm observed Cloud Top Temperature (CTT in Celsius). The relation between CTTs to precipitation rates in deep convection has been studied numerous times (e.g., Scofield and Oliver 1977). As a result, CTTs were applied here as well. Visibility was also used because of its greater precision in the absence of blowing snow or fog. A period of ten hours from

1. Corresponding author address: James G. LaDue, Operational Support Facility, Operations Training Branch, 3200 Marshall Ave., Suite 200, Norman, OK 73072; e-mail <jladue@nexrad.osf.uoknor.edu>.

0800 UTC to 1800 UTC was chosen along the south shore of Lake Erie during a time when there was a relatively unchanging boundary layer thermal profile.

Three stations were used, Cayuhoga (CGF), OH; Willoughby (LNN), OH; and Burkelake (BKL), OH. GOES-8 CTTs were derived from the average of a 2 X 3 pixel array nearest to the time of the observations. A 6 X 6 pixel array was used for the corresponding radar image. For this period, a relationship was derived between radar reflectivity, CTT and visibility. Similar comparisons were also made closer to 0000 UTC 5 January when significant cooling of the boundary layer occurred.

Finally, a technique was developed to integrate ground-truth, radar and satellite data to estimate snowfall intensity based on the second part of this study. This technique was tested by participants in two workshop lab environments.

3. SIX HOURLY AVERAGES

Six hour averages of satellite and radar imagery show good agreement on the location and persistence of the lake effect band coming off Lake Ontario. There was less agreement between the remote observations and analyzed snow spotter data.

Figure 1a and 1b show the satellite and radar location of the snow band on the border of Oswego and Jefferson counties between 0000 and 0600 UTC. The coldest CTT over the same area was -26°C while the radar showed -4 to -0 dBZ. Reflectivities were underestimated with the band almost 190 km away from the BGM radar. Reflectivities decreased and CTT's increased further east over Lewis County. However, this was the region that the contoured snow spotter reports showed the most significant accumulations.

The disagreements between the analyzed snow spotter reports and the satellite/radar only increased for later six hour periods. For example, the radar and satellite averaged data from 1200 to 1800 UTC in Figure 2a and 2b respectively indicated a significant increase in snowfall rates. However, the analyzed snow accumulations only showed light accumulations well southeast of the band. There were no reports underneath the band.

4. POINT COMPARISONS

Because of the poor spatial comparisons between remote and ground-based snow observations, single point comparisons were made over the south shore of Lake Erie. The SAO visibilities used this day were considered representative of snowfall intensity since there was only one report of blowing snow out of the stations used and fog was not a problem.

The relationship between visibility, CTT and reflectivity was better than expected. Visibility was positively (negatively) correlated with CTT (reflectivity), as shown in Figure 3. Out of this dataset, the satellite (correlation = 0.83) performed even slightly better than the radar (correlation = 0.63). The best correlations were made from log regression fits. At visibilities less than 0.5 nmi the fit was more uncertain because of the lack of observations with heavy snow.

Given these relationships, a threshold reflectivity and cloud top temperatures were made for light, moderate and heavy snow. The heavy snow CTT threshold (-25°C) was very close to the temperature near the top of the convective layer observed by the Buffalo 1200 UTC sounding for that day.

Much colder air passed over the eastern Great Lakes after 2000 UTC after the passage of a boundary layer shortwave (not shown). A consequence of this was the lowering of CTT's of all lake

effect bands. These phenomena did not result in an increase in snow intensity as measured by visibility for several stations along the south shore of Lake Erie. For example, a time trace of one station, Willoughby (LNN), OH was a good example of this (Figure 4). Note that the visibility, CTT and reflectivity were well correlated in the 0800 to 1800 UTC period. However, the CTT dropped to -26° to -28°C just before 0000 UTC 5 January while the visibility remained at a modest 3 nmi. The reflectivity seemed to be more related to visibility over the whole day. During the 0800 to 1800 UTC, an enlarged shoreline band (Holroyd 1971) with min CTT's of -26°C existed as the boundary layer flow was westerly. Upon the passage of the shortwave, the flow veered and the shoreline band broke up into multiple bands. At the same time, the whole boundary layer cooled resulting in colder CTT's with a lower snow rate.

It is hypothesized that the CTT's can only be related to snowfall rates given a relatively steady state boundary layer temperature profile. Upon changing that profile, a new CTT relation must be produced. The more stable nature of the radar reflectivity vs. snowfall rate gives hope that the radar can help provide the satellite with a new snowfall intensity to CTT relationship.

5. A COMBINED NOWCASTING TECHNIQUE

A technique was developed to combine satellite, radar and ground observations in order to improve nowcasts of snowfall intensity. It is a three-step process starting with:

A. Derive threshold reflectivity rates for light, moderate and heavy snow by comparing observed reflectivities to SAOs or snow spotters. This step is done at locations generally where the radar can accurately monitor the convective layer (within 90 km of a radar for this case).

B. Associate the reflectivity thresholds for each snow category to currently observed CTT's based on GOES-8 10.7μm data.

C. Use the radar reflectivity for areas within 90 km of a radar site and the CTT data for areas beyond the 90 km limit.

This technique was presented in a workshop environment at the NWS sponsored Winter Weather Workshop in Kansas City, MO during September 1995 and also at the Operational Support Facility in Norman, OK in October 1995. The participants worked in teams of two to three and used data from the 04 January 1995 case for three stations along the south shore of Lake Erie. Two stations, Cayuhoga Airport (CGF), and Willoughby (LNN), OH, were within 90 km of the WSR-88D radar in Ohio while Erie (ERI), PA was beyond 90 km. Threshold radar reflectivities (R) were given as: $R \leq 20$ dBZ for light snow, 20 dBZ$<R<$25 dBZ for moderate snow, and $R \geq 25$ dBZ for heavy snow. The threshold visibilities were less than 0.25 nmi for heavy snow, greater than .25 nmi for moderate snow and greater than 0.5 nmi for light snow. After receiving the background information, the participants used the combined technique to estimate the snow intensity for each station for two different periods, 1345 UTC and 1645 UTC.

The results were promising given that there was no correction for the horizontal displacement of falling snow or parallax error between the radar and satellite (Figure 5). Out of 11 teams for the 1345 UTC time, only one team was more than one snow category off for station LNN. And for the 1645 UTC time, all the teams were within one snow category except ERI where was a wide dispersion of snow estimates. Upon closer inspection of the satellite data, there was a gradient of CTTs over the station with values less than -26°C overhead and to the south of the station inferring the presence of heavy snow. This may have been one instance where parallax errors may have led to errors in snow intensity estimates.

6. SUMMARY

WSR-88D radar reflectivity and GOES-8 infrared imagery were compared to two types of ground-truth data in an effort to produce a technique for estimating snow intensity.

A. Time Averaged Comparisons

The first method of comparing spatially analyzed ground-truth data with time averaged infrared and reflectivity data failed east of Lake Ontario because of the lack of key observations around the lake effect band. However, radar to satellite comparisons showed excellent agreement on intensity trends and band location. Future comparisons with spotter observations should be done on a point-to-point basis. The 6 hourly spotter observations of snow accumulation should be extremely useful as long as they are compared to satellite and radar data averaged over the same period as the spotter reports.

B. Radar and Satellite Comparisons with Visibility

For the period analyzed, the radar and satellite data showed good correlation to observed visibility. The radar reflectivity was inversely proportional to visibility. Cloud top temperatures were proportional to visibility. However, there were big drops in visibility for small decreases in CTTs for visibilities under 0.5 nmi. These comparisons showed enough promise to develop a technique to be tested in a workshop environment.

C. A Combined Radar and Satellite Snowfall Intensity Technique

This technique showed good promise after being tested by meteorologists in two workshops. However, there was a large spread of estimates when Erie, PA was on the edge of a lake effect cloud band. This was possibly due to satellite parallax errors.

This technique will be tested more during the upcoming winter season for a variety of thermal profiles. In addition, snow spotter reports will be compared to radar and multi-spectral satellite on a point by point basis such that this technique may be tested in remote areas.

7. ACKNOWLEDGMENTS

Thanks go to Steve McLaughlin (WFO, BUF) and Bob LaPlante (WFO, CLE) for providing snow reports. Ed Mahoney and Tom Niziol (WFO, BUF) provided many insights. John Weaver, Ray Zehr (NESDIS) also were helpful with their thoughts. Pat Dills, Jim Cowie and Julie Hall (COMET) provided much needed data. Finally, Eileen Maturi and Jim Nelson (NESDIS) were thanked for their help.

8. REFERENCES

Holroyd, E.W., III, 1971: Lake-effect cloud bands as seen from weather satellites. *J. Atmos. Sci.*, **28**, 1165-1170.

Menzel, W.P., and J.F.W. Purdom, 1994: Introducing GOES-I: The first of a new generation of geostationary operational environmental satellite. *Bull. Amer. Meteor. Soc.*, **75**, 757-781.

Schrab, K.J., D. Molenar, J F.W. Purdom, L. Dunn, and B. Coleman, 1994: The use of digital satellite data via a menu system in NWS offices. *Preprint Volume, Seventh Conf. on Satellite Meteorology and Oceanography,* Monterey, CA, AMS (Boston), 448-451.

Scofield, R.A., and V.J. Oliver, 1977: A scheme for estimating convective rainfall from satellite imagery. NOAA Tech Memo. NESS-86, National Earth Satellite Service, Washington, D.C., 47 pp.

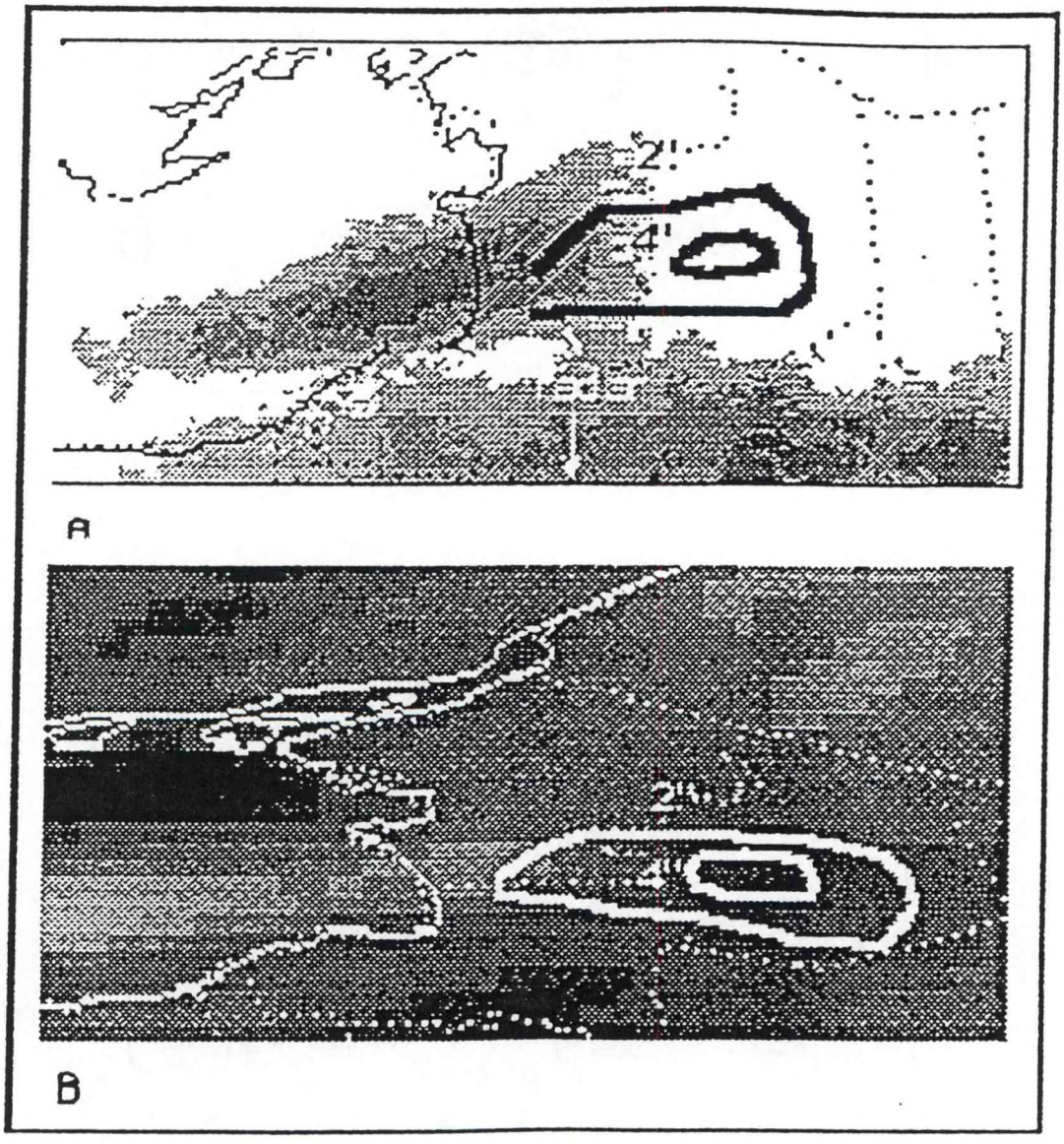

Figure 1. Averaged reflectivity in dBZ (a) and CTT (b) between 0000 and 0600 UTC 04 January, 1995. Contoured six hour snow accumulations are superimposed. The maximum reflectivities are 4 dBZ and decrease 8 dBZ for each lighter gray shade The brightest gray in 1b is CTTs between -25˚ to -30˚C and increase 5˚C for each darker shade of gray.

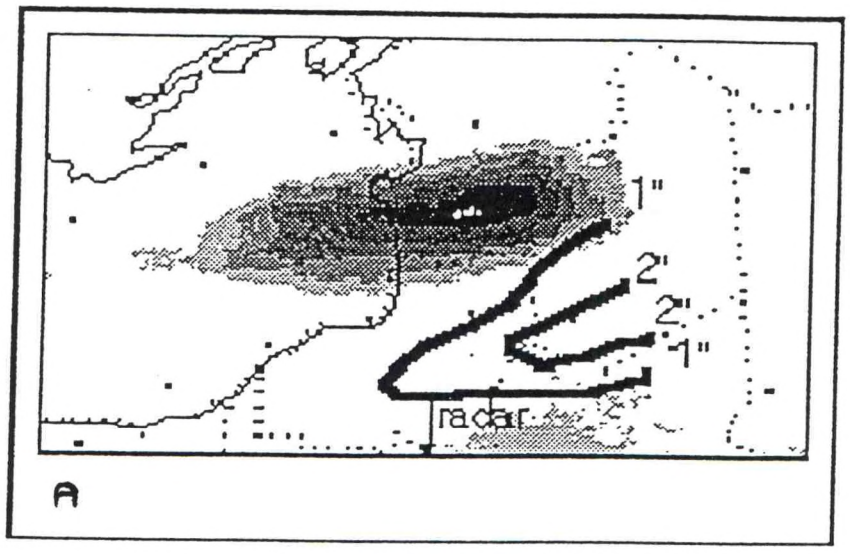

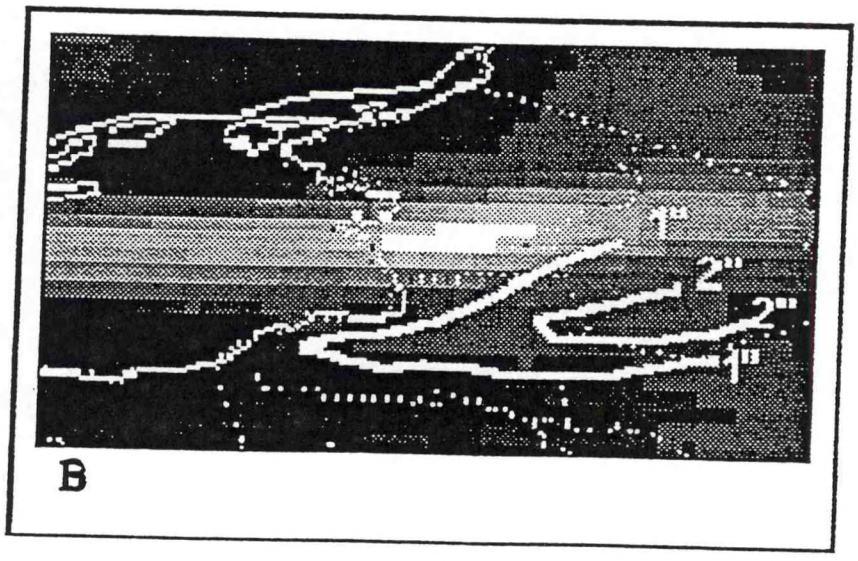

Figure 2. Same as Figure 1 except the times from 1200 to 1800 UTC are used in the averaged imagery. The maximum reflectivity on Figure 1b is 12dBZ with the same increments.

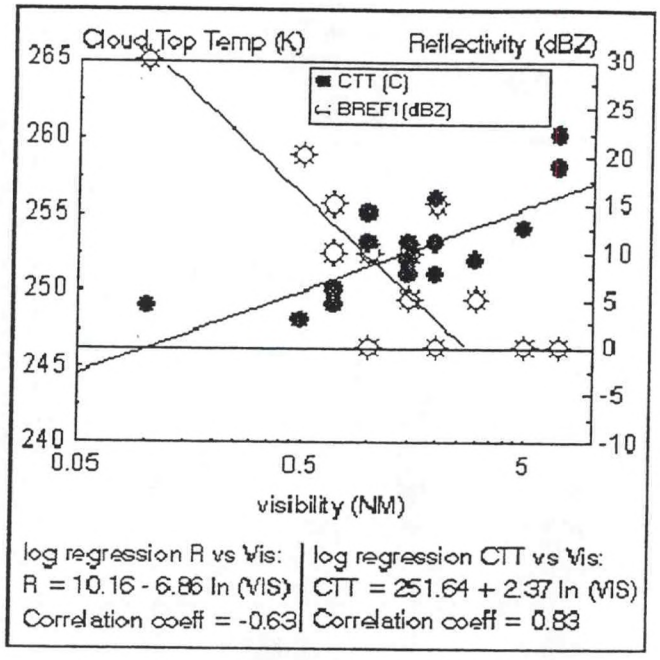

Figure 3. Scatter plot of visibility (VIS) vs. radar reflectivity (R) from CLE (sunburst symbols) and GOES-8 10.7 μm cloud top temperatures (CTT) (filled circles). The period was 0800 - 1800 UTC.

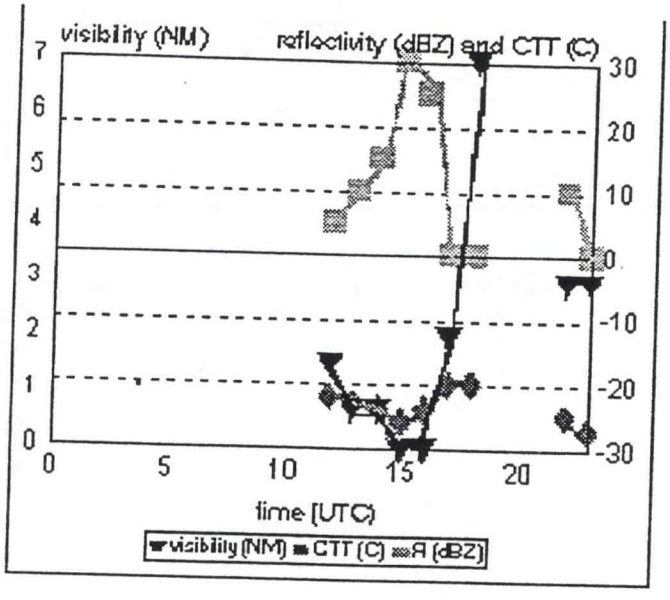

Figure 4. Time plot of visibility (wedges), reflectivity (boxes) and cloud top temperatures (diamonds) for Willoughby, OH 04 January 1995.

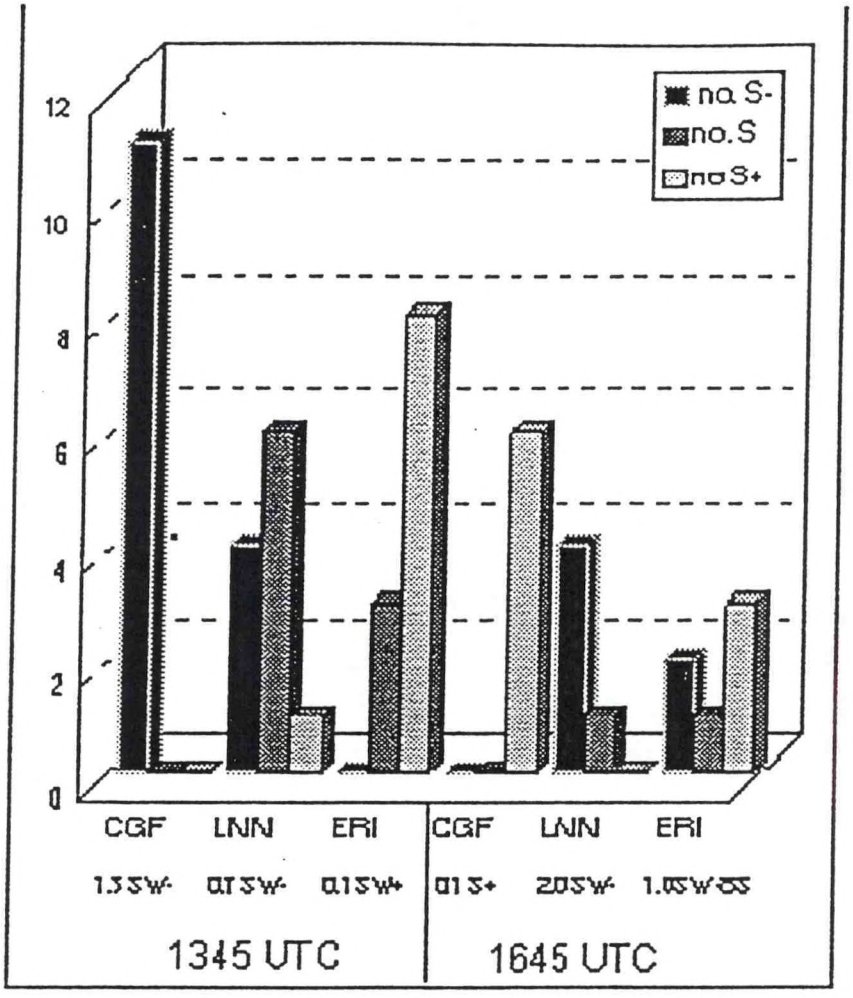

Figure 5. Histogram of workshop results in estimating snow intensity at stations, LNN, CGF, and ERI based on the 04 Jan 1995 data (see text). The vertical axis represents the number of teams in participation. The numbers below each station represent visibility (nm) and snow intensity.

National Severe Storms Laboratory and Storm Prediction Center Freezing Precipitation Forecast Experiment for Winter of 1993 - 1994

Charlie A. Crisp[1]

1. INTRODUCTION

The National Severe Storms Laboratory (NSSL) is committed to mesoscale applied research relating to the Storm Prediction Center's (SPC) (McPherson 1994) mission. Since the SPC will be forecasting freezing precipitation, NSSL conducted a freezing precipitation forecast experiment from December 1, 1993 through February 28, 1994. A description of the experiment and review of techniques used in preparing the forecast is given in the following sections. A case study of a particular freezing precipitation event on January 25-26, 1994 is presented to illustrate how forecast techniques and composite charts were used. Conclusions and a discussion regarding lessons learned are presented.

2. FORECAST EXPERIMENT

Forecasts during the experiment were issued between 2000 and 2100 UTC each day for that part of the central and southern plains west the Mississippi River and north of 31°N. Each day forecasters reviewed the synoptic situation to determine whether there was a reasonable chance for freezing precipitation in the forecast domain. If so, diagnostic and model prognostic packages were prepared.

The diagnostic package contained hand analyses of the surface, 850-, 700-, 500- and 300-mb charts for 1200 UTC, as well as low level (1000-850mb) thickness (LLT) and middle level (850-700mb) thickness (MLT) analyses from the Environmental Modeling Center's (EMC) 48km ETA model (Black et al. 1993) 1200 UTC initialization. Select parameters used to indicate areas having the potential for freezing precipitation were transferred to a composite analysis chart. The prognostic package was created using the ETA model 12, 24 and 36 hour forecasts. Composite charts were created for the respective times similar to that created in the diagnostic package. Forecasts were required to specify type of precipitation (freezing drizzle [ZL], freezing rain [ZR] or sleet [IP]), probability of occurrence, and amount. The forecasts assigned probability of occurrence expressed in multiples of 10% for each area in the forecast. Water equivalent amount of precipitation was forecast by category (0.01 inch - 0.1 inch, 0.1 inch -0.25 inch and 0.25 or more). The forecasts were divided into periods of 6,6 and 12 hours; 00-06 UTC, 06-12 UTC and 12-00 UTC, respectively. The forecast product (Section 5) consisted of a discussion and an area forecast chart for each forecast period. A general discussion described the current synoptic situation (1200 UTC diagnostics package) and how the forecaster interpreted the various meteorological variables evolving/interacting to produced the precipitation. For each forecast period, a specific discussion described the precipitation types, their probabilities and amounts and then described how/when each type would develop, change, move, and perhaps end. A chart was drawn for each of the forecast valid periods to indicate the areas where ZL, ZR or IP were expected.

1. Corresponding author address: Charlie A. Crisp, National Severe Storms Laboratory, 1313 Halley Circle, Norman, OK 73069. E-mail: crisp@nssl.uoknor.edu

3. FORECAST TECHNIQUES

Forecasts of precipitation type require the correct determination of the vertical configuration of freezing and melting layers. Location of the 850-mb 0°C isotherm relative to the surface 0°C isotherm was used as a first guess of precipitation type provided there was sufficient moisture and vertical motion present. Snow or IP (if a melting layer is above 850-mb) often occurs on the cold side of both the surface and 850-mb 0°C isotherms. Use of the 850-mb 0°C isotherms will not work for forecasting IP at locations who are near 850-mb in elevation because the surface based freezing layer will not be deep enough. ZL or ZR often occurs on the cold side of the surface 0°C but on the warm side of the 850-mb 0°C isotherms and liquid precipitation on the warm side of the surface and 850-mb 0°C isotherms (Figure 1a).

The second technique used to outline the precipitation type areas incorporate select LLT and MLT contours and their positions relative to the surface 0°C isotherm. This technique is not valid for the western U.S. or in higher terrain. In an unpublished report, Umpenhour (1968) associated the occurrence of liquid precipitation vs. freezing precipitation vs. snow with areas outlined by the surface 0°C and various LLT and MLT contours (Figure 1b). He also stated that there should be sufficient moisture and vertical motion to produce the precipitation. The intensities indicated in Figure 1b are dependent on the moisture availability and vertical motion. It should be noted that precipitation on the cold side of the 1300 meter LLT contour but on the warm side of the 1555 meter MLT will be freezing precipitation but since it could remain liquid in this area it is best to plot the surface 0°C isotherm to help determine the precipitation type.

Others such as Keeter and Cline (1991) have used partial thickness values to show precipitation type. Use of both techniques is demonstrated in Section 5.

4. SYNOPTIC SITUATION FOR JANUARY 25 & 26, 1994

At 25/1200 UTC a continental Polar (cP) front extended from southern Wisconsin through Wyoming (Figure 2). A surface low was located in southeast Kansas with a maritime Polar (mP) cold front extending from the low through central New Mexico with a warm front from the low through central Illinois. Surface dew points in the upper 40s to mid 50s (°F) were in western Missouri and eastern Kansas. The moisture at 850-mb (Figure 3) was being advected northeastward from Texas just east of the mP front and surface low. The 850-mb 0°C isotherms (Figure 3) were located about 120 miles north of the surface 0°C isotherm (Figure 2) in eastern Nebraska and northern Iowa where temperature dew point spreads were 5 degrees or less. A 500-mb short wave associated with the surface low was moving rapidly east-northeast (Figure 4). MLT values indicative of freezing precipitation were analyzed over the northern part of the experiment's forecast domain at this time (Figure 5). Upward motion associated with the 500-mb shortwave, low level moisture availability and favorable vertical thermal stratification explained why the freezing precipitation occurred from northern Illinois into eastern South Dakota and Nebraska (Figure 2).

The surface low in southeast Kansas moved east-northeast through the day and advanced the primary moist axis eastward. By 26/1200 UTC, a second surface low developed over southeastern Colorado and the mP front over Oklahoma (Figure 2) began to move northward as a warm front (not shown). The strong 500-mb short wave over the southwestern U.S. at 25/1200 UTC developed a closed circulation in Colorado by 26/1200 UTC and moved northeastward toward Nebraska. In response to the vigorous 500-mb short wave, 850-mb winds backed to a more southerly direction and increased to 45 knots. A new 850-mb axis of maximum moisture advection developed over eastern Oklahoma with dew points of 9°C at Oklahoma City and 7°C at Monett, Missouri by 26/1200 UTC. Surface dew points in the southern half of Oklahoma and most of Arkansas were in the upper 50s to low 60s (°F)

and strong low level warm and moist advection continued to the east and north of the surface low as it moved east and northeast beyond 27/0000 UTC.

5. FORECAST AND VERIFICATION FOR 26 JANUARY 1994

A. Forecast

The techniques described in Section 3 defined the parameters needed on the winter weather composite analysis (Figure 5) and composite prognoses (Figure 6) to outline the areas of forecast precipitation type. Other parameters the forecaster found useful were also included. Locations for the MLT (1555, 1540 and 1520 meters) contours were found by running a PCGRIDDS (Peterson 1992) macro on the ETA model 25/1200 UTC initialization. Since liquid precipitation will occur on the cold side of the 1300 meter LLT contour but on the warm side of the surface 0°C isotherm, the 1300 meter LLT contour was omitted in favor of using the surface 0°C isotherm to separate the areas where liquid and freezing precipitation would occur. The parameters were drawn on the composite analysis to determine locations for the precipitation types.

The 12, 24 and 36 hour composite prognoses were produced with the parameter locations based on forecaster experience and guidance from PCGRIDDS displays of various ETA model fields. Development of the 24-hour composite is described below and is shown in Figure 6. The B015 level (represents the midpt of the first 30mb above the surface) in the ETA model was more representative of surface conditions than any other level in the model using PCGRIDDS. The same parameters used on the composite analysis were used on the composite prognosis with some minor changes. The sea level pressure contours, 1000-500mb thickness contours and B015 level winds were used as guidance in deciding the location of the surface low and surface fronts. The ETA's B014 0°C isotherm was used as an approximation of the surface 0°C isotherm. ETA model 12 hour Quantative Precipitation Forecast (QPF) was noted as guidance for where the model expected precipitation during the period from 26/1200 to 27/0000 UTC. All of these parameters were drawn on a single chart to form the 24-hour composite prognosis (Figure 6). The techniques described in Section 3 were applied to the composite prognosis to arrive at an area forecast for that point in time.

The above procedure was repeated for 12 and 36 hour forecasts. This gave three snapshots showing where precipitation types should be occurring. The three area forecasts for freezing precipitation were then drawn on a single chart to show where the freezing precipitation would occur over the entire 24 hour forecast period (Figure 7). The northern area from each of the composite prognoses is the area likely to have IP and the southern area is likely to have ZR or ZL (Figures 6 and 7). Once this was completed, the forecasts had to be fitted to the forecast periods. At this point, forecaster judgment took over and the areas in Figure 7 were fitted to the forecast issued at 2100 UTC 25 January 1994 (Figure 8). Evaluation of the composite charts, 850-mb moisture advection, 700 vertical motion field, 500-mb trough movement, and 500-mb positive vorticity advection pattern lead to the forecast discussed below and shown in Figure 8.

DISCUSSION BULLETIN

EXPERIMENTAL FORECAST
FOR FREEZING RAIN

ISSUE TIME: 25/2100 UTC JANUARY 1994

GENERAL SYNOPTIC DIAGNOSTIC (1200 UTC) AND PROGNOSTIC DISCUSSION (FOR 24HR PERIOD 0000 - 0000 UTC):

Weak sfc low in SE KS at 25/12 UTC will move ENE to S Cent IL by 26/00 UTC and to SE IN by 26/06 UTC. The weak H5 short wave associated with this sfc low will also move eastward. Sufficient mstr has been pumped northward ahead of this low to produce ZR/ZL in IA and IL. Expect to see most of the ZR/ZL in IA end by 26/06 UTC as low and mstr move east. There will be enough mstr left to produce ZL in extreme Eastern MO as temps fall below freezing.

A stronger H5 short wave and its sfc low will be affecting KS, NE, and MO by 26/12UTC. Sfc low will be in SE CO by 26/12UTC and in NW OK by 27/00 UTC. Strong low level warm mst adv will occur ahead of the low and will be pumped north into KS over a below frz sfc. Significant ZR and ZL will occur in a 60NM wide band from SW KS to NW MO. This storm system has the potential to produce a MAJOR FREEZING RAIN EVENT and will probably produce heavy snow across parts of NW KS and the SE half of NE as the sfc low moves eastward tomorrow night. This system also has the potential to produce tstms, some possibly severe in parts of OK, S MO, and N AR. An interesting storm system to say the least. (Note: Figure 8 shows the forecast areas for each of the following forecast periods.)

PERIOD ONE VALID: 26/0000 UTC - 26/0600 UTC JANUARY 1994

As the first sfc low moves across IL and into IN and OH, mstr available for ZR/ZL will decrease from NW to SE thru the fcst area. Extreme E MO will probably have enough mstr to produce ZL late in this period and at the start of the next period.

AREA .."X".. (E IA/NE MO) 90% chance for ZL with a 20% chance for ZR accum less than 0.1 inch.
AREA .."O".. (IA/NE MO) 20% chance for ZL accum less than 0.1 inch.

PERIOD TWO VALID: 26/0600 UTC - 26/1200 UTC JANUARY 1994

The second sfc low (in SE CO by 26/12 UTC) will start affecting KS, NE and W MO. Warm mst low lvl adv will occur ahead of this low as colder sfc air sinks south into KS and MO. Expect mostly ZL in this pd with the possibility of sleet (ice pellets) in W NE where the cold air will be deeper. Used lower probabilities during this pd because mstr adv will just be getting started at the beginning of this period.

AREA .."X".. (80NM wide band thru Cent KS west to east) 40% chance for ZL accum less than 0.1 inch.
AREA .."O".. (NE KS/NW MO) 10% chance for ZL accum less than 0.1 inch.
AREA .."Z".. (W NE/NW KS) 10% chance for sleet mixed with ZL accum less than 0.1 inch.

PERIOD THREE VALID: 26/1200 UTC - 27/0000 UTC JANUARY 1994

This is the big one. As the sfc low moves from SE CO (26/12 UTC) to NW OK (27/00 UTC), warm moist air will be pumped north into KS over the well established cold air resulting in freezing rain in a 60NM wide band from SW KS to NW MO. By mid pd there will be wide spread ZL over parts of KS, MO, S IA, S and W NE. Also about mid pd hvy snow will most likely start in NE and NW KS.

!!!! THIS HAS THE POTENTIAL TO BE A VERY DANGEROUS STORM !!!!

AREA .."X".. (60NM wide band from SW KS to NW MO) 90% chance for ZL with a 60% chance for ZR accum. greater than 0.25 inch.
AREA .."O".. (SE NE, S IA, NE MO) 60% chance for ZL with a 30% chance for ZR accum. greater than 0.1 inch but less than 0.25 inch.
AREA .."Z".. (S Cent NE, NW KS) 10% chance for ZL accum. less than 0.1 inch.
AREA .."A".. (W NE, extreme NW KS) 10% chance for sleet mixed with freezing drizzle accum. less than 0.1 inch.

B. Verification

The current way that winter weather is being reported and recorded makes verifying a forecast product such as the one described here very difficult. Reports from Storm Data (1994), reports found in NWS special weather statements and observations from all available surface aviation observing (SAO) sites were used to verify the three period forecast. Actual amount of freezing precipitation and sleet could not be specifically determined and snowfall could only be determined in very general terms of amount and location. Using WMO standard weather symbols, observed weather was plotted at each observing site's location on a chart that displayed the location of each period's forecast areas. The weather represented by the symbols could have occurred any time during the forecast period or could have occurred throughout the period. Most of the weather did not occur continuously through the forecast period.

In PERIOD ONE valid 26/0000 to 26/0600 UTC (Figure 8a), ZL was observed in the northern half (Iowa) of areas "X" and "O" but the southern halves (Missouri) of both areas experienced drizzle and fog. The cold air did not move far enough south behind the first surface low as it crossed central Illinois. Below freezing surface temperature was experienced only in extreme northern Missouri. The ZL in Kansas (not anticipated) resulted from dense fog rather than being associated with warm moist advection ahead of the second low that was moving through Colorado.

In PERIOD TWO valid 26/0600 to 26/1200 UTC (Figure 8b), ZL was observed in the western half (Kansas) of area "O" but the eastern half (Missouri) experienced drizzle and fog. ZR was observed in Area "Z" rather than the ZL and IP that were forecast. Upslope type flow was expected to produce ZL from supercooled water droplets and late in the period warm moist advection over the deep cold surface layer was expected to produce IP. This didn't happen, instead ZR occurred in the southern part of the forecast area where the cold layer was too shallow for IP. ZR occurred in Area "X" rather than ZL. About 26/0700-0800 UTC thunderstorms moved out of southeast Colorado and northwest Oklahoma into southwest Kansas over the entrenched surface based cold air. At 26/0933 UTC thunderstorms moved into Garden City and by 26/1147 UTC they were moving through Dodge City, KS. These storms produced small hail, moderate to heavy ZR, IP and heavy snow. In a special weather statement issued at 26/1209 UTC, the Dodge City forecast office reported that significant accumulations of ice totaling .25 to .50 of an inch had already fallen in much of the area.

In PERIOD THREE valid 26/1200 to 27/0000 UTC (Figure 8c), the thunderstorms that moved into southwest Kansas in the previous forecast period continued to move northeast toward southeastern Nebraska. Thunderstorms in the warm air in southeastern Kansas produced damaging winds and large hail in the early part of the forecast period. Most of the heavy ZR occurred in the western two-thirds of Area "X" and rain fell in the extreme southeastern part of the area. ZR and ZL were observed in the northern half of Area "O" (Iowa and eastern Nebraska) while the southern half (Missouri) experienced drizzle and rain and not the ZL and ZR that were forecast. Late in the forecast period there were reports of .5 to 1 inch of sleet in east central Nebraska. Area "Z" experienced thunderstorms with ZR, ZL and IP with some heavy snow in the western part. Most of Area "A" experienced heavy snow with ZR, ZL and IP occurring in the extreme eastern and southern parts of the area.

The surface low was expected to move across northern Oklahoma and southern Missouri but instead turned northeast into south central Kansas. The low also moved faster than expected. It moved into northwest Oklahoma about 6 to 9 hours earlier than expected. All of this resulted in most of the winter weather occurring earlier and further north and west than anticipated. A combination of information in NWS special weather statements and from Storm Data (1994) indicated that over the whole 24 hour period of the forecast the heaviest freezing rain occurred in an area about 50

miles either side of an axis that extended from Liberal, KS to Omaha, NE to Lone Rock, WI. Heavy snow (six to twelve inches) occurred in the area from 50 miles northwest of the axis out to 200 miles northwest of the axis.

6. DISCUSSION

Forecasting winter weather can be particularly challenging. This experiment helped evaluate some techniques for forecasting winter weather, as well as a product that might be produced to discuss the threat. Although this experiment dealt only with ZR, ZL and IP events, most of these events also produced heavy snow. All of the events that occurred during this experiment appeared to be mesoscale in nature. Branick (1996), in his work on climatology of winter weather events also found that most of the winter weather events were mesoscale in nature. Although these events affect large areas over long time scales, much smaller areas were affected at short time scales. Many of the ZR events (12 to 24 hour duration) covered areas that might be hundreds of miles long but were only 30 (50) to 180 (300) miles (kilometers) wide. The width of the affected area varied from hour to hour as did the type of precipitation. During the entire experiment period there were cases when observing sites would report ZR one hour, IP the next, then a mix of both and repeat the cycle over a period of 3 to 12 or more hours. Trying to forecast precipitation type at short time scales is an extremely difficult task.

Verification of forecasts is essential if forecast quality is to be assessed and improved. In this experiment, the increased number of automated weather observations decreased the ability to verify the forecasts accurately. Lack of a standardized method of reporting hazardous winter weather is also detrimental. Reporting hazardous winter weather in Local Storm Reports (LSRs), the same way severe convective weather is being reported today, should be mandatory. The LSR method of reporting hazardous winter weather would also improve downstream weather forecast offices' ability to determine when hazardous winter weather is about to enter their area of responsibility.

For this experiment, numerical model data for the ETA model was only available using PCGRIDDS. The horizontal resolution was 190 kilometers between gridpoints, vertical resolution was the boundary layer and only the mandatory levels used in radiosonde data, and the time resolution was every 12 hours. This rather coarse resolution could allow some of the mesoscale processes causing hazardous winter weather to go undetected in the model data. Although higher resolution model data is now available, models still have considerable difficulty in forecasting free-forced mesoscale circulations and our ability to improve forecasts will progress not only as increasing time/space resolution improves, but as model physics, parameterization, etc. improves. This improved resolution should allow more mesoscale processes to be detected, and also enable refinements in the composting forecast technique for hazardous winter weather. Composite charts are a vital forecasting tool and with hourly model data, the forecaster could produce a sequence of composite charts that smoothly show how the atmosphere is changing in time. An operational forecaster couldn't possibly have time to construct composites manually for every hour through the forecast period so the computer must be used to facilitate and speed up the production of composite charts. Scripts have been written for the SPC workstations to do some, but not all of the composting. They do not yet allow the forecaster to interact with the data to adjust feature positions for model bias, to correct the speed of frontal movements, etc. Software must be developed to increase the speed and sophistication with which a forecaster can examine the model output or the full benefit of improvements such as increased resolution cannot be fully realized.

Much more mesoscale applied research is needed on forecasting hazardous winter weather. Use of composite charts will continue to play a major role in how we view the atmosphere in four dimensions. Thickness fields have been and are still used to estimate mean virtual temperature

through layers. Improved model resolution and computing ability should enable us to compute the mean virtual temperatures through layers directly. More research is needed on the thermal stratification needed for the different types of precipitation. Results from research on forecasting precipitation type (e.g., Schichtel 1988, Bourgouin 1992) needs to be tested and evaluated for possible use over the entire country.

Collaborative mesoscale applied research on forecasting hazardous winter weather by MAG/SPC should result in improved service to the public. A display of concern about our ability to forecast winter weather by the MAG/SPC will hopefully encourage other researchers/forecasters to work on improvement in this area of concern.

7. ACKNOWLEDGMENTS

Discussions with Dr. Robert A. Maddox and Douglas Forsyth of the NSSL and Phillip Bothwell of the SPC were extremely helpful in the design of the experiment and the forecast product. Paul Janish's (NSSL) assistance with some of the PCGRIDS macros was helpful throughout the experiment. Joan O'Bannon's (NSSL and Cooperative Institute for Mesoscale Meteorological Studies {CIMMS}) assistance with the complex figures made them much easier to read and understand. Suggestions from Dr. Harold Brooks (NSSL), Dr. John Cortinas (NSSL and CIMMS), Paul Janish (NSSL) and Joel Olson (SPC) who reviewed this paper resulted in a much improved presentation.

8. REFERENCES

Black, T., D. Deaven, and G. DiMego, 1993: The step-mountain Eta coordinate model. NWS Technical Procedures Bulletin, **412**. U.S. Dept. of Commerce, NOAA.

Bourgouin, P., 1992: Criteria for Determining Precipitation Types. Preprint, Fourth Workshop on Operational Meteorology, AES/CMOS, Whistler, BC, 460-469.

Branick, M., 1996: A Climatology of Winter Weather Events in the Continental United States, 1982-1993. Proceedings of the Fourth National Winter Weather Workshop, DOC, NOAA, NWS, Central Region, Kansas City.

Dept. of Commerce, 1994: Storm Data. National Climatic Data Center, Asheville, NC.

Keeter, K.K., and J. W. Cline, 1991: The Objective Use of Observed and Forecast Thickness Values to Predict Precipitation Type in North Carolina. *Wea. Forecasting*, **6**, 456-469.

McPherson, R.D., 1994: The National Centers for Environmental Prediction: operational climate, ocean, and weather prediction for the 21st century. *Bull. Amer. Meteor. Soc.*, **75**, 363-373.

Peterson, R.A., 1992: A PC-based system for the display of gridded WAFS data. Proceedings of the WMO technical Conference on Tropical Aeronautical Meteorology (TECTAM-92), Geneva, Switzerland, 1-6.

Schichtel, M.L., 1988: The Specification of Precipitation Type in Oklahoma Winter Storms. M.S. thesis, University of Oklahoma, 152 pp.

Umpenhour, C.M., 1968: Low Level Thickness Charts. [Available from author], 8pp.

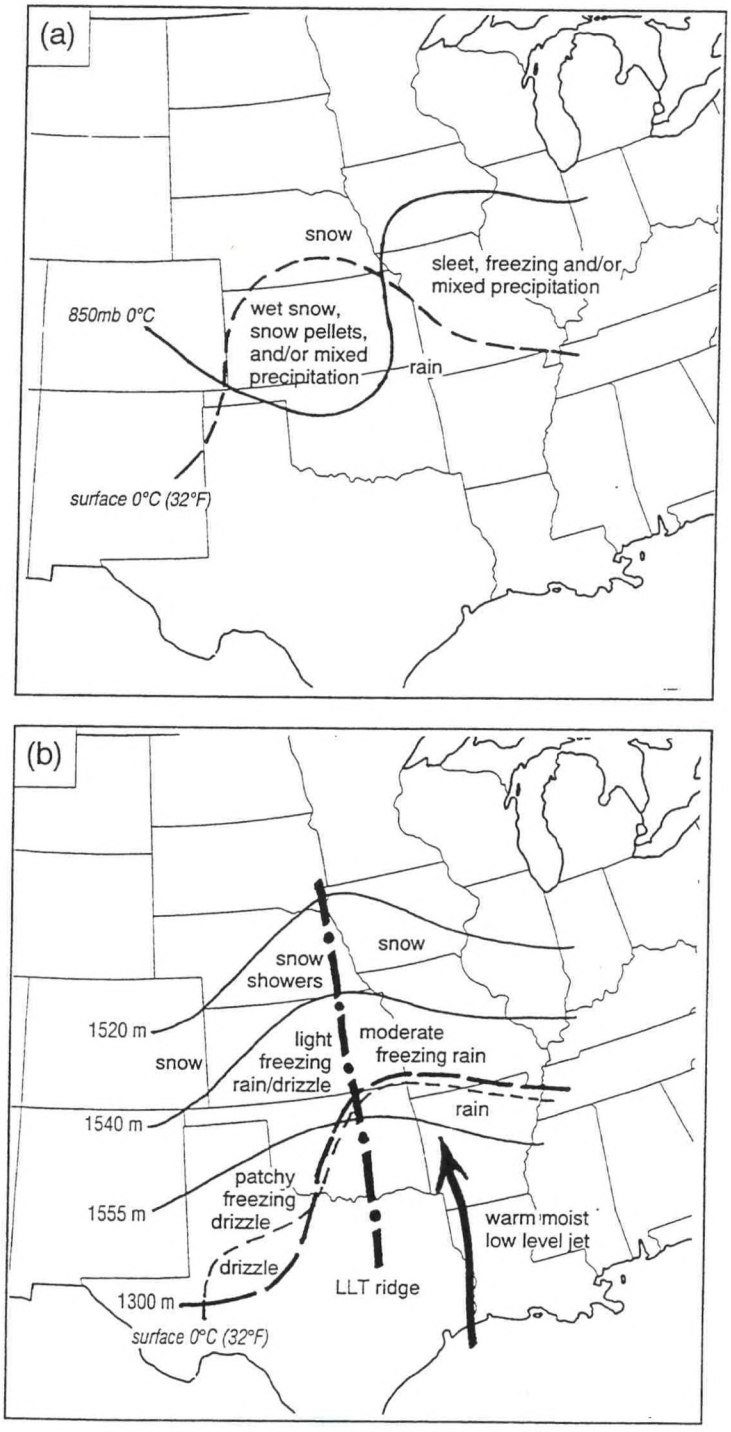

Figure 1. Favored areas for winter precipitation types. (a) Area locations for precipitation type relative to surface 0°C (dashed) and 850-mb 0°C (solid) isotherms. (b) Area locations for precipitation type relative to surface 0°C isotherms (thin dashed), 1300 meter LLT contour (thick dashed) and 1555, 1540, and 1520 meter MLT contours (solid).

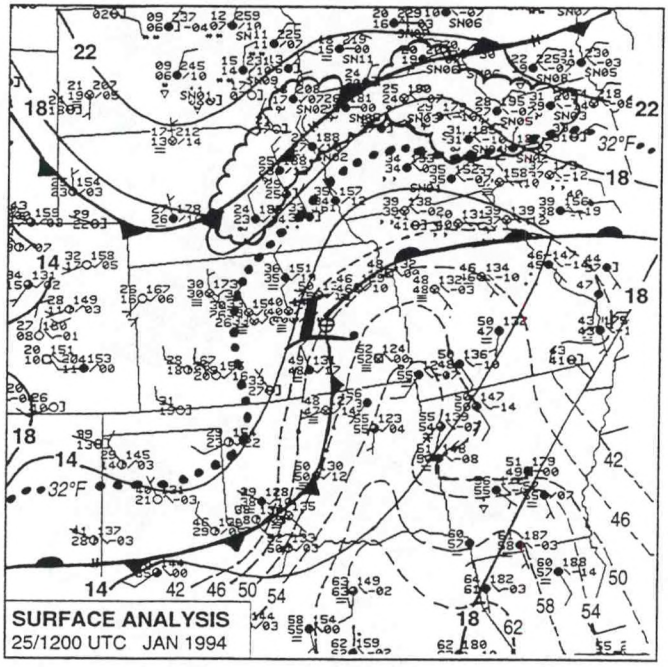

Figure 2. Surface synoptic analysis for 1200 UTC 25 January 1994. Sea level pressure isobars (solid) are drawn at a 4mb interval, 32°F isotherm is dotted, isodrosotherms (dashed) are drawn at an interval of 4°F for values ≥ 42°F and the area of freezing precipitation is enclosed by a scallop like contour. WMO standard weather symbols are used.

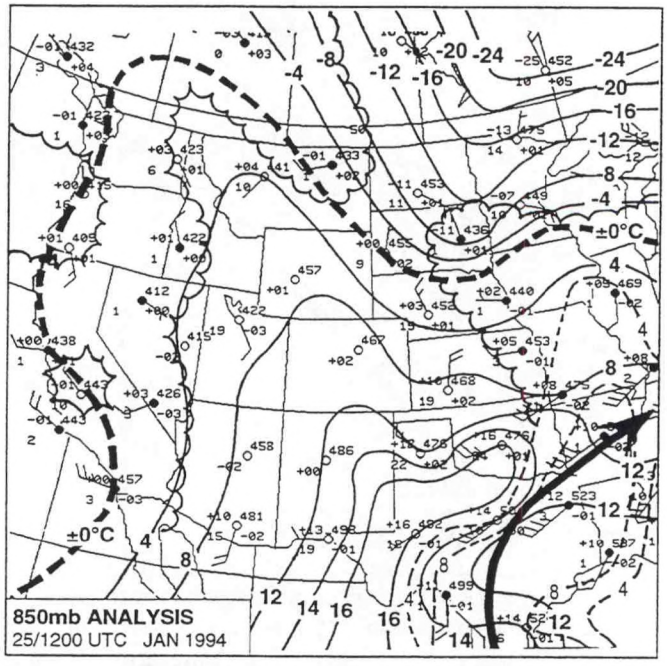

Figure 3. 850-mb analysis for 1200 UTC 25 January 1994. Isotherms (solid) are drawn at an interval of 4°C with the 0°C isotherm highlighted (thick dashed). Isodrosotherms (thin dashed) are drawn at an interval of 4°C for values ≥ 4°C and areas having temperature dew point spreads ≤ 5°C are enclosed by a scallop like contour.

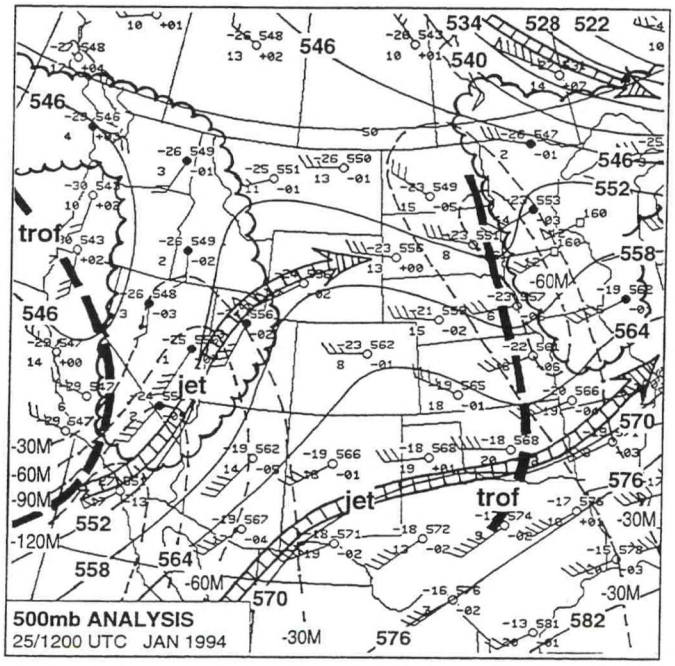

Figure 4. 500-mb analysis for 1200 UTC 25 January 1994. Height contours (solid) are drawn at an interval of 60 meters and 12 hr height change contours (dashed) are drawn at a 30 meter interval for values ≤ -30 meters. Areas having temperature dew point spreads ≤ 5°C are enclosed by a scallop like contour.

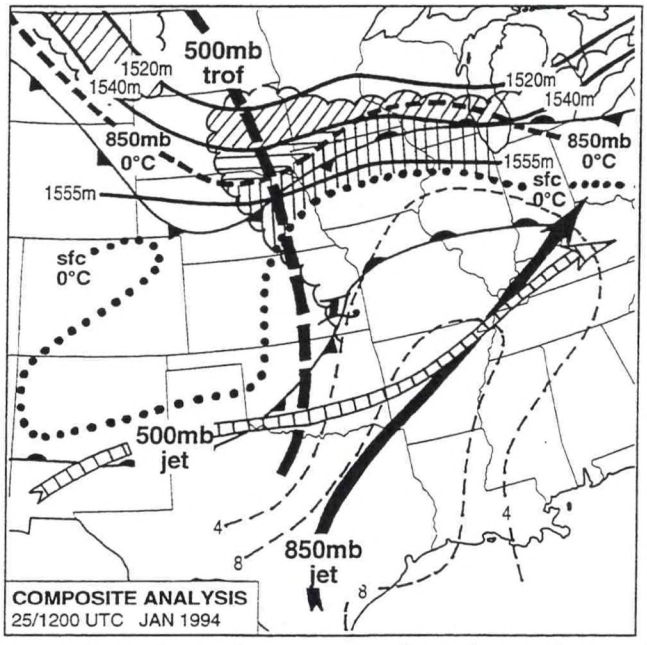

Figure 5. Composite analysis chart of parameters from the surface and upper air analyses for 1200 UTC 25 January 1994. 1555, 1540 and 1520 meter MLT contours are solid, 850-mb 0°C isotherm is a thick dashed contour, surface 0°C isotherm is a dotted contour and 850-mb isodrosotherms (thin dashed) are drawn at a 4°C interval for values ≥ 4°C. Areas having temperature dew point spreads ≤ 5°C are enclosed in a scallop like contour. Area with vertical hatching is where there is a potential for freezing precipitation, area with horizontal hatching is where there is a potential for sleet, and the areas with slanted hatching is where there is a potential for heavy snow.

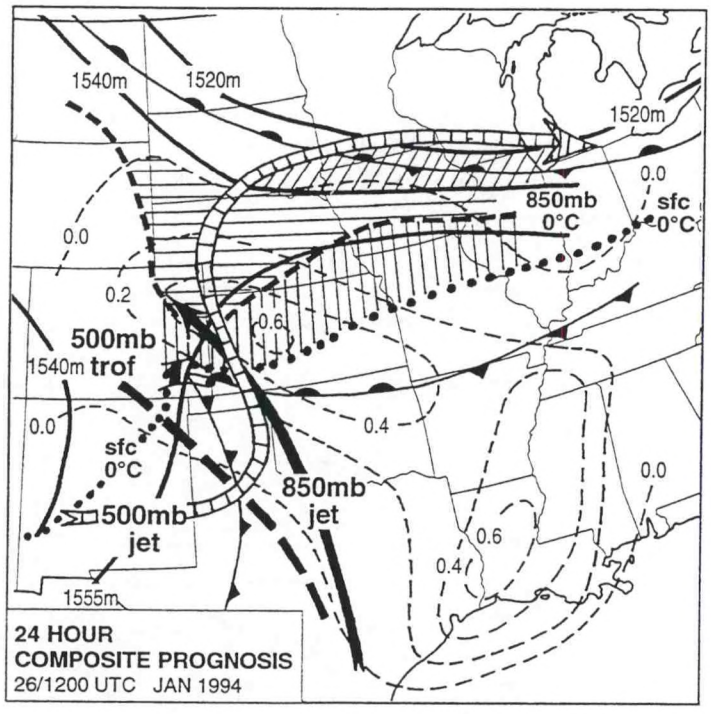

Figure 6. 24 hour composite prognosis chart of parameters from the surface and upper air prognoses for 1200 UTC 25 January 1994. 1555, 1540 and 1520 meter MLT contours are solid, 850-mb 0°C isotherm is a thick dashed contour, surface 0°C isotherm is a dotted contour and ETA model 12 hour QPF is indicated by thin dashed contours drawn at an interval of 0.2 inches for values greater than 0.0 inches. The QPF is valid for the period 26/1200 - 27/0000 UTC. Area with vertical hatching is where there is a potential for freezing precipitation, area with horizontal hatching is where there is a potential for sleet, and the area with slanted hatching is where there is a potential for heavy snow.

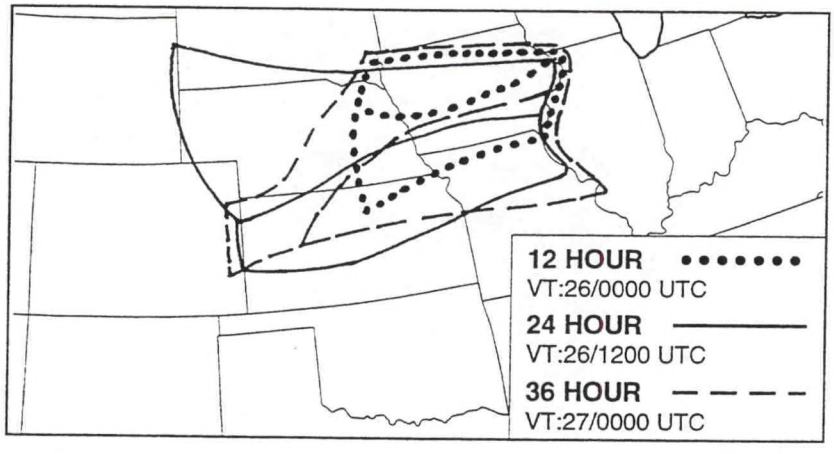

Figure 7. Probable sleet (northern most area for each) and freezing precipitation (southern most area for each) areas as indicated by the 12 hr (dotted), 24 hr (solid) and 36 hr (dashed) composite prognoses.

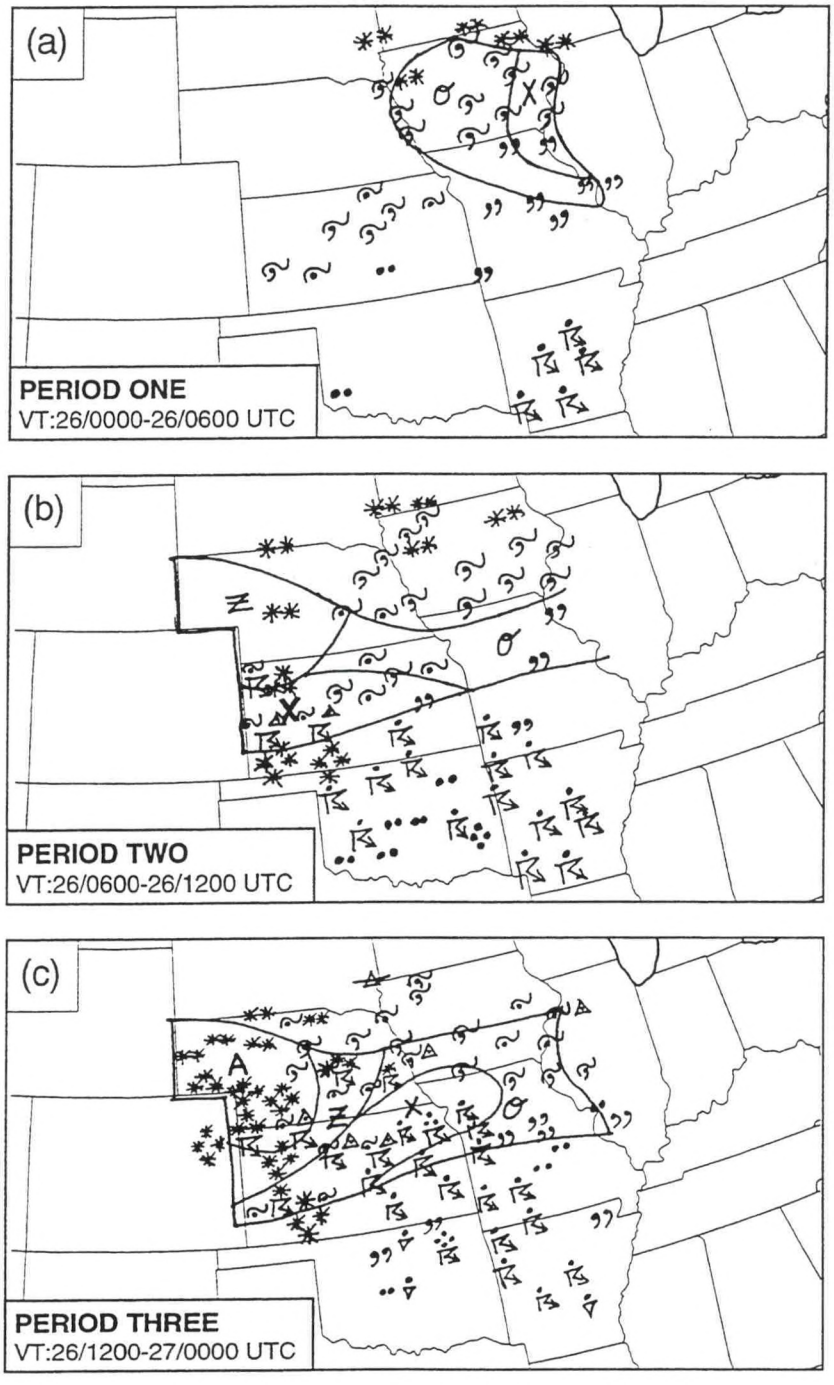

Figure 8. Example forecast areas (a) valid 26/0000 - 0600 UTC, (b) valid 26/0600 - 1200 UTC and © valid 26/1200 - 27/0000 UTC with observed WMO standard weather symbols superimposed for verification.

SESSION 6
HEAVY SNOW CASE STUDIES

16. An Isentropic Perspective of the January 19-20, 1995 Central Missouri Snowstorm

17. Dry Air Interactions with a Late Season Heavy Snow Event over Oklahoma

18. The March 8-9, 1994 Winter Storm over Southern Missouri: A Challenging Operational Forecasting Problem

19, Vertical Motion Forcing Mechanisms Responsible for the Production of a Mesoscale Very Heavy Snow Band Across Northern Kentucky

20. The Use of PCGRIDDS and New Forecast Techniques to Diagnose A Heavy Snow Event over Northeastern North Carolina - 8 February 1995

21. Evaluation of a Record Snowfall Event in the Lower Columbia Basin of Oregon and Washington Using PCGRIDDS

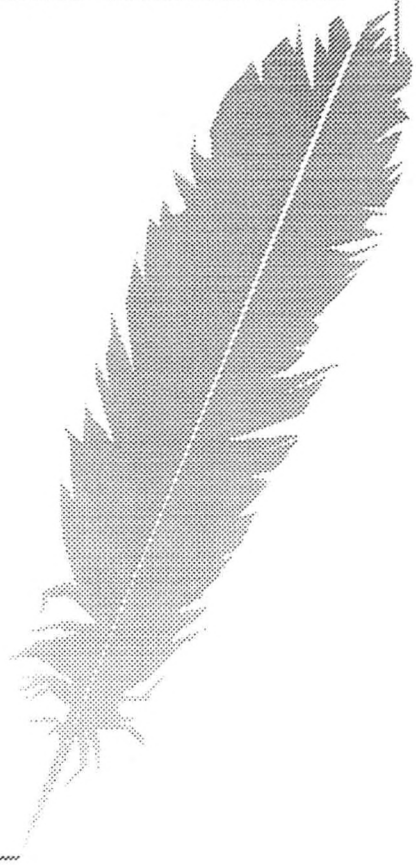

An Isentropic Perspective of the January 19-20, 1995 Central Missouri Snowstorm

James T. Moore[1] and Sean M. Nolan[2]

1. INTRODUCTION

On January 18-20, 1995, a fast developing extratropical cyclone moved northward through eastern Missouri and buried parts of central and southern Missouri with greater than 18 inches of snowfall. Columbia, Missouri received a record 20 inches in less than 24 hours.

There were many unique aspects of this heavy snowstorm that made it worthy of further study. First, the best dynamics appeared to remain well east of the region where the heavy snow fell. The greatest warm air and moisture transport were located within the warm conveyor belt near Tennessee, Kentucky, Illinois, while heavy snow was occurring in the "wrap around" area of the cyclone well west of the central low pressure.

Second, the low-level temperatures were relatively warm for mid-January. The freezing line at the surface bisected the state, running from southwest to northeast Missouri. Thus, a large area of mixed precipitation and rain fell less than 100 miles from where heavy snow occurred. In fact, temperatures were in the mid-40's in central and southern Missouri just two days before the heavy snowfall and no new air mass moved into the region before the development of the low pressure system.

Lastly, there was a heavy snow band approximately 80 miles wide from northeast Missouri to southwest Missouri (Figure 1). Numerous reports of thundersnow were observed within this snow band hinting that some form of elevated instability (conditional symmetric instability (CSI) and/or convective instability) was present above the stable boundary layer.

2. SYNOPTIC OVERVIEW OF THE SNOWSTORM

On January 18, 1995, a weak surface low in the western Gulf of Mexico moved northward and interacted with a deep trough in the central United States. The low rapidly intensified (10 mb/24h) and moved northeast through eastern Texas and southern Arkansas. By 1200 UTC 19 January, the low (998 mb) was centered over east-central Missouri (Figure 2). Infrared satellite imagery at 1200 UTC 19 January (Figure 3) reveals a pronounced dry slot moving into southern Illinois while the wrap around area was located over central and southern Missouri. At this time, heavy snow was falling at both Springfield and Columbia, Missouri. In fact, heavy snow fell for 12 consecutive hours up to 1200 UTC (Figure 4). The surface low proceeded to quickly move to the northeast into northern Indiana and the snow tapered off from southwest to northeast Missouri.

3. ISENTROPIC ANALYSIS OF THE SNOWSTORM

From a constant pressure perspective, the cause of the heavy snow is not explained sufficiently. In fact, heavy snow is occurring while cold air advection (CAA) is taking place over a deep layer from

1. Corresponding author address: James T. Moore, Dept. of Earth and Atmospheric Sciences, St. Louis University, St. Louis, Missouri.
2. Sean M. Nolan, Dept. of Earth and Atmospheric Sciences, St. Louis University, St. Louis, Missouri.

the surface-700 mb (a scenario where downward vertical motion should dominate). Thus, this study will accentuate the advantages of employing isentropic analysis, specifically concentrating on storm-relative isentropic motion, isentropic trajectories, isentropic potential vorticity and diagnosing instabilities on isentropic surfaces.

The 288 K isentropic surface was analyzed for ground-relative flow and storm-relative flow (a method where the preceding 12-hour storm motion, both speed and direction, is subtracted from the storm motion; Moore 1993). Upward vertical motion is optimized when streamlines are oriented normal to the isobars on an isentropic surface and flow from higher to low pressure.

At 0000 UTC 19 January, the surface low was centered over southern Arkansas. Figures for this time are not shown due to space limitations. The ground-relative flow analysis shows the streamlines crossing the isobars at small angles resulting in weak vertical velocities (-2 $\mu b\ s^{-1}$). For storm-relative flow at this time, the cross-isobar angle is greater resulting in upward vertical velocities of -4 $\mu b\ s^{-1}$ over the southern two-thirds of Missouri (-6 $\mu b\ s^{-1}$ covered the southeast quarter of Missouri). The moisture transport vectors (the product of the mixing ratio and the actual wind) on the 288 K surface revealed the greatest moisture transport taking place to the north of the surface low and wrapping around through southern Missouri.

The results at 1200 UTC 19 January were much more revealing as the storm began to strengthen. With the surface low centered over east-central Missouri, most of Missouri was experiencing northerly low-level flow. For ground-relative flow, the 288 K surface analysis showed that the streamlines were almost parallel to the isobars in central and southern Missouri (Figure 5). The corresponding vertical velocities reveal downward vertical motion over the southern half of Missouri and weak upward vertical motion (-2 $\mu b\ s^{-1}$) in extreme northern Missouri (Figure 6). The storm relative flow on the 288 K surface shows the streamlines crossing over the isobars throughout all of Missouri (Figure 7). The corresponding upward vertical velocities are more impressive as well, as -6 $\mu b\ s^{-1}$ is present throughout the northern half of Missouri (Figure 8). In southwest Missouri, upward vertical velocities exceeded -4 $\mu b\ s^{-1}$, which helped to explain the occurrence of heavy snow in Springfield, Missouri despite the surface low being positioned well to the east. Notice that significant moisture is present in southern Missouri as condensation differences are less than 50 mb. The moisture transport vectors on the 288 K surface revealed significant moisture from central Tennessee being wrapped around the cyclone into Missouri from north to south (Figure 9). Thus, the combination of strong upward vertical velocities with copious moisture transport explains why a large portion of Missouri experienced heavy snow for such long durations.

To highlight the advantage of isentropic even more, the calculated kinematic vertical velocities over Missouri for both 0000 and 1200 UTC 19 January were computed. At 0000 UTC, the kinematic vertical motions reveal downward vertical motion over the eastern half of Missouri despite the fact that all of Missouri was experiencing precipitation (snow, sleet, freezing rain, and rain) at this time. At 1200 UTC, the kinematic vertical velocities are even less impressive still as downward vertical motion is depicted through the southwestern two-thirds of Missouri (Figure 10). In fact, downward vertical velocities of +2 $\mu b\ s^{-1}$ are near Springfield, Missouri where heavy snow is occurring.

Isentropic trajectories illustrate the entire path that a single air parcel will travel over time along a particular isentropic surface. Figure 11 shows selected isentropic trajectories from 0000 to 1200 UTC 19 January on the 312 K surface. Initially, all of the trajectories have a southerly component. However, the trajectories in the vicinity of the low pressure center undergo a sharp turn to the west, while undergoing upward vertical motions of up to -3.6 $\mu b\ s^{-1}$.

Upper level isentropic surfaces are useful in calculating isentropic potential vorticity (IPV). IPV can be calculated as:

$$IPV = -g\frac{\zeta_\theta + f}{\frac{\partial p}{\partial \theta}} \quad (1)$$

as noted by Bluestein (1993). Thus, IPV is a function of the absolute vorticity and the dry static stability. In situations where tropopause undulations develop (Hirschberg and Fritsch 1990), a parcel of air moves from a stable stratospheric layer to a less stable tropospheric environment. Therefore, if IPV is conserved, as the static stability of the parcel decreases its cyclonic spin increases. Tropopause undulations are characterized by anomalously large values of IPV and warm air, since they represent extensions of stratospheric air that are "drawn" downward. Typically, any value greater than 2 PVU (where 1 PVU = 10e-06 m2 K s-1 kg-1) denotes stratospheric air. At 0000 UTC 19 January a large area of warm air (> 50° C) is present at 200 mb. The corresponding values of IPV show values greater than 4 PVU in Kansas (proximity to the developing low pressure system). At 1200 UTC 19 January, IPV values greater than 6 PVU are present down to 350 mb (Figure 12). The area of high values of IPV extending down into the southern plains is often referred to as an "isthmus of high IPV". The intrusion of stratospheric air (2 PVU surface) is almost down to the 450 mb level (Figure 13) and the warm air pocket (> 50° C) has closed off over the four corners of Missouri, Kansas, Oklahoma, and Arkansas (Figure 14). The addition of IPV is vital in aiding in the spin up of an extratropical cyclone. In this case, it appears that the rapid development of the cyclone is concurrent with the ingestion of high IPV from the stratosphere associated with a tropospause undulation and possible "fold".

As mentioned earlier, having a snow band only some 80 miles wide and reports of thundersnow suggested that some form of elevated instability may have been present in Missouri. To diagnose instability, cross-sections of equivalent potential temperature (θ_e) and absolute geostrophic momentum was created normally to the 1000-500 mb thickness. If the slope of the θ_e surface is greater than the absolute geostrophic momentum surface and θ_e does not decrease with height, then a parcel of air is unstable with respect to slantwise motions and CSI exists. If θ_e decreases with height convective instability is present and this form of instability dominates CSI since it has a shorter doubling time. Figure 15 shows that a broad area of convective instability was present between 800 and 700 mb from southern Illinois to central Missouri. Also, there was only a small nose of CSI present in central Missouri at this time. To reiterate this point, equivalent potential vorticity (EPV) was calculated to determine where CSI was located. If EPV < 0, then CSI is present (Moore and Lambert 1993). However, convective instability also creates region of EPV < 0, thus one must use this parameter carefully. These results were very similar to the cross-sections at 1200 UTC as negative EPV exists where convective instability exists on the cross-sections (Figure 16). Thus, it is suggested that convective instability be the dominant mechanism leading to convective snow bands and large snow totals while CSI played a very minor role.

4. CONCLUSIONS

Employing isentropic techniques to diagnose the central Missouri snowstorm of January 18-20, 1995 proved beneficial. The use of storm-relative versus ground-relative flow lead to more accurate calculations of the vertical motions fields within the storm. Upward vertical velocities of -6 $\mu b\ s^{-1}$ in Missouri corresponded well to where heavy snow was falling. In addition, computed kinematic vertical velocities were far less impressive as large areas of computed downward vertical motions were found where heavy snow was falling.

The use of isentropic trajectories presented a clear visualization of the movement of air parcels within the storm as cyclogenesis were occurring. Also, these parcels were experiencing upward vertical motions for the 12-hour period (0000-1200 UTC 19 January) where the heavy snow was falling in central and southwest Missouri.

The calculation of IPV was useful in explaining the rapid development of the cyclone while also illustrating the influence of stratospheric air on the system. Lastly, the diagnosis of convective instability within the storm was significant in explaining the mesoscale snow band present from southwest to central Missouri.

5. REFERENCES

Bluestein, H.B., 1993: *Synoptic-Dynamic Meteorology in Mid-Latitudes, Vol. II: Observations and Theory of Weather Systems.* Oxford University Press, New York, 594 pp.

Hirschberg P.A., and J.M. Fritsch, 1990: Tropopause Undulations and the Development of Extratropical Cyclones. Part I: Overview and Observations from a Cyclone Event. *Mon. Wea. Rev.*, **119**, 496-517.

Moore, J.T., 1993: Isentropic Analysis and Interpretation. Operational Applications to Synoptic and Mesoscale Forecast Problems. National Weather Service Training Center, Kansas City, Missouri, 99 pp.

_____, and T.E. Lambert, 1993: The use of equivalent potential vorticity to diagnose regions of conditional symmetric instability. *Wea. Forecasting*, **8**, 301-308.

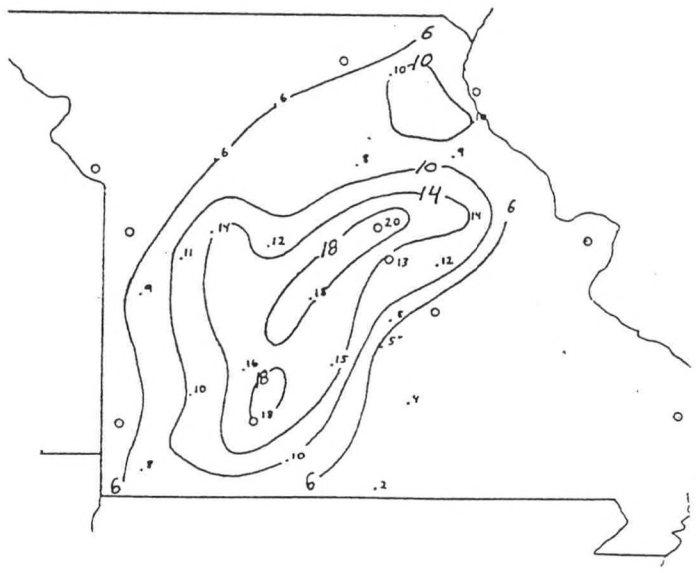

Figure 1. Total snowfall (in inches) over Missouri at 1200 UTC 20 January 1995.

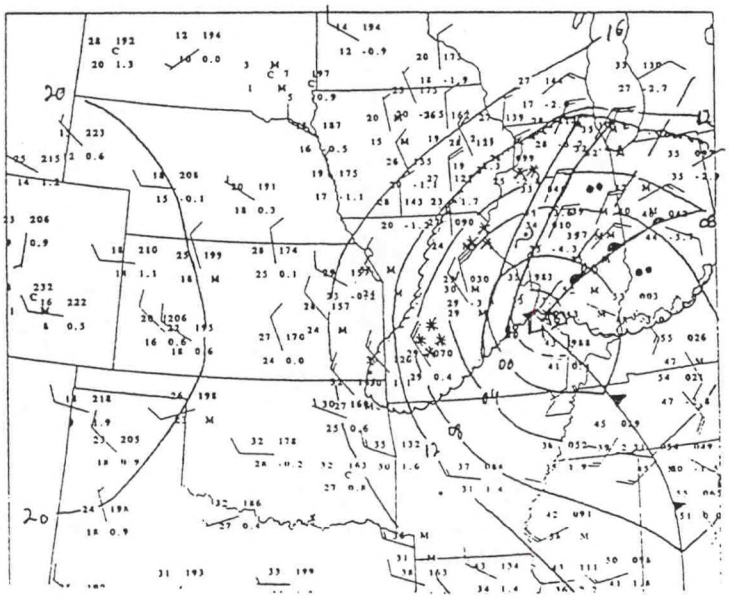

Figure 2. Surface map for 1200 UTC 19 January 1995. Solid lines are isobars. Station model follows standard notation.

Figure 3. Infrared satellite imagery for 1200 UTC 19 January 1995.

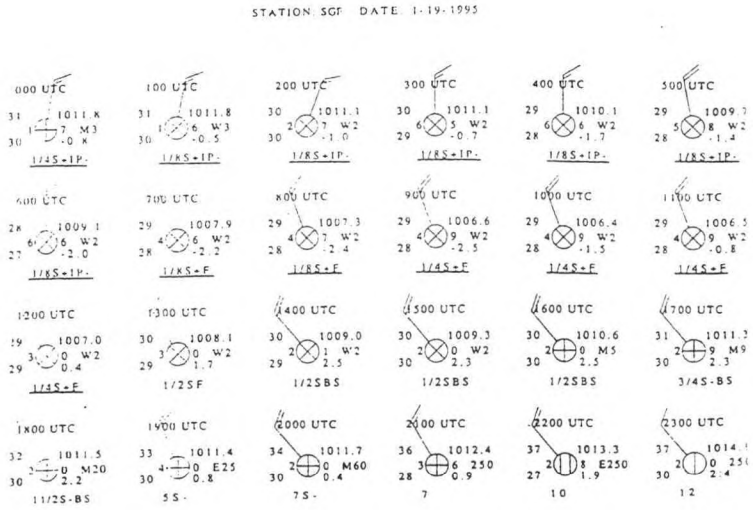

Figure 4. Station model plot for Springfield, MO (SGF) on 19 January 1995. Notice heavy snow being reported for 12 consecutive hours from 0000 to 1200 UTC.

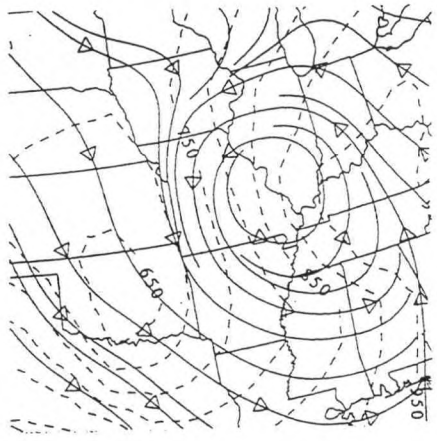

Figure 5. Ground relative flow of streamlines (solid lines) and isobars (dotted lines) on the 288 K isentropic surface for 1200 UTC 19 January 1995.

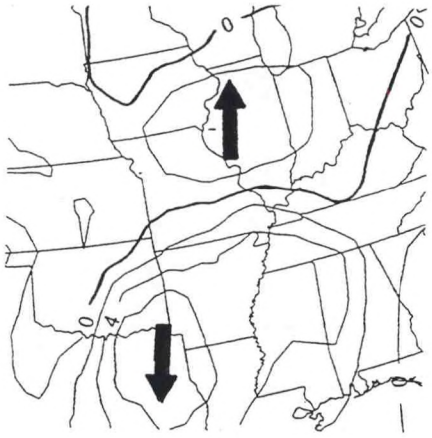

Figure 6. Vertical velocities derived from ground relative flow on the 288 K isentropic surface (μb s^{-1}) for 1200 UTC 19 January 1995.

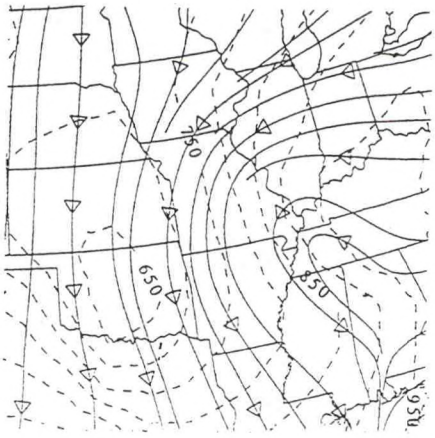

Figure 7. Storm relative flow of streamlines (solid lines) and isobars (dotted lines) on the 288 K isentropic surface for 1200 UTC 19 January 1995.

Figure 8. Vertical velocities derived from storm relative flow on the 288 K isentropic surface ($\mu b\ s^{-1}$) for 1200 UTC 19 January 1995. Dashed line encloses region of condensation difference < 50 mb.

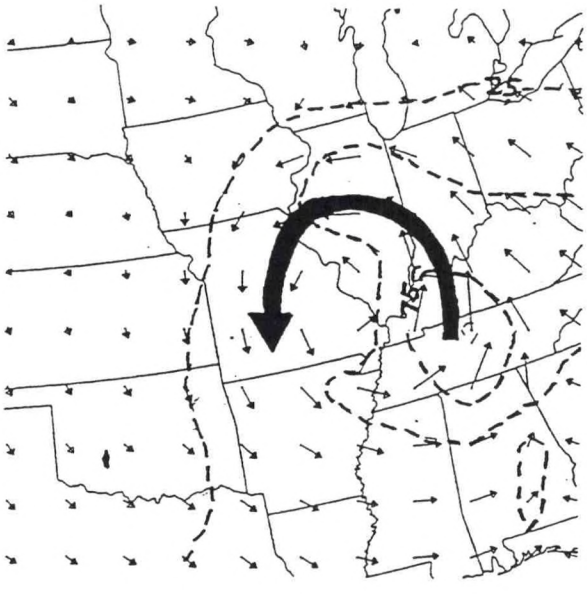

Figure 9. Moisture transport vectors (wind barbs) and magnitudes of moisture transport vectors (dashed lines) (gm m/kg s) on the 288 K isentropic surface for 1200 UTC 19 January 1995.

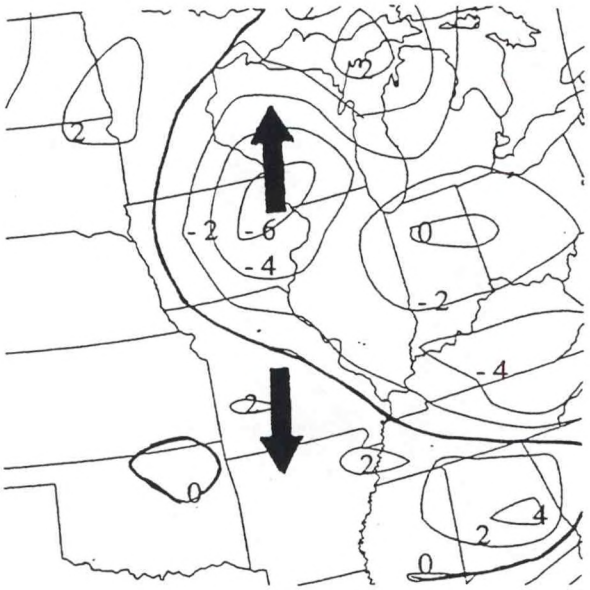

Figure 10. Kinematic vertical velocities ($\mu b\ s^{-1}$) at 700mb for 1200 UTC 19 January 1995.

Figure 11. Isentropic trajectories for the 12 hour period 0000-1200 UTC 19 January 1995 on the 312 K isentropic surface. Vertical velocities at 0600 UTC shown in $\mu b\ s^{-1}$.

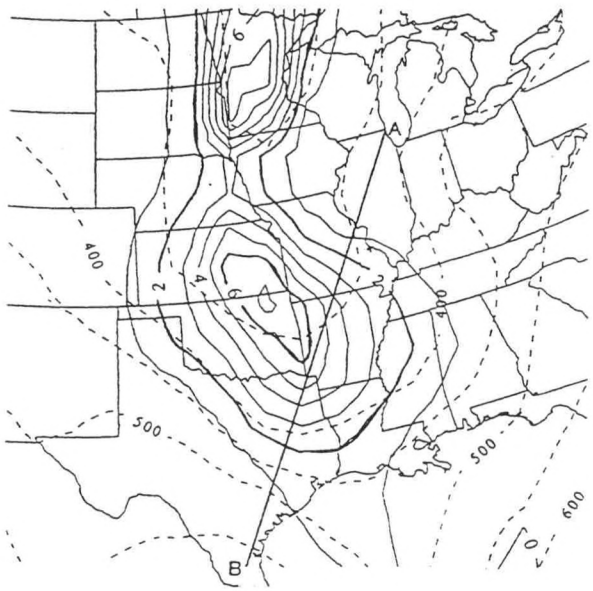

Figure 12. Isentropic potential vorticity (solid lines) in PVU (10e-06 m2 k/s kg) and isobars (dotted lines) on the 314 K isentropic surface for 1002 UTC 19 January 1995. Solid line denotes path of cross-section shown in Figure 13.

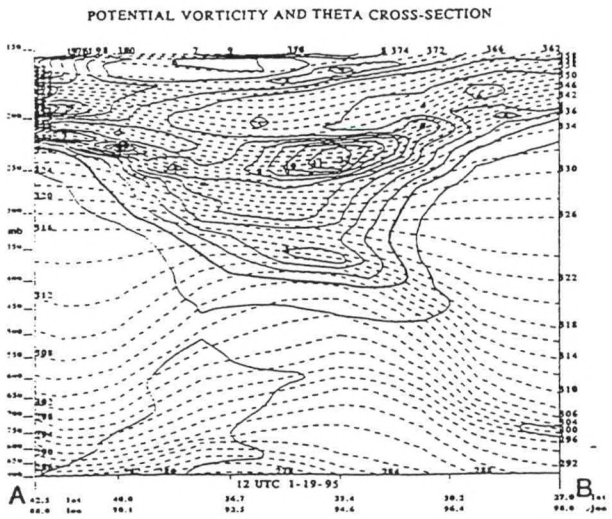

Figure 13. Cross-section of potential vorticity (solid lines) and potential temperature (dashed lines) from northern Illinois (left) to southern Texas (right) at 1200 UTC 19 January 1995. Note: 2 PVU surface denotes stratospheric air.

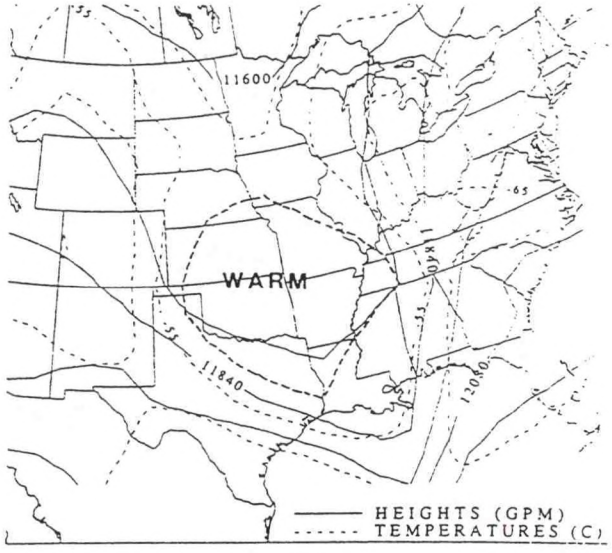

Figure 14. 200 mb plot at 1200 UTC 19 January 1995. Solid lines depict heights (gpm) and dashed lines depict temperatures (°C).

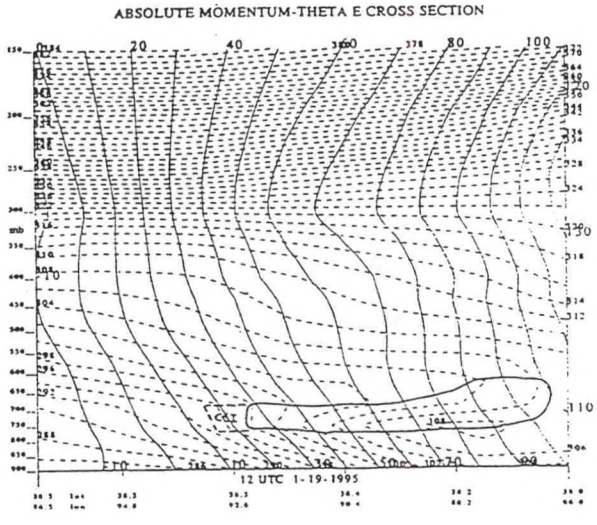

Figure 15. Cross-section of absolute momentum and equivalent potential temperature (K) from eastern Kansas (left) to central Kentucky (right) at 1200 UTC 19 January 1995. Convective instability is present inside bold solid line and CSI is present inside bold dashed line.

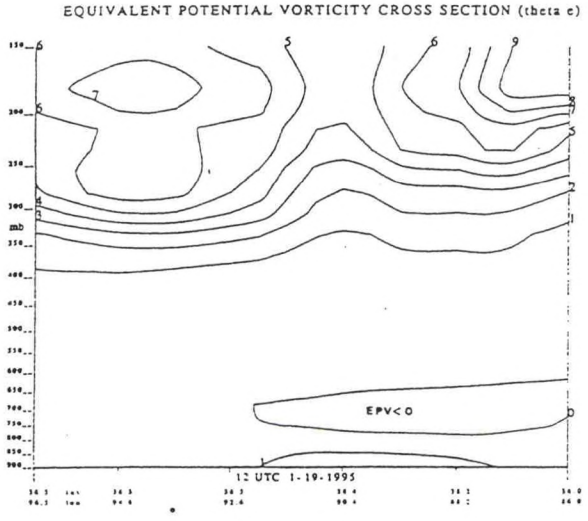

Figure 16. Cross-section of equivalent potential vorticity from eastern Kansas (left) to central Kentucky (right) at 12Z 19 January 1995. Negative values denote a region of CSI (see text for explanation).

Dry Air Interactions with a Late Season Heavy Snow Event over Oklahoma

Ryan C. McCammon[1]

1. INTRODUCTION

A strong late season winter snowstorm hit Oklahoma and the Texas panhandle during March 7-9, 1994, producing as much as 14 inches of snow over parts of northern Oklahoma (Figure 1). Factors that contributed to the evolution of this storm included: moisture from the Gulf of Mexico, isentropic uplift, coupled polar and subtropical jet streaks, and an environment favorable for Conditional Symmetric Instability (CSI). Also, relatively dry air at low levels from Kansas interacted with the storm, by wet-bulb cooling processes, and likely produced the cooling necessary to transform an environment favoring rain, to an environment favoring snow. Analyses of observational data as well as numerical weather prediction model forecasts using the PC-Gridded Display and Diagnostic System (PCGRIDDS, Petersen 1992) program will show these contributing factors.

Furthermore, a significant forecasting problem concerning precipitation type will be discussed. As a result of low-level dry air, model forecasts of thicknesses proved inadequate in determining the location of the liquid/frozen transition zone.

2. EVENT ANALYSIS AND EVOLUTION

At 0000 UTC 8 March 1994 (all time references refer to 8 March unless otherwise noted), a surface anticyclone was located over south central Nebraska with a cold front extending from central Arkansas through north central Texas to a low pressure center in extreme western Texas. A rich low-level moisture supply (greater than 60° dew points) was present south of the cold front with surface winds containing a strong southerly component. Available moisture was also evident at 850 mb with dew points exceeding 10°C over Texas.

Also, a closed low was located over Arizona at 500 mb with height falls occurring over the southwestern United States. A subtropical jet streak was noted at 300 mb over southern New Mexico and western Texas with a polar jet streak located farther north over the central Plains at 300 mb. Oklahoma was located between the subtropical and polar jet streaks.

At 1200 UTC, moderate to heavy snow was falling across the Oklahoma and Texas panhandles and northwest and north central Oklahoma. The surface rain/snow line was located from just north of Tulsa, Oklahoma westward through north central Oklahoma to just north of Amarillo, Texas. The cold front had moved south to a line from the Louisiana/Arkansas border to south of Waco, Texas to a low pressure center over the Big Bend area of western Texas. 1200 UTC surface observations also indicated that dry air (dew points in the teens and 20s) was found over northern Oklahoma and the southern half of Kansas. The 0°C isotherm at 850 mb was located from Springfield, Missouri to north central Oklahoma to south of Amarillo, Texas. Finally, the subtropical and polar jet streak positions remained nearly stationary at 300 mb (Figure 2) with the area of moderate to heavy snowfall located between the jet streaks (Uccellini and Kocin 1990).

Model analysis showed that the heavy snowfall area was enhanced by secondary circulations associated with coupled polar and subtropical jet streaks and with horizontal frontogenesis (Uccellini

1. Corresponding author address: Ryan C. McCammon, NOAA/NWS/WSFO 1200 Westheimer Dr. Room 101, Norman, Oklahoma 73069 (E-mail: CCMAIL: Ryan McCammon@W_SR_OUN) (Internet: mccammon@qns.com).

and Kocin 1990). A cross-section taken (Figure 3) across central Oklahoma at 1200 UTC indicated that upward vertical motion existed above the frontal surface (Figures 4 a, b) with horizontal frontogenesis (not shown) occurring at low levels during the event as well. Furthermore, the area of horizontal frontogenesis and coupled jet streak pattern played a role in maintaining a secondary direct circulation over Oklahoma, thus contributing toward increased synoptic scale upward vertical motion.

The environment favorable for CSI to occur over north central Oklahoma was also forecasted by the NGM for 1800 UTC. Cross-section analyses (Figure 5a) showed that equivalent potential temperature surface slopes were either greater than or equal to the momentum-surface (M-surface) slopes in an area with greater than 90 percent relative humidity (Figure 5b) over north central Oklahoma, thus indicating an environment favorable for slantwise convection (Snook 1992). Precipitation banding, associated with mesoscale processes via CSI, was observed using WSR-88D base reflectivities. These bands developed and propagated northeastward throughout the late morning and afternoon of March 8.

At 2100 UTC (Figure 6), surface observations showed that the surface rain/snow line had pushed south into central Oklahoma. The observations also showed dry air in southern Kansas with moderate to heavy snow occurring from the Texas panhandle through the northern half of Oklahoma to northwest Arkansas.

At 0000 UTC 9 March, moderate to heavy snow was falling from the Texas panhandle through central Oklahoma to southwest Missouri. Also, the closed low at 500 mb had "opened up" and a short wave trough was located from southwest Kansas to northern Mexico. Finally, the subtropical and polar jet streaks were located over central Texas and the Great Lakes region respectively, as northeastern Oklahoma and southwestern Missouri were now in the region of upward vertical motion associated with the coupled jet streaks.

3. FORECAST CHALLENGE

A key question facing forecasters prior to the event was: How would the dry air/wet-bulb cooling influence the precipitation type? This question was especially challenging since traditional model forecast thickness forecasts suggested an environment too warm for frozen precipitation. Given these circumstances, how could forecasters better anticipate the evolution of the event?

For Oklahoma, 850-700 mb thickness values less than 1540 m typically represent an environment cold enough to support snow versus liquid precipitation (Branick 1992, Szatkowski 1988). Similarly, 1000-500 mb thickness values less than 5430 m can be used as guidance in determining areas of frozen versus liquid precipitation. Comparisons of 850-700 mb thickness fields from observed data were made with numerical weather prediction model forecast fields. In this case, the 850-700 mb thickness forecasts were consistent with observations in the location of the 1540 m line. However, the surface rain/snow line was farther south than the observed 1540 m line and farther south than model forecast of the 1540 m thickness value (Figures. 7 a, b). The same observation is made for the 1000-500 mb thickness 5430 m value.

The models and real-time data portrayed the 1540/5430 m values correctly, however, the thickness technique in determining the rain/snow transition zone appears to have failed in this case. The presence of a layer of dry air, and its wet-bulb cooling potential, in central and southern Kansas is the likely explanation for the observed location of the rain/snow transition zone. Surface and upper air observations indicated a region of relatively low dew points (upper teens to lower 20s) in the lower troposphere. We assumed that the lower troposphere over north central Oklahoma was best

represented by the 0000 UTC Topeka sounding (Figure 8). Another assumption we made concerned the top of the dry air layer: the 1200 UTC winds at Norman (Figure 9) indicated that the frontal surface extended from the ground to approximately 800 mb, hence the upper boundary of the dry air layer. Temperatures within this layer were higher than 0°C, which on first inspection might suggest a liquid precipitation event, however, this layer played an important role with the storm because its wet-bulb temperature profile would become less than 0°C during the day of March 8. This cooling allowed liquid precipitation to transition to either snow or ice pellets. Furthermore, KTLX 88D data indicated that precipitation fell into this layer throughout the event. Surface observations also showed that dry air continued to advect southwest into the area of moderate to heavy snowfall depicted by observations at 2100 UTC. Additionally, the meteogram for March 8 at Bartlesville (Figure 10) depicted the overall trend of wet-bulb cooling by indicating dew points in the upper teens existing before the onset of precipitation. After precipitation started, the Bartlesville temperature dropped as the dew point increased. Furthermore, the 0000 UTC 9 March (Figure 11) Norman sounding showed that the temperature profile was below 0°C from the surface to 700 mb. It **appears** that the dry air layer provided a "source" of cold air through wet-bulb cooling processes resulting in the rain/snow line to be south of the model forecast thickness.

4. SUMMARY AND RECOMMENDATIONS

Results of this case study indicate that the winter storm of March 7-9, 1994 contained many "classic" elements necessary for heavy snowfall including: CSI, isentropic uplift, and ageostropic circulations associated with coupled jet streaks and frontogenesis. However, the crucial factor was the presence of dry air from Kansas. This is operationally important since proper preparation for a winter weather event by the public hinges on good forecasts before and during the event. Had the dry air not been present, the event may well have been a heavy rain producer instead of a heavy snowfall producer.

It is recommended that forecasters carefully consider the potential for diabatic (wet-bulb) cooling when formulating forecasts of winter weather. The increasing availability of high resolution gridded model data and advanced workstations (PCGRIDDS, N-AWIPS, etc.) in the operational environment offers new tools for this purpose. Even the Skew-T/Hodograph Analysis and Research Program (SHARP) (Hart and Korotky) can help the forecaster examine a sounding and modify it based on current observations and on model forecasts of temperature and moisture, much the same way forecasters use SHARP to modify soundings to determine severe thunderstorm potential. Using SHARP would seem a better option than relying solely on model forecasts of thicknesses. Furthermore, throughout an event, the forecaster could then modify a sounding based on current surface observations to obtain a more realistic picture of the atmosphere via the wet-bulb temperature curve and then make more accurate short-term forecasts as a result.

5. ACKNOWLEDGMENTS

I wish to thank David Andra (SOO WSFO Norman), the staff of WSFO Norman, the members of the Storm Prediction Center in Norman and the members of the Mesoscale Applications Group of the National Severe Storms Laboratory for their input in making this paper possible. I would also like to thank Dan Smith (SSD Southern Region Headquarters NWS) for providing requested data sets for this study.

6. REFERENCES

Branick, M., 1992: Winter Weather Forecasting Rules of Thumb at WSFO Norman. Norman forecast Office Internal Memo, 10pp.

Hart, J.A., and Korotky W.D., 1991: *The Sharp Workstation-V1.50. A Skew-T/hodograph analysis and research program for the IBM and compatible PC.* User's Manual. NOAA/NWS Forecast Office, Charleston, West Virginia. 62 pp.

Moore, J.T., 1993: Isentropic Analysis and Interpretation: Operational applications to synoptic and mesoscale forecast problems. National Weather Service Training Center, 99 pp.

Petersen, R.A., 1992: A PC-based system for the display of gridded WAFS data. *Proceedings of the WMO Technical Conference on Tropical Aeronautical Meteorology* (TECTAM-92), Geneva, Switzerland, 1-6.

Snook, J.S., 1992: Current techniques for real-time evaluation of conditional symmetric instability. *Wea. Forecasting,* 7, 430-439.

Szatkowski, G., 1988: The liquid/freezing/frozen precipitation decision. NWSFO Norman, OK. internal memo, 4pp.

Uccellini, L.W., and P.J. Kocin, 1990: The interaction of jet streak circulations during heavy snow events along the east coast of the United States. *Wea. Forecasting,* 2, 298-308.

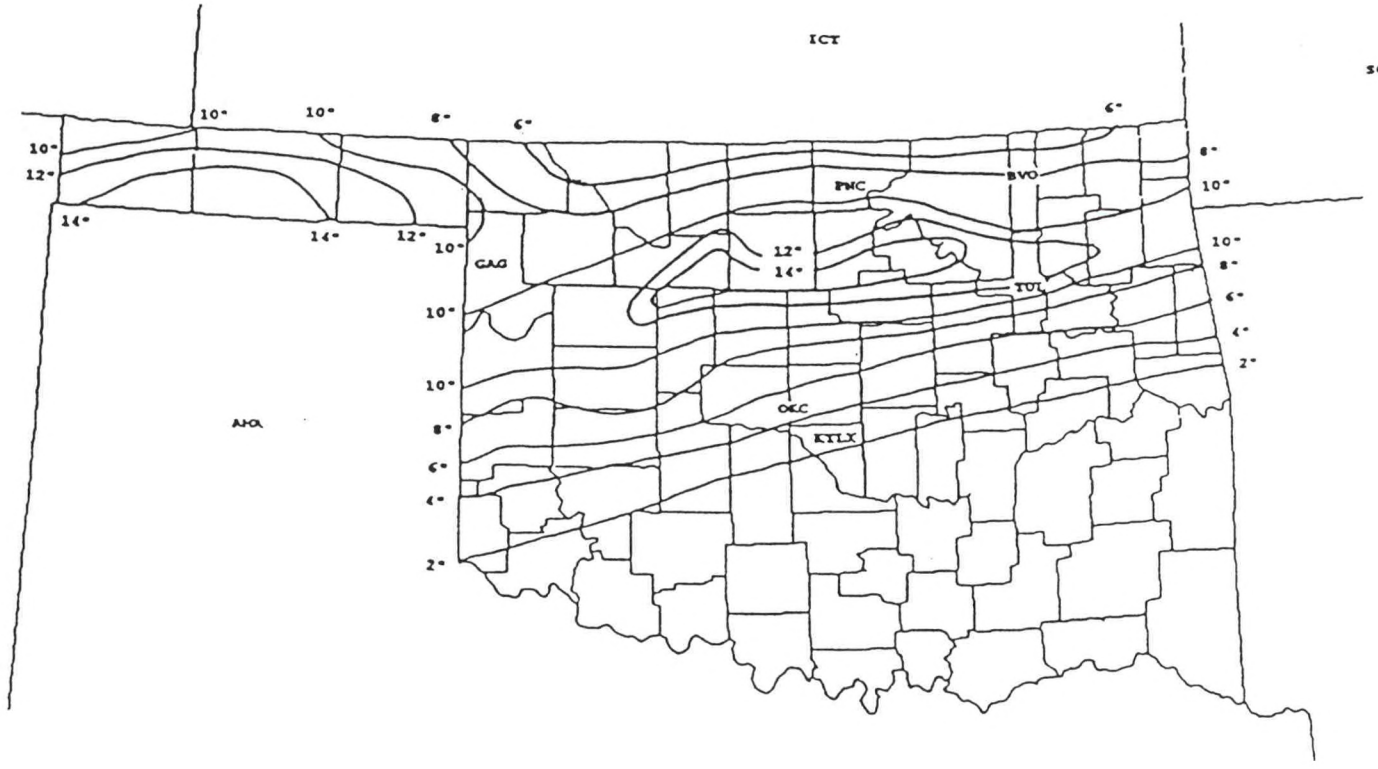

Figure 1. Total Snowfall (inches) March 7-9, 1994.

Figure 2. 300 mb NGM 1200 UTC 8 March 0 hr analysis. Wind barbs in knots. Isotachs (solid lines) in knots.

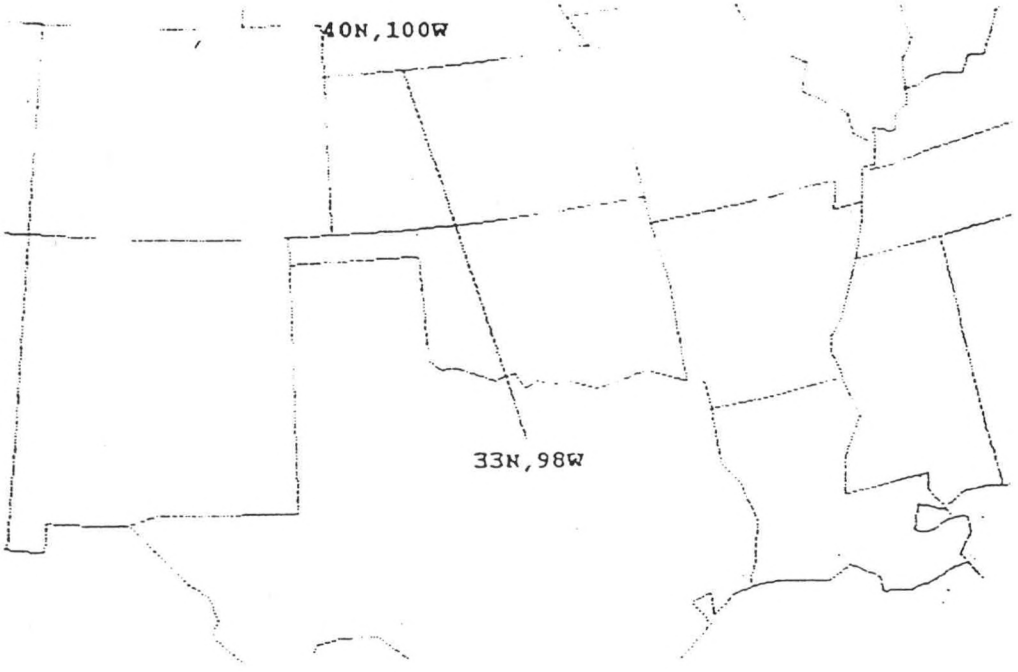

Figure 3. Cross-section line for all cross-sections.

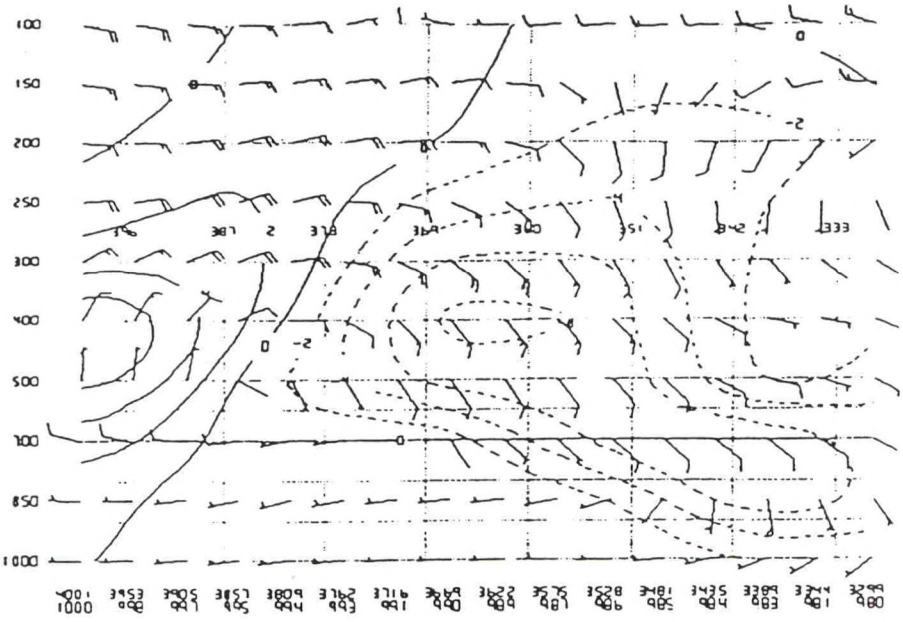

Figure 4a. NGM 0 hr analysis of vertical cross-section valid at 1200 UTC 8 March. Barbs are component of ageostrophic circulation parallel to cross-section plane. Dashed (solid) lines are upward (downward) vertical velocity. Units are microbars per second.

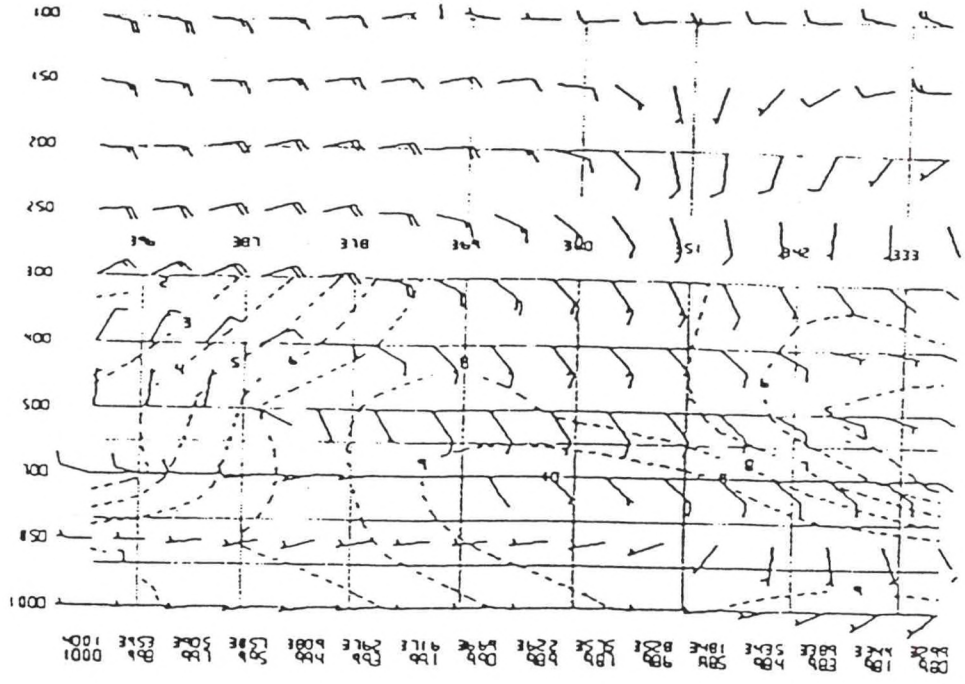

Figure 4b. Same as previous. Dashed lines are relative humidity Interval is 10 percent.

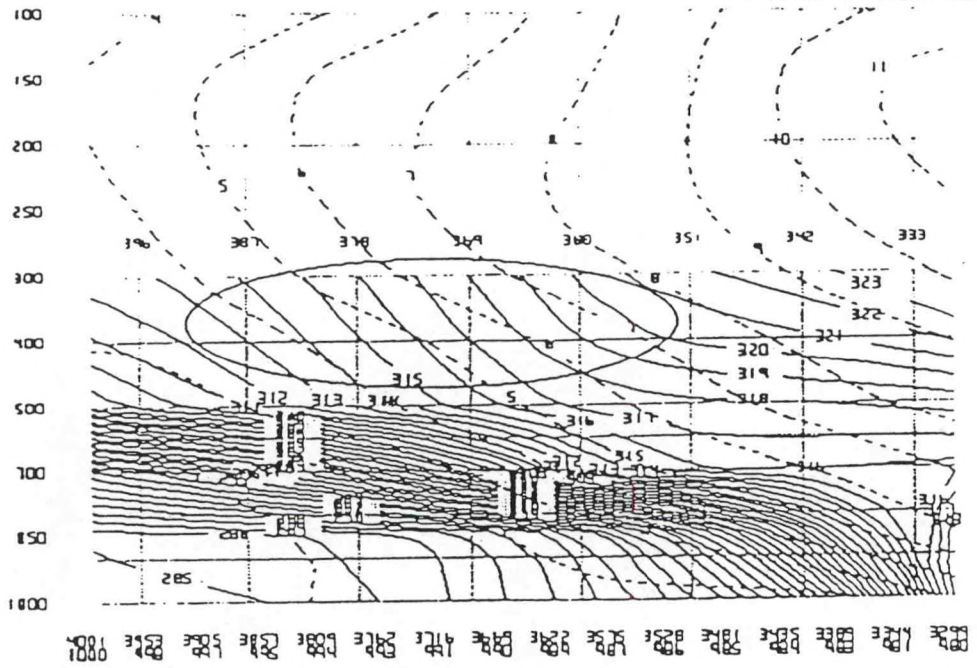

Figure 5a. Six hour NGM forecast valid 1800 UTC 8 March. Dashed lines are geostrophic momentum (meters per second). Solid lines are equivalent potential temperature (degrees Kelvin). The ellipse represents the region of CSI potential.

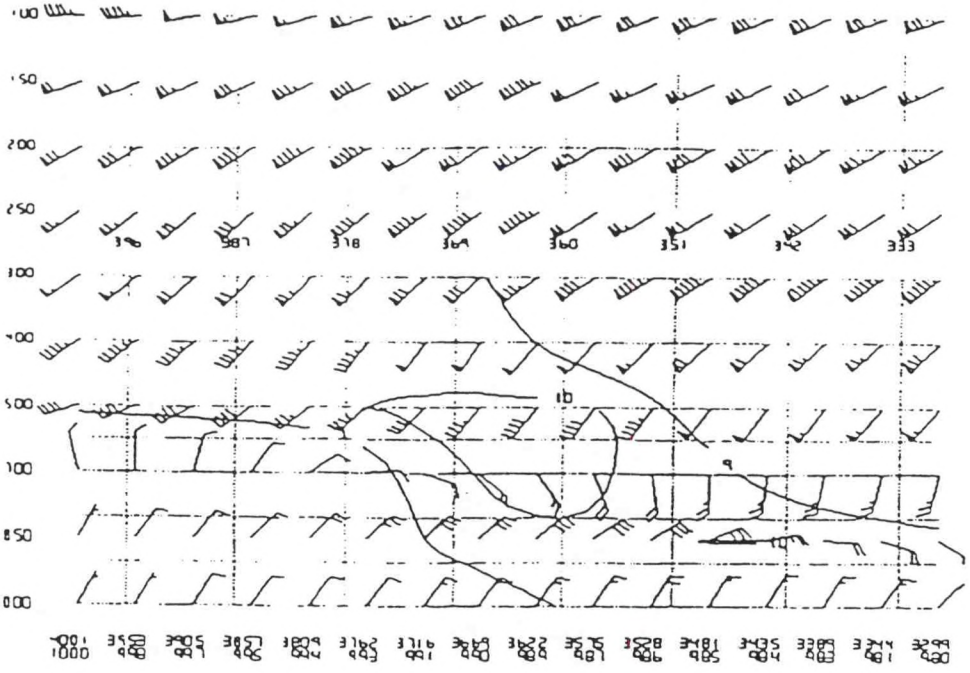

Figure 5b. Six hour NGM forecast valid 1800 UTC 8 March. Solid lines represent relative humidity values of 90 percent or greater. Wind barbs are in knots.

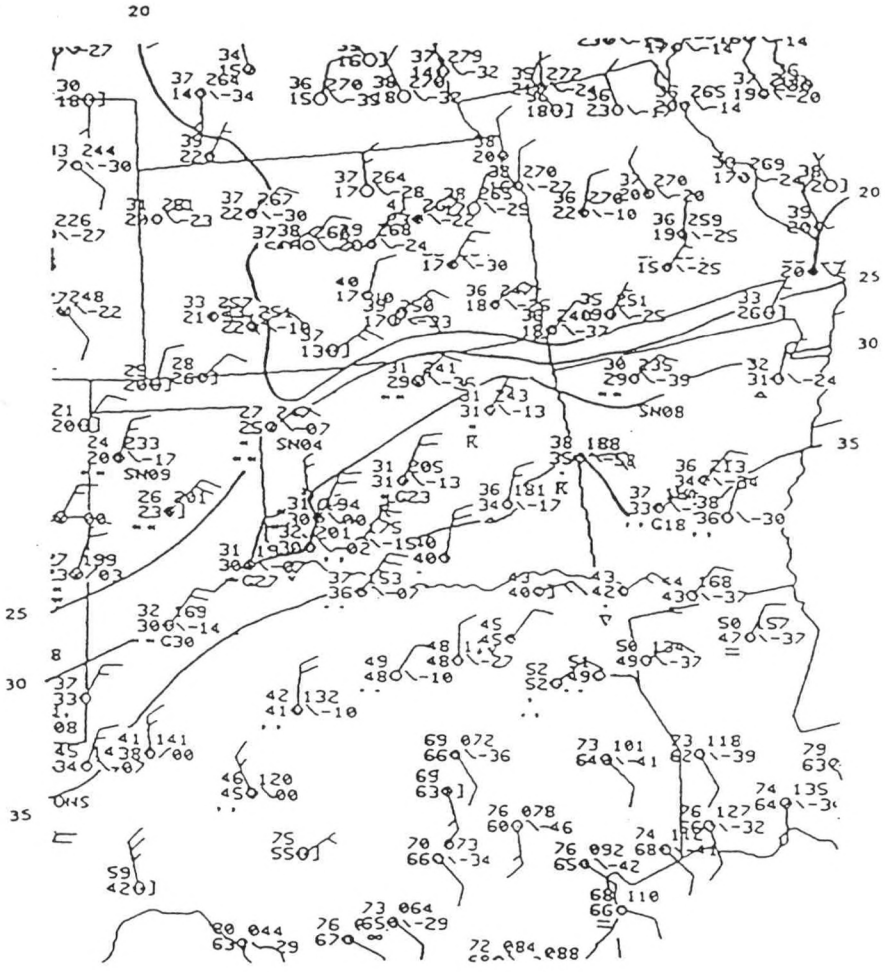

Figure 6. 2100 UTC 8 March surface plot solid lines are isodrosotherms. Contour interval is 5°F.

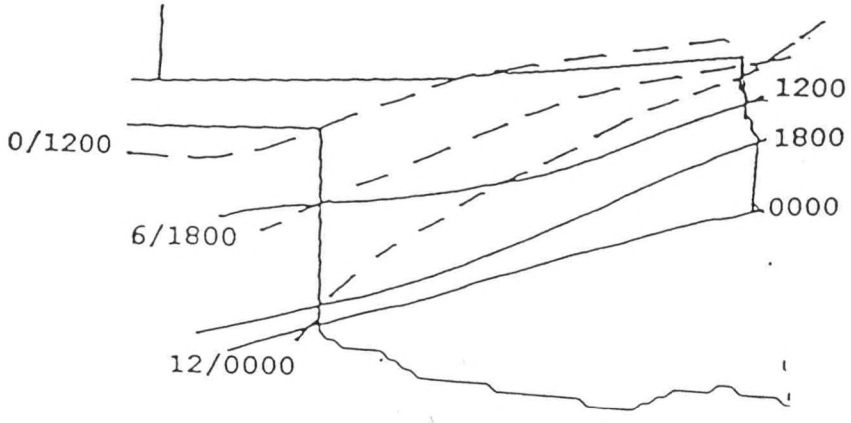

Figure 7a. NGM forecast of 1540 m 850-700 mb thickness (dashed). Solid lines represent observed rain/snow line.

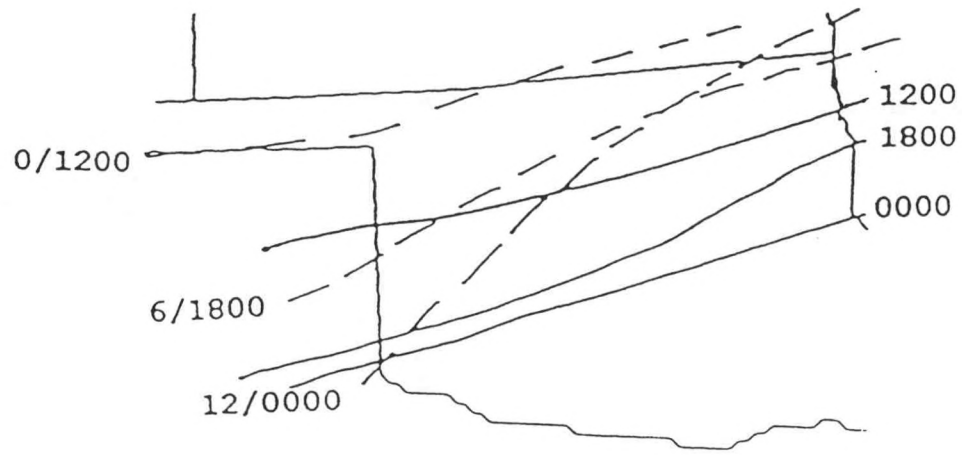

Figure 7b. ETA forecast of 1540 m 850-700 mb thickness (dashed). Solid lines represent observed rain/snow line.

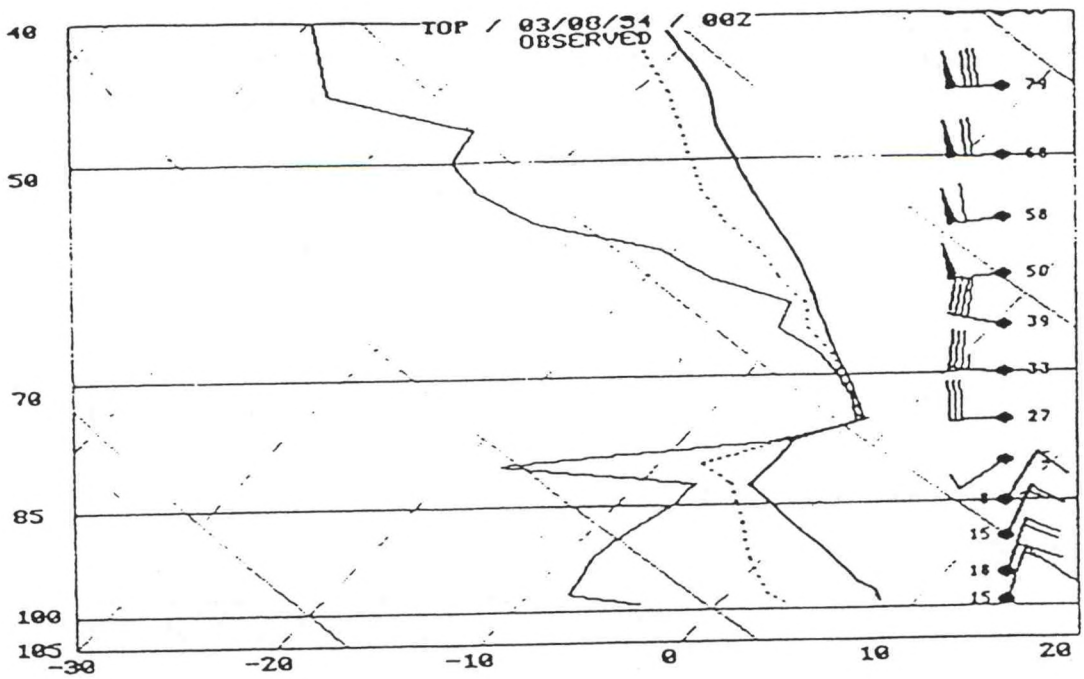

Figure 8. 0000 UTC 8 March Topeka, Kansas sounding. Right curve is temperature. Left curve is dew point. Dashed curve is wet-bulb temperature. All curves in °C.

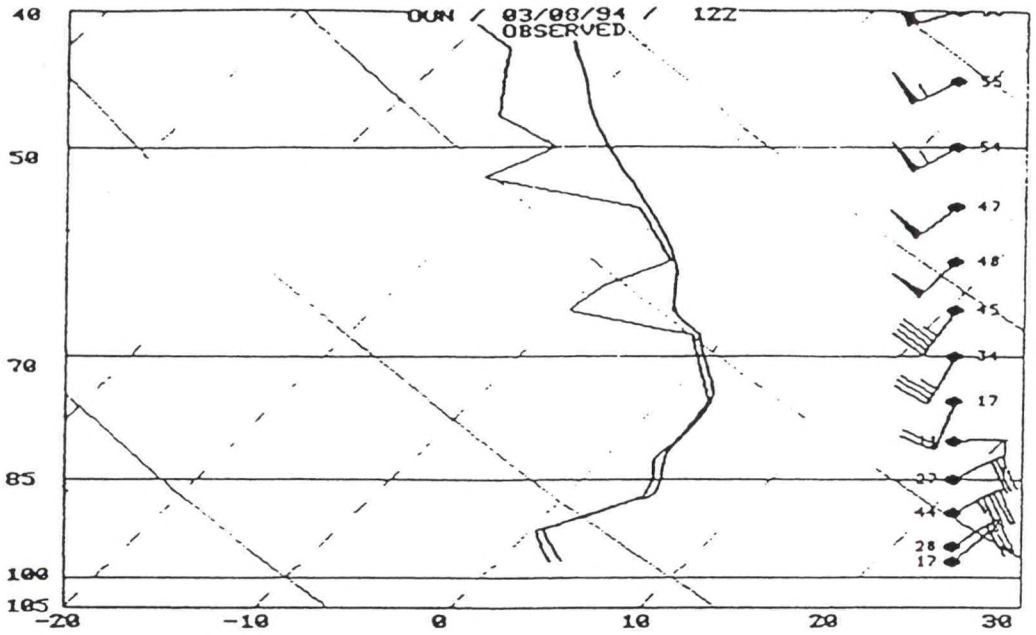

Figure 9. 1200 UTC 8 March Norman, Oklahoma sounding. Wet-bulb curve omitted.

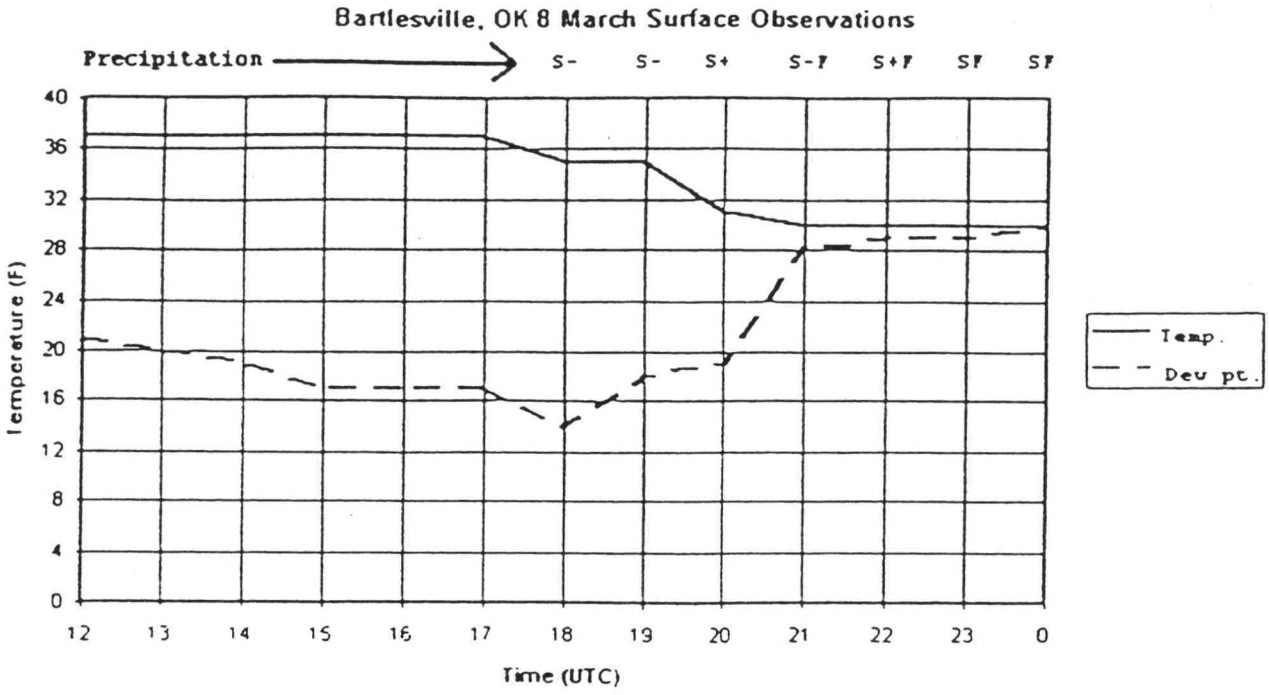

Figure 10. Bartlesville Meteogram.

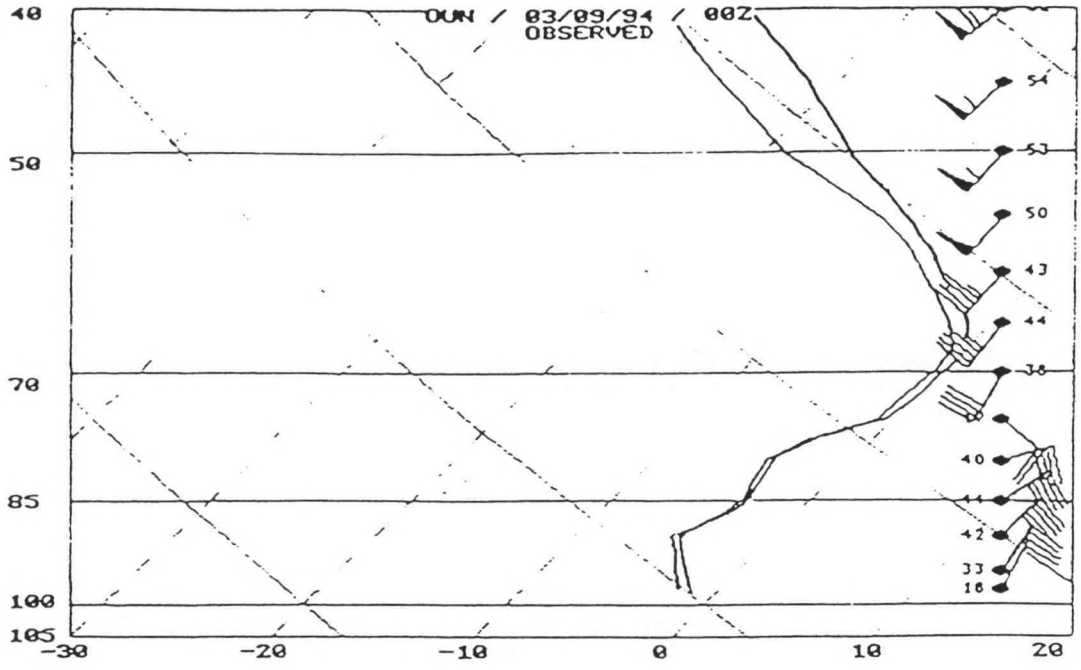

Figure 11. 0000 UTC 9 March Norman, Oklahoma sounding.

The March 8-9, 1994 Winter Storm over Southern Missouri: A Challenging Operational Forecasting Problem

Todd J. Shea[1], Ted Schroeder[2], Ron W. Przybylinski[3], James T. Moore[4], and Patrick S. Market[5]

1. INTRODUCTION

Operational forecasters are continuously challenged during the winter season in forecasting snow events over the continental United States. Mesoscale systems may produce a single narrow band of accumulating snow no wider than 60 to 80 km (32 or 45 nm), while other well-organized extratropical systems will often exhibit mesoscale structures within a large area of significant snowfall covering parts or even an entire state. The location and amount of heaviest snow will affect daily public activities, businesses, rush hour commutes, air travel, and will often place the general public in danger.

On March 8-9, 1994, a major winter storm traversed through the central U.S., and produced between 25.4 - 50.8 cm (10 to 20 inches) of snow across much of southern Missouri and far northern Arkansas (Figure 1). As the storm evolved, forecasters were challenged with the placement and the northern extent of the significant snowfall. Heavy snowfall initially occurred along a narrow band near the Missouri - Arkansas border between 1200 and 1500 UTC 8 March 1994. The snow area then gradually expanded and intensified during the late afternoon and evening hours over southern Missouri and northern Arkansas. Despite the heavy snow amounts over this region, a deep surface low center was not present. A post-mortem analysis of the event indicated that there was an abrupt northern edge to the area of significant snowfall across the southern third of Missouri. Several aspects of this storm appeared to be attributed to forcing mechanisms described by Uccellini and Kocin (1987), Hakim and Uccellini (1992), Shea and Przybylinski (1993), and Funk et al. (1995), where the ascending branches of two jet streaks may have contributed to the heavy snowfall. However, other forcing mechanisms including frontogenetical forcing (Moore and Blakley 1988; Shields et al. 1991) and isentropic up glide (down glide) (Moore and Kaster 1993) can play equally important roles in generating single banded snow structures which may last for several hours.

This paper will address those mechanisms which contributed to moderate-strong vertical motion and were responsible for enhancing the snowfall and defining the northern limits of the heavy snow area. The first part will describe the overall synoptic pattern at 0000 UTC 8 March 1994, leading up to the event. This will be followed by an overview of 0000 UTC 8 March 1994 derived fields computed by the St. Louis University (SLU) diagnostic analyses program and the GEnearl Meteorological PAcKage (GEMPAK) program. This section will be followed by an overview and comparison between the 24 h forecast Eta-X output from the Personal Computer-Gridded Display and Diagnostic System (PCGRIDDS) and the 00 Hour (0000 UTC 9 March 1994) SLU diagnostic output.

2. SYNOPTIC OVERVIEW

At 0000 UTC 8 March 1994, a stationary front extended across southern Arkansas and Oklahoma to a developing area of low pressure centered over the high plains of west Texas (Figure 2). Relatively cold, dry air was entrenched north of the front as temperatures ranged from -0 to -5°C

1. Corresponding author address: Todd J. Shea, NWS Forecast Office, St. Louis, MO.
2. Ted Schroeder, NWS Forecast Office, St. Louis, MO.
3. Ron Przybylinski, NWS Forecast Office, St. Louis, MO.
4. James T. Moore, St. Louis University, Dept. of Earth and Atmospheric Science, St. Louis, MO.
5. Patrick S. Market, St. Louis University, Dept. of Earth and Atmospheric Science, St. Louis, MO.

across Kansas, Missouri, and Illinois to +1 - +4°C across Arkansas and Oklahoma. Throughout the night-time hours, a steady northeast surface flow continued to transport colder air southwestward over this region.

The 850 mb front was marked by a trough, a strong temperature gradient and wind shift from the southern Great Lakes through southern Missouri and southwest into central Oklahoma (Figure 2). A moist but weak southerly flow was noted south of the front while drier air was being advected southeastward across the western Great Lakes through the mid-Mississippi Valley region. Overnight the 850 mb thermal gradient moved southward to a position from central Kentucky through southern Oklahoma by 1200 UTC. Compared to 0000 UTC initial analyses, wind speeds and the thermal gradient on both sides of the front increased at 1200 UTC over the southern plains through Arkansas.

At 500 mb (Figure 3), a broad trough extended from western Ontario through eastern Nebraska with a large area of height falls centered in the base of the trough. The broad trough structure was also revealed at 300 mb over this same area, while a closed low was positioned over far northern Baja (Figure 4). A strong polar upper-level jet streak (ULJS) with speeds exceeding 55 m s^{-1}, extended from the Great Lakes region through eastern Nebraska and Kansas while a subtropical jet core of equal magnitude (55 m s^{-1}), located near the base of the closed low, was entering southern New Mexico and western Texas.

3. 0000 UTC 8 MARCH, 1994 DIAGNOSTIC ANALYSES

The SLU diagnostic analyses program and GEMPAK diagnostics were used to show the utility of these programs in a near-real time evaluation and to capture the initial environmental settings of the developing system prior to the heavy snow event. At 850 mb, weak flow dominated much of Missouri while a strong northwesterly flow stretching from North Dakota through the Great Lakes region impinged upon a southwesterly flow over the Appalachian mountains (Figure 5). An axis of weak 850 mb convergence analyzed across Missouri through central Kentucky at 0000 UTC, evolved over the ensuing 24 hours. Frontogenesis at 850 mb was indicated along a broad swath from the Texas Panhandle region stretching eastward through Missouri and into northern Kentucky (Figure 6). This area of frontogenetic forcing was a response to the deformation of the flow at this level.

Further aloft, a broad region of 300 mb divergence was present over the Central Plains (Figure 7), upstream of the jet streak over northeast Kansas and central Iowa. Conversely, a large area of 300 mb convergence extended from the Upper Mississippi Valley region through the lower Great Lakes.

At this same time (0000 UTC 8 March 1994), isentropic analyses at 290 K showed this surface intersecting the earth's surface along the Gulf states and over the southern Rockies (Figure 8). However, significant isentropic down glide, signaling sinking motions and the penetration of colder air, was present from Iowa through much of the Great Lakes region.

4. COMPARISON OF THE 24-H FORECAST ETA-X GRIDDED DATA AND 0000 UTC 9 MARCH 1994 DIAGNOSTIC FIELDS

A major component of this study focused on comparing the 24 h forecast Eta-X output from PCGRIDDS and the 0000 UTC 9 March 1994 diagnostic fields from the SLU diagnostic analyses program. Comparisons between forecast Eta-X and RFS model output and diagnostic output from the SLU diagnostic package are planned for future winter weather events. Such comparisons will be used to reveal forecast model strengths and weaknesses with each event.

From 1500 UTC to 2100 UTC, heavy snow fell in a narrow band along the Missouri - Arkansas border mainly south of Springfield, Missouri (SGF). Amounts of 30.5 - 38.1 cm (12 to 15 inches) were already recorded across parts of extreme southwest and south-central Missouri. After 2100 UTC, the intensity of snowfall increased and expanded north and eastward across the southern third of Missouri. A sequence of WSR-88D images between 2028 UTC and 2344 UTC 8 March 1994 from (WSFO St. Louis) KLSX is shown in Figure 9. Reflectivity images revealed a general solid band, approximately 100 km wide, comprised of 10 to 25 dBZ echo. Isolated 30 dBZ echoes were detected within the larger band. This type of reflectivity structure persisted for over a 5 hour period. Springfield, Missouri experienced moderate to heavy snowfall during a five hour period ending at 0200 UTC 9 March 1994. Light to occasional moderate snow continued to fall across the SGF area and points east and northeast from 0200 to 0600 UTC. It is interesting to note that strong gradients of significant snowfall were revealed on the snowfall map (Figure 1) across parts of southwest and southeast Missouri.

A. Isentropic Perspective

The 24 h forecast 290 K isentropic surface valid for 0000 UTC 9 March 1994 and initial diagnostic analyses were used since this level was generally above the surface east of the Rockies. The forecast 290 K surface revealed a col from far southern Missouri through northern Oklahoma (Figure 10a). Weak isentropic down glide, associated with sinking motion, extended from central Kansas northeastward into the Ohio Valley region while isentropic up glide was present from northeast Texas through eastern Arkansas. The 24 h Eta forecast 290 K surface agreed fairly well with the SLU diagnostic package in locating the col and regions of isentropic down glide (up glide) (Figure 10b). The col represents a region of **deformation**. Vectors and pressures shown on the 290 K surface from the SLU package indicated more of a region of confluence than pure of deformation. The strength of the down glide (up glide) and region of confluence was not as significant on the 24 h forecast as on the SLU initial analyses at 0000 UTC. Moore (1993) has shown that strong isentropic up glide is associated with warm air advection and positive moisture advection, often resulting in the development of heavy precipitation. In contrast, the stronger isentropic down glide was one of several processes that defined the northern limits of the heavy snow area across south-central Missouri. Complementing the region of lower tropospheric confluence is a substantial moisture supply with condensation differences (not shown) of less than 50 mb over southern Missouri.

Garcia (1994) studied the relationship of isentropic mixing ratios and the amount of snowfall produced by different snow events. His technique centered on evaluating mixing ratios on isentropic surfaces within the 700 - 750 mb layer and correlating them to snowfall amounts. This layer was chosen since it typically contains the volumetric flow "conveyor belt" of moisture ascending isentropically into the middle levels of the atmosphere. In our study, the 295 K surface was chosen, since this layer bisected the region of snowfall and was at 700 - 750 mb over southern Missouri. Forecast average mixing ratio values of 4-5 g kg^{-1} was observed over the "area of concern" from southern Missouri through far northern Arkansas (Figure 10c). These values suggest that forecast snowfall amounts of 20.3 to 25.4 cm (8 to 10 inches) were possible during the duration of the snow event. The technique underestimated the total amount of snowfall, but did signal the potential for heavy snowfall to occur over the area of concern.

B. Moisture Transport Analyses

Moisture transport vectors (defined as Vq) were defined by Junker (1993) and have been shown to be an effective forecast tool in defining the region of heavy rainfall. The heaviest precipitation often falls north of the maximum moisture transport (in the gradient of the magnitude of moisture flux vectors; Nolan and Moore 1995; Market and Moore 1995; Rochette et al. 1995). Twenty-four hour

Eta forecast (Figure 11a) showed the axis of the strongest moisture transport vectors extending from extreme southeast Texas - far southern Louisiana through eastern and northeast Texas. In contrast, the initial 0000 UTC 9 March analyses of moisture transport vectors showed the axis of the strongest moisture transport vectors further east, extending from central Louisiana through eastern Oklahoma and northern Arkansas (Figure 11b). The marked differences in the placement of the axes lead to higher precipitation rates over much of Arkansas, southern Missouri and eastern and central Oklahoma. The 24 h Eta forecasts appeared to under-estimated the degree of moisture transport compared to the initial analyses. Magnitudes of moisture transport vectors were again slightly stronger with the initial 0000 UTC analysis compared to the 24 h forecast, suggesting that heavier amounts of precipitation would occur downwind of the maximum values of moisture transport than initially considered. This parameter has proven to be useful in heavy rainfall forecasting and was found to yield a similar signal in this scenario, with the heaviest precipitation amounts over Arkansas and southern Missouri.

C. Jet Streak Interactions

Several studies have documented the importance of jet streak interaction to the enhancement of vertical motions and heavy snowfall. Uccellini and Kocin (1987), Hakim and Uccellini (1992), and Shea and Przybylinski (1993) have all shown that vertical motions can be locally enhanced by the merger of the ascending branches of two ULJS. In our case the 24 h Eta-x forecast revealed a well-defined 300 mb polar ULJS exiting the lower Great Lakes region while a subtropical ULJS was entering central Texas (Figure 12a). The entrance region of the polar jet and exit region of the subtropical jet appeared coupled over southern Kansas through southern Missouri, with both showing substantial along-stream variation in the wind field. The result was an axis of strong upper-level divergence (ULD) extending from southern Kansas through southern Missouri.

The 24 hour Eta forecast position of the polar ULJS was slightly too far east compared to the initial analysis (Figure 12b), however the placement and magnitude of the 300 mb subtropical ULJS was in good agreement. The slight differences in the positioning of the polar ULJS between the Eta-X model and initial analysis lead to the placement of the max ULD being approximately 300 km east of the initial analyses. However, the overall placement of the forecast region of ULD was in good agreement with the initial analysis and would have given the forecaster valuable information in defining the region of maximum up glide.

Eta 850 mb model output indicated that the exit region of the southern subtropical jet may have intensified the southerly low-level jet (LLJ) across far eastern Texas. Convergent flow extended from far southern Missouri through southern Oklahoma. The 24 hour forecast Eta 850 mb isotach analysis (Figure 13a) showed the placement of the LLJ slightly too far west compared to the initial analysis at 0000 UTC (Figure 13b). Magnitudes of the LLJ over eastern Texas and the northeasterly LLJ across northern and central Oklahoma were also over-estimated by the model.

D. Frontogenesis

Shields et al. 1991 have shown that frontogenetic forcing is associated with a single band of enhanced precipitation within larger synoptic-scale storms. Moore and Blakely (1988) showed how both surface and 850 mb frontogenesis played a significant role in the January 30, 1982 snow storm over Missouri and Illinois. Frontogenesis results in the intensification of a thermal gradient near a front. The response to frontogenetic forcing is the evolution of a thermally direct circulation which will attempt to weaken the strong thermal gradient. In our case the 24 h Eta-X forecast of 850 mb geostrophic frontogenesis showed frontogenetical forcing extending from eastern Oklahoma through extreme southeast Missouri (Figure 14a). Diagnostic analyses of 850 mb frontogenesis from the

GEMPAK packaged showed nearly an identical placement to the 24 h forecast (Figure 14b). This area of frontogenesis, appeared to play an important role in enhancing heavy snowfall.

We also examined the 24 hour Eta-X forecast of geostrophic frontogenesis within the 850 - 700 mb layer and its response. The 24 h Eta forecast showed 850-700 mb frontogenesis extending from eastern Oklahoma through southern Indiana and Ohio (Figure 15a). The geostrophic frontogenetical forcing within the 850 - 700 mb layer is aligned along but slightly north of the 850 mb level frontogenesis and reflects the structure of the front tilting northward with height. The response to frontogenesis (Qn and the divergence of Qn) within a layer is shown in Figure 15b where a thermally direct circulation (frontal-scale circulation) is detected. The thermally direct circulation is the response to frontogenesis and acts to relax the strong temperature gradient. The area within the dashed contours represents ascent and cooling within a column while the area within the solid contours signifies descent and warming within the column. The thermally direct circulation (specifically the southern region of sinking motions) appeared to play an important role in defining the abrupt northern edge of the significant snowfall over southern Missouri. WSR-88D reflectivity images shown in Figure 9 revealed a relatively strong reflectivity gradient along the northern edge of the larger banded structure. This reflectivity gradient coincided with the northern edge of the significant snowfall area while the overall single banded reflectivity structure indicated that frontogenesis was present during this period.

E. Cross-Sectional Analyses

Cross-sectional analyses, oriented orthogonal to the strong westerly upper-level flow, were constructed to show the structure and magnitude of the ageostrophic transverse direct (indirect) circulations associated with the merger of the ascending branches of the two ULJS and the region of strong frontogenesis and vertical frontal structures. All cross-sections presented were oriented from 46°/94° lat/lon (near St. Cloud Minnesota (STC) to 27°/93° lat/lon, south of Lake Charles, Louisiana (LCH) or along a line that traverses the entrance region of the polar ULJS. Cross-sections generated from the PCGRIDDS program display pressure, potential temperature surfaces, total winds above 50 m s^{-1} (100 kts), tangential ageostrophic winds, and kinematic vertical motion fields.

Forecasters viewing the 24 h Eta-X cross-section would have discovered a strong transverse direct circulation (D) with strong ascending (descending) motion in the region of the polar ULJS's right rear (left rear) quadrant (Figure 16a). A weak transverse indirect circulation (I), associated with the exit region of the subtropical jet core can also be detected on the vertical plan near 30° N latitude. The slope of the ascending (descending) branches of the circulation are quite dramatic indicating deep-tropospheric motions rising over the frontal boundary over the southern third of Missouri and northern Arkansas. The region of maximum upward vertical motion extended from 650 mb to near 400 mb. This region is comparable to other winter storm cases where the region of maximum vertical motion associated with the transverse ageostrophic direct circulation resides within the 600 to 400 mb layer.

In contrast, a relatively deep layer of weak subsidence was detected beneath the region of rising motions at mid and upper altitudes. The sinking layer, also defined by the Divergence of Qn (Figure 15b) also appeared to be a critical feature in defining the northern limits of the heavy snow area by drying the atmospheric column.

The 0000 UTC initial cross-sectional analyses from the SLU diagnostic program showed a similar sloping structure of the ascending branch of the transverse direct circulation compared with the 24 h Eta-X forecast (Figure 16b). The altitude of strongest kinematic vertical motions on the 24 h Eta-X cross-section nearly matched the 00 hr initial analyses (550 - 450 mb). However, the magnitude of

vertical motion on the 00 hr analyses was slightly weaker (6 μb sec^{-1}) compared to the 24 hr Eta-X forecasts (8.1 μb sec^{-1}). A region of weak subsidence flow was detected beneath the ascending branch, similar to the 24 h forecast, however, its overall magnitude was not as strong compared to the 24 h Eta-X forecast. The northern edge of **significant snowfall** occurred near the northern edge of the area of maximum vertical motion detected between 550 and 450 mb. One interesting aspect with the 00 hr initial cross-sectional analyses was the detection of a second vertical motion maximum just north of 30° N latitude, embedded within the larger overall region of vertical motion. This region of upward motion appeared to be linked to the ascending branch of the transverse indirect ageostrophic circulation associated with the subtropical jet streak. Together, the larger region of vertical motion appeared to be locally enhanced by the merger of the ascending branches of the two jet streaks, similar to observations revealed by Hakim and Uccellini (1993). The orientation of the ULJSs combined with strong frontogenesis below 700 mb across southern Missouri appeared to play important roles toward enhancing and defining the northern edge of significant snowfall.

Figure 16c is a 00 hr cross-section (similar to the above cross-section) showing total winds (m s^{-1}) parallel to the plane and theta surfaces. Several interesting features were identified on this cross section. The isentropic analyses showed a strong temperature gradient, reflecting the frontal boundary, extending from central Louisiana (near Lake Charles (LCH) - 950 mb) through southern Missouri (north of Monett, Missouri (UMN) - 700 mb). A secondary frontal boundary was detected near 600 mb (near UMN) to near 400 mb (near Omaha, Nebraska (OMA). The wind field, parallel with the cross-section, revealed a northward moving low-level jet (15 m s^{-1}) along the strong thermal gradient. The structure of the wind and temperature field showed a nearly classic illustration of isentropic up glide. The steepest part of the frontal boundary is noted north of Little Rock, Arkansas (LIT) through UMN. Heavy snowfall occurred in the region where the frontal boundary was quite steep. Above the frontal boundary, the temperature field significantly weakens depicting a region of weaker (low) static stability. A component of the upper-level polar jet streak is detected between 250 and 325 mb near Topeka (TOP), Kansas. Above the jet core, the vertical potential temperature gradient significantly tightens, revealing a region of strong static stability.

5. SUMMARY

The March 8-9, 1994 snowstorm over southern Missouri and far northern Arkansas was studied to diagnose those physical mechanisms contributing to a long band of heavy snow that fell during the passage of a surface inverted trough. A number of derived fields from the 24 h Eta-X forecast (valid at 0000 UTC 9 March 1994) were compared to derived fields produced by the SLU diagnostic and GEMPAK software programs.

A number of forcing mechanisms, including frontogenesis within the 850-700 mb layer, interaction of two jet streaks and the merging of their associated transverse ageostrophic circulations, and isentropic up glide, appeared to be responsible for the heavy snowfall. Derived fields from the 24 h Eta-X forecasts were in general agreement with the 0000 UTC 9 March 1994 diagnostic analyses. Eta-X 24-h forecast placement of the 300 mb polar ULJ streak over the Great Lakes region was slightly too far east compared to the 00 hour 0000 UTC initial analyses. However, placement and magnitude of the 300 mb subtropical ULJS was in good agreement with the initial analyses. Merger of the ascending branches of both jet streaks likely contributed to locally enhanced vertical motion over parts of southern Missouri and northern Arkansas. The coupling of the subtropical ULJS and the 850 mb LLJ appeared to provide an efficient circulation pattern that induced a northward transport of heat and moisture.

Frontogenetical forcing was another important forcing mechanism enhancing the snowfall rate. The alignment of 850 - 700 mb geostrophic frontogenesis from the 24 h Eta-X forecast and the initial

00 h analysis were nearly identical agreement. The response to frontogenetical forcing was the development of a thermally direct circulation over Missouri and Arkansas, which attempted to weaken the strong thermal gradient across this region and helped define the northern edge of the area of significant snowfall.

It is critical for operational forecasters to examine a variety of gridded data fields to understand the science and atmospheric processes which contribute to heavy snowfall and other forms of precipitation associated with the winter storm. Without having this fundamental baseline of knowledge, and knowing the types of atmospheric processes at work, the forecaster will likely encounter difficulties in forecasting the location and intensity of snowfall. These troubling experiences have occurred in the past. It is also interesting to note how far we progressed in forecasting major snow events with the use of gridded data fields. Having these new capabilities to examine synoptic and sub-synoptic scale forcing mechanisms have brought forth a new dimension in forecasting winter storm events. It is hoped that this paper has shed new insights into understanding the synoptic and mesoscale atmospheric structures and implications of winter storm evolution.

6. ACKNOWLEDGEMENTS

The authors wish to thank Dr. Preston Leftwich (SSD/CR), and Scott Rochette of St. Louis University for their reviews and comments upon improving the manuscript. Additional thanks goes to Mr. Steve Thomas (MIC/AM) for his support in this study.

7. REFERENCES

Garcia, C. Jr., 1994: Forecasting snowfall using mixing ratios on an isentropic surface. NOAA Tech. Memo. NWS CR-105, 1-31.

Hakim, G.J., and L.W. Uccellini, 1992: Diagnosing coupled jet streak circulations for a Northern Plains snow band from Operational Nested-Grid Model. *Wea. Forecasting*, 7, 26-47.

Junker, N.W., R.S. Schneider, and R.A. Scofield, 1995: The meteorological conditions associated with the great Midwest flood of 1993. *Preprints, 14th Conf. Weather Analysis and Forecasting.* Dallas, TX., AMS (Boston), 13-17.

Market, P.S., and J.T. Moore, 1995: An isentropic perspective on elevated thunderstorms associated with heavy rainfall. *Preprints, Conf. on Isentropic Analysis and Forecasting.* Millerville Univ., 37-39.

Moore, J.T., 1993: Isentropic analysis and interpretation: Operational applications to synoptic and mesoscale forecast problems. Air Weather Service, AWS/TN-87/002, revised 1989, 87 pp.

_____, and P.D. Blakely, 1988: The role frontogenetical forcing and conditional symmetric instability in the Midwest snowstorm of 30-31 January, 1982. *Mon. Wea. Rev.*, **116**, 2155-2171.

_____, and M.A. Kaster, 1993: Physical processes organizing wintertime frozen precipitation events in the Midwest. *Preprints, 13th Conf. on Wea. Analysis and Forecasting*, Vienna, VA., AMS (Boston), 512-515.

Nolan, S.M., and J.T. Moore, 1995: An isentropic analysis of a heavy snow event associated with weak cyclogenesis. *Preprints, Conf. on Isentropic Analysis and Forecasting.* Millersville Univ. 5-7.

Rochette, S.M., J.T. Moore, P.S. Market, F.H. Glass, and D.L. Ferry, 1995: Heavy rain events associated with elevated thunderstorms in the Midwest. Post prints, 4th National Winter Weather Workshop (Tech Memo 112). DOC, NOAA, NWS, Central Region, Scientific Services Division, Kansas City, MO.

Shea, T.J., and R.W. Przybylinski, 1993: Assessing vertical motion fields in a winter storm using PCGRIDDS. *Preprints, 13th Conf. Wea. Analysis and Forecasting.* Vienna, VA., AMS (Boston), 10-14.

Shields, M.T., R.M. Rauber, and M.K. Ramamurthy, 1991: Dynamical forcing and mesoscale organization of precipitation bands in a Midwest winter cyclonic storm. *Mon. Wea. Rev.*, **119**, 936-964.

Uccellini, L.W. and P.J. Kocin, 1990: The interaction of jet streak circulations during heavy snow events along the east coast of the United States. *Wea. Forecasting*, **2**, 298-308.

_____, and D.R. Johnson, 1987: The coupling of upper and lower tropospheric jet streaks and implications for the development of severe convective storms. *Mon. Wea. Rev.*, **113**, 31-55.

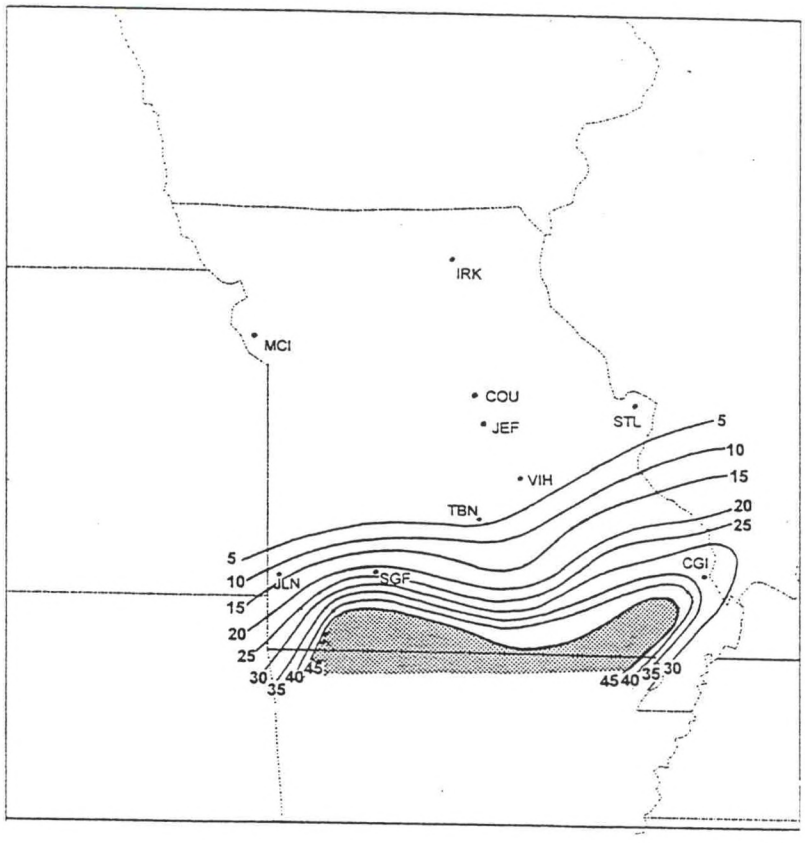

Figure 1. Observed snowfall (in cm) from March 8-9, 1994.

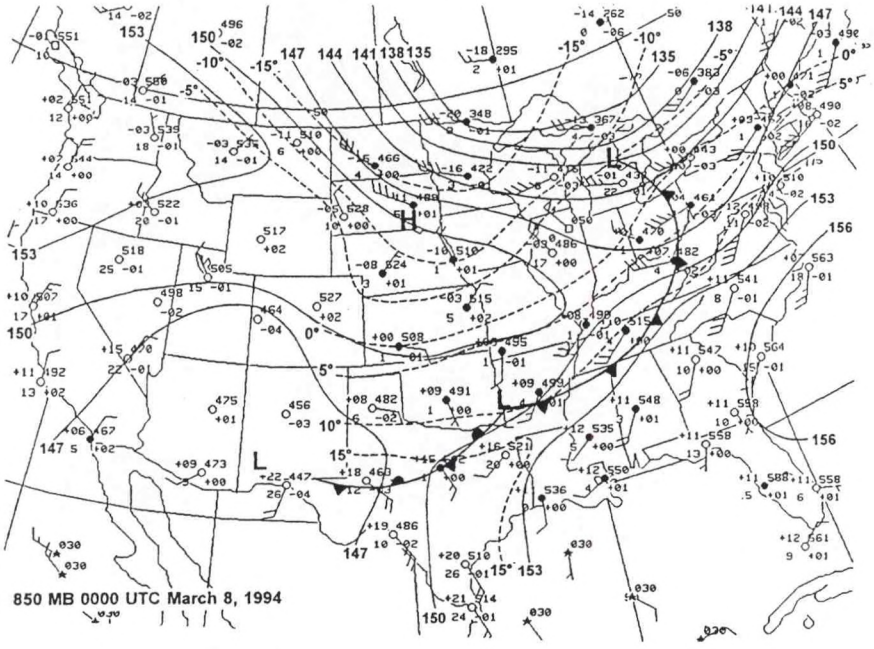

Figure 2. 850 hPa analysis for 0000 UTC 8 March 1994. Solid contours are heights (dam) and temperatures (°C) are dashed. Surface features are superimposed on chart.

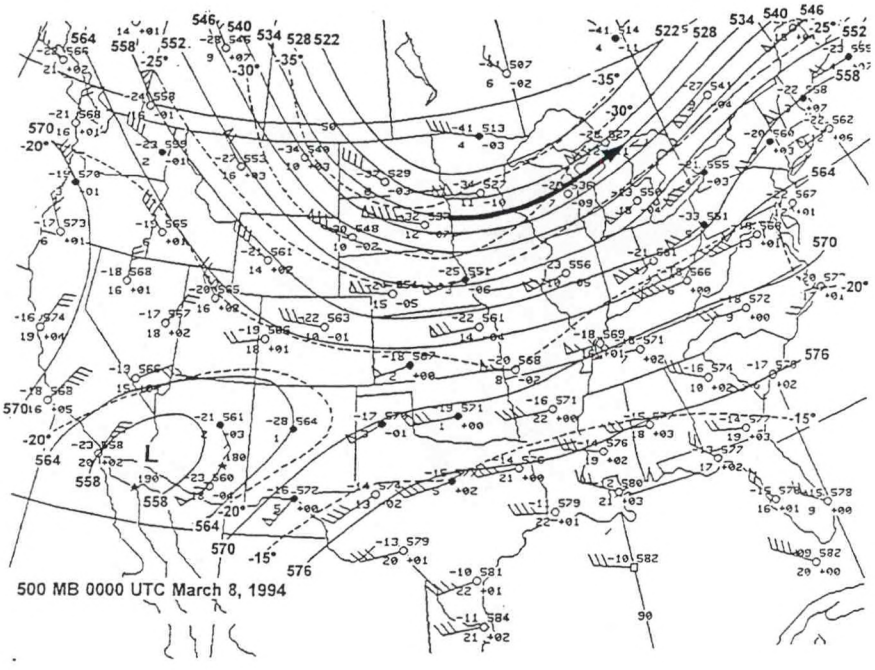

Figure 3. Same as Figure 2 except for 500 hPa. Bold arrows indicate jet axis.

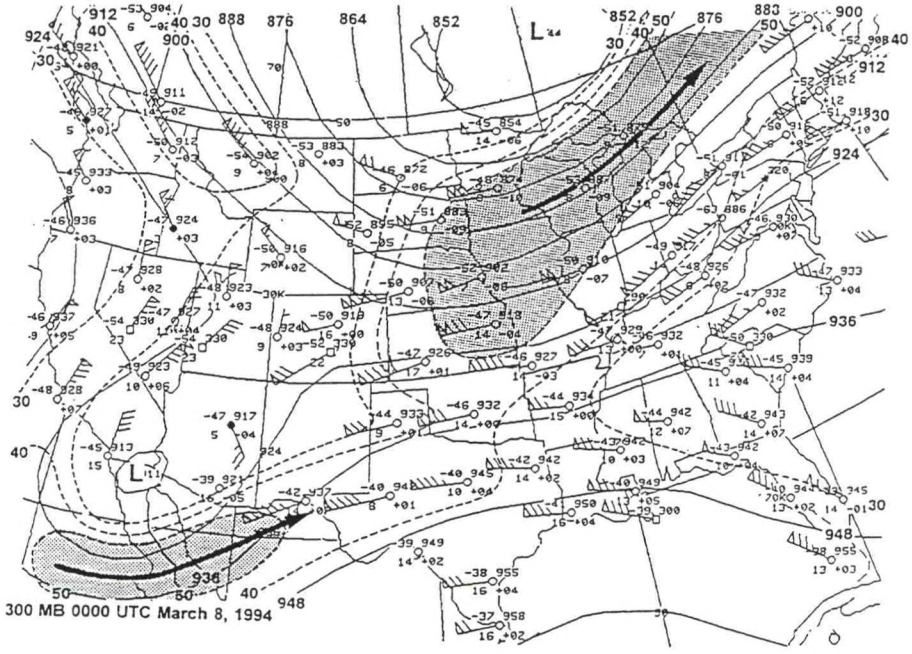

Figure 4. Same as Figure 2 except for 300 hPa. Isotachs (ms^{-1}) are dashed. Magnitude of winds greater than 50 ms^{-1} are stippled. Bold arrows indicate jet axis.

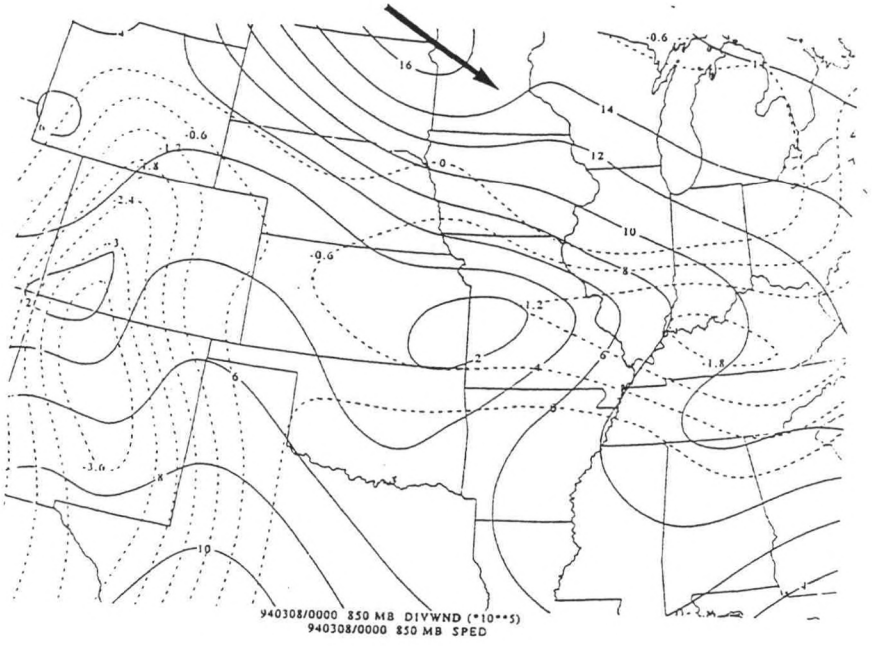

Figure 5. 850 hPa analysis for 0000 UTC 8 March 1994 from GEMPAK. Solid contours are isotachs (ms^{-1}). Areas of convergence (10^{-5} s^{-1}) are dashed (negative) contours.

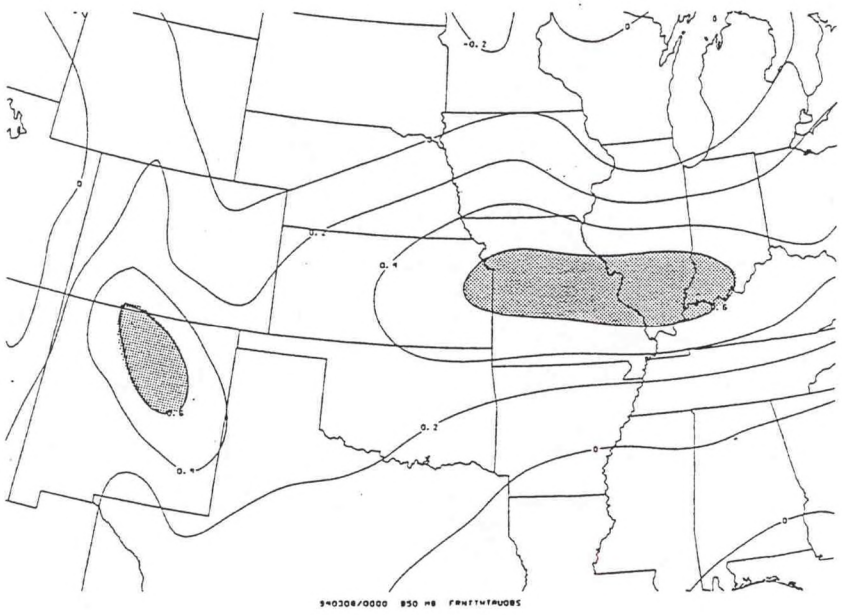

Figure 6. 850 hPa frontogenetical forcing (K 100 km^{-1} $3h^{-1}$) for 0000 UTC 8 March 1994 from GEMPAK. Hatched areas represents region of frontogenesis.

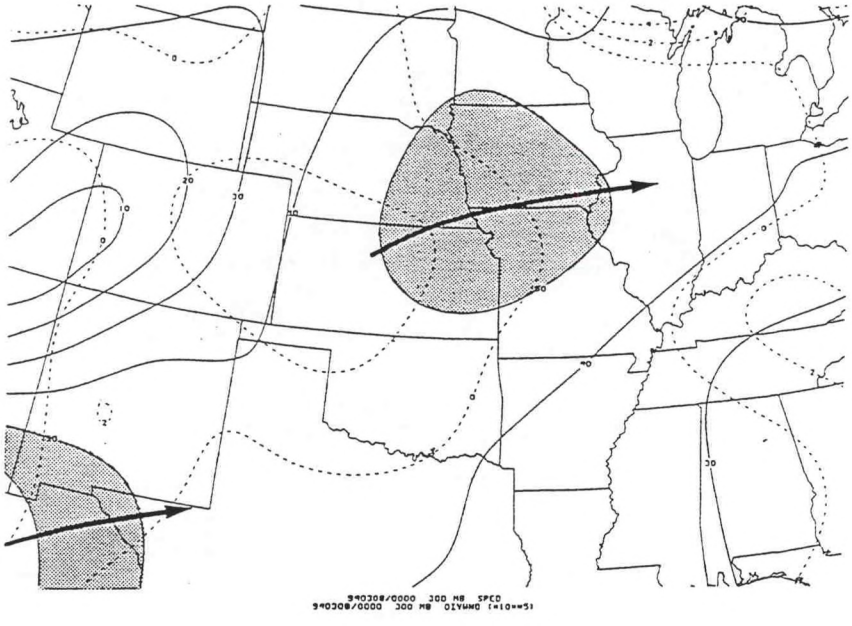

Figure 7. Same as Figure 5 except for 300 hPa. Areas of divergence are dashed contoured. Magnitude of winds greater than 50 ms^{-1} are stippled. Bold arrows indicate jet axis.

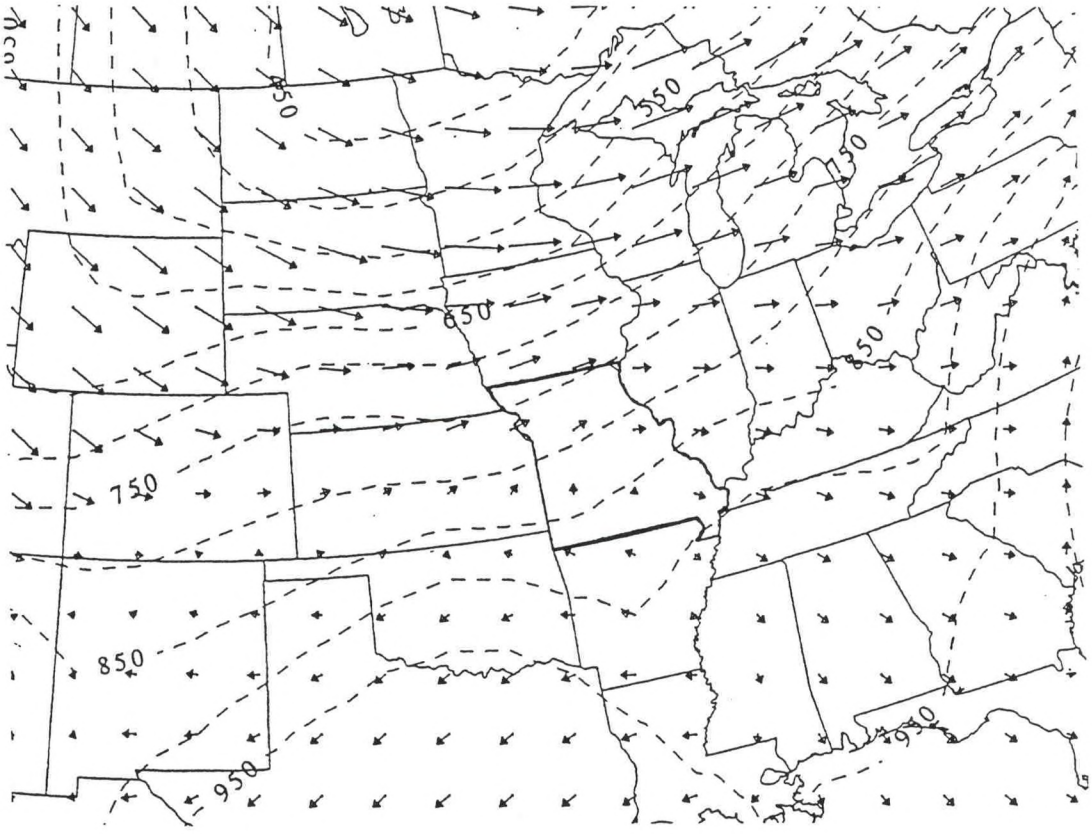

Figure 8. 290 K Isentropic surface for 0000 UTC 8 March 1994 from SLU diagnostic program. Vectors are proportional to the magnitude of the wind. Dashed lines are isobars (in mb).

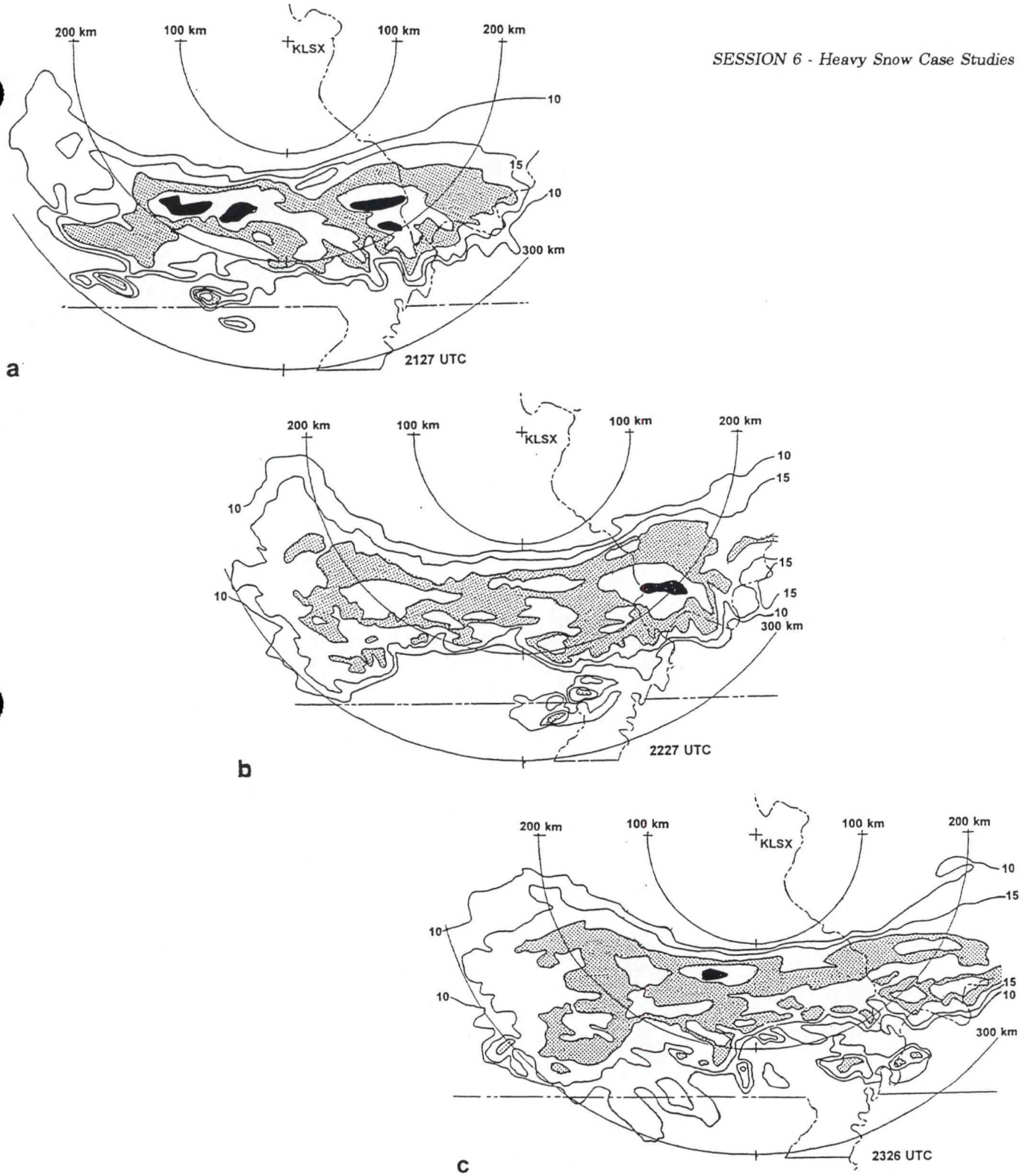

Figure 9. Sequence of WSR-88 reflectivity images at 0.5° elevation angle from WSFO St. Louis (KLSX). Contours are in dBz. Stippled areas represent values of 20 to 24 dBz while dark shaded regions signify reflectivity values greater than 30 dBz. (a) 2127 UTC, (b) 2227 UTC, and (c) 2326 UTC.

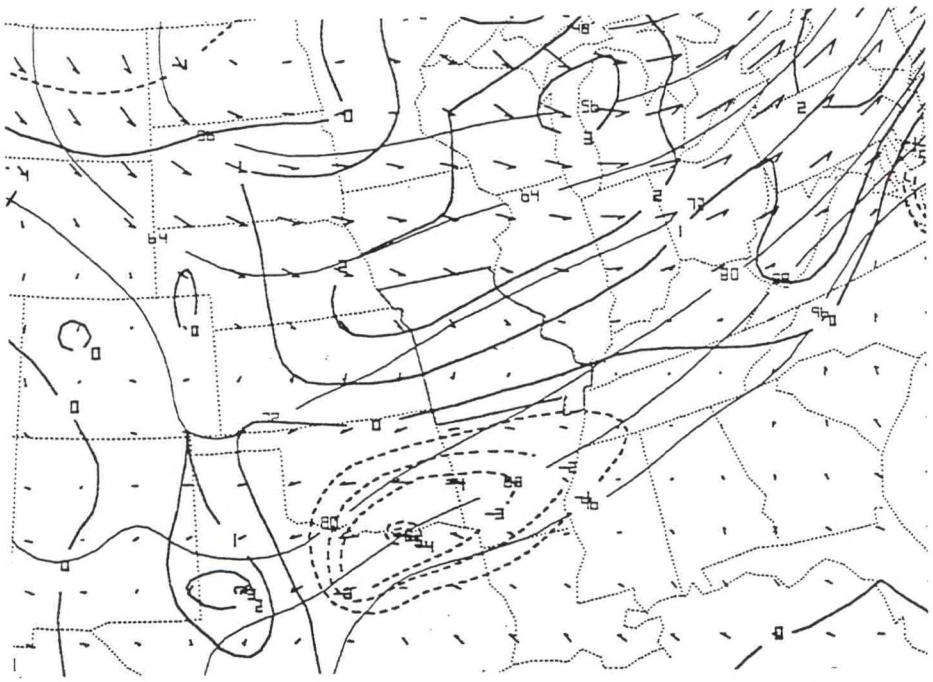

Figure 10a. Eta-X 24 h forecast of 290 K isentropic surface valid 0000 UTC 9 March 1994. Light solid contours are pressure (in mb). Heavy solid (dashed) contours are regions of vertical motion-isentropic down glide (isentropic up glide) (in bs^{-1}). Vectors are proportional to the magnitude of the wind (ms^{-1}).

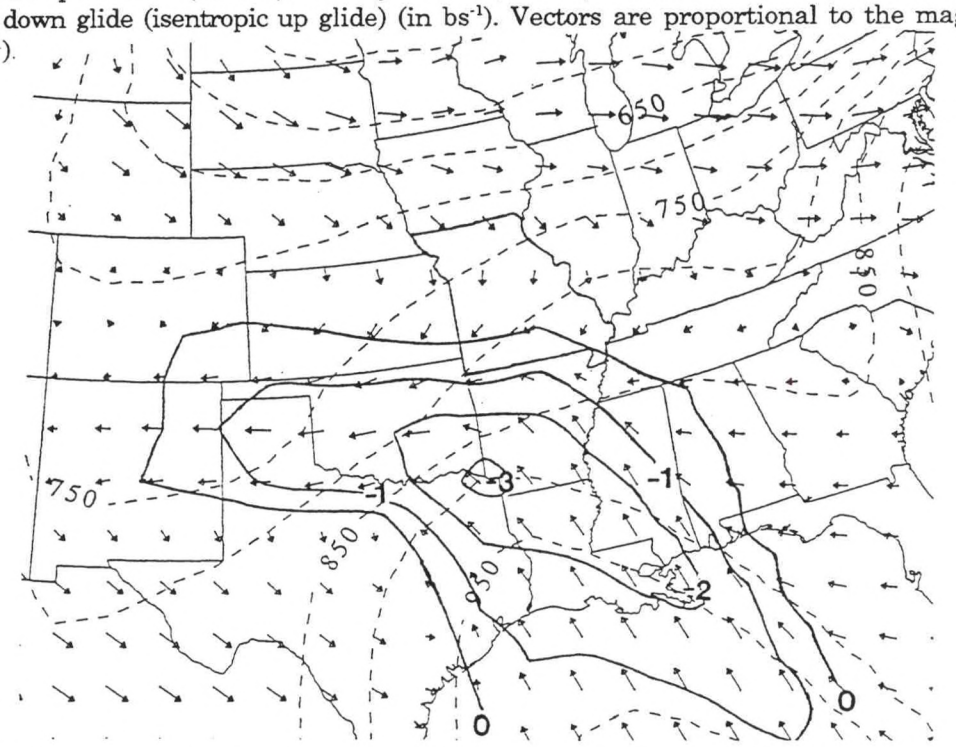

Figure 10b. 290 K isentropic surface for 0000 UTC 9 March 1994 from SLU diagnostic program. Dashed contours are isobars (in mb). Heavy solid contours signify area of vertical motion (isentropic up glide; in bs^{-1}).

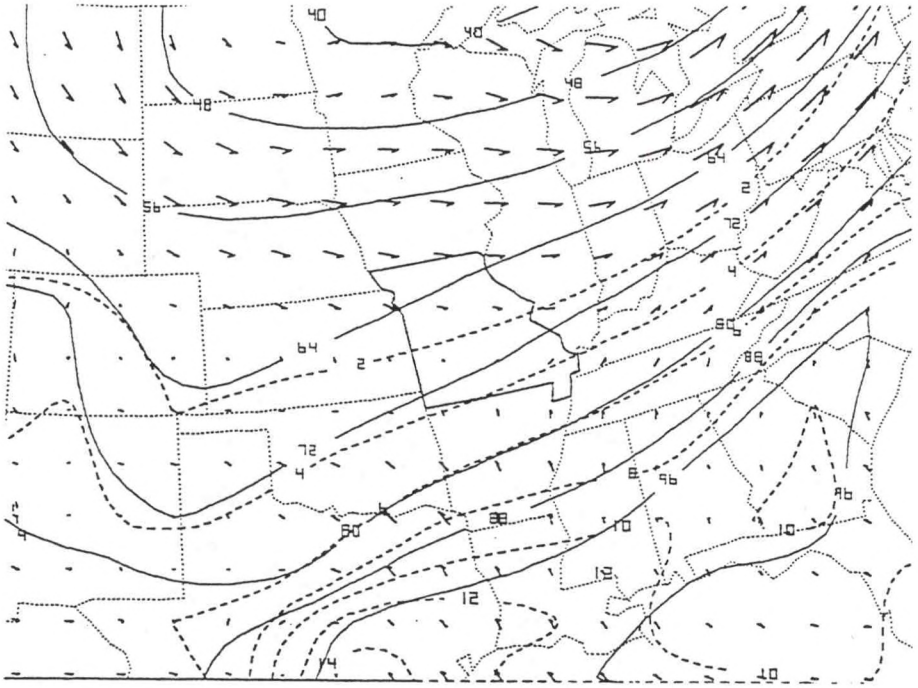

Figure 10c. Eta-X 24 h forecast of 295 K isentropic surface valid 0000 UTC 9 March 1994. Light solid contours are pressure (in mb). Dashed contours are mixing ratio (gm kg-1).

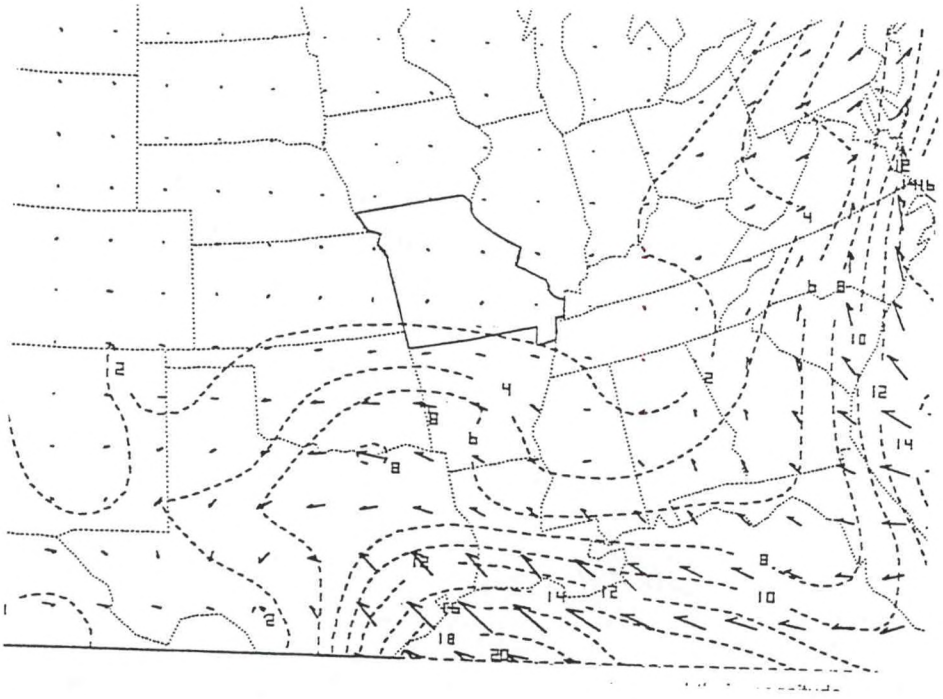

Figure 11a. Eta-X 24 h forecast of moisture transport vectors and their magnitude (dashed contours $x10^{-1}$ gm-m kg^{-1}-s^{-1}) on the 290 K isentropic surface valid for 0000 UTC 9 March 1994.

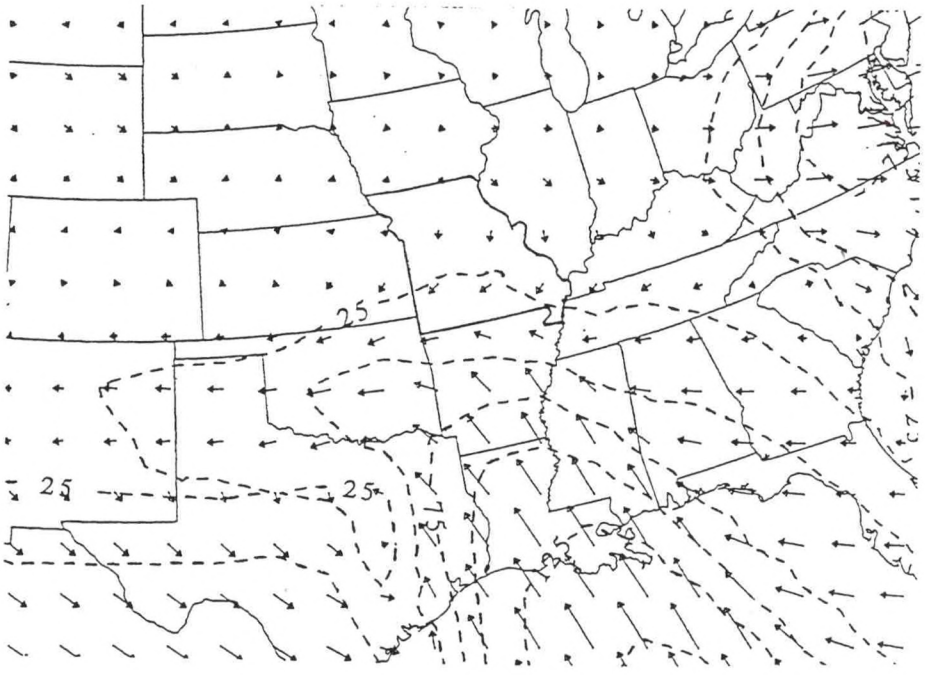

Figure 11b. Same as Figure 11a except for 0000 UTC 9 March 1994 from SLU diagnostic program (units gm-m kg^{-1}-s^{-1}).

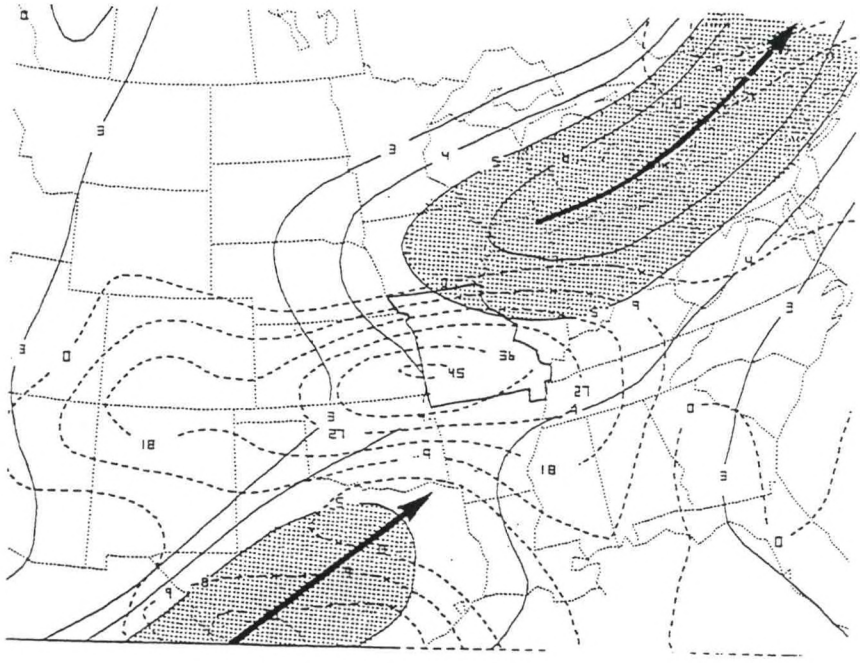

Figure 12a. Eta-X 24 h forecast 300 hPa chart valid time 0000 UTC 9 March 1994. Solid contours are isotachs (ms^{-1}) and dashed contours are magnitude of divergence (10^{-5} s^{-1}). Stippled area represents magnitude of winds greater than 50 ms^{-1}. Bold arrows indicate jet axis.

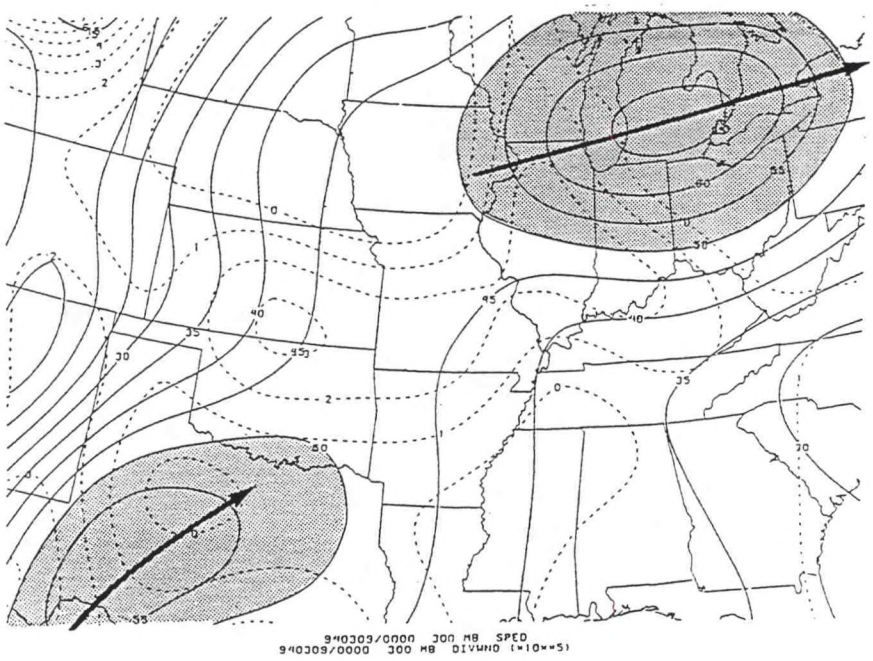

Figure 12b. 300 hPa diagnostic chart for 0000 UTC 9 March 1994 from GEMPAK. Solid contours are isotachs (ms^{-1}). Dashed contours are magnitude of divergence (10^{-5} s^{-1}). Stippled area represents magnitude of winds greater than 50 ms^{-1}. Bold arrows indicate jet axis.

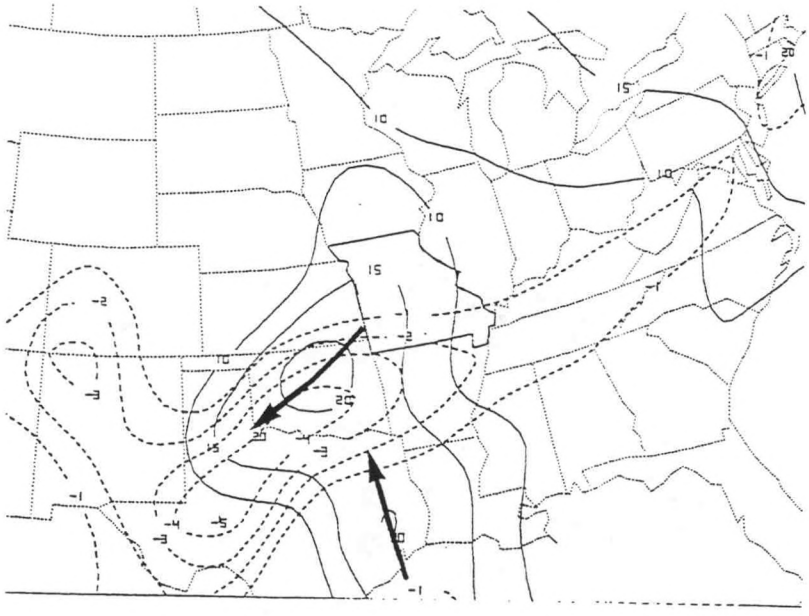

Figure 13a. Same as Figure 12a except for 850 hPa. Dashed contours are magnitudes of convergence (10^{-5} s^{-1}). Bold arrows indicate jet axis.

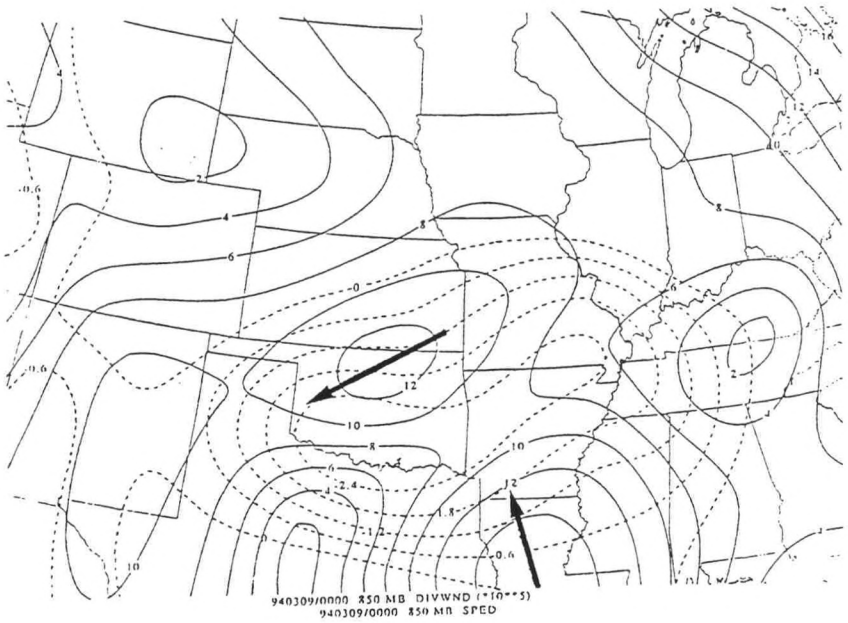

Figure 13b. Same as Figure 12b except for 850 hPa. Dashed contours are magnitudes of convergence (10^{-5} s^{-1}). Bold arrows indicate jet axis.

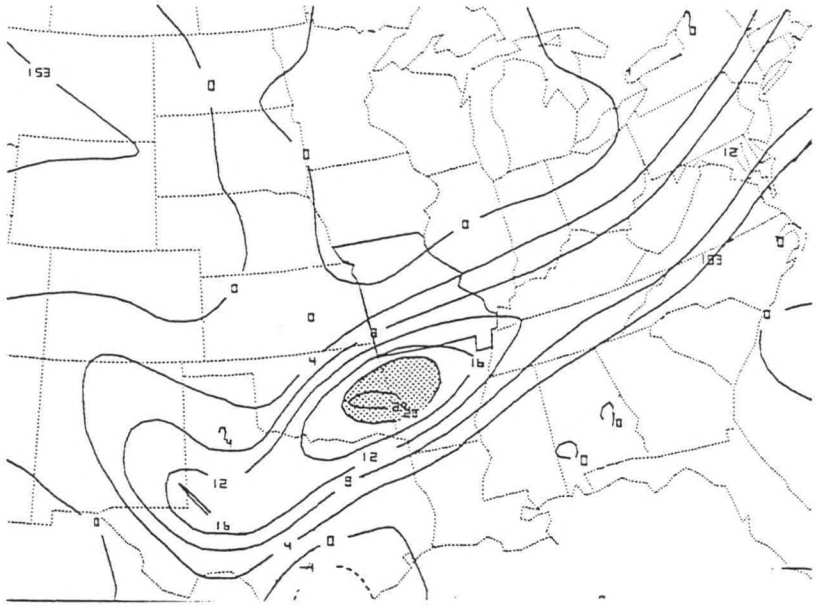

Figure 14a. Eta-X 24 h forecast 850 hPa frontogenetical forcing (x 10^{-10} K m-1 s^{-1}) valid for 0000 UTC 9 March 1994. Stippled area represents values greater than 20 x 10^{-10} K m^{-1} s^{-1}).

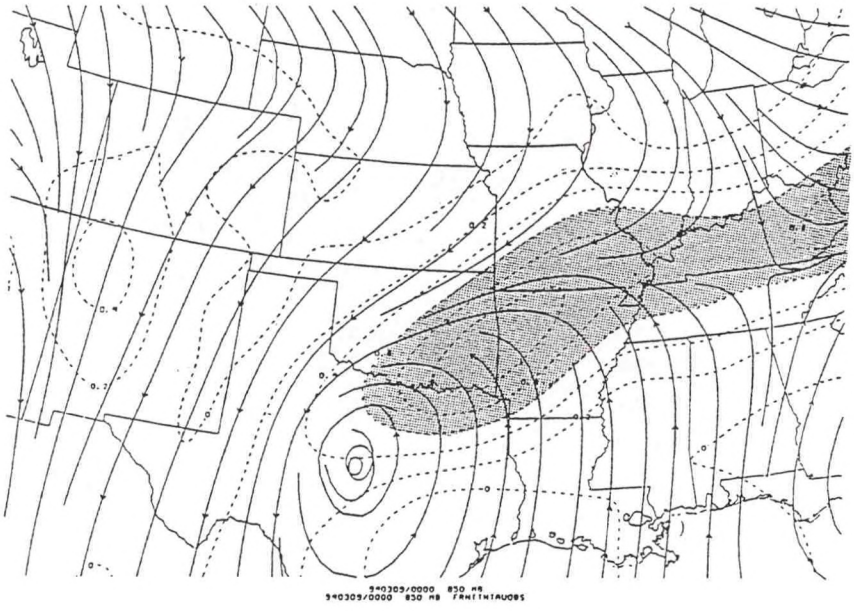

Figure 14b. 850 hPa frontogenetical forcing (K 100 km^{-1} $3h^{-1}$) for 0000 UTC 9 March 1994 from GEMPAK. Stippled area represents values greater than 0.6 K 100 km^{-1} $3h^{-1}$.

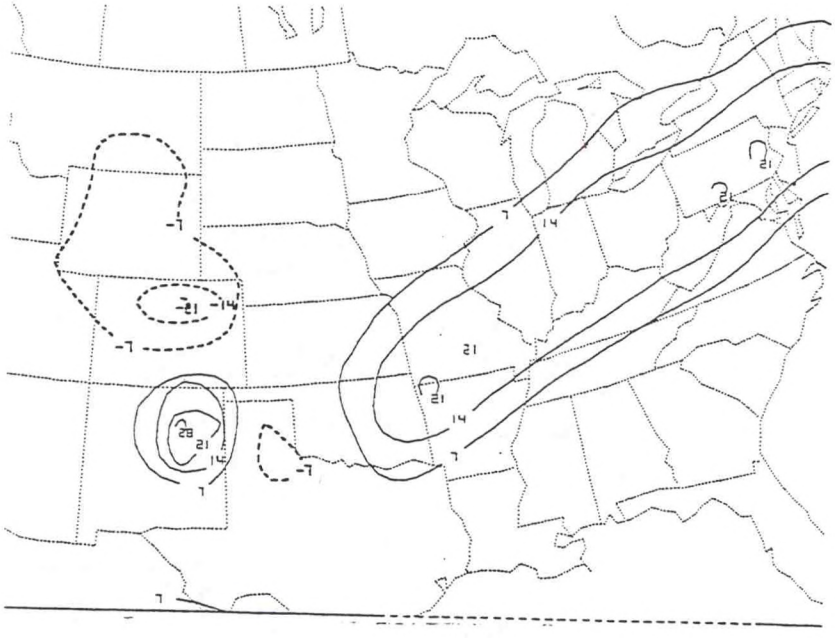

Figure 15a. Eta-X 24 h forecast layer-mean (850-700 hPa) frontogenesis function valid for 0000 UTC 9 March 1994. Dashed (solid) contours represents regions of frontolysis (frontogenesis). Units are 10^{-14} m Pa^{-1} m^{-1} s^{-1}.

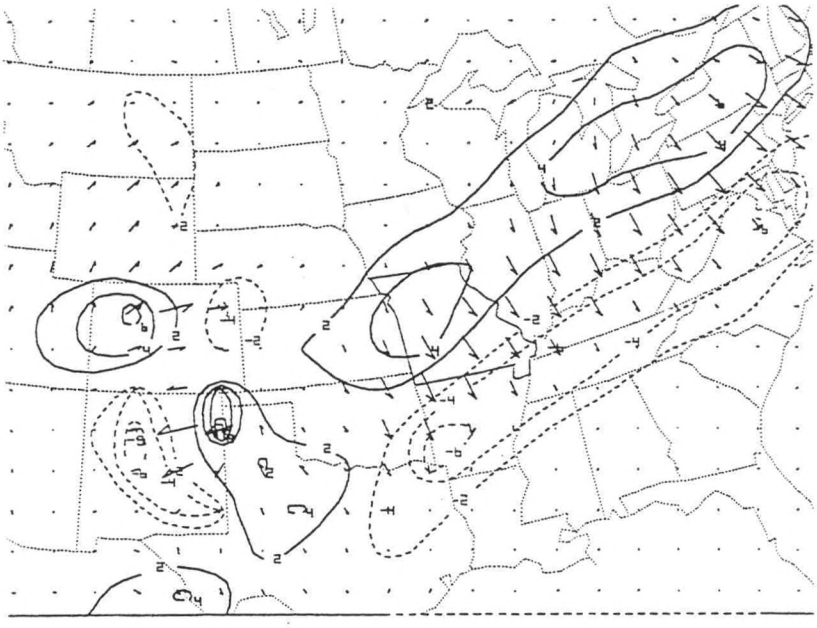

Figure 15b. Eta-X 24 h forecast layer mean (850-700 hPa) Qn Vectors and divergence of Qn valid for 0000 UTC 9 March 1994. Dashed (solid) contours represents region of rising (sinking) motions. Units are 10-19 m Pa^{-1} m^{-1} s^{-1}.

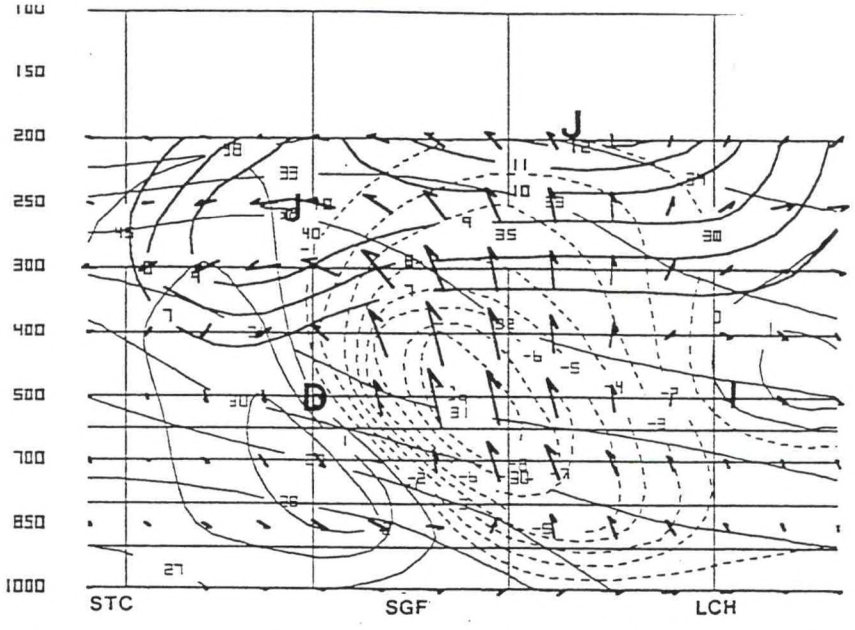

Figure 16a. Eta-X 24 h forecast cross-section from 46°N, 94°W to 27°N, 93°W of secondary circulations valid for 0000 UTC 9 March 1994. Vector representation of ageostrophic motions with isentropes every 10 K. Dashed (light solid) contours are rising (sinking) vertical motions (bs^{-1}). Heavy solid contours are isotachs (kts) greater than 70 kts. The center of the direct (indirect) circulation is indicated by D(I) and the jet core by J.

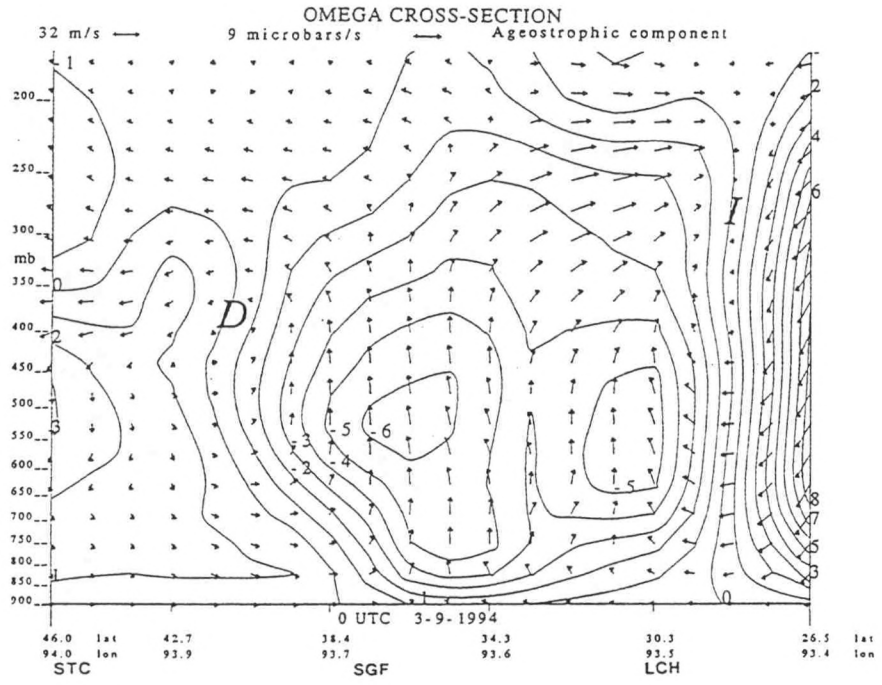

Figure 16b. Vertical cross-section from 46°N, 94°W to 27°N, 93°W of secondary circulation for 0000 UTC 9 March 1994 from SLU diagnostic program. Horizontal component of each arrow is proportional to the tangential ageostrophic wind component and vertical component is proportional to the vertical motion. Solid contours represent the magnitude of vertical motion (bs^{-1}). The center of the direct (indirect) circulation is indicated by D(I).

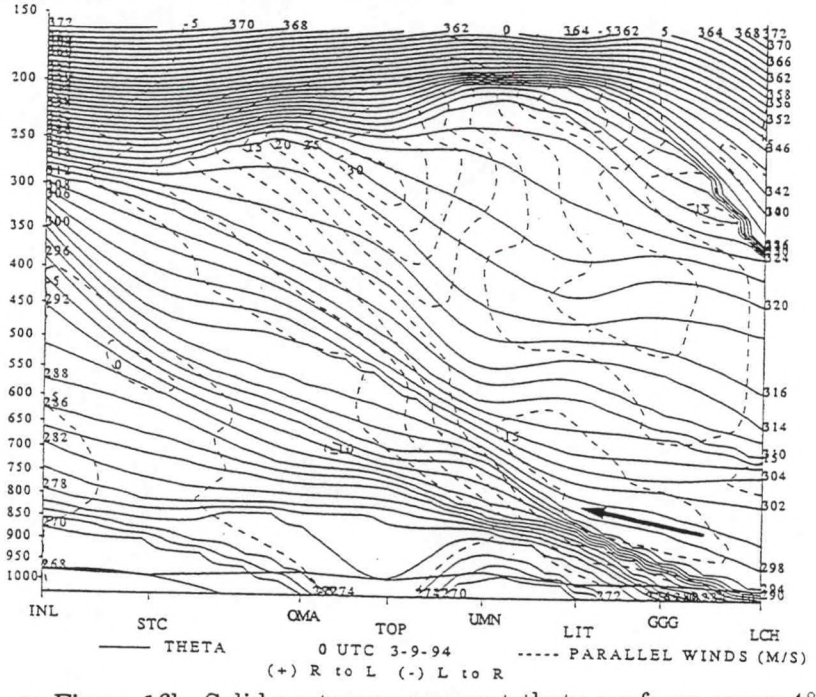

Figure 16c. Same as Figure 16b. Solid contours represent theta surfaces every 4° K and dashed contours represent the component of the wind parallel to the plane of the cross-section (ms^{-1}).

Vertical Motion Forcing Mechanisms Responsible for the Production of a Mesoscale Very Heavy Snow Band Across Northern Kentucky

Theodore W. Funk[1] and James T. Moore[2]

1. INTRODUCTION

Heavy precipitation within winter extratropical storm systems often exhibits mesoscale organization, evolution, and banding. Therefore, accurate prediction of the location, duration, and precipitation amounts associated with mesoscale banded structure is difficult. Numerical model data often indicate the potential for heavy precipitation, but usually lack the resolution to accurately forecast mesoscale banded structure. Several studies (e.g., Shields et al. 1991; Moore and Kaster 1993) have addressed the relationship of various forcing mechanisms to the development and evolution of mesoscale bands of heavy snow. These mechanisms include:

1. isentropic list
2. Conditional Symmetric Instability (CSI)
3. elevated upright convection
4. gravity wave propagation
5. jet streak interaction
6. frontogenesis
7. melting-induced circulation

Except for gravity waves, the above mechanisms are investigated in this study to determine their role and interaction in producing a zone of record-breaking snowfall across the northern half of Kentucky on January 16-17, 1994.

Precipitation began as freezing rain across northern Kentucky during the evening of the January 16, changed to heavy snow near midnight (in Louisville), then continued through the morning of the January 17. In less than 12-h, snowfall amounts of 1-2 feet occurred within a mesoscale east-west band across northern Kentucky (Figure 1). Louisville officially received 15.9 inches (a record), with isolated amounts up to 23 inches east of the city. Hourly snowfall rates within the band ranged from 1-3 inches during much of the storm, enhanced at times by embedded thunderstorms.

The case is somewhat unusual in that a deep low pressure center at the surface and aloft was not present. Instead, southerly surface flow existed on the backside of an arctic high pressure center, with a broad moist southwest flow from 850 to 300 mb ahead of an upstream "open" trough axis (not shown).

2. ISENTROPIC LIFT

Synoptic-scale upward vertical motion of moist air produced precipitation across the entire Ohio and Tennessee River Valleys. Much of this lift was accomplished through strong warm air advection and isentropic lift. The observed 296 K isentropic surface at 0000 UTC 17 January (Figure 2) indicated a tight gradient of pressure and mixing ratio across western Tennessee and Kentucky with strong cross-isobaric and cross-isohume flow from higher-to-lower values of pressure and mixing ratio. Thus, pronounced adiabatic upward motion and moisture advection were present in Kentucky along the warm conveyer belt. Gridded data from the NGM revealed that significant lift and moisture advection

1. Corresponding author address: Theodore W. Funk, NOAA/NWS Forecast Office Louisville, 6201 Theiler Lane, Louisville, Kentucky 40229.
2. James T. Moore, Earth and Atmospheric Sciences, Saint Louis University, St. Louis, Missouri 63103.

continued across central Kentucky between 0000 and 1200 UTC on several low-level isentropic surfaces. Latent heat release likely resulted in a diabatic contribution to vertical motion with respect to the isentropic surfaces (Moore 1993). Garcia (1994) has determined empirically those average isentropic mixing ratios of 4-5 g kg^{-1}, located across western Kentucky on the 292 K surface at 0000 UTC (not shown), are capable of generating 12-h snowfall amounts of 8-10 inches. While strong isentropic lift and moisture advection caused significant precipitation across the Ohio Valley, other mechanisms apparently concentrated very heavy snowfall amounts within a narrow mesoscale zone across northern Kentucky (Figure 1).

3. JET STREAK INTERACTION

Several studies have documented the importance of jet streak interaction to the production of enhanced vertical motion and heavy snowfall. The lift occurs in the ascending branch of the thermally direct transverse circulation within the entrance region, and the thermally indirect circulation within the exit region of a jet streak. Uccellini and Kocin (1987) have shown that upward motion is enhanced by the merger (coupling) of the ascending branches of two separate jet streaks, which often accompany heavy snowfall along the East Coast. Hakim and Uccellini (1992) documented jet streak coupling for a snow band across the northern Plains, while Shea and Przybylinski (1993) did likewise for a snowstorm in Missouri.

In this case, the 6-h NGM forecast valid 0600 UTC 17 January revealed a well-defined 300 mb jet streak across the Great Lakes and another across Texas and Arkansas (Figure 3). The entrance region of the northern jet and the exit region of the southern jet appeared coupled over the Lower Ohio Valley, with both exhibiting substantial along-stream variation in the wind field. As a result, the coupled ageostrophic wind response to the geostrophic deformation was significant, as evidence by divergent ageostrophic wind vectors (Figure 3) and NGM 300 mb divergence fields (not shown). The exit region of the southern upper-level jet also may have intensified the southerly low-level jet (e.g., 70 kts at 0000 UTC at Little Rock at 850 mb), resulting in enhanced low-level convergence and ascent across Kentucky.

A spatial-height cross-section, derived from the 6-h NGM forecast and defined by the line in Figure 3, depicts the transverse circulation of tangential ageostrophic winds valid at 0600 UTC (Figure 4). The direct (D) and indirect (I) thermal circulations, as well as a pronounced deep-tropospheric upward motion area clearly defined between the two jet streaks across western Kentucky. The location and timing of this enhanced ascent are coincident with an increase in precipitation intensity across western and northern Kentucky.

4. CONDITIONAL SYMMETRIC INSTABILITY (CSI)

CSI (also called "slantwise convection") has been studied by numerous researchers (e.g., Emanuel 1983; Bennetts and Hoskins 1979). CSI is an instability that results in slanted mesoscale circulations of saturated air parcels. CSI results from the combined effect of vertical (gravitational) and horizontal (inertial) forces. When CSI exists, the atmosphere often is weakly *stable* to both vertical (upright convection) and horizontal (inertial instability) displacements, but *unstable* to slanted movement. In other words, a parcel displaced vertically or horizontally eventually would come back to its original position; however, a parcel displaced slantwise would result in a titled upward acceleration. (Inertial instability and, therefore, CSI is possible near a significant anticyclonically-curved jet entrance region).

Several atmospheric conditions must be met to produce CSI, including 1) near saturated atmosphere, 2) near neutral stability (but slightly stable or else upright convection could develop), 3) strong vertical speed shear (baroclinic environment), and 4) large scale forcing for upward motion to produce parcel displacements. The Paducah 0000 UTC 17 January sounding (Figure 5), isentropic ascent (e.g., Figure 2),

and NGM forecast relative humidity and wind fields (not shown) indicated that these four conditions were met in this case.

An assessment of CSI can be made by evaluating spatial-height cross-sections of absolute momentum (M) (Emanuel 1988) and equivalent potential temperature (θ_e) surfaces. CSI is present in saturated areas where the slope of the θ_e surfaces is steeper than that of the M surfaces (i.e., near neutral stability and significant vertical speed shear exist). In the January 17 case, CSI criteria were met in the stippled area from northern and western Kentucky to eastern Louisiana at 0600 UTC (Figure 6). Note, however, that within the northern (left) portion of the shaded CSI region, θ_e and M lines actually are nearly parallel. However, given limited model resolution in PCGRIDDS, these model-depicted areas likely represent potential CSI zones as well.

CSI often results in the development of multiple bands of heavier precipitation within a general area of lighter precipitation. The heavier precipitation bands are caused by the enhanced slanted upward motion, whereby areas of lighter precipitation between bands may be due to a downward component in the mesoscale CSI circulation that partly counteracts the larger scale lift. CSI bands normally are about 100-300 miles in length and oriented parallel to the thermal wind (i.e., thickness field). Cross-sections to evaluate CSI should be made normal to 1000-500 (or 850-300) mb thickness lines. Recognition of CSI is meteorologically important because CSI can result in periods of heavy rainfall or snowfall, and higher precipitation amounts than may otherwise be expected.

5. FRONTOGENESIS

Frontogenetical forcing has been associated with mesoscale bands of enhanced precipitation within larger synoptic-scale storm systems (e.g., Locatelli et al. 1995; Shields et al. 1991). Frontogenesis (frontolysis) refers to an intensification (weakening) of a thermal gradient at the surface or aloft. Frontogenesis act to destroy thermal wind balance, so an atmospheric adjustment must take place to restore the balance. The adjustment is achieved through patterns of rising and sinking motion (vertical circulation) associated with the ageostrophic wind. The upward component of the frontogenetical circulation in low levels often is located near the warm side of the intensifying thermal gradient, i.e., displaced slightly away from the zone of maximum low-level frontogenesis. The ascent produces adiabatic cooling of air parcels. Meanwhile, parcels sink and warm adiabatically near the cool side of the thermal ribbon. Typically, frontogenetical zones are sloped with height toward cold air within baroclinic winter systems. Therefore, the responsive circulation may include sloped vertical motion, with ascent aloft often superimposed with the low-level maximum frontogenesis region. The horizontal ageostrophic components of this circulation consist of an acceleration of air parcels from cold to warm air in low levels and from warm to cold air at upper levels. This circulation is "thermally direct," and acts to relax the temperature gradient that frontogenesis attempts to strengthen. The opposite effect occurs for frontolysis.

In the January 17 snowstorm, frontogenesis played a role in forcing mesoscale vertical motion, but to what exact extent is still under investigation. For example, frontogenesis were evident across the Lower Ohio Valley to Arkansas at 850 mb at 0000 UTC 17 January (Figure 7), coincident with an area of enhanced precipitation (not shown). Gridded model forecast data (not shown) also indicated a zone of frontogenetical forcing in the 1000-700 mb layer across Kentucky during heavy precipitation between 0600 and 1200 UTC. In addition, low-level convergence over Kentucky may have contributed to deformation of the low-level thermal gradient, resulting in a frontogenetical contribution to the overall vertical motion field. However, while a strong thermal gradient existed at 850 mb across the Ohio Valley, the exact role of deformation in enhancing frontogenesis and subsequent vertical motion near the heavy snow band over northern Kentucky is still being examined. In addition, maximum frontogenesis values during the 0600-1200 UTC period (not shown) were predicted south of Kentucky

and the main snow band, which contributed to the development of a convective squall line across Tennessee and the Lower Mississippi Valley.

6. ELEVATED UPRIGHT CONVECTION

Upright convection can occur within warm advection/overrunning situations in the winter season. Colman (1990) studied these phenomena in detail. He suggested that these thunderstorms can occur in an environment characterized by very stable surface air, if strong baroclinicity, warm advection, and lift are present above a shallow, but significant inversion. Upstream source air may be even more conducive for thunderstorms and exhibit convective instability ($\partial\theta_e/\partial z<0$). The result is the development of "elevated" upright convection from the top of the inversion.

In the January 17 snowstorm case, embedded thunderstorms occurred periodically for a few hours over north-central Kentucky within the widespread precipitation, which enhanced snowfall rates. The Paducah sounding (Figure 5) showed that very stable surface air existed below a significant temperature inversion. Strong isentropic lift/warm advection also was present, along with convective instability upstream from Kentucky (right portion of stippled area at 0600 UTC in Figure 6). Finally, the Total Totals index at Little Rock at 0000 UTC was 51 indicating the potential for elevated convection. The CSI circulation also may have contributed to thunderstorm development (Bennetts et al. 1988). Thunderstorms dissipated later in the event as the temperature inversion was eroded by cooling aloft.

7. MELTING-INDUCED MESOSCALE CIRCULATIONS

Diabatic processes can have substantial dynamic and thermodynamic effects in the atmosphere. In particular, the melting of snow causes atmospheric cooling as ice crystals aloft fall into a warm layer above 0°C. This cooling then can result in a relatively deep (up to 1 km) isothermal layer at or below 0°C (Szeto et al. 1988). A saturated isothermal layer is important for heavy precipitation production since the layer will contain a larger absolute moisture content than one in which temperature, and thus mixing ratio, decrease with height.

The melting process also creates a mesoscale circulation driven by a melting-induced temperature gradient near a distinct rain-snow boundary (Szeto et al. 1988; Lin and Stewart 1986). This circulation (Figure 8), analogous to an elevated sea breeze, consists of descent on the warm (rain) side of the boundary and ascent on the cool (snow) side, resulting in a localized band of enhanced upward motion and snowfall. The circulation will persist as long as significant melting and the rain-snow boundary persist (Stewart and McPherson 1989). The small-scale circulation, like CSI, is superimposed on the larger scale vertical motion regime.

The melting process likely played an important role in the January 17, 1994 snowstorm, as the Paducah 0000 UTC sounding (Figure 5) indicated an above freezing layer from 900-750 mb while, at the same time, colder air existed north and east of Paducah. This created a distinct rain-snow boundary across northern Kentucky late on January 16 and early January 17, which contributed to a narrow zone of heavy precipitation ($dBZ \geq 35$) oriented east-west on the Louisville-Ft. Knox (KLVX) WSR-88D (not shown). Sleet was occurring within the band, with heavy snow on the band's northern (back) edge, and only light freezing rain immediately south (ahead) of the band.

The enhanced lift and snowfall rates just north of the transition zone and the lighter freezing rain just south of the band are consistent with and appear to be at least partly due to this mesoscale melting-induced circulation. Along with adiabatic cooling from strong ascent, the melting also eventually cooled the warm layer aloft resulting in a subfreezing isothermal layer and a changeover to heavy snow

across most of Kentucky during the morning of January 17. This cooling acted to diminish and terminate the melting-induced circulation later in the snowstorm event.

8. CLOUD MICROPHYSICS

Heavy snow rates are associated with large snowflakes consisting of dendritic crystals (Auer and White 1982). It is suggested that heavy snow can occur in events when the level of maximum vertical motion (i.e., the level of non-divergence) is near the level of maximum growth rate of dendritic crystals. This growth rate level typically occurs at temperatures of -13° to -17°C. A NGM-derived time-height cross-section for Louisville (Figure 9) showed that these two levels were coincident between 0600 and 1200 UTC 17 January (the 6-12-h model forecast), i.e., the period in which very heavy snow and large snowflakes occurred in Louisville.

9. SUMMARY AND CONCLUSION

Several mechanisms combined to produce very strong ascent and record-breaking snowfall across the northern half of Kentucky on January 16-17, 1994. Strong isentropic lift/warm air advection produced significant precipitation over a large area, although other processes apparently concentrated the heaviest snowfall into a mesoscale band over northern Kentucky.

The banding mechanisms in this event likely did not act independently from one another in producing strong ascent and heavy snow, although the exact mechanism interaction is not completely clear. However, *meteorologists must be aware that banding mechanisms exist within winter storm systems, and be able to recognize when these phenomena may act to significantly alter the ultimate accumulation of rainfall and snowfall.* Most of these phenomena can be evaluated qualitatively from observed and gridded model data. However, somewhat limited model resolution often prevents accurate model depiction of mesoscale organization and evolution, despite better prediction of general precipitation areas within winter storms. The WSR-88D can help greatly from a short-term forecast standpoint. It clearly can reveal 1) banded reflectivity structure, even in winter storms, 2) the presence, location, and trend of the bright band/melting layer, and 3) inversions aloft using the VAD Wind Profile (VWP) and radial velocity data. Training and experience is crucial in an effort to understand mesoscale atmospheric structure and the implications on storm evolution and precipitation.

10. ACKNOWLEDGEMENTS

The authors are grateful to the NWS Central Region's Scientific Services Division, particularly Preston Leftwich, for all the hard work put worth in making the Fourth NWS Winter Weather Workshop a great success, and the authors' two workshop sessions possible. The authors also thank Marilyn Scholz, WSFO Louisville; Chance Hayes, WFO Wichita; and Kenneth Kostura, WFO Blacksburg for their work on the original conference paper (*Preprints, 14th Conference on Weather Analysis and Forecasting*) from which this document was derived.

11. REFERENCES

Auer, A.H., Jr., and J.M. White, 1982: The combined role of kinematics, thermodynamics, and cloud physics associated with heavy snowfall episodes. *J. Meteor. Soc. Japan,* **60**, 500-507.

Bennetts, D.A., J.R. Grant, and E. McCallum, 1988: An introductory review of fronts. Part I: Theory and observations. *Meteor. Magazine,* **117**, 357-371.

_____, and B.J. Hoskins, 1979: Conditional symmetric instability-a possible explanation for frontal rainbands. *Quart. J. Roy. Meteor. Soc.,* **105**, 945-962.

Colman, B.R., 1990: Thunderstorms above frontal surfaces in environments without positive CAPE. Part A climatology. *Mon. Wea. Rev.,* **118**, 1103-1121.

Emanuel, K.A., 1988: Observational evidence of slantwise convective adjustment. *Mon. Wea. Rev.,* **116**, 1805-1816.

_____, 1983: On assessing local conditional symmetric instability from atmospheric soundings. *Mon. Wea. Rev.,* **111**, 2016-2033.

Garcia, C. ,Jr., 1994: Forecasting snowfall using mixing ratios on an isentropic surface. NOAA Technical Memorandum NWS CR-105, DOC/NOAA/NWS, Central Region, Scientific Services Division, 31 pp.

Hakim, G.J and L.W. Uccellini, 1992: Diagnosing coupled jet-streak circulations for a northern Plains snow band from the operational Nested Grid Model. *Wea. Forecasting,* 7, 26-48.

Lin, C.A. and R.E. Stewart, 1986: Mesoscale circulations induced by melting snow. *J. Geophys. Res.,* **91**, 13299-13302.

Locatelli, J.D., J.E. Martin, J.A. Castle, and P.V. Hobbs, 1995: Structure and evolution of winter cyclones in the central United States and their effects on the distribution of precipitation; Part III: The development of a squall line associated with weak cold frontogenesis aloft. *Mon. Wea. Rev.,* **123**, 2641-2662.

Moore, J.T., 1993: Isentropic analysis and interpretation: Operational applications to synoptic and mesoscale forecast problems. National Weather Service Training Center Training Manual, Kansas City, MO, 99 pp.

_____, and M.A. Kaster, 1993: Physical processes organizing wintertime frozen precipitation events in the Midwest. *Preprints, 13th Conf. on Weather Analysis and Forecasting,* Vienna, VA, AMS (Boston), 512-515.

Shea, T.J. and R.W. Przybylinski, 1993: Assessing vertical motion fields in a winter storm using PCGRIDDS. *Preprints, 13th Conf. on Weather Analysis and Forecasting,* Vienna, VA, AMS (Boston), 10-14.

Shields, M.T., R.M. Rauber, and M.K. Ramamurthy, 1991: Dynamical forcing and mesoscale organization of precipitation bands in a Midwest winter cyclonic storm. *Mon. Wea. Rev.,* **119**, 936-964.

Stewart, R.E. and S.R. McPherson, 1989: Winter storm structure and melting-induced circulations. *J. Atmos.-Ocean,* **27** *(1)*, 5-23.

Szeto, K.K., R.E. Stewart, and C.A. Lin, 1988: Mesoscale circulations forced by the melting of snow in the atmosphere. Part II: Application to meteorological features. *J. Atmos. Sci.,* **45**, 1642-1650.

Uccellini, L.W. and P.J. Kocin, 1987: The interaction of jet streak circulations during heavy snow events along the east coast of the United States. *Wea. Forecasting,* **2**, 289-308.

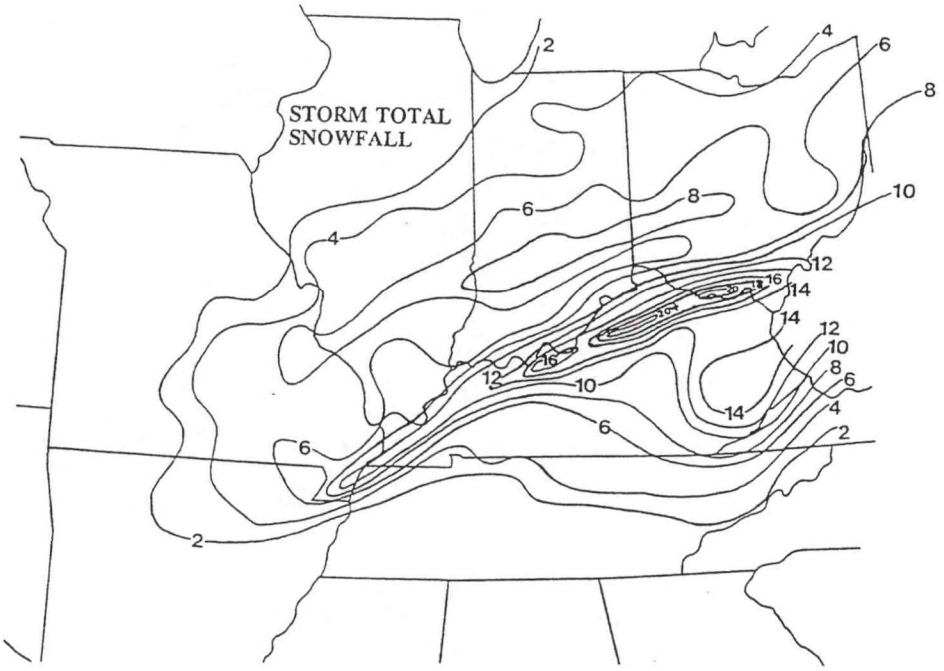

Figure 1. Storm total snowfall for the period 1200 UTC 16 January 1994 to 0000 UTC 18 January 1994. Amounts are reported in inches.

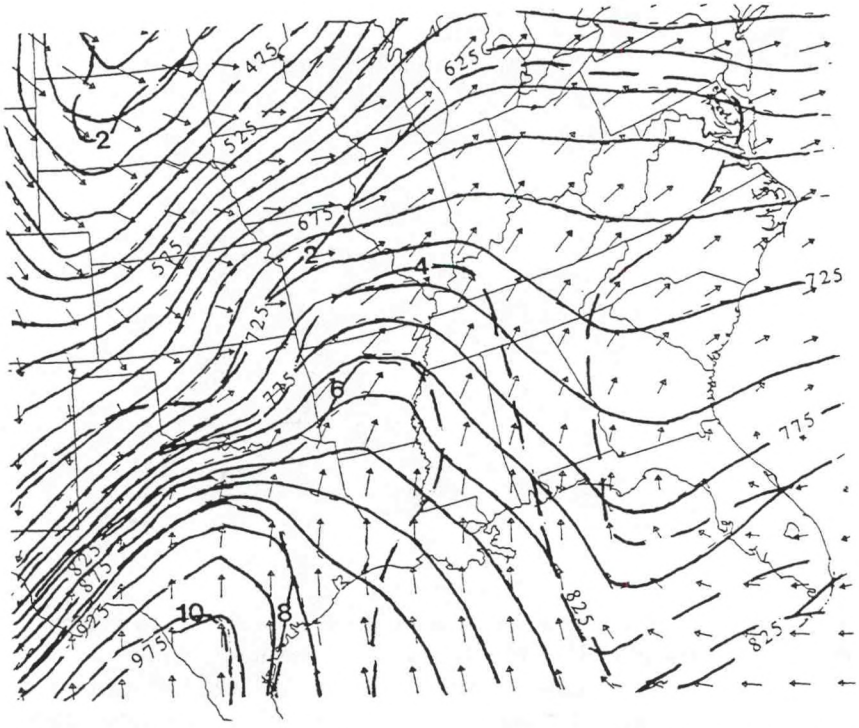

Figure 2. Wind vectors (arrows; m s^{-1}), isobars (solid; mb) and isohumes (dashed; g kg^{-1}) on the 296 K isentropic surface at 0000 UTC 17 January 1994.

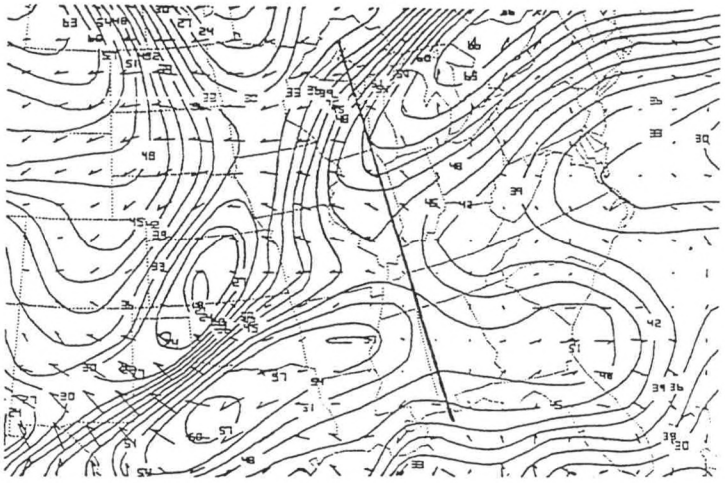

Figure 3. Nested Grid Model (NGM) 6-h forecast valid 0600 17 January 1994 of 300 mb isotachs (solid; m s^{-1}) and aeostrophic wind vectors (arrows; m s^{-1}). Solid line shows path of cross-section used to depict ageostrophic circulation shown in Figure 4.

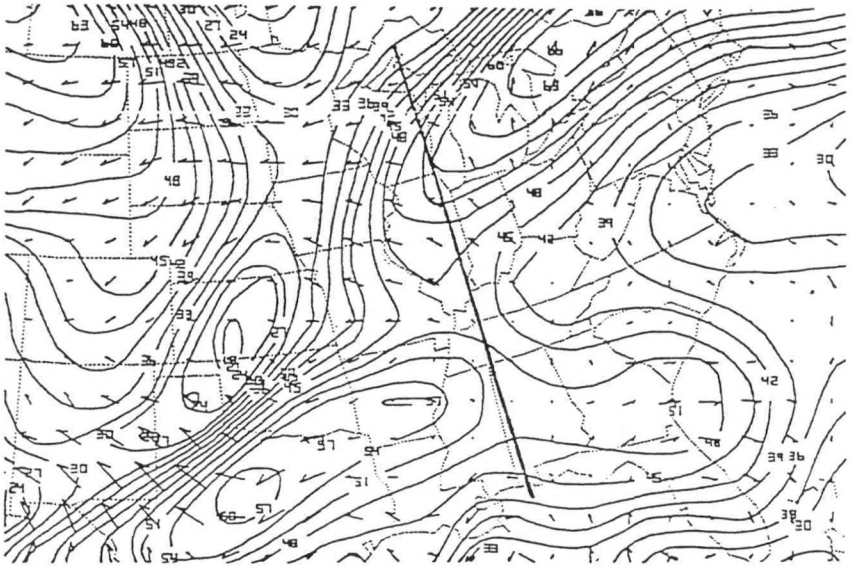

Figure 4. Vertical ageostrophic circulation along cross-section line shown in Figure 3 based on NGM 6-h forecast valid 0600 17 January 1994. Horizontal component of arrows is proportional to the ageostrophic wind component in the plane of the cross-section; vertical component of arrows is proportional to the vertical motion in the plane of the cross-section. Dashed lines are isopleths of upward vertical motion, solid lines are isopleths of downward vertical motion. "D" (I) indicates direct (indirect) thermal circulation.

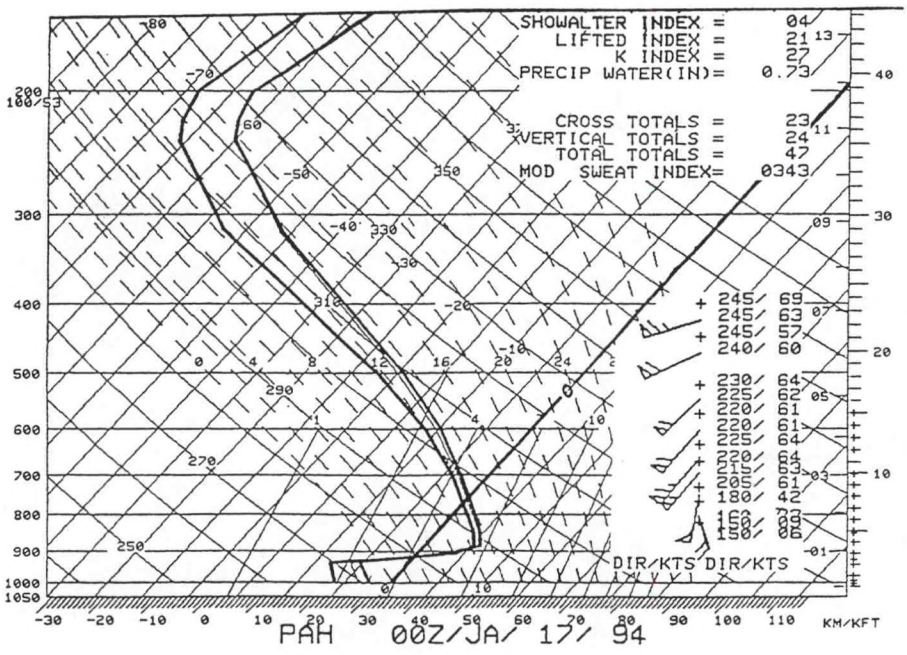

Figure 5. Sounding from Paducah (PAH), Kentucky valid 0000 UTC 17 January 1994.

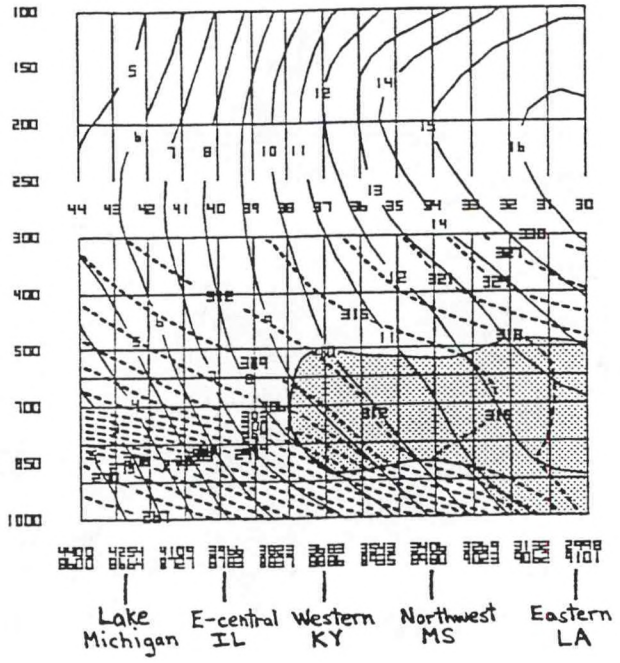

Figure 6. Cross-section of equivalent potential temperature (dashed; K) and absolute geostrophic momentum (solid; m s^{-1}) using NGM 6-h forecast gridded data valid 0600 17 January 1994. Cross-section was constructed from Michigan to Louisiana, normal to the 1000-500 mb thickness field. Stippled region denotes region of conditional symmetric instability.

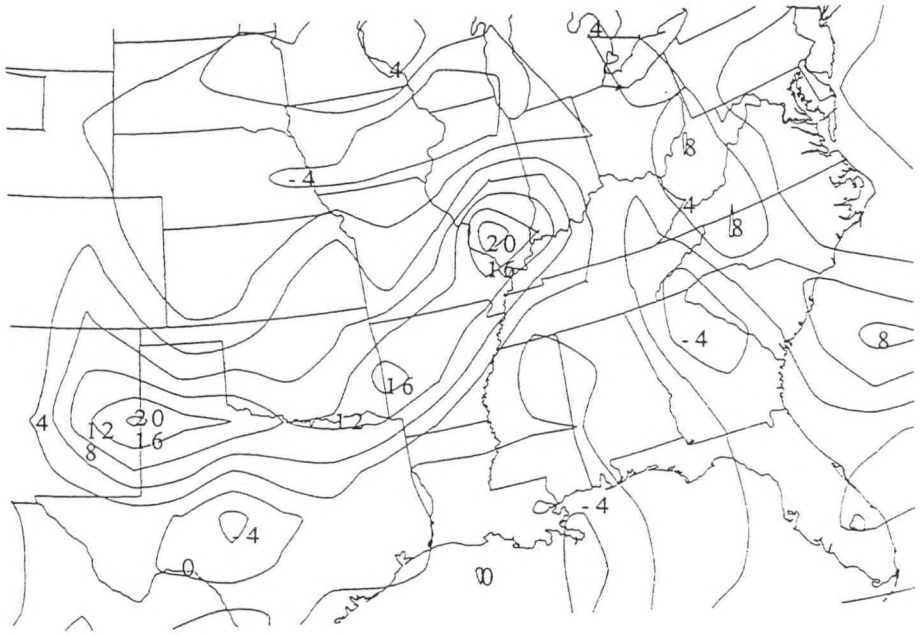

Figure 7. Frontogenesis function at 850 mb computed from observed data at 0000 UTC 17 January 1994. Units are 10^{-10} K m^{-1} s^{-1}.

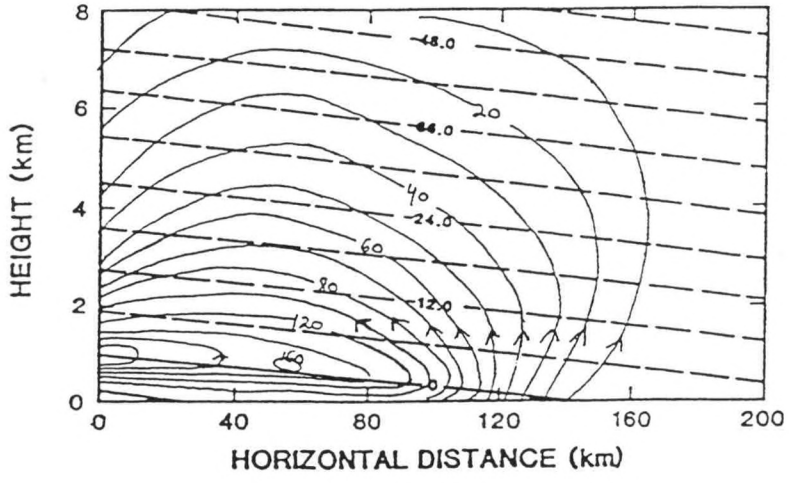

Figure 8. Schematic of indirect thermal circulation due to melting processes near the 0°C isotherm. Dashed lines are isotherms (°C) with colder air to the right, while solid lines are the perturbation stream functions for the rain/snow boundary at 1 hr into the simulation (adapted from Szeto et al. 1988).

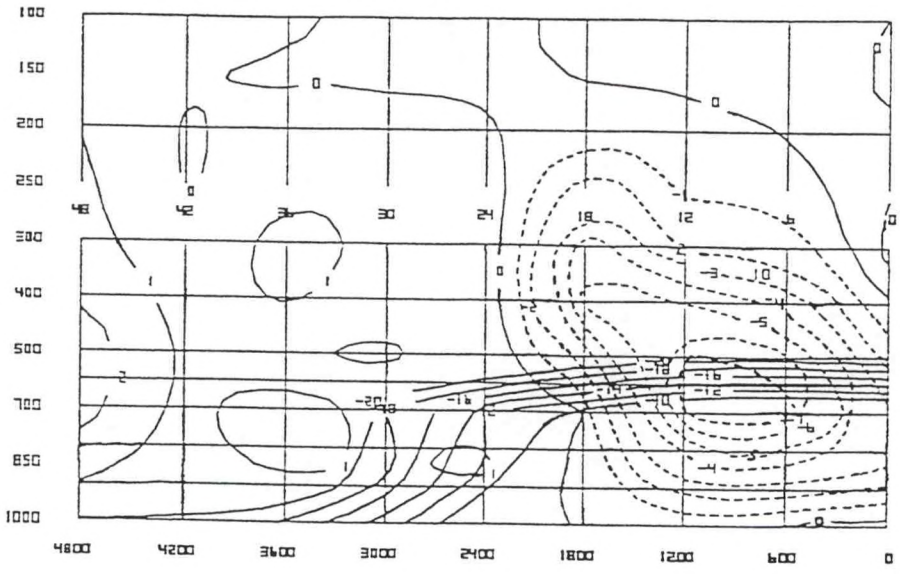

Figure 9. Time-height cross-section for Louisville, Kentucky from the 0000 UTC 17 January 1994 run of the NGM. Isotherms (solid; °C) and vertical motion dashed; μbars s^{-1}) are shown. Forecast hour (time) is along the abscissa and increases towards the left.

The Use of PCGRIDDS and New Forecast Techniques to Diagnose a Heavy Snow Event over Northeastern North Carolina - 8 February 1995

Hugh D. Cobb[1] and Wayne F. Albright[2]

1. INTRODUCTION

During the early morning of February 8, 1995, a 30 to 50-mile a wide swath of heavy snow fell across northeast North Carolina and extreme southeast Virginia. Snow accumulations, greater than 1 inch, occurred in this portion of the Nexrad Weather Service Office Wakefield, Virginia (NWSO AKQ) county warning area. The snowfall distribution for this event is shown in Figure 1. A few of the heaviest snow accumulations in northeast North Carolina included Elizabeth City receiving 4 inches, Hertford 6 inches and Point Harbor 7 inches. Even an isolated occurrence of 3 inches was found across the southern portion of Virginia Beach while only a trace of snow fell across the rest of the Hampton Roads.

In this paper, only a brief description of the synoptic conditions that caused the heavy snow to develop will be provided with most of the emphasis given to mesoscale analysis of numerical guidance utilizing the PC-GRidded Interactive Diagnostic and Display System software (PC-GRIDDS). The analysis using PC-GRIDDS will include determining atmospheric vertical motions and moisture content through the use of model time-sections. The diagnosis of ageostrophic jet streak circulations will also be included to illustrate the potential for heavy snow for northeast North Carolina and southeast Virginia on 8 February. In addition, the potential for conditional symmetric instability and corresponding banded mesoscale precipitation will be examined. As an aid with initial snowfall estimates, an empirical technique developed at the Nexrad Weather Service Forecast Office in Milwaukee, Wisconsin (NWSFO MKX) will be used (Garcia 1994). This technique relates snowfall to average mixing ratio values on an isentropic surface that intersects the 750-700 mb layer.

2. SYNOPTIC ENVIRONMENT

At 1200 UTC 7 February 1995, the 500 mb synoptic analysis indicated a broad longwave trough over the eastern United States with several weak shortwaves moving through the trough axis across the Tennessee Valley (Figure 2). Each shortwave was forecast to move quickly northeastward across North Carolina. The 1500 UTC surface analysis (Figure 3) indicated a weak area of low pressure over northern Alabama producing an area of light to moderate snow over the Tennessee and Ohio river valleys. This surface low moved steadily northeast, and reached southwestern North Carolina near Charlotte by 0000 UTC 8 February. At the same time, a strong jet streak at 300 mb became evident at 0000 UTC (not shown) moving through the base of the trough across Mississippi and Alabama. Based on the 18-hour forecast from the 1200 UTC NGM (valid 0600 UTC), this jet streak was to move over the South Carolina coast, placing North Carolina and southeast Virginia in the left exit region which favors divergence (Kocin and Uccellini 1990). The lower levels of the atmosphere that constitute 850 mb and below were conducive for snow. The 850 mb temperatures were forecast to be between -5 and -8°C from 0000 to 1200 UTC 8 February with 1000-850 mb thicknesses averaging 1280 to 1300 m.

1. Corresponding author address: Hugh D. Cobb, Nexrad Weather Service Office, Wakefield, VA.
2. Wayne F. Albright, Nexrad Weather Service Office, Wakefield, VA.

3. MODEL TIME-SECTIONS

An early indication of the potential for a heavy precipitation event was revealed through the use of PCGRIDDS time sections. These time-sections, which are centered on a specified location, are very useful in showing the vertical structure of the atmosphere given a particular data set. The time-sections used for this event are from the 1200 UTC 7 February run of the NGM. Figure 4 shows a time-section (in 6 hour forecast increments) for Cape Hatteras, North Carolina while Figure 5 shows a time section for Elizabeth City, North Carolina. Note the forecast of a rapid increase in vertical velocities for each location at 18-h into the model run (valid 0600 UTC 8 February). At Cape Hatteras, the vertical velocity increased to approximately -14 ubs^{-1} with an increase to about -9 ubs^{-1} found at Elizabeth City. In both instances, a substantial increase in relative humidity in the lower and middle levels of the troposphere corresponded with the onset of the strong upward velocities. A further investigation of the dynamic forces behind the strong vertical motion was needed.

4. ROLE OF AGEOSTROPHIC CIRCULATIONS AND Q-VECTOR DIAGNOSTICS

Ageostrophic circulations in the exit and entrance regions of jet streaks have played a major role in many east coast snowstorms (Kocin and Uccellini 1990). This was the case in this particular snow event except the ageostrophic circulations were in association with a singular jet streak of the polar jet.

Figure 6 shows the 18-h forecast of 300 mb winds and isotachs from the 1200 UTC 7 February cycle of the NGM. Note the forecast of two speed maxima, over Georgia and South Carolina and the western Atlantic ocean. As can be seen in Figure 6, eastern North Carolina was forecast to be under the left front quadrant (or exit region) of a jet speed max where thermally indirect circulations commonly develop (Kocin and Uccellini 1990). This case was an excellent illustration of this type of circulation. Figure 7 shows a PC-GRIDDS vertical cross-section that extends from Richmond, Virginia southward to near Wilmington, North Carolina. From this cross-section, the vertical ageostrophic circulations resulting from the exit region of a jet speed max over eastern North Carolina can be seen. The thermally indirect circulation is noted by the letter "I" in the cross section. The forecasted area of strong ageostrophic induced upward motion generally lies over northeast North Carolina. Figure 8 shows in plan view the resulting 850 mb ageostrophic winds overlaid with the 850-700 mb layer Q vector forcing from an NGM 18-h forecast valid at 0600 UTC 8 February. The 850 mb ageostrophic winds were strongly convergent off the Atlantic Ocean directed toward the North Carolina coast. This 850 mb ageostrophic flow served to advect moisture from the Atlantic ocean to the North Carolina coast. This moisture advection coupled with the fairly deep layered vertical motions as indicated by the Q-vector convergence centered over north central North Carolina, was sufficient to produce significant precipitation.

The total Q-vector can be broken into components oriented along the isotherms ($\mathbf{Q_s}$) and normal to the isotherms ($\mathbf{Q_n}$). The $\mathbf{Q_s}$ component is essentially a measure of geostrophic deformation and the $\mathbf{Q_n}$ component is a measure of geostrophic frontogenesis. Figure 9 shows the 18-h forecast of 850-700 MB layer $\mathbf{Q_s}$. Convergence of $\mathbf{Q_s}$ with the $\mathbf{Q_s}$ vector pointing with cold air to the left implies turning of the thermal field with time that is frontogenetic. The $\mathbf{Q_s}$ component also shows the forcing related to the synoptic scale middle and upper level vorticity maxima and corresponds closely to the position of the comma head in satellite imagery.

Figure 10 shows the 18-h forecast of 850-700 mb layer $\mathbf{Q_n}$. $\mathbf{Q_n}$ vectors pointing from cold to warm air implies geostrophic frontogenetic forcing while $\mathbf{Q_n}$ vectors pointing from warm to cold air implies geostrophic frontolytic forcing. Note the area of geostrophic frontolysis over eastern North Carolina.

The ageostrophic response would be a thermally indirect frontogenetic circulation that acts to tighten the thermal gradient over eastern North Carolina.

5. CONDITIONAL SYMMETRIC INSTABILITY

The relationship between heavy snowfall and conditional symmetric instability (CSI) was documented for the March 12-13, 1993 "Storm of the Century" (Bradshaw 1994) and by others for previous snow events. According to Moore (1993), CSI is determined by comparing the geostrophic angular momentum **(mg)** and equivalent potential temperature **(theta-e)** from a vertical cross-section of the atmosphere which is aligned perpendicular to the 1000-500 mb thickness. Overlaying relative humidity values onto this cross-section shows where the air is saturated, which results in moist symmetric instability. CSI is determined in saturated regions where the slope of the **mg** surface is less than **theta-e**. Figure 11 shows an NGM 18-h forecast cross-section displaying mg, theta-e and relative humidity. The orientation of the cross-section extends from around Elkins, West Virginia to 170 n mi southeast of Wilmington, North Carolina. The cross-section runs normal to an 850 mb theta-e ridge axis. The region of CSI is hatched and encompasses all of eastern North Carolina.

6. GARCIA TECHNIQUE

The Garcia Technique (Garcia 1994) was used to determine how much snowfall was possible for northeast North Carolina. The first two steps in this process are to determine the "area of concern" and to find the isentropic surface (°K), which intersected this area between 750 and 700 mb. Through model time sections and an analysis of ageostrophic circulations, it was concluded northeast North Carolina was the "area of concern". Plotting potential temperature surfaces on a cross-section that dissects the "area of concern" from north to south, showed that the best isentropic surface in this case would be 282K. Figure 12 shows the 12-h forecast pressure levels (valid 0000 UTC 8 February) on the 282K isentropic surface along with the winds along that surface. Note the air moving from higher pressure to lower pressure from South Carolina to off the Virginia/North Carolina coastline, which implies upward vertical motion along the isentropic surface. The best lift is achieved when winds blow perpendicular to the constant pressure surfaces. In this case, the air is moving at a 30° to 50° angle with respect to the constant pressure surfaces, and nearly perpendicular farther to the east toward the water. This cross contour flow was due in part to the ageostrophic circulation in the exit region of the jet streak moving toward South Carolina.

The third step of the Garcia Technique is to calculate an <u>average</u> mixing ratio value that would be over the "area of concern". Figure 10 shows that forecast mixing ratios valid at 0000 UTC were just below 1 g/kg. However, southwest winds along the isentropic surface were convergent and averaged 40 kt. This would likely result in advection of higher mixing ratios across northeast North Carolina during the next 12-h period. To approximate the highest mixing ratio value, the average wind speed was multiplied by 12-h. This calculation suggested that mixing ratios from about 480 n mi upstream could advect across northeast North Carolina by 1200 UTC 8 February. The highest mixing ratio in this time frame was found to be approximately 3 g/kg, with the <u>average</u> mixing ratio for the 12-h period estimated to be about 2 g/kg. The empirical formula for snow amounts used in the Garcia technique is roughly a 2:1 ratio of snowfall vs. the <u>average</u> mixing ratio values. Therefore, an average snowfall of 4 inches of snow was possible over northeast North Carolina during the 12-h period. It must be noted that this technique does not take into account the potential for additional low-level moisture advection from the Atlantic Ocean, so snow amounts over North Carolina could be higher.

7. SNOW EVENT

Light to moderate snow initially began over the mountains and western piedmont in North Carolina shortly after 0000 UTC 8 February. At 2345 UTC 7 February, a winter weather advisory was issued by the Nexrad Weather Service Forecast Office in Raleigh, North Carolina (NWSFO RAH) for the western piedmont, with expected snow accumulations of 1-2 inches. The snow spread eastward to the North Carolina coastal plain and expanded in coverage. Pockets of moderate snow became widespread over eastern North Carolina, mainly from near Elizabeth City south to the Albemarle Sound and east to the northern Outer Banks by 0800 UTC 8 February and continued through 1400 UTC. There were also indications that moderate snow fell for a short time across extreme southern sections of Virginia Beach resulting in the local 3 inch accumulations.

Snow accumulations of 2-4 inches were noted over a large area in eastern North Carolina extending from Raleigh eastward to the northeast coastal areas. Isolated amounts in excess of 6 inches were noted along the northern shore of the Albemarle Sound in Camden, Pasquotank and Currituck counties with Point Harbor in Currituck county measuring 7 inches of snow. Unofficial reports of 8 inches were received at the NWSO Wakefield from the northern North Carolina Outer Banks near Corolla. There was also a report of 3 inches of snow in Blackwater in extreme southern sections of Virginia Beach.

8. CONCLUSION

Snow events such as the one which occurred on February 8, 1995 and examined in this study are not very common for northeast North Carolina or extreme southeast Virginia. This event illustrates the importance of utilizing PC-GRIDDS and numerical gridded model data in diagnosing the potential for heavy precipitation. Although standard meteorological charts provided a quick but limited perspective of the model output, the versatility of PC-GRIDDS allowed for a more thorough analysis. The use of location specified time sections showed the vertical depth and timing of significant lift and moisture. From cross-section analyses, ageostrophic circulations and CSI potential were shown. Lastly, PC-GRIDDS also provides forecasters with a quick method to view isentropic surfaces. It has been shown in this study that based on the empirical technique of Garcia (1994), average mixing ratios values related to a specific isentropic surfaces provides an excellent starting point for forecasting possible snow accumulations.

9. ACKNOWLEDGEMENTS

The authors would like to thank NWSFO Raleigh, Science and Operations Officer Kermit Keeter and Warning Coordination Meteorologist George Lemons for their contributions. We would also like to thank Steve Kuhl of the ERH Scientific Services Division for his valuable assistance in revising this manuscript. Finally, special thanks go to Tony Siebers, Meteorologist-In-Charge at NWSO Wakefield for his assistance with the figures.

10. REFERENCES

Bradshaw, T., 1994: Relationships between conditional symmetrically instability, thunder and heavy snowfall during the "Storm of the Century". NOAA Technical Attachment NWS SR/SSD 94-21, DOC, NOAA, National Weather Service, Souther Region, Ft. Worth, Texas, 8pp.

Garcia, C., 1994: Forecasting snowfall using mixing ratios on an isentropic surface: An empirical study. NOAA Technical Memoranda, NWS CR-105, DOC, NOAA, National Weather Service, Central Region, Kansas City, MO, 31 pp.

Kocin, P.J., and L.W. Uccellini, 1990: *Snowstorms Along the Northeastern Coast of the United States: 1955-1985.* Lancaster Press, 280 pp.

Moore, J., 1993: Isentropic analysis and Interpretation: Operational Applications to synoptic and mesoscale forecast problems, DOC, NOAA, NWS Training Center, 73-82.

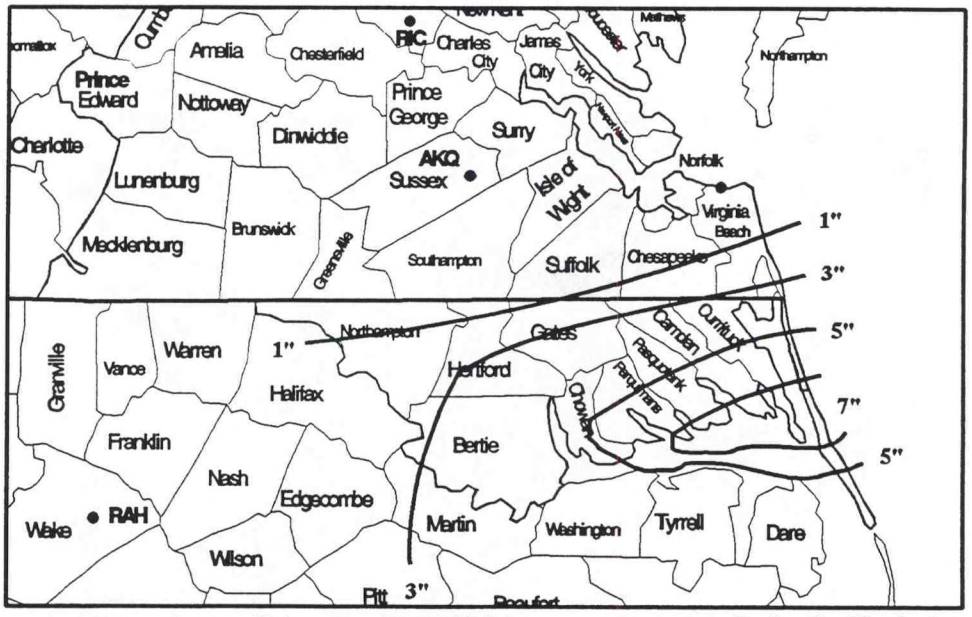

Figure 1. Snowfall totals for February 8, 1995 heavy snow event (inches). Shaded areas denote NWSO Wakefield warning area

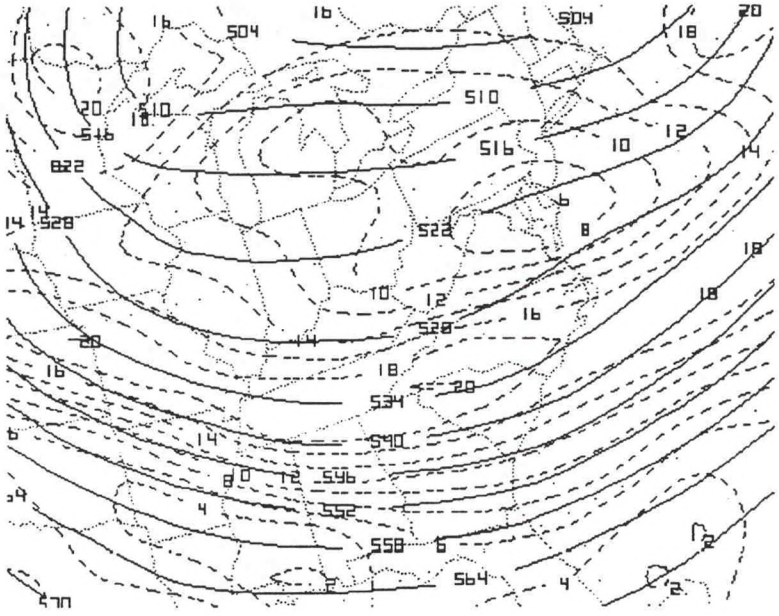

Figure 2. 1200 UTC 7 February 1995 NGM 500 mb (dm, solid lines) and vorticity ($x10^{-5}x^{-1}$, dashed lines) analysis. From PC-GRIDDS.

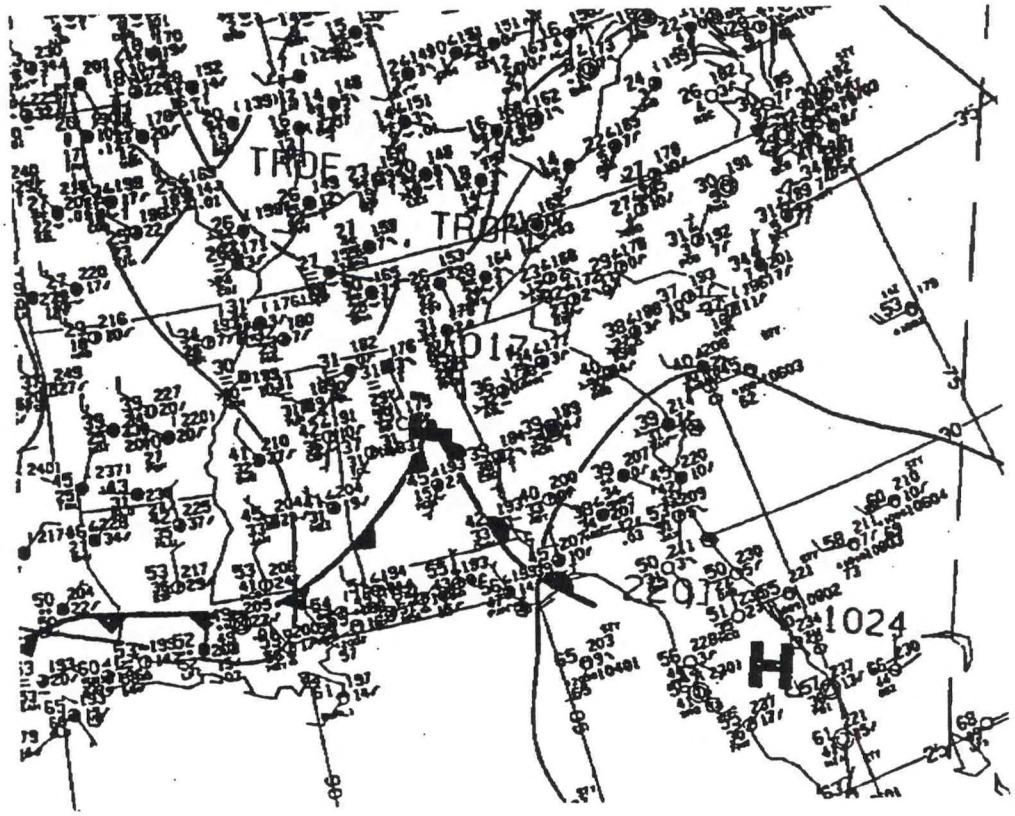

Figure 3. 1500 UTC 8 February 1995 surface plot and analysis.

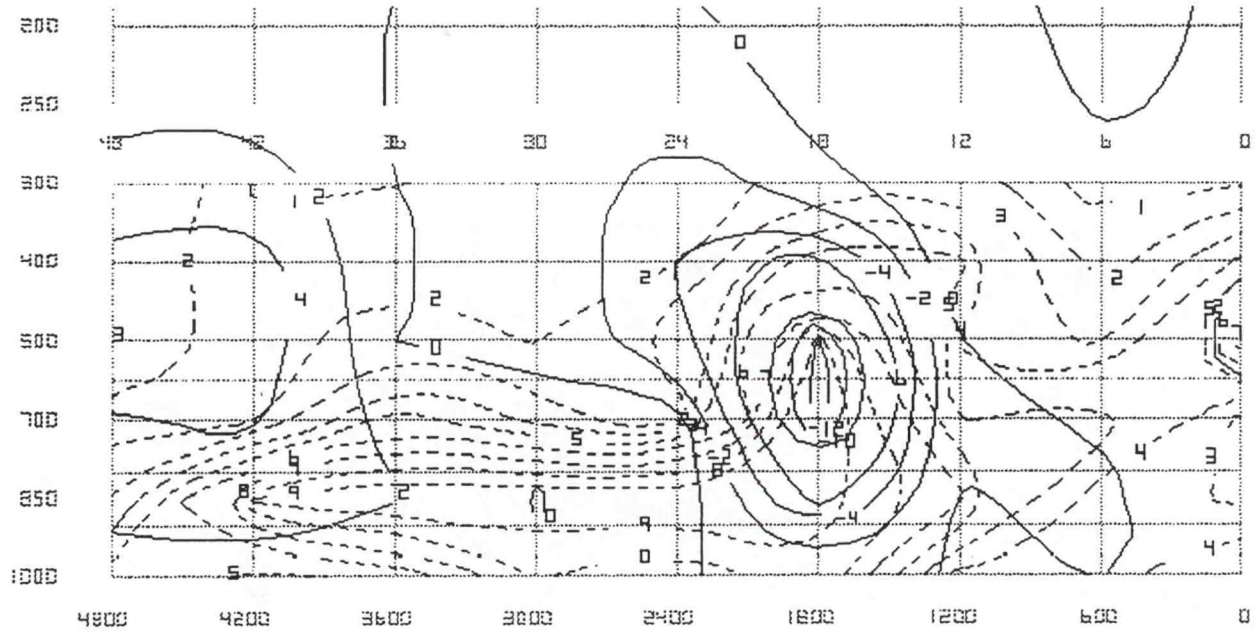

Figure 4. PC-GRIDDS time-section of vertical velocity (solid lines) and relative humidity (dashed lines) for Cape Hatteras, North Carolina, valid from 1200 UTC 7 February (00-h) to 1200 UTC 9 February, 1995 (4800-h). Note the upward vertical motion of -12 ubs^{-1} at approximately 18-h into the model run. The time increments are every 6-h.

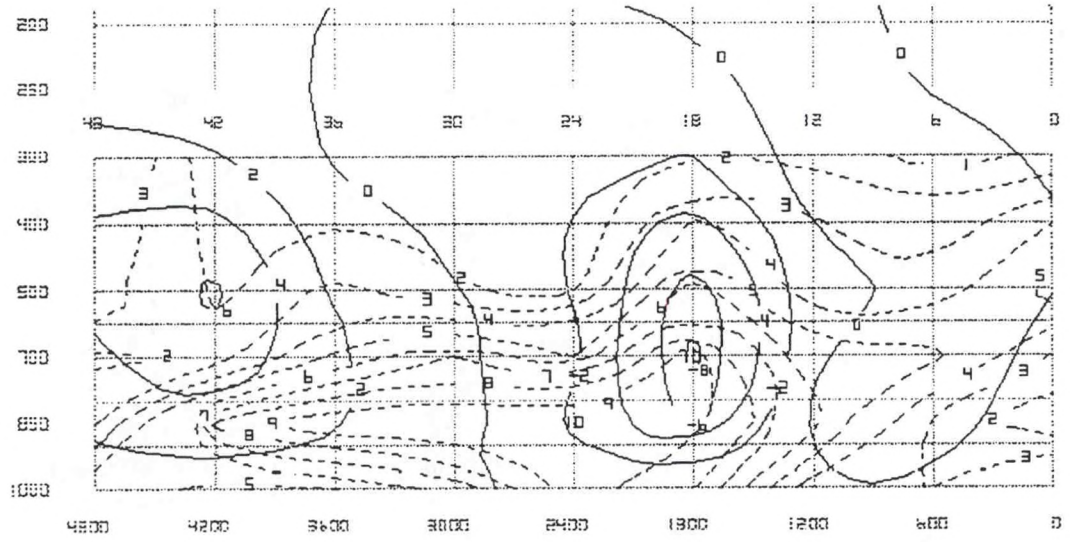

Figure 5. As in Figure 4, except Elizabeth City, North Carolina. Note the upward vertical motion of -10 ubs^{-1} at approximately 18-h.

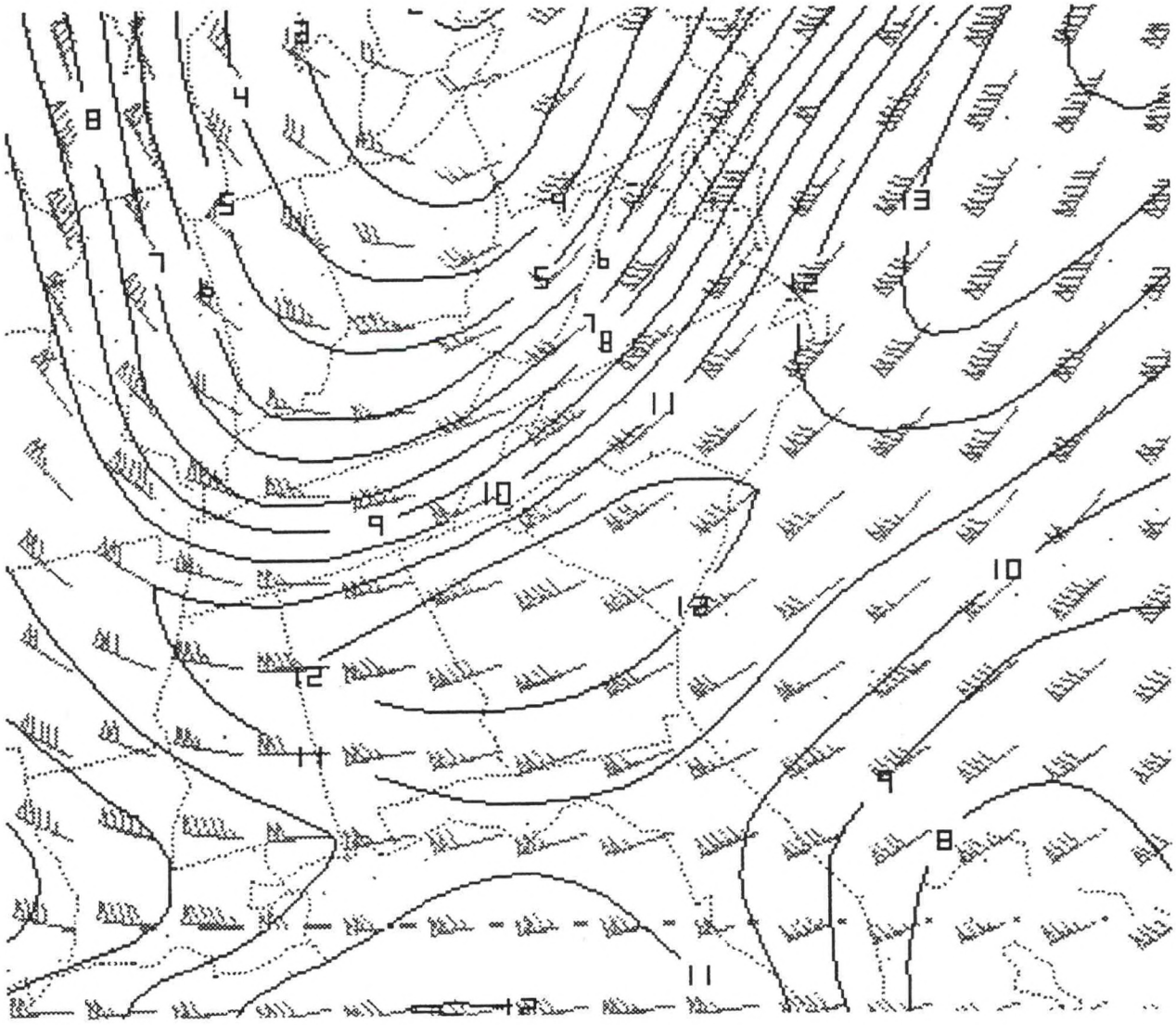

Figure 6. NGM 18-h forecast of 300 mb wind and isotachs (kt) valid at 0600 UTC 8 February, from the 1200 UTC 7 February 1995 run of the NGM. Note the speed maxima located over South Carolina and Georgia, and the western Atlantic Ocean.

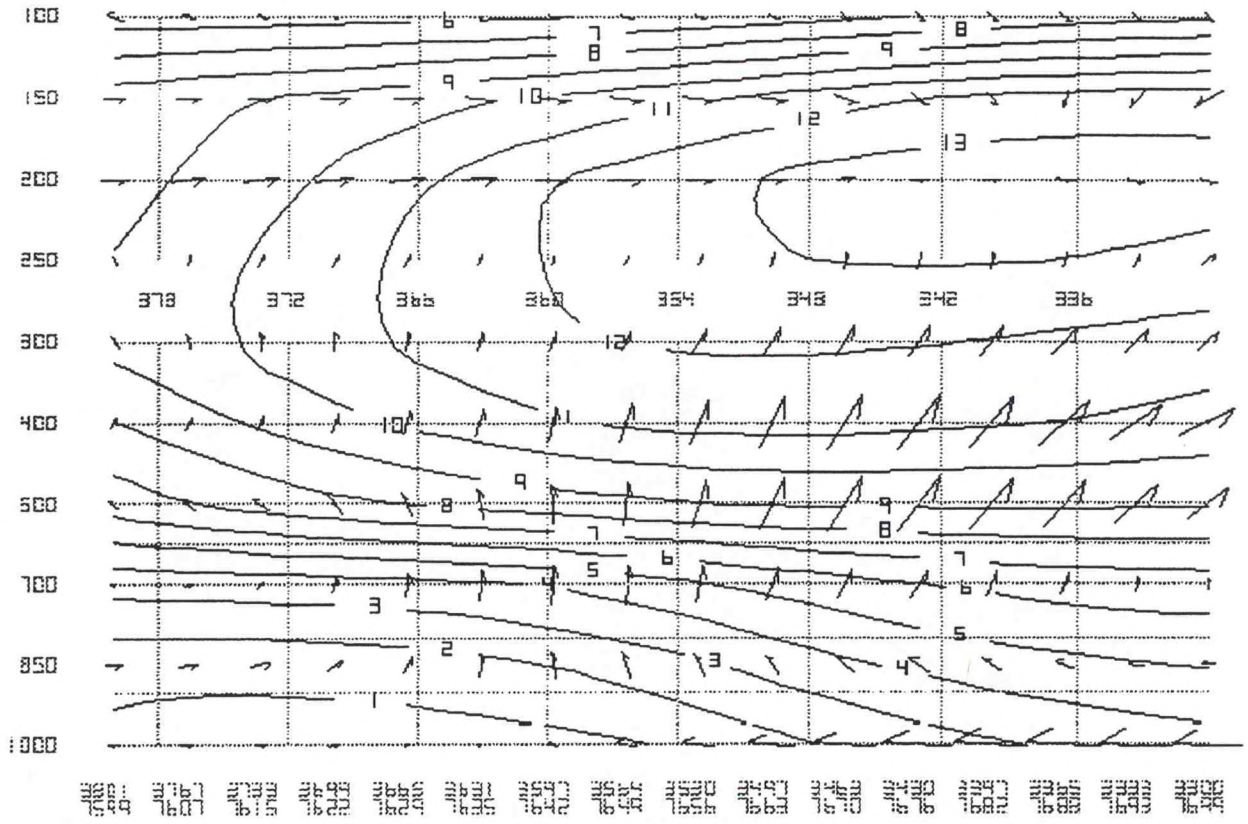

Figure 7. NGM 18-h forecast of ageostrophic circulations resulting from the exit region of a jet streak, valid at 0600 UTC 8 February 1995. The cross-section extends from A) Richmond, Virginia to near B) Wilmington, North Carolina. The thermally indirect circulation is marked by the letter "I".

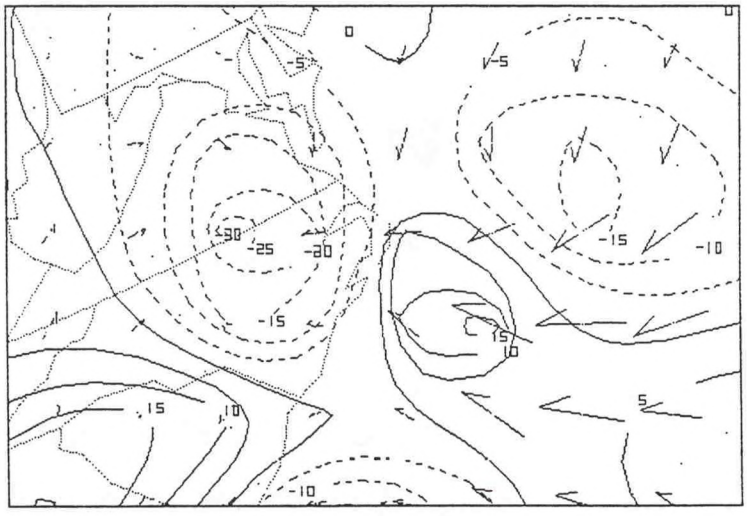

Figure 8. NGM 18-h 850 mb ageostrophic winds (arrows) and 850-700 mb Q-vector divergence, valid at 0600 UTC 8 February 1995 (dashed negative denotes Q-vector convergence).

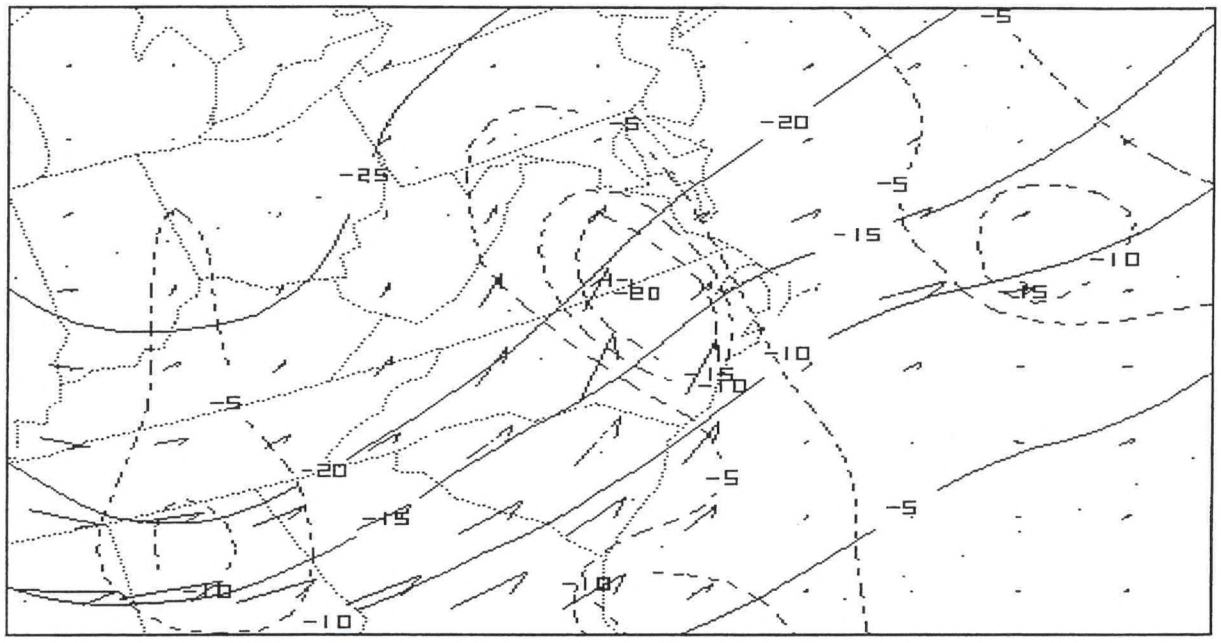

Figure 9. NGM 18-h forecast of divergence of Q_n pointing in the direction with cold air to the left implies a counterclockwise turning of the thermal wind.

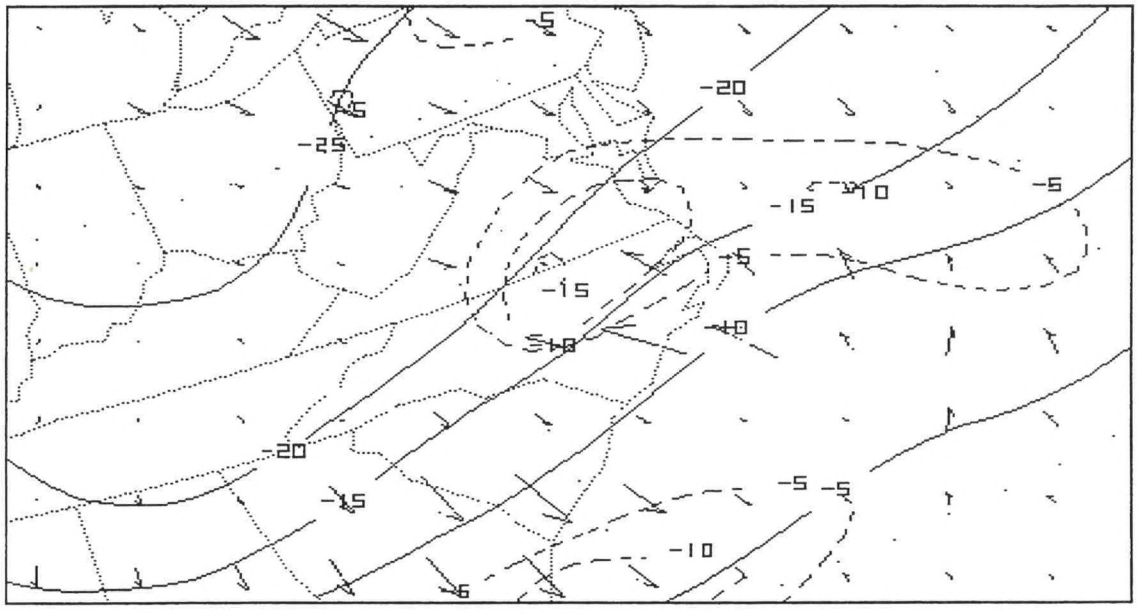

Figure 10. NGM 18-h forecast of divergence of Q_n (dashed negative = convergence). Q_n pointing from warm to cold air indicates frontolytic forcing over eastern North Carolina. The ageostrophic response is a thermally indirect frontogentic circulation.

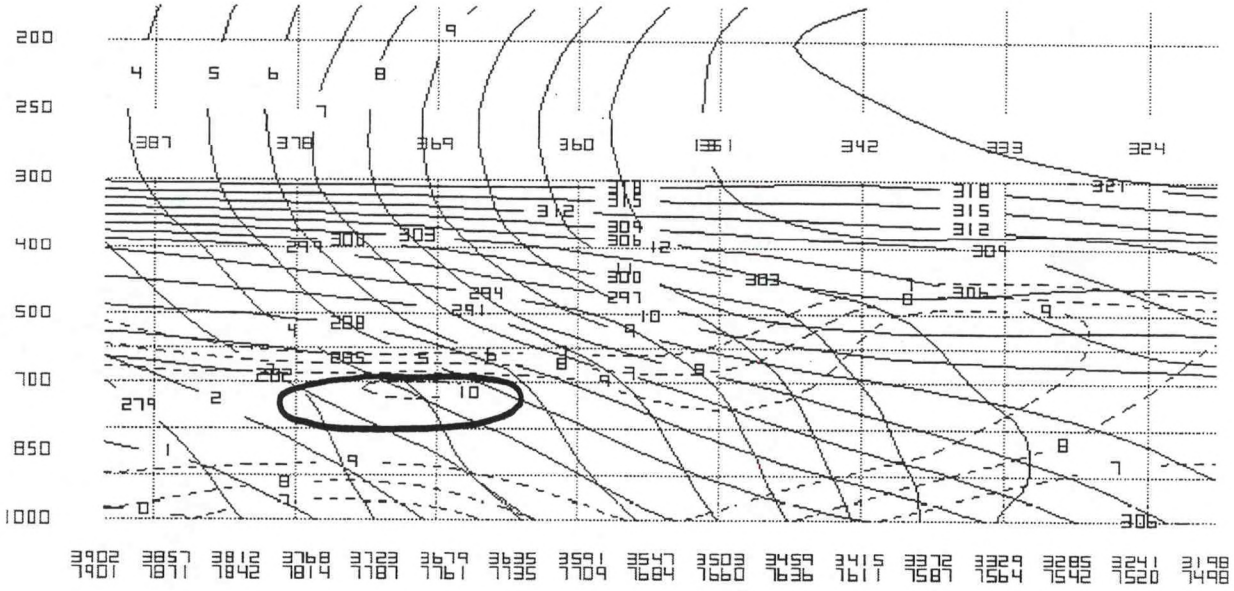

Figure 11. NGM 18-h forecast cross-section valid at 0600 UTC 0600 UTC 8 February showing areas of potential CSI. The geostrophic angular momentum (Mg; solid, semi-horizontal lines), theta-e surfaces (°K, solid, nearly vertical lines and mea relative humidity (dashed lines). CSI is determined to be possible in saturated regions where the slope of the mg surface is less than the slope of the theta-e surface.

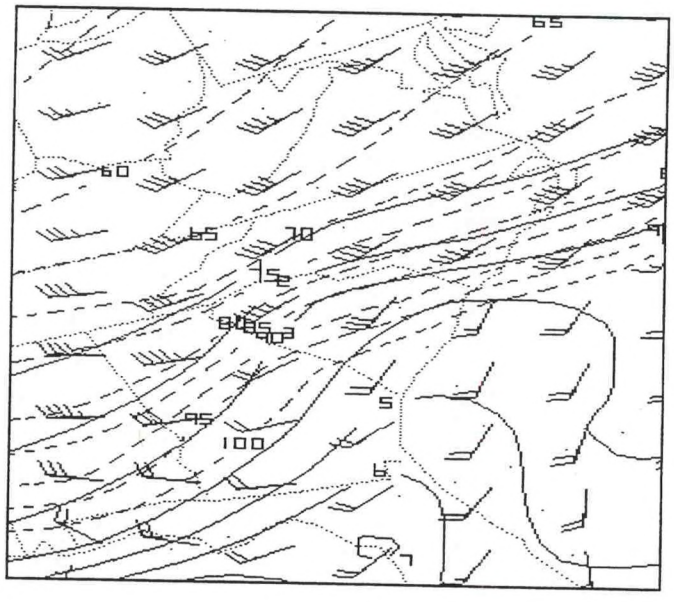

Figure 12. NGM 12-h forecast valid at 0000 UTC 8 February of 282K isentropic surface pressure level (dashed lines), winds along the 282K surface, and mixing ration contours (solid lines). Note the air moving from higher to lower pressure form the South Carolina coast to near Virginia coast. From PC-GRIDDS.

Evaluation of a Record Snowfall Event in the Lower Columbia Basin Using PCGRIDDS

Mark A. Tew[1]

1. INTRODUCTION

On the morning of February 24, 1994, an unexpected Winter Storm developed over the lower Columbia River basin of Oregon and Washington. This storm was not associated with major cyclogenesis, and conventional forecasting methods of estimating quasi-qeostrophic (QG) vertical motion such as: 500 mb PVA, positive isothermal vorticity advection (PIVA), and Q-vector analyses showed little or no dynamic support for a heavy snow event. Nevertheless, snowfall amounts across the region ranged from 6 to 16 inches (Figure 1) with most of the snow falling in less than 10 hours. The 16 inches of snow that was observed in Pendleton set a new all-time 24-hour snowfall record. This study will first show the failure of these conventional methods and then demonstrate by the use of PCGRIDDS, the combination of a jet-streak circulation pattern and conditional symmetric instability (CSI) to produce the sudden snowfall event.

2. BACKGROUND

Several studies have evaluated vertical motion associated with jet-streak circulation patterns that have produced winter precipitation. Hakim and Uccellini (1992) examined a heavy snow event in the Northern Plains produced by a coupled jet-streak circulation. The upper branch of a direct circulation pattern phased with the lower branch of an indirect circulation. Both combined to produce enhanced vertical motion that resulted in a heavy snow event. Another study evaluated by Uccellini and Kocin (1987) credited a coupled jet circulation to rapid cyclogenesis in eight East Coast snowstorms. Heavy snow in northwest Montana on March 15, 1989 was attributed to a coupled jet-streak circulation pattern by Blank (1989).

With the advent of PCGRIDDS, conditional symmetric instability (CSI) has become easier to diagnose and use as a forecast tool for banded winter precipitation. Snook (1992) explained CSI theory and applied a case study to illustrate the role of CSI in forming large snow bands in the Denver area. Dunn (1988) combined ageostrophic forcing with CSI to explain a 1985 September snowstorm over northeastern Colorado. Another snowstorm eight years later in northeastern Colorado was studied by Conger and Dunn (1993) using PCGRIDDS to apply CSI theory in forecasting real-time weather events.

3. SYNOPTIC OVERVIEW

The NGM gridded data initialized at 1200 UTC 23 February was chosen to determine the type of dynamics that existed to cause this snowstorm and the effectiveness of a 12- to 24-hour forecast. At 0000 UTC 24 February 1994, a deep upper-level low pressure system in southwest Alberta, Canada produced a strong westerly flow over the Pacific Northwest. The 12 hour forecast of 500 mb heights and vorticity (Figure 2a), the PVA band was forcast to be east of the Columbia Basin when

1. Corresponding author address: Mark A. Tew, NWSO Grand Rapids, Michigan (Formerly from WSFO Portland Oregon).

the snowstorm was at full strength. As a result, this forecasting method would not have been a useful tool in diagnosing the potential for a major winter storm.

Another estimation of vertical motion by QG forcing is positive isothermal vorticity advection (PIVA) or 500 mb vorticity advection by the thermal wind. The thermal wind can be depicted by the 1000-500 mb thickness field, which is readily available via AFOS graphics. By overlaying the 500 mb vorticity field on top of the thickness field, areas of QG forcing can be estimated. Since thickness contours were nearly parallel to height contours throughout the forecast period, vorticity advection by the thermal wind would be of little help in diagnosing the potential for strong vertical motion in this case (Figures 3a and 3b).

Finally, PCGRIDDS was utilized to examine Q-vector divergence that graphically shows synoptic scale upward vertical motion by incorporating both terms of the omega equation: differential vorticity advection and the laplacian of thickness advection (Dunn and Snellman 1994). Figure 4 shows rather weak QG forcing in central Washington at 12 and 24 hours and not centered over the area in question. However, one of the terms in the Q-vector formulation is the inverse of static stability. Therefore, the correlation of Q-vector convergence to values of vertical motion may not be valid in this case, since it maybe within an area of low static stability.

At the surface, a modified arctic cold front was advancing slowly southward during the 12- to 24-hour forecast period. The forecast problem was determining the southern extent of the front and whether cold air would move into the lower Columbia Basin. Figure 5 depicts very weak cold air advection and little southward movement of the 1000-500 thickness field (note the slight movement of the 528 dam thickness line). Use of this parameter alone, i.e., AFOS graphics, would be very difficult to discern the farthest point south the front would actually reach.

Statistical relationships have been developed to show rain/snow occurrence by utilizing differential thickness values (McNulty and Griffen 1993). By dividing the 1000-500 thickness into two layers (1000-850 mb layer and 850-700 mb layer), a more defined vertical temperature profile would result. When the 850-700 mb layer is less that 1540 m and the 1000-850 mb layer is less than 1300 m, the atmosphere is usually cold enough to support all snow down to the lowest elevation inside the lower Columbia basin (360 ft ASL in Richland, WA). Applying these values to this case, Figure 6 shows the forecasted 18-hour (solid line) and 24-hour (dashed line) 1300 m thickness line as it advanced slowly south through the night. This depicted quite accurately the path of the cold front as compared to surface observations. Looking at this figure alone, FROPA should occur in Pendleton between 0600 and 1200 UTC (FROPA did occur at 0800).

4. AGEOSTROPHIC ANALYSIS

The inadequacy of more conventional QG diagnostic methods to identify the potential for strong vertical motion, leads to an analysis of ageostrophic circulations. The NGM 12 (not shown) to 24-hour forecast of the 300 mb flow revealed a jet-streak tracking northwest to southeast over the region, which verified well with the initial 1200 UTC 24 February NGM gridded data file. By 1200 UTC (Figure 7) the lower Columbia Basin would be under the right entrance region of the jet. In response to this jet streak, the NGM indicated high values of model vertical velocity at 700 mb greater than 7 μbs^{-1} over the lower Columbia Basin lasting from 1800 UTC 23 February (not shown) through 0000 UTC 24 February (Figure 8a) before tapering off to near 3 $\mu b\ s^{-1}$ by 1200 UTC 24 February (Figure 8b). Typically during strong westerly flow episodes, areas east of Cascades receive little or no precipitation, even with large values of vertical velocities. As air flows over the Southern Washington Cascades, it decends from a crest of 6,000 ft down to 400 ft in the lower Columbia Basin. This is commonly called the *rain shadow effect* (Anthes et al. 1981), where the mesoscale downward forcing

east of the Cascades is often much greater in magnitude than any upward synoptic-scale forcing. However, note how the 700 mb flow is forecast to veer more towards the northwest by 1200 UTC (Figure 8b). By empirical knowledge through observations, a northwest flow aloft produces a lesser rain shadow effect than a westerly flow does.

A 12-hour forecast cross-section through the entrance region stretching from southeast British Columbia, Canada to southern Oregon, was created to depict the ageostrophic winds, model vertical motion, and potential temperature (Figure 9a). The ageostrophic circulation vectors reveal an upward direct circulation pattern derived from the jet streak entrance region over Pendleton. At the same time, there is bull's eye of model vertical velocity greater than 6 μb s^{-1}. The potential temperature field depicts the frontal zone north of Pendleton with the isentropes sloping down toward the warmer air. However, the synoptic scale lift was being canceled by the strong westerly flow over the Cascades.

Using the same cross-section 12 hours later (Figure 9b), the forecast ageostrophic circulation pattern continued to indicate strong upward motion, while the forecast vertical velocity values decreased slightly, and differed somewhat from the initial 1200 UTC NGM gridded data set which showed vertical velocity values in excess of 8 μb s^{-1}. The frontal zone depicted by the potential temperature field was projected to slide south of Pendleton by 1200 UTC 24 February, which matched the differential thickness prognosis. This dome of cold air that moved in behind the modified cold front, coupled with the veering to the 700 mb flow may have helped in weakening the downsloping effect off the Cascades, thus enabling the synoptic scale lift to commence. Snow began in Pendleton at 0800 UTC 24 February and continued heavily through 1800 UTC. During this time period 13 inches of snow fell, while 60 miles northwest of town near Hanford, WA less than 1 inch of snow was reported. Meanwhile, areas on the east slope of the Cascades like Yakima, WA and The Dallas, OR (Figure 1) received 6 to 8 inches of snow from this event.

5. CSI ANALYSIS

Another cross section was taken over the same area to examine the possibility of CSI that could contribute to banded areas of heavy snow due to slantwise convection. Remember, when using PCGRIDDS several steps must be taken to identify areas of CSI. First take a cross-section normal to the thermal wind (thickness field), then plot the momentum and Theta-E surfaces. Look for areas where Theta-E surfaces slope more than momentum surfaces. If this area is located in a moist atmosphere (RH> 70%) than this area can support CSI (Moore and Lambert 1993). The 24 hr forecast clearly shows a relatively large area of CSI (Figure 10a) over the same area that had large model vertical velocities and a vertical jet streak circulation pattern. The 00 h NGM initial analysis valid 1200 UTC 24 February 1994 (Figure 10b), matches well with the 24 h forecast valid at the same time.

5. SUMMARY

The sudden heavy snowstorm in February across the lower Columbia Basin proved not to be easily diagnosed by using more conventional forecasting methods such as 500 mb PVA, PIVA, Q-vector divergence, and the rain shadow effect. Even the ageostrophic forcing via a jet-streak circulation pattern did not take effect until the upper-level flow began to veer more towards the nrothwest at the time of the cold front's arrival. In addition, PCGRIDDS became a beneficial forecasting tool in recognizing the possibility of conditional symmetric instability, even 24 hours out. Once CSI is present over an area that has both frontogenetical and ageostrophic forcing occurring simultaneously, enhanced vertical motion would be expected. This explains the rapid development and banded nature of this snowstorm.

This case also proved that some forecasting methods that are commonly applied east of the continental divide, are also useful east of the Cascades. Consequently forecasters in the Pacific Northwest should be encouraged to utilize jet streak dynamics and CSI theory in differential thickness in diagnosing future real-time winter weather events.

6. REFERENCES

Anthes, R.A., J.J. Cahir, A.B. Fraser, and H.A. Panofsky, 1981: *The Atmosphere.* Charles E. Merril Publishing Co., 531 pp.

Blank, J., 1989: A heavy snow event associated with jet streak interaction. WR Tech. Attach. 89-36. DOC, NOAA, NWS, Western Region, Salt Lake, City, NV.

Conger, M.C., and L.B. Dunn, 1993: Using PCGRIDDS to forecast symmetric instability in a Northeast Colorado snowstorm. WR Tech. Attach. 94-02. DOC, NOAA, NWS Western Region, Salt Lake City, NV.

Darran, D.R., and L.W. Snellmann, 1987: The diagnosis of synoptic-scale vertical motion in an operational environment. *Wea. Forecasting,* **2**, 17-31.

Dunn, L.B., 1988: Vertical motion evaluation of a Colorado snowstorm from a synoptician's perspective. *Wea. Forecasting,* **3**, 261-272.

Hakim, G.J., and L.W. Uccellini, 1992: Diagnosing coupled jet-streak circulations for a Northern Plains snow band from the operational Nested-Grid Model. *Wea. Forecasting,* **7**, 26-48.

McNulty, R., and J. Griffen, 1993: Winter weather; precipitation type. National Weather Service Training Center, Kansas City, MO, 30 pp.

Moore, J.T., and T.E. Lambert, 1993: The use of equivalent potential vorticity to diagnose regions of conditional symmetric instability. *Wea. Forecasting,* **8**, 301-308.

Snook, J.S., 1992: Current techniques for real-time evaluation of conditional symmetric instability. *Wea. Forecasting,* **7**, 430-439.

Uccellini, L.W., and P.J. Kocin, 1987: The interaction of jet streak circulations during heavy snow events along the East Coast of the United States. *Wea. Forecasting,* **2**, 289-308.

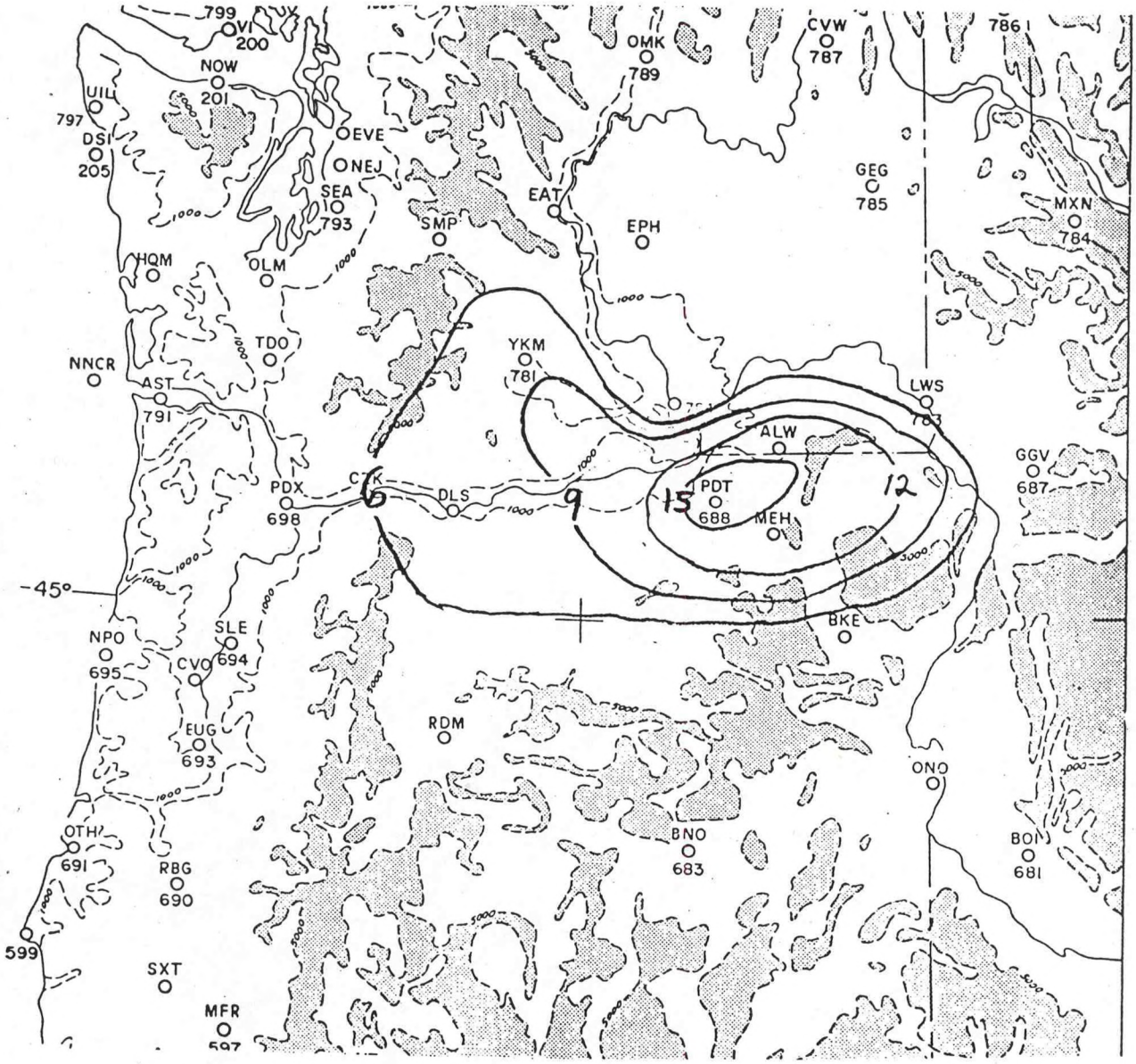

Figure 1. Subjective analysis of the 24-hour snowfall for February 24, 1994 based on National Weather Service and substation snow reports (contoured at 6, 9, 12, and 15 inch intervals).

(a)

(b)

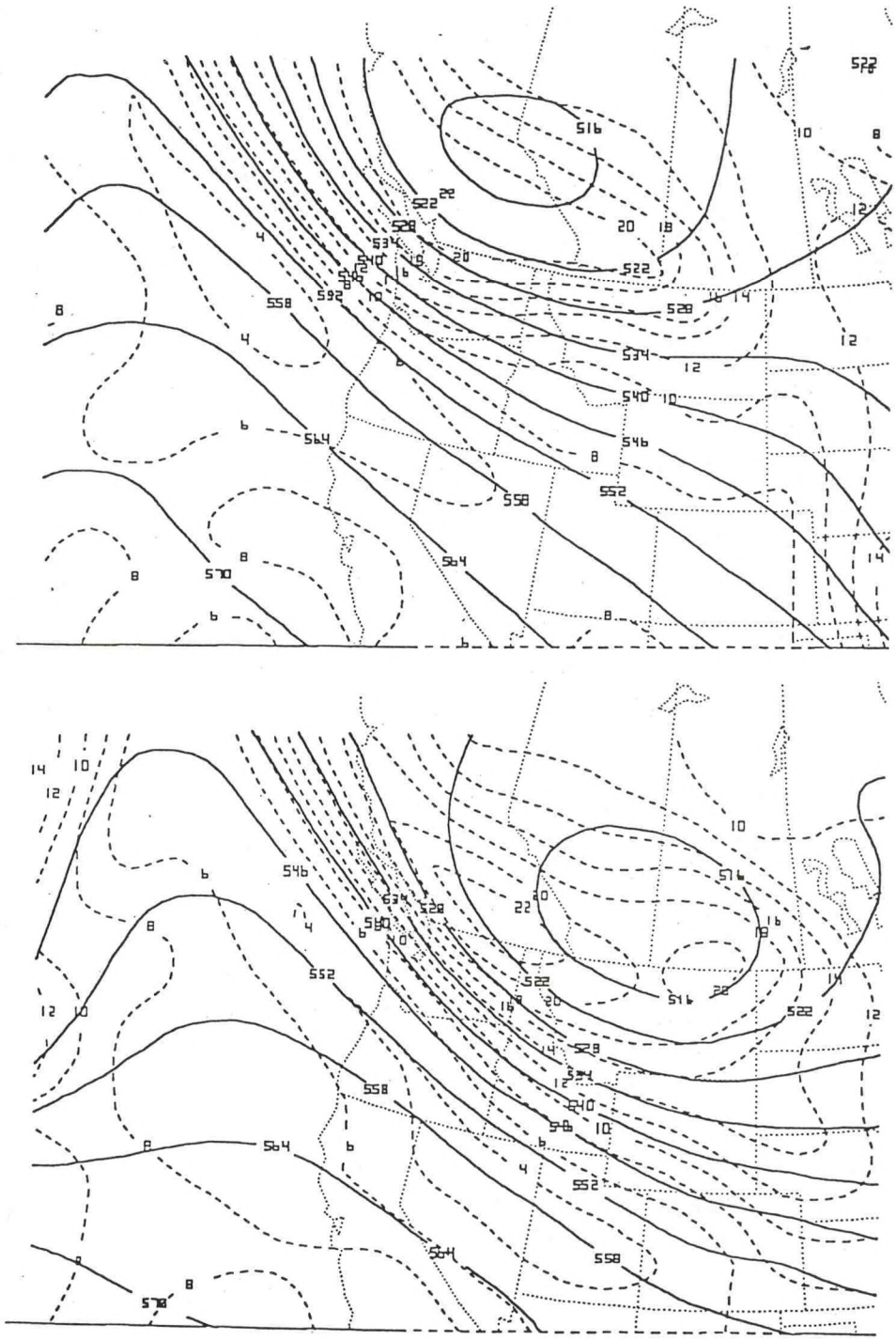

Figure 2 NGM and 24-hour forecast of 500 mb heights (solid, every 6 dam) and absolute vorticity (dashed, every $2x10^{-5}s^{-1}$) for (a) 0000 UTC and (b) 1200 UTC 24 February 1994.

(a)

(b)

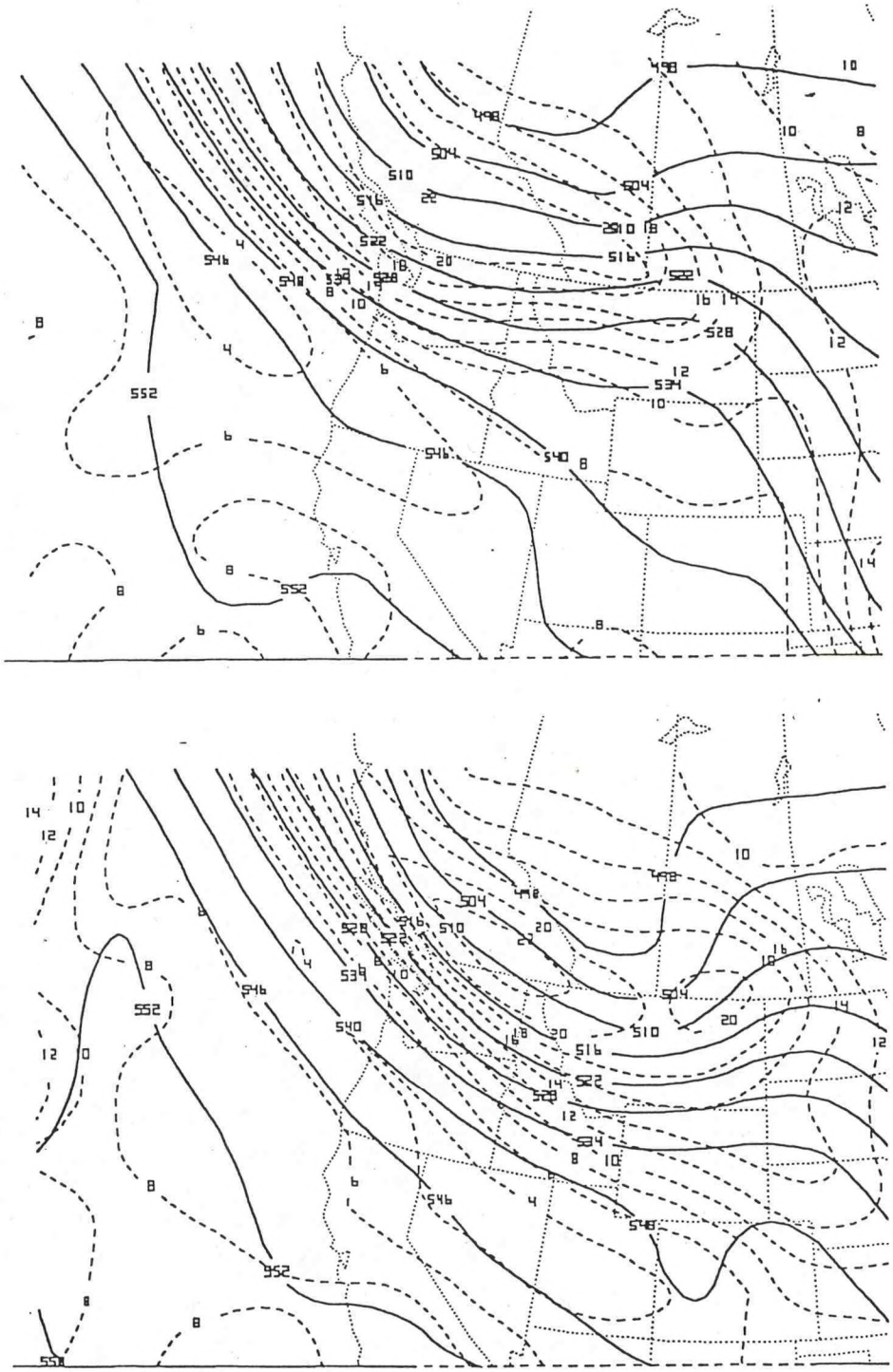

Figure 3. NGM 12- and 24-hour forecast of 1000-500 mb thickness (solid, every 6 dam) and absolute vorticity (dashed, every $2x10^{-5}s^{-1}$) for (a) 0000 UTC and (b) 1200 UTC 24 February 1994. Positive Isothermal Vorticity Advection (PIVA) technique.

(a)

(b)

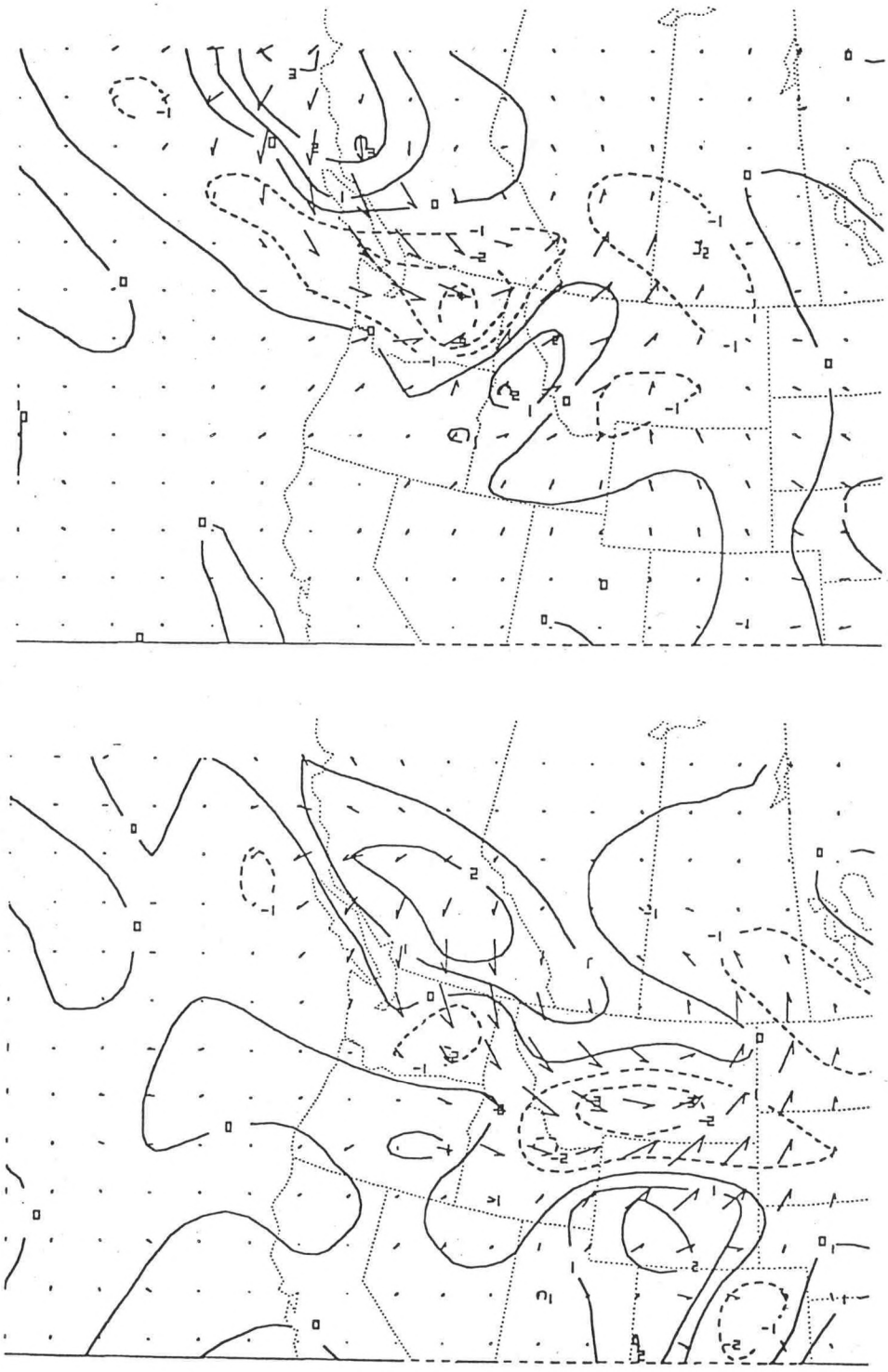

Figure 4. NGM 12 and 24-hour forecast of 500 mb Q-vectors (arrows) and divergency of Q (contoured every 10^{-17} m kg^{-1} s^{-1}) for (a) 0000 UTC and (b) 1200 UTC 24 February 1994.

(a)

(b)

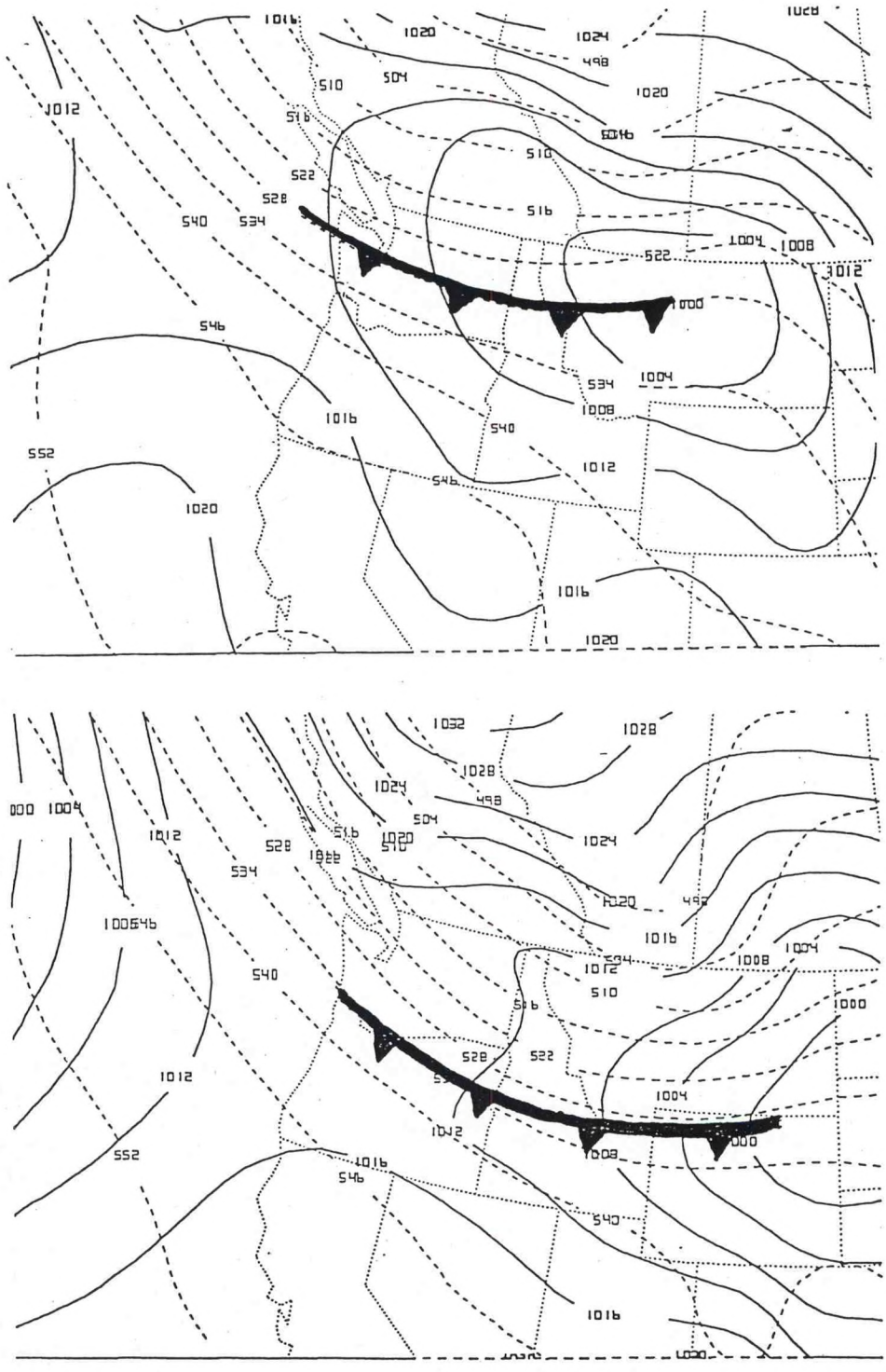

Figure 5. NGM 12- and 24-hour forecast of mean sea level pressure (solid, every 4 mb) and 1000-500 mb thickness (dashed, every 6 dam) for (a) 0000 UTC and (b) 1200 UTC 24 February 1994. Cold frontal position (barbed line).

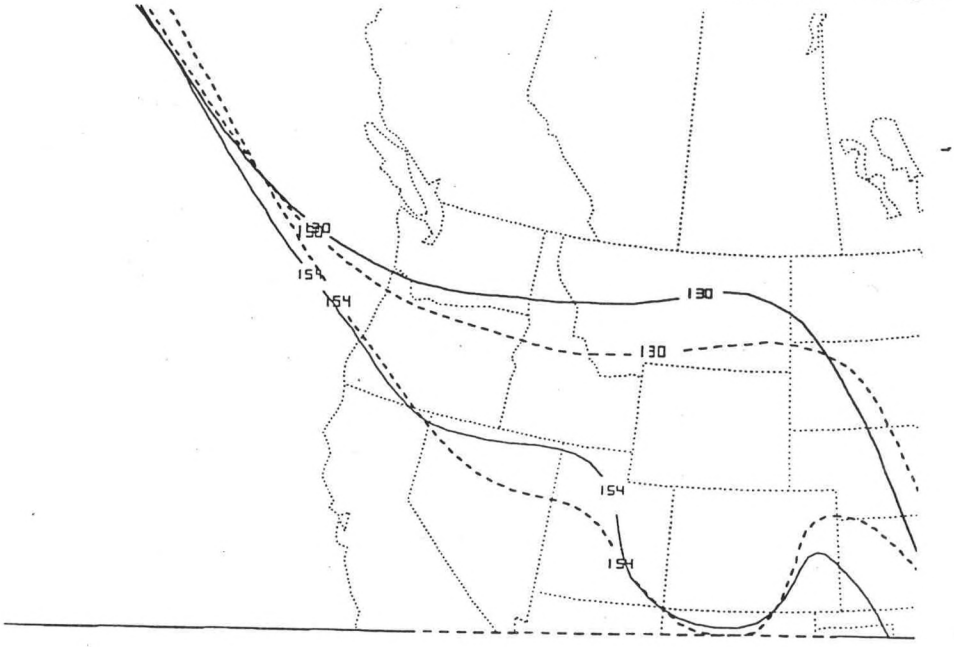

Figure 6. NGM 18-24-hour forecast of the 130 dam (1000-850 mb) and 154 dam (850-700 mb) differential thickness for 0600 UTC (line) and 1200 UTC (dashed) 24 February 1994.

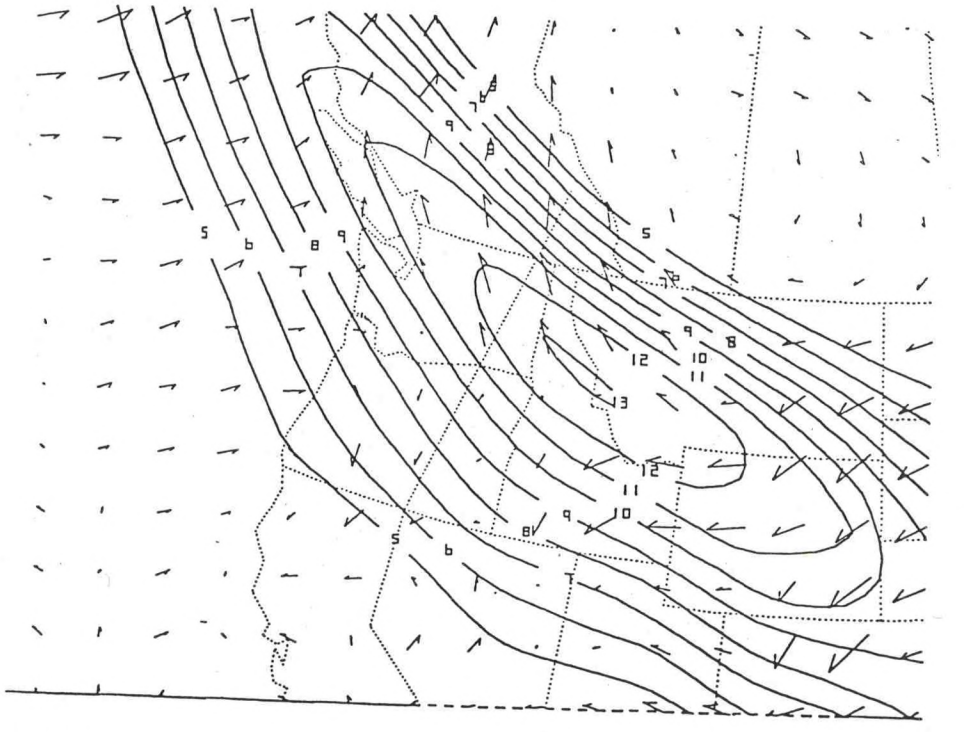

Figure 7. NGM 24-hour forecast of 300 mb isotachs (dark sold, every 10 knots), ageostrophic wind vectors (arrows) and line depicting cross-sections valid 1200 UTC 24 February 1994.

(a)

(b)

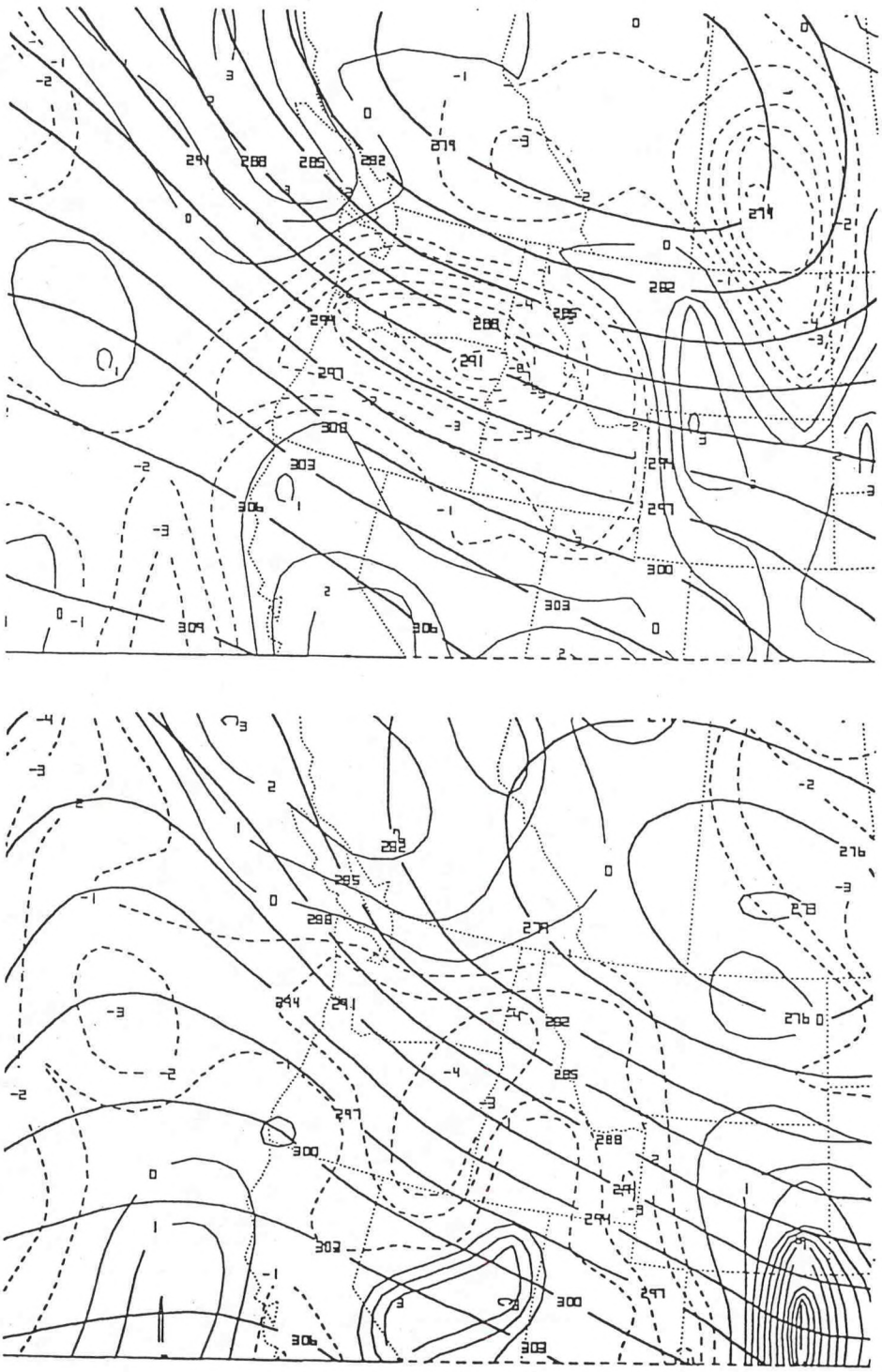

Figure 8. NGM 12- and 24-hour forecast of 700 mb heights (solid lines, every 3 dam) and 700 mb model vertical velocity (dashed, every μb s^{-1}) for (a) 0000 UTC and (b) 1200 UTC 24 February 1994.

(a)

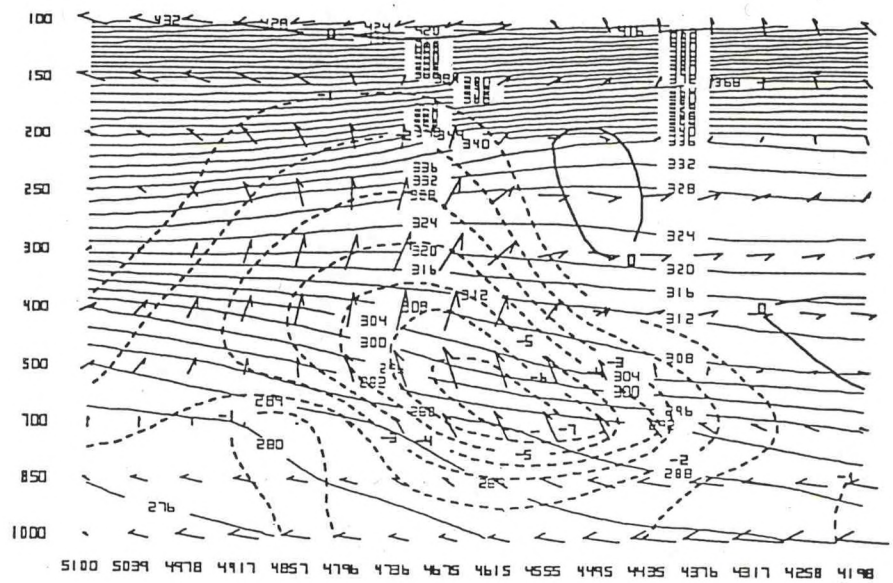

(b)

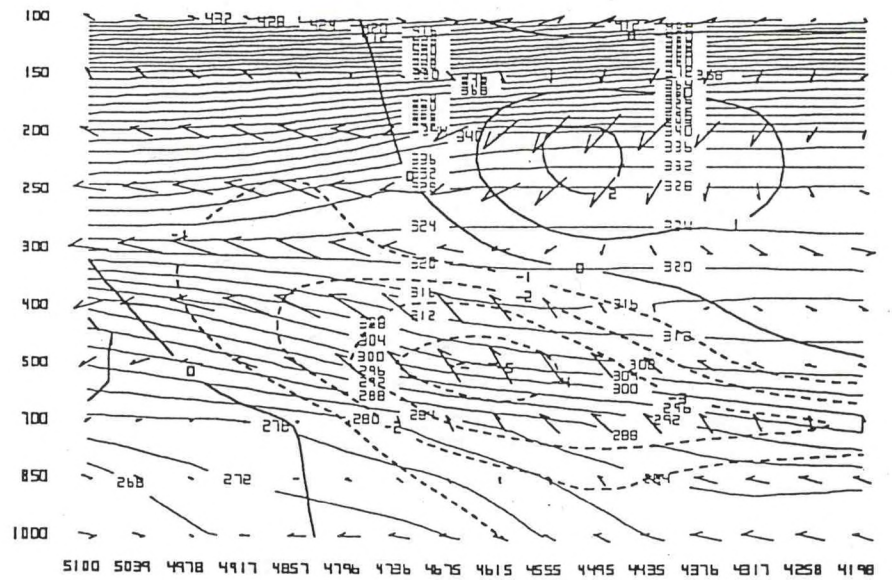

Figure 9. NGM 12 and 24-hour forecast cross-sections of potential temperature (thin solid lines, every 4K), model vertical velocity (dashed, every $\mu p\ s^{-1}$) and ageostrophic circulation vectors (thick arrows) for (a) 0000 UTC and (b) 1200 UTC 24 February 1994.

(a)

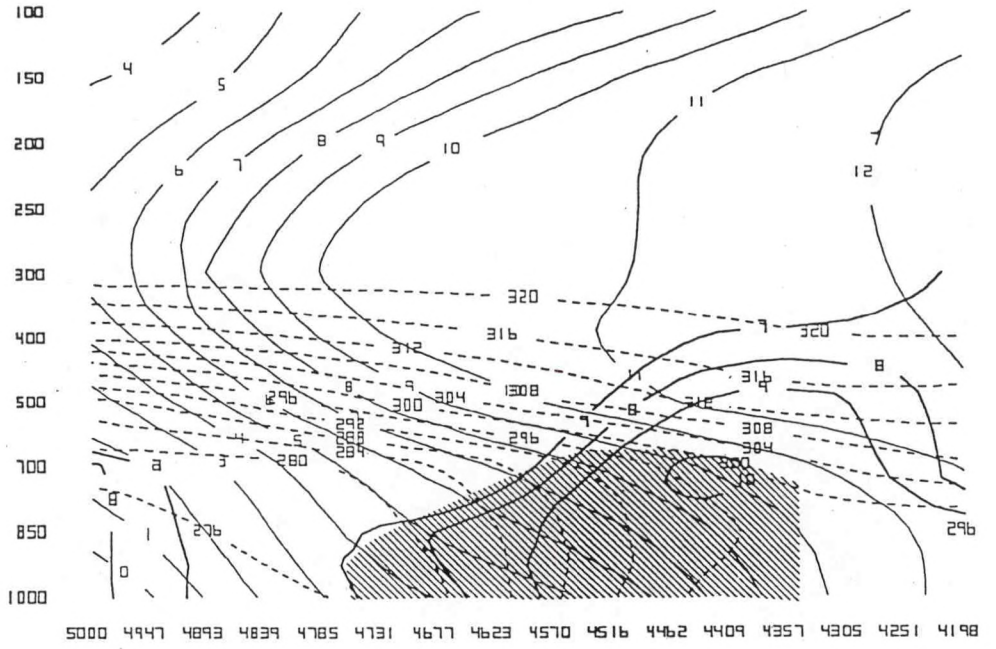

(b)

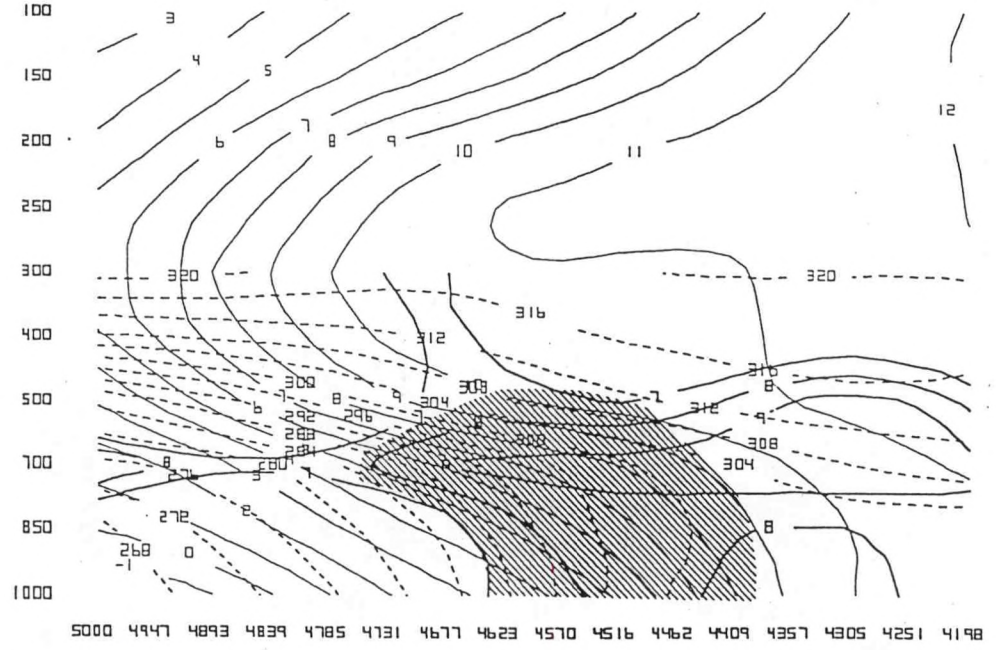

Figure 10. Cross-sections from the NGM model of equivalent potential temperature (dashed lines, every 4K), momentum (thin solid lines, every m s^{-1}) and relative humidity (thick solid lines ≥70 percent) for (a) 24 hour forecast and (b) 0000 hr forecast, both valid at 1200 UTC 24 February 1994. Shaded area represents region of conditional symmetric instability.

SESSION 7
WINTER WEATHER CLIMATOLOGY

22. A Climatology of Winter Weather Events over the Continental United States, 1982-1993

23. Climatology of Significant Snowfall Events in Southeast Arizona

24. Synoptic Climatology of Significant Weather Events In Northeast Nevada, Part I: Heavy Snow

A Climatology of Winter Weather Events in the Continental United States, 1982-1993

Michael L. Branick[1]

1. INTRODUCTION

As part of the National Centers for Environmental Prediction (NCEP), the Storm Prediction Center (SPC) will begin operational forecasting of severe winter weather for the Continental United States in the fall of 1997. This forecasting effort will be unprecedented in the National Weather Service (NWS), as forecasts will be short-term (6-12 h periods) and will address specific winter weather hazards (heavy snow, freezing precipitation, and blizzards) individually.

In order to determine operational requirements for the SPC winter weather forecast program, it is necessary to assess many climatological aspects of winter weather events--seasonal frequency, intensity, duration, and areal size distributions, to name a few. Data on these elements should assist SPC developers in planning issues such as staffing requirements, workloads, forecast formats, reasonable lead times, and forecast product schedules.

In this study, climatological data were assembled from all reported *Storm Data* winter weather entries from 1982-1993. Section 2 describes how state-by-state Storm Data entries and narratives were combined into events based on time-space continuity. In Section 3, results are presented from the database of over 1500 events. A discussion of forecast verification issues follows in Section 4, which addresses the suitability of Storm Data to serve as a source of verification data. Specific findings and recommendations, as related to the needs of SPC developers, are discussed in Section 5.

2. METHODOLOGY

All monthly Storm Data publications were scanned for entries with references to winter weather (heavy snow, blizzard, glaze, blowing snow, etc.). Since winter weather events often affect more than one state, there often are multiple entries for a given event (one from each area of Storm Data responsibility). Thus, it was necessary to determine which entries were part of the same event. This determination was made by passing through each monthly volume of Storm Data three times.

In the first pass, all winter weather entries were identified by date, type of event, and state. These entries were sorted chronologically and combined into events if it appeared obvious that they were continuous in time and space. Events were assigned titles ("Snow," "Ice," "Heavy Snow," "Ice Storm," "Ground Blizzard," "Blizzard," or "Extreme Cold") based on type of event and maximum reported snowfall or ice accumulation. A series of yes/no indicators was recorded in tabular form for each event indicating the reported presence or absence of heavy snow (HS), blowing/drifting snow (BS), freezing precipitation (ZR), wet snow (WS), high winds (HW), downed power lines (PL), and thunder/lightning with freezing or frozen precipitation (TS).

Each event identified in the first pass was examined more closely, entry by entry, in the second pass. To confirm time and space continuity, closer attention was paid to the dates and times of each entry and the geographical areas affected within each state. (During the period studied, most states reported these areas by referencing affected forecast zones within the respective state. A map of

1. Corresponding author address: Michael L. Branick, National Weather Service, 1200 Westheimer Drive, Norman, Oklahoma 73069.

these zones is published routinely in SD, making areal determinations simple.) Graphical outlines were drawn for each event, to document general size, shape, and geographic region affected. The second pass served to reinforce the listings obtained in the first pass, but sometimes led to refinements in event listings. Examples of refinements would be the combining of events that were originally listed separately, or splitting of single events into two, if closer inspection revealed that entries were or were not truly continuous.

Using the graphical outlines and the Storm Data narratives, each event was placed into one of four categories based on prevailing topographic influence and/or shape of the area affected: Elongated or banded (BA), circular or irregular in shape (CI), elevation-driven, (i.e., occurring mainly over mountainous terrain, M), or predominantly lake effect (L). (In most cases of lake effect, it was possible to separate lake effect and nonlake effect snowfall into separate events by examining the narratives closely. Some states routinely listed lake and nonlake effect components as separate entries, even when both were present around the same time and region.)

One should note that many aspects of this climatology involve some level of subjectivity. Some aspects are entirely subjective, and thus require subjective interpretation ("detective work") to transform the available information into useful climatological data. This is an unfortunate necessity when dealing with Storm Data winter weather entries. However, similar levels of subjectivity exist in the reporting of other severe weather elements (e.g., reported hail size, F-scale ratings), and yet such data are used extensively in climatological studies (e.g., Kelly et al. 1978, 1985).

To compensate as much as possible for subjectivity in the methodology, a third pass through Storm Data was conducted. Following completion of the second pass for the entire 12-year period, the second-pass procedure was repeated from the beginning of the database. Changes then were made to the database if analysis during the third pass seemed inconsistent with that during the second pass. This seeming redundancy was performed to ensure that the mostly-subjective method of combining and recording Storm Data entries and events remained consistent throughout the time the second-pass analysis was conducted. Few changes were found to be necessary during the third pass, lending support to the idea that the entire procedure was consistent and reliable despite the need to rely often on subjective data.

3. DATA SUMMARY.

Over the 12-year period, 1,521 events were identified (from an estimated 5,000-10,000 Storm Data entries). There were 1,867 "event days" days on which one or more events, or parts of events, occurred or 43 percent of all possible days. The number of events and event days was added up and examined by month, geographic area, size, intensity, and duration. Numbers also were broken down by type (heavy snow, blizzard, ice storm, etc.), yielding relative frequencies of these hazards.

A Types of Hazards

The breakdown of events by type is presented in Table 1. Heavy snow (defined here as a storm total of four inches or more from Texas and Oklahoma eastward to the Carolinas, and six inches or more elsewhere) has been the most frequent hazard by far, being present in 80 percent of all reported events. Significant ice (i.e., freezing rain or drizzle) was reported in only one-fourth of all events, and only half of those (or 13 percent of all events) qualified as ice storms by NWS definitions (glaze resulting in either structural damage or ice accumulations of 0.25 inches or more). Only 11 percent of all events qualified as blizzards (again, by NWS definition). Thunder was reported with freezing or frozen precipitation in five percent of all events, but the actual number of "thundersnow" and "thunder ice" events likely are larger since thunder is not a criterion for reporting in SD. The

high percentage of events that resulted in power outages (27 percent) is interesting, since less than half of them were ice storms. This finding shows that other factors, specifically wet snow and high winds, are the causal factors in more than half of all winter weather-related power outages.

TABLE 1
WINTER WEATHER EVENT DATA, 1982-1993

Type	Total #	Avg/yr	% of all events
All Events	1521	127	(100)
Event Days	1867	156	---
Events with heavy snow	1217	101	80
Events with significant ice	373	31	25
Ice storms	191	16	13
Blizzards	160	13	11
Events with thunder	79	7	5
Events with power outages	416	35	27

B. Yearly Trend

Figure 1 shows the number of reported events and event days by year. The steady increases in both reflect improvements in Storm Data reporting procedures over the years. Averages over the 12-year period are 127 events and 156 event days per year, but from Figure 1 it is apparent from the most recent years' data that actual averages likely are closer to 150 events and nearly 200 event days per year. Note that the number of events incorporates a certain amount of subjectivity (since one could debate whether a certain set of Storm Data entries constitutes one, two, or more events), but the number of event days is based only on calendar dates as reported in SD, and thus is less subject to debate. (A similar argument can be made for thunderstorm days vs. individual thunderstorms.) Therefore, the number of event days is particularly significant - especially when one notes from the nearly 200 day-per-year average that significant winter weather occurs within the Conterminous U.S. on more than half of all calendar days, averaged throughout the year.

C. Monthly and Seasonal Variations

Monthly variations in event frequency are shown in Figure 2. December had the highest frequency of events, followed closely by January. Note that events have occurred in every month, including July and August. (Summer events typically occur in the Rockies of Colorado, Wyoming, or Montana.) Events decrease steadily in number through the spring months, but the number of event days increases slightly from February into March. This finding suggests those late-winter events (i.e., in March) may be longer-lived, on average, than those in midwinter.

In order to examine seasonal variations in frequency in more detail, frequencies were calculated by calendar day. These numbers, expressed as percentages of possible days and smoothed by a seven-year running average, are shown in Figure 3. For any given calendar day, the data in Figure 3

approximate the probability of occurrence of significant winter weather somewhere within the Continental United States on that day. Peak frequencies are from late November through mid-January, exceeding 80 percent (roughly five days out of six) at several points. (Note, peaks in late November and middle to late December coincide with peak holiday travel periods, during which winter weather hazards are more likely to affect societal activities and thus are more likely to be reported.) In general, frequencies rise sharply from late October through mid-November, at which point they reach a relative plateau in the 70-80 percent range that persists through the end of March. High frequencies through March, April and early May are noteworthy, since these periods coincide with increasing frequencies of severe convective events (large hail and damaging convective winds; Kelly et al. 1985), also overlap the climatological peak for violent tornadoes (Kelly et al. 1978). Thus, the concurrence of severe winter weather and severe convective outbreaks appears inevitable, especially during early spring.

D. Horizontal Scale (Areal Coverage)

The "size" of a single winter weather event can vary by several orders of magnitude, from isolated local events (e.g., lake effect snow squalls) up to massive, paralyzing storms like the 1993 "Superstorm" (Kocin et al. 1995) that can affect a sizeable fraction of the Country. In order to evaluate this scale variation, all winter storms (i.e., those events that qualified as heavy snow events, ice storms, or blizzards) were rated based on the size of the area affected by winter storm conditions. Since objective measurement of such areas was virtually impossible (due to the qualitative nature of areal descriptions in many Storm Data entries, e.g., "Western South Dakota," "Northern mountains of Utah," "Southern third of Iowa"), this distribution was obtained by rating each winter storm subjectively into one of six areal size categories (0 to 5) as defined in Figure 4. While this approach is arguably imprecise, it actually was a simple matter to classify most events into one of the categories based on examination of the graphics produced during the second data pass.

Distribution of winter storms by size categories is shown in Figure 4. A vast majority of events were found to be confined to small areas: More than half-affected areas smaller than the state of Vermont ($\approx$9000 mi^2), and 85 percent affected areas smaller than Kansas ($\approx$82000 mi^2). This finding strongly indicates the importance of mesoscale processes in most winter weather systems. Effective short-term forecasting of such systems thus will require a thorough understanding of the mesoscale processes that produce and focus the often-localized areas of severe winter weather.

E. Local Duration

All events also were rated from 0 to 5 based on maximum reported local duration. Local duration is defined as the duration of the event at a given location (not to be confused with storm lifetime, which typically is considerably longer, especially for fast-moving or long-track systems.) As with areal coverage, one must deal with subjectivity in determining maximum duration since Storm Data time entries frequently are vague. Frequently, times of occurrence were given in qualitative terms such as "afternoon," "all day," etc., or only a single local time was given. In the latter case, it was not always clear whether the time was a start time or an end time for the event. And in cases where both start times and end times were given, there is no standard as to what constitutes the "start" and "end" of an event. However, in most events it is felt that Storm Data entries provided sufficient information to place events into one of the categories as defined in Figure 5.

As seen in Figure 5, most reported events (60 percent) lasted a maximum of 6 to 24 h locally. This finding has some bearing on viable forecast lead times and forecast intervals, suggesting that 24-h lead times and 12-h forecast intervals will be needed to "capture" most events in their entirety.

4. DISCUSSION - FORECAST VERIFICATION AND *STORM DATA* RELIABILITY

To improve forecast quality over time, and to document the level of improvement, forecasts must be verified systematically. This is true especially for new or "spin-up" forecast efforts, where forecast problems are more likely to arise. A structured verification effort, in turn, requires a reliable database with observed data on the element(s) being forecast. For the SPC winter weather program, verification will require observed data on snowfall and freezing rain measurements, and documentation of blizzard conditions. Yet, it is notable that no quantitative data exist anywhere regarding measurements of freezing rain accumulations or blizzard conditions. The only possible data source is SD, in which all such events (in theory) are reported and described, at least subjectively. Thus, one purpose of this research was to assess the quality and reliability of Storm Data as a database for verification of SPC (or any other) winter weather forecasts.

Several problems were found with winter weather documentation methods in SD. A few of these problems were discussed in the previous section (i.e., vague descriptions of areal coverage and start/end times). Other problems include variations in detail among entries from different states, regional differences in heavy snow criteria (12-h criteria vary locally and regionally from 4 to more than 12 inches), local economic factors (e.g., "blizzards" are never reported in the Colorado mountains, apparently due to the negative effect of that word on the ski industry; [Ruff, W. 1995, personal communication]), and general differences in reporting criteria from state to state. The latter problem sometimes led to sharp frequency gradients across state lines, as certain states seemed reluctant to report winter weather in Storm Data at all. While most entries included sufficient information in the narratives to assess the general impact of the event, the decidedly qualitative nature of most entries makes it difficult to evaluate many events objectively.

In general, improvements were noted in Storm Data winter weather reporting methods between the beginning and end of the period of study. It is felt that more improvements are needed before Storm Data can serve as a reliable source of forecast verification data. Improvements noted in recent years include more widespread inclusion of both start and end times of winter weather events (although exact definitions of what constitutes the start or end of an event remain elusive), increasing use of forecast zones or counties to better define areal coverage, and increasing numbers of reported winter weather events from several states or regions that rarely or never reported them previously. (This factor contributed heavily to the trend toward higher numbers shown in Figure 1). Needed improvements include definitions, or at least better guidelines, for determining when a winter weather event starts and ends; standardization in reporting of certain key elements such as maximum reported snowfall or ice accumulations; and more specific guidelines covering which events to report, so that similar events are reported similarly by each state or region affected. Perhaps a quality control program would ensure more standardization of reporting procedures and help to implement the above improvements. Since Storm Data is the only current source of ice and blizzard data (and that being mostly qualitative at present), it is vital to incorporate the above improvements. Alternatives are either a) develop an entirely new database and observing system for reporting freezing rain accumulations and blizzards, or b) forego verification of forecasts for these events. The first choice is considered impractical, and the second unacceptable.

5. FINDINGS AND RECOMMENDATIONS RELATED TO SPC OPERATIONS

The following preliminary findings and recommendations are tailored toward the primary purpose of this study, i.e. support of SPC operational planning. It is hoped that they will help in future decisions involving issues such as forecast content, staffing, forecast intervals, lead times, etc. Those findings that are not accompanied by recommendations are geared more toward forecasting (as opposed to forecast planning), and may be of greater use once forecast operations commence.

Finding 1: (ref. Figure 2): **Frequency peaks in early winter, but late-winter events tend to last longer.** See Section 3, Subsection C, for discussion.

Finding 2: (ref. Figure 3): **High frequency of wintertime events.** Nationally, hazardous winter weather occurs on average at least every other day from late October to late April. They are nearly daily occurrences from mid-November through March. *Recommendation: SPC should plan on at least one full-time winter weather forecaster on duty at all times beginning no later than November 1, and ending no sooner than April 30.*

Finding 3: (ref. Figure 3): **High winter event frequencies overlap severe convective season.** See Section 3, Subsection C, for discussion. *Recommendation: SPC should plan for multi-element events (with simultaneous winter weather, severe convection, and perhaps flash flooding), especially during late winter and early spring. There should be plans for extra staffing in the event of particularly severe or widespread multi-element events.*

Finding 4: (ref. Figure 4): **Most events affect very small areas.** See Section 3, Subsection D, for discussion. *Recommendations: 1) Emphasis at this time should be on spinning up the SPC Science Support Branch to develop short-term winter weather forecast skills (e.g. by assembling and testing techniques, studies, and applied research). 2) SPC products should adopt a probabilistic format (as opposed to, say, forecast isohyets or "yes/no" areal forecasts).*

Finding 5: (ref. Figure 5): **Most events last 12 hours or more locally.** See Section 3, Subsection E, for discussion. *Recommendation: "Routine" SPC winter weather forecasts should cover time periods of 0-12 and 12-24 hours.*

Finding 6: (ref. Figure 5): **Heavy snow is the predominant hazard.** See Section 3, Subsection A, for discussion.

Finding 7: SD, in its current state, is unsuitable as a verification source. See Section 4 for a detailed discussion. *Recommendations: 1] Remind offices with Storm Data responsibility that all significant weather events, including winter storms, should be reported in Storm Data per NWS Operations Manual (WSOM) Chapter F-42,* Storm Data *and Related Reports. 2] Incorporate guidelines into WSOM F-42 that standardize titles of winter weather events. 3] Incorporate enhancements into WSOM F-42 regarding detail levels. 4] Clarify procedures for reporting beginning and ending times of long-duration events. 5] Include forecast verification as an SPC function.*

Finding 8: There is no consistent procedure for real-time dissemination of most winter weather reports. Ground-truth information is needed in real time to track a forecast's performance. This is true for all NWS offices, not just the SPC. Currently, some states use special weather statements (AFOS category SPS) to report snowfall, ice, or significant "impact" reports (road closings, ice damage, etc.), but often do so well after the event is over. Other offices use public information statements (PNS). Still others use state or area weather summaries (SWS). Very few use local storm reports (LSRs) to report anything other than severe convective events (hail, tornadoes, etc.). Real-time winter reports could be standardized easily through guidelines calling for issuance of winter weather LSRs by all WFOs. *Recommendation: Develop guidelines for reporting and disseminating winter weather events in real time as LSRs.*

6. FUTURE WORK

The current database will be updated yearly as appropriate Storm Data volumes become available. (Data for 1994 currently is being analyzed, and will be added soon.) Data analysis will continue in several areas, most notably in the area of geographic distribution. Current ongoing

research involves computation of bi-monthly event frequencies over a 1-degree latitude-longitude grid. Results should help to locate areas or corridors of enhanced (or suppressed) winter weather activity, and shifts in such perturbations through the seasons. Other ongoing and/or planned research topics include a closer, more quantitative look at factors related to power outages, and development of an intensity rating system for use in comparing blizzards, ice storms, and heavy snow events. Other ideas doubtlessly will arise with time, perhaps involving local or regional tendencies.

The climatological database currently is stored in standard text format on a year-to year basis. Each event is condensed into two lines of data; the entire 12-year database "catalogue" is roughly 80 hard-copy pages . These data are available for anyone wishing to use them for local or regional studies. Prospective users should contact the author for further information. Graphic products are simple hand-drawn maps (about another 80 pages) which are color-coded based on type of event, and thus are not easy to reproduce for distribution in large quantities.

7. REFERENCES

Kelly, D.L., J.T. Schaefer, R.P. McNulty, C.A. Doswell III, and R.F. Abbey, Jr., 1978: An augmented tornado climatology. *Mon. Wea. Rev.*, **106**, 1172-1183.

_____, _____, and C.A. Doswell III, 1985: The climatology of non-tornadic severe thunderstorm events. *Mon. Wea. Rev.*, **113**, 1997-2014.

Kocin, P.J., P.N. Schumacher, R.F. Morales, Jr., and L.W. Uccellini, 1995: Overview of the 12-14 March 1993 Superstorm. *Bull. Amer. Meteor. Soc.*, **76**, 165-182

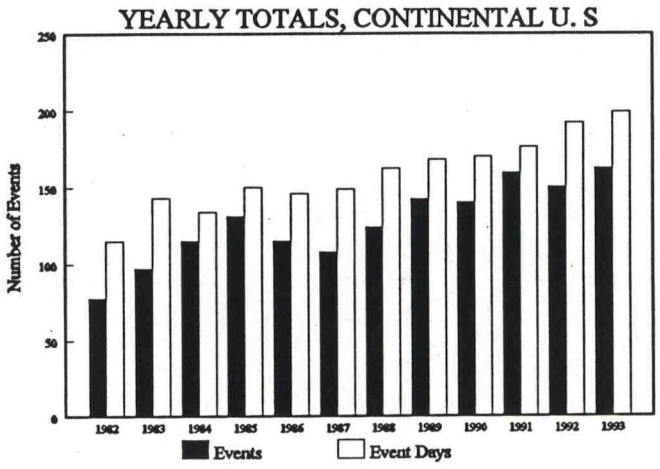

Figure 1. Yearly number of reported winter weather events and event days within the Continental United States, 1982-1993.

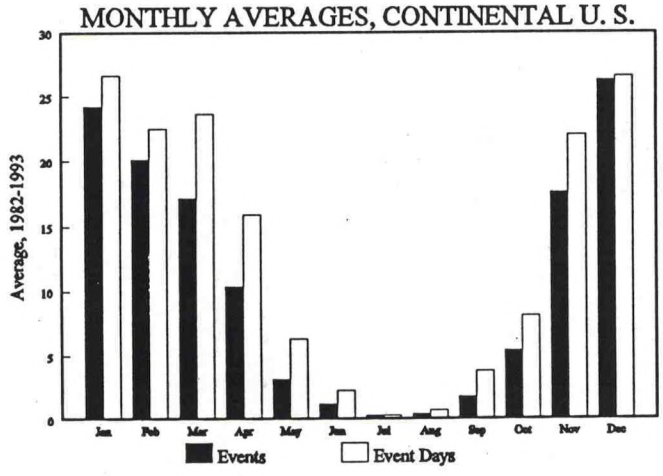

Figure 2. Monthly percentage of days with reported winter weather events within the Continental United States, 1982-1993.

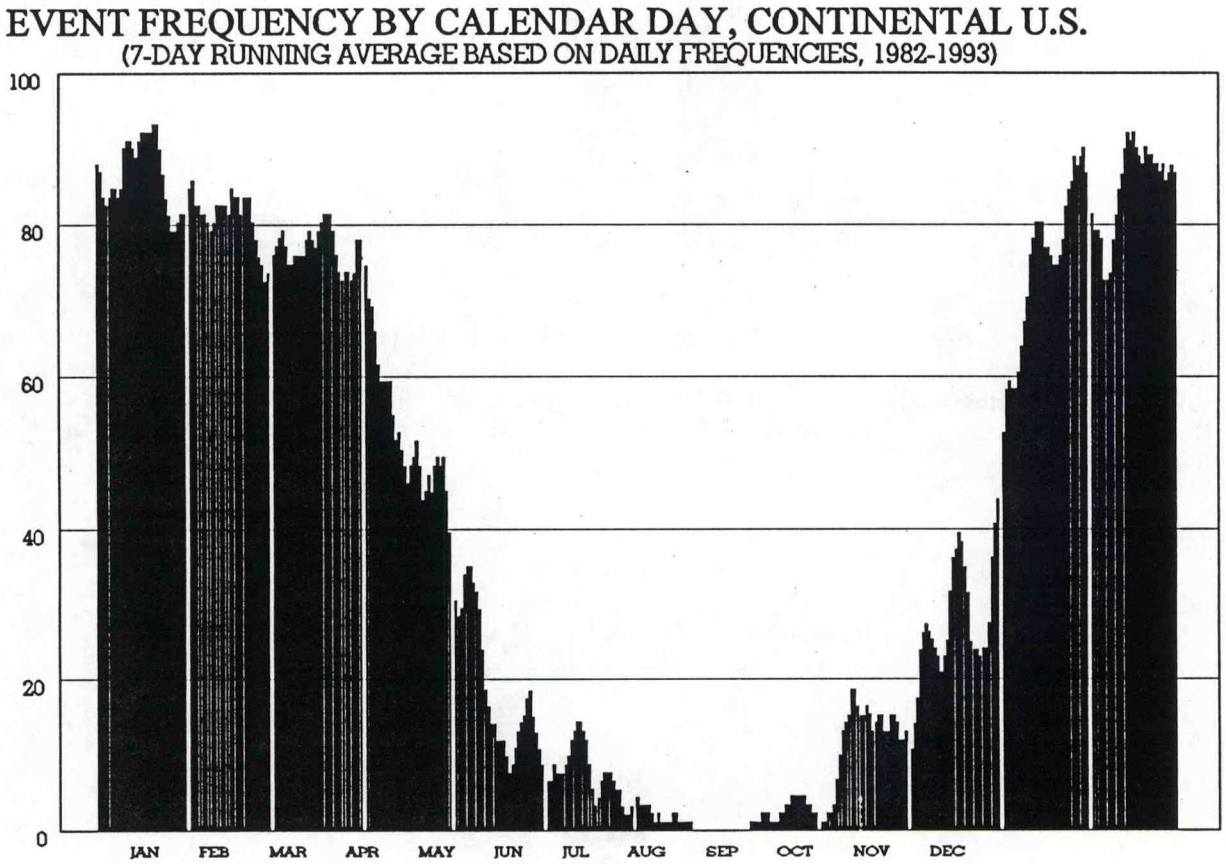

Figure 3. Percentage of winter weather days as a function of calendar day, based on a seven-day running average. Number for a given day represents the percent of time that significant winter weather occurred somewhere within the Continental U. S. on that day during the period 1982-1993.

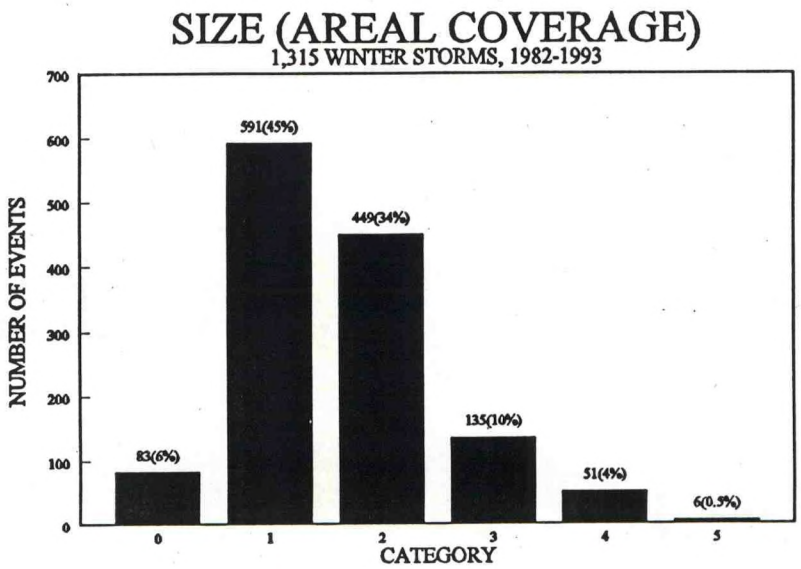

Figure 4. Distribution of winter storms by size of affected area. Size classifications are as follows: 0 - Isolated report, up to roughly the size of two average counties; 1- Larger than two counties but smaller than Vermont; 2 - Larger than Vermont, but smaller than Kansas; 3 - One to three times the size of Kansas; 4 - Three to six times the size of Kansas; 5 - More than six times the size of Kansas.

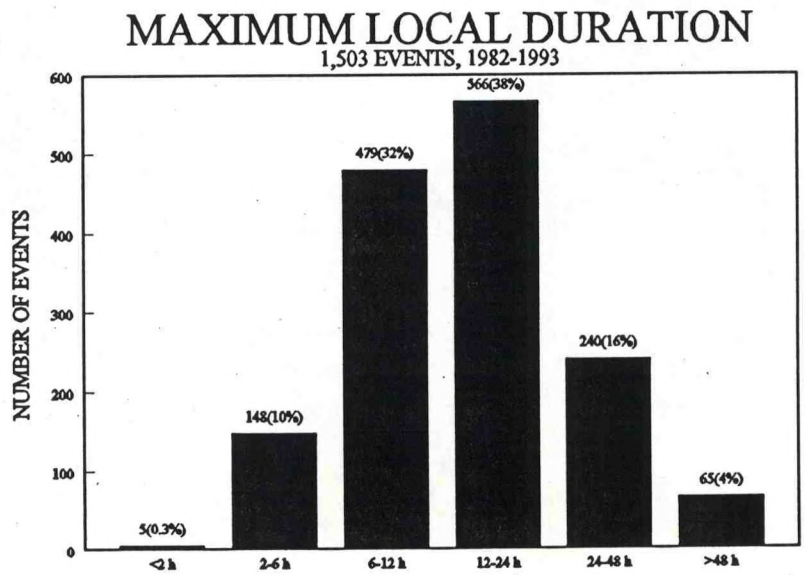

Figure 5. Distribution of winter weather events by maximum local duration. Categories refer to the maximum reported duration at a given location, and should not be confused with the lifetime of the event (which typically was considerably longer).

Climatology of Significant Snowfall Events in Southeast Arizona

Darren McCollum[1] and Jim Meyer[2]

1. INTRODUCTION

Forecasting significant winter snowfall events for southeast Arizona is a challenge. As a spin-up forecast office, this problem will soon fall to Tucson forecasters. While much of the area of responsibility for the Tucson forecast office is known for extreme summer temperatures and heavy "monsoon" thunderstorms, the higher elevation eastern portions of the area can experience significant snowfall during the winter months. These events occur less frequently in southeast Arizona than in the mountainous areas of northern Arizona and are poorly understood.

There are few references focusing on southeast Arizona winter forecasting. There are climatological overviews of winter weather in southeast Arizona (Green and Sellers 1964) but they are only of general seasonal use and do not address specific forecasting difficulties. The attempt in this study was to identify synoptic patterns and other related meteorological characteristics associated with significant snowfall events in southeast Arizona.

2. DATA ANALYSIS

Cases for analysis were selected using the publication CLIMATOLOGICAL DATA for Arizona and examining the record of cooperative station snowfall reports in southeast Arizona for the period 1985-94. Snowfall events were classified using the criteria listed in Table 1.

TABLE 1

MOUNTAINS	HIGH DESERT
normal <125 mm	normal <25 mm
125 mm≤heavy <200 mm	25 mm≤heavy <50 mm
extreme ≥ 200 mm	extreme ≥ 50 mm
One occurrence or greater constituted a case	

Using the set of snowfall events 1200 UTC 500, 700 and 850-hPa mean charts were composited using the NMC Upper Air Gridded data set (available on CD-ROM) for the period 1985 through 1989. Likewise, mean 1200 UTC soundings from Tucson were composited using the NCDC Historical North American RAOB data set (available on CD-ROM).

3. RESULTS

Analysis of the cooperative station snowfall data indicates that significant snowfall in the mountains of southeast Arizona (mean height 2160 m) and the high deserts (mean height 1190 m) occurs simultaneously only 29 percent of the time. Significant snowfall in southeast Arizona is most

1. Corresponding author address: Darren McCollum, NWSO, Tucson, Arizona.
2. Jim Meyer, NWSO, Tucson, Arizona,

likely to occur during the months of December, January and February. A significant snowfall event in the high desert ranges from 50 to 150 mm of accumulation. While significant snow accumulations in the mountain areas of southeast Arizona range from 125 to 250 mm.

The following is a presentation of the 1200 UTC 500-hPa charts and Tucson soundings preceding mountain and high desert snowfall events.

A. Mountain Snowfall Events

1.) 1200 UTC 500-hPa charts

Figure 1a, b, and c shows the 1200 UTC 500-hPa setting that precedes normal (Figure 1a), heavy (Figure 2a) and extreme (Figure 3a) mountain snowfall events. The charts indicate that, in general, when snow events occur in the mountains of southeast Arizona a split in the polar jet flow exists over the northwest United States with equally strong northern and southern branches. The southern branch typically contains a short wave that is amplifying as it enters the region of an existing long wave trough.

A general progression can be identified between the three charts. In the normal 1200 UTC mean 500-hPa chart (Figure 1a) there is a split in the flow just off the northwest United States coast with a vigorous short wave moving across the southwestern United States. This is a fast moving, medium amplitude system.

Figure 1b shows the heavy 1200 UTC mean 500-hPa setting. The main difference from the normal 500-hPa chart (Figure 1a) is that the split flow is shifted more inland over southwest British Columbia in Canada and the northwest United States. This pattern is higher amplitude than the normal chart (Figure 1a) with a more meridional orientation and a slower east-west progression of the short wave.

Figure 1c shows the 1200 UTC mean 500-hPa pattern for the extreme mountain snowfall events. The split in the flow is located over the northwest United States with an even higher amplitude pattern. In Figure 1c the short wave is deepening the long wave trough into southern California. The packing of the height gradient to the southwest of the shortwave suggests the potential for further deepening with this particular pattern and an even slower east-west progression of the short wave. Also, the 500-hPa heights for the extreme event are the lowest of the three types of snowfall events.

The 500-hPa charts show that significant mountain snowfall events are associated with higher amplitude patterns in the southern branch of the polar jet flow. A shortwave, imbedded within this high amplitude pattern, takes a north to south track just inland over the western United States. At this point low level moist and warm air from the Pacific is likely advected into the system resulting in elevated snow levels.

2.) 1200 UTC mean Tucson sounding

The 1200 UTC mean Tucson sounding (Figure 2) for extreme mountain snowfall events reveals that the mean freezing level is approximately 2430 m, well above the elevation of the high deserts. Also, if a near surface parcel is raised to the lifted condensation level saturation occurs at about -2.0 C. This is a prime temperature regime for the production of heavy snow. Also note that in the lowest layers of the 1200 UTC Tucson sounding (Figure 2) the flow is out of the southwest with temperatures well above freezing. This suggests that in the lowest layers a modified air mass of eastern Pacific origins is likely drawn into the system.

B. High Desert Events

1.) 1200 UTC 500-hPa charts

Figure 3a, b, and c shows the 1200 UTC mean 500-hPa chart for the high desert normal, heavy and extreme snowfall events respectively. The synoptic settings for high desert snowfall events are similar to those observed for the mountain snowfall events. With increasing snow accumulations in the high desert the amplitude of the 1200 UTC 500-hPa pattern increases, the depth of the system becomes greater, 500-hPa heights over southeast Arizona become progressively lower and the east-west progression of the associated short wave trough is slower.

However, there are important differences between the mountain and high desert snowfall 1200 UTC 500-hPa charts. The short wave associated with the desert snowfall events takes a track much further inland than in the mountain snowfall events. This is apparently due to the southwest to northeast ridge axis extending over western Canada in the high desert snowfall events, especially in the heavy and extreme cases. This results in the split in the polar jet flow being located over the lee side of the United States and Canadian Rockies. Short wave troughs deepening as they move southward over the inter-mountain west and Great Basin tap primarily cold continental air which accounts for the extremely low 500-hPa heights, especially in the extreme snowfall events. Also worth noticing is that the southern branch of the split flow is the much stronger than the northern branch for the high desert snowfall events.

2.) 1200 UTC Tucson sounding

The 1200 UTC mean Tucson sounding (Figure 4) for the extreme high desert snowfall events reveals a much colder low to mid level air mass. At 1200 UTC the temperature at Tucson is slightly above freezing with higher elevations below freezing. The lower level winds are distinctly weak with the suggestion that flow from the east or northeast is the most common wind during these events. This suggests drainage of cold air from the high terrain of eastern and northeastern Arizona the result of the cold air dome associated with the distinctly inland movement of the short wave. It is also much drier than the sounding for the mountain cases. If a parcel near the surface is lifted in the sounding it saturates at a temperature of approximately -8.0 C which is much colder than for the mountain event likely resulting in less efficient snow production.

4. CONCLUSIONS

Only 29 percent of the time does a significant snowfall event hit both the mountains and the high desert. This is due primarily to the difference between the synoptic patterns that bring snowfall to southeast Arizona.

The similarities between the synoptic settings for significant mountain and high desert snowfall events are they are both high amplitude medium wave length patterns with slow east to west movement of synoptic scale features (thus allowing for ample accumulations). The primary difference between the two types of events is that in the high desert events the digging short wave takes a much more inland track and is accompanied by a colder and drier air mass that inhibits significant snow accumulations in the mountains.

When the mountains get a heavy event the deserts rarely see significant accumulations because the digging short wave takes a path southward along the extreme western United States. The air mass is modified somewhat by trajectories over the Pacific Ocean (especially in the low levels) resulting in a more warm and moist air mass. The snow level is normally above the highest desert

locations and the mean 1200 UTC extreme mountain sounding suggests the potential for optimum snow production at the level of the mountain stations.

5. ACKNOWLEDGEMENTS

The authors would like to thank David Bright help in acquiring data sets and developing the graphics used in this paper.

6. REFERENCES

Green, C.R., and W.D. Sellers, 1964: *Arizona Climate*. University of Arizona Press, Tucson, 503 pp.

NOAA, NESDIS, NCDC, 1985-94: Climatological Data Arizona, 88-98.

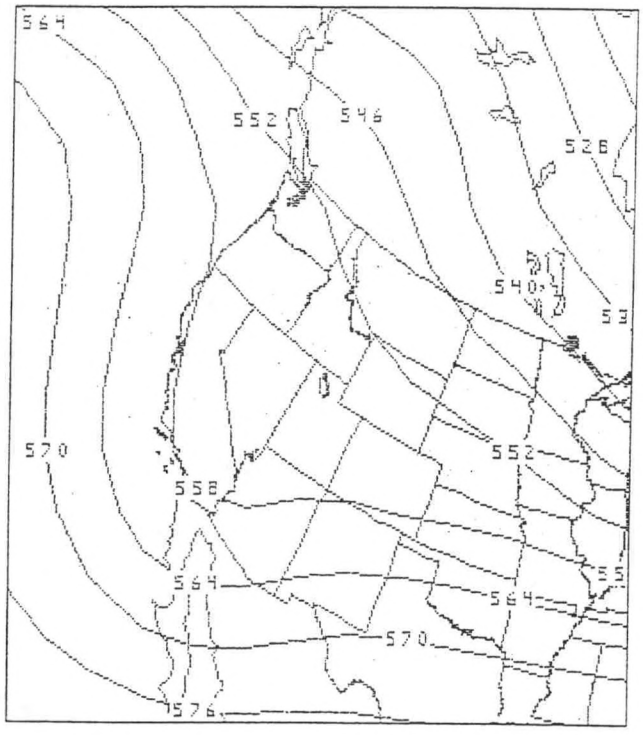

(A)

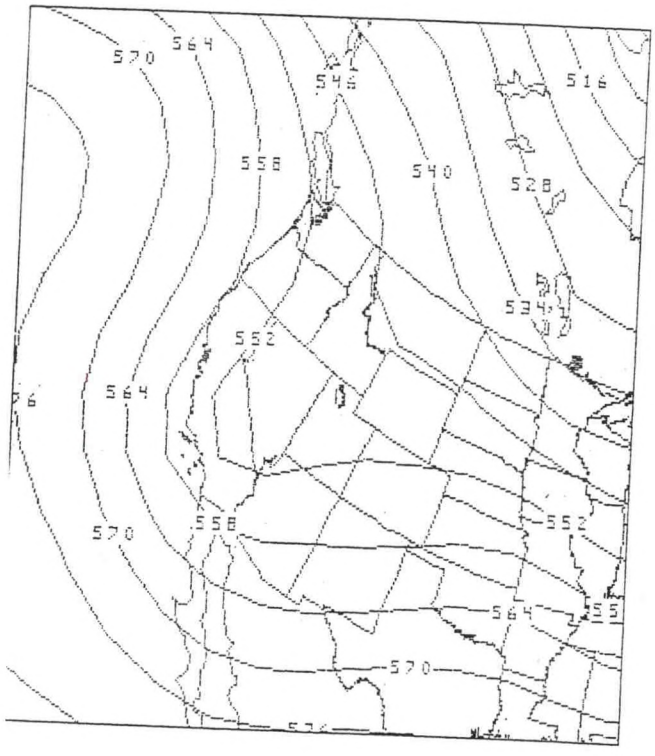

(B)

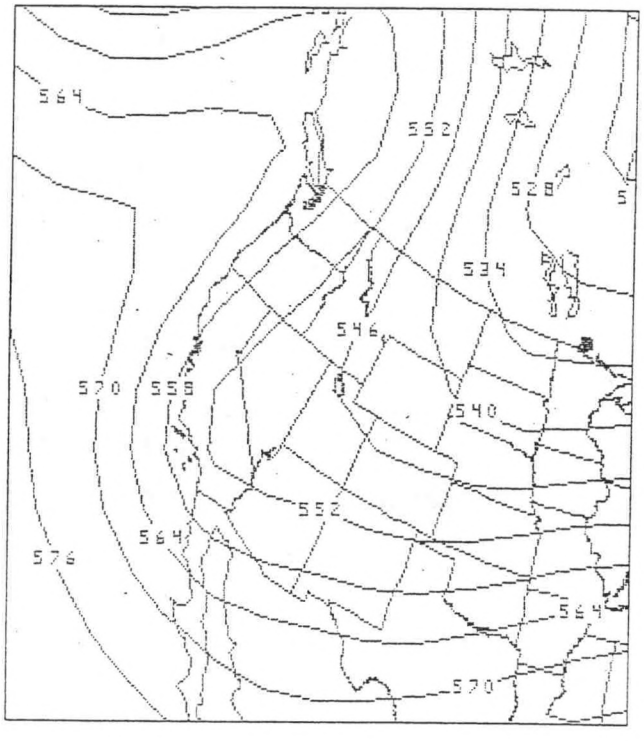

(C)

Figure 1. a) Normal, b) Heavy, and c) Extreme mountain snowfall 1200 UTC 500 hPa charts.

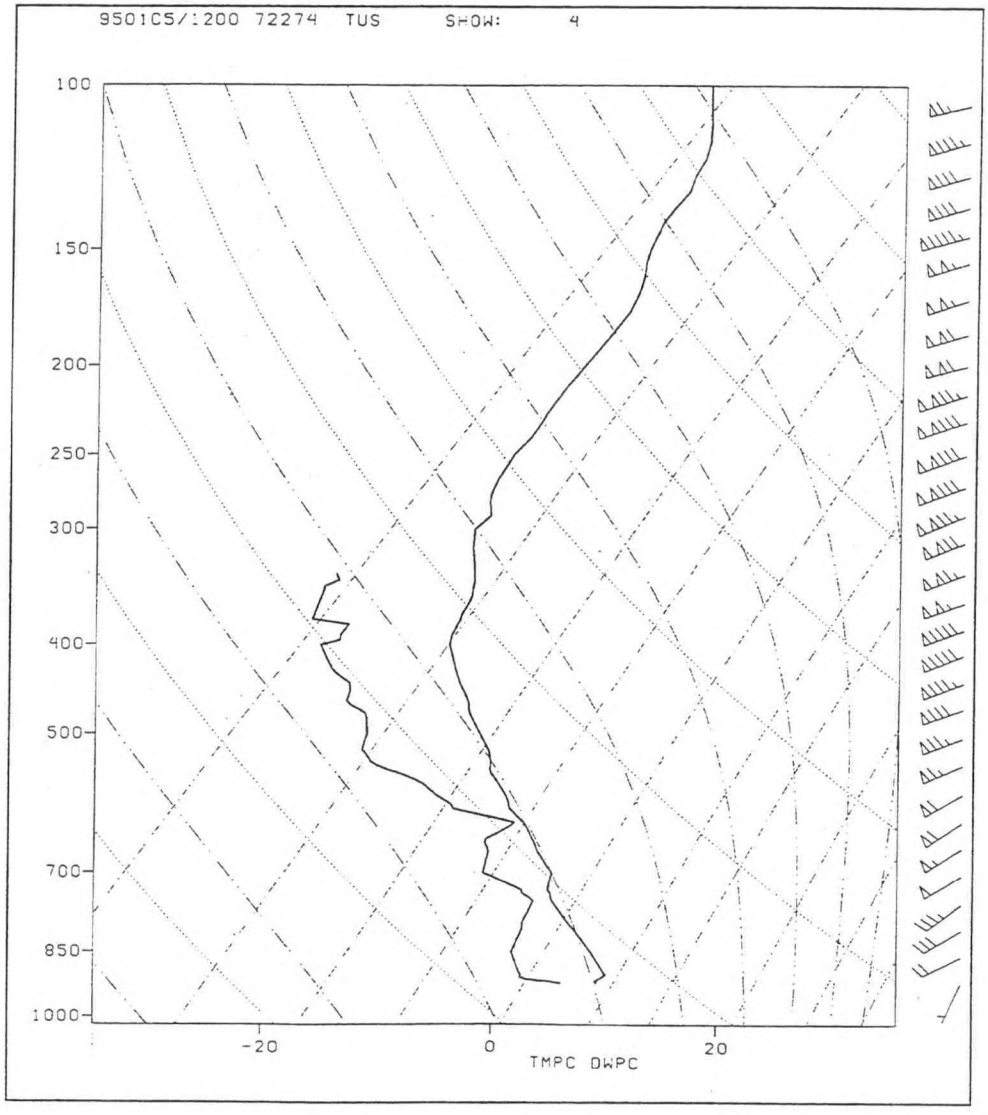

Figure 2. The 1200 UTC mean Tucson sounding preceding extreme mountain snowfall events.

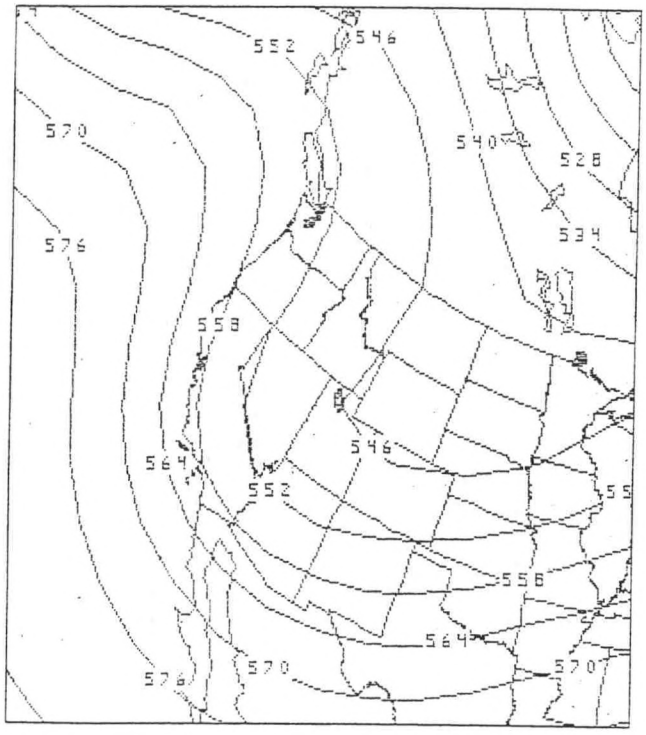

(A)

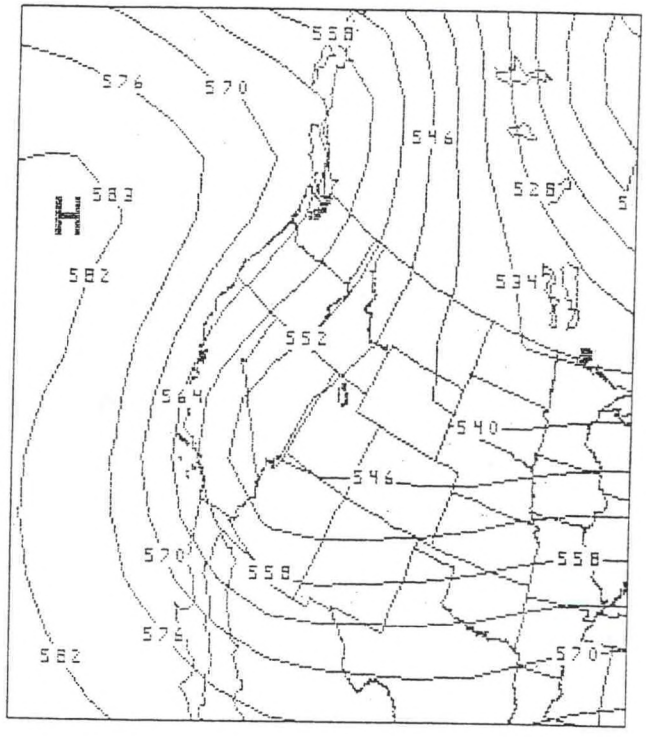

(B)

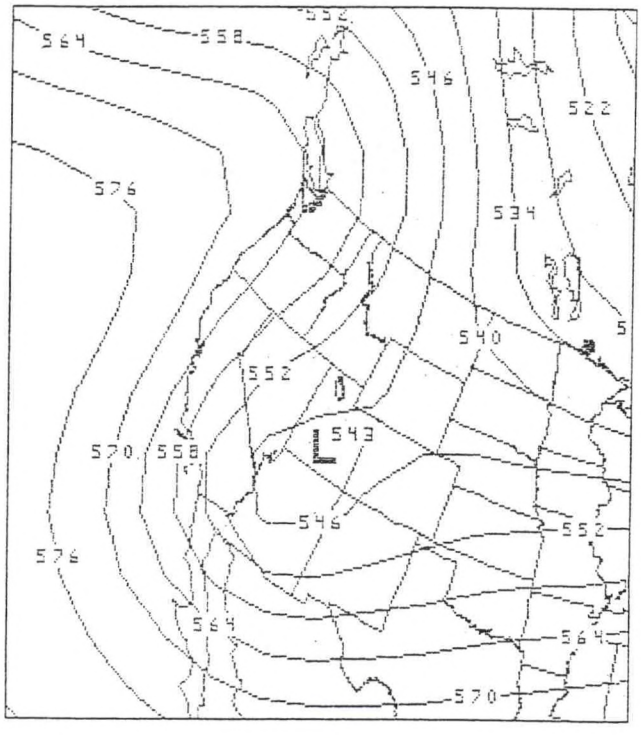

(C)

Figure 3. a) Normal, b) Heavy, and c) extreme desert snowfall 1200 UTC 500 hPa charts.

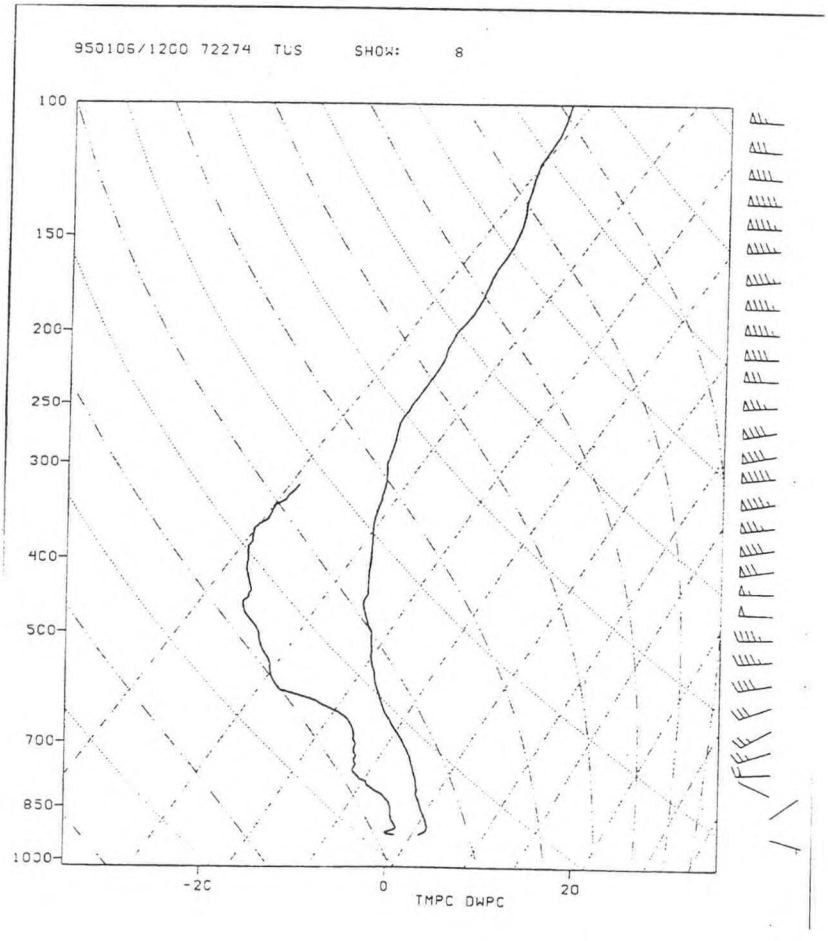

Figure 4. The 1200 UTC mean Tucson sounding preceding extreme desert snowfall events.

Synoptic Climatology of Significant Weather Events in Northeast Nevada, Part I: Heavy Snow

Jeffrey P. Craven[1] and Edwin C. Clark[2]

1. INTRODUCTION

The National Weather Service Modernization and Associated Restructuring (MAR) effort has created many training related challenges for each Science and Operations Officers (SOO). One such challenge occurs at "Spin-Up" offices, where meteorologists are usually new to the forecast area and may have little knowledge of local climatology. Well-documented case studies or climatologies of heavy snow events are often scarce or do not pertain to the specific areas of interest within the county warning area. The purpose of this study was to provide the incoming staff with a detailed analysis of the synoptic characteristics of significant snow events across Northeast Nevada.

A. Methodology

The basis of the study was the use of the NMCDraw program developed by Richard LeBlang of National Weather Service Forecast Office (NWSFO) Bismarck (Fors and LeBlang, 1993). The program was used to composite 20 years of data from 1970-1989, available on the National Meteorological Center Grid Point Data Set Version II CD-ROM. The study was motivated by a composite of heavy rainfall events in San Diego (Atkin and Reynolds, 1995). Another helpful paper looked at flow patterns favorable for producing heavy snow in the Big Horn Mountains of North Central Wyoming (Darrow, 1995). These studies categorized the events by certain temperature and flow pattern regimes for a small area of interest.

The current study separated snow events of 4 inches or more in a 24 hour period by month of occurrence, with events in the period of October through May included. No attempt was made to separate the events by flow patterns, and if any location in the county of interest met the snowfall criteria, then the event was included in the composites. The entire modern NWSO Elko County Warning Area was studied, divided into the following four geographic areas:

1. Northwest Nevada: Humboldt County including Winnemucca (seven reporting stations included).
2. Northeast Nevada: Elko County including Elko (15 reporting stations included).
3. East Central Nevada: Lander and Eureka Counties, including Battle Mountain (five reporting stations included).
4. East Central Nevada: White Pine County including Ely (five reporting stations included). A total of 32 stations were in the dataset.

The composited charts include 250 mb winds, 500 mb heights, 700 mb heights and temperatures, 850 mb heights and temperatures, and surface MSL pressure. This led to the creation of over 400 individual charts: mean monthly chart of snow events, mean monthly chart for all days in 20 year period, departures from the 20 year mean, and standard deviations.

1. Corresponding author address: Jeffrey P. Craven, National Weather Service Office, Elko Nevada. (Current affiliation Storm Prediction Center, Kansas City, Missouri.)
2. Edwin C. Clark, National Weather Service Office, Elko Nevada.

Table 1 lists the mean values of various useful parameters of height, temperature, and thickness for Elko, Winnemucca, and Ely. This data was derived from careful analysis and comparison of the mean charts created in the study. Using programs such as PCGRIDDS and N-AWIPS, forecast values of these various parameters can be easily compared with historic values to access the potential for heavy snow in a particular county.

TABLE 1
VARIOUS MEAN VALUES FOR 4"+ 24 HOUR SNOW EVENTS FROM 1970-1989

MEAN VALUES DURING HEAVY SNOW EVENTS

ELKO

			Thickness Values (mb)				
Month	50H	70T	1000-500	1000-850	1000-700	850-700	850-500
OCT	5590	-5	5470	1350	2910	1555	4120
NOV	5520	-7	5430	1350	2890	1540	4080
DEC	5500	-10	5400	1350	2870	1520	4045
JAN	5520	-8	5400	1335	2865	1530	4065
FEB	5500	-8	5410	1345	2880	1535	4065
MAR	5500	-8	5430	1360	2900	1540	4070
APR	5510	-7	5440	1360	2905	1545	4080
MAY	5540	-4	5490	1365	2930	1565	4125

WINNEMUCCA

			Thickness Values (mb)				
Month	50H	70T	1000-500	1000-850	1000-700	850-700	850-500
OCT	5590	-3	5500	1350	2925	1575	4150
NOV	5520	-7	5430	1335	2880	1545	4095
DEC	5500	-9	5400	1335	2865	1530	4060
JAN	5500	-9	5380	1325	2860	1535	4055
FEB	5450	-10	5370	1335	2860	1525	035
MAR	5410	-11	5360	1340	2870	1530	4020
APR	5460	-9	5400	1340	2875	1535	4055
MAY	5540	-6	5470	1360	2915	1555	4110

ELY

			Thickness Values (mb)				
Month	50H	70T	1000-500	1000-850	1000-700	850-700	850-500
OCT	5580	-4	5480	1360	2925	1565	4125
NOV	5500	-6	5470	1370	2920	1550	4100
DEC	5480	-10	5380	1335	2865	1530	4040
JAN	5500	-8	5410	1345	2880	1535	4065
FEB	5480	-8	5410	1350	2885	1535	4060
MAR	5480	-7	5430	1355	2900	1545	4075
APR	5490	-7	5450	1365	2910	1545	4085
MAY	5530	-5	5480	1370	2930	1560	4110

3. RESULTS

The enormous number of composite charts available for interpretation is beyond the scope of this paper, and will be used locally at the Elko office for training purposes. Some example charts for the month of November are included for Elko County (Figures 1 and 2) and White Pine County/Ely (Figures 3 and 4). Four panel displays of MSL pressure and departure from normal, 500 mb heights

and departure from normal, 700 mb heights and departure from normal, and 700 mb temperatures and standard deviation are included for the two areas.

A total of 38 charts were composited for White Pine County in November, with 116 for Elko County. A striking difference in flow patterns is evident. Elko County events are characterized by a broad long wave trough centered over the Four Corners states, with one short wave trough (at 700 mb and 500 mb) pulling out into the central plains and another digging into Northern California and Oregon from the northwest. One surface low is shown over the Texas Panhandle, while another is indicated west of the Washington Coast. Surface pressures are below normal over much of the Great Basin and Central Rocky Mountains, with the biggest departure near Wendover, Utah. Departures from normal are greatest at 700 mb and 500 mb over the Pacific Northwest, with a minimum around Pendleton, Oregon. The 700 mb temperature over the county is roughly -7°C.

White Pine County events in November (Ely area) indicate a much higher amplitude pattern, with a long wave trough over the Great Basin and a deep short wave trough at 700/500 mb digging down the California coast toward Nevada. The departures from normal are more-extreme than with the Elko County events, and are located farther southwest over southern Oregon and Northern California. The surface pressure anomaly is in about the same location, but is twice as deep. The pattern of 700 mb temperatures indicates a favored temperature of -6°C but the amplitude is much higher.

4. SUMMARY

Composite mapping of frequently used synoptic charts provides an excellent way to train a staff on the synoptic patterns associated with significant weather events in a particular area. When used in conjunction with individual case studies, the overall regimes necessary to produce the event can be better understood and hopefully anticipated in future forecast situations.

The composite charts can easily be arranged in a reference binder available to the staff in the operational area of a National Weather Service Office. Studies of Heavy Snow, Ice Storms, Severe Hail, Severe Convective Winds, Tornadoes, High Gradient Winds, Dense Fog, Heavy Rain/Flash Flooding, etc., can be completed at all the local offices as needed.

4. ACKNOWLEDGEMENTS

The authors would like to thank Summer Student Trainees' Melanie Carr and Chris Moore for the weeks of research that made the study possible. Also, thanks for the helpful tips on how to attack the composite chart problems from numerous NWS Western Region Science and Operations Officers.

5. REFERENCES

Atkin, D.V., and J.A. Reynolds, 1995: Composite Maps of Selected Rainfall Events in San Diego. Western Region Technical Attachment 95-06. National Weather Service, Scientific Services Division, Salt Lake City, UT.

Darrow, M.A, 1995: Flow Patterns Conducive for Heavy Snow in the Northern Big Horn Mountains of North Central Wyoming. *Natl Wea. Dig.*, **19**, 2-9.

Fors, J.R., and R.S. LeBlang, 1993: Synoptic Composites of Three Significant Weather Types in North Dakota Using NMC Gridded Data on CD-ROM. *Preprint, Weather Analysis and Forecasting Conference*, Vienna, VA, AMS (Boston)..

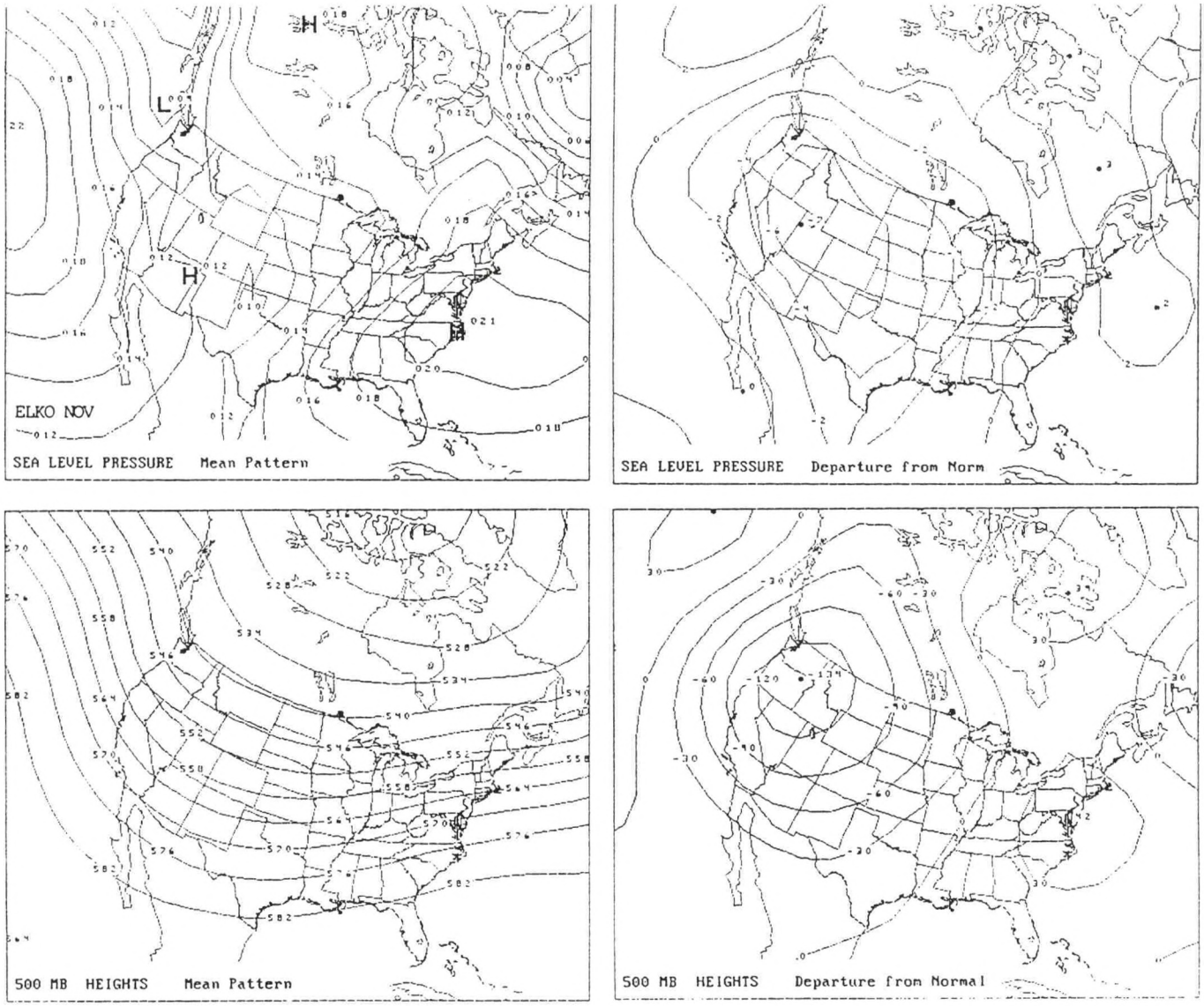

Figure 1. For Elko County in November: **top**-mean sea level pressure pattern and departure from 20 year mean pressure; **bottom**-mean 500 mb height and departure from 20 year mean 500 mb height.

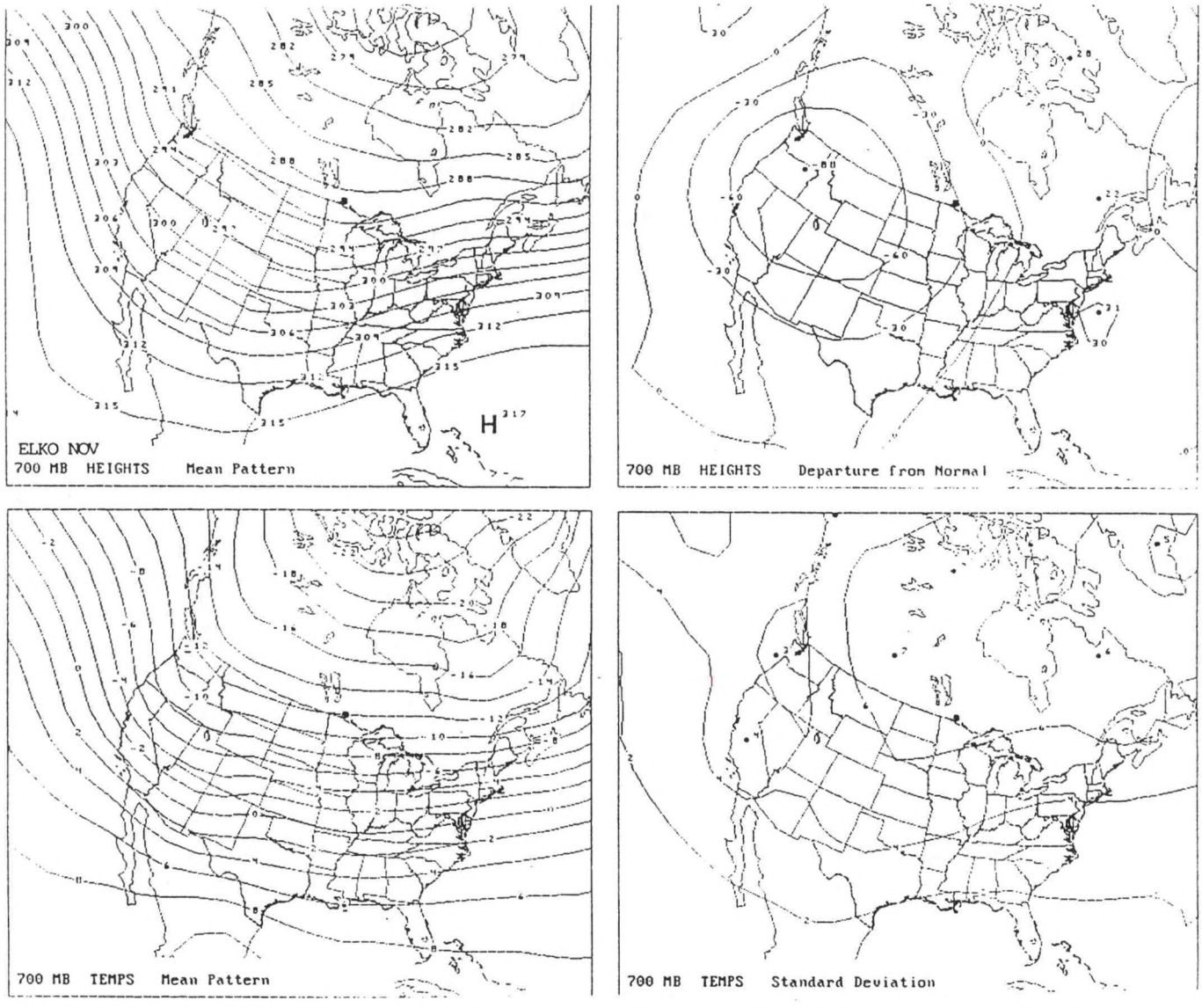

Figure 2. For Elko County in November: **top**-mean 700 mb height and departure from 20 year mean 700 mb height; **bottom**-mean 700 mb temperature in °C and standard deviation of 700 mb temperature in °C.

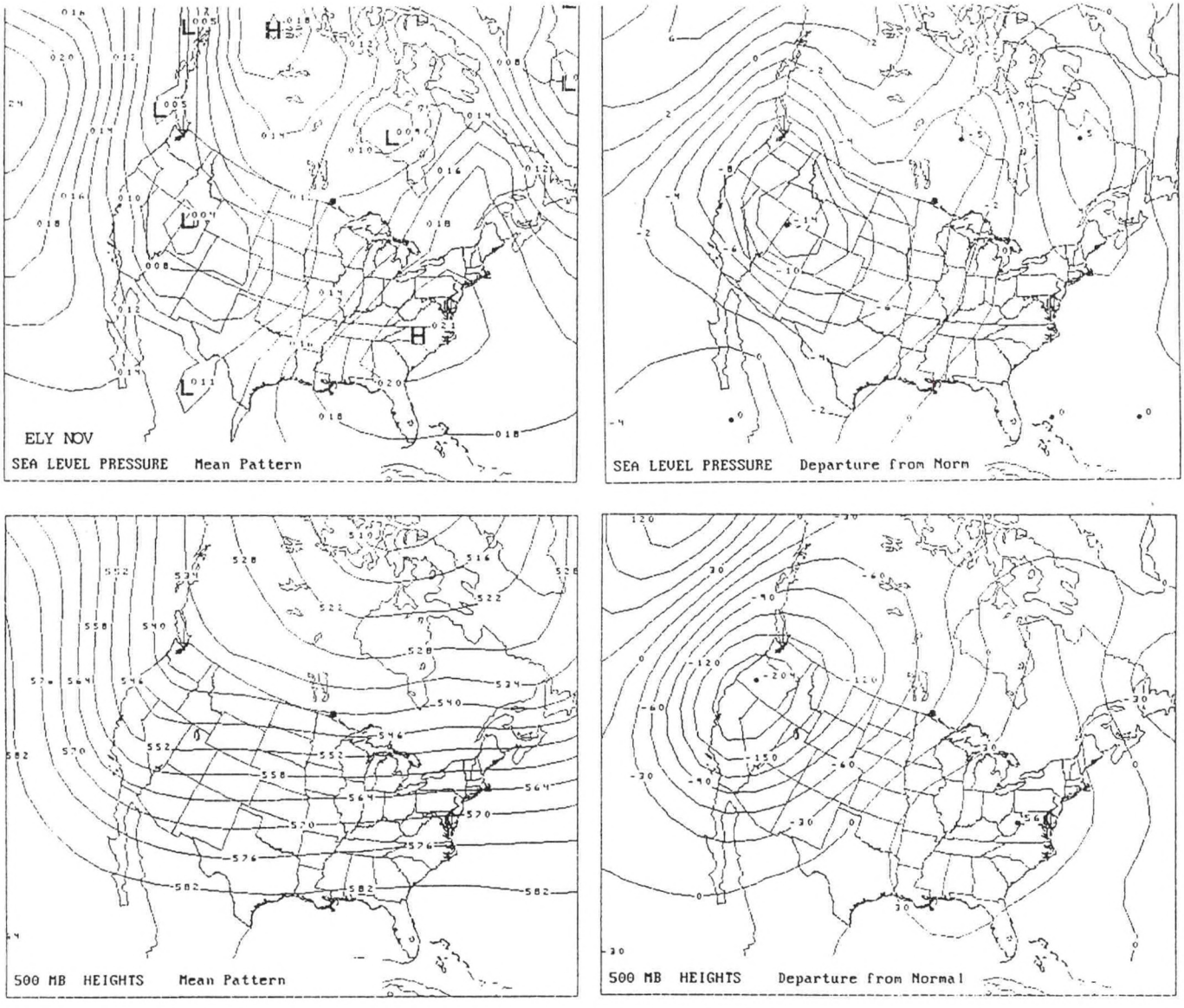

Figure 3. For White Pine County (Ely) in November: **top**-mean sea level pressure pattern and departure from 20 year mean pressure; **bottom**-mean 500 mb height and departure from 20 year mean 500 mb height.

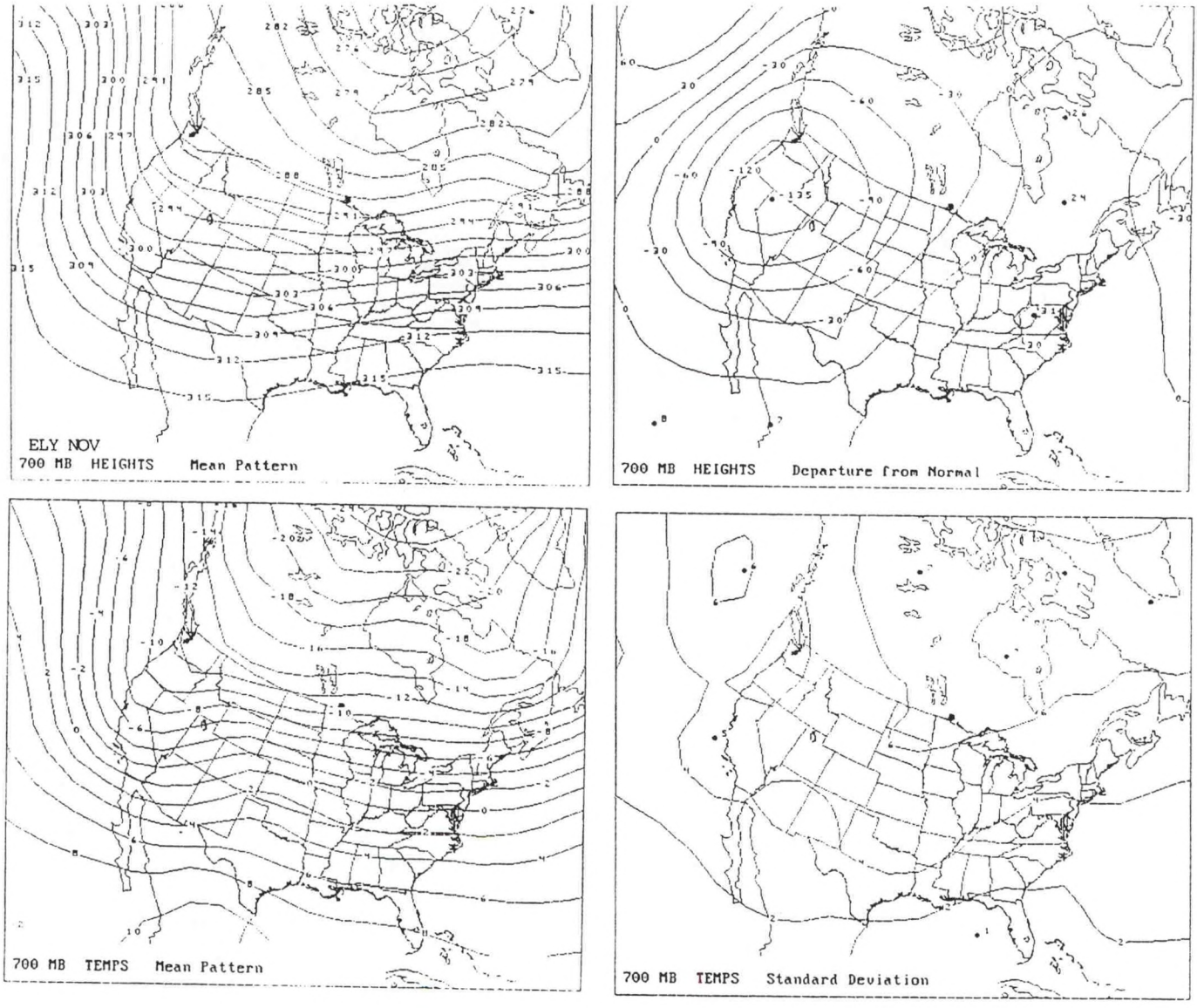

Figure 4. For White Pine County (Ely) in November: **top**-mean 700 mb height and departure from 20 year mean 700 mb height; **bottom**-mean 700 mb temperature in °C and standard deviation of 700 mb temperature in °C.

SESSION 8
WINTER CONVECTION/LIGHTNING

Heavy Rain Events Associated with Elevated Thunderstorms in The Midwest

Scott M. Rochette[1], James T. Moore[2], Patrick S. Market[3], Fred H. Glass[4], and Dan L. Ferry[5]

1. INTRODUCTION

Heavy convective rainfall has been in the headlines in the Midwestern United States for the past several years. Our cooperative group has been conducting research into this problem since 1993, and has archived numerous events of excessive precipitation and flash flooding around the central United States. Some of these events are characterized by mesoscale convective system (MCS) development on the cool side of a west-east oriented quasi-stationary surface boundary. Often these are comprised of *elevated* thunderstorms, which occur above a stable boundary layer and are isolated from surface diabatic effects (Colman 1990 a,b). His climatology of elevated thunderstorms indicates two separate and distinct maxima, with the primary maximum occurring in April and a second in September. In addition, Colman (1990a, b) explains that most winter season thunderstorms are of this type.

We have found that these types of MCS are a substantial source of heavy rainfall in the central Midwest. As a result, MCSs consisting of elevated thunderstorms and the conditions associated with their genesis deserve further investigation. The focus of this paper is to examine the synoptic-mesoscale environment leading to the development of organized elevated convection resulting in excessive rainfall.

2. PREVIOUS WORK

Examination of the large-scale conditions associated with elevated thunderstorms reveals that these MCSs initiate in scenarios that fit the "frontal" or "meso high" pattern described by Maddox et al. (1979). They note that in these situations the MCS forms to the north of a quasi-stationary surface boundary (front, outflow boundary), an environment characterized by a statically stable boundary layer. The present study focuses on seven individual MCS events that fit our criteria, which will be listed later in this paper. The research expands upon that of Maddox et al. (1979), where composite analyses of standard and derived fields are produced from rawinsonde data to quantitatively and qualitatively illustrate the typical synoptic-mesoscale features associated with the initiation of heavy rainfall-producing MCSs comprised of elevated thunderstorms.

In their study of nocturnal MCS development, Augustine and Caracena (1994) implemented compositing software to examine the lower-tropospheric precursors to the initiation of these thunderstorms. The emphasis of their research was on the evolution of the low-level jet (LLJ) and the role of lower-tropospheric frontogenetical forcing in the formation of large and small MCSs. Their composites centered either on the location of the initial storms or the cloud shield centroid at the time of maximum areal extent. Using observed surface and 850 mb data, they found that large, long-lived MCSs form during local early morning in the area where the LLJ intercepts a region of 850

1. Corresponding author address: Scott M. Rochette, Department of Earth and Atmospheric Sciences, Saint Louis, 3507 Laclede Ave., University, St. Louis, MO. St. Louis, MO 63103-2010; e-mail: rochette@eas.slu.edu.
2. James T. Moore, Department of Earth and Atmospheric Sciences, 3507 Laclede Ave., Saint Louis University, St. Louis, MO.
3. Patrick S. Market, Department of Earth and Atmospheric Sciences, 3507 Laclede Ave., Saint Louis University, St. Louis, MO.
4. Fred H. Glass, National Weather Service Forecast Office, St. Charles, MO.
5. Dan L. Ferry, National Weather Service Forecast Office, St. Charles, MO.

mb frontogenesis, north of a surface boundary. This frontogenetical forcing generally enhances the direct thermal circulation (DTC), and subsequent convective activity. Smaller MCSs were associated with a weak (if at all present) front, and *not* with frontogenetical forcing.

Glass et al. (1995) employed a similar approach, using gridded numerical data from the Nested Grid Model (NGM) to form a conceptual model for heavy rainfall events in the Mid-Mississippi Valley. They produced subjective 9x9 grid composite fields via the Personal Computer-Gridded Display and Diagnostic System (PC-GRIDDS) for 0000 and 1200 UTC initialization times. The parameter analyses were centered on MCS initiation areas that occurred within +/- 3h of the observation time. They utilized these storm-relative, non-temporal composites to produce a conceptual model of heavy rain-producing MCSs, which form north of a west-east oriented surface boundary and south of a 850 mb θ_e advection maximum, which is coupled with a southerly LLJ. This region is especially favored if the surface boundary is quasi-stationary and the 850-300 mb thickness contours are diffluent.

3. METHODOLOGY AND DATA SETS

In the current study compositing software was developed by the first two authors for use with observed rawinsonde data sets. Composite fields included both standard and derived fields, such as stability indices, thicknesses, and low-level moisture transport vectors (defined as the product of mixing ratio and wind velocity). Each parameter was first objectively analyzed via a Barnes (1973) scheme on a 31x23 LFM-type grid (190.5 km grid spacing; Figure 1). Each MCS event was examined to determine the point of initiation, which was approximated to the nearest grid point. A 9x9 subgrid centered on this grid point was computed for each parameter in each MCS event. Each subgrid was then averaged and plotted.

In order for an MCS to be considered for this study, it had to meet several criteria. To ensure representativeness of the data the MCS must have initiated within +/- 4h of rawinsonde observation time (0000/1200 UTC). An event was chosen if it was comprised of convection that displayed the three main characteristics of elevated thunderstorms defined by Colman (1990a, b):

A. thunderstorms develop on the cool side of a quasi-stationary surface boundary in relatively cool, stable air,
B. surface air on the warm side of the boundary has higher θ_e values than the air on the cool side of the front, and
C. surface wind, temperature and dew point fields proximal to the thunderstorms were qualitatively similar to the immediately surrounding values.

The MCS also had to occur in the "Midwest" region of the grid, and had to result in at least 100 mm (4 in.) of rain within 24h.

A difference between the elevated thunderstorms studied by Colman (1990a, b) and the storms in this study are the presence of *elevated* convective instability in the region of MCS initiation in all seven cases. Figure 2 is an illustration of this concept; this is a vertical profile of θ_e at Monett, MO (72349) for one of the MCS cases (1200 UTC 6 June 1993). Note the decrease of θ_e with height (convective instability) above a stable boundary layer marked by increasing θ_e from the surface to about 890 mb (convective stability). The elevated thunderstorms in Colman's study mainly occurred in environments characterized by convective stability. Table 1 lists the statistics of the seven MCS events involved in the composite study. Note that not all of the events occurred in what could be defined as the "cool" season. This paper marks a philosophy change that reflects this fact; the research group paid less attention to the time of year of the event and more to the position of the

MCS with respect to the surface boundary, collecting cases that occurred in the cool sector of the large-scale system.

TABLE 1.
HEAVY CONVECTIVE RAINFALL EVENTS ASSOCIATED WITH ELEVATED THUNDERSTORMS USED IN COMPOSITE STUDY.

Date	Init. Time	MCS Lat/Lon	Max. Rainfall
6 June 1993	1200 UTC	39.2N/93.6W	150 mm
21-22 September 1993	2000 UTC	41.0N/94.6W	225 mm
22-23 September 1993	2000 UTC	39.IN/91.7W	165 mm
10-11 April 1994	2100 UTC	38.3N/96.0W	270 mm
27-28 April 1994	2100 UTC	36.5N/96.0W	170 mm
29 April 1995	0200 UTC	36.5N/96.0W	150 mm
16 May 1995	0900 UTC	39.IN/91.7W	100 mm (est)

These elevated thunderstorm events bolster the concept of maximum parcel convective available potential energy (CAPE), as proposed by Doswell and Rasmussen (1994). They note that more energy is realized by using the most unstable parcel in the lowest 300 mb layer, as opposed to using a mean parcel from the lowest 100 mb. Figure 3 is a skew T-log P diagram for Monett, MO (72349) for the case listed above. The hatched region represents CAPE based on the mean 100 mb parcel, while the shaded region represents the additional energy realized based on the most unstable parcel. Mean parcel CAPE for this time and location is 2258 J kg^{-1}, while the CAPE based on the most unstable parcel increases by nearly 100 percent (4256 J kg^{-1}). This finding illustrates the gravity of using the most unstable parcel in cases of elevated convection, as the mean parcel CAPE may not be truly representative of the instability associated with the parcel that actually gets lifted.

4. COMPOSITE RESULTS

The figures show the storm-centered composite results based on the seven MCS cases listed in Table 1. The asterisk in the center of the diagrams represents the center of the composite MCS; it is located in north-central Missouri for scaling purposes only, as each MCS event initiated over a different location. The composites are intended to illustrate the spatial relation of synoptic and meso-α scale features in the standard and derived fields to the initiation point of the elevated MCS, and not with respect to a specific geographic location or point in time. It should also be noted that the magnitudes of the parameters could be diminished relative to actual event values due to the averaging of the compositing software and/or smoothing from the objective analysis.

Starting with the lower levels, Figure 4 illustrates composite 850 mb wind vectors and isotachs. The LLJ is instrumental in MCS development as it transports heat and moisture into the thunderstorm environment (Pitchford and London 1962; Bonner 1968). The average heavy rain-producing MCS develops about 200 km downstream from a 850 mb wind maximum (12 m s^{-1}) in the region of maximum low-level speed convergence. The effect of the LLJ is well depicted in Figures 5

and 6, average 850 mb θ_e advection and moisture convergence for the seven MCS cases. The MCS initiated in a region characterized by a maximum of θ_e advection (>+2.7 K h^{-1}) and moisture convergence (>+1.2 g kg^{-1} h^{-1}). Perhaps the transport of moisture-rich air into the initiation region is best illustrated by the use of 850 mb moisture transport vectors (Figure 7), defined as the product of the mixing ratio (q) and the vector wind ($\bar{v}$). Excessive rain-producing MCS development is favored about 400 km downstream and to the east of the moisture transport vector maximum. In the future we wish to reconstruct moisture transport vectors on isentropic surfaces, as this would be more representative of the preconvective environment. Similar but weaker patterns with respect to the initiation point were found at 700 mb (not shown).

The 500 mb composite height and vorticity analyses (not shown) indicate that the MCS is favored underneath anticyclonically curved height contours. In addition, there is a weak shortwave trough upstream of the MCS initiation point with weak positive vorticity advection (PVA). This closely resembles the frontal and meso high flash flood scenarios described by Maddox et al. (1979). Winds at this level (not shown) depict a small wind maximum (23 m s^{-1}) to the northeast of the MCS initiation point, with strong veering from 850 mb (southerly) to 500 mb (nearly westerly). Further aloft, the 200 mb wind pattern is generally from the west and west-southwest. Figure 8 reveals a 43 m s^{-1} jet streak to the north-northeast of the MCS initiation region, indicating that MCS formation is favored underneath the right entrance region of the upper-level jet (ULJ), an area of divergence aloft and enhanced upward vertical motion. This is confirmed in Figure 9, which shows that the MCS forms to the south of the 200 mb divergence maximum (+4.0 x 10^{-5} s^{-1}). This agrees with the results of work done by McNulty (1978), who found that severe convection tended to develop in the gradient region, typically south of an upper-level divergence maximum.

In addition, most stability parameters were also composited for the seven cases. lifted index (LI), computed from a mean lowest-100 mb parcel, is illustrated in Figure 10. The LI in the MCS initiation point is +1°C, indicating a modestly stable boundary layer associated with elevated thunderstorms. The Showalter index (SI; not shown) was also computed, giving a value of -2°C in the MCS region, which revealed that a parcel lifted from 850 mb was more unstable than its boundary layer counterpart, a result that was not surprising. More remarkable was the composited K index (KI), a helpful indicator of heavy rainfall potential (Funk 1991). Figure 11 reveals a value of 28°C in the region of MCS initiation; Funk (1991) noted that a value of ≥30 signifies the potential for heavy convective rainfall.

In order to estimate the degree of elevated convective instability, the algebraic difference between θ_e at 500 and 850 mb was computed (Figure 12). The MCS initiation region is characterized by a value of -9 K, indicative of convective instability. More negative values were found upstream of the MCS region, signifying greater instability. Admittedly this is a crude approximation, but the results are representative of the environment in which these MCSs develop. In short, while the lower-middle troposphere was modestly unstable (as judged by the SI), lifting the 850-500 mb layer to saturation would decrease its overall stability further. Such lift could easily be accomplished by low-level warm air advection and/or differential vorticity advection.

As one can deduce, heavy rain situations are usually characterized by environments rich in low-middle level moisture, which help to increase precipitation efficiency. Different parameters were composited to judge the degree of moisture present. Composited precipitable water (PW; Figure 13) shows that value exceeded 30 mm (1.2 in.) in the area of MCS initiation, with higher values upstream. In addition, surface-500 mb mean relative humidity (not shown) displays values > 60 percent over the MCS initiation point.

5. CONCLUSIONS

Standard, kinematic and thermodynamic atmospheric parameters were averaged for seven heavy rain episodes in the Midwest associated with elevated thunderstorms. These composite fields reveal that MCSs in these events are initiated:

A. About 200 km downstream from the nose of the LLJ, as denoted by the 850 mb wind field;
B. In a region characterized by strong positive θ_e advection and moisture convergence at 850 mb;
C. About 400 km downstream and to the east of the 850 mb moisture transport vector maximum;
D. In a region of mid-level anticyclonic curvature and downstream of a weak 500 mb short wave trough/PVA;
E. In an environment characterized by moderate speed shear and strong veering in the vertical;
F. Underneath the right entrance region of an ULJ, south of a 200 mb divergence maximum;
G. In a region characterized by positive LIs, slightly negative SIs, high KIs, and elevated convective instability;
H. In an area of high low to mid-level moisture (PW > 30 mm, mean $RH_{sfc\text{-}500}$ > 60%).

It must be noted that some composite values are weaker than those from the actual events for reasons addressed previously. More important than actual magnitudes are the patterns in each field and its relation to other fields. Future plans include the addition of new MCS events that meet the given criteria and the compositing of objectively-analyzed CAPE, both mean-parcel and most unstable, which was shown to be significantly increased in the case of elevated convection. It is also hoped that isentropic fields may be composited in the future. Finally, it is possible that the compositing software could be applied to the study of other meteorological phenomena.

6. ACKNOWLEDGEMENTS

The authors wish to thank Steven Thomas (MIC/AM, WSFO STL) and Ron Przybylinski (SOO, WSFO STL) for their comments and administrative support during this study. In addition, Ann McCarthy, Sean Nolan, and Jim O'Sullivan, graduate students at Saint Louis University, provided insight and helpful suggestions in many aspects of this research, and important feedback concerning the presentation of this paper by the lead author. This paper is funded from a Subaward under a cooperative agreement between the National Oceanic and Atmospheric Administration (NOAA) and the University Corporation for Atmospheric Research (UCAR). The views expressed herein are those of the authors and do not necessarily reflect the views of NOAA, its sub-agencies, or UCAR.

7. REFERENCES

Augustine, J.A., and F. Caracena, 1994: Lower-tropospheric precursors to nocturnal MCS development over the central United States. *Wea. Forecasting*, **9**, 116-135.

Barnes, S.L., 1973: Mesoscale objective map analysis using weighted time-series observations. NOAA Tech. Memo. ERL NSSL-62, 60 pp.

Bonner, W.D., 1968: Climatology of the low-level jet. *Mon. Wea. Rev.*, **96**, 833-850.

Colman, B.R., 1990a: Thunderstorms above frontal surfaces in environments without positive CAPE. Part I: A climatology. *Mon. Wea. Rev.*, **118**, 1103-1121.

_____, 1990b: Thunderstorms above frontal surfaces in environments without positive CAPE. Part II: Organization and instability mechanisms. *Mon. Wea. Rev.*, **118**, 1123-1144.

Doswell, C.A., III, and E.N. Rasmussen, 1994: The effect of neglecting the virtual temperature correction on CAPE calculations. *Wea. Forecasting*, **9**, 625-629.

Funk, T.W., 1991: Forecasting techniques utilized by the forecast branch of the National Meteorological Center during a major convective rainfall event. *Wea. Forecasting*, **6**, 548-564.

Glass, F.H., D.L. Ferry, J.T. Moore, and S.M. Nolan, 1995: Characteristics of heavy convective rainfall events across the Mid-Mississippi Valley during the warm season: Meteorological conditions and a conceptual model. *Preprints, 14th Conf. on Weather Forecasting and Analysis*, Dallas, TX, AMS (Boston), 173-180.

Maddox, R.A., C.F. Chappell, and L.R. Hoxit, 1979: Synoptic and meso-α scale aspects of flash flood events. *Bull. Amer. Meteor. Soc.*, **60**, 115-123.

McNulty, R.P., 1978: On upper tropospheric kinematics and severe weather occurrences. *Mon. Wea. Rev.*, **106**, 662-672.

Pitchford, K.L., and J. London, 1962: The low-level jet as related to nocturnal thunderstorms over Midwest United States. *J. Appl. Meteor.*, **1**, 43-47.

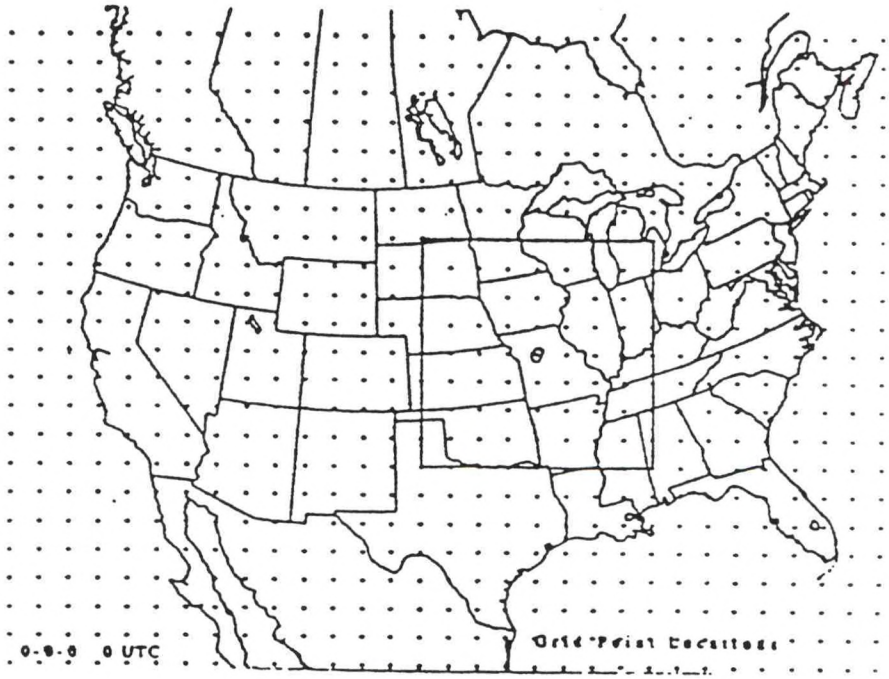

Figure 1. 31x23 grid used in compositing software. Squared area represents Midwest region of grid; central point is circled.

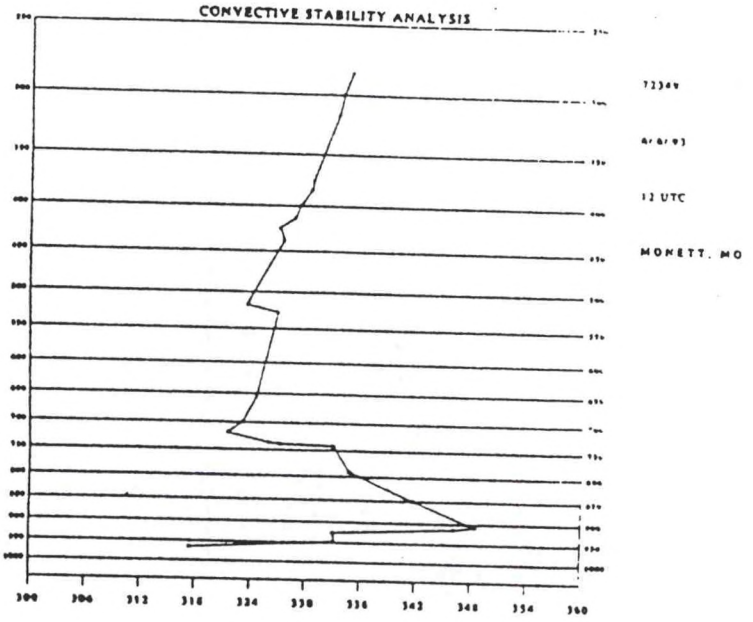

Figure 2. Vertical θ_e profile (K) for Monett, Missouri (72349) at 1200 UTC 6 June 1993.

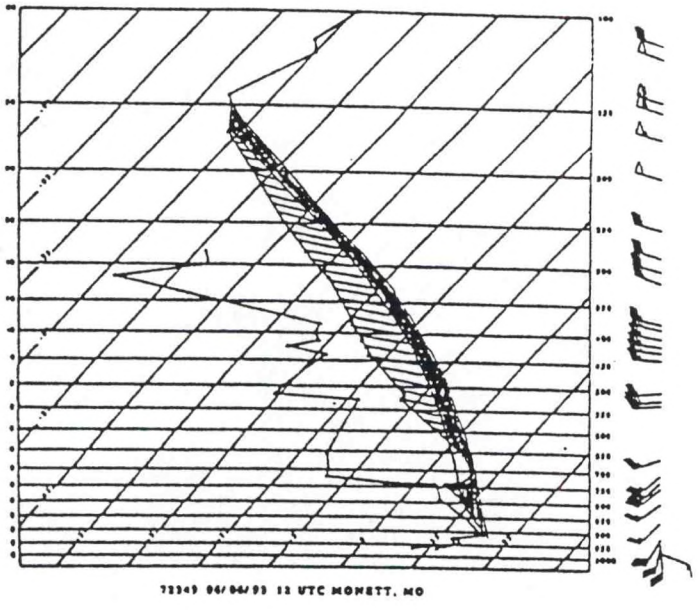

Figure 3. Skew T-log P diagram for Monett, Missouri (72349) at 1200 UTC 6 June 1993. Hatched region represents mean parcel CAPE, while shaded region represents additional CAPE from use of max θ_e parcel.

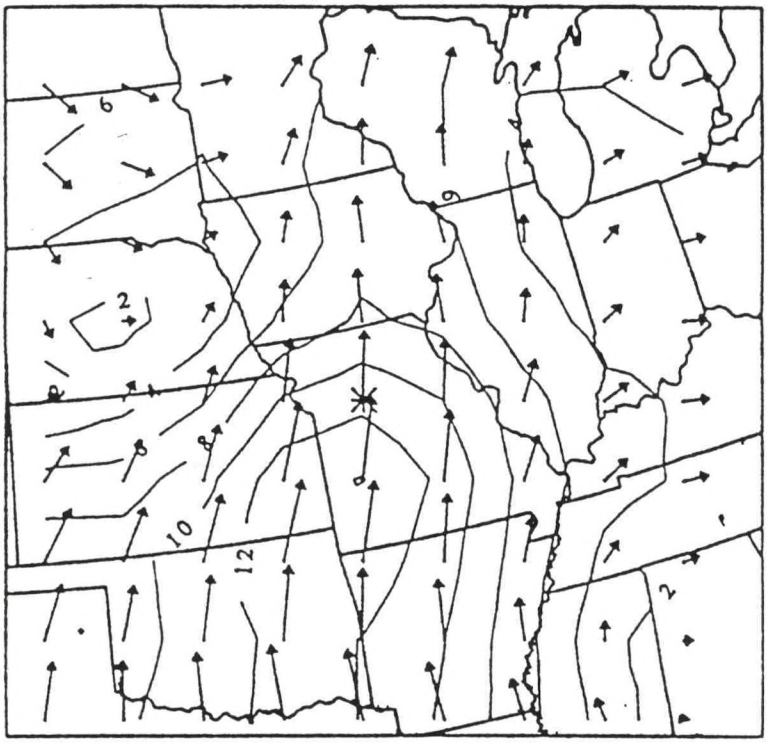

Figure 4. Composite of 850 mb wind vectors and isotachs (ms^{-1}). Asterisk in center of diagram denotes location of MCS initiation point.

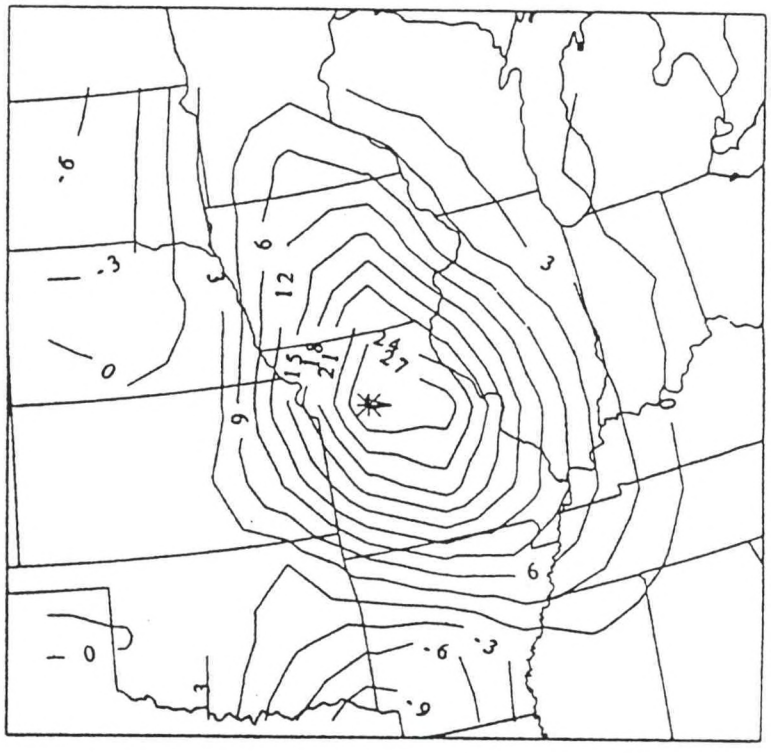

Figure 5. Same as Figure 4, except for 850 mb θ_e advection (10^{-1} K h^{-1}).

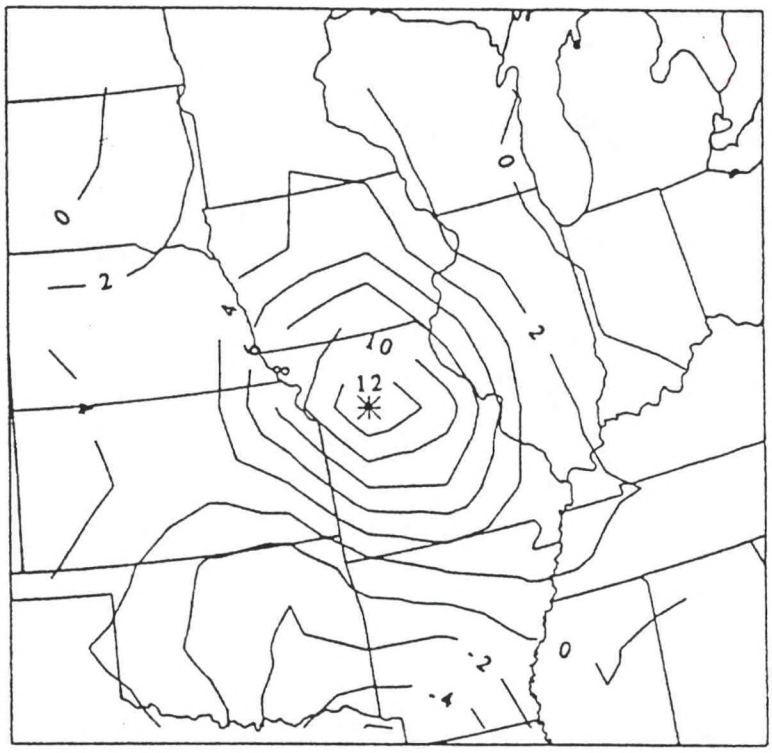

Figure 6. Same as Figure 4, except for 850 mb moisture convergence (10^{-1} g [kg h]$^{-1}$).

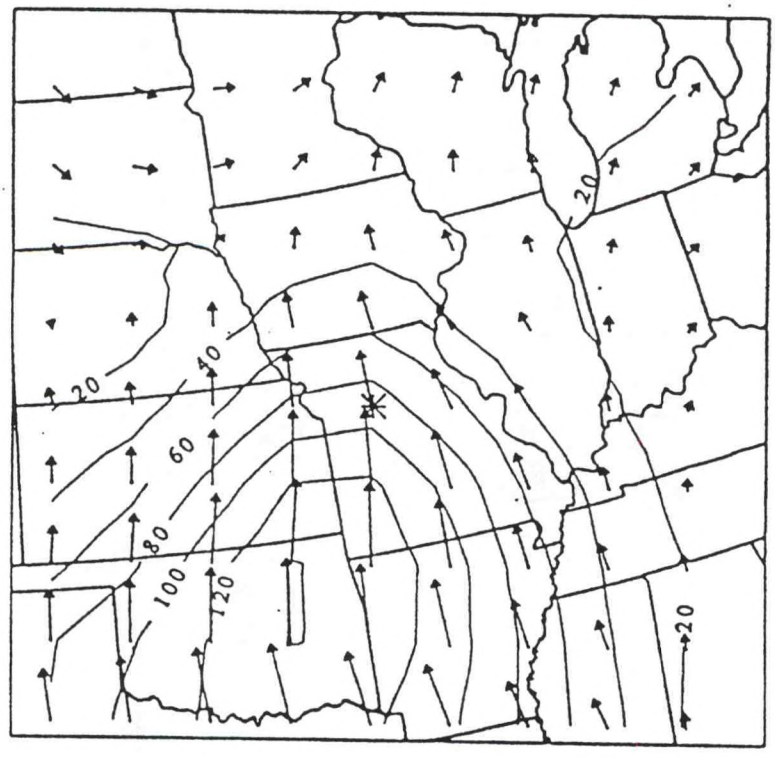

Figure 7. Same as Figure 4, except for 850 mb moisture transport vectors and their magnitudes (g m [kg s]$^{-1}$).

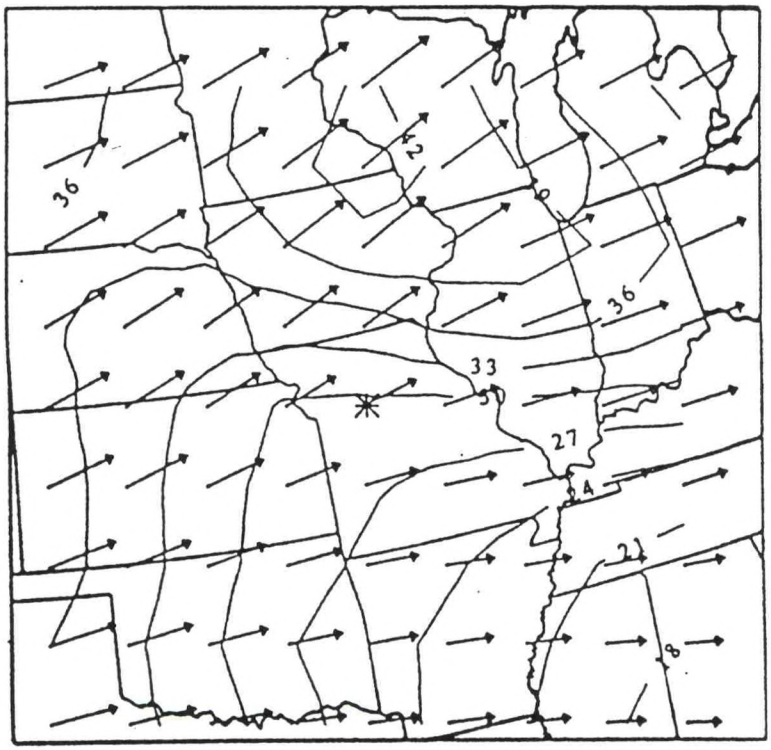

Figure 8. Same as Figure 4, except for 200 mb wind vectors and isotachs (m s^{-1}).

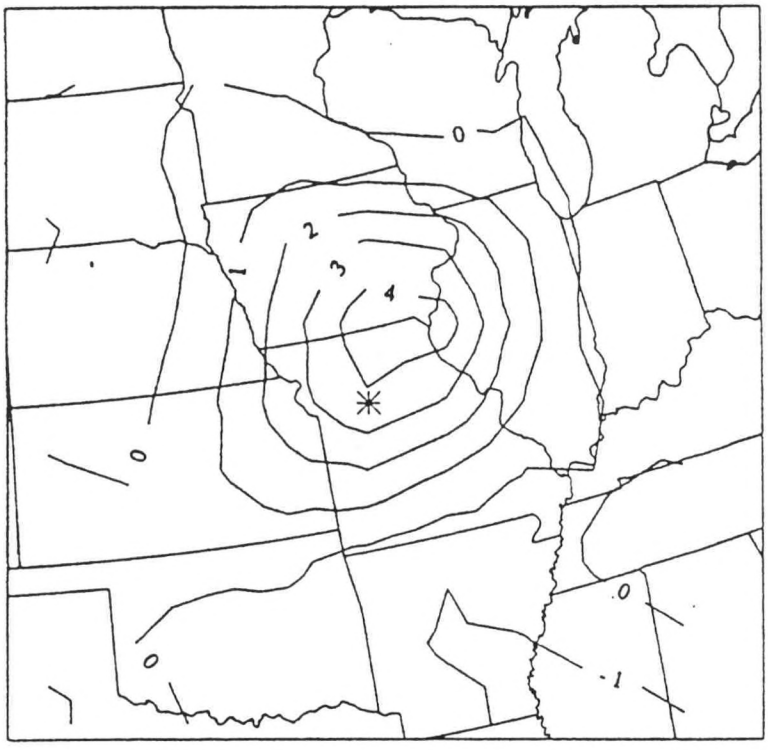

Figure 9. Same as Figure 4, except for 200 mb divergence ($10^{-5}s^{-1}$).

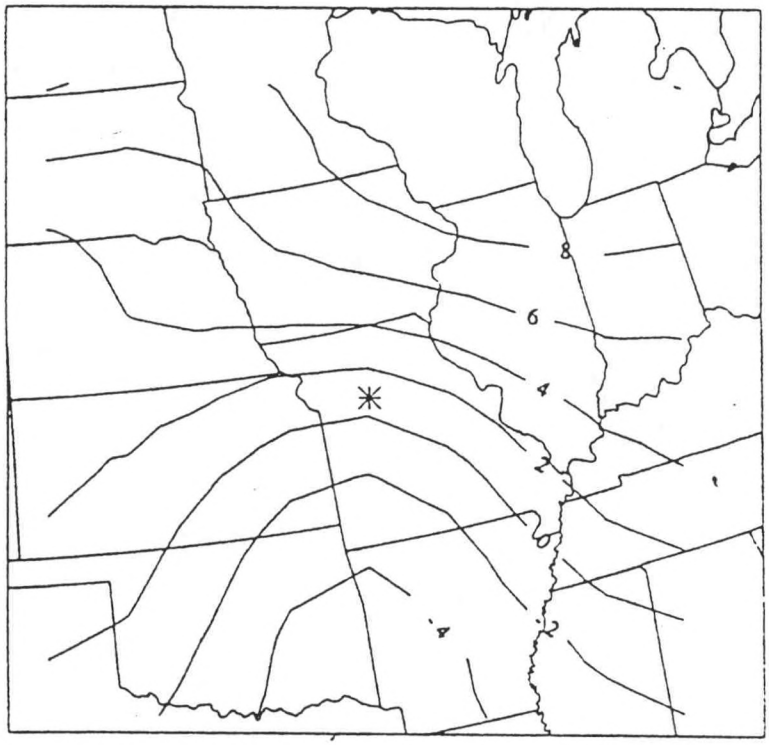

Figure 10. Same as Figure 4, except for lifted index (°C).

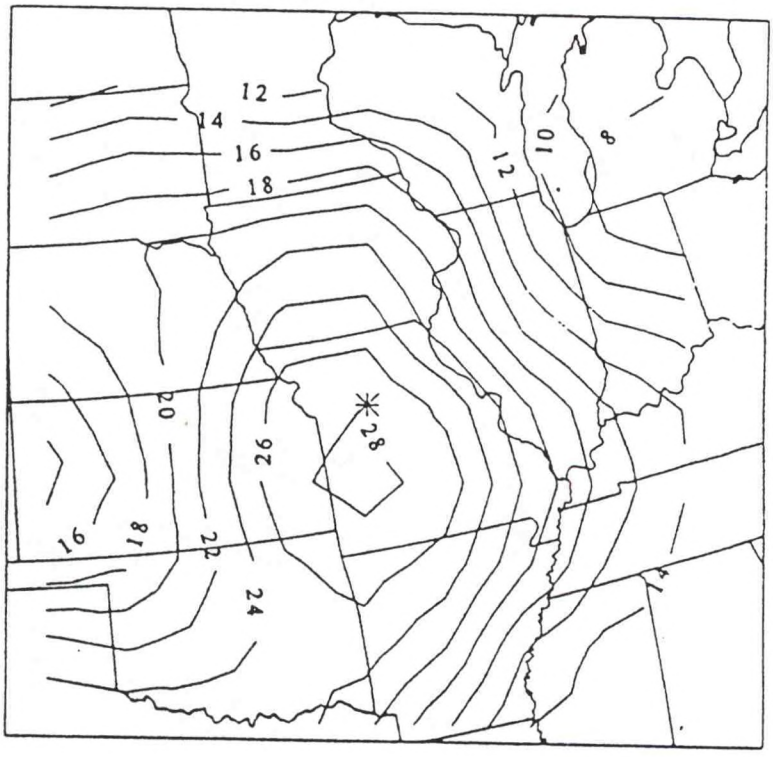

Figure 11. Same as Figure 4, except for K index (°C).

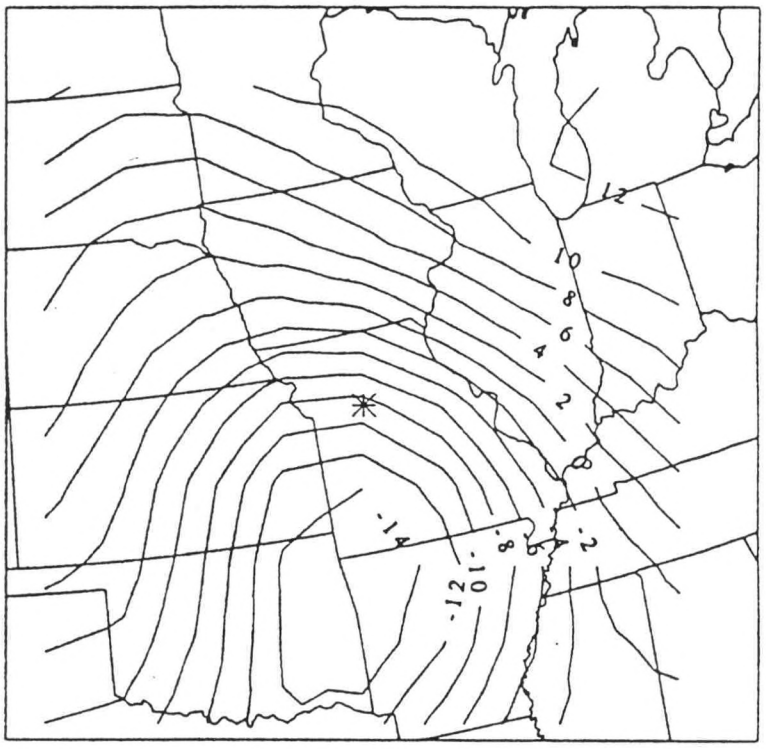

Figure 12. Same as Figure 4, except for convective instability ($\theta_{e\,500}$-θ_{e} 850; K).

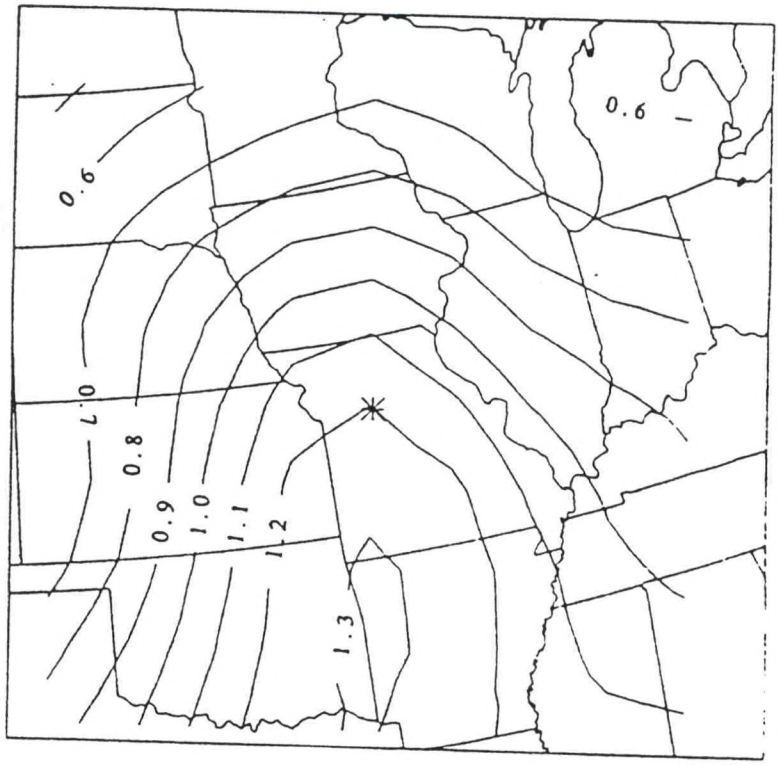

Figure 13. Same as Figure 4, except for precipitable water (inches).

Southwest Missouri Snowstorm of 18-19 January 1995

Daniel Riddle[1], John Gordon[2], Steve Lindenberg[3], Steve Shumway[4], and Mike Sutton[5]

1. INTRODUCTION

On January 18-19, 1995, an area of low pressure developed over eastern Texas and intensified as it moved northeast to southern Illinois. This storm produced a band of heavy snow from portions of northeast Oklahoma to northwest Illinois bringing transportation to a halt for two days. In Springfield, Missouri 14.4 inches fell, making it the heaviest 24 hour snowfall since 1980. The cost of clearing the main streets in Springfield alone was estimated at $50,000.

What made this storm unusual was the occurrence of thundersnow in many locations across southwest Missouri during the most intense period of the storm. This paper will examine how the models performed, and how the 300 mb jet and isentropic lift aided in the development of heavy snow across southwest Missouri. In addition, this paper will look into reasons why thundersnow developed by examining Conditional Symmetric Instability (CSI) and frontogenetic forcing.

2. SYNOPSIS

At 1200 UTC 17 January 1995, a strong 500 mb shortwave was diving south through the central Rockies. During the next 24 hours, the shortwave continued to deepen. By 1200 UTC 18 January, the shortwave was over southeast Oklahoma with the associated surface low over southeast Texas.

Light rain mixed with sleet began falling at the National Weather Service Office in Springfield, Missouri (NWSO SGF) at 1557 UTC 18 January. A changeover to snow was observed at 2200 UTC, and the snow quickly became heavy. At 0000 UTC 19 January, a 500 mb low was forming near the Arkansas and Oklahoma border close to Fort Smith with the accompanying surface low over southeast Arkansas. The area of heavy snow expanded across southwest Missouri during the evening as the 500 mb low continued to deepen rapidly over northwest Arkansas. By 0900 UTC, the 500 mb low was beginning to close off over northwest Arkansas. At 1200 UTC, a closed 500 mb low was located along the Missouri-Arkansas border, just south of SGF, (Figure 1) while the accompanying surface low had moved to southern Illinois. The snow ended across southwest Missouri by early afternoon.

KSGF WSR-88D radar showed distinct higher dBz bands moving north and northwest around the 500 mb low center between 0000 and 0800 UTC. Thundersnow with snowfall rates of 1 to 2 inches per hour was being reported in many locations from Joplin to Lebanon as these bands moved through. Storm total snowfall ranged from 10 to 20 inches in a 30 mile wide band from southwest to central Missouri (Figure 2). A cooperative observer in Ash Grove, 10 miles northwest of SGF reported 22 inches of snow.

3. MODEL DATA

1. Corresponding author address: Daniel Riddle, NWSO Springfield, Missouri.
2. John Gordon, NWSO Springfield, Missouri.
3. Steve Lindenberg, NWSO Springfield, Missouri.
4. Steve Shumway, NWSO Springfield, Missouri.
5. Mike Sutton, NWSO Springfield, Missouri.

3. MODEL DATA

A. Model Performance

PCGRIDDS data from the Eta-X and NGM showed that both models advertised this system well in advance. The relative humidity and vertical velocity time and height cross-sections two days prior to the storm indicated plenty of deep moisture and a tremendous amount of vertical lift from the evening of January 18 through the morning of January 19.

The Eta-X and AVN were the weakest and fastest while the NGM was the strongest and slowest. The NGM was the model of choice for this event as abundant moisture and warm temperatures with this system favored a stronger and deeper storm than either the Eta-X or AVN. It turned out that the NGM did a very good job, but was still a little too far east and not intense enough with the 500 mb low center and surface low.

B. Magic Chart

The Magic Chart (Sangster and Jagler, 1985) was developed as a guide to help forecasters estimate snowfall potential using 12 hr 700 mb net vertical displacement (NVD) from the trajectory model. For 0000 UTC 19 January, NVD was forecast to be +100 mb in the SGF area, 850 temperatures were forecast to be near -1 or -2°C, and mean relative humidity values were above 90 percent. The Magic Chart forecasted the potential for up to 10 inches of snow over southwest Missouri and, if it not for the thundersnow, would have worked out well.

C. Vertical Motion

The 300 mb analysis for 0000 UTC 18 January showed a rapidly deepening trough over the western Plains with a polar upper level jet streak of 100 kts along the base of the trough over New Mexico. Height falls of 80 to 110 m were common over the central and eastern plains. This polar jet streak would accelerate northeast through time and be a crucial forcing mechanism for southwest Missouri.

The NGM forecast for 0600 UTC 19 January predicted that southwest Missouri would be in the right rear entrance region of the polar jet. The forecast was accurate as the 300 mb analysis for 0000 UTC 19 January indicated a 90 kt jet core over Iowa. As a result, very strong upper level divergence was located over southwest Missouri underneath this right rear jet (Figure 3). The NGM identified the slope and intensity of the ascending branch of the transverse ageostrophic circulation, thereby indicating deep-tropospheric motions aloft over southwest Missouri (Uccelini, et al, 1988).

Figure 4 shows the vertical velocity cross section for SGF using data from the 1200 UTC 18 January NGM model run. At 700 mb, vertical velocities over southwest Missouri were forecast to be 13 to 16 microbars per second at 0000 UTC 19 January, corresponding to the start of the heavy snow.

Another way to examine vertical motion is by Q-vectors. From the $w \propto \nabla \cdot Q$ equation, we can see that the convergence of Q-vectors implies upward vertical motion (w) (Djuric, 1994). The authors set out to determine how deep the vertical motion was and to see if thundersnow was a possibility. The 700-300 mb Q-vector layer was chosen for this. Figure 5 shows strong Q-vector convergence over northwest Arkansas and southwest Missouri at 1200 UTC 19 January, just north of where the upper low was forming. Such strong vertical motions and large scale forcing associated with this storm led to the formation of heavy snow bands.

4. ISENTROPIC LIFT

A good correlation exists between isentropic mixing ratios and the maximum amount of snowfall during the ensuing 12 hours (Garcia, 1994). Garcia detailed one technique using isentropic analysis that can be used to forecast the amount of snow. This technique was used on this storm to see how well it worked in forecasting the heavy snow in southwest Missouri 12 to 24 hours ahead of time.

According to Garcia, the best isentropic surface to pick is one which best intersects the 700-750 mb layer over the area of concern, which in this case was southwest Missouri. The isentropic surface 294°K was chosen as the "best fit" over southwest Missouri.

An effective mixing ratio value for the 12 hour period can be calculated by averaging the mixing ratio over the area of concern and the highest mixing ratio that could be advected into this area. This average mixing ratio value will provide the basis for the maximum snowfall forecast. Multiplying the average wind speed by the time period of 12 hours will give the approximate distance to the point where the highest mixing ratio can be obtained.

Taking the average mixing ratio value and using the following table will give an estimate of snowfall for a 12 hour period:

TABLE 1
Snowfall Scale from Garcia (1994)

SNOWFALL SCALE (12 HOUR PERIOD)		
1-2 g/kg	=	2-4 inches of snow
2-3 g/kg	=	4-6 inches of snow
3-4 g/kg	=	6-8 inches of snow
4-5 g/kg	=	8-10 inches of snow
5-6 g/kg	=	10-12 inches of snow
6-7 g/kg	=	12-14 inches of snow

Figure 6 shows data for 0000 UTC 19 January using the 294°K isentropic surface. Mixing ratios over southwest Missouri were forecast to be around 4.0 g/kg. Southeast flow perpendicular to the constant pressure surface indicated good upward vertical motion, as air flowed from higher pressure to lower pressure. The air flow continued to transport Gulf moisture into southwest Missouri. The average wind speed was determined to be 15 kts and the estimated distance from the area of concern was 180 nm. The maximum mixing ratio was 7.0 g/kg. Taking the average of the mixing ratios (4.0 and 7.0 g/kg), gives an effective mixing ratio of 5.5 g/kg. According to Table 1, this means that 10 to 12 inches of snow is possible.

Garcia's method and the Magic Chart worked well in predicting general snow amounts, while PCGRIDDS data showed the amount of vertical motion needed to produce heavy snow. However, why did thunderstorms form? It is believed the presence of Conditional Symmetric Instability and frontogenetic forcing aided in the development of thunderstorms over southwest Missouri.

5. CONDITIONAL SYMMETRIC INSTABILITY (CSI)

Conditional Symmetric Instability (CSI) refers to the situation where a displaced parcel of air is stable when subjected to a horizontal or vertical displacement, but unstable if lifted in a diagonal, or slantwise manner. Past studies (Bennets and Sharp, 1982) indicated CSI-enhanced precipitation often occurs in narrow bands, on the order of 10-100 nm wide, that are oriented parallel to the wind.

Snowfall rates of 2 to 3 inches per hour may occur in CSI precipitation areas, with thunder and lightning observed in many cases.

To examine for CSI, the ambient environment must be deemed suitable for CSI. Snook (1992) listed the following factors as important conditions necessary for CSI:

A. Low static stability,
B. Wind increasing with height,
C. Wind veering with height, and
D. Layer near saturation and well mixed.

Moore and Lambert (1993) offer a theoretical value of 80 percent for the relative humidity in the area of CSI.

Angular Momentum (M_g) and Equivalent Potential Temperature (θ_e) surfaces were constructed via PCGRIDDS using a cross-section taken from southeast to west central Missouri. $M_g = v_g + fx$, where v_g is the component of geostrophic wind normal to the cross-section, x is the distance from the end of the cross-section, and f is the coriolis parameter. CSI exists in those saturated regions where the slope of M_g is equal or less than that of θ_e (Bradshaw, 1994). Investigation of the Eta-X data set from 0000 UTC on 19 January indicated weak CSI between 700 and 500 mb over southwest Missouri (not shown). Temperatures decreased with height between 400 and 500 mb indicating that advection had transported warm, moist air into the region above the frontal boundary. This created a layer of convective instability. Investigation of the 0000 UTC NGM and AVN data sets produced similar results.

6. FRONTOGENETIC FORCING

Another factor that can enhance vertical velocities is frontogenetic forcing. Frontogenetic forcing and CSI often work together to enhance the vertical motion field. Frontogenesis often forms in a thermally direct circulation. The thermally direct circulation is usually slanted toward cold air with upward vertical motion on the warm side and downward vertical motion on the cold side (Moore and Blakley, 1988). The gridded data sets were investigated for frontogenesis in the area of concern to look for the possible presence of a thermally direct circulation.

At 0000 UTC 19 January, strong frontogenetic forcing was indicated over northwestern and north central Arkansas and southern Missouri at 850 mb, over southwestern Missouri at 700 mb and over eastern Kansas at 500 mb. From this, one can imply a thermally direct circulation rising from near the surface on the warm side over northern Arkansas and south central Missouri, traveling west-northwest to near 500 mb on the cold side over eastern Kansas. This slanted path likely resulted in enhanced semi-vertical motion in the area of CSI, and while it may not have initiated convection, it may have acted to enhance its persistence and intensity. Figure 7 shows an area of maximum frontogenesis at 700 mb over southwest Missouri. Values of 6×10^{-10} °K m^{-1} s^{-1} were noted in the same location as where CSI was observed. Thus, frongenetical forcing and CSI worked together in this storm to enhance vertical motion over southwest Missouri.

7. CONCLUSION

Heavy snow fell across southwest Missouri from the afternoon of January 18, 1995 to the morning of January 19, 1995, with some locations receiving more than 20 inches. While storms of this magnitude have occurred in the past, this storm was unusual in that it was accompanied by thunderstorms. Strong warm advection accompanied by intense vertical lift caused this storm to

deepen rapidly. Isentropic lift played an integral part in the storm as very moist air was lifted north into the cold air over southwest Missouri. Weak CSI combined with strong frontogenetic to aid in the development of thunderstorm bands which moved through southwest Missouri dumping 1 to 2 inches of snow per hour.

8 .ACKNOWLEDGMENTS

The authors are grateful to Dave Gaede, SOO at NWSO Springfield for his help in gathering data and for his critique of the paper. Additional thanks goes to Douglas Kennedy, meteorologist intern at WSO Columbia, Missouri for his help in sending upper air and surface maps, and to Bill Davis, MIC and Steve Runnels, WCM, of NWSO Springfield, for their support in this study.

9. REFERENCES

Bennets, D.A., and J.C. Sharp, 1982: The Relevance of Conditional Symmetric Instability to the Prediction of Mesoscale Frontal Rainbands, *Quar. J. Roy. Meteor, Soc.*, **108**, 595-602.

Bradshaw, T., 1994: Relationships Between Conditional Symmetric Instability, Thunder, and Heavy Snowfall During the "Storm of the Century", SR Technical Attachment 94-21. DOC, NOAA, NWS, Southern Region, Scientific Services Division, Ft. Worth, TX, 8 pp.

Djuric, D., 1994: *Weather Analysis.* Prentice Hall, 304 pp.

Garcia, C., Jr., 1994: Forecasting Snowfall Using Mixing Ratios on an Isentropic Surface - An empirical study. NOAA Technical Memorandum NWS CR-105. DOC, NOAA, NWS, Central Region, Scientific Services Division, Kansas City, MO, 28 pp.

Moore, J.T., and P.D. Blakley, 1988: The Role of Frontogenetical Forcing and Conditional Symmetric Instability in the Midwest Snowstorm of 30-31 January 1982, *Mon. Wea. Rev.*, **116**, 2155-2171.

Moore, J.T., and T.E. Lambert, 1993: The Use of Equivalent Potential Vorticity to Diagnose Regions of Conditional Symmetric Instability, *Wea. and Forecasting*, **8**, 301-308.

Sangster, W.E., and E. Jagler, 1985: The (7WG,8WT) "Magic" Chart, CR Technical Attachment 85-1. DOC, NOAA, NWS, Central Region, Scientific Services Division, Kansas City, MO, 5 pp.

Snook, J.S., 1992: Current Techniques for Real-Time Evaluation of Conditional Symmetric Instability, *Wea. and Forecasting*, 7, 430-439.

Uccellini, L.W., K.F. Brill, P.J. Kocin, and J.S. Whitaker, 1988: Model Diagnostics of East Coast Storms, *Second National Winter Weather Workshop:* NOAA Technical Memorandum ER-32. DOC, NOAA, NWS, Eastern Region, Scientific Services Division, Bohemia, NY. 15 pp.

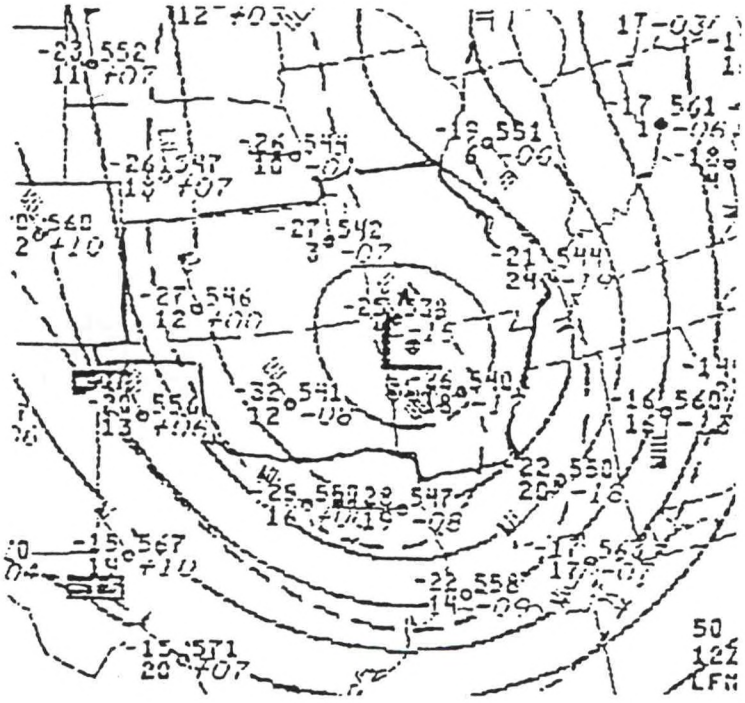

Figure 1. 500 mb analyses for 1200 UTC 19 January 1995.

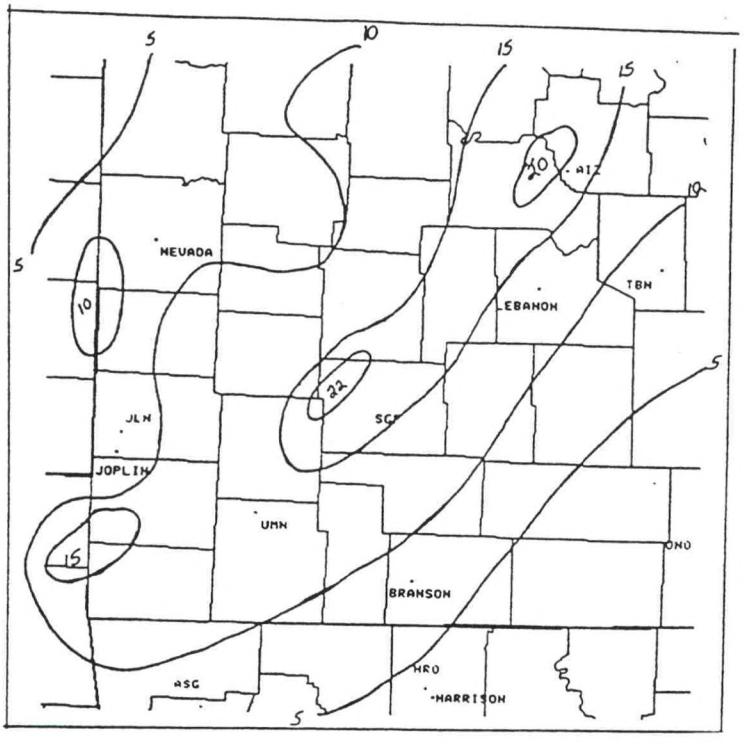

Figure 2. Snowfall totals (in) January 18-19, 1995 across southwest Missouri.

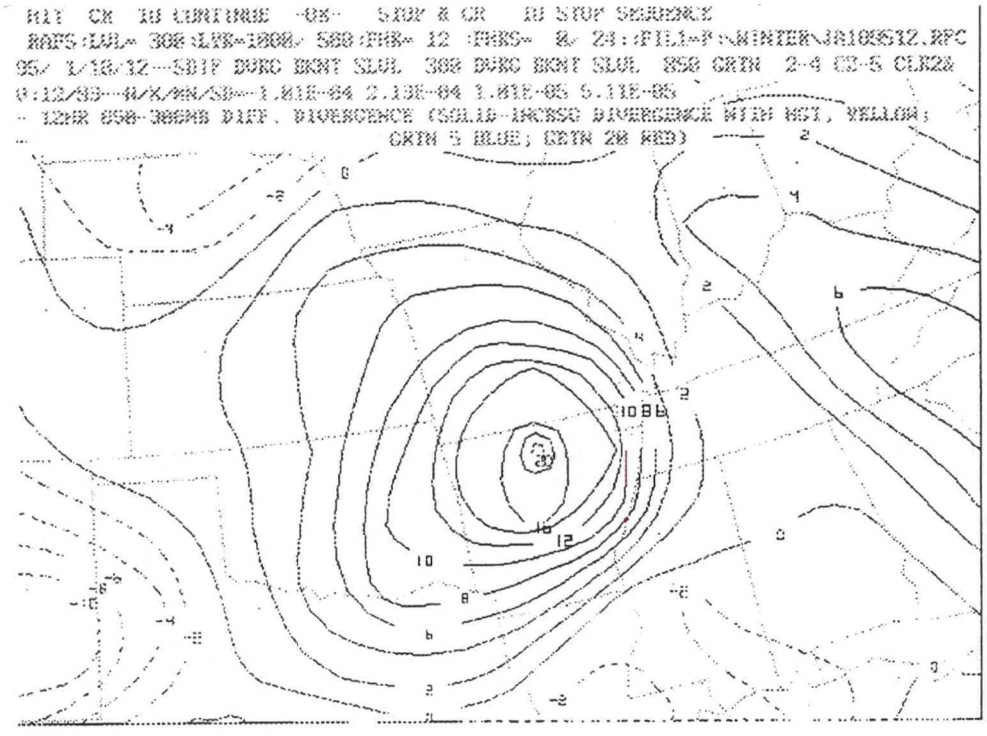

Figure 3. Upper level divergence (10^{-5} /sec) NGM forecast valid 0000 UTC 19 January 1995.

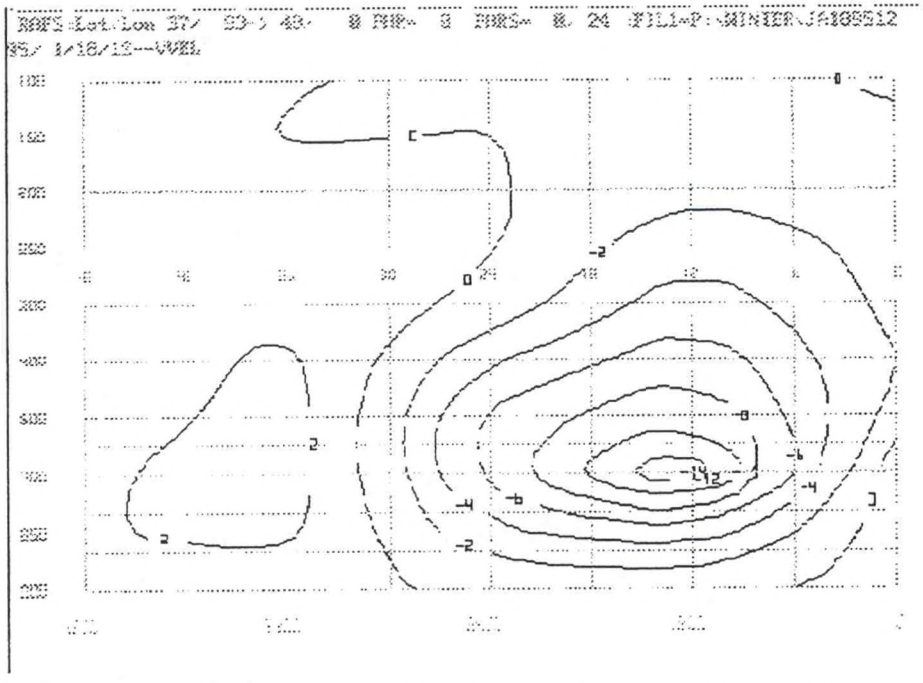

Figure. 4. Vertical velocity (μb/sec) cross-section for 37N/93W from 1200 UTC 18 January 1995.

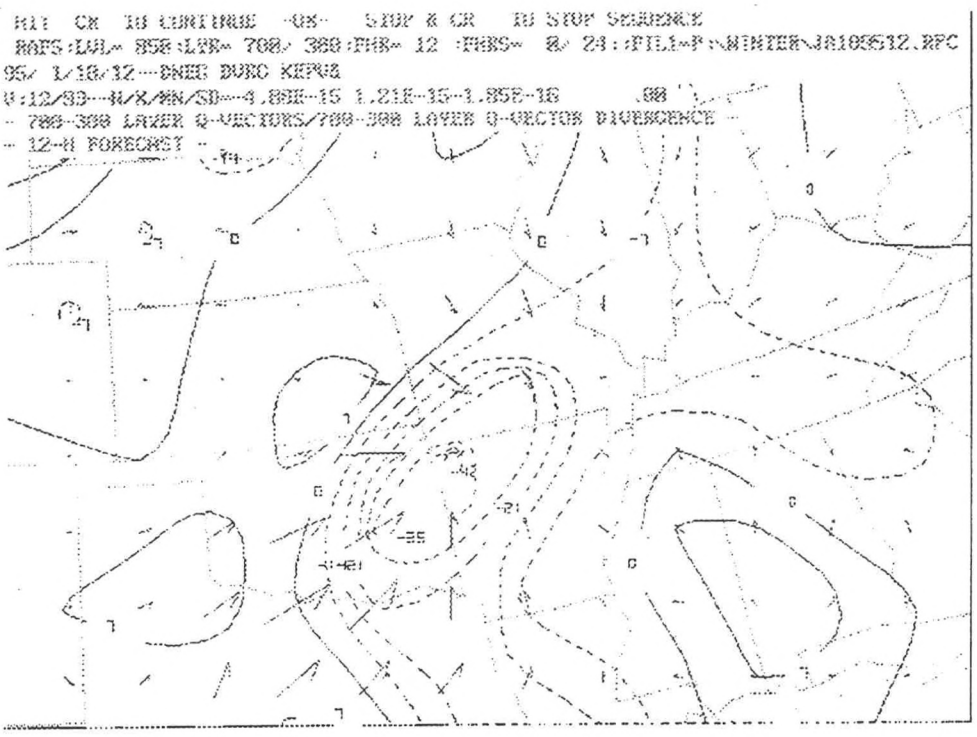

Figure 5. 700-300 mb Q-vector convergence valid 1200 UTC 19 January 1995.

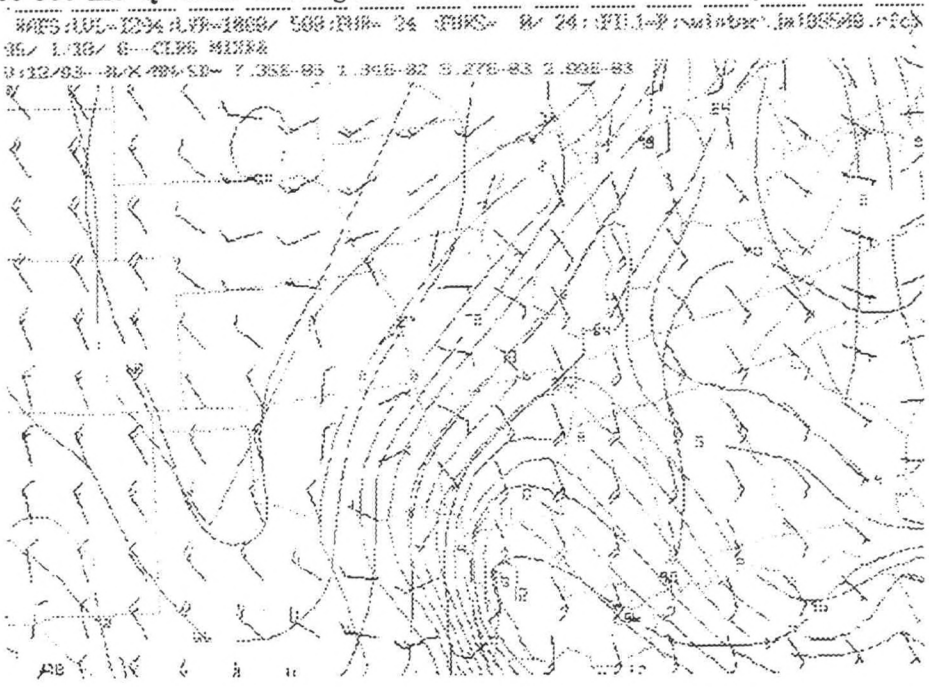

Figure 6. Isentropic surface 294°K analysis valid 0000 UTC January 1995. Mixing ratios in g/kg, wind speed in kts, and pressure surfaces in mb.

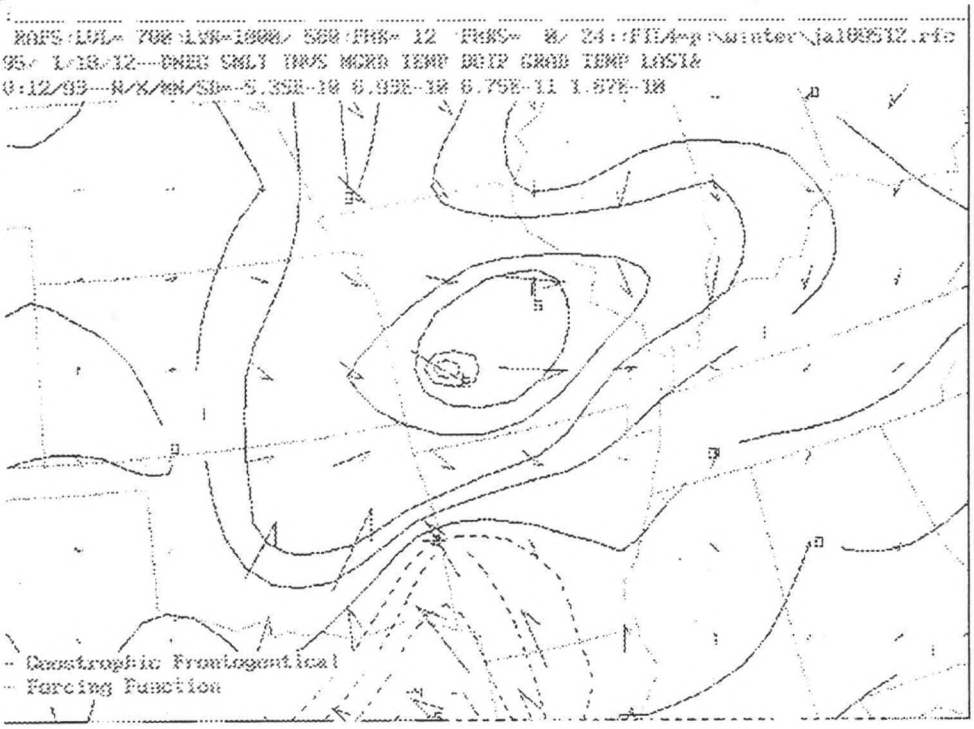

Figure. 7. 700 mb frontogenetic Forcing(x 10^{-10} °K m^{-1} s^{-1}) for 0000 UTC 19 January

A Convective Snowfall Event Across Central North Dakota

William Rasch[1] and James Scarlett[2]

1. INTRODUCTION

On March 22, 1995, the 1630 UTC forecast for south-central North Dakota, including Bismarck, called for rain showers with a high temperature of 45°F to 50°F. Rain mixed with snow was forecast for north-central North Dakota with accumulations of 1 to 2".

Despite observed and forecast thermal and dynamic data indicating a general rain event, this was not the case. Occasional rain occurred throughout the morning of March 22, 1995 over Bismarck and the surrounding areas. At 1935 UTC, a brief thundershower mixed with ice pellets occurred, changing to snow at 2007 UTC. The snow accumulated to 3" by 2300 UTC. During the next 12 to 18 hours, a band of heavy snow, (5 to 9") fell across central North Dakota (Figure. 1).

This paper will discuss the method in which strong evaporative and dynamic cooling interacting with a mesoscale area of strong isentropic lift produced a mesoscale heavy snow event across central North Dakota.

2. GENERAL SYNOPTIC SITUATION 1200 UTC 22 MARCH 1995

A. Upper-Level and Surface Analysis 1200 UTC 22 March 1995

A broad upper-level trough was located over the western half of the U.S. (Figure 2), with an embedded shortwave trough over western Nebraska. At the surface an area of low pressure was centered in central Nebraska with an inverted trough extending northwestward into the western Dakotas (Figure 3). At 850 mb, an associated baroclinic zone and region of warm air advection (WAA) was located across central North Dakota and South Dakota (Figure 4) with the 0°C isotherm extending north of North Dakota into Canada and the 10°C isotherm in central South Dakota perpendicular to a 30 to 35 knot jet.

B. Bismarck Sounding Analysis

The morning sounding from Bismarck (Figure 5) indicated a stable atmosphere with a Total Totals index of 34 and Lifted Index of +12. A cool and dry air mass over central North Dakota was represented by a strong inversion from the surface to 750 mb. The temperature in this layer was above 0°C from the surface to near 9,000 feet resulting in a large mass of air that had to be cooled for snowfall to occur. Above this layer, the moisture and potential instability increased. A shallow, conditionally unstable layer was located from 750 to around 660 mb, above which the sounding turned moist adiabatic forming a small positive energy area from 750 mb upward to 300 mb, when assuming saturation at the top of the inversion.

C. Isentropic Analysis

At 700 mb a well-defined θ_e ridge axis, indicative of an axis of heat and moisture (Figure 6), extended from eastern Nebraska northwestward to central North Dakota. Southerly winds of 20 to

1. Corresponding author address: William Rasch, NWSFO Bismarck, ND.
2. James Scarlett, NWSO Billings, MT.

30 knots were advecting mixing ratio values of 3 to 4 g kg^{-1} northward into south-central North Dakota.

3. MODEL FORECAST

The 6-hour data (valid 1800 UTC) from the Eta model and Nested Grid Model (NGM) forecast significant precipitation in south-central North Dakota in association to isentropic lift and PVA. Analysis of gridded data from both models indicated that isentropic lift was forecast to be the major source of vertical velocities in the event.

Analysis of the 6-hour Eta model had the 700 mb θ_e ridge continuing from Nebraska northwestward to central North Dakota (not shown). Analysis of the NGM 302K isentropic surface was showing a 60 mb gradient from south-central North Dakota to north-central South Dakota (Figure 7). (This level was used due to its proximity to the 700 mb level, putting it just along the cold air dome over the area.) Forecast winds of 30 to 35 knots were favorable for strong isentropic lift, as the directional component was nearly perpendicular to the geopotential heights on the 302K surface.

With the use of PCGRIDDS, the forecast of total vertical velocities was analyzed in a cross-section across the central parts of the Dakotas (Figure 8) and the portion of the total vertical velocities due to isentropic vertical motion on the 302K isentropic surface was calculated (Figure 7). Baumgardt (1993) explained the method in which isentropic coordinates can be used to assess vertical motion (ω) according to the equation:

$$\omega = \underset{A}{\left[\frac{\partial P}{\partial t}\right]_\theta} + \underset{B}{\vec{V} \cdot \nabla_\theta P} + \underset{C}{\frac{\partial P}{\partial \theta}\frac{d\theta}{dt}}$$

where term A is the local pressure tendency, term B refers to the advection of pressure along an isentropic surface, and term C is the diabatic heating component which is normally very small. We are interested in term B, which is the mathematical dot product of the total wind and the pressure gradient. As wind blows up an isentropic surface or from higher to lower pressures the result is $\omega < 0$. By comparing the forecast total vertical motion with the isentropic vertical motion forecast from term B, we can estimate the contribution of isentropic lift to the total vertical motion within the model.

Analysis of the total vertical motion field in south-central North Dakota indicated the NGM forecast 5-6 μb s^{-1} (Figure 8). Of this total, 4 μb s^{-1} of lift was forecast from the advection of pressure along the 302K isentropic surface (Figure 7) across south-central North Dakota.

With favorable moisture and vertical velocities in place, the rain versus snow aspect was a forecast problem. There are several different techniques of forecasting snow versus rainfall. Each traditional parameter was inspected. This included the 850 0°C isotherm, the 1000-500 mb thickness value of 540 dam, 850-700 mb thickness values of 152-154 dam, 1000-700 mb thickness value of 284 dam (Figure 9). Analysis of the 6 hours forecast for the Eta and NGM had all of these values well north of North Dakota and South Dakota into Canada.

The models cooled the atmosphere further at 12 hours but the rain/snow parameters were still north of Bismarck at 0000 UTC, the exception being the 850 mb 0°C isotherm which did sink south close to Bismarck.

Analysis of the model runs indicated a significant precipitation event was likely in the Bismarck area. Model analysis associated this event largely with isentropic lift along the 700 mb θ_e ridge axis, also forecasting some cooling, but not significant or timely enough to seriously consider snow.

4. DISCUSSION

By 1900 UTC the inverted surface trough moved eastward into central North Dakota and South Dakota. At the same time, the shortwave trough earlier in western Nebraska moved to south-central South Dakota. A low-level jet developed ahead of the inverted surface trough along the top of the cool air mass. This low-level jet could be seen on Bismarck's WSR-88D base velocity data from 1851 UTC (Figure 10). Upon closer examination, it was apparent the jet was ascending from south to north. The inbound region maxima was averaged at 31 kts, 9 nm south of Bismarck. The outbound average maxima was 43 kts, 13 nm north. Assuming a nearly homogenous wind direction and a quasi-steady state parcel trajectory, (Dunn 1991), an estimate of the vertical velocity over south-central North Dakota can be derived. Using an average velocity of 37 kts between the inbound and outbound maxima, a vertical velocity value of approximately -15 $\mu b\ s^{-1}$ was present. This value indicates that isentropic lift was occurring on a much stronger scale than forecast by the models.

This data somewhat supported the 6-hour model scenario. The models forecast 20 to 25 knot winds at low levels and a steep isentropic surface from north-central South Dakota north to south-central North Dakota. According to WSR-88D data, the isentropic lift was stronger, on the order of 15 $\mu b\ s^{-1}$. As parcels of air ascended up the isentropic surface, the small area of instability above 700 mb was encountered. The small area of conditional instability combined with strong vertical motion was enough to support convection. The equilibrium level was around 30,000 feet on Bismarck's morning sounding, which was the echo top heights shown on radar during the event (not shown). The area of initial development could seen on satellite as well as lightning data (Figure 11) in north-central South Dakota. This mesoscale area of convection then advected north with the thermal wind into south-central North Dakota. As the activity moved closer to Bismarck the tops of the clouds on enhanced infrared satellite imagery cooled to around -58°C (not shown) This cooling of cloud tops in the θ_e ridge indicated thundersnow was a possibility (Chaston 1994).

With the activity still in extreme south-central North Dakota, Bismarck WSR-88D velocity data was indicating strong bright banding. One hour precipitation estimates were ranging from 1 to 3 inches, likely due to the mixed state and freezing precipitation particles, indicative of cooling occurring in the low and mid levels (not shown).

Prior to the convective activity reaching Bismarck, the surface temperature had warmed to 43°F. According to Auer (1974), there is almost a 95 percent likelihood of rainfall occurring at that surface temperature. However, the low-level thermal profile must be examined. According to Penn (1957) if the wet bulb temperature is at or below 0°C, snow is likely. Referring to Bismarck's 1200 UTC sounding (Figure 5), the wet bulb was 1 to 2°C above the melting point, with apparent strong WAA occurring. Although the WAA appeared to be strong at lower levels, the WAA was offset by dynamic lifting and diabatic cooling processes, as it was ascending up an isentropic surface.

The strong cooling necessary for snowfall can be further examined by looking at the equation for temperature change over time:

$$\underset{A}{\delta T/\delta t = -(\vec{V} \cdot \vec{\nabla T})} \underset{B}{- W(Y_d - Y)} + \underset{C}{(1/C_p \cdot \delta Q/\delta t)}$$

where A is the horizontal temperature change, B is the vertical temperature change, and C is the temperature change due to non-adiabatic effects (diabatic heating, evaporative cooling). In this case term A was fairly strong due to the apparent WAA in the lower levels, and term B would imply cooling due to a lifting of the air parcel.

As the strong low-level jet encountered the steep isentropic slope, term B increased, offsetting term A (strong WAA). This probably resulted in some cooling of the column as the Positive Vorticity Advection (PVA) also increased lift, dynamically cooling the column. The most significant occurrence, however, was the decrease of term C. As convective heavy snow and rain fell into the fairly dry low levels, rapid evaporative cooling occurred.

According to Penn (1957), the actual evaporative cooling that is observed is often on the order of 5 to 10°F within an hour or two. For a rapid cooling of the column it is necessary to have heavy amounts of precipitation falling with little WAA. This was likely the occurrence near the steep isentropic surface as the WAA was neutralized by the isentropic lift. This was aided by dynamic cooling from PVA, but more strongly by strong evaporative cooling. This rapid cooling can be seen when comparing the 1200 UTC 22 March 1995 sounding to the 0000 UTC 23 March 1995 sounding (Figure 12). As can be seen, most of the cooling took place from the inversion to the surface. The sounding went from partially above zero to completely below freezing.

The result was a mesoscale area of convection that initially started as rain in north-central South Dakota. As the convective activity moved to the north, the heavy precipitation fell into the dry layer over south-central North Dakota. The majority of cooling over Bismarck occurred in the low levels from the surface to near 9,000 feet.

As convective activity reached Bismarck, the evaporative cooling began, with massive cooling in the lower levels of the sounding associated with the heavy convective precipitation falling into the dry layer over south-central North Dakota. As the convection propagated northeast with the thermal wind, it moved away from the steep isentropic slope into a much more stable environment, with weaker isentropic lifting present. This is evidenced somewhat by satellite imagery with warming tops in north- central North Dakota, with weakening convection spreading out into a moderate to heavy snow band. The majority of the heavy snow took place in the 700 mb θ_e ridge, with evaporative cooling, PVA, and weak isentropic lift making the atmosphere favorable toward a significant snow event.

5. SUMMARY AND CONCLUSIONS

The models showed slight cooling in the lower atmosphere and strong isentropic lift, but the presence of strong low-level WAA, surface temperatures in the low to mid 40s °F indicated that a heavy convective snow event was not likely. Traditional snowfall forecast methods also suggested a liquid precipitation event.

However, one must be cautious when dealing with isentropic lifting and evaporative cooling. This is probably most common in winter and early spring. In this case, a steep isentropic surface combined with some instability aloft was enough to initiate convection. This, combined with rapid evaporative cooling at the lower levels, resulted in a heavy snow event for much of central North Dakota, concentrated in the θ_e ridge.

This was a complex event with several meteorological parameters coming together at the same time. However, some key "flags" were present. They were:

1. **Theta-e ridge** represented available potential energy.

2. **Cloud tops cooling to -58°C** on the enhanced infrared MB satellite depiction curve. If occurs in the θ_e ridge axis during wintertime in the snowfall area of a low pressure, it is considered as a possible thundersnow threat area.

3. **Moderate to strong vertical velocities** combined with moisture advection. According to Garcia (1994) mixing ratio values of 3-4 gkg^{-1} can be correlated with 6-8 inches of snowfall given adequate vertical motion. Strong vertical velocities were also indicative of possible dynamic cooling.

4. **Ascending low level jet** indicated by WSR-88D velocity data with some assumptions was indicating strong vertical velocities as well as the presence of a sloped isentropic surface.

5. **Positive energy area** was indicating the potential for deep convection leading to moderate to heavy precipitation.

6. **Dry air** was susceptible to strong evaporative cooling to the wet bulb temperature, which was just above freezing, in the event of moderate to strong precipitation.

7. **Bright banding** indicated on WSR-88D reflectivity was indicating possible cooling of the low and middle levels.

In the future these factors or "flags" may be applied in real time to forecasts of similar conditions.

6. ACKNOWLEDGMENT

The authors would like to extend their appreciation to the entire staff at NWSFO Bismarck for their support and scientific contributions into this paper, in particular, Viggo Jensen III, Rich Van Ess, Jim Fors, Bill Abeling, Rich Leblang and Becky Nieuwsma, from NWSO Billings, Keith Meier for his extensive input on the final draft of this paper, and the North Dakota Atmospheric Resource Board for providing lightning data.

7. REFERENCES

Auer, A.H., Jr., 1974: The rain verses snow threshold temperature. *Weatherwise*, **27**, pg 67.

Baumgardt, D., 1993: Isentropic vertical motion using PCGRIDDS. Western Region Technical Attachment, DOC, NOAA, NWS, Western Region Headquarters, Scientific Services Division, Salt Lake City, UT, 11pp.

Chaston, P., 1994: Forecasting thundersnow. Graphical Guidance - 1994 edition. pg 138.

Dunn, L.B., 1991: Evidence of ascent in a sloped barrier jet and an associated heavy-snow band. *Mon. Wea. Rev.*, **120**, 914-924.

Garcia, C, 1994: Snowfall forecasting using mixing ratios on an isentropic surface. NOAA Technical Memorandum NWS CR-105. DOC, NOAA, NWS Central Region Headquarters, Scientific Services Division, Kansas City, MO.

Penn, S., 1957: The prediction of snow vs. rain. Forecasting Guide No. 2, U.S. Weather Bureau, U.S. Dept. of Commerce. 29 pp.

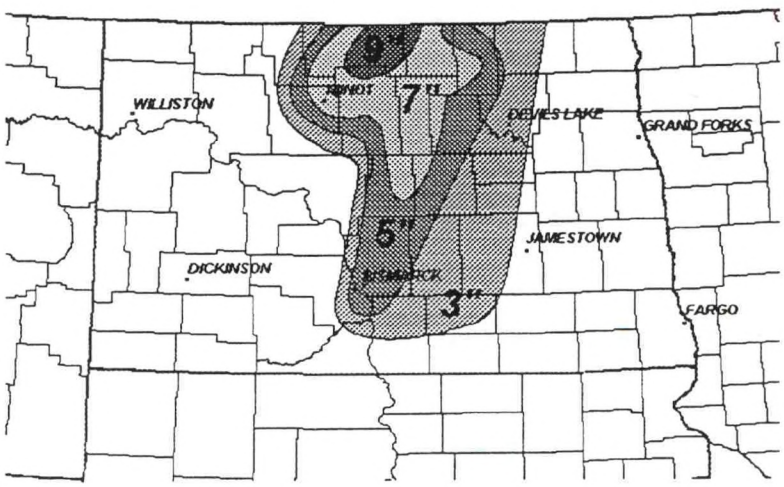

Figure 1. The 24 hour snowfall from 1200 UTC 22 March 1995 through 1200 UTC 23 March 1995.

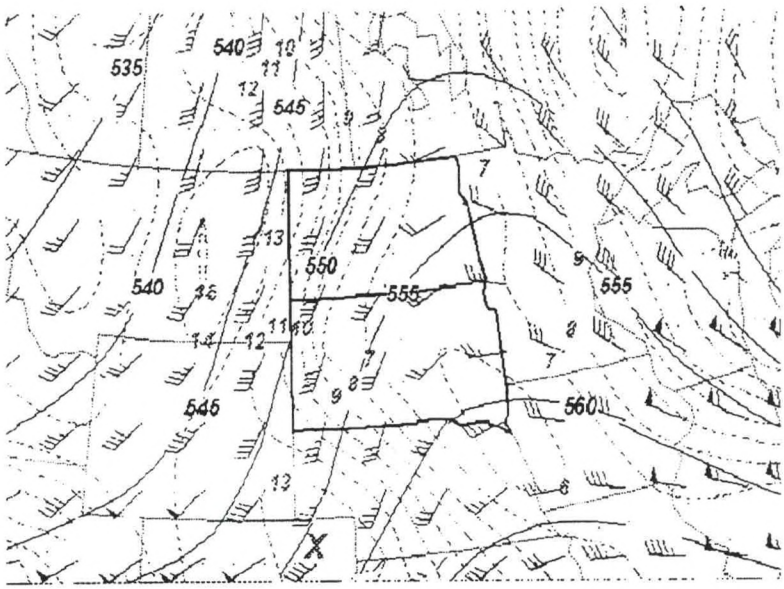

Figure 2. The 500 mb analysis for 1200 UTC 22 March 1995.

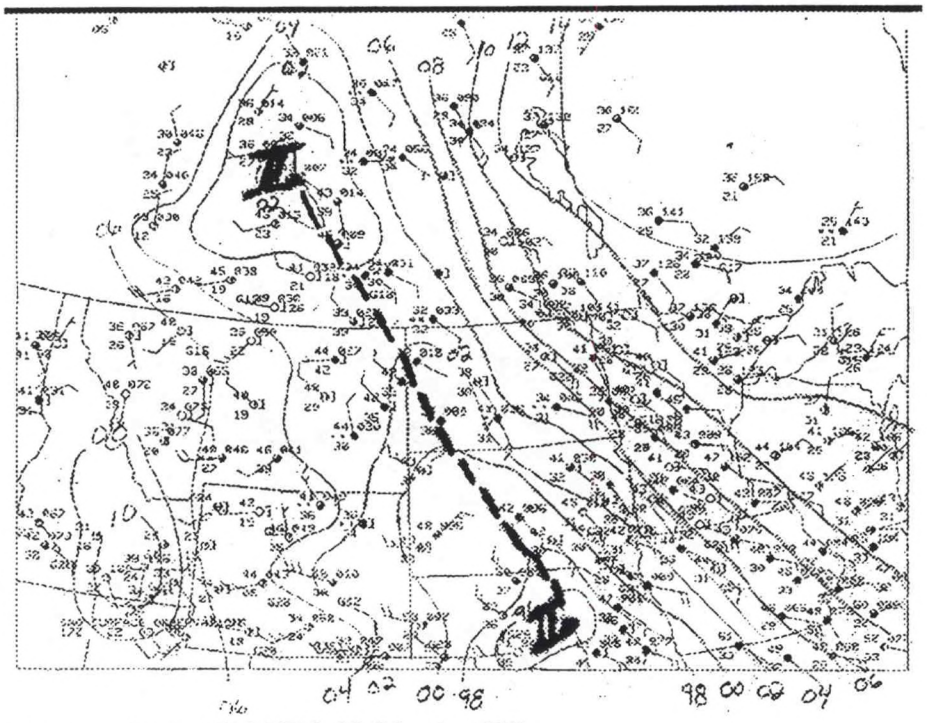

Figure 3. Surface analysis 1500 UTC 22 March 1995.

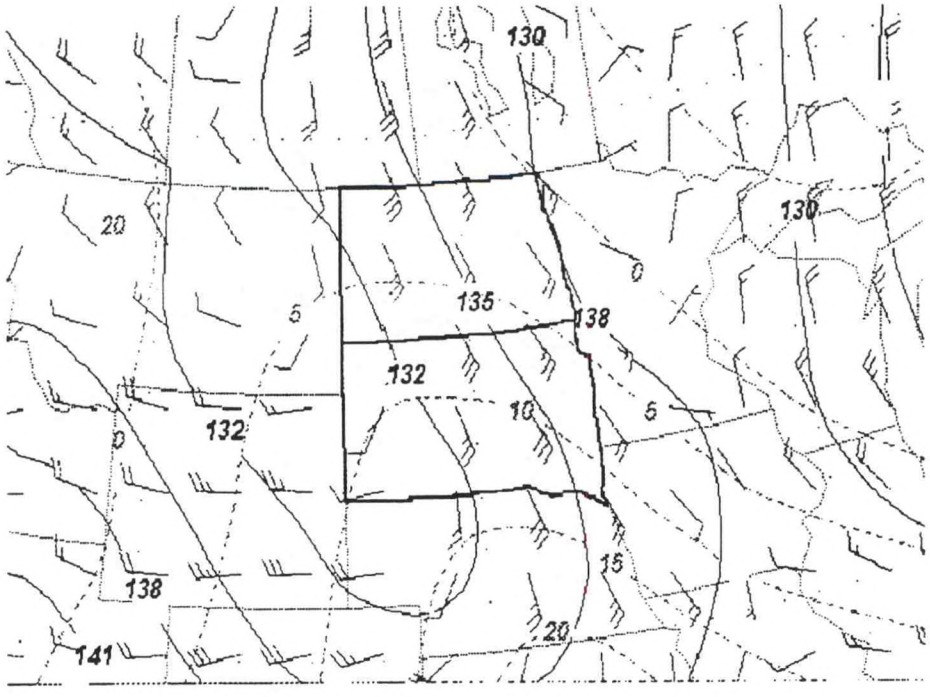

Figure 4. The 850 mb analysis for 1200 UTC 22 March 1995.

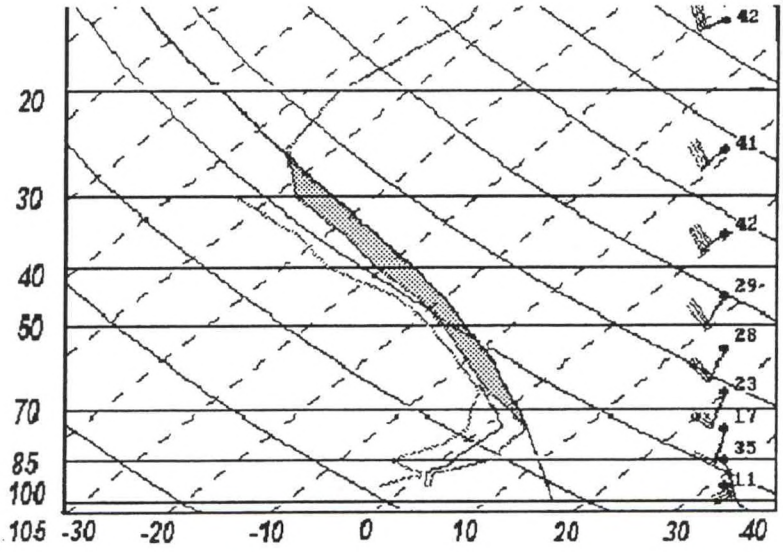

Figure 5. Sounding for Bismarck (BIS) at 1200 UTC 22 March 1995. Shaded area is positive energy assuming saturation at top of the inversion. also shown is wet bulb temperature.

Figure 5. Sounding for Bismarck (BIS) at 1200 UTC 22 March 1995. Shaded area is positive energy assuming saturation at top of the inversion, also shown is wet bulb temperature.

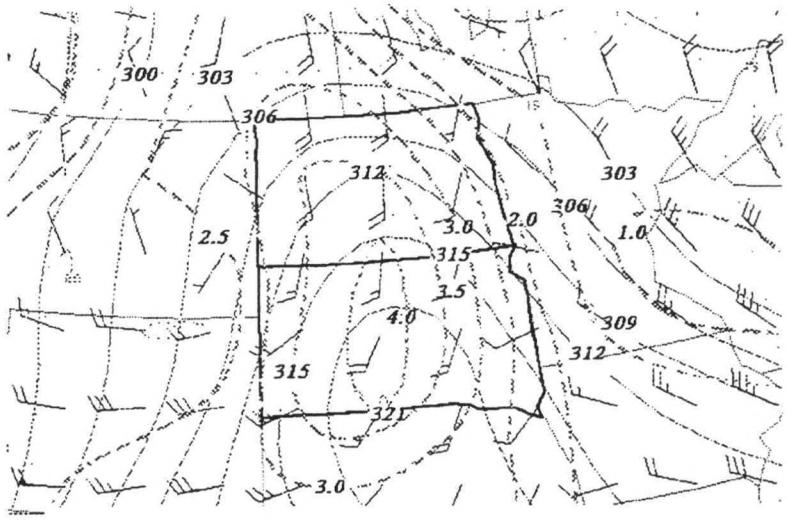

Figure 6. The 700 mb θe analysis (solid), mixing ratio (dashed g kg^{-1}) and wind (kt) for 1200 UTC 22 March 1995.

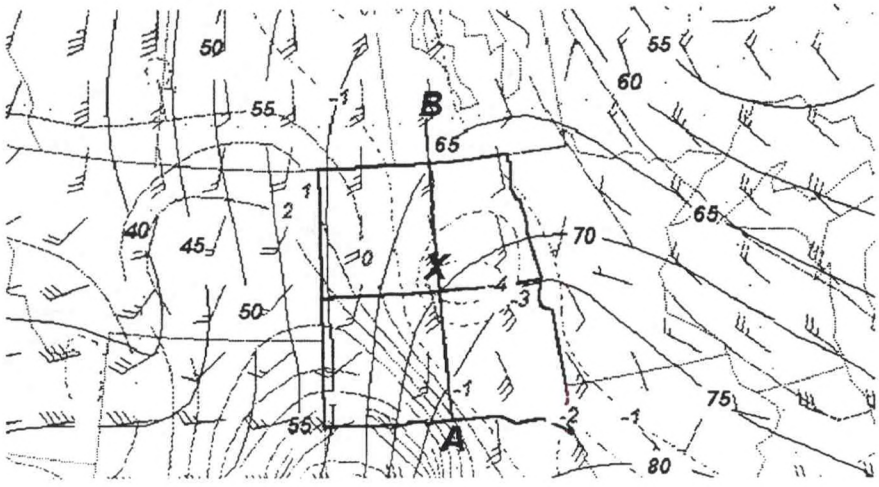

Figure 7. The NGM 6-hour forecast for 3402K isentropic surface valid 1800 UTC 22 March 1995. Pressure (solid), ω due to term B from PCGRIDDS (dashed μb s^{-1}), and wind (kt). A and B define cross-section area where X is near Bismarck, ND.

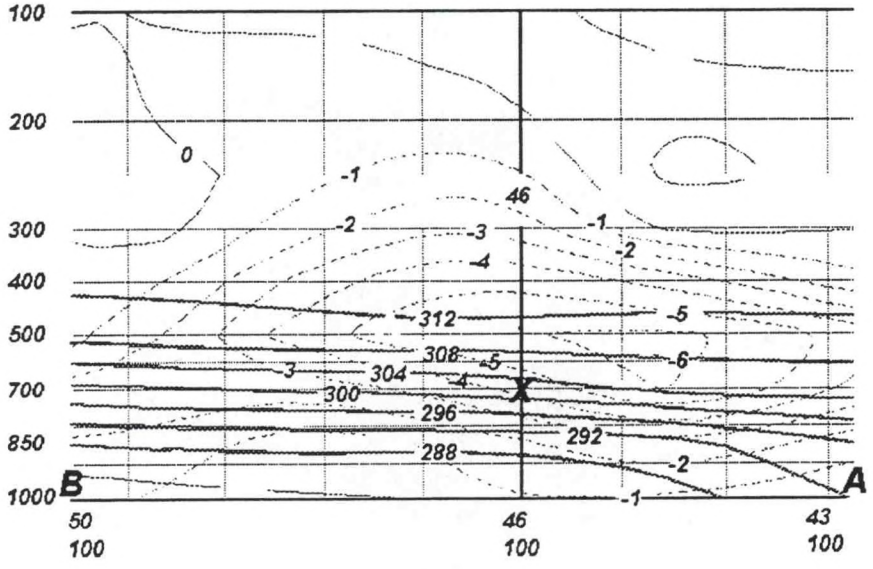

Figure 8. Vertical cross-section from A-B. The NGM 6-hour forecast to total ω (dashed μb s^{-1}) and isentropes (solid).

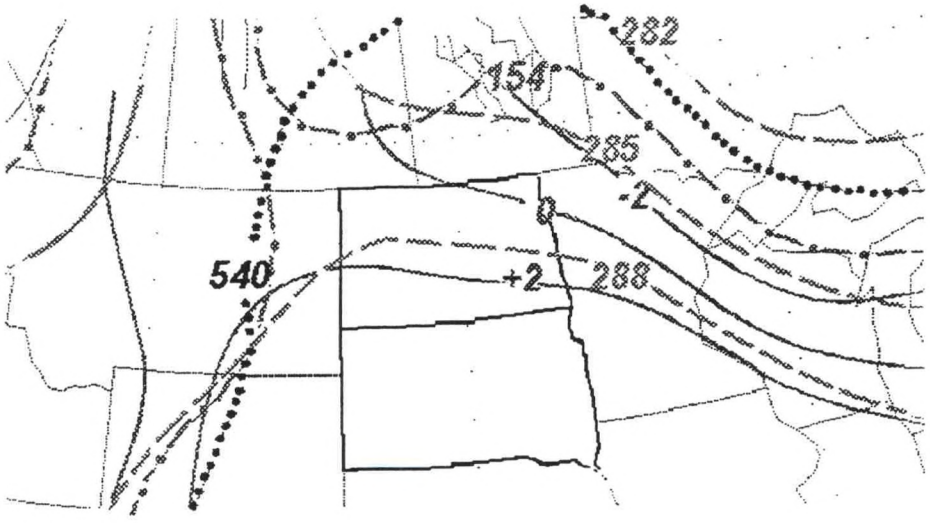

Figure 9. The NGM 6-hour forecast for 1000-500 mb thickness (dots), 850-700 mb thickness (dash-dot), 850 mb temperature (solid), and 1000-700 mb thickness (dash).

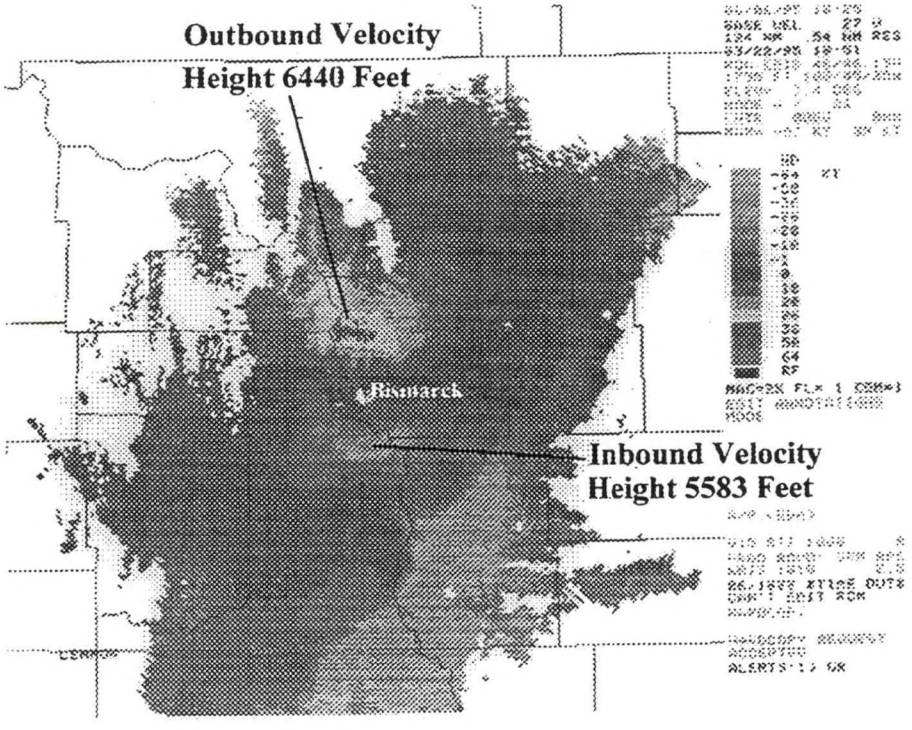

Figure 10. Bismarck 88D velocity data from 3.5° at 1851 UTC 22 March 1995.

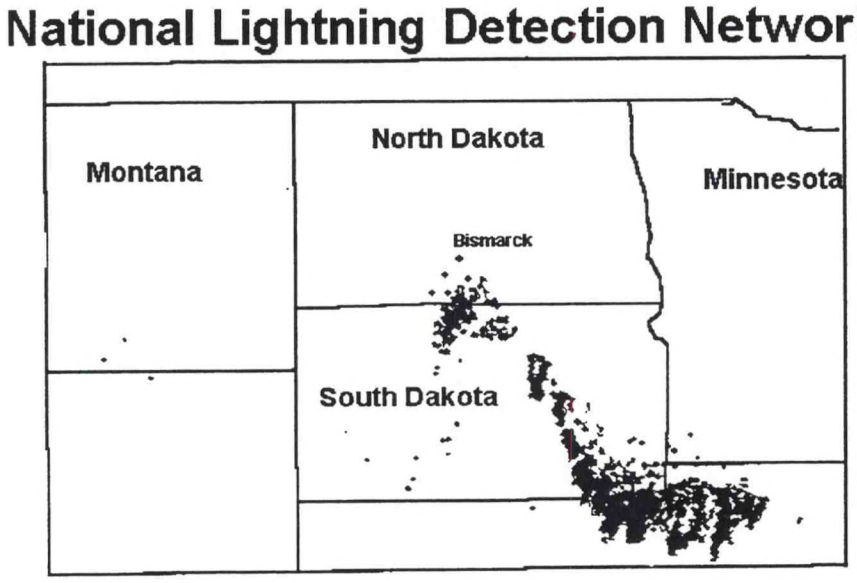

Figure 11. Lightning data from 1500 UTC to 2200 UTC 22 March 1995.

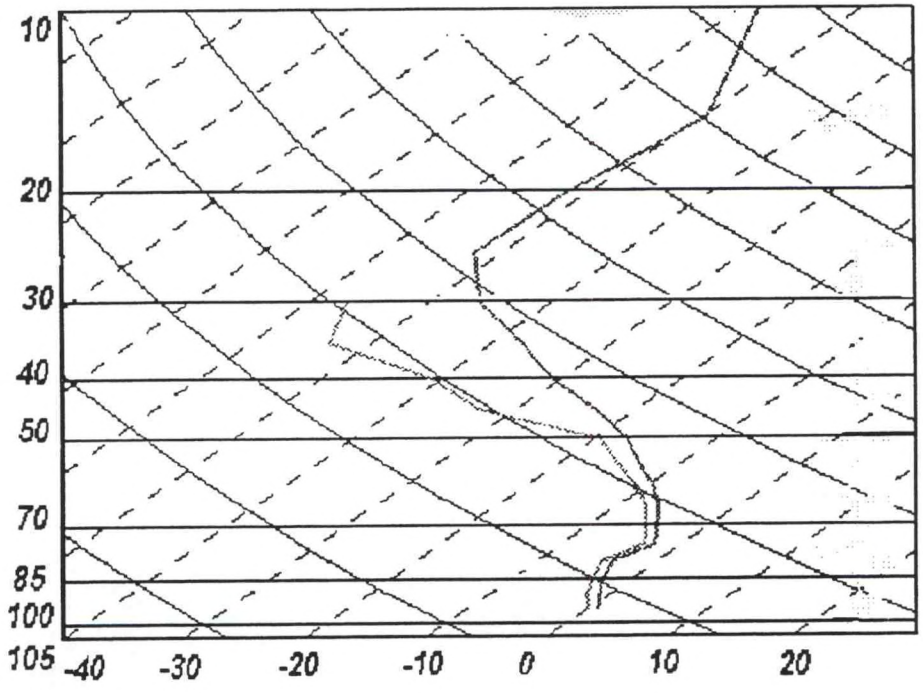

Figure 12. Sounding for Bismarck (BIS) at 0000 UTC 23 March 1995.

Mesoscale Convective Snow Shower Initiation Over The Central High Plains

Victor J. Nouhan[1] and Llyle Barker[2]

1. INTRODUCTION

During the late evening hours of January 17 and the early morning hours of January 18, 1995, a convective complex of snow showers developed along a weak frontal boundary across east central Colorado. The system initiated west and north of Limon and spread into much of western Kit Carson and southern Yuma counties. Subsequently, the snow shower complex quickly developed into a well structured Meso-gamma low, exhibiting both a well-defined "warm frontal" and a "cold frontal" structure. Snowfall amounts from this event ranged from one inch at Limon to locally as much as 4 to 6 inches over extreme northwest Kit Carson and extreme southwest Yuma county.

Although zone forecast products from Denver and Short Term Forecasts from Goodland mentioned widely scattered snow showers for this portion of the area, no accumulating snowfall was anticipated. This study will highlight the evolution of this snow shower complex and explain some of it's causes.

2. EVENT EVOLUTION

Development initially began just west and north of Limon Colorado at around 18/0400 UTC (Figure 1). Subsequently, the complex slowly intensified reaching maximum intensity as it moved east into northwest Kit Carson and southern Yuma counties by 0730 UTC (Figure 2). By this time the meso-scale low had developed a "warm frontal" structure extending east, a "cold frontal" structure south and an occluded-comma structure northwest of the low; features which are not normally associated with conditional symmetric instability (CSI) snow bands. Storm relative map velocity data at this time also indicated an area of weak cyclonic rotation near the comma head of the precipitation complex (Figure 3). WSR-88D reflectivities of up to 40 dBZ (and reported snow fall rates of up to 2 inches/hour) were associated with the meso "cold" front as it moved east. No lightning and thunder was reported at anytime during this event, though the low density of observing stations and poor visibility through heavy snow may have precluded such reports.

After remaining near maximum intensity through 0900 UTC, the line weakened and gradually became broken as it entered northwest Kansas and southwest Nebraska by 1000 UTC (Figure 4). The developmental and mature stages (0400-0800 UTC) of the event seemed to be marked by a multi-cell appearance, where new cells developed on the south flank of the line and propagated northeast. As the meso-cold front moved east, inflow was gradually cut-off and the low became "occluded".

3. OVERALL SYNOPTIC ENVIRONMENT

The overall surface synoptic pattern during the early morning hours of January 18, as shown by 0000 UTC NGM gridded data, was marked by a weak frontal zone extending from the western Dakotas, across eastern Colorado, into eastern New Mexico (Figure 5). At 500mb, a confluent trough also extended from the Front Range of the Rockies into the central high plains with weak negative vorticity advection progged over east central Colorado (Figure 6). Very cold 500mb temperatures accompanied the trough at 0000 UTC with the thermal trough over the central Rockies just slightly lagging the contour trough. Corresponding 700mb heights showed a similar trough axis position to

1. Corresponding author address: Victor J. Nouhan, NWS Goodland, KS.
2. Llyle Barker, NWS Goodland, KS.

500mb, however, the main thermal trough axis at 700mb (near the Colorado-Utah border) lagged the 500mb thermal trough by about 150 miles to the west. Consequently, winds at each level during this time indicated cold 500mb and near neutral 700mb thermal advection developing over east central Colorado (Figures 7 and 8), resulting in a negative differential thermal advection pattern and potential destabilization of the layer.

At initialization, the 0000 UTC NGM gridded data showed a maximum of 22°C difference between 500mb and 700mb temperatures across south central Colorado. As this area moved eastward and advected over the area of the frontal zone at around 0600 UTC, the lapse rate was becoming less steep, but was still greater than 20°C (Figure 9). This resulted in a progged shift of maximum mid-level instability, as depicted by 700-500mb lifted indices, from the Rockies at 0000 UTC into eastern Colorado by 0600 UTC (Figure 10). Mean surface to 400mb moisture near the time of the event was progged to be around 60 percent over east central Colorado; adequate for conditional instability. The lapse rate continued to slowly stabilize late in the event as the area of maximum instability moved into western Kansas and southwest Nebraska by 1200 UTC.

A thermal ridge apparent in the 200mb trough showed some potential for transport of stratospheric high potential vorticity air downward (Figure 11). Warm temperatures near the base of this trough in the southern Rockies and colder temperatures northeast through east central Colorado was indicative of a lowering of the tropopause near the frontal boundary. An isentropic cross-section taken perpendicular to the frontal zone (Fritsch and Hirschberg, 1991), shows the diffluence of the potential temperature contours with height from west to east across the boundary. Overlaying vorticity on this diagram shows the resultant increase in absolute vorticity attributed to the downward forcing of the stratospheric air (Figure 12). This increase of vorticity in the upper levels of the atmosphere resulted in a steeper gradient in vorticity with height, possibly adding to the lift (Holton 1979). Although the downward forcing of high potential vorticity air was more intense south of the region, the combination of mid level instability, meso-frontal position, possible influx of stratospheric air along the front, and topographic effects lead to the formation of the meso-scale low further north over east central Colorado.

4. MESOSCALE AND TOPOGRAPHICAL INFLUENCES

During the developmental phase of the snow shower complex prior to 0700 UTC, surface winds across eastern Colorado and parts of extreme western Kansas backed to the south in response to the development of a weak lee-side inverted surface trough. This allowed weak moisture advection from the south and subsequent moisture convergence over northwest Kit Carson and Yuma counties (Figure 13). The VAD Wind Profile from the Goodland WSR-88D (Figure 14) also showed a weak veering wind pattern from the surface to 4000 ft AGL, implying some low level warm thermal advection during this time. The combination of mid level cold advection with weak low level warm advection further helped destablize the local environment and contributed to the formation of the snow shower complex.

In addition, weak southerly surface winds flowing across the Palmer Divide provided some forced topographical ascent in a conditionally unstable environment, and also enhanced low-level cyclonic turning in the boundary layer, favoring the area north of the divide as the initial location of small-scale cyclogenesis (Szoke and Augustine 1990, Rasmussen 1992). The Palmer Divide is a ridge of land that separates the drainage area of the Platte River to the north, and the Arkansas River to the south. The divide extends from the front range of the Rockies east into northwest Kansas.

Reflectivities remained near maximum intensity prior to 0900 UTC as a result of relatively high surface dew points remaining in the vicinity of the snow shower complex. After 0900 UTC, surface

pressure rises over northern Colorado weakened the inverted lee side trough, cutting off the moist southerly inflow (Figure 15). Eventually, as northwest winds entrained over most of eastern Colorado and the axis of maximum mid-tropospheric instability moved east, the convection weakened and spread eastward as a broken line.

5. DISCUSSION AND SUMMARY

Synoptic, Mesoscale, and topographical factors over east central Colorado all contributed to an environment primed for the initiation of convection during the midst of winter. The resultant snow shower complex that formed was more analogous to an upright warm season convective system rather than a conditional symmetric instability (CSI) snow band. This event was probably a relatively rare winter occurrence for the Goodland county warning area, a region more known for explosive warm season convection. Events of this type, however, illustrate the importance of monitoring both the overall synoptic pattern and regional mesoscale influences, even during the "non-convective" season.

6. REFERENCES

Fritsch, J., and P. Hirschberg, 1991: Tropopause Undulations and the Development of Extratropical Cyclones, Part I: Overview and Observations from a Cyclone Event, *Mon. Wea. Rev.*, **119**, 496-517.

_____, and _____, 1991: Tropopause Undulations and the Development of Extratropical Cyclones, Part II: Diagnostic Analysis and Conceptual Models, *Mon. Wea. Rev.*, **119**, 518-550.

Holton, J., 1979: An Introduction to Dynamic Meteorology, Academic Press Inc. London.

Meier, K., 1993: PC-GRIDDS User's Manual. National Weather Service.

Ray, P (ed.), 1986: Mesoscale Meteorology and Forecasting, American Meteorological Society. Boston.

Rasmussen, R, 1992: Upstream Conditions Associated with the Denver Cyclone: March 14, 1991 Case Study, Fifth Conference on Mesoscale Processes, January, 1992, Atlanta, AMS (Boston).

Szoke, E. and Augustine, J., 1990: An Examination of the Mean Flow and Thermodynamic Characteristics of a Mesoscale Feature: The Denver Cyclone, Fourth Conference on Mesoscale Processes, June 1990, Boulder, AMS.

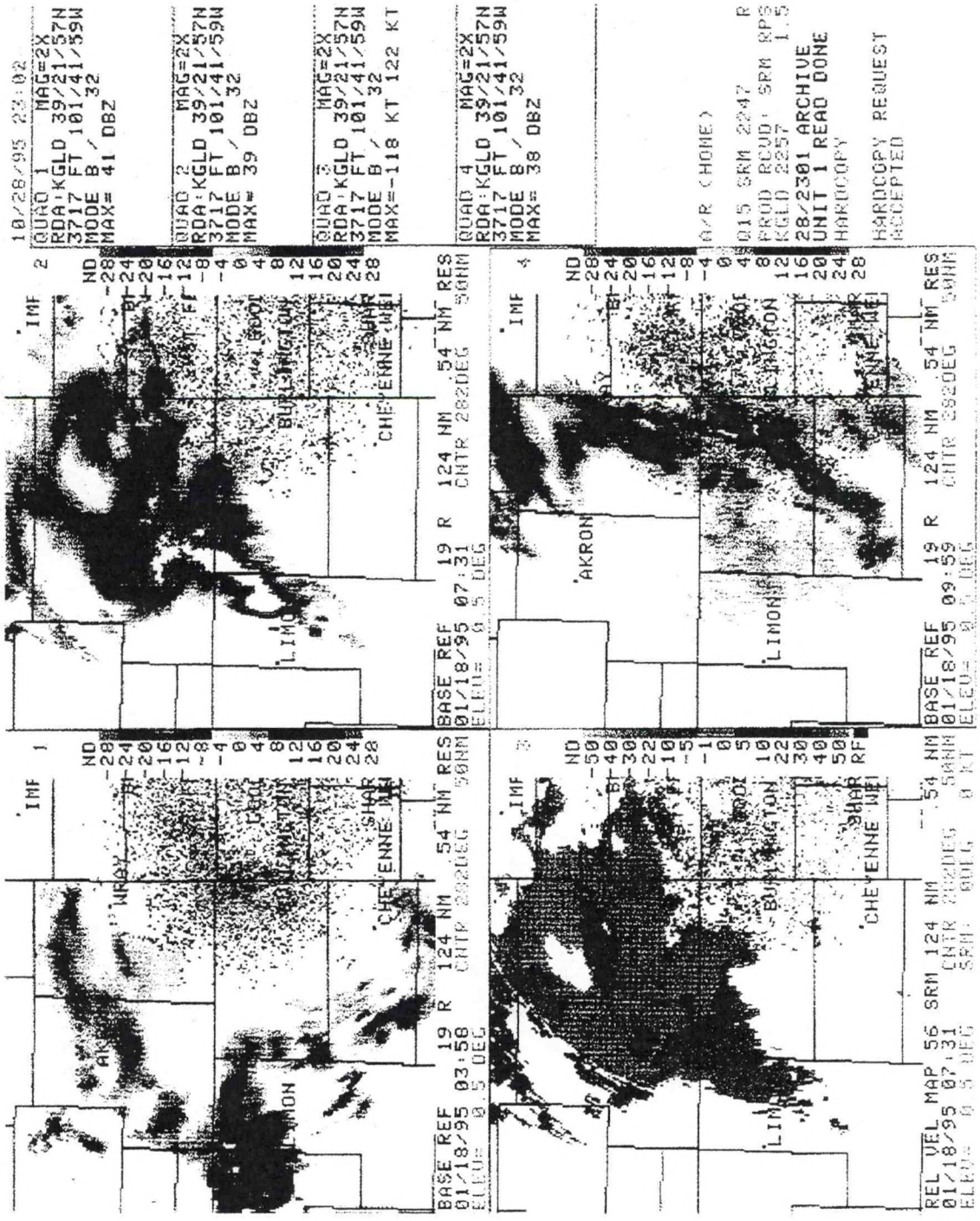

Figure 1

Figure 2

Figure 3

Figure 4

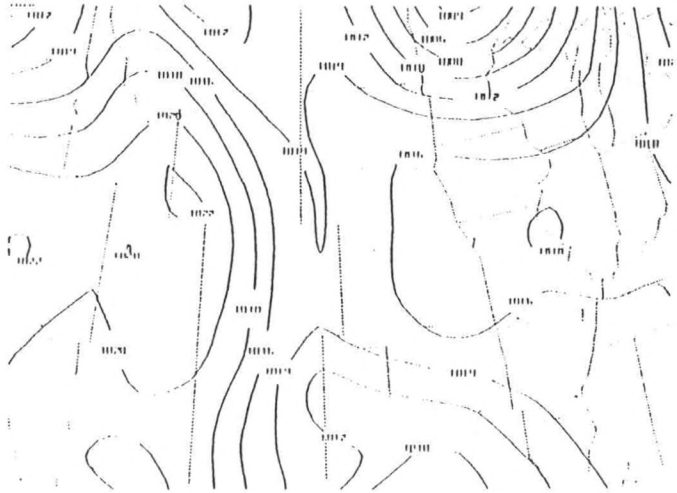

Figure 5. Mean sea level pressure (mb) forecast 6-hour forecast 0000 GMT 18 January 1995 NGM.

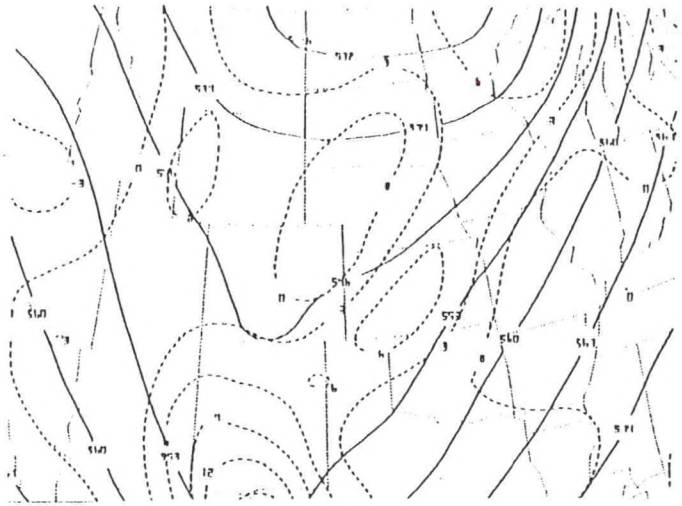

Figure 6. 500 millibar heights ($mx10^{-2}$), relative vorticity 6-hour forecast 0000 GMT 18 January 1995 NGM.

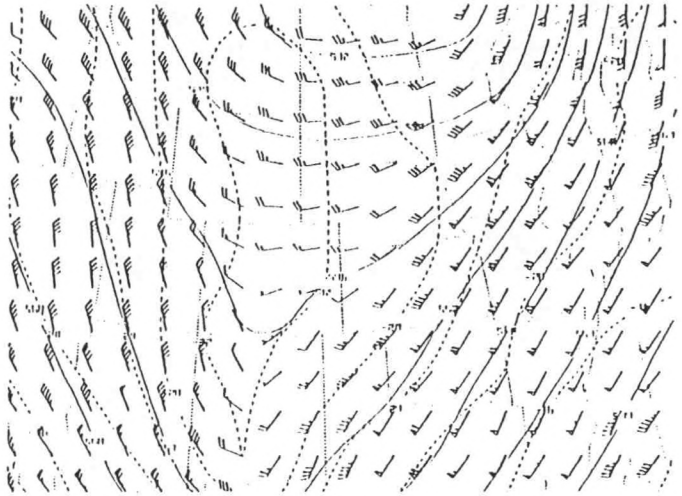

Figure 7. 500 millibar heights ($mx10^{-1}$), temperature (C), winds (Rts) 6-hour forecast 0000 GMT 18 January 1995 NGM.

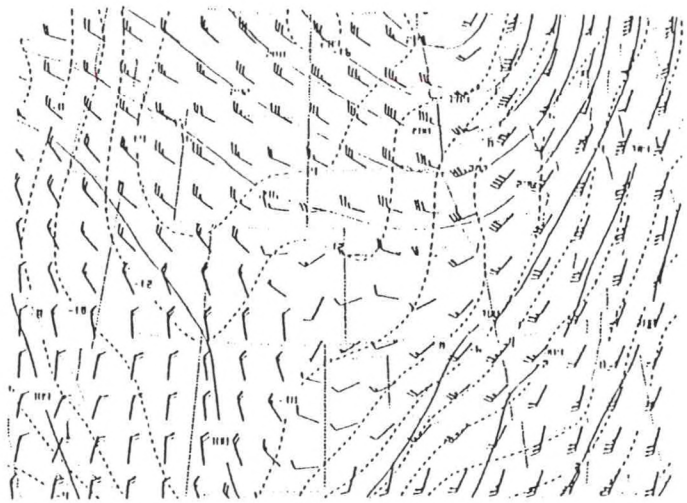

Figure 8. 700 millibar heights ($mx10^{1}$), temperature (C), winds (Rts) 6 hour forecast 0000 GMT 18 January 1995 NGM.

Figure 9. 700-500 millibar lapse rate (C). Initialization and 6-hour forecast 0000 GMT 18 January 1995 NGM. (Solid--18/00Z, Dash--18/06Z.)

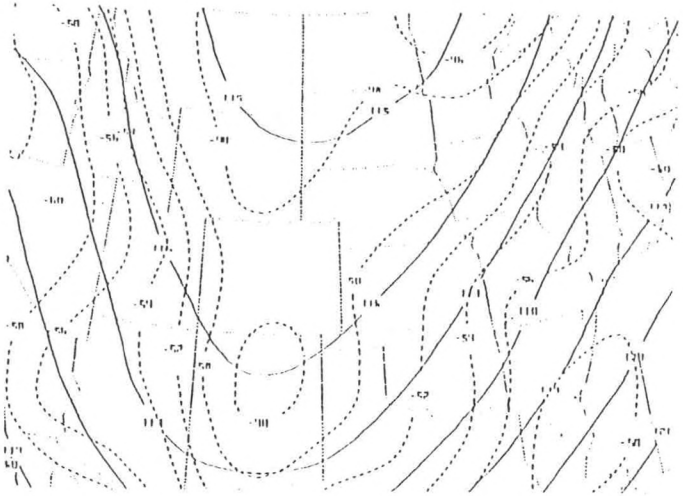

Figure 11. 200 millibar heights ($mx10^{-1}$), temperature (C) 6-hour forecast 0000 GMT 18 January 1995 NGM.

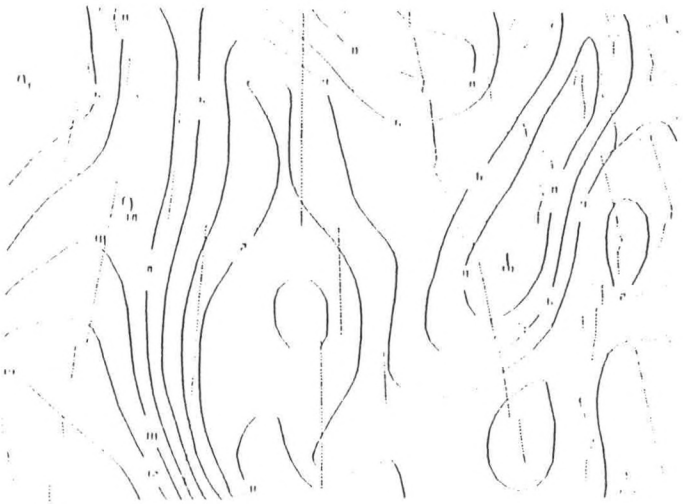

Figure 10. 700-500 millibar lifted index (C), 6 hour forecast 0000 GMT 18 January 1995 NGM.

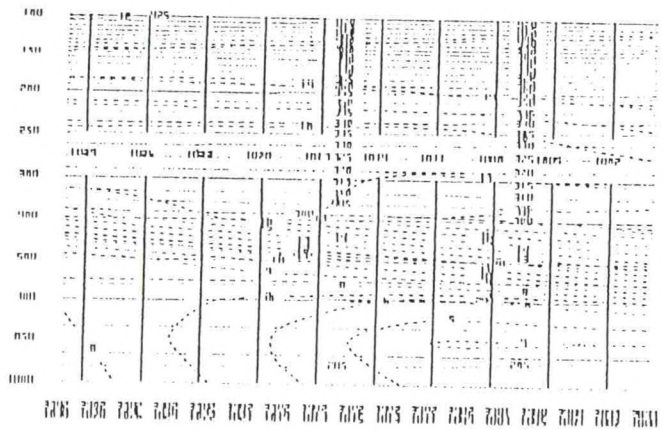

Figure 12. East-west cross-section (LIC-HLC) theta (K), relative vorticity 6-hour forecast 0000 GMT 18 January 1995 NGM.

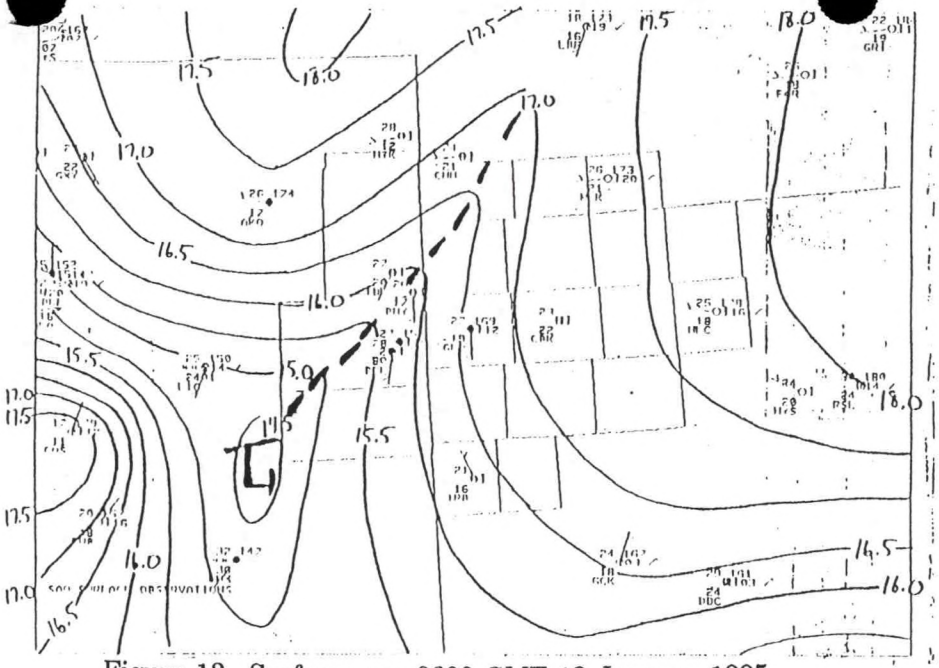

Figure 13. Surface map 0600 GMT 18 January 1995.

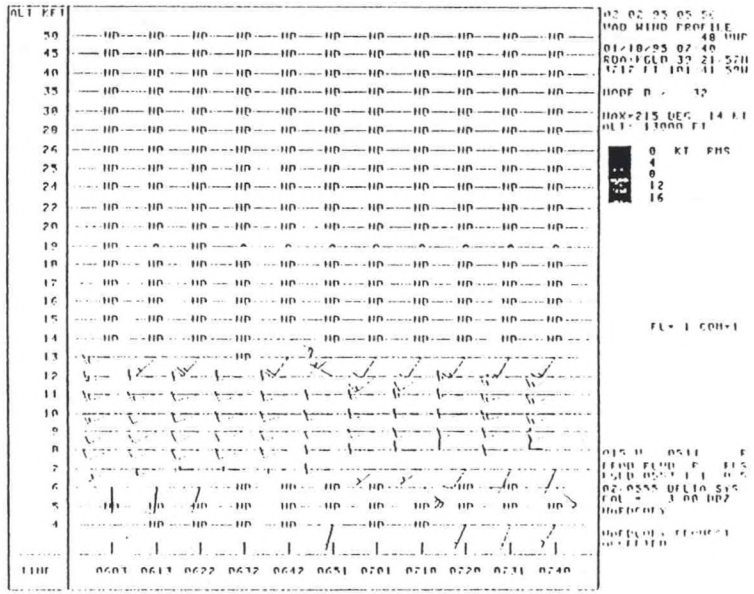

Figure 14

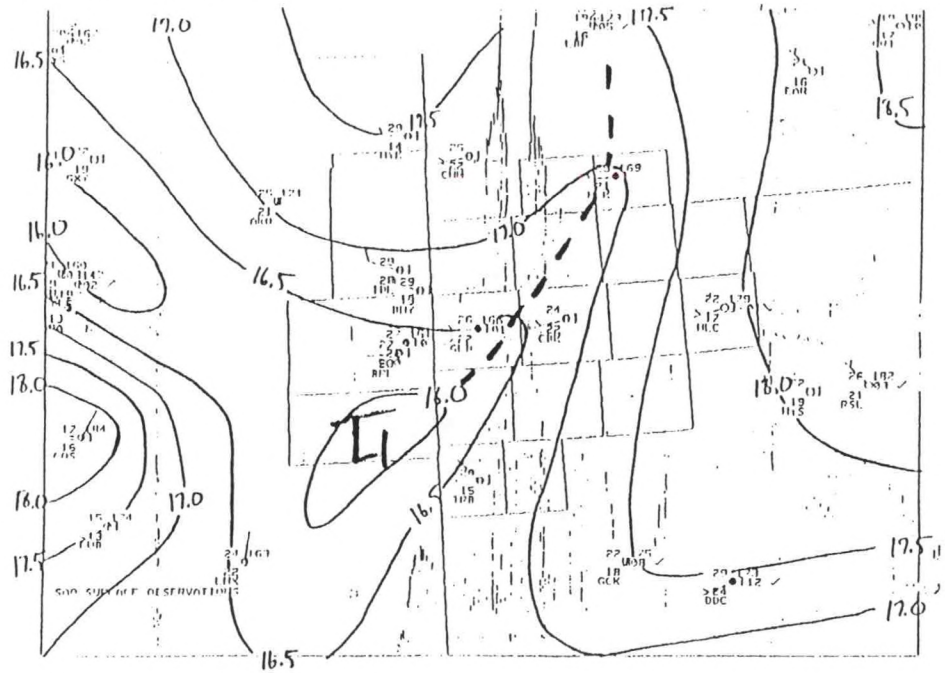

Figure 15. Surface map 0900 GMT 18 January 1995.

Lightning During Two January 1994 Winter Precipitation Events in the South Central United States

Ronald L. Holle[1] and Andrew I. Watson[2]

1. INTRODUCTION

Lightning was associated with two frozen precipitation events during January 1994 over Missouri and Arkansas. One isolated event had less than 30 flashes over Missouri, and the other had nearly 2000 flashes from Oklahoma into Arkansas. Significant frozen precipitation caused disruptions to air and ground traffic over several states, as well as power outages and fallen trees due to ice and snow.

The Storm Prediction Center (SPC) is being established in Norman, Oklahoma (McPherson 1994) to provide guidance, coordination, and short-term forecasting for winter and severe weather, and other significant meteorological events across the U.S. The extent to which lightning can play a role at SPC and other NWS offices for identifying locations and times of frozen precipitation is a major motivation for the study.

Cloud-to-ground (CG) lightning observed by detection networks has been associated with frozen precipitation at the surface in only a few publications described in Holle and Lopez (1993). Nearly all cases were during flow of cold air over large, unfrozen water bodies (Biswas and Hobbs 1990; Moore and Orville 1990; Orville 1990, 1993).

Winter thunderstorms were examined in other studies that did not use data from lightning detection networks. Curran and Pearson (1971) calculated a mean sounding in the vicinity of 76 thunder snow reports during four winters near radiosonde ascents in the U.S. There was a 100 mb subfreezing layer near the ground, topped by an 81-mb inversion whose upper half was warmer than freezing, then a deep layer with relative humidities above 90 percent; the mean sounding was moist adiabatic from 800 to 600mb. Using half-hour GOES imagery, Beckman (1986) found that clouds producing snow bursts may have originally been associated with thunder, but low-level warm advection, vertical motion and instability that generated thunderstorms weakened as clouds moved north into colder air. Colman (1990a, b) found cases of elevated thunderstorms in eastern U.S. synoptic observations during four winters on the cold side of fronts and examined their dynamic and thermodynarnic environments; Colman (1990a) said that lightning network data should be used to pursue issues raised by such observations. Stewart and King (1990) considered the region separating frozen from liquid precipitation in southern Ontario; thunder was heard by observers in one of two cases. Marwitz and Toth (1993) considered kinematic fields during a winter storm with a mixture of frozen precipitation and warm air flow ahead of a surface cold front; this is a similar situation to cases in this study.

During January 1994, a series of arctic fronts swept from northwest to southeast across the eastern two-thirds of the U.S. Low-temperature records for days, the month, and all time were set across the Midwest and Great Lakes states, especially on January 4-6 and 16-19, according to Storm Data. A complete version of this study is in Holle and Watson (1996).

1. Corresponding author address: Ronald L. Holle, National Severe Storms Laboratory, NOAA, Norman, Oklahoma.
2. Andrew I. Watson, National Severe Storms Laboratory, NOAA, Norman, Oklahoma. (Current affiliation: NWSO Tallahassee, Florida.

2. DATA

CG lightning data were collected by the National Lightning Detection Network (NLDN) described by Cummins et al. (1995) and Orville (1994). The NLDN during January 1994 was composed of direction finder antennas (Krider et al. 1980; Holle and Lopez 1993). Location accuracy for flashes within the NLDN at this time was estimated as 5-10 Ian (Cummins et al. 1995). System detection efficiency, the ratio of flashes detected by the network to the number of CG flashes that actually occurred, was estimated as 65-80 percent (Cummins et al. 1995). WSR-88D radar reflectivity and echo top heights were obtained in near real-time as products from WSI. NWS forecasts and discussions were obtained from the Experimental Forecast Facility collocated at the Norman NWS Forecast Office (Janish et al. 1995). Upper-air and surface data were obtained from NOAA's Forecast Systems Laboratory.

3. JANUARY 10, 1994 CASE

A. Lightning

Figure 1 shows locations of the 27 CG flashes observed in western Missouri on January 10 by the NLDN. There are 16 flashes lowering positive charge to ground, and 11 negative flashes from 1003 to 1340 UTC comprising the lightning event. The flashes are in regions with surface temperatures slightly above freezing. There is no recognizable organization to the flashes.

The ratio of 59 percent positive flashes is much higher than the 4 percent detected over the entire U.S. during three years (Orville 1994); the ratio is usually low in summer. High ratios of positive flashes have been noted late in the life cycle of large storms such as MCSs, during some severe storms, and cold conditions aloft. Prior cold-season results near water has shown that a majority were positive in lake-effect storms (Moore and Orville 1990), and a 13 percent ratio existed over a broad region during the East Coast Blizzard of 1993 (Orville 1993). A complete review of ratios is in Holle and Lopez (1993).

B. Winter Precipitation

A moderate pressure gradient producing south winds exists across the surface map (Figure 2). A north- south cold front is to the west, and a warm front is at the southwest corner of the map. No surface observing station in the region reported thunder or lightning any time during this event, but it is not especially unusual to have few observer reports of lightning or thunder in storms with low flash rates (Reap and Orville 1990; Changnon 1993).

Figure 2 shows freezing rain, sleet, and snow reported by observers in Nebraska, Iowa, Missouri and Illinois. Areas of mainly freezing rain and light snows are shown; sleet is reported within both regions. Several stations in the lightning region at 1300 (not shown) reported sleet at and just above the freezing point from the start of lightning at 1000 until 1200. Freezing rain is observed in Missouri starting at 1300; the area of lightning is in a region warmer than freezing at the ground 25 to 50 km southwest of the area with freezing surface temperatures. The large temperature dew point spreads to the south suggest that evaporative cooling from falling precipitation would inhibit daytime heating from warming the air to above freezing.

After lightning ended, an area of mainly freezing rain moved across Missouri. At St. Louis' Lambert Field, poor aircraft braking action was reported and several runways were closed for salt application. There were morning traffic disruptions in St. Louis until temperatures rose to above

freezing late in the morning. Frozen precipitation fell across central and northern Illinois later in the day, but there was no lightning.

C. Radar

WSR-88D radars near Kansas City and St. Louis observed the event. Radar reflectivity from Kansas City (not shown) before the lightning was in small, short lines in western Missouri, and mom continuous echoes from eastern Missouri were detected into western Illinois during the lightning event. Reflectivities were mostly 20 to 30 dBZ, but were above 35 in a few areas. The area of returns above 30 dBZ grew, reached a maximum, and dissipated during nearly the same time as lightning.

A few hours later at 1500, Figure 3 shows Kansas City reflectivity, and echo tops in western Missouri that reach 5.8 km (18,000 ft). Convective elements in the stratiform area are better identified by high tops east of Kansas City. In central Missouri, St. Louis (not shown) saw tops up to 6.1 km (20,000 ft). Over eastern Missouri, St. Louis detected reflectivities exceeding 35 dBZ over much larger areas than Kansas City.

Both radars show somewhat concentric features with different orientations in eastern Missouri. Higher reflectivities in central and northern Missouri observed from St. Louis are ascribed to the radar beam intersecting the melting level at the 0.5° elevation angle from 50 to 75 n mi (90 to 140 km) from the radar. The Monett sounding (Figure 4, right) is farther south and entirely above freezing from the surface to higher than 800 mb. Farther north in Missouri, the highest level where temperatures are above freezing and melting begins is in the altitude range of 0.8- 1.2 km according to maximum reflectivity in Figure 4.

D. Warm-Layer and Instability Formation

The sounding from Monett at 0000 UTC is warmer than freezing below 850 (Figure 4, left) but dry up to 550 mb. Twelve hours later, a layer warmer than freezing up to 800 is nearly saturated up to 650 mb (Figure 4, right), while the same temperatures remain above. A saturated parcel lifted just above 850 mb at 1200 gives a temperature difference from observed of 3°C at 700 mb. Southwest winds up to 28 m s^{-1} are in this layer at 1200.

The St. Louis NWS midmorning discussion on January 10 said that "0000 UTC model guidance did a poor job handling the overnight warming of the low levels due to a low-level jet exceeding 50 kt (26 m s^{-1}) from the Southern Plains into southwestern Missouri." This warm air aloft was in a narrow band ahead of the advancing arctic front. The advection at 1200 UTC 10 January (Figure 5) is shown in the middle of the lightning period with a combination of profiler winds at 1500 m and 850-mb data from upper-air stations. There is southwest flow over 30 kt over a large region, and winds are over 50 kt just upwind from the lightning.

The low-level jet was difficult to detect with the spacing of upper-air stations and the 12-h interval between soundings. But the jet was strong enough to produce an elevated warm moist layer. The steepest lapse rate from 850 to 500mb in western Missouri at the time of lightning was due mainly to warming near 850 mb; there was slight cooling at 500mb. Lightning occurred where precipitation developed with cloud tops reaching 6 km These taller and stronger radar echoes translated to the northeast into regions with surface temperatures colder than freezing where rain continued.

The progression of upper-air patterns on January 10 is shown by quasi-geostrophic (QG) analyses in Figure 6. Lightning is over western Missouri from 1003 to 1340 (Figure 1). The analyses at 0000

(top) and 1200 (bottom) show contributions to vertical motion due to temperature advection $-R\sigma^{-1}p^{-1}\nabla_p^2(-\mathbf{v}_g \cdot p\mathbf{T})$ at 700 mb with 700-mb contours. Vertical motion contributions due to differential vorticity advection $-f_0\,\sigma^{-1}\,\partial/\partial p[-\mathbf{v}_g \cdot \nabla p\,(\zeta_g + f)]$ in the 850-500 mb layer are in Holle and Watson (1996). At 0000, temperature advection is contributing to downward motion over eastern Oklahoma and Kansas and upward motion to the west, but there is no contribution to vertical motion from differential vorticity advection. At 1200 during the time of lightning over western Missouri, there is a large contribution from temperature advection in the region of the flashes and a small contribution to upward motion due to differential vorticity advection.

E. Forecast Issues

The NWS National Severe Storms Forecast Center in Kansas City included the possibility of thunderstorms in the region, and noted on the morning of January 10 a few strikes were in western Missouri. At 1220 UTC 10 January, the Kansas City NWS forecast mentioned the likelihood over the next hour of "a few thunderstorms producing brief periods of heavy sleet." Local NWS stations had access to gridded flash information, but not individual flash data as at the Center.

At 0345 CST/0945 UTC 10 January, the St. Louis NWSFO forecast discussion anticipated that there would be "a mixed bag of precipitation today . . once we see where it gets organized may have to go with advisory, however temperatures will remain generally above freezing today". The main concern was more with snow than freezing rain at this time. At 0955 CST/1555 UTC 10 January the St. Louis discussion mentioned the threat of frozen precipitation due in part to evaporative cooling, but expected it to end quickly through the day. Since no lightning or thunder was reported at any hourly observing site, staff may not have been aware of the existence of the flashes.

4. JANUARY 16-17, 1994 CASE

A. Lightning

Figure 7 shows locations of 2,417 cloud-to-ground flashes observed by the NLDN during 12 hours in the South Central US starting at 1800 UTC 16 January. Figure 7a shows that lightning during the first four hours are mainly in areas colder than freezing; the scattered flashes resemble January 10. During the next four hours (Figure 7b), lightning begins in areas warmer than freezing and ends in colder areas to the northeast; flashes tend to be aligned in a linear or banded structure from southwest to northeast. All flashes after 0200 (Figure 7c) are at above-freezing ground temperatures. Lightning was in a similar configuration to thunderstorms in Colman (1990a, b) that originated mainly in warm air south of the warm front and continued above the frontal surface. After 0600, flashes were in and near Louisiana.

Of the flashes, 52 percent during the first four hours were positive when lightning was mainly in regions of subfreezing surface temperatures. A similar value of 59% was shown for January 10 (Figure 1). For the 18-hour period ending at 1000, 29 percent of the flashes lowered positive charge to ground. There was a tendency for positive flashes to be more frequent on the northeast ends of individual lines. A higher positive ratio toward the end of a storm is often found in less severe convection such as MCSs, but severe storms can be dominated by positive flashes through a portion or all of their lifetime (MacGorman and Burgess 1994).

B. Winter Precipitation

A weak pressure gradient producing light southerly wind is across the surface map of Figure 8. A strong cold front is on the edge of the map to the northwest, and a warm front is across the

southern border of Arkansas. Fort Smith (FSM) reported thunder, freezing rain, and fog at 2200 and 2300 16 January (Figure 8) and at 0000 17 January. Freezing rain was light at 2200 and moderate at 2300 and 0000. McAlester reported a surface temperature of 1°C (34°F) with thunder and rain at 0300. Freezing rain was reported during this event in portions of seven states. Snow was to the north in Missouri and sleet was within portions of the freezing rain and snow areas. Warmer temperatures, fog, and rain were south of the frozen precipitation. Three Automatic Weather Observing System (AWOS) stations in northeast Arkansas had calm winds at 2300 (Figure 8) and for several hours around this time when adjacent stations reported freezing rain or rain; the wind sensors apparently were frozen due to accumulated ice. In addition, no present weather was observed or transmitted by these AWOS stations.

At 1030 UTC 16 January, Little Rock issued winter storm warnings over north and central Arkansas for total accumulations of 10 cm (4 in) of ice and snow. Oklahoma City on the afternoon of 16 January stated that "roadways throughout northeast and east-central Oklahoma remain icy and hazardous. Travel is discouraged." After 0100 17 January, freezing rain was in a band from northern Arkansas into southern Indiana.

Storm Data reported widespread accumulations of ice and snow up to 7.6 cm (3 in) in eastern Oklahoma and 12.7 cm (5 in) in northern Arkansas; a few parts of northeast Arkansas received up to 20 cm (8 in). A large number of trees and power lines were knocked down by the weight of ice and snow, and 15,000 electric customers were without power at the height of the storm. Traveling was described by the Little Rock NWSFO as "almost impossible in many areas" in the northern half of Arkansas during the night, and snow and ice remained on some roads for several days over northern Arkansas as cold air spread over the area.

C. Radar

The Little Rock radar at 0005 UTC 17 January (Holle and Watson 1996) had scattered echoes in southern Arkansas and more continuous echoes to the north; several short lines of higher reflectivity are evident. Frequent lightning had begun in western Arkansas during the previous two hours (Figure 7a). Reflectivities exceeded 35 dBZ in several regions to the north; one small area exceeded 50 dBZ within a large area of strong returns. However, locations of convective elements embedded in the stratiform precipitation are better shown by echo tops (not shown) as on January 10 (Figure 3). Cell tops exceed 11 km (30,000 ft) in western Arkansas where lightning was occurring (Figure 7b).

Five hours later at 0500 (Figure 9), radar shows a large area of reflectivity exceeding 35 dBZ some areas exceed 50 dBZ. Freezing rain, snow, and rain are reported at the surface. A few echo tops continue to reach over 11 km (30,000 ft) in the lightning area. The strong echo 75 km north of Little Rock at 0500 is just east of the cold front Arkansas and north of the warm front.

The high reflectivities in the east-west region across northern Arkansas (Figure 9) are ascribed to the radar beam intersecting the melting level at the 0.5° elevation angle from 40 to 70 n mi (75 to 130 km) from the radar. Upper-air soundings at Monett (not shown) taken to the north of the high reflectivities show temperatures at 0000 UTC entirely colder than freezing but close to 0°C from 810 to 750 mb. Over the region of strong reflectivity, some sounding was warmer than freezing, but not as much as at Little Rock (not shown). Farther north in Arkansas, then, a layer exists where melting is at temperatures a little warmer than freezing in the altitude range of 0.7-1.1 km according to the maximum in radar reflectivity in Figure 9.

In the January 10 case, lightning occurred at the same time as the increase in areal coverage on radar and the appearance of moderate reflectivity cores (Figure 3). For the January 16-17 case, stronger cores appeared near the time of first lightning before 1800 (Figure 7). However by this time the area of radar echoes was quite extensive, although maximum reflectivities were weak.

D. Warm-Layer and Instability Formation

The evening forecast discussion from Oklahoma City at 0310 UTC 16 January pointed out that "rich low-level moisture was flowing northward over the shallow cold air mass over the central plains." A series of three soundings at Little Rock (Holle and Watson, 1996) shows:

- At 1200 UTC 16 January, a shallow layer was above freezing between 800 and 875 mb. Strong veering of the wind, implying warm advection, was at low levels.

- 12 hours later, a deeper layer from 725 to 950 mb exceeded O°C while surface temperatures were below freezing. The warm moist layer was advected into the area by west-southwest flow at 25 to 36 ms-1, while it was very dry above 700 mb 12 hours earlier. Large-scale ascent may have assisted the moistening.

- After another 12 hours, all temperatures were below freezing again, drier conditions existed above 800 mb, and winds below 600 mb were from north to northwest after the cold front passed Little Rock.

These features are similar for both January 1994 events. The maximum temperature difference at Little Rock was 1.5°C at 685 mb when calculated by lifting a parcel from the top of the warm layer at 0000. The 850-500 mb lapse rate is 22°C at Fort Smith when thunder and freezing rain was reported, and 17°C from 700-500 mb. The 850-500 lapse rate was slightly higher 12 hours earlier at Fort Smith. Steepest lapse rates are due to warming from 850-700 mb and not to cooling at 500 mb. Trends and lapse rates are similar to January 10, but temperature differences are not as large. Warm air advection aloft was over a larger region than on January 10, so it was detected at several upper-air stations and 12-hourly sounding times.

A north-south cross section at 0000 UTC (Holle and Watson 1996) from near Kansas City into the Gulf of Mexico during the time when lightning occurred shows conditional symmetric instability (CSI) to the north below 800 mb. As required for CSI (Sanders and Bosart 1985; Snook 1992; Moore and Lambert 1993), conditions are near saturation, there is little directional shear in the vertical, and θ_e lines are somewhat more vertical than momentum lines. The linear lightning paths (Figure 7) may track an individual thunderstorm or a succession of convective updrafts that formed in the conditionally unstable environment and moved northeast in the unsheared flow. Browning and Foster (1995) shows radar images of narrow bands of significant icing at the surface and mentions the observation of thunder. The January 16-17 case is similar to thunderstorms associated with frozen precipitation in Colman (1990a, b); those storms also had their origins as upright convection in warm air south of the warm front. The air then traveled over a cold surface during CSI conditions; radar events averaged 200 km long and lasted 4.9 hours.

Major changes occurred at upper levels between 0000 and 1200 UTC 17 January as shown by QG analyses (Holle and Watson, 1996). Figure 7b shows lightning at 0000 over southeast Oklahoma and farther south and east. At 0000, temperature advection is the dominant contributor to upward vertical motion from central Texas northeast into eastern Oklahoma and is in nearly the same orientation as lightning at this one. The contribution from differential vorticity advection is minimal. In the same region of northeast Texas and eastern Oklahoma 12 hours later, temperature advection

contributes to downward motion while differential vorticity advection contributes to upward motion. While differential vorticity advection has strengthened, the arrival of colder and drier air at lower levels eliminated the possibility of continuing convection in the region. These QG results are similar to those found for January 10--low-level temperature advection made the main contribution to upward vertical motion in both cases at the times and places of flashes while the influence of differential vorticity advection was a much weaker factor.

E. Forecast Issues

The NWS National Severe Storms Forecast Center included the possibility of thunderstorms associated with snow or freezing rain from Texas into northern Arkansas and western Tennessee in its 1300 UTC 16 January convective outlook. In Oklahoma, the Tulsa area forecast discussion at 0425 CST/1025 UTC 16 January remarked that "gridded data show significant instability developing above the surface with Totals of 48 to 50 in southeast Oklahoma by this evening, so can't rule out thunder, even in the freezing rain areas near Fort Smith." In Arkansas, the Little Rock forecast discussion at 0330 UTC 16 January pointed out the need to "use some intuitive forecasting skills based on experience and interpretation" concerning the type and amount of precipitation that would occur as numerical models predicted southerly-component air to override the arctic air. Little Rock issued accurate winter storm watches at this time across the northern half of the state; winter storm warnings seven hours later stated that "significant ice accumulations are possible". At 1515 UTC 16 January, Little Rock noted that radar echo coverage "had increased considerably over the previous couple of hours". Lightning was not mentioned explicitly in Arkansas forecast products until the evening of 16 January for a chance of thunder in the above-freezing air over the southern half of the state.

5. CONCLUSIONS

Lightning began while the reflectivity cores reached moderate intensity for both cases, but areal coverage on radar became extensive several hours before first lightning in one event and at the same time in the other. On January 10 the national lightning network detected 27 CG flashes in portions of Missouri that were within 2°C on either side of the freezing point at the ground. A total of 2,417 flashes was detected during the January 16-17 event; flashes at the start were in regions below freezing at the ground, then new lines of flashes formed in above-freezing surface air to the southwest and ended in subfreezing surface air to the northeast. No organized configuration was evident on 10 January. Thunderstorms were not observed at any surface station on January 10 and at only two stations for a few hours on January 16-17. There was a high ratio (59 percent) of positive flashes to total on January 10, and a similar value of 52 percent during the first four hours of the January 16-17 event where surface temperatures were subfreezing. For the entire January 16-17 case, the positive ratio was 29 percent.

WSR-88D radar echoes had tops up to 6 km on January 10 and 10 km on January 16-17 near lightning and thunderstorms. Some reflectivity levels were strong and in partial concentric rings because of beam intersection with the bright band.

Upper-air soundings for both events showed layers between 800 and 900 mb that were warmer than freezing for less than 24 hours in the regions of lightning. These layers contained strong southwest flow advecting warmer, nearly saturated air. Lightning occurred in a CSI region on January 16-17, but not on January 10. For both cases, quasi-geostrophic analyses showed that low level temperature advection was a much more important contributor to upward motion in the area of lightning than was differential vorticity advection.

Analysis of these two events shows the potential for real-time lightning detection network data to provide information that, when combined with other meteorological data, shows where and when a thunderstorm exists that may not be otherwise detected. In both cases, standard upper-air data showed the low level jet and associated instability in a small area for a few sounding times, and thunder was observed infrequently or not at all at surface stations. These two factors made it difficult to identify with conventional approaches and datasets the important features that formed frozen precipitation.

6. ACKNOWLEDGMENTS

The assistance of John Cortinas, Charlie Crisp, Paul Janish, Robert Maddox, and Conrad Ziegler of NSSL in Norman is gratefully acknowledged.

7. REFERENCES

Beckman, S.K., 1986: Effects of convective type clouds on heavy snow as viewed by GOES satellite imagery. *Preprints, Second Conf. on Sat. Meteorology/Remote Sensing and Applications,* Williamsburg, VA, AMS (Boston), 212-217.

Biswas, K.R., and P.V. Hobbs, 1990: Lightning over the Gulf Stream. Geophys. Res. Lett., 17, 941-943.

Browning, W.D., and M.P. Foster, 1995: Forecast and detection of conditional symmetric instability: A case study. *Preprints, 14th Conf. on Wea. Anal. and Forecasting,* Dallas, TX, AMS (Boston), 199-203.

Changnon, S.A., 1993: Relationships between thunderstorms and cloud-to-ground lightning in the United States. *J. Appl. Meteor.,* **32**, 88-105.

Colman, B.R., 1990a: Thunderstorms above frontal surfaces in environments without positive CAPE. Part I: A climatology. *Mon. Wea. Rev.,* **118**, 1103-1121.

_____, 1990b: Thunderstorms above frontal surfaces in environments without positive CAPE. Part II: Organization and instability mechanisms. *Mon. Wea. Rev.,* **118**, 1123-1144.

Cummins, K.L., E.A. Bardo, W.L. Hiscox, R.B. Pyle, and A.E. Pifer, 1995: NLDN'95: A combined TOA/MDF technology upgrade of the U.S. National Lightning Detection Network. *Postprints, Intl. Aerospace and Ground Conf. on Lightning and Static Electricity,* Williamsburg, VA

Curran, J.T., and A. D. Pearson, 1971: Proximity soundings for thunderstorms with snow. *Preprints, 7th Conf. on Severe Local Storms,* Kansas City, MO, AMS, 118-119.

Holle, R.L., and R.E. Lopez, 1993: Overview of real-time lightning detection systems and their meteorological uses. NOAA Tech. Memo. ERL NSSL-102,68pp.

_____, and A.I. Watson, 1996: Lightning during two central United States winter precipitation events. *Wea. Forecasting* [conditionally accepted].

Janish, P.R., M.L. Branick, and L.J. Ruthi, 1995: The experimental forecast facility: Establishing collaboration between applied research and NWS operations. *Preprints, 14th Conf. on Wea. Analysis and Forecasting,* Dallas, AMS (Boston), 17-22.

Krider, E.P., R.C. Noggle, A.E. Pifer, and D.L. Vance, 1980: Lightning direction-finding systems for forest fire detection. *Bull. Amer. Meteor. Soc.*, **61**, 980-986.

MacGorman, D.R., and D.W. Burgess, 1994: Positive cloud-to-ground lightning in tornadic storms and hailstorms. *Mon. Wea. Rev.*, **122**, 1671-1697.

Marwitz, J.D., and J. Toth, 1993: A case study of heavy snowfall in Oklahoma. *Mon. Wea. Rev.*, **121**, 648-660.

McPherson, R.D., 1994: The National Centers for Environmental Prediction: Operational climate, ocean, and weather prediction for the 21st century. *Bull. Amer. Meteor. Soc.*, **75**, 363-373.

Moore, J.T., and T.E. Lambert, 1993: The use of equivalent potential vorticity to diagnose regions of conditional symmetric instability. *Wea. Forecasting*, **8**, 301-308.

Moore, P.K., and R.E. Orville, 1990: Lightning characteristics in lake-effect thunderstorms. *Mon. Wea. Rev.*, **118**, 1767-1782.

Orville, R.E., 1990: Winter lightning along the East Coast. Geophys. Res. Lett., 17, 713-715.

_____, 1993: Cloud-to-ground lightning in the Blizzard of '93. Geophys. Res. Lett., 20, 1367-1370.

_____, 1994: Cloud-to-ground lightning flash characteristics in the contiguous United States: 1989-1991. *J. Geophys. Res.*, **99**, 10,833-10,841.

Reap, R.M., and R.E. Orville, 1990: The relationships between network lightning locations and surface hourly observations of thunderstorms. *Mon. Wea. Rev.*, **118**, 94-108.

Sanders, F., and L.F. Bosart, 1985: Mesoscale structure in the megalopolitan snowstorm of 11-12 February 1983. Part 1: Frontogenetical forcing and symmetric instability. *J. Atmos. Sci.*, **42**, 1050-1061.

Snook, J.S., 1992: Current techniques for real-time evaluation of conditional symmetric instability. *Wea. Forecasting*, **7**, 430-439.

Stewart, R.E., and P. King, 1990: Precipitation type transition regions in winter storms over southern Ontario. *J. Geophys. Res.*, **95**, 22,355-22,368.

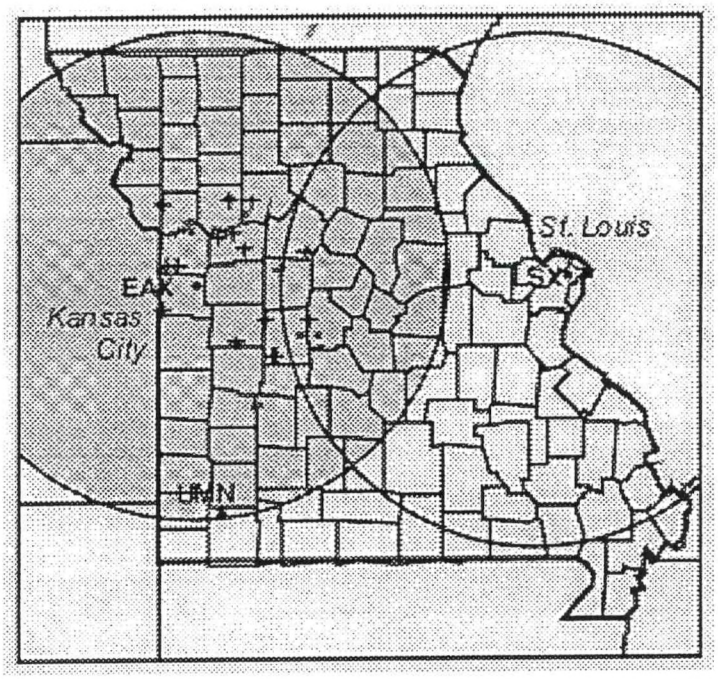

Figure 1. Missouri counties and 230-km (124-n mi) range from Kansas City (EAX, shaded) and St. Louis (LSX) radars. Negative cloud-to-ground flashes from 1003 to 1340 UTC 10 January 1994 are shown by a square; positive flashes, by a +. UMN locates Monett upper-air station.

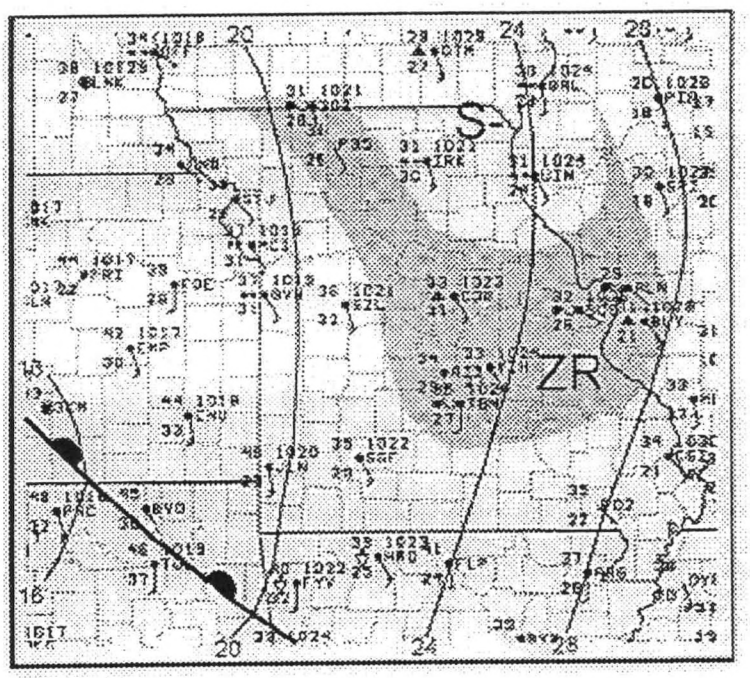

Figure 2. Surface map for middle Mississippi Valley at 1500 UTC 10 January. Shading and ZR shows regions with freezing rain; S- for mainly snow.

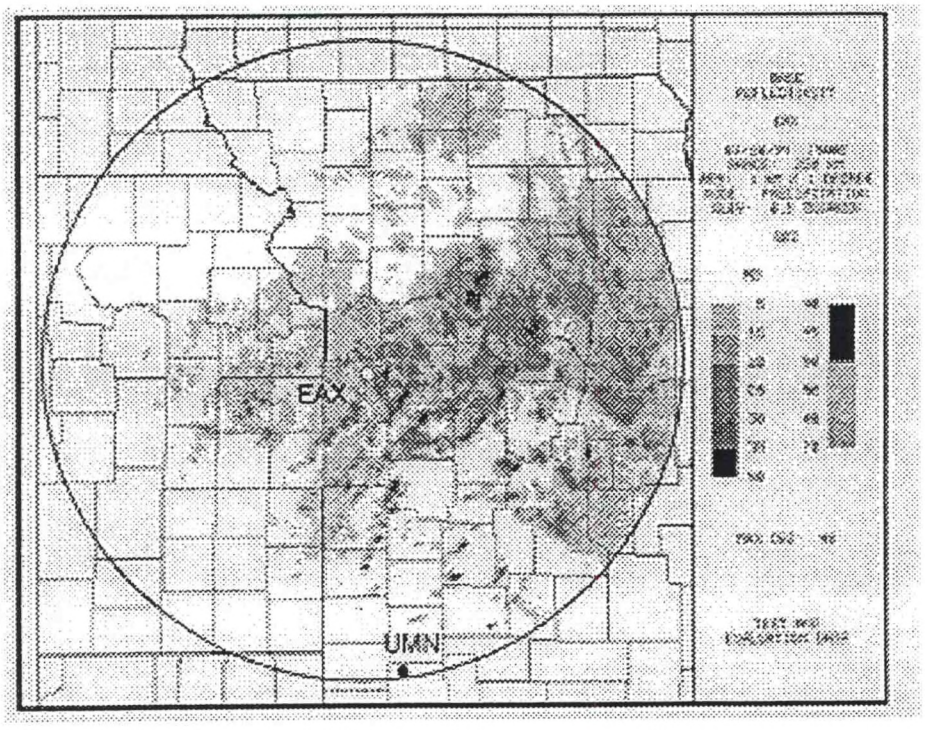

(A)

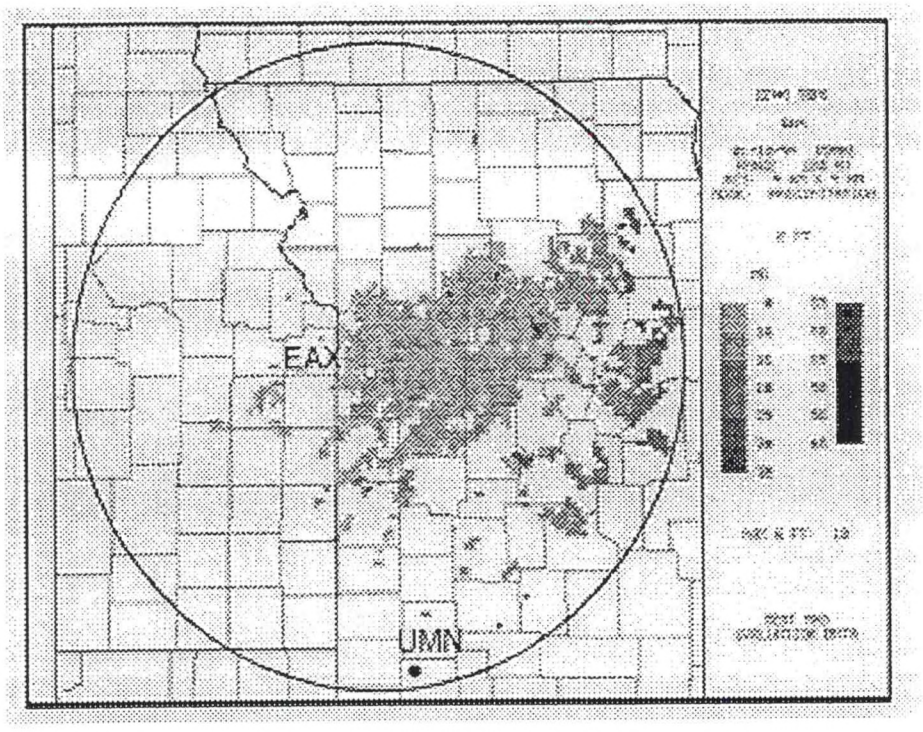

(B)

Figure 3. Radar reflectivity (A) and echo tops (B) from WSR-88D radar at Kansas City (EAX) at 1500 UTC 10 January. Circle is 230-km (124-n mi) range from radar.

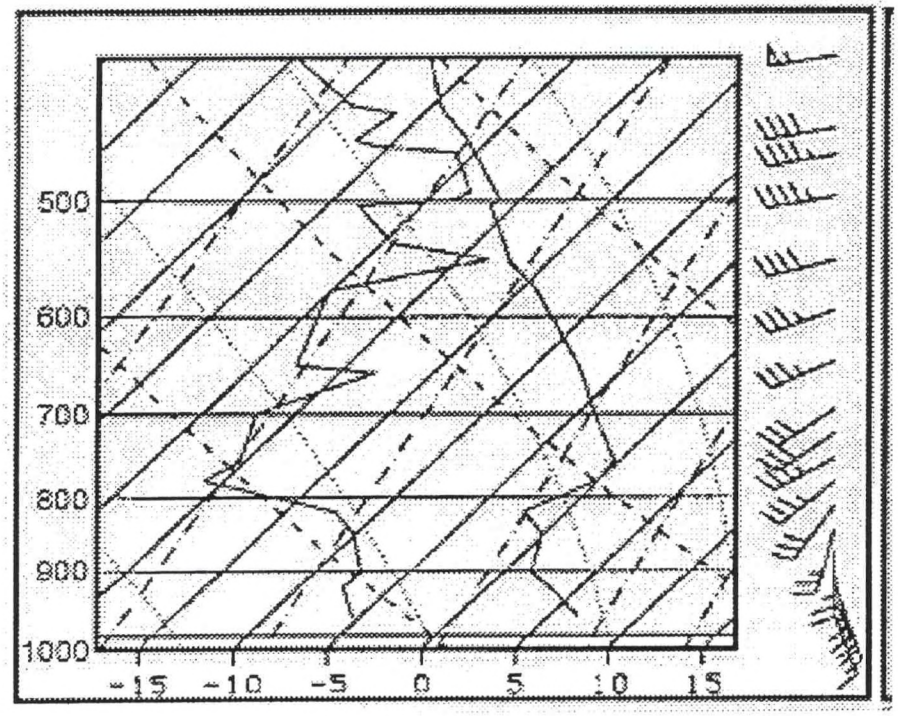

(A)

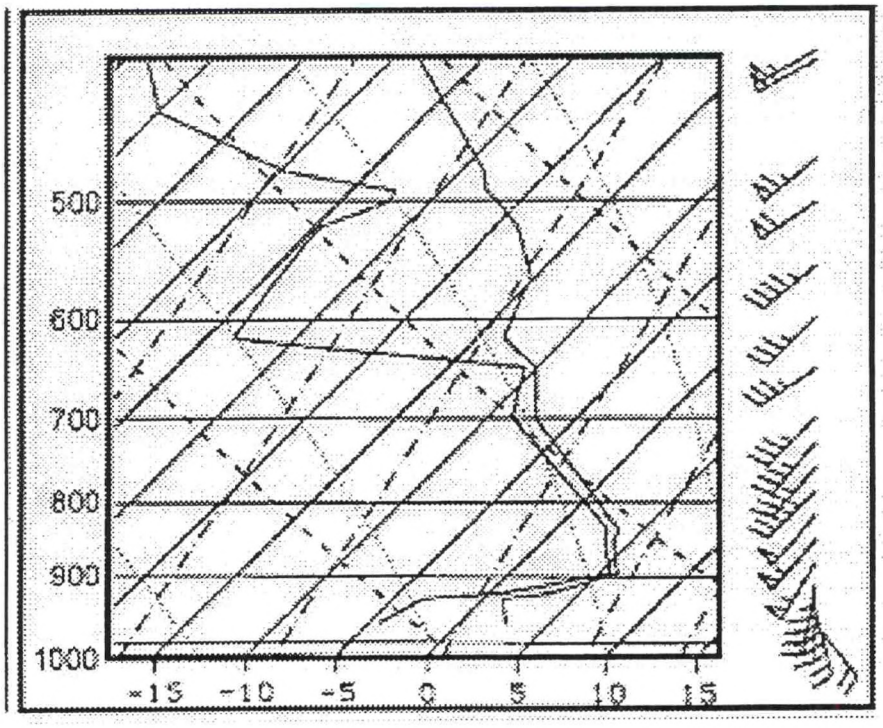

(B)

Figure 4. Temperature and dew point soundings at Monett at 0000 (A) and 1200 UTC (B) January 10, 1994. Solid lines are temperature and dew point.

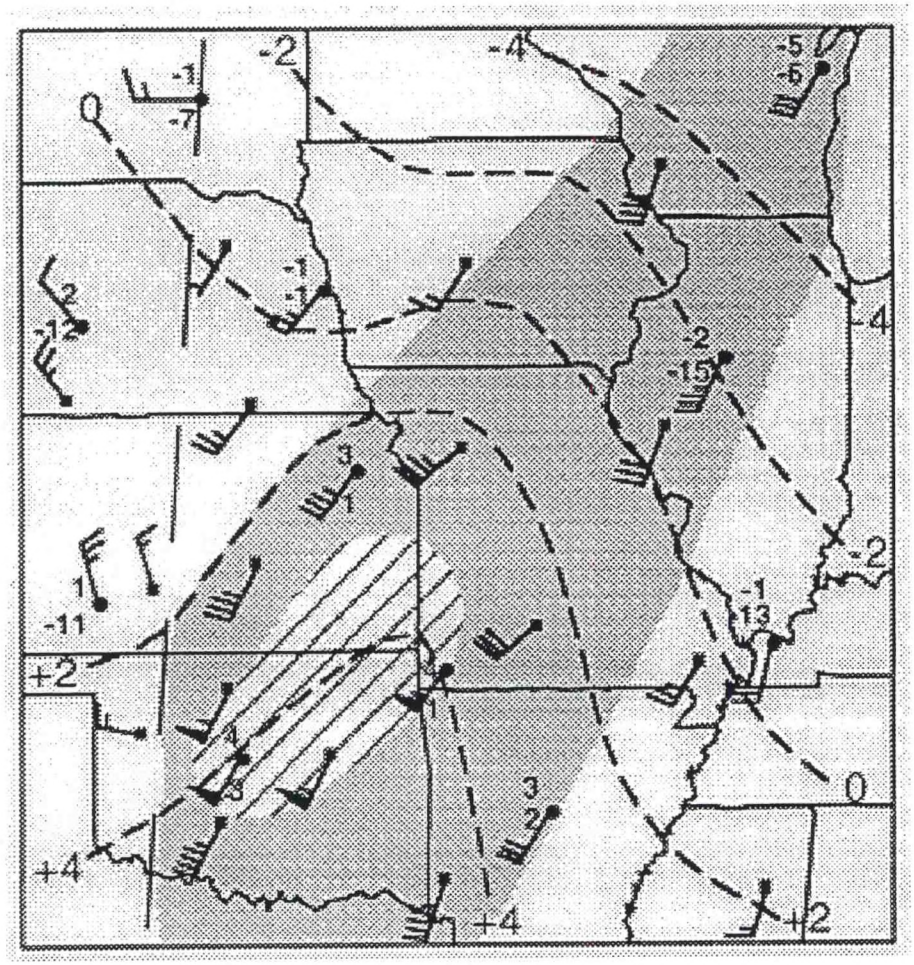

Figure 5. Wind at 1500 m from profilers (square station). 850-mb wind, temperature (upper number), and dew point (lower) at upper-air stations (circle) at 1200 UTC 10 January. Winds over 50 kt hatched horizontally, over 30 kt shaded. 850-mb temperatures shown by dashed isotherms. North-south dashed line is wind shift.

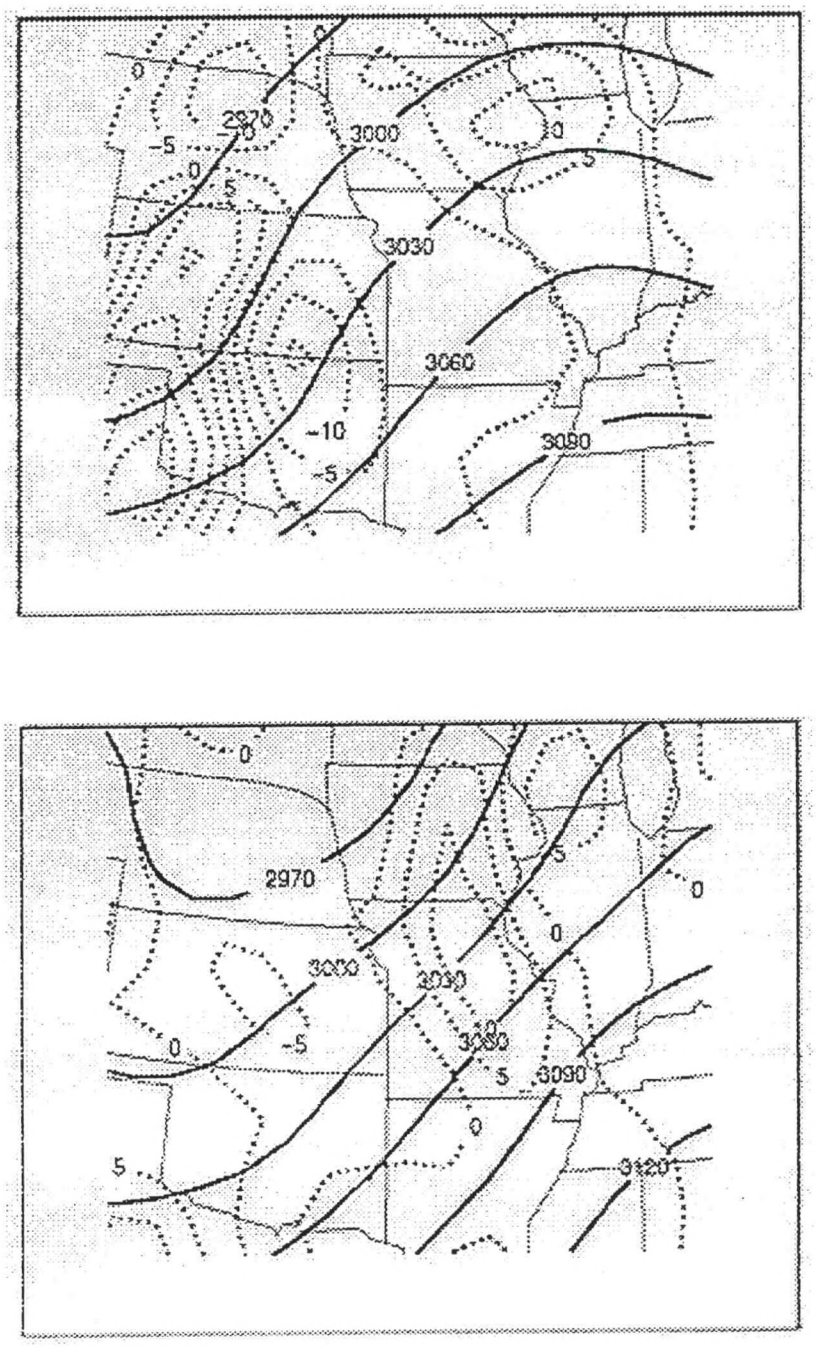

Figure 6 Upper-air data at 0000 (top) and 1200 UTC (bottom) 10 January. 700-mb height contours are solid. Contributions to upward (positive) and downward (negative) vertical motion from temperature advection is dotted and scaled by 10-14 mb s^{-1} m^{-2}.

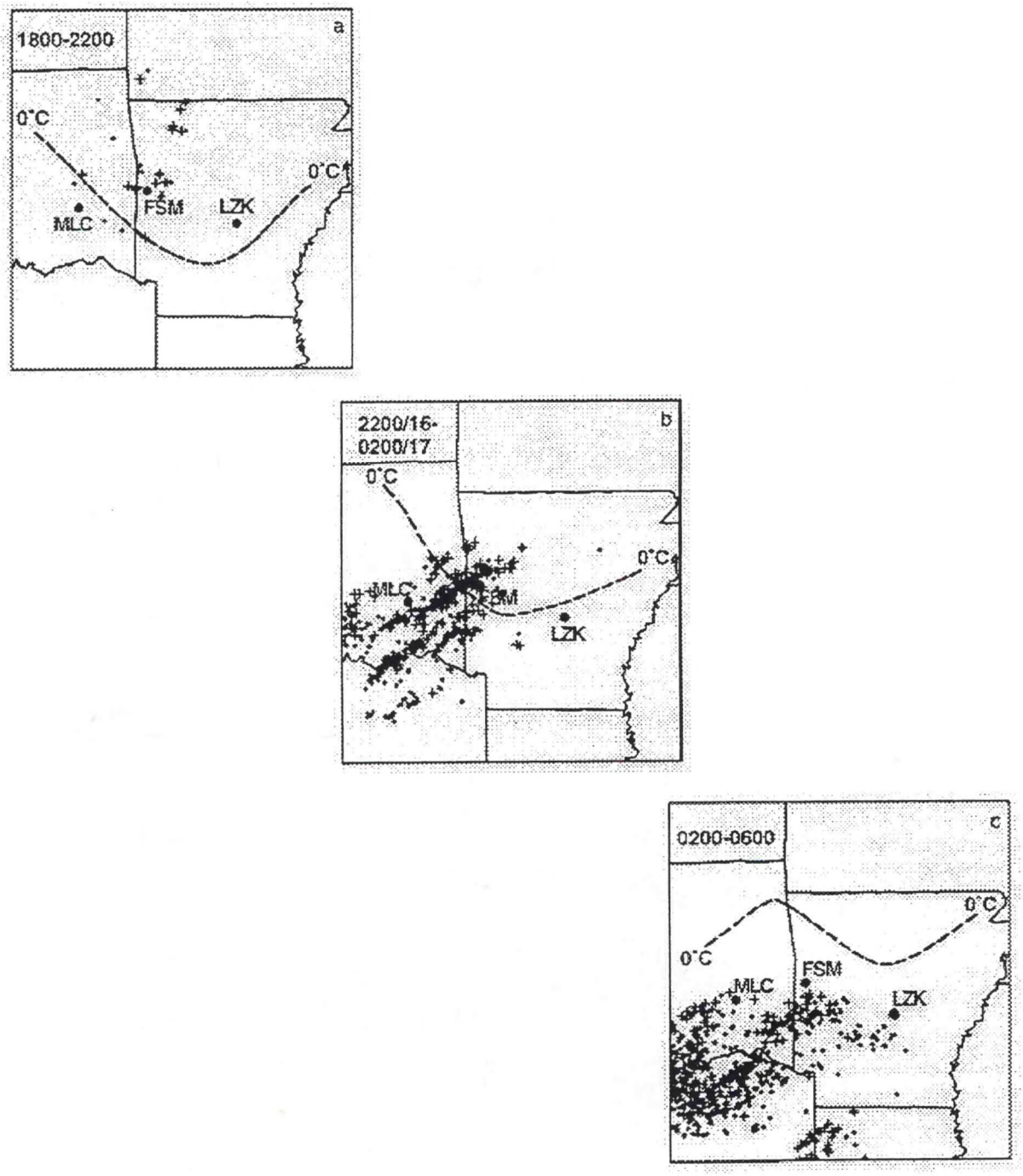

Figure 7. Lightning in South Central U.S. by 4-hour intervals from 1800 16 January to 0600 UTC 17 January. Negative flashes shown by small +; positive, by large +. MLC is McAlester, FSM is Fort Smith, and LZK is Little Rock. 0°C surface isotherm shown by dashed line for center of period.

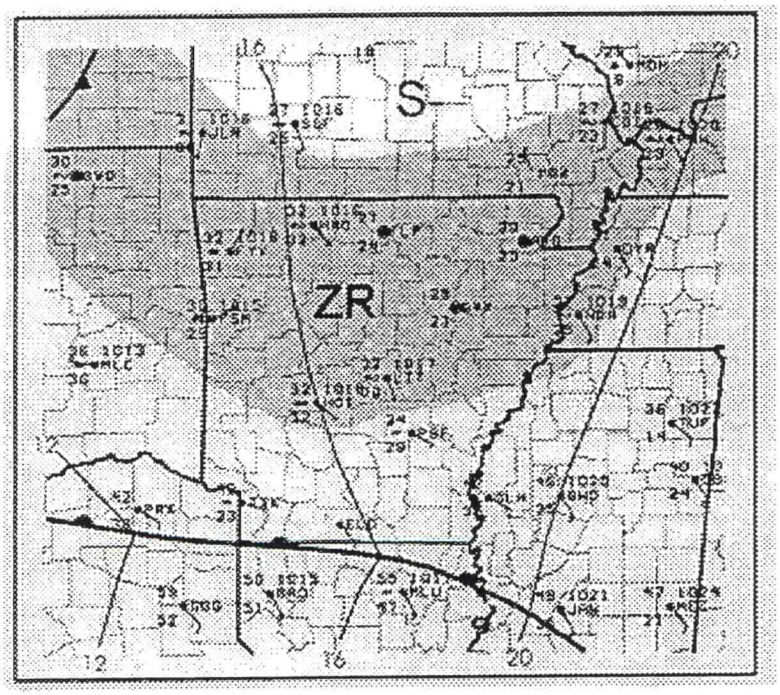

Figure 8. Surface map for Southern Plains at 2300 UTC 16 January 1994. Symbols as in Figure 2.

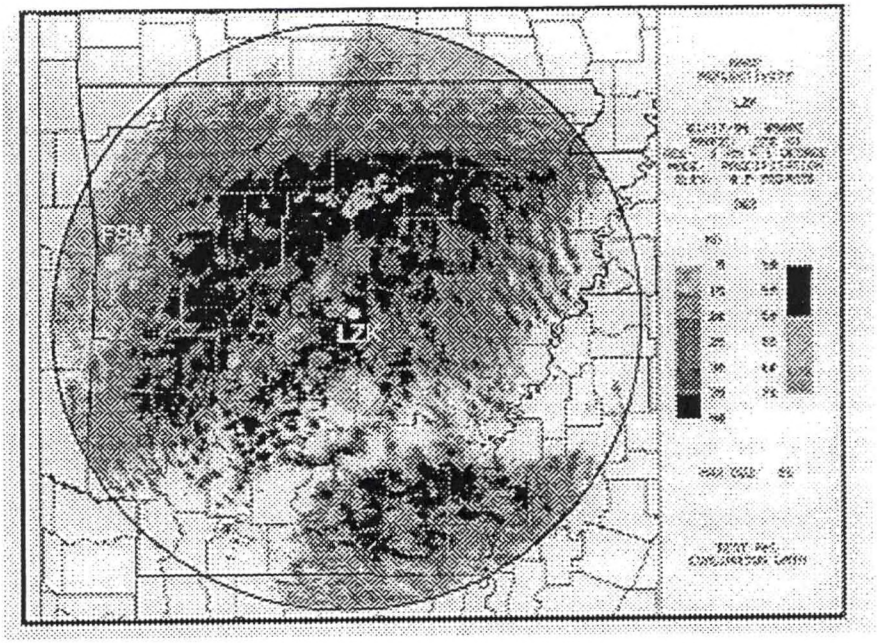

Figure 9. Radar reflectivity from the Little Rock WSR-88D (LZK) at 0500 UTC 17 January.

SESSION 9
MESOSCALE CASE STUDIES

A Case Study of Mesoscale Orographic Enhancement of Precipitation in the Santa Catalina Mountains of Arizona

David Bright[1] and Darren McCollum[2]

1. INTRODUCTION

During the early morning hours of January 5, 1995 (LST), a vigorous short wave trough was over Southern California approaching Arizona. As the system approached Southeast Arizona, synoptic scale ascent developed with a strong, moist low-level jet. Intense rainfall (and snowfall above 2550 meters) over the Santa Catalina mountains just north of Tucson was observed between 0600 UTC and 1200 UTC. Rainfall between 0000 UTC and 1200 UTC on January 5, totaled 0.13 inches at the NWS office in Tucson, while precipitation on Mt. Lemmon (40 kilometers north of Tucson at an elevation of 2791 meters) totaled 2 to 4 inches during roughly the same time. The exact Mt. Lemmon precipitation amount is ambiguous due to estimated measurements from a local ski area and a frozen automated precipitation gage located near the summit of Mt. Lemmon. Roads to the ski area were closed for several days due to many downed trees because of 20 inches of wet snow.

The south facing slopes of the Santa Catalina mountains drain into the Tucson valley where widespread flooding problems occurred during the morning hours of January 5, as numerous washes and normally dry rivers experienced swift runoff, prompting several road closures in and around Tucson. The regional scale numerical models (which for the purposes of this paper consists of only the NGM and Eta) handled the synoptic evolution satisfactorily, but were not capable of resolving the meso-beta scale (Orlanski 1975) processes that produced the heavy rainfall over the mountains north of Tucson. The deficiency of these models primarily resulted from the poor resolution of the small topographic features (about 25 to 50 km) that pepper the southeast Arizona landscape. See Dunn and Horel (1994) for a literature review regarding the NGM and Eta models, as well as previous precipitation studies utilizing these models. To illustrate the capability of mesoscale models employing high resolution terrain data, and to better understand the mesoscale processes associated with this precipitation event, a PSU-NCAR Mesoscale Model (MM5) version 1 (Grell et al. 1995) simulation was performed.

2. SYNOPTIC ANALYSIS AND THE REGIONAL MODELS FORECAST

The 0000 UTC and 1200 UTC 5 January 1995, Eta and NGM operational forecasts were revisited to determine the accuracy of their 6 to 12 hour guidance, and also to provide synoptic scale analysis of the event. Generally, the synoptic scale forecast produced by these models was of high quality and quasi-geostrophic diagnostics (Hoskins et al. 1978; Sanders and Hoskins 1990; Durran and Snellman 1987) would have benefited the forecaster in analyzing synoptic scale vertical motions. However, besides the poor terrain resolution, there were two notable weaknesses in both the NGM and Eta model forecasts that contributed to the heavy precipitation. First, the 12-hour forecast low-level wind field (below 700 hPa) was under forecast by 30 to 50 percent. A southwesterly low-level jet forecast by the 0000 UTC models in the 20 to 30 knot range over the southern Arizona verified in the 40 to 50 knot range. The verifying 1200 UTC 850 hPa wind field is shown in Figure 1. Second, the stronger than expected low-level jet was very effective at advecting low-level moisture northward into Southern Arizona. Both the NGM and Eta under forecast the low-level moisture flux into Southern Arizona.

1. Corresponding author address: David Bright, National Weather Service, Tucson, Arizona.
2. Darren McCollum, National Weather Service, Tucson, Arizona.

Figure 2 shows the surface pressure (as a proxy for model terrain) from the NGM model (horizontal resolution of approximately 80 km) and the 12-hour NGM QPF ending at 1200 UTC January 5. The NGM 12 hour QPF is less than 0.50 inch across Southern Arizona with the greatest precipitation amounts over the higher model terrain.

3. CONCEPTUALIZATION OF THE PRECIPITATION EVENT

Figure 3 shows the Tucson sounding from 1200 UTC 5 January 1995. Compared to the 0000 UTC sounding from the evening before (not shown), temperatures cooled at middle and upper levels about 3°C, and warmed 2 to 3 degrees below 700 hPa. Figure 4 shows 500 hPa quasi-geostrophic vertical velocity valid at 1200 UTC 5 January 1995 from the 00 hour Eta model forecast, indicating upward motion of 3 to 5 microbars/second over Eastern Arizona. Time-height cross-sections from the numerical models centered on Tucson showed slight mid-level warm air advection through the 0000 UTC to 1200 UTC period. Calculations based on the quasi-geostrophic thermodynamic equation (Holton 1979) (neglecting temperature advection and using a static stability derived from the 1200 UTC Tucson sounding) indicate that a time averaged omega of 1.5 microbars/second for 12 hours is sufficient to cool temperatures by approximately 3°C. Thus, despite the weak warm air advection in the middle levels of the atmosphere, cooling due to synoptic scale upward vertical motion dominated the local temperature tendency resulting in destabilization of the atmosphere. At lower levels, both the warm air advection and positive moisture advection contributed to the destabilization.

Errors in the forecast low-level moisture and wind field become significant when the mountains of Southeast Arizona, whose horizontal resolutions are about 25 to 50 km, are considered. Computation of the up-slope flow over the steep south facing slopes of the Santa Catalina mountains assuming a 50 knot low-level jet yields an upward vertical velocity of roughly 1.2 m/s. Analysis of the sounding in Figure 3 shows that parcels lifted from the 700 to 850 hPa layers (i.e., the layer of air forced to ascend over the Santa Catalina mountains) are slightly unstable to moist adiabatic ascent. The strong low-level jet not only created forced ascent in excess of 1 m/s allowing parcels to reach their level of free convection, but also served as a continuous source of moisture. Infrared satellite pictures (not shown) showed occasional localized convection over the Santa Catalina's during the 0600 UTC to 1200 UTC period.

4. MESOSCALE MODEL SIMULATION

A. Model Description

To better understand this rainfall event, and explore the capability of high resolution mesoscale models for operational use, a 12-hour MM5 simulation was performed. The authors would like to thank Jordan Powers of NCAR for his support and assistance in the modeling effort. The initial conditions of the atmosphere and sea surface temperature fields were obtained by interpolation of the NMC operational global analyses to the model grid. These course resolution fields were then enhanced through a Barnes objective analysis scheme (Barnes 1973, 1964) of surface and rawinsonde data. To simulate a real-time operational run of the MM5, no additional processing of the initial data was performed (i.e., no data not routinely available through automated procedures by operational run time were utilized). The simulation was carried out for 12 hours to capture the heavy precipitation event that occurred primarily within the 0600 UTC to 1200 UTC window. This also allowed sufficient time for the model to "spin-up" and generate cloud water during the first few hours of the simulation (Powers, personal communication). For this particular run of the MM5, an explicit moisture scheme (Hsie et al. 1984) for grid-resolvable precipitation was used with a convective parameterization (Arakawa-Schubert 1974; Grell et al. 1991) for subgrid-scale convective precipitation processes. The grid resolution utilized a 15 km course grid and a 5 km nested fine grid with 27 vertical levels. The

size and location of these grids are shown in Figure 5a. The fine grid terrain is shown in Figure 5b and captures many detailed terrain features of Southern Arizona, including the Santa Catalina mountains.

B. Model Results

Before the heavy rainfall, the MM5 showed blocked flow and a meso-high immediately upstream of Mt. Lemmon over the Tucson area through 0700 UTC. National Weather Services (NWS) surface observations from Tucson International Airport showed light easterly winds out of this meso-high (through 0600 UTC) before southwesterly momentum mixing downward to the surface. As the stability decreased and the southwesterly low level jet intensified, up-slope flow developed over the windward slopes of the Santa Catalina's. Figure 6 shows a cross-section (Figure 5b shows location of the cross-section) of vertical velocity (m/s) and equivalent potential temperature at forecast hour 10 of the simulation (valid time: 1000 UTC 5 January 1995). The model simulation shows 1.22 m/s up-slope flow just above the south slopes of the Santa Catalina's. In the 500 hPa to 800 hPa layers, equivalent potential temperature is nearly constant implying very weak to neutral stability for moist parcel displacement. Figures 7a-c shows the MM5 total precipitation (explicit and convective precipitation combined) ending at 0600 UTC, 0900 UTC, and 1200 UTC, respectively. In Figure 7d is the MM5 12 hour accumulated convective precipitation (ending at 1200 UTC). The MM5 simulation maintains intense orographic precipitation over the Santa Catalina mountains during the 0600 UTC to 1200 UTC period producing a 12-hour QPF of 68.9 mm (2.71 inches) on Mt. Lemmon. Note that the convective parameterization did turn on, but the convective scheme contributed less than 1 mm to the total Mt. Lemmon precipitation. Based on satellite imagery (not shown), it is believed that brief convective bursts did occur over the mountain although the model did not simulate significant convective precipitation. The detailed gravity wave fields produced by the MM5 and their role in the orographic precipitation event, as well as the significance of the feeder-seeder process (Bluestein 1993) remains to be investigated for this case.

5. SUMMARY

Regional scale numerical weather prediction models (in this case the NGM and Eta) did a reasonable job forecasting the synoptic scale evolution of the trough that moved across Arizona on January 5, 1995. Notable model deficiencies included an under forecast low level jet and under forecast low level moisture flux into Southern Arizona. Despite the meteorological deficiencies in the regional scale models forecasts, it is believed that the most significant deficiency resulted from poor terrain resolution.

An MM5 simulation utilizing a fine grid of 5 km over Southern Arizona was run to investigate the mesoscale processes and aid in determining the usefulness of high resolution mesoscale models during a significant orographic precipitation event in Southern Arizona. The MM5 results further suggest that the primary deficiency of the regional scale numerical model in a Southern Arizona orographic precipitation event is their poor terrain resolution.

In order for future events of this magnitude to be better forecast, either (1) mesoscale numerical models capable of resolving the small but significant mountain ranges of Southeast Arizona must be employed, or (2) techniques must be derived which allow forecasters to recognize and anticipate the development of similar conditions based on available regional scale numerical model guidance.

6. ACKNOWLEDGMENTS

The authors are grateful to Jordan Powers at the National Center for Atmospheric Research for his time and assistance. The discussion and assistance of Robert Gall at the National Center for Atmospheric Research are also greatly appreciated.

7. REFERENCES

Arakawa, A., and W.H. Schubert, 1974: Interaction of a cumulus cloud ensemble with the large-scale environment. Part I. *J. Atmos. Sci.*, **31**, 674-701.

Barnes, S.L., 1964: A technique for maximizing details in numerical weather map analysis. *J. Appl. Meteor.*, **3**, 396-409.

_____, 1973: Mesoscale objective map analysis using weighted time-series observations. 60 pp. [NTIS Rep. No. COM-73-10781, Springfield, VA.]

Bluestein, H.B., 1993: *Synoptic-Dynamic Meteorology in Midlatitudes - Volume II*, Oxford University Press, 594 pp.

Dunn, L.B., and J.D. Horel, 1994: Prediction of Central Arizona convection. Part I. Evaluation of the NGM and ETA model precipitation. *Wea. Forecasting.*, **9**, 495-507.

Durran, D.R., and L.W. Snellman, 1987: The diagnosis of synoptic-scale vertical motion in an operational environment. *Wea. Forecasting.*, **2**, 17-31.

Grell, G.A., Y.-H. Kuo, and R.J. Pasch, 1991: Semiprognostic tests of cumulus parameterization schemes in middle latitudes. *Mon. Wea. Rev.*, **119**, 5-31.

_____, J. Dudhia, and D.R. Stauffer, 1995: A description of the fifth generation Penn State/NCAR Mesoscale Model (MM5), NCAR Tech. Note TN-398 + STR, 122 pp.

Holton, J.R., 1979: *An Introduction to Dynamic Meteorology*. 2nd ed., Academic Press, 391 pp.

Hoskins, B.J., I. Draghici and H.C. Davies, 1978: A new look at the omega-equation. *Quart. J. Roy. Meteor. Soc.*, **104**, 31-38.

Hsie, E.-Y., R.A. Anthes, and D. Keyser, 1984: Numerical simulation of frontogenesis in a moist atmosphere. *J. Atmos. Sci.*, **41**, 2581-2594.

Orlanski, I., 1975: A rational subdivision of scale for atmospheric processes. *Bull. Amer. Meteor. Soc.*, **56**, 527-530.

Sanders, F., and B.J. Hoskins, 1990: An easy method for estimation of Q-vectors from weather maps. *Wea. Forecasting.*, **5**, 346-353.

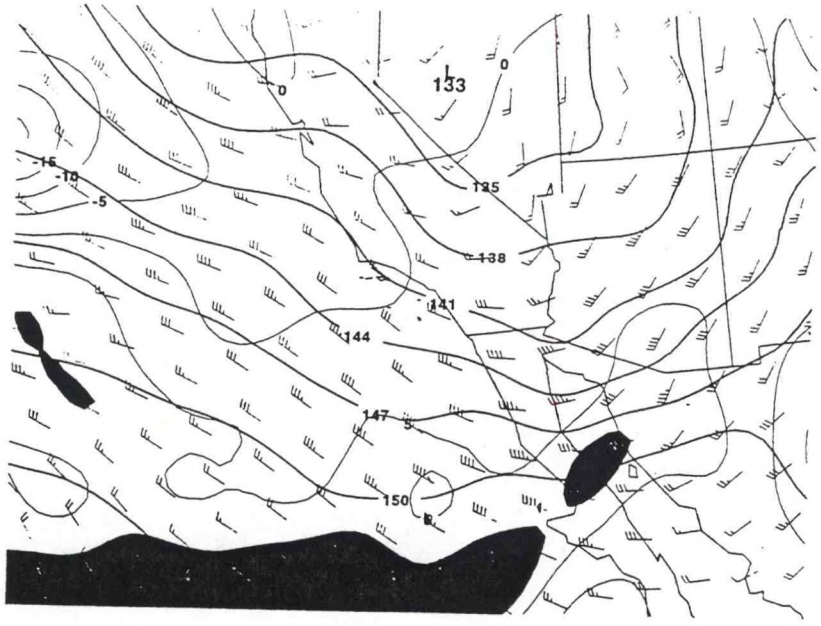

Figure 1. Eta 00 hour forecast 850 hPa height (bold solid; contour interval 3 dam), wind (knots), and dew point (thin solid; contour interval 5°C) valid 1200 UTC 5 January 1995. Dew points greater than 10°C are shaded.

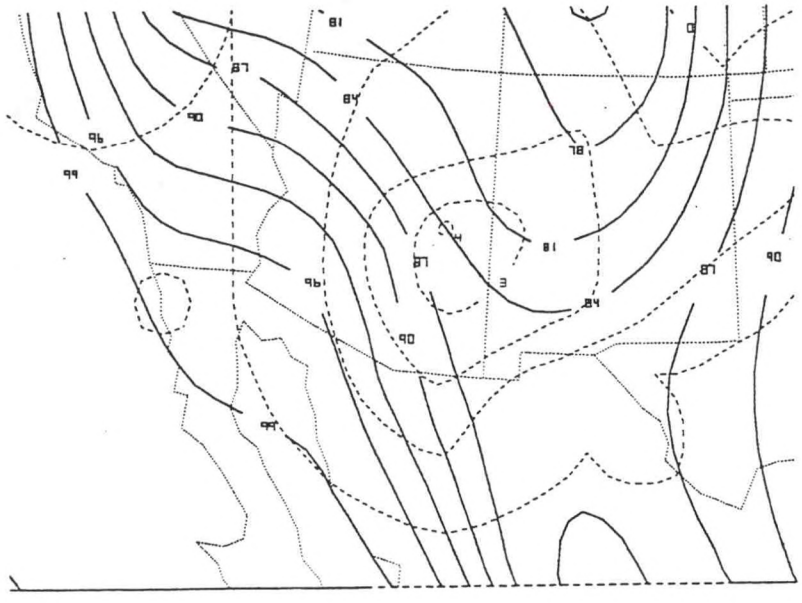

Figure 2. NGM surface pressure (bold solid; contour interval 3 kPa) and NGM 12 hour QPF (dashed; contour interval in tenths of inches) valid 1200 UTC January 5, 1995.

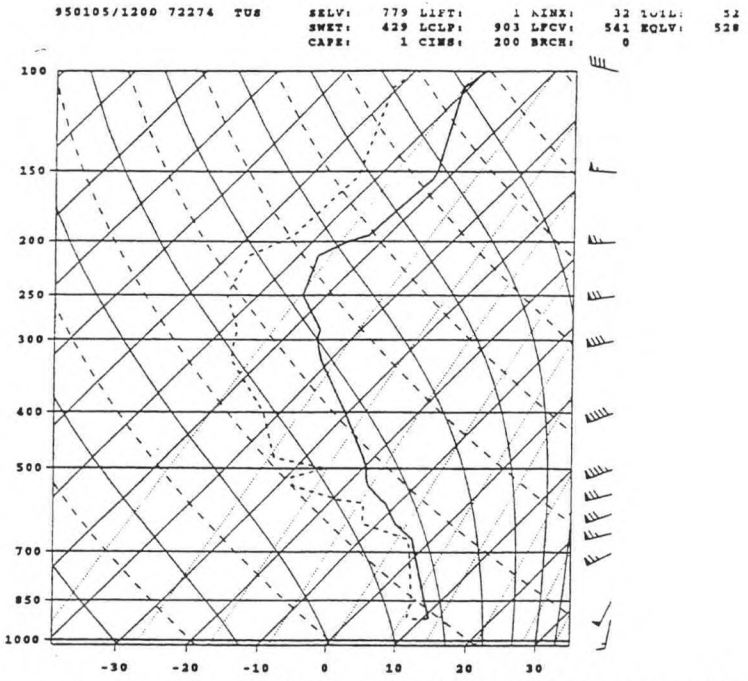

Figure 3. NWS Tucson sounding valid 1200 UTC 5 January 1995.

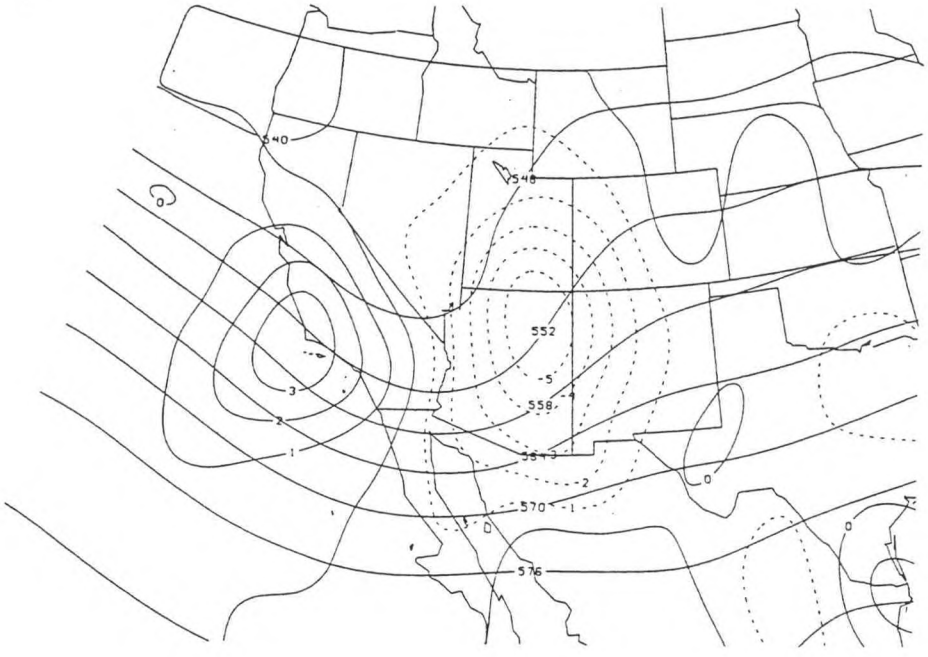

Figure 4. Eta 00 hour forecast 500 hPa height (solid; contour interval 6 dam) and Eta 00 hour forecast 500 hPa quasi-geostrophic omega (dashed/solid: contour interval 1 microbar/second) valid 1200 UTC 5 January 1995.

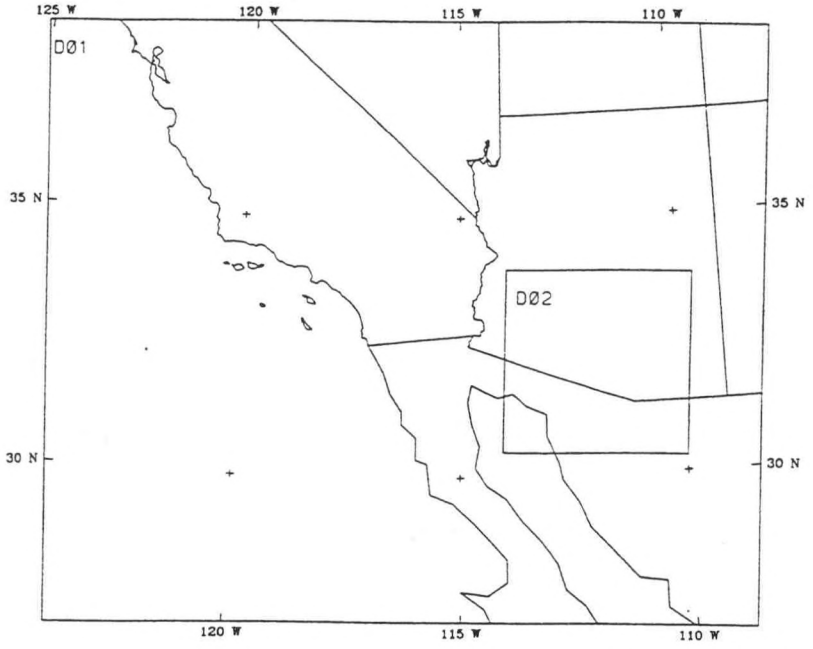

Figure 5a. The course domain (labeled DO1) and fine domain (labeled DO2) used in the MM5 simulation of the January 5, 1995 heavy precipitation event. Horizontal resolution of the course domain is 15 km, and the fine domain 5 km.

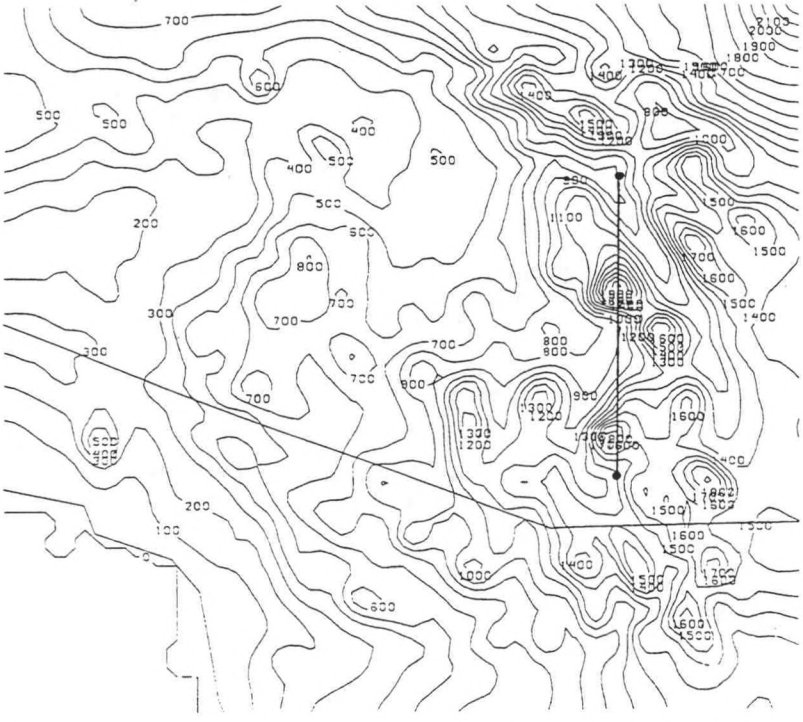

Figure 5b. Model fine grid terrain (horizontal resolution of 6 km; contour interval 100 meters). The solid line represents the cross-section referenced in Figure 6.

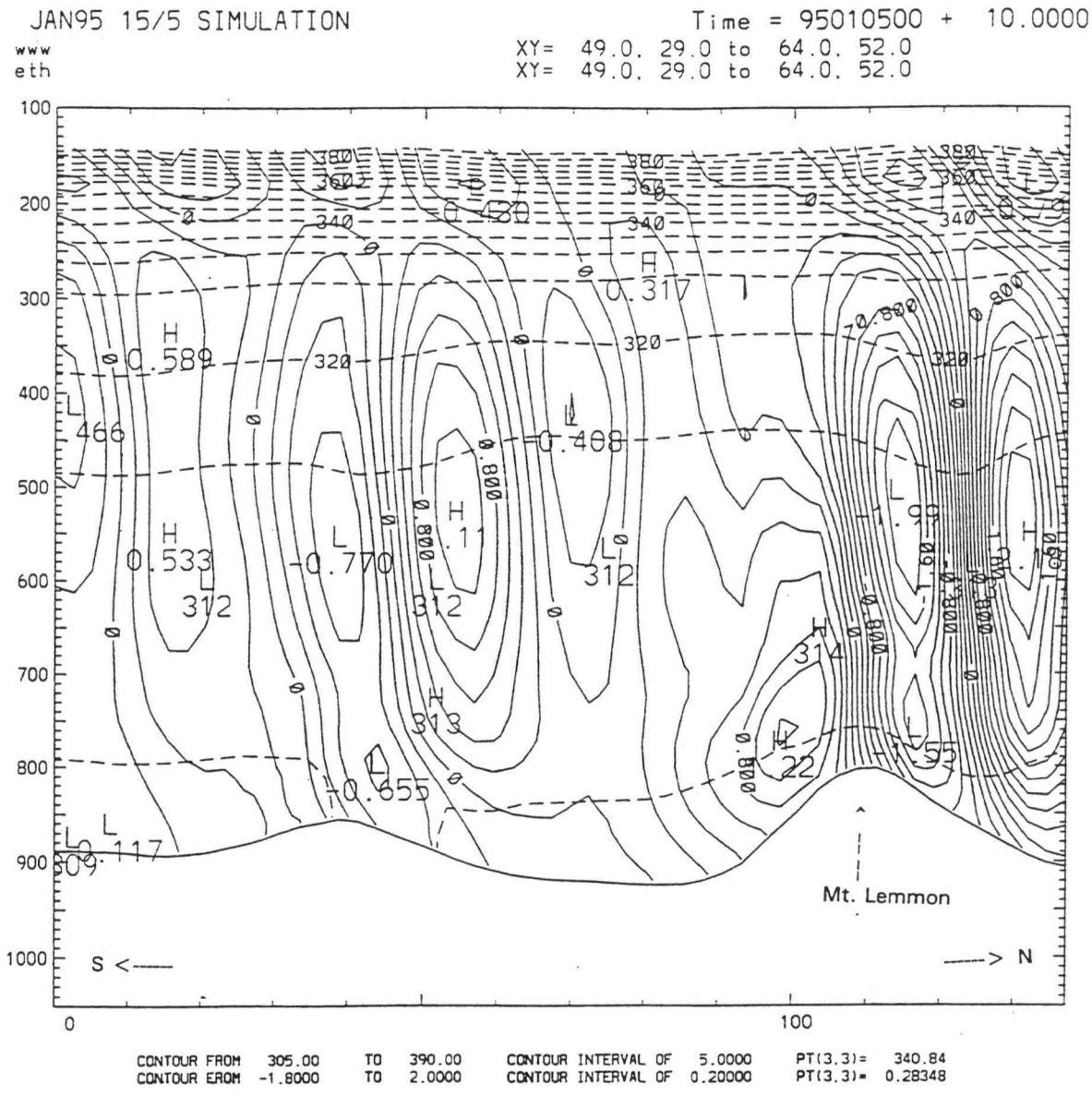

Figure 6. Cross-section (Figure 5b shows locations) running North to South through heavy precipitation over Mt. Lemmon. Vertical velocity (solid; contour interval 0.2 m/s) and equivalent potential temperature (dashed; contour interval 5K).

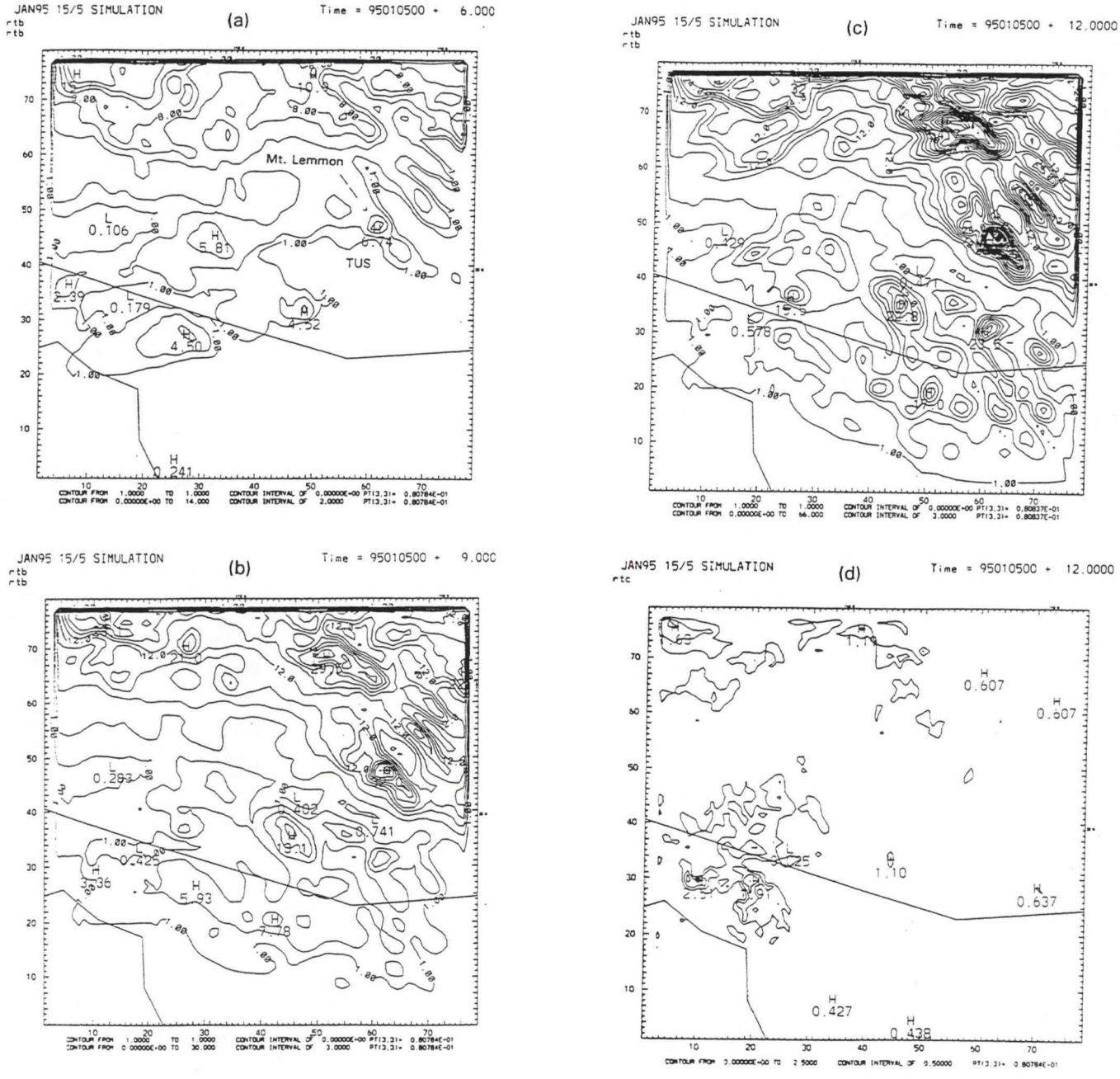

Figure 7a-d. MM5 fine grid total (explicit and convective combined) QPF ending at 0600 UTC, 0900 UTC, and 1200 UTC January 5, 1995, respectively. (Contours interval in (a): 1, 2, 4, 6 mm...; Contour interval in (b) and (c): 1, 3, 4, 6, 9 mm...) Location of Mt. Lemmon and Tucson (TUS) is shown in (a). (d) MM5 fine grid convective QPF ending at 1200 UTC 5 January 1995. (Contour interval 0.5 mm).

An Analysis of the Central Kansas Ice Storm of December 6, 1994

John Stoppkotte[1] and Michael L. Moritz[2]

1. INTRODUCTION

On December 6, 1994, significant ice accumulations were recorded across central Kansas. One-third to one-half inch (water equivalent) of ice fell from southwest into eastern Kansas. As the modernization of the National Weather Service (NWS) progresses, new technologies are becoming available to the operational forecaster which allow detailed analysis of meteorological parameters once not readily available. Primarily through the use of PCGRIDDS, the intent of this paper is to apply some of this new technology to a freezing precipitation event, and depict its value to the operational forecaster for enhancing real-time forecast techniques and results.

2. SYNOPTIC OVERVIEW

A. Surface Features

At 1200 UTC 6 December 1994, a stationary boundary, separating shallow Arctic air to the north and warmer, moisture laden air to the south, stretched from the Texas panhandle, across southern Kansas and into central Illinois. Well north of the front, high pressure was moving east across southern Canada. Low pressure developed in northern New Mexico, and by 2100 UTC, the low had deepened to 1004 mb and moved into extreme southeast Colorado.

Surface temperatures (°F) were in the teens and 20s north of the front with 40s and 50s noted south of the front. Widespread freezing and frozen precipitation was observed in the colder air with rain further south. The Dodge City, Kansas (DDC) sounding on the morning of December 6 depicted the shallow nature of the cold air trapped below in an inversion near 860 mb.

During the day, the freezing line remained nearly stationary from southwest Kansas into northeast Missouri. A light easterly flow prevailed across Kansas into the early afternoon.

B. Upper Levels

Though surface temperatures north of the front were below freezing, temperatures at 700 mb were above freezing as far north as southern Nebraska. Soundings from the area were nearly saturated to 400 mb and warmed to above 0°C within 50 mb of the surface. Warm advection was evident above 900 mb with south to southwest winds above the front advecting temperatures as warm as 9°C into the region.

A shortwave was moving into western New Mexico with 60 meter heights falls at 500 mb ahead of the feature. A pair of jet segments in the upper levels were evident near the area. A 120 kt jet core was located over the Great Lakes while a speed maximum of 90 kts was rounding the base of the western states long wave trough. Further examination of the role of these jet features will be discussed later.

1. Corresponding author address: John Stoppkotte, National Weather Service Office, North Platte, Nebraska.
2. Michael L. Moritz, National Weather Service Office, Hastings, Nebraska.

3. GRIDDED DATA APPLICATIONS

A. Overview

Gridded data was obtained for December 5-7, 1994 from the NGM and the ETA model, when available. Using the operational forecast software PCGRIDDS, a detailed post-storm analysis could be done. Various fields indicated the potential for enhanced precipitation with this definitive overrunning synoptic pattern.

The general trend of both models was to track the surface low primarily across southern Kansas when in reality it followed the boundary created by the southward plunging Arctic air. The initial surface low pressure system deepened more than the models had initially forecasted and thus, both models under estimated the amount of warm advection ahead of the low in central Kansas. Yet, each model did indicate 850 mb frontogenesis in southwest Kansas by 1200 UTC 6 December, with the best frontogenetic forcing moving across Kansas with time.

B. Advection Patterns

Early detection of strong advection patterns within the developing storm was a key indicator to the intensity of the storm. Figure 1 is a time cross section for 48 hours located in central Kansas. During the first 6 to 18 hours of the forecast, strong cold advection associated with the Arctic front can be seen below 850 mb. On the strength of 30 kt winds, warm advection began by 24 hours. The warm air, primarily above 900 mb, was lifted over the cold air dome at the surface creating a profile adherent to freezing precipitation development.

With PCGRIDDS, isentropic fields were created. The 30-hour forecast from the December 5, 1994 00Z Eta model, depicted strong pressure advection or vertical lift throughout the isentropic layer from 302-310 K over Oklahoma and Kansas. Moisture was also transported from the Gulf of Mexico into the system on the isentropic surfaces.

Using PCGRIDDS, the forecaster can view advection fields in the vertical and with time. Isentropic charts can be quickly created for detailed examination. Yet, it is the potential to analyze and implement more complex parameters which give the operational forecaster the insight and facility to significantly "fine tune" the forecast.

C. Conditional Symmetric Instability

Numerous papers have been written concerning the topic of Conditional Symmetric Instability (CSI). Lussky (1987), Sanders and Bosart (1985), and Moore and Lambert (1993) are a few of the more recent. Analysis of the pre-storm environment for the December 6 storm indicated the presence of CSI.

With PCGRIDDS, parameters once abstract to the operational forecaster, can be viewed almost instantaneously. This allows forecasters to analyze precipitation enhancing elements, such as CSI, in real-time.

Using the method described by Conger and Dunn (1993) to view CSI via PCGRIDDS, a cross-section was taken normal to the lines of constant thickness, or perpendicular to the thermal wind, using NGM gridded data. Upon the addition of equivalent potential temperature (θe), geostrophic momentum (Mg), and relative humidity (RH) to the overlay, an area of CSI is shown in Figure 2 (near Dodge City) between 850 and 700 mb. The air in this area was becoming saturated

as moisture was advected into south central Kansas. This region of CSI corresponds to the sector of the DDC sounding above 0°C. Using NGM gridded data from 1200 UTC December 5, the potential for CSI was shown to exist 24 to 30 hours earlier as seen in Figure 3, illustrating the value of this technique in making real-time forecast decisions.

D. Jet Streak Vertical Motions

Further analysis of the ETA gridded data from the 0000 UTC run on December 5 showed early indications of enhanced vertical motion due to jet streak interactions. Labas (1994) used gridded data and PCGRIDDS exclusively to study vertical motions associated with jet streaks. Similar characteristics occurred on December 6. A 120 kt jet was near the Great Lakes while a 90 kt jet pushed into the west central Texas.

The 42-hour forecast from the 1200 UTC 4 December NGM model run depicted a developing ageostrophic circulation, just south of central Kansas (near 38°N 99°W), possibly enhanced by the coupled jets. Evidence of this vertical motion over central Kansas can be seen in Figure 4. The 30-hour forecast from the next NGM run (Figure 5) showed a similar result, with the enhanced lift moving into central Kansas. This feature, combined with a forecast 30 kt low level jet advecting high mixing ratios (6-9 gkg^{-1}) into the region, may have helped focus and intensify the freezing precipitation event.

4. CONCLUSION

Events like the December 6, 1994 ice storm in Kansas are often difficult to forecast. However, as the NWS Modernization continues, offices around the country should continue to see a stream of new data, systems and technological advances which can potentially make forecasts of such events easier, faster and more accurate. Not only does technology like PCGRIDDS allow for early identification of features once abstract to the operational forecaster, it also allows one a chance to look at consistency, or lack of, between model runs. Other advances, such as the WSR-88D, have granted many forecasters their first look at parameters critical for prediction of meteorological and hydrological conditions. Benefits of improved forecasts and longer lead time have already begun, and will likely continue to improve for years to come.

5. ACKNOWLEDGEMENTS

We thank Mr. Rick Ewald, Science and Operations Officer (SOO) at Hastings NWSO, for his valuable time and suggestions for this paper.

6. REFERENCES

Conger, M.C., and L.B. Dunn, 1993: Using PCGRIDDS to Forecast Symmetric Instability in a Northeast Colorado Snowstorm. NWS Western Region Technical Attachment 94-02. DOC/NOAA/NWS/Western Region, Scientific Service Division, Salt Lake City , UT.

Labas, K.M., 1994: Views of Vertical Motion Associated with a Jet Streak Through the Eyes of PCGRIDDS. NWS Central Region Technical Attachment 94-10. DOC/NOAA/NWS/Central Region, Scientific Service Division, Kansas City, MO.

Lussky, G.R., 1987: Heavy Rains and Flooding in Montana: A Case for Slantwise Convection. NWS/NOAA Technical Memorandum NWS WR-199. DOC/NOAA/NWS/Western Region, Scientific Service Division, Salt Lake City , UT.

Moore, J.T., and T.E. Lambert, 1993: The Use of Equivalent Potential Vorticity to Diagnose Regions of Conditional Symmetric Instability. *Wea. Forecasting*, **8**, 301-308.

Sanders, F., and L.F. Bosart, 1985: Mesoscale Structure in the Megalopolitan Snowstorm of 11-12 February 1983. Part I: Frontogenetic Forcing and Symmetric Instability. *J. Atmos. Sci.*, **42**, 1050-1061.

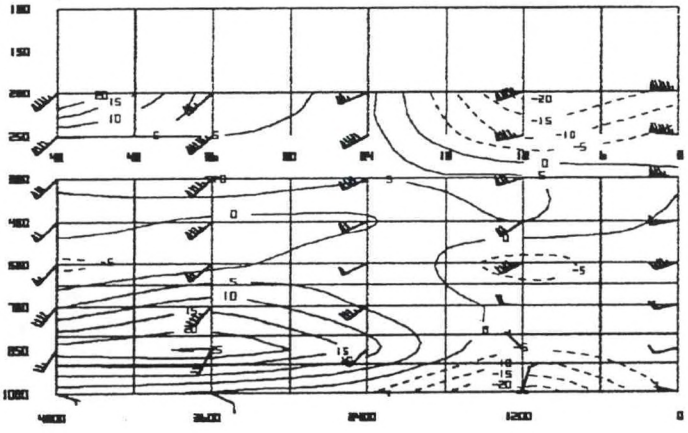

ETAX:Lon/Lat 99/37-> 0/48:FHR= 0 :FHRS= 0/ 24::FILE=DE059400.ETC
94/12/ 5/ 0--ADVT TEMP WIND C5-5 DNEG

ETAX:Lon/Lat 99/37-> 0/48:FHR= 0 :FHRS= 0/ 24::FILE=DE059400.ETC
94/12/ 5/ 0--BKNT&

Figure 1. Time height cross-section in south central Kansas of temperature advection (solid lines) and wind.

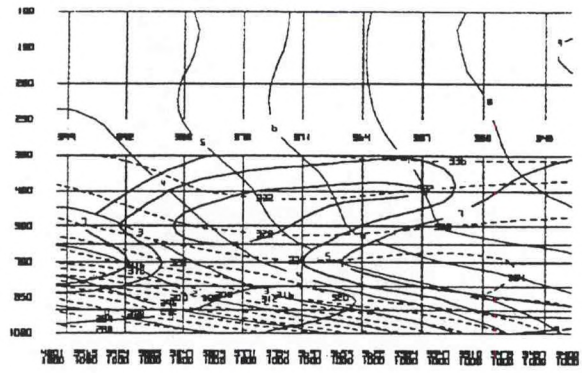

RAFS:Lon/Lat100/40->100/34:FHR= 0 :FHRS= 0/ 24::FILE=DE069412.RFC
94/12/ 6/12--SSUM NORM GEOS SMLT PFPF DIST CLR1

RAFS:Lon/Lat100/40->100/34:FHR= 0 :FHRS= 0/ 24::FILE=DE069412.RFC
94/12/ 6/12--THTE CI04 DASH CLR2&

RAFS:Lon/Lat100/40->100/34:FHR= 0 :FHRS= 0/ 24::FILE=DE069412.RFC
94/12/ 6/12--RELH GRTN 70.0 CI10 CLR6&

Figure 2. Cross-sections of (a) equivalent potential temperature (4K), (b) geostrophic momentum (solid, every 1 m s^{-1}) and © relative humidity (≥ 70%).

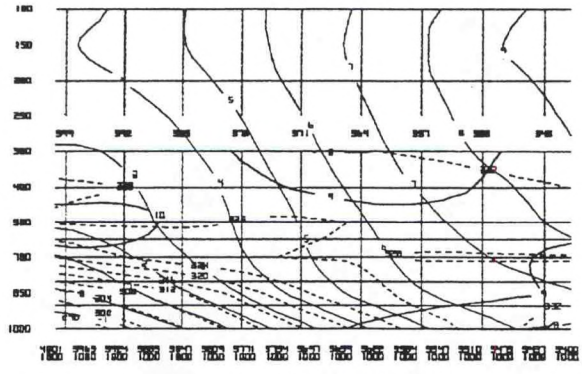

RAFS:Lon/Lat100/40->100/34:FHR= 30 :FHRS= 0/ 24::FILE=DE059412.RFC
94/12/ 5/12--SSUM NORM GEOS SMLT PFPF DIST CLR1

RAFS:Lon/Lat100/40->100/34:FHR= 30 :FHRS= 0/ 24::FILE=DE059412.RFC
94/12/ 5/12--THTE CI04 DASH CLR2&

RAFS:Lon/Lat100/40->100/34:FHR= 30 :FHRS= 0/ 24::FILE=DE059412.RFC
94/12/ 5/12--RELH GRTN 70.0 CI10 CLR6&

Figure 3. 30-hour forecast cross-section of (a) equivalent potential temperature (4K), (b) geostrophic momentum (solid, every 1 m s^{-1}) and © relative humidity (≥ 70%).

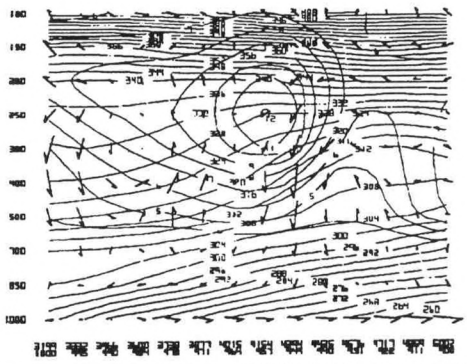

```
 RAFS:Lon/Lat100/31-> 90/50:FHR= 12 :FHRS=  0/ 24::FILE=DE059400.RFC
94/12/ 5/ 0--THTA CI04

 RAFS:Lon/Lat100/31-> 90/50:FHR= 12 :FHRS=  0/ 24::FILE=DE059400.RFC
94/12/ 5/ 0--XLBL PRES CLR7&

 RAFS:Lon/Lat100/31-> 90/50:FHR= 12 :FHRS=  0/ 24::FILE=DE059400.RFC
94/12/ 5/ 0--XLBB DATT ALAT CLR7&

 RAFS:Lon/Lat100/31-> 90/50:FHR= 12 :FHRS=  0/ 24::FILE=DE059400.RFC
94/12/ 5/ 0--XLBB DATA ALON CLR7&

 RAFS:Lon/Lat100/31-> 90/50:FHR= 12 :FHRS=  0/ 24::FILE=DE059400.RFC
94/12/ 5/ 0--MAGN WKNT GRTN 40.0 CI10 CLR5&

 RAFS:Lon/Lat100/31-> 90/50:FHR= 12 :FHRS=  0/ 24::FILE=DE059400.RFC
94/12/ 5/ 0--ACRC&
```

Figure 4. 42-hour forecast cross-section of (a) potential temperature (4K), (b) isotachs (solid, every 10 kts) and (c) ageostrophic circulation (arrows) in plane of cross-section.

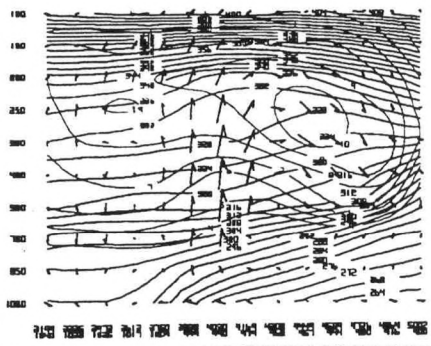

```
 RAFS:Lon/Lat104/31-> 90/50:FHR= 30 :FHRS=  0/ 24::FILE=de059412.rfc
94/12/ 5/12--THTA CI04 CLR2

 RAFS:Lon/Lat104/31-> 90/50:FHR= 30 :FHRS=  0/ 24::FILE=de059412.rfc
94/12/ 5/12--XLBL PRES CLRF&

 RAFS:Lon/Lat104/31-> 90/50:FHR= 30 :FHRS=  0/ 24::FILE=de059412.rfc
94/12/ 5/12--XLBB DATT ALAT CLRF&

 RAFS:Lon/Lat104/31-> 90/50:FHR= 30 :FHRS=  0/ 24::FILE=de059412.rfc
94/12/ 5/12--XLBB DATA ALON CLRF&

 RAFS:Lon/Lat104/31-> 90/50:FHR= 30 :FHRS=  0/ 24::FILE=de059412.rfc
94/12/ 5/12--MAGN WKNT GRTN 40.0 CI10 CLR5&

 RAFS:Lon/Lat104/31-> 90/50:FHR= 30 :FHRS=  0/ 24::FILE=de059412.rfc
94/12/ 5/12--ACRC CLR3&
```

Figure 5. 30-hour forecast cross-section of (a) potential temperature (4K), (b) isotachs (solid, every 10 kts) and (c) ageostrophic circulation (arrows) in plane of cross-section.

Disastrous Mississippi Ice Storm of 1994

Russell L. Pfost[1]

1. INTRODUCTION

The following quote concisely sums up the terrible ice storm that plagued 26 counties in north and northwest Mississippi February 9-11, 1994. The storm damage resulted in a Federal Disaster Declaration from President Clinton for 26 counties and total damage estimates exceeding three hundred million dollars. For Mississippians, the ice accumulation was the heaviest since the "Great Southern Glaze Storm" in January, 1951 (Harlin, 1952).

"I haven't seen damage this widespread since Hurricane Camille!"

Miss. Power & Light spokesperson
Edd Jussely quoted in the Jackson
Clarion-Ledger

According to Mississippi Power and Light (M. P. & L.) estimates, 500,000 persons in roughly 200,000 homes had no electricity at the height of the storm and 175,000 homes had no water. Consequently, in a state with about 2.5 million residents, 20 percent of Mississippians lost power for at least a day. M.P.& L. estimates that even on Monday, February 14, three days after the storm, 151,000 homes were still without power. In areas serviced by smaller power companies, electricity was out for three weeks or more due to the ice. People had to resort to fireplaces for heat and candles and flashlights for light. Food that was refrigerated had to be eaten quickly or thrown out, and travel was impossible. Water systems were also severely affected for a week or more with over 300,000 customers of about 300 water systems advised to boil the water before use.

Agriculture, Mississippi's livelihood for most of its history, took a severe blow. Five percent of the state's pecan trees were reported destroyed and 6,000 acres severely damaged as most of the state's commercial pecan orchards are located in the hard hit counties of Coahoma, Bolivar, and Tallahatchie (delta counties located between the Mississippi River and Interstate 55 in northwest Mississippi). It will be at least 3 and more likely 5 years before pecan production can recover. Huge losses to commercial tree crops were front page news across the state the week following the storm. The state's education system, from grammar schools to large state universities, sustained severe damage, with schools in the disaster area forced to cancel classes for up to two weeks after the storm.

Ice storms are very difficult to forecast anywhere, and especially so in the deep south. NWSFO Jackson forecasters did an outstanding job of providing early warning of this event. Early notice of a potential ice problem was provided for the fourth period (Thursday) forecast at 4:20 PM (all local times CST) Tuesday, February 8. The mention of freezing rain was carried through the 9:20 PM Tuesday and 4:20 AM Wednesday February 9 packages. Forecasters at Jackson were also concerned with the potential for heavy rain (a Flash Flood Watch was issued for the northwest third of Mississippi early Tuesday) and very dense sea fog that moved north from the Gulf of Mexico across the three Mississippi coastal counties. The sea fog contributed to a 17 car accident on the Pascagoula River bridge in Jackson County (a Dense Fog Advisory was in effect).

1. Corresponding author address: Russell L. Pfost, NEXRAD Weather Service Forecast Office, Jackson, Mississippi.

With temperatures falling and persistent reports of icing from Arkansas and the Memphis area, a Freezing Rain Advisory was issued in the 10:20 AM Wednesday, February 9, forecast package. Map discussion, held routinely at NWSFO Jackson, was an open exchange with the possibility of a major ice storm for the northern counties the main topic. It was a group decision led by the Forecaster-In-Charge to issue an Ice Storm Warning for 39 counties north of a Hollandale-Kosciusko-Macon line and a Freezing Rain Advisory for central Mississippi north of a Port Gibson-Magee-Quitman line (Figure 1). Specific cities were mentioned in the text and people warned of significant ice accumulations. Advice was offered concerning preparations for downed power lines. State utility companies and the highway patrol were notified individually.

As the event continued, forecasters tailored the warned area to those counties northwest of a Greenville to Tupelo line and extended the time period through Friday morning. The 10:20 AM zone forecast product Thursday, February 10, trumpeted damaging ice accumulations of 3 to 6 inches and reiterated that this was a dangerous situation. As power was lost to NOAA Weather Radio sites, utility companies made numerous calls for updated weather information to the Jackson office. To make the situation even more difficult, a Tornado Watch was issued for southeast Mississippi that afternoon in advance of the developing wave in the northern Gulf.

The counties which suffered the worst damage were under a Freezing Rain Advisory from 10:20 AM to 4:20 PM Wednesday, February 9, and an Ice Storm Warning from 4:20 PM Wednesday through 10:20 AM Friday, February 11, a total of 48 hours.

In spite of the severity and broad scale in both time and space (icing occurred in northeast Texas, north Louisiana, northwest Mississippi, southeast Arkansas, west Tennessee (including the Memphis metro area), and northwest Alabama) there was a curious lack of attention from the national media concerning this event. In fact, most Americans outside the affected area knew little about the storm and its effect on area residents. This lack of attention was detrimental to recovery efforts by utilities and civil defense offices.

2. SYNOPTIC SCALE OVERVIEW

The synoptic meteorological situation at 0000 UTC 9 February 1994, showed a split flow in the middle and upper troposphere over the contiguous United States (Figures 2 and 3). The northern branch showed a strong northwest to southeast flow down the lee side of the Canadian Rockies and a southwest to east-northeast flow through the Great Lakes region; the mean trough extended into the Dakotas from central Canada. The southern branch was generally oriented southwest to northeast over the southwest quadrant of the United States; a relatively strong storm system was beginning to move ashore over southern California. At the surface, a shallow (generally less than 1 km) but very cold Arctic air mass had moved southward across the high plains from central Canada behind a strong surface cold front (Figure 4). A 7.5 C / 100 km temperature gradient existed across the front and surface winds behind the front were generally 8 m/s from the north; ahead of the front were generally 6 m/s from the south.

The frontogenesis function as defined by Bluestein (1992) states that the geostrophic total derivative of the gradient of temperature on a constant pressure surface is equal to the geostrophic frontogenesis. Near the surface (1000 mb), a more meaningful result is obtained by using the total wind to obtain a measurement of the actual frontogenesis. Using PCGRIDDS (Personal Computer GRIdded Data Display System - which in NWS field offices is a program widely used to display and analyze model gridded output - Petersen, 1991; Meier, 1993) to calculate this function at 1000 mb yields maximum frontogenesis of about 1°C 100 km^{-1} h^{-1} across southern Arkansas, northeast Texas, and northwest Mississippi at 12 UTC 9 February (not shown), increasing to 2°C 100 km^{-1} h^{-1} near

the Mississippi Gulf coast at 12 UTC 10 February (not shown). The frontogenesis function thus shows a horizontal deformation field tending strongly toward strengthening the front.

The cold front entered extreme northwest Mississippi around 0800 UTC 9 February and moved steadily through the north and central counties, only to stall across south Mississippi as a wave began to develop in the Gulf of Mexico. Temperatures in northern Mississippi dropped steadily behind the front and became subfreezing in the northwest corner of the state by mid morning 9 February. Cold air advection (approaching $2^{\circ}C\ hr^{-1}$) existed behind the surface cold front across southeast Arkansas while warm air advection (0° to $0.5^{\circ}C\ h^{-1}$ at the 850 mb level) existed ahead of the surface front.

Moisture flux convergence was strong at the 850 mb level across the ice storm area (not shown). A strong vorticity center (valued at $28 \times 10^{-5}\ sec^{-1}$) moved east across Texas and then northeast through the Lower Mississippi Valley; at the same time weaker vorticity lobes passed across the ice storm area (ahead of this vorticity center - Figure 5). These weak short waves provided additional dynamic lift to complement the mechanical lift of the very cold air moving under the warm, moist air already in place, and consequently light rain began to fall across the extreme northwest counties Wednesday morning.

As the strong California system began to move across the southern Rockies and into Texas, a wave developed along the front in the northern Gulf of Mexico off the Louisiana coast. Ahead of this developing low pressure system, very warm, moist air from the Gulf increased temperatures to the $20\text{-}25^{\circ}C$ range across the southeast and coastal counties of Mississippi, and enhanced the overrunning of the cold surface air in the north. From the Little Rock, Arkansas, rawinsonde sounding, the cold air in north Mississippi was only 300 to 1,200 meters thick at most, with a pronounced "nose" of very warm, moist air at 850 to 800 mb. This "nose" is classically associated with freezing rain (Harlin, 1952, Williams, 1960). Comparison of Little Rock rawinsonde soundings at 0000 UTC (Figures 6 and 7) show increases in temperature and dew point in the 850-800 mb layer, presumably due to advection.

Heavy rains fell over all but extreme southeast Mississippi, and, where icing did not occur, some minor flooding was reported. With northwest Mississippi well below freezing, damaging ice accumulations of 50 to 120 mm (2 to 5 in) were common. The freezing rain reached its peak intensity Wednesday night and Thursday, February 9-10, with rainfall totals in the 26 county disaster area ranging from 63 to over 127 mm (2.5 to 5 in) (Figure 8). The rainfall finally ended early in the morning on Friday, February 11.

3. NATIONAL METEOROLOGICAL CENTER MODEL FORECASTS AND INTERPRETATION

Overall, NMC's three operational models, the 80 km Eta, the Nested Grid (NGM), and the Aviation (AVN), did a good job in providing advance notice of the impending ice storm for north Mississippi. The overall split flow pattern and the subsequent forecasts of the California system were consistent and reasonable, and JAN forecasters were able to use the models to correctly forecast heavy rain. Temperature forecasts were very difficult, because the Model Output Statistics (MOS) had trouble with the very shallow cold air mass at the surface; thus, MOS forecasts were too warm. Even so, forecasters at JAN were able to key in on the PCGRIDDS gridded data for the Eta, Nested Grid Model (NGM), and Aviation models and use the 1000 mb forecast temperatures and winds to successfully position advisories and warnings.

Of the three gridded data models, the 80 km resolution Eta model provided the best and most consistent forecast of the freezing and subfreezing temperatures for northwest Mississippi. As early

as the 1200 UTC run on Tuesday, February 8, the models showed possibly heavy rain with temperatures below freezing over the northwest half of the state. The problem was how much of the state would have temperatures below freezing and how long such conditions would last. The early Eta model initially was too fast and too far south with the freezing temperatures, as was the NGM's 1000 mb temperature forecast. By 0000 UTC 9 February, about 12 h before the beginning of the ice storm, the Eta and NGM still placed the freezing temperatures too far south, and the NGM showed a dramatic warmup at 48 h that neither of the other models showed. The Ice Storm Warning was issued with the benefit of the 1200 UTC model runs on February 9, with all models reasonably consistent and correctly targeting the Delta and northern counties for the main ice accumulations. The NGM, however, still showed a dramatic warmup in the 36 and 48 h period forecasts that did not show up in the other two model runs (Figures 9 and 10). NWSFO Jackson forecasters commendably rejected this dramatic warmup and accepted the Eta and AVN solutions for low level temperatures. Overall, the Eta model did the best with the low level shallow cold air forecast.

Precipitation amounts were substantially underforecast by all three models, and all three models had precipitation centers too far south. Junker (1990) has shown that the NGM will underforecast precipitation amounts over the southern U.S. in the presence of moderate to strong southerly flow from the Gulf. However, it was surprising that the newer 80 km Eta (Figure 11), with its better resolution of lower levels and Betts parameterization scheme, also underforecast this event. Comparison of the actual reported 48 hour precipitation totals for the ice storm area with total model precipitation forecasts shows that the models were underpredicting the precipitation by as much as a factor of 2, consistent with Junker's findings for the NGM (Figure 12, Aviation model Figure 13). It must be noted that the model resolution constraints cannot be blamed for the underforecast of the rain amounts since the affected area for this case was large and stretched across several states.

4. MESOSCALE CONSIDERATIONS

A. General

Beginning 12 UTC 9 February, a strong upper atmospheric jet in excess of 80 m /sec over the Midwest and Ohio Valley moved such that its right rear entrance region was over the ice storm area for much of the event (Figure 3 shows initial position, other figures not shown). As explained in Bluestein (1993), vertical motion is enhanced by this jet position, and a direct circulation develops that results in heavier precipitation totals.

B. Model Soundings

Model-predicted soundings, which were not available in real-time (but were analyzed through the General Meteorological Package (GEMPAK) on workstations at the Center for Operational Meteorological Education and Training (COMET) laboratories in Boulder, CO) would have been a huge help to line forecasters during the critical stages of the ice storm. Most interestingly, the model sounding verification for Little Rock, Arkansas, showed wind anomalies at 300 and 250 mb which, when displayed via PCGRIDDS, revealed a weak anticyclonic ageostrophic circulation centered over the Gulf of Mexico with ridging north into east Texas, west Louisiana, and southwest Arkansas (Figure 14). This anticyclonic ageostrophic circulation may be similar to that shown by Maddox (1982) to be associated with Mesoscale Convective Complexes (MCCs). The circulation, in this writer's opinion, is related to vigorous convection that occurred in the warm air south of the front. Lightning data also supports this conclusion.

C. WSR-88D Observations

As Memphis (KNQA) WSR-88D data was not available, products from Little Rock (KLZK) and Jackson were analyzed for this storm (Figure 15 shows relative WSR-88D 230 km ranges). These products accurately depicted the stratiform type precipitation in the ice storm disaster area, and the more convective type precipitation to the south. Echo tops for the stratiform area were generally 6.0 to 7.6 km while in the more convective area echo tops were 9.1 km and higher. Cross sections were taken of the convective cells, but unfortunately none were available for the stratiform area. Higher reflectivities at fairly uniform distances from the JAN WSR-88D (Figure 16 is where higher reflectivities are shown from southeast Arkansas into north central Mississippi), lead to the determination of the melting level. As indicated by the bright band, this level is approximately 3,230 m (10,600 ft) agl (using the WSR-88D displayed height above mean sea level and subtracting the radar site elevation). WSR-88D reflectivity data from Little Rock (Figure 17), confirmed this melting level as well as did the Little Rock soundings.

WSR-88D rainfall products (as generated by the Jackson WSR-88D) substantially underestimated the rainfall in spite of possible contamination by bright banding. However, 88D rainfall products generated by the Little Rock radar grossly *over*estimated the rainfall. A possible explanation of this dichotomy (compare Figures 18 and 19) is that the bright band persisted on Little Rock's reflectivity products far longer than on Jackson's, since Little Rock was behind the front in the cold shallow air mass for the duration of the freezing rain episode. Notice also the double heavy rainfall signatures on the Little Rock Storm Total Precipitation (STP) product for the ice storm period. (The rainfall period for the STP product is from the beginning of the precipitation in northwest Arkansas late on February 8 to the time of the product, 11:42 UTC 11 February.) A maximum of 215.9 mm (8.5 inches) is estimated just southeast of Pine Bluff (PBF), Arkansas, in Jefferson County, but the reported rainfall for Pine Bluff Airport (which is also southeast of the city and very close to the estimated maximum) was only 82.3 mm (3.24 inches), a very large error. A second possible explanation that is just now beginning to be discussed is calibration error between the two WSR-88Ds. A discrepancy of only 2 or 3 dBz between two radars can produce significant differences in rainfall estimates, as discussed by Ricks, Graschel, and Jones (1995).

In spite of the understimation of the Jackson STP product, the 11:08 UTC 11 February Storm Total Precipitation product (the rainfall period for the STP product is from the beginning of the precipitation in southeast Arkansas early February 9 to the time of the product) did show a relative maximum of precipitation over Holmes and Attala counties but underestimated the amount by 25 to 50 mm (1 to 2 inches) or 20 to 40 percent. The maximum rainfall estimated by the WSR-88D algorithm was 106.7 mm (4.2 inches), but the maximum reported storm total rainfall reported up to that time was 140.0 mm (5.51 inches) at Vaiden. Vaiden is in Carroll County, which is about 30 miles north of the radar indicated maximum.

Mesoscale banding was observed on short pulse Doppler velocity products just southeast of Little Rock at 11:55 UTC 10 February (Figure 20) at approximately 300 to 1500 m (1000 to 5000 ft) agl oriented somewhat perpendicular to the thermal wind. This banding was occurring below the base of the frontal inversion with directional shear (backing winds) but little speed shear at all, and was probably due to small ripples or gravity waves propagating along the 'roof' of the frontal surface. Other interesting waves were visible on the Velocity Azimuth Display (VAD) wind profile product from Little Rock at 11:55 UTC on 10 February. Beginning at 11:32 UTC at 3700 m (12,000 ft) (Figure 21) a progressive veering and backing is evident as the cloud base or descending precipitation dropped to 3350 m (11,000 ft). These waves are in a layer that is obviously becoming more moist and that has significant speed shear.

D. Conditional Symmetric Instability Considerations

Conditional Symmetric Instability (CSI) combines the effects of inertial and gravitational forces and has been observed in association with extratropical fronts (Snook, 1992). CSI depends on either or both horizontal and vertical shear in the wind and whether or not the atmosphere is saturated (Bluestein, 1993). We use conditional symmetric instability if the atmosphere is symmetrically stable with respect to dry parcels, but symmetrically unstable with respect to saturated parcels. CSI theory has been explained in previous works by Bennetts and Hoskins (1979) and Emanuel (1983a, 1983b). Applying this theory, Emanuel (1985) and Rauber et al. (1994) showed that CSI was a factor in the ice storms they analyzed. Using a method suggested by Snook and diagnosed through PCGRIDDS (Figure 22), the momentum and theta-e surfaces on a cross section from 38°N 95°W to 30°N 88°W (or roughly from southeast Kansas, to the mouth of Mobile Bay) were analyzed. The slope of the momentum surfaces was shallower than the slope of the theta-e surfaces through most of Arkansas and northwest Mississippi as high as 730 mb. This means that parcels moving along the momentum surface would encounter lower theta-e temperatures and be unstable along a slantwise path. The upper air sounding from Little Rock for the time 12 UTC on 9 February showed strong vertical wind shear above 700 mb but the sounding was not saturated. At 0000 UTC 10 February, PCGRIDDS momentum and theta-e surface analyses showed the best potential for CSI somewhat southeast of the Little Rock area; however, at this time the sounding was more favorable for CSI (or had already had responded to CSI) with near zero static stability and near saturated conditions in addition to the strong vertical wind shear. The response to CSI by the atmosphere could also be evident here. The atmosphere responds fairly rapidly to CSI conditions and results in a saturated neutral or weakly stable environment. This environment is ripe enough for frontogenetic forcing to produce enhanced vertical circulations necessary for convection (i.e. thunderstorms).

Bradshaw (1994) applied this CSI diagnosis to help explain the 'Storm of the Century' thundersnows in Birmingham, Alabama, in March of 1993. Lightning data, examined at 6 hourly increments from 18 UTC 9 February to 12 UTC 11 February, shows a number of flashes in the ice storm area between 12 UTC 10 February and 00 UTC 11 February (most active times, 12 UTC 10 February through 00 UTC 11 February, shown in Figures 23 and 24). A significant number of the flashes were positive, and a study by Studwell and Orville (1994) has suggested a relationship between positive cloud-to-ground lightning and the location of freezing rain. Thus the environment just north of a slow moving or nearly stationary cold front including:

1) sharp, shallow inversion
2) little or no convective available potential energy (CAPE) above the inversion
3) slightly positive lifted indices within the layer
4) neutral or weak stability with respect to CSI
5) presence of lightning

all point to an example of elevated thunderstorms as discussed by Colman (1990a, b). The best explanation, as concluded by Colman, of the convection and subsequent heavy rains and ice accumulations associated with this storm, is that enhanced vertical circulations (as a result of strong frontogenetical forcing) existed in the presence of weak or neutral symmetric stability.

5. SUMMARY AND CONCLUSIONS

Several synoptic and mesoscale features worked in tandem to enhance ice accumulations across northwest Mississippi:

1) Positive Isothermal Vorticity Advection ahead of weak short waves and ultimately the vorticity maxima over California
2) Mechanical lift of the warm, moist air overrunning the shallow, cold air at the surface
3) Thermally direct circulation under the right rear entrance region of the 300-250 mb jet
4) Possible mesoscale anticyclonic circulation aloft imposed on the mean synoptic flow
5) Frontogenesis in a region of weak or neutral symmetric stability.

As far as the new technology available to field forecasters, the WSR-88D was an effective tool in diagnosis of the bright banding structure, but was somewhat inadequate for rainfall amounts, underestimating from one radar site and overestimating from another radar site. Dual Radar analysis, through the Little Rock and Jackson WSR-88Ds, verified the presence of the melting level near 3.230 m. The VAD Wind Profile product from Little Rock showed the frontal structure well, and gave continuous updates on its depth and movement. The profiler network was not as helpful as it could have been, due to power failure from ice accumulation at Okolona, MS, but did provide continuous updates on the depth and movement of the colder air at Winnfield, LA, Dequeen, AR, and Palestine, TX.

Model soundings should be made available to field personnel in these critical situations. Had model soundings been available, watch and warning decisions would have been easier and issue times could have been earlier. This would provide the public and power companies a much longer lead time. The advent of the Science Applications Computers (SAC) as workstations for NWS offices, and ultimately AWIPS, will provide the capability to analyze model soundings in the near future.

6. ACKNOWLEDGEMENTS

The author is indebted to Dr. John M. Brown of the NOAA Forecast Systems Laboratory in Boulder, Colorado, for many helpful sessions and suggestions concerning this disastrous event. Dr. Brown is a volunteer mentor for students at the COMET Meteorological Analysis and Prediction Course held in Boulder. Additional appreciation is extended to George Wilken, SOO at the NWSFO Little Rock, Arkansas; Kevin Pence, SOO at the NWSFO Birmingham, Alabama, Dr. Brad Colman, SOO at the NWSFO Seattle, Washington; and Mike Koziara, SOO at the NWSFO New Orleans Area, for data and helpful suggestions. Lightning data and helpful advice was supplied by Dr. Richard Orville and Aaron Studwell at Texas A&M University, as well as by Ron Holle at the National Severe Storms Laboratory. Precipitation data was supplied by Jay Grymes at the Southern Regional Climatic Center at Louisiana State University.

7. REFERENCES

Bennetts, D.A., and B.J. Hoskins, 1979: Conditional Symmetric Instability - A Possible Explanation for Frontal Rainbands, *Quart. J. Roy. Meteor. Soc.*, **105**, 945-962.

Bluestein, H.B., *Synoptic-Dynamic Meteorology in Midlatitudes*, Vol. I, Principles of Kinematics and Dynamics, Oxford Univ. Press, New York, N.Y., 1992, pp. 367-368.

Bluestein, H.B., *Synoptic-Dynamic Meteorology in Midlatitudes*, Vol. II, Observations and Theory of Weather Systems, Oxford Univ. Press, New York, N.Y., 1993, pp. 397 ff.

Bradshaw, T, 1994: Relationships Between Conditional Symmetric Instability, Thunder, and Heavy Snowfall During the "Storm of the Century", National Weather Service Southern Region Administrative Notes, April 1, 1994, Technical Attachment.

Colman, B.R., 1990: Thunderstorms above Frontal Surfaces in Environments without Positive CAPE, Part I, A Climatology, and Part II, Organization and Instability Mechanisms, *Mon. Wea. Rev.*, **118**, 1103-1144.

Emanuel, K.A., 1983a: The Lagrangian Parcel Dynamics of Moist Symmetric Instability, *J. Atmos. Sci.*, **40**, 2368-2376.

_____, 1983b: On Assessing Local Conditional Symmetric Instability from Atmospheric Soundings, *Mon. Wea. Rev.*, **111**, 2016-2033.

_____, 1985: Frontal circulations in the presence of small moist symmetric instability, *J. Atmos. Sci.*, **42**, 1062-1071.

Harlin, B.W., 1952: The Great Southern Glaze Storm of 1951, *Weatherwise*, 10-13.

Maddox, R.A., 1983: Large-Scale Meteorological Conditions Associated with Midlatitude, Mesoscale Convective Complexes, *Mon. Wea. Rev.*, **111**, 1475-1493.

Meier, K.,1993 : *PCGRIDDS - A User's Manual*, Western Region Scientific Services Division, National Weather Service.

Petersen, R., 1991: *PCGRIDDS*, original program, National Meteorological Center,

Rauber, R.M., M.K. Ramamurthy, and A. Tokay, 1994: Synoptic and Mesoscale Structure of a Severe Freezing Rain Event: The St. Valentine's Day Ice Storm, *Wea. and Fcstg.*, **9**, 183-208.

Ricks, R., J. Graschel, and E. Jones, 1995: A Comparison of Adjacent WSR-88D Precipitation Estimates Along the Mississippi Gulf Coast National Weather Service Southern Region Administrative Notes, May 1, Technical Attachment.

Snook, J.S., 1992: Current Techniques for Real-Time Evaluation of Conditional Symmetric Instability, *Wea. and Fcstg.*, 7, 430-439.

Studwell, A.M., and R.E. Orville, 1994: Characteristics of Cloud-to-Ground Lightning in a Severe Winter Storm, 9-12 February, 1994, advance copy of paper presented at the 6th Conference on Aviation Weather Systems, AMS Annual Meeting, 15-20 January, 1995.

Williams, B.B., 1960: The 1960 Ice Storm in Northern Alabama, *Weatherwise*, October, 1960, 196-199,203.

Figure 1. Mississippi ice storm area locator map.

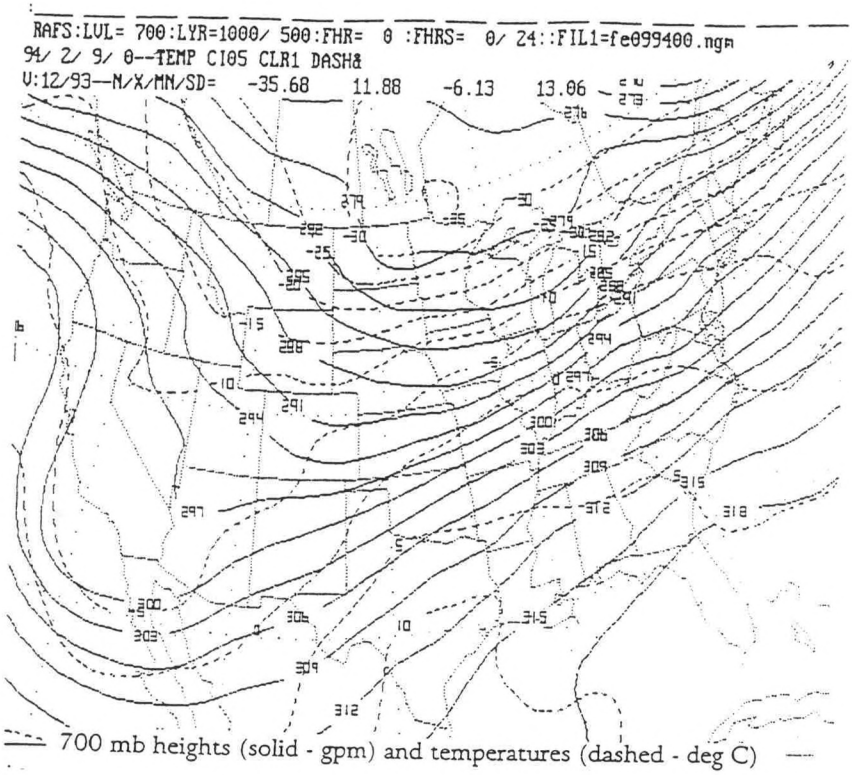

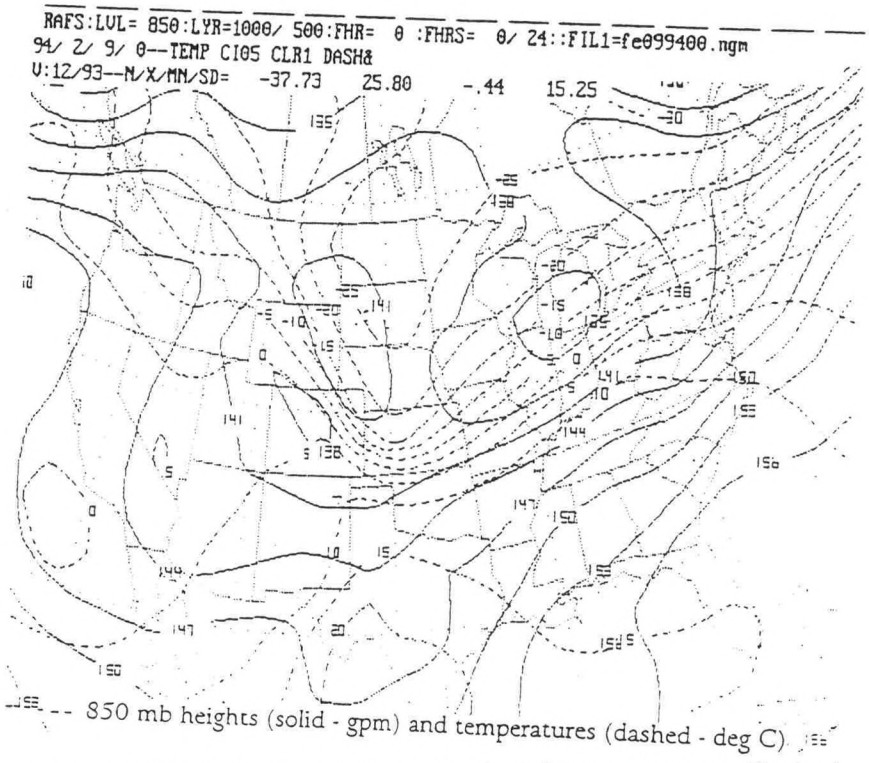

Figure 2. 0000 UTC 9 February 1994; a) 700 mb heights (solid - gpm) and temperatures (dashed - deg C) and b) 850 mb heights (solid - gpm) and temperatures (dashed - deg C).

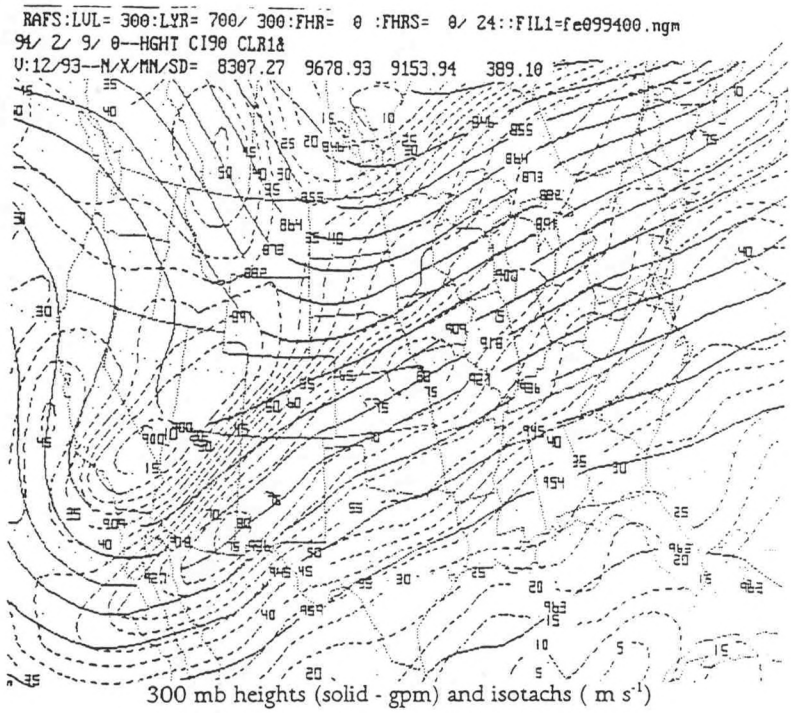

300 mb heights (solid - gpm) and isotachs (m s^{-1})

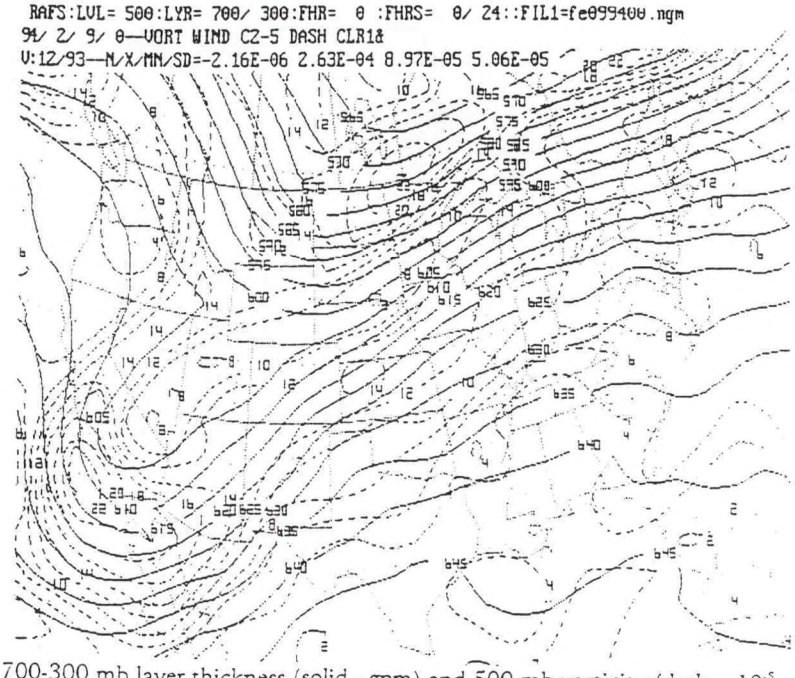

700-300 mb layer thickness (solid - gpm) and 500 mb vorticity (dash - 10^{-5} s^{-1})

Figure 3. 0000 UTC 9 February 1994; a) 300 mb heights (solid - gpm) and isotachs (m s^{-1}) and b) 700 - 300 mb layer thickness (solid - gpm) and 500 mb vorticity (dash - 10^{-5} s^{-1}).

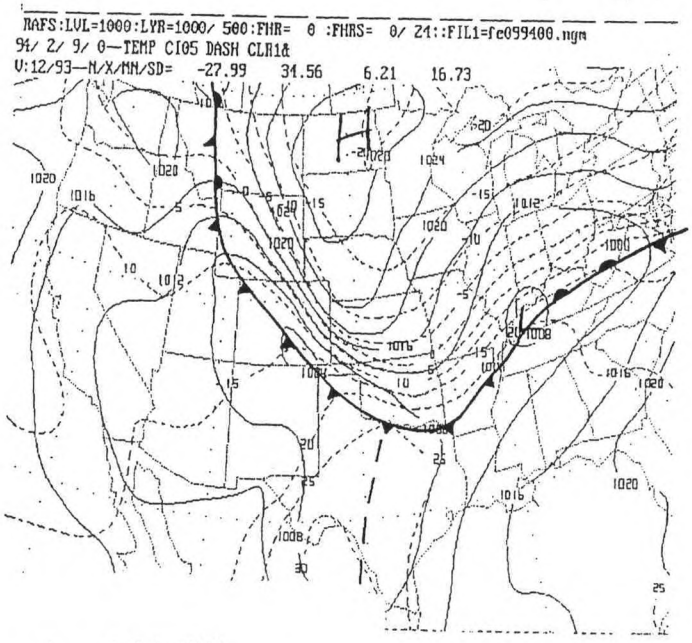

Figure 4. 0000 UTC 9 February 1994 surface anaylsis isobars (mb) and temperatures (°C) with fronts and pressure centers.

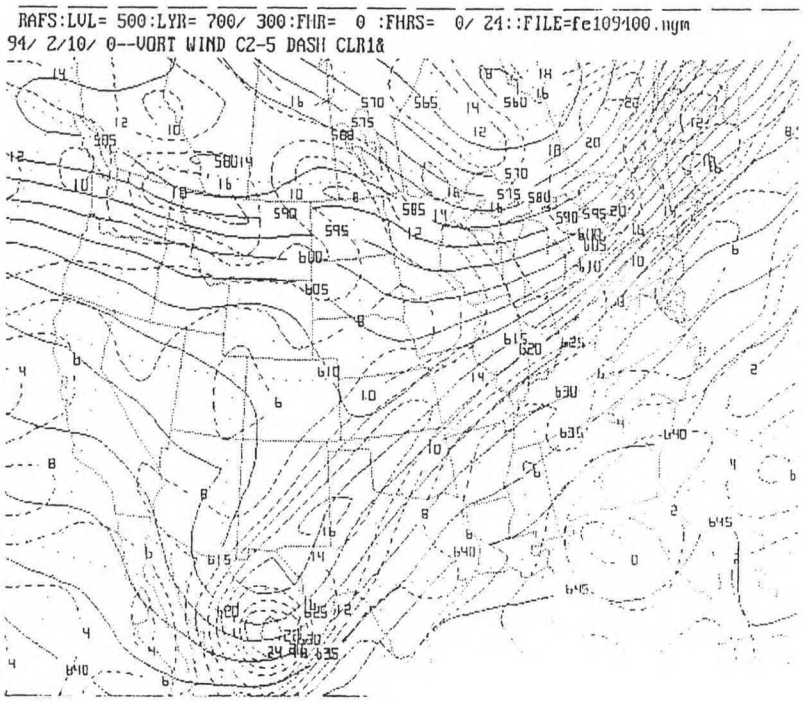

Figure 5. 0000 UTC 10 February 1994, 700 - 300 mb layer thickness (solid - gpm) and 500 mg vorticity (dash - 10^{-5} s^{-1}).

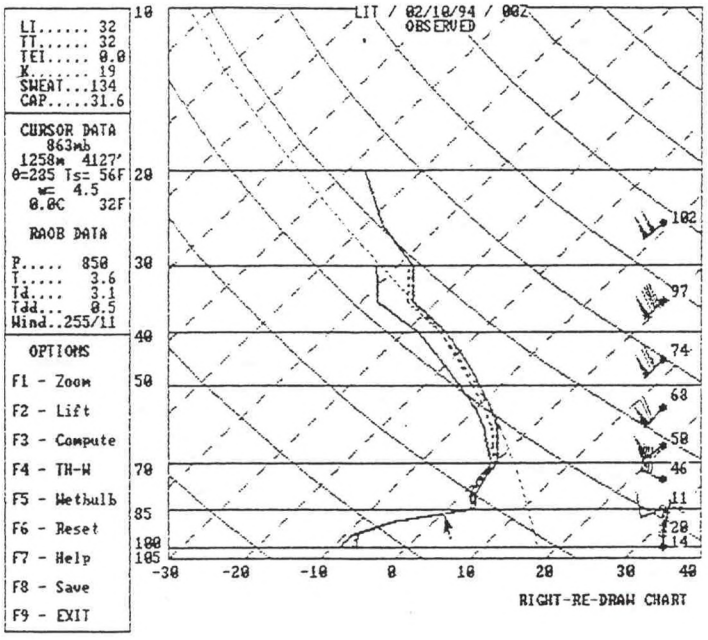

Figure 6. 0000 UTC 10 February 1994 Little Rock sounding from SHARP workstation isotherms dashed, adiabats solid, pseudoadiabat dotted.

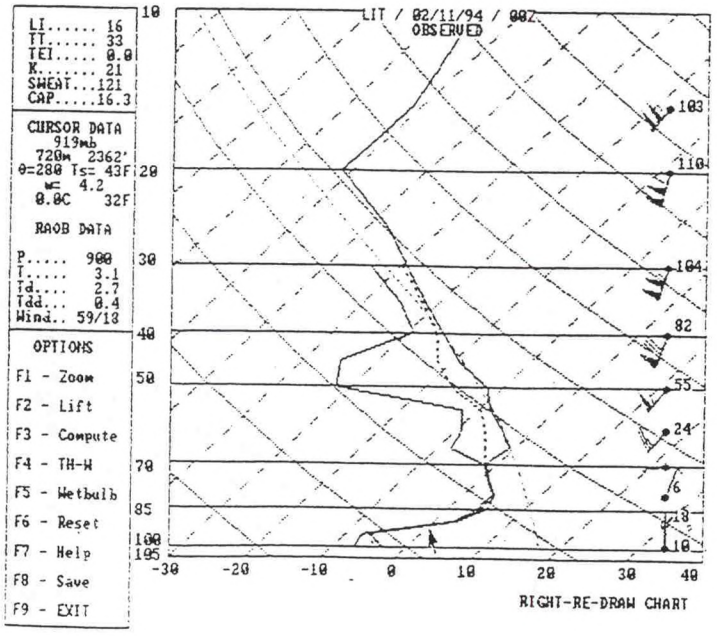

Figure 7. 0000 UTC 11 February 1994 Little Rock sounding from SHARP workstation isotherms dashed, adiabats solid pseudoadiabat dotted.

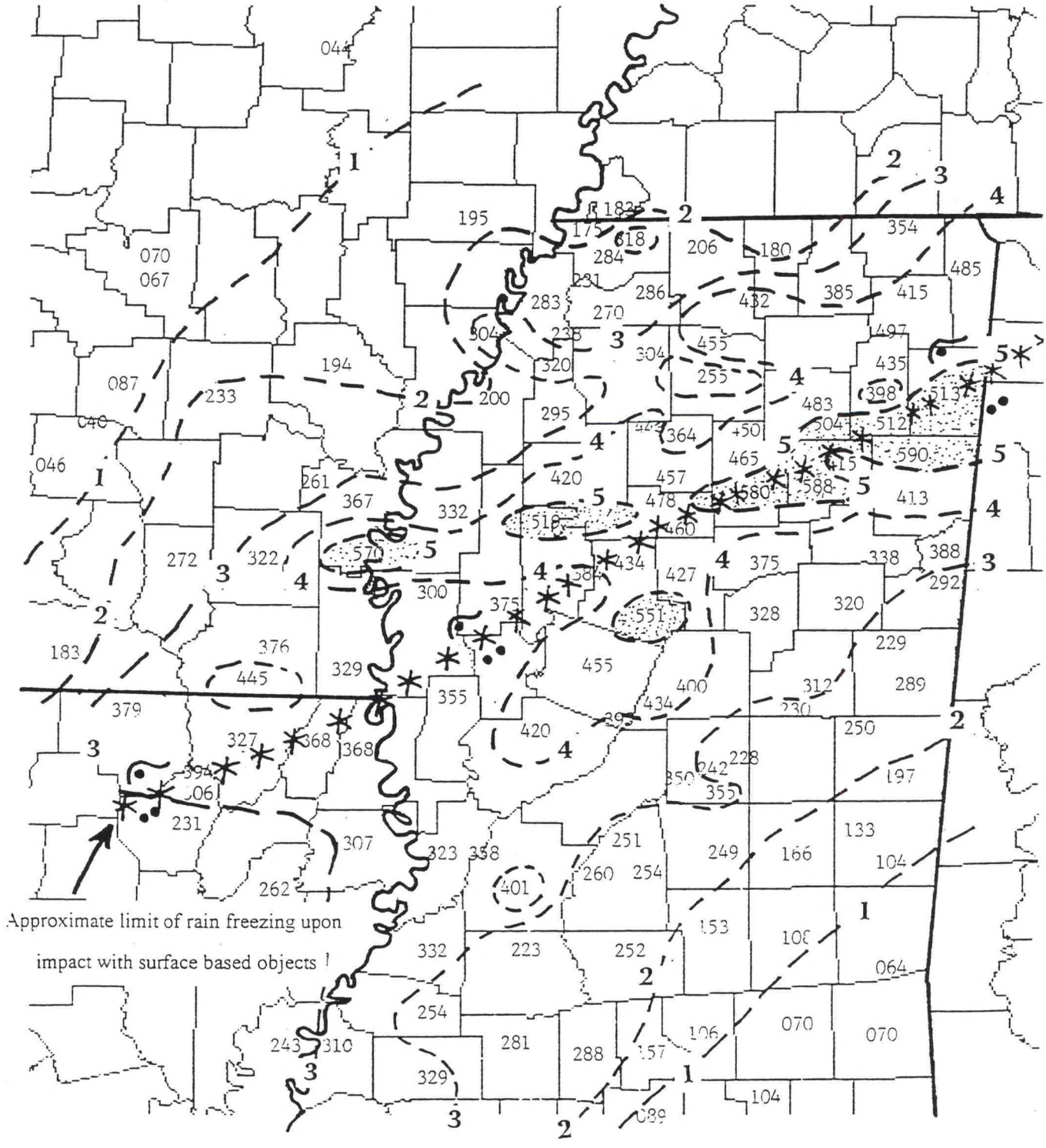

Figure 8. Storm total rainfall 1200 UTC 9 February to 1200 UTC 11 February 1994. 48-hour total in inches and hundredths (e.g., 395 = 3.95 inches).

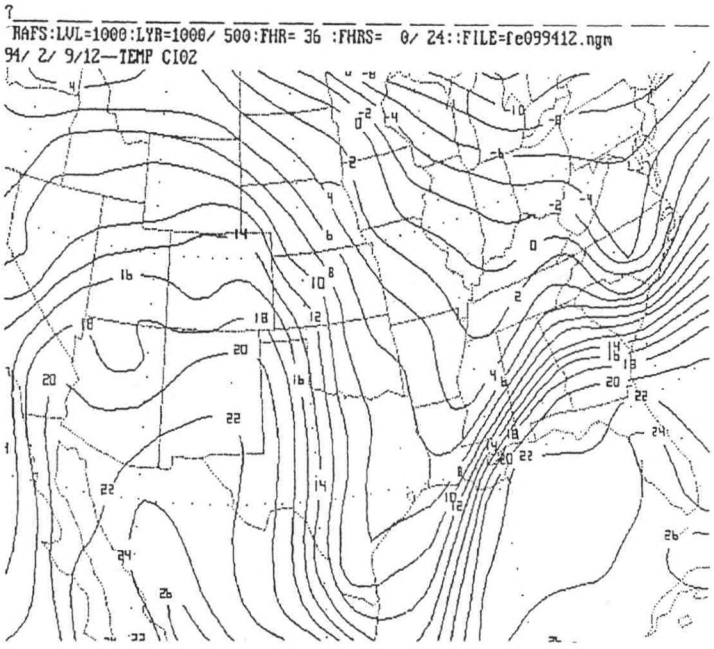

Figure 9. 1000 mb leel temperature forecast (°C) at 36 hours from the NGM model run at 1200 UTC 9 February 1994.

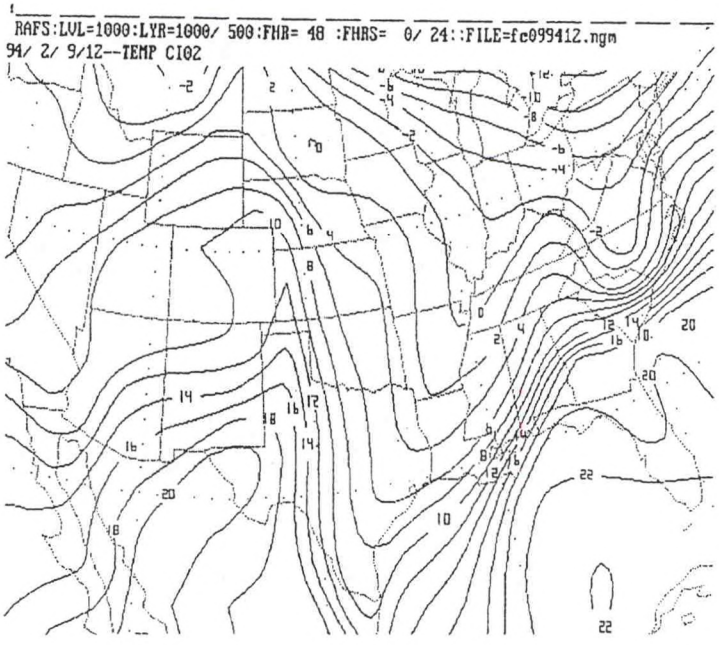

Figure 10, 1000 mb level temperature forecast (°C) at 48 hours from the NGM model run at 1200 UTC 9 February 1994.

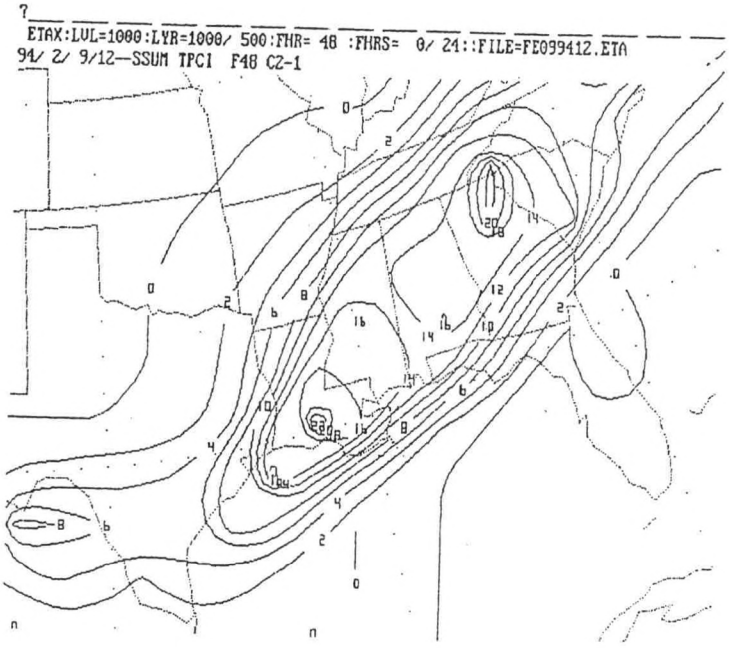

Figure 11. Forecast of 48 hour precipitation (tenths of an inch) from the Eta model run at 1200 UTC 9 February 1994.

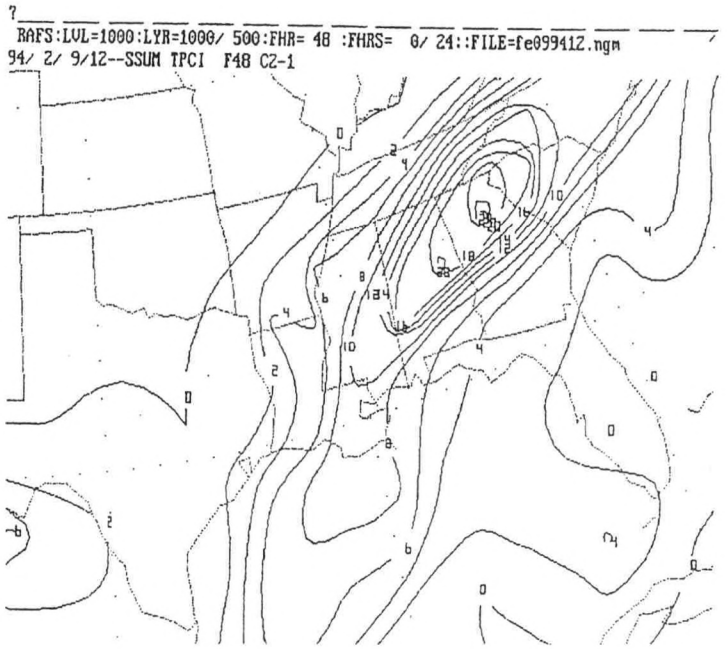

Figure 12. Forecast of 48 hour precipitation (tenths of an inch) from the NGM model run at 1200 UTC 9 February 1994.

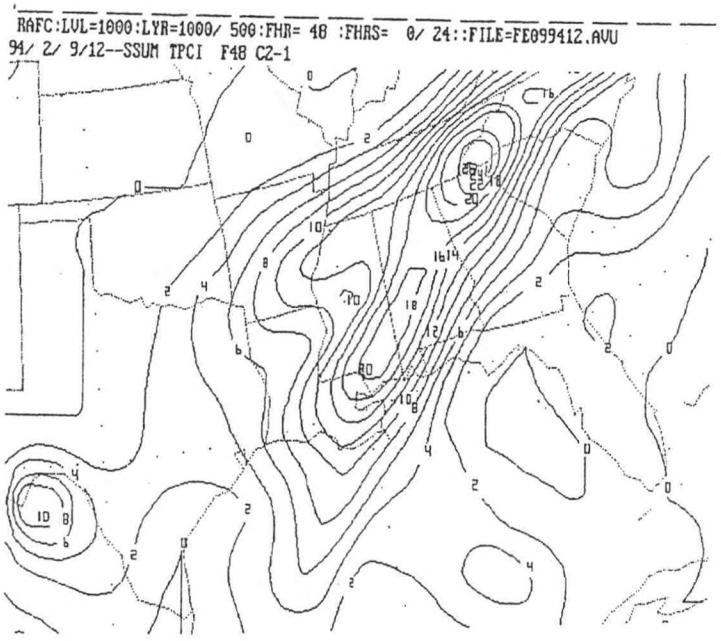

Figure 13. Forecast of 48 hour precipitation (tenths of an inch) from the AVN model run at 1200 UTC 9 February 1994.

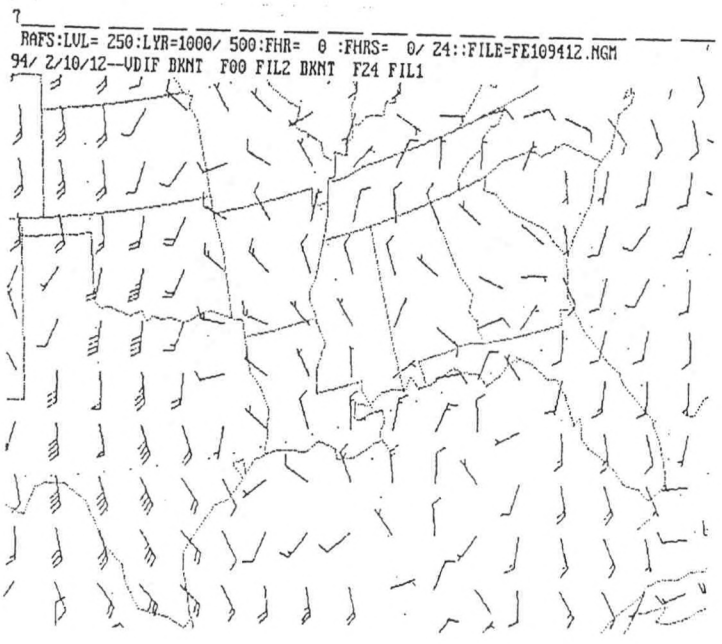

Figure 14. Vector difference of total wind at 250 mb. (Total wind analysis from NGM run 1200 UTC 10 February 1994 minus 24-hour forecast of total wind from NGM run 1200 UTC 9 February 1994; 24-hour earlier).

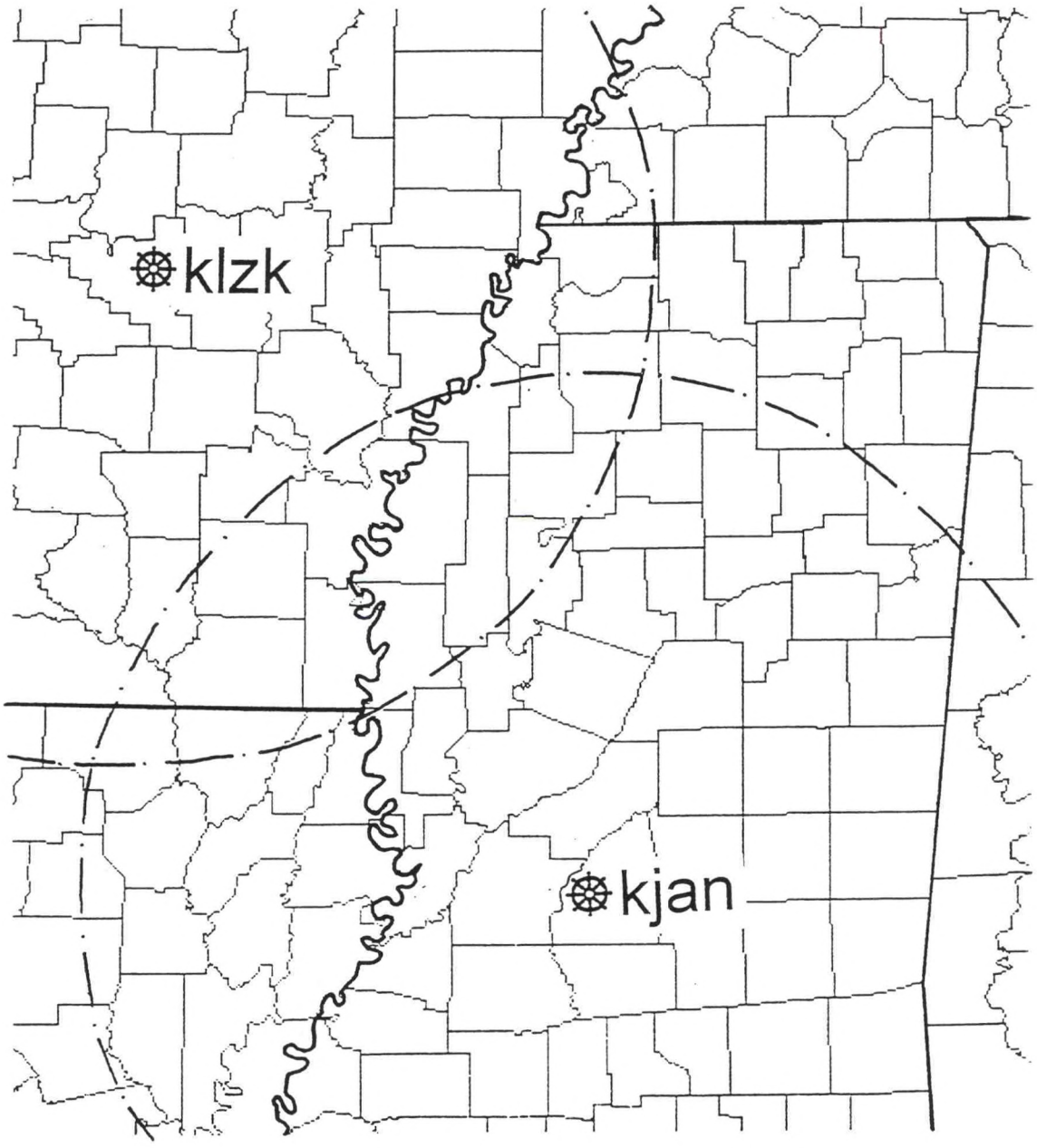

Figure 15. Relative 230 km ranges from WSR-88D sites at KJAN and KLZK.

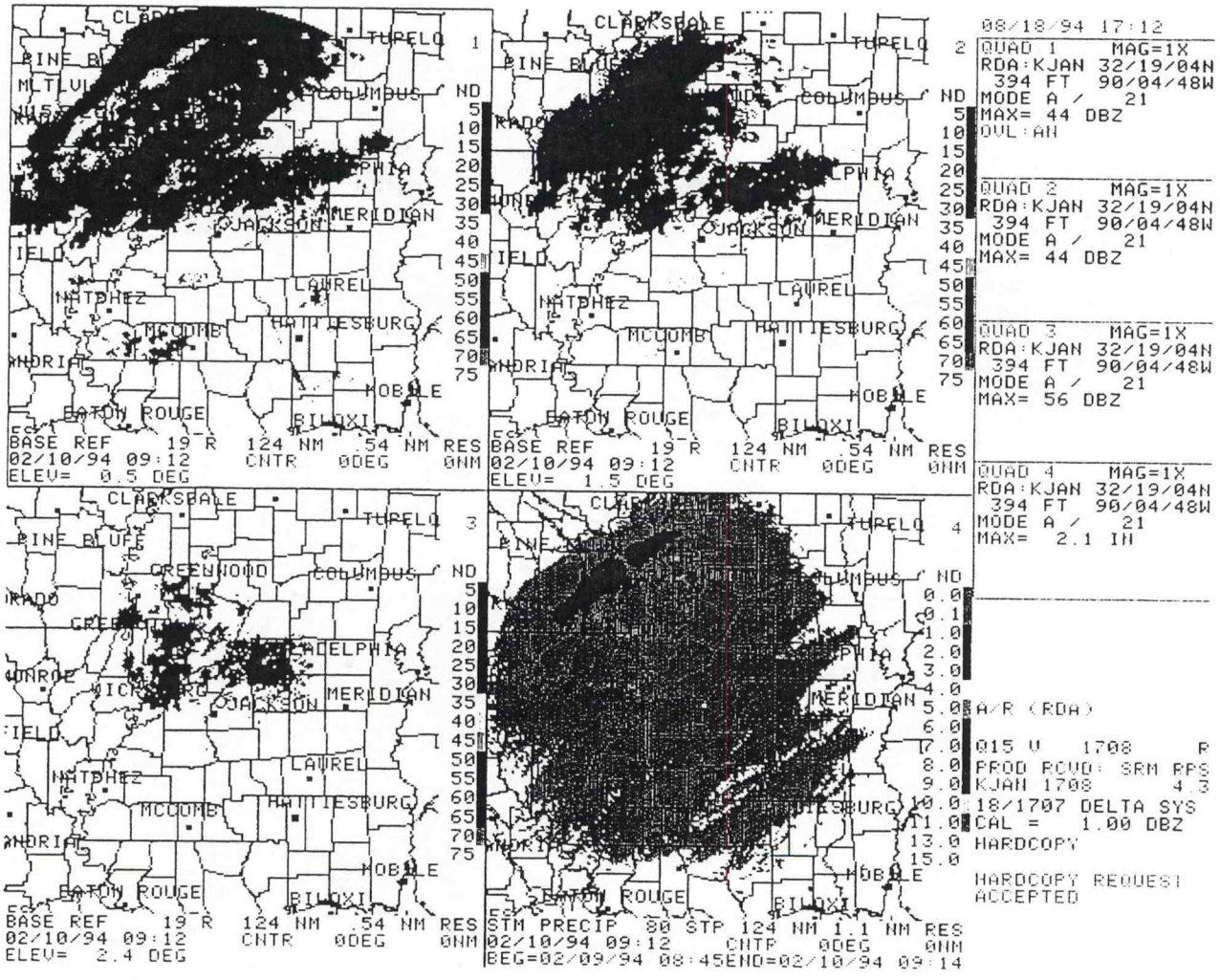

Figure 16. Four-panels of reflectivity (0.5, 1.5, 2.4 degrees) and STP KJAN 0912 UTC 10 February 1994).

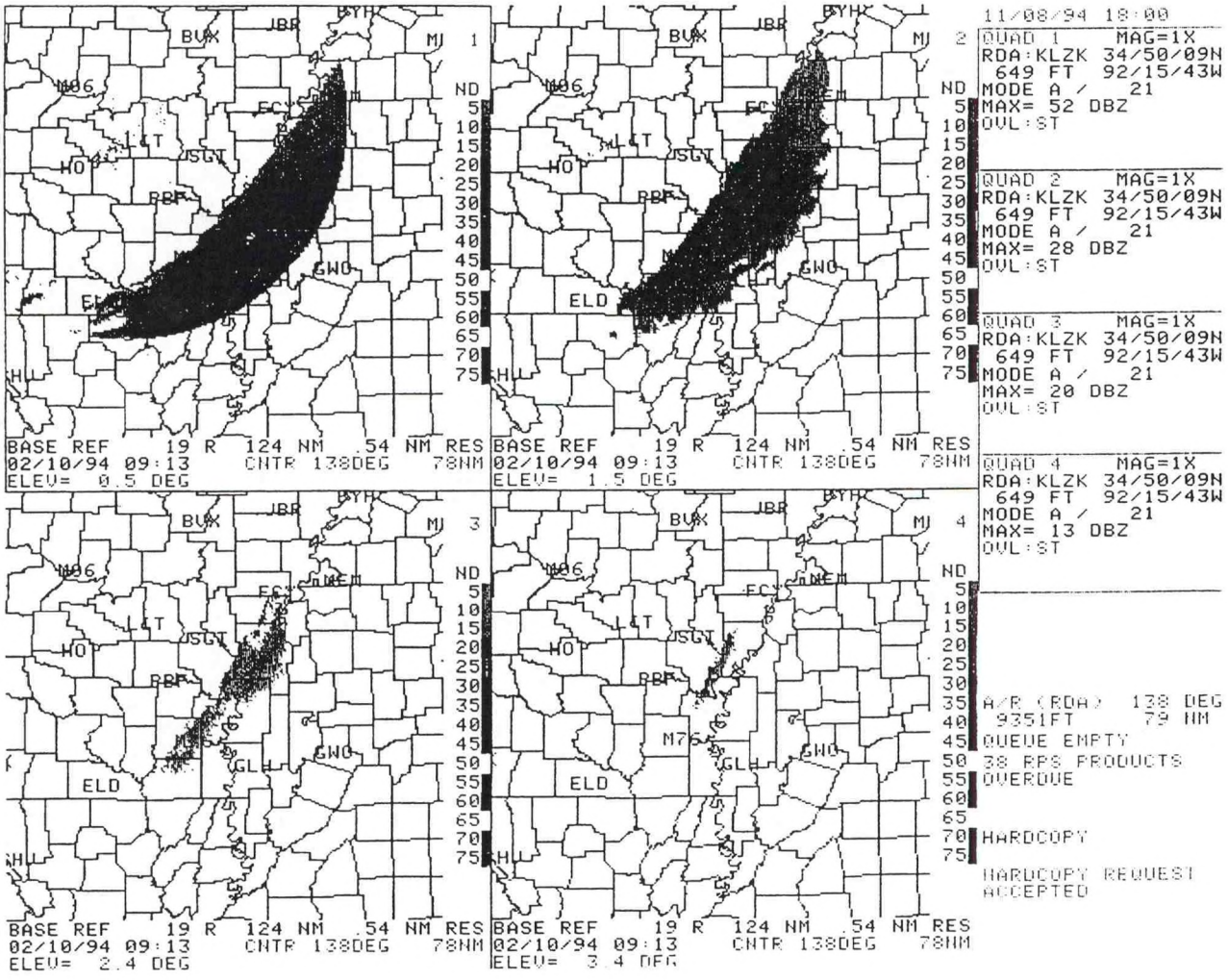

Figure 17. Four-panels of reflectivity (0.5, 1.5, 2.4, 3.4 degrees) KLZK 0913 UTC 10 February 1994.

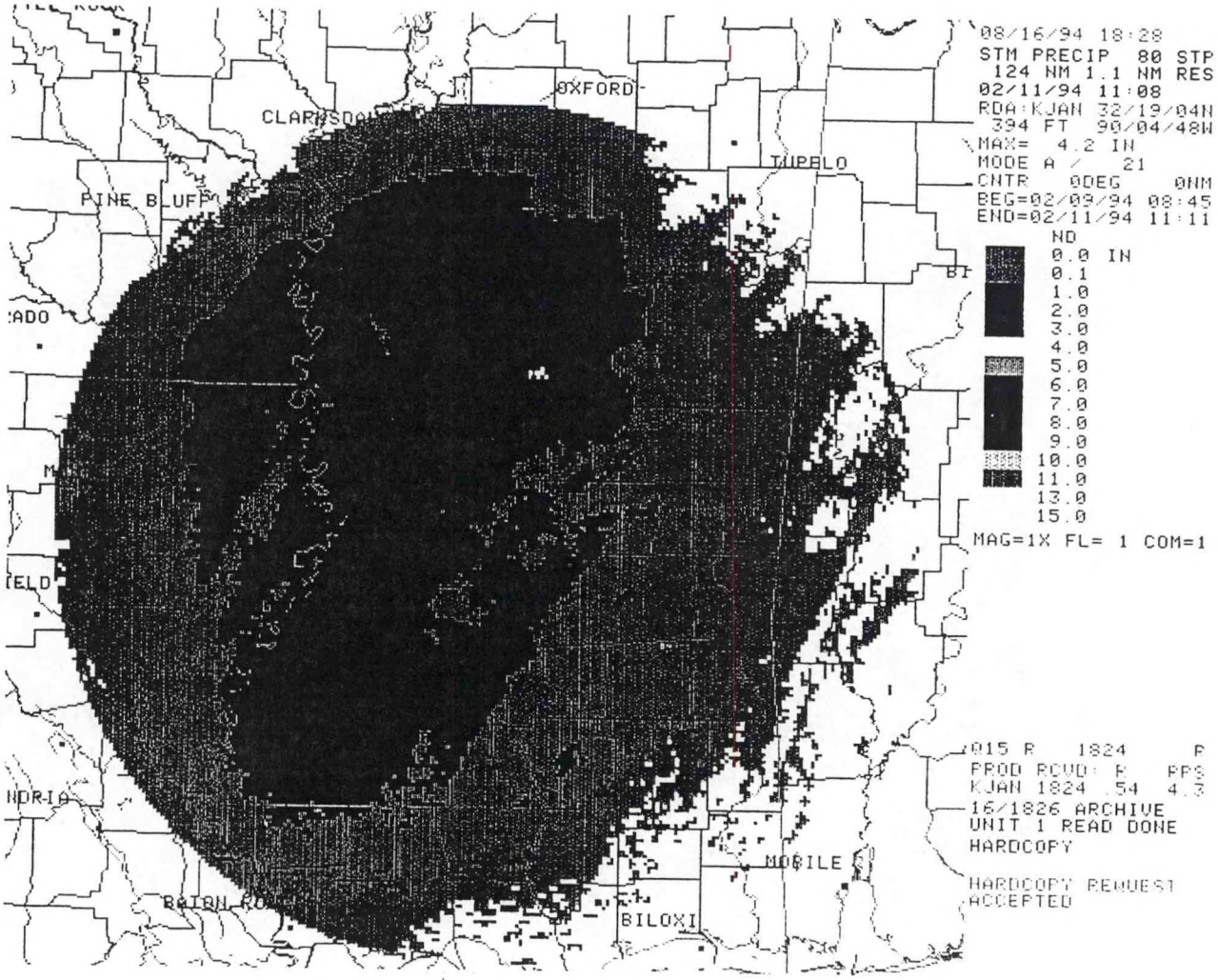

Figure 18. Storm totap precipitation (STP) KJAN 1108 UTC 11 February 1994.

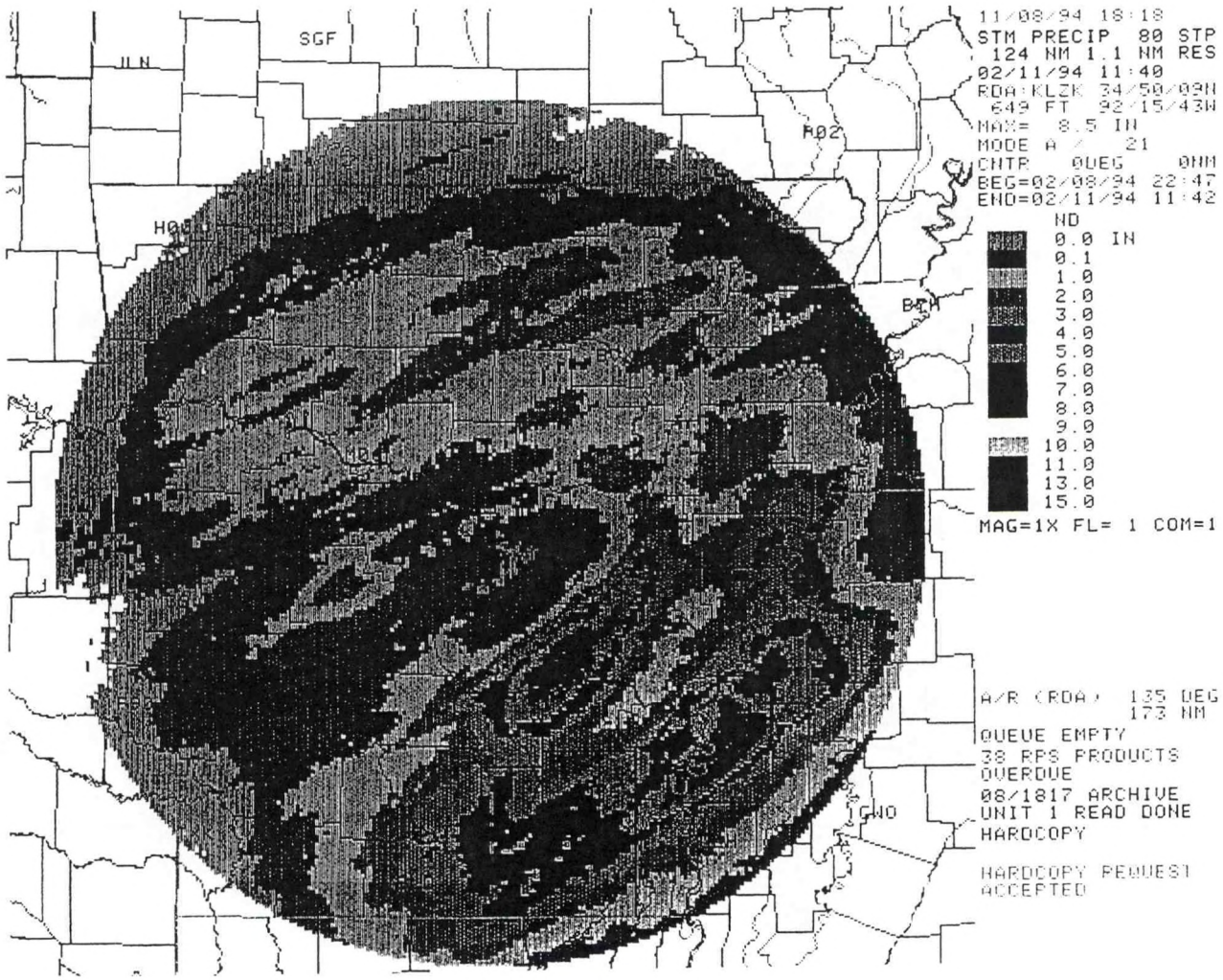

Figure 19. Storm total precipitation (STP) KLZK 1140 UTC 11 February 1994.

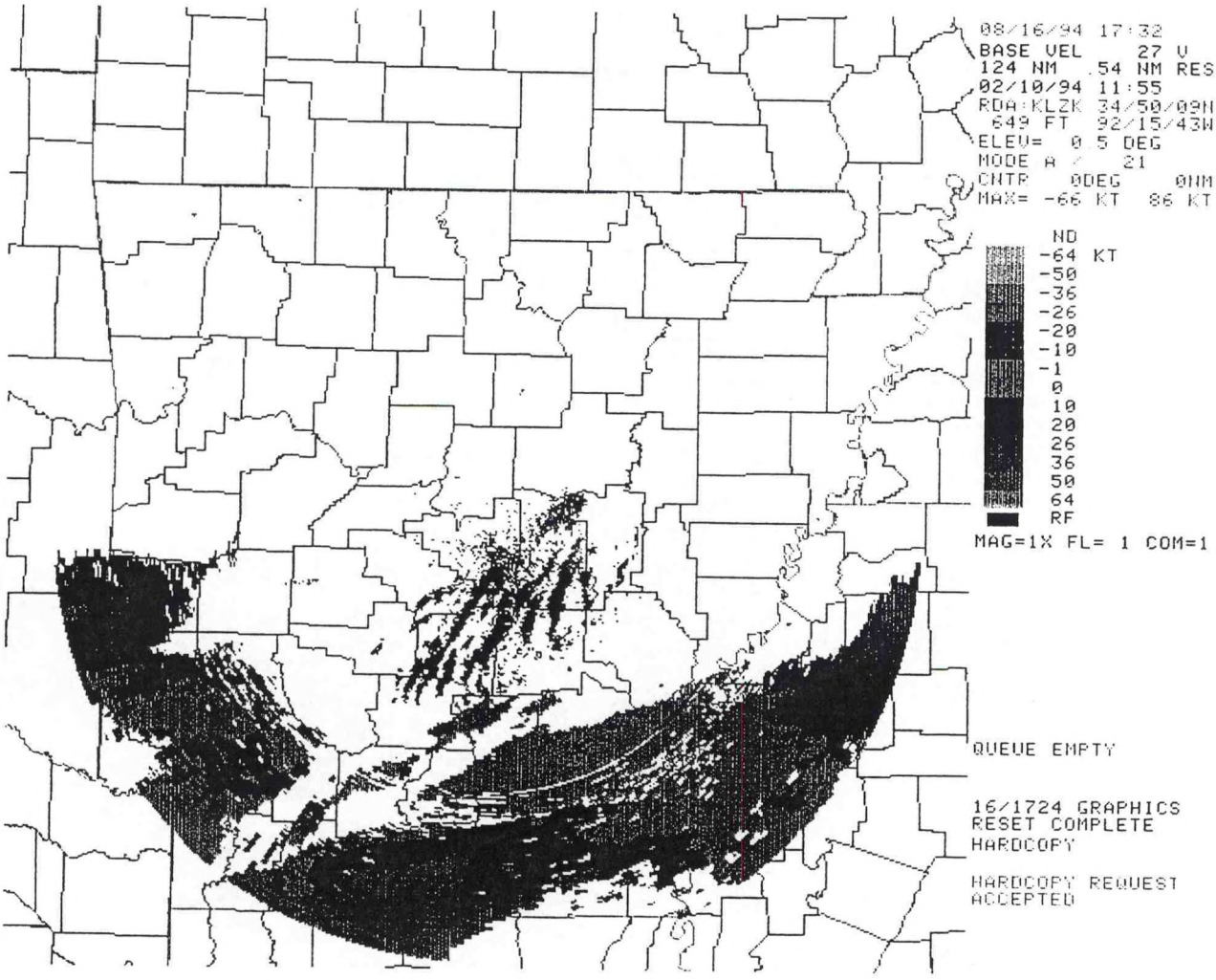

Figure 20. Velocity (0.5°) KLZK 1155 UTC 10 February 1994.

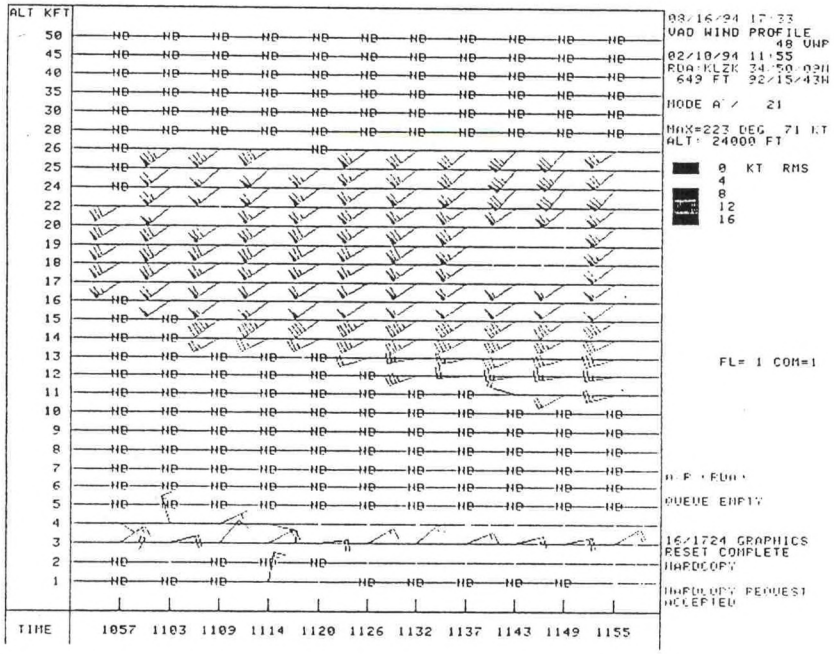

Figure 21. VAD wind profile (VWP). KLZK 1155 UTC 10 February 1994.

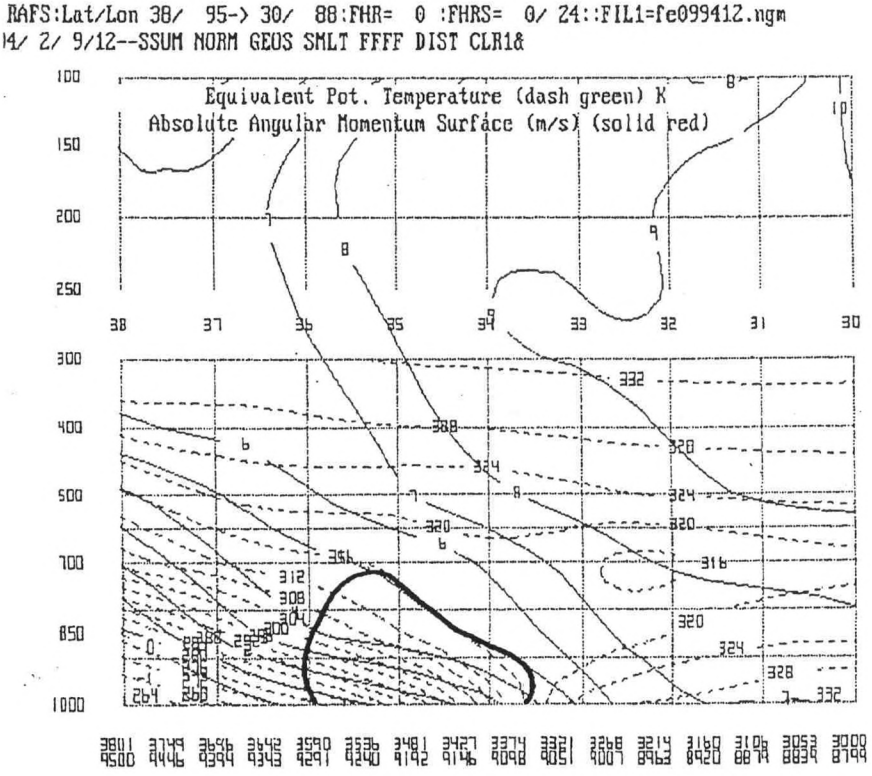

Figure 22. Cross-section from 38°N 95°W (approx MKC) to 30°N 88°W (approx Mobile Bay) showing equivalent potential temperature (θ_e) in deree Kelvin and absolute angular momentum (m s^{-1}). Region of CSI is outlined.

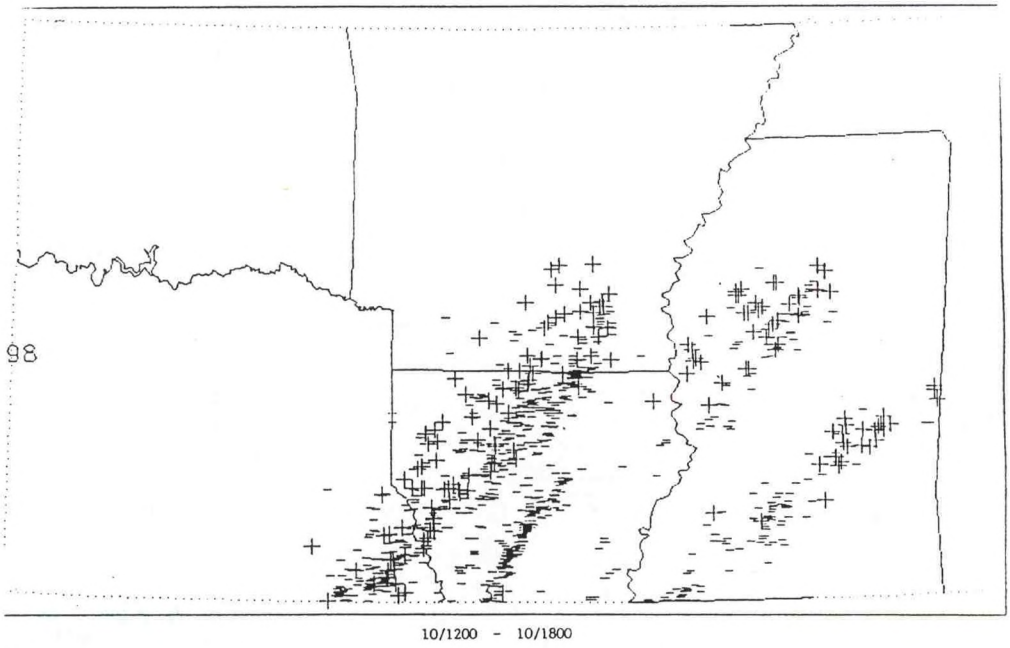

Figure 23. Lightning strikes (positive and negative polarity).

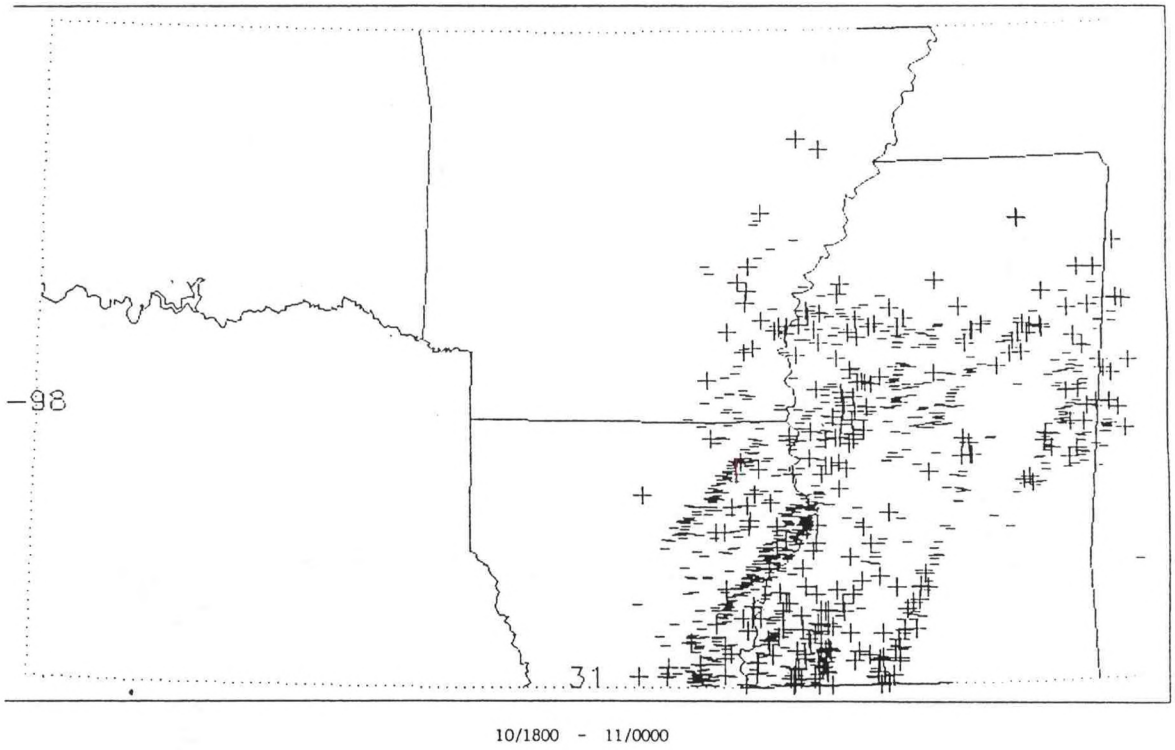

Figure 24. Lightning strickes (positive and negative polarity).

SESSION 10
FORECAST TECHNIQUES I

33. Physical Rationale Associated with Various Minneapolis, Minnesota Heavy Snow Checklist Parameters

34. A Comparison of Snow Amount Forecasting Techniques for Kansas Heavy Snowstorms During the Winter of 1994-1995

35. The Forecasting of Precipitation Phase Change: a Case Study

36. The Influence of Coniferous Forest Albedo on Wintertime Maximum Temperatures

37. A Winter Storm Forecast: from the Science to the Public

Physical Rationale Associated with Various Minneapolis, Minnesota Heavy Snow Checklist Parameters

Glenn R. Lussky[1]

1. INTRODUCTION

After a forecast for 1 inch of snow for Minneapolis, Minnesota (MSP) in January 1982 verified at 17 inches, Lead Forecaster Rich Naistat developed a checklist of forecast parameters upon which to help identify the appropriate location and amount of snow to forecast. Portions of this checklist have been revised and refined some over the past decade. The most recent version of the checklist is shown in Figure 1.

Many concepts associated with the MSP Heavy Snow Checklist are similar to most of the discussions presented at this workshop, and at earlier workshops such as the December 1992 Milwaukee Winter Weather Workshop. Knowledge of the relationship between the heavy snow band and the low-level cyclonic and mid-tropospheric vorticity maxima is prevalent across much of the country. A number of methods have been demonstrated which appear to have operational utility.

Therefore, instead of discussing *what* methods seem to work in heavy snow forecasting, this paper will consider a few aspects associated with *why* some of these methods work. That is the main purpose of this study: to consider the physical mechanisms that are acting in an organized synoptic-scale system, and to discern how these mechanisms effect the production of heavy snow. As a byproduct, it is hoped that this understanding will reduce the dependence on the simple interpretation of geometric lines in the snowfall forecast process.

We will lay the groundwork for examination of the physical mechanisms by surveying the dynamics associated with the Colorado lee-side cyclogenesis systems. We will explore why the heavier snow bands form where they do concerning the circulations present. This discussion will provide the foundation for understanding the importance of cloud physics, as it applies to the snow development problem and the location of heavy snow.

2. PHYSICAL FACTORS

A. Position of the Surface Low

The position of the surface low has long been recognized as a key feature in identifying the axis of heavy snow. The existence of an organized surface low is not essential for significant snow events to occur (Hakim and Uccellini, 1992). However, when heavy snow is expected with an organized system, the location and track of the surface low can be used to identify the expected snow band location.

With situations that involve moist baroclinic lee-enhanced cyclogenesis (under southwesterly mid- to upper-tropospheric flow), the heaviest snow will typically be around 150 miles to the left of the track. (This distance tends to decrease as the system undergoes occlusion). In general, if the low track could be forecast well, so could the snow axis.

1. Corresponding author address: Glenn R. Lussky, WFO La Crosse, Wisconsin.

Figure 2 shows a well-known schematic illustration of conceptual isentropic conveyor belt flows around a developing cyclone (Carlson, 1980). The image presented shows the warm conveyor belts rising to near 500 mb in the vicinity of the warm front and then turning eastward in the deformation zone of the comma head's cirrus cloud shield (i.e., along the axis of dilatation). It also indicates that air wrapping around the low originates in the cold conveyor belt flow north of the warm front *and at a lower altitude than the warm frontal boundary.*

While this applies for that isentropic surface, the image gives a very incomplete 3-D representation of the full flow field for the air originating in the cyclone's warm sector. For instance, what is the flow structure of the air originating in the lowest 200 mb above the surface just south of the warm front? This figure does not show it. That low-level air parcels are backing rapidly with height around the circulation center as they ascend over the warm frontal boundary. The warm air wraps around the cyclone center throughout the lower atmospheric layers, and thermal advections do the same. The 850 mb "S-shaped" thermal pattern is a characteristic feature of these systems, and is a direct result of the warm advection wrapping north (and even west) of the system and cold air wrapping to the south.

An example of such a S-shaped thermal pattern is shown in Figure 3, from the Midwestern snowstorm at 0000 UTC 26 November 1992. No state backgrounds are given since the figure has been oriented such that the 850 mb low is moving toward the top of the page. The low cloud edge and enhanced IR comma are denoted by scalloped lines. The area of moderate snow (from surface reports) is indicated within the enhanced comma region. Isotherms are dashed and streamlines are shown in solid. Clearly, the warm advection is strongest just ahead (and to the left) of the 850 low track.

So, what causes the precipitation to become heaviest where it does? To understand this, we go back to the Quasi-Geostrophic (QG) Omega Equation, in which we note that the thermal advective support for upward velocities is not related to the warm advection *per se*, but the *Laplacian* of warm advection (Holton, 1979).

Consider Figure 3 again. A broad area of warm advection exists ahead of and to the left of the 850 mb low. However, the Laplacian is maximized in the lower part of the comma head, since that area of warm advection is immediately adjacent to an area of neutral advection and even cold advection. Based on the thermal portion of the Omega Equation alone, this analysis suggests that the vertical motion would maximize in that zone of the system. This area coincides with the location of heaviest snow shown on Figure 3. It also is consistent with previous work by Morrison (1988) and others, who related the heavy snow bands to the lower portion of the satellite sensed IR comma head.

Based on this discussion, we might believe that upward vertical motion due to the thermal advections is maximized where the heaviest snow falls. But, does the upward vertical motion gradient within the comma cloud shield warrant the gradient of snowfall that typically occurs there? Is the relationship between vertical motion and snowfall rate perfectly correlated? (No). Numerical guidance regularly shows broad areas of upward motion throughout the comma head region, yet only very light amounts of snow tend to fall in the upper portion of the comma, while a heavy band of snow falls in the lower portion of the comma (Morrison, 1988). Rationale for this will be examined in the next section of this paper, where other processes are described which play an additive role in creating the heavy band of snowfall.

B. The Vertical Temperature Structure

Here we move away from the surface features to look at some thermal considerations as we go up vertically through the storm. For most Midwestern meteorologists, or at least those who gained their initial meteorological education in the Midwest, one of the first things you learned regarding the rain/snow demarcation line is to identify the location of the "540 line" (or, the 5400m thickness between 1000-500 mb).

In general, this is a quick and easy "first look" which is often used to estimate the rain/snow line. The heaviest snow falls tend to accumulate between the 534 and 540 thicknesses, partially because this is the area where precipitable water loading is greatest among the thicknesses in which precipitation *tends to* fall as snow. However, approximating the heavy snow band by the 534-540 thickness lines doesn't always work well. The vertical stratification of temperature plays a significant role in determining whether the falling precipitation will be rain, snow or freezing precipitation near the 540 line. Thus, additional thickness checks were added to the checklist.

2.1 The 1000-850 mb thickness

An established checklist criterion says that for heavy snowfall to occur, the 1000-850 mb thickness should normally be less than 1300 meters. This limit ensures that the mean virtual temperature in this layer is less the 0°C. Obviously, a thickness greater than this would allow too much melting of the crystals through the layer, which would normally create either rain at the surface or a mixture of rain and snow.

2.2 The 850-700 mb thickness

The checklist also says that the preferred thickness for the 850-700 mb layer ranges from 1520 to 1540 meters. This requirement helps ensure that the vertical temperature profile is appropriate for snowfall within the 534-540 thickness between 1000-500 mb. If the 850-700 mb thickness is greater that 1540 meters, chances increase that the precipitation will melt before reaching the ground (ergo, no snow - though freezing precipitation could be a problem). Additionally, the thickness range of 1520-1540 meters helps ensure that the mean virtual temperature through that layer is around -5°C.

2.3 The impact of cloud microphysics at -5°C

Earlier in this paper, we discussed how vertical motion is maximized in the lower portion of the IR cloud shield. In that section, the question was raised about whether vertical motion differences in the cloud shield would warrant the strong gradient of snowfall that often occurs within the shield. The suggestion was made that the correlation between vertical motion and snowfall was not perfect, and that the snowfall gradient around the heavy snow band was strong relative to the vertical motion gradient.

The justification for saying relates at least in part to the microphysical processes (in particular, ice crystal growth processes) which occur in this cloud shield. Laboratory observations by Hallett (1965), Mason (1957) and Todd (1964) indicated that there are two peaks in the crystal growth curve, relative to temperature. The primary growth area occurs around -14°C, with a secondary maximum near -5 C (bottom panel of Figure 4). More recent studies indicate that the maximum near -5°C is due to the production of ice nuclei near that temperature, a result of the shattering of the partially frozen exteriors of supercooled droplets (Hallett and Mossop, 1974; Mossop, 1976). This large increase

in nuclei provides an excellent medium for the early development of many snow crystals near that temperature. This is important because crystals tend to require existing ice structures to grow.

Mossop (1985) also notes that a key factor in this shattering process is the existence of droplets which are sufficiently large. In general, droplets need to be greater than 25 microns in diameter to produce droplet splintering. This presents a dilemma, of sorts, for the operational forecaster, who knows little about the droplet spectrum inside the clouds.

According to aufm Kampe and Weickmann (1957), stratus clouds typically have droplets with diameters which reach up to around 40 microns (though most of the stratus clouds droplets are smaller than 25 microns). Mossop (1985) documents literature in which thin stratus clouds (only 600 meters thick) have produced crystals. It is clear that stratus clouds, by themselves, can support the splintering process.

However, we also know that clouds created in an environment with stronger vertical velocities have more droplets that are large enough to produce ice splinters (aufm Kampe and Weickmann, 1957). This is important, since knowing that enhanced vertical velocities will increase the number of ice nuclei due to splintering around -5°C, we can start to shed additional light on some essential details of the aforementioned checklist parameters. In particular, consider what was stated earlier:

a. The 534-540 thickness exists to the left of the surface low and through the lower portion of the IR comma shield in Colorado storms.

b. There is kinematic rationale that indicates that vertical velocities may be maximized through that portion of system.

c. When virtual temperatures in that location tend to be around -5°C in the 850-700 mb layer, heavy snow is favorable.

Is it coincidence that these circumstances are consistent with the maximization of ice crystal nuclei around -5°C, as determined by the mean virtual temperature between 850-700 mb? Probably not, since the enhanced vertical velocities will in turn increase the ice splintering effectiveness in that area by producing a greater number of cloud droplets that are larger than 25 microns in diameter.

Now that we've established a satisfactory mechanism for ice nuclei production between 850 and 700 mb in the lower portion of the IR cloud shield, how does this help produce heavier snows? The answer to this leads us to our next topic.

2.4 Cloud microphysics in the primary crystal growth temperature region

Recall that there are *two* favored thermal areas of crystal growth. The *primary area of crystal growth* extends between the -12 to -17°C thermal region, and is maximized at -14°C. This primary area exists because in this temperature interval, the pressure differential between the ice crystal and supercooled vapor is maximized (Rogers, 1979). In other words, at this temperature range, there is a strong attraction of vapor to the ice crystals, simply due to this pressure differential. These are the temperatures at which this attraction is most significant.

Indeed, Braham (1968) notes that crystal growth rates between -12 and -17°C are as much as two orders of magnitude greater than those found at warmer and colder temperatures, and that growth rates in this range overshadow that at all other levels. (Is it any wonder that most snow falls in the dendritic form, since crystal growth in this temperature range is dendritic?)

Auer (1987) has noted that the existence of temperatures in the -12 to -17°C range between 600 and 700 mb *strongly assists* heavy snow development. That is very consistent with what you'd expect based on Braham's comments. From the Skew T-log P diagram in Figure 5, raising a -5°C parcel pseudo adiabatically from the midpoint of the 850-700 mb layer (much as a parcel would ascend in the lower portion of the IR enhanced comma area), these familiar -12 to -17°C temperatures are encountered between 620 to 680 mb (right in the heart of the range noted by Auer). Thus, there is an excellent correlation between the production of ice nuclei at lower levels (850 to 700 mb) and crystal growth at higher levels (between 700 and 600 mb).

Finally, this whole connection leads back to the main synoptic scale system. When these microphysical processes occur within a baroclinic system, in an area of sufficient upward vertical motion, efficient snowfall production is very likely. Therefore, when the conditions described above are met, the gradient of snowfall is likely greater than the gradient of synoptic scale ascent through the IR comma cloud shield.

3. SUMMARY

This paper concentrated on some significant physical processes which play into the location and development of heavy snow areas. These include relevance of the surface low track (and what goes on aloft relative to the surface low), why the lower portion of the comma head is a favorable location, how thickness considerations play into the forecast and how cloud microphysics assist in snow development.

Though this paper used the lee-side situation to demonstrate the microphysical processes that impact snowfall development, application of this information is much broader. Certainly, any situation with a thermal structure in which the microphysical process described herein applies has the potential for heavier snowfall development than might otherwise be expected. Operational forecasters can use this information to help assess where the heaviest snowfall potential exists. An understanding of the 3-dimensional thermal structure associated with baroclinic systems and the recognition of the pertinent microphysics described in this paper can provide an important framework from which forecasters can improve their heavy snow forecasting abilities.

4. ACKNOWLEDGEMENTS

The discussion here was developed in large part from efforts by WSFO MSP Lead Forecaster Richard Naistat, who not only has developed and refined the Heavy Snow Checklist over the past decade, but also provided considerable insight into the physical processes as well. Thanks also to Doug Streu, Met Intern at the NWS Neenah, WI radar site (current location???), for his efforts in providing information on the cloud microphysical processes described in section 2.B.iii.

5. REFERENCES

Auer, A.H., 1987: An Aid to Forecasting Heavy Snowfall Episodes. *Nat. Wea. Dig.,* **12.**

aufm Kampe, H.J., and H.K. Weickmann, 1957: *Physics of Clouds.* Meteor. Monograph, **3,** 18. AMS, Boston, pp. 182-225.

Braham, R.R., 1968: Meteorological Bases for Precipitation Development. *Bull. Amer. Meteor. Soc.,* **49,** 343-353.

Carlson, T.N., 1980: Airflow Through Midlatitude Cyclones and the Comma Cloud Pattern. *Mon. Wea. Rev.*, **108**, 1498-1509.

Hakim, G.J. and Uccellini, L.W., 1992: Diagnosing Coupled Jet-Streak Circulations for a Northern Plains Snow Band from the Operational Nested-Grid Model. *Wea. Forecast.*, **7**, 26-48.

Hallett, J., 1965: Field and Laboratory Observations of Ice Crystal Growth from the Vapor. *J. Atmos. Sci.*, **22**, 64-69.

Hallett, J. and S.C. Mossop, 1974: Production of Secondary Ice Crystals During the Riming Process. *Nature*, **249**, 26-28.

Holton, J.R., 1979: *An Introduction to Dynamic Meteorology*. 2nd ed., Int'l Geophysics Series, 23, Academic Press, New York, 391 pp.

Mason, B.J., 1957: *The Physics of Clouds*. 1st ed., Oxford University Press, London.

Morrison, A., 1988: A Method to Determine the Width of a Snow Band Associated with Winter Storms by Using Infrared Satellite Data. NOAA Tech Memo NWS ER-82, Postprints of the Second National Winter Weather Workshop, Raleigh, NC. DOC/NOAA/NWS/Eastern Region Headquarters

Mossop, S.C., 1976: Production of Secondary Ice Particles During the Growth of Graupel by Riming. *Quart. J. Roy. Meteor. Soc.*, **102**, 45-57.

Mossop, S.C., 1985: The Origin and Concentration of Ice Crystals in Clouds. *Bull. Amer. Meteor. Soc.*, **66**, 264-273.

Rogers, R.R., 1979: *A Short Course in Cloud Physics*, 2nd ed., Int'l Series in Natural Philosophy, **Vol. 96**, Pergamon Press, Oxford, 235 pp.

Todd, C.J., 1964: A System for Computing Ice Phase Hydrometeor development. *Flagstaff Cumulus Studies*, Final Report on NSF Grants G8334 and G11969 by Meteorology Research, Inc., Altadena, California.

MSP HEAVY SNOW FORECASTER CHECKSHEET

1. Check progged position of surface low.
   A. If a Colorado Low, prior to occlusion, heaviest snow axis usually is centered 150 nmi to the left of the track of the Low.
   B. If an Alberta Clipper, heaviest snow axis usually lies just left of the track of the Low.
   C. If an inverted trough, heaviest snow axis frequently occurs 150 nmi left of the surface geostrophic vorticity center located at the north end of the inverted trough.

2. Locate favorable thickness. Given that the 1000-850 mb thickness is less than 1300 meters, heaviest snow axis usually occurs:
   A. between 1520-1540 meters on the 850-700 mb thickness, AND
   B. between 5340-5400 meters on the 1000-500 mb thickness.

3. Check the B. J. Cook Index.
   A. Within the favorable thickness fields noted above, compute the 200 mb temperature difference (°C) from the point in question to a point about 15 degrees latitude upstream. Note that the area usually lies close to the 164 contour at 200 mb, but in very warm systems, the heavy snow threat area could exist up to the 188 contour.
   B. Is warm advection occurring/going to occur at 700 mb? If yes, divide the value in 3A by 2. If no divide the value in 3A by 4.
   C. Over the threat area, is the 700 mb temperature between -12 and -17°C? If yes, double the value in 3B.
   D. The value obtained is the average expected snowfall for the threat area in a 12-hour period.

4. Other factors to examine
   A. Check the progged 850 mb warm advection. Can also check the surface isotherms and Sangster winds.
   B. Check synoptic scale lift due to PIVA, Q-vector convergence fields and/or diffluent mid-level thickness.
   C. Check precipitable water and forward speed of the 850 mb low.
   D. Check the 500 mb vorticity center track.
      ⇒ When associated with an upper level circulation center, the heavy snow in an ensuing 12-hour period tends to fall 7 degrees downstream and 150 nmi left of the vorticity track.
      ⇒ When associated with an open trough or shear zone into an upper low, the heavy snow in an ensuing 12-hour period tends to fall 7 degrees downstream and 60 nmi left of the vorticity center track.
   E. Check the satellite images. Heavy snow usually falls in the lower half of the comma head and the upwind half of the comma tail.

5. Unfavorable factors to examine.
   A. Heavy snow usually <u>does not</u> fall to the right of the 850 mb low track.
   B. Heavy snow usually <u>does not</u> fall to the right of the 500 mb vorticity maximum track.

Figure 1. Naistat's heavy snow checklist.

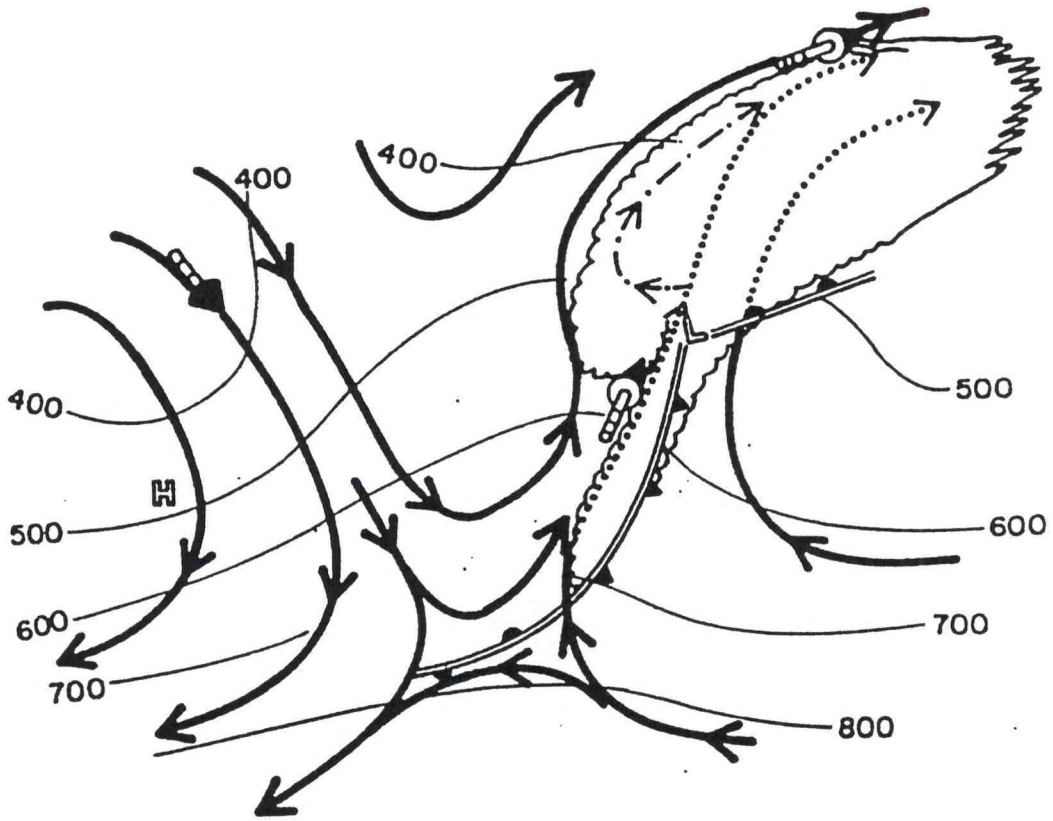

FIG. 10. Schematic illustration of relative flow on a dry isentropic surface. Thin solid lines are isobars; these are discontinued in regions of saturation where the flow is drawn dotted for the warm conveyor belt, and dot-dashed for the cold conveyor belt. The dry airstream originates at high levels in the northwest and descends toward the trough axis. There it splits into two branches, one branch descending into low levels west of the trough and the other flowing around the trough to ascend in a narrow stream over the western extension of the cloud shield (scalloped border). The symbols L and H, respectively, refer to the locations of the surface high and low pressure centers. Fronts are depicted in conventional symbols. Jet maxima are represented by solid arrow segments.

Figure 2. From Carlson (1980).

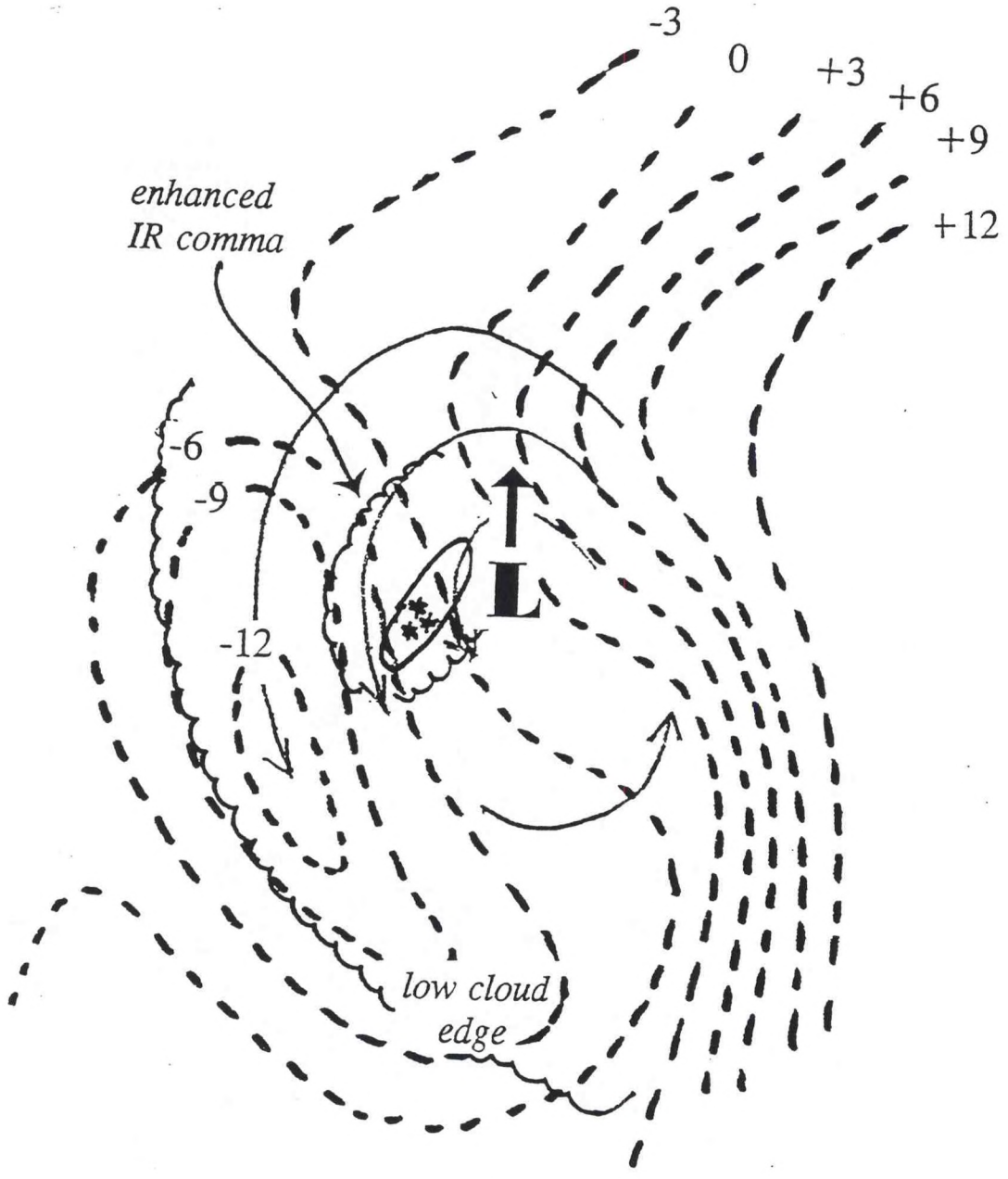

Figure 3. Schematic representation of 850 mb temperature, streamlines and cloud depiction from 0000 UTC 26 November 1992.

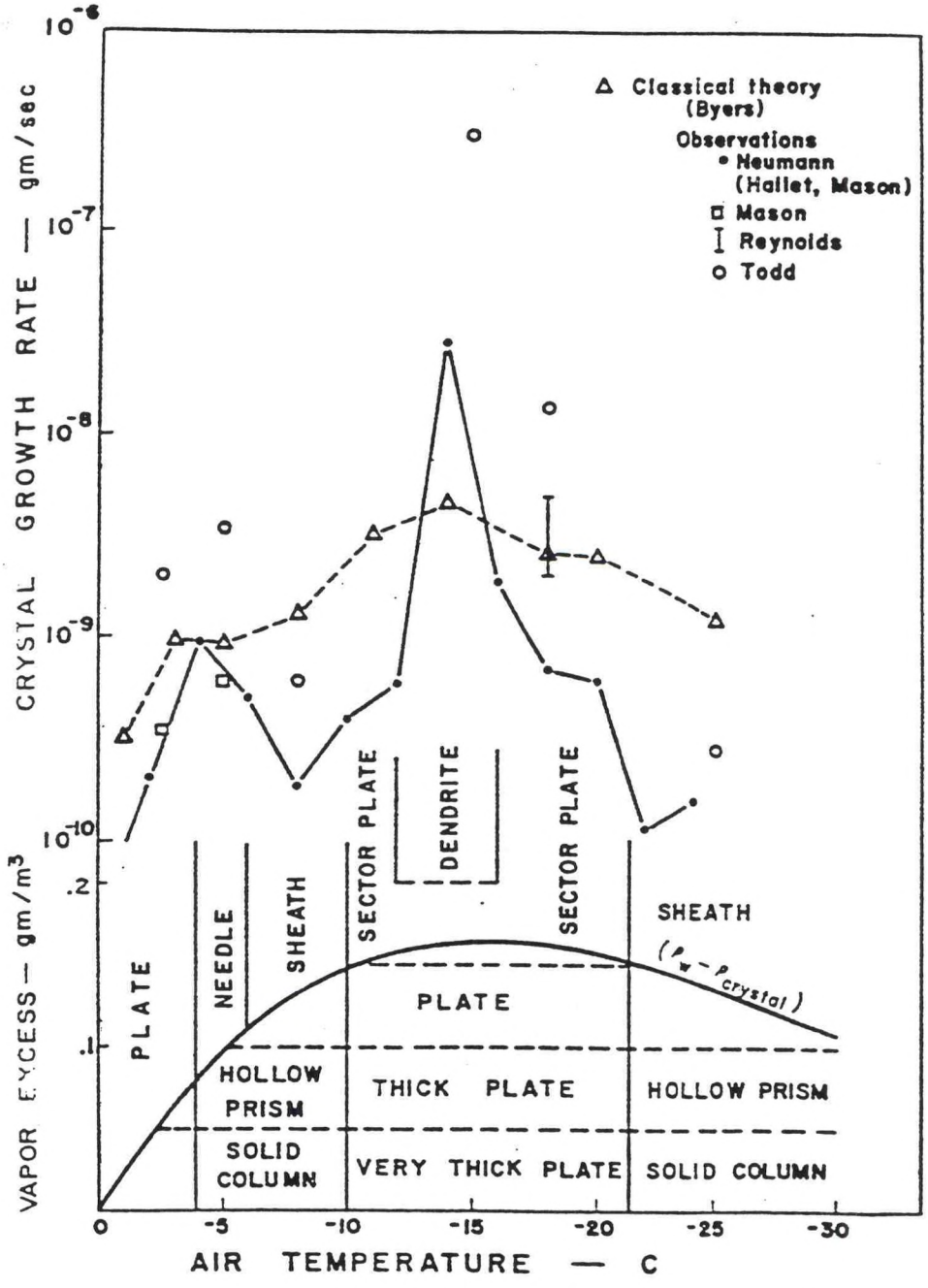

Figure 4. Ice crystal growth rates (top) and ice crystal habit regions (bottom) as a function of temperature. From Braham (1968).

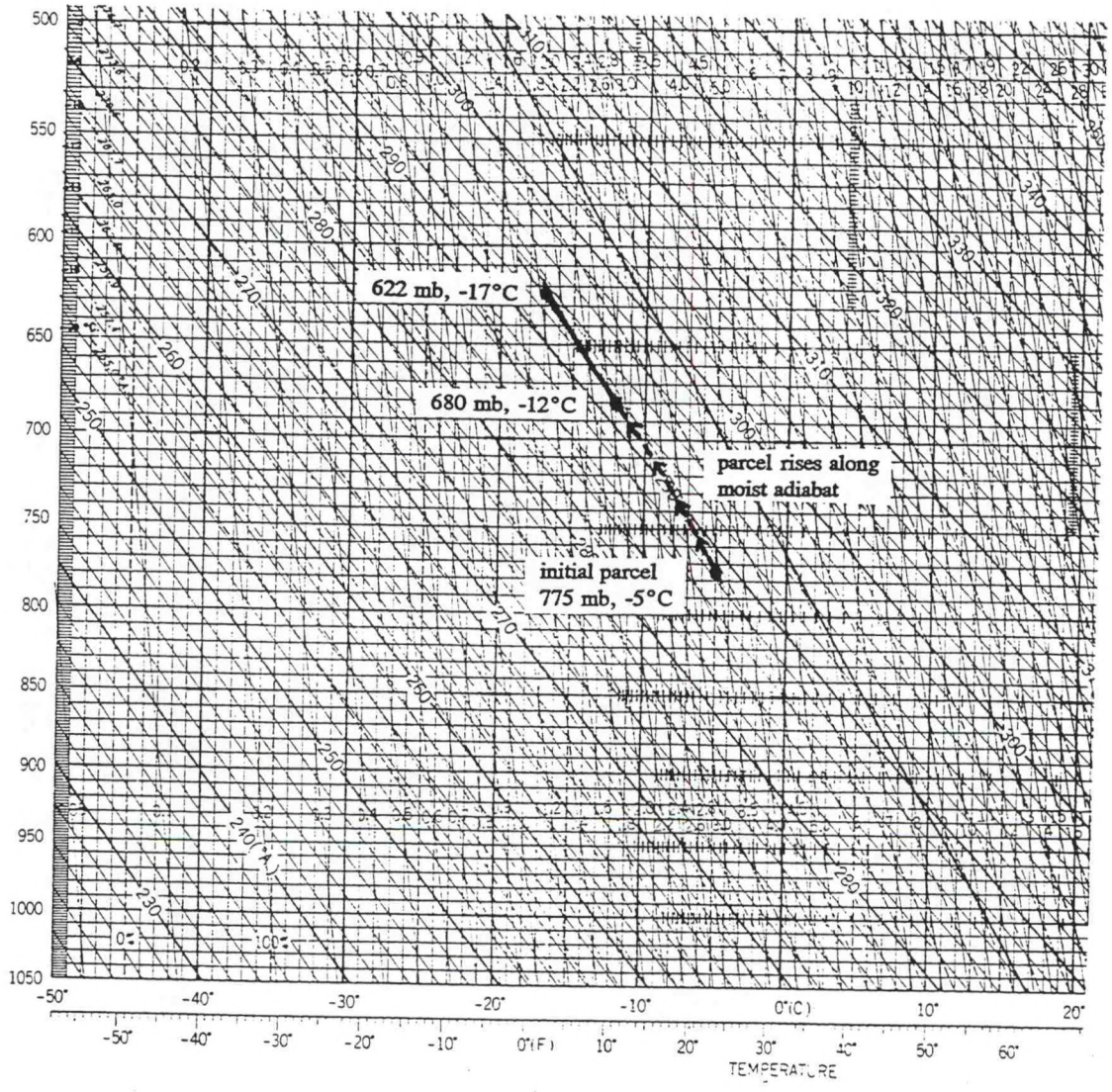

Figure 5. Pseudo-adiabatic chart representation of moist layer ascent from -5°C in the middle of the 850-700 mb layer through the -12°C to -17°C layer.

A Comparison of Snow Amount Forecasting Techniques for Kansas Heavy Snowstorms During the Winter of 1994-1995

Daniel D. Nietfeld[1]

1. INTRODUCTION

One of the most important forecasts a meteorologist makes is that related to heavy snow prediction. While the meteorological ingredients for heavy snow are well known (strong upward vertical motion, sufficient moisture, the right thermodynamic environment), forecasting specific snowfall amounts is quite difficult. Precipitation amount forecasts from numerical prediction models combined with the empirically derived relationship of snow amount to liquid water equivalent can be quite useful in this task. However, other empirical methods have been developed that have been found useful in most synoptic settings. This paper will focus on the evaluation of the utility of these techniques for the eight heavy snowstorms that occurred across Kansas during the winter of 1994-1995.

Each of the eight heavy snow events was reviewed, and three snow amount forecasting methods were applied to determine which technique verified most accurately in each case (using the NWS Central Region definition of heavy snow as six inches in 12 hours or eight inches in 24 hours). The three techniques examined were: the Cook Method (Cook 1980), the Magic Chart Method (Sangster and Jagler 1985, Chaston 1989), and the Garcia Method (Garcia 1994), from now on called CM, MCM, and GM respectively. These techniques were chosen because they are the most widely used at NWS Forecast Office (NWSFO) Topeka, Kansas.

The synoptic setting in each case was closely examined, and it was noted if the case was associated with various features or processes such as: a surface low, upslope boundary layer flow, mid level warm or cold advection, isentropic lift, positive vorticity advection, strength of upper level dynamics, etc. Through examining the characteristics of the storm, it was determined whether each of the three techniques could be applied to the event (i.e., was each methods' assumptions met?).

Two of the eight cases will be examined in detail. The first was not a classic (atypical) High Plains snowstorm while the second was associated with a well-developed shortwave more typical of the classic mid-latitude extratropical cyclone. In this paper the term "classic" snowstorm will refer to one associated with a well-developed shortwave trough and accompanying mean sea level (MSL) low pressure system. Other systems lacking these features will be referred "non classic", or "atypical". These two cases will illustrate the utility of each technique, and should offer some insight about why the methods were, or were not, applicable.

2. BRIEF REVIEW OF TECHNIQUES

A thorough review of the CM, the MCM, and the GM would require much more than the scope of this paper allows. Therefore, the following review will be brief.

The CM relates the magnitude of 200-mb warm air advection to snowfall amounts. Approximately one-half of the value of the indicated warm air advection (°C) at 200-mb is used for the amount in inches, assuming warm air advection is also occurring at 700-mb. If cold air advection is occurring

1. Corresponding author address: Daniel D. Nietfeld, National Weather Service Forecast Office, Topeka, Kansas 66616.

at 700-mb, one-quarter of the value is used. This technique carries several assumptions with it, the four most restrictive beings:

A. location of surface low
B. best not to use with northwest flow aloft or under areas of strong confluent 200-mb flow
C. unreliable in spring and fall
D well-developed system is necessary to generate the warm and cold pockets.

The MCM uses the forecast of 850-mb critical temperatures combined with the 12-hour net vertical displacement (NVD) of parcels arriving at 700-mb (Reap, 1992) to predict a snowfall amount. For example, the AFOS chart 7WG, which is the 12-hour NVD for air that will arrive at the 700-mb level 24 hours after initial time is overlaid with the AFOS chart 82T, which is the 12-hour 850-mb temperature prognosis from the NGM (Chaston, 1989). Where the greatest NVD overlays the region between -3°C and -5°C is where the heaviest snowfall is likely to occur. This method's assumptions are similar to the assumptions of the CM, in that developed or developing upper and surface systems are necessary, and at least 90 percent relative humidity (RH) in the layer from 1000-500 mb is required by the technique. An inherent limitation of this method is the temperature range between -3°C and -5°C, which makes the technique inappropriate in events involving an arctic air mass.

The GM is the newest of the techniques, having been developed from the late 1980s into the early 1990s. The GM uses an empirical relationship between mixing ratios on isentropic surfaces and snowfall amount. The technique examines the isentropic environment over the area of concern within the layer between 700-mb and 750-mb. The value of the mixing ratio that is found on an isentropic surface that is within the critical layer at the onset of the event is averaged with the highest mixing ratio value that could be advected into the area in the next 12 hours. The only assumptions are that there must be some type of forcing to provide upward vertical motion. What makes this technique unique is that it is the only method that attempts to account for the quantity of moisture available to the system, not just the relative humidity. Also, it is much less limiting in terms of the character of the forcing mechanism for upward vertical motion responsible for generating the snow.

3. APPLICATION OF THE METHODS

For each event, archived data was reviewed which consisted of, but was not limited to: snowfall records for all available stations, surface and mandatory level analysis, NCEP AFOS charts such as those required for use with the MCM, gridded model output, and various NWS text products (i.e., State Forecast Discussions, Zone Forecasts, Winter Storm Warnings, etc.) The three techniques were applied to each of the eight cases, and the 24-hour forecast snowfall amount was determined. For this study, the 24-hour forecast snowfall amount refers to the event beginning in about 12 hours, lasting for about 12 hours, then ending 24 hours from the forecast issuance time. The 24-hour forecast snowfall amount was chosen because at 24 hours, important decisions need to be made by the forecaster such as what type of warning or advisory may be needed, and what snowfall amounts should be in the zone forecast.

In evaluating these techniques, standard AFOS charts were used for determining snowfall forecast amounts for the MCM. While the Cook and Garcia Methods were developed using observational data, gridded model output, as displayed on PCGRIDDS (Peterson, 1992) allows for employing these methods for longer range forecasts. Forecasters are now able to adjust the techniques slightly by using a prognosis as the zero hour conditions. For example, if the event were to begin in 12 hours, instead of waiting for the observed data from the onset of the event, one could use the 12-hour prognosis to determine the forecast conditions, then apply the technique on those fields. Often,

this study assumed the event would begin in about 12 hours. Thus, the appropriate model run was examined.

It was not possible to recreate each event and apply each method exactly the way it was meant to be applied. Adjustments could have been made in a real-time operational forecast setting to account for various factors. Obviously, the model run examined needed to be somewhat accurate, and any errors or biases in the model would contribute to errors in the forecast amount. Another complicating factor was the precipitation phase change observed sometimes. If the event began as rain, then later changed to accumulating snow, the techniques would not be entirely accurate because they assume the precipitation type is accumulating snow. This was difficult to consider. However, the start of each event was still defined as the beginning time of the snowfall.

The observed duration of each event did not always correspond to the assumed duration of the method. For example, the GM was designed to give the snowfall amount over a 12-hour period. However if the event lasted for 18 hours, the techniques were adjusted to account for the longer duration.

4. COMPILATION OF RESULTS

Table 1 show various parameters collected for each event. Besides notes concerning the synoptic environment, also shown are the values of the observed snowfall, the forecast snowfall, as well as the error for all three techniques. Of most importance is the calculated error for each technique, which is illustrated in Figure 1. The GM clearly yielded a more accurate forecast overall with no error for two events and a maximum error of 1.5 inches. The CM consistently had the highest errors, with the MCM errors varying from of one-half inch to four inches.

The bias to over forecast or under forecast snowfall in these events is shown in Figure 2. The CM and MCM often under forecast the snowfall amount, while the GM over forecast snowfall about as much as it under forecast snowfall. The magnitude of error is most clearly shown using the absolute error. Figure 2 displays the average absolute error, which better reflects the accuracy of each technique.

The very large errors forecasted by the CM and MCM was typically a result of the event not fitting the assumptions of the techniques. These cases were generally atypical of Midwest snow storms in their synoptic setting. If the event was not characterized by a well-developed shortwave or a defined surface low, the physical reasoning behind the techniques could not be applied. However, in particular with High Plains snow storms, these classic features are not always present.

In the following section, two of the eight case studies will be examined. The first was a non-classic High Plains snow storm, while the second was associated with a well-developed shortwave more typical of the common mid-latitude extratropical cyclone. These two cases will illustrate the utility of each technique, and should offer some insight about why the methods were, or were not, applicable.

5. ATYPICAL HIGH PLAINS EVENT

On February 12, 1995, the High Plains experienced a snowstorm that brought a great deal of challenge to forecasters. A shallow arctic airmass had moved into the region from the north, with 850-mb temperatures ranging from -12°C in southern Kansas to -15°C in northern Kansas (not shown). The ridge axis of the MSL high pressure area that accompanied the arctic air had moved into central Kansas, with boundary layer southeast flow of 10 to 20 knots (not shown). This created

boundary layer upslope flow over the High Plains, thus establishing terrain-induced upward vertical motion.

TABLE 1
Summary of events and parameters collected for each case

Date	Nov 20	Dec 30	Jan 05	Jan 18	Jan 21	Feb 11	Mar 6	Mar 25
Hours	6am-6pm	6pm-12n	6am-6pm	3pm-7am	6am-6pm	12m-9pm	6am-9pm	6pm-12n
Amt	6.5"	6.5"	6.0"	11"	7.0"	11.0"	6.2"	9.0"
Sec of KS	NW/WC	NC	C/NC	SE	SC	WC	NRN Tier	NW
ShrtWv	Y-STG	Y	Y	Y	Y-WK	N	Y	Y-STG
PVA	Y-STG	Y	Y	Y	Y-WK	N	Y	Y-STG
DynForcing	Y-STG	Y	Y	Y	Y-WK	Y-WK	Y	Y
H7 VVEL	UP-WK	UP-STG	UP	UP	UP-STG	UP	UP-STG	UP-STG
H7 WAA	Y-WK	Y-WK	Y-WK	Y-WK	Y-WK	Y-STG	Y	Y-WK
H85 Temp	+3	-8	-5	-2	-3	-14	-1	+4/-2
H10-H5 Mean RH	90%	90-95%	90%	90%	65-85%	85%	95%	80%
SfcLow	Y	Y	Y	Y	N	N	Y	Y-STG
SfcWdDir	50 DEG	70 DEG	150 DEG	10 DEG	130 DEG	150 DEG	40-130 D	90 DEG
SfcWndSpd	15 KTS	15 KTS	20 KTS	20 KTS	5 KTS	15 KTS	10-20 KTS	10 KTS
Cook	4"	2"	8"	5"	0"	1"	5"	4"
FitCook	Y	Y	Y	Y	N (H2CAA	N	Y	Y
DelCook	**-2.5**	**-4.5**	**2**	**-6**	**-7**	**-10**	**-1.2**	**-5**
Garcia	8.0"	6.5"	6.0"	10"	5.5"	10"	6/7"	10"
FitGarcia	Y	Y	Y	Y	Y	Y	Y	Y
DelGarcia	**1.5**	**0**	**0**	**-1**	**-1.5**	**-1**	**0.4**	**1**
ISNLift	Y	Y	Y-WK	Y	Y	Y-STG	Y	Y-STG
Majic	4"	7"	4"	8"	3"	7"	8"	7"
FitMajic	N	N	Y	Y	N	N	Y	N
DelMajic	**-2.5**	**0.5**	**-2**	**-3**	**-4**	**-4**	**1.9**	**-2**

Only a weak mid level shortwave trough was present with broad cyclonic 500-mb flow (Figure 3). A 500-mb vorticity maximum was located about 800 miles upstream. Thus, traditional pattern recognition would not alert the forecaster to a threat of heavy snow.

A thermodynamic analysis revealed more need for concern however, particularly at the 700-mb level. Strong warm air advection was occurring over western Kansas (Figure 4). Therefore flow on isentropic surfaces between 286K and 288K in this region was indicating moderate isentropic lift (Figure 5). There was significant quasi-geostrophic forcing for upward vertical motion as indicated by the 700-850-mb layer Q-vector convergence (Figure 6). Also at 700-mb, significant geostrophic frontogenesis were occurring with Q_n convergence maximizing over western Kansas indicating possible banding of the precipitation field (Figure 7). With this implied forcing considered, the forecaster had sufficient evidence that snow would be produced, so the next challenge was to determine the snowfall amount.

The CM is first applied, however; Figure 8 shows the obvious problems with this technique. This synoptic pattern does not result in a distinct warm pocket upstream from a cold pocket at 200-mb. In fact, the temperature advection into the area of concern is neutral or slightly cold. Thus, the CM would show no snowfall in the area of concern. This event could be considered a northwest flow event, which Cook stated is one of the several situations the method does not work. The MCM was also not applicable in this case, because the 850-mb temperature is much colder than the specified -5°C to -3°C range used in the MCM technique. The other requirement that the 1000-500-mb mean relative humidity be at least 90 percent was also not met, as adequate moisture was available below 700-mb, but fairly dry air was shown above 700-mb (not shown). In addition, the poorly defined dynamics of the system only resulted in a forecast NVD of about 20 MB for the first 12 hours (not shown), which would suggest about 2 inches of snow for that period, if the other prerequisites had been met.

The GM requires moderate to strong upward vertical motion, which is not surprising if heavy snow is to be produced. This requirement was met, as shown in the isentropic fields and from a quasi geostrophic forcing perspective. The next step in this method is to determine the mixing ratio values that will be used to compute the snowfall amount. At the start of the snow event, Figure 9 shows about 1.5 gkg^{-1} is found in the 700-750-mb layer over the area of concern, and about 3.0 gkg^{-1} are available to be advected into that area. The technique would suggest about 4.5 inches of snow with this moisture. However, the forcing was forecast to continue beyond a duration of 12 hours, possibly as much as 24 hours (not shown). The GM can be reapplied to every 12-hour period, as illustrated in Garcia (1994). The next 12-hour period would begin with a mixing ratio value of 1.5 gkg^{-1} over the area of concern, with about 3.5 gkg^{-1} available to be advected in throughout the following 12 hours (Figure 10). This would suggest an additional 5 inches, or a total of 9.5 inches. The forecaster might keep in mind that the airmass is very cold, so the snow to liquid water ratio may be higher than normal, so an additional inch or two may be added to the forecast value.

The highest observed snowfall for this event was 11.0 inches that fell in Gove, Kansas in the west central section of the state (not shown). The actual duration of the snowfall was only 21 hours, so an inch or two may be taken off the forecast snow amount calculated for a 24-hour duration. Thus the amount compensated for by the shorter duration is nearly equal to the adjustment made for the higher water equivalent ratio, making the GM in error by -1 to -1.5 inches. The GM would still show snow amounts in the heavy snow category, therefore suggesting a warning.

6. CLASSIC CENTRAL PLAINS SNOWSTORM

On March 6, 1995, a widespread area of the Central Plains received heavy snow, extending from northwest Kansas into northern Nebraska. Around six inches of snow was reported across much of northern Kansas, from the northwest corner to the northeast corner (not shown). Figure 11 shows that this storm system involved a well defined mid level shortwave trough moving into the Plains, with very strong upward vertical motion indicated by the model forecast omega. The forcing was centered over central and north central Kansas, so the area of concern was quickly identified. A second feature of this system was a well defined MSL low pressure center located in the climatologically favored area of the Oklahoma Panhandle (Figure 12). These two features give obvious indications that a relatively strong mid-latitude extratropical cyclone is poised to threaten the region with adverse weather. A saturated airmass is in place as the 1000-500-mb mean layer relative humidity was approximately 95 percent in the identified area of concern (not shown).

The synoptic setting of this event met many prerequisites stated in all three of the snow amount forecast techniques, including the important well-developed short wave trough necessary for the CM and MCM. The dynamics of the system were reflected by a tropopause fold, with a warm pocket of

stratospheric air found at 200-mb over the western United States (Figure 13). The 200-mb plot (not shown) revealed an observed temperature of -46°C at Salt Lake City, Utah, which was even warmer than the model analysis. This warm air was upstream from Nebraska, with the warmest air upstream from Kansas about -56°C. A cold pocket of -66°C was found over eastern Kansas. The CM was showing a maximum snowfall amount of about 10 inches that would occur in Nebraska, with about 5 inches over Kansas. The snowfall amount forecast from the CM was in error only -1 inch over northern Kansas.

The MCM verified reasonably well in this case with an error of 2 inches. The NVD indicated about 8 inches of snow would fall in the area between -5°C and -3°C (not shown) over northern Kansas.

The GM was still the most accurate with this event, which had an error of only 0.5 inches. The average mixing ratios on the isentropic surfaces between 700 and 750-mb (not shown) indicated about 6.5 inches of snow would fall in northern Kansas.

This case was a successful forecast, foreseen several days in advance. The characteristic synoptic pattern contained more traditional features than the February 12 case. Consequently, all three of the snow amount forecast techniques were designed to work with this scenario, and all three did reasonably well.

7. CONCLUSIONS

This study reviewed eight heavy snow events that occurred during the winter of 1994-95 in Kansas. Three snow amount forecast techniques were applied to each case to determine how each technique did in that setting. One result common to each event was the accurate performance of the GM. Figure 1 shows that the method gave a good indication of the heaviest snow to expect in every event, however this could not be said for the other two techniques.

The CM depends on a strong enough low pressure system that extends through much of the troposphere to produce a tropopause fold, thus creating a warm pocket of stratospheric air at the 200-mb level. The CM was shown to verify reasonably well with these well-developed systems, although still less accurate than either the MCM or the GM overall. However, for any case in which this warm pocket was not evident, the method was entirely not applicable. Unfortunately, many High Plains snowstorms are produced without this type of system.

The MCM performed better overall than the CM. This was due, in part, to its superior performance with well-developed systems. For non-classic storm systems, which occur frequently over the High Plains, the MCM did poorly, and often, was not applicable.

What makes the performance of the GM rather remarkable was its ability to predict reasonably accurate snow amounts in a diverse realm of synoptic settings. It not only handled the heavy snows resulting from the warm air advection or strong differential positive vorticity advection typical of a well developed mid-latitude extratropical cyclone, but it also did well in atypical settings where the forcing mechanisms were less obvious. In the first case study discussed, the forcing was primarily due to boundary layer upslope flow and isentropic lift around the 700-mb level, besides frontogenetical forcing. The event did not involve a surface low, nor a well developed mid level shortwave trough. Because of the lack of these features, the system did not meet the assumptions of the CM or the MCM, and thus neither of these methods was applicable to the event. An attempt to apply these methods resulted in gross errors of under forecast snow amounts.

The GM does not involve rigid requirements as to the type of storm system, with the only requirement that of moderate to strong upward vertical motion. This simplicity allows flexible application. It is also unique in that it is the only technique that attempts to relate the actual amount of moisture going into a system to the amount of moisture that may fall out of that system. Other techniques involve checking for a saturated airmass with at least 90 percent relative humidity, but do not incorporate specific humidity. While the results indicate that the GM was the superior snowfall amount prediction tool in this study, more research in other areas of the country will be needed to determine if these results can be generalized to other geographic areas.

8. ACKNOWLEDGEMENTS

Special thanks goes to George Phillips, Science and Operations Officer at NWSFO Topeka, Kansas for his thorough and constructive reviews and assistance.

9. REFERENCES

Chaston, P.R., 1989: The Magic Chart for Forecasting Snow Amounts. *Natl. Wea. Dig.*, **14**, 20-22.

Cook, B.J., 1980: A Snow Index Using 200-mb Warm Advection. *Natl. Wea. Dig.*, **5**, 29-40.

Garcia, C., Jr., 1994: Forecasting Snowfall Using Mixing Ratios on an Isentropic Surface - An Empirical Study, NOAA Tech. Memo. NWS-CR-105. DOC, NOAA, NWS, Central Region, Scientific Services Division, Kansas City, MO, 28 pp.

Peterson, R.A., 1992: A PC based system for the display of gridded WAFS data, *Proceedings of the WMO Technical Conf. on Tropical Aeronautical Meteor.* **(TECTAN-92)**, Geneva, Switzerland, 1-6.

Reap, R.M., 1992: The techniques development laboratory three-dimensional trajectory model. NWS Technical Procedures Bulletin **No. 397**, 11 pp.

Sangster, W., and E.C. Jagler, 1985: The (7WG, 8WT) Magic Chart. NWS Central Region Technical Attachment No. 85-1, 5pp.

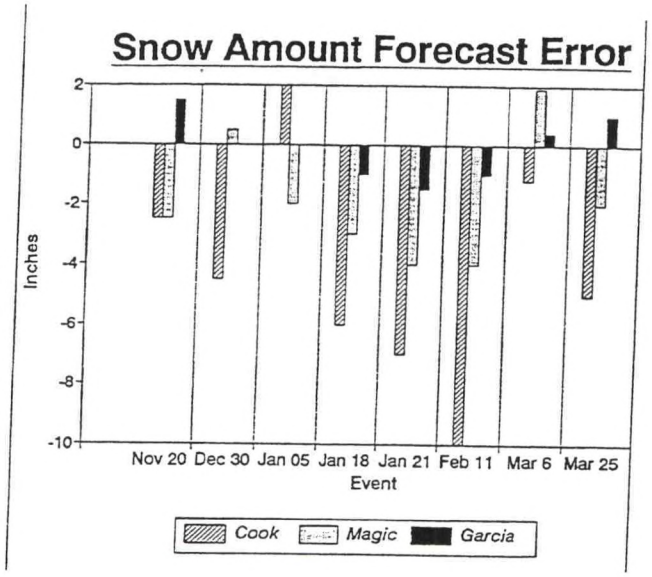

Figure 1. Forecast error for each event (observed snowfall subtracted from forecast snowfall in inches).

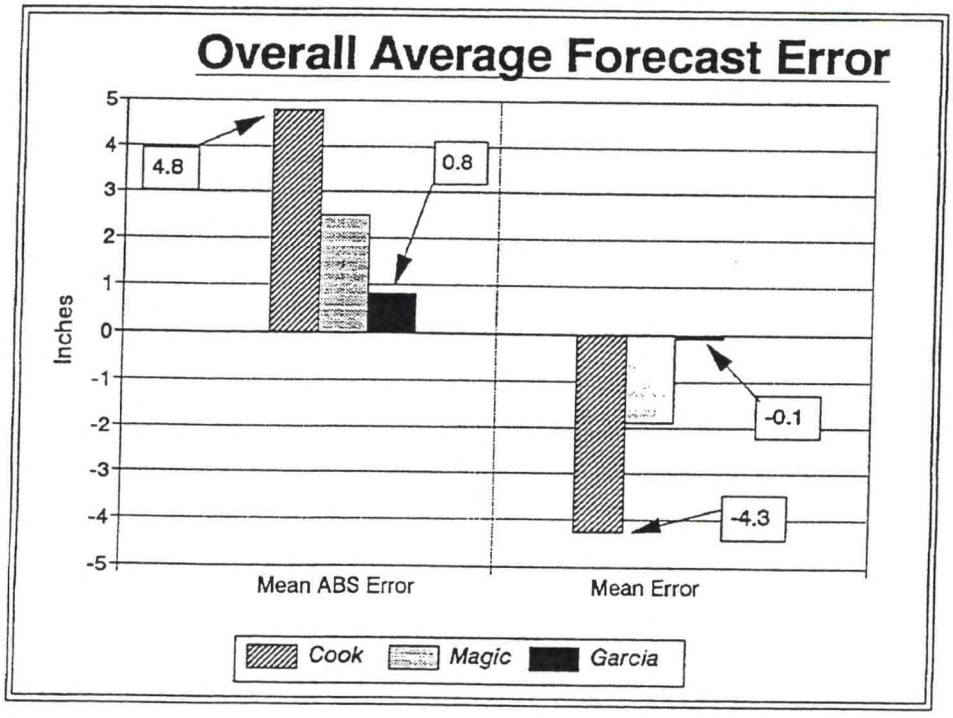

Figure 2. Mean absolute error and mean algebraic error each technique (inches).

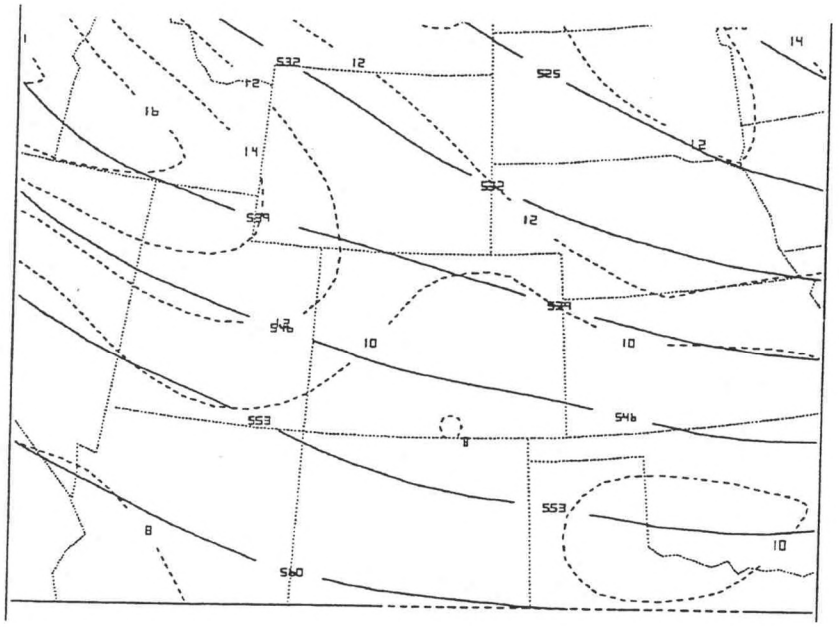

Figure 3. Eta model 6-hour forecast of the 500-mb heights (solid contours every 7 decimeters) and absolute vorticity (dashed contours every 2 x 10^{-5} s^{-1}) for 0600 UTC 12 Feb. 1995.

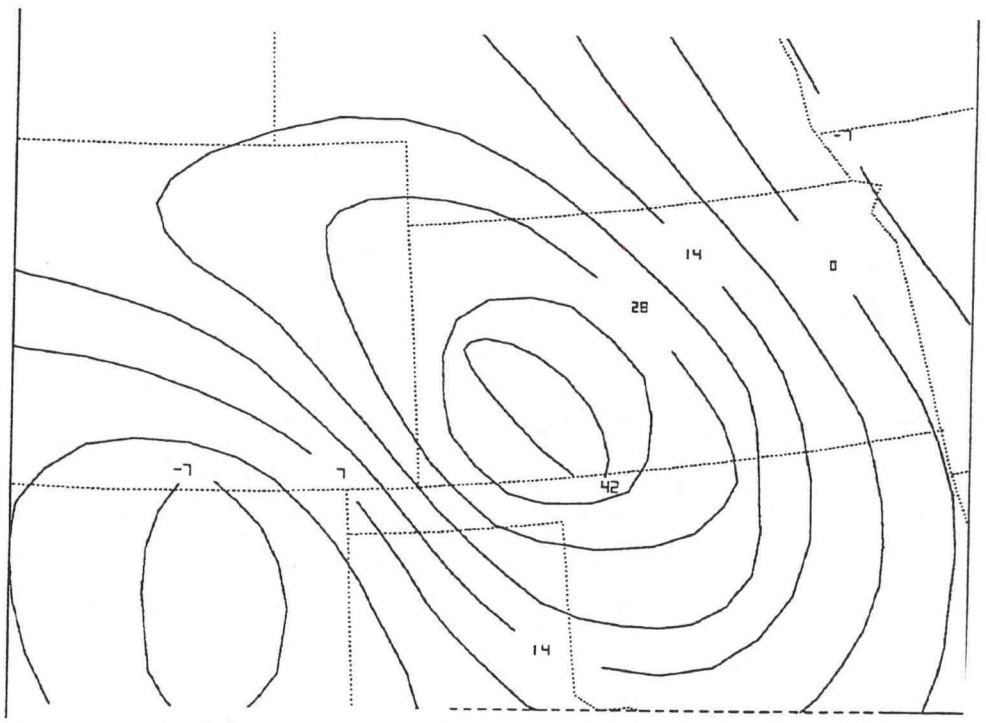

Figure 4. Eta model 12-hour forecast of the 700-mb temperature advection by the total wind (contours every 7 x 10°C $12hr^{-1}$) for 1200 UTC 12 Feb. 1995.

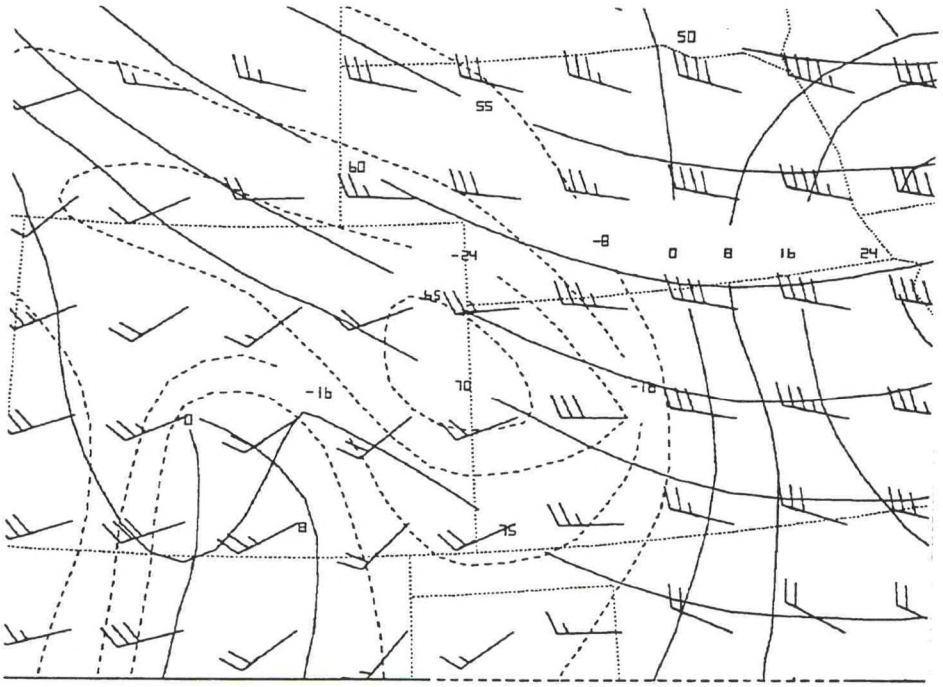

Figure 5. Eta model 6-hour forecast of the 286K isentropic surface omega (contours every 8 μbs^{-1} dashed is negative solid is positive), pressure (solid contours every 5 $x10^{-1}$ mb), and the total wind barb (knots) for 0600 UTC 12 Feb. 1995.

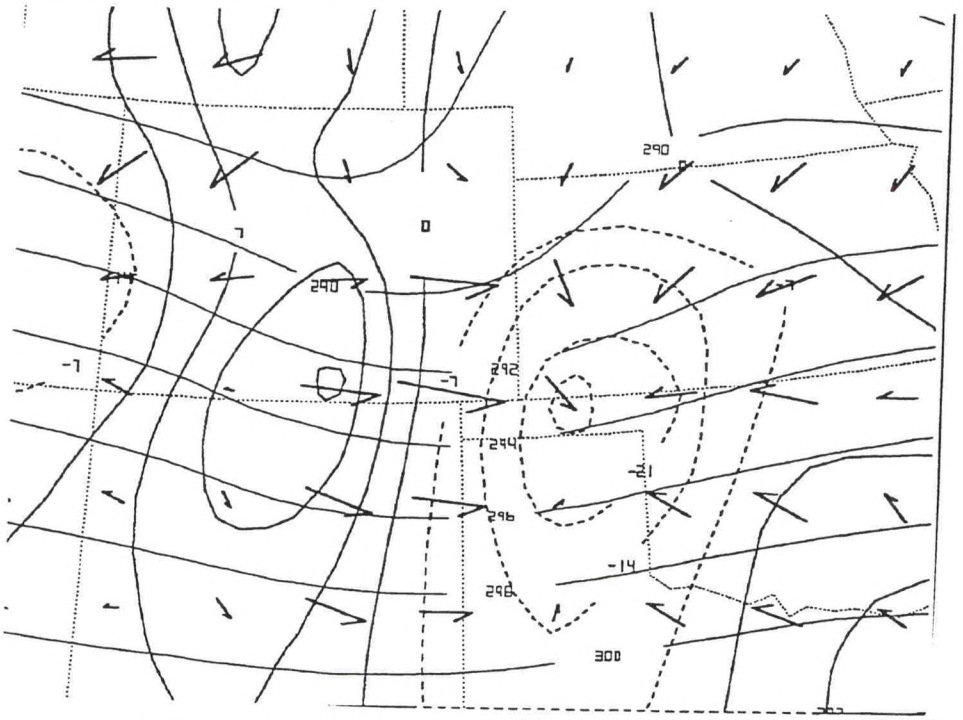

Figure 6. Eta model 12-hour forecast of the 850-700-mb layer Q-vectors and the divergence of the Q-vectors (dashed contours indicate convergence and solid contours show divergence) and the 700-500-mb layer thickness (solid contours every 2 decimeters) for 1200 UTC 12 Feb. 1995.

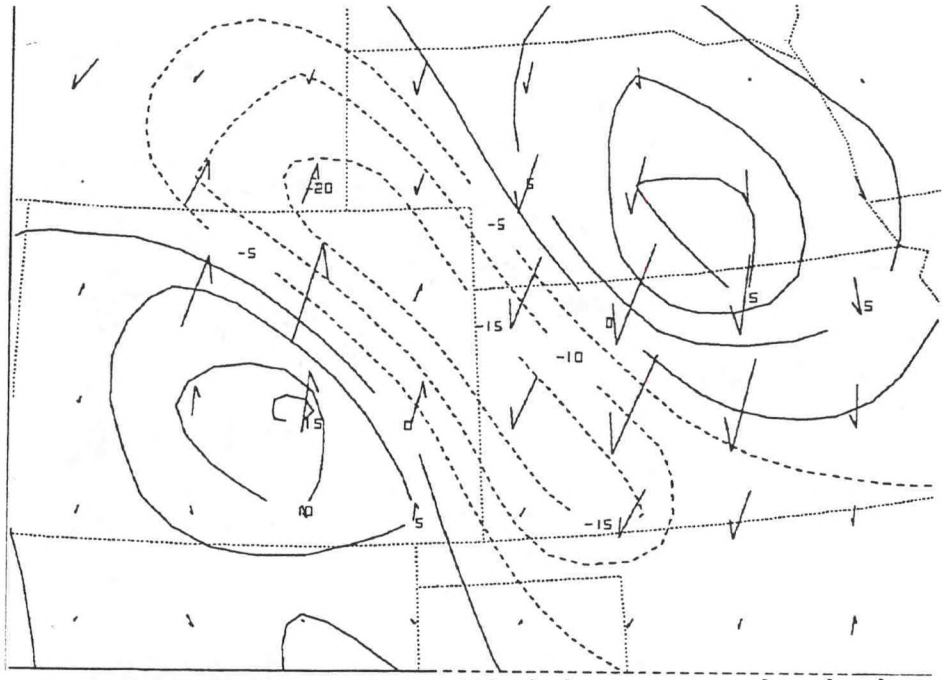

Figure 7. Eta model 12-hour forecast of the 700-mb Q-vectors normal to the thermal wind and the divergence of the Q-vectors normal to the thermal wind (dashed contours show convergence and solid contours indicate divergence) for 1200 UTC 12 Feb. 1995.

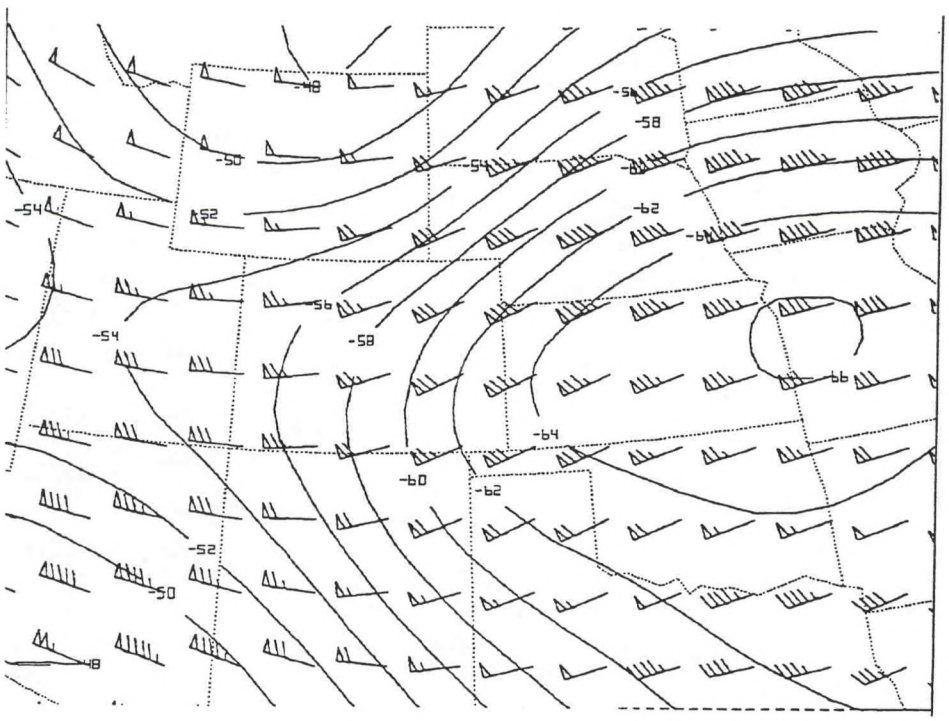

Figure 8. Eta model 6-hour forecast of the 200-mb temperature (solid contours ever 2 °C) and the total wind barb (knots) for 0600 UTC 12 Feb. 1995.

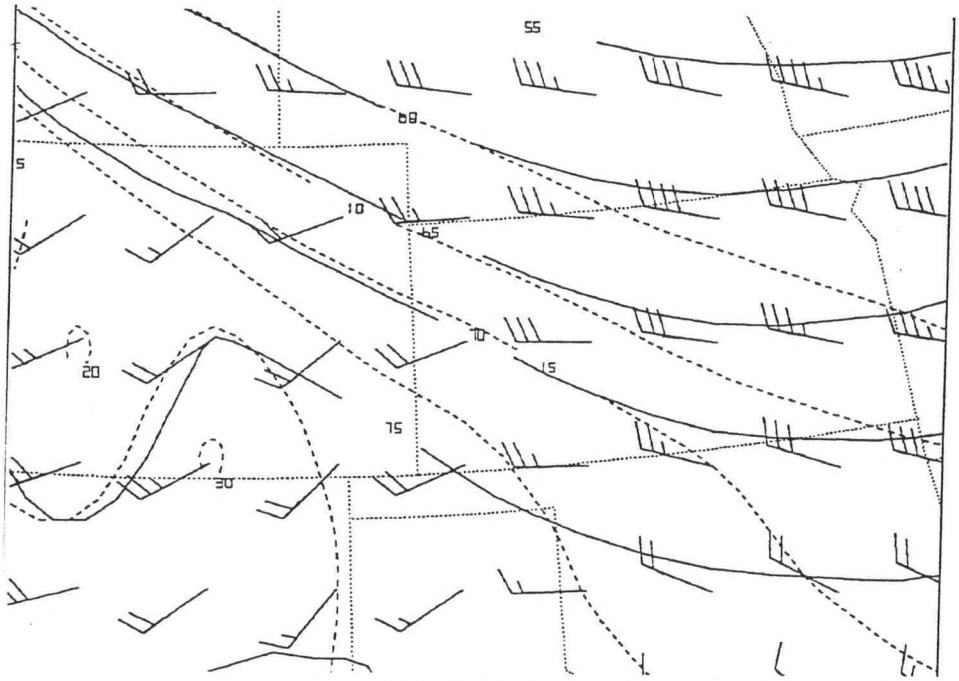

Figure 9. Eta model 6-hour forecast of the 286K isentropic surface pressure (solid contours every 5 x 10^{-1} mb), mixing ratio (dashed contours every 5 x 10 gkg^{-1}) and total wind barb (knots) for 0600 UTC 12 Feb. 1995.

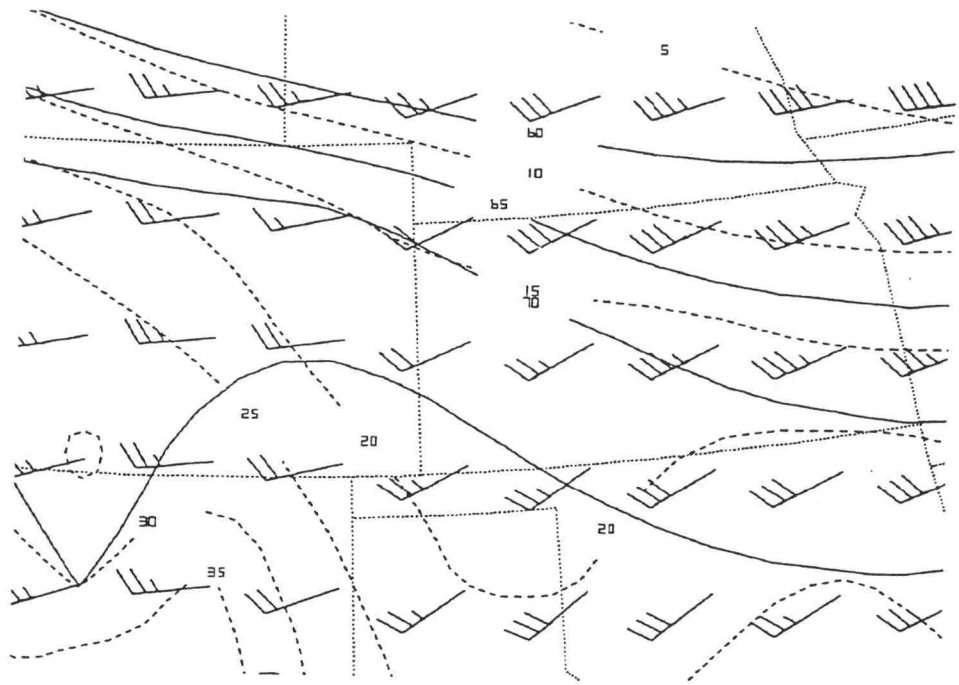

Figure 10. The same as Figure 9 except the 18-hour forecast.

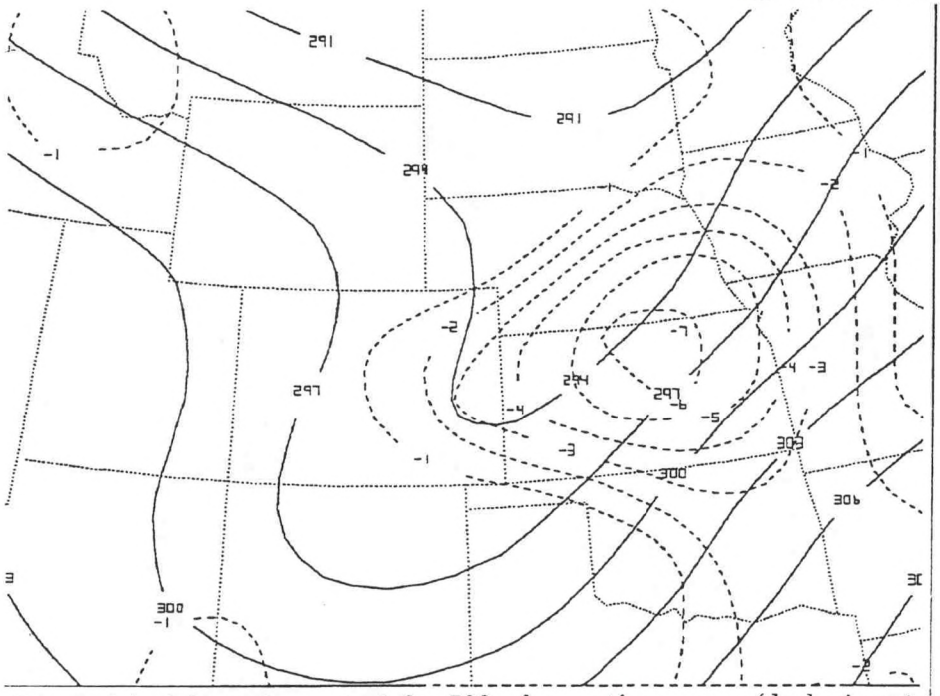

Figure 11. Eta model 18-hour forecast of the 700-mb negative omega (dashed contours every μbs^{-1}) and heights (solid contours every 3 decimeters) for 1800 UTC 6 March 1995.

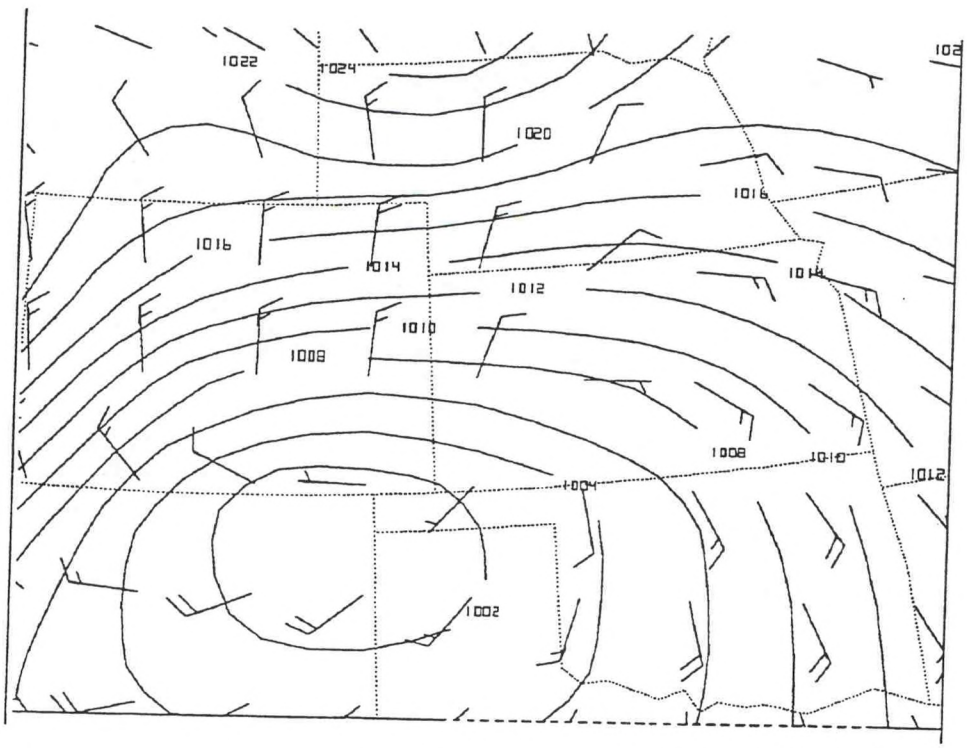

Figure 12. Eta model 18-hour forecast of the boundary layer total wind barb (knots) and the MSL pressure (solid contours every 2 mb) for 1800 UTC 6 March 1995.

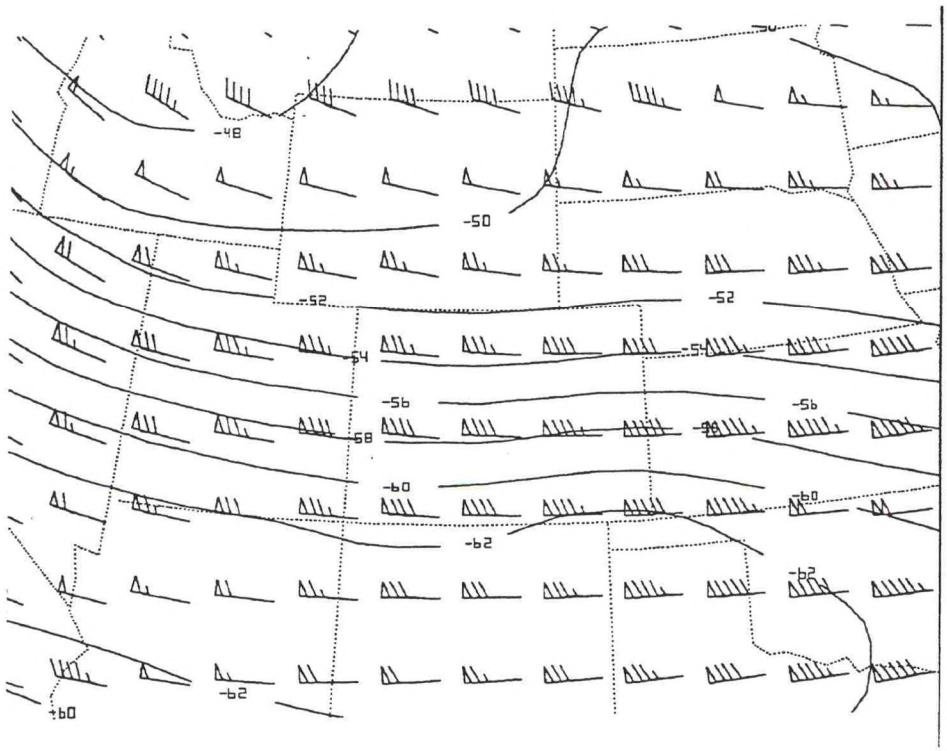

Figure 13. Eta model 12-hour forecast of the 200-mb temperature (solid contours ever 2 °C) and total wind barb (knots) for 1200 UTC 6 March 1995.

The Forecasting of Precipitation Phase Change: A Case Study

William Wilson[1] and Kenneth Kostura[2]

1. INTRODUCTION

During the winter, forecasting the change of state of precipitation is a problem faced by most forecasters. The WSR-88D radar data and other meteorological data can be used to forecast precipitation phase change. This study of a winter precipitation event over northern Kentucky will address this problem.

2. SYNOPSIS

A surface cold front moved southeast across Kentucky on the night of October 29, 1993 (Figure 1). As the low-level cold air was spreading into Kentucky, strong upward vertical motion behind the front and overrunning of warm air caused widespread post frontal precipitation across northern Kentucky. The vertical motion was located east of a 700-mb wave at 0000 UTC (Figure 2). A 200-mb jet streak of 150 KTS centered over West Virginia provided upper air support for upward lift (Figure 3). Isentropic analysis on the 290 K surface at 0000 UTC showed the significant ascent over Kentucky (not shown). The VAD Wind Profile (Figure 4) from the (KLVX) WSR-88D radar at Louisville, 0439 UTC, showed north winds up to 4,000 ft and south winds above. This VAD Wind Profile and the 0000 UTC Paducah sounding clearly showed the height of the low-level cold air and the overrunning warmer air (Figure 5). Precipitation started as rain early in the evening on October 29, and changed to snow by the morning of October 30.

3. RADAR ANALYSIS

The Louisville WSR-88D radar showed a bright band on base reflectivity products at several elevation slices (Figures 6 and 7) and on the reflectivity cross-sections (not shown). Bright bands are layers of high reflectivity due to the melting of snow (Battan 1973). A bright band circle forms on base reflectivity products because of the tilt of the radar beam at an elevation angle as it goes through a melting layer. The larger the distance from the radar to the bright band (melting layer), the higher the bright band (melting layer). From 0439 UTC to 0855 UTC, the radius of the bright band circle at the 4.3° elevation angle decreased over Jefferson county Kentucky and remains the same length southwest of the radar (Figures 6 and 7). Jefferson County is just northeast of the KLVX radar and Louisville covers' the northern two-thirds of the county. The radius decreases between the radar site and bright band shows a lowering of the bright band, and thus the lowering of the melting level. The circle on the 2.4° elevation disappeared from 0439 UTC to 0855 UTC (Figures 6 and 7). The 2.4° elevation angle was lower, so over Louisville the bright band had reached the ground showing there no longer was an elevated melting level. By 0800 UTC, the airport in Louisville reported ice pellets and a surface analysis of temperature showed the warmer air south of Louisville (Figure 8).

Forecasters noted the change in circle radius early in the evening of October 29 and concluded that the melting layer was slowly decreasing in height over Jefferson County. Since the melting layer

1. Corresponding author address: William Wilson, National Weather Service Office, Louisville KY.
2. Kenneth Kostura, National Weather Service Office, Blacksburg Virginia.

was lowering forecasters inferred that a change in precipitation phase from liquid to frozen likely was going to occur (Mason 1975).

Another indication that the cold air depth was increasing was the change of wind direction on successive base velocity products. On base velocity pictures, red (warm colors) shows an outgoing wind and green (cool colors) represents an incoming wind. The base velocity picture at 0439 UTC showed a north wind at low levels (Figure 9). This low-level wind was followed by a calm wind or else winds perpendicular to the radar beam axis, while at higher levels farther from the radar a southwest wind prevailed. As with the VAD wind profile mentioned earlier, the velocity products showed an inversion that, in this case, was nearly coincident with the melting layer. However, base velocity products give a plan view from which a vertical view can be inferred. By 0814 UTC (Figure 10) low level wind increased in speed (more intense reds and greens) as did the area of outbound and inbound winds. The north wind increased in depth because the radar can detect a north wind farther away from the radar site. As the depth of the north wind increased, deeper, colder air moved into Louisville, and by 1100 UTC the ice pellets had changed to snow.

4. SUMMARY AND CONCLUSION

There were several atmospheric processes that may have been responsible for the change of rain to snow in this case. These include: 1) cooling due to melting of snow in the bright band region, and its induced circulation (Szeto et al 1988), 2) adiabatic cooling due to strong lift, and 3) the deepening of the low-level cold layer (Stewart and Patenabe, 1988).

The temperatures fell in lower levels of the atmosphere, which lowered the melting level causing the bright band to decrease in elevation in the reflectivity data. A deepening of the cold layer was reflected in the height increase of the northerly winds on base velocity data. Forecasters at the WSFO Louisville used this radar information and the inferred rate of cold air advection in the lower troposphere to forecast when rain would change to snow. Forecasts of the phase change to snow over Louisville were incorporated in the terminal forecast for the airport and in nowcasting.

The WSR-88D is an excellent tool to bridge the gap between 12 hour upper air soundings. Using an "old friend", the bright band, one can determine the depth of cold or warm layers by showing where the melting level is located. The base velocity products can give an idea of where wind changes occur in relation to the area of forecast interest. The WSR-88D radar data, and surface and upper air analyses can be used to imply processes aloft and near the surface such as adiabatic and diabatic cooling, cold air advection and evaporative cooling. The methods described in this paper with conceptual models of precipitation processes aloft is a potential solution to solving some precipitation phase change problems.

5. ACKNOWLEDGEMENTS

The authors thank Ted Funk, SOO, WSFO Louisville and Preston Leftwich, CRH/SSD for their help with this paper.

6. REFERENCES

Battan, L.J., 1973: *Radar observation of the atmosphere,* University of Chicago Press, 324 pp.

Mason, B.J., 1975: *Clouds, rain, and rainmaking,* Cambridge University Press, 189 pp.

Stewart, R.E., and L.M. Patenabe, 1988: Rain-snow boundaries and freezing precipitation in Canadian east coast winter storms, *Atmosphere-Ocean,* **26**(3), 377-398.

Szeto K.K., R.E. Stewart, and C.A. Lin, 1988: Mesoscale circulations forced by the melting of snow in the atmosphere. Part II: Applications to meteorological features, *J. Atmos. Sci.,* **45**, 1642-1650

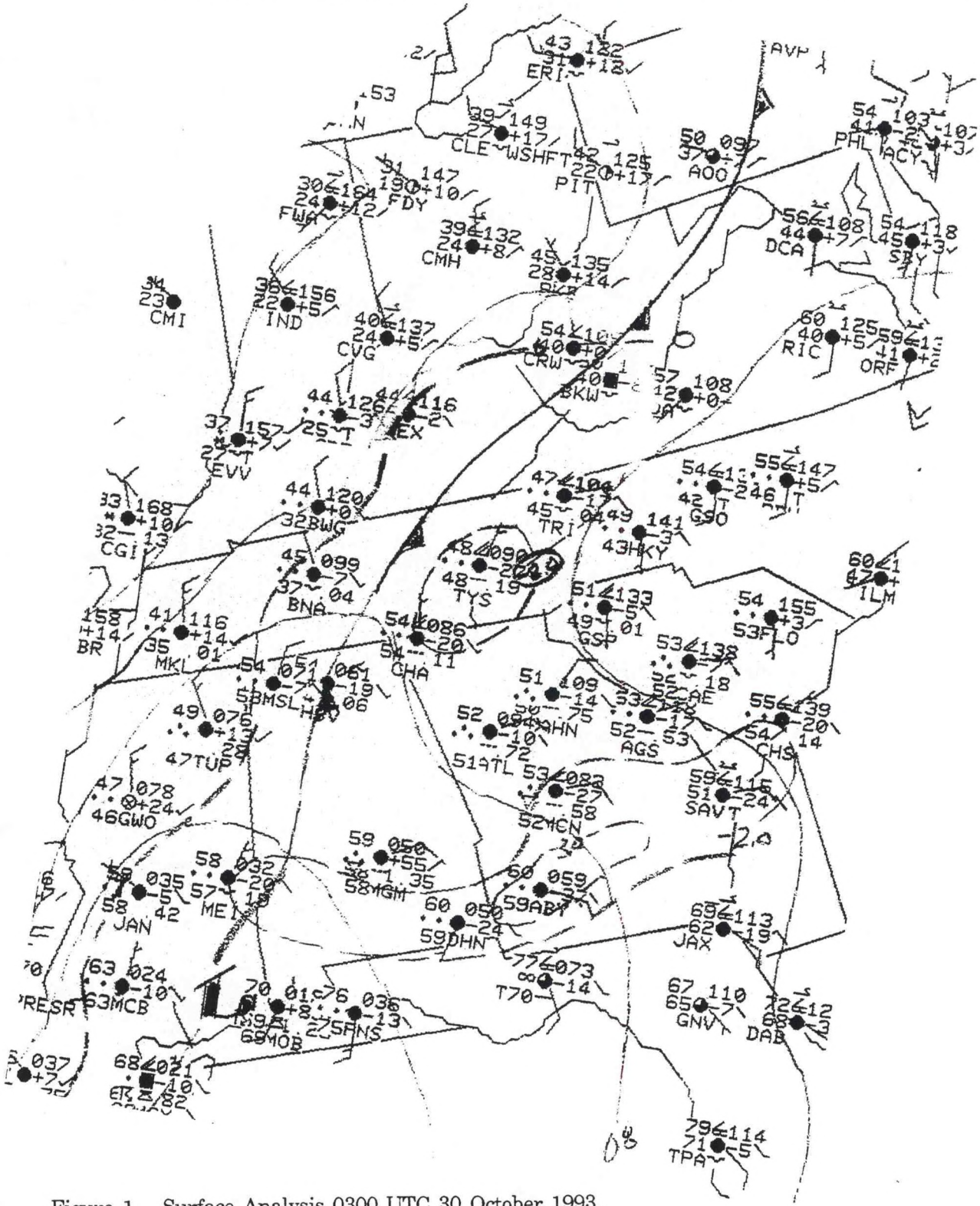

Figure 1. Surface Analysis 0300 UTC 30 October 1993.

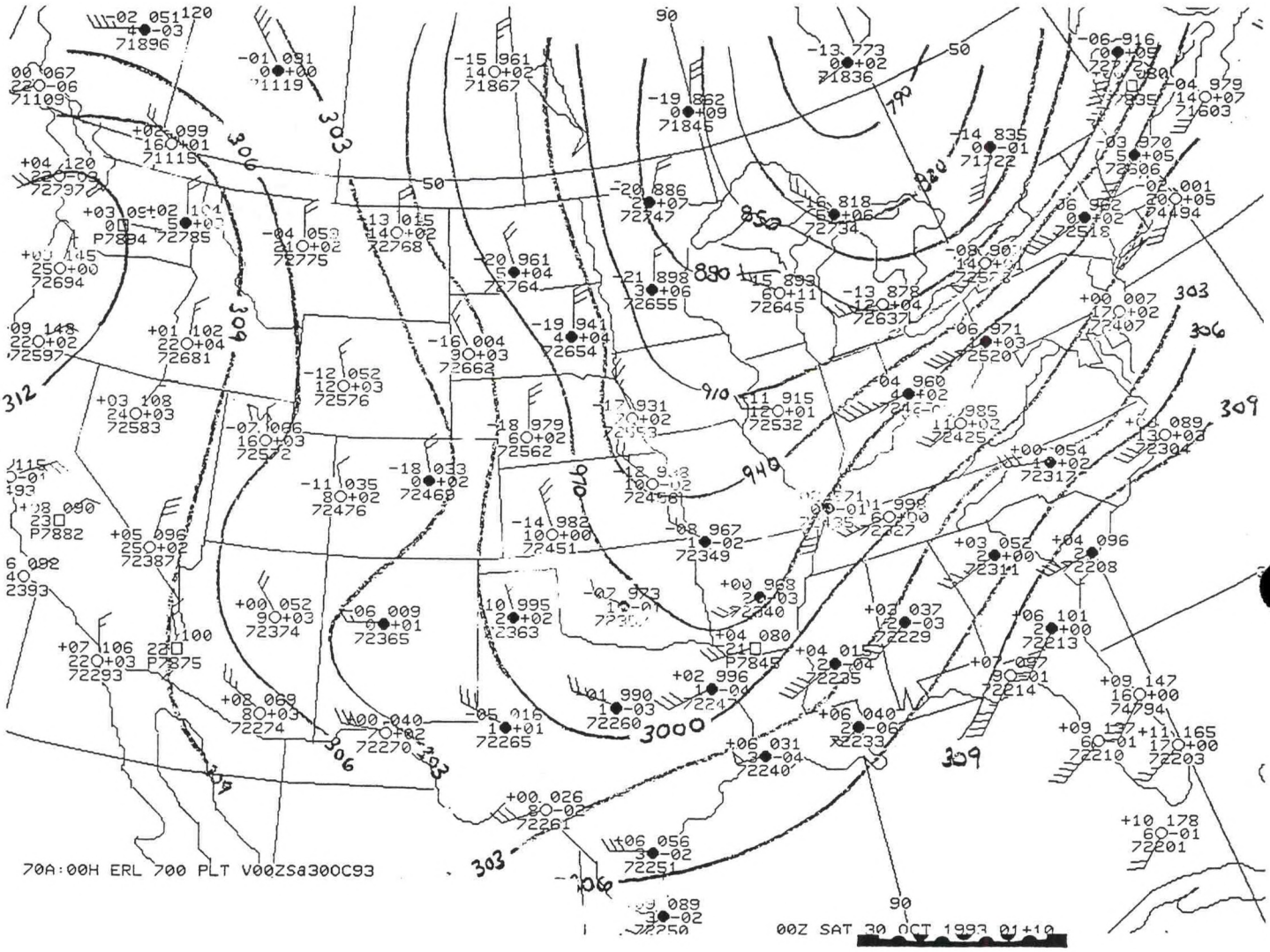

Figure 2. 700 mb 0000 UTC 30 October 1993. Black lines - height meters 2 and 3 omitted every 30 meters.

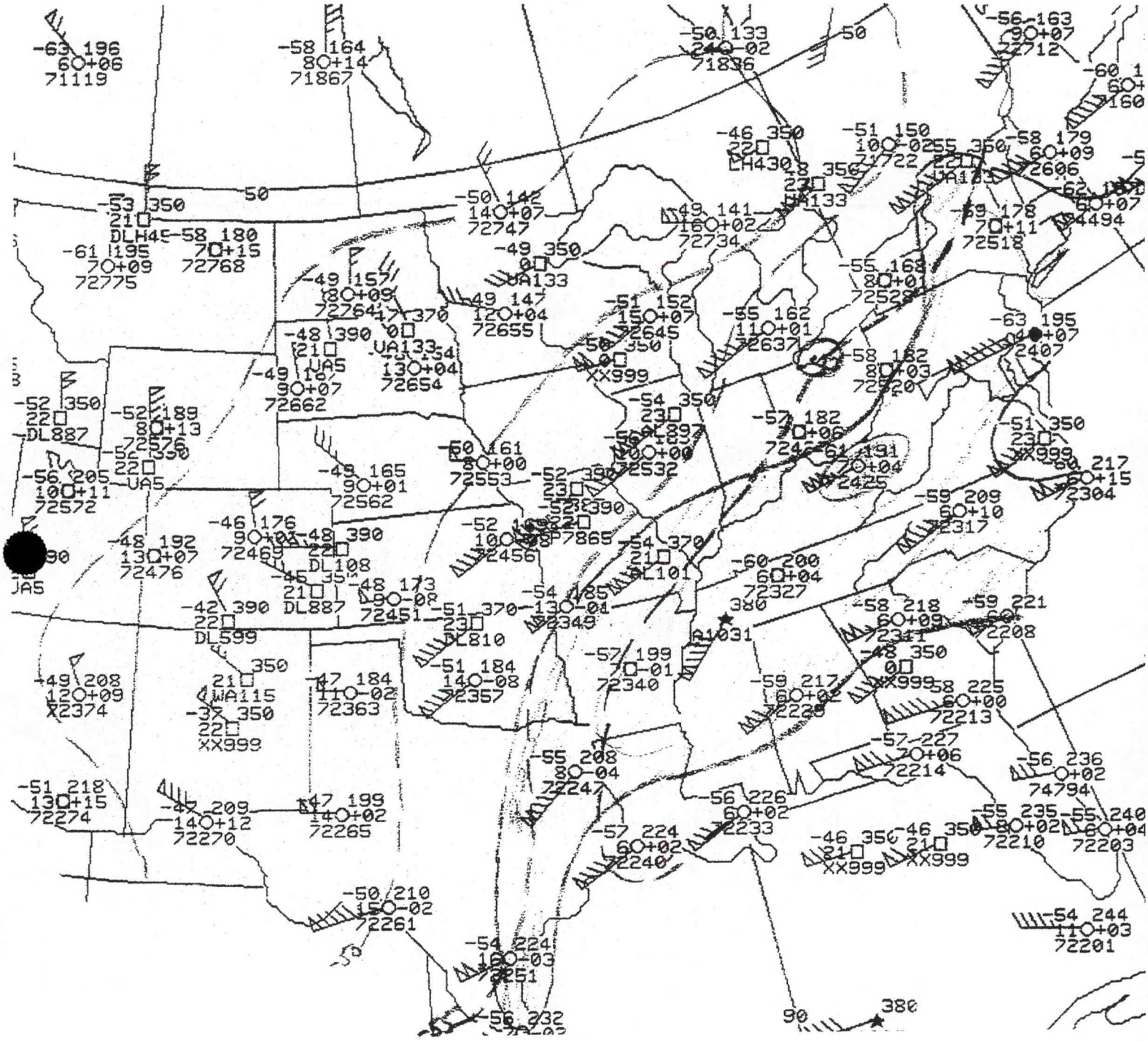

Figure 3. 200 mb 0000 UTC 30 October 1993. Purple - 150 kts.

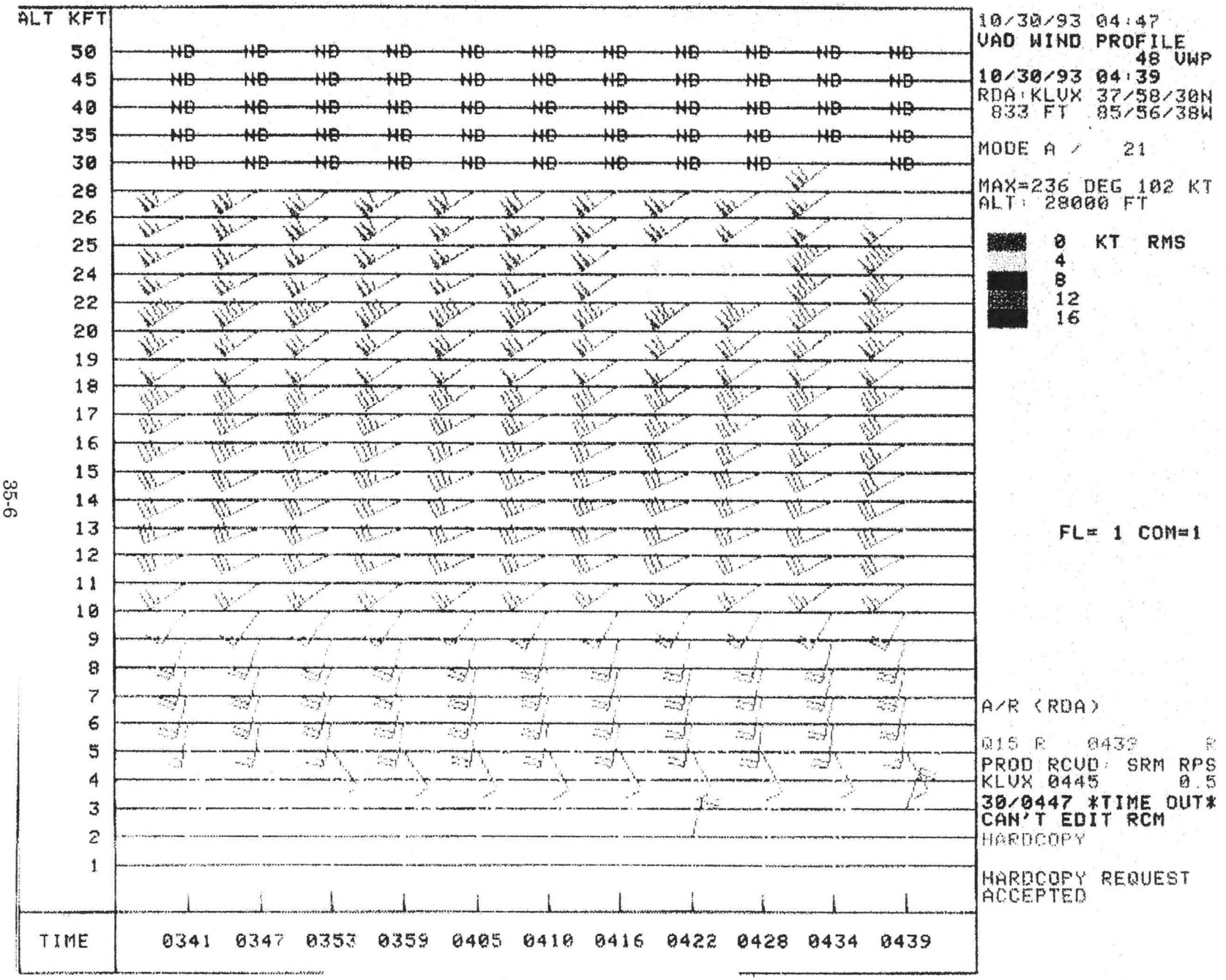

Figure 4. VAD Wind Profile 0439 UTC 30 October 1993.

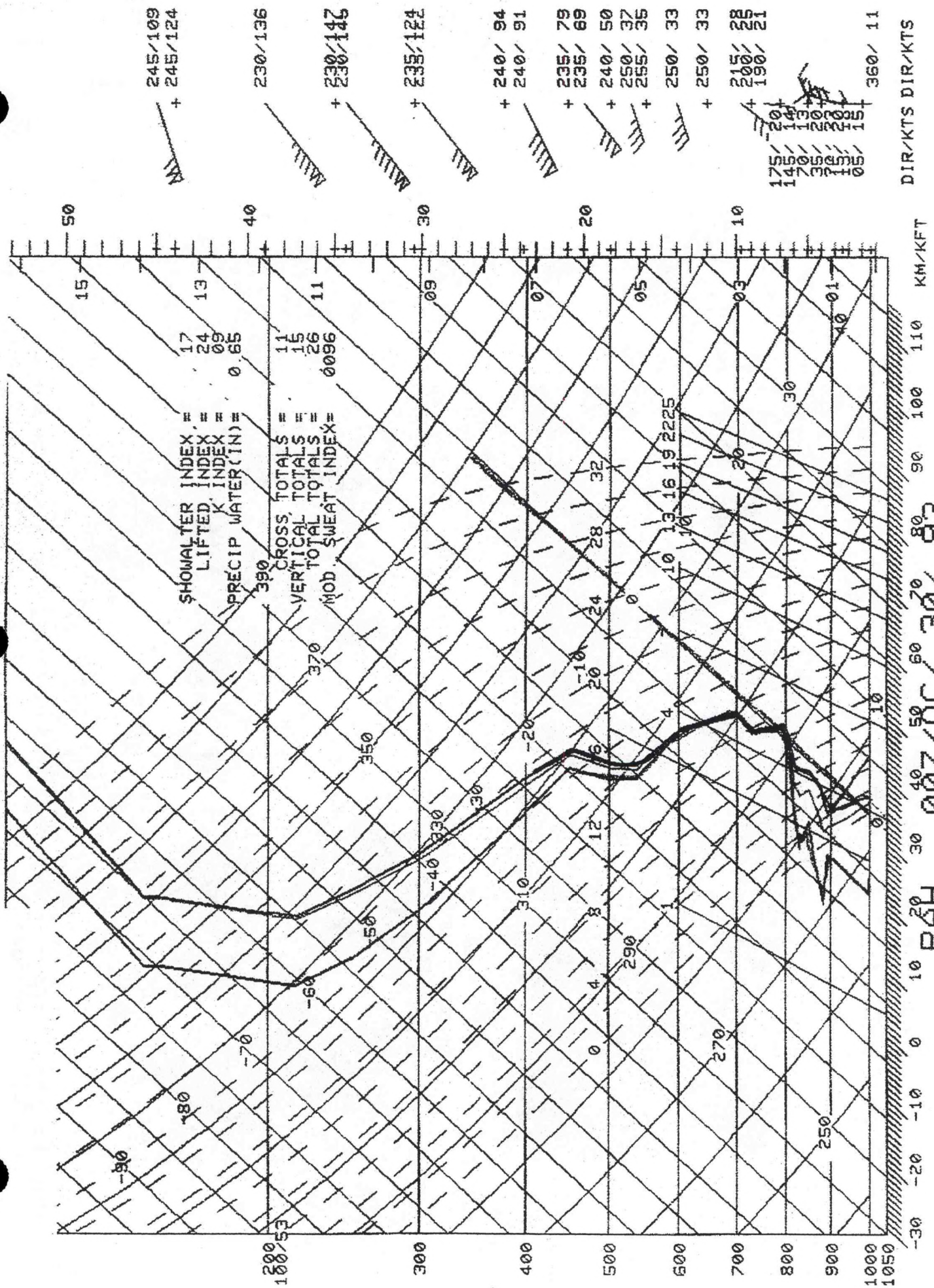

Figure 5. Paducah, Kentucky sounding 0000 UTC 30 October 1993.

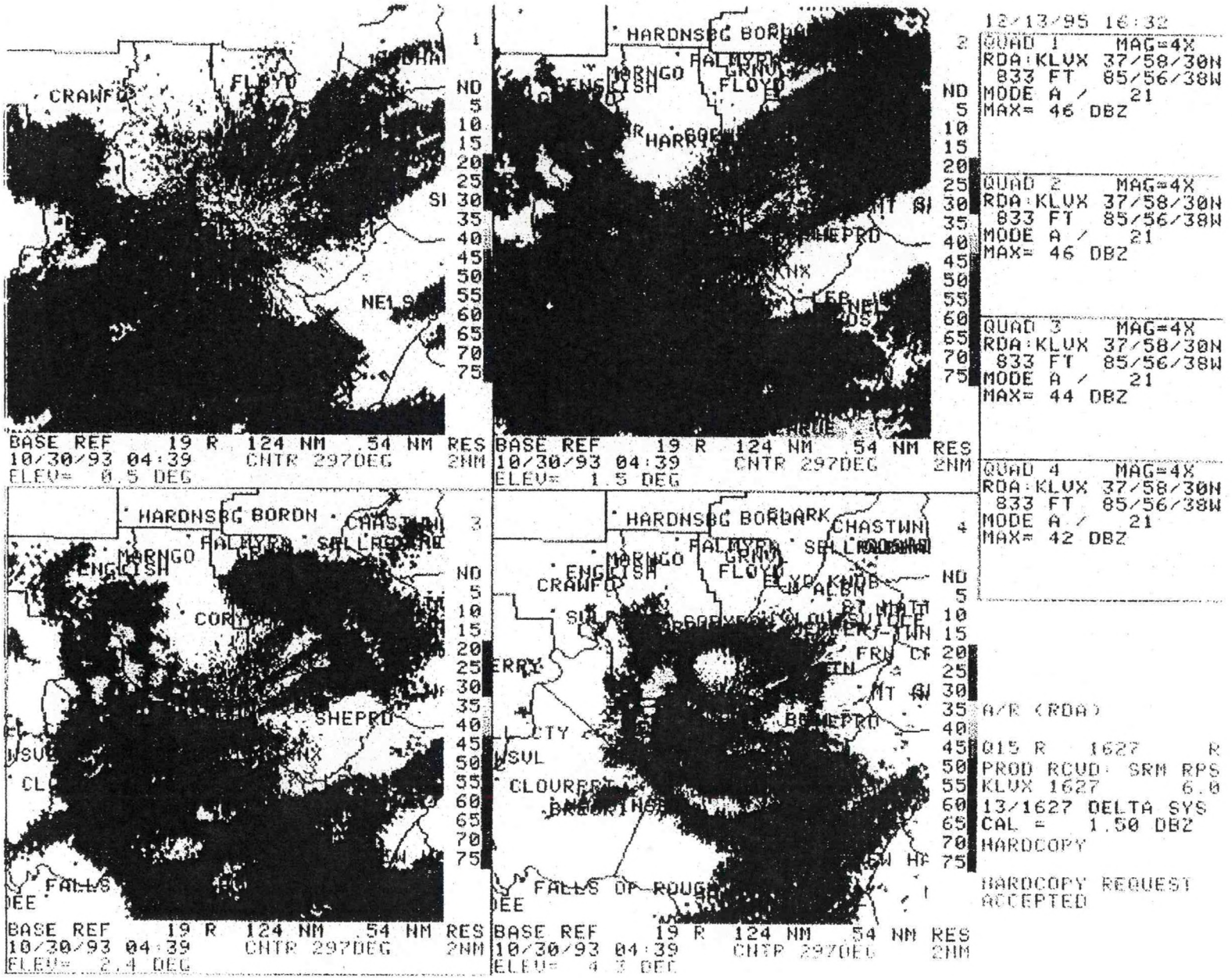

Figure 6. Four panel base reflectivity KLVX WSR-88D 0439 UTC 30 October 1993. (2.4˚ on bottom left - 4.3˚ on bottom right.)

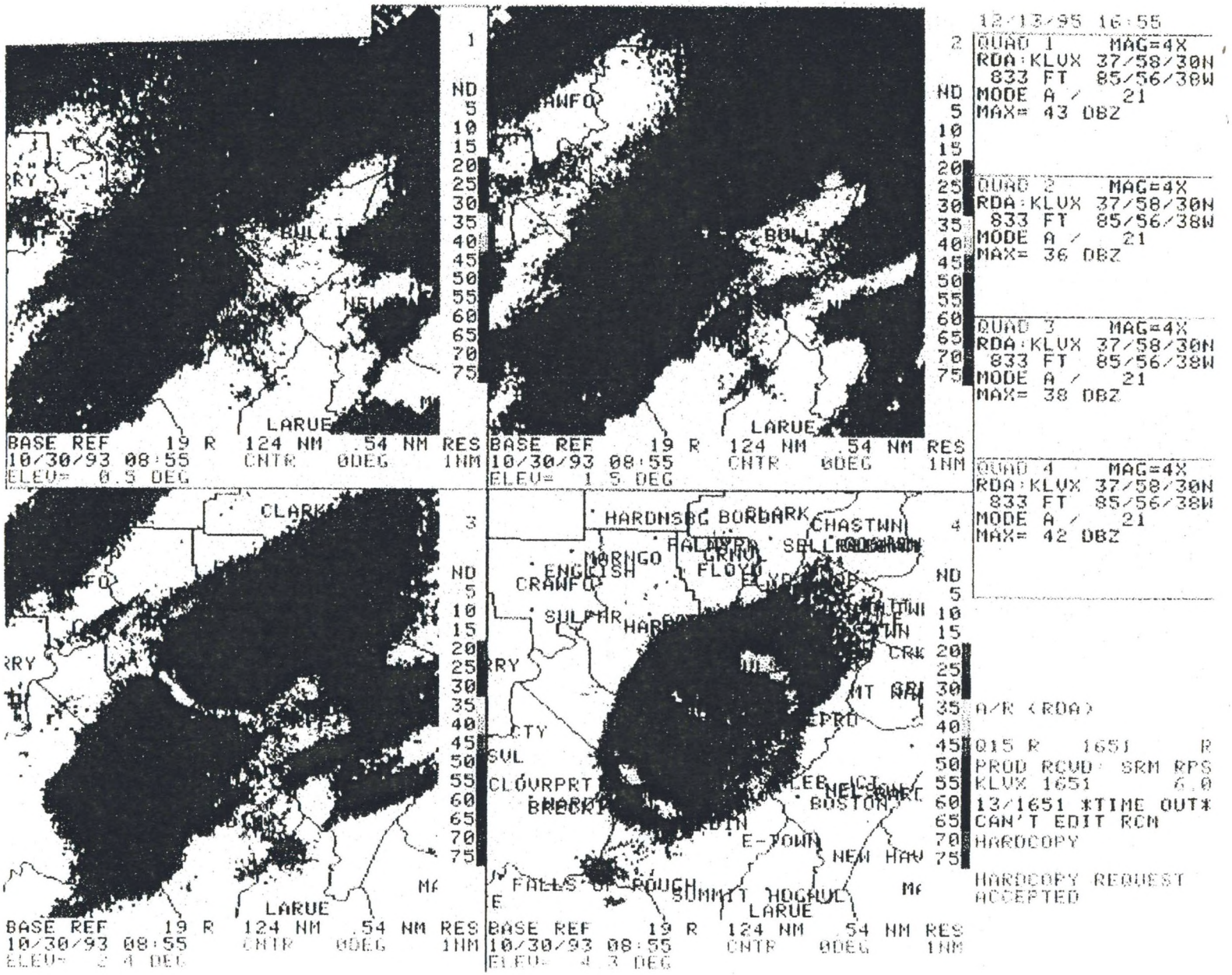

Figure 7. Four panel base reflectivity KLVX WSR-88D 0855 UTC 30 October 1993. (2.4° on bottom left - 4.3° on bottom right.)

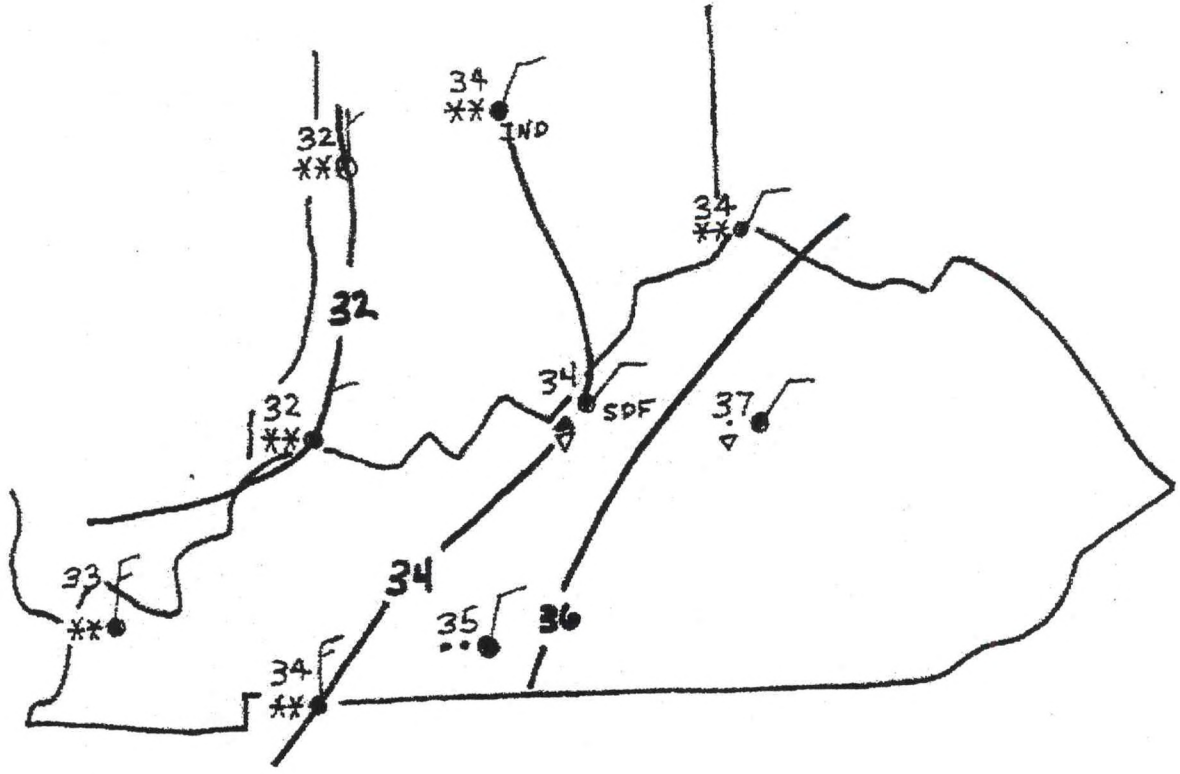

Figure 8. Surface analysis of temperature 0800 UTC 30 October 1993. (Temperature in red.)

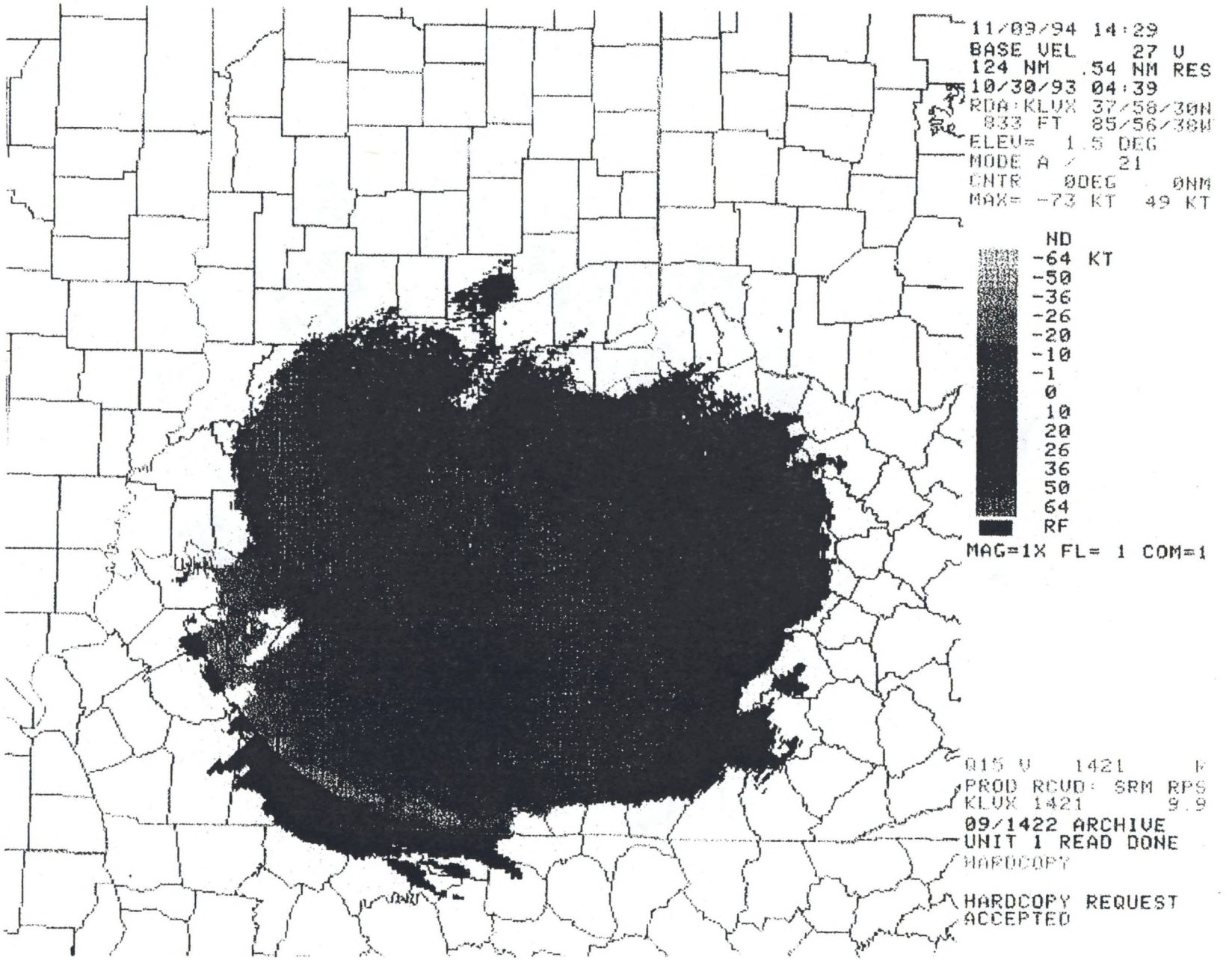

Figure 9. Base velocity - KLVX WSR-88D 0439 UTC 30 October 1993.

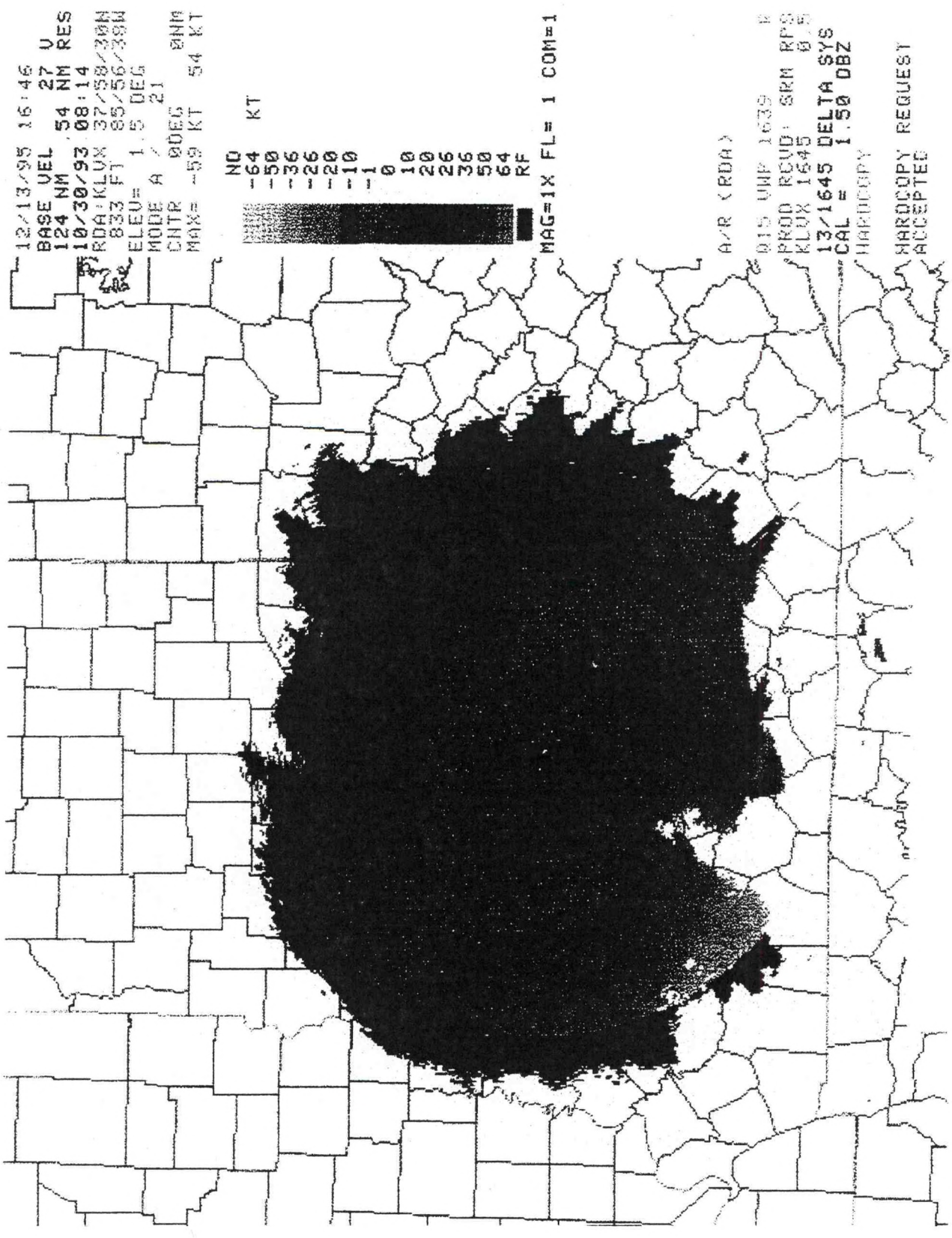

Figure 10. Base velocity - KLVX WSR-88D 0814 UTC 30 Oct 1993.

The Influence of Coniferous Forest Albedo on Wintertime Maximum Temperatures

Bradley J. Bramer[1]

1. INTRODUCTION

The extensive coniferous forest stands in the northern portions of the continental United States can have a significant influence on mesoscale meteorological conditions. Richardson (1990) described an interesting case study in which maximum temperatures were profoundly elevated in the northern portion of Minnesota, compared to the southern section of the state, in spite of a significant snow cover present. Because of a nearly homogeneous synoptic scale pattern across the region, he attributed the temperature paradox to the lower albedo of the forested areas in the north negating the impact of a substantial snow pack.

This study is an expansion of the work of Richardson (1990) to include an overview of recent scientific results, an examination of March 2, 1993 case and a highlight of some synoptic scale parameters which operational meteorologists can look for to modify their maximum temperature forecasts.

2. THE ALBEDO FACTOR

The cooler climate in the higher latitude locations of the United States allow coniferous tree species to dominate the forest ecosystems. An example of the distribution of black spruce is shown in Figure 1. Berglund and Mace (1972) found this to be a representative species of far northern Minnesota. They obtained mean monthly albedo values for black spruce under various levels of cloud cover. As an example, with clear skies during March, the average albedo of the black spruce canopy was found to be 10 percent. This agreed well with the albedo range of 5 to 15 percent that Sellers (1965) generalized for conifer forests. Other factors, such as the albedo of the surface snow cover and patches of snow within the canopy were found to have only minor impacts on the mean albedo. The measured albedo value of Berglund and Mace (1972) was assumed to be typical of the forested areas of northern Minnesota for this study.

As a contrast to the low albedo of forested regions, a location which had extensive open areas of deep snow cover would also have to be examined in order to obtain a mean snow albedo value. Baker et al. (1991) examined the snow depth that would be required to mask the albedo of the underlying surface cover. They found that the snow cover would have to be at least 7.5 cm (3 inches) deep in order to hide the reflectance of grass sod. For the prairie grassland area of central Minnesota, a somewhat more stringent value of 10.2 cm (4 inches) was used in this study as a minimum snow depth criterion to obscure the underlying cover.

The age of the snow cover is another important factor to consider when determining a representative albedo value. In an earlier study, Baker et al. (1990) measured the mean albedo decay rates of prairie snow covers in Minnesota for each of the months of the snow season. They assumed the total snow depth was at least 10.2 cm (4 inches) and the initial albedo of freshly fallen snow of a measurable depth was 80 percent. For the month of March, Baker et al. (1990) found the average decay rate in the snow's albedo was 2.9 percent per day. The case of March 2, 1993, used in this

1. Corresponding author address: Bradley J. Bramer, National Weather Service Duluth, MN.

study, had measurable snowfall seven days earlier. A reasonable albedo value for the week old snow would be on the order of 60 percent. This is consistent with the albedo range of 40 to 70 percent that Sellers (1965) assigned to snow cover that was several days old.

The impact of the large difference in albedo values between areas with extensive snow cover and forested locations on air temperature is quite dramatic. Baker et al. (1992) looked at the mean temperature and radiation depressions associated with a significant snow cover (at least 10 cm) compared to a bare ground situation. They found that mean maximum daily temperatures for the period March 1-15 were 6°C (10.8°F) colder than conditions where no snow was present.

Modeling studies in Japan (Yamazaki and Kondo (1992) and Yamazaki (1995)) have revealed the connection between the albedo of a dense coniferous forest canopy to increases in boundary layer air temperatures. The models showed that a tall coniferous forest canopy (common in northern Minnesota) was an efficient mechanism, during sunny days with light winds, of transferring heat to the lowest layers of the atmosphere.

3. THE SYNOPTIC SITUATION

In order to isolate the albedo effect from other possible influences, a number of specific synoptic scale meteorological conditions must be present. These factors help to minimize the possibility that "synoptic scale contamination" is responsible for differences in maximum temperatures between locations with vastly different surface albedos.

The most important factor to consider is the amount of solar radiation which will reach the surface. Due to the difficulty in determining the amount of cloud cover present over the course of the daylight hours, Baker and Ruschy (1985) used percent of possible sunshine as a proxy indicator. By examining the situation presented in Richardson (1990), the case March 2, 1993, in this study and other examples, it was found that the percent of possible sunshine for the day must be at least 90 percent. This allows a maximum amount of shortwave radiation from the sun to be intercepted by the coniferous canopy and re-radiated to the surface layer of the atmosphere as infrared energy which, in turn, results in the elevated maximum temperatures.

The amount of cloud cover may also be determined by using the mean surface-500 mb relative humidities as another proxy indicator. Generally, mean lower tropospheric relative humidities of less than 50 percent indicate that mostly sunny sky conditions are likely.

The magnitude of temperature rises also depends on when in the winter season a situation develops. Due to the lower solar zenith angle in January, compared to March, the elevation of the maximum temperature in the forest from snow field locations is significantly lower. Forested areas in January are typically around 5°F warmer than surrounding non-forested locations. However, due to the increased shortwave energy input during the month of March, forest stations may be as much as 10°F warmer than areas with just snow cover.

A second consideration is the lack of any significant warm air advection in the lower troposphere. The situations when moderate to strong warm air advection were taking place would mask the mesoscale influence of the forested region.

An additional factor that must be accounted for is the limitation of significant wind-induced mixing in the surface layer. This helps maintain the sub-layer of warm air beneath the forest canopy. The 1200 UTC soundings examined in the March 2, 1993 case had surface radiation inversions present which implied light winds. Wind speeds of less than 10 knots during the daylight hours

enhanced the heating of the sub-canopy layer. This reduced mechanical mixing of the cold sub-layer of air, in contact with the snow surface, throughout the surface layer.

Model output statistical (MOS) temperature forecasts tend to underestimate the maximum temperatures in forested regions during the previously mentioned synoptic conditions. This may be due to two primary factors which influence the statistical predictor. The first condition is the simple snow/no snow ground cover coefficient term which is present during the winter season. If a sufficient snow depth is indicated by surface observations, the coefficient will assume a standard snow albedo value. However, this is not representative for regions of coniferous forest during these specialized meteorological conditions. A second factor is the relative rarity of these events. Only a handful of days each winter meet these criteria. This would mean their infrequency of occurrence would not be statistically significant.

4. THE CASE OF MARCH 2, 1993

A "classic" example of the "conifer albedo effect" can be seen in the situation of March 2, 1993. The meteorological conditions on that date resulted in a rather dramatic demonstration of the elevation of maximum temperatures on the mesoscale due to lower albedo of forested regions. A comparison was made between two National Weather Service stations in Minnesota: International Falls (INL) in the coniferous forested area and St. Cloud (STC) in a prairie/deciduous environment.

The lower tropospheric synoptic situation for 1200 UTC 2 March 1993 can be seen in Figure 2. An 850 mb ridge (as part of a rex block pattern) was firmly established over northern Minnesota resulting in no appreciable low-level temperature advection over the state. Surface radiational inversions at both stations are evident in the 1200 UTC soundings (Figure 3). Clear skies, wind speeds less than 10 knots and mean surface 500 mb relative humidities of 50 percent or less were present at both locations (not shown). Snow cover at the stations (INL: 8 inches and STC: 11 inches) was also adequate to cover the underlying surface.

The resulting time series of station temperatures (Figure 4) indicated similar values at 0600 CST. However, during the daylight hours, the temperature rise at INL was significantly more rapid than at STC despite homogeneous synoptic conditions. Maximum temperatures across northeastern Minnesota, northern Wisconsin and the Upper Peninsula of Michigan were noticeably higher than those of more southern locations (Figure 5). A record high temperature for March 2 was also set at INL due to the direct impact of the coniferous forest albedo. By contrast, the MOS 48 and 24 hour maximum temperature forecasts for INL on March 2, 1993 were 41° and 43°F, respectively.

5. SUMMARY AND RECOMMENDATIONS

The lower albedo of an extensive coniferous forest canopy during the snow season can result in a significant elevation of maximum temperatures on the mesoscale compared to snow field locations. This is due to the emission of infrared radiation energy by the forest canopy into the atmospheric surface layer (Figure 6). Forecasters can anticipate the onset of such events by keying on such factors as:

A. Percent of possible sunshine expected to be at least 90 percent.
B. Mean surface-500 mb relative humidities less than 50 percent.
C. Snow depth at least 10.2 cm (4 inches) across the region.
D. Average surface wind speeds less than 10 knots during the daylight hours. This is usually preceded by a surface radiation inversion present on nearby 1200 UTC soundings.
E. No significant lower tropospheric warm air advection is present.

In predicting the maximum temperatures for forested areas during these synoptic conditions, forecasters should consider raising the MOS temperature estimates by anywhere from 5° to 10°F. Smaller temperature rises are expected in January with higher maximum temperatures later in the snow season as the solar zenith angle increases.

6. ACKNOWLEDGMENTS

The author thanks the Department of Atmospheric and Oceanic Sciences at the University of Wisconsin-Madison for the use of their map archive facilities. The copy of Richardson (1990) provided by Rich Naistat (SOO MPX) was also appreciated. The author also thanks Gary Austin (SOO DLH) for his review of the manuscript and Dean and Tracy Packingham for their preparation of computer generated figures.

7. REFERENCES

Baker, D.G., and D.L. Ruschy, 1988: Historical albedo values at St. Paul, Minnesota, 1969-1985. *J. Appl. Meteor.*, **27**, 244-253.

_____, _____, R.H. Skaggs, and D.B. Wall, 1992: Air temperature and radiation depressions associated with a snow cover. *J. Appl. Meteor.*, **31**, 247-254.

_____, _____, and D.B. Wall, 1990: The albedo decay of prairie snows. *J. Appl. Meteor.*, **29**, 179-187.

_____, R.H. Skaggs and D.L. Ruschy, 1991: Snow depth required to mask the underlying surface. *J. Appl. Meteor.*, **30**, 387-392.

Berglund, E.R., and A.C. Mace, 1972: Seasonal albedo variation of black spruce and sphagnum-sedge bog cover types. *J. Appl. Meteor.*, **11**, 806-812.

Burns, R.M. and B.H. Honkala, 1990: Silvics of North America: Volume 1, Conifers. Agriculture Handbook 654. U.S. Forest Service, 675 pp.

Richardson, J.P., 1990: A comparison of afternoon/maximum temperatures over snow cover: forest areas vs. open country. Central Region Technical Attachment 90-10. DOC, NOAA, NWS Central Region Scientific Services Division, Kansas City, MO.

Sellers, W.D., 1965: *Physical Climatology*. The University of Chicago Press, 272 pp.

Yamazaki, T., 1995: The influence of forests on atmospheric heating during the snowmelt season. *J. Appl. Meteor.*, **34**, 511-519.

_____, and J. Kondo, 1992: The snowmelt and heat balance in snow-covered forested areas. *J. Appl. Meteor.*, **31**, 1322-1327.

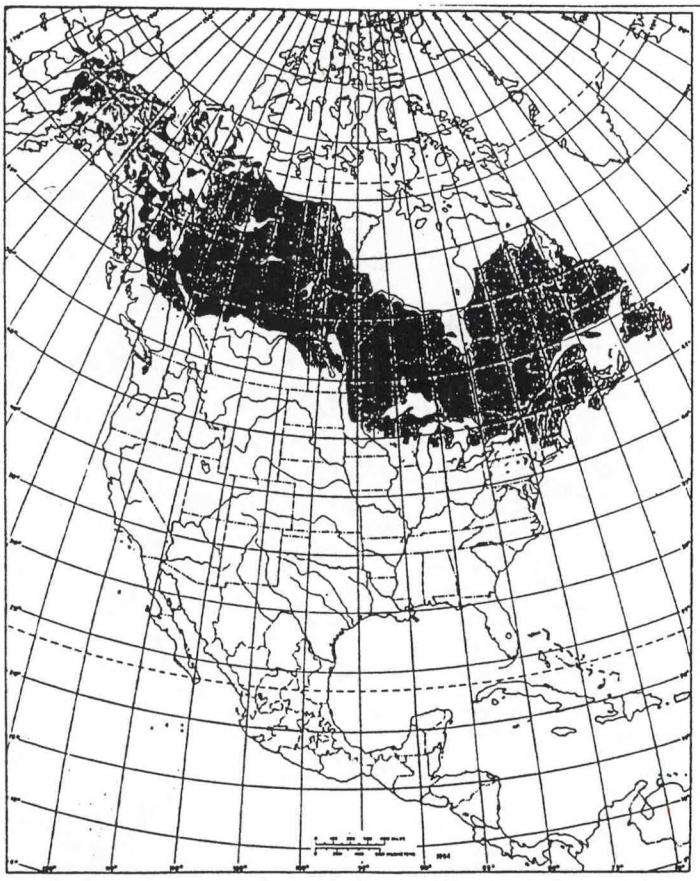

Figure 1. Distribution of black spruce (*Pinus mariana*) across North America (black shading). From urns and Honkala (1990).

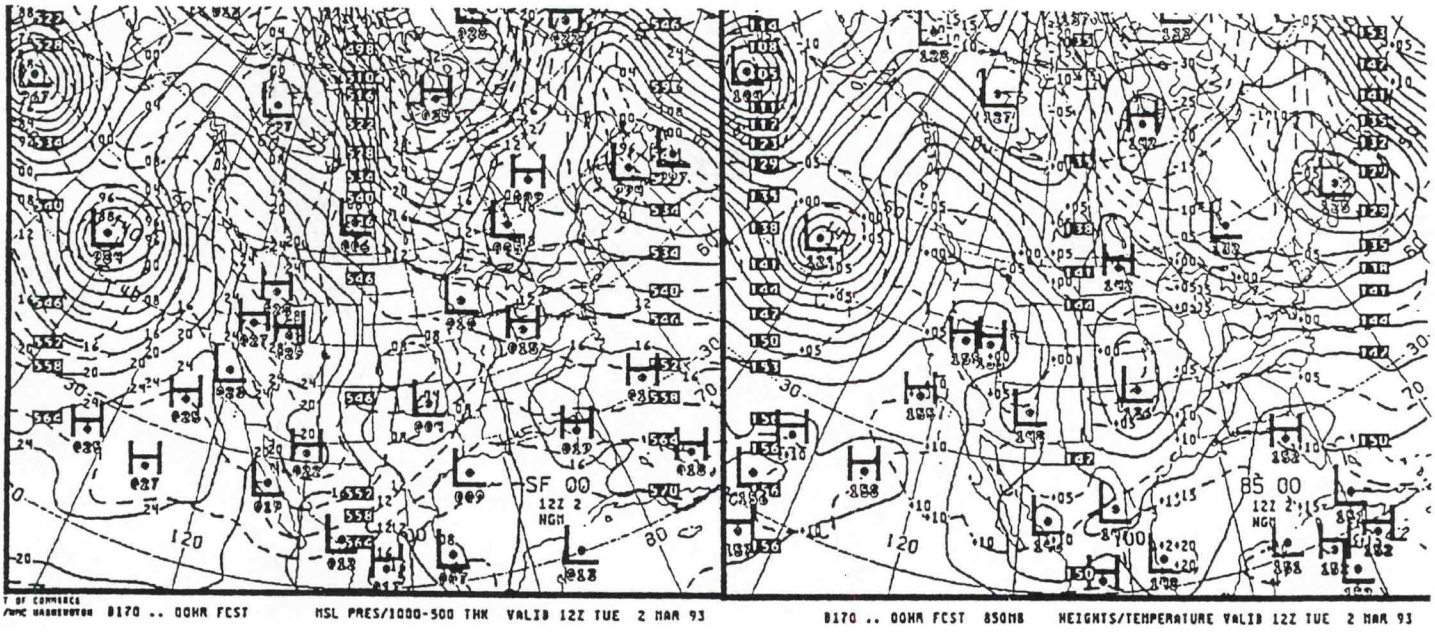

Figure 2. Nested Grid Model 00 Hr analysis valid 1200 UTC 2 March 1993.

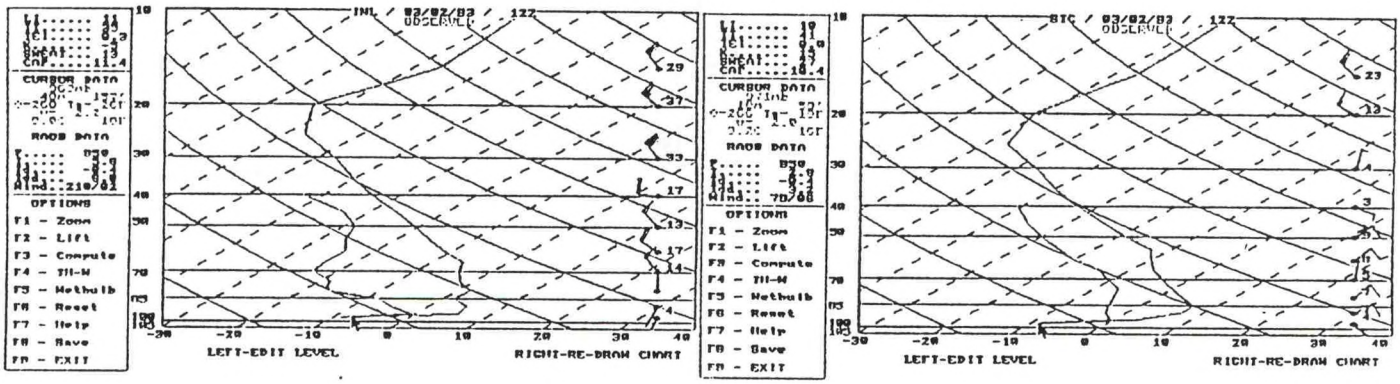

Figure 3. 1200 UTC soundings of 2 March 1993 for INL (left) and STC (right).

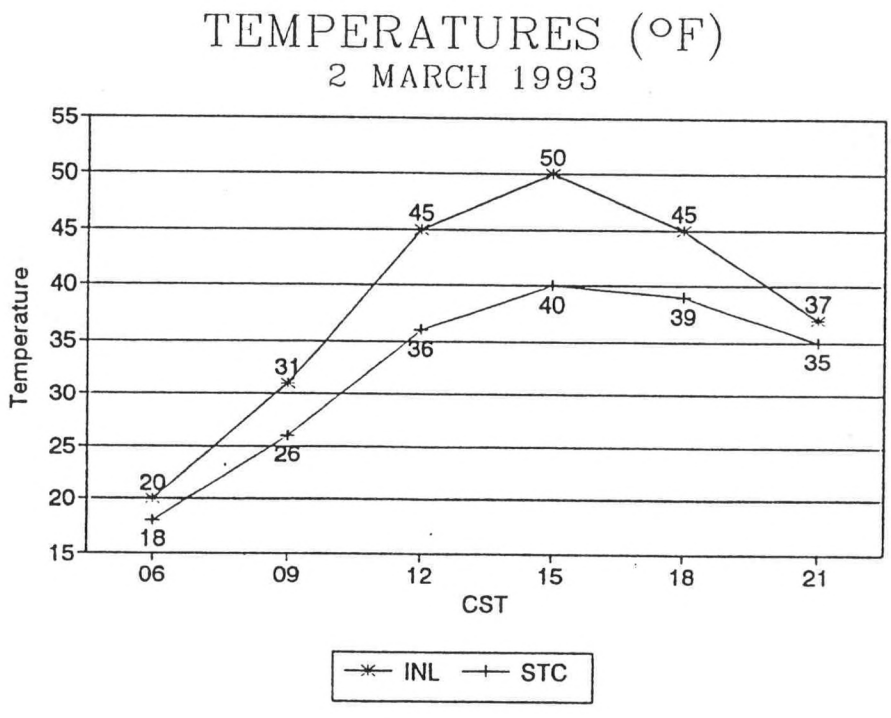

Figure 4. Temperature plots on March 2, 1993 for INL and STC.

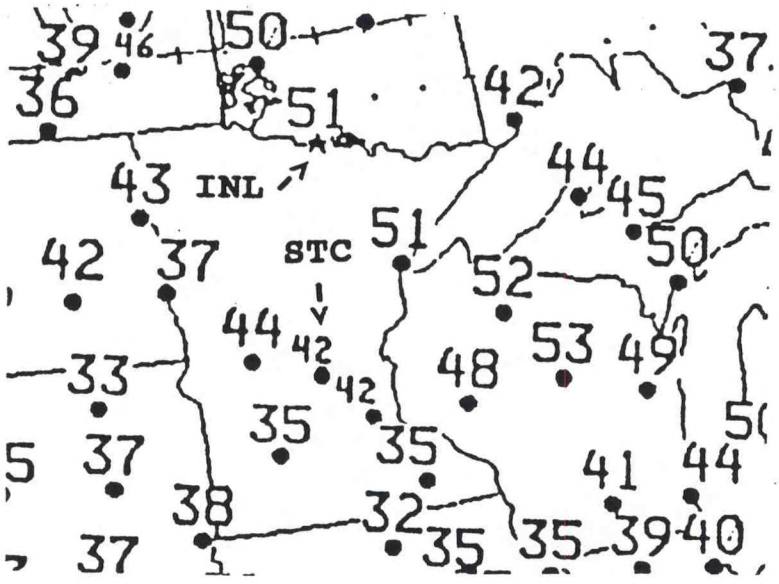

Figure 5. Maximum temperature plot for the 12 hours prior to 0000 UTC 3 March 1993.

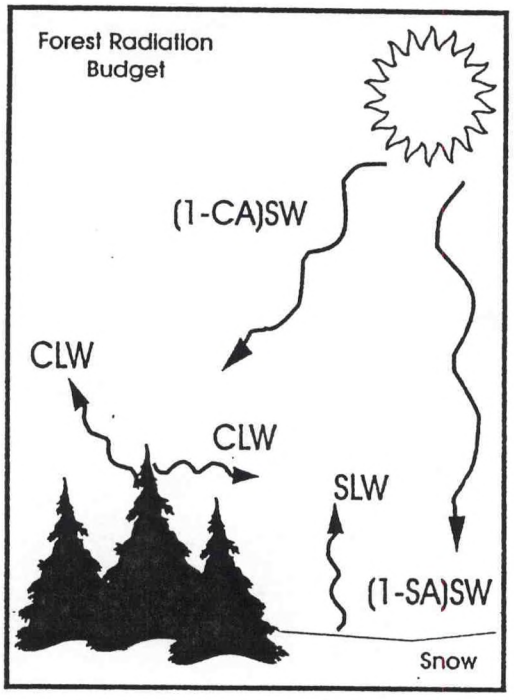

Figure 6. Simplified schematic of the forest radiation budget. CA = Canopy albedo, SA = Snow surface albedo (SA >> CA), CLW = Canopy longwave radiation (CLW > SLW) , SLW = Snow surface, longwave radiation, SW = Shortwave radiation from the sun.

A Winter Storm Forecast: From the Science to the Public

Stephen F. Byrd[1]

1. INTRODUCTION

Meteorologists should have a systematic approach to determining and solving the forecast problem of the day. The funnel forecast concept as described in COMET Computer Based Learning Module number 4 by Snellman et al (1992) is a good foundation for development of a strategy. Because of the increasing amount of real-time data and model output, the forecaster will refine the selection of parameters to examine while moving down the funnel from the hemispheric to the mesoscale.

SCIENTIFIC METHODOLOGY TO FORECASTING

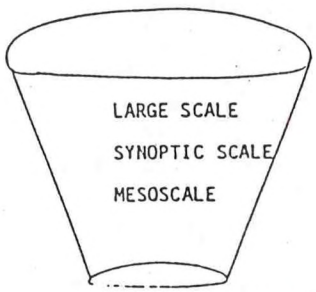

Caution is advised against making quick decisions based on a limited analysis, diagnosis and synthesis. The use of "rules of thumb" can lead to a poor forecast if physics and good conceptual models are not utilized.

The purpose of examining the March 6, 1995 heavy snow event will not be to second guess a forecast, to show a case that was well handled by the model, nor to be a complete case study. The Nested Grid model (NGM) gridded data examined will be confined primarily to initialized fields and 6 hour forecasts. The utility of using some diagnostic and forecast tools of Q-G theory, cross-sections, and real-time data will be emphasized.

Using suggested scientific techniques should not only lead to a better understanding of what is happening in the atmosphere, but should also enable the forecaster to determine more precisely "what the people want to know". Suggestions for communicating the developed forecast information to the public will be presented. What good is the science if the written (or graphically displayed) forecast is confusing to the user?

2. DISCUSSION

Figure 1 shows heavy snow amounts that fell from around 0900 UTC 6 March to about 0600 UTC 7 March in a 290 km (160 nmi) wide band across central Nebraska northeast into northwest Iowa and southeast South Dakota. The 9.8 inches of snowfall at Norfolk Nebraska for March 6 was a 24-hour record amount. This winter storm will be used to illustrate some important aspects of using gridded data (PCGRIDDS) in forecasting.

1. Corresponding author address: Steve F. Byrd, NWSFO Valley, Nebraska.

Integration of several data sources (WSR-88D, Satellite, Profiler, and surface observations) is necessary to refine the zone forecasts in the first period. The integration process will also provide the opportunity to write timely and accurate short term forecasts (nowcasts-NOW) of significant weather changes in the 1 to 3 hour period.

A "traditional" examination of the 6 hour forecast of 500 hPa heights and absolute vorticity in Figure 2 show a progressive positively tilted trough. If a limited forecast is applied the weak 1800 UTC vorticity advection pattern in central and eastern Nebraska could erroneously lead a person to forecast small snow amounts. The sea-level pressure analysis in Figure 3. from the Daily Weather Map showed a southward moving arctic front from extreme northwest Iowa into southwest Nebraska near North Platte at 1200 UTC 6 March 1995. The low pressure in extreme southeast Colorado was predicted by the nested grid model (NGM) to move southward through the day. This solution of the surface low track is reasonable when considering the effect of urography described by Blastin (1993).

The NGM 6 hour predicted field of vertical velocity at 700 hPa (Figure 4) showed an area of upward vertical motion greater than 4 microbars/sec into much of eastern Nebraska by 1800 UTC, thus indicating broad scale synoptic lift is spite of the lack of positive vorticity (PVA) at 500 hPa. The NGM 12 hour quantitative precipitation forecast (QPF) (Figure 5) showed a .30 inch water equivalent contour from near Grand Island Nebraska to Sioux City Iowa. Using the simple 10:1 snow to water equivalent 3 to 4 inches of snow would be expected over much of eastern Nebraska. However Mote (1991) found in a statistical study that the average water equivalent ratio for 25 winters in Nebraska was 14.5:1. Using this mean water equivalent would have suggested that the forecaster boost amounts based on model QPF to 4 to 6 inches of snow. The average water equivalent ratio for the March 6 storm was 13:1 based on the average from a dense cooperative observer network. Determining this ratio empirically from upper air soundings and cross-sections is a suggested area of further study.

The initial 850-700 hPa thickness pattern in Figure 6 suggested ideal thickness values (1550 m to 1520 m) for significant snow across our area of interest. The 6 hour predicted field of the 850-700 thickness suggested an increase in the temperature gradient with time implying frontogenesis.

Quantitative precipitation techniques such as the Magic chart (Chaston 1989) would have implied that up to 6 inches of snow was possible, except that the well-defined surface low required by the technique was missing. The Cook (1980) 200 hPa warm advection technique indicated that up to 10 inches could fall in central and eastern Nebraska. It was noticed in applying this technique that using the actual 200 hPa analysis is preferred to the initialized 200 hPa temperature field. Smoothing of isotherms in the initial 200 hPa gridded data resulted in a 5°C error at both Salt Lake City (SLC) and Omaha (OAX). The actual warm pocket of was -46°C at Salt Lake City at 1200 UTC 6 March 1995. The observed OAX 200 hPa temperature was -66°C. Using the track of the 500 hPa height fall center as a heavy snow predictor (Weber 1979) was of little use here because the main height fall center was well south of Nebraska in north Texas.

3. THE IMPORTANCE OF USING QUASI-GEOSTROPHIC THEORY AND CROSS-SECTIONAL ANALYSIS IN THE FORECAST PROCESS

The Numerical Models are based on the primitive equations as described in Carr (1988) and Haltiner and Williams (1980). The equations are used to generate the model graphics displayed on AFOS. With the wide availability of gridded data in the field, the forecaster can display initial and prognostic fields relating to quasi-geostrophic (QG) theory described extensively in Bluestein (1992).

Dunn (1991) points out that mesoscale process such as conditional symmetric instability, or cases of strong frontogenesis and their associated vertical motion is either poorly resolved or entirely absent in current operational numerical models. Using quasi-geostrophic (QG) theory forecasters can subjectively anticipate precipitation generated by these processes.

QG theory reduces the primitive equations to a simpler set of equations that can be interpreted on operational meteorological charts. The quasi-geostrophic system was developed to be utilized with typical synoptic-scale motions in which a near balance exits between the pressure gradient force and the coriolis force. Hence the term "quasi-geostrophic" has become synonymous with atmospheric dynamics in modern meteorology, and has guided the development of many conceptual models of mid-latitude motion. Some of the most useful quasi-geostrophic (QG) equations are:

- The thermodynamic equation
- The vorticity equation
- The omega equation
- The geopotential tendency equation

For a complete development and explanation of these equations see Chapter 5 of volume I of *Synoptic-Dynamic Meteorology in Midlatitudes* by Howard Bluestein, or Chapter 6 of *An Introduction to Dynamic Meteorology*, 2nd edition, by James Holton. This paper will concentrate on the omega equation.

How does an atmosphere in near geostrophic balance produce vertical motions? Advection of vorticity and (or) temperature by the geostrophic wind disrupt the geostrophic and hydrostatic balances. The atmosphere acts to restore equilibrium by reducing the effects of the advections. The response occurs through the development of vertical motions and convergence/divergence patterns called secondary circulations. For an example see Durran and Snellman (1987). Think about the many ways that nature tries to remain in various types of balance. After your hot shower you open the bathroom door and you would find a circulation through the door opening attempting to reestablish thermal and moisture balance in that area of the house. Of course this is an oversimplified analogy since your house is not spinning on its foundation and your bathroom is not moving.

There are some assumptions incorporated into QG theory. It is important that forecasters are aware of these assumptions to properly use QG diagnostics as a forecast tool. It is assumed that the static stability (σ) is constant and that meteorological parameters are advected by the geostrophic wind - not the total wind (geostrophic + ageostrophic components). Diabatic and terrain effects are not considered. Both vertical advection and friction are neglected. In addition, it is assumed that the rotational part of the wind remains in geostrophic balance. Keep these assumptions in mind when using QG diagnostics in forecasting vertical motion and cyclogenesis. The release of latent heat in widespread precipitation before a developing cyclone is a significant diabatic effect. Resulting diabatic heat sources will increase thickness values, build constant pressure heights ahead of the developing cyclone, increasing warm advection, moisture advection and upward vertical motion. The result is a deepening low pressure system and generally a self development process involving cyclogenesis. Recognition of these effects will help us to better use QG theory and to better interpret predicted model evolution.

The quasi geostrophic-omega equation is shown below from Bluestein (1992):

$$(\nabla_p^2 + \frac{f_0^2}{\sigma}\frac{\partial^2}{\partial p^2})\omega = \frac{f_0}{\sigma}\frac{\partial}{\partial p}[-v_g \cdot \nabla_p(\zeta_g + f)] - \frac{R}{\sigma p}\nabla_p^2(-v_g \cdot \nabla_p T). \quad (1)$$

(A) (B) (C)

where ω is the vertical motion (dp/dt) in the left side of the equation. Term A (the three dimensional "Laplacian" of ω is proportional to -ω. Term B is the change in height (pressure) of the absolute vorticity advection. Term C is the two dimensional "Laplacian" of the temperature advection. Temperature "T" can be written in terms of the thickness of a layer ($-\partial\Phi/\partial p$). Thus using UA Diagnostics - Foster (1988), and PCGRIDDS - Petersen (1992) terms B and C can be displayed and evaluated to give the forecaster an idea of where upward forcing ($\omega<0$) is expected. Thus favored areas of upward vertical motion occur in association with warm advection maxima, and with increasing cyclonic vorticity advection with height. A problem using this solution to the ω equation is that attempting to determine ω for identical systems, moving at different speeds results in different values in the forcing terms (not Galilean invariant). Evaluation of vertical forcing using the two graphic fields can be confusing when they oppose each other.

Trenberth (1978) presented a solution to the ω equation in which -ω is proportional to the advection of vorticity by the thermal wind + terms involving deformation of the wind field. The isothermal vorticity advection can be viewed easily using gridded data but the deformation terms can be significant, especially in cases of frontogenesis.

A. Q Vectors

Rather than weighing the separate effects of differential vorticity advection and the Laplacian of the thermal advection Hoskins et al. (1978) have suggested the using Q-vectors defined as:

$$Q = [\frac{\partial V_g}{\partial x}\cdot\nabla\frac{\partial \phi}{\partial p}, \frac{\partial V_g}{\partial y}\cdot\nabla\frac{\partial \phi}{\partial p}] \quad (2)$$

where the Q vector has the x and y components as showed. It is essentially the dot product of the gradient of the geostrophic wind and the horizontal gradient of the layer thickness or mean temperature. The Q vector is equal to the rate of change of the potential temperature gradient that would develop in a fluid parcel moving with the geostrophic wind, if the vertical velocity were zero. It is convenient to visualize the Q vector as proportional to the horizontal ageostrophic wind in the lower branch of a circulation that developed to restore the thermal wind balance. It represents a complete solution to the QG-ω equation (with all of the assumptions) in the form from Nuss and Titley (1994):

$$(\sigma\nabla^2 + f_0^2\frac{\partial^2}{\partial p^2})\omega = -2h\nabla_p \cdot Q \quad (3)$$

Where the static stability parameter $\sigma = -(\alpha/\Theta)\partial\Theta/\partial p$, and $h = (R/p)(p/p_0)^{\kappa}$, where R is the gas constant, p pressure, ρ is the density of the air, and $\kappa = R/C_p$ (specific heat at a constant pressure). Since $\nabla^2\omega \propto -\omega$, and $\nabla^2\omega \propto -\nabla\bullet\mathbf{Q}$, then $\omega \propto \nabla\bullet\mathbf{Q}$ (the divergence of Q). Converging Q vectors are associated with upward vertical motion ($\omega<0$) and diverging Q vectors are associated sinking motion ($\omega>0$).

Figure 7 shows an initial 1200 UTC 6 March 1995 and 6 hour forecast of the 700 hPa to 500 hPa layer divergence of Q. Areas of converging Q vectors indicate favorable upward vertical motion. Other layers of divergence of Q should be examined and compared with both the model derived ω, and the vertical motion derived from isentropic lift. Figure 8 shows the initial 1200 UTC 850-700 hPa layer divergence of Q vectors with the mean layer potential temperature overlaid.

The static stability parameter σ shows up in different places in various forms of the QG-ω equation. It is easier to lift air with low static stability than air with high static stability. The static stability parameter $\sigma \propto -\partial\theta/\partial p$ is also modified by lifting. To get a complete picture of the forcing function in a layer $F_Q = 2h\nabla\bullet\mathbf{Q}$ Tapp (1988) has suggested dividing F_Q the layer static stability σ. A command file that divides the layer divergence of Q by $\Delta\Theta/\Delta p$ (an approximation of the static stability - the change in potential temperature with the vertical pressure coordinate) is used at NWSFO Omaha. While the magnitude of the "forcing" is changed, little change in the location of the area of upward vertical motion is indicated (figure not shown).

B. Q-Vectors and Frontogenesis

Frontogenesis are the intensification of the thermal gradient in the frontal zone, and is also associated with a direct thermal circulation (Shea and Przybylinski 1984). The mean potential temperature field may be overlaid with the layer Q/div-Q using PCGRIDDS. The orientation of the Q-vectors with reference to the thermal field enables the forecaster to gain some further insight into Q-G forcing. If converging Q-vectors are parallel to layer mean potential temperature (or thickness) then the upward forcing is typical before approaching short waves. Figure 8 shows a diagnosis of the 850 - 700 hPa layer Q-vectors and the layer average potential temperature pattern. Notice that the Q vectors are aligned at an angle to the mean thermal pattern across most of Nebraska at 1200 UTC 6 March 1995. When Q-vectors are directed at an angle to the mean thermal field then the normal component of layer Q can change the magnitude of the thermal field. The result can be either frontogenesis or frontolysis. Bluestein (1992) shows that of the frontogenetical function, $D/Dt|\nabla_p T| \propto (\nabla_p T\bullet\mathbf{Q})$. If Q-vectors are directed from cold air to warm air ($\nabla_p T\bullet\mathbf{Q} >0$) then the magnitude of the temperature gradient is increasing. Frontogenesis are shown in Figure 8. As a consequence of this frontogenetical pattern there is lifting in the warm air and sinking in the cold air - a thermally direct circulation. If Q-vectors are directed from warm air to cold air ($\nabla_p T\bullet\mathbf{Q}<0$), then the magnitude of the temperature gradient is decreasing and the pattern is frontolytical, inducing lifting in the cold air and sinking in the warm air - a thermally indirect circulation. These secondary circulations result from the atmosphere responding to restore the thermal wind balance.

The total Q vector at a level can be expressed as $\mathbf{Q} = \mathbf{Qs} + \mathbf{Qn}$, where **Qs** is the "streamwise" component along isotherms, and **Qn** is the component normal to the isotherms. Just as the Q vector can be split into components along and normal isotherms, so also can forcing F_Q. Thus, $F_Q = \nabla_p\bullet\mathbf{Q} = F_{Qs}+F_{Qn} = \nabla_p\bullet\mathbf{Qs}+\nabla_p\bullet\mathbf{Qn}$. F_{Qn}, the frontogenetical forcing is described by Sawyer (1956) and Eliassen (1962).

Figures 9 shows the initial 850 - 700 hPa layer **Qs** and **Qn** valid at 1200 UTC 6 March 1995. The Divergence of **Qs** is and **Qn** is also shown. Notice in Figure 14 that a direct circulation is indicated in eastern Nebraska and western Iowa, and southwest Kansas because of frontogenetical forcing. With sufficient moisture mesoscale single banded type precipitation parallel to the thickness field is

often associated with areas of convergence of Qn, while the more general widespread precipitation is associated with convergence of Qs. Keyser et al (1988) point out that convergence of Qs results in rising branches of the flow in the direction of the isotherms, and in that configuration any circulation can only rotate $\nabla\theta$ - it cannot change the magnitude of the gradient. The movement of short-wavelength troughs and ridges is reflected in the quantity $\nabla \bullet Q_s$. In the snow storm of March 6, 1995 figures showed that both divergence of Qs and Qn was present. However, the divergence of Qn dominated especially in the 850 to 700 hPa layers. It is advisable to examine Q vectors and Q vector divergence in several layers to evaluate forcing through the troposphere. Notice the significant frontogenetical 700 - 500 hPa forcing shown across the heavy snow area in the 6 hour Qn/divergence of Qn shown in Figure 10. A weakness of quasi geostrophic frontogenesis is that the process is slow in comparison to what is typically observed (since the total wind is not used - no ageostrophic component). Frontogenetical effects due to differential heating or the release of latent heat are not included in QG frontogenesis. These effects will need to be evaluated independently by the forecaster.

Atmospheric stability will of course be important in determining the character (convective vs stratiform) of the precipitation. The forecaster should examine lapse rates in layers that Q and $\nabla \bullet Q$ are evaluated. The stronger the static stability, the less the vertical displacement through a layer a layer of converging Q vectors.

There are alternate ways to viewing frontogenetical forcing rather than Qn. Layer scalar frontogenesis command files have been developed by Eric Thaler (1995), SOO NWSFO Denver that include frontogenetical forcing by the total wind (geostrophic + ageostrophic). Often the ageostrophic wind components contribute significantly to frontogenesis. Thaler also developed command files for the Petterssen (1936) two-dimensional frontogenesis function:

$$D/Dt\ |\nabla\Theta| = -1/2\ |\nabla\Theta|\ (D - E\cos 2\beta) \qquad (4)$$

where Θ is the potential temperature, D is the divergence of the total wind, E is the total deformation, and β is the angle between the axis of dilatation and the isentropes. The frontogenesis function quantifies the amount of change in the potential temperature following air parcel motion. Consider the function in a reference frame moving along with the front. Figure 11 shows the 6 hour forecasts of 700 hPa - 500 hPa layer frontogenesis in the Plains using Petterssen's equation.

The significant frontogenetical forcing across south central Nebraska into northwest Iowa through 1800 UTC enables the forecaster to anticipate (or recognize) the development of a mesoscale band of heavier snow. Satellite imagery and the WSR-88D can be used to monitor the location and evolution of this mesoscale snow band. Figure 12 shows infrared (IR) imagery at both 1200 UTC and 1800 UTC. Note that colder cloud tops were advancing northeast in the southwest flow aloft and that banded colder tops (-52°C to -58°C) evolved from south central Nebraska into west central Iowa by 1800 UTC. These satellite images suggest both an increase in large scale lift toward 1800 UTC as predicted in the Qs fields. In addition there was enhancement of the existing frontogenetic band Qn between 1200 UTC and 1800 UTC.

Studies by Moore and Kaster (1993) and Shields et al. (1991) suggest that the strongest and widest precipitation bands in winter storms occur in strong frontogenetical environments.

4. THE USE OF CROSS-SECTIONS AND APPLICATION OF CLOUD PHYSICS

The use of cross-sections in weather diagnosis and forecasting enhances our three dimensional views of what is occurring and what is expected to occur. It is an area that has opened up to the operational meteorologist with the capability of manipulating gridded data sets.

It is important to examine cross-sections normal to jet streak patterns that are (or will be) affecting the area of concern (AOC). Barnes and Coleman (1994) say that air circulates not only in plains transverse to a jet axis, but also along the axis. Complexities such as interacting jets limit the general application of the conceptual jet-streak model Beebe and Bates (1955) and the correct visualization of the associated vertical motions. Coupled jet-streak circulations can be diagnosed using cross-sections. These coupled transverse circulations have been found significant in producing enhanced mesoscale bands of heavy snow in studies by Uccellini and Kocin (1987) and Hakim and Uccellini (1992).

Figure 13 shows the predicted 1800 UTC cross-section taken in the right entrance quadrant of the jet. Note the contribution of the jet to a transverse direct circulation that enhanced upward vertical motion, and frontogenesis across eastern Nebraska, our area of concern (AOC). It is useful to use cross-sectional analysis and forecasts to locate the level of non-divergence (LND) and note where the maximum vertical velocity occurs. Figure 14 shows 6 hour forecast cross-sections across eastern Nebraska of both divergence of the total wind and the vertical motions through the -12°C to -18°C layer, along with relative humidity. Auer and White (1983) have discovered that heavy snowfall episodes are frequent when the level of maximum vertical velocity (near the LND) is coincident with saturation in the temperature layer between -13°C and -17°C. This is not surprising since a large amount of saturated air is moving through the layer in which dendritic snow crystal growth is at a maximum. Growth by diffusion is prolific in the layer because the difference between the saturation vapor pressure over ice and water is at a maximum between -12°C and -18°C.

Cross-sections can be helpful when using Garcia's (1994) snow amount forecast technique with short range model forecast gridded data. Cross-sections taken from the warm moist inflow source up into the forecast area show the level of best moisture advection. The forecaster can determine the best isentropic level to use in estimating expected snow amounts, since moisture advection can be viewed in three dimensions. Note the forecast advection of moisture along isentropic surfaces shown in the cross-section in Figure 15 from Emporia, Kansas (EMP), north to Norfolk, Nebraska (OFK),

According to Snook (1992) frontogentical forcing can explain the existence of a single band of precipitation. However, multiple bands of precipitation are often caused by convective instability or conditional symmetric instability (CSI). Frontogenetical forcing can help actuate CSI. As stated by Moore and Lambert (1993), in convectively stable regions it is possible to develop elevated convection in an area of weak symmetric instability with significant frontogenetic forcing.

Decreasing equivalent potential temperature (Θ_e) with height is called either potential instability or convective instability but does not necessarily imply conditional instability. Potential instability can be easily diagnosed on a cross-sectional analysis by identifying areas where Θ_e "folds over". Emannuel (1994) points out that the instability is potential in this sense: was the entire air mass lifted bodily until it became saturated, then the upward decrease of Θ_e implies instability. Note however upward forcing through the convectively unstable layer is necessary. Potential instability was not present in the March 6, 1995 snow event, but CSI was.

A cross-section taken normally to the thermal wind in a layer is useful in determining whether CSI or convective instability exists or is forecast. CSI like potential instability requires large scale

forcing to initiate slantwise convection that we have shown existed. Surfaces of Θ_e and M_g (geostrophic absolute momentum) as defined by Emannuel (1994) are overlaid normal to the 1000-500 hPa thickness pattern. CSI is located in areas where M_g surfaces are flatter than the Θ_e surfaces. There should be no convective instability as that condition would support upright rather than slantwise convection. Upright convection would dominate in a potentially unstable environment because of the faster growth rate when compared with slantwise convection. CSI requires near saturated conditions, i.e., relative humidity (RH) $\geq$ 80%. Figure 16 shows the 6 hour forecasts of M_g, Θ_e and the relative humidity. Note that near dynamically neutral conditions or the existence of CSI was forecast to exist at 1800 UTC in the AOC. While the model cannot tell the forecaster the specific locations of a given CSI band, it is useful to assess the potential of these bands of heavier convective snow embedded in a synoptic scale snow area. Both the WSR-88D and visible satellite imagery are useful in displaying convective bands. It best to not be surprised by the thief in the night. An excellent summary of several mesoscale mechanisms that produce enhanced banded snowfall is described in Funk et al (1994).

5. THE ZONE FORECAST PRODUCT

The main forecast demands for the mid-shift early March 6, 1995 were to assure that the ongoing forecast was valid. The importance of an accurate diagnosis by the previous shift was essential. March 6, 1995 observations from Norfolk Nebraska showed snow (1 mile visibility) after 0800 UTC. The visibility fell to ½ mile with an inch of snow from 0900 UTC to 1000 UTC. An inch an hour accumulated between 1200 UTC and 1800 UTC. The frontogenetic band remained quasi stationary throughout the period. The WSR-88D can be used to identify the location of the coarse PCGRIDDS predicted frontogenetic band. Figures 17 shows WSR-88D highly sensitive volume coverage patterns (VCP) 32 reflectivities. Reflectivity values of 24 to 28 dBz 40 to 45 km wide were displayed from west southwest to east northeast across OFK by 0832 UTC, thus helping the forecaster verify the frontogenetic process on the morning of March 6, 1995. Isentropic lift was also causing snow south to Grand Island and Hebron.

Recognition by the forecaster of the cause of the mesoscale band was essential to a well worded forecast, which transformed knowledge into a well-worded zone forecast product (ZFP). What good is use of the science if the final product is poorly written, or not informative? The WSR-88D and observations made it easier to issue the winter storm warning where it was needed when the anticipated frontogenetical mesoscale band developed.

For the 415 A.M. zone forecasts use of the gridded forecast data as described in this paper enabled the forecaster to determine the trend of the observed frontogenetical band. Also the recognition of forcing mechanisms such as CSI required informing the public of some heavier amounts than showed by the larger scale forcing. Suggestions for wording the zone forecast based on integrated real-time data and model gridded forecast data are shown below:

- Arrange zones (counties) into as many representative groups as is necessary to precisely describe significant differences.
- Let the zone grouping be time and event driven rather than convenience based.
- Avoid the use of Probabilities of Precipitation (POPS) in the first period when you have a high degree of confidence. You may use a temporal term such as OCCASIONAL SNOW. OR...LIGHT SNOW BEGINNING AFTER 10 AM...
- Use as few hedge words as the situation allows. Be bold when writing the text. Competent diagnosis and application of proven scientific techniques allow us to be more specific in area and time.

- Address the problem presented by mesoscale bands with more specific areal and temporal forecasts based on the frontogenetic band, however allow for wider ranges of amounts with the possibility of CSI.
- Explain what you know that will be useful and understandable to the users in your Winter Storm Warning (WSW) or Special Weather Statements (SPS). Advertise your short term forecasts.
- Use beginning and ending times of significant events. While these can be most specifically addressed in a short term forecast, a range of times can be used in the ZFP.
- Use total amounts of snow for an ongoing event in the zones.

An example for the Norfolk Nebraska zone group:

> ...WINTER STORM WARNING TODAY...
> .TODAY...HEAVY SNOW DIMINISHING AFTER 10 AM WITH 8 TO 12 INCH TOTAL SNOW ACCUMULATIONS. WINDY WITH SLOWLY FALLING TEMPERATURES TO 5 TO 10 ABOVE BY 4 PM. NORTH WIND 15 TO 25 MPH WILL INCREASE TO 20 TO 30 MPH THIS AFTERNOON CAUSING BLOWING AND DRIFTING SNOW.

6. THE SHORT TERM FORECAST - NOWCAST (NOW)

The short term forecast (STF) program began the day of the March 6, 1995 storm in Nebraska. Thus, WSFO Omaha personnel started a learning and growing experience. The purpose of the STF is to refine the zone forecast both in time and area during a 1 to 3 hour period when precipitation is occurring. During a snow event such as this winter storm, it is important to let the public know in precise and understandable language the information they want and need to know.

Well-written Nowcasts should be based on a foundation of the synoptic and mesoscale pattern. Science and the communication skills must be integrated. When this is done, the forecaster can maximize the short term forecast tools such as surface observations (both human and automated), WSR-88D, satellite imagery and wind profilers. The mesoscale analysis and prediction system (MAPS) products can be generated at H+25 for those on the frame relay network (FRN). Figure 18 (1300 UTC to 1600 UTC) showed the increase in areal coverage in snow across east central and southeast Nebraska as the snow became more banded in appearance from Lincoln (LNK) to Omaha (OMA). The WSR-88D also showed that the people in the OFK area could continue to expect heavy snow. This showed that processes suggested by the gridded data and anticipated in earlier discussions were at work. Large scale lift was increased and frontogenesis continued to cause a heavy snow band.

Forecast layer Q vectors showed southward shifting frontogenesis in the lower layers as deduced from viewing Q vector components and divergence of these components **Qs** and **Qn**. The multiple banding in Figure 18 parallel to the thermal pattern suggested CSI had resulted in slantwise convection.

When viewing WSR-88D reflectivities indicating heavy snow the VAD wind profiler data should be examined. Craven (1993) points out that because of winds in the layer through which the snow is falling, the heaviest snow can be displaced up to 20 miles. Thus, the heaviest snow may not always be below the highest reflectivity.

The wind profile network is very useful in mesoscale forecasting. Detection of the passage of troughs, trends in low level winds, and detection of thermal advection are some of the uses. Snook (1992) showed that observing changing vertical shear patterns can show the increasing favorability

of CSI (increasing speed shear with height) or the end of slantwise convection (decreasing vertical wind shear).

A single profiler site can show whether the depth of overrunning cold air is deepening or becoming more shallow. This could be important in determining precipitation type (ZR vs. S). Observing low level winds from two profiler sites with a North South frontal boundary (such as with NLG and FBY in northeast and southeast Nebraska respectively) can show the change in frontal tilt, and thus frontogenesis can be inferred.

Use of these tools enable us to better determine what is happening in the short term forecast periods. Some suggestions for writing the NOWCAST are given:

- Use brief headline as an eye catcher with the "key" information
- Avoid repetition of the zone forecast. Be specific!
- Refine zone forecast information. For example - zone:

> TODAY...HEAVY SNOW WITH ACCUMULATIONS 8 TO 12 INCHES...DIMINISHING TO FLURRIES LATE THIS AFTERNOON.
>
> STF - HEAVY SNOW WILL CONTINUE TO ACCUMULATE AN INCH PER HOUR THROUGH NOON ACROSS THE AREA...ESPECIALLY FROM MADISON AND NORFOLK TO WAYNE. ALTHOUGH SNOWFALL WILL DIMINISH DURING THE AFTERNOON...SNOW AND BLOWING SNOW WILL CONTINUE TO CAUSE VISIBILITIES FROM 1/4 TO ½ MILE IN NEAR BLIZZARD CONDITIONS. A DANGEROUS WINDCHILL OF 35 BELOW IS EXPECTED.

- Group as best meets the public needs. This could be uniform weather driven, but could overlap weather driven zones to call attention to important changes in CWA eg. a rain/freezing rain boundary.
- Consider your customers, the NOAA Weather Radio broadcast area, and local media users.
- Do not use the STF as a substitute for a needed zone forecast update, unless a condition described is expected to be very localized (one county or part of a county) or very short term (1 hour).
- The STF is not a radar summary and should not be written as a substitute.
- Give the users an idea of expected rainfall or snowfall rates using the WSR-88D.

An example of an STF for the Omaha and Lincoln areas written at 1400 UTC 6 March 1995:

> NOW...
> ...SNOW EXPANDING AND INCREASING...
> SNOWFALL WILL INCREASE ALONG INTERSTATE-80 FROM OMAHA TO LINCOLN THROUGH 10 AM. SNOWFALL RATES WILL BE VARIABLE WITH SOME LOCATIONS RECEIVING ONE INCH PER HOUR. VISIBILITIES WILL RANGE FROM 2 MILES TO AS LOW AS ½ MILE. THE TEMPERATURE WILL FALL SLOWLY TO AROUND 20 BY 10 AM AS WINDS SHIFT TO THE NORTH AND INCREASE TO 15 TO 25 MPH.

7. SUMMARY AND FUTURE CONSIDERATIONS

It is important to develop a forecast process that leads the meteorologist to a scientifically based solution of expected weather conditions, especially in the first 12 to 24 hours. Use of the funnel forecast technique, the applications of QG theory, and the use of cross-sectional analysis are important to a successful forecast.

We must use our capabilities with new data sets to improve our confidence and understanding of the atmospheric processes at work. Improved model resolution is becoming available as MAPS/Rapid update cycle (RUC) data on the FRN, and in the future the meso-eta model with 29 km resolutions. These models must not be used blindly but must be integrated with automated and human surface observations, satellite imagery, WSR-88D data, and wind profiler data.

The increase in the abundance of real-time data and gridded numerical forecast data from several models can be overwhelming to the point that the forecaster has little time to devote to the product. Worse yet, he or she becomes unable to resolve various model differences and writes a forecast as vague as any pre-1980 zone forecast product.

Since we are in a revolutionary period in the weather services, all the answers cannot be arrived at this moment. However, we can set the direction to be one of thorough scientific diagnosis and recognition. Look for the synoptic patterns that drive mesoscale features, then work to become expert mesoscale forecasters. We need to maximize real-time data to refine model trends without attempting to look at every parameter from each model and must allow time for the composition of improved and more specific public products concentrating on the zero hour to 24 hour forecast.

8. ACKNOWLEDGEMENTS

I wish to thank Ralph Meigas, NCDC for making satellite imagery available. Thanks also to Eric Thaler, Paul Janish and Steve Zubrick, whose PCGRIDDS command files were utilized. I wish to express appreciation to Bill Gavers, lead forecaster at WSFO Omaha, who proofread this manuscript. Thanks also to the staff at Central Region Scientific Services Division, especially Preston Leftwich and Deborah White for their help.

9. REFERENCES

Barnes, S.L., and B.R. Coleman, 1994: Diagnosing an Operational Numerical Model Using Q-vector and Potential Vorticity Concepts, *Weather and Forecasting*, **9**, pp 85-102.

Beebe, R.G. and F.C. Bates, 1955: A mechanism for releasing convective instability. *Mon. Wea. Rev.* **83**, pp1-10.

Bluestein, H.B., 1992: *Synoptic-Dynamic Meteorology in Midlatitudes*, Volume I, Principles of Kinematics and Dynamics, Oxford University Press Inc., pp 285-296.

_____, 1993: *Synoptic-Dynamic Meteorology in Midlatitudes*, Volume II, Observations and Theory of Weather Systems, Oxford University Press Inc.

Chaston, P.R., 1989: The magic chart for forecasting snow amounts, *Natl. Wea. Digest* **14**, pp 20-23.

Carr, F.H, 1988: Introduction to Numerical Weather Prediction Models at the National Meteorological Center.

Craven, J.P., 1993: A quick glance at reflectivities may be misleading. Central Region WSR-88D Operational Note 93-04. DOC, NOAA, NWS, Central Region, Scientific Services Division, Kansas City, MO.

Dunn, L.B., 1991: Evaluation of vertical motion: Past, present and future. *Wea. and Forecasting*, **6**, pp 65-75.

Durran, D.R., and L.W. Snellman, 1987: The Diagnosis of Synoptic Scale Vertical Motion in an Operational Environment, *Wea. and Forecasting*, **2**, pp 17-32.

Eliassen, A., 1962: On the vertical circulations in frontal zones, *Geofys. Publ..*, **24**, pp 147-160.

Emannuel, K.A. 1994, *Atmospheric Convection*, Oxford University Press, p 185, and pp 392-417.

Foster, M.P., 1988: Upper air analysis and quasi-geostrophic diagnosis for personal computers. DOC, NOAA, NWS, Southern Region, Scientific Services Division., Fort Worth, TX.

Funk, T.W., C.W. Hayes, M.B. Scholz, and K. A. Kostura, 1994: Vertical motion forcing mechanisms responsible for the production of a mesoscale very heavy snow band. *Preprint 14th Conf. on Wea. Analysis and Forecasting*, AMS (Boston), Dallas, TX, pp 176-181.

Garcia, C., Jr., 1994: Forecasting snowfall using mixing ratios on an isentropic surface - an empirical study. *NOAA Tech. Memo.* NWS-CR-105. DOC, NOAA, NWS, Central Region, Scientific Services Division, Kansas City, MO.

Hakim, G.J., and L.W. Uccellini, 1992: Diagnosed coupled jet-streak circulations for a plains snow band from the operational nested grid model, *Wea. and Forecasting* **7**, pp 26-48.

Holton, J.R., 1979: *An Introduction to Dynamic Meteorology*, Second Edition, Academic Press, pp 119-142.

Hoskins, B.J., I. Draghici, and H.C. Davies, 1978: A New Look at the ω-Equation, *Quart. J. Roy. Meteor. Soc.* 104, 31-38.

Keyser, D., M.J. Reeder, and R.J. Reed, 1988: A Generalization of Petterssen's Frontogenesis Function and its Relation to the Forcing of Vertical Motion, *Mon. Wea. Rev.*, **120**, pp 698-730.

Moore, J.T. and T.E. Lambert, 1993: The use of equivalent potential vorticity to diagnose regions of conditional symmetric instability, *Weather and Forecasting* **8**, number 3, pp 512-517.

Mote, T.C., 1991: A statistical investigation of atmospheric thermodynamics and kinematics associated with the intensity of snowfall at Omaha, NE, A Thesis under the supervision of Mark R. Anderson Ph.D., University of Nebraska, Lincoln, NE.

Nuss W.A., and D W. Titley, 1994: Diagnosis of oceanic cyclogenesis using surfaced-based Q Vectors. *Wea. and Forecasting* **9**, p 137.

Petersen, R.A., 1992: PC Gridded Interactive Display and Diagnostic System, NOAA-NMC, Camp Springs, MD.

Petterssen, S., 1956: *Weather Analysis and Forecasting,* **Volume I.** McGraw-Hill Book Co. Inc. pp 189-209.

Sawyer, J.S., 1956: The vertical circulation at meteorological fronts and its relation to frontogenesis, *Proc. Roy. Soc. London,* **A234**. pp 346-362.

Shields, M.T., R.M. Rauber, and M.K. Ramanmurthy, 1991: Dynamical forcing and mesoscale organization of precipitation bands in a Midwest winter cyclonic storm. *Mon. Wea. Rev.* **119,** pp 936-964.

Shea, T.J., and R.W. Przybylinski, 1994: Forecasting the northern extent of significant snowfall in a major winter storm: An operational forecast problem. *Preprints 14th Conf. on Wea. Analysis and Forecasting,* AMS, (Boston) Dallas, TX, pp 335-342.

Snellman L., E. Thaler and COMET Staff, 1992: Forecast Process. COMET CBL Module 4, Boulder, CO

Snook, J.S., 1992: Current techniques for real-time evaluation of conditional symmetric instability. *Wea. and Forecasting* 7, 430-439.

Trenberth, K.E., 1978: On Interpretation of the Diagnostic Quasi-geostrophic Omega Equation, *Mon. Wea. Rev.* **106,** pp 131-137.

Uccellini, L.W., and P.J. Kocin, 1987: The interaction of jet-streak circulations along the East Coast of the United States, *Wea. and Forecasting* 2, pp 289-308.

Weber, E.M., 1979: Major Midwest snowstorms. *3WW Tech. Note* 79-2, 3rd Wea. Wing, Offutt AFB, NE.

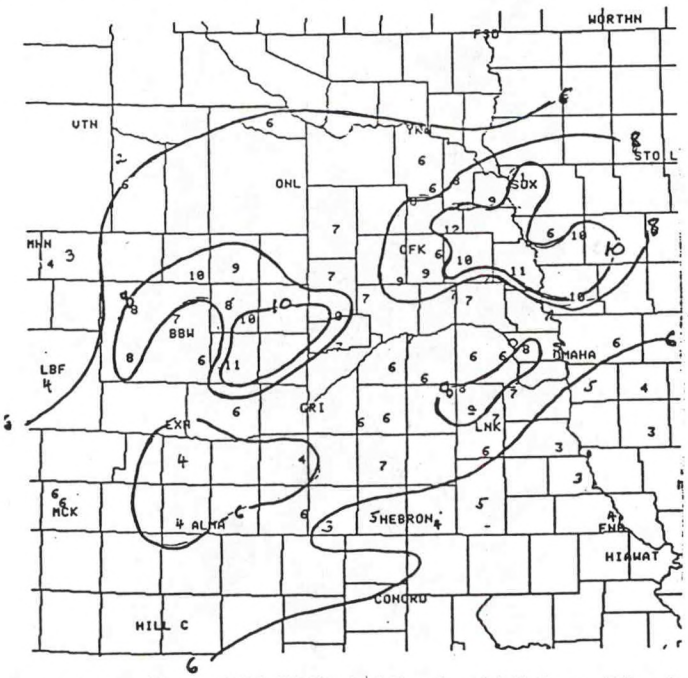

Figure 1. Snowfall amounts ending 1200 UTC 7 March 1995 from March 6-7, 1995 storm across eastern and central Nebraska and adjacent areas.

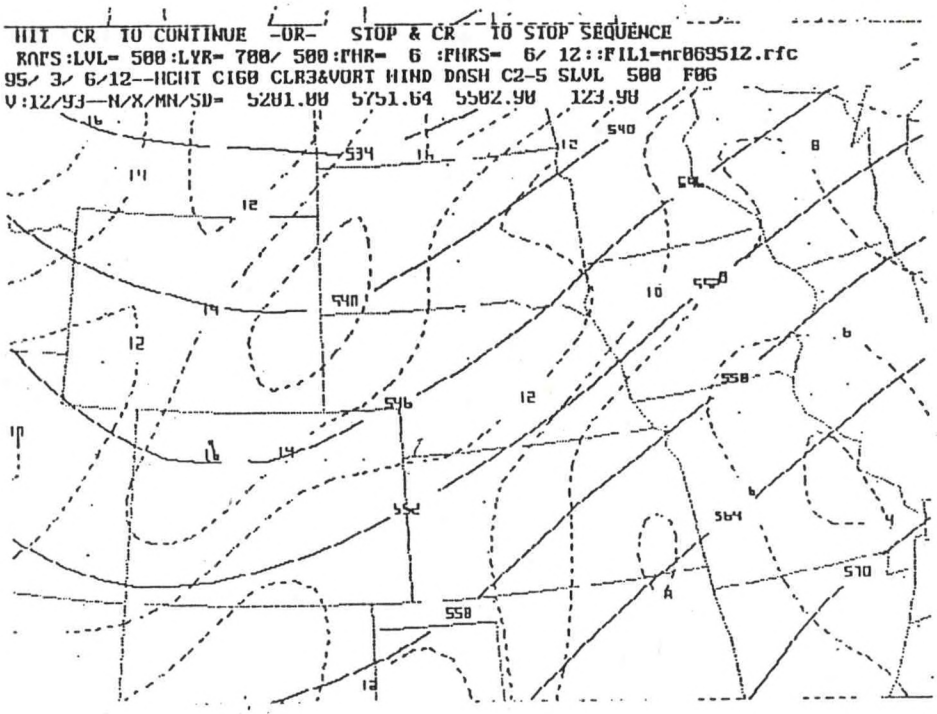

Figure 2. NGM Model 6 hour forecast of 500 hPa heights in decimeters (solid), and vorticity 10^{-4}sec^{-1} (dashed).

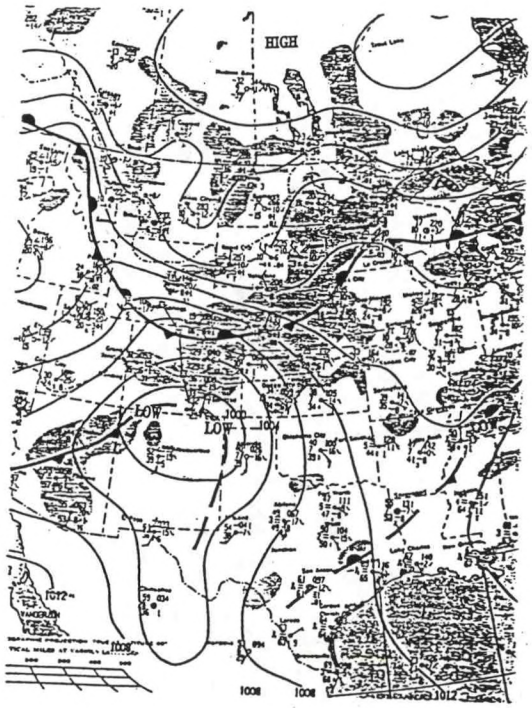

Figure 3. Sea level pressure plot and analysis from the 1200 UTC 6 March 1995 Daily Weather Map.

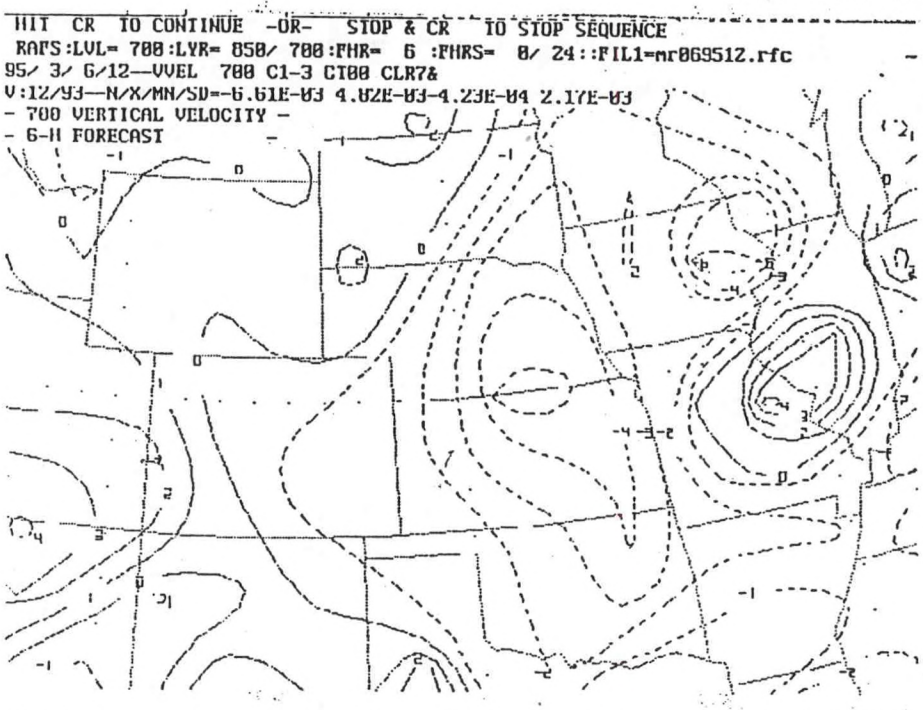

Figure 4. NGM 6 hour forecast of vertical velocity in μbars/sec valid at 1800 UTC 6 March 1995. Dashed lines indicate upward vertical motion.

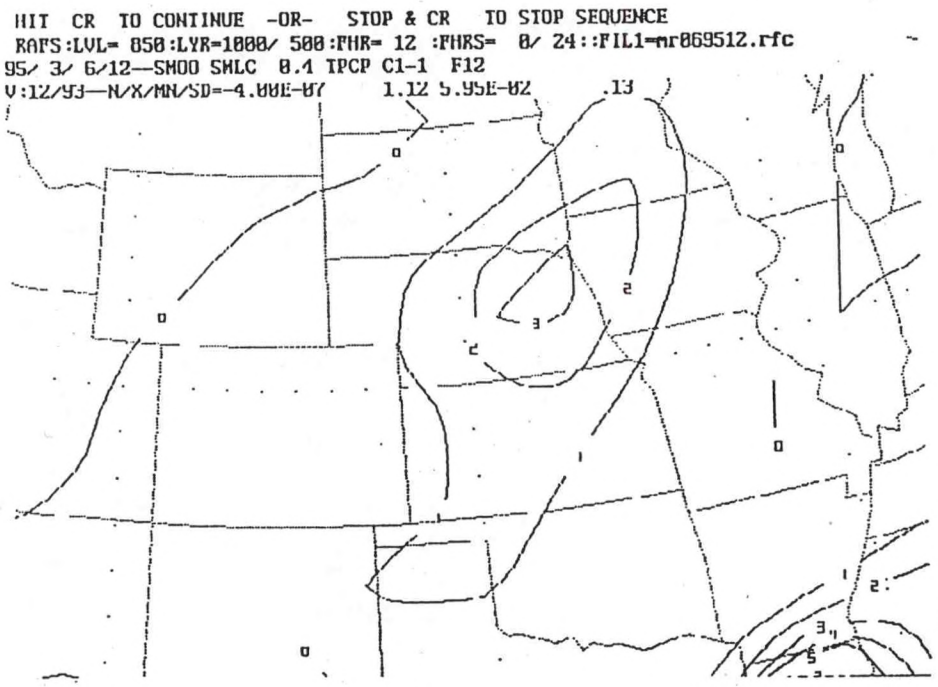

Figure 5. NGM 12 hour water equivalent precipitation forecast in tenths of an inch.

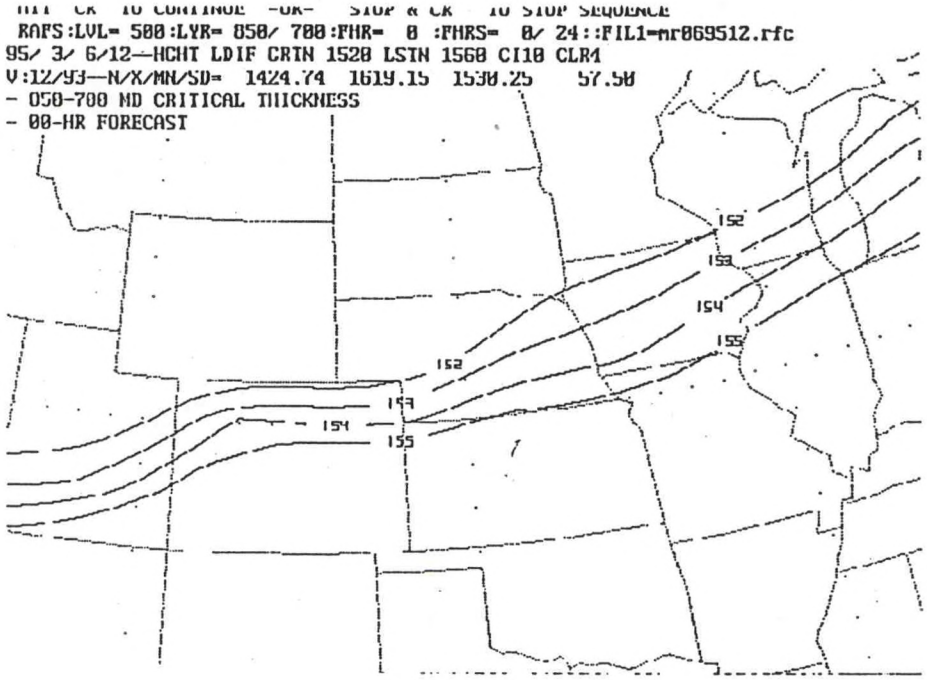

Figure 6. Thickness for the 850-700 hPa layer from the initial gridded NGM data at 1200 UTC 6 March 1995.

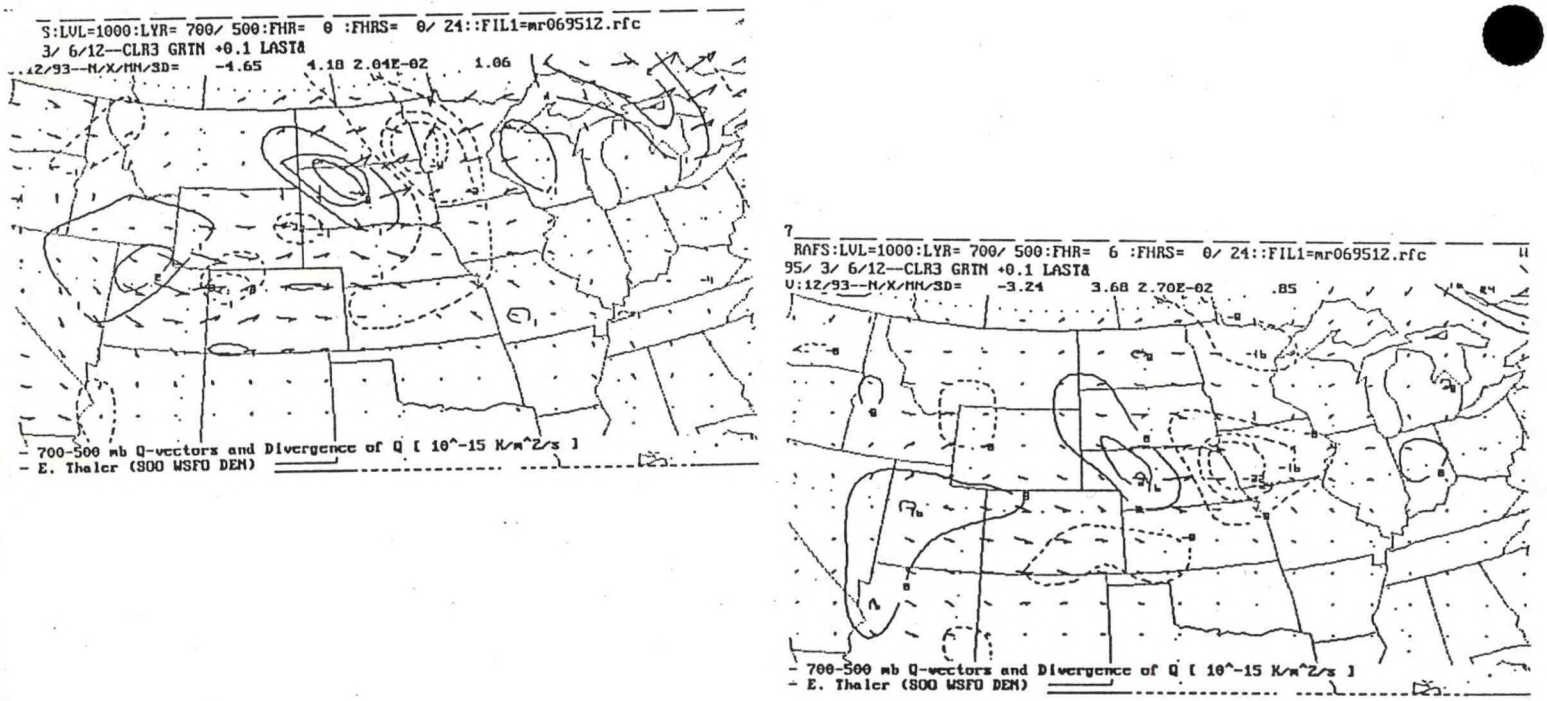

Figure 7. Initial (a) and 6 hour (b) NGM forecast from the 1200 UTC NGM of 700 - 500 hPa layer Q vectors and layer divergence of Q (10^{-15}°K/m^2 sec^{-1}. Areas of Q vector convergence are dashed and indicate upward forcing.

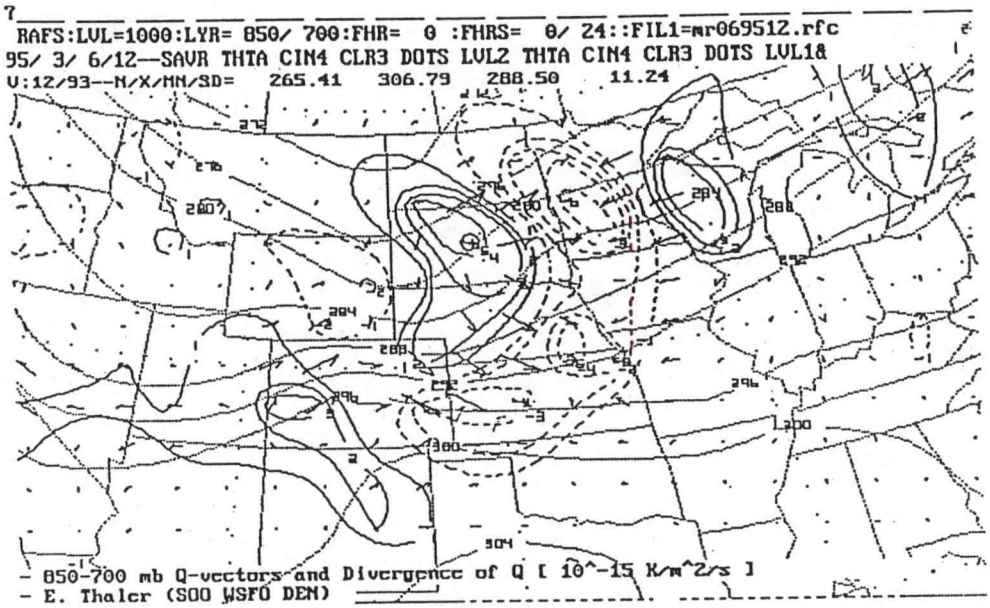

Figure 8. Initial NGM 1200 UTC, Mar 6, 1995 850 - 700 hPa Q vectors, layer divergence of Q (10^{-15}°K/m^2 sec^{-1}), and the layer mean potential temperature in °K.

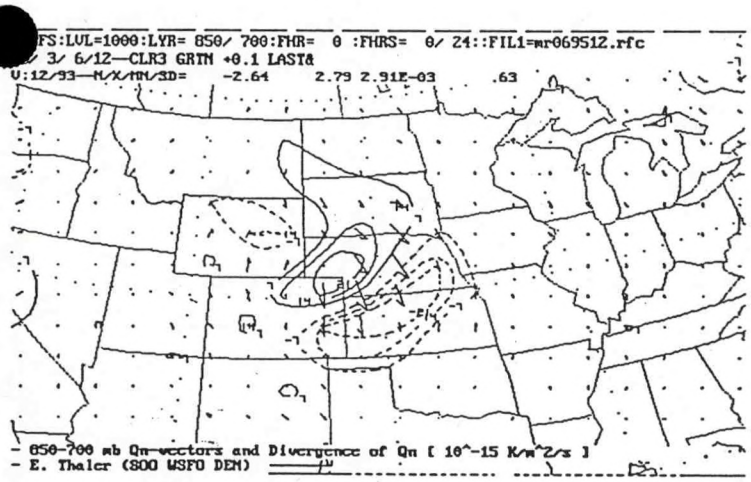

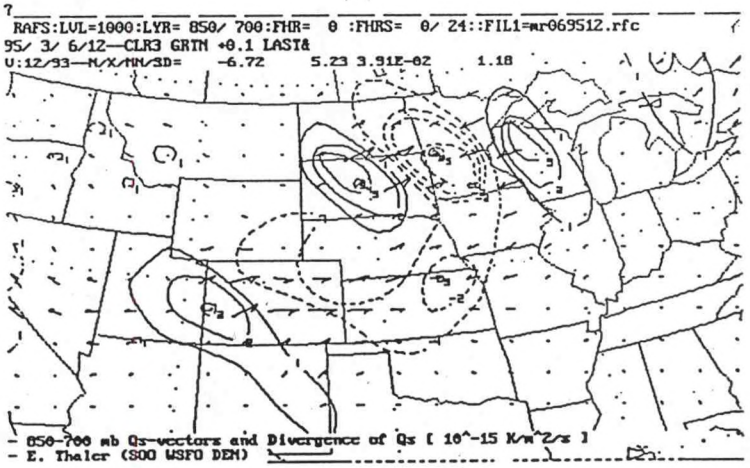

Figure 9. Initial NGM 1200 UTC 6 March 1995 850 - 700 hPa layer divergence of Qn (a) and Qs (b). Units 10^{-15}°K/m^2 sec^{-1}, with dashed areas indicating upward forcing.

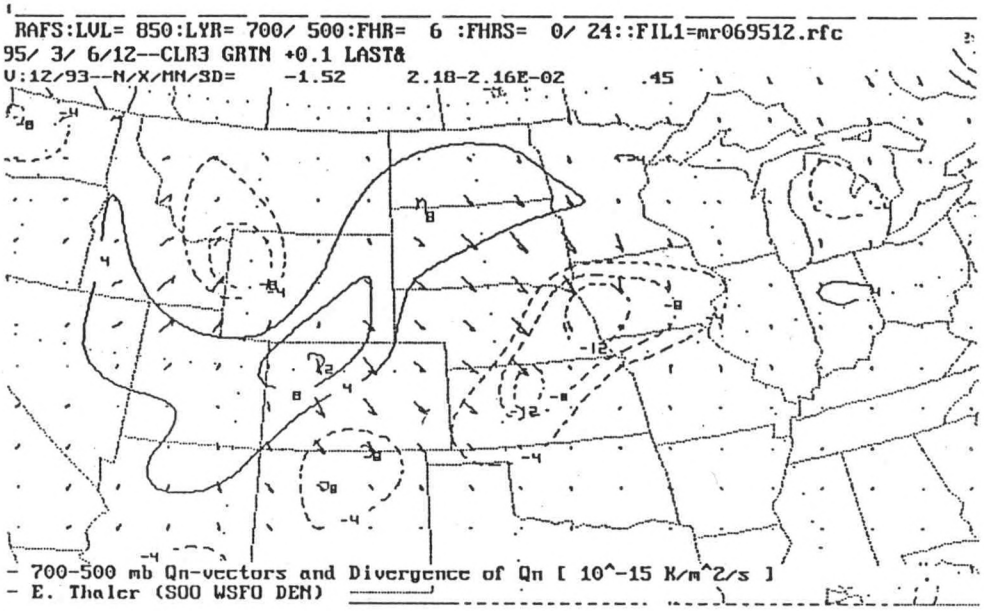

Figure 10. NGM 6 hour forecast of 700 - 500 hPa layer divergence of Qn (10^{-15}°K/m^{2}sec^{-1}) valid 1800 UTC 6 March 1995.

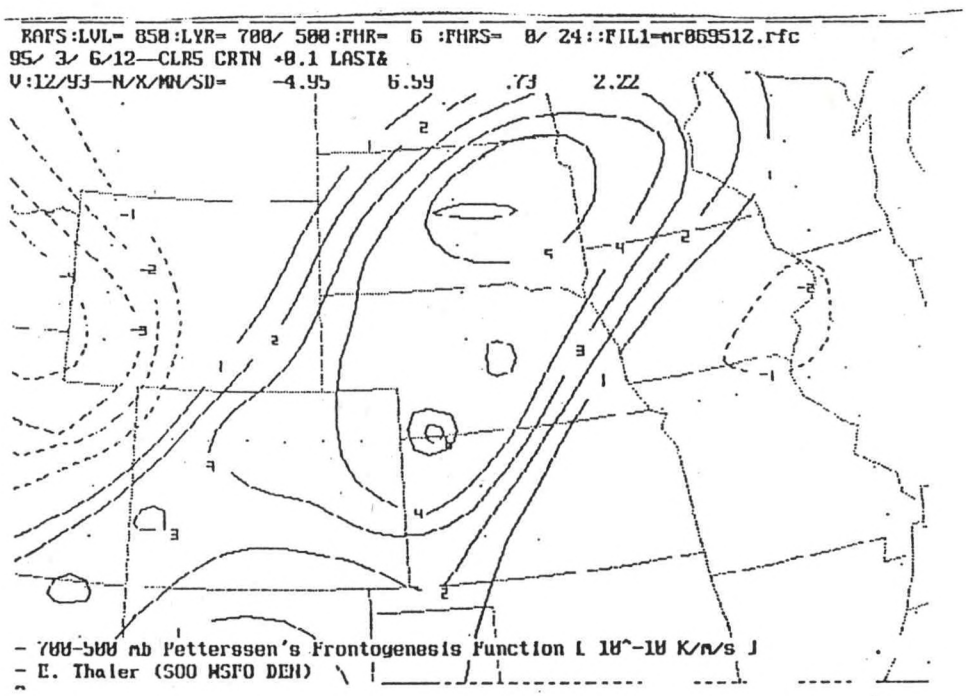

Figure 11. NGM 6 hour forecast valid 1800 UTC 6 March 1995 of 700 - 500 hPa layer Petterssen's frontogenesis. Units are 10^{-10}°K/m sec^{-1} with positive values indicating frontogenesis, and negative value frontolysis. Direct thermal circulation is gradient to the right of the axis of maximum frontogenesis from north central Iowa into southwest Kansas.

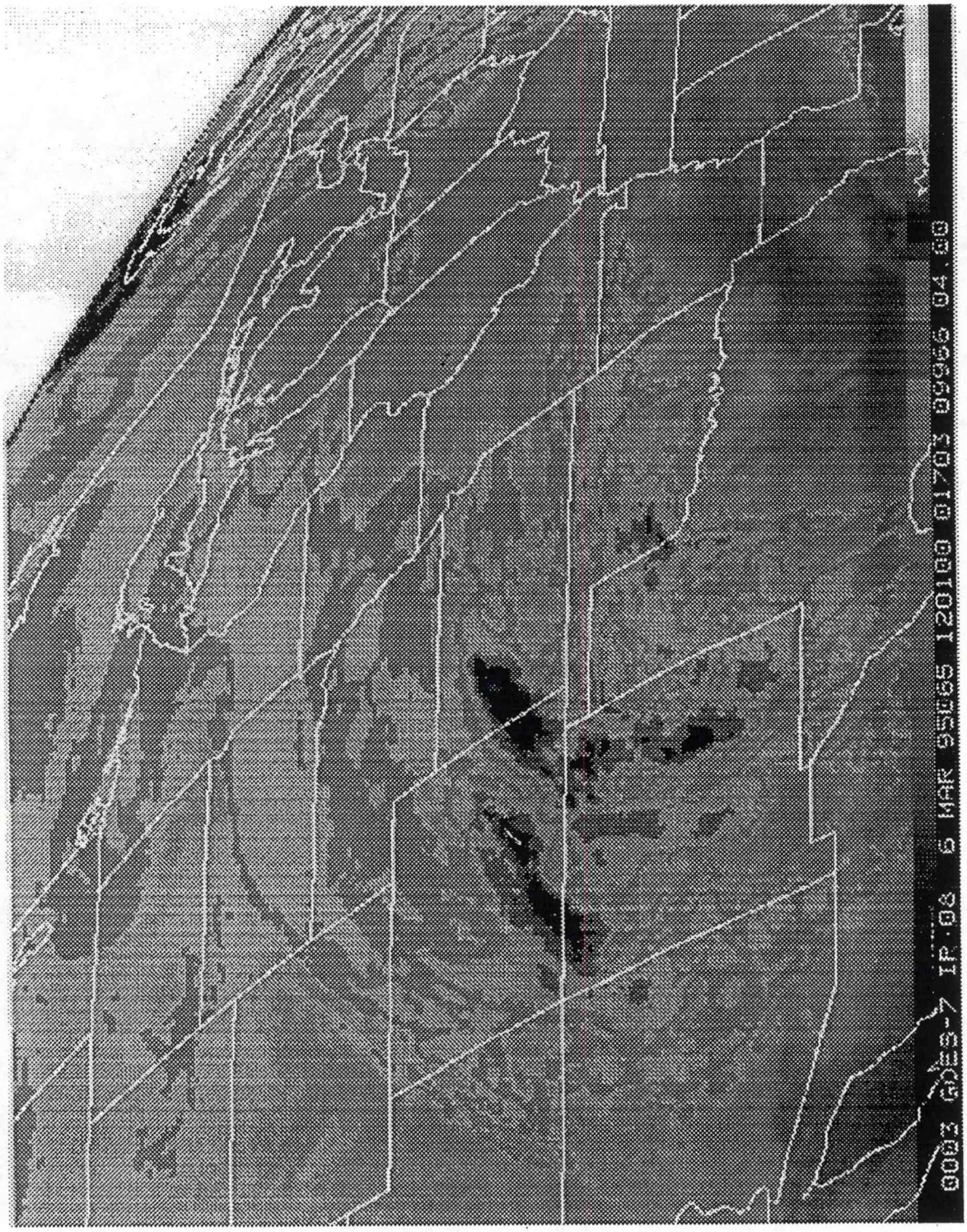

Figure 12a. Infrared satellite imagery GOES-7 MB curve at 1200 UTC 6 March 1995.

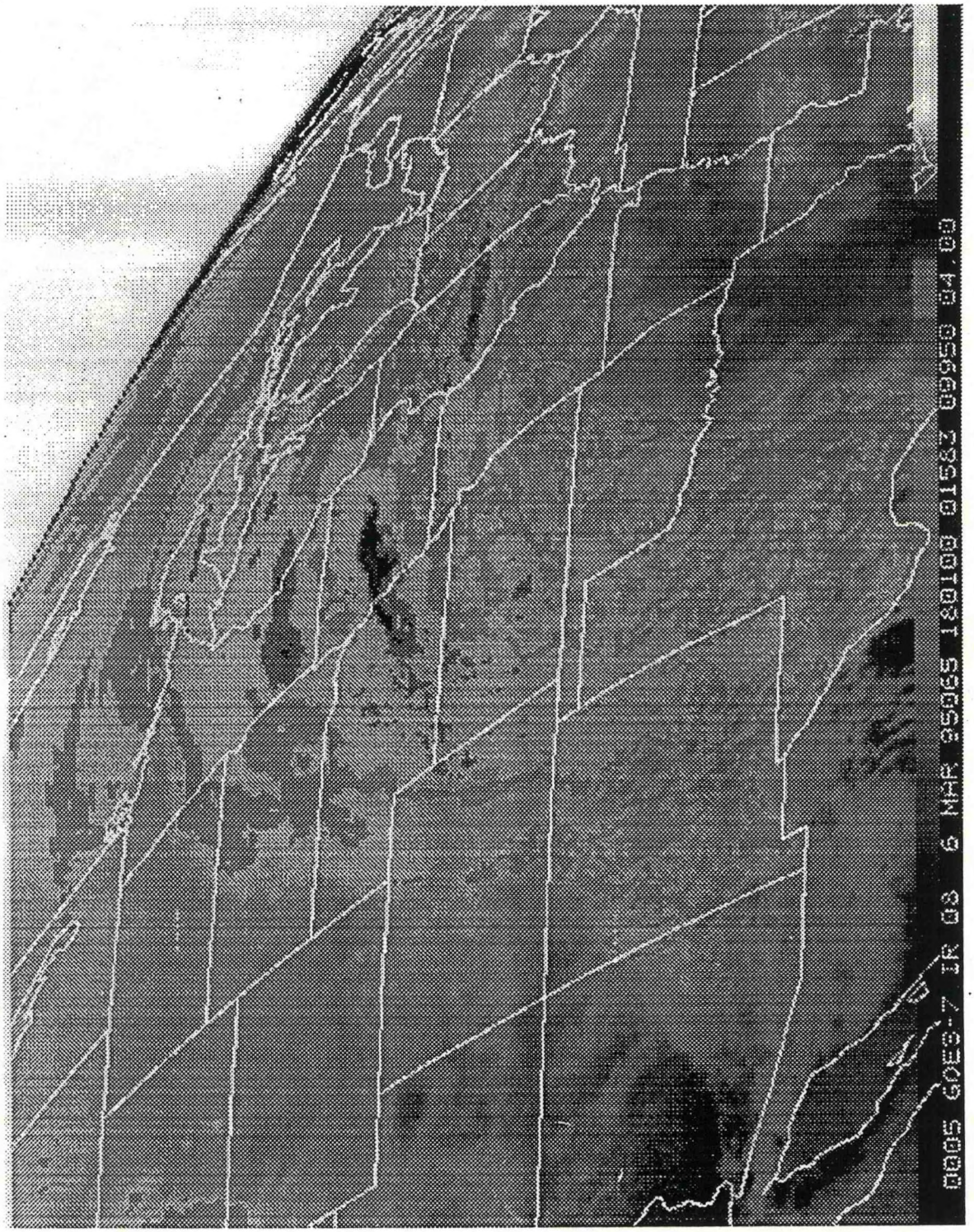

Figure 12b. Infrared satellite imagery GOES-7 MB curve at 1800 UTC 6 March 1995. Cold tops have developed in across frontogenetic area of eastern Nebraska and western Iowa.

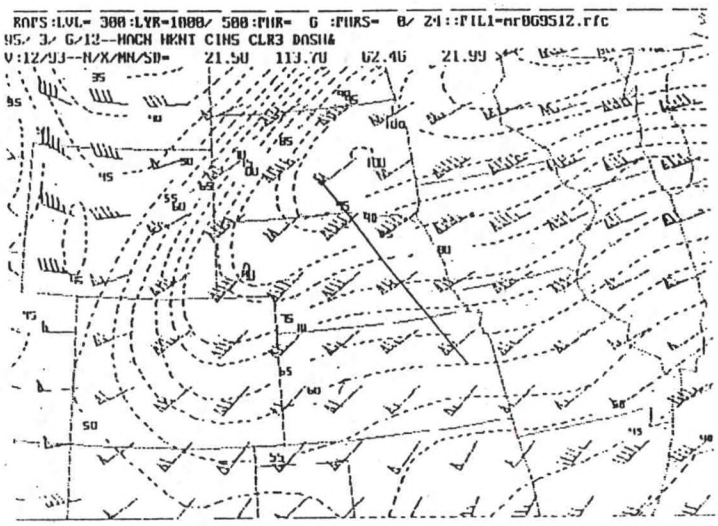

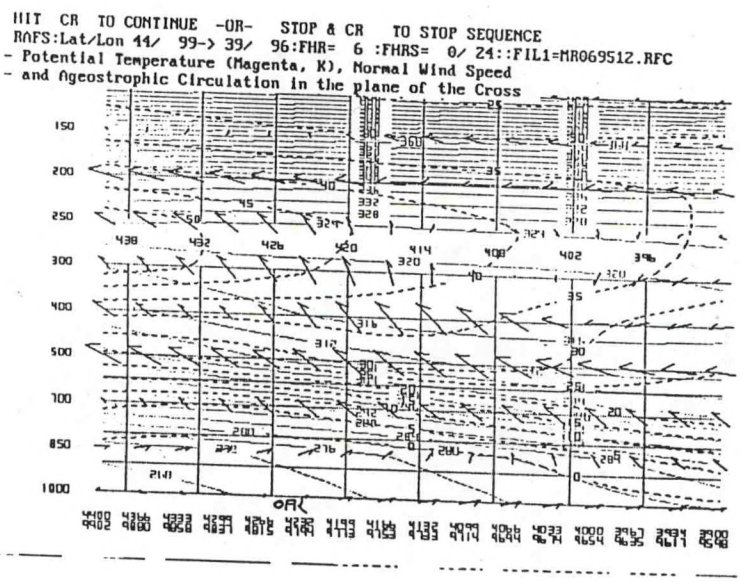

Figure 13. (a) NGM 6 hour forecast of 300 hPa winds in knots and isotachs. Cross section location is indicated. (b) cross-section from near Topeka (TOP) to near Norfolk (OFK) and north to just southeast of Pierre, SD. Winds normal to and into the plane of cross section dashed (m/sec), Potential temperature dotted (°K), and arrows are vector representation of ageostrophic in the plane of the cross section.

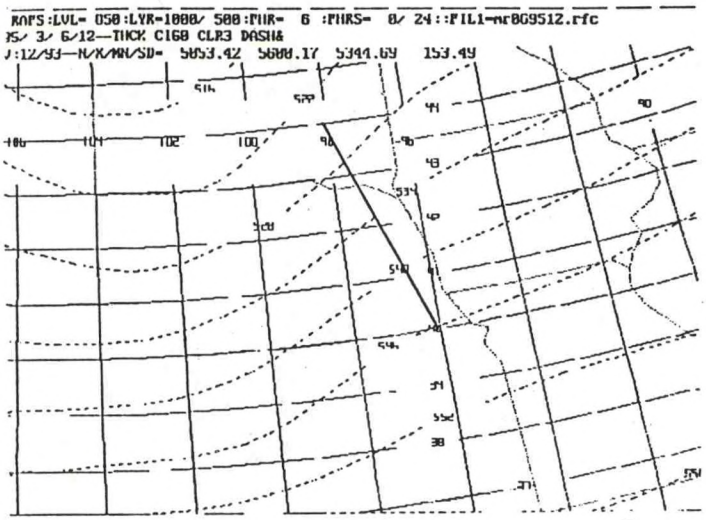

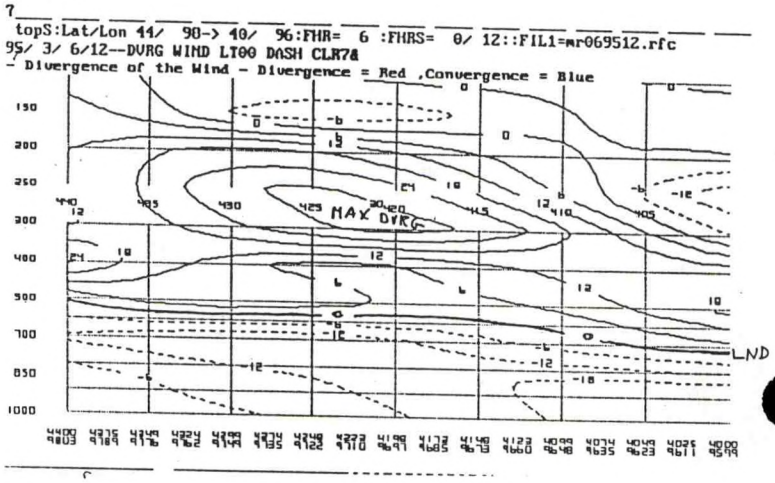

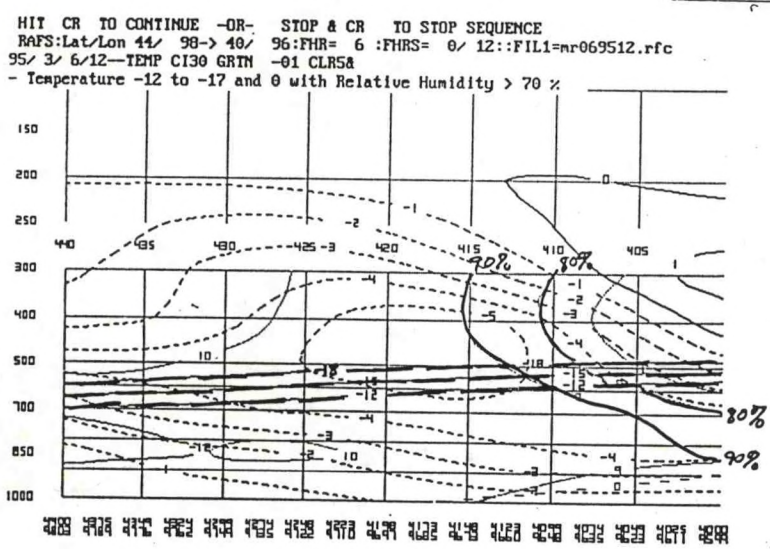

Figure 14. (a) Location of NGM 6 hour forecast cross section taken normal to the 1000 - 500 hPa in eastern Nebraska. (b) Divergence of the wind with solid positive and dashed negative. Note the well-defined level of non divergence between 500 and 700 hPa. (c) Vertical velocity in μmars/sec - dashed upward, temperature layer -12°C and -18°C heavy dashed, and heavy solid lines show relative humidity.

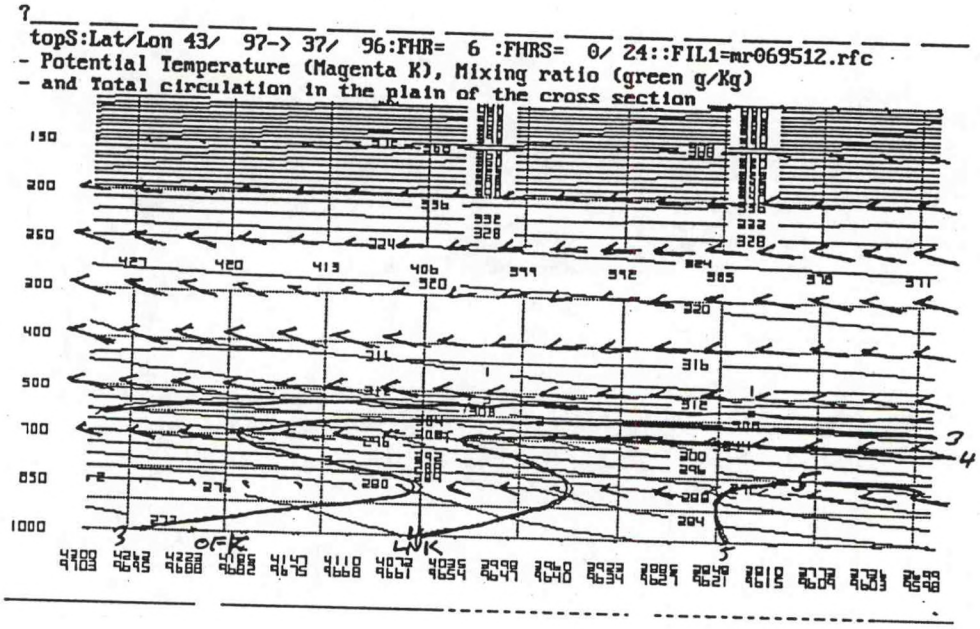

Figure 15. NGM 6 hour forecast cross section valid at 1800 UTC 6 March 1995 from Emporia, KS (EMP) to Norfolk, NE (OFK) showing mixing ratios (g/Kg), isentropes dotted °K, and arrows are vectors representing total circulation in the plan of the cross section. Advection of the mixing ratio up isentropic surfaces is easily seen.

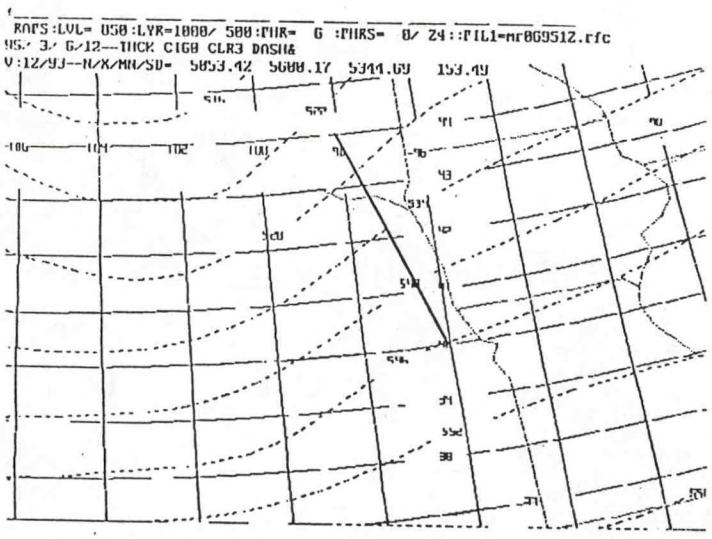

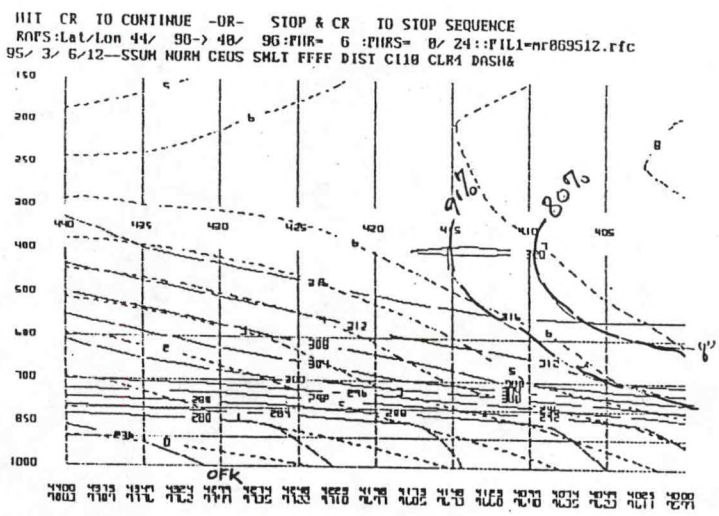

Figure 16. (a) NGM 6 hour forecast of 1000 - 500 hPa thickness and indication of cross section taken normally to the thermal wind. (b) Associated cross section valid 1800 UTC 6 March 1995. Light dashed lines are the geostrophic momentum in m/sec, and solid lines are the equivalent potential temperature in °K. Heavy dashed lines are the relative humidity. CSI is shown in areas where the relative humidity is greater than 80%, and geostrophic momentum surfaces are about the same slope or flatter than equivalent potential temperature surfaces.

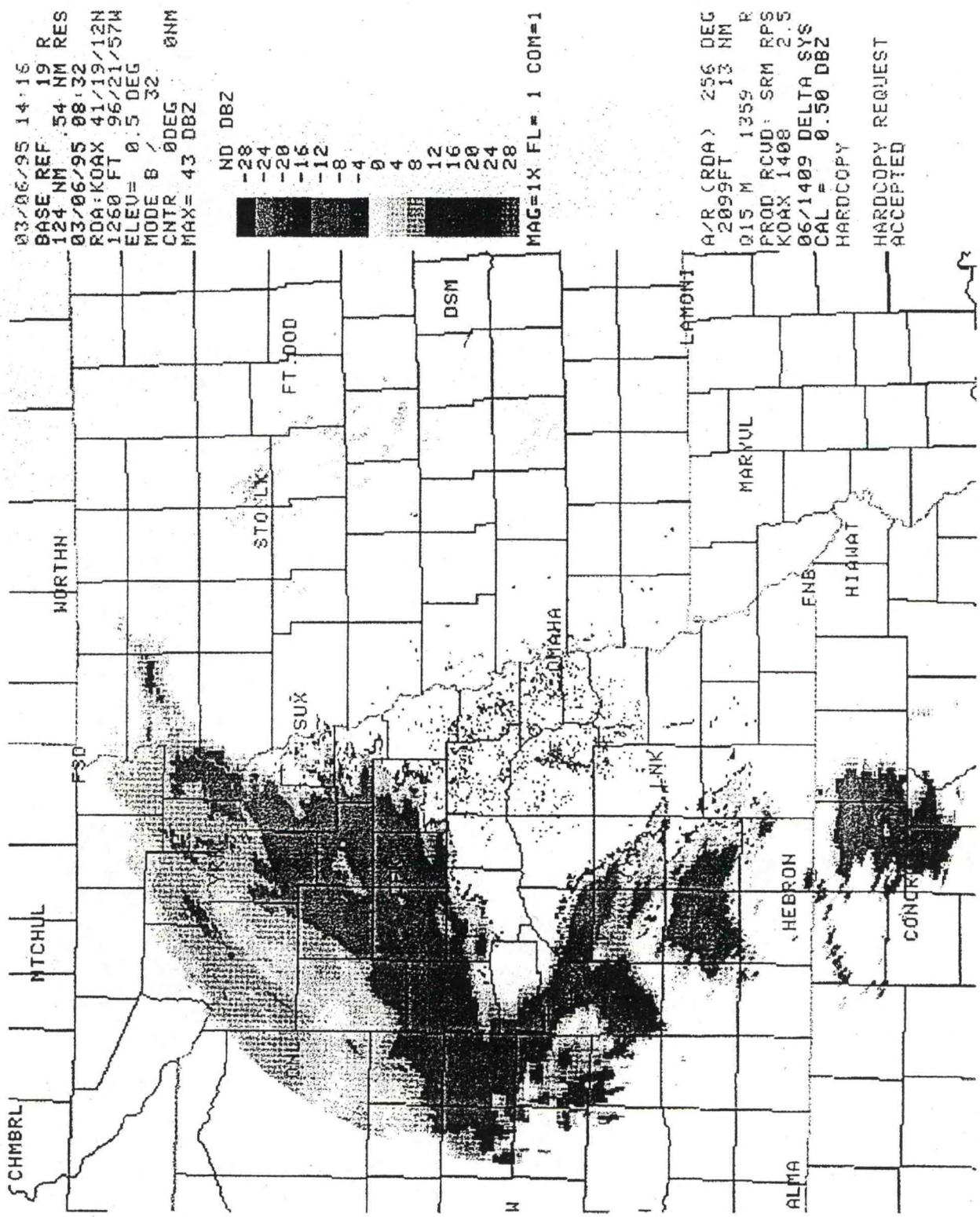

Figure 17a. WSR-88D 0832 UTC 6 March 1995 reflectivity displays in the "clear air mode".

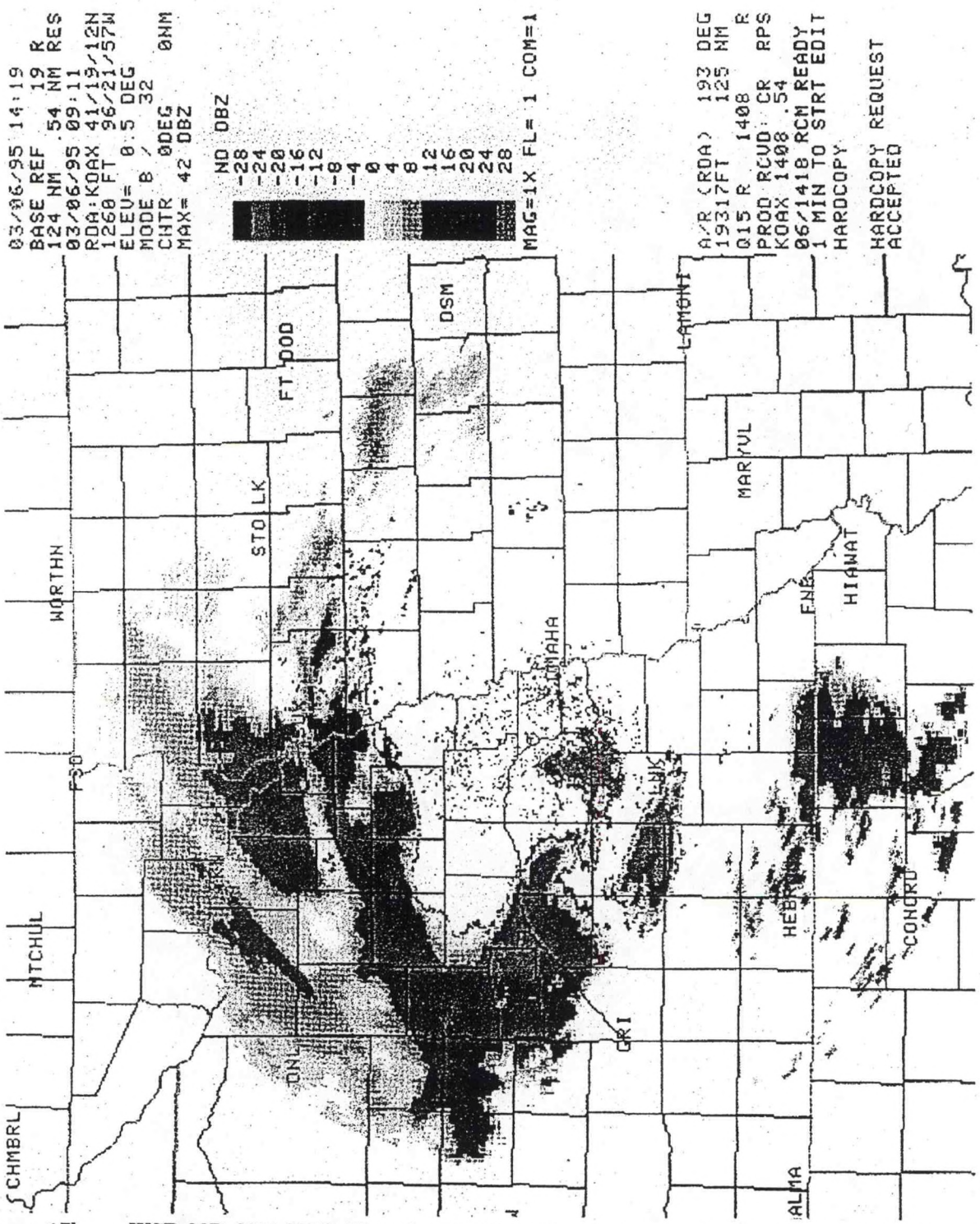

Figure 17b. WSR-88D 0911 UTC. Note the significant band of snow that is occurring from central into northeast Nebraska, giving the forecaster an idea of where the anticipated frontogenetic band has developed.

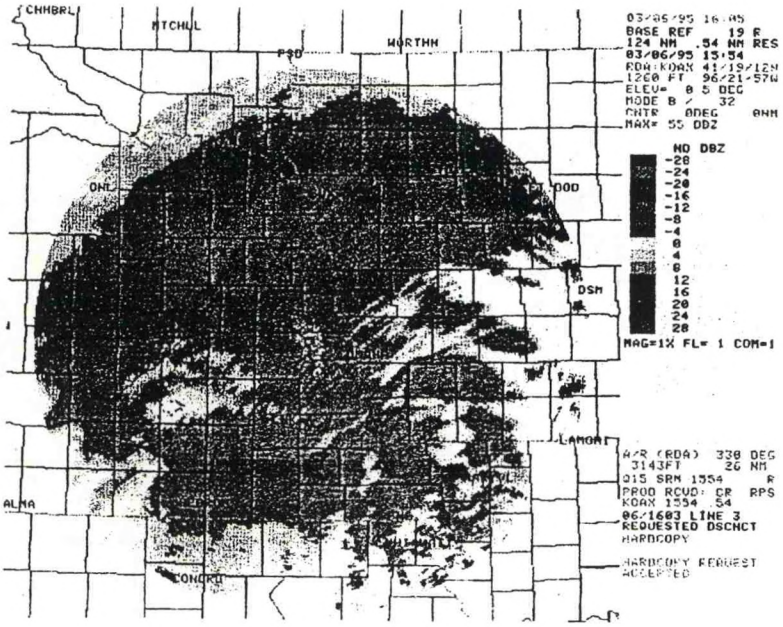

(A)

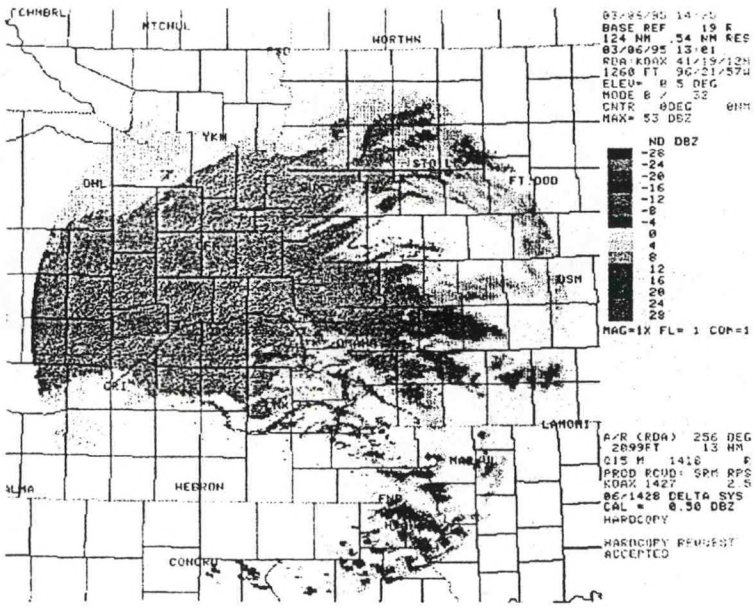

(B)

Figure 18. WSR-88D Reflectivity pattern showing the evolution of the snow pattern on March 6, 1995 from 1301 UTC (a) to (b) 1554 UTC. Note that by 1605 UTC the wide frontogenetical band persists across northeast Nebraska with intensities > 28 dBz. In addition banded snowfall in east central Nebraska and southwest Iowa suggests that slantwise convection have developed as anticipated.

SESSION 11
FORECAST TECHNIQUES II

38. Operational Applications of Hovmöller Diagrams to Forecasting a Snowstorm in the Medium-Range

39. A Simple Technique to Identify and Separate Upward Vertical Motion from 500mb Height Falls, a Useful Tool for Medium Range Winter Storm Forecasting

40. Forecasting Hydrologically Critical Storms in Northern and Central California

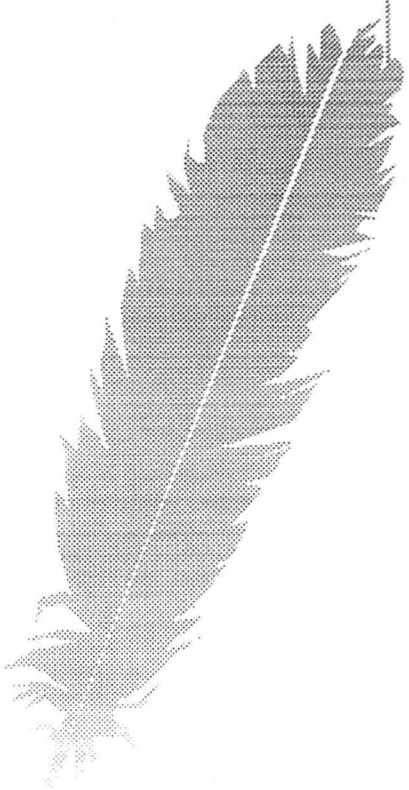

Operational Applications of Hovmöller Diagrams to Forecasting a Snowstorm in the Medium-Range

Edward Berry[1]

1. INTRODUCTION

On February 22-23, 1994 a widespread and significant snowfall event occurred across the Central and Northern Plains of the United States. Storm total snowfall amounts were mostly between 6 to 12 inches, with the largest accumulations generally occurring from southern Nebraska through most of Iowa into southern Wisconsin/northern Illinois (Figure 1). In addition to the snowfall, surface winds with sustained speeds of 25 to 35 mph, with gusts to near 45 mph, caused considerable blowing and drifting snow.

While the occurrence of this event was well predicted during the day 1 and 2 forecast periods, such was not the case for days 3 through 5 (the National Meteorological Center's (NMC) operational medium-range forecast period). The latter were true for much of the operational medium-range numerical weather prediction (NWP) model guidance, which was utilized as input to the manual forecasts generated by NMC's medium-range forecast desk.

The purpose of this presentation is to show that a fairly easy to use diagnostic tool may have helped to more accurately predict this important snowfall event during the medium-range (which would have been useful information to the public). This tool is the representation of the atmosphere (observed and predicted) utilizing three-dimensional Hovmoller (3D Hovs) diagrams (Hovmoller 1949), supplemented with computations of 500-mb geostrophic kinetic energy (GKE), done for various wave number groups.

A brief discussion of the methodology employed follows. Afterwards, the snowstorm case of February 22-23, 1994 will be addressed. Regarding the latter, emphasis is made on (1) that this was a case of wave number transition (Berry et al. 1993, 1995), (2) the differences in the operational medium-range NWP, (3) the NMC manual forecasts and (4) the utility of the 3D Hovs to provide a *priori* information (as a supplement to ensemble prediction (Tracton and Kalnay 1993)) for scales of motion that can be predictable out to day 5. Finally, a concluding discussion is given.

2. METHODOLOGY

Three-dimensional Hovs for the observed and predicted 500-mb constant pressure surface were generated, for various zonal wave number groups (such as waves 1-3, 4-9, etc.). The forecasts were done utilizing NMC's deterministic operational T126 Medium-Range Forecast model (MRF). The domain of all the Hovmöllers was from 25°-75° North latitude, with hemispheric longitudinal extent. Computations included GKE from the height field and 5-day running mean 500-mb heights. The GKE was areal averaged on a 2.5° latitude/longitude grid.

The purpose of these 3D Hov computations was to isolate spatial teleconnection structures (and other signatures of low frequency variability (LFV)) such as the Pacific North American Teleconnection (PNA) and the North Atlantic Oscillation (NAO), and observe behaviors such as curved

1. Corresponding author address: Edward K. Berry, DOC, NOAA, NWS, Central Region, Scientific Services Division, 601 E. 12th Street, Kansas City, MO.

baroclinic energy propagations (which cannot be observed with ordinary two-dimensional traditional Hovmöllers), wave number and regime transitions. The MRF-based predicted 3D Hovs were useful to see if the model forecast trajectory was consistent with the real atmosphere.

3. DISCUSSION

A. Differences in the Operational NWP

To highlight the variabilities of forecast solutions for the medium-range period, emphasis will be made on the differences between the operational global model from the European Center for Medium-Range Weather Forecasts (ECMWF) and the MRF, for day 5. Output from the operational global model from the Meteorological Office of the United Kingdom (UKMET) will not be shown. However, observationally (and shown by objective verification skill scores) its forecasts were similar to the MRF. Further, only a few prediction charts will be shown so that important points can be addressed quickly.

Figure 2 is the MRF 132-hour 500-mb heights/height tendency forecast valid 1200 UTC 23 February 1994, for the region of the lower 48 states. This chart would be used as input for NMC's day 5 manual sea-level prediction. It is important to observe that the greatest height falls are located across the Northern High Plains, in association with the forecasted position of the polar jet stream westerlies. Figure 3 is the MRF predicted mean sea-level pressures (MSLP) (and 1000 to 500-mb thicknesses) response (same initial conditions) to what is shown in Figure 1. Observe the sea-level cyclone over eastern Montana.

Figure 4 is the ECMWF 144-hr 500-mb heights/absolute vorticity valid 1200 UTC 23 February 1994. When comparing with Figure 1, it can be seen that the ECMWF model was more suggestive of predicting an energetic southern branch of the westerlies. Further, and recalling that quasi-geostrophic height tendency equation, etc., at 1200 UTC 23 February, while the MRF was predicting the bulk of the cyclonic vorticity advection (CVA) to be across the western Dakotas, the ECMWF model was forecasting the greatest CVA to be across New Mexico. Clearly, the latter solution was much farther south.

Later numerical integrations of both models displayed similar trends in their respective forecasts. For instance, Figure 5 is the 120-hr ECMWF MSLP/1000 to 500-mb thickness forecast valid 1200 UTC 23 February. Observe the sea-level cyclone near the intersection of the states of Indiana, Illinois and Kentucky.

Suppose now that you are a forecaster that MUST issue a deterministic MSLP day 5 prediction for the lower 48 states (especially the central part of the country). Given the whole array of possibilities that the operational NWP presented, what do you forecast? Indeed, an ensemble (Berry 1995 and references therein) would quantify forecast uncertainty such as this, in real time. For this case, there would be large spread among the members, with several clusters (of just about all forecast fields).

Figure 6 is the manual MSLP/fronts forecast for day 5, valid 1200 UTC 23 February 1994, issued by NMC. As can be seen from this figure, the forecast was very much "MRF-like", and would not suggest a significant snowfall event for the "Iowa region". In the following, it will be seen what did evolve in reality, including any *a priori* information.

B. Diagnostic Information Derived from 3D Hovs

As a supplement to ensemble prediction, diagnostic tools can be useful, even in situations when forecast uncertainty is high and confidence low. For this presentation, information derived from 3D Hovs will be shown (other diagnostic tools are being studied as part of ongoing work).

Figure 7 is a 3D Hovmöller representation of 5-day mean 500-mb geopotential height anomalies. The graphical representation shown in Figure 7 is called a 3D Hov because latitude, longitude and time are given. The dateline is represented by 180 degrees, and the North American continent is located to the right.

February 18, roughly, would be the date for the initial conditions of any NWP model valid for day 5, February 23. From the Hov, through February 18, observed the large negative 500-mb height anomalies increasing in magnitude just to the west of the U.S, with downstream positive height anomalies across the eastern part of the country. Furthermore, the careful reader can observe a signature of curved downstream baroclinic energy propagation from the Asian land mass to the U.S. Given the meridional extent of these height anomalies, if one wishes to be "deterministic", a better ECMWF solution would be likely (Figure 4) (or any ensemble clusters like the ECMWF).

Figure 8 is a 3D Hov representation of 500-mb heights, for zonal wave number group 4-9 (medium-scale waves, for our purposes). With the zonal mean subtracted out, this wave group appears like height anomalies. Also given are computations of GKE, written to the right of the date-time group. The period of record is from February 18-20. Upon comparison of these charts with other Hovmöller presentations and GKE computations for this case (including predicted), it was easy to observe there was a rapid down scale transfer of GKE, from the planetary-scale (waves 1-3 in this study) to the medium-scale (waves 4-9). That is a signature of a low to high zonal wave number transition, and a source of numerical model forecast error (which was true here, Berry et al. 1993, 1995; part of ongoing work).

Given this was a case of low to high wave number transition, with a great deal of meridional extent, as shown by the 3D Hov presentations above, an ECMWF-like solution seems more logical. *This type of prior information could have been supplied to the operational NMC forecaster doing the medium-range prediction for day 5, February 23, if other resources were available.*

C. What Did Evolve

Figure 9 is the 500-mb geopotential height analysis valid 1200 UTC 22 February 1994 (about the time sea-level cyclogenesis was occurring across the Southern Plains). Comparison with Figures 2 and 4 will show that indeed, the ECMWF model was the correct deterministic solution. Granted, the ECMWF was "slow" with the progression of the short-wave trough in the southern branch of the westerlies (NWP predictability skill for wave numbers 13 and greater falls off rapidly after Day 3, which is quite applicable here).

Figure 10 is the "surface analysis" valid at 1200 UTC 23 February 1994. Note the MSLP cyclone near southwestern Indiana. Comparison with Figure 5, the ECMWF solution, will show that this model verified quite well for the day 5 MSLP cyclone near southwestern Indiana. Also shown on Figure 10 is the track of the "surface low" during the 48-hour period from 1200 UTC 22-24 February 1994. As can also be seen from comparing Figures 6 and 10, the NMC manual forecast was well too far to the northwest with the MSLP cyclone.

4. CONCLUSION

A case study presentation was shown where information derived from 3D Hov representations of the atmosphere, including computations of GKE, may have been beneficial for a day 5 forecast. .Specifically, for the prediction of a significant snowfall event across the central U.S.

The case given was a low to high zonal wave number transition event. The rapid down scale GKE transfers that occurred were likely a source of numerical model forecast error (Tracton 1990, Berry 1995 and references therein). Of the three operational global models that were available for the NMC medium-range forecaster to examine, the ECMWF forecast model best captured the evolution of the real atmosphere out to day 5.

Diagnostic tools such as 3D Hovs can be useful supplements to the method of ensemble prediction (not only for just medium-range, but all time/space scales). The integration of these kinds of diagnostic and prediction methods will further link forecast operations with theory. Of course, these techniques can only be most effective on workstations, such as AWIPS.

5. ACKNOWLEDGEMENTS

Deborah White, CRH SSD, carefully prepared this manuscript for post print publication. Michael Manker, also of CRH SSD, provided graphical support. The author extends considerable appreciation to these folks for their help.

6. REFERENCES

Berry, E.K., 1995: Ensemble prediction. Central Region Technical Attachment 95-06. DOC/NOAA/NWS/Central Region, Scientific Services Division, Kansas City, MO.

_____, J.A McGinley, and P. Schultz, 1993: Global model errors associated with rapid low to high zonal wave number transitions. *Preprints, 13th Conf. on Wea. Anal. and Fcstg.* and incl. *Sym. on Flash Floods,* Vienna, VA, AMS (Boston), 117-120.

_____, _____, and _____, 1995: Global model errors associated with rapid low to high zonal wave number transitions. NOAA Technical Memorandum NWS-111, DOC/NOAA/NWS/Central Region, Scientific Services Division, Kansas City, MO.

Hovmöller, E., 1949: The trough-and-ridge diagram. *Tellus,* **1**, 62-66.

Tracton, M.S., 1990: Predictability and its relationship to scale interaction processes in blocking. *Mon. Wea. Rev.,* **118**, 1666-1695.

_____, and E. Kalnay, 1993: Operational ensemble prediction at the National Meteorological Center: Practical aspects. *Wea. Forecasting,* **9**, 457-465.

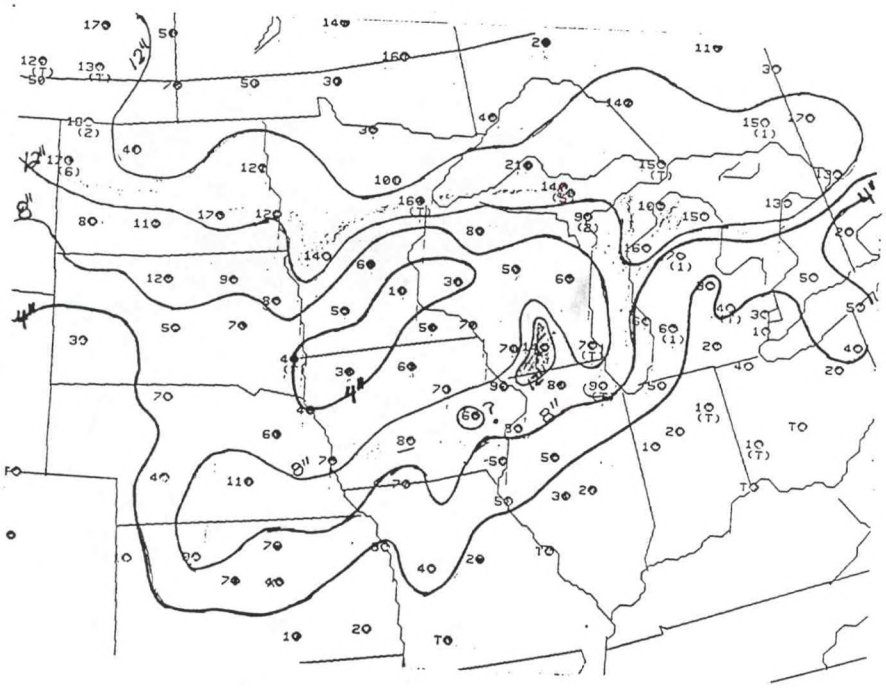

Figure 1. Snow depth chart valid at 1200 UTC 24 February 1994.

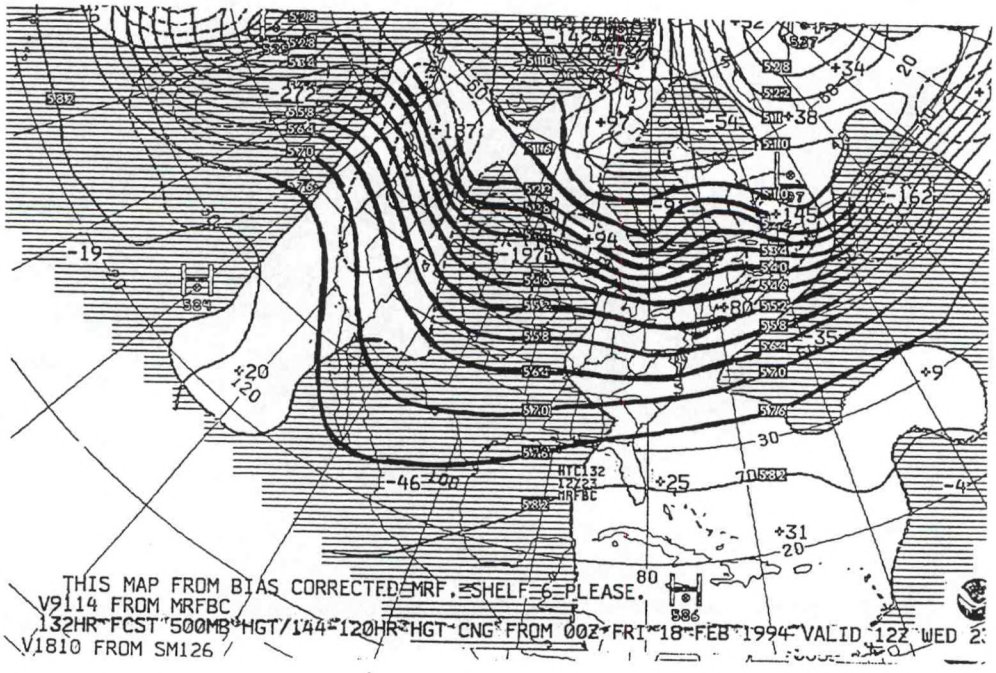

Figure 2. 132-hr 500-mb MRF model prediction valid 1200 UTC WED 23 February 1994. Solid isopleths are height contours in gpdm (interval every 6 gpdm) while dashed are height tendencies in gpm (interval every 30 gpm). Algebraic signs for the height rise (+) and fall (-) centers are also given.

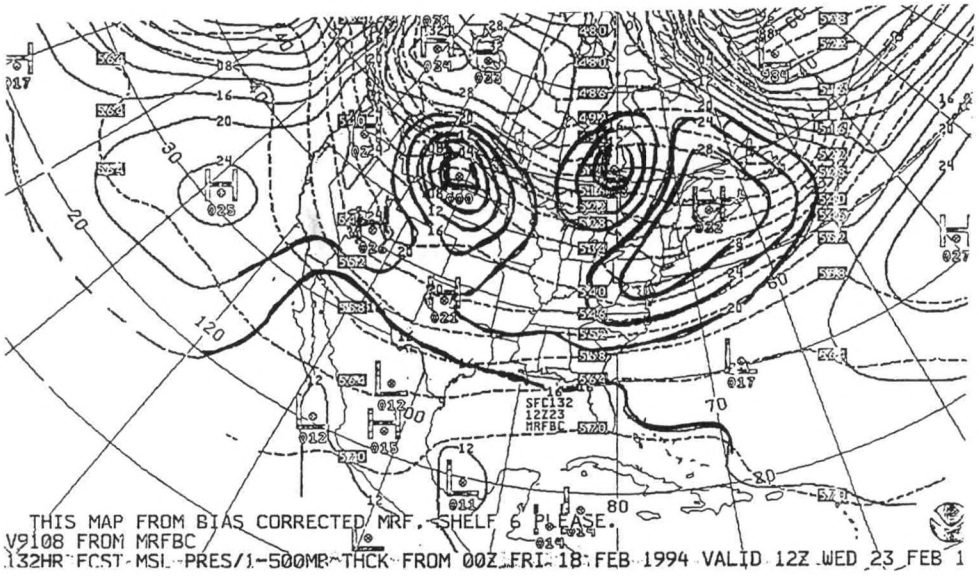

Figure 3. 132-hr MRF MSLP (mb, CI=4 mb) and 1000 to 500-mb thicknesses (gpdm, CI=6 gpdm).

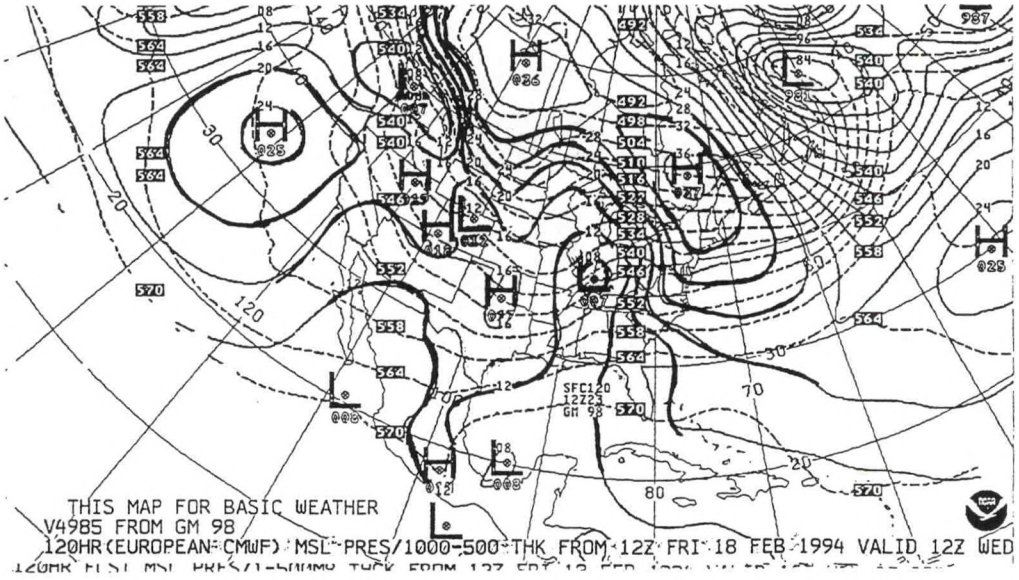

Figure 4. 144-hr 500-mb ECMWF model prediction valid 1200 UTC WED 23 February 1994. Same presentation as Figure 2, except dashed isopleths are absolute vorticities, units 10 **-5 sec^{-1} (CI=2*10**-5sec^{-1}).

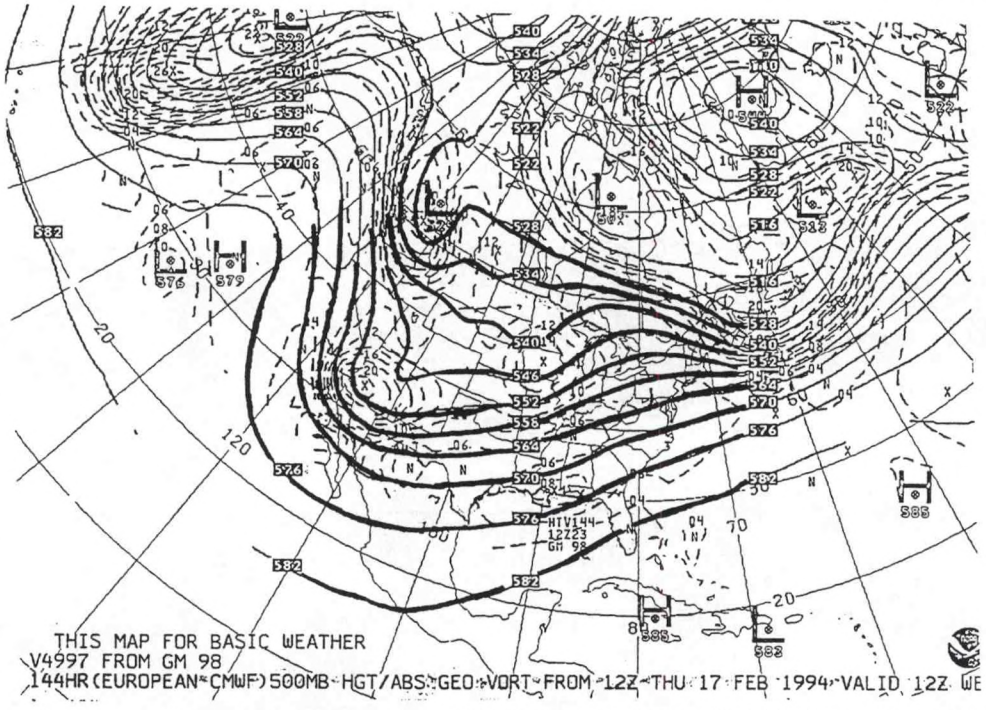

Figure 5. Same as Figure 3, but for the ECMWF valid 1200 UTC 23 February 1994.

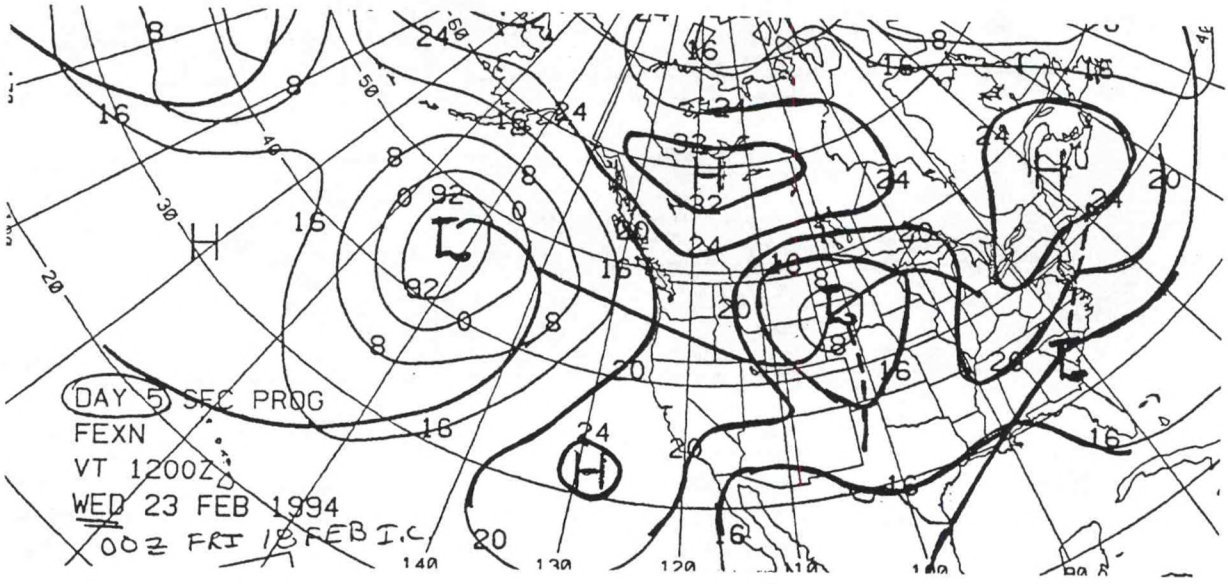

Figure 6. NMC man sea-level forecast, day 5, valid 1200 UTC 23 February 1994.

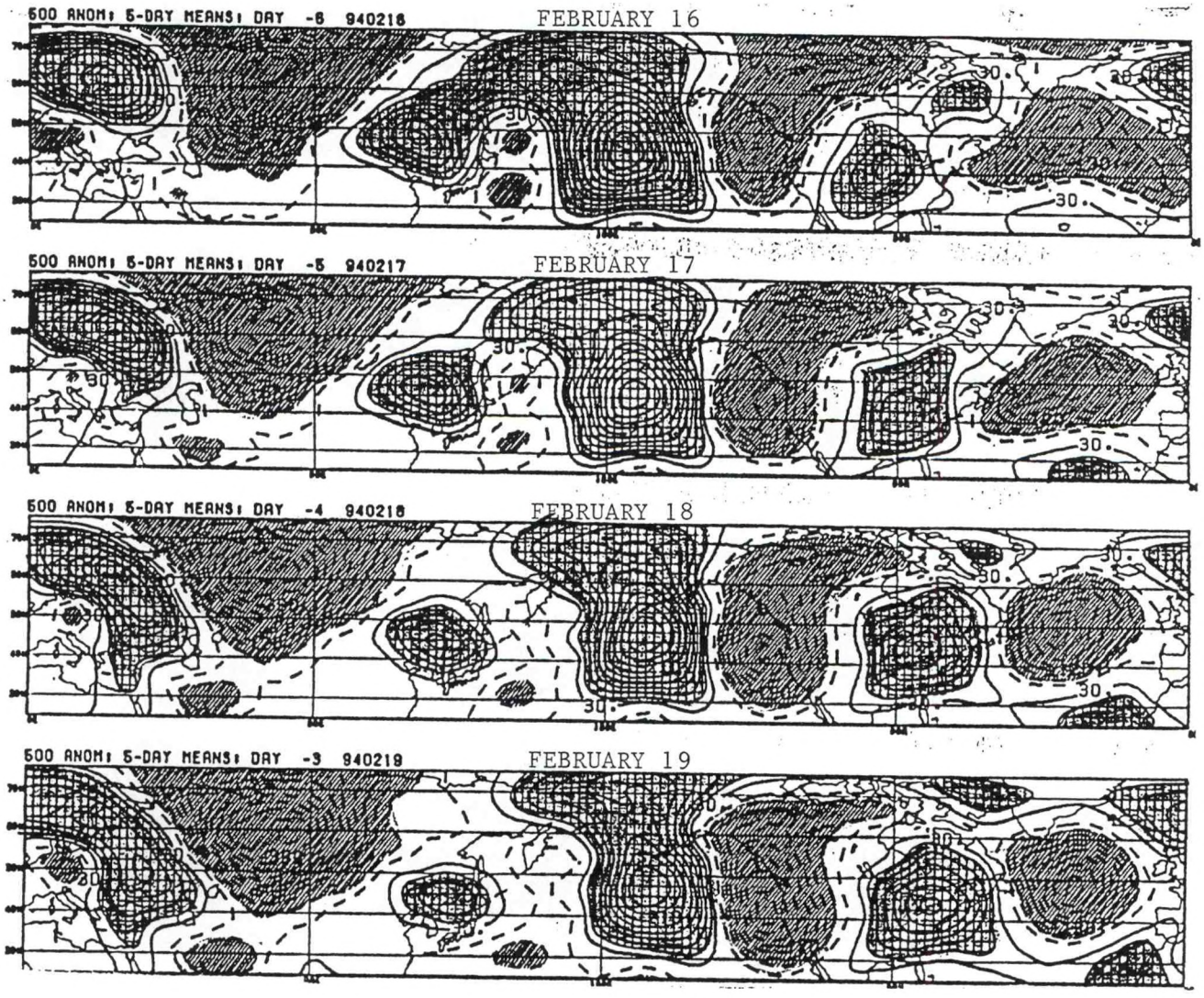

Figure 7. Three dimensional (x, y, t) Hovmoller charts that display 5-day 500-mb mean height normalities. Units are in gpm (CI=30 gpm); hatched (with solid contours) areas are positive and shaded with dashed contours) are negative. Dates are shown at the top of each chart, all valid at 0000 UTC.

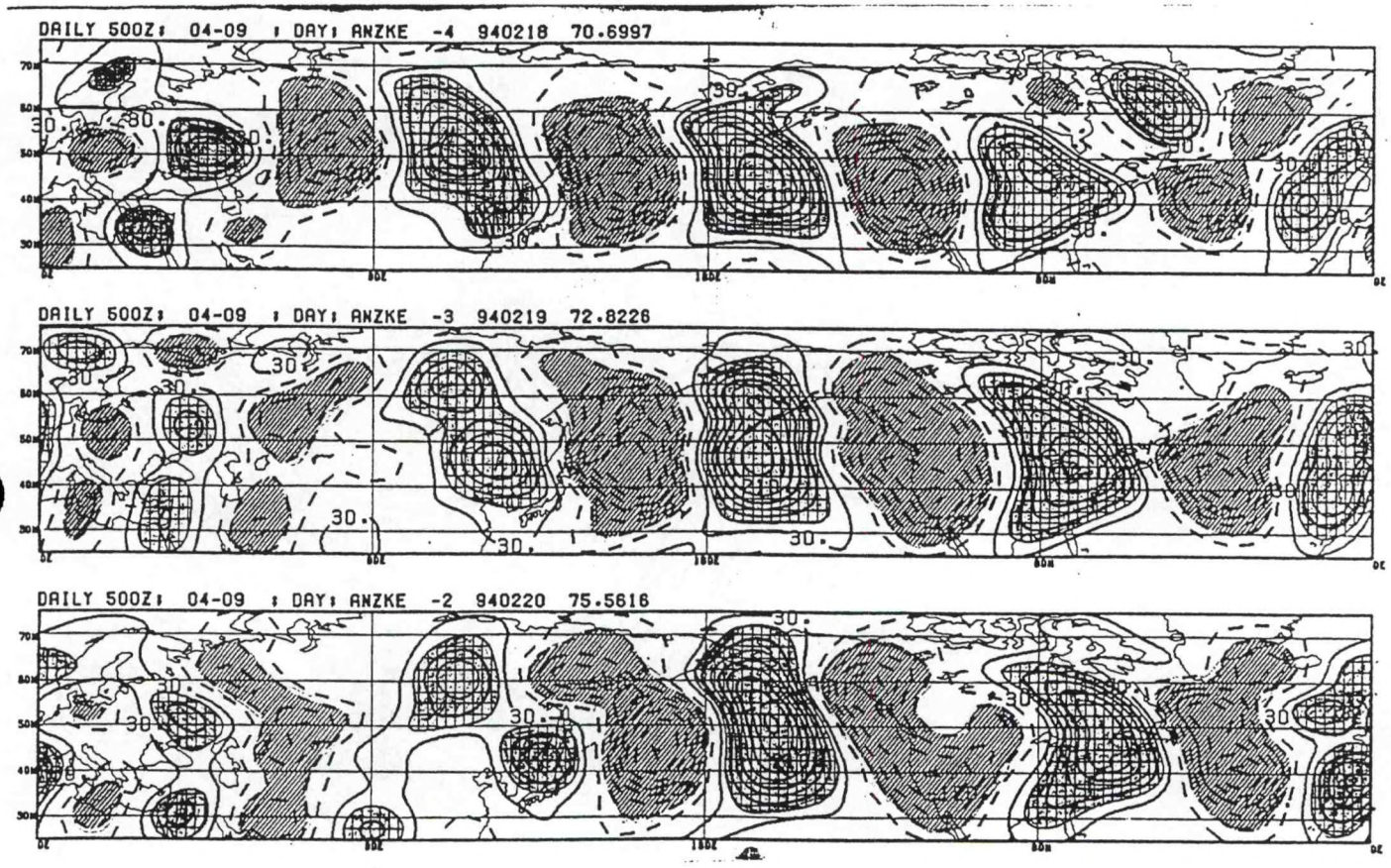

2

Figure 8. Same as Figure 7. However, what is displayed are analyzed 500-mb heights for zonal wave number group 4-9, with the zonal mean removed. Thus, the appearance is like height anomalies. Hatched are areas with heights greater than the zonal mean and vice-versa for shaded (just like Figure 7). Date/time group is given such as 940218 ==> 0000 UTC 18 February 1994. Areal averaged GKE, for wave number group 4-9 (units of J/Kg; 2.5° lat/long grid), is the last number farthest to the right. For February 18, the GKE is about 71 J/Kg.

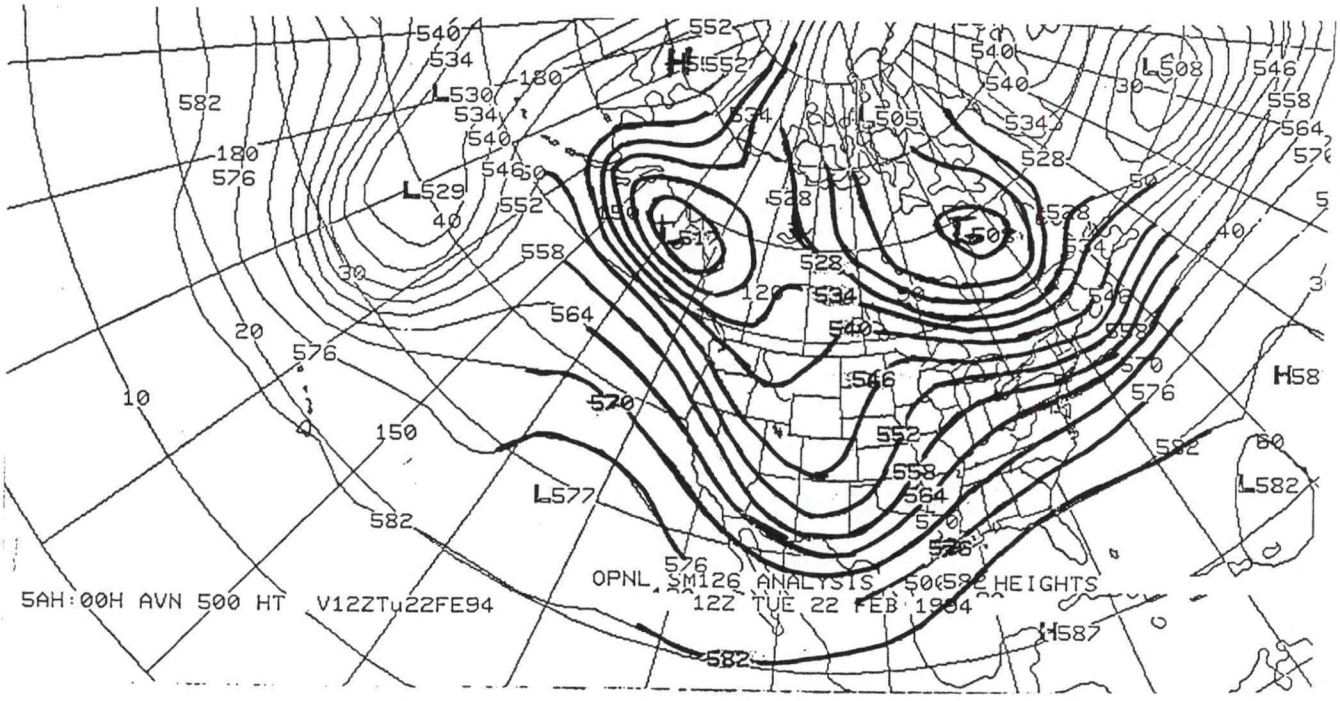

Figure 9. 500-mb northern hemispheric analysis valid 1200 UTC 22 February 1994 ("day earlier" chart is shown to illustrate that there was baroclinic development). CI=6 gpdm.

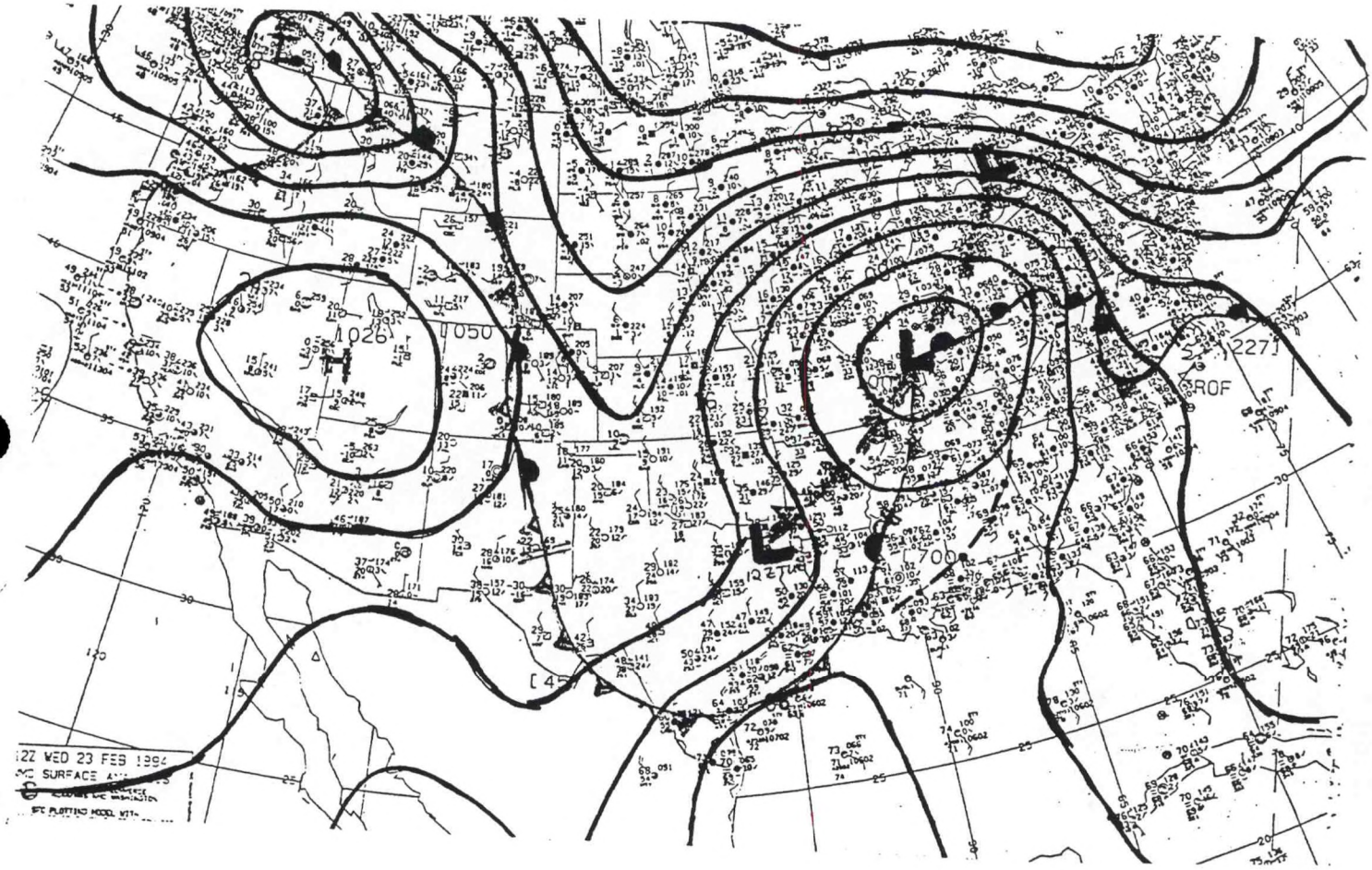

Figure 10. NMC MSLP/fronts analysis valid 1200 UTC 23 February 1994. Note the "track" of the cyclone for the 48-hr period from 1200 UTC Tuesday to Thursday, is shown.

A Simple Technique to Identify and Separate Upward Vertical Motion from 500mb Height Falls, a Useful Tool for Medium Range Winter Storm Forecasting

Hector R. Vasquez[1]

1. INTRODUCTION

Generations of operational meteorologists have used 500 mb height falls to forecast characteristics of winter storms. Height changes at 500mb can be used to estimate movement of mid-latitude synoptic systems (Figure 1), or to generally imply upward vertical velocity (UVV) and storm intensity. As an example, daily NMC hemispherical discussions often allude to the predicted location of the greatest height falls. However, given a height field change, how can a forecaster operationally identify areas of UVV within the fall region. This paper will discuss the relationship between 500 mb height falls and UVV, and show a simple empirical technique to identify UVV from height changes useful for medium range forecasting.

2. GEOPOTENTIAL TENDENCY EQUATION AND ITS RELATIONSHIP BETWEEN 500MB HEIGHT FALLS AND VERTICAL MOTION

The 500mb heights falls imply atmospheric cooling. For example, in Figure 4a, the entire area within the contoured height fall region represents airmass cooling. Two mechanisms, cold advection and UVV, are primarily responsible for atmospheric cooling. (Note: diabatic cooling is normally small compared with synoptic scale temperature advection and adiabatic motion). Since cold advection and UVV are both coincident within the height fall region, a technique to separate the UVV component would be useful, especially for the medium range forecast period.

The geopotential Tendency equation,

$$\text{where} \equiv \partial\Phi/\partial t \qquad \underbrace{\frac{\partial \chi}{\partial p}}_{\substack{\text{Geopotential}\\ \text{Rise/Fall}}} = \underbrace{-\,V_g \cdot \nabla\left(\frac{\partial \Phi}{\partial p}\right)}_{\substack{\text{Thickness or}\\ \text{Temp Advection}}} \underbrace{-\,\sigma\omega}_{\substack{\text{Vertical}\\ \text{Motion}}}$$

Geopotential Tendency

a simple diagnostic equation derived from the thermodynamic energy equation, is used to show that vertical motion is proportional to geopotential tendency and temperature advection. With assumptions that vorticity is constrained to be geostrophic and temperature hydrostatic, vertical motion can be uniquely determined from a changing geopotential or height field. **Therefore, to the first approximation, The evolution of synoptic systems can be predicted without direct measurement of the velocity field!** (Holton, 1972).

Falling (rising) heights in Figure 2 implies cooling (warming) of the atmosphere through cold (warm) advection and vertical motion. Without cold advection, cooling can be accomplished through rising adiabatic motions. Adiabatic expansion from rising motion is a secondary circulation required

1. Corresponding author address: Hector R. Vasquez, WSFO Phoenix, Arizona.

to keep the atmosphere hydrostatic. Conversely if heights rise, warming of the atmosphere increases through compressional heating. Without warm advection, heating from downward motion expands the column to maintain hydrostatic balance.

2. A SIMPLE TECHNIQUE TO SEPARATE UVV FROM HEIGHT FALLS

With the coming of PCGRIDDS technology, the usefulness of determining 12 to 48 hour UVV from height falls is moot, but sometimes useful! The technique used to separate the UVV component from height falls involves, 1) overlaying two height forecasts at 12 hour intervals (e.g. 48-60 hour, 60-72 hour, 72-84 hour, etc.), 2) subtracting the height difference and displaying the change in contour form. In the area where the height fall contour lines cross the 2nd period height field, usually in the north and east quadrants of the height fall region (Figure 3), UVV can be implied. The greatest local rate of change in height field, and strongest UVV, increases toward the height fall center.

3. EXAMPLES OF SEVERAL 1993-1994 WINTER STORMS

A. 0000Z Friday 12 November 1993

The Aviation Model (AVN) 48-60 hour forecast showed the greatest height change in southeast Utah (Figure 4). The height fall UVV forecast estimated most of the UVV would occur over northwest New Mexico, eastern Utah, the western half of Colorado, and Wyoming. The 12-hour AVN height forecast, from the model run just before the event (Figure 4b), showed this system was slightly deeper and slower than the 60-hour forecast. Both height fall regions however covered the same area except Wyoming. Satellite imagery at 2300 UTC (Figure 4c), and 00 hour NGM and ETA model 500-300 mb layered Q-Vector divergence (Figure 4d), showed that mid and upper-level forcing, and resultant weather, correlated well with the medium and short range height fall UVV forecast.

B. 0000Z Sunday 12 December 1993

The AVN 48-60 hour forecast showed the greatest height change over west-central Nevada (Figure 5a). Height fall UVV forecasts estimated that most of the UVV would occur over the northern half of Nevada, northern Utah, eastern Oregon, eastern Washington, Idaho, and most of Montana and Wyoming. The 12-hour AVN height forecast from the model run just before the event (Figure 5b) closely resembled the 60-hour forecast, except UVV coverage was smaller. Satellite imagery at 0100 UTC (Figure 5c), and 00 hour NGM and ETA model 500-300 mb layered Q-vector divergence (Figure 5d), showed that mid- and upper-level forcing, and resultant weather, correlated well with medium and short range height fall UVV forecasts.

C. 0000Z Friday 18 February 1994

The AVN 36-48 hour forecast showed the greatest height change over the Inter-mountain region from western Montana to northwest Utah (Figure 6a). The height fall UVV forecast showed most of the UVV was estimated to develop over the Inter-mountain and northern Rocky Mountain region south to Arizona. The AVN 12-24 hour height forecast from the model run before the event (Figure 6b) nearly resembled the old 48-hour forecast. Satellite imagery at 2300 UTC (Figure 6c), and 00 hour NGM and ETA model 500-300 mb layered Q-vector divergence (Figure 6d), showed that most of the mid and upper-level forcing, and resultant weather, correlated well with the height fall UVV forecasts.

4. CONCLUSION

When numerical models are performing well, to the first approximation, this height fall technique can be used to identify UVV from broad sweeping synoptic systems moving into the Western Region. As might be expected, this technique also accounts for a decrease (increase) in UVV associated with positive (negative) tilt troughs.

This empirical study was started in the late 1980s and finalized in the early 1990s before the availability of gridded data sets. Quasi-geostrophic theory, including the geopotential and omega diagnostic equations, showed it could be done. The author has also noticed that 500mb height fall maximum of greater than 80 meters in 12 hours can be used to forecast winter convection in Arizona. Height falls greater than 150 meters in 12 hours are associated with high wind events particularly during the spring and fall seasons.

5. REFERENCES

Holton, J.R., 1972: *An Introduction to Dynamic Meteorology.* Academic Press, pp. 103-118.

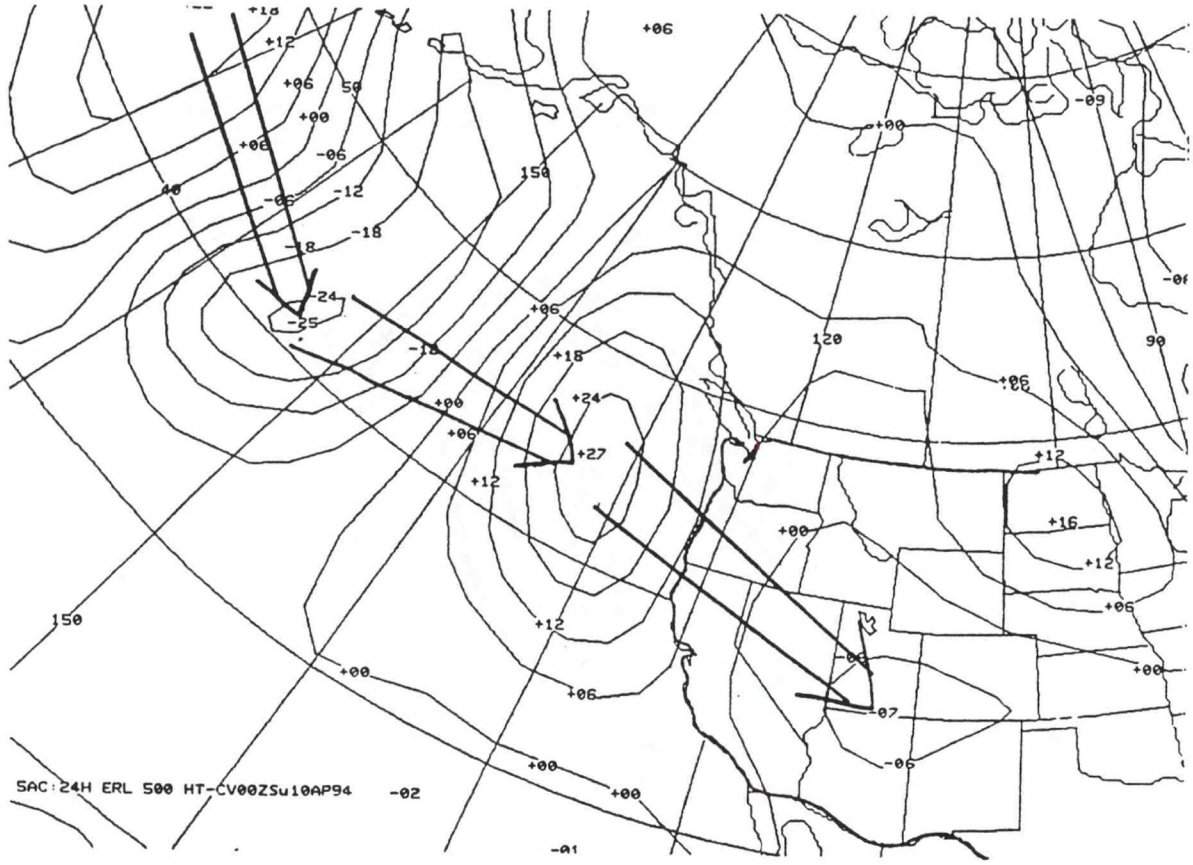

Figure 1. Example of estimated movement of synoptic systems based on geopotential height changes at 500 mb.

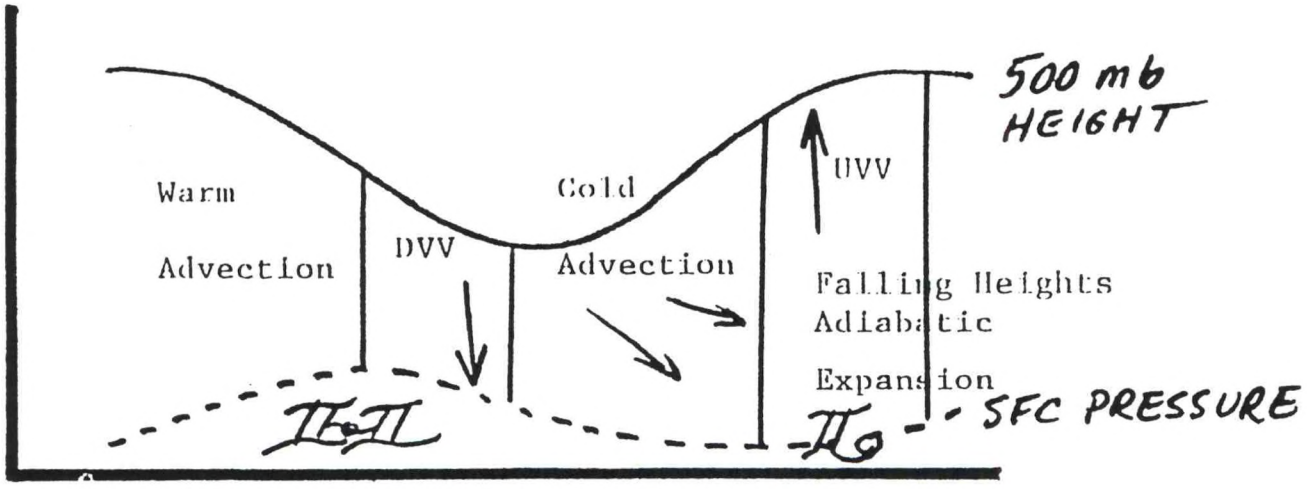

Figure 2. Qualitative relationships among height tendency, thermal advection and vertical motions.

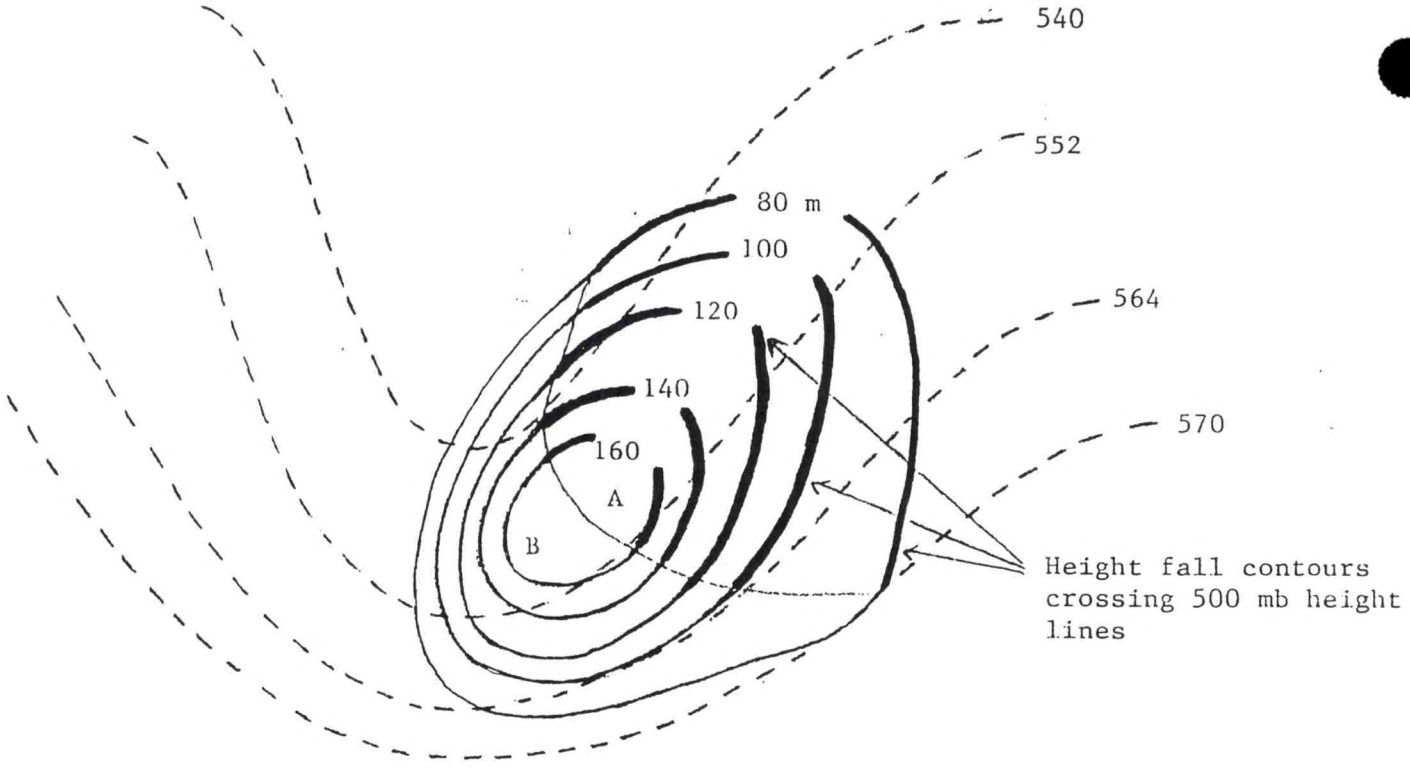

Figure 3. 500 mb Height Fall Contours (solid lines). Crossing 500 mb Height Lines (dashed). Area A denotes the UVV region. Area B is the cold advection side.

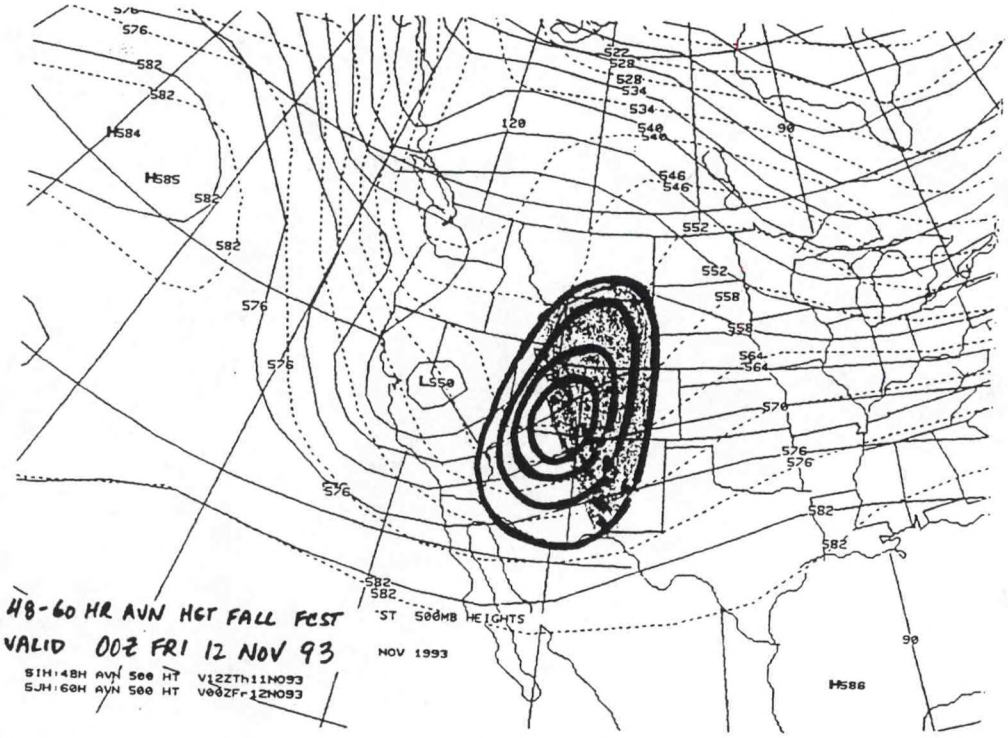

Figure 4a

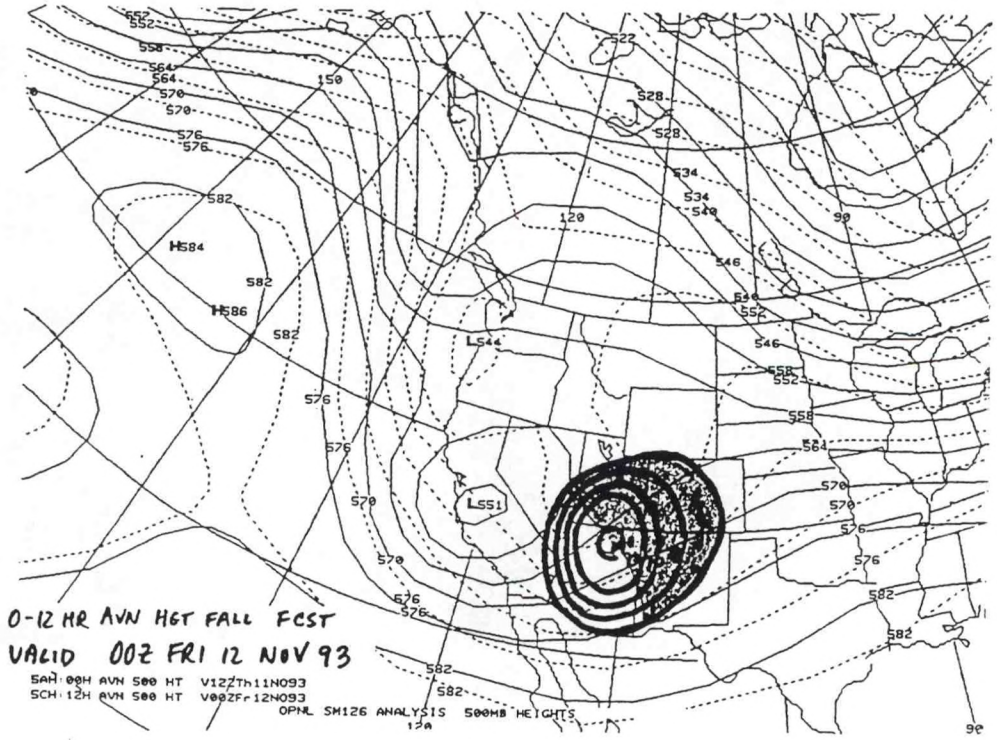

Figure 4b

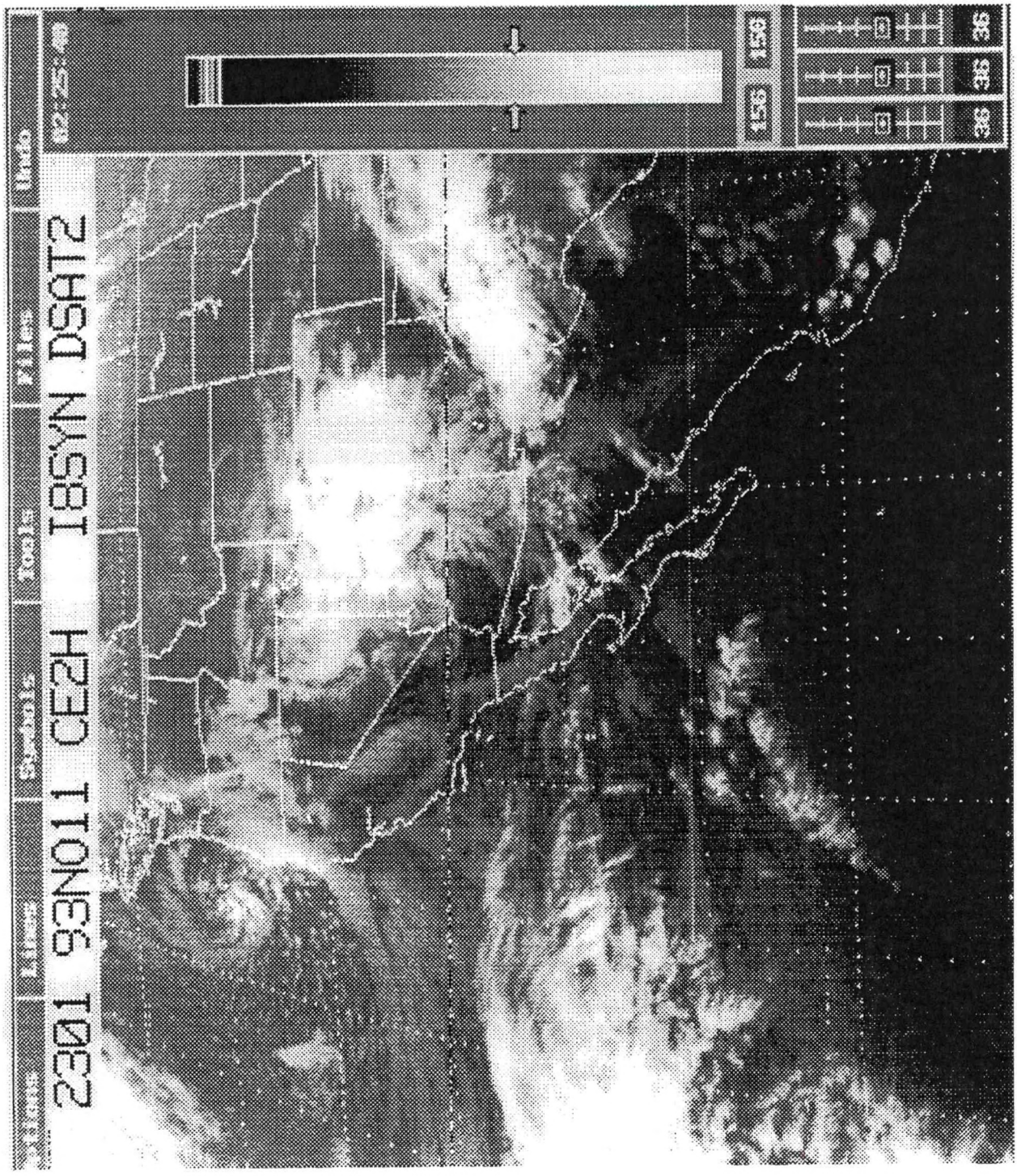

Figure 4c. IR satellite imagery for 2300 UTC 11 November 1993.

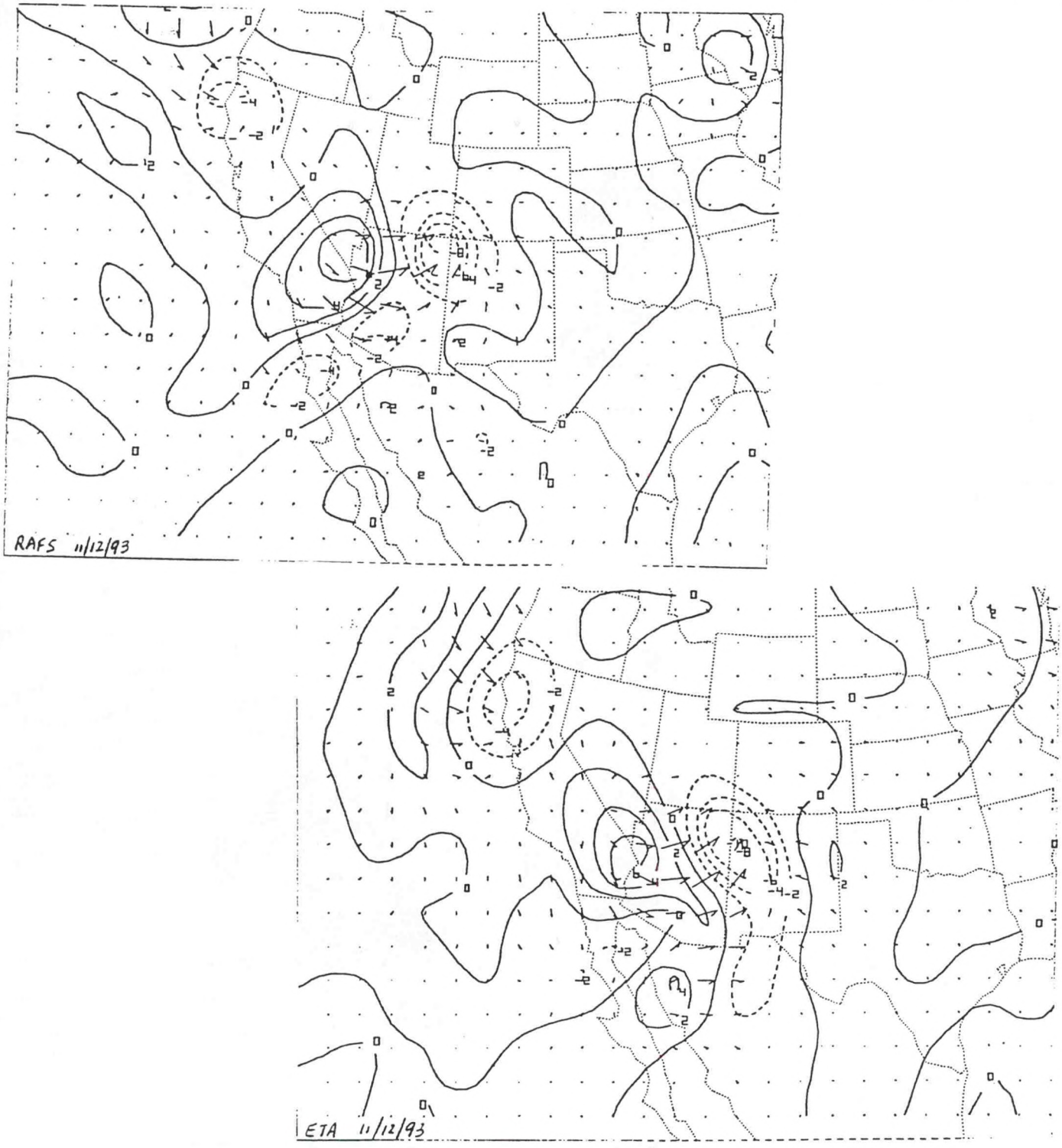

Figure 4d. 0000 hour NGM (top) and ETA (bottom) 500-300 mb layer Q-vector/layer Q-vector divergence. Negative values (Q-vector convergence), which imply UVV, are represented by dashed lines.

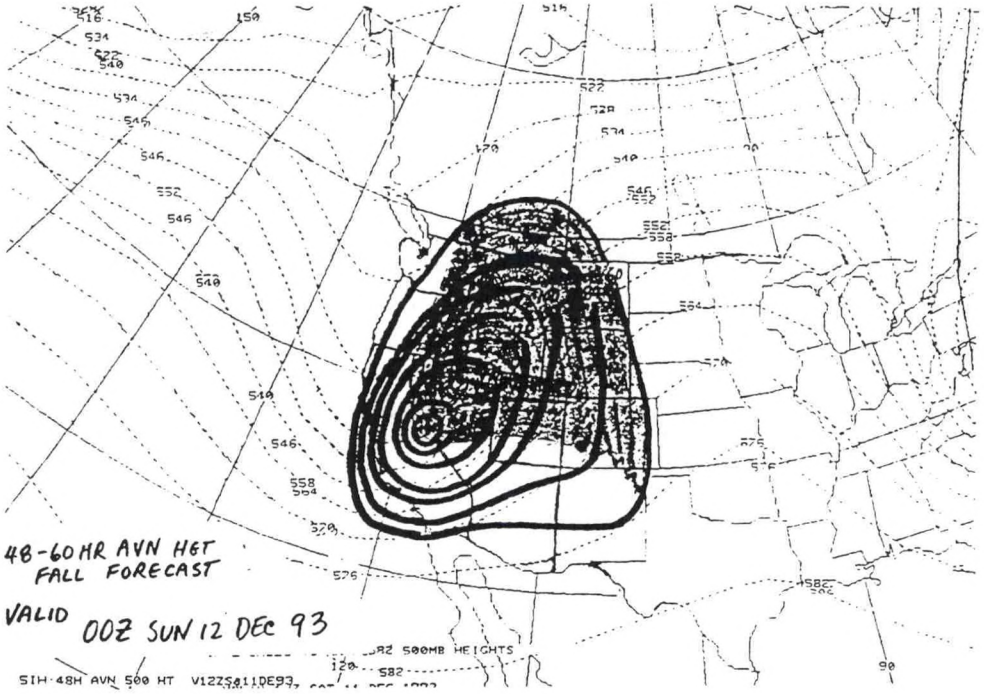

Figure 5a

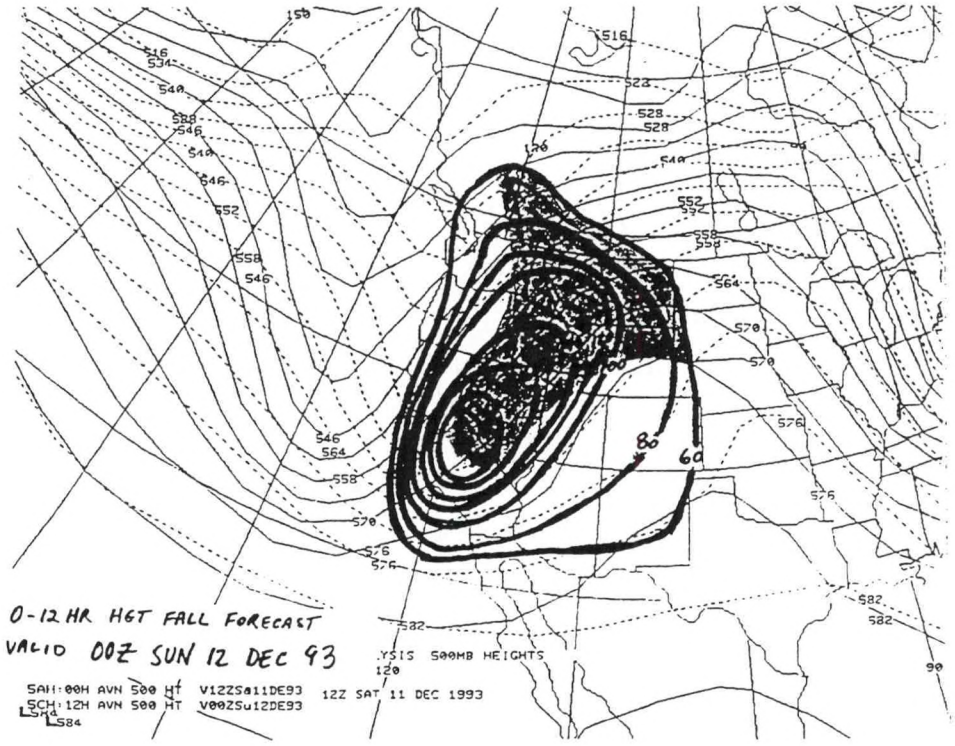

Figure 5b

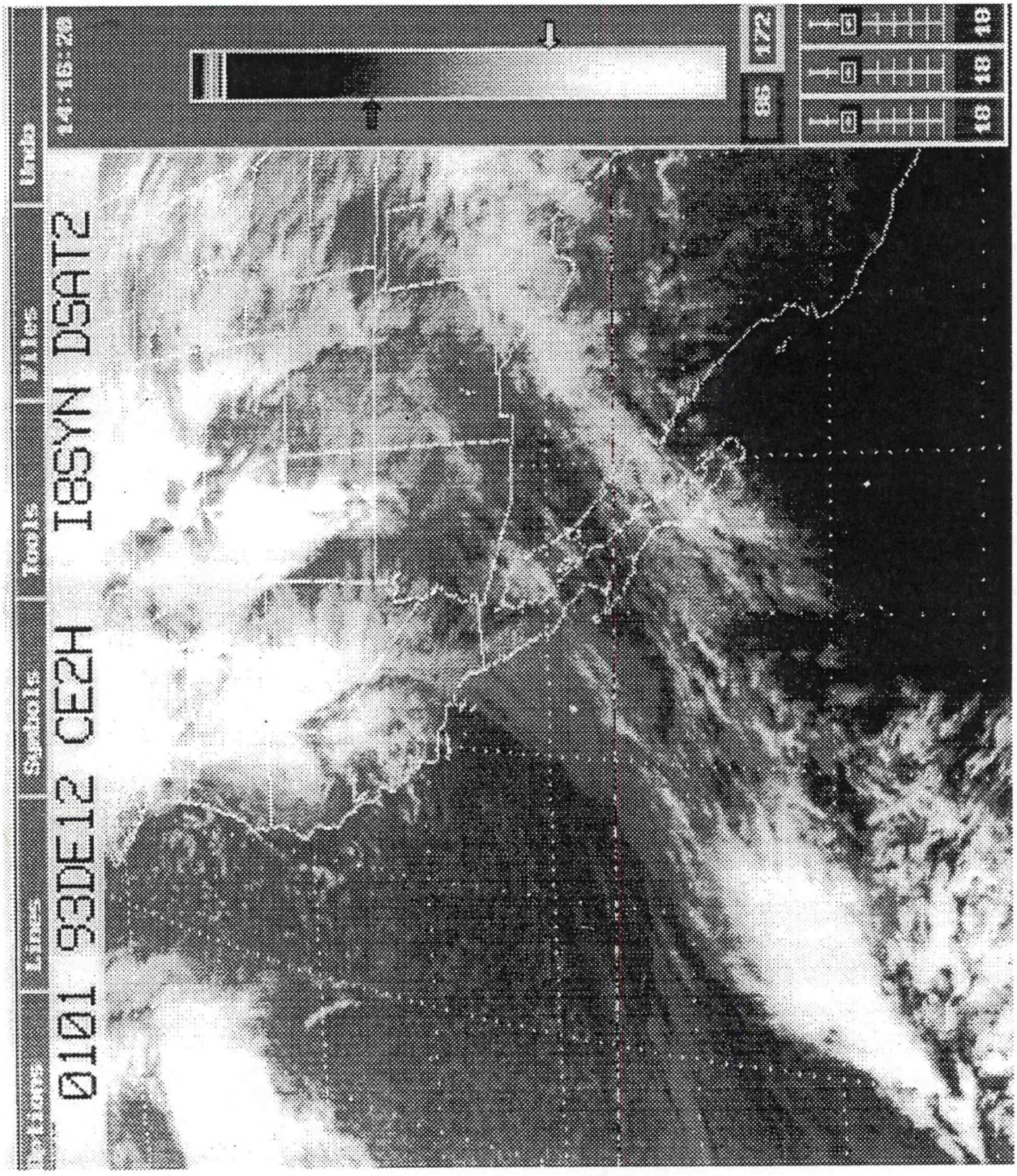

Figure 5c. IR satellite imagery for 0100 UTC 12 December 1993.

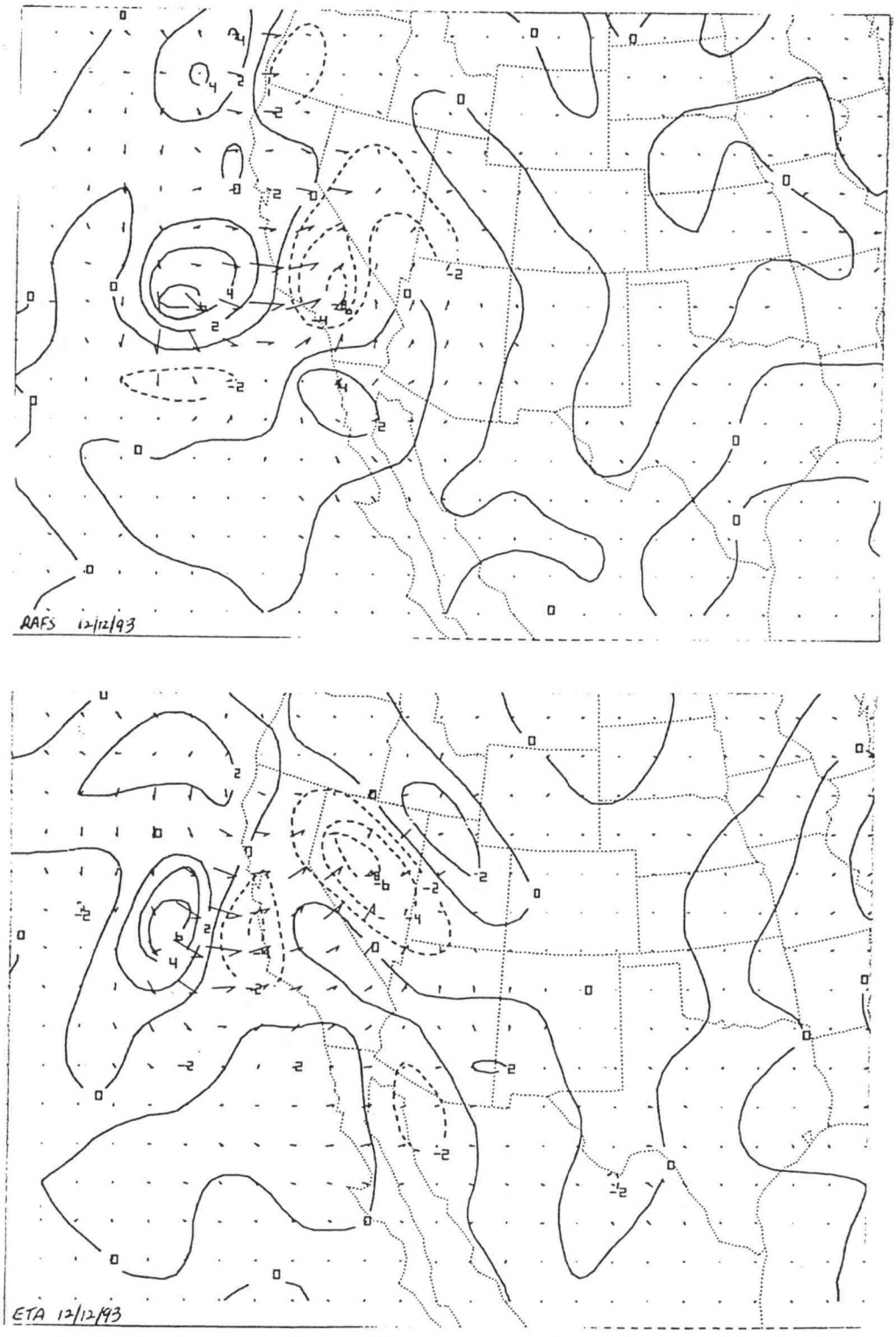

Figure 5d. 0000 hour NGM (top) and ETA (bottom) 500-300 mb layer Q-vector/layer Q-vector divergence. Negative values (Q-vector convergence), which imply UVV, are represented by dashed lines.

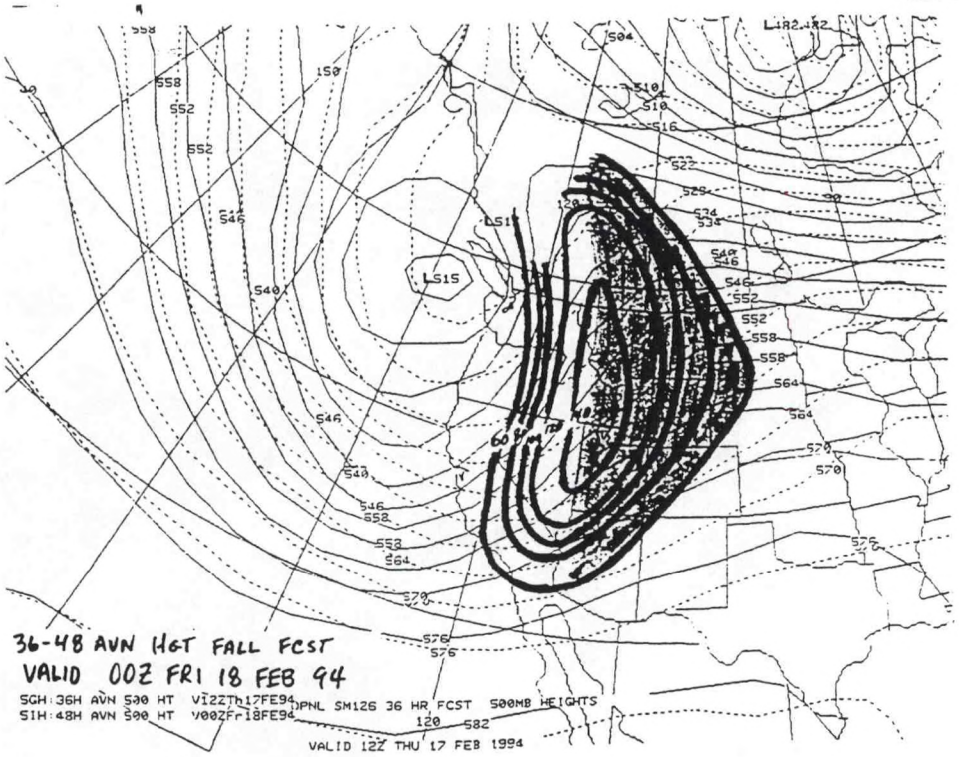

Figure 6a

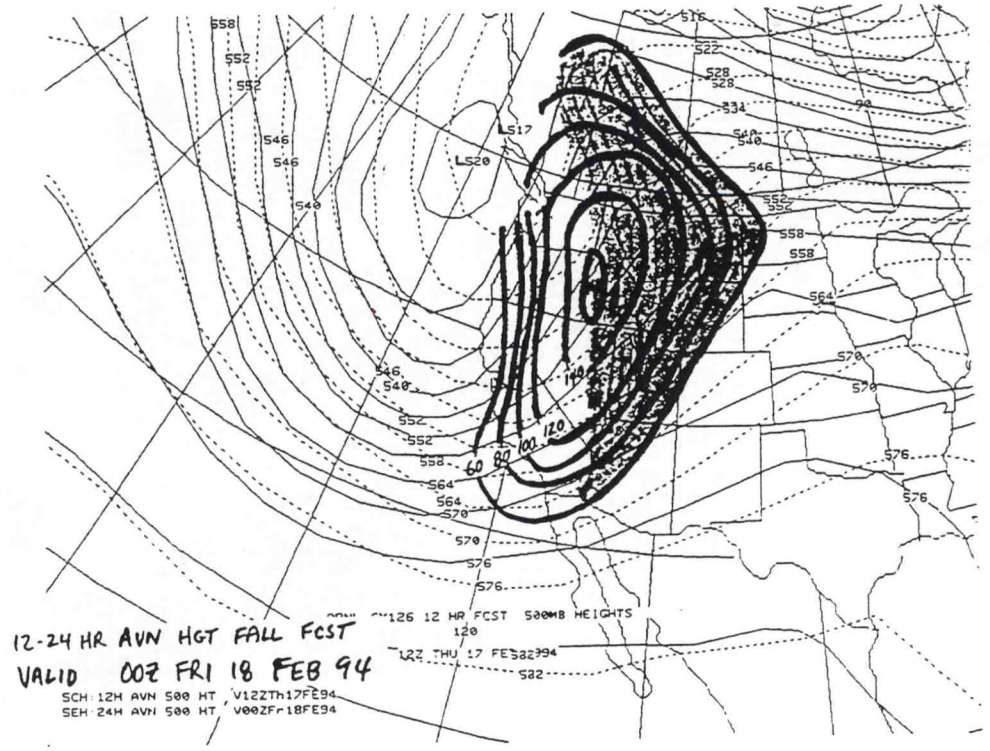

Figure 6b

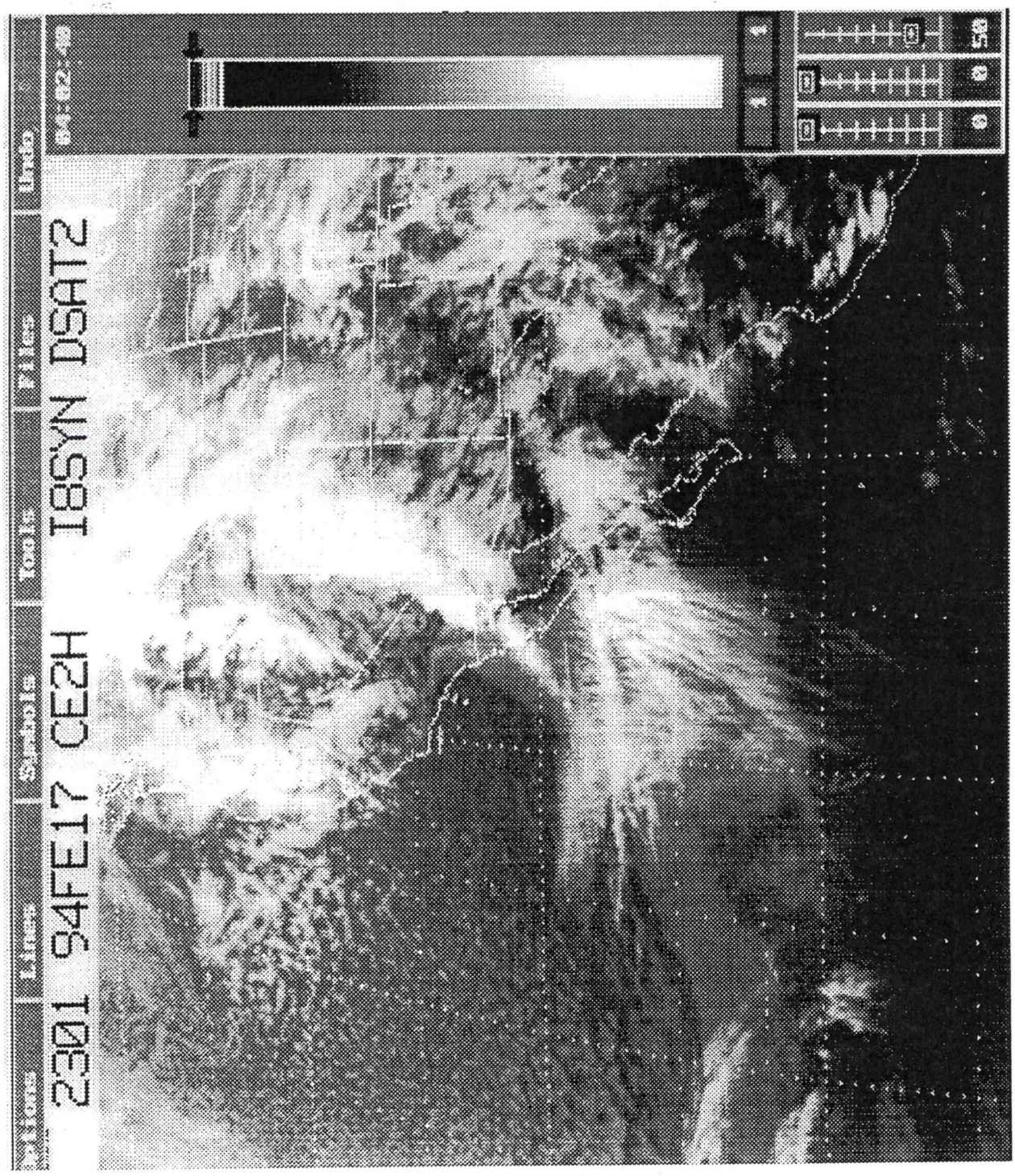

Figure 6c. IR satellite imagery for 2300 UTC 17 February 1994.

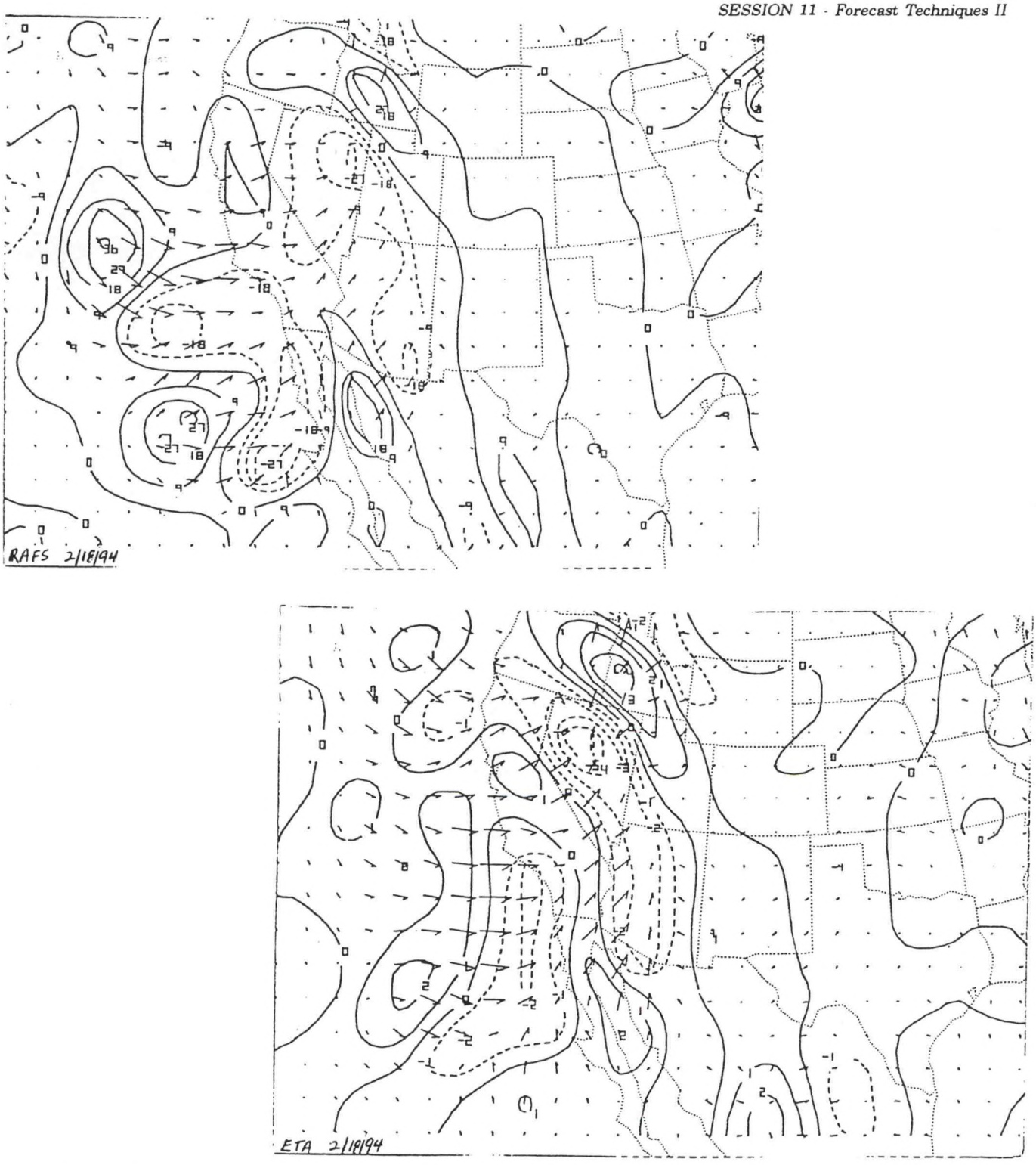

Figure 6d. 0000 hour NGM (top) and ETA (bottom) 500-300 mb layer Q-vector/layer Q-vector divergence. Negative values (Q-vector convergence), which imply UVV, are represented by dashed lines.

Forecasting Hydrologically Critical Storms in Northern and Central California

Mark H. Strobin[1] and David W. Reynolds[2]

1. INTRODUCTION

What is a hydrologically critical storm? In this paper, a hydrologically critical storm is one with heavy rain that has the potential for widespread flooding. Of vital importance in defining hydrologically critical storms is not so much the total amount of rain but the intensity of rain and the antecedent conditions.

Floods are the number one weather-related killers in the United States. The National Weather Service, Office of Meteorology, Warning and Forecast Branch have estimated that on average, 140 people die each year, and 300,000 are forced from their homes. Property damage averaged $3 billion per year in the early and middle 1980s (LaPenta et al, 1995a). To reduce losses, the Quantitative Precipitation Forecast (QPF) needs to be as accurate as possible. Knowledge of past significant flooding events, recognition of the meteorological patterns that led to these events, careful analysis of current observations including satellite and radar data, atmospheric soundings, and analysis of gridded model output are important factors in the QPF process.

This paper was developed to assist forecasters, hydrologists and staff in the northern and central California WFO's to become familiar with the meteorology associated with hydrological critical storms in their respective areas of coverage. It will help forecasters prepare emergency personnel and the public before the threat of heavy rain. The California floods of January and March 1995 show the importance of advance warning.

2. TYPICAL SYNOPTIC PATTERN OF HYDROLOGICALLY CRITICAL STORMS IN NORTHERN AND CENTRAL CALIFORNIA

Historically, most of the storms that have produced the greatest amount of rain in northern and central California are low latitude type storms that have a strong infusion of tropical/subtropical air. Some of these storms are occluded by the time they reach California with diffuse frontal systems (Monteverdi, 1976). These systems produce heavy rain primarily due to orographic enhancement, which occurs with low level flow oriented perpendicular to the mountain ranges. An example of this type of system is the storm of February 11-20, 1986 in which extensive flooding occurred in the Napa and Russian Rivers and the American River in the Sacramento Valley (Goodridge, 1992). In addition, some heavy precipitation producing storms exhibit a tremendous amount of baroclinicity with major frontal bands, such as the January and March 1995 storms.

During the beginning of the rainy season these heavy rain events are not typically hydrologically critical storms, unless they have excessive rain rates (> 1 "/hr). As the antecedent conditions change during the rainy season, it is more likely that these heavy rain events will become hydrologically critical storms.

Figure 1 shows one of the synoptic patterns of heavy rain events that can become hydrologically critical storms. This pattern is represented by a high latitude blocking ridge located over either

1. Corresponding author address: Mark H. Strobin, WSFO Monterey, California (Current affiliation: NWS Spokane, Washington).
2. David W. Reynolds, WSFO Monterey, California.

Alaska or western Canada. Strong undercutting of the ridge occurs forming a long southwesterly fetch into California from the Hawaiian Islands or even further south and west into the InterTropical Convergence Zone (ITCZ). In this scenario, the polar jet forms along 35°N, and could be quite strong with winds in excess of 75 ms-1. Northern and central California are often located in the left front exit region of this jet that greatly enhances the large scale vertical motion field. There is also a very strong 700 mb flow from the south and southwest, advecting very warm moist air into northern and central California. Condensate supply rates are maximized by a saturated lower troposphere having temperatures above 0°C to the 700 mb level and wind speeds greater than 25 ms-1. An example of a sounding from Oakland, CA during the March 1995 storm showed precipitable water of more than 200 percent of the March normal. This was almost entirely due to a very warm, moist lowest 3000 meters of atmosphere (Figure 2).

3. ANTECEDENT CONDITIONS

The antecedent conditions must be considered in determining flood potential and the need for appropriate watches or warnings. These conditions include the following: 1) the antecedent soil moisture content and degree of foliation; 2) the river channel's current base flow; and 3) the basin's topography.

In northern and central California almost all major flood-producing storms have closely followed previous heavy and/or prolonged rainfall creating saturated soil moisture conditions. Any subsequent rain will then quickly run off, adding to already swollen streams and rivers. Excessive precipitation rates are more important than rainfall totals. Flash floods are possible if precipitation rates exceed 1-3"/hr no matter how dry the soil conditions. In November 1994, San Francisco received more than 6" of rain during a period of 24-hours, yet there was very little flooding reported. Soil conditions were dry from the long summer season, and more importantly, precipitation rates were not excessive. During the January and March 1995 storms, the soil was saturated from recent previous rain. Given the high rain rates produced by these two storms, there was a tremendous amount of runoff into creeks and rivers. In addition, these waterways were overgrown with trees and other vegetation that encouraged the flooding.

River flooding from a prolonged heavy rain event can last several days after the rain has stopped due to the runoff from higher elevations. The varied topography of northern and central California can augment heavy rain events from orographic lift that will be described further in Section 4. A flood's severity can be greatly intensified by dam and levee failures as in the town of Pajaro, California (near Monterey) during the March 1995 storm.

4. PHYSICAL PROCESSES

Understanding and identifying the physical processes leading to heavy rain is important in determining hydrologically critical storms. These processes include: 1) large scale vertical motion; 2) orographic lift or shadowing; 3) precipitation mechanisms including the warm rain process; and 4) an active seeder-feeder mechanism.

The large scale vertical motion field can be enhanced by direct and indirect circulations associated with ageostrophic flow around upper level jet streaks. At times, two jet streaks can interact to produce significant vertical motions. In addition, enhanced localized regions of vertical motion can be established by what is called convective symmetric instability or CSI. Under strong vertical wind shear, near neutral stability, and a relatively moist airmass, narrow bands of enhanced precipitation can develop that may double precipitation rates over areas away from the bands.

Orographic lift can substantially enhance vertical motion. When the westerlies establish themselves over California, the low level wind speeds can approach 25 ms-1 from the south and southwest. Given the orientation of the Sierra Nevada and coastal ranges the component of the wind orthogonal to the mountain can approach 15 to 20 ms-1 and thus induce vertical motions of 0.3 to 0.4 ms-1 over the windward side of the Sierra Nevada and coastal mountains. Besides upward motions, the mechanism for precipitation formation is important in determining how the condensate produced by vertical motions will be converted to precipitation. Precipitation can be classified in two main categories; the Bergeron process which includes ice particles and the warm rain process that exclusively deal with liquid droplets (Reynolds, 1995). The heaviest precipitation will occur when both processes are active.

In complex terrain like California, an important precipitation process is the seeder-feeder mechanism (Figure 3). This occurs when mid to high level clouds form precipitating ice or rain that falls through low level liquid water produced either by large scale lift or topographic lift. This low level water is scavenged by the falling particles (Houze and Hobbs, 1982). It is estimated that the seeder cloud produces about 20-35% of the total mass of precipitation while the feeder cloud adds the additional 65-80% of the mass. In the coastal mountains of California the feeder cloud can itself produce substantial amounts of precipitation if the cloud base temperature is warmer than +10°C and there is a sufficient depth of cloud to allow time for coalescence growth to take place. This would be an exclusive warm rain process. A substantial portion of the precipitation occurring during November 6-7, 1994 when SFO set their all-time 24 hour precipitation record of over 6", was produced from the warm rain process.

5. FUTURE PRECIPITATION FORECASTING APPLICATIONS

A checklist of important meteorological features to look for in forecasting hydrologically critical storms is shown in Table 1. As the list implies, many of these features are keyed to identifying aspects of the warm rain process or to enhanced vertical motions. Empirical precipitation rates could be associated with each predictor in Table 1 based on extensive analysis of precipitation events. Based on an expected duration of each event and these processes that are active at any given time, a total rain rate could be developed. This checklist follows a similar methodology developed in 1980 at WSFO Pittsburgh and is currently used at WSFO Philadelphia (LaPenta et al, 1995b).

TABLE 1
WSFO SAN FRANCISCO HYDROLOGICALLY CRITICAL STORM FORECAST CRITERIA CHECKLIST FOR NORTHERN AND CENTRAL CALIFORNIA

1. Is airmass saturated between +10°C and 0°C?
2. Do the 700 mb winds equal or exceed 50 knots from a direction perpendicular to well defined topographic features?
3. Is the 700 mb temperature within 2°C of 0°C?
4. Is the cloud base temperature >15°C?
5. Is convection present in bands? Can these be classified into cold or warm frontal bands?
6. Does QG Omega support strong upward vertical motion over the area? Can a cross-section be constructed that would show the interaction of jet streaks over the forecast area?
7. Is CSI present or expected?
8. Are cloud tops colder than -40°C?
9. Does satellite imagery show a long continuous cloud band extending from California to subtropical latitudes?

* The more criteria in this list met, the higher the probability that a significant precipitation event is likely to occur. Other factors such as the antecedent conditions in the capture basin and the duration of the precipitation event must be investigated before forecasting a hydrologically critical storm.

6. CONCLUSION

Many factors must be considered in forecasting hydrologically critical storms. Northern and central California must be in an area of large scale vertical motion, with strong 700 mb flow from the south and southwest advecting warm, moist air into northern and central California, with a large depth of cloud warmer than 0°C. The long fetch to the subtropics allows the front to align itself with the upper flow, either stalling the front or moving it very slowly extending the duration of the event. An understanding of the antecedent soil and river conditions is very important as is the role of topography in augmenting heavy rain events. Knowledge of the various physical processes involved is also important.

Using all of this information, a hypothetical checklist was developed (Table 1). The more criteria in this list met, the higher the probability that a significant precipitation event will occur. Other factors such as the antecedent conditions in the capture basin and the duration of the precipitation event then need to be investigated to determine if this is indeed a hydrologically critical storm.

7. REFERENCES

Goodridge, J.D., 1992: A study of 1000-year storms in California. Ninth Annual Paclim Workshop.

Houze, R.A., Jr., and P.V. Hobbs, 1982: Organization and structure of precipitating cloud systems. *Advances in Geophysics*, **24**, 225-315.

Klemp, J.B., 1992: Mountains, effect on airflow and precipitation. *Encyclopedia of Earth System Science*, **3**, 251-261.

LaPenta, K.D., B.J. McNaught, S.J. Capriola, L.A. Giordano, C.D. Little, S.D. Hrenbenach, G.M. Carter, M.D. Valverde, D.S. Frey, 1995a: The challenge of forecasting heavy rain and flooding throughout the Eastern Region of the National Weather Service. Part 1: Characteristics and Events. *Wea. and Forecasting*, **10**, 78-90.

_____, _____, _____, _____, _____, _____, _____, _____, _____, 1995b: The challenge of forecasting heavy rain and flooding throughout the Eastern Region of the National Weather Service. Part 11: Forecast Techniques and Applications. *Wea. and Forecasting*, **10**, 91-104.

Monteverdi, J.P., 1976: The single airmass disturbance and precipitation characteristics at San Francisco. *Mon. Wea. Rev.*, **104**, 1289-1296.

Reynolds, D.W., 1995: The warm rain process and WSR-88D. Western Region Technical Attachment, No. 95-08. DOC/NOAA/NWS/Western Region, Scientific Services Division, Salt Lake City, UT.

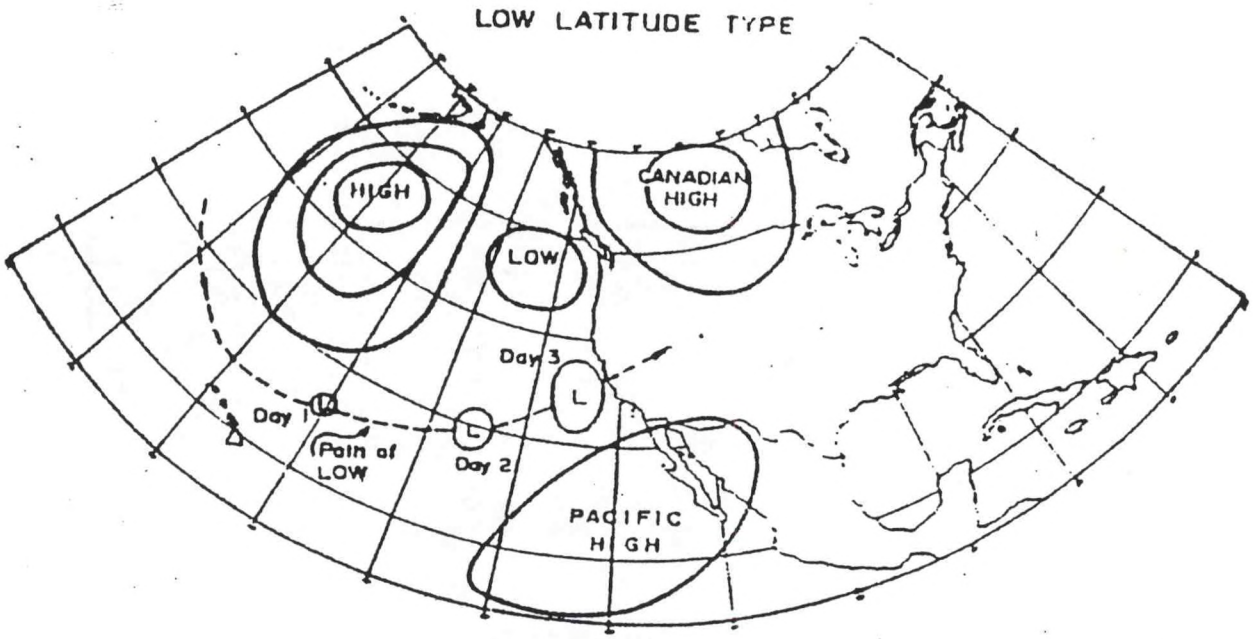

Figure 1. Schematic diagram showing Low Latitude type storm. Blocking in the Gulf of Alaska is an integral feature of this synoptic type. Disturbances pass north and south of the blocking anticyclone with southern breakthrough occurring near Hawaii. A quasi-stationary front with waves at various stages of development extends from the latitude of Hawaii northeastward into California (Monteverdi 1976).

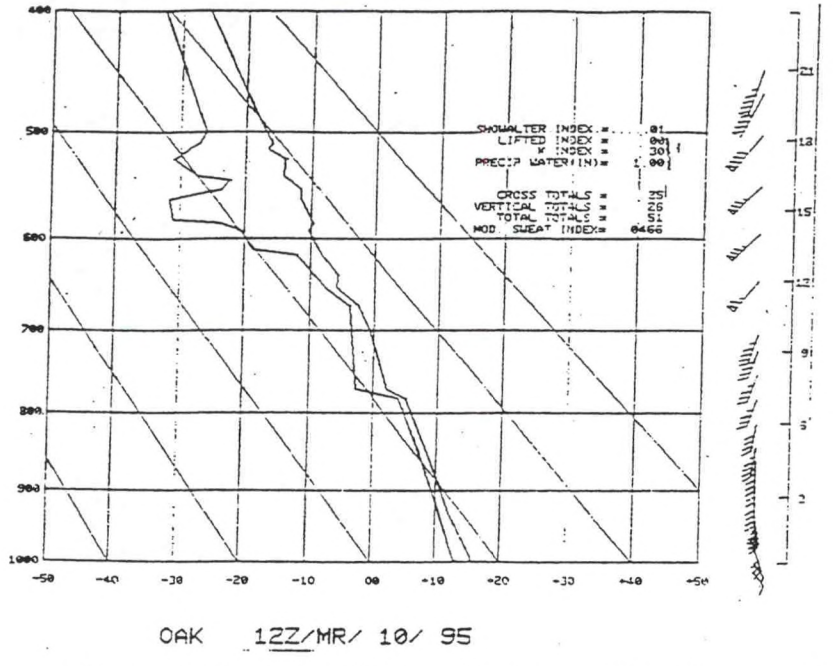

Figure 2. Sounding from Oakland, California for 1200Z on March 10, 1995. The normal precipitable water for this date is 0.46 inches.

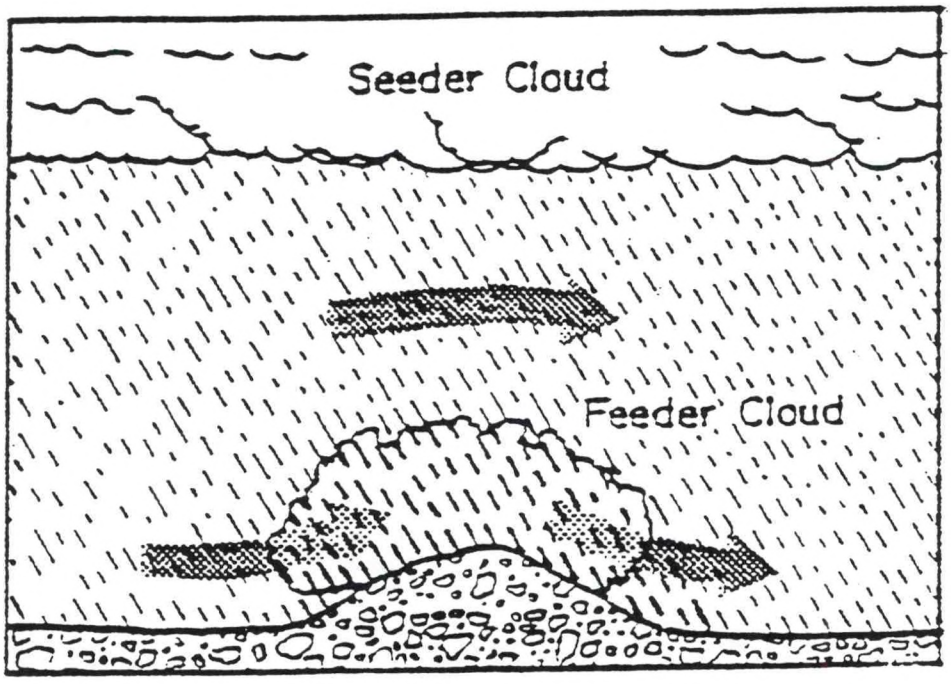

Figure 3. Seeder-feeder mechanism for the enhancement of orographic precipitation (Klemp 1992)

SESSION 12
SURVEY SESSION

41. Training Survey Results

Results of the Winter Weather Survey

Richard P. McNulty[1]

1. INTRODUCTION

A survey on winter weather was conducted during the Fourth National Winter Weather Workshop held in Kansas City, Missouri, from September 19-22, 1995. The purpose of this report is to summarize the results of that survey.

2. THE RESULTS

Tables of results are presented at the end of this report. A brief analysis is given below.

Forty-eight (48) workshop attenders responded to the winter weather survey distributed during the workshop registration process. Results from Question 7 that asked for demographic information on the group showed most responders were in their early or mid-career (5 to 14 years in meteorology and worked for the National Weather Service (37 of 48). The university community and the Atmospheric Environment Service (AES) of Canada were also represented in the group.

Question one asked the group to indicate which three weather events were the "**most difficult to forecast**" during the winter months. Precipitation type (R, ZR, IP, S, ZL) was the overwhelming winner. Heavy snow amount, heavy snow location and time of precipitation events (onset/ending) had a strong showing. All four of these events showed strong marks independent of the experience level of the responder. From a training perspective, it is good to see that the Forecasters' Development Course lesson on winter weather focuses on those areas of most concern to forecasters, i.e., heavy snow and precipitation type.

Question two asked the group that three weather events were it "**most important to forecast correctly**" during the winter season. The same four events that peaked in question one also peaked here.

Question three asked forecasters to rate the three tools or guidance "**most frequently used**" to forecast winter weather successfully. Surface and upper air data and numerical model output were the most used. Radar data, satellite data, and personal experience had a moderate second place showing.

Question four asked forecasters to indicate the "**availability of forecasting techniques**" for a variety of winter weather events. The terms none, few, some and many were used for the rating scheme. Due to the somewhat relative nature of these terms, interpretation needs to look at the distribution of results rather than the numbers in each category. Those events that have distributions shifted toward the high side (some or many) included:

- heavy snow amount
- heavy snow location
- precipitation type
- lake effect snow
- orographic snow
- convective severe weather
- storm track

1. Corresponding author address: Richard P. McNulty National Weather Service Training Center, Kansas City, MO..

Those showing a more middle ground included:

- thunder show
- ceiling and visibility
- cloud amount/occurrence
- frost/freeze
- blowing snow/blizzard
- timing of precip events.

Those showing distributions toward the low side included glazing.

It was interesting to observe that several events had distribution covering the spectrum from high to low, that is, with three or more forecasters indicating either "none" or "many" techniques were available. These events included: ceilings and visibility, cloud amount/occurrence, frost/freeze, and blowing snow/blizzard. Only ceiling and visibility showed a trend toward more techniques with more experience.

Question seven: Demographics

Years in Meteorology	Met	Other	NWS	Govern	AES	Univ	Total
		Other					
less than 5	3	1	3	--	--	1	4
5 to 9 yrs	14	1	10	1	2	2	15
10 to 14 yrs	9	1	7	1	--	2	10
15 to 19 yrs	9	--	8	1	--	--	9
20 to 24 yrs	5	--	4	--	--	1	5
more than 25 yrs	5	--	5	--	--	--	5
	45	3	37	3	2	6	48

Question 1: On the following list, mark the 3 items that you consider the most difficult to forecast during the winter months.

	YEARS IN METEOROLOGY						
	<5	5-9	10-14	15-19	20-25	>25	Total
heavy snow amount	--	7	2	5	4	2	20
heavy snow location	3	7	7	4	2	2	25
precip type (R, ZR, IP, S, ZL)	3	8	6	6	3	4	30
thundersnow	--	3	--	--	1	2	6
ceilings & visibility	1	6	1	1	--	1	10
cloud amount/occurrence	--	--	--	--	1	--	1
glazing (non-precip event)	--	1	4	--	1	1	7
lake effect snows	--	1	--	1	1	--	3
storm track	1	4	1	3	--	--	9
frost/freeze	--	1	--	--	--	--	1
blowing snow/blizzard	--	--	1	--	--	--	1
timing of precip events (onset/ending)	3	2	7	5	2	2	21
convective severe weather	--	1	--	1	--	1	3
orographic snows	--	3	--	1	--	--	4
no response	1	1	1	--	--	--	3
	12	45	30	27	15	15	144

Question 2: On the following list, mark the 3 items you feel it is most important to forecast correctly during the winter season.

	YEARS IN METEOROLOGY						
	<5	5-9	10-14	15-19	20-25	>25	Total
heavy snow amount	1	10	6	6	4	2	29
heavy snow location	4	11	8	7	3	4	37
precip type (R,ZR,IP,S,ZL)	2	10	6	7	4	3	32
thundersnow	--	--	--	--	1	1	2
ceilings & visibility	1	3	--	1	1	--	6
cloud amount/occurrence	--	--	--	--	--	--	--
glazing (non-precip event)	--	--	1	--	--	--	1
lake effect snows	--	--	--	--	1	--	1
storm track	1	2	2	1	--	--	6
frost/freeze	--	--	--	--	--	--	--
blowing snow/blizzard	--	2	1	--	--	1	4
timing of precip events (onset/ending)	3	6	4	4	1	3	21
convective severe weather	--	--	2	--	--	--	2
orographic snows	--	1	--	--	--	--	1
other/no response	--	--	--	1	--	1	2
	12	45	30	27	15	15	144

Question 3: What tools or guidance do you use most frequently to forecast winter weather successfully. Choose 3 from the following list and rank them with 1 = most used.

	1s	2s	3s	No Rank	Total
Climatology	--	2	1	--	3
Surface/Upper Air Data	18	6	5	10	39
Radar Data	1	3	4	2	10
Satellite Imagery	--	4	8	6	18
Numerical Model Output	16	12	3	9	40
NMC Discussions	--	1	4	1	6
QPF Guidance	--	--	1	1	2
MOS	1	1	--	1	3
Personal Experience	--	5	6	2	13
Past Trends/Persistence	--	1	2	-	3
Other/No response	1	2	3	1	7
	37	37	37	33	144

Question 4: For each of the following winter events, how would rate the availability of forecasting techniques:

Heavy Snow Amount	Msg	None	Few	Some	Many
less than 5 yrs	--	--	2	1	1
5 to 9 yrs	1	--	5	7	2
10 to 14 yrs	--	--	1	7	2
15 to 19 yrs	--	--	1	6	2
20 to 25 yrs	--	--	3	2	--
more than 25 yrs	--	--	1	3	1
Total	1	--	13	26	8

Heavy Snow Location	Msg	None	Few	Some	Many
less than 5 yrs	--	-	2	1	1
5 to 9 yrs	1	--	4	7	3
10 to 14 yrs	--	--	4	5	1
15 to 19 yrs	--	--	2	5	2
20 to 25 yrs	--	--	1	3	1
more than 25 yrs	--	--	1	1	3
Total	1	--	14	22	11

Precip Type (R,ZR,IP,S,ZL)	Msg	None	Few	Some	Many
less than 5 yrs	--	--	--	3	1
5 to 9 yrs	1	--	3	9	2
10 to 14 yrs	--	--	2	8	--
15 to 19 yrs	--	--	3	4	2
20 to 25 yrs	--	--	--	5	--
more than 25 yrs	--	--	2	1	2
Total	1	--	10	30	7

Lake Effect Snows	Msg	None	Few	Some	Many
less than 5 yrs	1	--	--	2	1
5 to 9 yrs	2	--	3	9	1
10 to 14 yrs	--	--	5	4	1
15 to 19 yrs	--	--	3	4	2
20 to 25 yrs	--	--	3	2	--
more than 25 yrs	---	--	1	1	3
Total	3	--	15	22	8

Orographic Snows	Msg	None	Few	Some	Many
less than 5 yrs	1	--	1	2	--
5 to 9 yrs	1	--	8	5	1
10 to 14 yrs	--	1	4	4	1
15 to 19 yrs	--	--	2	7	--
20 to 25 yrs	--	--	2	3	--
more than 25 yrs	1	--	--	2	2
Total	3	1	17	23	4

Thundersnow	Msg	None	Few	Some	Many
less than 5 yrs	--	--	2	2	--
5 to 9 yrs	1	2	12	--	--
10 to 14 yrs	--	--	4	6	--
15 to 19 yrs	--	2	5	2	--
20 to 25 yrs	--	--	5	--	--
more than 25 yrs	--	--	4	1	--
Total	1	4	32	11	--

Ceilings & Visibility	Msg	None	Few	Some	Many
less than 5 yrs	--	--	3	1	--
5 to 9 yrs	1	3	7	4	--
10 to 14 yrs	--	3	5	1	1
15 to 19 yrs	--	1	7	1	--
20 to 25 yrs	--	--	3	1	1
more than 25 yrs	--	--	2	2	1
Total	1	7	27	10	3

Cloud Amt/occurrence	Msg	None	Few	Some	Many
less than 5 yrs	--	--	3	1	--
5 to 9 yrs	2	1	8	3	1
10 to 14 yrs	--	1	5	2	2
15 to 19 yrs	--	1	6	1	1
20 to 25 yrs	--	1	2	2	--
more than 25 yrs	--	-	3	1	1
Total	2	4	27	10	5

Glazing (non-precip event)	Msg	None	Few	Some	Many
less than 5 yr	--	1	3	--	--
5 to 9 yrs	2	7	6	--	--
10 to 14 yrs	--	6	2	2	--
15 to 19 yrs	--	5	3	1	--
20 to 25 yrs	--	4	1	--	--
more than 25 yrs	--	-	3	2	--
Total	2	23	18	5	--

Frost/Freeze	Msg	None	Few	Some	Many
less than 5 yrs	--	--	3	1	--
5 to 9 yrs	1	2	8	4	--
10 to 14 yrs	--	1	3	4	2
15 to 19 yrs	--	1	6	2	--
20 to 25 yrs	--	1	3	1	--
more than 25 yrs	--	--	2	3	--
Total	1	5	25	15	2

Blowing Snow/blizzard	Msg	None	Few	Some	Many
less than 5 yrs	--	--	1	3	--
5 to 9 yrs	1	--	8	4	2
10 to 14 yrs	-	1	2	6	1
15 to 19 yrs	--	1	4	4	--
20 to 25 yrs	--	--	3	2	--
more than 25 yrs	--	--	2	2	1
Total	1	2	20	21	4

Timing of Precip. Events	Msg	None	Few	Some	Many
less than 5 yrs	--	--	1	3	--
5 to 9 yrs	1	--	6	7	1
10 to 14 yrs	--	--	5	5	--
15 to 19 yrs	--	--	6	3	--
20 to 25 yrs	--	1	2	2	--
more than 25 yrs	--	--	1	4	--
Total	1	1	21	24	1

Convective Severe Weather	Msg	None	Few	Some	Many
less than 5 yrs	--	--	1	2	1
5 to 9 yrs	1	--	--	6	8
10 to 14 yrs	--	--	2	5	3
15 to 19 yrs	--	1	1	2	5
20 to 25 yrs	--	--	4	1	--
more than 25 yrs	--	--	1	1	3
Total	1	1	9	17	20

Storm Track	Msg	None	Few	Some	Many
less than 5 yrs	--	--	--	2	2
5 to 9 yrs	1	--	2	8	4
10 to 14 yrs	--	--	-2	-5	3
15 to 19 yrs	--	--	2	5	2
20 to 25 yrs	--	1	1	2	1
more than 25 yrs	---	1	-	2	2
Total	1	2	7	24	14

LAB SESSIONS

42. WSR-88D Winter Applications
(Lab Sessions A&C)

43. Heavy Snow Forecasting at the NMC
(Lab Sessions A&D)

44. Lake-Effect Snow Forecasting
(Lab Session A)

45. Wintertime Applications of GOES-8 Imagery
(Lab Sessions B&C)

46. Utilization of Local Data Sets in Winter Weather Forecasting
(Lab Session D)

WSR-88D Winter Weather Applications Workshop

(Sessions A & C)

John Ferree[1]

The lab session began with a review of ongoing work at the Operations Support Facility pertaining to winter weather topics. This review included a discussion of the Snow Algorithm development, a field survey, and WATADS. The handout included more information on these subjects.

A video tape of time lapses of WSR-88D data from the following winter events were shown:

1. KDDC (Dodge City, KS) 11/24/92,
2. KTLX (Twin Lakes, OK) and KSTL (St. Louis, MO) 3/8/94,
3. KSTL (St. Louis, MO) 1/16-17/94,
4. KCCX (State College, PA) 10/30-31/94,
5. KCCX (State College, PA) 12/5/93,
6. KCCX (State College, PA) 3/2-3/94,
7. KGLD (Goodland,CO) 2/12/95,
8. KLOT (Chicago,IL) 2/9-10/94,
9. KFTG (Denver, CO) 12/21-22/93, and
10. KFTG (Denver, CO) 1/29-30/94.

Participants were asked to make snowfall accumulation estimates using the radar data and hourly surface observations. The major points from this exercise are included as a Summary of Strengths and Limitations of the WSR-88D in Winter Weather Situations.

1. Corresponding author address: John Feree, Operational Support Facility, Operations Training Branch, 3200 Marshall Avenue, Norman, OK.

WSR-88D Algorithms Testing and Display System (WATADS)

Why?

WATADS will give users the capability to conduct WSR-88D algorithm studies in-house. Investigations could include case studies, adaptable parameter studies, algorithm performance evaluations, user interface evaluations, etc.

What?

A software package ported to the NWS SACs that will run the WSR-88D baseline algorithms, and the Enhanced NSSL algorithms using recorded Archive Level II data. The package will use the NSSL RADS (Radar Algorithm Display System) display software. NSSL algorithms included in the first release will include the Storm Cell ID/Tracking (SCIT), Hail Detection (HDA), Tornado Detection, and Mesocyclone Detection. Baseline algorithms included will be Meso/TVS, Storm Series, Precipitation Processing Subsystem, Hail Detection, VAD/VWP, Storm Relative Velocity, and Velocity Dealiasing. This package will include an Algorithm Cookbook containing information on algorithms and adaptable parameters. This Cookbook will include the ranges of values allowed, expected effects of changing adaptable parameters, and the verification/scoring methods suggested by the OSF.

Who?

The OSF will release the software to all NWS forecast offices and RFCs, NEXRAD agencies requesting the software, COMET, Universities in collaborative work with NEXRAD agencies, and other government agencies. Follow-on support will be provide by NSSL with the OSF Applications Branch acting as focal point. Participation will be voluntary, but participants will be asked to share results with the OSF to insure a core of consistent verification methodology and criteria. The OSF will then merge results enabling regional applications, and the crossfeeding of results to other users.

When?

The test plan approach is similar to that used in WSR-88D software releases. OSF operations testing are currently in progress. Beta tests at select sites are currently planned for October and November. Final release is currently planned as a Christmas present. Limited funds are available, but upgrades are expected to include corrections, VIL Cross Sections, time lapses, map enhancements, and enhanced algorithms (i.e., damaging downburst).

For more information:
Applications Branch WSR-88D OSF
Voice: (405) 366-6530 (xtn 2226)
email: jdavis@nexrad.osf.uoknor.edu

WSR-88D Snow Accumulation Algorithm

- 3-YEAR MOU ESTABLISHED WITH U. S. BUREAU OF RECLAMATION TO DEVELOP A LIQUID WATER EQUIVALENT AND A SNOW DEPTH ACCUMULATION ALGORITHM
- PPS-LIKE PRODUCTS
- WILL USE Z-S RELATIONSHIPS
- WILL CONSIDER WIND ADVECTION EFFECTS

==========

Year #1 (June '95 - May '96)

- DEVELOP BASIC PROTOTYPE ALGORITHM FOR ESTIMATION OF **SNOWFALL WATER EQUIVALENT (S)**
- INITIAL ALGORITHM (CODE DUE 1 JUNE '96)
  - BASED ON RADAR VS. GAGE MEASUREMENTS (**Z** vs. **S**)
  - WILL CONSIDER HORIZONTAL DRIFT OF SNOW USING WSR-88D VWP
  - WILL CONSIDER RANGE EFFECTS
  - WILL CONSIDER GROUND CLUTTER AND TERRAIN BLOCKAGE
  - USE LEVEL II DATA INPUT
- COLLECT GAGE MEASUREMENTS OF **S**, SNOW BOARD/STAKE OBS OF **SD**, AND CORRESPONDING WSR-88D REFLECTIVITIES (**Z**) AT THREE SITES (ONE OF THESE SITES WILL BE AT CLEVELAND IN SUPPORT OF THE LAKE EFFECT SNOW STUDY).

==========

Year #2 (June '96 - May '97)

- REFINE ALGORITHM BASED ON RADAR VS. SURFACE MEASUREMENTS
- EXPAND ALGORITHM TO INCLUDE ESTIMATION OF **SNOW DEPTH (SD)**
- BASIC PRODUCTS (**S** AND **SD** ACCUMULATIONS)
  - ONE-HOUR
  - THREE-HOUR
  - STORM-TOTAL
- DELIVERABLE - DUE 1 NOVEMBER '96
  - CODE OPERATIONAL ON SUN UNIX "PROOF OF CONCEPT" DATA-INGEST WORKSTATION
  - COMPATIBLE WITH NSSL RADS
  - SUITABLE FOR TESTING AT SELECTED WSR-88D SITES

- EXPAND ALGORITHM TO AUTOMATICALLY ADJUST **RADAR-ESTIMATED S** BY INCORPORATION OF REAL-TIME **SURFACE MEASUREMENTS OF S**

- DELIVERABLE - DUE 1 JUNE '97
  - 1 NOV '96 OPERATIONAL CODE PLUS CAPABILITY FOR AUTOMATIC ADJUSTMENTS BASED ON SURFACE MEASUREMENTS

- DEVELOP PARTITIONS OF Z-S RELATIONSHIPS AS FUNCTION OF:
  - PREDOMINANT ICE PARTICLE TYPES AND FALL SPEEDS
  - RAWINSONDE AND SURFACE OBSERVATIONS
  - STORM TYPES
  - STORM PHASE
  - CLOUD TOP HEIGHT

- COLLECT GAGE MEASUREMENTS OF **S**, SNOW BOARD/STAKE OBS OF **SD**, AND CORRESPONDING WSR-88D REFLECTIVITIES (**Z**) AT ADDITIONAL SITES

==========

Year #3 (June '97 - May '98)

- TEST AND REFINE ALGORITHM WITH DIVERSE DATA SETS

- PROVIDE RECOMMENDATIONS ON OPTIMUM ADAPTABLE PARAMETERS
  - FOR ALL MAJOR SNOW REGIMES OF U.S.
  - BASED ON LOGICAL PARTITIONS OF Z-S RELATIONSHIPS

- DELIVERABLE - DUE 30 MAY '98
  - FINAL VERSION OF ALGORITHM
  - COMPREHENSIVE DOCUMENTATION

Summary of Strengths and Limitations of the WSR-88D in Winter Weather Situations

STRENGTHS

☺ The WSR-88D detects snow better than conventional radar due to increased transmitter power, increased antenna gain, and a narrow beam width (0.95°).

☺ Precipitation Processing Subsystem (PPS) estimates rainfall accumulations, which may be useful in estimating snowfall accumulations.

☺ Numerous adaptable parameters in the PPS allows for improvements and local adaptations.

☺ Observations of bright band trends are an indication of the slope of the freezing level, and can be used in "Nowcasting" a change in precipitation phase.

☺ A Snow Algorithm is under development.

LIMITATIONS

☹ The radar beam overshoots shallow phenomena.

☹ Reflectivities vary due to mixed state, not intensity (i.e., Bright Band Contamination).

☹ Strong low level winds can cause snow to fall several miles from the radar echo.

☹ Reflectivity to snow relationships (Z-S) are much more difficult to establish than Z-R relationships, often varying over short distances in the same area.

☹ Gage and observer measurements of snow are difficult

Heavy Snow Forecasting at the NMC
(LAB SESSIONS A&D)

Bruce Terry[1]

MODEL PERFORMANCE SUMMARY OF MAJOR BIASES

- NGM, AVN, AND ETA TOO FAR NORTH AND TOO STRONG WITH SYSTEMS COMING OUT OF THE ROCKIES
- NGM GROSSLY UNDER FORECASTING RAINS ACROSS THE SOUTH DURING THE COOL SEASON
- AVN (AND OFTEN NGM) OVER FORECASTING UPSLOPE PCPN OVER THE CENTRAL/SOUTHERN ROCKIES
- AVN PREMATURELY WEAKENING SEPARATE SOUTHERN STREAM SYSTEMS: OR TOO OFTEN PHASING THE TWO SEPARATE STREAMS
- NGM UNDER FORECASTING PCPN AMOUNTS INTO THE WEST COAST WITH A BLOCKING RIDGE OVER THE GULF OF AK
- ETA (AND NGM) TOO FAR WEST WITH SIGNIFICANT SURFACE CYCLONES COMING UP THE EAST COAST
- MODELS TOO SLOW (ETA BETTER) WITH ARCTIC AIR MASSES PLUNGING SOUTHWARD DOWN THE PLAINS
- MODELS (ESPECIALLY NGM) HOLD ON TO TOO MUCH PCPN IN TX (USUALLY SPRING AND/OR FALL/EARLY WINTER) WHEN MID LEVEL FLOW IS SOUTHWESTERLY AND FRONT IS STILL IN TX BUT ON THE MOVE; ORGANIZED RAINS SWEEP OUT WELL AHEAD OF FRONT ALONG PRE-FRONTAL SQUALL LINE

1. Corresponding author address: Bruce Terry, WFB, HPC, Camp Springs, MD.

HEAVY SNOW AND THE SURFACE PATTERN
EASTERN AND CENTRAL U.S.

HEAVY SNOWS OCCUR:

- AROUND 2° TO 2.5° LATITUDE TO THE LEFT OF THE TRACK OF THE LOW
- ABOUT 5° LATITUDE AHEAD OF THE LOW
- WHEN THE LOW DEEPENS--WHEN THE LOW BEGINS TO FILL AND BECOME VERTICAL, THE HEAVY SNOW USUALLY ENDS
- WHEN THE COLD SURFACE ANTICYCLONE IS TO THE NORTH OR NORTHWEST--TYPICALLY ENHANCED BY CONFLUENT MID LEVEL FLOW

GOREE AND YOUNKIN, 1966

==========

12-HOUR HEAVY SNOW - SURFACE PATTERN
LOW AT ORIGIN; MOVEMENT ALONG X-AXIS

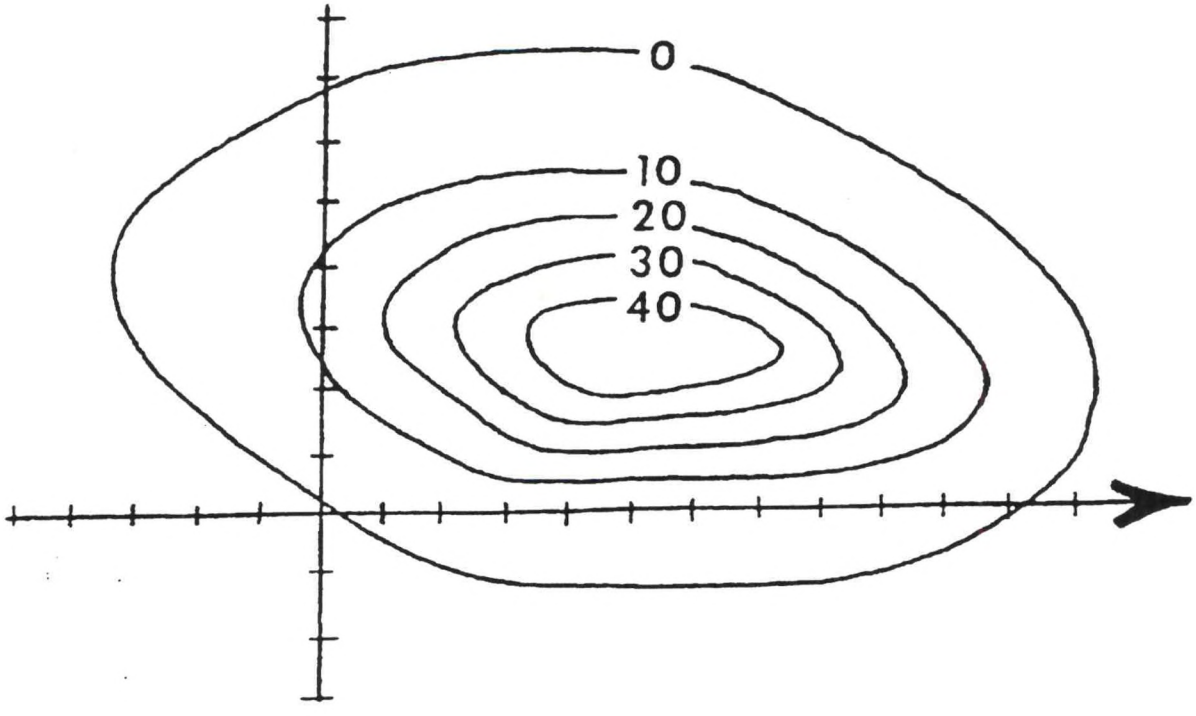

HEAVY SNOW AND THE 850MB PATTERN
EASTERN AND CENTRAL U.S.

HEAVY SNOWS OCCUR:

- ABOUT 1.5° TO THE LEFT OF THE TRACK OF THE H85 LOW
- WHEN THE MEAN CIRCULATION DEEPENS SIGNIFICANTLY
- WHEN COOLING OCCURS IN THE REAR QUADRANT OF THE LOW DURING THE EARLY STAGES OF DEVELOPMENT
- ABOUT THE INITIALLY OBSERVED -5°C ISOTHERM I.E. HEAVY SNOW DURING THE NEXT 12 HOURS WOULD OCCUR WHERE THE -5°C ISOTHERM WAS OBSERVED
- WITH LOWS THAT GENERALLY MOVE NORTHEASTWARD--HEAVY SNOWS ARE MORE RARE WITH LOWS DROPPING SOUTH OF EAST

BROWNE AND YOUNKIN, 1970

12-HOUR SNOW - 850MB PATTERN
LOW AT ORIGIN; MOVEMENT ALONG X-AXIS

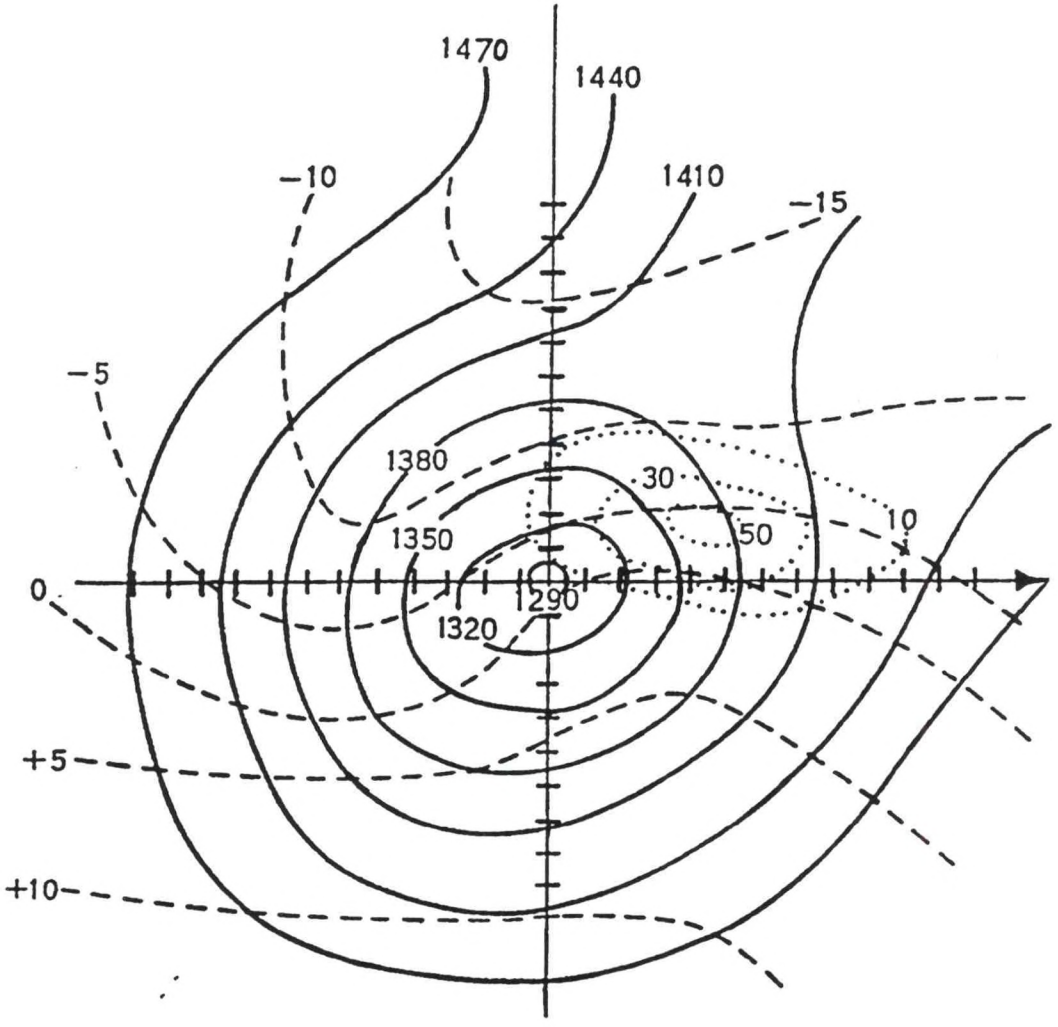

HEAVY SNOW AND THE 500MB PATTERN
EASTERN AND CENTRAL U.S.

HEAVY SNOWS OCCUR:

- ABOUT 7° LATITUDE DOWNSTREAM OF THE VORT MAX
- SLIGHTLY LEFT OF THE TRACK OF THE CLOSED LOW/STRONG VORT MAX (AROUND 2°)
- SLIGHTLY DOWNSTREAM FROM WHERE THE CURVATURE CHANGES FROM CYCLONIC TO ANTICYCLONIC
- WHEN THE 500MB TROF OR LOW DEEPENS
- WHEN THE AVERAGE LOWEST 500MB TEMP WITHIN A DISTANCE OF 3° OF THE VORT MAX IS -30°C

GOREE AND YOUNKIN, 1966

12-HOUR HEAVY SNOW - 500MB PATTERN
VORT MAX AT ORIGIN; MOVEMENT ALONG X-AXIS

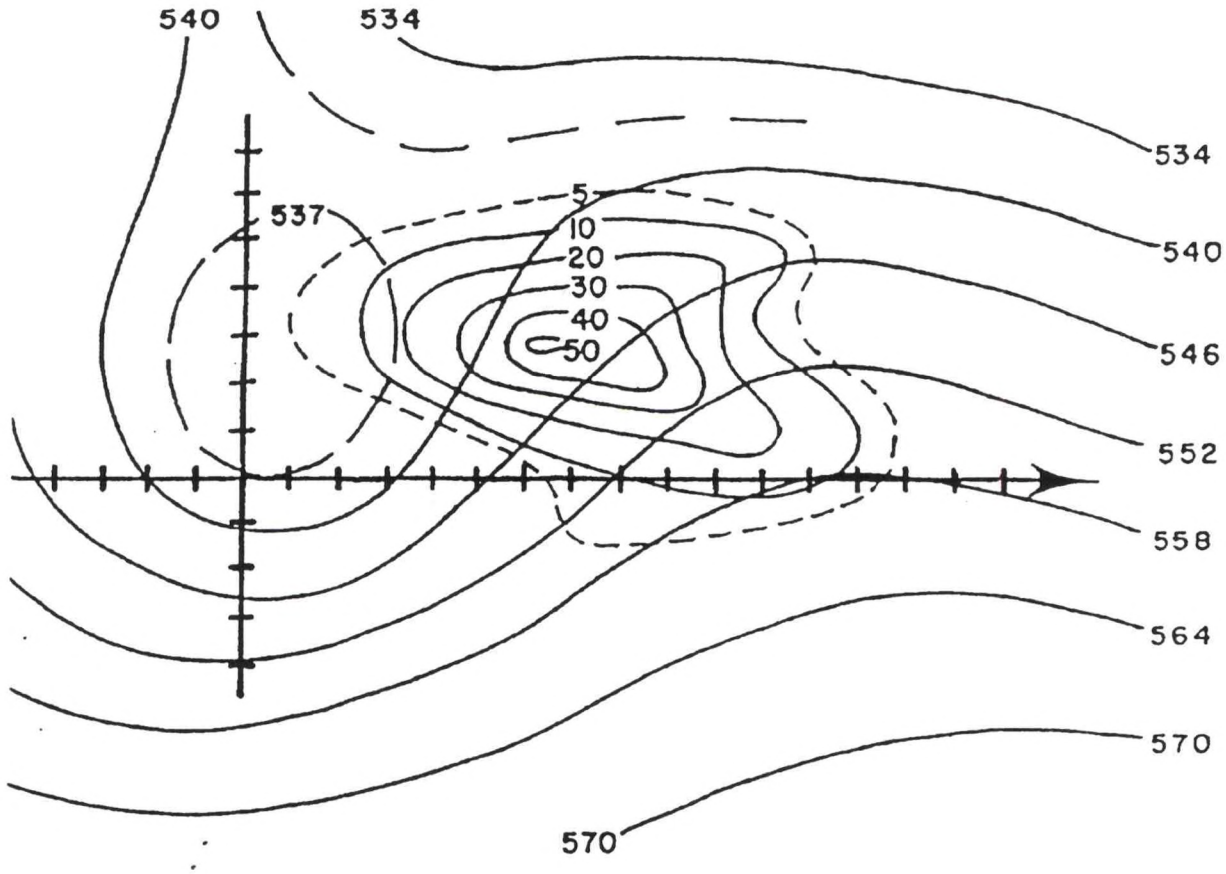

HEAVY SNOW AND CLIPPER TYPE STORMS

- SNOWFALL AMOUNTS USUALLY RELATE TO HOW MANY CLOSED CONTOURS THERE ARE AROUND THE SURFACE LOW AND HOW STRONG THE VORT MAX IS--STRONGER, MORE DEFINED FEATURES PRODUCE HEAVIER SNOW
- HEAVIEST SNOWS OCCUR WHEN BOTH ARE DEEPENING
- USUALLY HIGH SNOW TO LIQUID RATIO--UP TO 20 TO 1-- WHICH RESULTS IN HEAVY SNOWS WITH MEAGER WATER EQUIVALENTS
- WIND DRIVEN SNOW CAN BE A BIG PROBLEM

==========

LAKE EFFECT SNOWS

- STRONG FLOW OF ARCTIC AIR ACROSS WARMER LAKES
- CYCLONIC FLOW AND A DEFINABLE, PROGRESSIVE SHORT WAVE PREFERRED FOR HEAVIER SNOWS
- BOUNDARY LAYER FLOW DIRECTED ACROSS THE LONGEST FETCH OF THE LAKE(S) GREATLY ENHANCES SNOW AMOUNTS--MAINTAINS HIGHER TRANSPORT OF MOISTURE
- DIFFERENCE IN TEMPERATURE BETWEEN THE LAKES AND 850MB SHOULD BE AT LEAST 13°C. HEAVY SNOWS BECOME MUCH MORE LIKELY WHEN AIR-LAKE TEMPERATURE DIFFERENCE APPROACHES 20°C.
- "OPEN" LAKES MUCH MORE CONDUCIVE TO HEAVY SNOWS--ICE COVERED LAKES (GREATER THAN 65% ICE) CAN AND WILL CUT SNOW AMOUNTS DRAMATICALLY

HEAVY SNOW--GENERAL RULES
WESTERN U.S.

- HEAVY SNOWS IN THE WEST ARE OFTEN OROGRAPHICALLY ENHANCED, PARTICULARLY BY DEEP UPSLOPE FLOW
- MANY OF THE "SYNOPTIC" SITUATION SNOWS ARE RELATED TO 500MB PARAMETERS AND FURTHER CLASSIFIED AS EITHER "DIGGING" OR "COMING OUT" TYPES
- IN GENERAL, GREATEST PREDOMINANCE OF HEAVY SNOW OCCURRED BETWEEN -20° AND -30°C 500MB ISOTHERM
- FOR "DIGGING" SYSTEMS THE GREATEST PROBABILITY OF HEAVY SNOW WAS 4° TO 5° LATITUDE DOWNSTREAM AND 3° LEFT OF THE VORT TRACK. FOR "COMING OUT" SYSTEMS HEAVY SNOWS OCCURRED 3° TO 5° LATITUDE DOWNSTREAM AND 3° LEFT OF THE VORT TRACK WITH A SMALLER MAXIMUM OF SNOW ABOUT 7° LATITUDE DOWNSTREAM AND 1° TO 2° LEFT OF THE TRACK
- OCCURRED MAINLY IN THE 534-546 THICKNESS CHANNEL

YOUNKIN, 1968

==========

HEAVY SNOW
PACIFIC NORTHWEST TYPE

- DIFFERENT FROM OTHER WESTERN TYPES
- 500 MB TROF POSITION ABOUT 10° OF LATITUDE DISTANCE (WEST) FROM CENTER OF HEAVY SNOW (USUALLY MUCH LESS IN OTHER TYPES)
- HEAVY SNOW OCCURRED MOSTLY BETWEEN 528-540 DM THICKNESS CHANNEL, SOME 60 M LESS THAN IN OTHER WESTERN TYPES
- MORE OF A "WARM ADVECTION" TYPE SNOW EVENT, AS EVIDENCED BY FLOW AND ISOTHERM STRUCTURE

YOUNKIN, 1968

12-HOUR HEAVY SNOW-500MB PACIFIC NORTHWEST CENTROID OF HEAVY SNOW AT ORIGIN

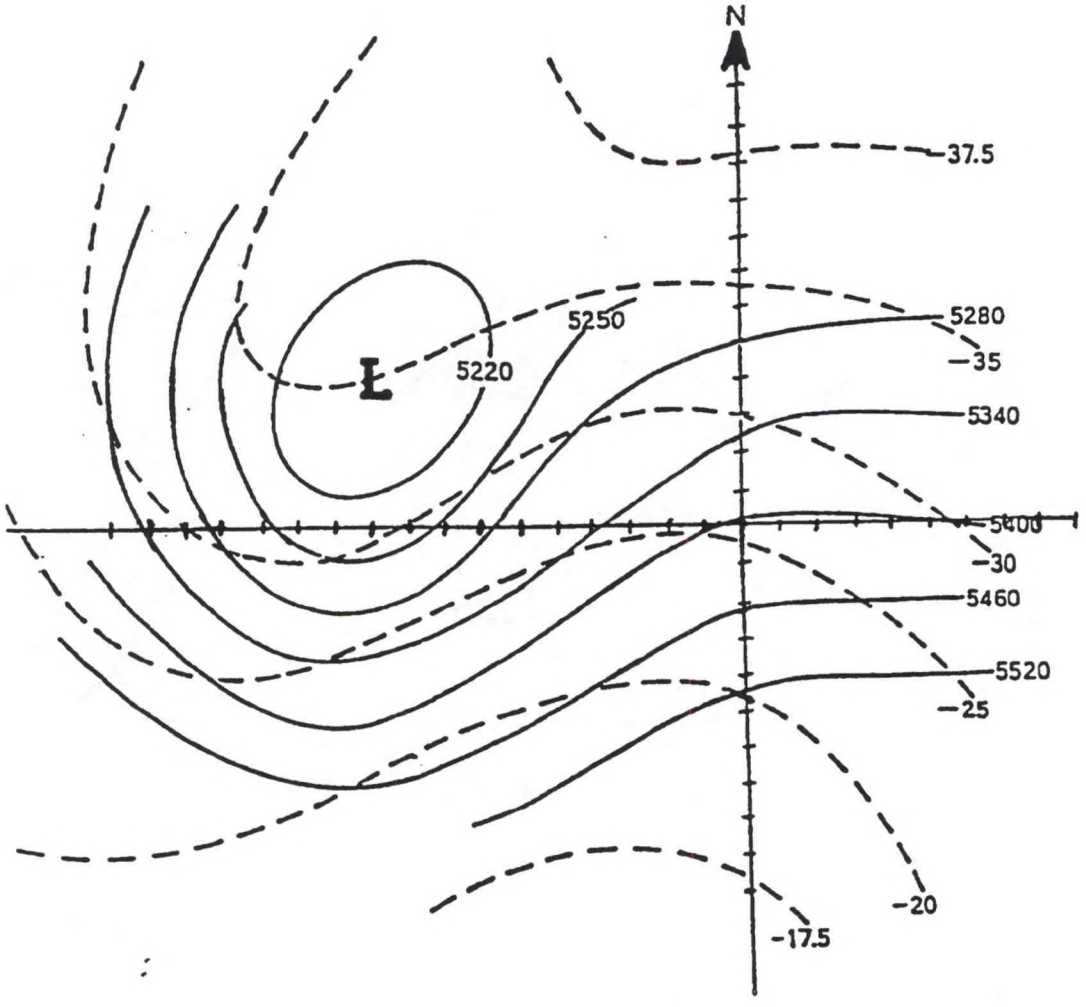

YOUNKIN, 1968

12-HOUR HEAVY SNOW - 1000-500MB THICKNESS PACIFIC NORTHWEST CENTROID OF HEAVY SHOW AT ORIGIN

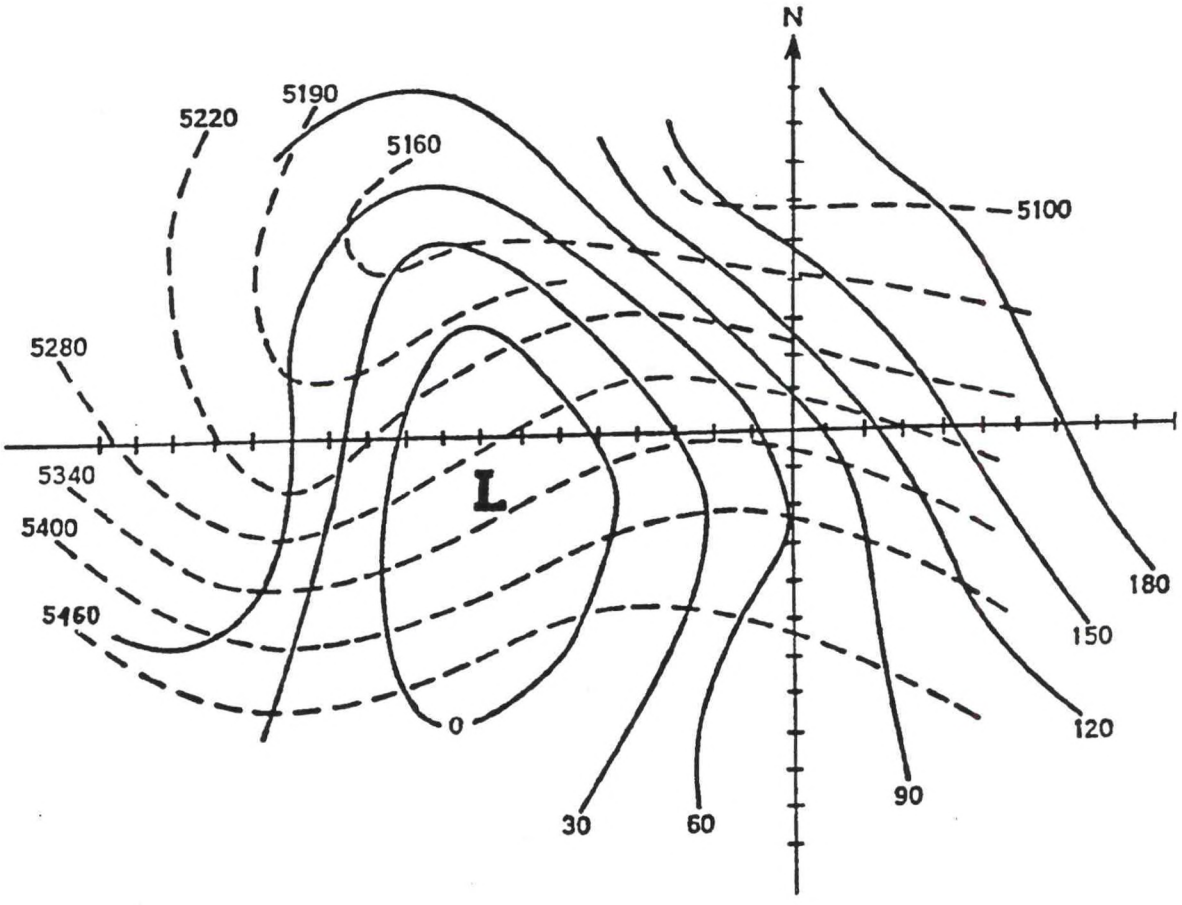

NWS Winter Weather Workshop, Sept. 19-22

Lake Effect Snow Forecasting

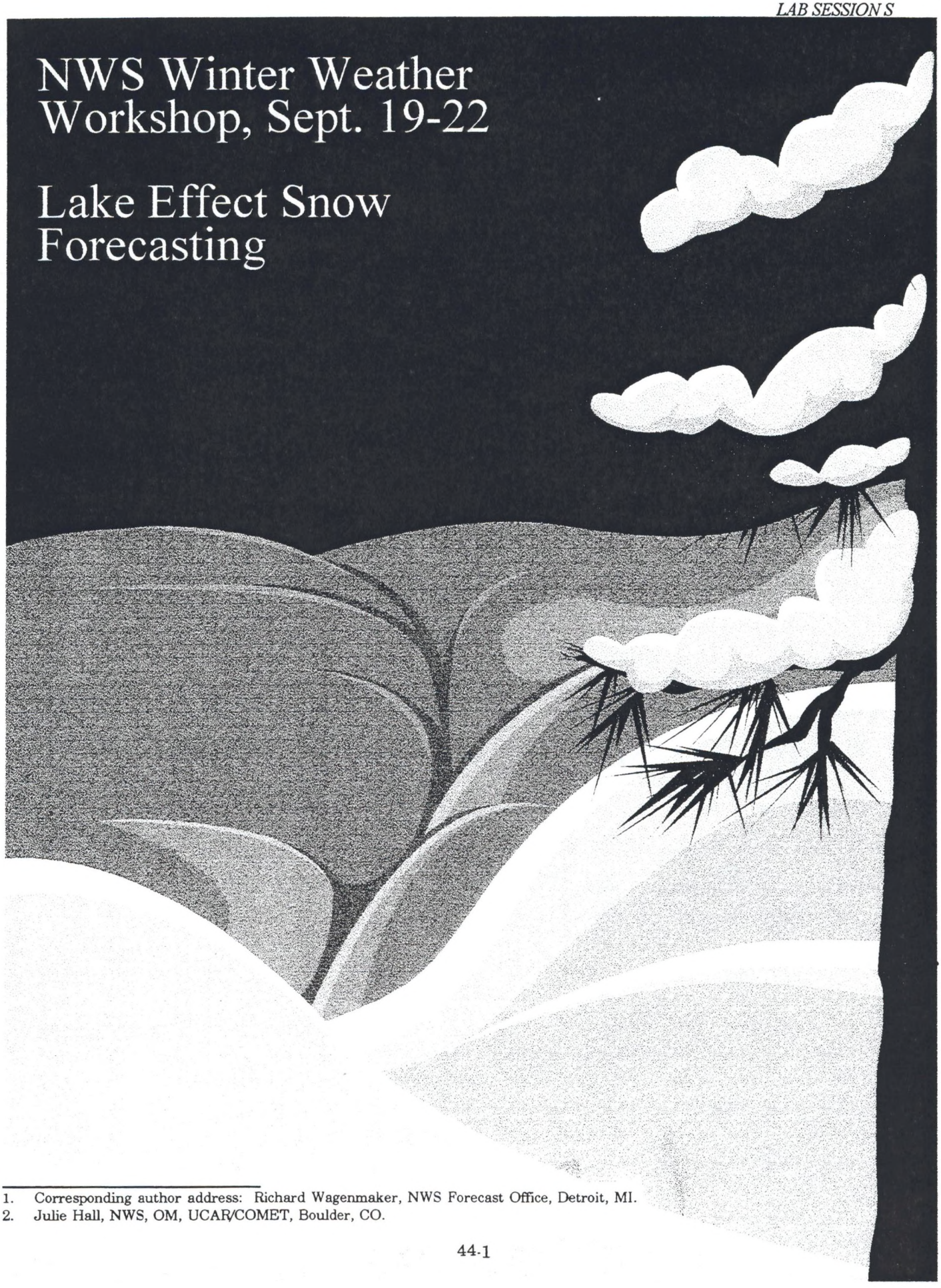

1. Corresponding author address: Richard Wagenmaker, NWS Forecast Office, Detroit, MI.
2. Julie Hall, NWS, OM, UCAR/COMET, Boulder, CO.

Definitions:

"Lake Effect" Precipitation:

Precipitation that is primarily generated via convection, the result of destabilization of the convective boundary layer (CBL) by the turbulent flux of heat and moisture from a body of water.

"Lake Enhanced" Precipitation:

Precipitation that is primarily generated or enhanced by superimposing an external large scale forcing mechanism upon a shallow layer of conditional instability.

The single most important parameter governing the generation of "Lake Effect" or "Lake Enhanced" precipitation is -- *THERMAL INSTABILITY.*

Many other factors are important for modulating the strength of convection, but are secondary for its generation.

Instability can be created through:

- *Differential temperature advection*

- *Physical lifting of an entire layer*

- *Heat and moisture flux from water into the bottom of a layer*

- *Horizontal moisture advection into the bottom of the CBL*

Historically, forecasters have represented stability in the CBL via empirically-derived proxy. Although this approach is not the most desirable, it has been a necessity in operational forecasting due to:

a) lack of radiosonde data in and near "Lake Effect" environments.

b) the inability of coarse numerical weather prediction models to simulate the meso-beta and meso-gamma scale "Lake Effect" environment.

The most commonly used methods for estimating overwater stability include:

1- Temperature difference between the water surface and 850-mb (Rothrock 1969, Holroyd 1971).

$\Delta T_{(water-850)}$ >= 13C for lake effect snow generation
$\Delta T_{(water-850)}$ >= 20C for heavy lake effect snow
$\Delta T_{(water-850)}$ >= 8C for lake-enhanced snow generation

2- 850-mb temperature (Dockus 1985)

T <= -10C for lake effect snow generation
T <= -5C for lake-enhanced snow generation

3- Comparison of $\Delta T_{(water - 850)}$ and $\Delta T_{(water - 700)}$. (Niziol 1987)

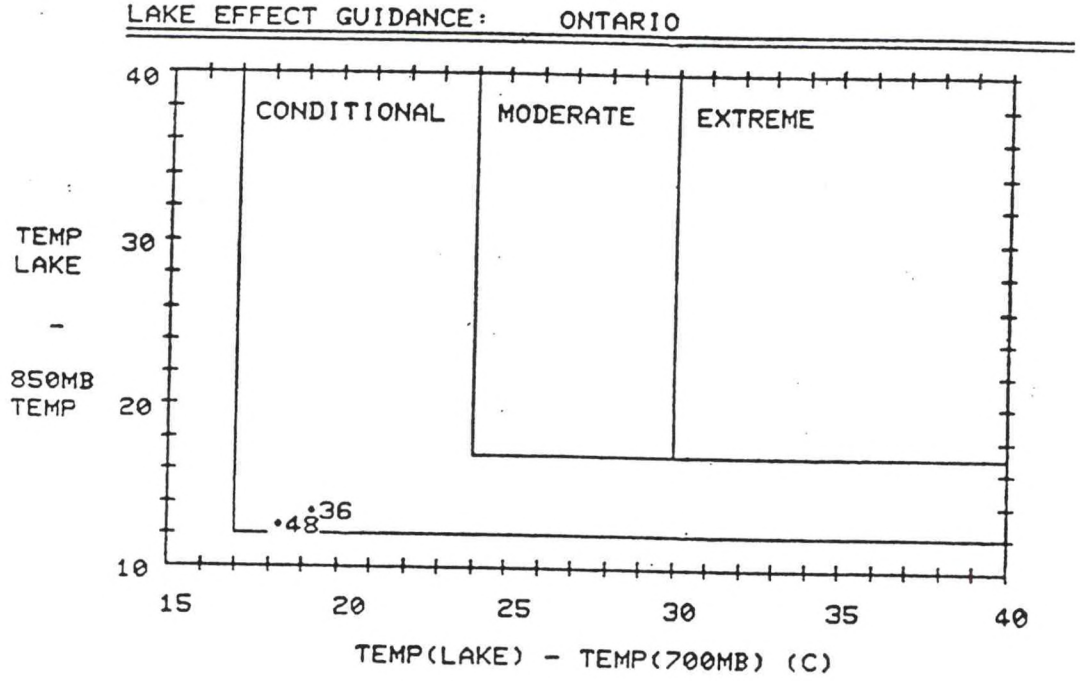

Modulation of Lake Effect Precipitation

1- Depth of Moist Convection

a) Found to be as important as instability in controlling the maintenance, intensity, and decay lake effect storm bands.

b) Minimum depth of 3000 feet for "significant snows".

c) Inversion heights lower than 3000 feet AGL usually "cap" significant convection.

d) Inversion heights greater than 7500 feet AGL usually (not always) favorable for heavy snow.

e) Affected by upstream relative humidity.

f) Ascending moist air parcels that cool to -15C or colder will be able to maximize ice crystal (dendritic) growth rates.

2- Fetch

a) Provides adequate distance/time over water to allow sensible heat and moisture flux to destabilize the CBL.

b) Distances of 80 km or more are usually considered favorable for significant snow.

c) Can be less if an external lifting mechanism is acting to bring parcels to saturation earlier in their trajectories.

d) Approximately 50 percent of total modification occurs in a parcel's first 10 minutes over water.

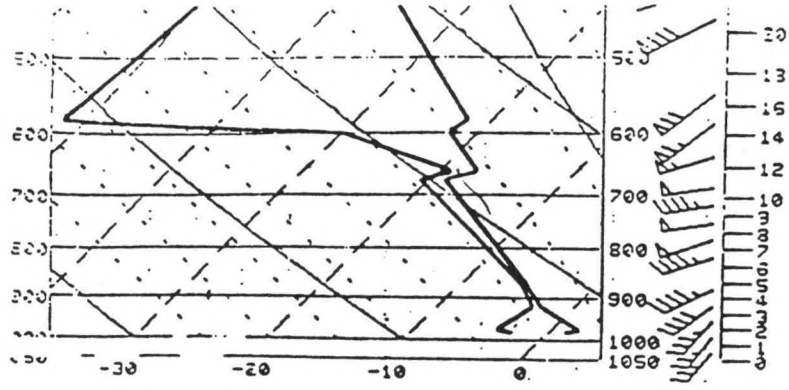

DATE: 11/29 TO 12/1 1983

T(LAKE)..... +8 C
T(850-LAKE)..... 16 C
INVERSION HEIGHT..... 11,800FT.
FETCH..... LONG
MAXIMUM SNOWFALL..... 22 TO 24 I

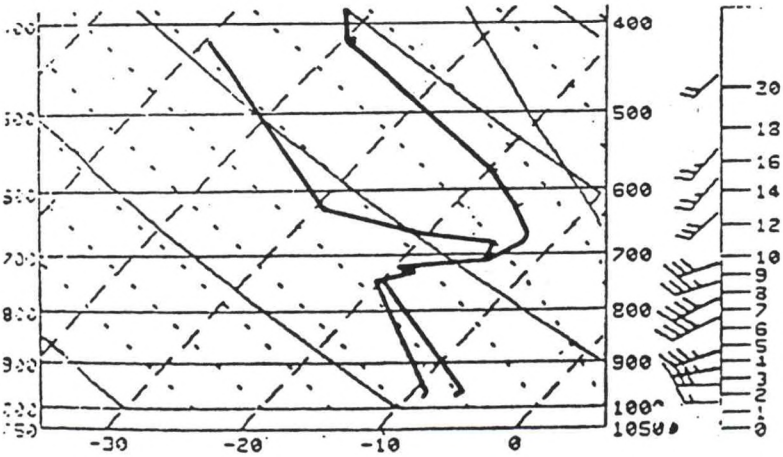

DATE: 3/22 1983

T(LAKE)..... +2 C
T(850-LAKE)..... 16 C
INVERSION HEIGHT..... 8500FT.
FETCH..... LONG
MAXIMUM SNOWFALL..... 6 TO 12 I

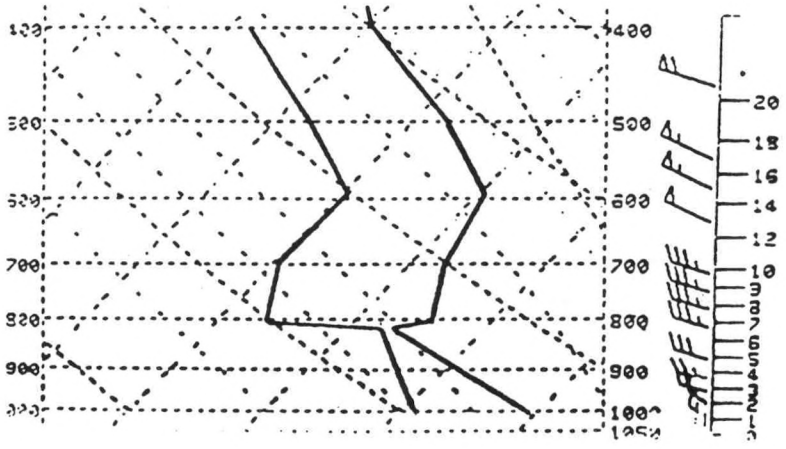

DATE: 11/24/82

T(LAKE)..... +9 C
T(850-LAKE)..... 21 C
INVERSION HEIGHT..... 6800FT.
FETCH..... SHORT
MAXIMUM SNOWFALL..... 1 TO 2 IN.

Fig 7

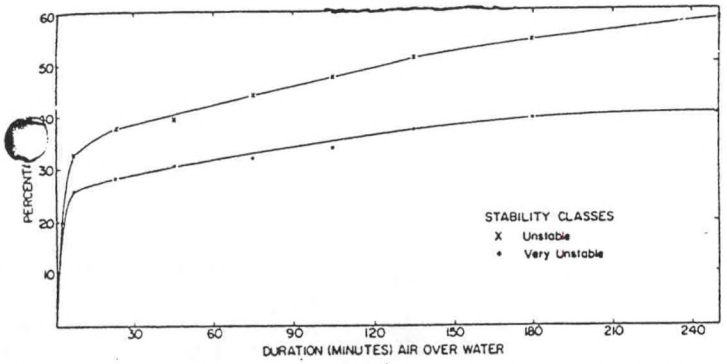

FIGURE 4.—Modification of surface air temperature when air flows from land out over Lake Ontario, as a percentage of total possible change [i.e., $(T_{AW}-T_{AL})/(T_{AL}-T_W)$] as limited by water temperature for unstable and very unstable conditions.

R. R. BRAHAM, Jr. AND R. D. KELLY

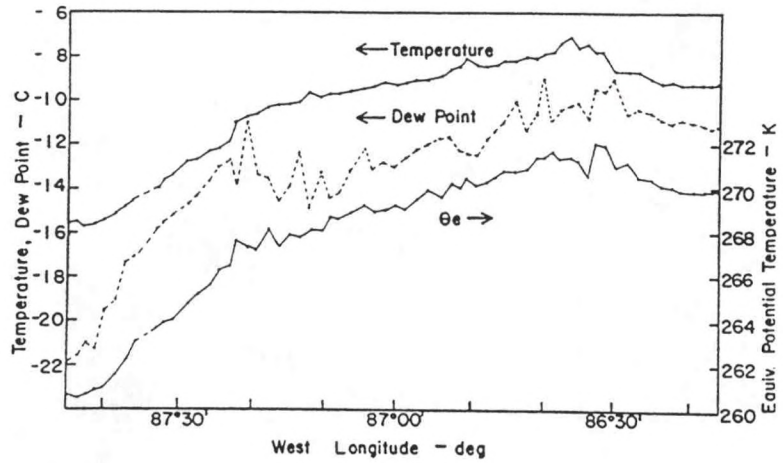

Figure 9. Horizontal profiles of temperature, dew point, and equivalent potential temperature for the south leg of Flight 19, 10 December 1977 across Lake Michigan. Refers to a sub-cloud flight level of about 250 m above the lake surface.

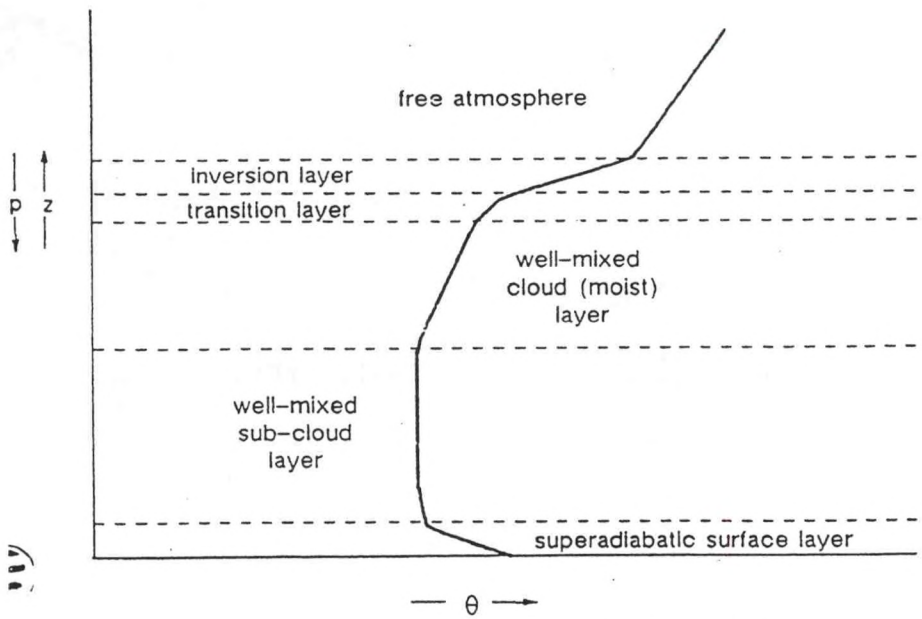

FIG. 18. Vertical profile of potential temperature for a Type I CTBL which includes the transition layer where penetrative convection occurs.

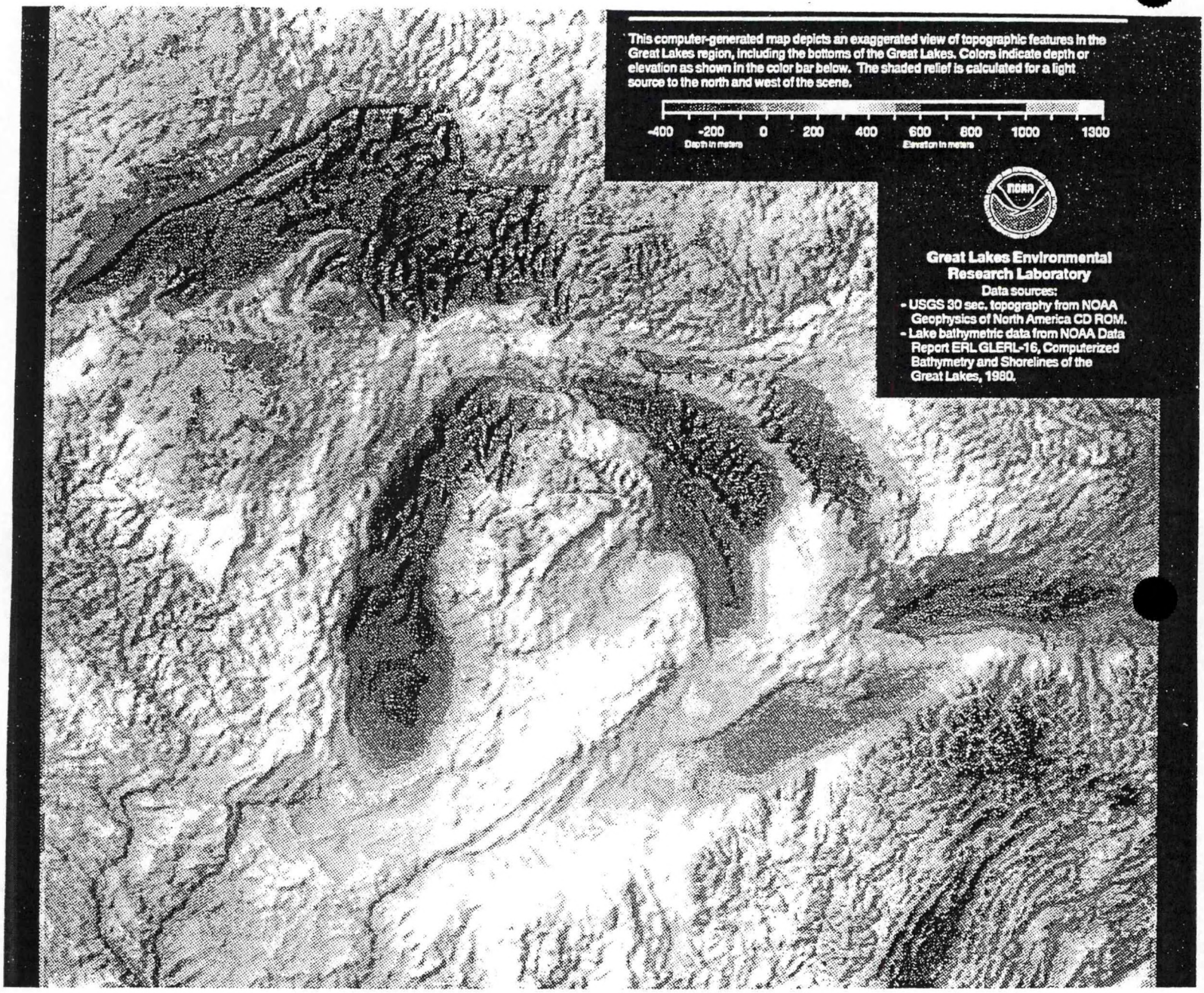

Image 2.0 Topographic Relief Map of the Great Lakes Region

3- Directional Wind Shear

a) Can have a significant impact on character of snow bands.

b) Surface to 700 mb directional turning of less than 30 degrees favors strong, well-organized bands.

c) Often, in a well-mixed CBL, shear tends toward unidirectional through redistribution of momentum.

d) Direction of shear vector is indicative of orientation of snow bands. In unidirectionally sheared environments snow bands are generally oriented along the layer wind vector.

4- Orography

a) Can greatly enhance snowfall rates by forcing greater vertical penetration of ascending parcels.

b) Significantly affects snowfall patterns in west Upper Michigan, northwest Lower Michigan, northeast Ohio, northwest Pennsylvania, and western New York.

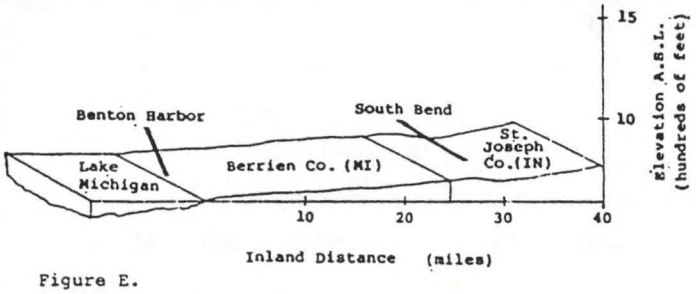

Figure E.

Elevation rise southeast of Lake Michigan, from Benton Harbor, MI. Note that height is exaggerated to amplify relief change.

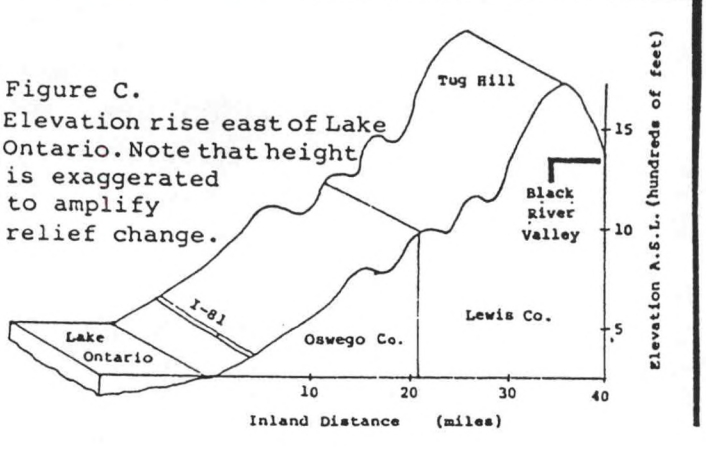

Figure C.
Elevation rise east of Lake Ontario. Note that height is exaggerated to amplify relief change.

5- External Forcing and Control Mechanisms

a) Differential Cyclonic Vorticity Advection

1. May help lift parcels to saturation earlier in their trajectories.

2. Lift on the synoptic-scale also enhances lake snow by deepening moist convection via raising or erasing capping inversions.

b) Surface confluent or convergent zones.

1. Key to forecasting where single or dominant bands may occur.

2. Frictional convergence - due to backing winds and slower speeds or downwind shores. If occurring at the right angle relative to shore, can be frontogenetic.

3. Thermal convergence. Density currents driven by horizontal pressure (density) gradients across land/water boundaries. Propogation is offshore is related to depth of cold air over land and large-scale pressure gradient. Often diurnally driven.

4. Overwater horizontal stability and vertical motion gradients. Often establishes convergent bands near genesis regions for convection which may be perpetuated downstream. Latent heat release within bands may contribute to meso-low formation and maintenance over water. Convection > vertical motion/latent heat release > sfc pressure falls > low level convergence > more convection.

5. Items 2-4 often act in concert with one another in the development and maintenance of convergence zones.

A

Frictional Convergence

(Smooth Lake and Rough Land)

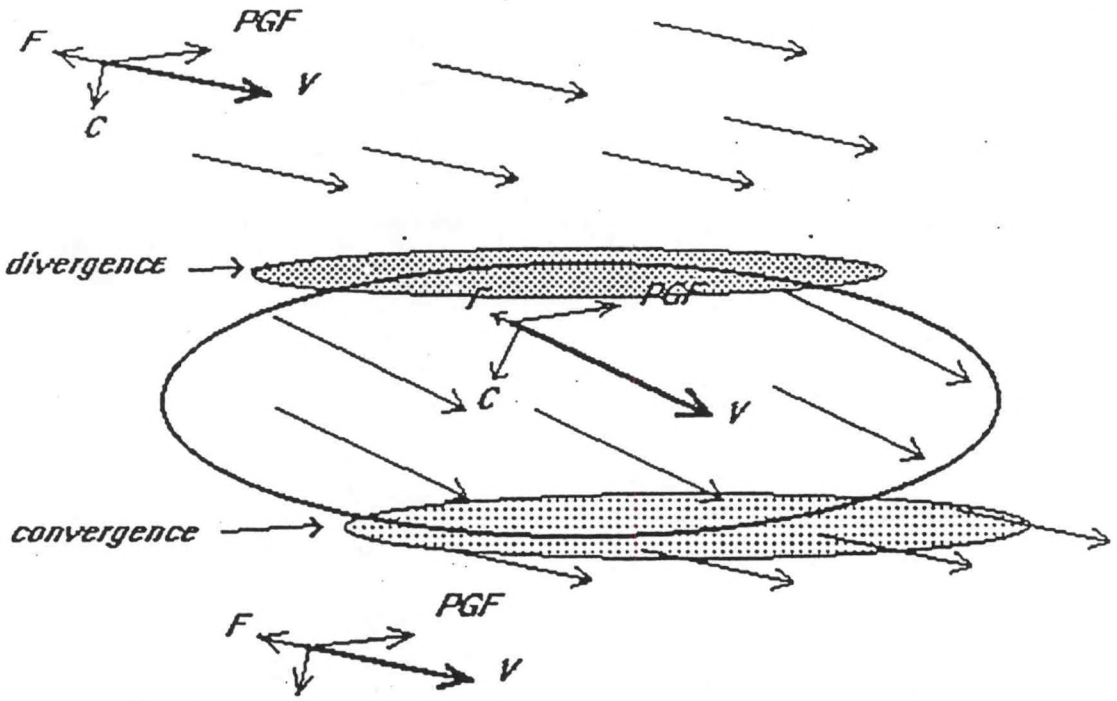

B

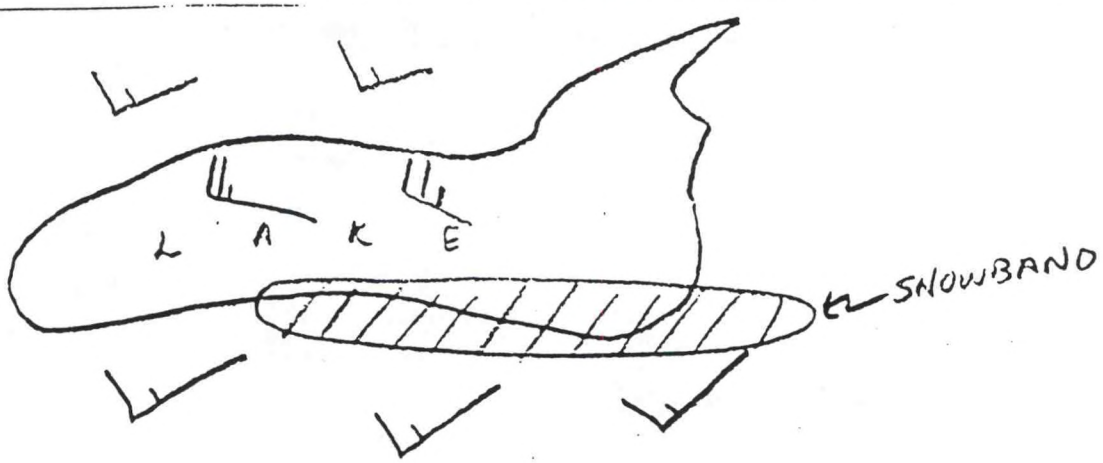

Warm core of snowband is stretched out over land by prevailing synoptic scale wind. Pronounced convergence near edge of elongated band. Strongest press gradient on south side of band.

As warm air in snowband moves onshore, it rides up over the dense cold air, forming a sloping "overrunning" frontal surface.

Thermal Convergence

Synoptic Flow = Light NE

(Elliptically Shaped Lake)

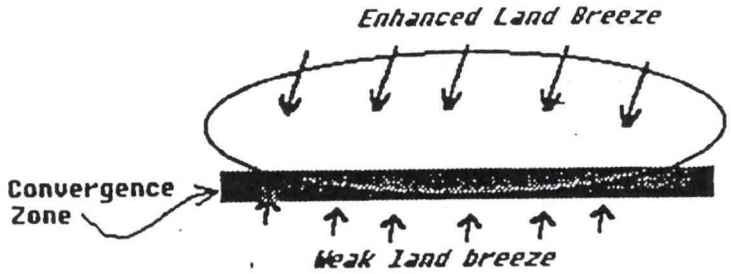

Synoptic Flow = Calm Wind

(Elliptically Shaped Lake)

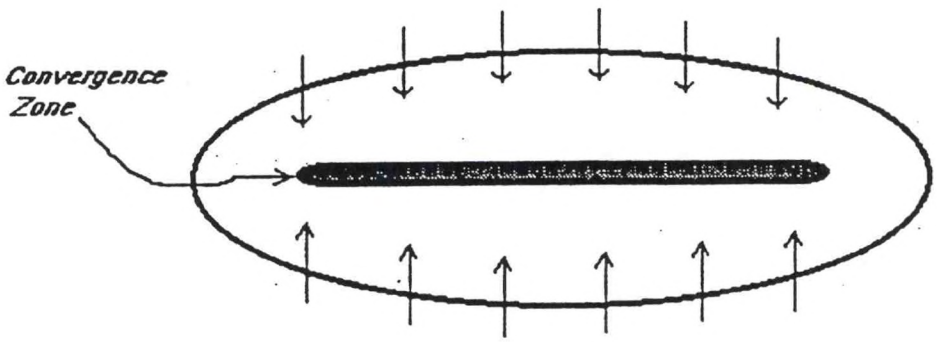

Synoptic Flow = Calm Wind

(Bowl Shaped Lake)

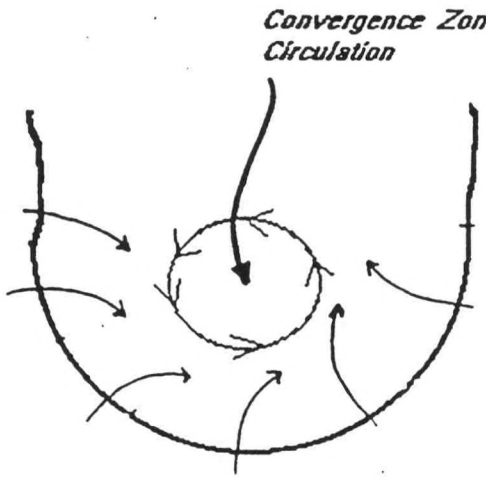

Upwind bay preferences for band formation

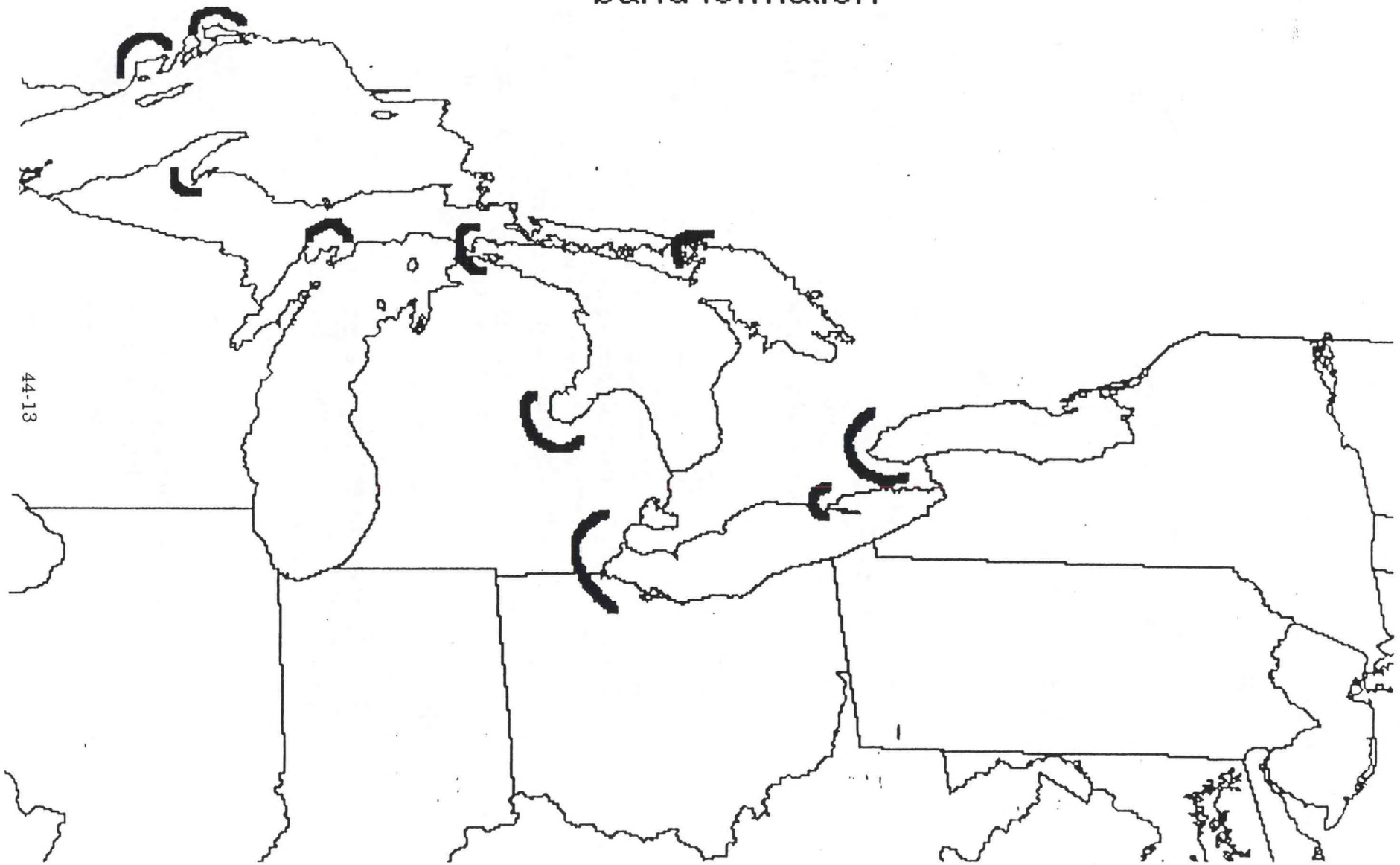

6- Morphological Types of Lake Effect Storms

a- Wind Parallel Bands (major-axis of a lake)

1. Most often occur in the eastern Great Lakes.
2. Favorable for development of strong convergence zones due to long fetches, frictional/thermal effects.
3. Usually single band events (5-50 km wide).
4. The most significant type of Lake Effect Storm.

b- Wind Parallel Bands (minor-axis of a lake)

1. More common in western Great Lakes.
2. Multiple, less intense, shallower banding (1-15 km wide).
3. Large areal coverage.
4. Over large lakes (Superior, Huron) a few dominant bands often embedded among families of weaker bands.

c- Shoreline Parallel Bands

1. Prevailing wind often roughly along major axis of lake.
2. Light to moderate gradient wind.
3. Thermal and frictionally induced circulations play a big role in organizing convergence zones.
4. Convergence zones usually near shore due to land breeze pentration being limited by larger scale pressure gradients.

d- Mid-Lake Convergence Bands

1. Very weak surface pressure gradients.
2. Primarily occur as a result of strong land breeze circulations.
3. Sometimes referred to as "tea-kettle" bands.

e- Mid-Lake Mesoscale Vortices

1. Weak surface pressure gradient
2. Occurs in "bowl-shaped" lakes via land breeze circulations from surrounding shorelines.

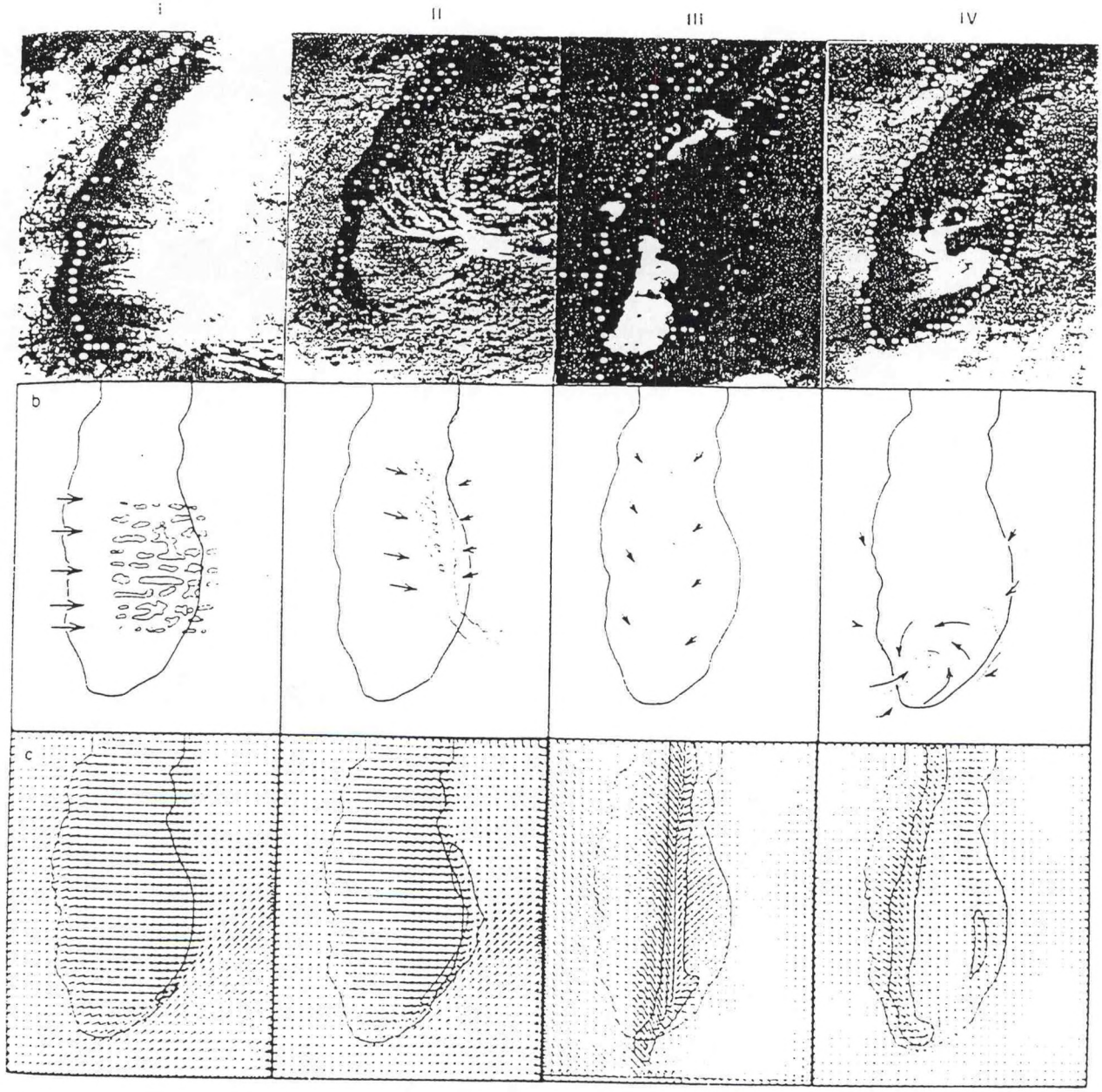

FIG. 1. Morphological types of lake effect snowstorms: (I) Broad area, (II) shoreline band, (III) midlake band, and (IV) vortex. (a) Satellite pictures of examples of each type (photos courtesy of R. R. Braham, Jr.); (b) schematic depiction; (c) numerical simulation examples. Grid spacing is 8 km and results are shown for 20 h simulated time except for (III) at 9 h. Vectors are scaled to 1 km = 1 m s^{-1}; shading is cloud cover at 1800 m height. The contour shows vertical velocity = 20 cm s^{-1} at 1 km. Heavy dark contour is Lake Michigan shoreline.

Single Banded Storm

Synoptic Flow = Moderate W →

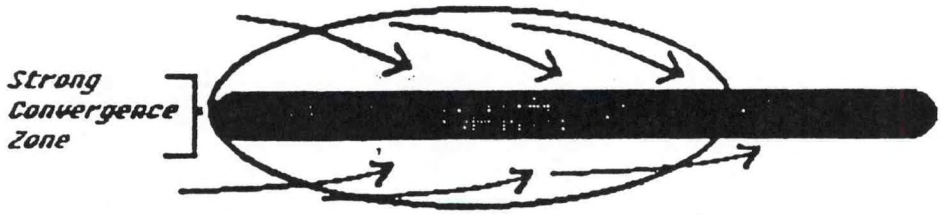

Multiple banded Event

Synoptic Flow = Moderate NW ↘

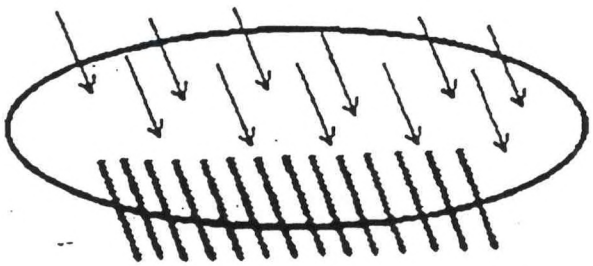

Parallel Roll Convection

"First-Guess Accumulations" Guide

"Main Lake Effect" Branch

1- Initial Temperature Check

Is T(water) - T(850) >= 13C ?

YES ↓

NO → Go to Lake Enhanced Branch (Step 1)

2- Fetch Check

Is Trajectory Over Open Water >= 100 Miles ?

YES ↓

NO → Go to Lake Enhanced Branch (Step 2)

3- Synoptic Scale Lift

Is Synoptic Scale Vertical Motion aoa 700 mb Expected to be Neutral or Downward ?

YES ↓

NO → Go to Combination Branch

4- Final Temperature Check

Is T(water) - T(850) >= 20C ?

YES ↓

NO → Is T(water) - T(850) >= 17C ?

YES ↓

NO ↓ **Little or No Accumulation**

5- Depth of Moist Convection ↓

Inversion < 3000 Feet
Estimated 6 hr amounts
1-3 inches

Inversion >= 3000 ft < 7500 ft
Estimated 6 hr amounts
2-4 inches
3-6 inches terrain

Inversion >= 7500 ft
Estimated 6 hr amounts
3-5 inches
5-8 inches terrain

Depth of Moist Convection ↓

Inversion < 3000 Feet
Estimated 6 hr amounts
Little or no accumulation

Inversion >=3000 ft < 7500 ft
Estimated 6 hr amounts
1-3 inches
2-4 inches terrain

Inversion >= 7500 ft
Estimated 6 hr amounts
2-4 inches
4-6 inches terrain

* If broad-scale surface flow is anticyclonic, decrease amounts by 50 percent.
* In light winds beware of shoreline parallel bands moving onshore.

"Lake Enhanced" Branch

1- Initial Temperature Check

Is T(water) - T(850) >= 8C ?

YES ↓

NO → No Accumulation

2- Fetch Check

Is Trajectory Over Open Water >= 40 Miles ?

YES ↓

NO → Accumulation Unlikely

3- Synoptic Scale Lift

Is Synoptic Scale Upward Motion Expected to Occur ?

YES ↓

NO → Accumulation Unlikely

4- Depth of Moist Convection

Will the Inversion Height be >= 3000 feet AGL ?

YES ↓

NO → Accumulation Unlikely

5- Final Temperature Check

Is T(water) - T(850) >= 17C ?

YES ↓

NO →

6- Degree of Synoptic Scale Lift

Will Upward Vertical Velocity aoa 700 mb be >= 2μb/sec ?

YES ↓

Estimated 6 hr amounts
3 inches or more
5 inches or more terrain

NO →

Estimated 6 hr amounts
1-3 inches

Degree of Dynoptic Scale Lift

Will Upward Vertical Velocity aoa 700 mb be >= 2μb/sec ?

YES ↓

Estimated 6 hr amounts
2 inches or more

NO →

Estimated 6 hr amounts
1-2 inches

"Combination" Branch

<u>1- Synoptic Scale Lift</u>

Is Upward Vertical Velocity aoa 700 mb Expected to be >= 2μb/sec ?

YES → **Estimated 6 hr total snowfall amounts**
6 inches or more
8 inches or more terrain

NO → <u>3- Final Temperature Check</u>

Is T(water) - T(850) >= 20C ?

YES → **Estimated 6 hr amounts**
4-6 inches
6-8 inches terrain

NO → Is T(water) - T(850) >= 17C ?

YES → **Estimated 6 hr amounts**
2-3 inches
3-5 inches terrain

NO → **Estimated 6 hr amounts**
1-2 inches

* Inversion heights less than 3000 feet AGL will severely limit convective contribution to snowfall totals.

Wintertime Applications of GOES-8 Imagery
(LAB SESSIONS B&C)

Ray Zehr[1] and Jim LaDue[2]

OUTLINE - LAB SESSION

1.	Using 3.9 -micrometer Images	30 min	Ray Zehr
2.	East Coast Winter Storm: February 4, 1995	20 min	Ray Zehr
3.	Forecasting Lake Effect Snowfall	50 min	Jim LaDue

1. Corresponding author address: Ray Zehr, NESDIS, Fort Collins, CO.
2. James LaDue, Operational Support Facility, Operations Training Branch, 3200 Marshall Avenue, Norman, OK.

GOES-7 Characteristics

Wavelength µm	IGFOV km (E/W x N/S)	SSRes km (E/W x N/S)	Noise
0.55-0.75	.75 x .86	.75 x .86	6 bit data + 2 counts 3σ
3.84-4.06	13.8 x 13.8	3.0 x 13.8	0.25 K @ 300 K, 6.0 K @ 230
6.40-7.08	13.8 x 13.8	3.0 x 13.8	1.0 K @ 230 K
10.2-12.0	6.9 x 6.9	3.0 x 6.9	0.10 K @ 300 K, 0.2 K @ 230
12.5-12.8	13.8 x 13.8	3.0 x 13.8	0.40 K @ 300 K, 0.8 K @ 230

GOES-8 Characteristics

Wavelength µm	IGFOV km (E/W x N/S)	SSRes km (E/W x N/S)	Noise
0.52-0.72	1.0 x 1.0	.57 x 1.0	10 bit data + 6 counts 3σ
3.78-4.03	4.0 x 4.0	2.3 x 4.0	0.23 K @ 300 K, 5.52 K @ 230
6.47-7.02	8.0 x 8.0	2.3 x 8.0	0.22 K @ 230 K
10.2-11.2	4.0 x 4.0	2.3 x 4.0	0.14 K @ 300 K, 0.28 K @ 230
11.5-12.5	4.0 x 4.0	2.3 x 4.0	0.26 K @ 300 K, 0.52 K @ 230

4/7
Aspect RATIO

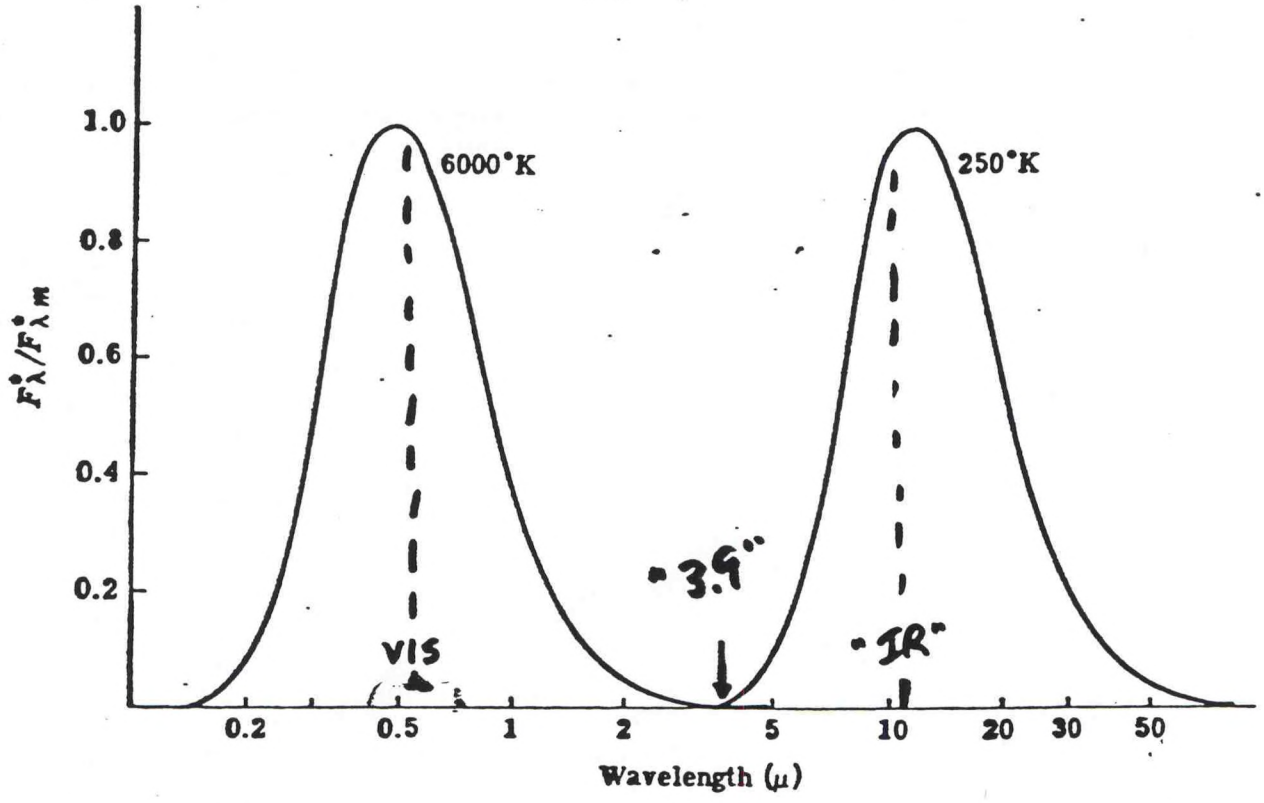

FIG. 4.11. Normalized black-body flux density per unit wavelength calculated from Eqs. (4.3) and (4.17) for temperatures of 6000° and 250°K.

CHARACTERISTICS OF 3.9-MICROMETER SATELLITE IMAGES

3.9-micrometer temperatures are nearly the same or warmer than corresponding 11-micrometer temperatures (conventional IR images), EXCEPT with fog/stratus at night, when they are colder.

This is because of the emissivity differences between the two wavelengths and the temperature profile of fog/status (inversion).

Thin cirrus clouds at night have 3.9-micrometer temperatures significantly warmer than the 11-micrometer temperatures.

During the daytime, 3.9-micrometer temperatures are strongly influenced by reflected solar energy, and thus have characteristics of visible imagery combined with infrared imagery. Liquid water clouds are particularly strong reflectors of sunlight at 3.9-micrometers.

This characteristic is useful for distinguishing low cloud from snow cover in the daytime. The low clouds will appear significantly warmer.

UTILIZATION OF LOCAL DATA SETS IN WINTER WEATHER FORECASTING

BY

JOHN A. MCGINLEY

FORECAST SYSTEM LAB, NOAA

OUTLINE

- **BACKGROUND**
- **LOCAL DATA**
- **LOCAL PROCESSING**
- **DISSEMENATION**
- **CASE STUDIES**

1985: 3,200 Total Observations per Day

Rawinsonde

Surface Station

800/day

2400/day

Observations per Day

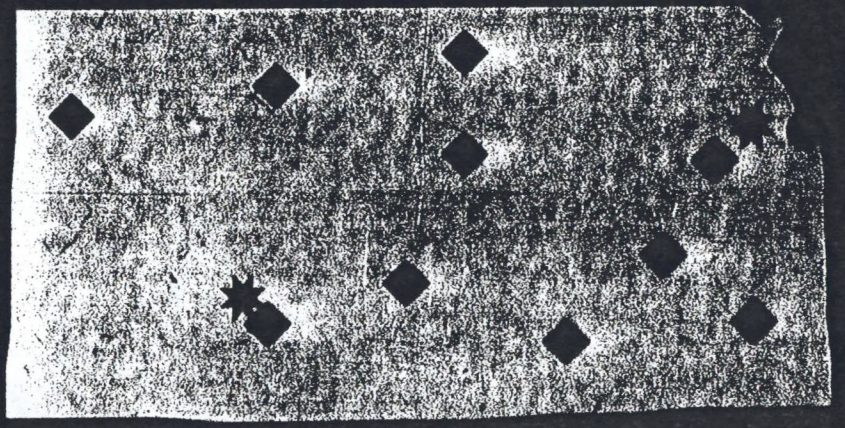

Kansas City

FORECAST SYSTEMS LABORATORY

BOULDER, COLORADO

BM 1 94-2

1995: 86,600 Total Observations per Day

Rawinsonde	Surface Station	Wind Profiler	Radar	Satellite	Aircraft
800/day	9600/day	6000/day	48000/day	7200/day	15000/day

Observations per Day

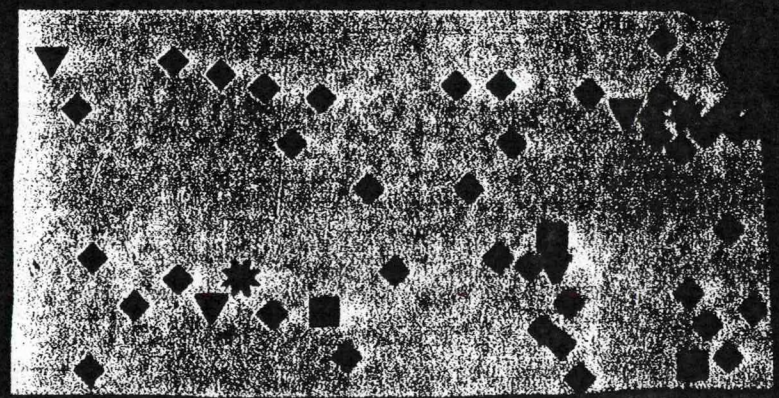

Kansas City

FORECAST SYSTEMS LABORATORY

BOULDER, COLORADO

BM 1.94-3

RELEVANT SCALES FOR FORECASTING

SYNOPTIC

L ~ 2000 - 10000 KM
V ~ 10 M/SEC
T ~ 2 DAYS - 11 DAYS

OBSERVATIONAL SPACING — 500 KM
PRODUCT CYCLE — 12 HRS

MESO-ALPHA

L ~ 200 - 2000 KM
V ~ 10 M/SEC
T ~ 6 HRS - 2 DAYS

OBSERVATIONAL SPACING — 100 KM
PRODUCT CYCLE — 3 HOURS

MESO-BETA

L ~ 20 - 200 KM
V ~ 10 M/SEC
T ~ 30 MIN - 6 HR

OBSERVATIONAL SPACING — 10 KM
PRODUCT CYCLE — 15 MIN

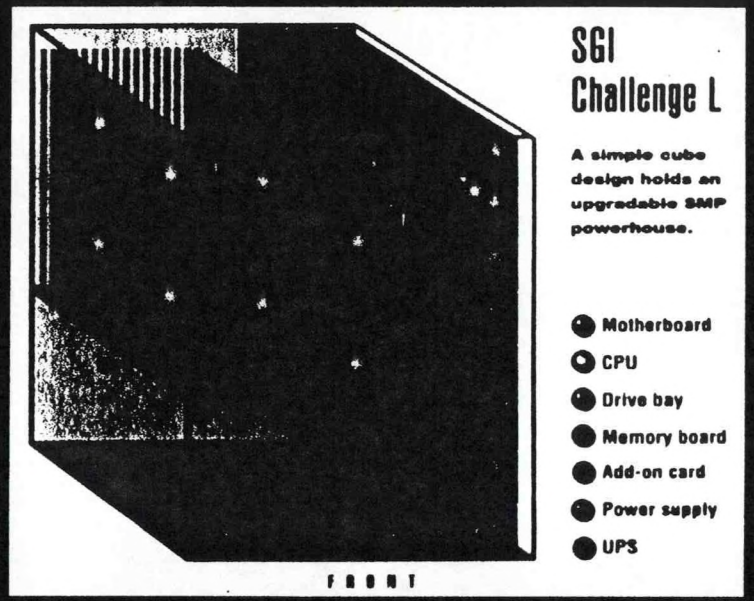

SGI Challenge L

A simple cube design holds an upgradable SMP powerhouse.

- Motherboard
- CPU
- Drive bay
- Memory board
- Add-on card
- Power supply
- UPS

UNIX/RISC Workstations

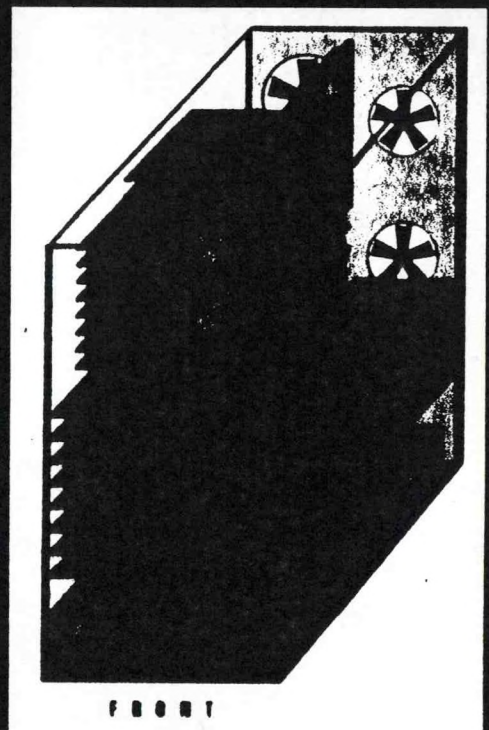

IBM POWERserver 580

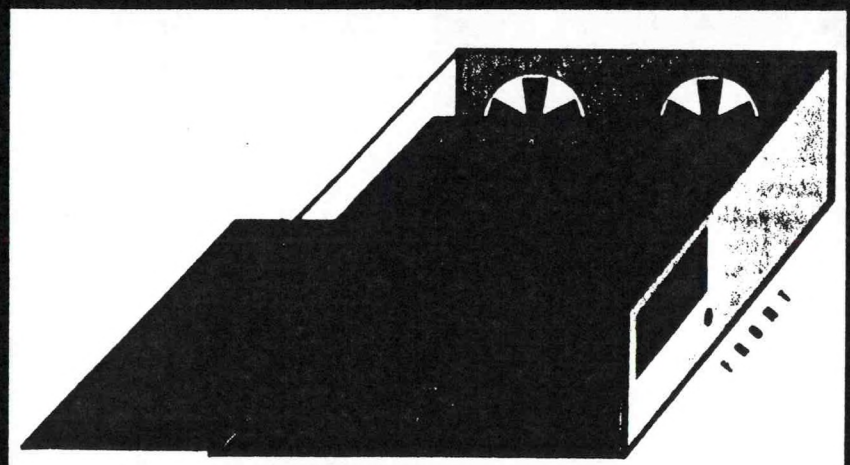

Sun SPARCserver 1000

FORECAST SYSTEMS LABORATORY

BOULDER, COLORADO

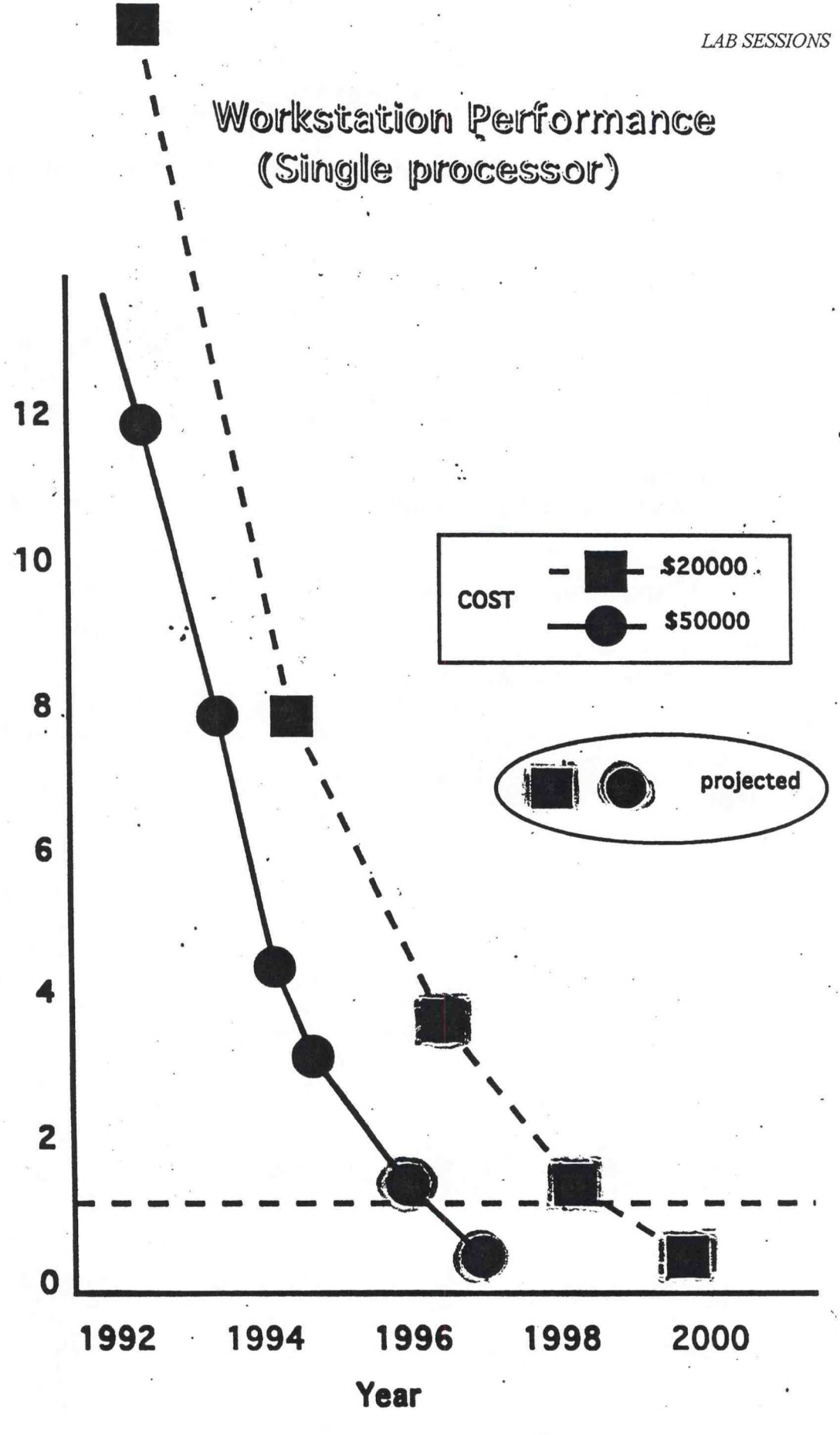

* 61 x61 x25
One-way single
nest

Local Data

Local Data may be defined as that data not entering into the National Database

- **Sources**

  - **Highway Departments**
    - 22 States with full or partial networks
  - **Agricultural Networks**
    - State run, sometimes private
  - **Universities**
    - Experimental observations
  - **Private Industry**
    - Environmental monitoring

- **Links**

  - **Telephone Modem**
  - **Dedicated communications**
  - **Internet**

- **Costs and Payback: What we can offer**

  - **Quality Control Checking**
  - **User-Friendly Products**

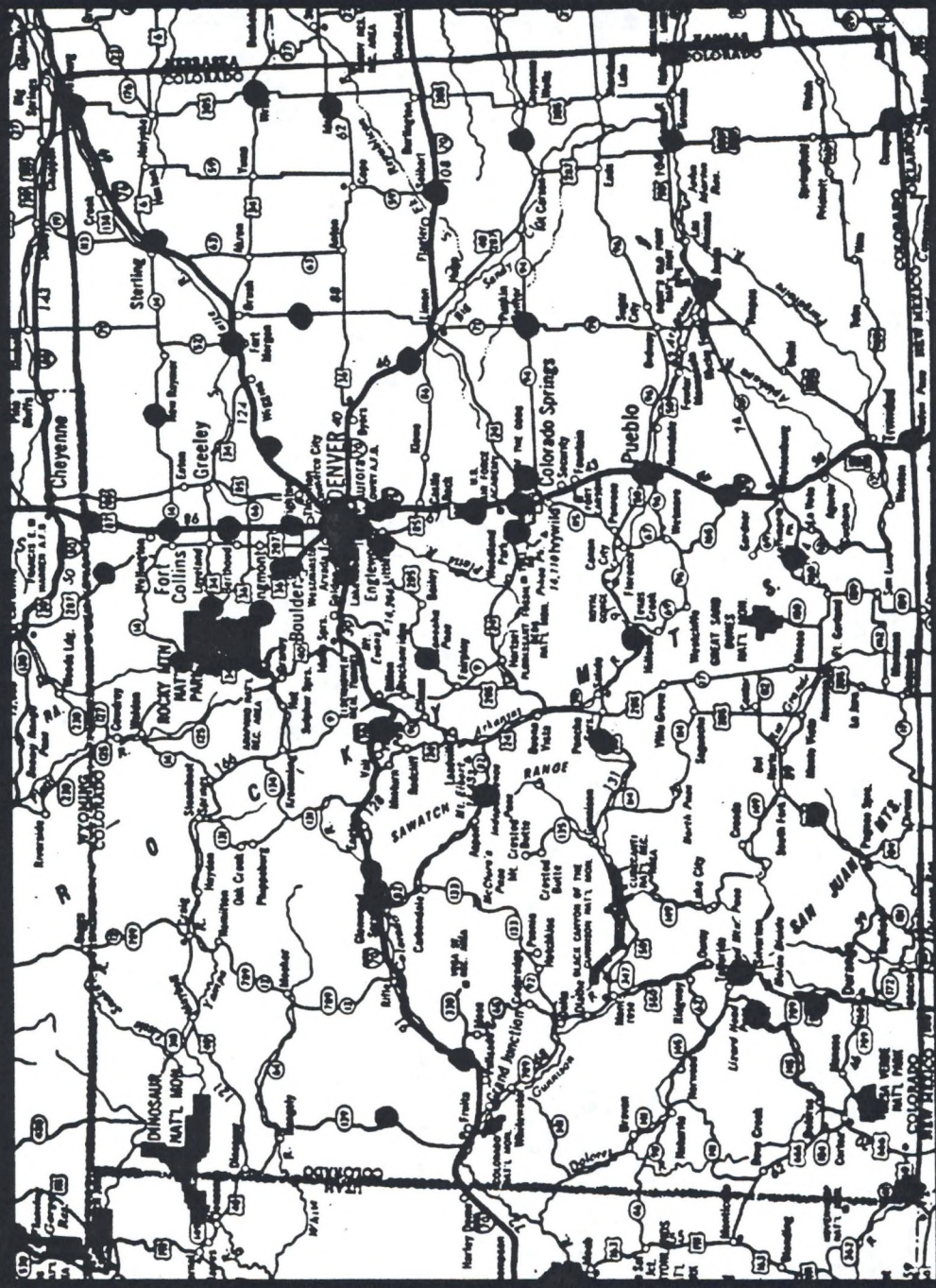

FORECAST SYSTEMS LABORATORY
BOULDER COLORADO

Mesonet Sites

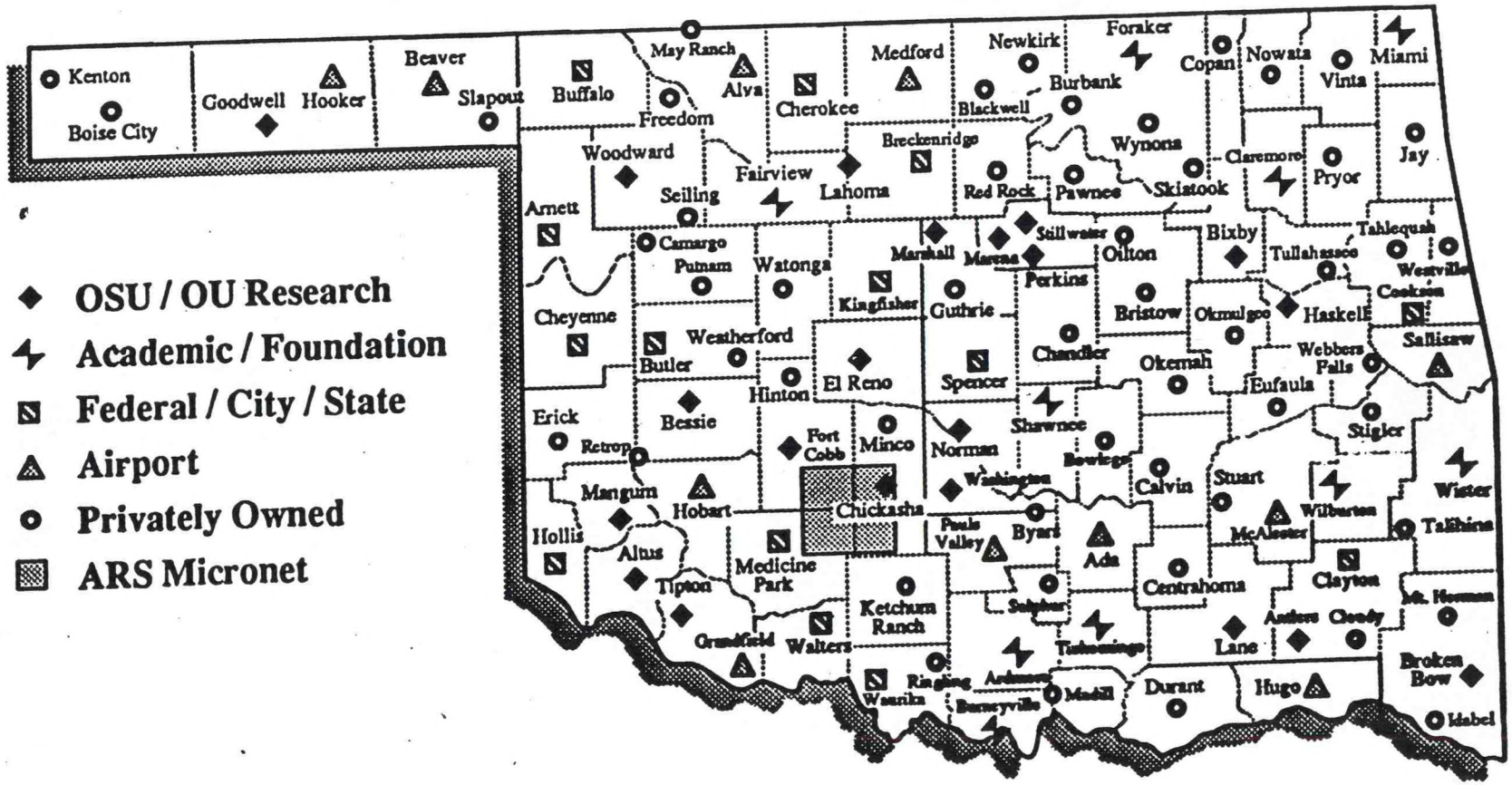

LAPS Domain & Data

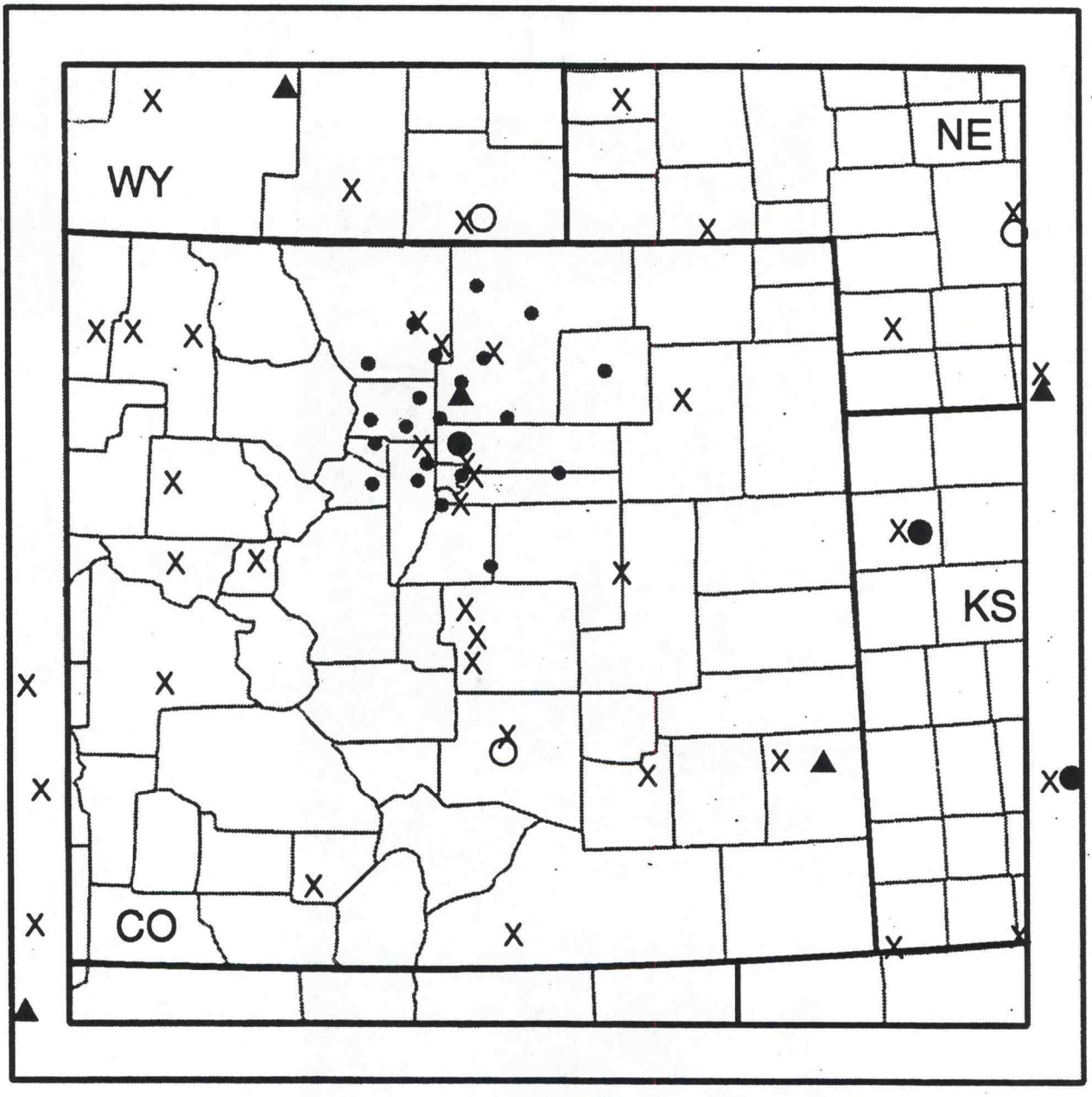

X SAO (Includes ASOS)

• FSL MESONET

▲ PROFILER

WSR-88D DOPPLER RADAR

● OPERATIONAL (as of Spring 1993)

○ PLANNED

FSL Systems

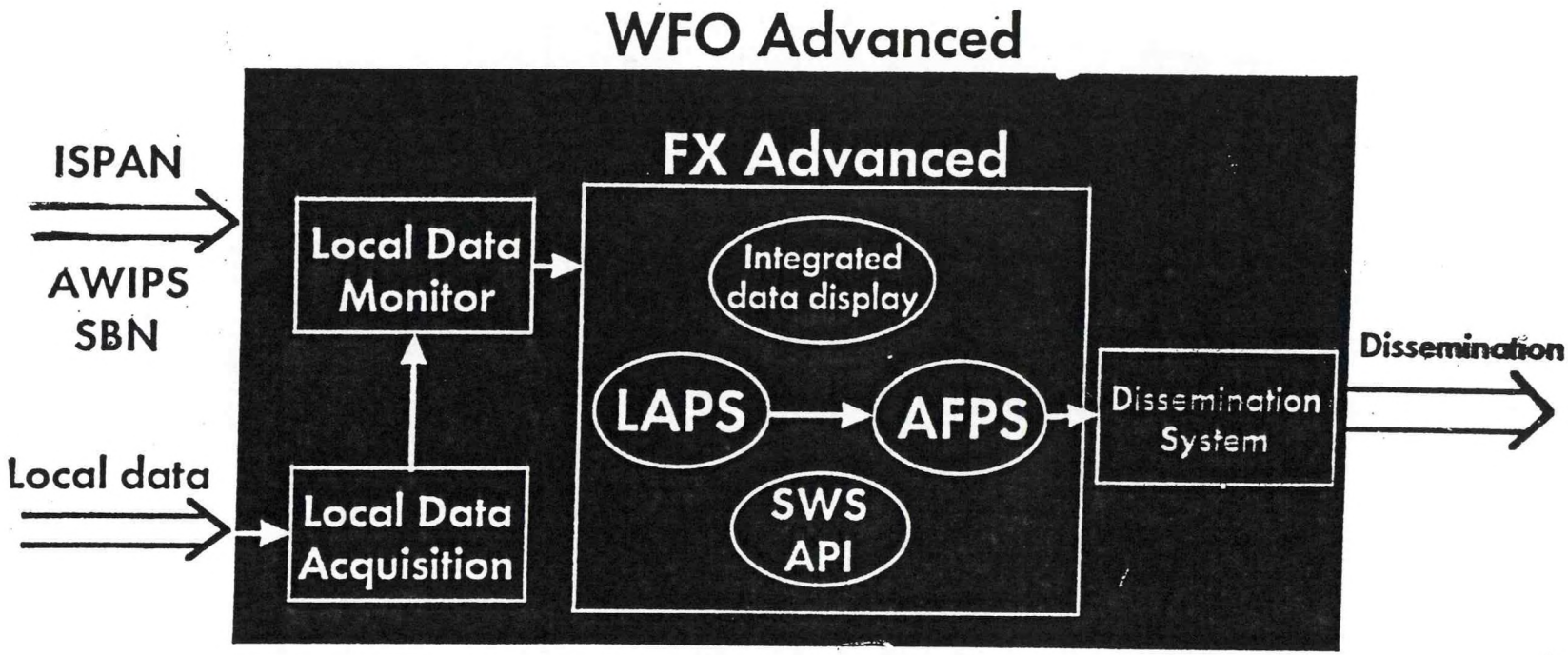

FORECAST
SYSTEMS
LABORATORY
BOULDER, COLORADO

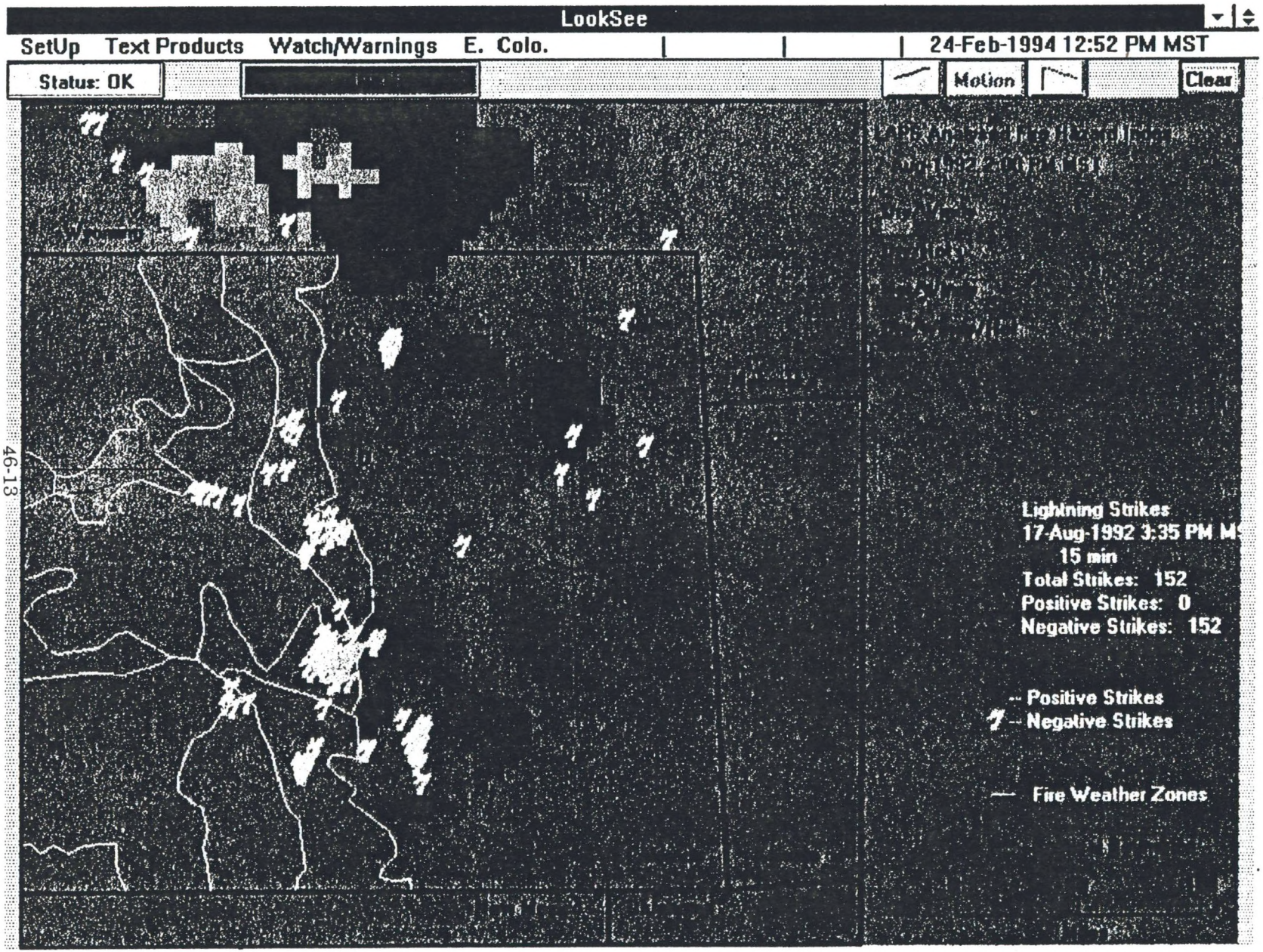
LookSee
SetUp
Text Products
Watch/Warnings
E. Colo.
24-Feb-1994 12:52 PM MST
Status: OK
Motion
Clear
Lightning Strikes
17-Aug-1992 3:35 PM M
15 min
Total Strikes: 152
Positive Strikes: 0
Negative Strikes: 152
-- Positive Strikes
-- Negative Strikes
Fire Weather Zones

LOCAL PROCESSING

- **Fusion**

Creating the database, formats, directories, input

- **Analysis**

The nowcasting product set, standard and derived products

- **Forecasting**

Use of meso-beta models in the weather office

LAPS

A system designed to:

Exploit all available data sources

Create analysed and forecast grids

Build products for specific forecast applications

Use advanced display technology

...All within the local weather office

JM 6.93.2

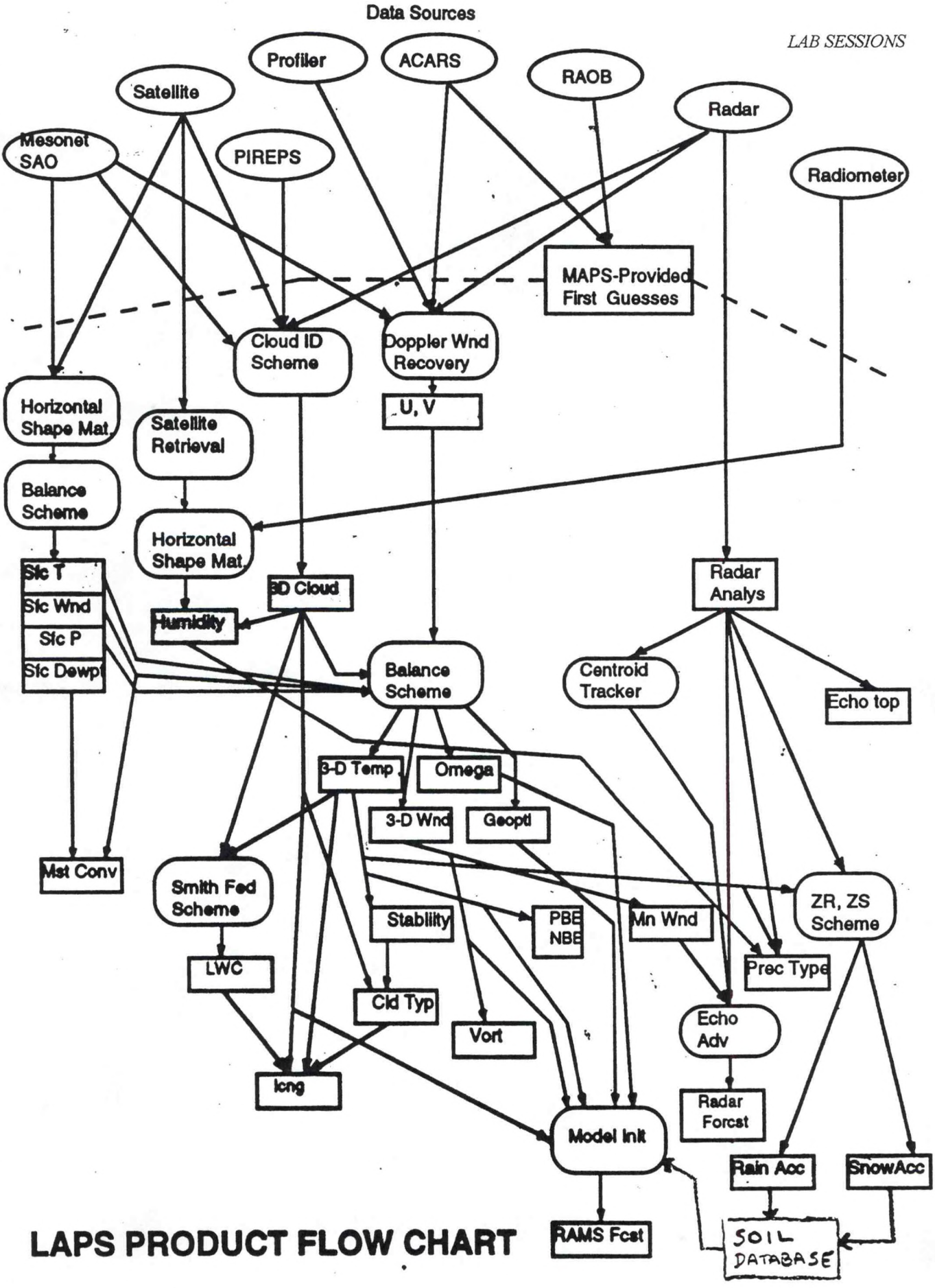
Data Sources
Profiler
ACARS
RAOB
Satellite
Radar
Mesonet SAO
PIREPS
Radiometer
MAPS-Provided First Guesses
Cloud ID Scheme
Doppler Wnd Recovery
U, V
Horizontal Shape Mat.
Satellite Retrieval
Balance Scheme
Horizontal Shape Mat.
Sfc T
Sfc Wnd
Sfc P
Sfc Dewpt
3D Cloud
Humidity
Radar Analys
Balance Scheme
Centroid Tracker
Echo top
3-D Temp
Omega
3-D Wnd
Geopti
Mst Conv
Smith Fed Scheme
Stability
PBE NBE
Mn Wnd
ZR, ZS Scheme
LWC
Prec Type
Cld Typ
Vort
Echo Adv
Icng
Radar Forcst
Model Init
Rain Acc
SnowAcc
RAMS Fcst
SOIL DATABASE
LAPS PRODUCT FLOW CHART

LAPS BASIC DESIGN

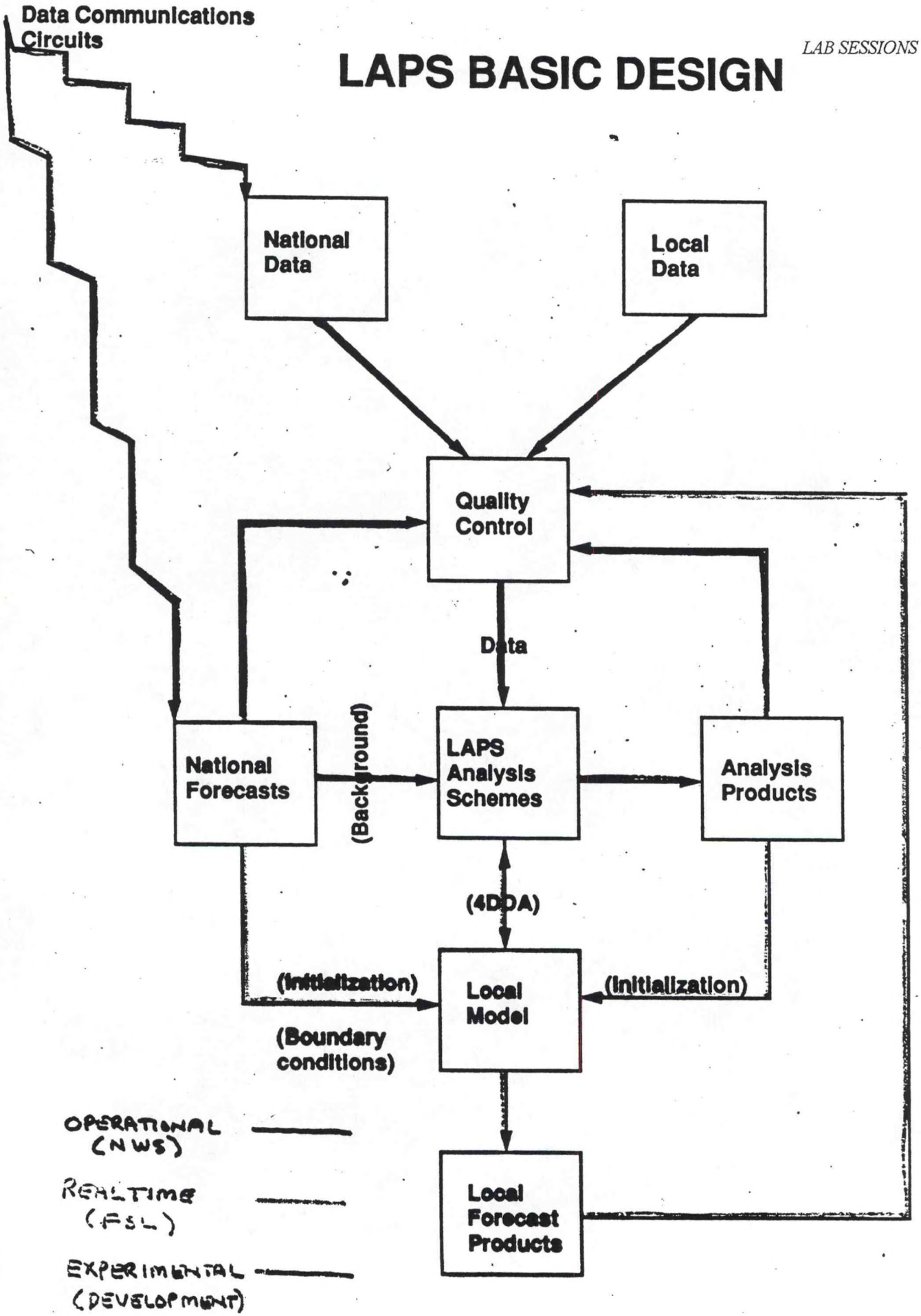

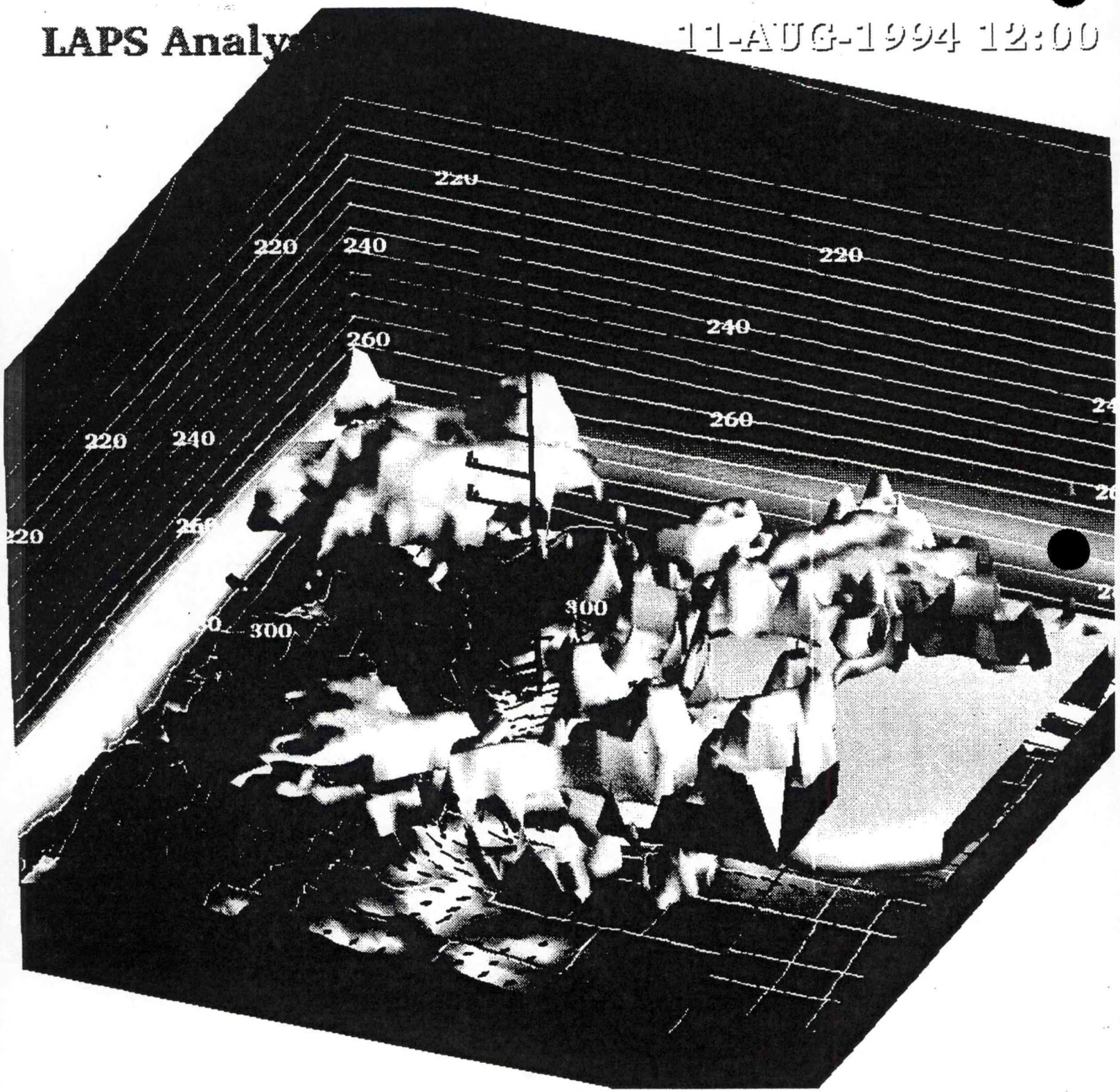
LAPS Analy
11-AUG-1994 12:00
220
220
240
260
220
240
260
220
240
260
300
300

DISSEMINATION

- **Internal**

Products for the forecast staff

- **External**

Products for outside users (non-meteorologists)

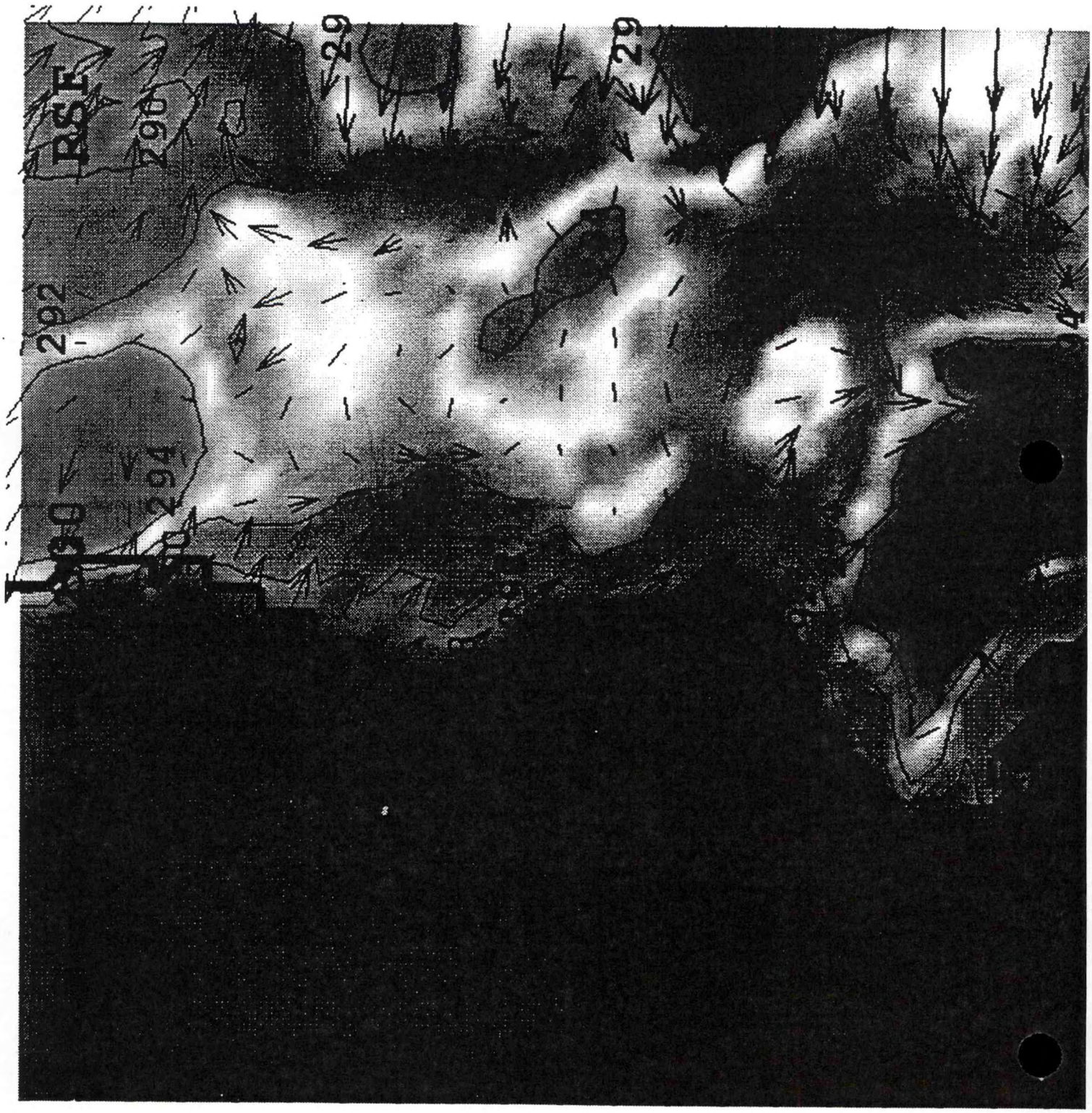
RSF
296
29
29
292
294
30

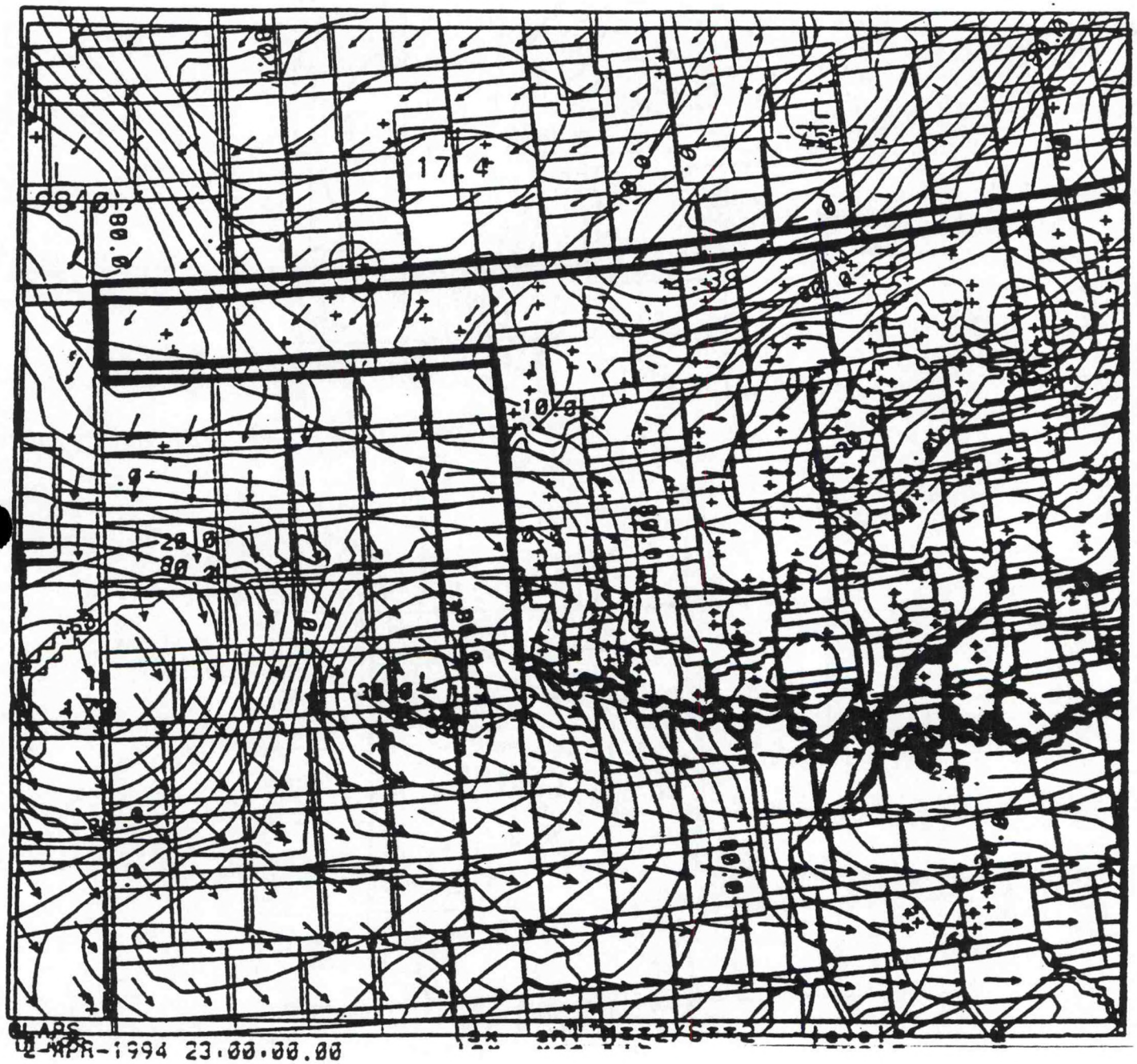
17.4
10.8
2-APR-1994 23:00:00.00

CAPE

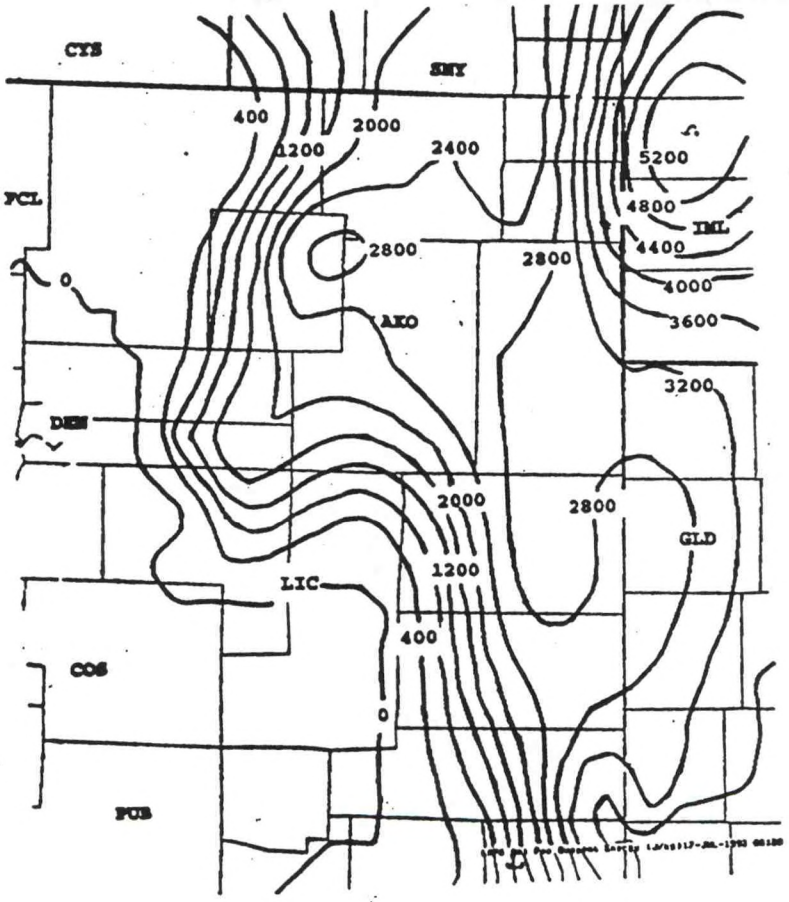

8

CIN

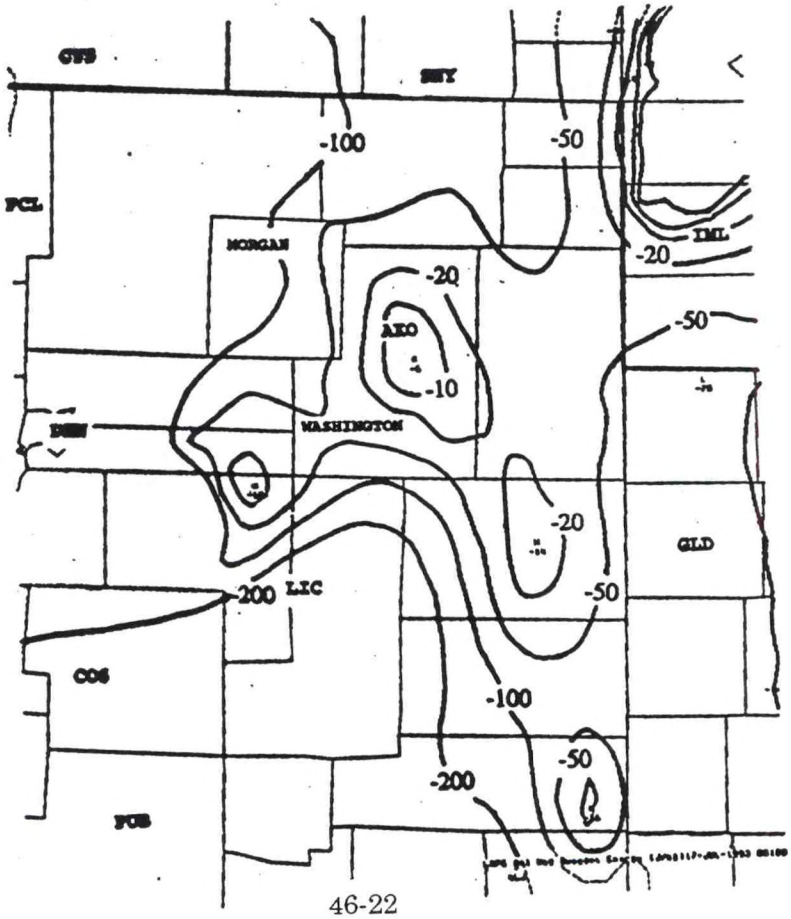

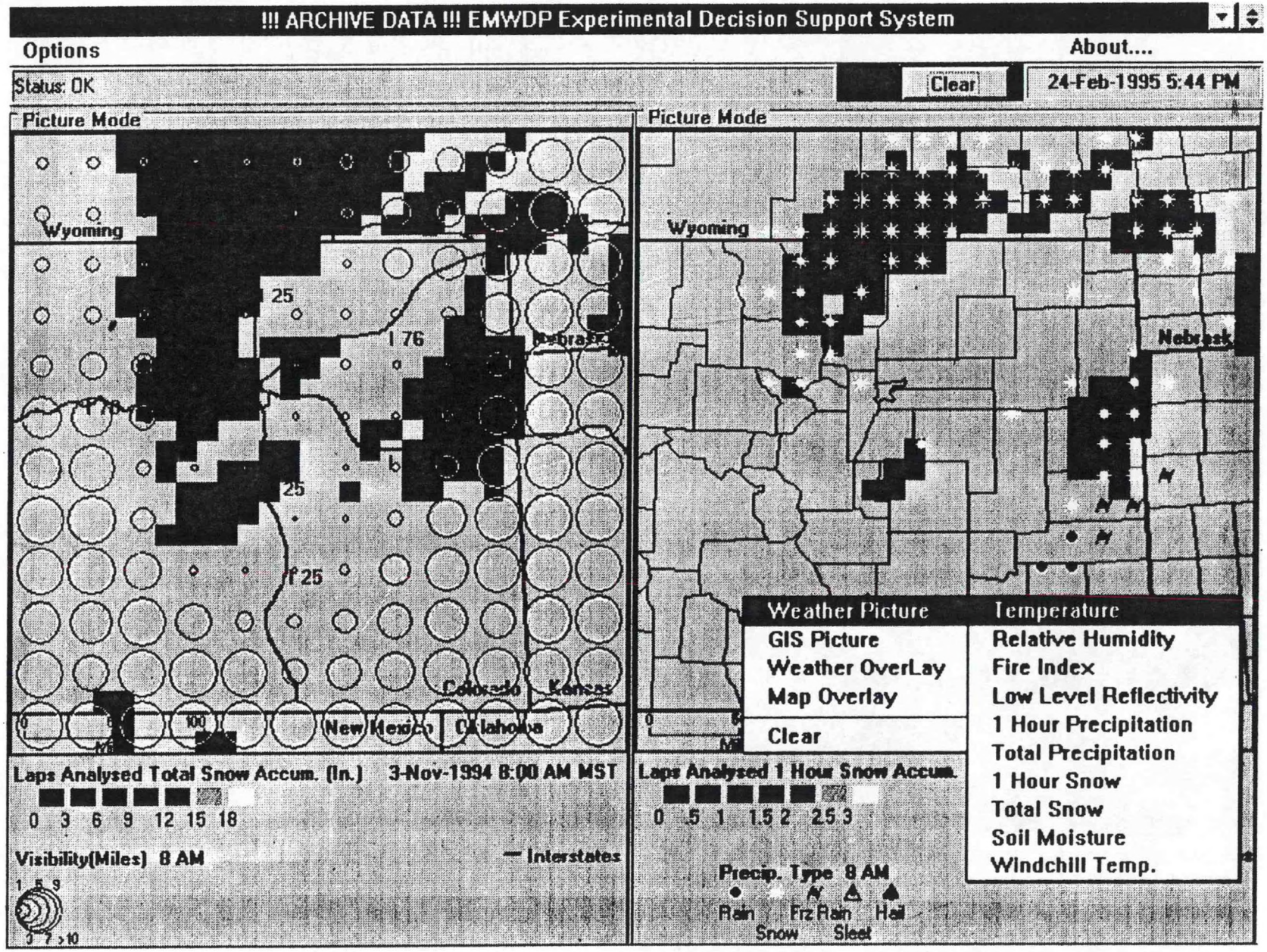
!!! ARCHIVE DATA !!! EMWDP Experimental Decision Support System
Options
About....
Status: OK
Clear
24-Feb-1995 5:44 PM
Picture Mode
Wyoming
25
I 76
Nebraska
25
I 25
Colorado
Kansas
New Mexico
Oklahoma
Laps Analysed Total Snow Accum. (In.)
3-Nov-1994 8:00 AM MST
0 3 6 9 12 15 18
Visibility(Miles) 8 AM
1 5 9
3 7 >10
— Interstates
Picture Mode
Wyoming
Nebraska
Weather Picture
GIS Picture
Weather OverLay
Map Overlay
Clear
Temperature
Relative Humidity
Fire Index
Low Level Reflectivity
1 Hour Precipitation
Total Precipitation
1 Hour Snow
Total Snow
Soil Moisture
Windchill Temp.
Laps Analysed 1 Hour Snow Accum.
0 .5 1 1.5 2 2.5 3
Precip. Type 8 AM
Rain
Snow
Frz Rain
Sleet
Hail

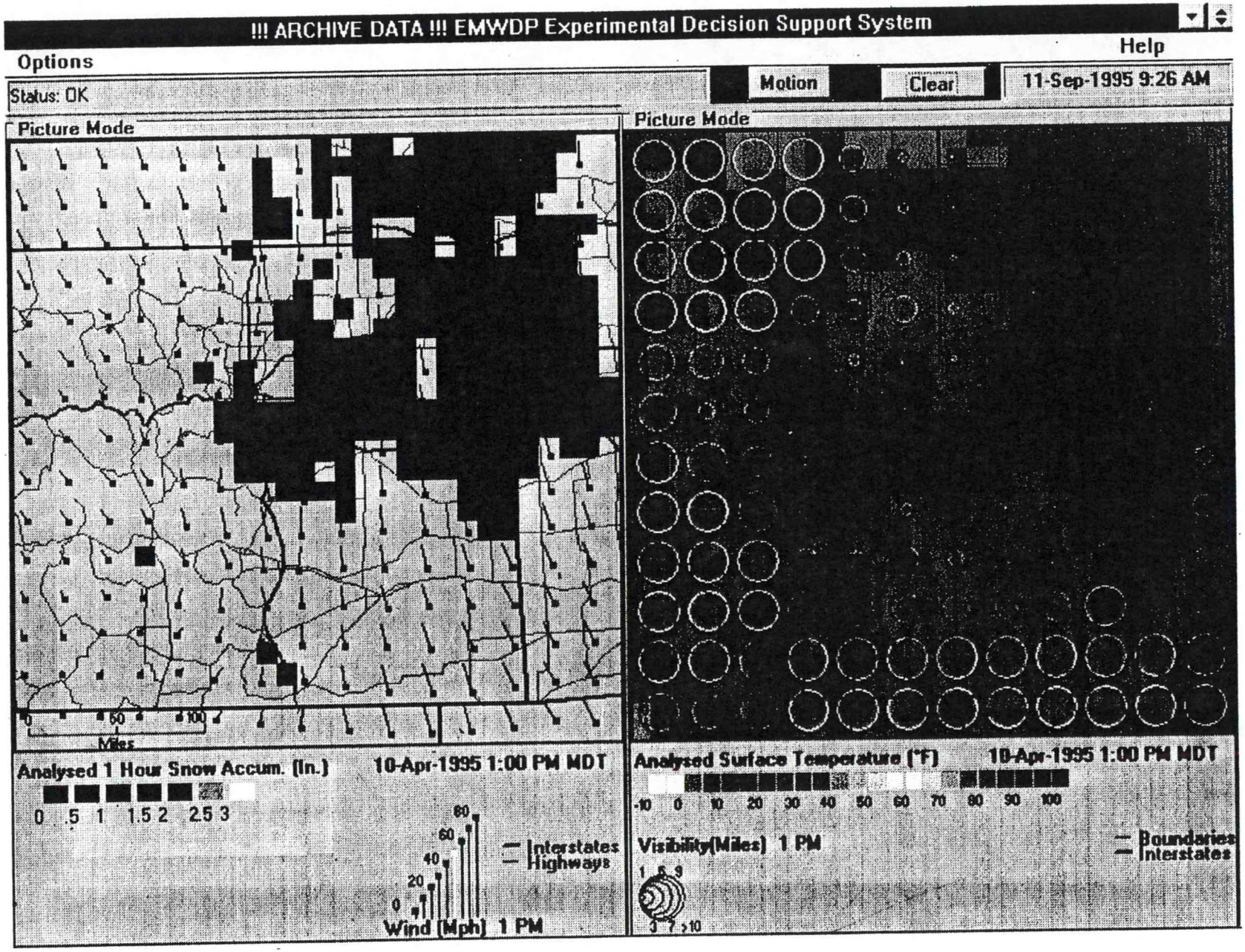
!!! ARCHIVE DATA !!! EMWDP Experimental Decision Support System
Options
Help
Status: OK
Motion
Clear
11-Sep-1995 9:26 AM
Picture Mode
Picture Mode
0 50 100
Miles
Analysed 1 Hour Snow Accum. (In.)
10-Apr-1995 1:00 PM MDT
0 .5 1 1.5 2 2.5 3
Interstates
Highways
0 20 40 60 80
Wind (Mph) 1 PM
Analysed Surface Temperature (°F)
10-Apr-1995 1:00 PM MDT
-10 0 10 20 30 40 50 60 70 80 90 100
Visibility(Miles) 1 PM
Boundaries
Interstates
1 5 9
3 7 >10

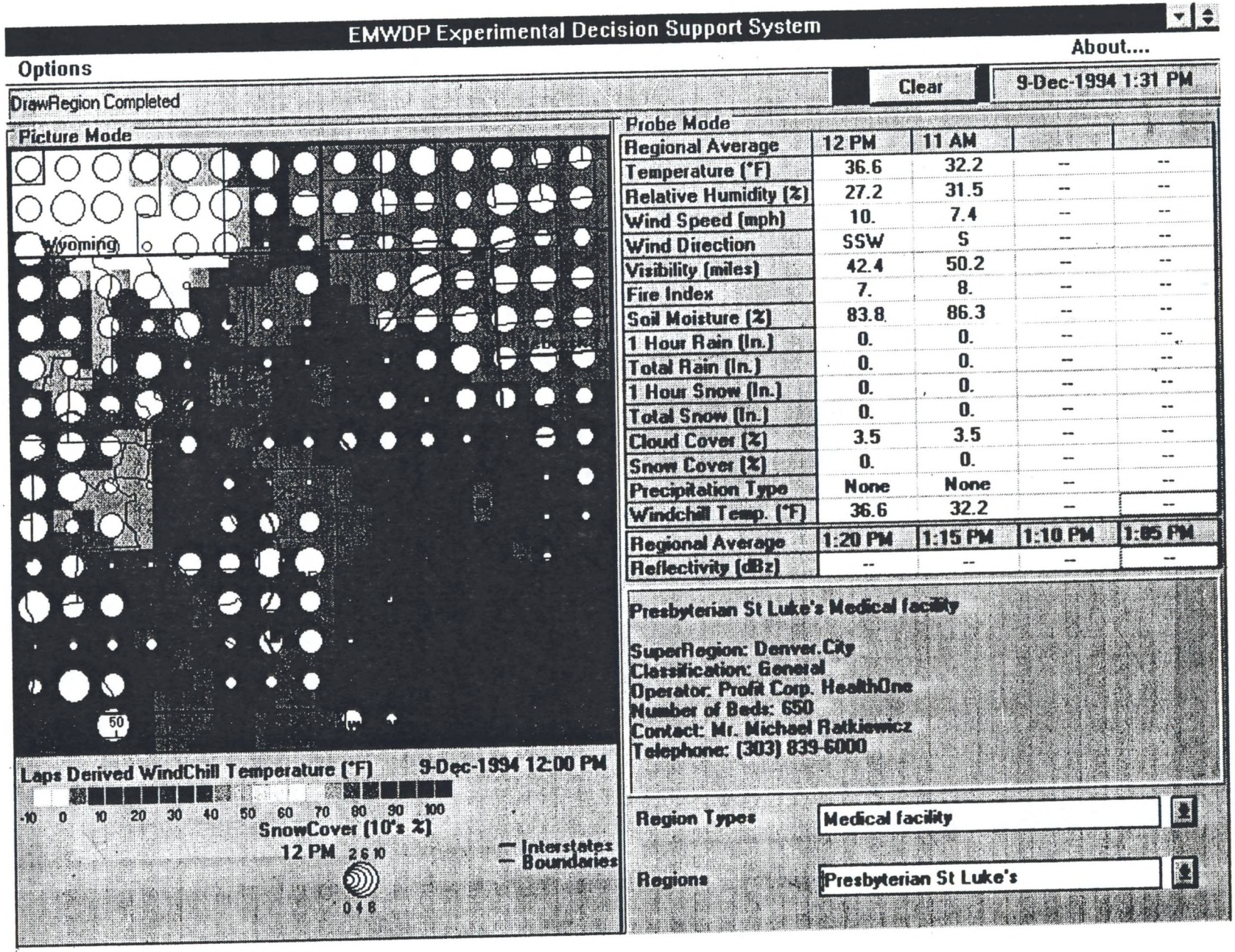
EMWDP Experimental Decision Support System
About....
Options
DrawRegion Completed
Clear
9-Dec-1994 1:31 PM
Picture Mode
Wyoming
50
Laps Derived WindChill Temperature (°F)
9-Dec-1994 12:00 PM
-10 0 10 20 30 40 50 60 70 80 90 100
SnowCover (10's %)
12 PM 2 6 10
0 4 8
Interstates
Boundaries
Probe Mode
Regional Average | 12 PM | 11 AM
Temperature (°F) 36.6 32.2 -- --
Relative Humidity (%) 27.2 31.5 -- --
Wind Speed (mph) 10. 7.4 -- --
Wind Direction SSW S -- --
Visibility (miles) 42.4 50.2 -- --
Fire Index 7. 8. -- --
Soil Moisture (%) 83.8 86.3 -- --
1 Hour Rain (In.) 0. 0. -- --
Total Rain (In.) 0. 0. -- --
1 Hour Snow (In.) 0. 0. -- --
Total Snow (In.) 0. 0. -- --
Cloud Cover (%) 3.5 3.5 -- --
Snow Cover (%) 0. 0. -- --
Precipitation Type None None -- --
Windchill Temp. (°F) 36.6 32.2 -- --
Regional Average | 1:20 PM | 1:15 PM | 1:10 PM | 1:05 PM
Reflectivity (dBz) -- -- -- --
Presbyterian St Luke's Medical facility
SuperRegion: Denver.City
Classification: General
Operator: Profit Corp. HealthOne
Number of Beds: 650
Contact: Mr. Michael Ratkiewicz
Telephone: (303) 839-6000
Region Types
Medical facility
Regions
Presbyterian St Luke's

CASE STUDIES

- **7 January 1992**
- **8-9 March 1992**
- **14 November 1994**

COLORADO

ZONE FORECAST BOUNDARIES

CO Zones 1–23, 30–50, 60–81 and 90–92 prepared by WSFO Denver, CO
CO Zone numbers 24–29, 51–59 and 82–89 reserved for future use.

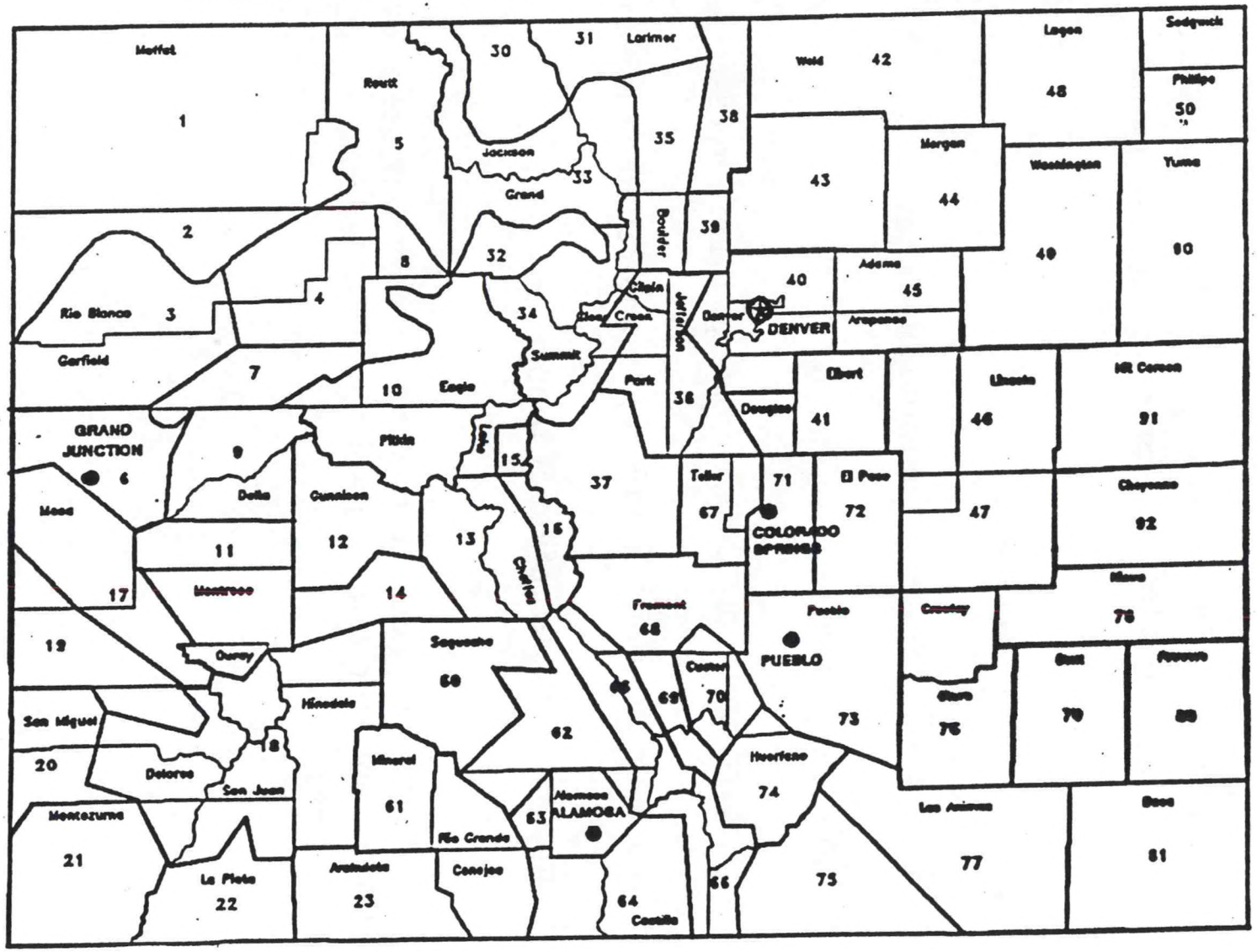

WEATHER SERVICE FORECAST OFFICE
WEATHER SERVICE OFFICE

NATIONAL WEATHER SERVICE
CENTRAL REGION

Real-Time High-Resolution Forecasting

High resolution (LAPS) analyses provide excellent data for the start-up of sophisticated meteorological forecast models.

Benefits of higher resolution:

- More detailed state of the atmosphere predictions
- Explicit representation of clouds
- Improved and more detailed precipitation forecasts
- Representation of soil improves boundary layer forecasts
- Improved representation of topography

*** Rapid improvements in computer technology are allowing the implementation of high-resolution forecast models in real-time systems.

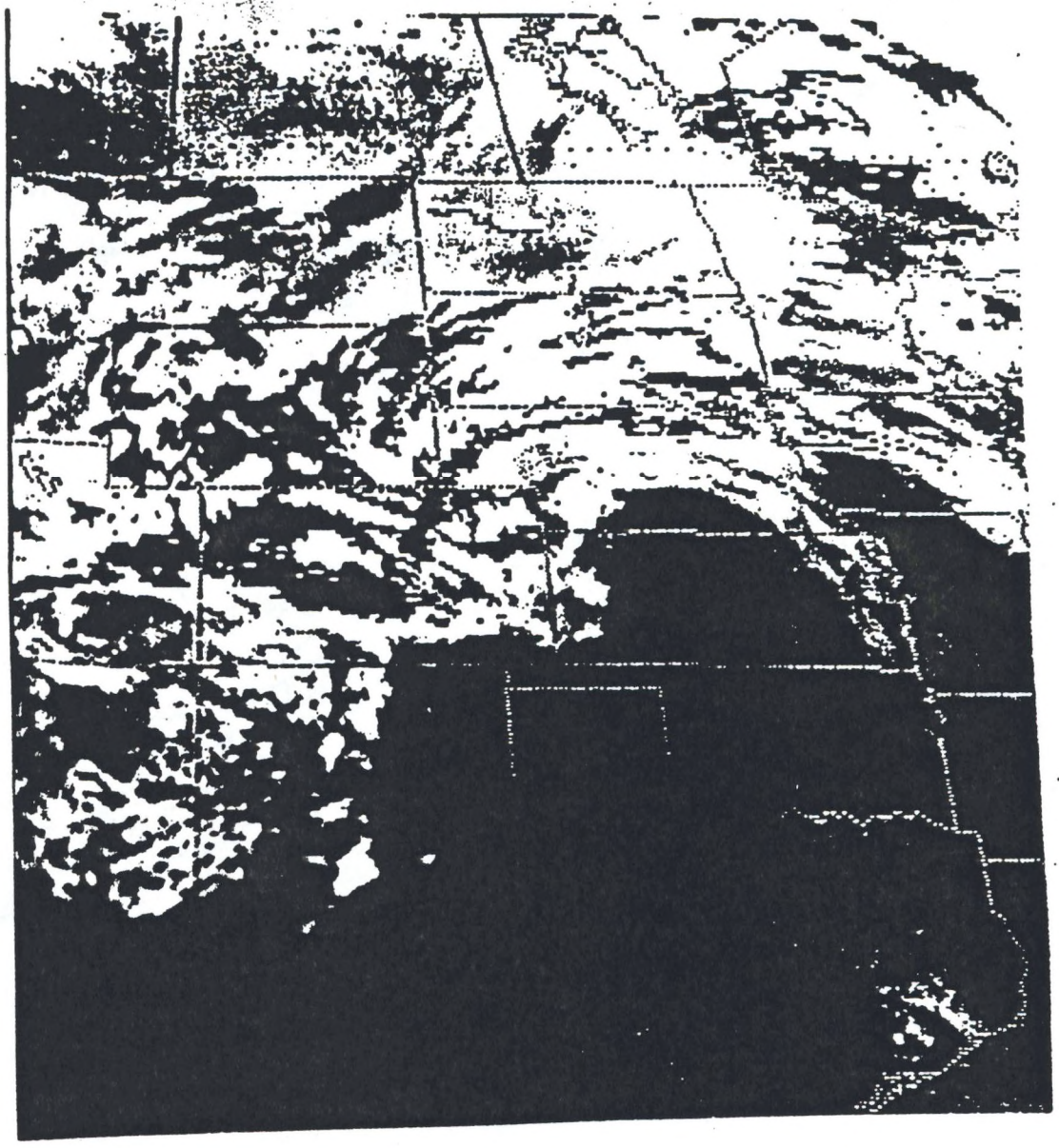

MODELING
CASE

18Z
7 JAN 92

F 3

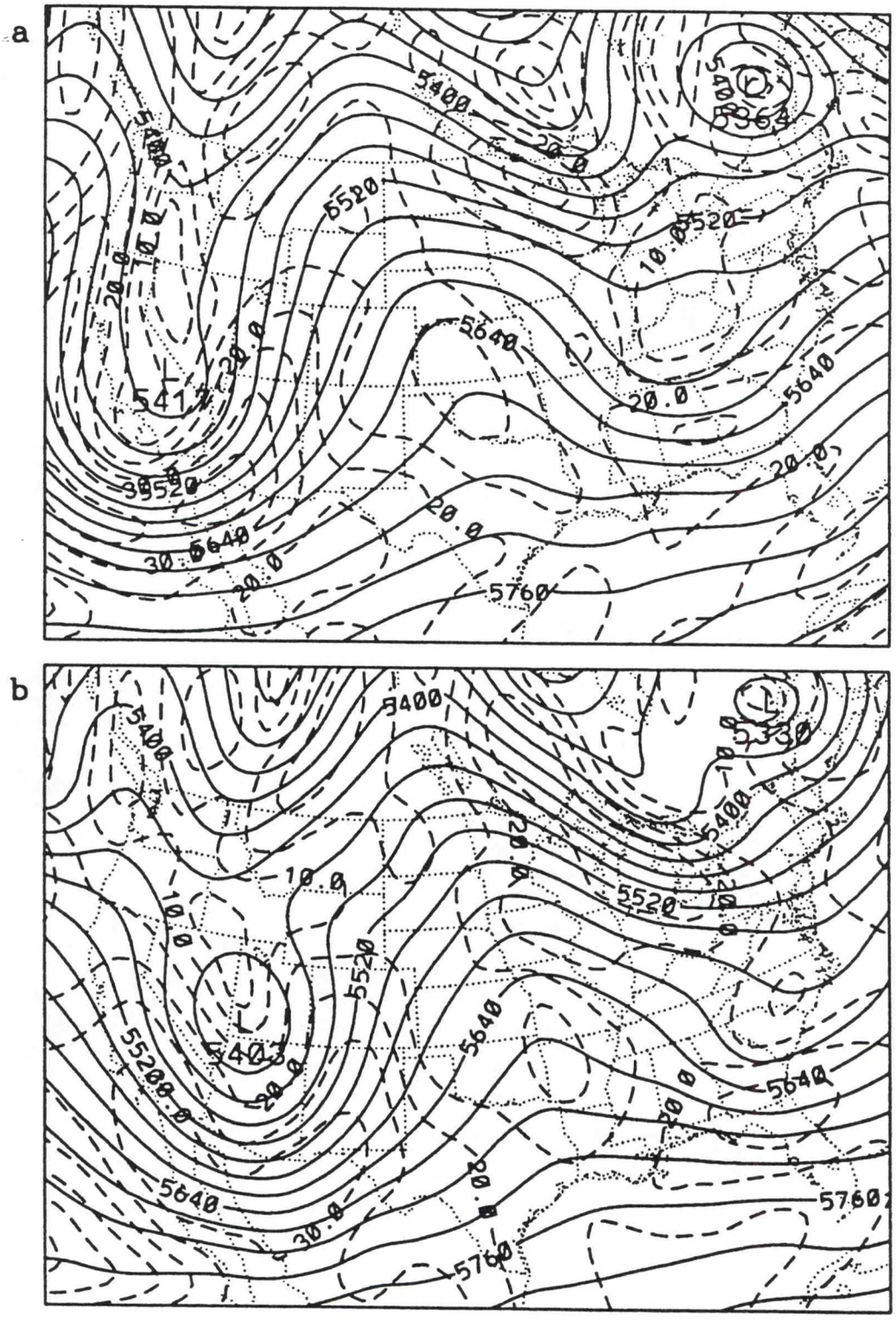

Figure 4.2: NGM 500 mb height (m, solid contours) and isotach (m s^{-1}, dashed contours) analyses from (a) 1200 UTC 6 January and (b) 0000 UTC 7 January 1992.

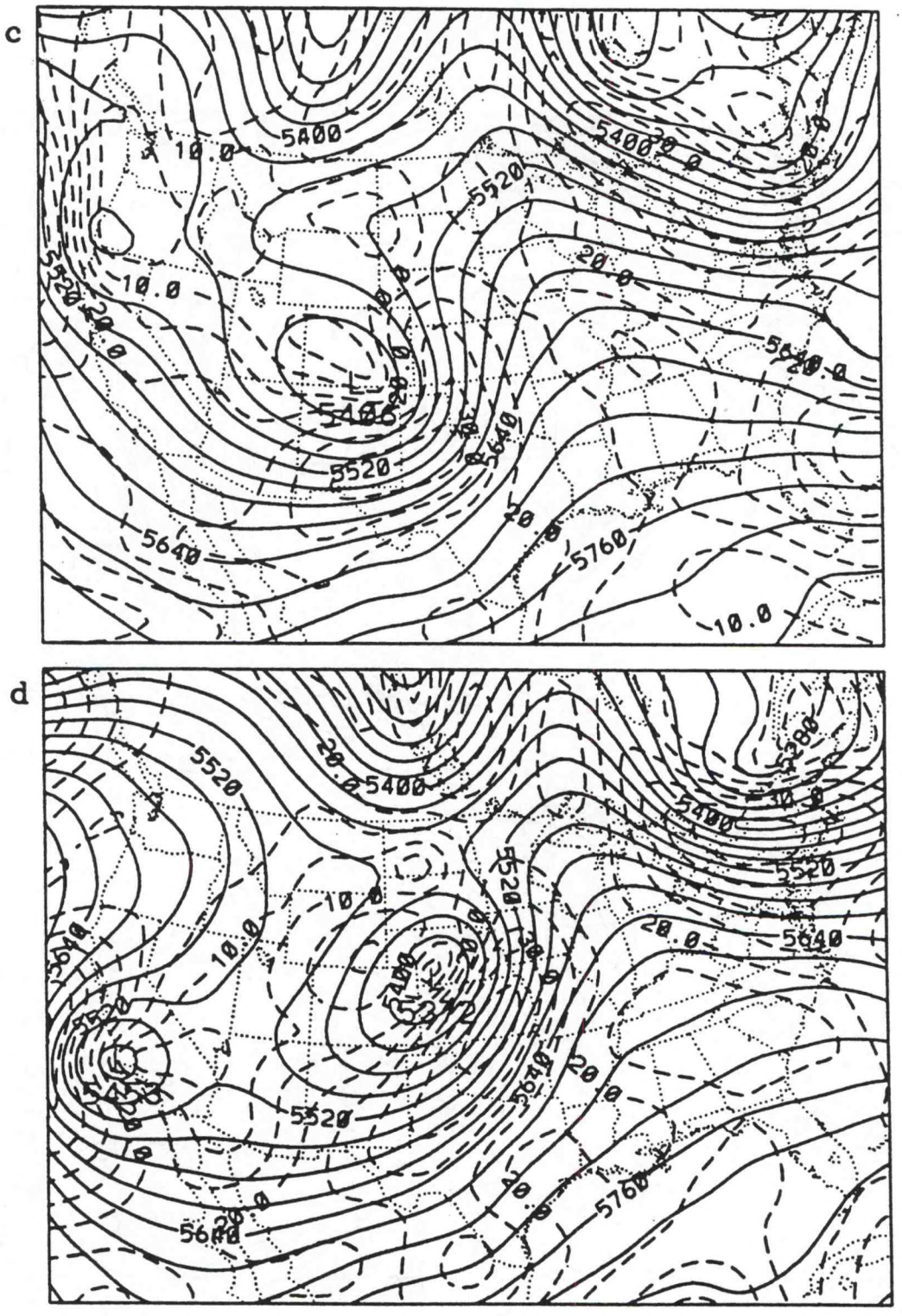

Figure 4.2: Continued: (c) 1200 UTC 7 January and (d) 0000 UTC 8 January 1992.

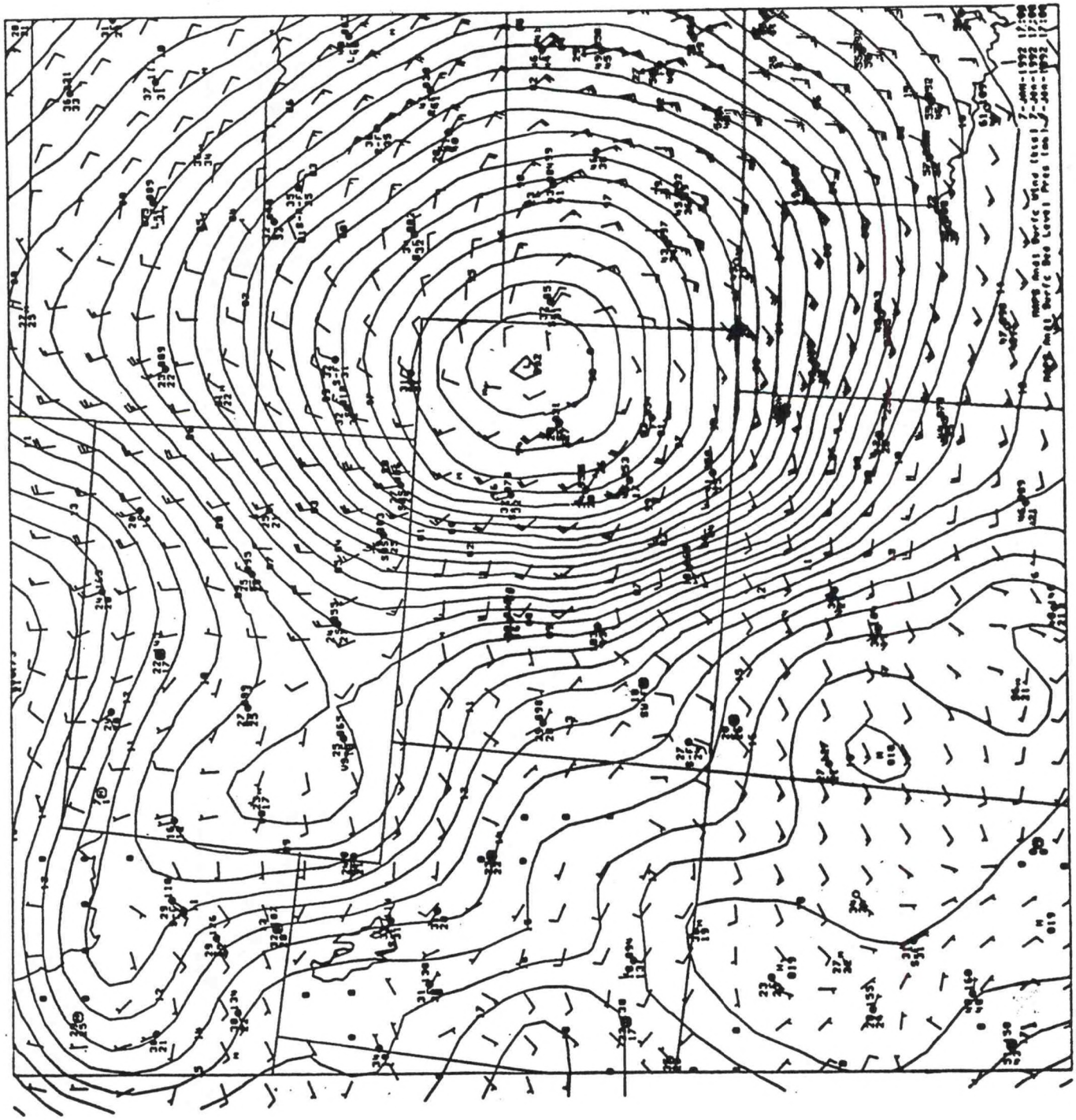

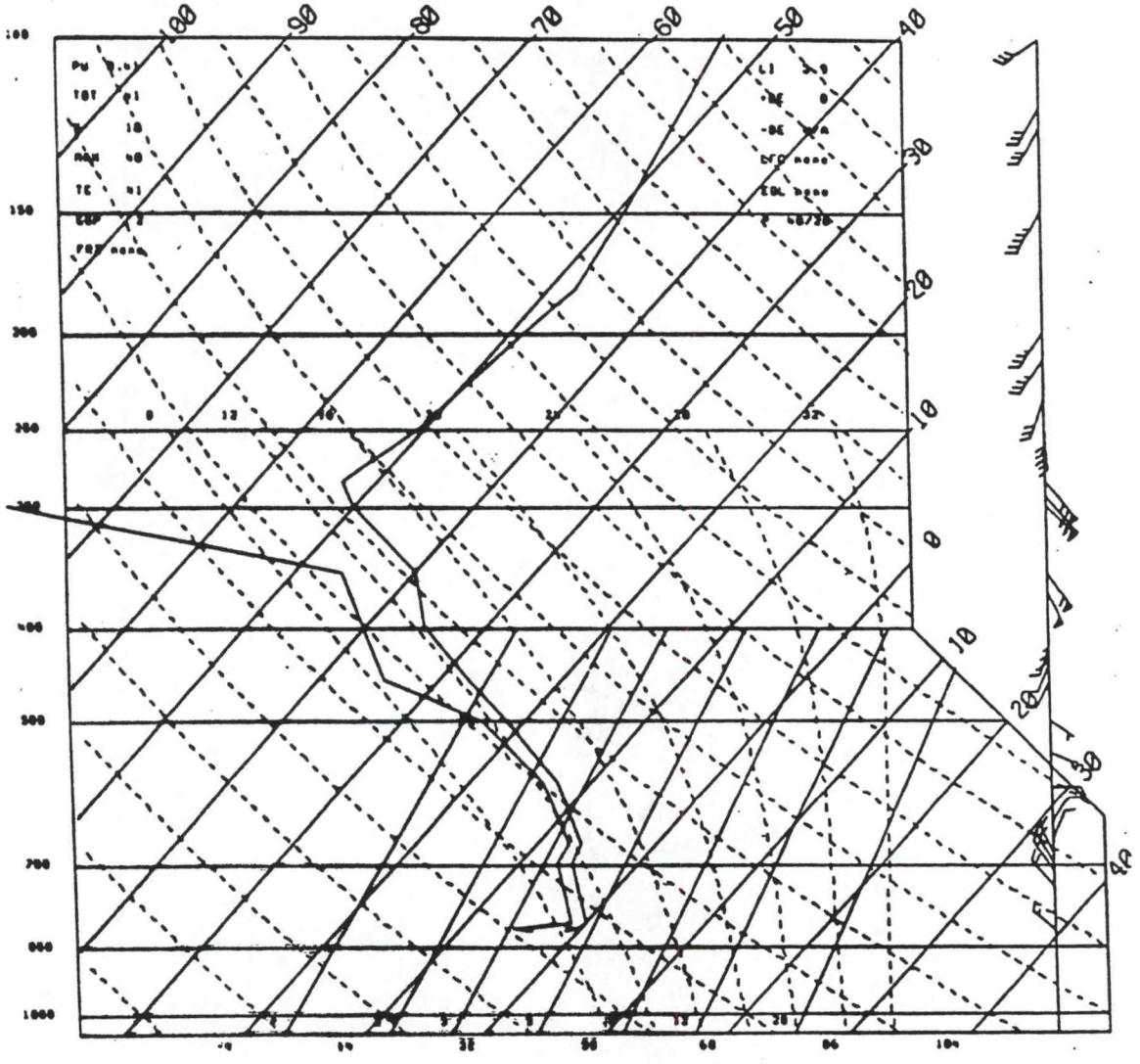

Figure 4.11: Rawinsonde observations from 1200 UTC 7 January 1992 at (a) Denver, CO.

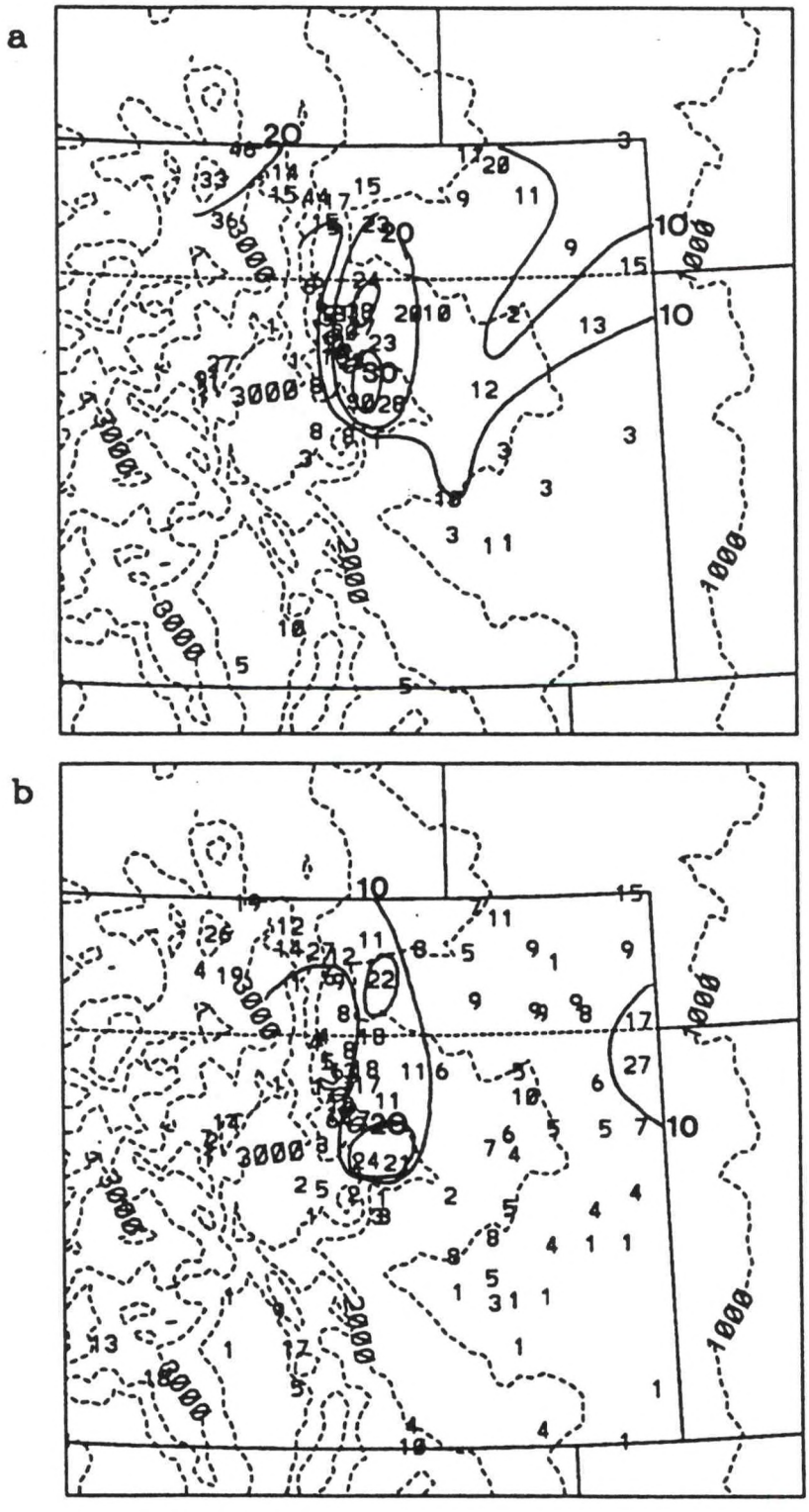

Figure 4.1: Observed precipitation during the 7 January 1992 snow storm, (a) snowfall (cm) and (b) melted water equivalent (mm).

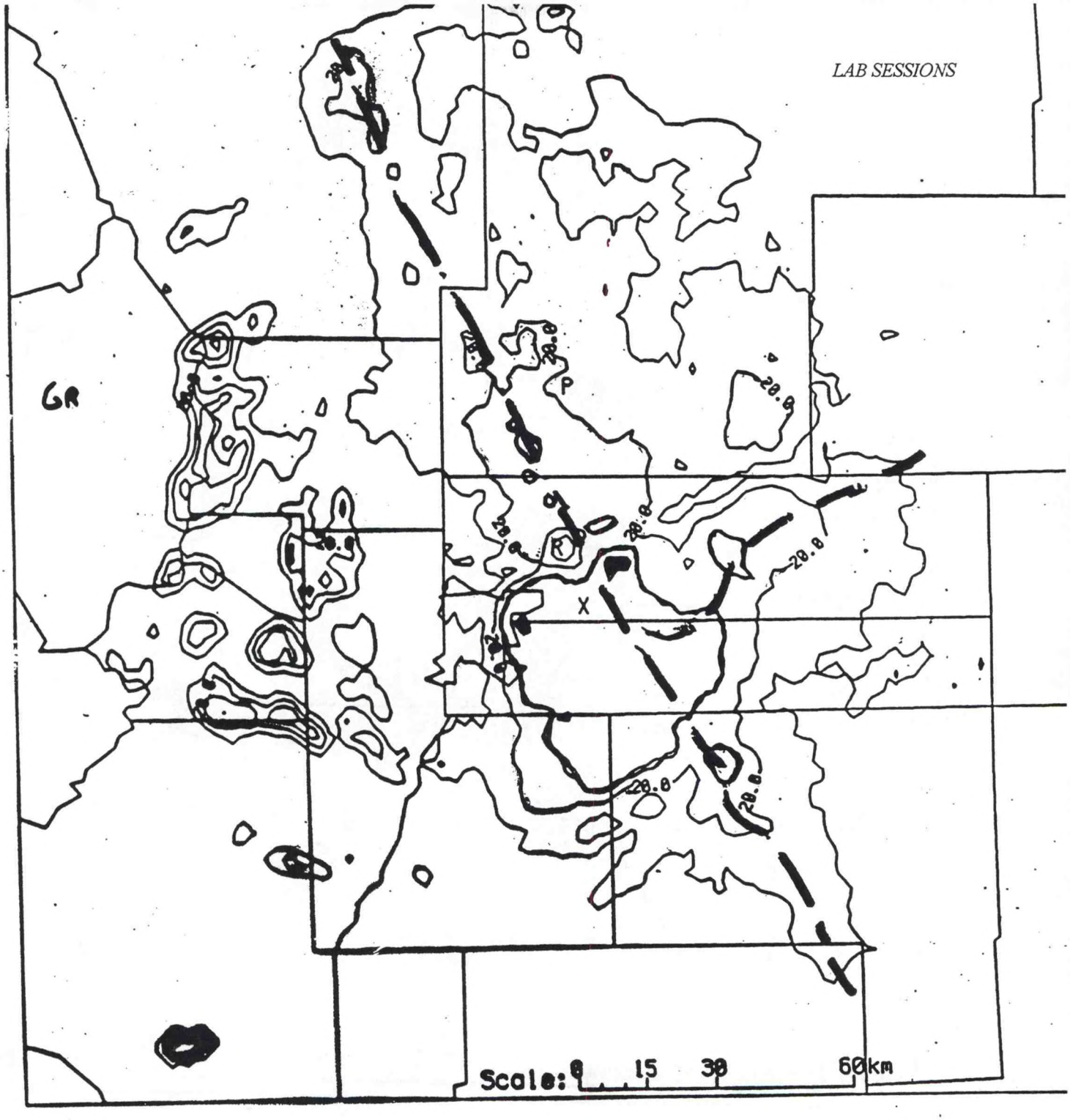

18Z
RADAR

1800 LTC

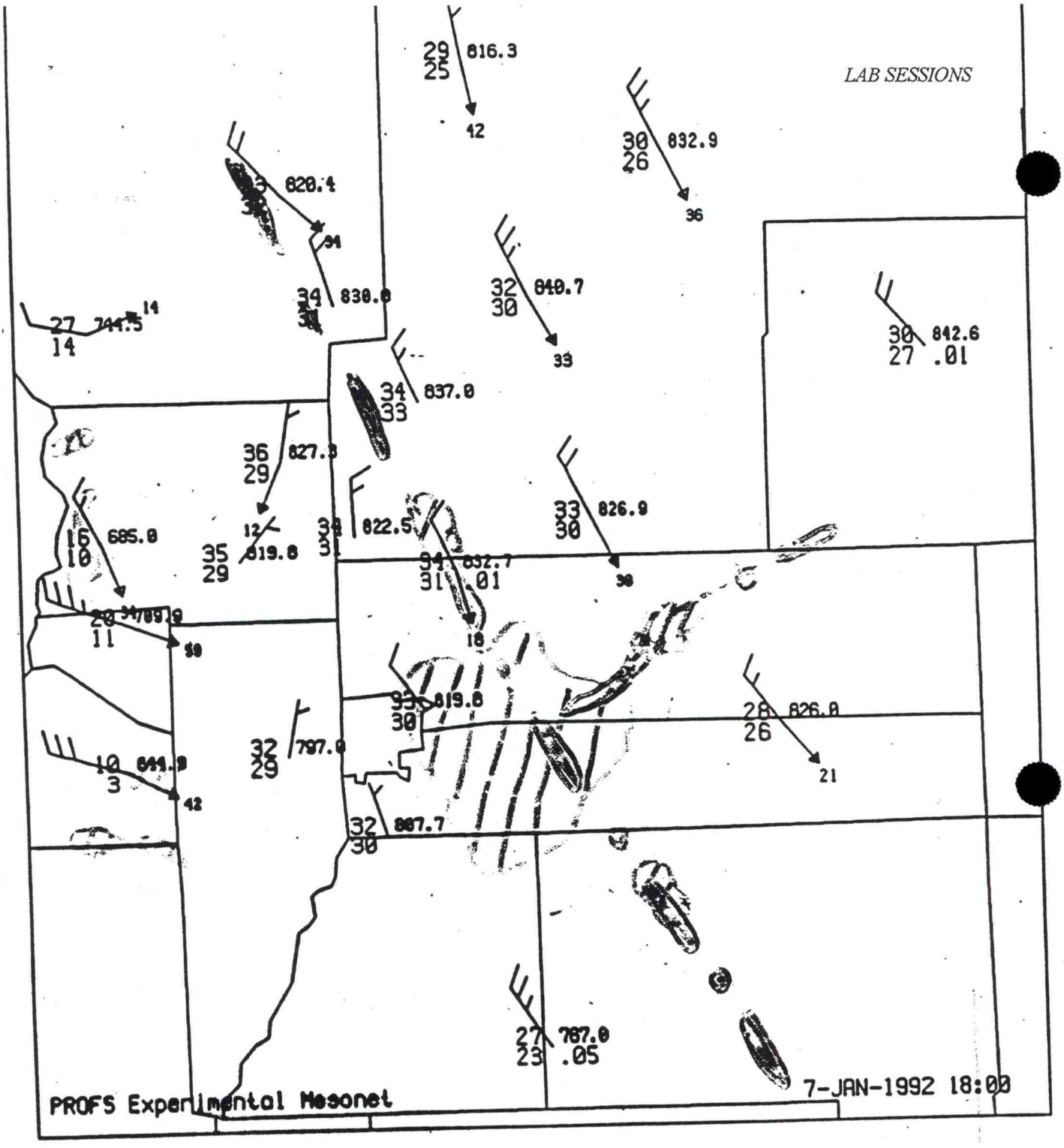
29 816.3
25
12
30 832.9
26
36
820.4
34
32 840.7
30
33
30 842.6
27 .01
34 837.0
33
36 827.8
29
33 826.9
30
16 685.0
10
12
35 819.8
29
822.5
34 832.7
31 .01
36
18
20 34/889.9
11
39
33 819.8
30
28 826.8
26
21
32 787.8
29
10 844.9
3
42
32 867.7
30
27 787.0
23 .05
PROFS Experimental Mesonet
7-JAN-1992 18:00

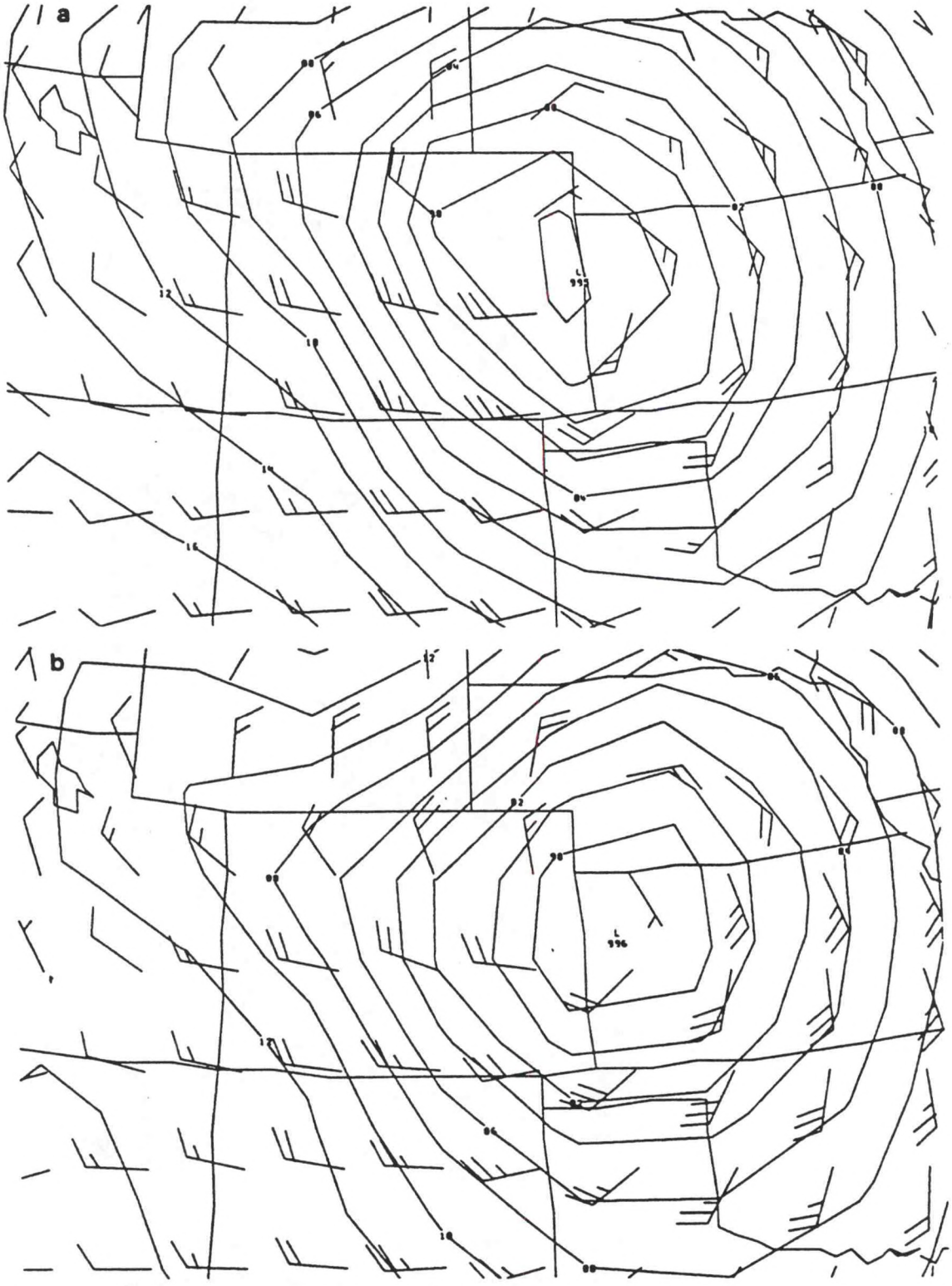

Figure 4.52: NGM mean sea-level pressure (mb) and surface wind (knots) predictions from (a) the 6 h forecast valid at 1800 UTC 7 January and (b) the 12 h forecast valid at 0000 UTC 8 January 1992.

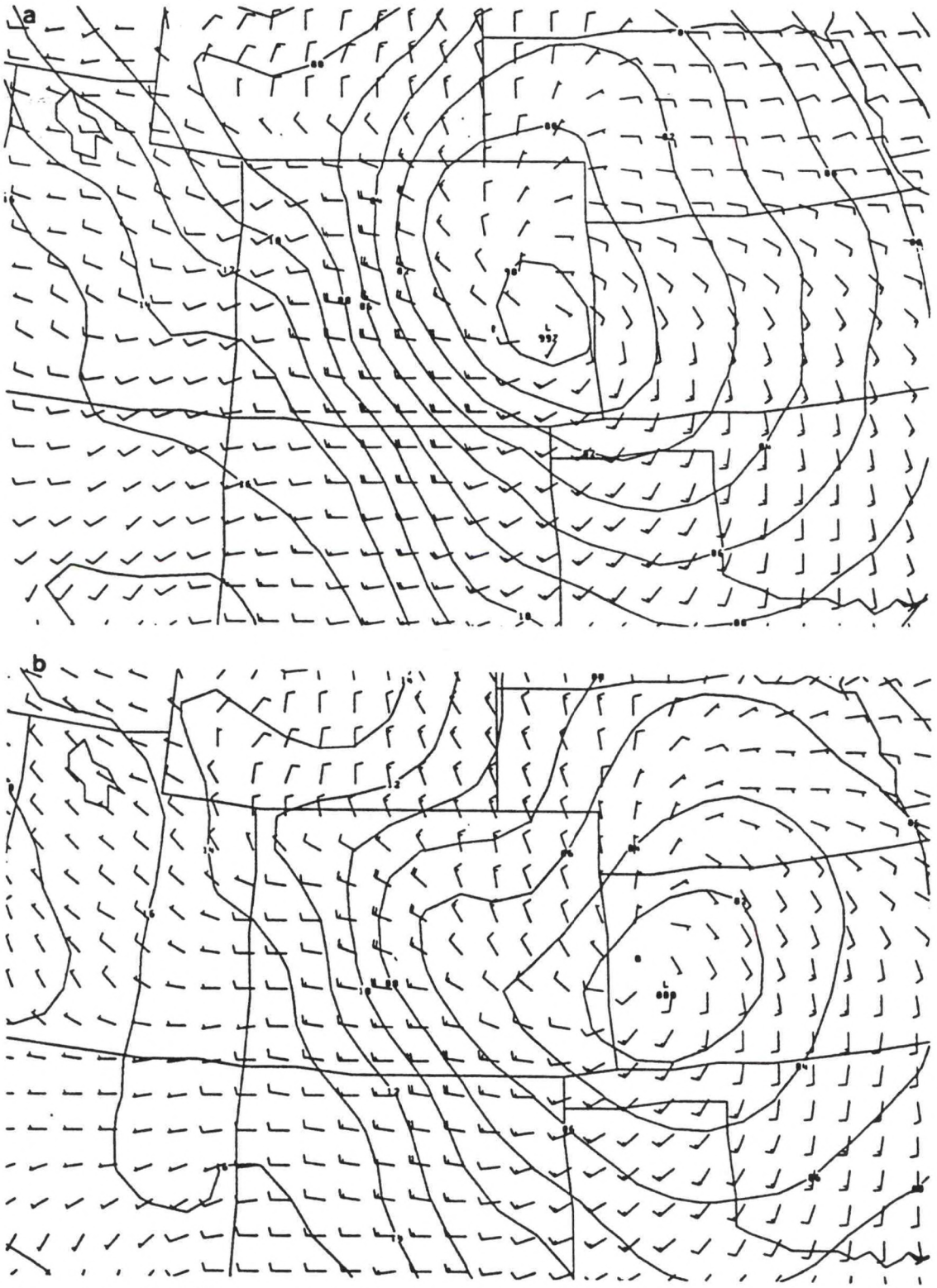

Figure 4.51: MAPS mean sea-level pressure (mb) and surface wind (knots) predictions from (a) the 6 h forecast valid at 1800 UTC 7 January and (b) the 12 h forecast valid at 0000 UTC 8 January 1992.

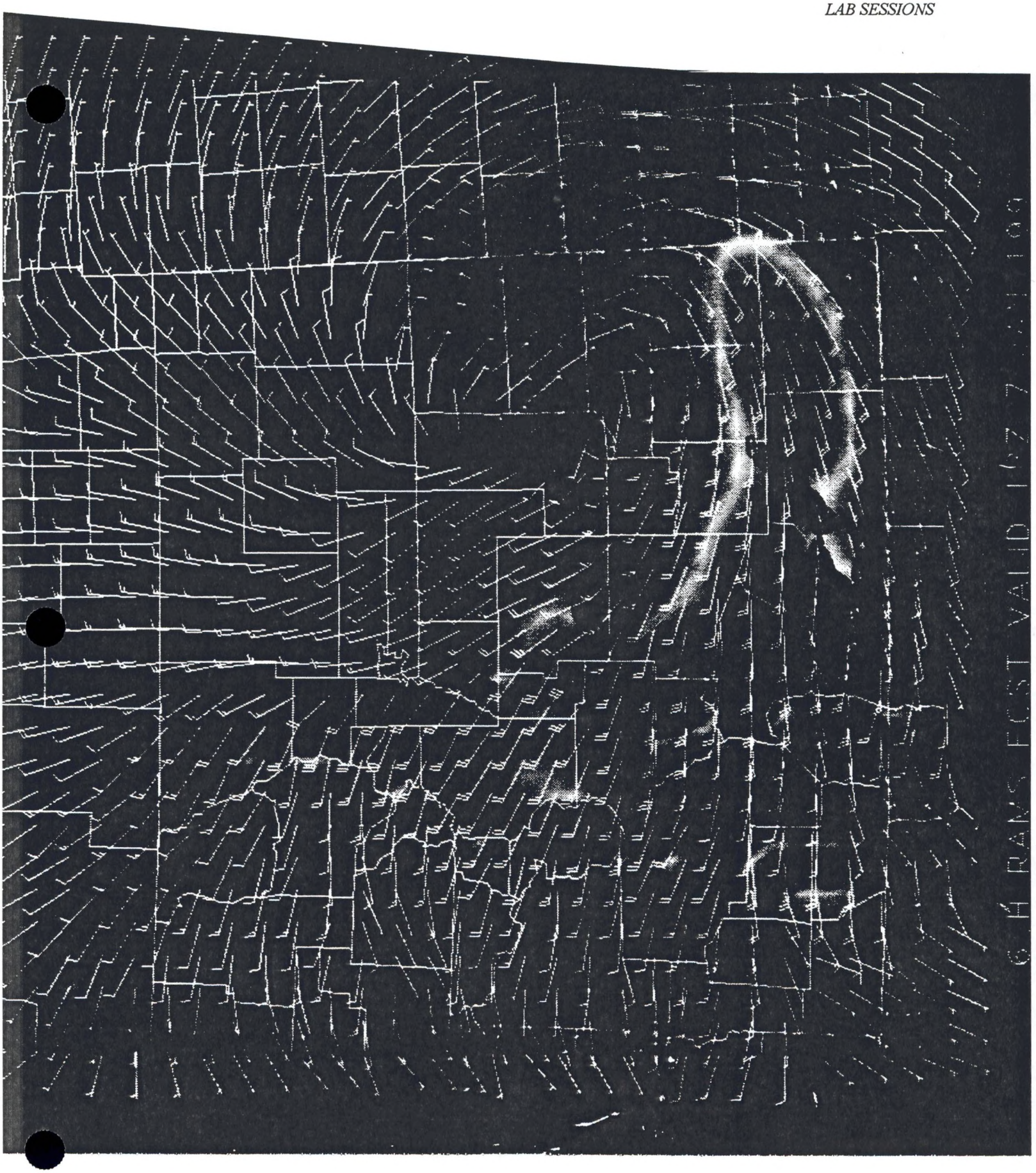
6 H RAMS FCST VALID 12Z 7 JAN 199

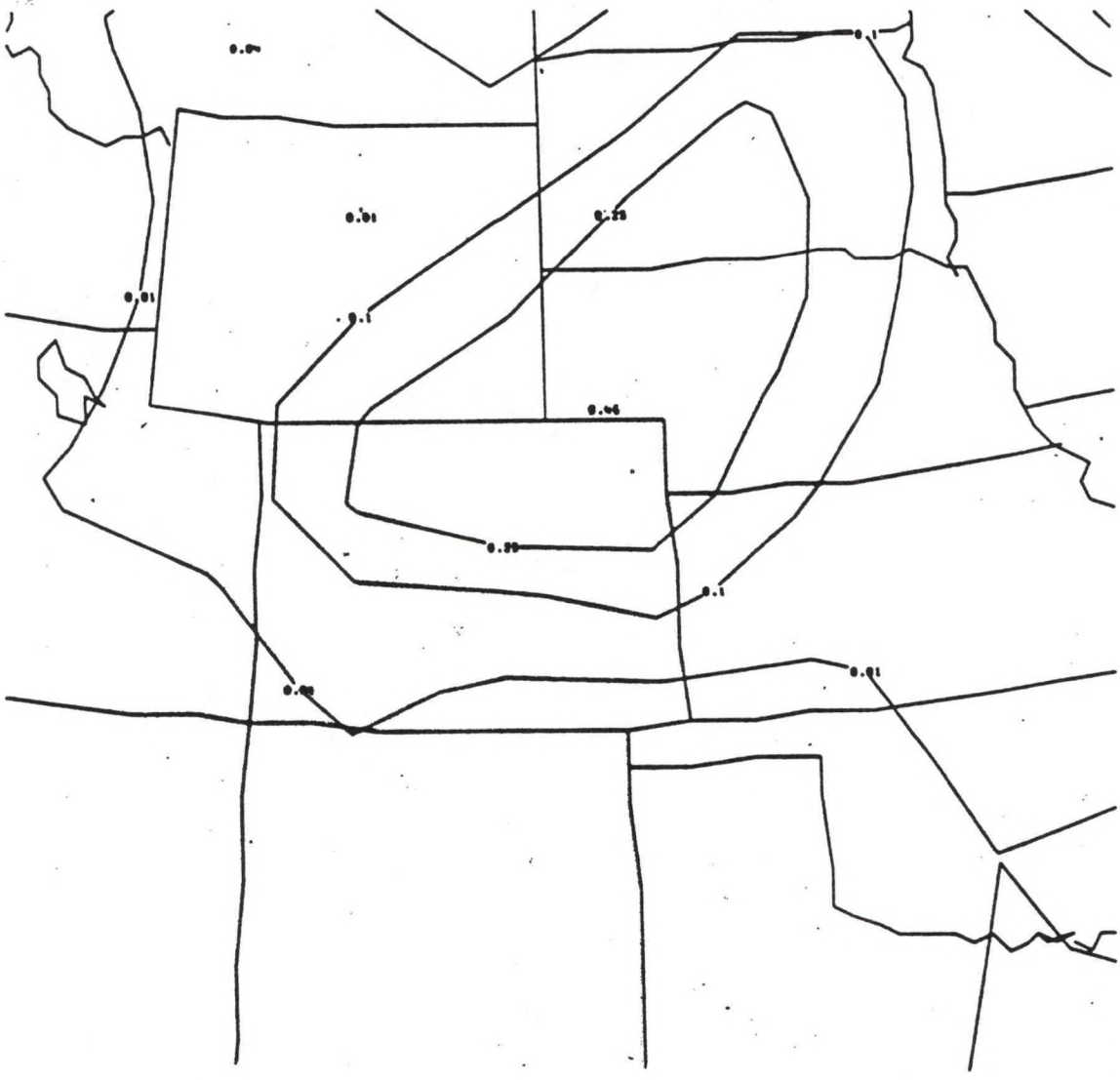

Figure 4.55: NGM 12 h melted precipitation (inches) forecast valid at 0000 UTC 8 January 1992.

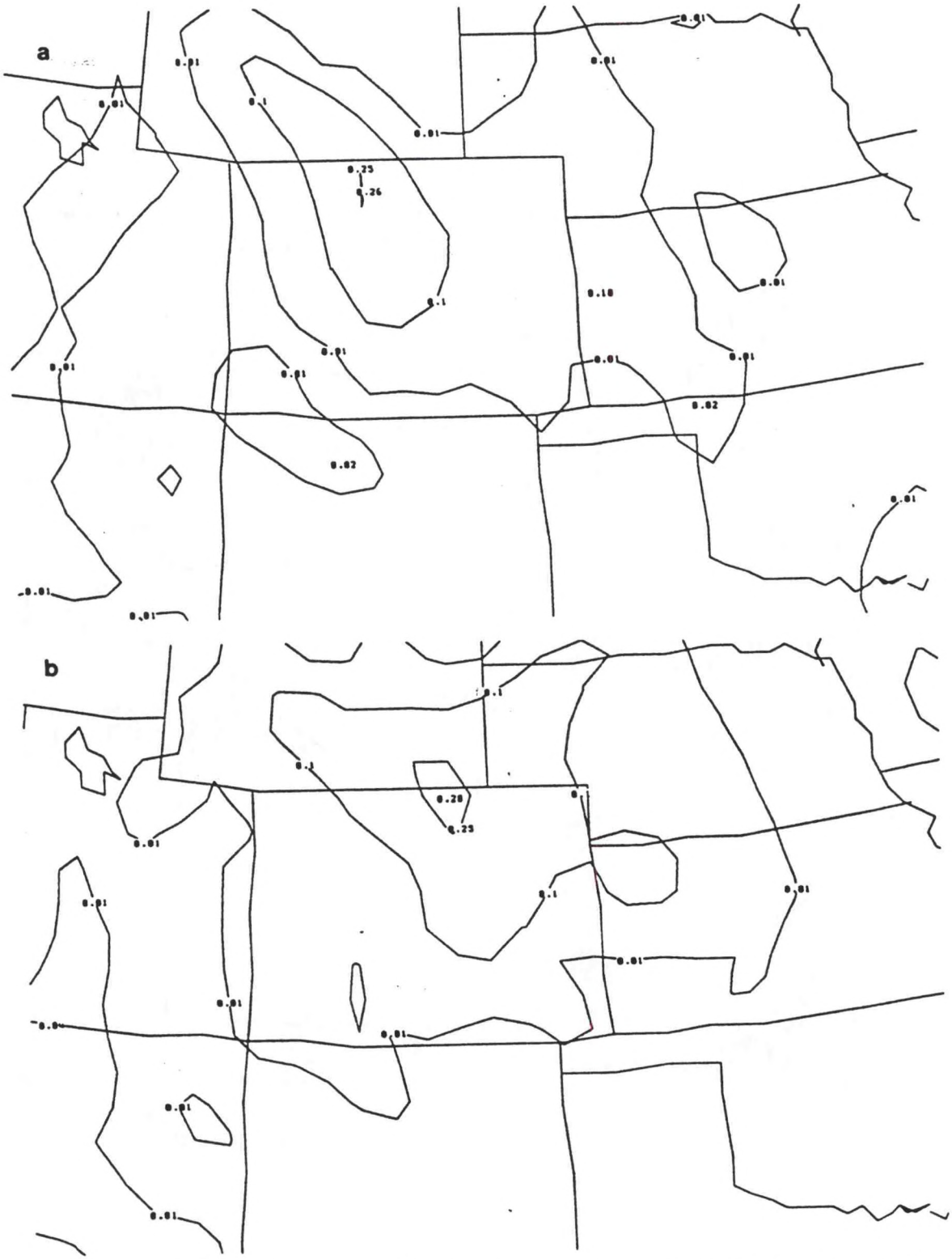

Figure 4.56: MAPS 3 h melted precipitation (inches) forecasts from (a) the 3 h prediction valid at 1500 UTC and (b) the 6 h prediction valid at 1800 UTC 7 January 1992.

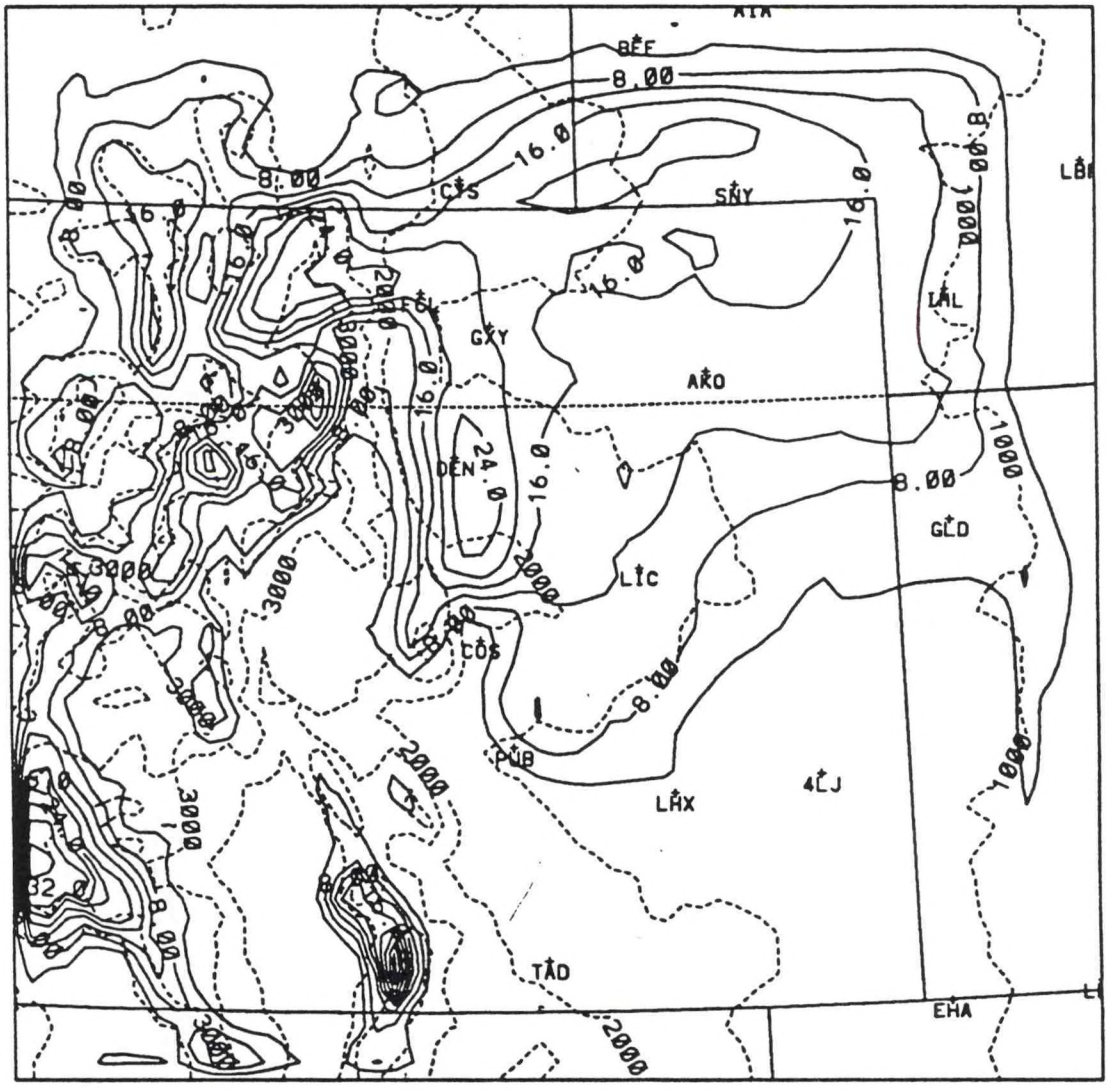

Figure 4.34: RAMS (LMIC) 12 h melted precipitation (mm) forecast.

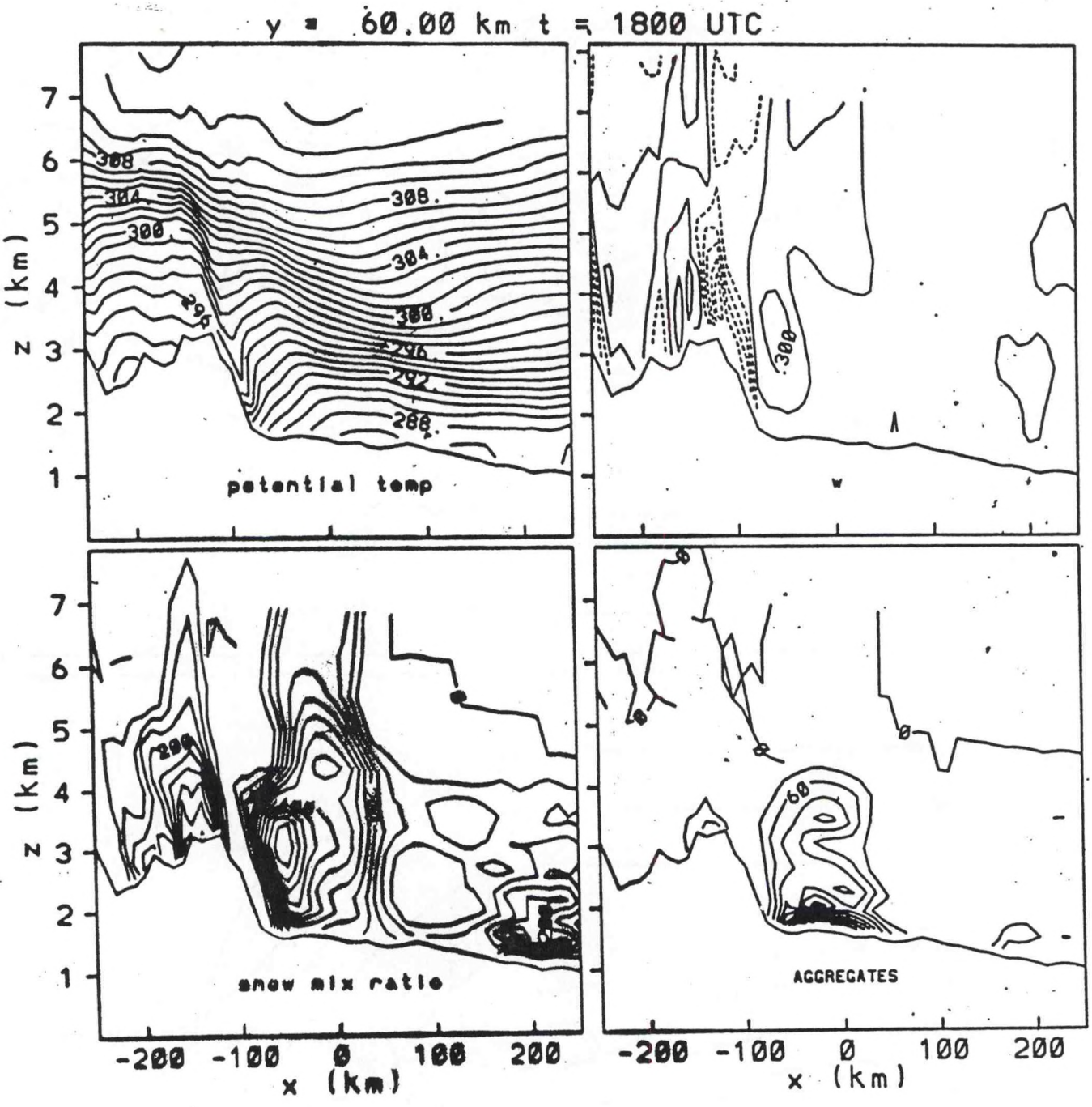
y = 60.00 km t = 1800 UTC
potential temp
w
snow mix ratio
AGGREGATES
z (km)
x (km)
-200 -100 0 100 200
1 2 3 4 5 6 7

4.29

Schematic Diagrams of 7 Jan 1992 Snow Event

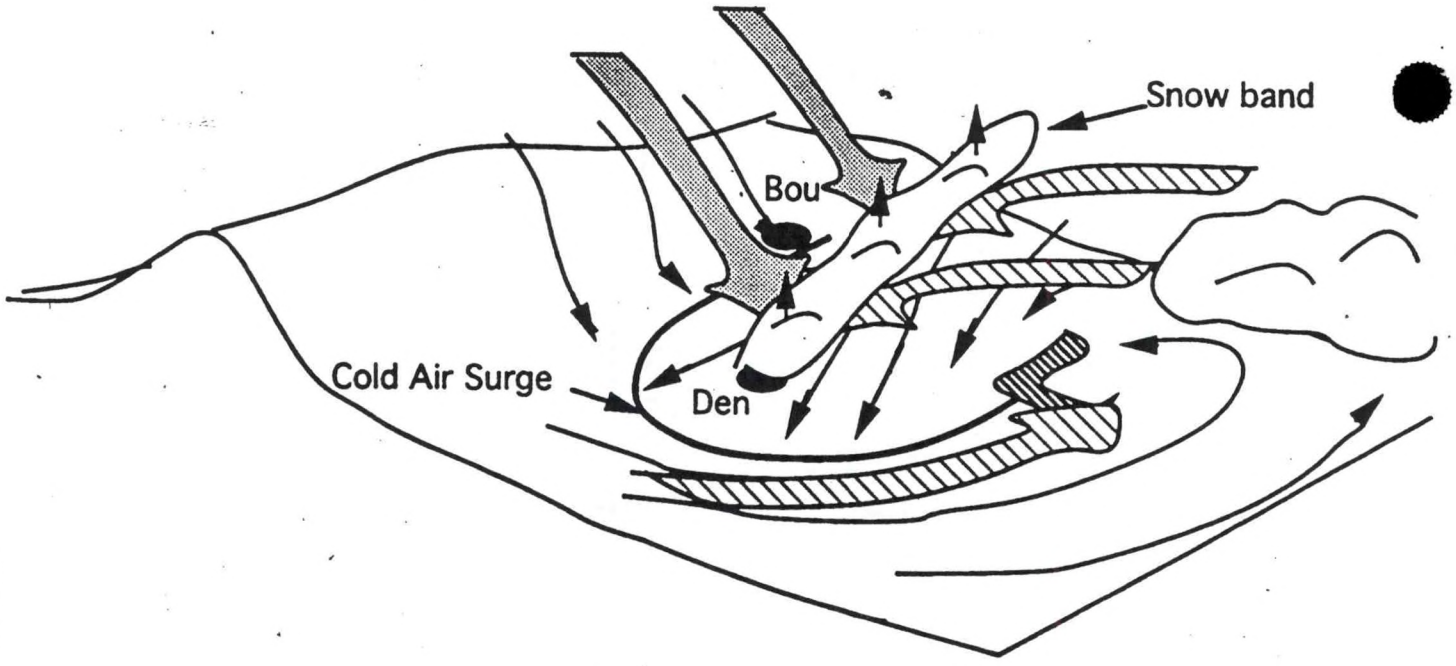

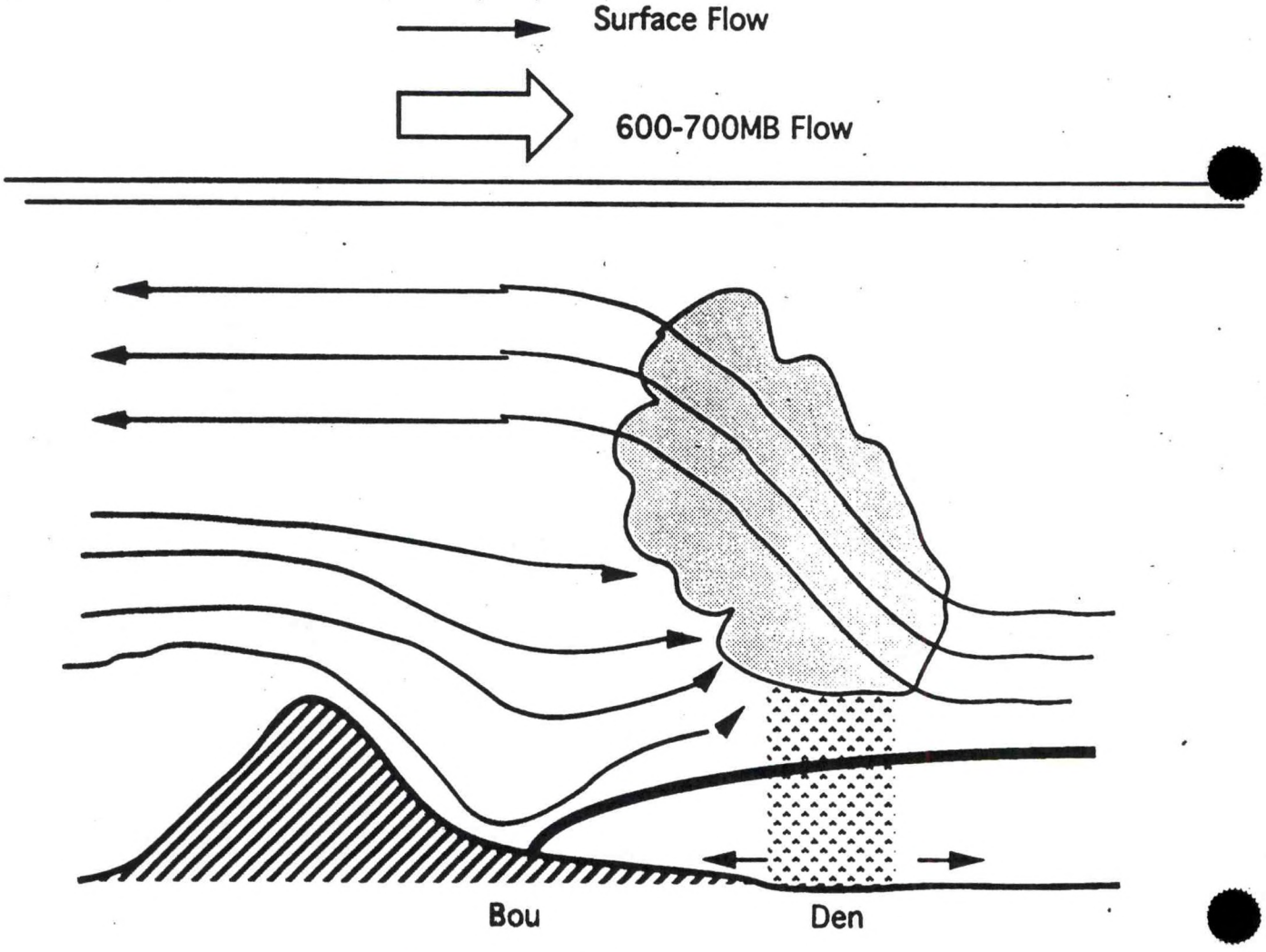

West to East Cross-section

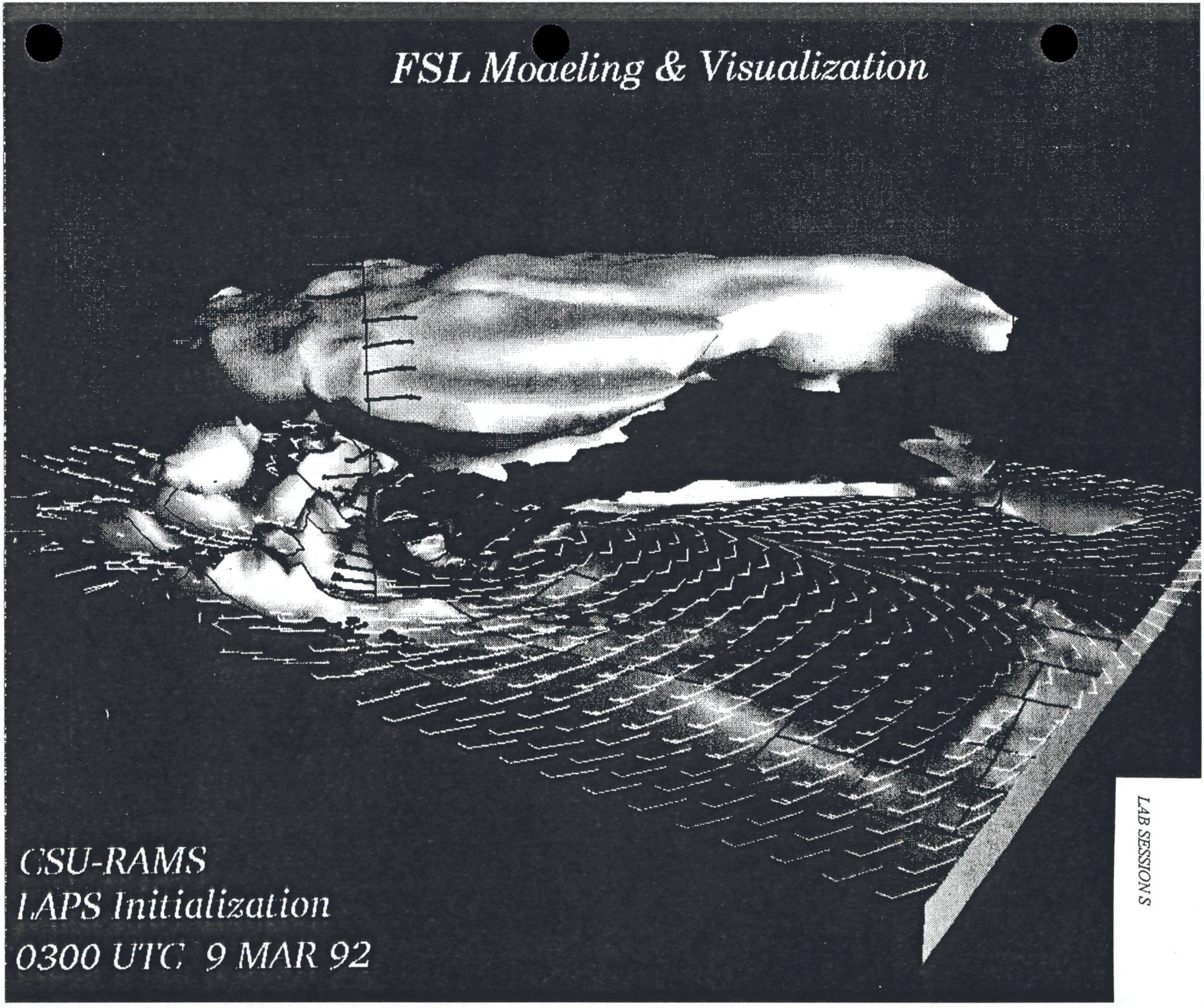
FSL Modeling & Visualization
CSU-RAMS
LAPS Initialization
0300 UTC 9 MAR 92

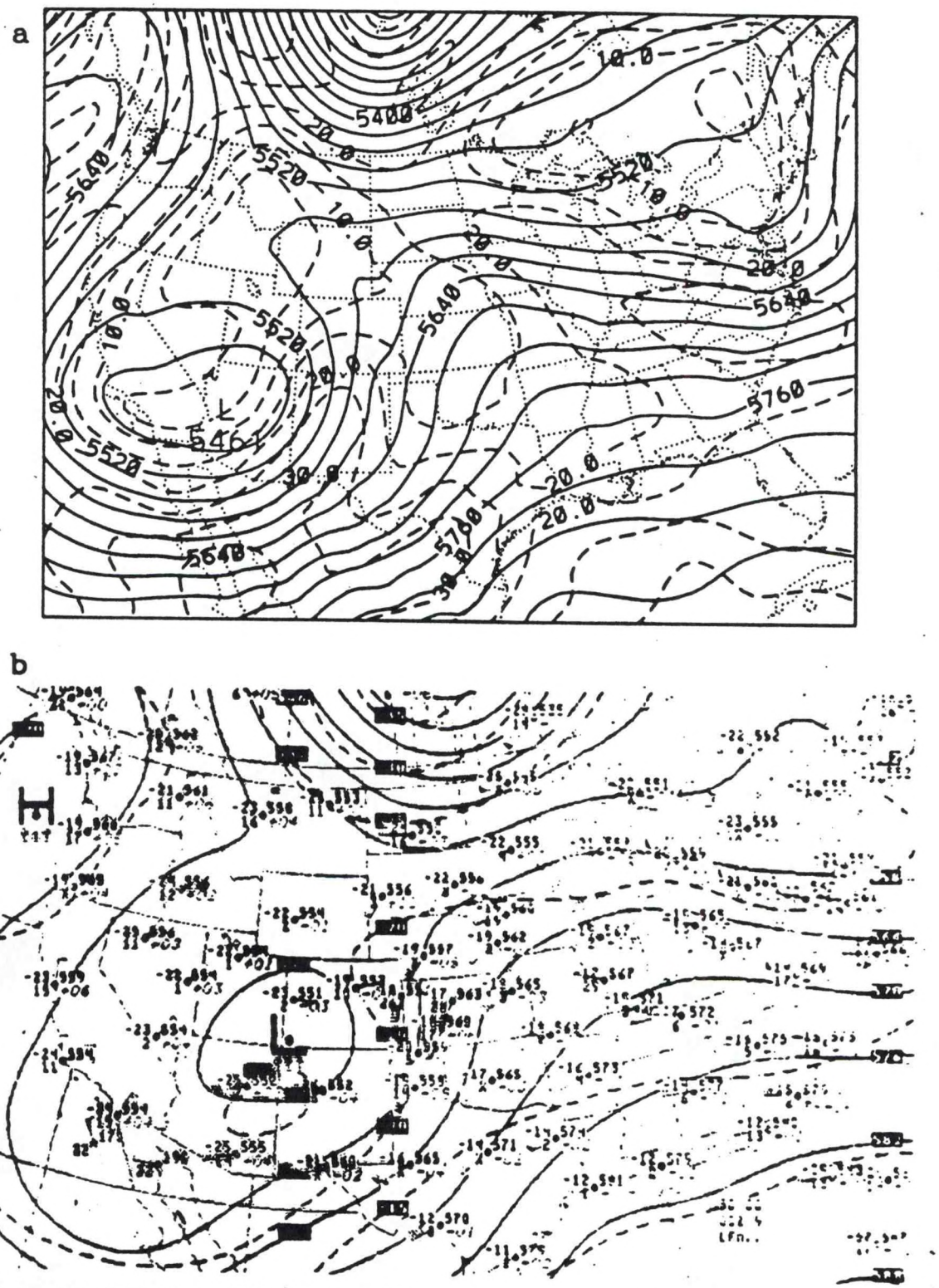

Figure 5.2: NGM 500 mb height (m, solid contours) and isotach (m s^{-1}, dashed contours) analyses from (a) 1200 UTC 8 March and (b) 0000 UTC 9 March 1992.

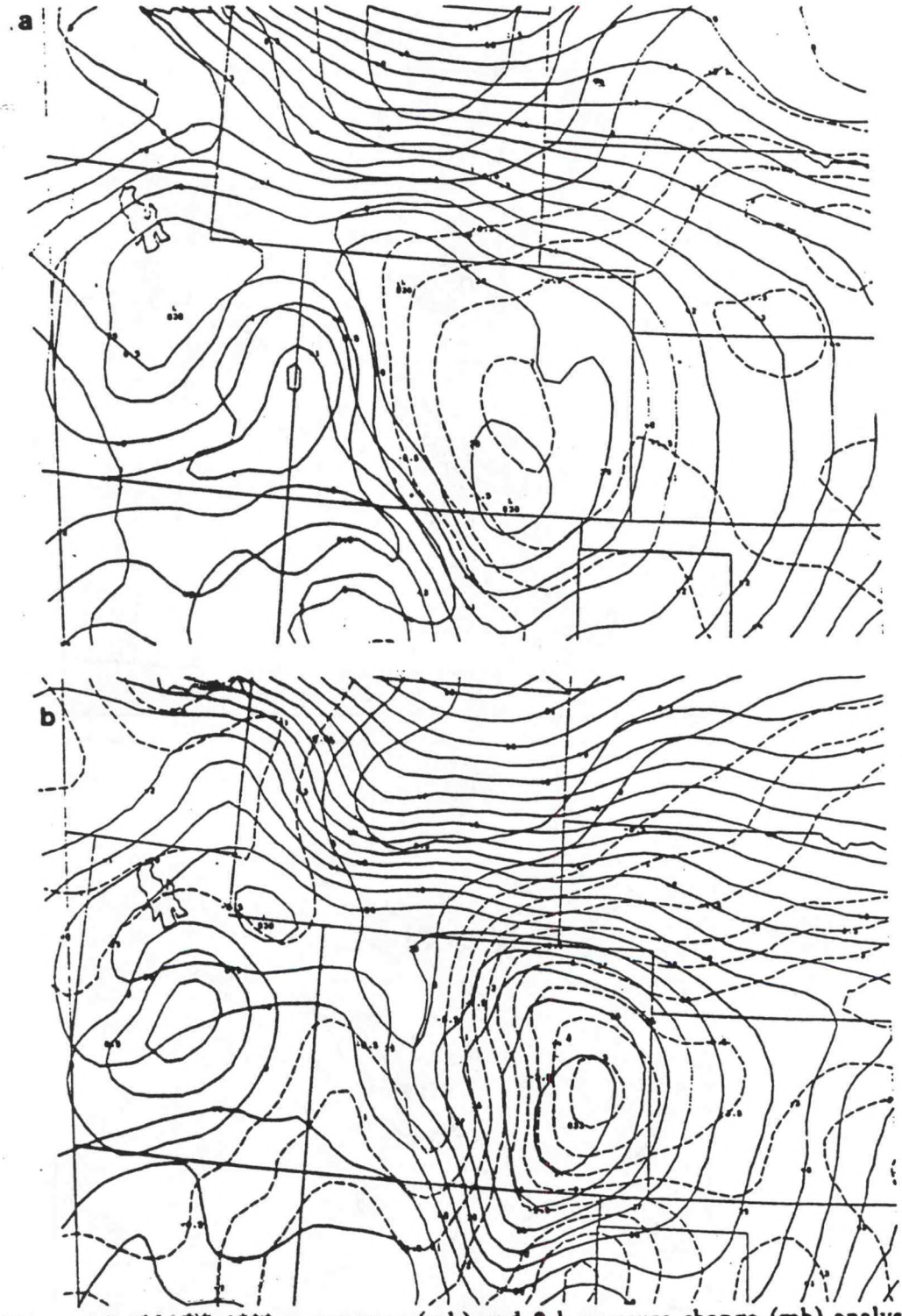

Figure 5.5: MAPS 1500 m pressure (mb) and 3 h pressure change (mb) analyses from (a) 1800 UTC and (b) 2200 UTC 8 March 1992.

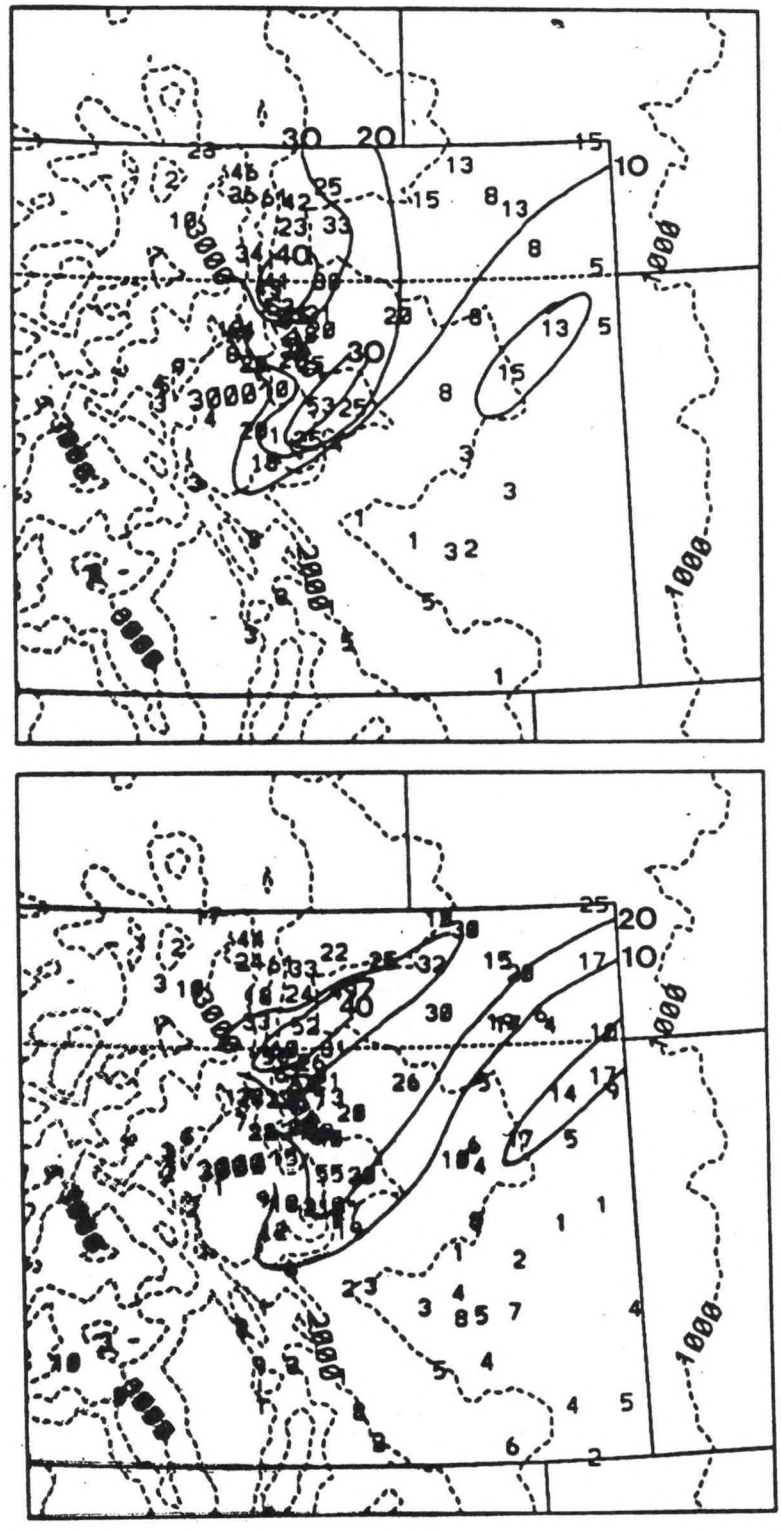

Figure 5.1: Observed precipitation during the 8-9 March 1992 snow storm, (a) snowfall (cm) and (b) melted water equivalent (mm).

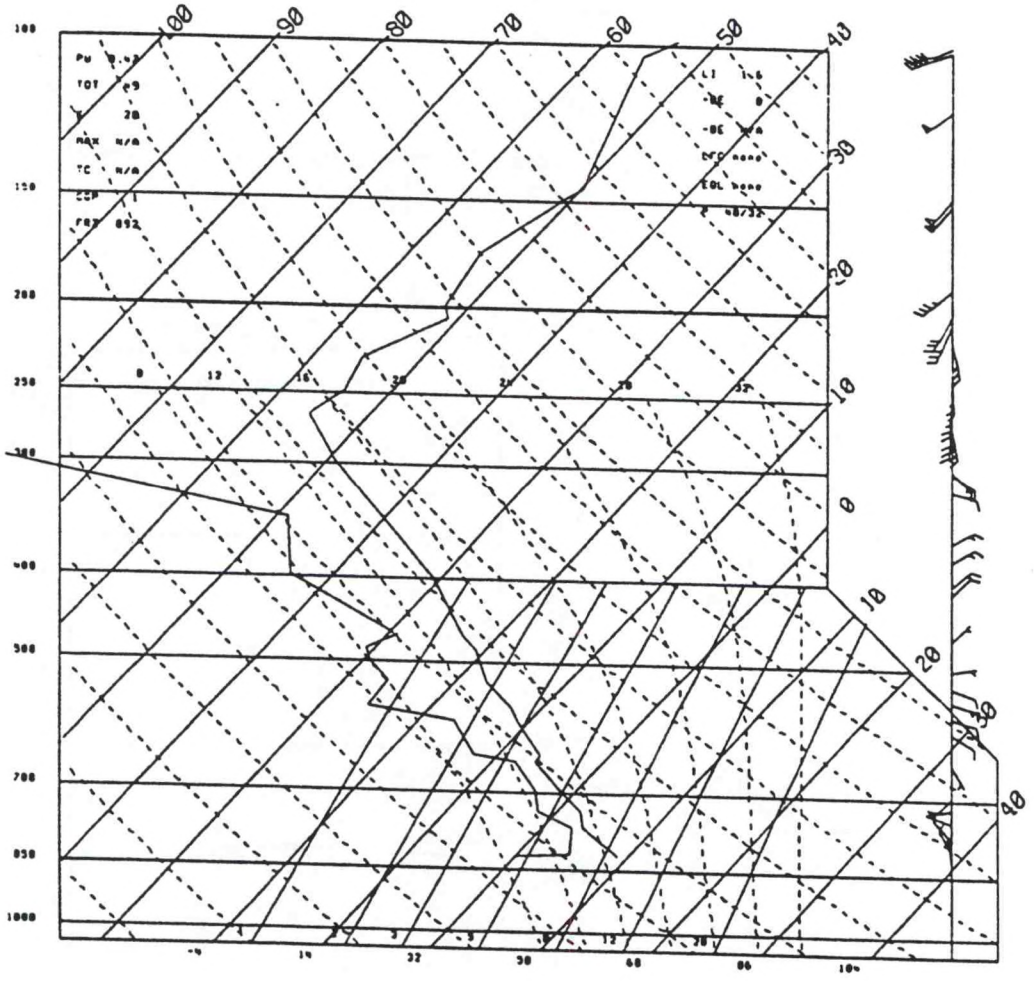

Figure 5.9: Continued: Rawinsonde observations from 0000 UTC 9 March 1992 at (d) Denver, CO.

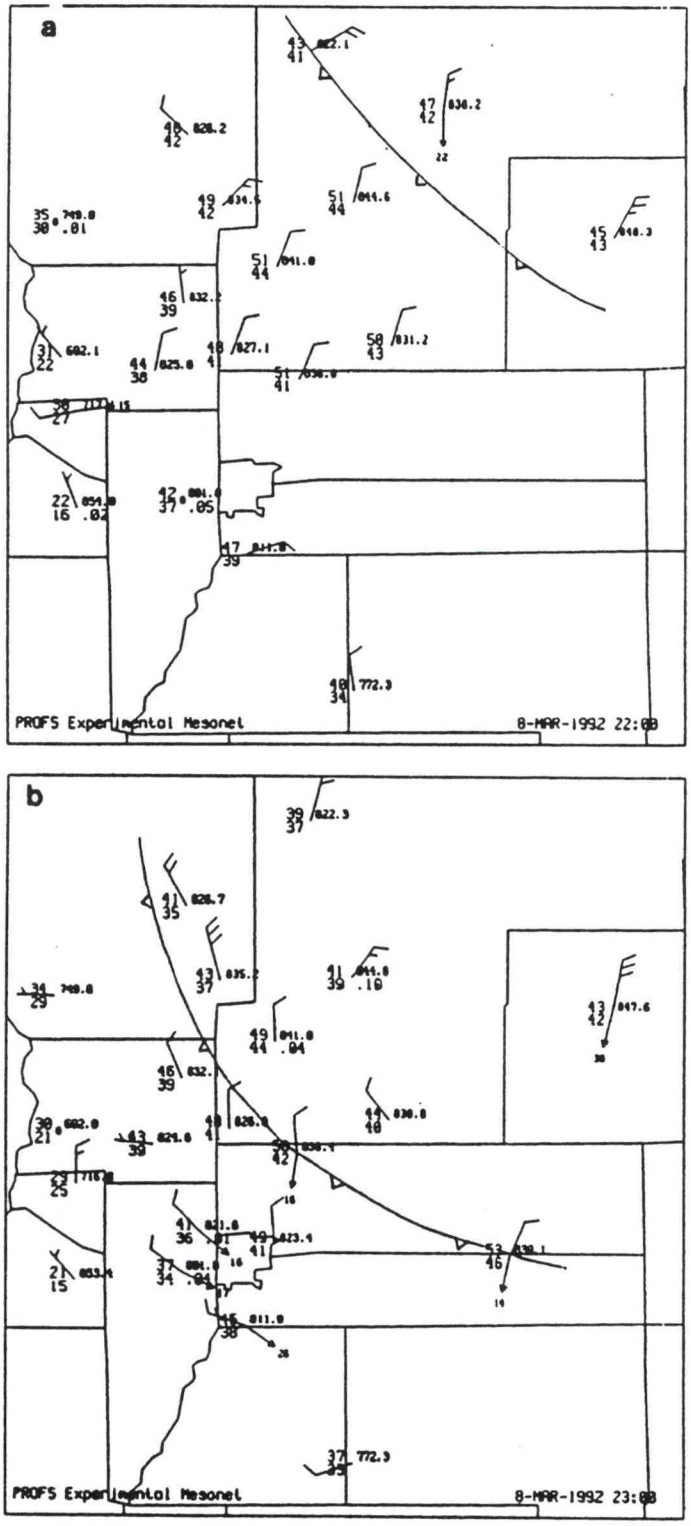

Figure 5.10: Automated surface observations from the FSL mesonet for (a) 2200 UTC and (b) 2300 UTC 8 March 1992 (winds are in knots).

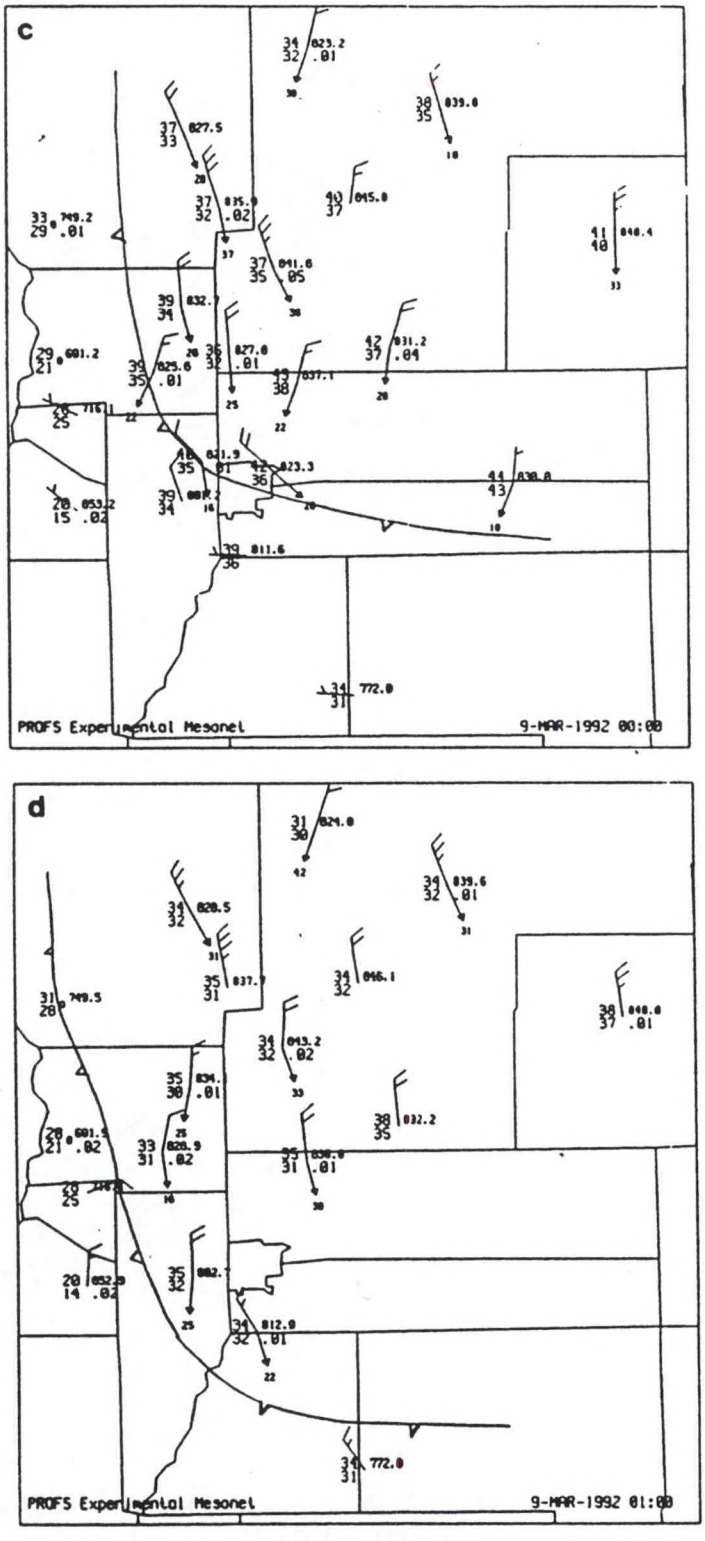

Figure 5.10: Continued: (c) 0000 UTC and (d) 0100 UTC 9 March 1992

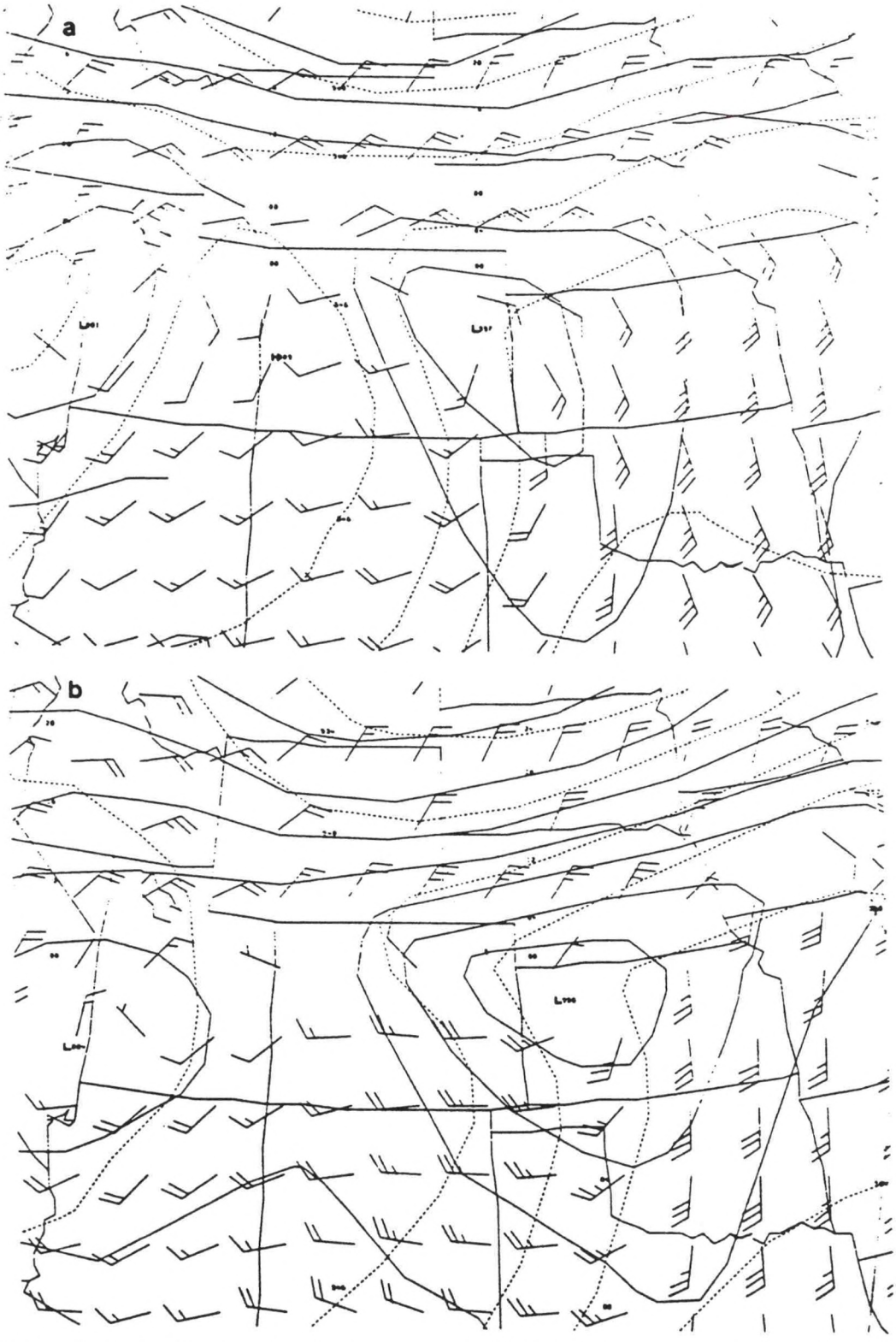

Figure 5.49: NGM mean sea-level pressure (mb), 1000-500 mb thickness (m), and surface wind (knots) predictions from (a) the 12 h forecast valid at 0000 UTC and (b) the 18 h forecast valid at 0600 UTC 9 March 1992.

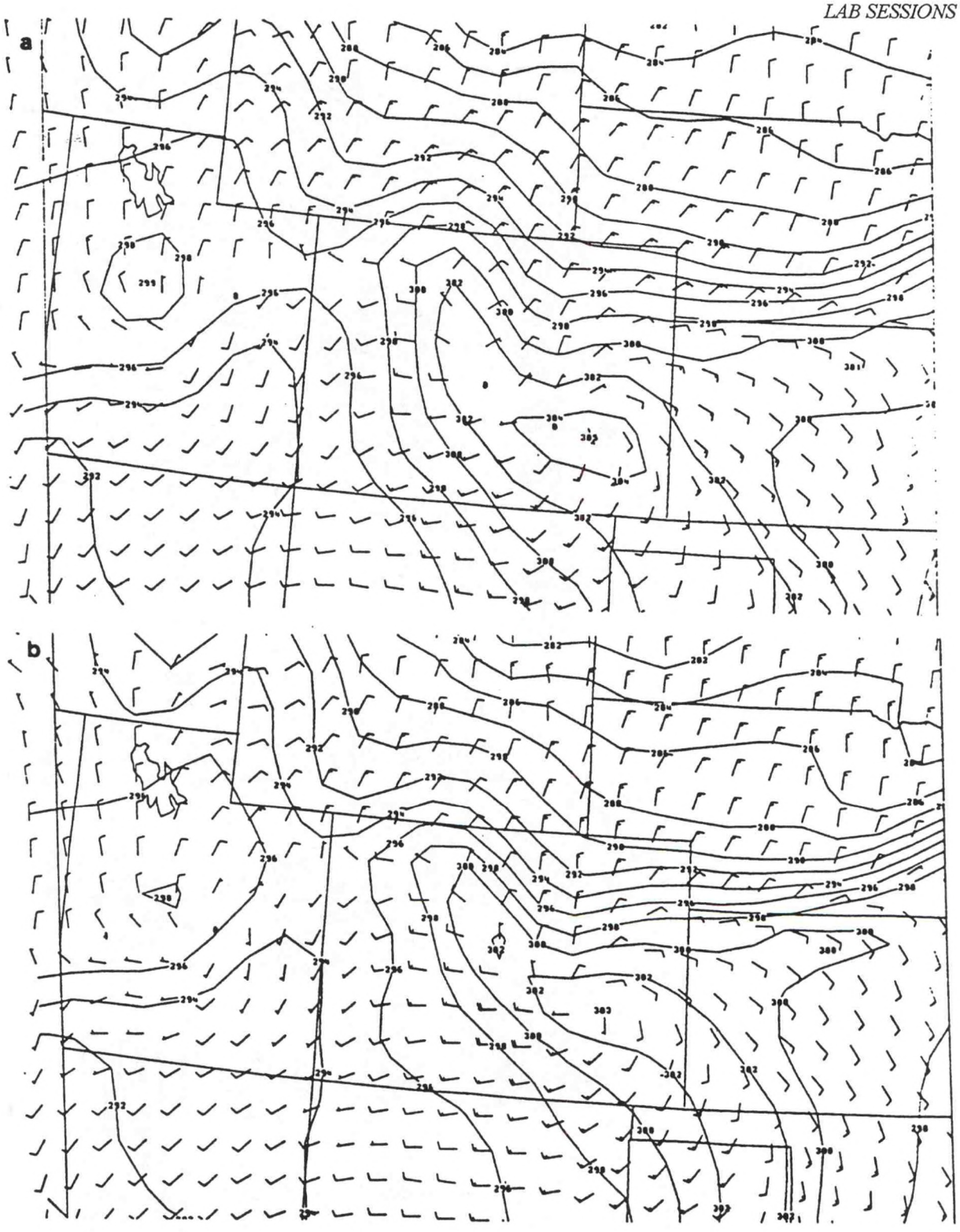

Figure 5.48: MAPS potential temperature (K) and surface wind (knots) predictions from (a) the 3 h forecast valid at 0000 UTC and (b) the 6 h forecast valid at 0300 UTC 9 March 1992.

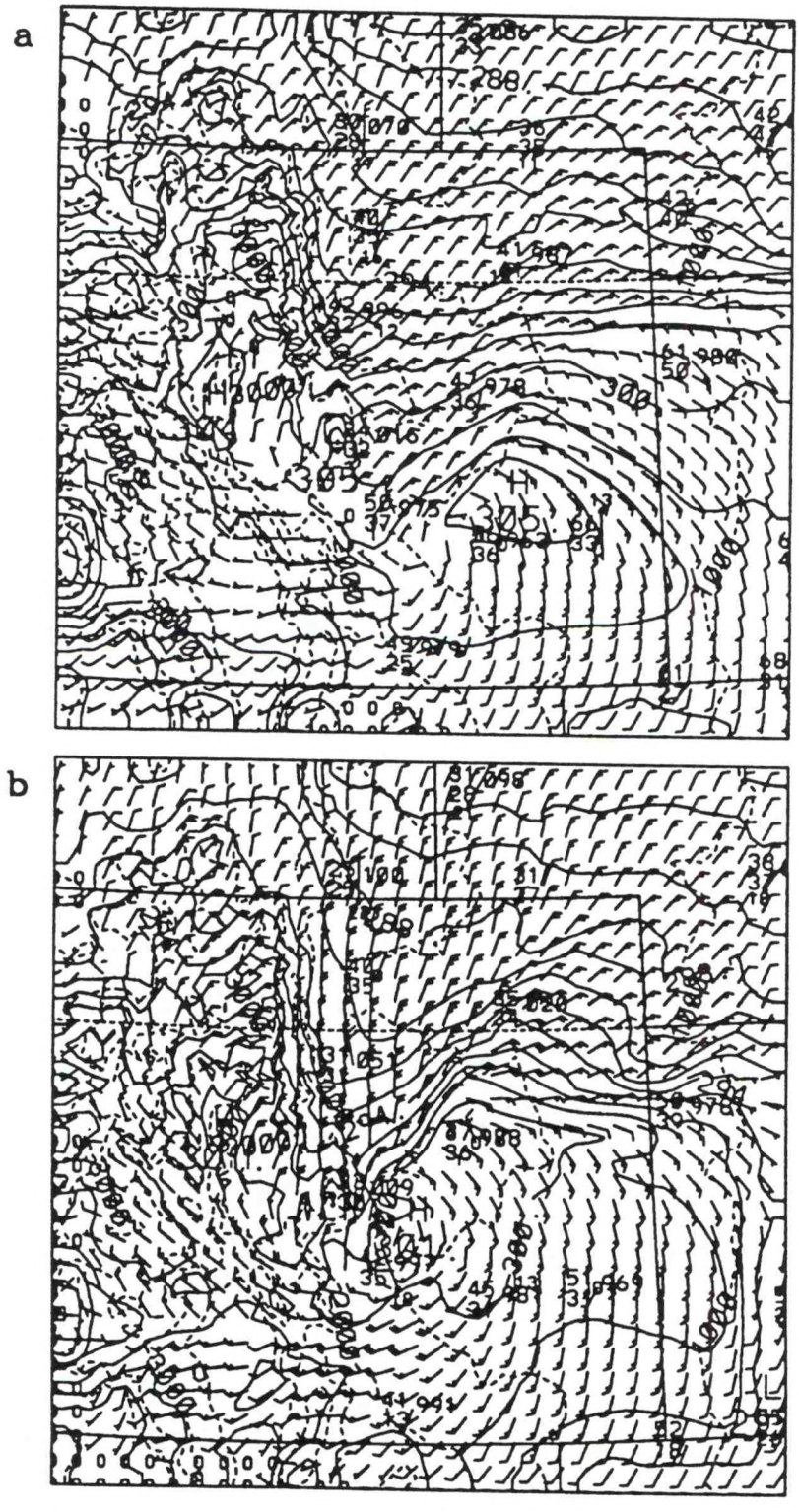

Figure 5.14: RAMS (LSFC) low-level (146 m AGL) potential temperature (K, contour interval = 1.5 K) and wind ($m\ s^{-1}$) predictions and actual SAO reports at model validation time from (a) the 3 h forecast valid at 0000 UTC and (b) the 6 h forecast valid at 0300 UTC 9 March 1992. Dashed contours represent model topography. Wind barbs are displayed at every other grid point.

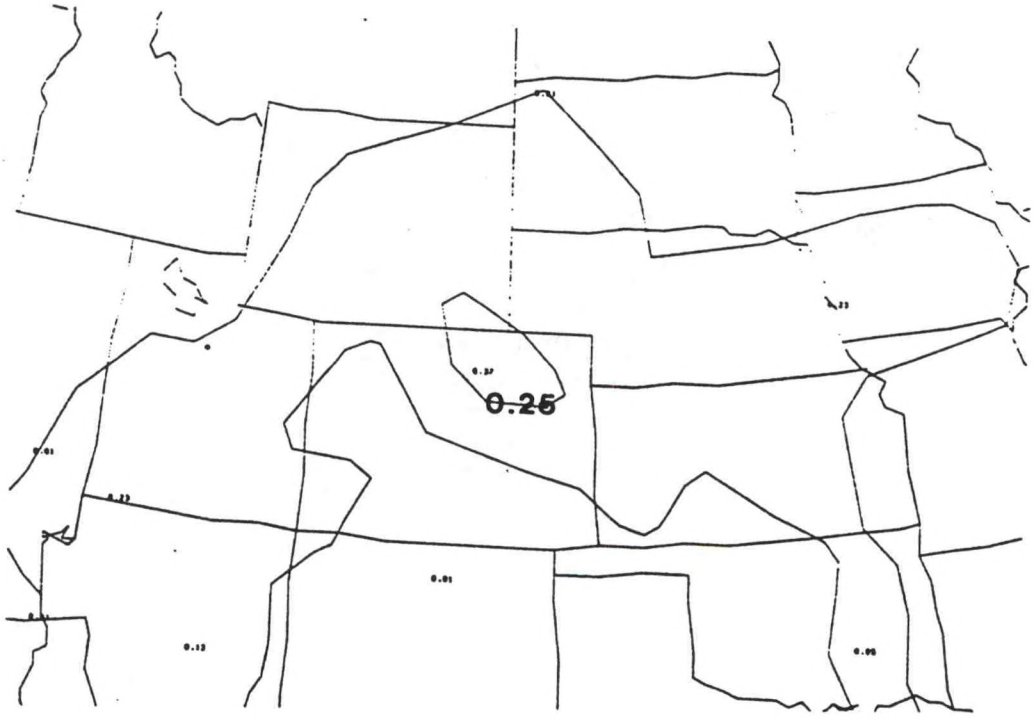

Figure 5.50: NGM 12 h melted precipitation (inches) forecast valid at 0000 UTC 9 March 1992

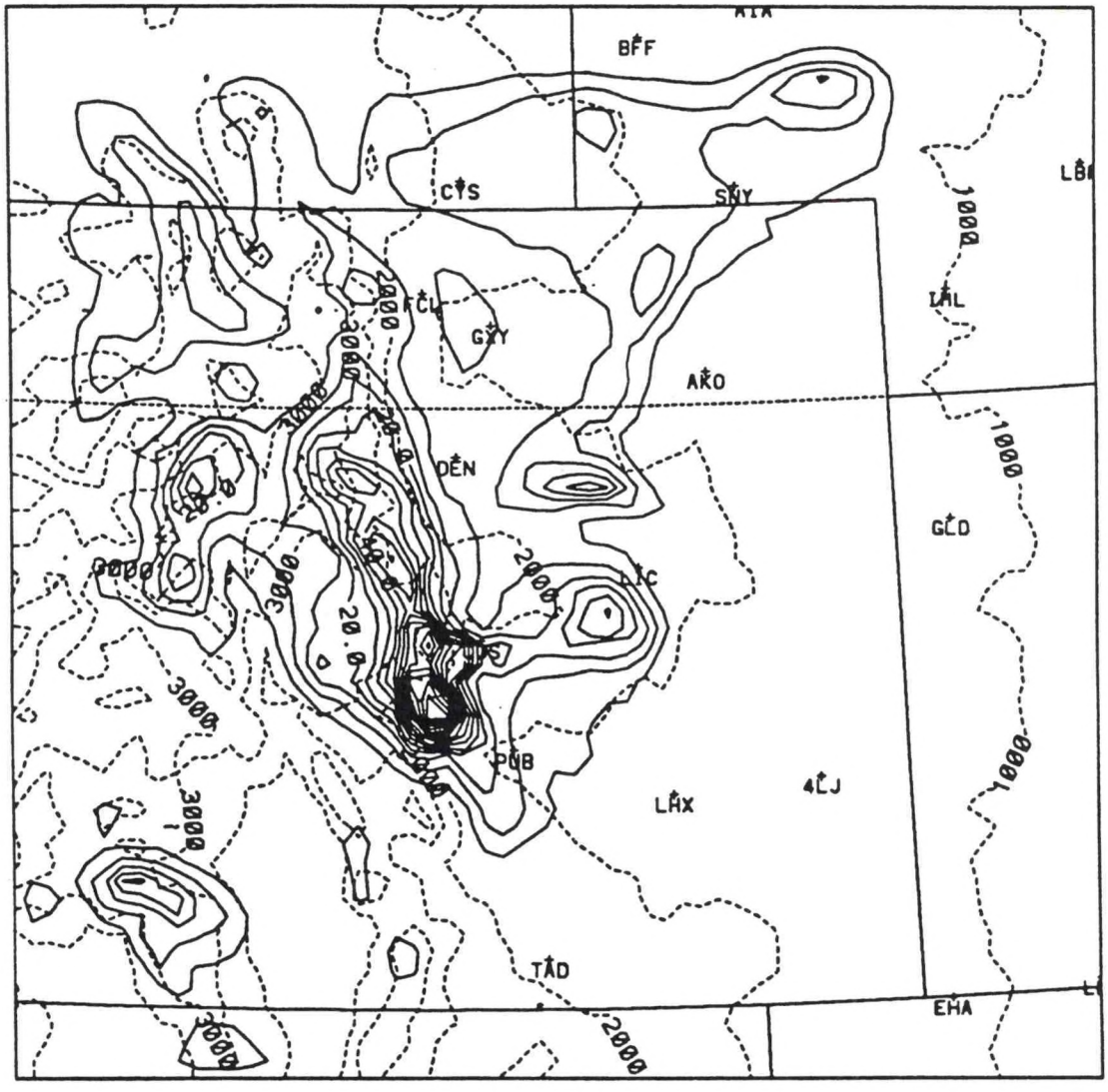

Figure 5.33: RAMS (LMIC) 12 h melted precipitation (mm) forecast. Contour interval is 5 mm.

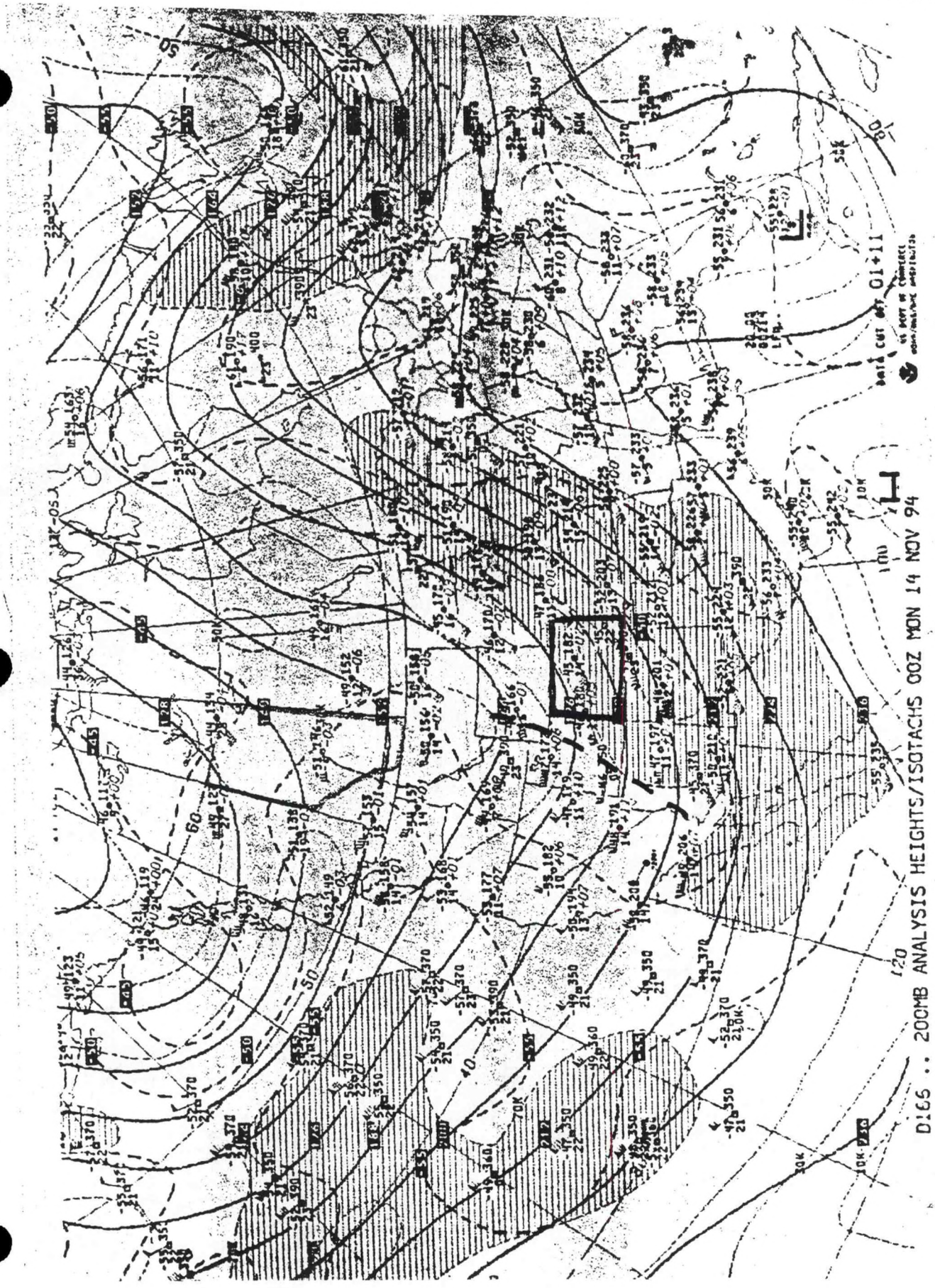
D166 .. 200MB ANALYSIS HEIGHTS/ISOTACHS 00Z MON 14 NOV 94

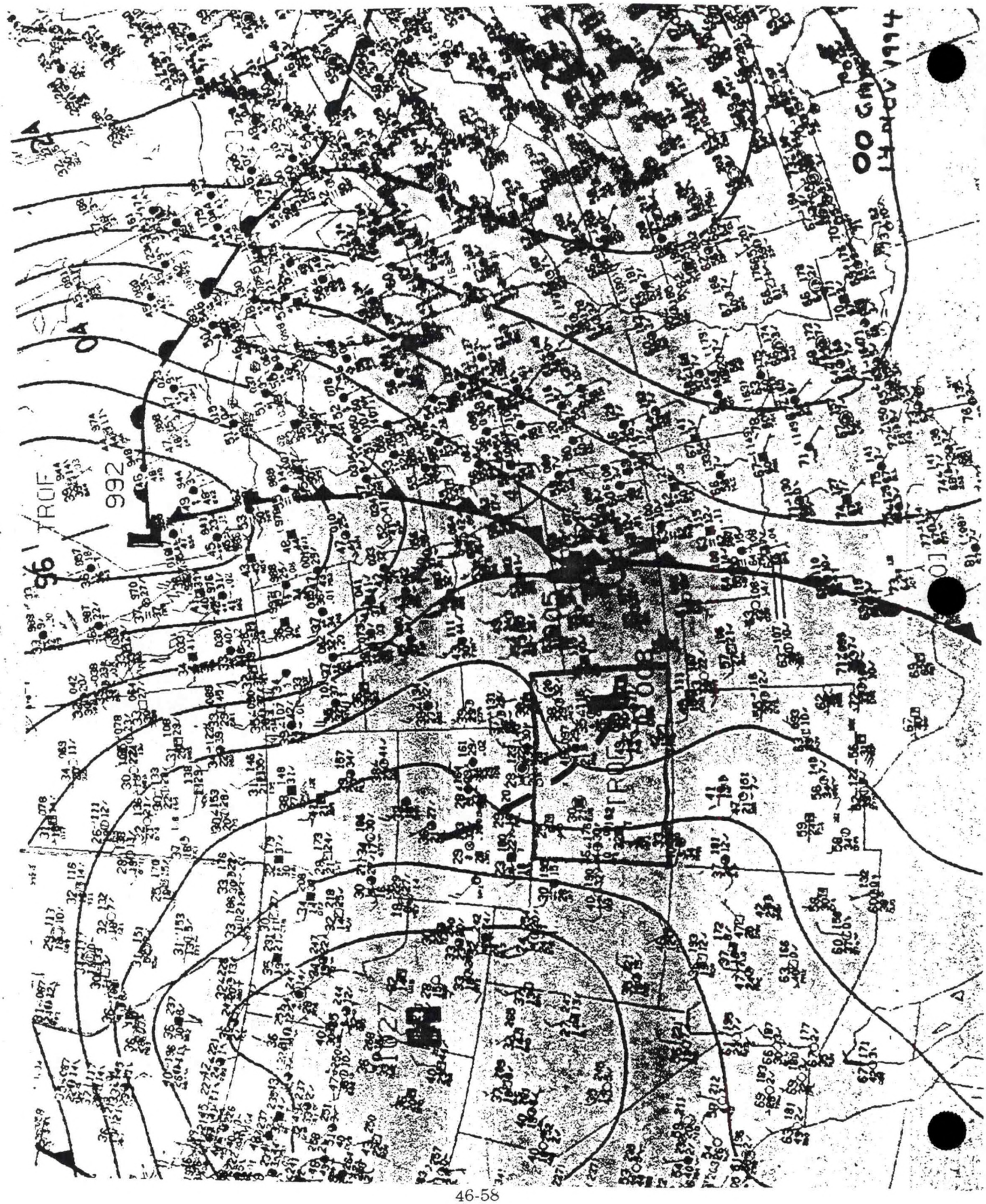

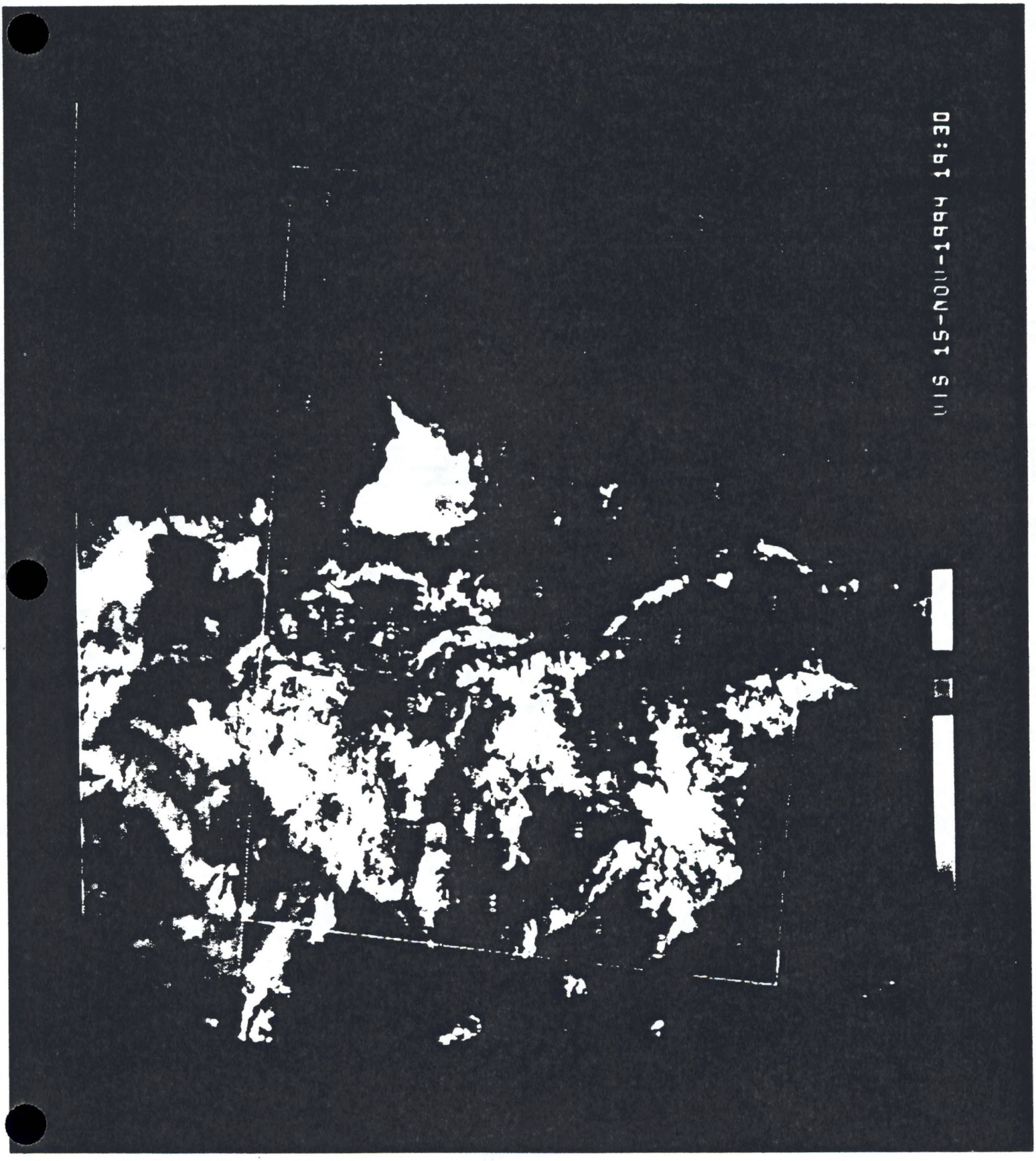
UIS 15-NOV-1994 19:30

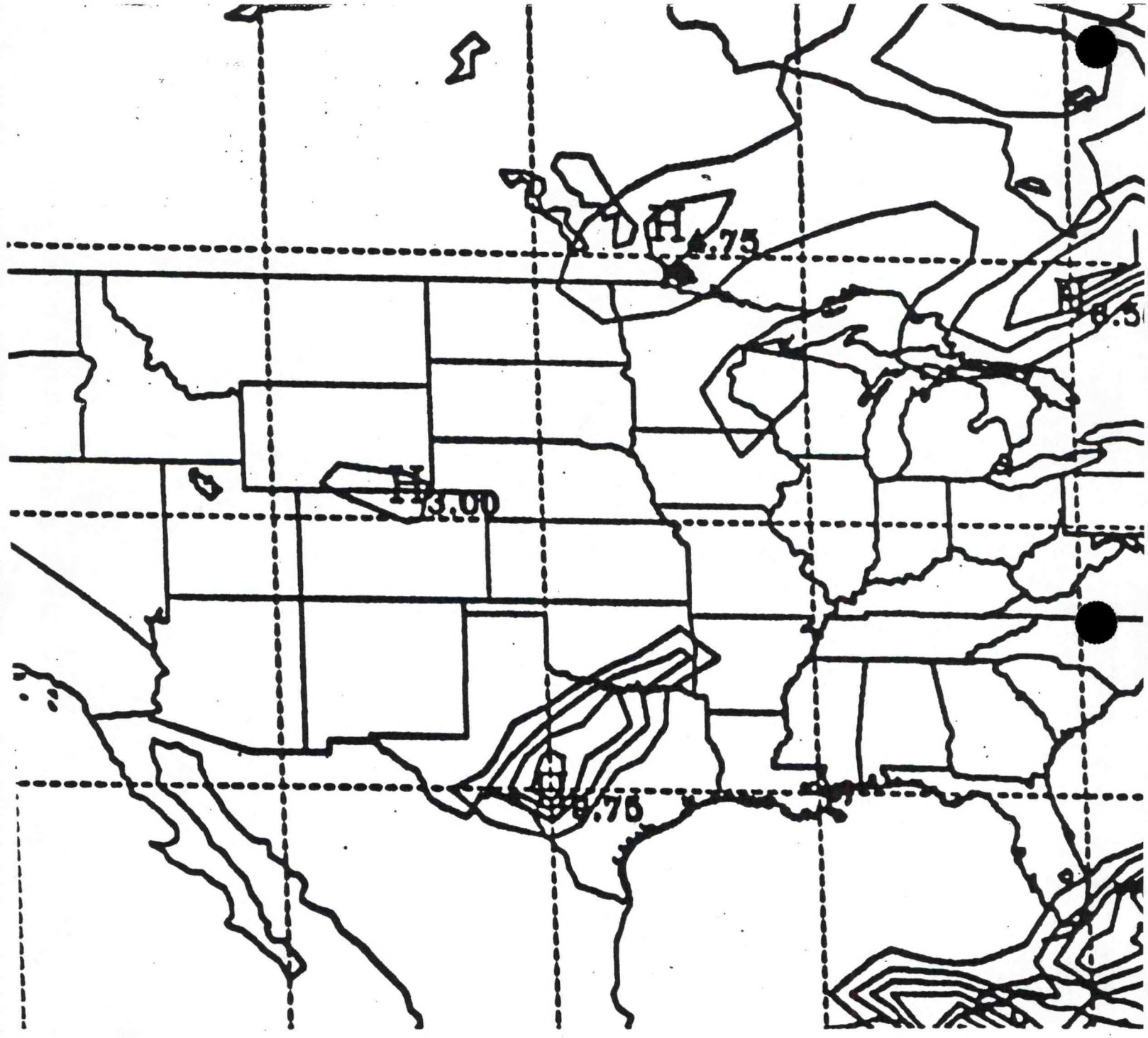

INIT 943180000 1000 MB

NGM 12 HR FCST PRECIP (MM)

MAPS 12 HR FCST
INIT 943180000

LARGE SCALE PRECIP (MM)

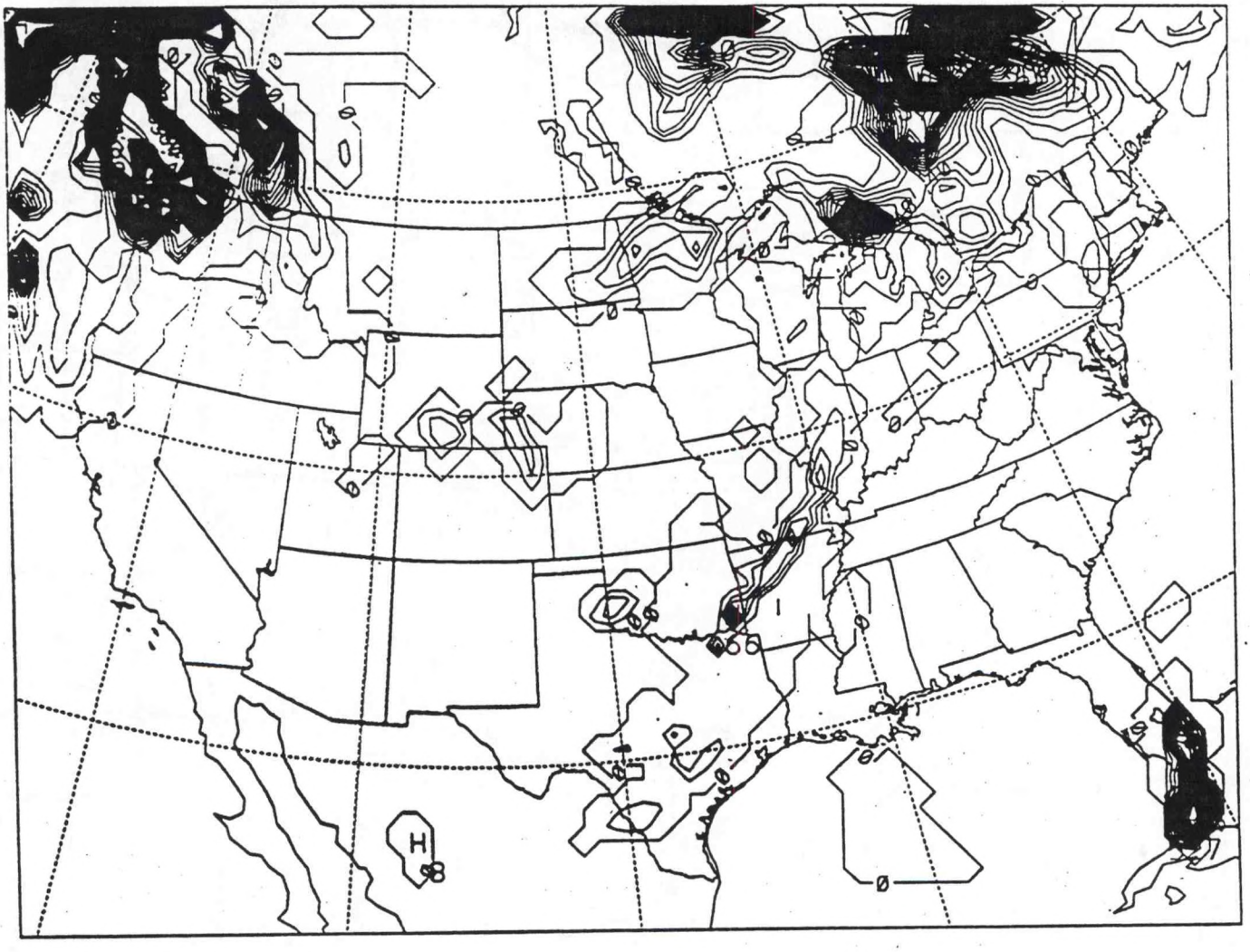

CONTOUR FROM .10000E-03 TO 3.9001 CONTOUR INTERVAL OF .10000 PT(3,3)= .00000E+00 LABELS SCALED BY 100.00

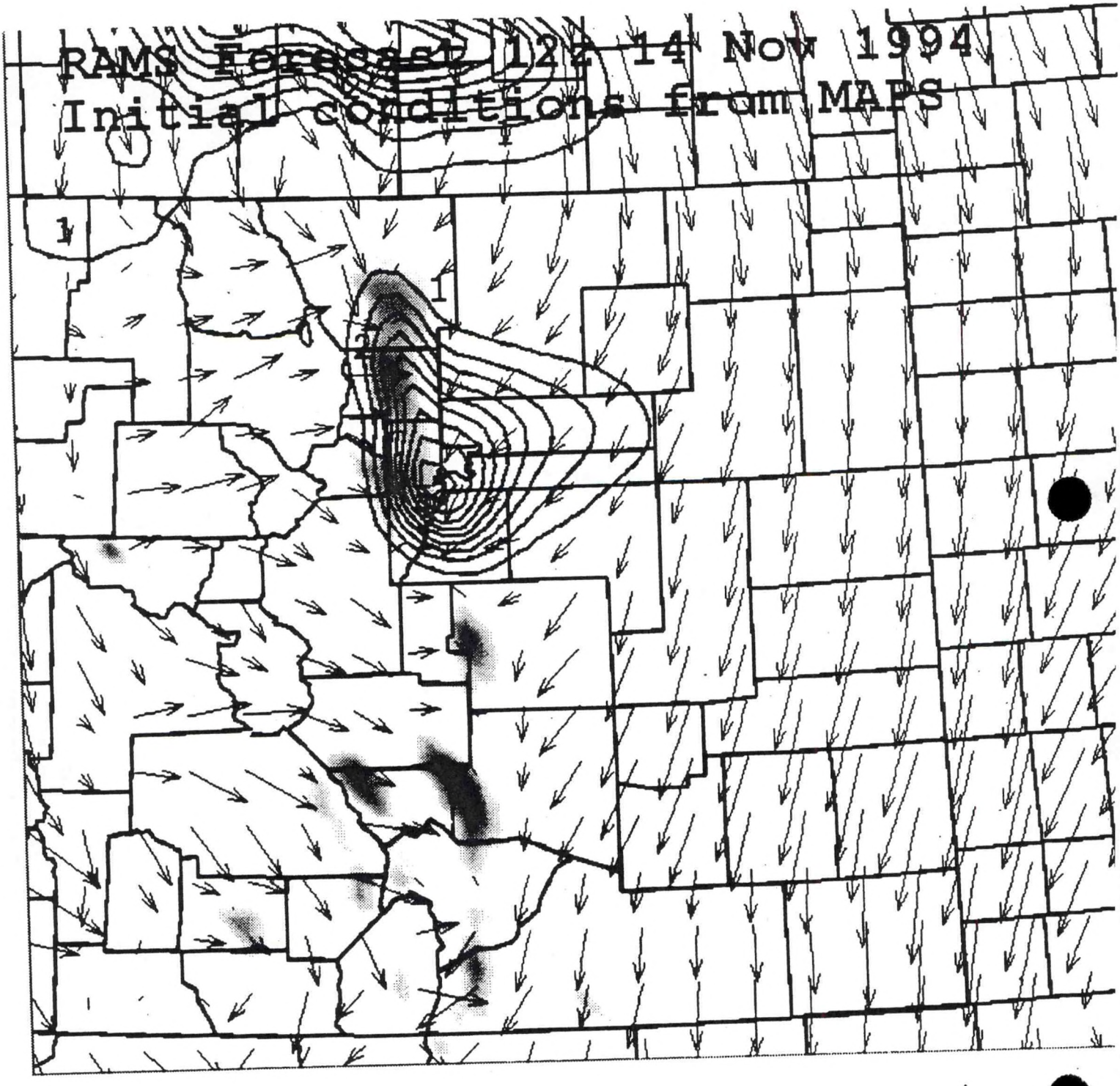
RAMS Forecast 12Z 14 Nov 1994
Initial conditions from MAPS

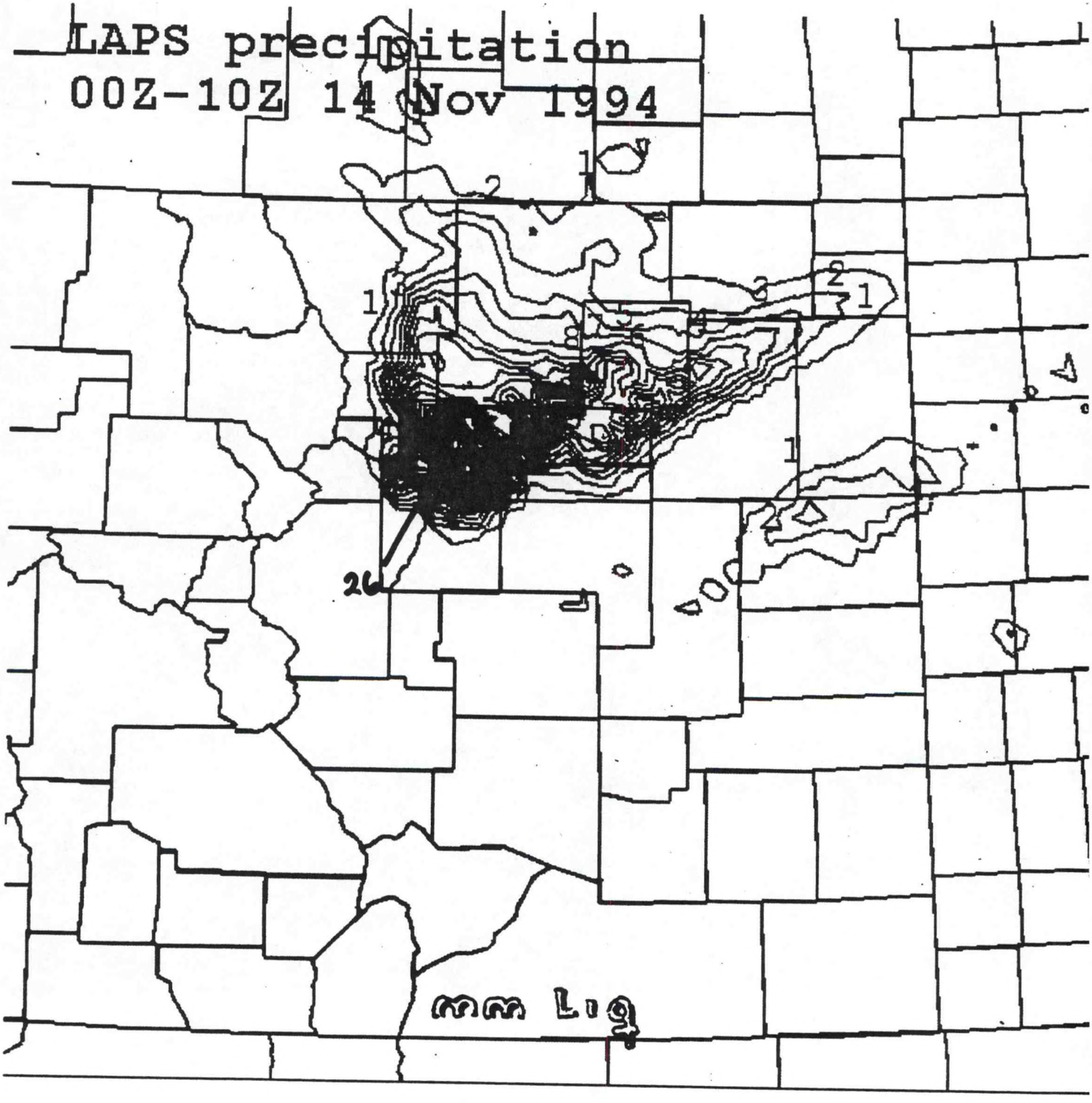
LAPS precipitation
00Z-10Z 14 Nov 1994
1
2
1
1
2
1
2
mm Liq

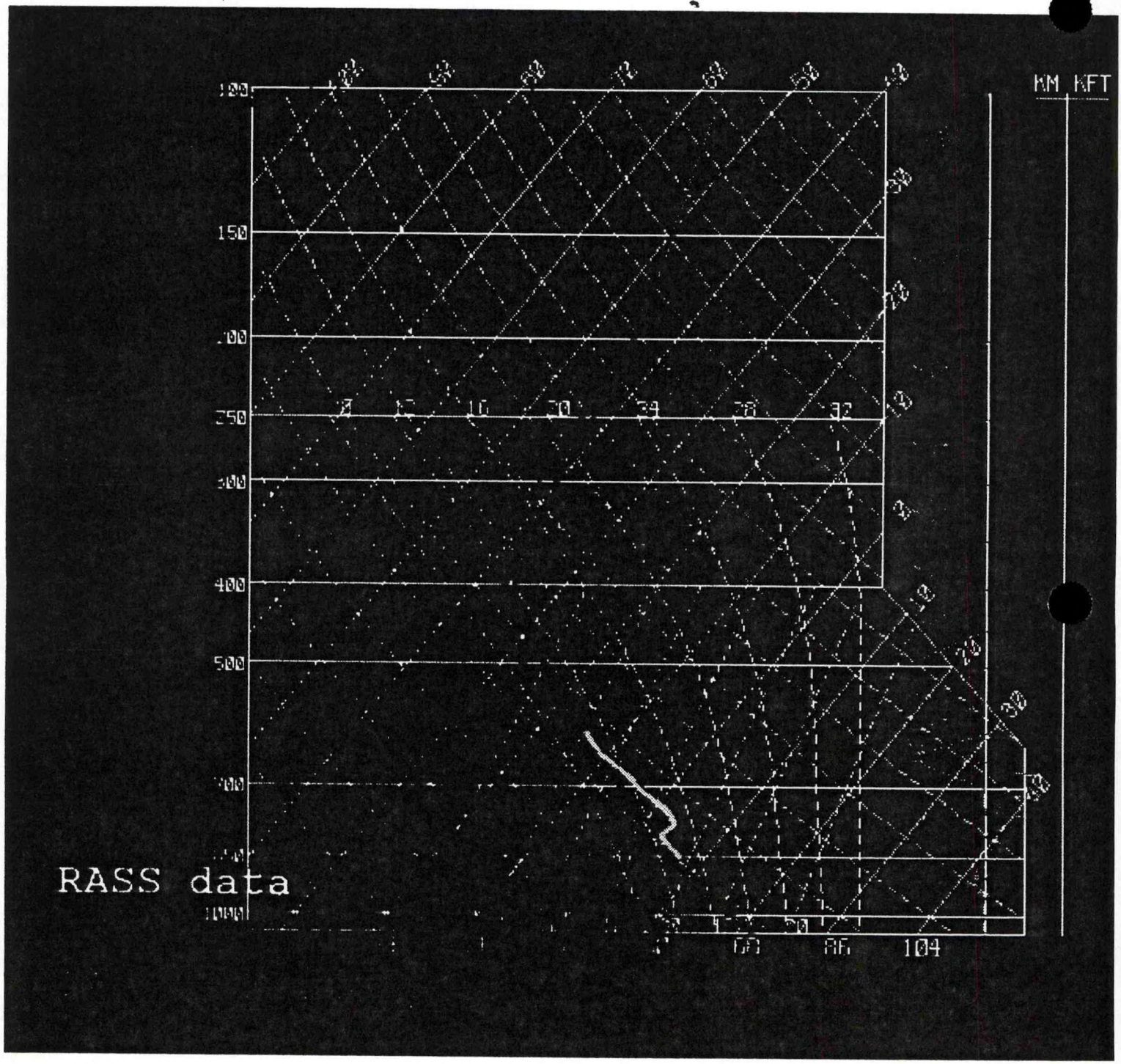
KM KFT
RASS data

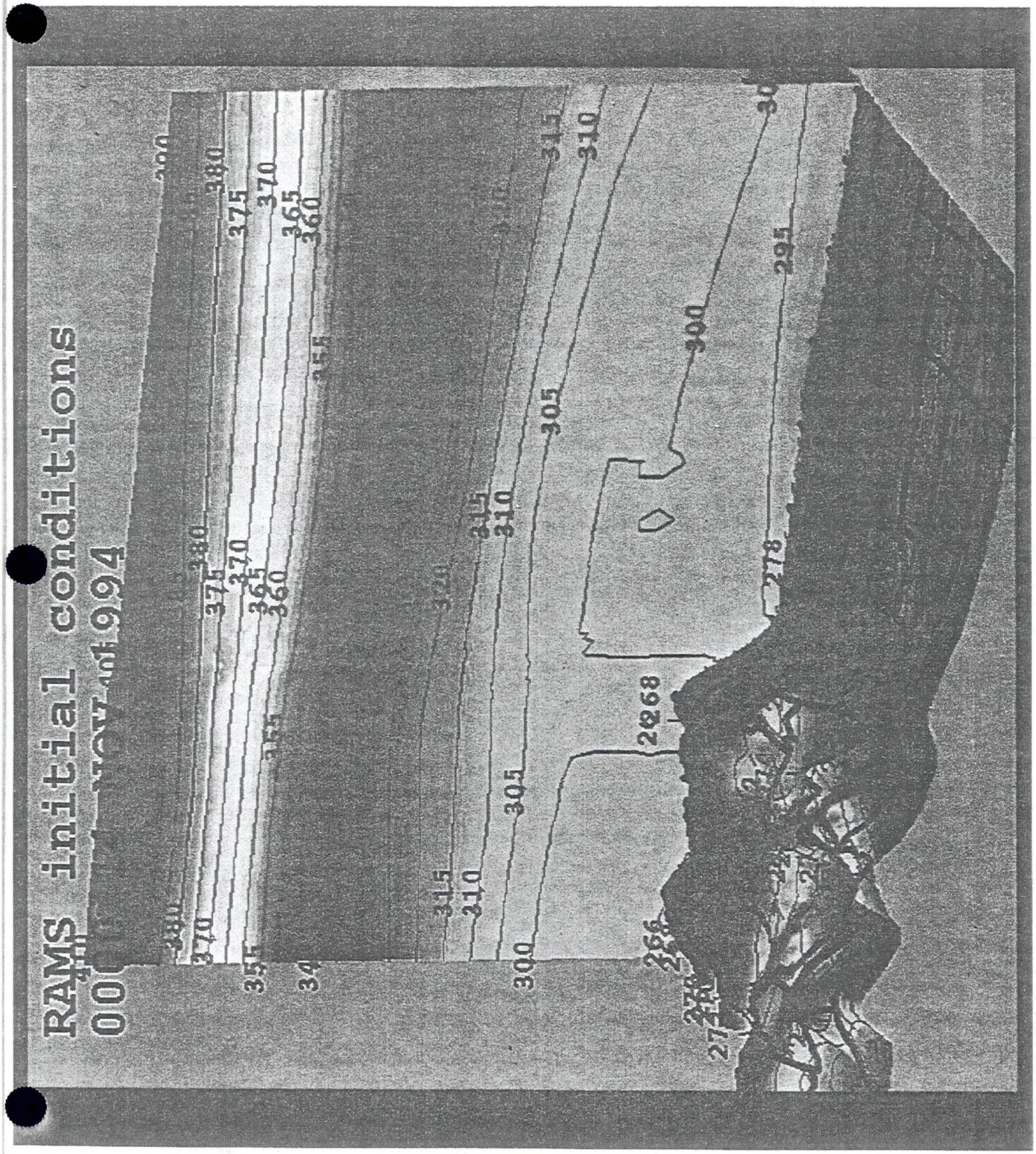
RAMS initial conditions
00
994
380
375
370
365
360
355
350
345
340
335
330
325
320
315
310
305
300
295
290
285
280
275
270
268
266
278

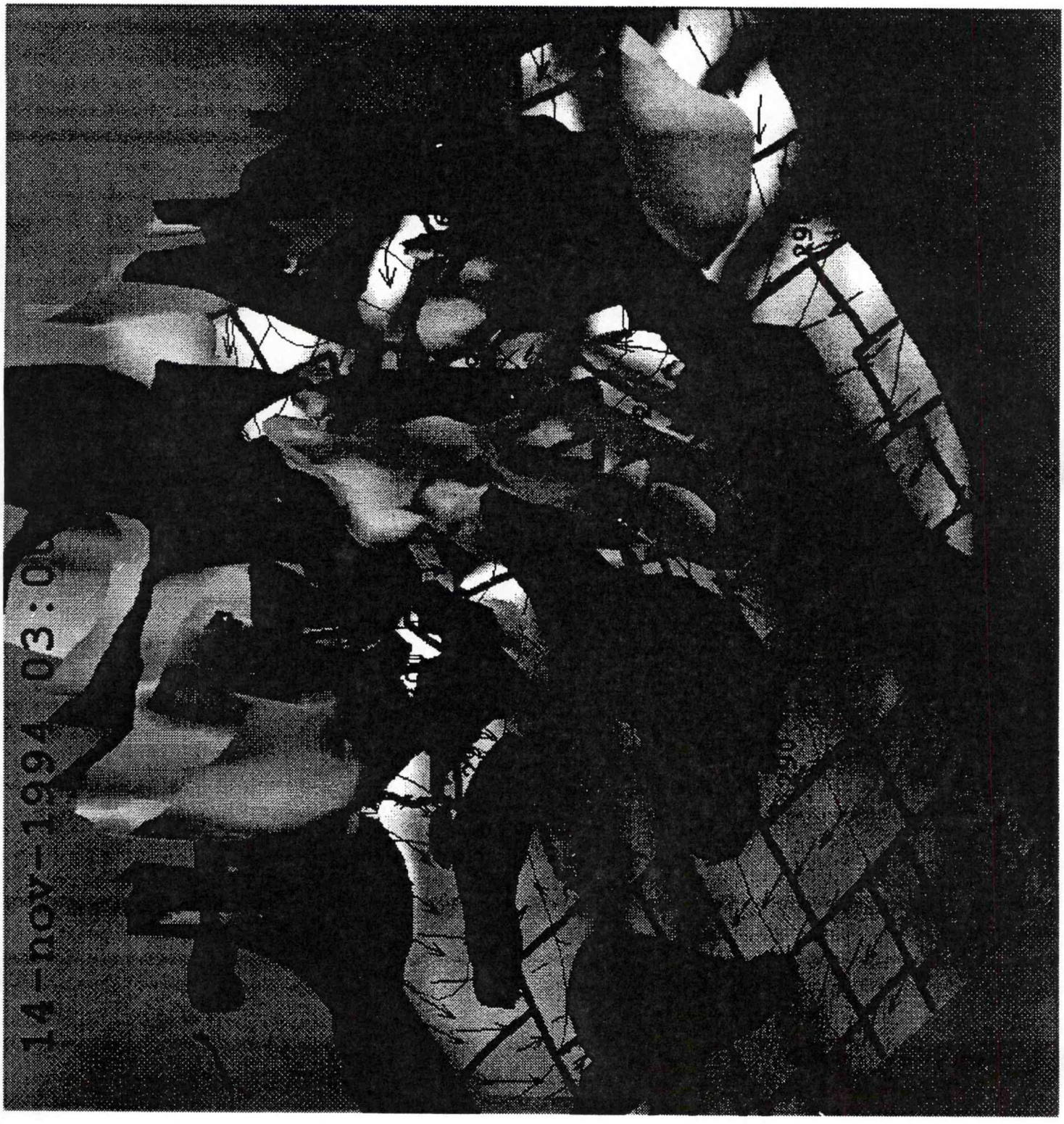
14-NOV-1994 03:0

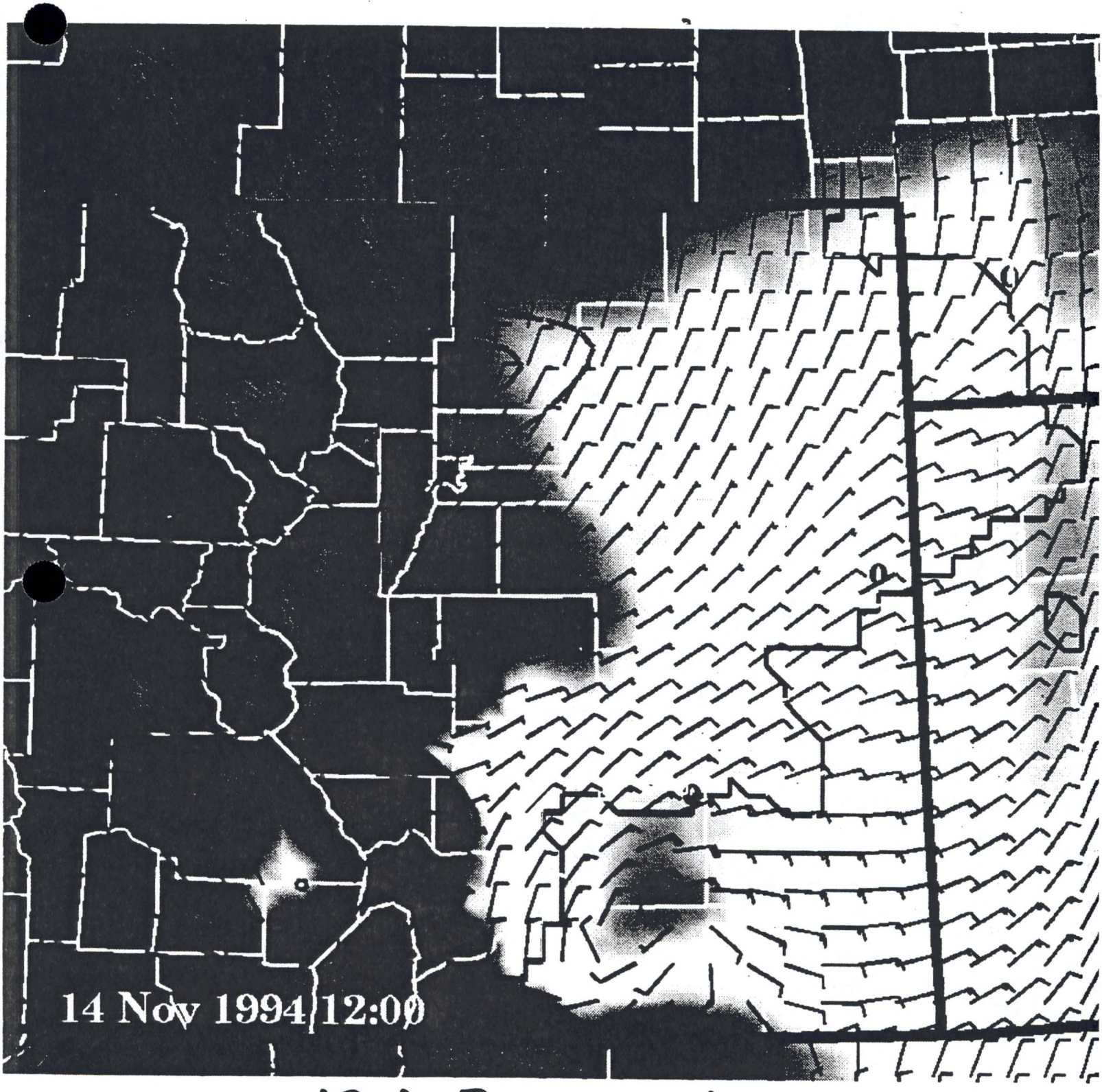

12 h Forecast

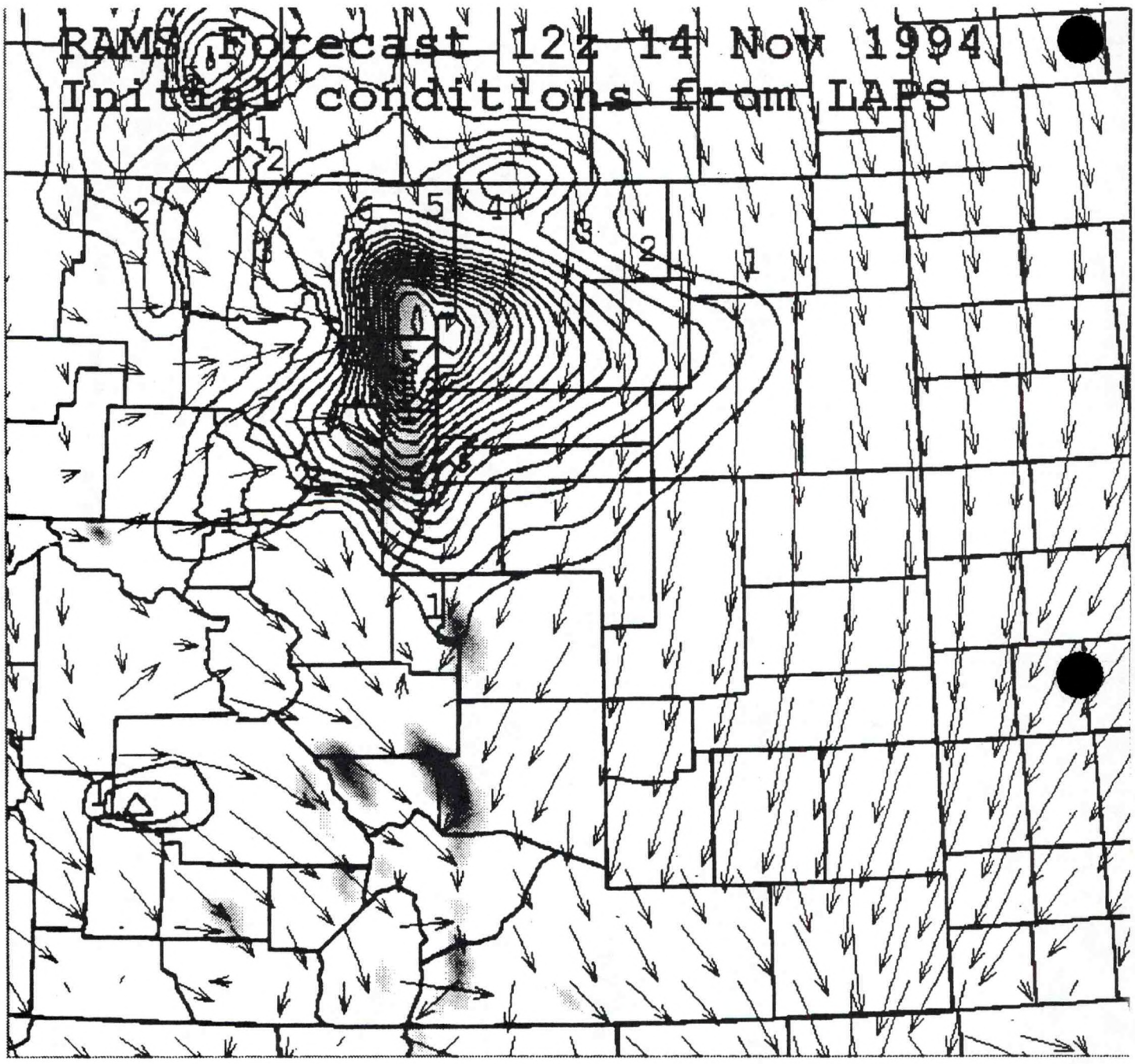
RAMS Forecast 12Z 14 Nov 1994
Initial conditions from LAPS

Differences between MAPS and LAPS initial conditions for 14 Nov 1994 snowstorm simulations

- LAPS vertical profile more unstable (due to RASS).
- LAPS low-level wind convergence more focused over Boulder County area - MAPS convergence strong but spread over large frontal boundary area.
- LAPS had more low level moisture over snowstorm area.

CONCLUSIONS

SUBJECTIVE VERIFICATION OF LAPS MODEL

12-h forecasts from 1200 UTC, initialized from LAPS analysis

COOL SEASON

Reliably predicts meso-beta terrain-induced flow features.

Vertically propagating mountain waves (but not windstorms)
Denver cyclone
Anticyclonic turning in northwest flow (example: 13-14 Nov 94)

Heating-driven daytime upslope is consistently too strong.

WARM SEASON

Reliably forecasts meso-beta terrain-induced flow features.

Reliably indicates an upper bound on overall amount of convection and precipitation.

Is helpful at indicating where initial convection will form.

Not trustworthy once precipitation begins.

NWS CR 47 Practical Application of a Graphical Method of Geostrophic Wind Determination. C.B. Johnson, November 1971 (COM 71-01084).

NWS CR 48 Manual of Great Lakes Ice Forecasting. C. Robert Snider, December 1971 (COM 72-10143).

NWS CR 49 A Preliminary Transport Wind and Mixing Height Climatology, St. Louis, Missouri. Donald E. Wuerch, Albert J. Courtois, Carl Ewald, Gary Ernst, June 1972 (COM 72-10859).

NWS CR 50 An Objective Forecast Technique for Colorado Downslope Winds. Wayne E. Sangster, December 1972 (COM 73-10280).

NWS CR 51 Effect on Temperature and Precipitation of Observation Site Change at Columbia, Missouri. Warren M. Wisner, M[redacted] 1973 (COM 73-10734).

NWS CR 52 Cold Air Funnel Clouds. Jack R. Cooley and Marshall E. Soderberg, September 1973, (COM 73-11753/AS).

NWS CR 53 The Frequency of Potentially Unfavorable Temperature Conditions in St. Louis, Missouri. Warren M. Wisner, October 1973.

NWS CR 54 Objective Probabilities of Severe Thunderstorms Using Predictors from FOUS and Observed Surface Data. Clarence A. David, May 1974 (COM 74-11258/AS).

NWS CR 55 Detecting and Predicting Severe Thunderstorms Using Radar and Sferics. John V. Graff and Duane C. O'Malley June 1974 (COM 74-11335/AS).

NWS CR 56 The Prediction of Daily Drying Rates. Jerry D. Hill, November 1974 (COM 74-11806/AS).

NWS CR 57 Summer Radar Echo Distribution Around Limon, Colorado. Thomas D. Karr and Ronald L. Wooten, November 1974 (COM 75-10076/AS).

NWS CR 58 Guidelines for Flash Flood and Small Tributary Flood Prediction. Lawrence A. Hughes and Lawrence L. Longsdorf, October 1975 (PB247569/AS)

NWS CR 58 (Revised) March 1978 (PB281461/AS)

NWS CR 59 Hourly Cumulative Totals of Rainfall - Black Hills Flash Flood June 9-10, 1972. Don K. Halligan and Lawrence L. Longsdorf, April 1976 (PB256087).

NWS CR 60 Meteorological Effects on the Drift of Chemical Sprays. Jerry D. Hill, July 1976 (PB259593).

NWS CR 61 An Updated Objective Forecast Technique for Colorado Downslope Winds. Wayne E. Sangster, March 1977 (PB266966/AS).

NWS CR 62 Design Weather Conditions for Prescribed Burning. Ronald E. Haug, April 1977 (PB268034).

NWS CR 63 A Program of Chart Analysis (With Some Diagnostic and Forecast Implications). Lawrence A. Hughes, December 1977 (PB279866/AS).

NWS CR 64 Warm Season Nocturnal Quantitative Precipitation Forecasting for Eastern Kansas Using the Surface Geostrophic Wind Chart. Wayne E. Sangster, April 1979 (PB295982/AS).

NWS CR 65 The Utilization of Long Term Temperature Data in the Description of Forecast Temperatures. Arno Perlow, November 1981

(PB82 163064).

NWS CR 66 The Effect of Diurnal Heating on the Movement of Cold Fronts Through Eastern Colorado. James L. Wiesmueller, August 1982 (PB83 118463).

NWS CR 67 An Explanation of the Standard Hydrologic Exchange Format (SHEF) and Its Implementation in the Central Region. Geoffrey M. Bonnin and Robert S. Cox, April 1983 (PB83 193623).

NWS CR 68 The Posting of SHEF Data to the RFC Gateway Database. Geoffrey M. Bonnin, April 1983 (PB83 222554).

NWS CR 69 Some Basic Elements of Thunderstorm Forecasting. Richard P. McNulty, May 1983 (PB83 222604).

NWS CR 70 Automatic Distribution of AFOS Products Created at the NOAA Central Computer Facility via Hamlet (RJE) Punch Stream. Billy G. Olsen and Dale G. Lillie, November 1983 (PB84 122605).

NWS CR 71 An Investigation of Summertime Convection Over the Upper Current River Valley of Southeast Missouri. Bartlett C. Hagemeyer, July 1984 (PB84 222389).

NWS CR 72 The Standard SHEF Decoder Version 1.1. Geoffrey M. Bonnin, August 1984 (PB85 106508).

NWS CR 73 The Blizzard of February 4-5, 1984 Over the Eastern Dakotas and Western Minnesota. Michael Weiland, October 1984 (PB85 120087).

NWS CR 74 On the Observation and Modeling of the Slope Winds of the Upper Current River Valley of Southeast Missouri and Their Relationship to Air-Mass Thunderstorm Formation. Bartlett C. Hagemeyer, June 1985 (PB85 226926/AS).

NWS CR 75 Complete Guide to Canadian Products in AFOS. Craig Sanders, July 1985 (PB85 228153/AS).

NWS CR 76 The Reliability of the Bow Echo as an Important Severe Weather Signature. Ron W. Przybylinski and William J. Gery, September 1985 (PB86 102340).

NWS CR 77 Observation of Bow Echoes with the Marseilles Radar System. John E. Wright, Jr., September 1985 (PB86 102340).

NWS CR 78 Statistical Analysis of SHEF Coding Errors. Robert S. Cox, Jr., January 1986 (PB86 145141).

NWS CR 79 On the Midwestern Diurnal Convergence Zone on the West Side of the Warm Season Bermuda High. Bartlett C. Hagemeyer, March 1986 (PB86 171378).

NWS CR 80 Some Characteristics of Northeast Kansas Severe Weather 1963-1984. Larry W. Schultz, March 1986 (PB86 173952/AS).

NWS CR 81 The Severe Thunderstorm Outbreak of July 6, 1983 in Southeast Idaho, Western Wyoming and Southwest Montana. Gary L. Cox, April 1986 (PB86 184322/AS).

NWS CR 82 Some Proposals for Modifying the Probability of Precipitation Program of the National Weather Service. Wayne E. Sangster and Michael D. Manker, July 1986 (PB86 226636/AS).

NWS CR 83 Deformation Zones and Heavy Precipitation. Henry Steigerwaldt, August 1986 (PB86 229085/AS).

NWS CR 84 An Overview of the June 7, 1984 Iowa Tornado Outbreak. Charles H. Myers, August 1987.

NWS CR 85 Operational Detection of Hail by Radar Using Heights of VIP-5 Reflectivity Echoes. Richard B. Wagenmaker, September 1987.

NWS CR 86 Fire Weather Verification: The Forecaster Does Make a Difference. Therese Z. Pierce and Scott A. Mentzer, December 1987 (PB88 140744).

NWS CR 87 Operational Use of Water Vapor Imagery. Samuel K. Beckman, December 1987 (PB88 140751).

NWS CR 88 Central Region Applied Research Papers 88-1 Through 88-7. NWS Central Region, Scientific Services Division, May 1988 (PB88-210836).

NWS CR 89 Compendiums of Information for the Missouri Basin River Forecast Center and the North Central River Forecast Center. NWS Central Region, Scientific Services Division, June 1988 (PB88-226204).

NWS CR 90 Synoptic-Scale Regimes Most Conducive to Tornadoes in Eastern Wyoming - A Link Between the Northern Hemispheric Scale Circulation and Convective-Scale Dynamics. William T. Parker and Edward K. Berry, July 1988 (PB88-231337).

Continued on Back Cover.

NWS CR 91 Heavy Snowfall in Northwest Wyoming. Michael S. Weiland, September 1988 (PB89 109524).

NWS CR 92 On the Utility of a Geographic Information System in Modelling Climatic Suitability. Bartlett C. Hagemeyer, September 1988 (PB89 109516).

NWS CR 93 The Synoptic and Meso-Alpha Scale Meteorology of Wyoming Flash Floods. Joseph A. Rogash, October 1988 (PB89 117709)

NWS CR 94 The Removal of Stagnant Winter Air Masses From Wyoming's Wind River Basin. Gary L. Cox and Jeffrey M. Graham, November 1988 (PB89 128664).

CR 95 Floods Along Des Plaines and Fox Rivers: September-October 1986. Thomas L. Dietrich, February 1989 (PB89 152797/AS)

CR 96 A Case Study Evaluation of Satellite-Derived Rainfall Estimates and Their Application to Numerical Model Precipitation Forecast Verification. Glenn A. Field, May 1989 (PB89 194591).

NWS CR 97 Central Region Applied Research Papers 97-1 through 97-6. NWS Central Region, Scientific Services Division, July 1989 PB89 213375/AS).

NWS CR 98 The Record Rainfall of August 13-14, 1987 at Chicago, Illinois. Paul Merzlock, November 1989.

NWS CR 99 Central Region Applied Research Papers 99-1 through 99-7. NWS Central Region, Scientific Services Division, November 1989 (PB90 151325).

NWS CR 100 A Guide to Forecasters in Judging Weather Impact on Growth Environments and Farm Operations in the Midwest. John W. Kottke, December 1989 (PB90 141011).

NWS CR 101 Numerical Solutions to the Shallow Water Equations as Applied to a Local Meteorological Forecast Problem. Eric R. Thaler, March 1990 (PB90 191230).

NWS CR 102 Postprint Volume National Weather Service Aviation Workshop Kansas City, Missouri, December 10-13, 1991. NWS Central Region, Scientific Services Division, March 1992 (PB92-176148).

NWS CR 103 An Investigation of Two Microburst Producing Storms Using A Microburst Recognition Algorithm. David Eversole, January 1994 (PB94-156577).

NWS CR 104 Lincoln ASOS Temperature Test January 13-15, 1993, Gregory Grosshans and Phil Clark, March 1994 (PB94-159993).

NWS CR 105 Forecasting Snowfall Using Mixing Ratios on an Isentropic Surface "An Empirical Study", Crispin Garcia, Jr, May 1994 (PB94-188760).

NWS CR 106 The Use of Profiler Data for Analysis and Nowcasting of a Winter Season Extratropical Cyclone, Bradley S. Small, June 1994 (PB94-187804).

NWS CR 107 Flood Forecasting for the Lower Missouri River Basin: June - September, 1993, John F. Pescatore, September 1994 (PB95-123568).

NWS CR 108 Heterogeneous Nucleation and its Relationship to Precipitation Type, Gregory Smith, April 1995 (PB95-217170).

NWS CR 109 Synoptic, Mesoscale and Radar Aspects of the Northeast Kansas Supercell of September 21, 1993, Kenneth Labas and Brian Walawender, October 1995 (PB96-125075).

NWS CR-110 The Effect of Quantitative Precipitation Forecasts on River Forecasts, Noreen O. Schwein, January 1996 (PB96-154893)

NWS CR-111 Global Model Errors Associated with Rapid Low to High Zonal Wave Number Transitions, Edward K. Berry, March 1996 (PB96-166509).